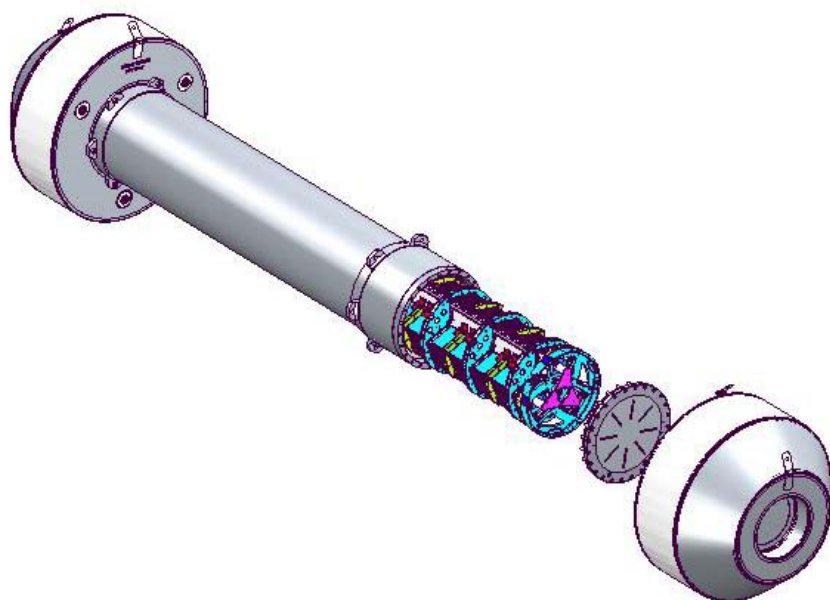




DOCKET 71-9295

Mixed Oxide Fresh Fuel Package



Safety Analysis Report

Volume 1
Revision 7
July 2008

This page left intentionally blank.

TABLE OF CONTENTS

1.0	GENERAL INFORMATION	1.1-1
1.1	Introduction.....	1.1-1
1.2	Package Description	1.2-1
1.2.1	Packaging	1.2-1
1.2.1.1	Body	1.2-1
1.2.1.2	Strongback	1.2-2
1.2.1.3	Impact Limiters	1.2-3
1.2.1.4	Gross Weight	1.2-4
1.2.1.5	Neutron Moderation and Absorption	1.2-4
1.2.1.6	Receptacles, Valves, Testing and Sample Ports	1.2-4
1.2.1.7	Heat Dissipation.....	1.2-4
1.2.1.8	Coolants	1.2-4
1.2.1.9	Protrusions	1.2-4
1.2.1.10	Lifting and Tie-down Devices	1.2-5
1.2.1.11	Pressure Relief Systems.....	1.2-5
1.2.1.12	Shielding	1.2-5
1.2.2	Containment System.....	1.2-5
1.2.3	Contents of Packaging.....	1.2-5
1.2.3.1	Radionuclide Inventory.....	1.2-6
1.2.3.2	Maximum Payload Weight	1.2-6
1.2.3.3	Maximum Decay Heat	1.2-6
1.2.3.4	Maximum Pressure Buildup	1.2-6
1.2.4	Operational Features.....	1.2-6
1.3	General Requirements for All Packages.....	1.3-1
1.3.1	Minimum Package Size.....	1.3-1
1.3.2	Tamper-Indicating Feature	1.3-1
1.3.3	Positive Closure.....	1.3-1
1.3.4	Chemical and Galvanic Reactions.....	1.3-1
1.3.5	Valves.....	1.3-1
1.3.6	Package Design	1.3-1
1.3.7	External Temperatures	1.3-2
1.3.8	Venting	1.3-2
1.4	Appendices.....	1.4-1
1.4.1	Nomenclature	1.4.1-1
1.4.2	Packaging General Arrangement Drawings	1.4.2-1

2.0	STRUCTURAL EVALUATION.....	2.1-1
2.1	Structural Design	2.1-1
2.1.1	Discussion	2.1-1
2.1.2	Design Criteria	2.1-1
2.1.2.1	Analytic Design Criteria (Allowable Stresses).....	2.1-2
2.1.2.2	Miscellaneous Structural Failure Modes	2.1-3
2.1.3	Weights and Center of Gravity.....	2.1-6
2.2	Materials	2.2-1
2.2.1	Material Properties and Specifications.....	2.2-1
2.2.2	Chemical and Galvanic Reactions.....	2.2-2
2.2.3	Effects of Radiation on Material	2.2-2
2.3	Fabrication and Examination	2.3-1
2.3.1	Fabrication.....	2.3-1
2.3.2	Examination.....	2.3-1
2.4	Lifting and Tie-down Standards for All Packages	2.4-1
2.4.1	Lifting Devices	2.4-1
2.4.2	Tie-down Devices.....	2.4-1
2.4.2.1	Doubler Plate Weld Stress	2.4-1
2.4.2.2	Doubler Plate Bearing Stress	2.4-2
2.4.2.3	Tie-down Device Overload Condition.....	2.4-2
2.4.2.4	Summary	2.4-3
2.5	General Considerations.....	2.5-1
2.5.1	Evaluation by Test.....	2.5-1
2.5.2	Evaluation by Analysis.....	2.5-1
2.6	Normal Conditions of Transport.....	2.6-1
2.6.1	Heat	2.6-1
2.6.1.1	Summary of Pressures and Temperatures.....	2.6-1
2.6.1.2	Differential Thermal Expansion	2.6-2
2.6.1.3	Stress Calculations	2.6-2
2.6.2	Cold	2.6-8
2.6.3	Reduced External Pressure.....	2.6-9
2.6.4	Increased External Pressure	2.6-10
2.6.5	Vibration and Shock.....	2.6-10
2.6.6	Water Spray	2.6-12
2.6.7	Free Drop.....	2.6-12
2.6.8	Corner Drop.....	2.6-12

2.6.9	Compression.....	2.6-12
2.6.10	Penetration.....	2.6-12
2.7	Hypothetical Accident Conditions.....	2.7-1
2.7.1	Free Drop.....	2.7-1
2.7.1.1	Technical Basis for the Free Drop Tests.....	2.7-2
2.7.1.2	Summary of Results from the Free Drop Testing.....	2.7-3
2.7.2	Crush	2.7-7
2.7.3	Puncture.....	2.7-7
2.7.3.1	Technical Basis for the Puncture Drop Tests.....	2.7-7
2.7.3.2	Summary of Results from the Puncture Drop Tests	2.7-8
2.7.4	Thermal	2.7-8
2.7.4.1	Summary of Pressures and Temperatures.....	2.7-8
2.7.4.2	Differential Thermal Expansion	2.7-9
2.7.4.3	Stress Calculations.....	2.7-9
2.7.5	Immersion – Fissile Material.....	2.7-10
2.7.6	Immersion – All Packages.....	2.7-11
2.7.7	Deep Water Immersion Test (for Type B Packages Containing More than 10^5 A ₂).....	2.7-11
2.7.8	Summary of Damage.....	2.7-12
2.8	Accident Conditions for Air Transport of Plutonium.....	2.8-1
2.9	Accident Conditions for Fissile Material Packages for Air Transport.....	2.9-1
2.10	Special Form.....	2.10-1
2.11	Fuel Rods	2.11-1
2.12	Appendices.....	2.12-1
2.12.1	Impact Limiter Evaluation.....	2.12.1-1
2.12.1.1	Material Properties.....	2.12.1-1
2.12.1.2	Force-Deflection Relations	2.12.1-3
2.12.1.3	Force-Deflection Curves.....	2.12.1-4
2.12.1.4	Impact Analysis Method	2.12.1-4
2.12.1.5	Impact Analysis at Cold Temperature	2.12.1-5
2.12.1.6	Impact Analysis at Hot Temperature	2.12.1-6
2.12.1.7	Worst-Case Slapdown Angle.....	2.12.1-6
2.12.2	Certification Test Plan.....	2.12.2-1
2.12.2.1	Initial Test Conditions	2.12.2-1
2.12.2.2	Certification Test Unit (CTU).....	2.12.2-2
2.12.2.3	Identification of Worst-Case Drop Tests	2.12.2-3

2.12.2.4	Summary of Selected Certification Drop Tests	2.12.2-6
2.12.2.5	Acceptance Criteria.....	2.12.2-8
2.12.3	Certification Test Results	2.12.3-1
2.12.3.1	Introduction.....	2.12.3-1
2.12.3.2	Summary	2.12.3-1
2.12.3.3	Test Facilities.....	2.12.3-2
2.12.3.4	Instrumentation	2.12.3-2
2.12.3.5	Initial Test Conditions	2.12.3-2
2.12.3.6	Test Unit Description.....	2.12.3-3
2.12.3.7	CTU Payloads	2.12.3-5
2.12.3.8	Test Results.....	2.12.3-5
2.12.3.9	Pre-Test and Post-Test Leakage Rate Tests.....	2.12.3-15
2.12.4	Engineering Test Results.....	2.12.4-1
2.12.4.1	Engineering Test Unit Configuration	2.12.4-1
2.12.4.2	Pre-Test Activities	2.12.4-3
2.12.4.3	Summary of Engineering Test Results	2.12.4-4
2.12.5	Fuel Control Structure Evaluation.....	2.12.5-1
2.12.5.1	Summary of Results.....	2.12.5-1
2.12.5.2	Conditions Analyzed.....	2.12.5-2
2.12.5.3	FCS Geometry	2.12.5-2
2.12.5.4	FCS Material Properties.....	2.12.5-3
2.12.5.5	FCS Stress Criteria.....	2.12.5-4
2.12.5.6	FCS Stability Criteria.....	2.12.5-5
2.12.5.7	FCS Vertically Loaded Fuel Load Determination	2.12.5-5
2.12.5.8	FCS Horizontal Loaded Fuel Load Determination.....	2.12.5-8
2.12.5.9	Evaluation Assumptions and Methodology	2.12.5-9
2.12.5.10	FCS Finite Element Analysis (FEA)	2.12.5-10
2.12.5.11	Pinned Connection Elastic Analysis.....	2.12.5-11
2.12.5.12	Fastener Analysis.....	2.12.5-13
2.12.5.13	Lock Plate and Hinge Mounting Brackets.....	2.12.5-15
2.12.5.14	Strongback Global Stability.....	2.12.5-21
2.12.5.15	Strongback Local Stability.....	2.12.5-22
2.12.5.16	Strongback Width-Thickness Ratio - Triangular Core	2.12.5-23
2.12.5.17	Strongback Width-Thickness Ratio - Plate Extensions	2.12.5-24
2.12.5.18	Strongback Axial Stress.....	2.12.5-24
2.12.5.19	Evaluation of Strongback Response to FCS Loads	2.12.5-25
2.12.5.20	Strongback Stress Calculations – Horizontal Loads.....	2.12.5-27
2.12.6	CASKDROP Computer Program.....	2.12.6-1

2.12.6.1	Using CASKDROP to Determine Impact Limiter Deformation Behavior	2.12.6-1
2.12.6.2	An Example Problem for the CASKDROP Program	2.12.6-3
2.12.7	Impact Limiter Weld Joint Test Results.....	2.12.7-1
2.12.7.1	Packaging Weld Joint Design	2.12.7-1
2.12.7.2	Certification Test Unit Weld Joint Design	2.12.7-1
2.12.7.3	Bench Test Results.....	2.12.7-1
2.12.7.4	Conclusions.....	2.12.7-2
2.12.8	Effect of Bounding Weight on Package Structural Responses	2.12.8-1
2.12.8.1	Component Weights.....	2.12.8-1
2.12.8.2	Evaluations.....	2.12.8-1
2.12.8.3	Conclusions.....	2.12.8-7
3.0	THERMAL EVALUATION.....	3.1-1
3.1	Description of Thermal Design.....	3.1-1
3.1.1	Design Features	3.1-1
3.1.1.1	Body	3.1-1
3.1.1.2	Impact Limiters.....	3.1-2
3.1.1.3	Strongback	3.1-2
3.1.1.4	Neutron Moderation and Absorption.....	3.1-3
3.1.1.5	Receptacles, Valves, Testing and Sample Ports	3.1-3
3.1.2	Content's Decay Heat.....	3.1-3
3.1.3	Summary of Temperatures	3.1-3
3.1.4	Summary of Maximum Pressures	3.1-4
3.2	Material Properties and Component Specifications.....	3.2-1
3.2.1	Material Properties	3.2-1
3.2.2	Component Specifications.....	3.2-2
3.3	General Considerations.....	3.3-1
3.3.1	Evaluation by Analysis.....	3.3-1
3.3.1.1	NCT Analytical Model	3.3-2
3.3.1.2	HAC Analytical Model.....	3.3-4
3.3.2	Evaluation by Test.....	3.3-5
3.3.3	Margins of Safety	3.3-5
3.4	Thermal Evaluation for Normal Conditions of Transport.....	3.4-1
3.4.1	Heat and Cold.....	3.4-1
3.4.1.1	Heat.....	3.4-1
3.4.1.2	Cold.....	3.4-3

3.4.2	Maximum Normal Operating Pressure.....	3.4-3
3.4.3	Maximum Thermal Stresses.....	3.4-5
3.4.4	Evaluation of Package Performance for Normal Conditions of Transport.....	3.4-5
3.5	Thermal Evaluation Under Hypothetical Accident Conditions	3.5-1
3.5.1	Initial Conditions.....	3.5-1
3.5.2	Fire Test Conditions	3.5-1
3.5.2.1	Analytical Model	3.5-1
3.5.2.2	Performance of Rigid Polyurethane Foam Under HAC Fire Conditions	3.5-3
3.5.3	Maximum Temperatures and Pressures	3.5-6
3.5.3.1	Maximum Temperatures.....	3.5-6
3.5.3.2	Maximum Pressures.....	3.5-7
3.5.4	Accident Conditions for Fissile Material Packages for Air Transport.....	3.5-8
3.5.5	Evaluation of Package Performance for Accident Conditions of Transport	3.5-8
3.6	Appendices.....	3.6-1
3.6.1	Computer Analysis Results	3.6.1-1
3.6.2	Thermal Model Details.....	3.6.2-1
3.6.2.1	Convection Coefficient Calculation.....	3.6.2-1
3.6.2.2	Effective Thermal Conductivity of MOX Fuel Assemblies	3.6.2-3
4.0	CONTAINMENT.....	4.1-1
4.1	Description of the Containment System	4.1-1
4.1.1	Containment Boundary.....	4.1-1
4.1.1.1	Containment Penetrations	4.1-1
4.1.1.2	Closure	4.1-1
4.1.1.3	Seals	4.1-1
4.1.1.4	Welds	4.1-2
4.1.2	Special Requirements for Plutonium.....	4.1-2
4.2	General Considerations.....	4.2-1
4.2.1	Type A Fissile Package	4.2-1
4.2.2	Type B Packages	4.2-1
4.3	Containment Requirements for Normal Conditions of Transport	4.3-1
4.3.1	Containment of Radioactive Material	4.3-1
4.3.2	Pressurization of the Containment Vessel.....	4.3-1
4.3.3	Containment Criterion.....	4.3-1
4.4	Containment Requirements for Hypothetical Accident Conditions	4.4-1

4.4.1	Fission Gas Products	4.4-1
4.4.2	Containment of Radioactive Material	4.4-1
4.4.3	Containment Criteria	4.4-1
4.5	Leakage Rate Tests for Type B Packages	4.5-1
4.5.1	Fabrication Leakage Rate Tests	4.5-1
4.5.2	Maintenance/Periodic Leakage Rate Tests	4.5-1
4.5.3	Preshipment Leakage Rate Tests.....	4.5-1
5.0	SHIELDING EVALUATION.....	5-1
6.0	CRITICALITY EVALUATION	6.1-1
6.1	Description of Criticality Design	6.1-1
6.1.1	Design Features Important for Criticality	6.1-1
6.1.2	Summary Table of Criticality Evaluation	6.1-1
6.1.3	Criticality Safety Index	6.1-2
6.2	Fissile Material Contents.....	6.2-1
6.3	General Considerations	6.3-1
6.3.1	Model Configuration	6.3-1
6.3.1.1	Contents Model.....	6.3-1
6.3.1.2	Packaging Model	6.3-1
6.3.2	Material Properties	6.3-3
6.3.3	Computer Codes and Cross-Section Libraries	6.3-3
6.3.4	Demonstration of Maximum Reactivity	6.3-4
6.3.4.1	Single Package.....	6.3-4
6.3.4.2	Arrays of Undamaged Packages	6.3-4
6.3.4.3	Arrays of Damaged Packages	6.3-5
6.4	Single Package Evaluation	6.4-1
6.4.1	Single Package Configuration.....	6.4-1
6.4.1.1	NCT Configuration	6.4-1
6.4.1.2	HAC Configuration.....	6.4-1
6.4.2	Single Package Results.....	6.4-3
6.5	Evaluation of Package Arrays Under Normal Conditions of Transport.....	6.5-1
6.5.1	NCT Array Configuration	6.5-1
6.5.2	NCT Array Results.....	6.5-1
6.6	Package Arrays Under Hypothetical Accident Conditions.....	6.6-1
6.6.1	HAC Array Configuration.....	6.6-1
6.6.2	HAC Array Results	6.6-1

6.6.3	Impact of Niobium Content in the Cladding	6.6-2
6.7	Fissile Material Packages for Air Transport.....	6.7-1
6.8	Benchmark Evaluations	6.8-1
6.8.1	Applicability of Benchmark Experiments	6.8-1
6.8.2	Bias Determination.....	6.8-2
6.9	Appendices.....	6.9-1
6.9.1	Single Package Model	6.9.1-1
6.9.2	Infinite Array Model	6.9.2-1
7.0	OPERATING PROCEDURES.....	7.1-1
7.1	Package Loading.....	7.1-1
7.1.1	Preparation for Loading.....	7.1-2
7.1.1.1	Removal of MFFP from the Transport Conveyance.....	7.1-2
7.1.1.2	Removal of the Closure Lid.....	7.1-2
7.1.1.3	Removal of the Strongback from the MFFP	7.1-3
7.1.2	Loading of Contents	7.1-4
7.1.2.1	Loading of Fuel Assemblies into Strongback.....	7.1-4
7.1.2.2	Loading of the Strongback into the MFFP	7.1-5
7.1.2.3	Closure Lid Installation	7.1-7
7.1.3	Preparation for Transport (Loaded).....	7.1-9
7.2	Package Unloading	7.2-1
7.2.1	Receipt of Package from Carrier	7.2-1
7.2.2	Removal of Contents	7.2-1
7.2.2.1	Removal of MFFP from the Transport Conveyance.....	7.2-1
7.2.2.2	Removal of the Closure Lid.....	7.2-1
7.2.2.3	Removal of the Strongback from the MFFP	7.2-3
7.2.2.4	Unloading of FAs from the Strongback.....	7.2-3
7.2.2.5	Loading of the Empty Strongback into the MFFP.....	7.2-4
7.2.2.6	Closure Lid Installation	7.2-6
7.2.2.7	Final Package Preparations for Transport (Unloaded)	7.2-8
7.3	Preparation of an Empty Package for Transport.....	7.3-1
7.4	Preshipment Leakage Rate Test.....	7.4-1
7.4.1	Gas Pressure Rise Leakage Rate Test Acceptance Criteria	7.4-1
7.4.2	Determining the Test Volume and Test Time	7.4-1
7.4.3	Performing the Gas Pressure Rise Leakage Rate Test	7.4-2
7.4.4	Optional Preshipment Leakage Rate Test	7.4-2

8.0	ACCEPTANCE TESTS AND MAINTENANCE PROGRAM	8.1-1
8.1	Acceptance Tests	8.1-1
8.1.1	Visual Inspection and Measurements	8.1-1
8.1.2	Weld Examinations	8.1-1
8.1.3	Structural and Pressure Tests	8.1-1
8.1.3.1	Lifting Device Load Testing	8.1-1
8.1.3.2	Pressure Testing	8.1-1
8.1.4	Fabrication Leakage Rate Tests	8.1-2
8.1.4.1	Fabrication Leakage Rate Test Acceptance Criteria	8.1-2
8.1.4.2	Helium Leakage Rate Testing the Containment Structure Integrity	8.1-2
8.1.4.3	Helium Leakage Rate Testing the Main O-ring Seal	8.1-3
8.1.4.4	Helium Leakage Rate Testing the Vent Port Plug O-ring Seal	8.1-3
8.1.4.5	Helium Leakage Rate Testing the Fill Port Plug O-ring Seal	8.1-4
8.1.5	Component and Material Tests	8.1-5
8.1.5.1	Polyurethane Foam	8.1-5
8.1.5.2	Neutron Poison Plates	8.1-13
8.1.6	Shielding Tests	8.1-13
8.1.7	Thermal Tests	8.1-13
8.2	Maintenance Program	8.2-1
8.2.1	Structural and Pressure Tests	8.2-1
8.2.2	Maintenance/Periodic Leakage Rate Tests	8.2-1
8.2.2.1	Maintenance/Periodic Verification Leakage Rate Test Acceptance Criteria	8.2-1
8.2.2.2	Helium Leakage Rate Testing the Main O-ring Seal	8.2-1
8.2.2.3	Helium Leakage Rate Testing the Vent Port Plug O-ring Seal	8.2-2
8.2.2.4	Helium Leakage Rate Testing the Fill Port Plug O-ring Seal	8.2-3
8.2.3	Component and Material Tests	8.2-3
8.2.3.1	Fasteners	8.2-3
8.2.3.2	Seal Areas and Grooves	8.2-3
8.2.3.3	Impact Limiters	8.2-4
8.2.3.4	Strongback	8.2-4
8.2.3.5	Fuel Control Structures	8.2-4
8.2.3.6	Seals	8.2-4
8.2.4	Thermal Tests	8.2-4
8.2.5	Miscellaneous Tests	8.2-4

APPENDIX A: ARB-17 CONTENTS

A1.0 GENERAL INFORMATION	A1.1-1
A1.1 Introduction.....	A1.1-1
A1.2 Package Description	A1.2-1
A1.2.1 Packaging	A1.2-1
A1.2.2 Containment System.....	A1.2-1
A1.2.3 Contents of Packaging.....	A1.2-1
A1.2.3.1 Radionuclide Inventory.....	A1.2-2
A1.2.3.2 Maximum Payload Weight	A1.2-2
A1.2.3.3 Maximum Decay Heat	A1.2-2
A1.2.3.4 Maximum Pressure Buildup	A1.2-2
A1.2.4 Operational Features.....	A1.2-2
A1.3 General Requirements for All Packages.....	A1.3-1
A1.4 Appendices.....	A1.4-1
A1.4.1 Nomenclature	A1.4-1
A1.4.2 General Arrangement Drawings.....	A1.4-1
A2.0 STRUCTURAL EVALUATION	A2-1
A2.1 Structural Design	A2-1
A2.1.1 Discussion	A2-1
A2.1.2 Design Criteria	A2-1
A2.1.3 Weights and Center of Gravity.....	A2-1
A2.2 Materials	A2-2
A2.3 Fabrication and Examination	A2-2
A2.4 Lifting and Tie-down Standards for All Packages	A2-2
A2.5 General Considerations.....	A2-2
A2.6 Normal Conditions of Transport.....	A2-2
A2.6.1 Heat	A2-2
A2.6.2 Cold	A2-2
A2.6.3 Reduced External Pressure.....	A2-2
A2.6.4 Increased External Pressure	A2-2
A2.6.5 Vibration and Shock.....	A2-3
A2.6.6 Water Spray	A2-3
A2.6.7 Free Drop.....	A2-3

A2.6.8	Corner Drop.....	A2-3
A2.6.9	Compression.....	A2-3
A2.6.10	Penetration.....	A2-3
A2.7	Hypothetical Accident Conditions.....	A2-3
A2.7.1	Free Drop.....	A2-3
A2.7.2	Crush	A2-3
A2.7.3	Puncture.....	A2-3
A2.7.4	Thermal	A2-4
A2.7.4.1	Summary of Pressures and Temperatures.....	A2-4
A2.7.4.2	Differential Thermal Expansion	A2-4
A2.7.4.3	Stress Calculations.....	A2-4
A2.7.5	Immersion – Fissile Material.....	A2-4
A2.7.6	Immersion – All Packages.....	A2-4
A2.7.7	Deep Water Immersion Test (for Type B Packages Containing More than 10^5 A ₂).....	A2-4
A2.7.8	Summary of Damage.....	A2-5
A2.8	Accident Conditions for Air Transport of Plutonium.....	A2-5
A2.9	Accident Conditions for Fissile Material Packages for Air Transport.....	A2-5
A2.10	Special Form.....	A2-5
A2.11	Fuel Rods	A2-5
A2.12	Appendices.....	A2-6
A3.0	THERMAL EVALUATION.....	A3.1-1
A3.1	Description of Thermal Design.....	A3.1-1
A3.1.1	Design Features	A3.1-1
A3.1.2	Content's Decay Heat.....	A3.1-1
A3.1.3	Summary of Temperatures	A3.1-1
A3.1.4	Summary of Maximum Pressures	A3.1-2
A3.2	Material Properties and Component Specifications.....	A3.2-1
A3.2.1	Material Properties	A3.2-1
A3.2.2	Component Specifications.....	A3.2-1
A3.3	General Considerations.....	A3.3-1
A3.3.1	Evaluations by Analysis	A3.3-1
A3.3.1.1	NCT Analytical Model	A3.3-1
A3.3.1.2	HAC Analytical Model	A3.3-2
A3.3.2	Evaluation by Test.....	A3.3-2

A3.3.3	Margins of Safety	A3.3-2
A3.4	Thermal Evaluation for Normal Conditions of Transport	A3.4-1
A3.4.1	Heat and Cold	A3.4-1
A3.4.1.1	Heat	A3.4-1
A3.4.1.2	Cold	A3.4-1
A3.4.2	Maximum Normal Operating Pressure	A3.4-1
A3.4.3	Maximum Thermal Stresses	A3.4-3
A3.4.4	Evaluation of Package Performance for Normal Conditions of Transport	A3.4-4
A3.5	Thermal Evaluation under Hypothetical Accident Conditions	A3.5-1
A3.5.1	Initial Conditions	A3.5-1
A3.5.2	Fire Test Conditions	A3.5-1
A3.5.2.1	Analytical Model	A3.5-1
A3.5.3	Maximum Temperatures and Pressures	A3.5-1
A3.5.3.1	Maximum Temperatures	A3.5-1
A3.5.3.2	Maximum Pressures	A3.5-1
A3.5.4	Accident Conditions for Fissile Material Packages for Air Transport ...	A3.5-3
A3.5.5	Evaluation of Package Performance for Accident Conditions of Transport	A3.5-3
A3.6	Appendices	A3.6-1
A3.6.1	Computer Analysis Results	A3.6-1
A4.0	CONTAINMENT	A4-1
A5.0	SHIELDING	A5-1
A6.0	CRITICALITY EVALUATION	A6.1-1
A6.1	Description of Criticality Design	A6.1-1
A6.1.1	Design Features Important for Criticality	A6.1-1
A6.1.2	Summary Table of Criticality Evaluation	A6.1-1
A6.1.3	Criticality Safety Index	A6.1-1
A6.2	Fissile Material Contents	A6.2-1
A6.3	General Considerations	A6.3-1
A6.3.1	Model Configuration	A6.3-1
A6.3.1.1	Contents Model	A6.3-1
A6.3.1.2	Packaging Model	A6.3-1
A6.3.2	Material Properties	A6.3-1
A6.3.3	Computer Codes and Cross-Section Libraries	A6.3-1

A6.3.4	Demonstration of Maximum Reactivity	A6.3-1
A6.4	Single Package Evaluation	A6.4-1
A6.4.1	Single Package Configuration	A6.4-1
A6.4.1.1	NCT Configuration	A6.4-1
A6.4.1.2	HAC Configuration	A6.4-1
A6.4.2	Single Package Results	A6.4-2
A6.5	Evaluation of Package Arrays Under Normal Conditions of Transport.....	A6.5-1
A6.6	Package Arrays Under Hypothetical Accident Conditions.....	A6.6-1
A6.6.1	HAC Array Configuration	A6.6-1
A6.6.2	HAC Array Results	A6.6-1
A6.7	Fissile Material Packages for Air Transport.....	A6.7-1
A6.8	Benchmark Evaluations	A6.8-1
A6.9	Appendices.....	A6.9-1
A6.9.1	Single Package Model	A6.9.1-1
A6.9.2	Infinite Array Model	A6.9.2-1
A7.0	PACKAGE OPERATIONS	A7-1
A7.1	Package Loading	A7-1
A7.2	Package Unloading	A7-1
A7.3	Preparation of an Empty Package for Transport.....	A7-1
A7.4	Preshipment Leakage Rate Test	A7-1
A8.0	ACCEPTANCE TESTS AND MAINTENANCE PROGRAM	A8-1
A8.1	Acceptance Tests	A8-1
A8.1.1	Visual Inspections and Measurements	A8-1
A8.1.2	Weld Inspections	A8-1
A8.1.3	Structural and Pressure Tests	A8-1
A8.1.4	Fabrication Leakage Rate Tests	A8-1
A8.1.5	Component and Material Tests.....	A8-1
A8.1.6	Shielding Tests	A8-1
A8.1.7	Thermal Tests	A8-1
A8.2	Maintenance Program	A8-2

APPENDIX B: EXCESS MATERIAL ASSEMBLY AND AFS-B WITH MOX RODS

B1.0 GENERAL INFORMATION	B1.1-1
B1.1 Introduction.....	B1.1-1
B1.2 Package Description	B1.2-1
B1.2.1 Packaging	B1.2-1
B1.2.2 Containment System.....	B1.2-1
B1.2.3 Contents of Packaging.....	B1.2-2
B1.2.3.1 Radionuclide Inventory.....	B1.2-2
B1.2.3.2 Maximum Payload Weight	B1.2-2
B1.2.3.3 Maximum Decay Heat	B1.2-3
B1.2.3.4 Maximum Pressure Buildup	B1.2-3
B1.2.4 Operational Features.....	B1.2-3
B1.3 General Requirements for All Packages.....	B1.3-1
B1.4 Appendices.....	B1.4-1
B1.4.1 Nomenclature	B1.4-1
B1.4.2 Packaging General Arrangement Drawings	B1.4-1
B2.0 STRUCTURAL EVALUATION	B2-1
B2.1 Structural Design	B2-1
B2.1.1 Discussion	B2-1
B2.1.2 Design Criteria	B2-1
B2.1.3 Weights and Center of Gravity.....	B2-2
B2.2 Materials	B2-2
B2.3 Fabrication and Examination	B2-3
B2.4 Lifting and Tie-down Standards for All Packages	B2-3
B2.5 General Considerations.....	B2-4
B2.6 Normal Conditions of Transport.....	B2-4
B2.6.1 Heat	B2-4
B2.6.1.1 Differential Thermal Expansion	B2-4
B2.6.2 Cold	B2-5
B2.6.3 Reduced External Pressure.....	B2-5
B2.6.4 Increased External Pressure	B2-5
B2.6.5 Vibration and Shock.....	B2-5

B2.6.6	Water Spray	B2-5
B2.6.7	Free Drop	B2-5
B2.6.8	Corner Drop	B2-5
B2.6.9	Compression	B2-5
B2.6.10	Penetration	B2-6
B2.7	Hypothetical Accident Conditions	B2-6
B2.7.1	Free Drop	B2-6
B2.7.2	Crush	B2-9
B2.7.3	Puncture	B2-9
B2.7.4	Thermal	B2-9
B2.7.4.1	Summary of Pressures and Temperatures	B2-9
B2.7.4.2	Differential Thermal Expansion	B2-10
B2.7.4.3	Stress Calculations	B2-10
B2.7.5	Immersion – Fissile Material	B2-10
B2.7.6	Immersion – All Packages	B2-10
B2.7.7	Deep Water Immersion Test (for Type B Packages Containing More than 10^5 A ₂)	B2-10
B2.7.8	Summary of Damage	B2-10
B2.8	Accident Conditions for Air Transport of Plutonium	B2-10
B2.9	Accident Conditions for Fissile Material Packages for Air Transport	B2-10
B2.10	Special Form	B2-11
B2.11	Fuel Rods	B2-11
B2.12	Appendices	B2-11
B3.0	THERMAL EVALUATION	B3.1-1
B3.1	Description of Thermal Design	B3.1-1
B3.1.1	Design Features	B3.1-1
B3.1.2	Content's Decay Heat	B3.1-1
B3.1.3	Summary of Temperatures	B3.1-1
B3.1.4	Summary of Maximum Pressures	B3.1-2
B3.2	Material Properties and Component Specifications	B3.2-1
B3.2.1	Material Properties	B3.2-1
B3.2.2	Component Specifications	B3.2-1
B3.3	General Considerations	B3.3-1
B3.3.1	Evaluations by Analysis	B3.3-1
B3.3.1.1	NCT Analytical Model	B3.3-1

B3.3.1.2	HAC Analytical Model	B3.3-5
B3.3.2	Evaluation by Test	B3.3-5
B3.3.3	Margins of Safety	B3.3-6
B3.4	Thermal Evaluation for Normal Conditions of Transport	B3.4-1
B3.4.1	Heat and Cold	B3.4-1
B3.4.1.1	Heat	B3.4-1
B3.4.1.2	Cold	B3.4-1
B3.4.2	Maximum Normal Operating Pressure	B3.4-2
B3.4.3	Maximum Thermal Stresses	B3.4-3
B3.4.4	Evaluation of Package Performance for Normal Conditions of Transport	B3.4-3
B3.5	Thermal Evaluation under Hypothetical Accident Conditions	B3.5-1
B3.5.1	Initial Conditions	B3.5-1
B3.5.2	Fire Test Conditions	B3.5-1
B3.5.2.1	Analytical Model	B3.5-1
B3.5.3	Maximum Temperatures and Pressures	B3.5-1
B3.5.3.1	Maximum Temperatures	B3.5-1
B3.5.3.2	Maximum Pressures	B3.5-2
B3.5.4	Accident Conditions for Fissile Material Packages for Air Transport	B3.5-2
B3.5.5	Evaluation of Package Performance for Accident Conditions of Transport	B3.5-3
B3.6	Appendices	B3.6.1-1
B3.6.1	Computer Analysis Results	B3.6.1-1
B4.0	CONTAINMENT	B4-1
B5.0	SHIELDING	B5-1
B6.0	CRITICALITY EVALUATION	B6.1-1
B6.1	Description of Criticality Design	B6.1-1
B6.1.1	Design Features Important for Criticality	B6.1-1
B6.1.2	Summary Table of Criticality Evaluation	B6.1-1
B6.1.3	Criticality Safety Index	B6.1-2
B6.2	Fissile Material Contents	B6.2-1
B6.3	General Considerations	B6.3-1
B6.3.1	Model Configuration	B6.3-1
B6.3.1.1	Contents Model	B6.3-1

B6.3.1.2 Packaging Model.....	B6.3-1
B6.3.2 Material Properties	B6.3-1
B6.3.3 Computer Codes and Cross-Section Libraries	B6.3-1
B6.3.4 Demonstration of Maximum Reactivity	B6.3-1
B6.4 Single Package Evaluation	B6.4-1
B6.4.1 Single Package Configuration	B6.4-1
B6.4.1.1 NCT Configuration	B6.4-1
B6.4.1.2 HAC Configuration.....	B6.4-1
B6.4.2 Single Package Results.....	B6.4-3
B6.5 Evaluation of Package Arrays Under Normal Conditions of Transport.....	B6.5-1
B6.6 Package Arrays Under Hypothetical Accident Conditions.....	B6.6-1
B6.6.1 HAC Array Configuration.....	B6.6-1
B6.6.2 HAC Array Results	B6.6-1
B6.7 Fissile Material Packages for Air Transport.....	B6.7-1
B6.8 Benchmark Evaluations	B6.8-1
B6.9 Appendices.....	B6.9-1
B6.9.1 Single Package Model	B6.9.1-1
B6.9.2 Infinite Array Model	B6.9.2-1
B7.0 PACKAGE OPERATIONS	B7-1
B7.1 Package Loading	B7-1
B7.2 Package Unloading	B7-1
B7.3 Preparation of an Empty Package for Transport.....	B7-1
B7.4 Preshipment Leakage Rate Test.....	B7-2
B8.0 ACCEPTANCE TESTS AND MAINTENANCE PROGRAM.....	B8-1
B8.1 Acceptance Tests	B8-1
B8.1.1 Visual Inspections and Measurements	B8-1
B8.1.2 Weld Inspections	B8-1
B8.1.3 Structural and Pressure Tests	B8-1
B8.1.4 Fabrication Leakage Rate Tests	B8-1
B8.1.5 Component and Material Tests.....	B8-1
B8.1.6 Shielding Tests	B8-1
B8.1.7 Thermal Tests	B8-1
B8.2 Maintenance Program	B8-2

APPENDIX C: AFS-C WITH TA-18 MOX RODS

C1.0 GENERAL INFORMATION	C1.1-1
C1.1 Introduction.....	C1.1-1
C1.2 Package Description	C1.2-1
C1.2.1 Packaging	C1.2-1
C1.2.2 Containment System.....	C1.2-2
C1.2.3 Contents of Packaging.....	C1.2-2
C1.2.3.1 Radionuclide Inventory.....	C1.2-2
C1.2.3.2 Maximum Payload Weight	C1.2-2
C1.2.3.3 Maximum Decay Heat	C1.2-3
C1.2.3.4 Maximum Pressure Buildup	C1.2-3
C1.2.4 Operational Features.....	C1.2-3
C1.3 General Requirements for All Packages.....	C1.3-1
C1.4 Appendices.....	C1.4-1
C1.4.1 Nomenclature	C1.4-1
C1.4.2 Packaging General Arrangement Drawings	C1.4-1
C2.0 STRUCTURAL EVALUATION.....	C2-1
C2.1 Structural Design	C2-1
C2.1.1 Discussion	C2-1
C2.1.2 Design Criteria	C2-1
C2.1.3 Weights and Center of Gravity.....	C2-2
C2.2 Materials	C2-2
C2.3 Fabrication and Examination	C2-3
C2.4 Lifting and Tie-down Standards for All Packages	C2-3
C2.5 General Considerations.....	C2-4
C2.6 Normal Conditions of Transport.....	C2-4
C2.6.1 Heat	C2-4
C2.6.1.1 Differential Thermal Expansion	C2-4
C2.6.2 Cold	C2-5
C2.6.3 Reduced External Pressure.....	C2-5
C2.6.4 Increased External Pressure	C2-5
C2.6.5 Vibration and Shock.....	C2-5
C2.6.6 Water Spray.....	C2-5

C2.6.7	Free Drop.....	C2-5
C2.6.8	Corner Drop.....	C2-5
C2.6.9	Compression.....	C2-5
C2.6.10	Penetration.....	C2-6
C2.7	Hypothetical Accident Conditions.....	C2-6
C2.7.1	Free Drop.....	C2-6
C2.7.2	Crush	C2-11
C2.7.3	Puncture.....	C2-11
C2.7.4	Thermal	C2-12
C2.7.4.1	Summary of Pressures and Temperatures.....	C2-12
C2.7.4.2	Differential Thermal Expansion	C2-12
C2.7.4.3	Stress Calculations.....	C2-12
C2.7.5	Immersion – Fissile Material.....	C2-12
C2.7.6	Immersion – All Packages.....	C2-12
C2.7.7	Deep Water Immersion Test (for Type B Packages Containing More than 10^5 A ₂).....	C2-12
C2.7.8	Summary of Damage.....	C2-12
C2.8	Accident Conditions for Air Transport of Plutonium.....	C2-13
C2.9	Accident Conditions for Fissile Material Packages for Air Transport.....	C2-13
C2.10	Special Form.....	C2-13
C2.11	Fuel Rods	C2-13
C2.12	Appendices.....	C2-13
C3.0	THERMAL EVALUATION.....	C3.1-1
C3.1	Description of Thermal Design.....	C3.1-1
C3.1.1	Design Features	C3.1-1
C3.1.2	Content’s Decay Heat.....	C3.1-1
C3.1.3	Summary of Temperatures	C3.1-2
C3.1.4	Summary of Maximum Pressures	C3.1-2
C3.2	Material Properties and Component Specifications.....	C3.2-1
C3.2.1	Material Properties	C3.2-1
C3.2.2	Component Specifications.....	C3.2-1
C3.3	General Considerations.....	C3.3-1
C3.3.1	Evaluations by Analysis	C3.3-1
C3.3.1.1	NCT Analytical Model	C3.3-1
C3.3.1.2	HAC Analytical Model.....	C3.3-5

C3.3.2	Evaluation by Test.....	C3.3-6
C3.3.3	Margins of Safety	C3.3-6
C3.4	Thermal Evaluation for Normal Conditions of Transport	C3.4-1
C3.4.1	Heat and Cold.....	C3.4-1
C3.4.1.1	Heat.....	C3.4-1
C3.4.1.2	Cold.....	C3.4-2
C3.4.2	Maximum Normal Operating Pressure.....	C3.4-2
C3.4.3	Maximum Thermal Stresses.....	C3.4-4
C3.4.4	Evaluation of Package Performance for Normal Conditions of Transport	C3.4-4
C3.5	Thermal Evaluation under Hypothetical Accident Conditions.....	C3.5-1
C3.5.1	Initial Conditions.....	C3.5-1
C3.5.2	Fire Test Conditions	C3.5-1
C3.5.2.1	Analytical Model	C3.5-1
C3.5.3	Maximum Temperatures and Pressures	C3.5-1
C3.5.3.1	Maximum Temperatures.....	C3.5-1
C3.5.3.2	Maximum Pressures.....	C3.5-2
C3.5.4	Accident Conditions for Fissile Material Packages for Air Transport....	C3.5-2
C3.5.5	Evaluation of Package Performance for Accident Conditions of Transport	C3.5-3
C3.6	Appendices.....	C3.6.1-1
C3.6.1	Computer Analysis Results	C3.6.1-1
C4.0	CONTAINMENT.....	C4-1
C5.0	SHIELDING.....	C5-1
C6.0	CRITICALITY EVALUATION	C6.1-1
C6.1	Description of Criticality Design	C6.1-1
C6.1.1	Design Features Important for Criticality	C6.1-1
C6.1.2	Summary Table of Criticality Evaluation	C6.1-1
C6.1.3	Criticality Safety Index	C6.1-2
C6.2	Fissile Material Contents.....	C6.2-1
C6.3	General Considerations.....	C6.3-1
C6.3.1	Model Configuration.....	C6.3-1
C6.3.1.1	Contents Model.....	C6.3-1
C6.3.1.2	Packaging Model	C6.3-1
C6.3.2	Material Properties	C6.3-1

C6.3.3	Computer Codes and Cross-Section Libraries	C6.3-1
C6.3.4	Demonstration of Maximum Reactivity	C6.3-2
C6.4	Single Package Evaluation	C6.4-1
C6.4.1	Single Package Configuration	C6.4-1
C6.4.1.1	NCT Configuration	C6.4-1
C6.4.1.2	HAC Configuration	C6.4-1
C6.4.2	Single Package Results	C6.4-6
C6.5	Evaluation of Package Arrays Under Normal Conditions of Transport.....	C6.5-1
C6.5.1	NCT Array Configuration	C6.5-1
C6.5.2	NCT Array Results	C6.5-1
C6.6	Package Arrays Under Hypothetical Accident Conditions.....	C6.6-1
C6.6.1	HAC Array Configuration	C6.6-1
C6.6.2	HAC Array Results	C6.6-2
C6.7	Fissile Material Packages for Air Transport.....	C6.7-1
C6.8	Benchmark Evaluations	C6.8-1
C6.9	Appendices	C6.9-1
C6.9.1	Single Package Model	C6.9.1-1
C6.9.2	Infinite Array Model	C6.9.2-1
C7.0	PACKAGE OPERATIONS	C7-1
C7.1	Package Loading	C7-1
C7.2	Package Unloading	C7-1
C7.3	Preparation of an Empty Package for Transport.....	C7-2
C7.4	Preshipment Leakage Rate Test.....	C7-2
C8.0	ACCEPTANCE TESTS AND MAINTENANCE PROGRAM.....	C8-1
C8.1	Acceptance Tests	C8-1
C8.1.1	Visual Inspections and Measurements	C8-1
C8.1.2	Weld Inspections	C8-1
C8.1.3	Structural and Pressure Tests	C8-1
C8.1.4	Fabrication Leakage Rate Tests	C8-1
C8.1.5	Component and Material Tests.....	C8-1
C8.1.6	Shielding Tests	C8-1
C8.1.7	Thermal Tests	C8-1
C8.2	Maintenance Program	C8-2

This page left intentionally blank.

1.0 GENERAL INFORMATION

This chapter of the Mixed Oxide Fresh Fuel Package (MFFP) Safety Analysis Report (SAR) presents a general introduction and description of the package. The MFFP is utilized for transport of mixed oxide (MOX) fresh fuel assemblies in accordance with the requirements of 10 CFR 71¹ and 49 CFR 173². The major components of the packaging system are shown in Figure 1.1-1. The containment boundary is identified in Figure 1.1-2. Additional figures and schematics are presented in support of the discussion within this chapter. Terminology used throughout this SAR is presented in Section 1.4.1, *Nomenclature*. General arrangement drawings of the packaging are provided in Appendix 1.4.2, *Packaging General Arrangement Drawings*.

The main body of the SAR provides the analysis for the contents of three (3) intact fuel assemblies. Three Appendices have been added to the main SAR to address three additional contents:

Appendix A: Replacing up to three (3) standard fuel assemblies with Areva Rod Box 17 (ARB-17) containers. Each ARB-17 may contain up to 17 standard MOX fuel rods. The fuel rods may be undamaged or slightly damaged. Slightly damaged rods are defined as rods that may be bent, scratched, or dented, but under no circumstances exhibit cladding breach.

Appendix B: Contents of up to one (1) AFS-B rod container, and one (1) Excess Material Assembly (EMA). The AFS-B may contain up to 175 standard MOX fuel rods. For transportation purposes, the EMA is equivalent to a MOX fuel assembly.

Appendix C: Contents of up to three (3) AFS-C rod containers containing two types of rods currently stored at Los Alamos Technical Area 18 (TA-18), Exxon rods and Pacific Northwest Laboratory (PNL) rods. TA-18 rods are MOX rods but are not the same as standard MOX rods. Each AFS-C may contain up to 116 Exxon rods and 69 PNL rods.

Each Appendix has eight chapters and follows the same format as the main body of the SAR, referring to the main body of the SAR for information common to both.

1.1 Introduction

The Mixed Oxide Fresh Fuel Package, Model: **MFFP**, is designed to transport fresh MOX pressurized water reactor (PWR) reactor fuel assemblies. The packaging is designed to provide a safe means of transporting up to three fresh MOX PWR fuel assemblies, with or without burnable poison rod assemblies (BPRAs) installed.

This SAR contains the information required to conclusively demonstrate that when the MFFP is subjected to the applicable tests described in Subpart F of 10 CFR 71, the applicable requirements of Subpart E of 10 CFR 71 have been met. A combination of analytical and full-scale prototypic testing is used to demonstrate that the MFFP satisfies these requirements. A full-scale, prototypic certification test unit (CTU) was subjected to a series of hypothetical

¹ Title 10, Code of Federal Regulations, Part 71 (10 CFR 71), *Packaging and Transportation of Radioactive Materials*, Final Rule, 01-26-04.

² Title 49, Code of Federal Regulations, Part 173 (49 CFR 173), *Shippers-General Requirements for Shipments and Packagings*, Final Rule, 01-26-04.

accident condition (HAC) free and puncture drop tests. A detailed discussion of the CTU and certification tests is provided in Appendix 2.12.3, *Certification Test Results*. These tests, coupled with supplementary analytical evaluations, conclusively demonstrated the leaktight³ containment boundary integrity and criticality control performance of the MFFP.

Based on the shielding and criticality assessments provided in Chapter 5.0, *Shielding Evaluation*, and Chapter 6.0, *Criticality Evaluation*, the Criticality Safety Index (CSI) for the MFFP is zero (0.0), and the Transport Index (TI) is determined at the time of shipment.

Authorization is sought for shipment of the MFFP by all modes of conveyance, except for aircraft, as a Type B(U)F package per the definitions delineated in 10 CFR §71.4.

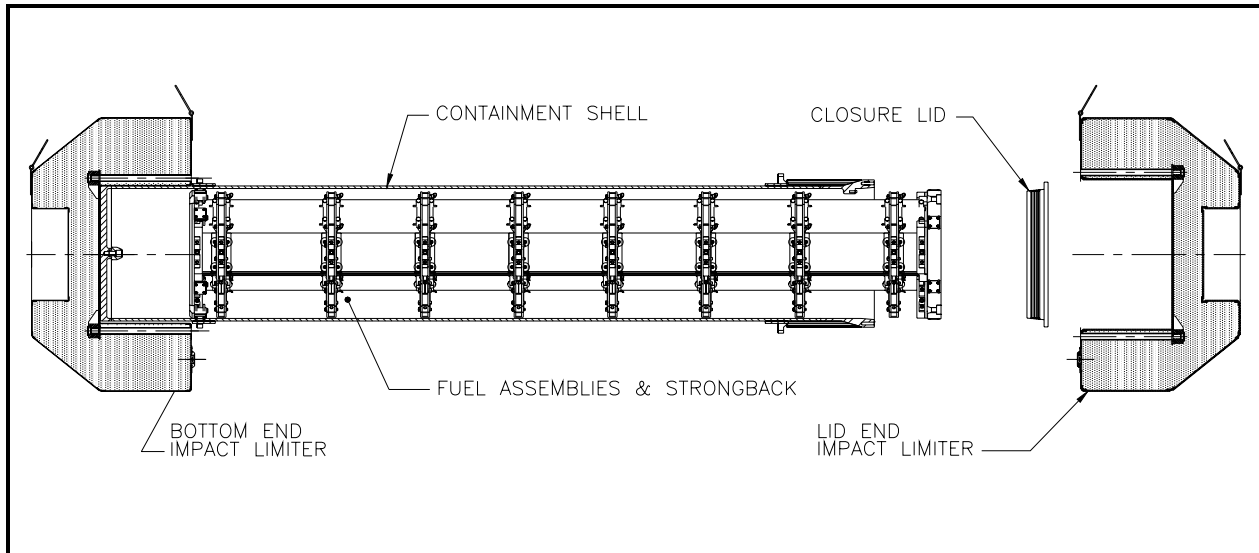


Figure 1.1-1 – Major MFFP Components

³ Leaktight is defined as 1×10^{-7} standard cubic centimeters per second (scc/s), or less, air leakage per ANSI N14.5-1997, *American National Standard for Radioactive Materials – Leakage Tests on Packages for Shipment*, American National Standards Institute, (ANSI), Inc

Security Related Information
Figure Withheld Under 10 CFR 2.390

Figure 1.1-2 – MFFP Body Major Containment Boundary Structures (inches)

This page left intentionally blank.

1.2 Package Description

This section provides a basic description of the MFFP design. General arrangement drawings of the packaging are provided in Appendix 1.4.2, *Packaging General Arrangement Drawings*. Following the descriptions, supporting figures are provided as necessary to illustrate the discussion.

1.2.1 Packaging

The MFFP includes an austenitic stainless steel cylindrical containment body and closure lid that provide leaktight containment for a payload of up to three fresh MOX PWR commercial reactor fuel assemblies (FAs). The FAs are supported during operations and transportation by the strongback. In addition to supporting the fuel, the strongback provides geometric stability and neutron poisoning for criticality control. Impact limiters are installed at each end of the MFFP body for impact force mitigation and thermal protection of the containment O-ring seals. The MFFP has no component whose function is to provide biological shielding. Shown in Figure 1.1-1 are the primary components of the MFFP and detailed drawings are provided in Appendix 1.4.2, *Packaging General Arrangement Drawings*.

The maximum permissible gross shipping weight of the MFFP is 14,260 pounds including maximum payload, body, strongback, and impact limiters. Details of the component weights are provided in Section 2.1.3, *Weights and Centers of Gravity*, of this document. The MFFP may be shipped with one to three MOX FAs. The width of the MFFP is the impact limiter diameter of 60 inches; the length is 201.33 inches. The outer envelope dimensions of the package are shown in Figure 1.2-1.

1.2.1.1 Body

The containment body shell is 9/16-inches thick, and is fabricated from Type XM-19 austenitic stainless steel. The shell may be fabricated from multiple sections, which are joined using full penetration, volumetrically-inspected welds. A circumferentially continuous doubler plate, constructed of Type XM-19 austenitic stainless steel, is welded to each end of the shell, near the end of each impact limiter. Welded to the doubler plate are impact limiter attachment lugs, six per impact limiter. The doubler plate also serves to provide a tiedown interface with the transportation skid for longitudinal loads. The seal flange is located at the open end of the body, and consists of a locally thicker wall section to accommodate the closure lid sealing area and the closure bolt threaded holes. The transition between the shell and the seal flange section is at least a 3:1 taper.

To provide complete support for the lid end impact limiter, an annulus of relatively strong polyurethane foam is used to build the outer diameter of the body out to the full diameter of the sealing flange and closure lid. The foam annulus has a density of 30 pounds per cubic foot (pcf), a radial thickness of approximately 1¼ inches, and is protected by a 16-gauge sheet of Type 304 or Type XM-19 austenitic stainless steel. The end of the annulus is protected by a 1/4-inch thick plate of Type 304 or Type XM-19 austenitic stainless steel, which contains plastic fire-consumable plugs to prevent over-pressurization in the HAC thermal event.

The bottom end plate, constructed of Type XM-19 or Type FXM-19 austenitic stainless steel, is a simple machined circular plate. The thickness of the end plate is 1½ inches and has a machined transition to the body shell weld. The transition allows for an easily examined full

penetration weld. Also machined into the bottom end closure is a threaded interface for the internal trunnion that engages with the end of the strongback.

The closure lid is a weldment constructed of Type XM-19, and has a construction which provides significant strength and stiffness while also being weight efficient. The closure lid is constructed of a 3/4-inch thick outer plate and 5/8-inch thick inner plate, stiffened with eight, 1/2-inch thick radial ribs that are three inches deep. A 1/2-inch thick, 6 inch inner diameter cylinder forms a hub at the inner end of the radial ribs. The ribs are welded on all four edges to the adjacent structure. Each rib has a projection that passes through a slot in the outer plate, and the ribs and outer plate are securely welded together using 1/2-inch groove welds. The closure lid inner plate is welded to the outer ring using a full-penetration, volumetrically inspected weld. The seal flange of the closure lid has a minimum thickness of one inch, and provides locations for three closure O-ring seals, as well as providing a location for the vent, fill, and test ports. The closure lid is attached to the body using twenty four (24) 3/4-10UNC socket head cap screws (SHCS) fabricated from ASTM A564, Grade 630, Condition H1100, nickel plated bolting material. Hardened washers are utilized with the closure lid SHCS, which engage threaded inserts in the receiving flange. A cut-away view of the closure lid, showing the internal reinforcements, is shown in Figure 1.1-2.

The closure lid design provides for three, 3/8-inch diameter butyl rubber O-ring seals in a bore seal type arrangement. The middle O-ring seal provides containment. O-ring seals of similar construction are located on either side of the middle containment O-ring seal for leakage rate testing purposes. The sealing interface is the inner diameter of the seal flange, which has a 5 degree taper for the O-ring bore seals. For leaktight verification of the closure, the cavity formed between the containment and the inner test O-ring seals is flooded with helium, while the cavity formed between the containment and the outer test seals is evacuated and tested for the presence of helium. The fill port connects to the inner, helium-filled cavity, and the test port connects to the outer, test cavity. A vent port is provided to vent the containment cavity during closure lid insertion or removal. Both the fill and vent ports are containment penetrations. All three ports are closed using 3/8-16UNC socket head cap screw plugs, fabricated of ASTM B16, half-hard brass, and sealed with butyl rubber sealing washers. Each port is an integral part of the closure lid, and is recessed for protection. Sealing and port details are shown in Figure 1.2-3.

Not considering the closure lid flange area and the impact limiter tie-down lugs, the body has a nominal external diameter of 29⁵/₈ inches and a nominal length of 171.33 inches, with the closure lid installed. The nominal external diameter of the closure lid flange area is 32.3 inches. The nominal external diameter including the tie-down lugs is 38¹/₂ inches.

1.2.1.2 Strongback

The strongback assembly, shown in Figure 1.2-4 through Figure 1.2-10, consists primarily of a longitudinal weldment, clamp arm assemblies, fuel control structure (FCS), and top and bottom end plates. The strongback top and bottom end plates restrain the fuel longitudinally. The clamp arms and longitudinal weldment provide restraint at each FA grid strap location normal to the axial length of the FA. The FCS provides lateral fuel deflection restraint for HAC conditions and supports additional neutron poison plates.

The strongback longitudinal weldment is constructed of 1/4-inch thick, ASTM A240, Type 304 stainless steel, and provides support for the neutron poison plates and for the MOX fuel assemblies. The longitudinal plates are welded in a triangular arrangement, as can be seen in

Figure 1.2-7 and Figure 1.2-9. A triangular-shaped reinforcement weldment is used at each grid strap location, as shown in Figure 1.2-9.

The clamp arm assemblies are attached to the strongback longitudinal weldment at each fuel assembly grid location using 5/16-18UNC flat head machine screws. Each clamp arm assembly is hinged to facilitate FA loading and unloading. When closed, the clamp arms are secured in place by two 1/2-inch nominal diameter quick-release pins. Each clamp arm assembly contains two clamp pads and adjustment screws, used to securely clamp the fuel assemblies against the strongback. The clamp arm is constructed of two 3/8-inch thick plates, separated by the fuel clamping mechanism and welded stiffening components which provide stability during in-plane loading. Rubber pads provide a cushion between the clamp pads and the fuel grids.

The strongback fuel control structure (FCS) provides geometric control of the FA during vertical and near-vertical HAC free drops. Additionally, the FCS provides support of neutron poison plates. The FCS assemblies are constructed of a 1/8-inch thick Type 304 austenitic stainless steel angle plate. In the center of the longitudinal span of each FCS is a stiffener, constructed of 1/4-inch thick Type XM-19 austenitic stainless steel channel. Each FCS assembly is hinged to assist FA loading and unloading. When closed, the FCSs are secured in place by a single 3/8-inch nominal diameter quick-release pin.

The top and bottom end plates secure the top and bottom FA nozzles in the same way that the grids are secured, as well as provide axial restraint of the FA. The loaded strongback is slid into and out of the package horizontally, aided by anti-friction Delrin[®] pads located in the top and bottom end disks. The end disks support the strongback such that the somewhat smaller support disks have no contact with the inner wall of the body shell. The top end disk also includes a feature used to retain the optional burnable poison rod assemblies (BPRAs).

When installed in the body, the bottom end of the strongback is supported on a 2³/₄ inch diameter trunnion fabricated from UNS S21800 stainless steel that is bolted to the center of the body bottom plate using a 7/8-9UNC bolt fabricated from ASTM A540 B23, Class 1 bolting material. Due to support by the trunnion, the strongback bottom end plate outer diameter does not contact the body shell during transport. The top end of the strongback is secured by bolts to three lugs machined into the MFFP body weldment. The lugs prevent axial motion of the strongback under normal over-the-road transportation forces, as shown in Figure 1.2-10.

In the fully assembled condition, the nominal external diameter of the strongback is 28¹/₄ inches and a nominal overall length of 164.9 inches.

1.2.1.3 Impact Limiters

As shown in Figure 1.2-1, impact limiters are installed at each end of the MFFP for thermal and impact protection during transport. The impact limiters are comprised of cylindrical and conical sections. The cylindrical sections correspond to the body-to-impact limiter interface length of 20 inches, and have an outer diameter of 60 inches. The adjacent conical section is 15 inches long with a minimum diameter of 36 inches. The bottom hole is designed to reduce end drop impact loads, and has a diameter of 20 inches and a depth of eight inches. The impact limiter shells are constructed of Type 304 stainless steel. The closure lid end impact limiter has 1/4-inch thick shells (5/16-inch thick for the end-hole plate) to resist perforation from the HAC puncture drop, and to protect the closure lid and sealing area from puncture and HAC fire damage. The bottom impact limiter has 11-gauge (0.12 inch) thick shells. Within the impact limiter shells is closed cell, rigid

polyurethane foam. The polyurethane foam provides the majority of the energy absorption during the HAC drop events, and thermal protection of the containment seals during the HAC fire event. Each impact limiter is attached to the body using six (6), 1-8UNC \times 24½ inches, ASTM A320, Grade L43 SHCS, with the shank reduced to a diameter of 0.81 inches. The impact limiter bolts are nickel or cadmium plated to preclude corrosion.

1.2.1.4 Gross Weight

The gross weight of a MFFP is 14,260 pounds maximum. A summary of overall component weights is delineated in Section 2.1.3, *Weights and Centers of Gravity*.

1.2.1.5 Neutron Moderation and Absorption

Criticality control is provided in the MFFP package by the geometric spacing of the fuel assemblies and by borated neutron absorbing material contained on the strongback assembly. The strongback weldment and clamp arm assemblies maintain the geometric spacing. The borated neutron poison plates on the longitudinal strongback weldment are secured by cover plates at ten locations corresponding to the fuel assembly clamping locations. The borated neutron poison plates on the FCS are secured by the center stiffener and outer angles at each end. The neutron absorbing material does not support any structural loading except its own weight.

1.2.1.6 Receptacles, Valves, Testing and Sample Ports

The MFFP closure lid design includes a seal test port, a fill port, and a vent port. The seal test port accesses the cavity between the middle (containment) and upper O-ring bore seals on the closure lid, thereby allowing leakage rate testing prior to shipping the loaded package. The fill port allows leakage rate testing of the containment O-ring seal. The vent port permits venting of the containment cavity during loading and unloading of the package. Each port is an integral part of the closure lid, and each port plug is recessed into the closure lid for protection. There are no receptacles or valves utilized on this package. A more detailed discussion of the package test and vent port features is provided in Chapter 4.0, *Containment*.

1.2.1.7 Heat Dissipation

The package maximum internal thermal load is 240 watts (80 watts per fuel assembly), as shown in Chapter 3.0, *Thermal Evaluation*. There are no active devices utilized on the MFFP for the transfer or dissipation of heat. Heat dissipation from the package is entirely passive. Heat dissipation is achieved by convection and radiation from the exposed surfaces of the package and impact limiters. A more detailed discussion of the package thermal characteristics is provided in Chapter 3.0, *Thermal Evaluation*.

1.2.1.8 Coolants

No coolants are utilized within the MFFP.

1.2.1.9 Protrusions

There are no protrusions on the outer surface of the MFFP other than the impact limiter attachment lugs and the shock indicators. These lugs are located at both ends of the MFFP,

inboard of the impact limiters. The shock indicators are attached to brackets that are welded to the package shell.

1.2.1.10 Lifting and Tie-down Devices

There are no lifting devices integral to the MFFP. The only tie-down devices integral to the MFFP are the doubler plates that attach the impact limiter attachment lugs. The doubler plates serve as an interface between the shipping skid and the MFFP, and provide axial restraint for tie-down. The shipping skid for MFFP is shown in Figure 1.2-11.

1.2.1.11 Pressure Relief Systems

There is no pressure relief system included in the MFFP to relieve pressure from within the containment boundary. Fire-consumable vents in the form of plastic pipe plugs are employed on the exterior surface of the impact limiters. These vents are included to release any gases generated by charring polyurethane foam in the HAC thermal event (fire). During the HAC fire, the plastic pipe plugs melt allowing the release of gases generated by the foam as it flashes to a char. Three vents are used on each impact limiter, located on the inside surface. For optimum performance, the vents are equally spaced around the circumference of the impact limiters.

1.2.1.12 Shielding

The MOX fresh FA payload is not a significant source of radiation. Thus, use of shielding specific components is not required. Further detail of the shielding evaluation is provided in Chapter 5.0, *Shielding Evaluation*.

1.2.2 Containment System

The containment boundary for MFFP is provided by the containment body, closure lid and bolts, and associated sealing components. The containment boundary of the package consists of the cylindrical shell and bottom forging, sealing flange, the inner plate and sealing ring of the closure lid, the vent port plug and elastomeric seal, the fill port plug and elastomeric seal, and the closure lid elastomeric containment O-ring seal. The body has an inner diameter of 28½ inches and an inside length of 165.45 inches. The outer diameter in the closure lid flange area is 32.3 inches, while a majority of the body outer diameter is 29⅞ inches. The overall length of the body with the closure lid, excluding impact limiters, is 171.33 inches. The containment boundary is shown in Figure 1.1-2.

1.2.3 Contents of Packaging

The MFFP is designed to carry up to three fresh MOX PWR FAs. The FAs are based on the MK-BW/MOX1 17 × 17 PWR design. For shipping less than three MOX FAs, non-fuel dummy assemblies are utilized in the strongback locations not occupied by the MOX FAs. The physical size and weight of the non-fuel dummy assemblies are nominally the same as the MK-BW/MOX1 17 × 17 design. For criticality analyses, a maximum loading of 6.0^w% plutonium (Pu) is assumed. FA physical parameters are provided in Table 1.2-1.

Burnable poison rod assemblies (BPRAs) may be inserted into a FA as an option. Therefore, a loaded package may contain up to three BPRAs. The 17 × 17 BPRA (Figure 1.2-12) consists of

an arrangement of poison rods and thimble plugs suspended from a flat plate and held in place by a spring-loaded holddown assembly. The holddown assembly fits within the fuel assembly upper nozzle and rests on the adapter plate. To ensure that the cluster remains seated in the fuel assembly during operation, the holddown springs are compressed by the upper core plate, thereby providing a downward force in excess of the hydraulic lift forces from the reactor coolant. The holddown assembly and the holddown springs are fabricated of Type 304 stainless steel and Inconel[®] 718, respectively.

The burnable poison rod design contains an absorber stack of $\text{Al}_2\text{O}_3\text{-B}_4\text{C}$ pellets. The pellets are encased in cold-worked, stress-relieved annealed Zircaloy-4 cladding with Zircaloy-4 end plugs welded to each end. The upper end plug provides a threaded attachment to the holddown assembly plate, and a bullet nose lower end plug provides lead-in guidance for the rods. A stainless steel spring is located in the plenum above the poison pellet column. Prior to the final seal weld, each rod is pressurized with helium to reduce the pressure differential across the clad wall during operation.

The pellets consist of a uniform sintered dispersion of boron carbide (B_4C) in an alumina (Al_2O_3) matrix. The boron-10 concentrations are adjusted by varying the boron carbide content of the pellets.

In addition to the boron-10 concentration being variable, the number of burnable poison rods on a FA can vary up to a maximum of twenty-four (24) rods. The locations that do not contain a burnable poison rod typically will contain a short thimble plug rod that serves to reduce the coolant flow up the empty guide thimble. The approximate weight of a BPRA with twenty-four poison rods is 65 pounds.

1.2.3.1 Radionuclide Inventory

The nuclear parameters for the MFFP payload are provided in Table 1.2-2. Impurities (e.g., americium) are chemically cleaned from the MOX powder in an aqueous polishing process prior to fuel fabrication and reduced to acceptable processing levels.

1.2.3.2 Maximum Payload Weight

The maximum payload weight of the MFFP is 4,740 pounds, based on three MOX PWR fuel assemblies (including BPRAs) with a weight of 1,580 pounds each.

1.2.3.3 Maximum Decay Heat

The maximum heat load for the MFFP is 240 watts for three fuel assemblies.

1.2.3.4 Maximum Pressure Buildup

The maximum normal operating pressure (MNOP) is established at 10 psig. The design pressure of the MFFP is 25 psig. The MFFP is evaluated for the design pressure in Chapter 2.0, *Structural Evaluation*.

1.2.4 Operational Features

The MFFP is not considered to be operationally complex. All operational features are depicted on the drawings provided in Appendix 1.4.2, *Packaging General Arrangement Drawings*. Operating procedures and instructions for loading, unloading, and preparing an empty MFFP for transport are provided in Chapter 7.0, *Package Operations*.

Table 1.2-1 – Fuel Assembly Physical Parameters

Parameter	Value
Fuel Rod Cladding Material	M5
Fuel Rod Array	17 × 17
Fuel Rods per Fuel Assembly	264
Guide Tubes per Fuel Assembly	24
Instrument Tubes per Fuel Assembly	1
Fuel Assembly Length, inches	161.61
Fuel Assembly Maximum Width, inches	8.565
Fuel Rod Pitch, inches	0.496
Fuel Rod Length, inches	152.4
Fuel Rod OD, inches	0.374
Fuel Rod Clad Thickness, inches	0.023
Active Fuel Length, inches	144.0
PuO ₂ + UO ₂ weight, pounds	1,157
Heavy Metal Weight, pounds	1,020
Maximum Fuel Assembly Weight (including BPRA), pounds	1,580
Maximum Initial Pu Loading, weight percent	6.0
Temperature Limits, °F	392 (NCT) 1,337 (HAC)

Table 1.2-2 – Nuclear Design Parameters

Parameter	Value
Pellet Diameter	0.323 inch
Effective Pellet Density	10.31 g/cc
Burnable Poison Rods	Yes – as separate removable assembly
Uranium Concentration Ranges (w/o)	<u>Total Uranium 94.0^{w/o} or greater of which:</u> ²³⁴ U: 0 to 0.05 w/o ²³⁵ U: 0 to 0.30 w/o ²³⁸ U: 99.65 to 100 w/o
Plutonium Concentration Ranges (w/o)	<u>Total Plutonium up to 6.0^{w/o} of which:</u> ²³⁸ Pu: 0 to 0.05 w/o ²³⁹ Pu: 90 to 95 w/o ²⁴⁰ Pu: 5 to 9 w/o ²⁴¹ Pu: 0 to 1 w/o ²⁴² Pu: 0 to 0.1 w/o

Security Related Information
Figure Withheld Under 10 CFR 2.390

Figure 1.2-1 – MFFP Overall Assembly (inches)

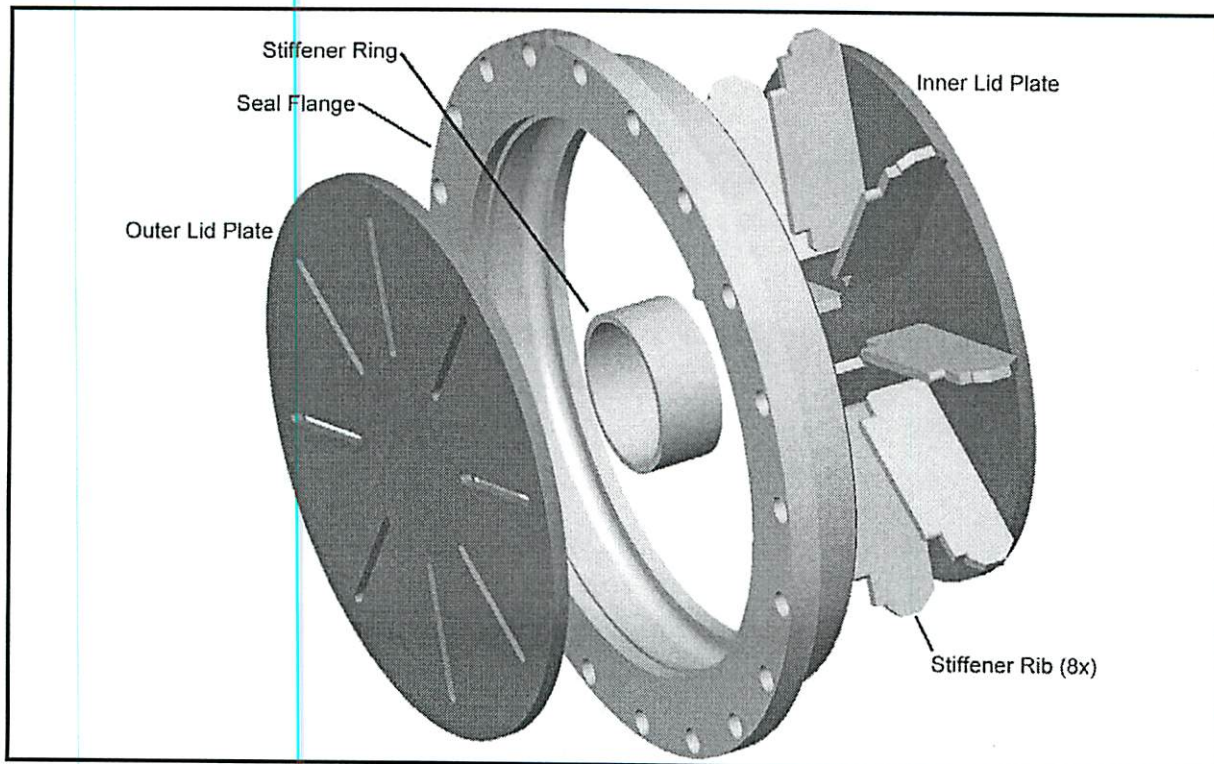


Figure 1.2-2 – Closure Lid (O-Ring Grooves and Ports Removed for Clarity)

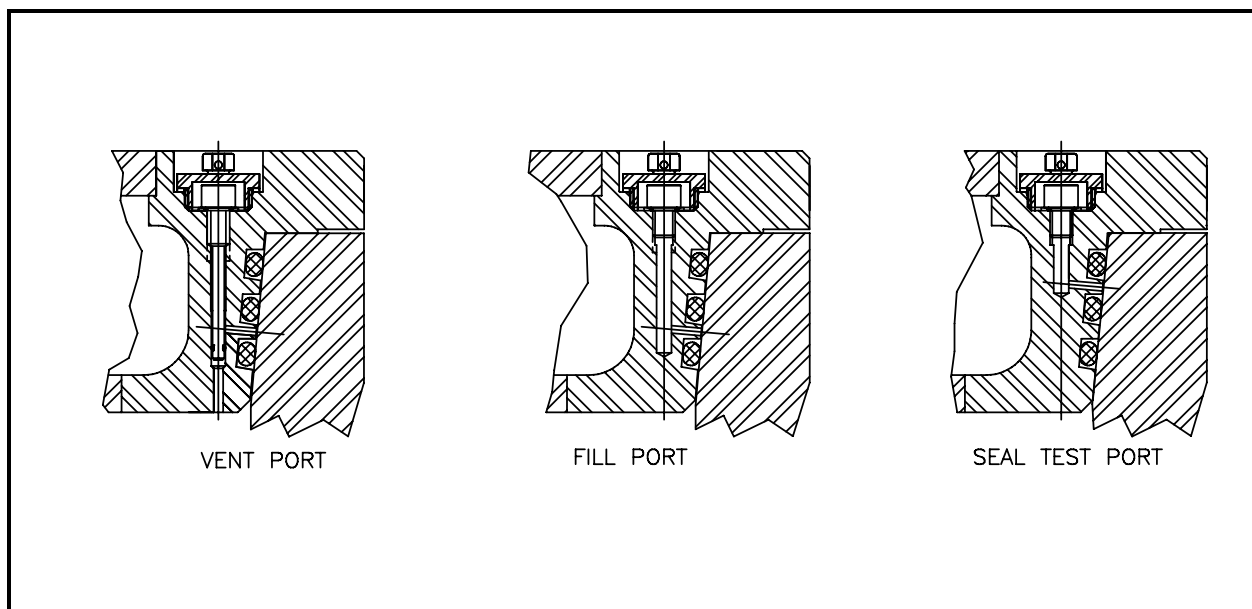


Figure 1.2-3 – MFFP Port Details

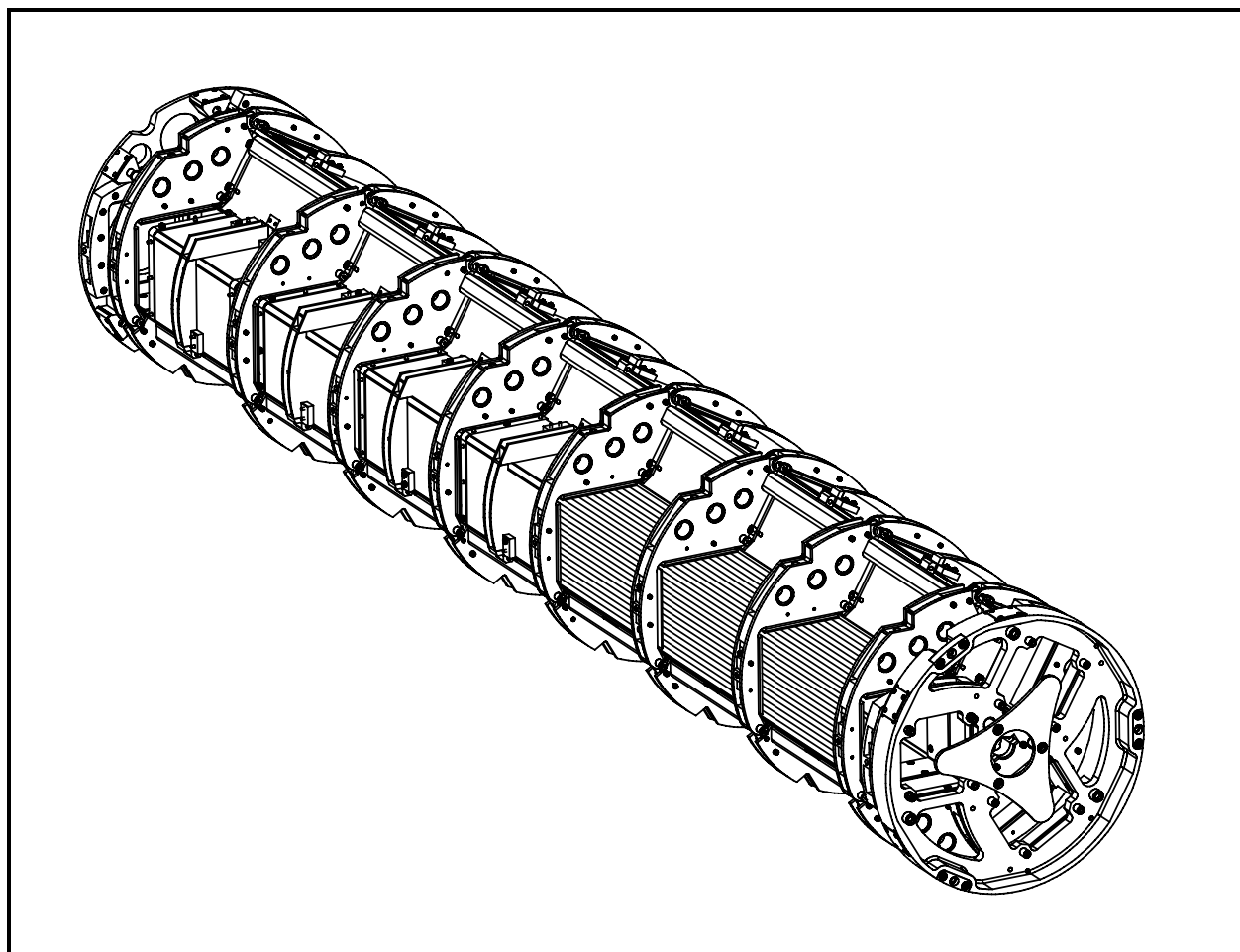


Figure 1.2-4 – Strongback (Shown with FAs installed, Upper (3) FCS Segments Removed)

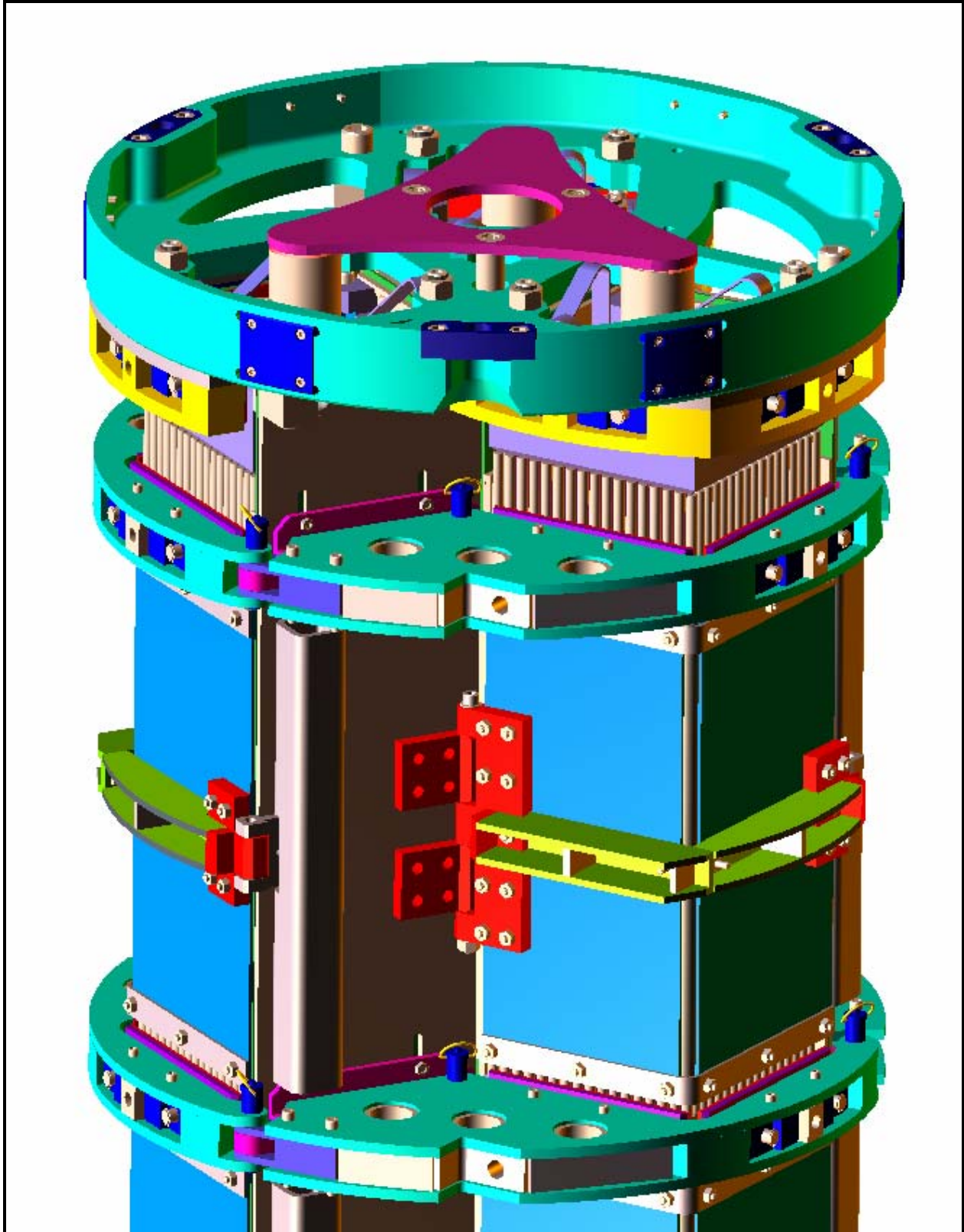


Figure 1.2-5 – Strongback, Top End (Shown with FAs Installed)

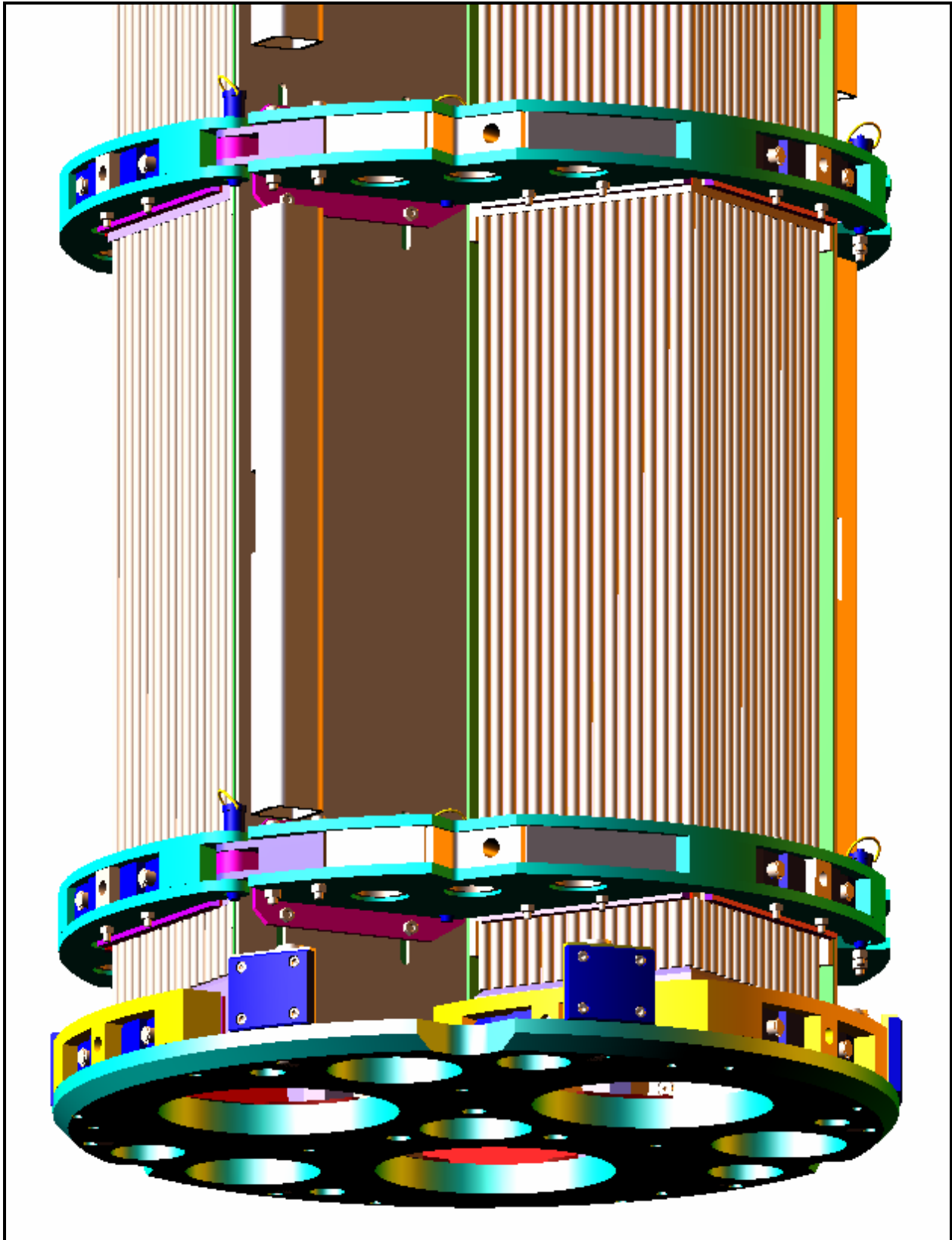


Figure 1.2-6 – Strongback, Bottom End with FAs, (FCSs Removed for Clarity)

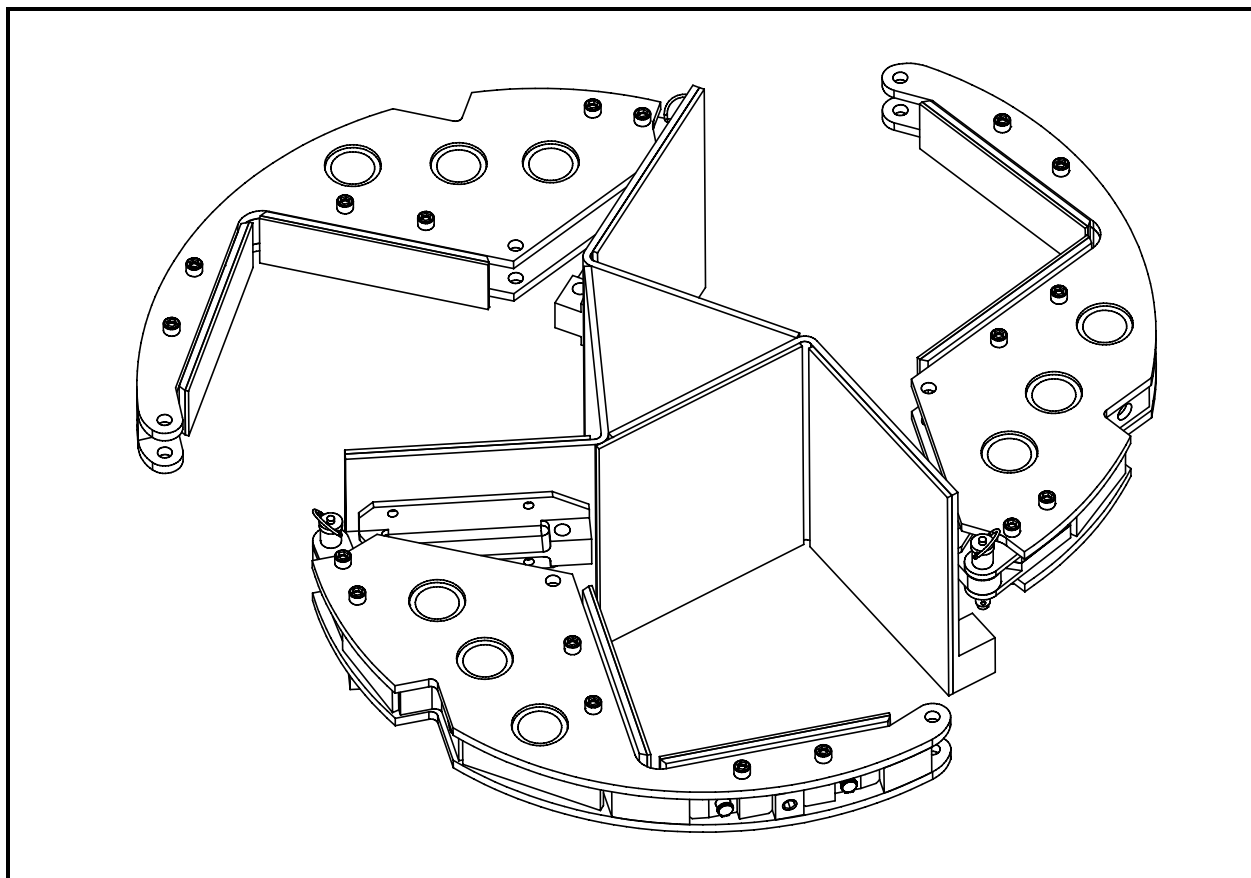


Figure 1.2-7 – Strongback Sectional View (Clamp Arms Shown Partially Open, FCSs Removed)

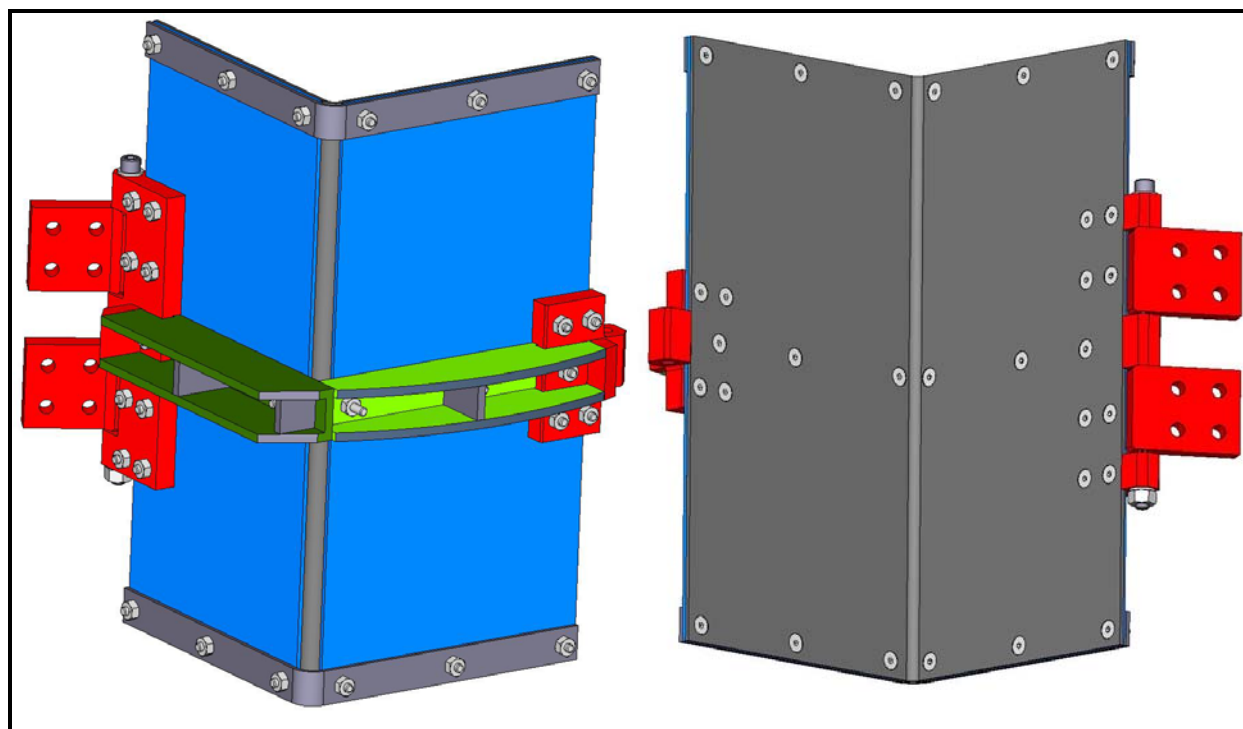


Figure 1.2-8 – Fuel Control Structure, Outside and Inside Views

Security Related Information
Figure Withheld Under 10 CFR 2.390

Figure 1.2-9 – Strongback Cross-Section (Clamp Arms and FCSs Removed for Clarity)

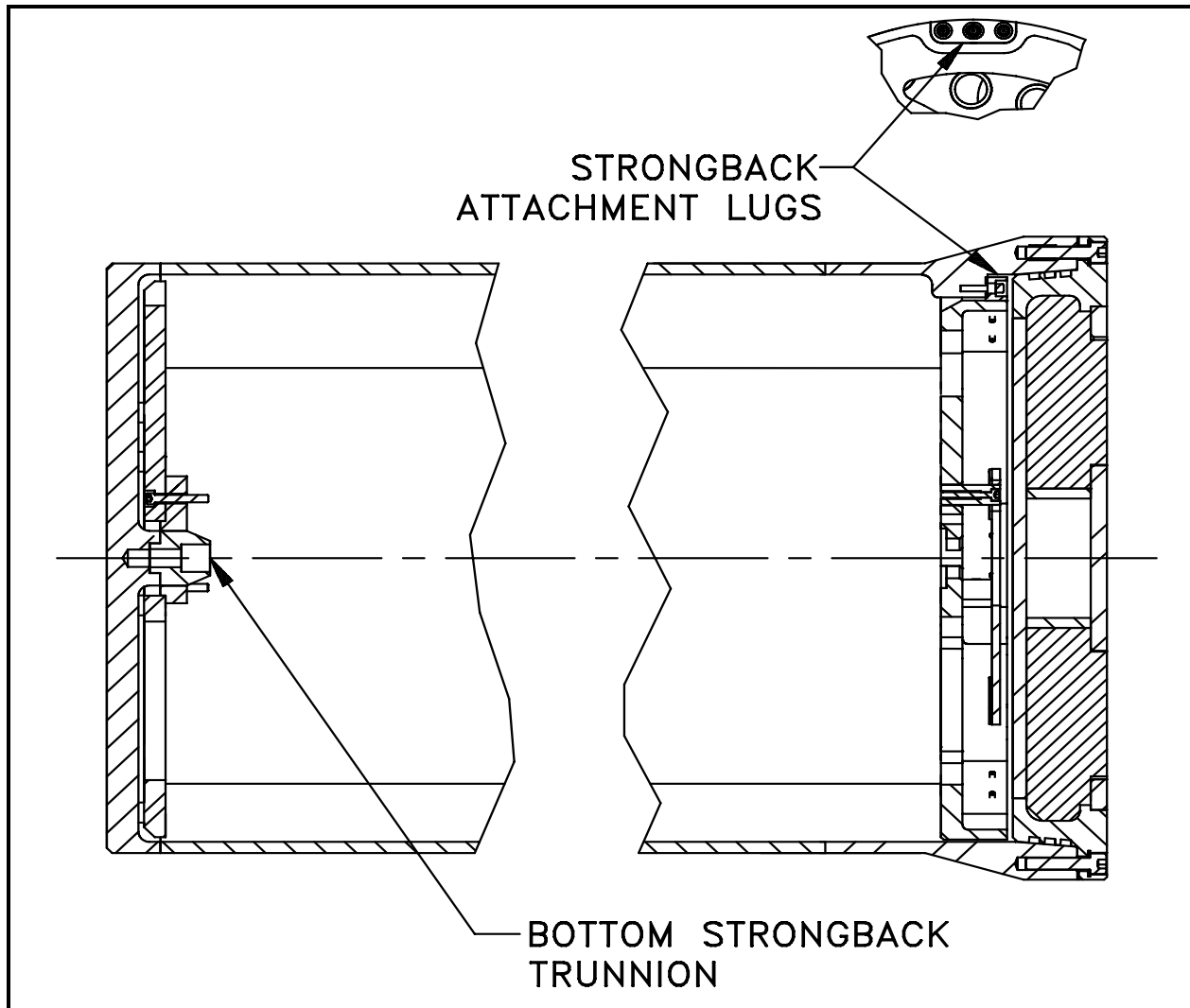


Figure 1.2-10 – Strongback Top Plate-to-Body Interface

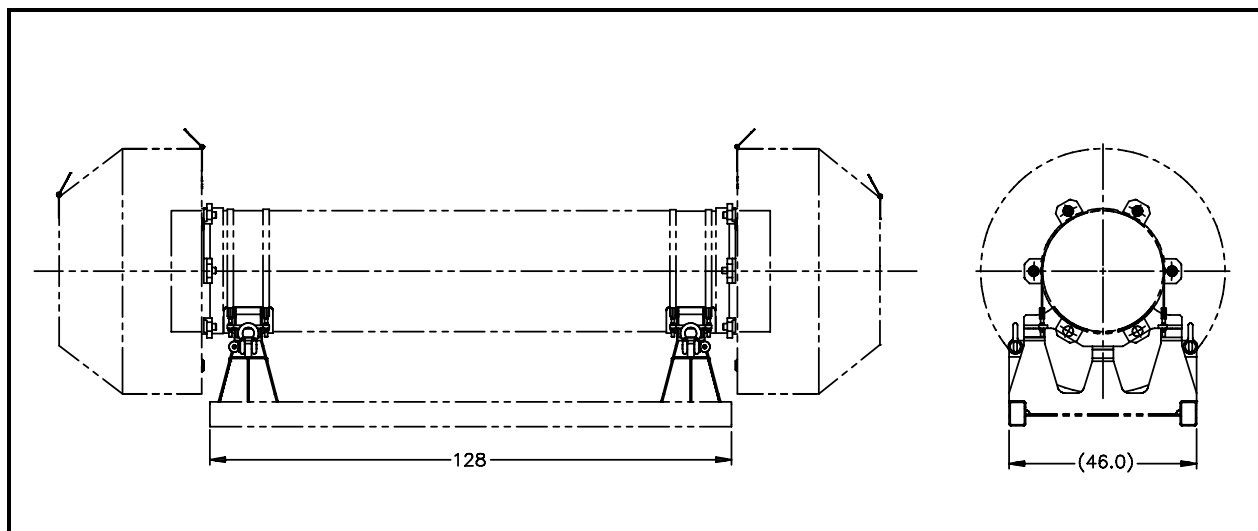


Figure 1.2-11 – MFFP Shipping Skid

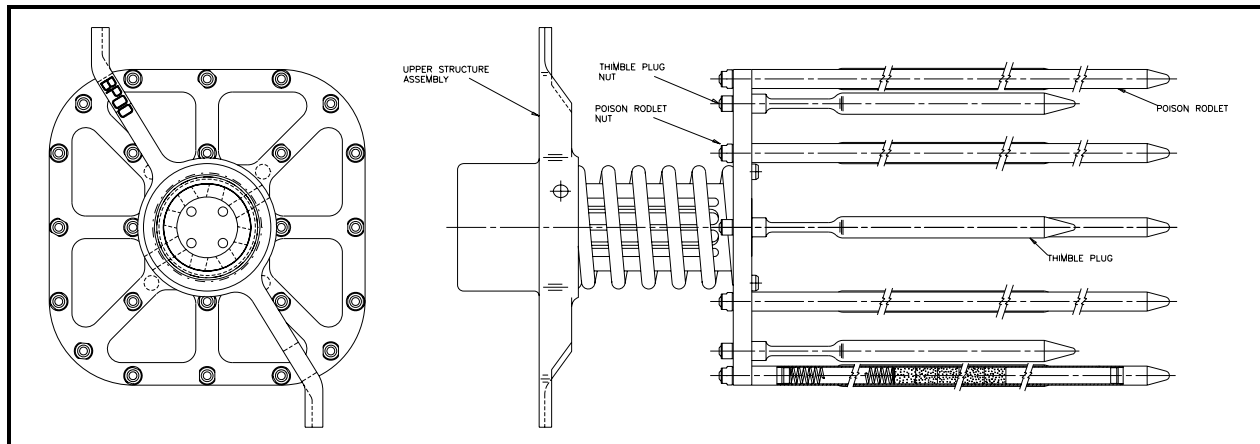


Figure 1.2-12 – BPR Assembly

This page left intentionally blank.

1.3 General Requirements for All Packages

1.3.1 Minimum Package Size

The minimum transverse dimension of the MFFP is 29⁵/₈ inches, and the minimum longitudinal dimension is approximately 201.33 inches. Therefore, the 4-inch requirement of 10 CFR §71.43(a)¹ is satisfied.

1.3.2 Tamper-Indicating Feature

A tamper-indicating seal is installed between two adjacent impact limiter bolts after installation of the lid end impact limiter, as delineated on the drawings in Appendix 1.4.2, *Packaging General Arrangement Drawings*. Failure of the tamper-indicating device provides evidence of possible unauthorized access. Therefore, the requirement of 10 CFR §71.43(b) is satisfied.

1.3.3 Positive Closure

Inadvertent opening of the package closure cannot occur for the MFFP. The closure lid is secured by twenty-four (24), 3/4-10 UNC-2A socket head cap screws (SHCS), thereby eliminating access to the containment cavity. The impact limiters are then installed onto each end of the package using six (6), 1-8UNC-2A SHCS. Once installed, the lid end impact limiter prevents all access to the closure lid, and the vent and fill port plugs. Thus, inadvertent opening of the package cannot occur, and the requirement of 10 CFR §71.43(c) is satisfied.

1.3.4 Chemical and Galvanic Reactions

The potential for material chemical and galvanic reaction of the major materials of construction of the MFFP are discussed in Section 2.2.2, *Chemical and Galvanic Reactions*. As noted in that section, the requirements of 10 CFR §71.43(d) are met.

1.3.5 Valves

The MFFP does not contain valves. However, beside the closure lid, the vent and fill ports penetrate the containment boundary. Both ports are recessed, fitted with brass protective caps, and are covered by the lid end impact limiter. Access to the vent and fill ports is prevented by the lid impact limiter during transport, as discussed in Section 1.3.3, *Positive Closure*. Therefore, these penetrations cannot be accessed during transport. Thus, the requirements of 10 CFR §71.43(e) are met.

1.3.6 Package Design

As shown in Chapter 2.0, *Structural Evaluation*, Chapter 3.0, *Thermal Evaluation*, Chapter 5.0, *Shielding Evaluation*, and Chapter 6.0, *Criticality Evaluation*, the structural, thermal, shielding, and criticality requirements, respectively, of 10 CFR §71.43(f) are satisfied for the MFFP.

¹ Title 10, Code of Federal Regulations, Part 71 (10 CFR 71), *Packaging and Transportation of Radioactive Materials*, Final Rule, 01-26-04.

1.3.7 External Temperatures

As shown in Table 3.4-1 from Section 3.4, *Thermal Evaluation Under Normal Conditions of Transport*, the maximum accessible surface temperature with maximum internal decay heat load and no insolation is 110 °F. Since the maximum external temperature does not exceed 122 °F, the requirements of 10 CFR §71.43(g) are satisfied for nonexclusive use shipments.

1.3.8 Venting

The MFFP does not include any features intended to allow continuous venting of the containment boundary during transport. Thus, the requirements of 10 CFR §71.43(h) are satisfied.

1.4 Appendices

1.4.1 Nomenclature

1.4.2 Packaging General Arrangement Drawings

This page left intentionally blank.

1.4.1 Nomenclature

B&PV – Boiler and Pressure Vessel Code, typically referring to the ASME B&PV Code

Body – A welded cylindrical shell and bottom end plate of the MFFP.

Bottom End – The closed end of the body.

BPRA – Burnable poison rod assembly, may optionally be shipped installed in a MOX FA.

Clamp Arms – The arms that secure the fuel assemblies to the strongback.

Closure Bolts or Closure Lid Bolts – Fasteners that secure the closure lid to the body.

Closure Lid – A weldment that closes the upper end of the body; contains vent, fill, and test ports, and three O-ring seals.

Containment O-ring Seal – The middle elastomeric O-ring seal, inserted into a groove in the closure lid, which forms a part of the containment boundary.

FA – Fuel assembly.

FCS – Fuel control structure.

Fill Port – An opening in the closure lid, communicating with the annular region between the containment (middle) and fill (inner) O-ring seals, to facilitate helium leakage rate testing of the containment seal.

Fill O-ring Seal – The innermost elastomeric O-ring, inserted into a groove in the closure lid that facilitates helium leakage rate testing of the containment seal.

Fuel Control Structure – A right-angle assembly that encloses the fuel assembly between the clamp arms.

HAC – Hypothetical accident conditions.

Impact Limiter – A device used to limit deceleration of the transportation package upon impact.

Leaktight – Defined by ANSI¹ N14.5 as 1×10^{-7} standard cubic centimeters per second (scc/s), or less, air leakage.

Lid End – The open end of the body.

MFFF – MOX Fuel Fabrication Facility.

MFFP – MOX Fresh Fuel Package, consisting of the body, closure lid, strongback, and impact limiters.

MNOP – Maximum normal operating pressure.

MOX – Mixed oxide.

Neutron Poison Plates – Neutron-absorbing material, mounted as plates on the FCSs and the strongback.

¹ ANSI N14.5-1997, *American Nation Standard for Radioactive Materials – Leakage Test on Packages for Shipment*, American Nation Standards Institute (ANSI), Inc.

NCT – Normal conditions of transport.

Packaging – The assembly of components necessary to ensure compliance with packaging requirements as defined in 10 CFR §71.4. Within this SAR, the packaging is denoted as the MFFP.

Package – The packaging with its radioactive contents, or payload, as presented for transportation as defined in 10 CFR §71.4. Within this SAR, the package is denoted as the MFFP with its fresh fuel assembly payload.

Payload – The MOX fresh fuel assemblies (FAs).

Strongback – An assembly that supports and restrains the payload.

Strongback Bottom End Plate – A plate assembly that attaches to the bottom end of the strongback and secures the bottom nozzle on the FA.

Strongback Top End Plate – A plate assembly that attaches to the top end of the strongback and secures the top nozzle on the FA.

Seal Test Port – An opening in the closure lid, communicating with the annular region between the containment (middle) and test (outer) O-ring seals, to facilitate helium leakage rate testing of the containment seal.

Shipping Skid – A weldment used to support the package within the conveyance, and during handling operations.

Test O-ring Seal – The outermost elastomeric O-ring seal, inserted into a groove in the closure lid, which facilitates helium leakage rate testing of the containment O-ring seal.

Vent Port – An opening in the closure lid, communicating with the internal cavity, which allows venting of the cavity during package opening and closing operations.

Vent, Seal Test, or Fill Port Plug – Brass fittings which, together with their elastomer sealing washer, close and seal the corresponding ports.

1.4.2 Packaging General Arrangement Drawings

This section presents the MFFP general arrangement drawings¹, consisting of the following drawings:


- 99008-10, Rev. 4, 1 sheet, *MFFP Shipping Package*
- 99008-20, Rev. 3, 6 sheets, *MFFP Body Assembly*
- 99008-30, Rev. 5, 7 sheets, *MFFP Strongback Assembly*
- 99008-31, Rev. 1, 3 sheets, *MFFP Strongback Top Plate Assembly*
- 99008-32, Rev. 1, 2 sheets, *MFFP Strongback Bottom Plate Assembly*
- 99008-33, Rev. 3, 4 sheets, *MFFP Strongback Clamp Arm Assembly*
- 99008-34, Rev. 4, 2 sheets, *MFFP Strongback Fuel Control Structure Assembly*
- 99008-40, Rev. 2, 3 sheets, *MFFP Impact Limiters*

Within the packaging general arrangement drawing, dimensions important to the packaging's safety are dimensioned and toleranced (e.g., shell thicknesses, polyurethane foam thicknesses, and the sealing regions on the seal flanges). All other dimensions are provided as a reference dimension, and are toleranced in accordance with the general tolerance block on the drawings.

¹ The MFFP general arrangement drawings utilize the uniform standard practices of ASME Y14.5M, *Dimensioning and Tolerancing*, American National Standards Institute, Inc. (ANSI).

This page left intentionally blank.

Security Related Information
Figure Withheld Under 10 CFR 2.390

 PACTEC		PACKAGING TECHNOLOGY, INC. TACOMA, WA	
MFFP SHIPPING PACKAGE SAR DRAWING			
SCALE: 1/8		WT. N/A	
REV: 4		SHEET 1 OF 1	
DWG NO. D		99008-10	
CADFILE: 99008-1014.DWG			

8

7

6

5

4

3

99008-20

1 3

1

D

D

Security Related Information
Figure Withheld Under 10 CFR 2.390

C

C

B

B

A

A



PACKAGING TECHNOLOGY, INC.
TACOMA, WA

MFFP
BODY ASSEMBLY
SAR DRAWING

SCALE: N/A	WT. N/A
REV: 3	SHEET 1 OF 6
DWG NO. 99008-20	
DWG SIZE D	CADFILE: 99008_2013.DWG

8

7

6

5

4

3

2

1

8

7

6

5

4

3

99008-20 2 3

1

D

D

Security Related Information
Figure Withheld Under 10 CFR 2.390

C

C

B

B

A

A

8

7

6

5

4

3

2

1



PACKAGING TECHNOLOGY, INC.
TACOMA, WA

MFFP
BODY ASSEMBLY
SAR DRAWING

SCALE: 1/8	WT. N/A
REV. 3	SHEET 2 OF 6
DWG NO.	
SIZE D	99008-20
CAD FILE: 99008_2031.DWG	

8

7

6

5

4

3

99008-20

3

1

D

D

C

C

B

B

A

A

8

7

6

5

4

3

2

1

Security Related Information
Figure Withheld Under 10 CFR 2.390



PACKAGING TECHNOLOGY, INC.
TACOMA, WA

MFFP
BODY ASSEMBLY
SAR DRAWING

SCALE: 1/4	WT. N/A
REV: 3	SHEET 3 OF 6
DRG NO.	
D	99008-20
SIZE	CADFILE: 99008_2033.DWG

8

7

6

5

4

3

99008-20

4

3

1

D

D

C

C

B

B

A

A

8

7

6

5

4

3

2

1

Security Related Information
Figure Withheld Under 10 CFR 2.390



PACKAGING TECHNOLOGY, INC.
TACOMA, WA

MFFP
BODY ASSEMBLY
SAR DRAWING

SCALE: FULL	WT. N/A
REV. 3	SHEET 4 OF 6
DWG NO. D	99008-20
CADFILE: 99008_2043.DWG	

8

7

6

5

4

3

99008-20

5 3

1

D

D

C

C

B

B

A

A

Security Related Information
Figure Withheld Under 10 CFR 2.390



PACKAGING TECHNOLOGY, INC.
TACOMA, WA

MFFP
BODY ASSEMBLY
SAR DRAWING

SCALE: FULL	WT. N/A
REV: 3	SHEET 5 OF 5
DWG NO.	
SIZE	
D	99008-20
CADFILE:	99008_2053.DWG

8

7

6

5

4

3

2

1

8

7

6

5

4

3

99008-20

6 3

1

D

D

C

C

B

B

A

A

Security Related Information
Figure Withheld Under 10 CFR 2.390



PACKAGING TECHNOLOGY, INC.
TACOMA, WA

MFFP
BODY ASSEMBLY
SAR DRAWING

SCALE: FULL	WT. N/A
REV. 3	SHEET 5 OF 5
DWG NO.	
SIZE	
D	99008-20
CAD FILE: 99008_2063.DWG	

99008-30

1 5

1

Security Related Information
Figure Withheld Under 10 CFR 2.390

**PACTEC**PACKAGING TECHNOLOGY, INC.
TACOMA, WAMFFP
STRONGBACK ASSEMBLY
SAR DRAWING

SCALE: N/A	WT. N/A
REV: 5	SHEET 1 OF 7
DWG NO.	
DWG SIZE	
D	99008-30
CADFILE: 99008_3015.DWG	

Security Related Information
Figure Withheld Under 10 CFR 2.390



PACTEC

PACKAGING TECHNOLOGY, INC.
TACOMA, WA

MFFP
STRONGBACK ASSEMBLY
SAR DRAWING

SCALE: 1/8"	WT. N/A
REV. 5	SHEET 2 OF 7
DWG NO.	
SIZE	
D	99008-30
CADFILE: 99008_3025.DWG	

Security Related Information
Figure Withheld Under 10 CFR 2.390

99008-30

3 5

1



PACKAGING TECHNOLOGY, INC.
TACOMA, WA

MFFP
STRONGBACK ASSEMBLY
SAR DRAWING

SCALE: 1/8	WT. N/A
REV: 5	SHEET 3 OF 7
DWG NO.	
D	99008-30
CADFILE: 99008_3035.DWG	

99008-30

4

5

1

Security Related Information
Figure Withheld Under 10 CFR 2.390



PACKAGING TECHNOLOGY, INC.
TACOMA, WA

MFFP
STRONGBACK ASSEMBLY
SAR DRAWING

SCALE: 1/2	WT. N/A
REV: 5	SHEET 4 OF 7
DWG NO.	99008-30
DWG SIZE	D
CADFILE: 99008_3045.DWG	

99008-30

5 5

1

Security Related Information
Figure Withheld Under 10 CFR 2.390




PACKAGING TECHNOLOGY, INC.
TACOMA, WA

MFFP
STRONGBACK ASSEMBLY
SAR DRAWING

SCALE: 1/2	WT. N/A
REV: 5	SHEET 5 OF 7
DWG NO.	
D	99008-30
CADFILE: 99008_3055.DWG	

Security Related Information
Figure Withheld Under 10 CFR 2.390

		PACKAGING TECHNOLOGY, INC. TACOMA, WA	
MFFP STRONGBACK ASSEMBLY SAR DRAWING			
SCALE: 1/2	WT. N/A		
REV. 5	SHEET 6 OF 7		
DWG NO.			
D	99008-30		
CAD FILE: 99008_3065.DWG			

99008-30

7

5

1

Security Related Information
Figure Withheld Under 10 CFR 2.390



PACKAGING TECHNOLOGY, INC.
TACOMA, WA

MFFP
STRONGBACK ASSEMBLY
SAR DRAWING

SCALE: 1/2	WT. N/A
REV: 5	SHEET 7 OF 7
DWG NO. 99008-30	
DWG SIZE D	
CAD FILE: 99008_3075.DWG	

Security Related Information
Figure Withheld Under 10 CFR 2.390

99008-31

1

1



PACKAGING TECHNOLOGY, INC.
TACOMA, WA

MFFP
TOP PLATE ASSEMBLY
SAR DRAWING

SCALE: N/A	WT. N/A
REV. 1	SHEET 1 OF 3
DWG NO.	
D	99008-31
CHGFILE: 99008_3111.DWG	

8

7

6

5

4

3

99008-31

2 1

1

D

D

C

C

B

B

A

A

Security Related Information
Figure Withheld Under 10 CFR 2.390



PACKAGING TECHNOLOGY, INC.
TACOMA, WA

MFFP
TOP PLATE ASSEMBLY
SAR DRAWING

SCALE: 1/2	WT. N/A
REV: 1	SHEET 2 OF 3
DWG NO.	
DWG SIZE	
D	99008-31
CADFILE: 99008_3121.DWG	

8

7

6

5

4

3

2

1

8

7

6

5

4

3

99008-31

3

1

1

D

D

C

C

→

←

B

B

A

A

8

7

6

5

4

3

2

1

Security Related Information
Figure Withheld Under 10 CFR 2.390



PACKAGING TECHNOLOGY, INC.
TACOMA, WA

MFFP
TOP PLATE ASSEMBLY
SAR DRAWING

SCALE: 1/2	WT. N/A
REV: 1	SHEET 3 OF 3
DWG NO.	
DWG SIZE	
D	99008-31
CADFILE: 99008_3131.DWG	

8

7

6

5

4

3

99008-32

1

1

1

D

D

C

C

B

B

A

A

Security Related Information
Figure Withheld Under 10 CFR 2.390



PACKAGING TECHNOLOGY, INC.
TACOMA, WA

MFFP
BOTTOM PLATE ASSEMBLY
SAR DRAWING

SCALE: FULL	WT. N/A
REV: 1	SHEET 1 OF 2
DWG NO. 99008-32	
DWG SIZE D	
CADFILE: 99008_3211.DWG	

8

7

6

5

4

3

2

1

8

7

6

5

4

3

99008-32

2

1

1

D

D

C

C

B

B

A

A

Security Related Information
Figure Withheld Under 10 CFR 2.390



PACKAGING TECHNOLOGY, INC.
TACOMA, WA

MFFP
BOTTOM PLATE ASSEMBLY
SAR DRAWING

SCALE: 1/2	WT. N/A
REV: 1	SHEET 2 OF 2
DWG NO. 99008-32	
DWG SIZE D	CADFILE: 99008_3221.DWG

99008-33

1 3

1

Security Related Information
Figure Withheld Under 10 CFR 2.390



PACKAGING TECHNOLOGY, INC.
TACOMA, WA

MFFP
CLAMP ARM ASSEMBLY
SAR DRAWING

SCALE: N/A	WT. N/A
REV. 3	SHEET 1 OF 4
DWG NO. 99008-33	
DWG SIZE D	
CAD FILE: 99008_3313.DWG	

99008-33

2 3

1

Security Related Information
Figure Withheld Under 10 CFR 2.390



PACTEC

PACKAGING TECHNOLOGY, INC.
TACOMA, WAMFFP
CLAMP ARM ASSEMBLY
SAR DRAWING

SCALE: 1/2	WT. N/A
REV. 3	SHEET 2 OF 4
DWG NO. 99008-33	
DWG SIZE D	CAD FILE: 99008_3323.DWG

Security Related Information
Figure Withheld Under 10 CFR 2.390

99008-33 3 3



PACKAGING TECHNOLOGY, INC.
TACOMA, WA

MFFP
CLAMP ARM ASSEMBLY
SAR DRAWING

SCALE: FULL	WT. N/A
REV: 3	SHEET 3 OF 4
DWG NO.	
D	99008-33
CADFILE: 99008_3333.DWG	

99008-33

4 3

Security Related Information
Figure Withheld Under 10 CFR 2.390



PACKAGING TECHNOLOGY, INC.
TACOMA, WA

MFFP
CLAMP ARM ASSEMBLY
SAR DRAWING

SCALE: 1/2	WT. N/A
REV: 3	SHEET 4 OF 4
DWG NO. 99008-33	
DWG SIZE D	
CAD FILE: 99008-33.dwg	

8

7

6

5

4

3

99008-34

1 4

1

D

D

C

C

B

B

A

A

Security Related Information
Figure Withheld Under 10 CFR 2.390



PACKAGING TECHNOLOGY, INC.
TACOMA, WA

MFFP
FUEL CONTROL STRUCTURE ASSEMBLY
SAR DRAWING

SCALE: 1/2	WT. N/A
REV. 4	SHEET 1 OF 2
DWG NO.	
D	99008-34
CADFILE: 99008_3414.DWG	

8

7

6

5

4

3

2

1

99008-34 2 4

Security Related Information
Figure Withheld Under 10 CFR 2.390



PACKAGING TECHNOLOGY, INC.
TACOMA, WA

MFFP
FUEL CONTROL STRUCTURE ASSEMBLY
SAR DRAWING

SCALE: 1/2	WT. N/A
REV: 4	SHEET 2 OF 2
DWG NO. 99008-34	
DWG FILE: 99008_342.DWG	

8

7

6

5

4

3

99008--40

1 2

1

D

D

C

C

B

B

A

A

8

7

6

5

4

3

2

1

Security Related Information
Figure Withheld Under 10 CFR 2.390




PACKAGING TECHNOLOGY, INC.
TACOMA, WA

MFFP
IMPACT LIMITER
SAR DRAWING

SCALE: 1/2	WT. N/A
REV. 2	SHEET 1 OF 3
DWG NO.	
SIZE	
D	99008-40
CADFILE: 99008_4012.DWG	

Security Related Information
Figure Withheld Under 10 CFR 2.390

 PACTEC		PACKAGING TECHNOLOGY, INC. TACOMA, WA	
MFFP IMPACT LIMITER SAR DRAWING			
SCALE: 1/8	WT. N/A		
REV. 2	SHEET 2 OF 3		
DWG NO.			
DWG SIZE			
D	99008-40		
CAD FILE: 99008_4022.DWG			

Security Related Information
Figure Withheld Under 10 CFR 2.390



PACKAGING TECHNOLOGY, INC.
TACOMA, WA

MFFP
IMPACT LIMITER
SAR DRAWING

SCALE: 1/8	WT. N/A
REV: 2	SHEET 3 OF 3
DWG NO.	99008-40
DWG SIZE	CADFILE: 99008_40.32.DWG

2.0 STRUCTURAL EVALUATION

This chapter presents the package weights, mechanical properties of materials, and structural evaluations that demonstrate that the MOX Fresh Fuel Package (MFFP) design meets all applicable structural criteria. The package, which is designed to transport up to three fresh MOX fuel assemblies, consists of a strongback to secure the fuel assemblies, a body including the containment shell and closure lid, and two impact limiters. Structural evaluations of normal conditions of transport (NCT) and hypothetical accident conditions (HAC) are performed using analytical and experimental techniques to address 10 CFR 71¹ performance requirements. All NCT events are evaluated analytically. The HAC fire and immersion events are also evaluated analytically. HAC free drop and puncture events are evaluated by a combination of analysis and full-scale certification testing.

2.1 Structural Design

2.1.1 Discussion

A comprehensive discussion of the MFFP design and configuration is provided in Section 1.2, *Package Description*. The MFFP drawings show the detailed geometry of the package, as well as the dimension, tolerances, materials, and fabrication requirements, and are provided in Appendix 1.4.2, *Packaging General Arrangement Drawings*.

- The MFFP assembly of components is shown on Drawing 99008-10.
- The containment body, which includes the closure lid, closure bolts, and containment body weldment, is described in Section 1.2.1.1, *Body*, and is shown on Drawing 99008-20.
- The closure requirements of the package are described on the package drawings and in Chapter 7.0, *Package Operations*.
- The containment boundary is identified in Section 1.2.2, *Containment System*, and is shown on Figure 1.1-2.
- The strongback, which supports the payload and provides criticality control, is described in Section 1.2.1.2, *Strongback*, and is shown on Drawing 99008-30.
- The impact limiters, which mitigate free drop impact loads and thermally protect the containment O-rings during the postulated accident fire conditions, are described in Section 1.2.1.3, *Impact Limiters*, and are shown on Drawing 99008-40.

Specific discussions relating to the aspects important to demonstrating the structural configuration and performance to design criteria for the MFFP are provided in the following sections.

2.1.2 Design Criteria

Proof of performance of the MFFP is achieved by a combination of analytical evaluations and certification testing of a prototypic package. The acceptance criterion for analytical assessments is in

¹ Title 10, Code of Federal Regulations, Part 71 (10 CFR 71), *Packaging and Transportation of Radioactive Materials*, Final Rule, 01-26-04.

accordance with Regulatory Guide 7.6² and Section III of the ASME Boiler and Pressure Vessel (B&PV) Code³. The acceptance criteria associated with certification testing of free drop and puncture is primarily a demonstration that the containment boundary remains leaktight (leakage rate of less than 1×10^{-7} standard cubic centimeters per second (scc/sec), air) following the imposed load conditions. Additionally, package deformations obtained from testing must be such that deformed geometry assumptions used in criticality and thermal analyses are validated or bounded.

The remainder of this subsection presents the detailed acceptance criteria used for analytical evaluations of the MFFP.

2.1.2.1 Analytic Design Criteria (Allowable Stresses)

2.1.2.1.1 Containment Structures

The design criteria used for containment structure analyses are provided in Table 2.1-1. The containment body is classified as a Section III, Subsection NB, Class 1 component by NUREG/CR-3854⁴ and NUREG/CR-3019⁵. The analytical design criteria presented in Table 2.1-1 are consistent with Regulatory Guide 7.6 and the ASME B&PV Code, Section III, Subsection NB-3000, and Appendix F.

2.1.2.1.2 Criticality Control Structures

The acceptance criteria applicable to criticality control structural component analyses are provided in Table 2.1-2. The criticality control structures are classified as a Section III, Subsection NG, core support structure by NUREG/CR-3854 and NUREG/CR-3019. The analytical design criteria presented in Table 2.1-2 are consistent with the ASME B&PV Code, Section III, Subsection NG-3000, and Appendix F.

2.1.2.1.3 Other Structures

Impact limiter components are permitted to exceed the material's yield strength for all conditions. The acceptance criterion for impact limiters is that all of the kinetic energy associated with the free drop event be absorbed without contact of a solid (non-energy absorbing) package component with the "unyielding" impact surface.

For evaluation of tie-down devices, the allowable stresses are limited to the material yield strength, consistent with the requirements of 10 CFR §71.45(b).

² U.S. Nuclear Regulatory Commission, Regulatory Guide 7.6, *Design Criteria for the Structural Analysis of Shipping Cask Containment Vessels*, Revision 1, March 1978.

³ American Society of Mechanical Engineers (ASME) Boiler and Pressure Vessel Code, Section III, *Rules for Construction of Nuclear Power Plant Components*, 2001 Edition, 2002 and 2003 Addenda.

⁴ L. E. Fischer, W. Lai, *Fabrication Criteria for Shipping Containers*, NUREG/CR-3854, UCRL-53544, U.S. Nuclear Regulatory Commission, March 1985.

⁵ R. E. Monroe, H. H. Woo, and R. G. Sears, *Recommended Welding Criteria for Use in the Fabrication of Shipping Containers for Radioactive Materials*, NUREG/CR-3019, UCRL-53044, March 1985.

2.1.2.2 Miscellaneous Structural Failure Modes

2.1.2.2.1 Brittle Fracture

With the exception of the closure lid bolts, some bolts and pins on the strongback, and energy absorbing foam, all structural components of the MFFP are fabricated of austenitic stainless steels. Austenitic stainless steels do not undergo a ductile-to-brittle transition in the temperature range of interest (i.e., down to -40 °F), and thus do not need to be evaluated for brittle fracture. Further, Regulatory Guide 7.11⁶ states, “*Since austenitic stainless steels are not susceptible to brittle failure at temperatures encountered in transport, their use in containment vessels is acceptable to the staff and no tests are needed to demonstrate resistance to brittle fracture.*”

The closure lid bolts are fabricated from ASTM A564, Type 630, Condition H1100, precipitation hardened stainless steel bolting material. Per Section 5 of NUREG/CR-1815⁷, bolts are not considered as fracture-critical components because multiple load paths exist and bolting systems are generally redundant, as is the case with the MFFP. Therefore, brittle fracture is not a failure mode of concern.

2.1.2.2.2 Fatigue Assessment

2.1.2.2.2.1 Normal Operating Cycles

Normal operating cycles do not present a fatigue concern for the MFFP components over a 20-year service life. The basis for this conclusion is reached using the six criteria of Article NB-3222.4(d) of the ASME B&PV Code. For the following analysis, the containment boundary design temperature (as identified in Section 2.6.1, *Heat*) of 160 °F is used. The material properties described in Section 2.2, *Materials*, are used. A summary of the six criteria and their application are discussed below.

(1) Atmospheric to Service Pressure Cycle: The total number of atmospheric-to-operating pressure cycles during normal operations does not exceed the number of cycles on the fatigue curve corresponding to a value of $S_a = 3S_m$ for Type XM-19 stainless steel. From Section 2.2, *Materials*, the S_m value for Type XM-19 stainless steel at a temperature of 160 °F is 33,180 psi, corresponding to an alternating stress value of $S_a = 3S_m = 99,540$ psi. The corresponding number of cycles for a value of $S_a = 99,540$ psi is approximately 2000 from Figure I-9.2.1 and Table I-9.1 of the ASME B&PV Code⁸. The MFFP has a design life of 20 years, and the maximum number of shipments is estimated at 65 per year. The containment boundary undergoes one atmospheric-to-operating pressure cycle per shipment, therefore the package will experience $20 \times 65 = 1,300$ atmospheric-to-operating pressure cycles in its life. Since $2,000 > 1,300$, the first criterion is therefore satisfied.

⁶ U.S. Nuclear Regulatory Commission, Regulatory Guide 7.11, *Fracture Toughness Criteria of Base Material for Ferritic Steel Shipping Cask Containment Vessels with a Maximum Wall Thickness of 4 Inch (0.1 m)*, June 1991.

⁷ W.R. Holman, R. T. Langland, *Recommendations for Protecting Against Failure by Brittle Fracture in Ferritic Steel Shipping Containers Up to Four Inch Thick*, NUREG/CR-1815, UCRL-53013, August 1981.

⁸ ASME Code, Subsection III, Division 1 Appendices, Appendix I, *Design Stress Intensity Values, Allowable Stresses, Material Properties, and Design Fatigue Curves*, Figure I-9.2.1, *Design Fatigue Curve for Austenitic Steels, Nickel-Chromium-Iron Alloy, Nickel-Iron-Chromium Alloy, and Nickel-Copper Alloy for $S_a > 28.2$ ksi, for Temperatures not Exceeding 800 °F*, and Table I-9.1, *Tabulated Values of S_w , ksi, from Figure I-9.0*.

(2) Normal Service Pressure Fluctuation: The specified full range of pressure fluctuations during normal service does not exceed the quantity $1/3 \times \text{Design Pressure} \times (S_a/S_m)$, where the Design Pressure is 25 psig, S_a is the value obtained from the Type XM-19 stainless steel design fatigue curve for the total specified number of significant pressure fluctuations, and S_m is the allowable stress intensity for the material at the service temperature. The total number of service cycles is less than 10^6 cycles. From Figure I-9.2.1, $S_a = 89,000$ psi for 2,600 cycles. The value of S_m was defined above as 33,180 psi at service temperature. The significant pressure fluctuation (SPF) becomes:

$$\text{SPF} = 1/3 \times \text{Design Pressure} \times (S_a/S_m) = 22.4 \text{ psid}$$

Next, the maximum pressure fluctuations in the package will be determined. The bulk average fill gas temperature (see Table 3.4-1 of Chapter 3.0, *Thermal Evaluation*) varies between the extremes of $T_1 = -40^\circ\text{F}$ to $T_2 = 166^\circ\text{F}$, the increase in internal pressure from atmospheric, $P_1 = 14.7$ psia, is:

$$\frac{P_2}{P_1} = \frac{T_2}{T_1} \Rightarrow P_2 = P_1 \left(\frac{T_2}{T_1} \right) = 14.7 \left(\frac{166 + 460}{-40 + 460} \right) = 21.9 \text{ psia}$$

The resulting pressure fluctuation is $21.9 - 14.7 = 7.2$ psid, which is less than 22.4 psid presented above and therefore, not significant. Thus, the second criterion is satisfied.

(3) Temperature Difference — Startup and Shutdown: The temperature between adjacent points of a package component during normal service does not exceed $S_a/2E\alpha$, where S_a is the design fatigue value taken from Table I-9.1 for Figure I-9.2.1 of the ASME Code for Type XM-19 stainless steel for the total specified number of temperature difference fluctuations, $E = 27.8 \times 10^6$ psi is the modulus of elasticity, and $\alpha = 8.9 \times 10^{-6}$ in/in/ $^\circ\text{F}$ is the instantaneous coefficient of thermal expansion, all evaluated at temperature. The total number of temperature fluctuations will not exceed the number of uses of the package and is conservatively taken as 1,300. The value of S_a , from Figure I-9.2.1 of the ASME Code, for 1,300 cycles is 109,000 psi. The value of $S_a/2E\alpha$ corresponding to 1,300 cycles is 220°F . Since the containment boundary design temperature is 160°F under ambient conditions of 100°F , the temperature difference between any two adjacent points cannot approach the 220°F value. Thus, the third criterion is satisfied.

(4) Temperature Difference — Normal Service: The temperature difference between any two adjacent points does not change during normal service by more than the quantity $S_a/2E\alpha$, where S_a , E , and α are as defined above. However, normal operating temperatures of the containment boundary are largely determined by the steady heat load, and any changes in temperature due to changes in ambient conditions, warm-up, or cool-down will be relatively slow and even due to the large thermal mass of the package. Therefore, the fourth criterion is satisfied.

(5) Temperature Difference — Dissimilar Materials: The fifth criterion addresses dissimilar materials, which is not a concern. The containment boundary is constructed entirely of Type XM-19 austenitic stainless steel. Therefore, the fifth criterion is satisfied.

(6) Mechanical Loads: The only repeating mechanical loads will be those associated with lifting and handling. Since the containment boundary is handled twice for each transport cycle (load and unload), the maximum number of cycles is $2 \times 1,300 = 2,600$. From Figure I-9.2.1, $S_a = 89,000$ psi for 2,600 cycles. Lifting stress is limited by 10 CFR §71.45(a) to a value of one-third of the material's minimum yield strength. For a lifting temperature of 160°F , the

minimum yield strength of Type XM-19 stainless steel is 50,260 psi. Thus, one-third of the minimum yield strength is $50,260/3 = 16,753$ psi. Since 89,000 psi \gg 16,753 psi, the sixth criterion is satisfied.

The previous discussion verifies that fatigue failure of the containment boundary due to normal operating cycles is not a concern, per Section III, Subsection NB, Article NB-3222.4(d) of the ASME B&PV Code. Therefore, the MFFP containment boundary resistance to fatigue is adequate to ensure a minimum 20-year service life.

The maximum stress developed in the closure bolts during normal operations (reported in Section 2.6.1.3.4, *Closure Bolt Evaluation*) is $S_{\max} = 92,512$ psi. This stress includes stresses due to pressure and thermal effects, and a conservative inclusion of 50% of the applied preload torque as a residual torsional stress. From Table I-9.1 for Figure 1-9.4 of the ASME Code for ASTM A564, Type 630, Condition H1100 bolting material, the allowable number of cycles for a corresponding alternating stress of one-half the value of S_{\max} above ($92,512/2 = 46,256$ psi) is over 5,000 cycles. Since closure bolts are tightened once per service cycle, and there are 1,300 service cycles as determined above, fatigue of closure bolts is not of concern.

2.1.2.2.2.2 Normal Vibration Over the Road

Fatigue associated with normal vibration over the road is addressed in Section 2.6.5, *Vibration*.

2.1.2.2.2.3 Extreme Total Stress Intensity Range

Per paragraph C.7 of Regulatory Guide 7.6:

The extreme total stress intensity range (including stress concentrations) between the initial state, the fabrication state, the normal operating conditions, and the accident conditions should be less than twice the adjusted value (adjusted to account for modulus of elasticity at the highest temperature) of S_a at 10 cycles given by the appropriate design fatigue curves.

Since the response of the MFFP to accident conditions is typically evaluated empirically rather than analytically, the extreme total stress intensity range has not been quantified. However, the full-scale certification test unit (see Appendix 2.12.3, *Certification Test Results*) was tested at relatively low ambient temperatures during free drop and puncture testing. The CTU was also fabricated in accordance with the drawings in Appendix 1.4.2, *Packaging General Arrangement Drawings*, thus incurring prototypic fabrication induced stresses, increased internal pressure greater than 150% of MNOP during fabrication pressure testing, and reduced internal pressure (i.e., a full vacuum during leak testing) conditions as part of initial acceptance. Exposure to these extreme conditions, while demonstrating leaktight containment resulting from certification testing satisfy the intent of the previously defined extreme total stress intensity range requirement.

2.1.2.2.3 Buckling Assessment

Buckling, per Regulatory Guide 7.6, is an unacceptable failure mode for the containment vessels. The intent of this provision is to preclude large deformations that would compromise the validity of linear analysis assumptions and quasi-linear allowable stress, as given in Paragraph C.6 of Regulatory Guide 7.6.

Buckling prevention criteria are applicable to the containment boundary of the MFFP. The containment vessel incorporates a cylindrical shell with essentially flat heads at each end. The

methodology of ASME B&PV Code Case N-284-1⁹ is applied to the cylindrical body section. Buckling analysis details are provided in Section 2.6.4, *Increased External Pressure*, and Section 2.7.7, *Deep Water Immersion Test (for Type B Packages Containing More than 10⁵ A₂)*.

Consistent with Regulatory Guide 7.6 philosophy, factors of safety corresponding to ASME Boiler and Pressure Vessel Code, Level A and Level D service conditions are employed. For NCT (Service Level A) and HAC (Service Level D), the factors of safety are 2.00 and 1.34, respectively.

It is also noted that 30 foot drop tests performed on a full-scale model with the package in various orientations produced no evidence of buckling of the containment boundary shell (see Appendix 2.12.3, *Certification Test Results*). Certification testing does not provide a specific determination of the margin of safety against buckling, but is considered as evidence that buckling will not occur.

2.1.3 Weights and Center of Gravity

The maximum gross weight of the MFFP, including a maximum payload weight of 4,740 pounds, is 14,260 pounds. The longitudinal center of gravity (CG) of the package is located 103.7 inches from the end of the bottom end impact limiter. A detailed breakdown of the MFFP component weights and CG is summarized in Table 2.1-3.

Note that the location of the CG (103.7 inches from the datum in the fully loaded transport configuration) is only $(103.7 - 201.33/2) = 3.0$ inches from the geometric center of the package, where 201.33 inches is the overall length of the package. Since this distance is small, the difference between the location of the geometric center and the CG may be neglected.

⁹ American Society of Mechanical Engineers (ASME) Boiler and Pressure Vessel Code, Section III, *Rules for Construction of Nuclear Power Plant Components*, Division 1, Class MC, Code Case N-284-1, *Metal Containment Shell Buckling Design Methods*, 2001 Edition, 2002 and 2003 Addenda.

Table 2.1-1 – Containment Structure Allowable Stress Limit Criteria

Stress Category	NCT	HAC
General Primary Membrane Stress Intensity	S _m	Lesser of: 2.4S _m 0.7S _u
Local Primary Membrane Stress Intensity	1.5S _m	Lesser of: 3.6S _m S _u
Primary Membrane + Bending Stress Intensity	1.5S _m	Lesser of: 3.6S _m S _u
Range of Primary + Secondary Stress Intensity	3.0S _m	Not Applicable
Pure Shear	0.6S _m	Not Applicable
Peak	Per Section 2.1.2.2.2, <i>Fatigue Assessment</i>	
Buckling	Per Section 2.1.2.2.3, <i>Buckling Assessment</i>	
Fastener Allowable Stress Limits ^{①②}		
Average Tensile Stress	S _m	Lesser of: S _y 0.7S _u
Average Shear Stress	0.6S _m	Lesser of: 0.6S _y 0.42S _u
Average Tensile + Average Shear	R _t ² + R _s ² < 1	R _t ² + R _s ² < 1
Average Tensile + Average Shear + Bending + Residual Torsion Stress Intensity	1.50S _m for S _u <100,000 psi	N/A
	1.35S _m for S _u >100,000 psi	N/A

Notes:

- ① Containment fastener stress limits are in accordance with NUREG/CR-6007.
- ② S_m is defined as $(2/3)S_y$ as recommended by NUREG/CR-6007.

Table 2.1-2 – Criticality Control Structure Allowable Stress Limit Criteria

Stress Category	NCT	HAC	
		Elastic Analyses ^①	Plastic Analyses ^②
General Primary Membrane Stress Intensity	S_m	Lesser of: $2.4S_m$ $0.7S_u$	Greater of: $0.7S_u$ $S_y + 1/3(S_u - S_y)$
Local Primary Membrane Stress Intensity	$1.5S_m$	Lesser of: $3.6S_m$ S_u	$0.9S_u$
Primary Membrane + Bending Stress Intensity	$1.5S_m$	Lesser of: $3.6S_m$ S_u	$0.9S_u$
Range of Primary + Secondary Stress Intensity	$3.0S_m$	Not Applicable	Not Applicable
Pure Shear Stress	$0.6S_m$	$0.42S_u$	$0.42S_u$
Fatigue	S_a	Not Applicable	Not Applicable

Notes:

- ① Elastic Analysis: ASME B&PV Code, Section III, Appendix F, F-1331.
- ② Plastic Analysis: ASME B&PV Code, Section III, Appendix F, F-1341.2.

Table 2.1-3 – MFFP Weight and Center of Gravity

Item	Weight, pounds		CG Location, inches ^①	
	Component	Assembly	Component	Assembly
Body, Closure Lid/Bolts	3,900		109.6	
Strongback ^②	3,030		98.0	
Lid End Impact Limiter	1,490		181.7	
Bottom End Impact Limiter	1,100		19.4	
<i>Total Empty Package</i>		<i>9,520</i>		<i>106.8</i>
Payload (3 FA's)	4,740		97.4	
<i>Total Loaded Package (Maximum)</i>		<i>14,260</i>		<i>103.7</i>

Notes:

- ① The reference datum is the outer end surface of the bottom impact limiter. The CG radial location is located along the package longitudinal axis.
- ② The strongback weight includes 160 pounds for the neutron poison plates.

2.2 Materials

2.2.1 Material Properties and Specifications

Mechanical properties of the structural materials utilized for the MFFP are presented in Table 2.2-1 through Table 2.2-8. Temperature dependent material properties for metallic components are obtained primarily from Section II, Part D, of the ASME B&PV Code¹⁰. High temperature dependent material properties for Type XM-19 and Type 304 materials are obtained from steel manufacturer's data bulletins and ASME B&PV Code, Section III, Subsection NH¹¹, respectively. Material properties are linearly interpolated or extrapolated from these tables as necessary. The body components and closure lid are fabricated from Type XM-19 stainless steel. The closure lid bolts are made from ASTM A564, Grade 630, Condition H1100 stainless steel. The strongback components are primarily fabricated from Type 304 and XM-19 stainless steel. The fasteners used on the strongback are ASTM A574 (alloy steel socket head cap screws) or F835 (alloy steel flat head cap screws). The impact limiter attachment bolts are fabricated from ASTM A320, Grade L43 bolting material. The central trunnion at the bottom of the package is fabricated from ASTM A479, UNS S21800. Threaded inserts used with the closure lid bolts are fabricated from austenitic stainless steel.

The impact limiter shells are fabricated from Type 304 stainless steel. The primary energy absorbing material is closed-cell polyurethane foam. The polyurethane foam is cast in-place in the impact limiter shells. The polyurethane foam for the top impact limiter has a nominal density of 10 lb_m/ft³ and the bottom impact limiter has a nominal density of 11½ lb_m/ft³. The data summarized in Table 2.2-7 and Table 2.2-8 are established in accordance with the acceptance testing requirements outlined in Section 8.1.5.1, *Polyurethane Foam*.

Several non-structural materials are used in the MFFP. The vent, fill, and test port plugs are fabricated from ASTM B16, 360 alloy, half-hard brass, and are sealed with butyl rubber stat-o-seals. The plugs are protected by brass covers, which may optionally be sealed with Teflon[®] gaskets. The containment (middle), inner, and outer closure lid O-ring seals are fabricated from butyl rubber. The washers used beneath the closure lid bolts are fabricated from hardened alloy steel. The neutron absorbing material used on the strongback is a boron/aluminum matrix. Contact between the strongback and fuel assemblies is made through pads made of neoprene elastomer. Anti-friction wear pads made from Delrin[®] are used on the strongback top and bottom end plates.

The density of stainless steel and carbon steel is taken as 0.290 lb_m/in³ and 0.283 lb_m/in³, respectively¹². Poisson's Ratio is taken as 0.3 for both steel types.

¹⁰ American Society of Mechanical Engineers (ASME) Boiler and Pressure Vessel Code, Section II, *Materials*, Part D, *Properties*, 2001 Edition, 2002 and 2003 Addenda.

¹¹ American Society of Mechanical Engineers (ASME) Boiler and Pressure Vessel Code, Section III, *Rules for Construction of Nuclear Power Plant Components*, 2001 Edition, 2002 and 2003 Addenda.

¹² Baumeister, et al, *Mark's Standard Handbook for Mechanical Engineers*, Ninth Edition, McGraw Hill Book Company, 1987

2.2.2 Chemical and Galvanic Reactions

The major materials of construction of the MFFP (i.e., stainless steel, polyurethane foam, butyl rubber, aluminum clad poison, brass, and alloy steel fasteners) will not have significant chemical, galvanic, or other reactions in air, inert gas, or water environments. These materials have been previously used, without incident, in radioactive materials (RAM) packagings for the transport of fresh fuel assemblies. Thus, significant chemical, galvanic, or other reactions will not occur, and the requirements of 10 CFR §71.43(d) are met.

2.2.3 Effects of Radiation on Material

The structural materials of construction of the MFFP are not significantly affected by radiation. These materials have been previously used, without incident, in radioactive materials (RAM) packagings for the transport of fresh fuel assemblies. Thus, significant radiation effects will not occur, and the requirements of 10 CFR §71.43(d) are met.

Table 2.2-1 – Type XM-19 Stainless Steel Material Properties^⑥

Material Specification	Temperature, °F	Yield Strength ^{①⑦} (S _y), psi	Ultimate Strength ^{②⑦} (S _u), psi	Design Stress Intensity ^③ (S _m), psi	Elastic Modulus ^④ , ×10 ⁶ psi	Coefficient of Thermal Expansion ^⑤ , 10 ⁻⁶ in/in/°F
SA-240/A240, SA-479/A479, Type XM-19 UNS S20910 SA-182/A182, SA-336/A336, Grade FXM-19 UNS S20910	-40	55,000	100,000	33,300	28.9	7.8
	-20	55,000	100,000	33,300	28.8	7.8
	70	55,000	100,000	33,300	28.3	8.2
	100	55,000	100,000	33,300	28.1	8.2
	200	47,100	99,400	33,100	27.6	8.5
	300	43,300	94,200	31,400	27.0	8.7
	400	40,700	91,100	30,400	26.5	8.9
	500	38,800	89,100	29,700	25.8	9.1
	600	37,400	87,700	29,200	25.3	9.2
	700	36,300	86,400	28,800	24.8	9.3
	800	35,300	84,800	28,300	24.1	9.4
	900	34,500	82,600	--	23.5	9.5
	1,000	33,700	79,700	--	22.8	9.6
	1,200	<i>31,000</i>	<i>74,000</i>	--	22.0	9.8
	1,350	<i>31,000</i>	<i>66,000</i>	--	19.75	10.0
	1,500	<i>30,000</i>	<i>52,000</i>	--	18.1	10.2

Notes:

- ① ASME B&PV Code, Section II, Part D, Table Y-1.
- ② ASME B&PV Code, Section II, Part D, Table U.
- ③ ASME B&PV Code, Section II, Part D, Table 2A.
- ④ ASME B&PV Code, Section II, Part D, Table TM-1, Material Group G (22Cr-13Ni-5Mn).
- ⑤ ASME B&PV Code, Section II, Part D, Table TE-1, Material Group 4 (22Cr-13Ni-5Mn), Coefficient B (mean from 70 °F).
- ⑥ When necessary, values are linearly interpolated or extrapolated and given in **bold** text.
- ⑦ Yield and ultimate strength values for temperatures of 1,200 °F to 1,500 °F are shown in *italic* text and are extracted from High Performance Alloys *HPA Nitronic[®] 50 Product Bulletin*.

Table 2.2-2 – Type 304 Stainless Steel Material Properties^⑥

Material Specification	Temperature, °F	Yield Strength ^{①⑦} (S _y), psi	Ultimate Strength ^② (S _u), psi	Design Stress Intensity ^③ (S _m), psi	Elastic Modulus ^④ , ×10 ⁶ psi	Coefficient of Thermal Expansion ^⑤ , 10 ⁻⁶ in/in/°F
ASTM A182 ASTM A213 ASTM A240 ASTM A249 ASTM A276 ASTM A312 ASTM A479 Type 304	-40	30,000	75,000	20,000	28.9	8.2
	-20	30,000	75,000	20,000	28.8	8.2
	70	30,000	75,000	20,000	28.3	8.5
	100	30,000	75,000	20,000	28.1	8.6
	200	25,000	71,000	20,000	27.6	8.9
	300	22,400	66,200	20,000	27.0	9.2
	400	20,700	64,000	18,600	26.5	9.5
	500	19,400	63,400	17,500	25.8	9.7
	600	18,400	63,400	16,600	25.3	9.8
	700	17,600	63,400	15,800	24.8	10.0
	800	16,900	62,800	--	24.1	--
	900	16,200	60,800	--	23.5	--
	1,000	15,500	57,400	--	22.8	--
	1,200	<i>14,100</i>	--	--	22.0	--
	1,300	<i>13,200</i>	--	--	20.3	--
	1,400	<i>11,600</i>	--	--	19.2	--
	1,500	<i>9,500</i>	--	--	18.1	--

Notes:

- ① ASME B&PV Code, Section II, Part D, Table Y-1.
- ② ASME B&PV Code, Section II, Part D, Table U.
- ③ ASME B&PV Code, Section II, Part D, Table 2A.
- ④ ASME B&PV Code, Section II, Part D, Table TM-1, Material Group G (18Cr-8Ni).
- ⑤ ASME B&PV Code, Section II, Part D, Table TE-1, Material Group 3 (18Cr-8Ni), Coefficient B (mean from 70 °F).
- ⑥ When necessary, values are linearly interpolated or extrapolated and given in **bold** text.
- ⑦ Yield strength values for temperatures of 1,200 °F to 1,500 °F are shown in *italic* text and are taken from ASME B&PV Code, Section III, Subsection NH, Appendix I, Table I-14.5.

Table 2.2-3 – Alloy UNS S21800 Stainless Steel Material Properties

Material Specification	Temperature, °F	Yield Strength^① (S_y), psi	Ultimate Strength^① (S_u), psi	Elastic Modulus^②, ×10⁶ psi
ASTM A479, UNS S21800	70 to 100	50,000	95,000	28.2

Notes:

- ① ASTM A479, Table 2, *Standard Specification for Stainless Steel Bars and Shapes for Use in Boilers and Other Pressure Vessels*.
- ② ASME B&PV Code, Section II, Part D, Table TM-1, Material Group G (18Cr-8Ni).

Table 2.2-4 – ASTM A574 Alloy Bolting Material Properties^⑥

Material Specification	Temperature, °F	Yield Strength ^① (S _y), psi	Ultimate Strength ^② (S _u), psi	Maximum Allowable Stress ^③ (S), psi	Elastic Modulus ^④ , ×10 ⁶ psi	Coefficient of Thermal Expansion ^⑤ , 10 ⁻⁶ in/in/°F
ASTM A574 Grade 4037, or 4042, or 4140 (Size ≥ 5/8 in)	-40	135,000	170,000	33,800	29.7	6.0
	-20	135,000	170,000	33,800	29.6	6.1
	70	135,000	170,000	33,800	29.2	6.4
	100	135,000	170,000	33,800	29.0	6.5
	200	126,900	170,000	33,800	28.5	6.7
	300	121,700	170,000	33,800	28.0	6.9
	400	117,600	170,000	33,800	27.4	7.1
	500	114,000	170,000	33,800	27.0	7.3
	600	110,400	170,000	...	26.4	7.4
	700	106,200	170,000	...	25.3	7.6
ASTM A574 Grade 4037, or 4042 (Size ≤ 1/2 in)	-40	140,000	180,000	35,000	29.7	6.0
	-20	140,000	180,000	35,000	29.6	6.1
	70	140,000	180,000	35,000	29.2	6.4
	100	140,000	180,000	35,000	29.0	6.5
	200	131,600	180,000	35,000	28.5	6.7
	300	126,200	180,000	35,000	28.0	6.9
	400	121,900	180,000	35,000	27.4	7.1
	500	118,200	180,000	35,000	27.0	7.3
	600	114,500	180,000	...	26.4	7.4
	700	110,100	180,000	...	25.3	7.6

Notes:

- ① ASME B&PV Code, Section II, Part D, Table Y-1.
- ② ASME B&PV Code, Section II, Part D, Table U.
- ③ ASME B&PV Code, Section II, Part D, Table 3.
- ④ ASME B&PV Code, Section II, Part D, Table TM-1, Material Group A (C-1/4Mo).
- ⑤ ASME B&PV Code, Section II, Part D, Table TE-1, Material Group A (C-1/4Mo), Coefficient B (mean from 70 °F).
- ⑥ When necessary, values are linearly interpolated or extrapolated and given in **bold** text.

Table 2.2-5 – ASTM A564, Grade 630, Condition H1100, Bolting Material Properties^⑥

Material Specification	Temperature, °F	Yield Strength ^① (S _y), psi	Ultimate Strength ^② (S _u), psi	Design Stress Intensity ^③ (S _m), psi	Elastic Modulus ^④ , ×10 ⁶ psi	Coefficient of Thermal Expansion ^⑤ , 10 ⁻⁶ in/in/°F
ASTM A564 Grade 630 Condition- H1100 UNS S17400	-40	115,000	140,000	76,667	29.8	5.0
	-20	115,000	140,000	76,667	29.7	5.0
	70	115,000	140,000	76,667	29.2	5.3
	100	115,000	140,000	76,667	29.0	5.4
	200	106,300	140,000	70,867	28.5	5.5
	300	101,800	140,000	67,867	27.9	5.7
	400	98,300	136,100	65,533	27.3	5.8
	500	95,200	133,400	63,467	26.7	5.9
	600	92,700	131,400	61,800	26.1	6.0
	700	90,300	128,400	...	25.6	6.1

Notes:

- ① ASME B&PV Code, Section II, Part D, Table Y-1.
- ② ASME B&PV Code, Section II, Part D, Table U.
- ③ S_m is defined as (2/3)S_y as recommended by NUREG/CR-6007.
- ④ ASME B&PV Code, Section II, Part D, Table TM-1, Material Group F (17Cr-4Ni-4Cu).
- ⑤ ASME B&PV Code, Section II, Part D, Table TE-1, for 15Cr and 17Cr steels, Coefficient B (mean from 70 °F).
- ⑥ When necessary, values are linearly interpolated or extrapolated and given in **bold** text.

Table 2.2-6 – A320, Grade L43 Alloy Bolting Material Properties[®]

Material Specification	Temperature, °F	Yield Strength ^① (S _y), psi	Ultimate Strength ^② (S _u), psi	Design Stress Intensity ^③ (S _m), psi	Elastic Modulus ^④ , ×10 ⁶ psi	Coefficient of Thermal Expansion ^⑤ , 10 ⁻⁶ in/in/°F
ASTM A320 Grade L43	-40	105,000	125,000	35,000	28.3	6.0
	-20	105,000	125,000	35,000	28.2	6.1
	70	105,000	125,000	35,000	27.8	6.4
	100	105,000	125,000	35,000	27.6	6.5
	200	99,000	125,000	33,000	27.1	6.7

Notes:

- ① ASME B&PV Code, Section II, Part D, Table Y-3.
- ② According to ASME B&PV Code, Section III, Code Case N-249, Table 5, for Specification No. SA-354, Grade BC, for AISI 4340 bolting material, the material composition of ASTM A320, Grade L43, the ultimate tensile strength value S_u is constant versus temperature.
- ③ ASME B&PV Code, Section II, Part D, Table 4.
- ④ ASME B&PV Code, Section II, Part D, Table TM-1, Material Group B (1 $\frac{3}{4}$ Ni- $\frac{3}{4}$ Cr- $\frac{1}{4}$ Mo).
- ⑤ ASME B&PV Code, Section II, Part D, Table TE-1, Material Group 1 (1 $\frac{3}{4}$ Ni- $\frac{3}{4}$ Cr- $\frac{1}{4}$ Mo), Coefficient B (mean from 70 °F).
- ⑥ When necessary, values are linearly interpolated and given in **bold** text.

Table 2.2-7 – Nominal Material Properties of 11½ pcf Polyurethane Foam

Property	Direction	Room Temperature Value
Compressive Strength, S	Axial (Parallel-to-Rise)	470 psi @ 10% Strain 555 psi @ 40% Strain 1,660 psi @ 70% Strain
	Radial (Perpendicular-to-Rise)	435 psi @ 10% Strain 540 psi @ 40% Strain 1,725 psi @ 70% Strain

Table 2.2-8 – Nominal Material Properties of 10 pcf Polyurethane Foam

Property	Direction	Room Temperature Value
Compressive Strength, S	Axial (Parallel-to-Rise)	358 psi @ 10% Strain 416 psi @ 40% Strain 1,124 psi @ 70% Strain
	Radial (Perpendicular-to-Rise)	330 psi @ 10% Strain 398 psi @ 40% Strain 1,115 psi @ 70% Strain

Note for Table 2.2-7 & Table 2.2-8:

The foam is installed so that it rises parallel to the axis of revolution of the impact limiter.

2.3 Fabrication and Examination

2.3.1 Fabrication

The fabrication requirements for the MFFP are detailed on the drawings in Appendix 1.4.2, *Packaging General Arrangement Drawings*. All material acceptance tests required prior to installation or use are specified in Chapter 8.0, *Acceptance Tests and Maintenance Program*.

2.3.2 Examination

The examination requirements for the MFFP are detailed on the drawings in Appendix 1.4.2, *Packaging General Arrangement Drawings*. All material acceptance tests required prior to installation or use are specified in Chapter 8.0, *Acceptance Tests and Maintenance Program*.

This page left intentionally blank.

2.4 Lifting and Tie-down Standards for All Packages

For analysis of the lifting and tie-down components of the MFFP, material properties from Section 2.2.1, *Mechanical Properties and Specifications*, are taken at a bounding temperature of 160 °F per Section 2.6.1.1, *Summary of Pressures and Temperatures*. The primary structural material is XM-19 stainless steel.

A loaded MFFP is secured to the transport skid with formed steel straps. Longitudinal forces are reacted against the impact limiter doubler plates made from XM-19 stainless steel. Properties of XM-19 stainless steel at 160 °F are summarized below.

Material Property	Value	Reference
Elastic Modulus, E	27.8×10^6 psi	Table 2.2-1
Ultimate Strength, σ_u	99,640 psi	
Yield Strength, σ_y	50,260 psi	
Shear Strength, equal to $(0.6)S_m$	19,908 psi	

2.4.1 Lifting Devices

During operations, the MFFP is normally handled by the shipping skid. If the package is lifted off of the skid, or if the package and skid are lifted together, it will be performed with lifting slings that are positioned around the package body. For this reason, there are no lifting devices which are a structural part of the package. Therefore, per 10 CFR §71.45(b)(1), no analysis of lifting devices is required.

2.4.2 Tie-down Devices

During transport, the MFFP is secured to a shipping skid, as shown in Figure 2.4-1. The package is held in two cradles situated near each impact limiter. The package is retained in the cradles by means of two steel straps that pass over the top of the package. Together, the straps and the cradles retain the package in the vertical and lateral directions, without the aid of any tie-down devices that are a structural part of the package. Axially, the longitudinal tie-down loads are carried between the shipping skid cradle and the package body by means of the impact limiter attachment lug doubler plates that encircle the body shell. There are two doubler plates, one bearing against the forward cradle, and one bearing against the rear cradle. Note, that the entire axial load is carried by one doubler plate. Since the doubler plates are structurally attached to the package, they must be analyzed according to 10 CFR §71.45(b).

2.4.2.1 Doubler Plate Weld Stress

Each doubler plate is 1/2-inch thick and 5 inches wide. The shipping skid cradle extends 108° ($\theta = 1.88$ radians) about the lower surface of the package, which has a radius of $r = (1/2)(29.63) = 14.82$ inches, where 29.63 inches is the outer diameter of the package body. The length of contact between the cradle and the doubler plate is then:

$$s = r \theta = 27.86 \text{ inches}$$

The doubler plate is attached to the package with a 1/4-inch groove weld along the side that contacts the skid cradle, and a 1/4-inch fillet weld on the opposite side. The welds are continuous, but conservatively considering only the length in contact with the cradle, the length of both welds is $L_g = L_f = 27.86$ inches. For the 45 degree, 1/4-inch groove weld, the unit weld area, $A_g = 0.25 \text{ in}^2/\text{in}$. The unit area of the fillet weld $A_f = 0.25 \times 0.707 = 0.177 \text{ in}^2/\text{in}$. Therefore, the total weld area, A_t , is:

$$A_t = L_f A_f + L_g A_g = 11.90 \text{ in}^2$$

The gross weight of the MFFP is 14,260 pounds. The required applied loading in the axial direction, per 10 CFR §71.45(b), is 10g, which loads the doubler plate welds in shear. Therefore, the shear stress in the welds, τ_{weld} , is:

$$\tau_{\text{weld}} = \frac{14,260(10)}{A_t} = 11,983 \text{ psi}$$

The allowable shear stress for XM-19, which applies to the weld material, is 19,908 psi. The margin of safety (MS) for pure shear stress in the welds is:

$$MS = \frac{19,908}{11,983} - 1.0 = +0.66$$

2.4.2.2 Doubler Plate Bearing Stress

The contact area between the skid cradle and the doubler plate is shown in Figure 2.4-2. A nominally 1/8-inch thick rubber pad is located inside the cradle, and thus, contact between the cradle and the doubler plate begins at a radius of $r_i = r + 0.13 = 14.95$ inches, and ends at the outside radius of the doubler plate, $r_o = r + 0.50 = 15.32$ inches. Circumferentially, the cradle covers an arc of 1.88 radians as shown above. Therefore, the contact area, A_c , is:

$$A_c = \left(\frac{1.88}{2\pi} \right) \pi (r_o^2 - r_i^2) = 10.53 \text{ in}^2$$

The contact stress, σ_c , is:

$$\sigma_c = \frac{14,260(10)}{10.53} = 13,542 \text{ psi}$$

The allowable yield stress is 50,260 psi. The margin of safety is:

$$MS = \frac{50,260}{13,542} - 1.0 = +2.71$$

2.4.2.3 Tie-down Device Overload Condition

In accordance with the requirements of 10 CFR §71.45(b)(3), tie-down devices must be designed so that failure of any tie-down device under excessive load will not impair the ability of the package to meet other requirements. Since the doubler plate is welded to the body shell, it must fail before damage to the shell occurs.

The load applied to the doubler plate is transferred to the package shell as a surface traction, since the doubler plate is relatively thin and the axial load is located very near to the surface of the shell. The load is transferred into the shell by compression, tension, and shear loads, applied along the sides of the doubler plate. However, it may be assumed that the entire load is transferred into the shell by only the tension and compression loads, evenly distributed along the two circumferential edges of the doubler plate. The cross-sectional area of the shell, A_{shell} , along the 1.88 radian arc segment is:

$$A_s = \left(\frac{1.88}{2\pi} \right) \frac{\pi}{4} (d_o^2 - d_i^2) = \left(\frac{1.88}{2\pi} \right) \frac{\pi}{4} (29.63^2 - 28.50^2) = 15.44 \text{ in}^2$$

where the package shell outer diameter, $d_o = 29.63$ inches, and the shell inner diameter, $d_i = 28.50$ inches. For a yield stress of 50,260 psi, the minimum yield load of the shell is equal to:

$$F_y = 2A_s(50,260) = 1,552,029 \text{ pounds}$$

where twice the cross-sectional area is used to account for both the tension and compression sides of the load into the shell. The maximum load that can be developed by the doubler plate welds, F_w , can be estimated by using the ultimate strength, or 99,640 psi for XM-19 steel, or:

$$F_w = A_t(99,640) = (11.90)(99,640) = 1,185,716 \text{ pounds}$$

Note that this value very conservatively overestimates the weld strength by neglecting the shear reduction factor of 0.6. Therefore, since the maximum load (conservatively overestimated) that can be developed by the weld is less than the minimum yield load of the shell (conservatively underestimated), the weld will fail prior to any permanent deformation of the package shell.

Another method of determining the ability of the package to withstand excessive tie-down loads is to consider the bearing of the cradle against the doubler plate. Because of the pad between the shell wall and the cradle, the bearing surface includes only the upper 3/8 inches of the doubler plate. Shear stresses are maximum along a 45° shear plane, as shown in Figure 2.4-2. The shear area, where $r_o = 15.32$ inches is the outer diameter of the doubler plate, is:

$$A_s = 1.414(0.375) \left(\frac{1.88}{2\pi} \right) (2(15.32)\pi) = 15.27 \text{ in}^2$$

The maximum force that can be resisted by the shear area for 99,640 psi ultimate strength of the XM-19 steel is:

$$F_s = 0.6A_s(99,640) = 912,902 \text{ pounds}$$

This value is less than calculated above for either the shell or weld limits affording another layer of assurance that the shell will not be damaged.

2.4.2.4 Summary

All margins of safety for the tie-down loads are positive. The minimum margin of safety, $MS = +0.66$, is for shear weld failure of the doubler plate, indicating that this item will be the mode of failure for tie-down devices under excessive load condition. This failure mode does not compromise the performance capabilities of the MFFP since no main structural part of the package is affected. Thus, the requirements of 10 CFR §71.45(b) are met.

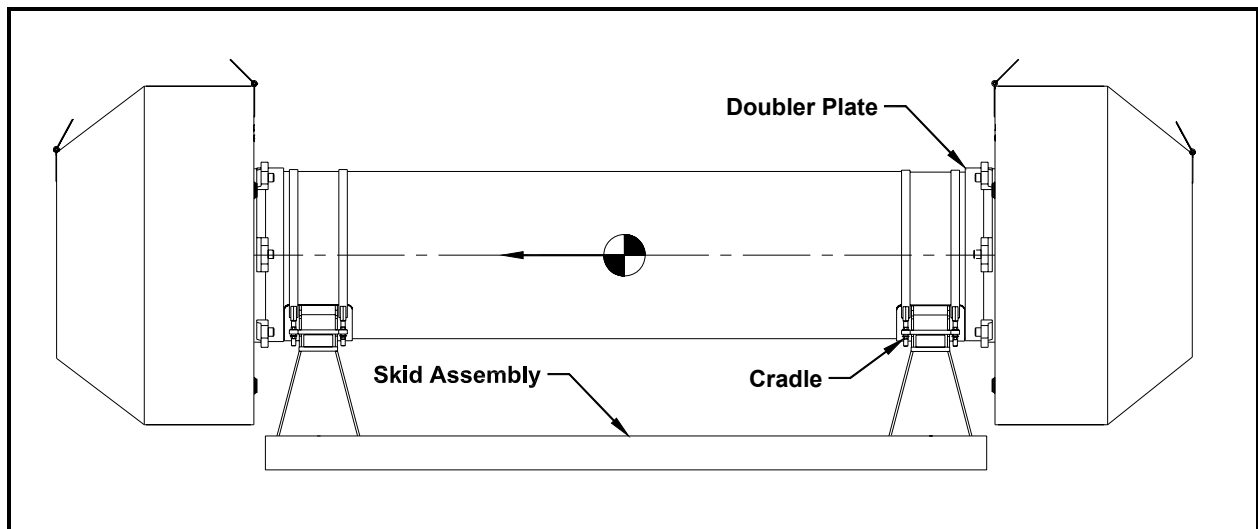


Figure 2.4-1 – MFFP and Shipping Skid

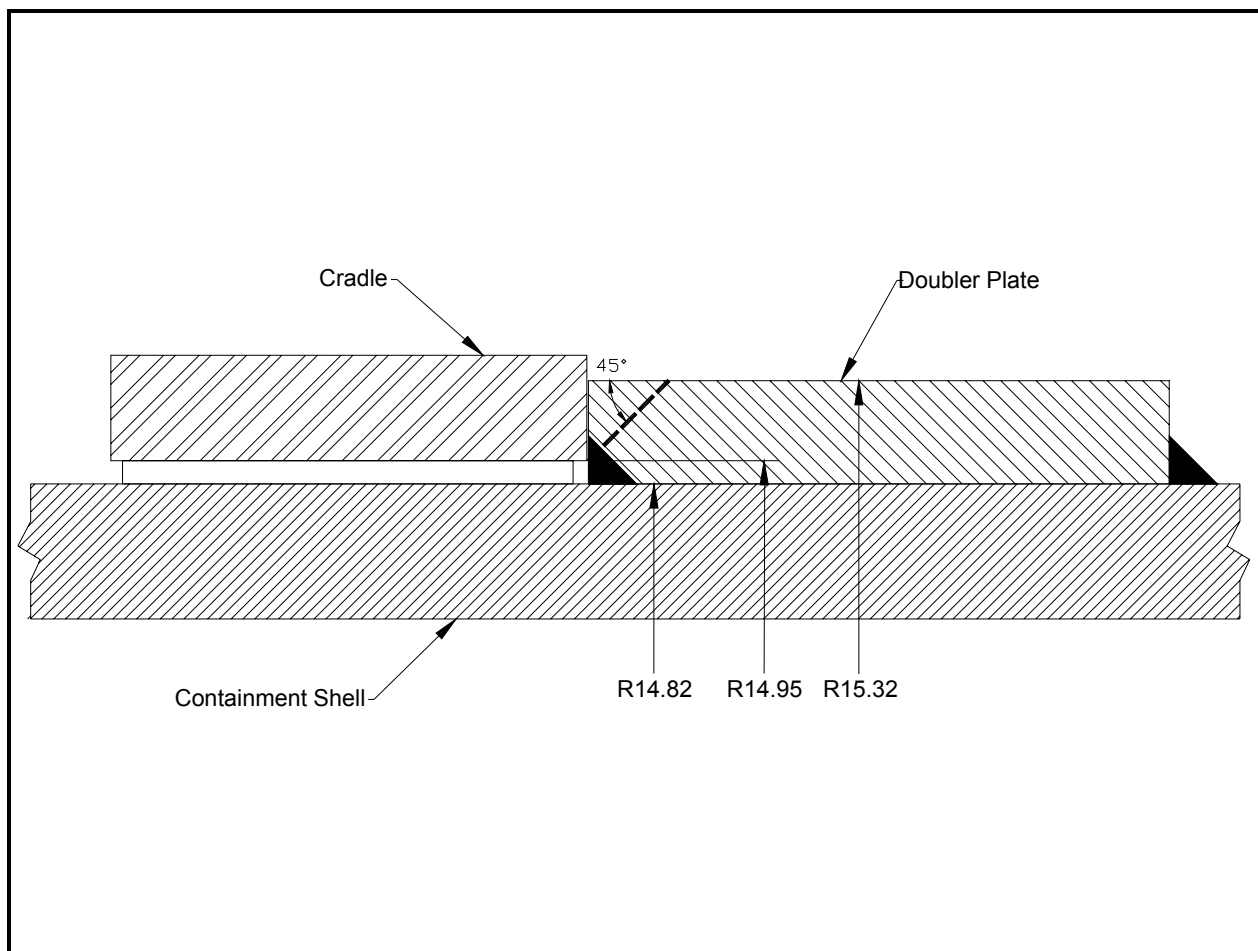


Figure 2.4-2 – Skid Cradle and Doubler Plate Details

2.5 General Considerations

2.5.1 Evaluation by Test

Full-scale certification tests were performed on the MFFP as the primary demonstration of performance for HAC free drop and puncture drop tests. In order to conclusively and conservatively address package performance capabilities, the certification test unit (CTU) was subjected to multiple free and puncture drop tests. The basis for the certification tests performed is provided in Appendix 2.12.2, *Certification Test Plan*. A summary of the tests performed is provided in Table 2.5-1, which also contains the primary performance aspect of the MFFP being addressed in each test. Details of the tests, including results, are provided in Appendix 2.12.3, *Certification Test Results*.

2.5.2 Evaluation by Analysis

Analytical evaluations are provided within this SAR as the primary demonstration of the MFFP performance for NCT and for structural HAC that are not demonstrated by test (such as immersion), and HAC thermal. The fuel control structure (FCS) assembly was added to the strongback design following the certification testing. Section 2.7.1.2, *Summary of Results from the Free Drop Testing*, discusses the functional purpose of the FCS. Appendix 2.12.5, *Fuel Control Structure Evaluation*, presents a detailed structural evaluation of the FCS and its effects on the strongback. Analytic demonstration techniques, where used, comply with the design criteria described in Section 2.1.2, *Design Criteria*. A summary of the analyses performed is given in Table 2.5-2.

Table 2.5-1 – Certification Test Series Summary

No.	Test Description	Addresses
Series No. 1		
1	Horizontal 30-ft free drop	Containment shell buckling
2	Puncture drop axial to limiter	Impact limiter retention. Corner weld attack.
3	Oblique puncture drop on tapered skin	Perforation of lid end impact limiter skin
4	Oblique puncture drop on bottom disk	Perforation of lid end impact limiter skin
Series No. 2		
1	C.G.-over-corner (near-vertical) 30-ft free drop	Closure lid and prototypic FA integrity
2	C.G.-over-corner puncture on free drop damage	Effect of puncture on prior damage; puncture load on closure region
Series No. 3		
1	15° Slapdown 30-ft free drop, lid primary	Strongback deformations
2	15° Slapdown 30-ft free drop, lid secondary	Strongback deformations, closure lid integrity
3	Horizontal puncture drop on containment shell	Containment shell leaktight integrity
4	Oblique puncture drop on containment shell	Containment shell leaktight integrity
Series No. 4 (duplicate of Series No. 2, Test No. 1)		
1	C.G.-over-corner (near-vertical) 30-ft free drop	Gather detailed impact information

Table 2.5-2 – Summary of Analyses

Analysis Condition	Refer to Section
All NCT	2.6, <i>Normal Conditions of Transport</i>
HAC Thermal	2.7.4, <i>Thermal</i>
HAC Immersion	2.7.5, <i>Immersion – Fissile Material</i> 2.7.6, <i>Immersion – All Packages</i> 2.7.7, <i>Deep Water Immersion (for Type B Packages Containing More than 10⁵ A₂)</i>
Warm Ambient Effect on Impact Limiters	2.12.1, <i>Impact Limiter Evaluation</i>
HAC Free Drop (effect of FCS)	2.12.5, <i>Fuel Control Structure Evaluation</i>

2.6 Normal Conditions of Transport

The MFFP, when subjected to the normal conditions of transport (NCT) specified in 10 CFR §71.71¹, is shown to meet the performance requirements specified in Subpart E of 10 CFR 71. As discussed in the introduction to this chapter, the primary proof of NCT performance is via analytic methods. Regulatory Guide 7.6² criteria are demonstrated as acceptable for all NCT analytic evaluations presented in this section. The load combinations used herein are consistent with Regulatory Guide 7.8³. Specific discussions regarding brittle fracture and fatigue are presented in Section 2.1.2.2, *Miscellaneous Structural Failure Modes*, and are shown not to be limiting cases for the MFFP design.

NCT analyses for heat, cold, reduced external pressure, increased external pressure, vibration, and free drop are performed in this section. Allowable stress limits are consistent with Table 2.1-1 and Table 2.1-2 in Section 2.1.2.1, *Analytic Design Criteria (Allowable Stresses)*, using temperature-adjusted material properties taken from the tables in Section 2.2.1, *Material Properties and Specifications*. The design temperatures bound the maximum NCT temperature for the components, as determined in Chapter 3.0, *Thermal Evaluation*. Parameters at the design temperatures are summarized in Table 2.6-1 for the appropriate materials.

2.6.1 Heat

The thermal evaluation for the normal heat condition is presented in Chapter 3.0, *Thermal Evaluation*. The NCT heat condition is evaluated by applying a 100 °F ambient temperature, maximum insolation, and maximum decay heat per Regulatory Guide 7.8 and 10 CFR §71.71(c)(1).

2.6.1.1 Summary of Pressures and Temperatures

The maximum temperatures for the 100 °F ambient NCT condition of the MFFP containment body and strongback are presented in Table 3.4-1 of Chapter 3.0, *Thermal Evaluation*. The resulting maximum temperature of the containment body and closure lid is 159 °F, located near the top of the containment body at the interface with the strongback top end plate. The region of peak temperature is relatively small; most of the containment shell has a temperature of approximately 150 °F. The closure lid and closure bolt maximum temperatures are both 147 °F. Conservatively, both the containment body and closure bolt design temperature is set at 160 °F. The maximum temperature of the strongback is 178 °F in the middle of each longitudinal weldment plate. Conservatively, the strongback design temperature is set at 180 °F.

The initial pressure in the package at assembly is ambient, i.e., 14.7 psia. As determined in Section 3.4.2, *Maximum Normal Operating Pressure*, the maximum normal operating pressure (MNOP) is conservatively defined to be 10 psig. The MFFP has a design pressure of 25 psig, which is significantly higher than the MNOP. The design temperatures and pressure discussed

¹ Title 10, Code of Federal Regulations, Part 71 (10 CFR 71), *Packaging and Transportation of Radioactive Material*, Final Rule, 01-26-04.

² U. S. Nuclear Regulatory Commission, Regulatory Guide 7.6, *Design Criteria for the Structural Analysis of Shipping Cask Containment Vessels*, Revision 1, March 1978.

³ U.S. Nuclear Regulatory Commission, Regulatory Guide 7.8, *Load Combinations for the Structural Analysis of Shipping Casks for Radioactive Material*, Revision 1, March 1989.

above are used in the analyses discussed in Sections 2.6.1.2, *Differential Thermal Expansion*, through 2.6.1.3, *Stress Calculations*.

2.6.1.2 Differential Thermal Expansion

The design temperature of the strongback, which is conservatively assumed to apply to the entire strongback, is $T_{SB} = 180$ °F. The thermal expansion coefficient of Type 304 stainless steel at this temperature is $\alpha_{SB} = 8.8 \times 10^{-6}$ in/in/°F from Table 2.6-1. Since the overall length of the strongback is $L_{SB} = 164.90$ inches, the thermal expansion of the strongback is:

$$\delta_{L-SB} = (\alpha_{SB})(T_{SB} - 70)(L_{SB}) = (8.8 \times 10^{-6})(180 - 70)(164.90) = 0.16 \text{ inches}$$

The package shell will also expand thermally. From Figure 3.4-2, the average shell temperature T_{SH} may be estimated as 154 °F. A conservative value of 150 °F may be used to bound this temperature. At a temperature of 150 °F, Table 2.2-1 gives the thermal expansion coefficient of XM-19 stainless steel as $\alpha_{SH} = 8.35 \times 10^{-6}$ in/in/°F. Therefore, the thermal expansion of the shell over the strongback length is:

$$\delta_{L-SH} = (\alpha_{SH})(T_{SH} - 70)(L_{SB}) = (8.35 \times 10^{-6})(150 - 70)(164.90) = 0.11 \text{ inches}$$

The top of the strongback plate is 0.4 inches from the closure lid, and the overall cavity length $L_{CAV} = 165.45$ inches with the lid installed. Therefore, the ambient temperature axial gap between the containment bottom plate and the strongback bottom plate is:

$$\text{gap}_{TROOM} = L_{CAV} - L_{SB} - 0.4 = 165.45 - 164.90 - 0.4 = 0.15 \text{ inches}$$

The room temperature axial gap, gap_{TROOM} , will decrease as a result of thermal expansion. This gap at hot NCT temperature is therefore:

$$\text{gap}_{HOT} = \text{gap}_{TROOM} - \delta_{L-SB} + \delta_{L-SH} = 0.15 - 0.16 + 0.11 = 0.10 \text{ inches}$$

Thus, because the hot NCT axial gap is greater than zero, axial clearance is maintained under NCT.

The design temperature of the strongback top end plate is $T_{TEP} = 180$ °F. The thermal expansion coefficient of Type 304 stainless steel at this temperature is $\alpha_{SB} = 8.8 \times 10^{-6}$ in/in/°F from Table 2.6-1. Since the diameter of the strongback top end plate is $D_{TEP} = 28.25$ inches, the thermal expansion of the strongback is:

$$\delta_{TEP} = (\alpha_{SB})(T_{TEP} - 70)(D_{TEP}) = (8.8 \times 10^{-6})(180 - 70)(28.25) = 0.027 \text{ inches}$$

The inner diameter of the containment body is $ID_{cb} = 28.50$ inches. The minimum room temperature diametrical gap between the inside cavity wall and the strongback top end plate is $ID_{cb} - D_{TEP} = 0.25$ inches. Thus, because the room temperature diametrical clearance is greater than the diametrical thermal expansion of the strongback, clearance is maintained under NCT.

The clearance at the bottom end plate, which has slightly more room temperature diametrical clearance than the top end plate, is bounded by the top end plate analysis. Similarly, the diameter of the support disks, composed of three clamp arms, is equal to 27.5 inches, which is a full inch smaller than the inner diameter of the body. Therefore, diametrical clearance at the support disks is not of concern.

2.6.1.3 Stress Calculations

2.6.1.3.1 Stresses Due to Pressure Loading

Shell stresses in the structural components of the MFFP due to the internal design pressure of 25 psig are calculated using classical shell methods. The hoop stress (σ_θ), axial stress (σ_ϕ), and radial stress (σ_r), are found from:

$$\begin{aligned}\sigma_\theta &= \frac{Pr}{t} & \sigma_\phi &= \frac{Pr}{2t} & \sigma_r &= -P \\ \sigma_\theta &= \frac{25(14.53)}{0.56} = 649 \text{ psi} & \sigma_\phi &= \frac{25(14.53)}{2(0.56)} = 324 \text{ psi} & \sigma_r &= -25 \text{ psi}\end{aligned}$$

where the design pressure, $P = 25$ psig, the shell mean radius, $r = 14.53$ inches, and the shell thickness, $t = 0.56$ inches. The shell mean radius is found simply by adding the inner radius of the containment shell and one-half of the shell thickness. The resulting stress intensity (SI) is equal to the difference between the maximum and minimum principal stresses, or:

$$SI = \sigma_\theta - \sigma_r = 649 - (-25) = 674 \text{ psi}$$

For the NCT design temperature of 160 °F, the allowable general primary membrane stress of Type XM-19 stainless steel is 33,180 psi. Therefore, the shell stress margin of safety (MS) is:

$$P_m : MS = \frac{33,180}{674} - 1.0 = +48.2$$

Stress analysis for the bottom end closure plate is performed using Table 24, Case 10a of Roark⁴. Considering the bottom end closure plate as a simply supported circular plate with uniform thickness, the maximum bending moment is located in the center of the plate and is found from:

$$M_{\text{center}} = \frac{qr^2(3+\nu)}{16} = \frac{25(14.53)^2(3+0.3)}{16} = 1,089 \text{ in} \cdot \text{lb/in}$$

Using Table 24, Case 10b of Roark and considering the bottom end closure plate as a fixed edge circular plate with uniform thickness, the maximum bending moment is located at the plate outer fixed edge and is found from:

$$M_{\text{edge}} = \frac{qr^2}{8} = \frac{25(14.53)^2}{8} = 660 \text{ in} \cdot \text{lb/in}$$

In both above cases, $q = 25$ psig is the design pressure, and $r = 14.53$ inches is conservatively taken as the diameter of the lid. Since $1,089 > 660$, the assumption of a simply supported edge governs. The maximum possible bending stress in the bottom closure plate, where $t_{bp} = 1.5$ inches, considering the maximum of the above calculated moments is found from:

$$\sigma = \frac{6M}{t_{bp}^2} = \frac{6(1,089)}{1.5^2} = 2,904 \text{ psi}$$

⁴ Young, Warren C., *Roark's Formulas for Stress & Strain, Sixth Edition*, McGraw-Hill, Inc, 1989.

For the NCT containment body design temperature of 160 °F, the allowable primary membrane-plus-bending stress of Type XM-19 stainless steel is 49,770 psi (see Table 2.6-1). The bottom closure plate stress margin of safety is:

$$MS_{P_m+P_b} = \frac{49,770}{2,904} - 1.0 = +16.1$$

Stress analysis for the closure lid inner plate is performed using Table 24, Case 27 of Roark. Considering the lid inner plate as a simply supported circular solid sector with uniform thickness, with uniformly distributed load, q , over the entire surface, the radial stress, σ_r , is found from:

$$\sigma_r = \beta \frac{qr^2}{t^2} = 0.102 \frac{25(14.5)^2}{0.63^2} = 1,351 \text{ psi}$$

The tangential stress, σ_t , is found from:

$$\sigma_t = \beta_1 \frac{qr^2}{t^2} = 0.114 \frac{25(14.5)^2}{0.63^2} = 1,510 \text{ psi}$$

In both above cases, $q = 25$ psig is the design pressure, $r = 14.5$ conservatively taken as the diameter of the lid, interior to the bolting flange, and $t = 0.63$ is the thickness of the inner plate. The β and β_1 are defined by Roark for angle of the sector is 45°, which is the angle between two lid rib stiffeners.

For the NCT containment body design temperature of 160 °F, the allowable primary membrane plus bending stress of Type XM-19 stainless steel is 49,770 psi (see Table 2.6-1). The minimum closure stress margin of safety is:

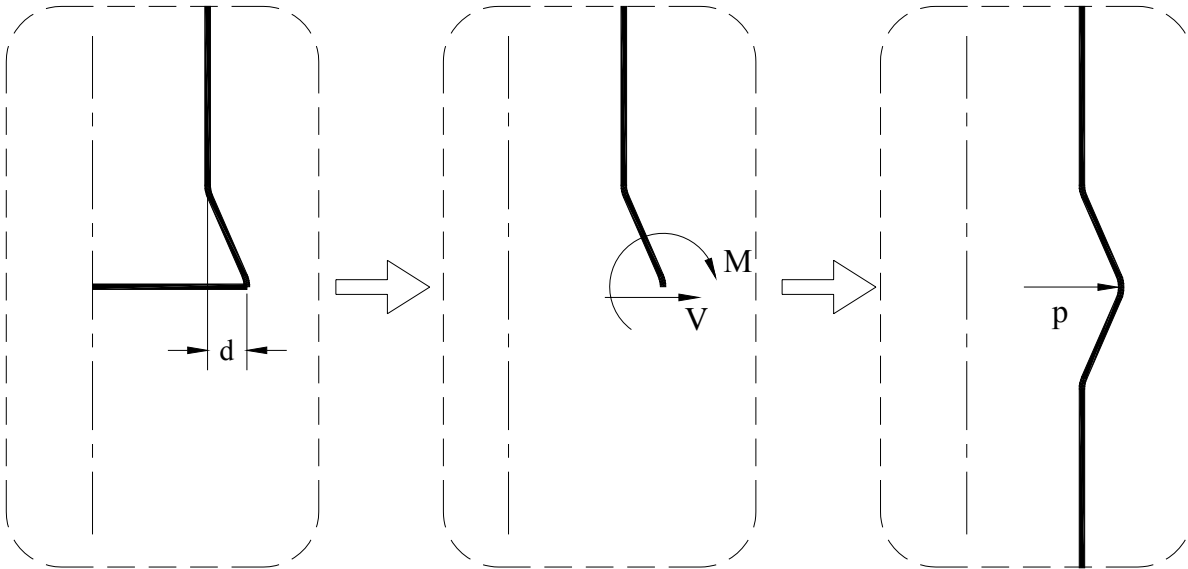
$$MS_{P_m+P_b} = \frac{49,770}{1,510} - 1.0 = +32.0$$

Therefore, stresses in the containment bottom plate and closure lid are within acceptable limits under the 25 psig design pressure.

2.6.1.3.2 Stresses Due to Thermal Gradients

As shown in Figure 3.4-2 of Chapter 3, the total thermal gradient of approximately 13 °F in the MFFP is small and well distributed. Treating the closed end as rigid, the maximum thermal stress in the containment shell is determined as follows. This method is extremely conservative because it assumes a step temperature change in the shell. For the containment shell, the imposed radial displacement, where $\alpha = 8.4 \times 10^{-6}$ in/in/°F is the coefficient of thermal expansion at 160 °F, $r = 14.53$ inches is the mean radius of the containment shell, and $\Delta T = 13$ °F is the thermal change, is determined by:

$$\delta = \alpha \cdot r \cdot \Delta T = (8.4 \times 10^{-6})(14.53)(13) = 0.0016 \text{ in}$$



Assuming the end closure restrains the containment shell rigidly, the rotation, θ , of the end of the shell is zero. Using Table 29, Case 15 from Roark accurately models this condition.

$$\text{Max } y = \frac{-p}{8D\lambda^3}, \text{ in}$$

For the containment shell:

$$D = \frac{Et^3}{12(1-\mu^2)} = \frac{27.8 \cdot 10^6 (0.56^3)}{12(1-0.3^2)} = 447,081 \text{ in} \cdot \text{lb}_f$$

and

$$\lambda = \left(\frac{3(1-\mu^2)}{r^2 t^2} \right)^{\frac{1}{4}} = \left(\frac{3(1-0.3^2)}{(14.53^2)(0.56^2)} \right)^{\frac{1}{4}} = 0.450 \text{ in}^{-1}$$

Where $R = 14.53$ inches is the average radius of the containment shell, $t = 0.56$ inches is the shell thickness, $E = 27.8 \times 10^6$ psi is the modulus of elasticity at 160 °F, and $\mu = 0.3$ is the material Poisson ratio. Solving the above equation for p , using $y = \delta = 0.0016$ inches (calculated above), yields $p = -521 \text{ lb}_f/\text{in}$.

From Table 29, Case 15 of Roark:

$$\text{Max } V = \frac{-p}{2} = \frac{-(-521)}{2} = 261 \frac{\text{lb}_f}{\text{in}} \text{ (maximum unit shear load)}$$

$$\text{Max } M = \frac{p}{4\lambda} = \frac{-521}{4(0.450)} = -289 \frac{\text{lb}_f \cdot \text{in}}{\text{in}} \text{ (maximum unit moment load)}$$

Also from Table 29, Case 15 of Roark:

$$\sigma_1 = 0 \text{ (axial membrane stress)}$$

$$\sigma_2 = \frac{yE}{R} + \nu\sigma_1 = \frac{0.0016(27.8 \times 10^6)}{14.53} + 0.3 \times 0 = 3,061 \text{ psi (hoop membrane stress)}$$

$$\sigma_1' = \frac{-6(M)}{t^2} = \frac{-6(-289)}{0.56^2} = 5,529 \text{ psi (axial bending stress)}$$

$$\sigma_2' = \nu\sigma_1' = 0.3(5,529) = 1,659 \text{ psi (hoop bending stress)}$$

$$\tau = \frac{V}{t} = \frac{261}{0.56} = 466 \text{ psi (hoop shear stress)}$$

Since thermal stresses are deformation limited, they are classified as secondary stresses. The NCT allowable is $3.0S_m$, or 99,540 psi for the XM-19 containment boundary material, from Table 2.6-1. Conservatively combining the highest normal condition secondary stress determined above (5,529 psi) with the highest primary membrane-plus-bending stress, regardless of location (2,904 psi in the bottom closure due to pressure, see Section 2.6.1.3.1, *Stresses Due to Pressure Loading*) results in a primary membrane-plus-bending-plus-secondary stress of:

$$P_m + P_b + Q = 5,529 + 2,904 = 8,433 \text{ psi}$$

The corresponding margin of safety for this stress combination is:

$$MS = \frac{99,540}{8,433} - 1.0 = +10.8$$

Because the above calculated thermal stress is much less than the increase in allowable given when considering thermal stresses, the remainder of the NCT evaluations do not specifically consider thermal stresses for load combination.

2.6.1.3.3 Range of Primary-Plus-Secondary Stress Intensities

Per Paragraph C.4 of Regulatory Guide 7.6, the maximum range of primary-plus-secondary stress intensity for NCT must be less than $3.0S_m$. This limitation on stress intensity range applies to the entire history of NCT loadings and not only to the stresses from each individual load transient. To conservatively encompass the maximum stress intensity range, the maximum stress condition in the MFFP was doubled to account for the worst possible stress reversal. From the result above, the maximum MFFP stress is 8,433 psi. Doubling this value results in a maximum stress intensity range of 16,866 psi. The allowable stress, at NCT temperatures, is $3.0S_m$, or 99,540 psi. The margin of safety is then:

$$MS = \frac{99,540}{16,866} - 1.0 = +4.90$$

Therefore, the criterion of Paragraph C.4 of Regulatory Guide 7.6 is met.

2.6.1.3.4 Closure Bolt Evaluation

The closure bolts are tightened to a maximum of 220 lb_f-ft torque (minimum torque is 175 lb_f-ft). From Subsection 4.2 of NUREG/CR-6007⁵, the maximum non-prying tensile force per bolt due to preload, $F_{a_{max}}$, is found from:

$$F_{a_{max}} = \frac{Q_{max}}{(K)(Db)} = \frac{12(220)}{(0.157)(0.75)} = 22,420 \text{ lb}_f$$

where $Q_{max} = 220 \text{ lb}_f\text{-ft}$ is the maximum applied closure bolt preload, $K = 0.157$ is the nut factor (based the average K for lubricated bolts from Table 4.1 of NUREG/CR-6007), and $Db = 0.75$ inches is the closure bolt nominal diameter. The closure lid has a step located at the bolt circle diameter which precludes prying forces.

The maximum residual torsion is 50% of the applied torsion:

$$M_{tr} = 0.5(Q_{max}) = 0.5(12 \times 220) = 1,320 \text{ in-lb}_f$$

From Subsection 4.4 of NUREG/CR-6007, utilizing appropriate temperature dependent material properties from Section 2.2.1, *Material Properties and Specifications*, the maximum non-prying tensile force per bolt, F_a , due to pressure loads are based on the following formula:

$$F_a = \frac{\pi(Dlg)^2(Pli - Plo)}{4Nb} = \frac{\pi(28.97)^2(39.7 - 14.7)}{4 \cdot 24} = 687 \text{ lb}_f$$

where $Dlg = 28.97$ inches is the closure lid diameter at the location of gasket load reaction (i.e., the O-ring seal diameter), $Pli = 39.7$ psia is the pressure inside the closure lid, $Plo = 14.7$ psia is the pressure outside the closure lid, and $Nb = 24$ is the total number of closure bolts.

The bolt diameter used for stress calculations is based on the stress diameter of the closure bolts, i.e., $Db_a = 0.653$ inches⁶. The closure bolt tensile stress, S_{ba} , is defined as:

$$S_{ba} = (1.2732) \frac{\sum F_a}{Db_a^2} = (1.2732) \frac{22,420 + 687}{0.653^2} = 68,994 \text{ psi}$$

From Table 2.1-1, for NCT the allowable average tensile stress is $S_m = (2/3)S_y$. The allowable tensile stress is therefore 73,187 psi at a conservative temperature of 160 °F, from Table 2.6-1. The corresponding margin of safety on average tensile stress, σ_{t-ave} , is:

$$MS_{\sigma_{t-ave}} = \frac{73,187}{68,994} - 1.0 = +0.06$$

While the temperature of the closure bolts and the closure lid are essentially identical in all cases, a thermally induced load is applied to the bolts since the thermal expansion coefficient of the ASTM A564, Grade 630 Condition H1100, alloy steel closure bolts and Type XM-19 stainless steel closure lid differ. From Subsection 4.5 of NUREG/CR-6007, utilizing appropriate

⁵ G.C. Mok, L.E. Fischer, S.T. Hsu, *Stress Analysis of Closure Bolts for Shipping Casks*, NUREG/CR-6007, UCRL-ED-110637, U.S. Nuclear Regulatory Commission, April 1992

⁶ From Table 5.1 of NUREG/CR-6007: $Db_a = Db - 0.9743 p$, where Db is the nominal diameter of the closure bolt and p is the pitch = 0.1 inches per thread.

temperature dependent material properties from Section 2.2.1, *Material Properties and Specifications*, the maximum non-prying tensile force per bolt due to thermal differential expansion of the closure bolt and the closure lid is based on the following formula:

$$F_{a_{\text{therm}}} = \left(\frac{\pi}{4} \right) (Db)^2 (Eb) [(al)(Tl) - (ab)(Tb)]$$

$$F_{a_{\text{therm}}} = \left(\frac{\pi}{4} \right) (0.75)^2 (28.8 \times 10^6) [(8.4 \times 10^{-6})(90) - (5.5 \times 10^{-6})(90)] = 3,321 \text{ lb}_f$$

where Db is the bolt diameter, Eb = 28.8 × 10⁶ psi is the elastic modulus of the closure bolt material, al = 8.4 × 10⁻⁶ in/in/°F is the thermal expansion coefficient of the closure lid material, ab = 5.5 × 10⁻⁶ in/in/°F is the thermal expansion coefficient of the closure bolt material, Tl = 90 °F is the temperature change of the closure lid from a reference temperature of 70 °F, and Tb = 90 °F is the temperature change of the closure bolt from a reference temperature of 70 °F.

The closure bolt thermal stress, Sb_{therm}, is defined as:

$$Sb_{\text{therm}} = (1.2732) \frac{\sum F_a}{Dba^2} = (1.2732) \frac{3,321}{0.653^2} = 9,916 \text{ psi}$$

The closure bolt shear stress due to torsion, Sbt, is defined as:

$$Sbt = (5.093) \frac{\sum Mt}{Dba^3} = (5.093) \frac{1,320}{0.653^3} = 24,144 \text{ psi}$$

Finally, the maximum closure bolt stress intensity, Sbi, is defined as:

$$Sbi = \sqrt{(Sba + Sb_{\text{therm}})^2 + 4Sbt^2} = \sqrt{(68,994 + 9,916)^2 + 4(24,144)^2} = 92,512 \text{ psi}$$

Note that there are no applied shear stresses since the shear load is carried by the closure lid.

For tension-plus-residual torsion, and closure bolts having a minimum ultimate stress, Su, greater than 100,000 psi, the maximum stress intensity is 1.35Sm. The allowable stress intensity is 98,802 psi and the corresponding margin of safety on average tensile + residual torsion stress (σ+τ) is:

$$MS_{(\sigma+\tau)} = \frac{98,802}{92,512} - 1.0 = +0.07$$

2.6.1.3.5 Strongback Securement Bolts

The three 1/2-13UNC socket head cap screws (SHCS) that secure the strongback into the body are tightened to a maximum of 75 lb_f-ft torque (minimum torque is 70 lb_f-ft). Since these SHCS only react normal transportation forces (not regulatory NCT forces), the preload is the only applied load to be evaluated. The maximum tensile force per bolt due to preload, Fa_{max}, is found from:

$$F_{a_{\text{max}}} = \frac{Q_{\text{max}}}{(K)(Db)} = \frac{12(75)}{(0.157)(0.50)} = 11,465 \text{ lb}_f$$

where Q_{max} = 75 lb_f-ft is the maximum applied closure bolt preload, K = 0.157 is the nut factor, and Db = 0.50 inches is the SHCS nominal diameter.

The bolt diameter used for stress calculations is based on the stress diameter of the closure bolts, i.e., $D_t = 0.425$ inches⁷. The closure bolt tensile stress, σ_t , is defined as:

$$\sigma_t = \frac{Fa_{\max}}{\frac{\pi}{4} D_t^2} = (1.2732) \frac{11,465}{0.425^2} = 80,815 \text{ psi}$$

From Table 2.1-1, for NCT the allowable average tensile stress is $S_m = (2/3)S_y$. From Table 2.2-4, the yield strength of the ASTM A574 material at a conservative temperature of 180 °F (Table 2.6-1), is 133,280 psi. Therefore, the allowable tensile stress is 88,853 psi. The corresponding margin of safety on average tensile stress, $\sigma_{t\text{-ave}}$, is then:

$$MS_{\sigma_{t\text{-ave}}} = \frac{88,853}{80,815} - 1.0 = +0.10$$

2.6.2 Cold

For the cold condition, a -40 °F steady state ambient temperature is utilized per 10 CFR §71.71(c)(2), with zero insolation and zero decay heat. This results in a uniform temperature of -40 °F throughout the package. The materials of construction for the transportation package are not adversely affected by the -40 °F condition, including brittle fracture, which is evaluated in Section 2.1.2.2.1, *Brittle Fracture*.

The closure bolts are fabricated of ASTM A564, Grade 630 Condition H1100, and have a coefficient of thermal expansion which is lower than that of the body and closure lid. Therefore, under cold conditions, the initial bolt preload force is reduced below the value at room temperature. The following evaluation demonstrates the pre-load on the bolts is maintained at the cold condition.

The closure bolts are tightened to a minimum of 175 ft-lb_f torque. From Subsection 4.2 of NUREG/CR-6007, the minimum non-prying tensile force per bolt due to minimum preload, Fa_{\min} , is found from:

$$Fa_{\min} = \frac{Q_{\min}}{(K)(Db)} = \frac{12(175)}{(0.157)(0.75)} = 17,834 \text{ lb}_f$$

where $Q_{\min} = 175 \text{ lb}_f\text{-ft}$ is the minimum applied closure bolt preload, $K=0.157$ is the nut factor, and $Db=0.75$ inches is the closure bolt nominal diameter.

While the temperature of the closure bolts and the closure lid are essentially identical in all cases, a thermally induced load is applied to the bolts since the thermal expansion coefficient of the alloy steel closure bolts and Type XM-19 stainless steel closure lid differ. From Subsection 4.5 of NUREG/CR-6007, utilizing appropriate temperature dependent material properties from Section 2.2, *Materials*, the maximum change in force per bolt due to thermal differential expansion of the closure bolt and the closure lid is based on the following formula:

$$Fa = \left(\frac{\pi}{4} \right) (Db)^2 (Eb) [(a_l)(T_l) - (a_b)(T_b)]$$

⁷ From Table 5.1 of NUREG/CR-6007: $D_t = Db - 0.9743 p$, where Db is the nominal diameter of the closure bolt and p is the pitch = 0.08 inches per thread.

$$F_a = \left(\frac{\pi}{4} \right) (0.75)^2 (29.8 \times 10^6) \left[(7.8 \times 10^{-6})(-110) - (5.0 \times 10^{-6})(-110) \right] = -4,055 \text{ lb}_f$$

where D_b is the bolt diameter, $E_b = 29.8 \times 10^6$ psi is the elastic modulus of the closure bolt material, $\alpha_l = 7.8 \times 10^{-6}$ in/in/°F is the thermal expansion coefficient of the closure lid material, $\alpha_b = 5.0 \times 10^{-6}$ in/in/°F is the thermal expansion coefficient of the closure bolt material, $T_l = -110$ °F is the temperature change of the closure lid from a reference temperature of 70 °F, and $T_b = -110$ °F is the temperature change of the closure bolt from a reference temperature of 70 °F. Thus the preload is reduced by 4,055 lb_f. Since the room temperature minimum preload force is 17,834 lb_f, the preload at a temperature of -40 °F is 17,834 - 4,055 = 13,779 lb_f. This is over 75% of the minimum room temperature value and demonstrates that adequate preload is maintained.

2.6.3 Reduced External Pressure

The effect of a reduced external pressure of 3.5 psia, per 10 CFR §71.71(c)(3), is negligible for the MFFP. This conclusion is based on the analyses presented in Section 2.6.1, *Heat*, addressing the ability of the containment vessel to withstand a design pressure of 25 psig. The MNOP of the MFFP is 10 psig, or 14.7 + 10 = 24.7 psia. For an external pressure of 3.5 psia, the internal gage pressure is 24.7 - 3.5 = 21.2 psig, and thus less than the design pressure of 25 psig.

2.6.4 Increased External Pressure

The MFFP has been demonstrated to have a positive margin of safety against buckling for a 20 psia increased external pressure, utilizing ASME Code Case N-284-1⁸.

Consistent with Regulatory Guide 7.6 philosophy, a factor of safety corresponding to ASME Code, Service Level A conditions is employed. In this case, the applicable factor of safety is 2.00 for normal conditions, as specified in ASME Code Case N-284-1.

Buckling analysis geometry parameters are provided in Table 2.6-2, and loading parameters are given in Table 2.6-3. The buckling analysis conservatively utilizes MFFP shell temperatures consistent with Section 2.6.1, *Heat*, i.e., 160 °F. The stresses are determined using the increased external pressure of 20 psia which, conservatively assuming an internal pressure of 0 psia, corresponds to 20 psig. The hoop stress, σ_θ , axial stress, σ_ϕ , and in-plane shear stress, $\sigma_{\phi\theta}$, are found from:

$$\sigma_\theta = \frac{Pr}{t} \quad \sigma_\phi = \frac{Pr}{2t} \quad \sigma_{\phi\theta} = \frac{Pr}{4t}$$

where P is the applied pressure, r is the mean shell radius, and t is the shell thickness. As shown in Table 2.6-4, all the interaction check parameters are less than 1.0, as required. Therefore, buckling of the shell is not a concern.

⁸ American Society of Mechanical Engineers (ASME) Boiler and Pressure Vessel Code, Section III, *Rules for Construction of Nuclear Power Plant Components*, Case N-284-1, *Metal Containment Shell Buckling Design Methods*, Section III, Division 1, Class MC, 2001 Edition, 2002 and 2003 Addenda.

2.6.5 Vibration and Shock

The effects of vibration normally incident to transport are shown to be insignificant. Draft ANSI N14.23⁹ identifies peak truck trailer vibration inputs. Table 2 of ANSI N14.23 shows peak vibration accelerations of a trailer bed as a function of package and tie-down system natural frequency. For the frequency range 0 to 5 Hz, and conservatively assuming a light package, Table 2 of ANSI N14.23 gives peak accelerations (99% level) of 2g in the vertical direction, and 0.1g in both the lateral and longitudinal directions. All other frequency ranges give significantly lower acceleration levels. Further, due to package symmetry, the vertical load of $\pm 2g$ governs the $\pm 0.1g$ in the lateral and longitudinal directions.

Design fatigue curves are taken from Figure I-9.2.2 and Table I-9.2.2 of the ASME Code¹⁰, Section III, Appendix I for the Type XM-19 stainless steel shell material, from which the allowable amplitude, S_a , of the alternating stress component (1/2 of the alternating stress range) as a function of number of loading cycles may be obtained. Table I-9.2.2 extends the fatigue allowable data to the endurance limit, which is used in the fatigue assessment of transportation vibration. The allowable amplitude, S_a , from Table I-9.2.2 for Type XM-19 stainless steel shell material at 10^{11} cycles is 13,600 psi. This value is adjusted based on the ratio of room temperature elastic modulus of 28.3×10^6 psi, which is the basis for Table I-9.2.2, and the elastic modulus at 160 °F, 27.8×10^6 psi from Table 2.6-1, as follows:

$$S_a = 13,600 \left[\frac{27.8(10^6)}{28.3(10^6)} \right] = 13,360 \text{ psi}$$

An analysis of the MFFP shows that fatigue of the containment boundary is not of concern. The body can be modeled as a simply supported beam, with concentrated loads at each end, supported by the cradles of the transport skid, and with a distributed load equal only to the weight of the shell. The load at each end is equal to the sum of the weight of the impact limiter, body end structure, and one-half of the weight of the loaded strongback (since the strongback weight is supported by the strongback endplates, the strongback and payload weight is applied to the body at the ends). The beam model of the MFFP is shown in Figure 2.6-1.

The cross-sectional area of the shell is:

$$A_s = \frac{\pi}{4} (d_o^2 - d_i^2) = 51.59 \text{ in}^2$$

and the area moment of inertia is:

$$I_s = \frac{\pi}{64} (d_o^4 - d_i^4) = 5,450 \text{ in}^4$$

where d_o is the shell outer diameter of 29.63 inches and d_i is the inner diameter of 28.5 inches. For a material density of $0.29 \text{ lb}_m/\text{in}^3$, the distributed weight of the shell is $w = 15 \text{ lb}_m/\text{in}$. For an

⁹ ANSI N14.23, *Design Basis for Resistance to Shock and Vibration of Radioactive Material Packages Greater Than One Ton in Truck Transport*, 1980, American National Standards Institute, Inc. (ANSI).

¹⁰ ASME Code, Subsection III, Division 1 Appendices, Appendix I, *Design Stress Intensity Values, Allowable Stresses, Material Properties, and Design Fatigue Curves*, Figure I-9.2.2, *Design Fatigue Curve for Austenitic Steels, Nickel-Chromium-Iron Alloy, Nickel-Iron-Chromium Alloy, and Nickel-Copper Alloy for $S_a \leq 28.2$ ksi, for Temperatures not Exceeding 800 °F*, and Table I-9.2.2, *Tabulated Values of S_a , ksi, from Figure I-9.2.2*.

overall length of shell of 168.2¹¹ inches, the total shell weight is $168.2 \times 15 = 2,523$ pounds. The maximum gross weight of the MFFP is 14,260 pounds. The remaining weight, which is divided equally between each end, is $14,260 - 2,523 = 11,737$ pounds, or 5,869 pounds per end. The reaction (under static, 1g conditions) at each cradle support is $14,260/2 = 7,130$ pounds. The maximum bending moment, which occurs at the skid cradle support, is:

$$M_{\max} = 5,869(L_e) + w \frac{L_e^2}{2} = 190,730 \text{ lb}_f - \text{in}$$

where $L_e = 31.25$ inches (the distance from the end to the cradle support centerline). The shell bending stress is:

$$\sigma = \frac{Mc}{I_s} = \frac{190,730(14.82)}{5,450} = 519 \text{ psi}$$

where $c = 29.63/2 = 14.82$ inches. Multiplying the stress by a factor of 2 to account for the $\pm 2g$ alternating load condition results in a conservative fatigue stress amplitude of $2 \times 519 = 1,038$ psi. This stress is considerably less than the minimum value of the fatigue limit found above to be 13,360 psi. The margin of safety is:

$$MS = \frac{13,360}{1,038} - 1.0 = +11.9$$

2.6.6 Water Spray

The materials of construction utilized for the MFFP are such that the water spray test identified in 10 CFR §71.71(c)(6) will have a negligible effect on the package.

2.6.7 Free Drop

Because the maximum gross weight of the MFFP is 14,260 pounds, a three-foot free drop is required per 10 CFR §71.71(c)(7). The MFFP is designed to withstand the effects of a 30-foot HAC free drop, while maintaining leaktight containment and criticality control of the payload. However, the NCT free drop is from a height of 3 feet, which represents a potential energy of impact of only 10% that of the 30-foot hypothetical accident condition (HAC) free drop tests. HAC free drop performance of the containment boundary and strongback was demonstrated to be within acceptable limits by full-scale testing of the MFFP certification test unit (CTU), as discussed in Appendix 2.12.3, *Certification Test Results*. Leakage rate testing following certification testing demonstrated the ability of the MFFP to maintain leaktight (i.e., 1.0×10^{-7} standard cubic centimeters per second (scc/sec), air) containment boundary integrity. Therefore, the requirements of 10 CFR §71.71(c)(7) are met.

¹¹ The actual length is 168.45 inches instead of 168.2 inches. Because the difference is small and would not affect the results significantly, the analysis is not revised.

2.6.8 Corner Drop

This test does not apply, since the package weight is in excess of 220 pounds, and the materials do not include wood or fiberboard, as delineated in 10 CFR §71.71(c)(8).

2.6.9 Compression

This test does not apply, since the package weight is in excess of 11,000 pounds, as delineated in 10 CFR §71.71(c)(9).

2.6.10 Penetration

The 40-inch drop of a 13 pound, hemispherically-headed, 1½ inch diameter, steel cylinder, as delineated in 10 CFR §71.71(c)(10), is of negligible consequence to the MFFP. This conclusion is due to the fact that the MFFP is designed to minimize the consequences associated with the much more limiting case of a 40-inch drop of the entire package onto a puncture bar as discussed in Section 2.7.3, *Puncture*.

Table 2.6-1 – Summary of NCT Design Parameters

Parameter	Body, Closure Lid (XM-19)	Closure Bolts (A564, Grade 630, Condition H1100)	Strongback (Type 304)
NCT Hot Bounding Temperature, °F	160	160	180
Coefficient of Thermal Expansion, α , (in/in/°F)	8.4×10^{-6}	5.5×10^{-6}	8.8×10^{-6}
Elastic Modulus, psi	27.8×10^6	28.8×10^6	27.7×10^6
Design Stress, S_m , psi	33,180	73,187	20,000
Yield Stress, S_y , psi	50,260	109,780	26,000
Primary Membrane Stress Intensity (P_m), psi	$S_m = 33,180$	n/a ^①	$S_m = 20,000$
Primary Membrane + Bending Stress Intensity ($P_m + P_b$), psi	$1.5S_m = 49,770$	n/a ^①	$1.5S_m = 30,000$
Primary Membrane + Bending + Secondary Stress Intensity ($P_m + P_b + Q$), psi	$3.0S_m = 99,540$	n/a ^①	$3.0S_m = 60,000$
NCT Cold Bounding Temperature, °F	-40	-40	-40
Coefficient of Thermal Expansion, α , (in/in/°F)	7.8×10^{-6}	5.0×10^{-6}	8.2×10^{-6}
Elastic Modulus, psi	28.9×10^6	29.8×10^6	28.9×10^6

Notes: ① Bolting allowable stresses are discussed in the sections where they are used.

Table 2.6-2 – Shell Buckling Geometry Parameters per Code Case N-284-1

Geometry, Temperature, and Material Input	Cylindrical Shell
Outside Diameter, inch	29.63
Inside Diameter, inch	28.50
Length, inch	168.20
Temperature, °F	160
Material	Type XM-19
Geometry Output	
R =	14.533
t =	0.565
R/t =	25.72
$\lambda_\phi =$	168.2
$\lambda_\theta =$	91.31
$M_\phi =$	58.70

Table 2.6-3 – Shell Load Input for 20 psig Increased External Pressure

Direction	Stress, psi
Axial Stress, σ_ϕ	260
Hoop Stress, σ_θ	519
Shear Stress, $\sigma_{\phi\theta}$	130

Table 2.6-4 – Buckling Summary for 20 psia Increased External Pressure

Condition	Shell	Remarks
Capacity Reduction Factors (-1511)		
$\alpha_{\phi L} =$	0.5094	
$\alpha_{\theta L} =$	0.8000	
$\alpha_{\phi\theta L} =$	0.8000	
Plasticity Reduction Factors (-1610)		
$\eta_{\phi} =$	0.1509	
$\eta_{\theta} =$	1.0000	
$\eta_{\phi\theta} =$	0.3567	
Theoretical Buckling Values (-1712.1.1)		
$C_{\phi} =$	0.6050	
$\sigma_{\phi eL} =$	653,895	
$C_{\theta r} =$	0.0137	
$\sigma_{\theta eL} = \sigma_{reL} =$	14,809	
$C_{\theta h} =$	0.0137	
$\sigma_{\theta eL} = \sigma_{heL} =$	14,809	
$C_{\phi\theta} =$	0.0974	
$\sigma_{\phi\theta eL} =$	105,239	
Elastic Interaction Equations (-1713.1.1)		
$\sigma_{za} =$	166,539	
$\sigma_{ha} =$	5,924	
$\sigma_{ra} =$	5,924	
$\sigma_{ta} =$	42,096	
Axial + Hoop \Rightarrow Check (a):	...N/A	
Axial + Hoop \Rightarrow Check (b):	...N/A	
Axial + Shear \Rightarrow Check (c):	0.0016	<1 \therefore OK
Hoop + Shear \Rightarrow Check (d):	0.0876	<1 \therefore OK
Axial + Hoop + Shear \Rightarrow Check (e):	...N/A	
Axial + Hoop + Shear \Rightarrow Check (f):	...N/A	
Inelastic Interaction Equations (-1713.2.1)		
$\sigma_{xc} =$	25,130	
$\sigma_{rc} =$	5,924	
$\sigma_{tc} =$	15,015	
Axial + Hoop \Rightarrow Check (a):	0.0876	<1 \therefore OK
Axial + Shear \Rightarrow Check (a):	0.0104	<1 \therefore OK
Hoop + Shear \Rightarrow Check (b):	0.0877	<1 \therefore OK

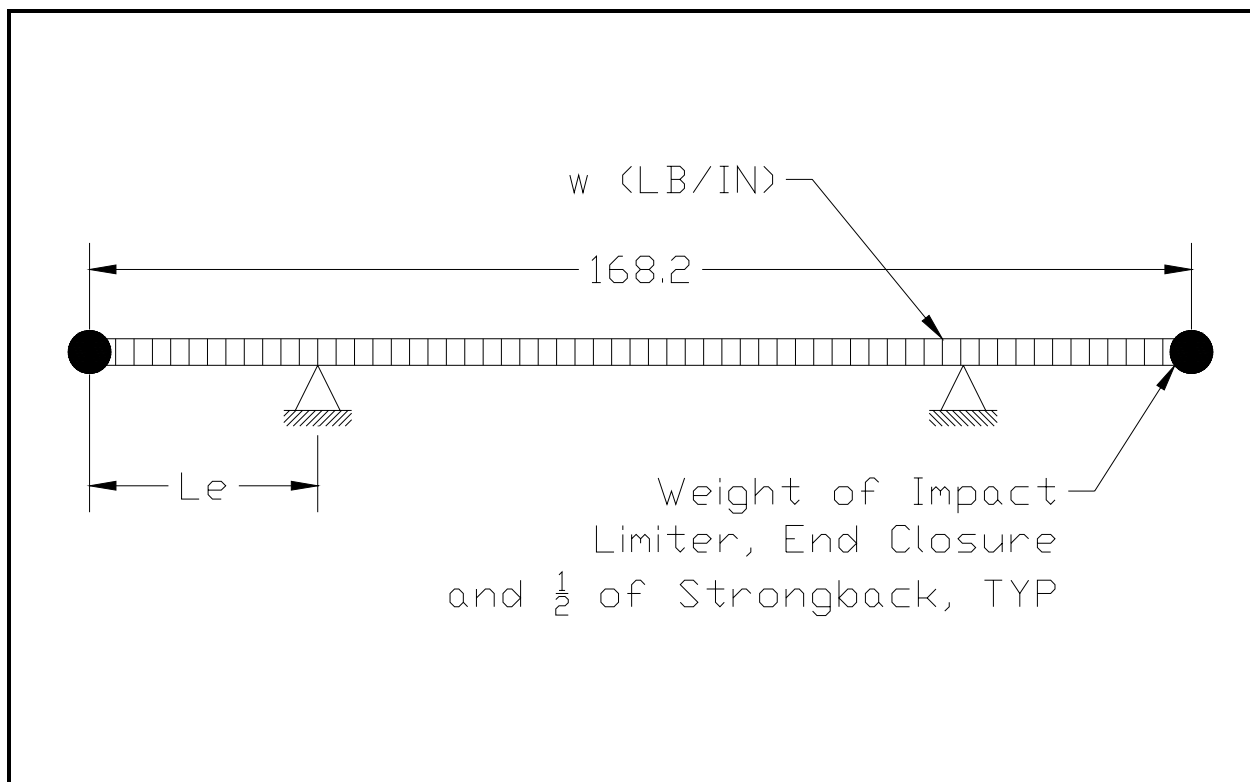


Figure 2.6-1 – Vibration Model of Package

2.7 Hypothetical Accident Conditions

The MFFP, when subjected to the sequence of hypothetical accident condition (HAC) tests specified in 10 CFR §71.73¹, subsequent to the sequence of normal conditions of transport (NCT) tests specified in 10 CFR §71.71, is shown to meet the performance requirements specified in Subpart E of 10 CFR 71. As indicated in the introduction to Chapter 2.0, *Structural Evaluation*, with the exception of the thermal and immersion tests that are demonstrated by analysis, the primary proof of performance for the HAC tests is via the use of full-scale testing. In particular, free drop and puncture testing of the MFFP certification test unit (CTU) confirms that the containment boundary will remain leaktight after a worst case HAC sequence. Observations from testing of the CTU also confirm the conservative nature of deformed geometry assumptions used in the thermal and criticality assessments.

Specifically, the certification test program demonstrated the following objectives:

1. **No loss of containment:** The leaktight containment boundary was maintained throughout repeated regulatory test sequences. Additionally, HAC structural loads did not result in deformations (including buckling) that would lead to the degradation of containment under the subsequent HAC fire event.
2. **Maintaining subcriticality:** The strongback structure retained its geometry and retained the neutron poison in their respective positions. Together with the certification testing and the analytical evaluations provided herein, the geometry of the payload is controlled and the MFFP payload remains subcritical.

The basis for the certification testing performed is summarized in the following sections. For a detailed discussion of the basis of the structural certification performed, refer to Appendix 2.12.2, *Certification Test Plan*. The results of the certification testing program are presented in Appendix 2.12.3, *Certification Test Results*. Analyses necessary to supplement or expand the tests results are also presented, as necessary. Development of the MFFP design was facilitated by a half-scale engineering test unit. The engineering tests were focused on development of the puncture resistant impact limiters, but also included a 30-foot free drop (side drop orientation). The results of the engineering test are summarized in Appendix 2.12.4, *Engineering Test Results*.

2.7.1 Free Drop

Subpart F of 10 CFR 71 requires performing a free drop test in accordance with the requirements of 10 CFR §71.73(c)(1). The free drop test involves performing a 30-foot, HAC free drop onto a flat, essentially unyielding, horizontal surface, with the package striking the surface in a position (orientation) for which maximum damage is expected. The ability of the MFFP to adequately withstand this specified free drop condition is demonstrated via testing of a full-scale, certification test unit (CTU) and analytical evaluations. Specifically, the analytical evaluations include:

- Structural analyses of the fuel control structure (FCS), provided in Appendix 2.12.5, *Fuel Control Structure Evaluation*.
- Structural analyses of package weight not accounted for in the certification tests, provided in Appendix 2.12.8, *Effect of Bounding Weight on Package Structural Responses*.

¹ Title 10, Code of Federal Regulations, Part 71 (10 CFR 71), *Packaging and Transportation of Radioactive Material*, Final Rule, 01-26-04.

- Maximum deformation of impact limiters under warm conditions, provided in Appendix 2.12.1, *Impact Limiter Evaluation*.

2.7.1.1 Technical Basis for the Free Drop Tests

Items that could compromise the containment integrity or criticality safety of the package were identified when selecting the worst case package orientations for the 30-foot free drop event. Shielding integrity is not addressed since the MFFP design does not include any components whose primary purpose is shielding. For the MFFP containment body, its ability to remain leaktight is of primary importance. For the strongback, geometric stability, including support of the fuel assemblies and poison plates, is of primary importance.

The types of damage that are the most likely candidates to compromise the leaktight capability of the MFFP are as follows:

- Excessive deformation of the sealing surfaces that would cause reduced seal compression,
- Failure of the closure lid bolts,
- Buckling of the containment shell, and
- Thermal degradation of the seal material resulting from the HAC fire event.

Types of damage that could affect criticality safety are as follows:

- Deformations of the strongback that could change the relative geometric relationships between the fuel assemblies (FAs) and the neutron absorbing material which exceed the bounds established in the criticality analyses, and
- Buckling of the containment shell.

From the above considerations, a total of four 30-foot free drops were selected, including horizontal, vertical, and two near-horizontal slapdown orientations. In the course of testing, an additional free drop test was performed. Multiple tests have been performed to ensure that the most vulnerable package features were subjected to “worst case” loads and deformations, as required by 10 CFR §71.73(c)(1). The certification tests were exceedingly conservative for the containment boundary since a single containment body structure was subject to all the free drops (and punctures). Table 2.7-1 summarizes the free drops performed and the primary aspect of the MFFP performance being tested. Appendix 2.12.2, *Certification Test Plan* discusses, in detail, the justification for the selection of each free drop orientation and the objectives for each test, as well as describing the sequence of free drop and puncture tests, the initial test conditions, the data to be gathered from the test, and the test unit and payload configuration for each test.

As shown in Table 2.7-1, there were three (3) test series. Each series employed a different test payload configuration as subsequently noted. Each series consisted of at least one 30-foot free drop followed by at least one puncture drop, such that each series fulfilled the regulatory requirements for HAC drop testing, i.e., free drop followed by puncture drop. In keeping with the regulatory series philosophy, the containment boundary closure seals were leakage rate tested prior to, and following each series to demonstrate the containment boundary remained leaktight. The entire boundary was leakage rate tested prior to and following the entire set of test series.

For the certification test free drops the CTU impact limiters were chilled to the minimum temperature (-20 °F ambient) condition, in order to maximize crush strength of the foam and

consequent impact magnitude. Since the impact limiters do not “bottom-out” under maximum temperature conditions, see Appendix 2.12.1, *Impact Limiter Evaluation*, maximum impact accelerations are associated with the increased crush stress of chilled foam.

As noted above, three payload configurations were used for certification testing. The mock payload was comprised of a simple bundle of 1/2-inch diameter carbon steel rods. The mock payload was used in lieu of the strongback and FAs in the first test series, which consisted of a HAC side drop and multiple puncture drops. This first test series focused upon demonstrating the behavior of the impact limiters and the integrity of the package containment and structural shells. The details of the mock Payload are presented in Appendix 2.12.2, *Certification Test Plan*. The second and third payload configurations both included the strongback assembly. The second payload configuration consisted of the strongback loaded with two dummy FAs plus one prototypic FA, whereas the third payload configuration consisted of three dummy FAs. The purpose of the second test series was to assess the behavior of an actual MOX FA under hypothetical accident conditions. The purpose of the third test series was to assess the behavior and demonstrate the integrity of the strongback assembly itself.

The dummy FAs were designed to accurately represent the way that an actual MOX FA would apply loads to the strongback, but were not intended to accurately represent the behavior characteristics of the individual fuel rods. The details of the dummy FA are presented in Appendix 2.12.2, *Certification Test Plan*. The prototypic FA was designed to be exactly representative of a MK-BW MOX FA. The only difference between an actual MOX FA and the prototypic FA was that the fuel pellets of the prototypic FA were tungsten carbide. The burnable poison rod assembly (BPRA), optionally shipped assembled with the MOX FA, was not represented. However, the weight of the tungsten carbide pellets was greater than the weight of the actual MOX fuel pellets. Therefore, the prototypic FA included the weight of a BPRA, and thus conservatively represented the actual MOX FA.

2.7.1.2 Summary of Results from the Free Drop Testing

The certification testing successfully demonstrated the robust nature of the containment boundary and stability of the strongback. The containment structure was subjected to five HAC free drops (and six puncture drops, as described in Section 2.7.3) and remained leaktight throughout the testing. Appendix 2.12.3, *Certification Test Results*, contains the details of the free drop results. Significant results of the free drop testing, with respect to the containment boundary, are as follows:

- Containment
 - Following a total of five, 30-foot free drops and six puncture drops, the containment boundary, which was used for all drops, demonstrated its robustness and capability to remain leaktight. The only components of the containment boundary replaced between test series were the butyl O-ring seals.
 - The containment boundary structure did not buckle or permanently deform due to any of the free drops.
 - The side and secondary slapdown impacts (both are effectively 0° impacts) resulted in weld failure in the outside top angle corner of the closure lid end impact limiter (see Figure 2.12.3-7, Appendix 2.12.3, *Certification Test Results*). The impact limiter weld failure was subjected to a subsequent puncture test (see Figure 2.12.3-9, Appendix 2.12.3, *Certification Test Results*). Although the resulting cumulative damage is evaluated in Chapter 3.0, *Thermal Evaluation*, and shown to have no effect on the integrity of the

containment O-ring seals, the fillet weld joint design was revised to a groove butt weld for the packaging design. Demonstration of the weld joint designs is presented in Appendix 2.12.7, *Impact Limiter Weld Joint Test Results*.

- The maximum gross weight of the MFFP, as presented in Section 2.1.3, *Weights and Center of Gravity*, is 14,260 pounds and represents the bounding weight of the package. The CTU Series 1, 2, and 3 configurations weighed 13,815, 13,234, and 13,217 pounds, respectively. These are somewhat lighter than the maximum gross weight, primarily because they are actual fabricated weights (not worst-case maximums) and also do not include the FCS, which was not present in the CTUs. An evaluation of the effect of the additional weight is given in Appendix 2.12.8, *Effect of Bounding Weight on Package Structural Responses*. The effect of the bounding weight on maximum impact limiter deformations under hot conditions is evaluated by analysis in Appendix 2.12.1, *Impact Limiter Evaluation*, where the maximum gross weight is conservatively used to demonstrate that the impact limiters will not 'bottom out'.
- Based on the certification tests and structural analyses, and the conclusions of the thermal analyses in Chapter 3.0, *Thermal Evaluation*, the containment boundary is maintained when the MFFP is subjected to the applicable tests described in Subpart F of 10 CFR 71.

As noted above, the FCS was not present during the certification tests. Presence of the FCS could have an effect on the axial movement of the fuel rods in a top end drop, since the degree of the rod's lateral buckling is strictly limited by the FCS. However, since the degree of buckling of the rods was very small in the absence of the FCS, a further small restriction is unlikely to alter the behavior of the rods significantly. As shown in Figure 2.12.3-23, some rods did pass through the top nozzle plate as a result of the end drop, and some may have struck the closure lid containment plate. Although no significant change to this configuration is expected to occur in the presence of the FCS, a bounding analysis will be performed to evaluate the worst-case loading of the closure lid by the axial movement of fuel rods. This evaluation focuses on the local effect of rods on the closure lid containment plate. The more global effect of the package contents weight on the closure system is discussed in Appendix 2.12.8, *Effect of Bounding Weight on Package Structural Responses*.

Figure 2.12.3-23 shows a view of the top nozzle of the fuel assembly. There are a total of 56 holes through which a fuel rod could pass through. The hole size allows only a single rod to come through each hole. Therefore, the maximum number of fuel rods per FA that could strike the closure lid in an end drop is 56. This analysis will conservatively neglect any friction of the rod with the grids, with other rods that do not move, or with the top nozzle itself. The analysis further assumes that each hole is adequately aligned with a fuel rod to permit passage. Additionally, to ensure that all rods that can move are accounted, the quantity of rods striking the closure lid will be arbitrarily increased by 25%, thus $1.25 \times 56 = 70$ rods will be considered. Per Table 2.12.5-1, the weight of a fuel rod is $W_R = 5.33$ pounds, and from Section 2.12.5.2, *Conditions Analyzed*, the bounding axial impact load is 120g. The maximum load for a FA that could be applied to the lid by the rods is:

$$F = 70W_R(120) = 44,772 \text{ lb}_f$$

The closure lid is a weldment with eight radial ribs. Each 45° segment between the ribs is bounded by the inner diameter of the outer forging of 26.38 inches and the outer diameter of the central support pipe of 7.0 inches. The area of one segment is:

$$A = \left(\frac{1}{8}\right) \frac{\pi}{4} (26.38^2 - 7.0^2) = 63.51 \text{ in}^2$$

The entire load of the displaced rods, F , is conservatively applied to a single segment, so that the pressure loading on the segment is:

$$q = \frac{F}{A} = \frac{44,772}{63.51} = 705 \text{ psi}$$

The maximum stress in the containment plate for a solid circular sector is found using Table 24, Case 27 of Roark¹, and bounded by the tangential stress, σ_t :

$$\sigma_t = \beta_1 \frac{qr^2}{t^2} = 36,478 \text{ psi}$$

where: $q = 705 \text{ psi (impact load)} + 25 \text{ psi (design pressure)} = 730 \text{ psi}$
 $r = 26.38/2 = 13.19 \text{ inches}$
 $t = 0.63 \text{ inches}$
 $\beta_1 = 0.114 \text{ for } 45^\circ \text{ sector}$

From Table 2.1-1, the allowable primary membrane plus bending stress intensity is equal to the lesser of $3.6S_m$ and S_u , but since this region is near to the closure O-ring seals, a value equal to the yield stress will be conservatively used, equal to 47,100 psi from Table 2.2-1 at a bounding temperature of 200 °F. The margin of safety is:

$$MS = \frac{47,100}{36,478} - 1.0 = +0.29$$

Thus, any additional movement of the fuel rods in an end drop due to the introduction of the FCS is not of concern.

The fuel rods themselves will not be significantly damaged by impact with the lid. As shown in Figures 2.12.3-22 and 2.12.3-23, the damage incurred by the fuel rods in the certification test bounds any damage that could occur in the presence of the FCS.

The burnable poison rod assembly (BPRA) which can optionally be shipped with the fuel was not present during the certification tests. As described in Section 1.2.3, *Contents of Packaging*, the BPRA may be inserted into the top of the FA and weighs up to 65 pounds. During normal transport, it is restrained by the BPRA restraint, shown as Assembly A3 on General Arrangement Drawing Number 99008-30. In a top end drop, the BPRA restraint weldment comes into contact with the inner plate of the closure lid. Therefore, the weight of the BPRA is transferred to the closure lid through the BPRA restraint weldment. Since the surface area of the restraint weldment is relatively large, and since contact between the BPRA, the restraint weldment, and the closure lid is flat without protrusions, the BPRA cannot inflict significant damage to the closure lid inner plate. As stated in Section 2.7.1.1, *Technical Basis for the Free Drop Tests*, the weight of the prototypic and dummy FAs was conservatively slightly greater than the total FA plus BPRA weight. Thus, the presence of a BPRA in any or all of the FAs is not of concern.

¹ Young, W. C., *Roark's Formulas for Stress and Strain*, Sixth Edition, McGraw-Hill, 1989.

The principal criticality control structure for the MFFP is the strongback. Two strongbacks were used for the certification testing program. Table 2.7-1 summarizes the performance aspect being tested in the respective series.

The first strongback was used in Series 2 and was assembled with two dummy FAs and one prototypic FA. This strongback was subjected to one HAC free drop (and one puncture drop).

The second strongback was used in Series 3 and for the 'Additional Test', and was assembled with three dummy FAs. This strongback was subjected to two HAC free drops (and two puncture drops) as part of Series 3, and then the 'Additional Test' HAC free drop.

Both strongbacks exhibited no significant deformations as a result of the test series. The effectiveness of the neutron poison plates was preserved through maintenance of its integrity and position. Following Series 2, the clamp arms, which restrain the fuel assemblies to the longitudinal strongback plates, were operational following the test and retained both the prototypic and dummy fuel assemblies in position. Although the strongback was not removable from the containment body following Series 3, a borescope inspection of the structure revealed no significant damage or re-configuration of the strongback.

The purpose of Series 2 was to demonstrate the longitudinal stability of the strongback during axial accelerations, and to determine the stability of the prototypic FA as assembled to the strongback. As described above, the strongback performance is acceptable. The fuel rods of the prototypic FA exhibited unacceptable lateral deformations. The lateral fuel rod deformations are best characterized as first mode Euler buckling between the clamp arms nearest the top nozzle (nearest the ground in the near-vertical orientation, see Figure 2.12.3-22, Appendix 2.12.3, *Certification Test Results*). In addition to lateral fuel rod deformations, a number of prototypic fuel rods also slid through the grid straps. An undetermined number of rods contacted the top nozzle, and 8 rods slid through the flow openings in the top nozzle (see Figure 2.12.3-23, Appendix 2.12.3, *Certification Test Results*). To ensure that this lateral fuel rod deformation is positively bounded, a fuel control structure (FCS) has been incorporated into the strongback design. The FCS is analytically evaluated in Appendix 2.12.5, *Fuel Control Structure Evaluation*. As shown in that evaluation, the geometry of the fuel is confined to a maximum cross-section of 8.7 inches square. In addition, since the FCS contains two neutron poison plates, the FAs are surrounded on all four sides by neutron poison materials. Chapter 6.0, *Criticality Evaluation*, concludes that with the neutron poison and geometric control afforded by the strongback/FCS structure, an optimally moderated FA, arranged in the most reactive credible configuration, remains subcritical with significant margin.

Significant results of the free drop testing, with respect to criticality safety, are as follows:

- Criticality safety
 - The strongback structure did not significantly reconfigure. The position of the neutron poison relative to the FAs, and the global position of the FAs relative to each other were maintained.
 - The post-drop configuration of the fuel rods is bounded by the FCS (refer to Section 2.12.5, *Fuel Control Structure Evaluation*), which ensures the assumptions used in the criticality evaluation are valid.
 - Based upon the structural tests and analyses, and upon the conclusions of the criticality analyses, the MFFP, when optimally moderated, remains subcritical when subjected to the applicable tests described in Subpart F of 10 CFR 71.

2.7.2 Crush

Subpart F of 10 CFR 71 requires performing a dynamic crush test in accordance with the requirements of 10 CFR §71.73(c)(2). Since the MFFP weight exceeds 1,100 pounds, the dynamic crush test is not required.

2.7.3 Puncture

Subpart F of 10 CFR 71 requires performing a puncture test in accordance with the requirements of 10 CFR §71.73(c)(3). The puncture test involves a 40-inch free drop of a package onto the upper end of a solid, vertical, cylindrical, mild steel bar mounted on an essentially unyielding, horizontal surface. The bar must be six inches in diameter, with the top surface horizontal and its edge rounded to a radius of not more than 1/4 inch. The package is to be oriented in a position for which maximum damage will occur. The minimum length of the bar is to be eight inches. The ability of the MFFP to adequately withstand this specified puncture drop condition is demonstrated via testing of a full-scale, MFFP certification test unit.

2.7.3.1 Technical Basis for the Puncture Drop Tests

Items that could compromise containment integrity or criticality safety of the package were identified when selecting a worst case package orientation for the puncture drop event. For the MFFP containment body, its ability to remain leaktight is of primary importance. For the strongback, geometric stability, including support of the fuel assemblies and neutron poison plates is of primary importance. Criticality safety could be impacted by excessive deformation of the containment boundary shell which might cause a significant reconfiguration of the fuel and strongback geometry relationship.

The types of damage that are the most likely to compromise the leaktight capability of the MFFP are as follows:

- Excessive deformation of the sealing surfaces that would result in excessive reduction of seal compression caused by a direct puncture impact to the sealing area,
- Puncture of the containment boundary shell, and
- Thermal degradation of the O-ring seal butyl material resulting from the HAC thermal event resulting from the removal of, or excessive damage to, the impact limiter.

Types of damage that could affect criticality safety are as follows:

- Deformations of the strongback that would result in change of the relative geometric relationships between the FAs and the neutron absorbing material, which exceed the limits established in the criticality analyses, and
- Deformation or reconfiguration of the FAs that exceeds the bounds established in the criticality analysis.

From the above considerations, six puncture drops were selected, as shown in Table 2.7-3. Each puncture test was performed following at least one HAC 30-foot free drop. The same MFFP body (body, closure lid, and closure bolts) was conservatively subjected to all six tests. Appendix 2.12.2, *Certification Test Plan*, contains further discussion and provides the detailed logic behind the choice of puncture orientations and test sequence. Section 2.7.3.2, *Summary of Results from the Puncture Drop*

Tests, summarizes the puncture test results and Appendix 2.12.3, *Certification Test Results*, describes the results in detail.

2.7.3.2 Summary of Results from the Puncture Drop Tests

The certification testing successfully demonstrated the robust nature of the containment boundary and stability of the strongback. Appendix 2.12.3, *Certification Test Results*, contains the details of the free drop results.

- Containment
 - The containment boundary shell did not perforate due to any of the puncture drops, including both perpendicular and oblique orientations.
 - The lid end impact limiter shell prevented the puncture bar from directly applying loads to the sealing region. Thus, containment is not affected by direct puncture attack.
 - The lid end impact limiter shell resisted gross perforation, thus preventing excessive removal of polyurethane foam or exposure of the containment seal region to the fire temperatures.
 - The puncture damage, added to the free drop lid end impact limiter weld damage, did not result in loss of containment in the analysis of the HAC thermal event.
- Criticality safety
 - The strongback structure did not significantly reconfigure. The position of the neutron poison relative to the FAs, and the global position of the FAs relative to each other were maintained.
 - The puncture bar was unable to deform the shell body sufficiently to significantly reconfigure the FA rods.

Based upon the puncture tests, the MFFP maintains containment and remains subcritical when subjected to the applicable tests described in Subpart F of 10 CFR 71.

2.7.4 Thermal

Subpart F of 10 CFR 71 requires performing a thermal test in accordance with the requirements of 10 CFR §71.73(c)(4). To demonstrate the performance capabilities of the MFFP when subjected to the HAC thermal test specified in 10 CFR §71.73(c)(4), the worst-case damage from the HAC, 30-foot free drop and puncture tests, as discussed in Section 2.7.1, *Free Drop*, and Section 2.7.3, *Puncture*, was included in the MFFP thermal model, as discussed in Chapter 3.0, *Thermal Evaluation*.

2.7.4.1 Summary of Pressures and Temperatures

Package pressures and temperatures due to the HAC thermal event are presented in Section 3.5.3, *Maximum Temperatures and Pressures*. A brief summary of the thermal analysis results are provided in the following sections.

2.7.4.1.1 Summary of Pressures

From Table 3.5-2, the maximum internal pressure during the HAC thermal event, which includes an assumption of 100% rupture of the fuel rods and the complete combustion of all of the polymer

materials utilized in the strongback, is 123.5 psig, with the package initially at atmospheric pressure. For stress analysis purposes, a pressure of 130 psig is used, which conservatively bounds the maximum internal pressure.

2.7.4.1.2 Summary of Temperatures

From Table 3.5-1, the maximum shell wall temperature is 1,361 °F, and the maximum closure lid temperature is 301 °F, both of which occur at the end of the 30-minute HAC thermal event. The closure lid temperature bounds the bottom end closure temperature. The maximum temperature of the strongback is 599 °F. The maximum temperature in the closure lid sealing region is 339 °F.

2.7.4.2 Differential Thermal Expansion

The maximum temperature of the strongback is $T_{SB} = 599$ °F, but a value of 700 °F is conservatively used and applied to the entire strongback. From Section 2.2.1, *Material Properties and Specifications*, the thermal expansion coefficient of Type 304 stainless steel at this temperature is $\alpha_{SB} = 10.0 \times 10^{-6}$ in/in/°F. Since the length of the strongback is $L_{SB} = 164.90$ inches, the thermal expansion of the strongback is:

$$\delta_{L-SB} = (\alpha_{SB})(T_{SB} - 70)(L_{SB}) = 1.04 \text{ inches}$$

The bounding minimum temperature of the MFFP shell, which is conservatively assumed to apply to the entire shell, is $T_{SH} = 1,200$ °F, a value well below the calculated maximum temperature of 1,361 °F. The linearly extrapolated thermal expansion coefficient of XM-19 is $\alpha_{SH} = 9.8 \times 10^{-6}$ in/in/°F from Section 2.2.1, *Material Properties and Specifications*, using data for 600 °F and 700 °F. Since the length of the shell cavity, L_{SH} , is 165.25 inches, the minimum thermal expansion of the shell is:

$$\delta_{L-SH} = (\alpha_{SH})(T_{SH} - 70)(L_{SH}) = 1.83 \text{ inch}$$

For the HAC thermal event, the strongback grows 0.79 inches less than the cavity, increasing axial clearance. Thus, axial clearance is maintained for the HAC thermal event.

2.7.4.3 Stress Calculations

As discussed in Section 2.7.4.1.1, *Summary of Pressures*, a conservative maximum internal pressure of 130 psig is assumed for the HAC thermal. Shell stresses due to the design pressure of 25 psig are calculated in Section 2.6.1, *Heat*. Therefore, the stress in the shell due to the HAC maximum pressure is found from:

$$\sigma_{HAC} = \frac{130}{25} \sigma_{NCT}$$

The results of this scaling for the shell, bottom end closure, and closure lid are shown in Table 2.7-4. For simplicity, the bottom end and closure lid stresses used in the scaling are peak values, but allowable stresses for membrane-only stress (the lesser of $2.4S_m$ or $0.7S_u$) are conservatively used.

The allowable stress for the bottom end and closure lid is extracted from Section 2.2.1, *Material Properties and Specifications*, for the XM-19 material at a temperature of 301 °F, and is governed by $0.7S_u$, equal to 65,940 psi. Since its temperature exceeds the values given in Section II, Part D of the ASME B&PV Code, the allowable stress for the Type XM-19 shell material is developed by comparing the yield strength behavior versus temperature to Type 304 material, which is included in

the high-temperature ASME B&PV Code. As illustrated in Figure 2.7-1, the yield strengths of Type XM-19 and Type 304 austenitic stainless steels behave similarly up to 1,500 °F. However, the Type XM-19 material is significantly stronger than Type 304 material at all temperatures. Therefore, utilizing the allowable stress extracted from ASME B&PV Code, Section III, Subsection NH² for Type 304 is conservative for evaluating the shell at elevated temperature. The value of the rupture stress, S_R , for Type 304 is 16.5 ksi for an upper bound shell temperature of 1,400 °F and an exposure of one hour, from Table I-14.6A. The selection of a one-hour temperature duration is conservative since the shell wall temperature falls rapidly after the 30-minute HAC thermal event. The governing allowable stress is equal to $0.67S_R = 11,055$ psi.

The minimum margin of safety for the HAC thermal pressure case, including the significant conservative assumptions described above, is +2.15, as shown in Table 2.7-4. Therefore, stresses in the body shell, bottom end, and closure lid are within acceptable limits.

Per Regulatory Guide 7.6, Paragraph C.7, the extreme range of stress must be considered. Of all the various allowable stresses corresponding to the different conditions evaluated (including fabrication stresses and normal conditions of transport), the largest allowable stress is equal to the material ultimate strength, S_u . It is therefore conservative to assume that S_u bounds all stresses actually developed in the structure. For Type XM-19 stainless steel, $S_u = 100,000$ psi at 70 °F. The maximum possible stress intensity range is twice this value, or 200,000 psi. Applying a factor of four to account for possible stress concentrations at structural discontinuities gives a total stress range of 800,000 psi. The alternating component is one-half of this value, or 400,000 psi. To account for temperature effects, this value of alternating stress is factored by the ratio of modulus of elasticity. This ratio is formed between the modulus of elasticity at room temperature (at which the test data applies directly) and the modulus of elasticity at the design temperature of 160 °F. The adjusted stress is:

$$S_{alt} = 400,000 \frac{E_{70^\circ F}}{E_{160^\circ F}} = 407,194 \text{ psi}$$

where $E_{70^\circ F} = 28.3 \times 10^6$ psi and $E_{160^\circ F} = 27.8 \times 10^6$ psi. Per Figure I-9.2.1 and Table I-9.1 of the ASME B&PV Code, the allowable value for S_{alt} at 10 cycles is 708,000 psi. The margin of safety is:

$$MS = \frac{708,000}{407,194} - 1.0 = +0.74$$

Considering the significant conservatism used in the underlying assumptions (e.g., use of allowable stress rather than smaller actual stresses, assuming worst case stresses are fully reversing, use of the maximum factor of stress concentration), it is apparent that the actual margin of safety is larger than +0.74. Thus, the requirement of paragraph C.7 of Regulatory Guide 7.6 is met.

2.7.5 Immersion – Fissile Material

Subpart F of 10 CFR 71 requires performing an immersion test for fissile material packages in accordance with the requirements of 10 CFR §71.73(c)(5). The criticality evaluation presented in Chapter 6.0, *Criticality Evaluation*, assumes optimum hydrogenous moderation of the contents, thereby conservatively addressing the effects and consequences of water in-leakage.

² American Society of Mechanical Engineers (ASME) Boiler and Pressure Vessel Code, Section III, *Rules for Construction of Nuclear Power Plant Components*, 2001 Edition, 2002 and 2003 Addenda.

2.7.6 Immersion – All Packages

Subpart F of 10 CFR 71 requires performing an immersion test for all packages in accordance with the requirements of 10 CFR §71.73(c)(6). For the MFFP, this external pressure condition is bounded by the requirements of 10 CFR §71.61, which requires that the undamaged containment system withstand an external water pressure of 290 psi for a period of not less than one hour without collapse, buckling, or in-leakage of water. Section 2.7.7, *Deep Water Immersion Test (for Type B Packages Containing More than 10⁵ A₂)*, demonstrates that the transportation package meets the requirements of 10 CFR §71.61, which bounds the requirements of 10 CFR §71.73(c)(6).

2.7.7 Deep Water Immersion Test (for Type B Packages Containing More than 10⁵ A₂)

Subpart E of 10 CFR 71 specifies performance of a deep immersion test in accordance with the requirements of 10 CFR §71.61. Since the MFFP contains more than 10⁵ A₂ of any isotope, a buckling evaluation for the 200 meter deep immersion test is performed. The evaluation is performed utilizing ASME Code Case N-284-1 and considers an external pressure of 290 psig, which exceeds the pressure of 200 meters of water.

Consistent with Regulatory Guide 7.6 philosophy, a factor of safety corresponding to ASME B&PV Code, Service Level D conditions for the hypothetical accident condition pressure loading is employed. In this case, the applicable factor of safety is 1.34 for accident conditions, as specified in ASME B&PV Code Case N-284-1.

Buckling analysis geometry parameters are provided in Table 2.7-5, and loading parameters are given in Table 2.7-6. The buckling analysis conservatively utilizes shell temperatures consistent with Section 2.6.1, *Heat*, i.e., 160 °F. The stresses are determined using the external pressure of 290 psi. The hoop stress, σ_{θ} , axial stress, σ_{ϕ} , and in-plane shear stress, $\sigma_{\phi\theta}$, are found from:

$$\sigma_{\theta} = \frac{Pr}{t} \quad \sigma_{\phi} = \frac{Pr}{2t} \quad \sigma_{\phi\theta} = \frac{Pr}{4t}$$

where P is the applied pressure, r is the mean radius, and t is the shell thickness. As shown in Table 2.7-7, all the interaction check parameters are less than 1.0, as required. Therefore, buckling of the shell due to a deep immersion is not of concern.

The same analytical methods presented in Section 2.6.1.3.1, *Stresses Due to Pressure Loading*, which are used to determine the stress due to the 25 psig design pressure, are applicable for the 290 psig deep immersion pressure. The stress results are linear and therefore the stress results of Section 2.6.1.3.1, *Stresses Due to Pressure Loading*, are multiplied by the ratio of 290/25 = 11.6. For the HAC MFFP containment design temperature of 160 °F, the allowable primary membrane stress for Type XM-19 stainless steel is the lesser of (2.4)S_m and 0.7S_u, which is equal to 69,748 psi. The allowable primary membrane-plus-bending stress of Type XM-19 stainless steel is the lesser of (3.6)S_m and S_u, which is equal to 99,640 psi. The bottom closure plate, closure lid, and shell stress and resulting margins of safety are shown in Table 2.7-8, which lists the minimum margin of safety as +1.96.

2.7.8 Summary of Damage

As discussed in the previous sections, the cumulative damaging effects of free drop and puncture drop tests are satisfactorily withstood by the MFFP, as demonstrated by certification testing (see Appendix 2.12.3, *Certification Test Results*) and analysis (see Sections 2.7.1, *Free Drop*, through 2.7.7, *Deep Water Immersion (for Type B Packages Containing More than 10⁵ A₂)*, and Appendix 2.12.5, *Fuel Control Structure Evaluation*). Helium leak testing performed prior to and subsequent to each test series confirmed that containment integrity was maintained throughout the test series. The thermal analyses presented in Chapter 3.0, *Thermal Evaluation*, demonstrate that the containment seals, which are the most temperature sensitive material in the MFFP, remain below the limiting temperature of 400 °F. The thermal evaluation includes the effect of accumulated damage from the free and puncture drop tests (conservatively neglecting the improvement to the impact limiter welded corner joint design, described in Appendix 2.12.7, *Impact Limiter Weld Joint Test Results*). The fuel assembly payload remains subcritical, as demonstrated in Chapter 6.0, *Criticality Evaluation*. Therefore, the requirements of 10 CFR §71.73 have been met.

Table 2.7-1 – Free Drop Test Summary

Test No.	Test Description	Addresses
Series 1, Test 1	Horizontal 30-ft free drop	Containment shell buckling
Series 2, Test 1	C.G.-over-corner (80° from horizontal) 30-ft free drop	Closure lid integrity; prototypic fuel integrity
Series 3, Test 1	15° Slapdown 30-ft free drop, lid primary	Strongback deformations
Series 3, Test 2	15° Slapdown 30-ft free drop, lid secondary	Strongback deformations, closure lid integrity
Additional Test (Repeat of Series 2, Test 1)	C.G.-over-corner (80° from horizontal) 30-ft free drop	Using accelerometers to gather more acceleration data for this orientation.

Table 2.7-2 – Summary of Payload Used for Certification Testing

Series No.	Payload
Series 1	Mock Payload, criticality control not tested
Series 2	Strongback, 1 Prototypic FA, 2 Dummy FAs
Series 3	Strongback, 3 Dummy FAs
Additional Test (single free drop)	Strongback, 3 Dummy FAs

Table 2.7-3 – Puncture Drop Test Summary

Test No.	Test Description	Addresses
Series 1, Test 2	Puncture drop axial to limiter	Impact limiter retention, impact limiter shell weld integrity.
Series 1, Test 3	Oblique puncture drop on bottom disk	Perforation of lid end impact limiter skin
Series 1, Test 4	Oblique puncture drop on tapered skin	Perforation of lid end impact limiter skin
Series 2, Test 2	C.G.-over-corner puncture drop on free drop damage	Effect of puncture on prior damage; puncture load on closure region
Series 3, Test 3	Horizontal puncture drop on containment shell	Containment shell leaktight integrity
Series 3, Test 4	Oblique puncture drop on containment shell	Containment shell leaktight integrity

Table 2.7-4 – HAC Thermal Pressure Stresses and Margins of Safety

Component	Stress at 25 psi Internal Pressure (psi)	Stress at 130 psi Internal Pressure (psi)	Allowable Stress (psi)	Margin of Safety
Shell	674	3,505	11,055	+2.15
Closure Lid	1,510	7,852	65,940	+7.40
Bottom End Closure	2,904	15,101	65,940	+3.37

Table 2.7-5 – Buckling Geometry Parameters per Code Case N-284-1

Geometry, Temperature, and Material Input	Shell
Outside Diameter, inch	29.63
Inside Diameter, inch	28.50
Length, inch	168.20
Temperature, °F	160
Geometry Output (nomenclature consistent with ASME Code Case N-284-1)	
R =	14.53
t =	0.56
R/t =	25.72
$\lambda_\phi =$	168.20
$\lambda_\theta =$	91.31
$M_\phi =$	58.70

Table 2.7-6 – Stress Results for 290 psig External Pressure

Direction	Stress (psi)
Axial Stress, σ_ϕ	3,762
Hoop Stress, σ_θ	7,524
Shear Stress, $\sigma_{\phi\theta}$	1,881

Table 2.7-7 – Buckling Summary for 290 psig External Pressure

Condition	Shell	Remarks
Capacity Reduction Factors (-1511)		
$\alpha_{\phi L} =$	0.5094	
$\alpha_{\square L} =$	0.8000	
$\alpha_{\phi \theta L} =$	0.8000	
Plasticity Reduction Factors (-1610)		
$\eta_{\phi} =$	0.1509	
$\eta_{\theta} =$	1.0000	
$\eta_{\phi \theta} =$	0.3567	
Theoretical Buckling Values (-1712.1.1)		
$C_{\phi} =$	0.6050	
$\sigma_{\phi e L} =$	653,895	psi
$C_{\theta r} =$	0.0137	
$\sigma_{\theta e L} = \sigma_{r e L} =$	14,809	psi
$C_{\theta h} =$	0.0137	
$\sigma_{\theta e L} = \sigma_{h e L} =$	14,809	psi
$C_{\phi \theta} =$	0.0974	
$\sigma_{\phi \theta e L} =$	105,239	psi
Elastic Interaction Equations (-1713.1.1)		
$\sigma_{xa} =$	248,565	psi
$\sigma_{ha} =$	8,841	psi
$\sigma_{ra} =$	8,841	psi
$\sigma_{ta} =$	62,829	psi
Axial + Hoop \Rightarrow Check (a):	...N/A	
Axial + Hoop \Rightarrow Check (b):	...N/A	
Axial + Shear \Rightarrow Check (c):	0.0160	<1 ∴ OK
Hoop + Shear \Rightarrow Check (d):	0.8519	<1 ∴ OK
Axial + Hoop + Shear \Rightarrow Check (e):	...N/A	
Axial + Hoop + Shear \Rightarrow Check (f):	...N/A	
Inelastic Interaction Equations (-1713.2.1)		
$\sigma_{xc} =$	37,507	psi
$\sigma_{rc} =$	8,841	psi
$\sigma_{tc} =$	22,411	psi
Axial + Hoop \Rightarrow Check (a):	0.8510	<1 ∴ OK
Axial + Shear \Rightarrow Check (a):	0.1073	<1 ∴ OK
Hoop + Shear \Rightarrow Check (b):	0.8581	<1 ∴ OK

Table 2.7-8 – Deep Water Immersion Test Stresses (psi) and Margins of Safety

Component	25 psi Internal Pressure Stress	290 psi External Pressure Stress	Allowable Stress	Margin of Safety
Shell	674	7,818	69,748	+7.92
Closure Lid	1,510	17,516	99,640	+4.69
Bottom End Closure	2,904	33,686	99,640	+1.96

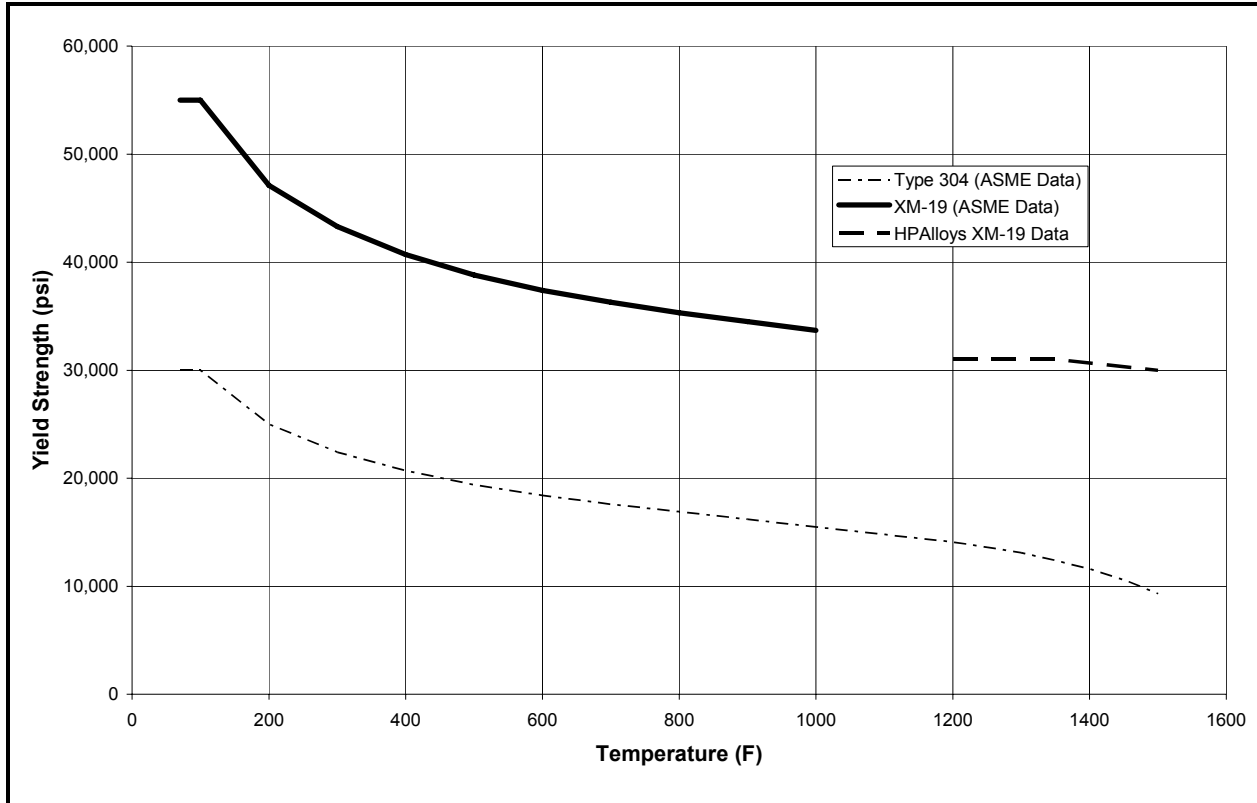


Figure 2.7-1 – Yield Strength vs. Temperature for Type 304 and XM-19 Materials

2.8 Accident Conditions for Air Transport of Plutonium

This section does not apply for the MFFP, since air transport is not claimed.

This page left intentionally blank.

2.9 Accident Conditions for Fissile Material Packages for Air Transport

This section does not apply for the MFFP, since air transport is not claimed.

This page left intentionally blank.

2.10 Special Form

This section does not apply for the MFFP, since special form is not claimed.

This page left intentionally blank.

2.11 Fuel Rods

This section does not apply for the MFFP, since containment by the fuel rod cladding is not claimed.

This page left intentionally blank.

2.12 Appendices

- 2.12.1 Impact Limiter Evaluation
- 2.12.2 Certification Test Plan
- 2.12.3 Certification Test Results
- 2.12.4 Engineering Test Results
- 2.12.5 Fuel Control Structure Evaluation
- 2.12.6 CASKDROP Computer Program
- 2.12.7 Impact Limiter Weld Joint Test Results
- 2.12.8 Effect of Bounding Weight on Package Structural Responses

This page left intentionally blank.

2.12.1 Impact Limiter Evaluation

The following appendix evaluates and extrapolates the certification test results of the 30-foot free drops with cold (-20 °F) impact limiters, in order to provide analytical determination that the polyurethane foam crush strain will remain within design limits during warm conditions.

Bounding force-deflection curves are developed for both the lid and bottom end impact limiters for a variety of drop orientations. Each force-deflection relation is based on the impact limiter design and on dynamic, temperature-adjusted material properties of the energy-absorbing materials used. The development of material properties and the force-deflection relations are described in the following subsections.

2.12.1.1 Material Properties

The MFFP impact limiters consist of polyurethane foam within Type 304 stainless steel shells. The limiter shape is tapered at the outer end to reduce end drop forces and to eliminate limiter attachment separation loads.

The crush strength of the polyurethane foam varies with temperature. From Chapter 3.0, *Thermal Evaluation*, the bulk average foam temperature under NCT is bounded by 145 °F, which is used to evaluate warm foam properties. The use of bulk average temperature is conservative, since the foam actually crushed is located in the outer region of the impact limiter, where the material temperature is below the bulk average. The minimum foam temperature for HAC is -20 °F.

Measurements of the crush strength at cold (-20 °F) and hot (140 °F) temperatures for both perpendicular and parallel rise directions were performed and are provided in Table 2.12.1-1.

Note: This analysis is performed for a hot temperature of 140 °F; however the average bulk temperature of limiters from Table 3.4-1 of Chapter 3.0, *Thermal Evaluation*, is 145 °F. Effect of this temperature difference is discussed in Section 2.12.1.2, *Force-Deflection Relationships*.

The design crush strength data in Table 2.12.1-1 is given at three strains: 10%, 40%, and 70%. This data is adequate to fully characterize the foam. However, more information is required to perform calculations required for this evaluation. The design stress-strain curve is resolved between the design data points given using a ‘shape factor’. The ‘shape factor’ is developed using published data from the foam manufacturer (General Plastics¹). Table 2.12.1-2 provides the inputs and results of the ‘shape factor’ calculation. These factors illustrate the relationship between the published crush strength at 10%, 40%, and 70% strain and the intermediate values of strain. The column headed “Calculation Method” shows which data is used to calculate the shape factor at any given strain.

For example, the perpendicular-to-rise crush strength at a strain of 30% is 327 psi, and at 40% strain, it is 354 psi. The shape factor is the ratio of these two values, or:

¹ *General Plastics Last-a-Foam® for Crash and Fire Protection of Nuclear Material Shipping Containers*, General Plastics Manufacturing Company.

$$SF_{\text{PERP}} = \frac{\sigma_{30}}{\sigma_{40}} = \frac{327}{354} = 0.9237$$

In other words, the perpendicular-to-rise crush strength of 10 lb/ft³ foam at 30% strain and ambient temperature is equal to 0.9237 times the crush strength at 40% strain. Similarly, to take another example, the parallel-to-rise crush strength of the same foam at a strain of 65% is 0.7309 times the crush strength at a strain of 70%. In this way, a smooth curve can be generated for analysis using the shape factors and crush data at 10%, 40%, and 70% strain.

To validate this method for the used range of foam densities and temperatures, a comparison is made between published crush strengths and the design crush strengths generated using shape factors. The results are shown in Table 2.12.1-3. Crush strengths for 10 lb_m/ft³ foam at -20 °F and 140 °F, and 12 lb_m/ft³ foam at ambient temperature, -20 °F and 140 °F, are listed. In the first two columns, the published crush strength data is listed as extracted from the database. In the second two columns, the computed crush strength data is generated by applying the shape factors to the published values at 10%, 40%, and 70% strain. The last two columns document the percentage difference which was achieved. For strain levels of 75% and below, the difference never exceeds 5%, and therefore the resolved design stress-strain curves generated by applying the shape factors are sufficiently accurate for the analysis. The difference is greater for 80% strain, but since the highest strain calculated in this evaluation is 76%, the 80% strain data is not used.

Moreover, the variation of crush strength due to manufacturing tolerance is also taken into account. The strength of the polyurethane foam used in the impact limiter is controlled by three test specimens for each production batch pour. The maximum allowable variation in crush strength (tested at 10%, 40%, and 70% strains) for the average variation of crush strength for all pours used in the impact limiter is held to ±15%.

Conservative application of the polyurethane foam manufacturing tolerance requires that the low strength material (nominal-minus-15%) be applied at warm conditions (to maximize deformation), and that the higher strength material (nominal-plus-15%) be applied at cold conditions (to maximize impact load).

In the same manner, the crush strength of polyurethane foam can also vary between static and dynamic conditions. The dynamic effect for polyurethane foam is found from:

$$D = 1.32S + 0.00015(S^2), \text{ psi}$$

where S is the static crush strength and D is the dynamic crush strength. This relationship is extracted from General Plastics' data and applies at ambient (75 °F) temperature for strain rates between approximately 30 in/sec/in and 100 in/sec/in.

Results of manufacturing and dynamic effects are provided in Table 2.12.1-4.

Finally, as the foam properties vary with the direction of crush, the preceding curves for both perpendicular (D_{per}) and parallel (D_{par}) directions are combined to include the drop test orientation using an ellipse function, as described in Appendix 2.12.6, *CASKDROP Computer Program*.

If θ is the drop test angle with the horizontal, the crush strength at any orientation will be:

$$D_{\theta} = \frac{1}{\sqrt{\left(\frac{\sin \theta}{D_{\text{par}}}\right)^2 + \left(\frac{\cos \theta}{D_{\text{per}}}\right)^2}}$$

2.12.1.2 Force-Deflection Relationships

The impact experienced by the MFFP in NCT or HAC free drops is a direct function of the force-deflection relations of the impact limiters. These force-deflection relations vary as the orientation to the impact surface is varied, and are a function of the limiter geometry and impact-absorbing material properties. The force-deflection curve is determined as a sum of the force contribution of the foam and the shell for the lid end limiter in which the stainless steel envelope is 1/4-inch. For the bottom limiter, the effect of the stainless steel envelope is neglected as it is thinner (1/8-inch).

The force-deflection contribution of the foam portion is calculated using the computer program CASKDROP. Given an impact limiter external geometry, orientation to the impacting surface, and material properties, CASKDROP performs a two-dimensional integration over the crush area of the foam for increment of deflection. The integration process sums the force contribution from each differential element by determining each deflection increment for the crush strain in that element. Given the crush strain, the program consults a stress-strain table of the impact limiter material to determine crush stress. The differential element's force is simply the product of the crush stress and the element's area. The output consists of total foam crush force as a function of deflection from the point of initial contact with the impact surface and is extracted directly from CASKDROP output. However, this output does not include the effect of the impact limiter's 1/4-inch thick steel shell. The method for determining the "foam with steel" force-deflection curve is detailed below:

Stainless Steel Shell: To take into account the 1/4-inch thick stainless steel shell of the lid end impact limiter, a 1.47 bias (equivalent to a 47% strength increase) is applied to the foam crush strength at ambient temperature. This bias is based on the results of the engineering tests and is confirmed by the comparison of the results with the drop test measurements (see Table 2.12.1-7).

1. In order to isolate the effect of the steel, CASKDROP is run for the MFFP geometry at a given primary impact angle for "with shell" (which includes the 47% strength increase) and "without shell" cases for a nominal 10 lb_m/ft³ foam at ambient temperature.
2. The difference of the two resulting force-deflection curves is equal to the force-deflection curve of the steel shell at the appropriate drop angle.
3. The resulting "steel only" force-deflection curve may be added to "foam only" force-deflection curves resulting from CASKDROP runs at bounding temperatures and manufacturing tolerances.
4. The net force-deflection curve may be used to predict deflections and impact level for the various temperatures and drop angles.

The input data for the CASKDROP program are tabulated in Table 2.12.1-5.

Effect of temperature: As stated previously, the analysis is performed with foam properties at 140 °F instead of 145 °F according to Table 3.4-1 of Chapter 3.0, *Thermal Evaluation*. The CASKDROP program has a polyurethane foam database of crush strength function of an input temperature. When running two input files differing just on the temperature (one at 140 °F, the other at 145 °F), the difference on the force-deflection results is about 1%, which is negligible, and will not significantly change the results of this analysis.

2.12.1.3 Force-Deflection Curves

Plots of force-deflection relations are provided in Figure 2.12.1-1 through Figure 2.12.1-7 for the lid end impact limiter, and in Figure 2.12.1-8 through Figure 2.12.1-14 for the bottom end impact limiter, for orientations of the axis relative to the impact surface of 0° (horizontal), 15°, 30°, 45°, 60°, 80°, and 90° (vertical). The upper bound (cold) and lower bound (warm) curves are given in each plot. The force-deflection curves are a direct result of adding the “steel only” force-deflection data to the “foam only” force-deflection curves.

As the force-deflection curves at hot temperature (145 °F) are below the cold temperature (-20 °F) ones, the free drop tests at hot temperature will result in a lower impact force and therefore, lower acceleration on the package components. A higher crush of the impact limiter will result at the hot temperature.

The foam crush should remain below an acceptable strain level (below 75%) to avoid the “lock up” phenomena. “Lock-up” occurs when foam density approaches a solid polymer condition, which could result in higher accelerations. The following section calculates the crush of the impact limiters at hot temperature conditions to demonstrate that “lock up” does not occur.

2.12.1.4 Impact Analysis Method

The SLAPDOWN² program is used to analyze the impact of transportation packages with an unyielding surface during a free drop. It is particularly useful when the center of gravity is not directly over the impact point. Under these circumstances, the package will generally hit, begin to rotate, and strike the ground a second time as a “slapdown” impact. SLAPDOWN conducts a time-integration analysis using a model of the package as a rigid rod, and of the impact limiters as non-linear springs. Given a drop height, the package has an initial velocity at impact. The energy is absorbed first by the primary spring (called the “Nose” limiter), which imparts a rotational force to the model, until the secondary spring comes in contact (called the “Tail” limiter). Most of the energy absorbed by the springs is lost, except the portion that is restored by springback. The position, angle, velocity, and acceleration in both linear and rotational modes are calculated for each time step.

For the case at cold temperature, the objective is to compare the results from SLAPDOWN program to the test measurements performed after the drop tests at -20 °F (see Appendix 2.12.3, *Certification Test Results*). For a valid comparison, the input data in SLAPDOWN program are close to the CTU data, as follow:

- Breakdown of mass representing CTU (difference with measurements is negligible):
 - body = 10,790 pounds (1.2% greater than Test Series 2 and 3 CTUs, and 4.3 % less than Test Series 1 CTU)
 - lid end limiter = 1,480 pounds (0.4% greater than CTU measurements)
 - bottom end limiter = 1,080 pounds (1.3% greater than CTU measurements)
 - total = 13,350 pounds (maximum difference of 3% with CTU measurements).
- For “slapdown” cases (drop angles from 15° to 30°), a friction coefficient of 0.3 is added in the input file of the SLAPDOWN program. Indeed, during the drop test performed on the

² G. D. Sjaardema and G. W. Wellman, *Numerical and Analytical Methods for Approximating the Eccentric Impact Response (Slapdown) of Deformable Bodies*, Sandia Report SAND88-0616 UC-71, Sandia National Laboratories.

CTU, the package is seen sliding on the impact surface after the first impact and during its rotation. This assumption is validated by good agreement between calculated and test measurements (refer to Section 2.12.1.5, *Impact Analysis at Cold Temperature*).

For the case at hot temperature, the aim is to determine the maximum deformation of the limiters. Then, the input data in SLAPDOWN program are the design data, as follow:

- Breakdown of mass:
 - body = 11,540 pounds
 - lid end limiter = 1,490 pounds
 - bottom end limiter = 1,100 pounds
 - total = 14,130 pounds

The body and in turn the total weight used for the analysis is 130 lbs less than the weights listed in Table 2.1-3 of Section 2.1.3, *Weights and Center of Gravity*. However, it is reasonable to conclude that the difference in weights would have an insignificant affect on the results because the missing weight corresponds to only 0.9% of the total weight.

- For “slapdown” cases (drop angles from 15° to 45°), a friction coefficient of 0.3 is added in the input file of the SLAPDOWN program.

The input data for the SLAPDOWN program is stated in Table 2.12.1-6.

The rotational moment of inertia³ of a solid cylinder about a perpendicular axis, through the center of gravity is:

$$J = \frac{M}{12}(3R^2 + H^2), \text{ in}^4$$

The total rotational moment of inertia is determined by combination of 3 parts:

1. The body is defined as a cylinder with an outer radius $R = 14.81$ inches, a length $H = 171.3$ inches.
2. The lid end impact limiter defined as cylinder with a radius $R = 30$ inches, a length $H = 35$ inches, distant from the center of gravity of the package of $L = 85.67$ inches.
3. The bottom end impact limiter defined as cylinder with a radius $R = 30$ inches, a length $H = 35$ inches, distant from the center of gravity of the package of $L = 85.67$ inches.

The total rotational moment of inertia is:

$$J_{\text{total}} = J_{\text{body}} + (J_{\text{upper}} + M_{\text{upper}} L^2) + (J_{\text{lower}} + M_{\text{lower}} L^2), \text{ in}^4$$

2.12.1.5 Impact Analysis at Cold Temperature

To validate the method of analysis, the SLAPDOWN program results are compared to the test measurements performed after the drop tests at -20 °F (see Appendix 2.12.3, *Certification Test Results*).

³ J.L. Meriam, L.G. Kraige, *Engineering Mechanics – Dynamics*, Fourth Edition.

The results in Table 2.12.1-7 demonstrate that the SLAPDOWN results are conservative on displacement compared to the drop test measurements, especially for the secondary impact during “slapdown” drop tests (i.e., 15° orientation).

2.12.1.6 Impact Analysis at Hot Temperature

The results in Table 2.12.1-8 show that the crush of the foam in the impact limiters during drop tests at hot temperature remain acceptable (below 75%), except for the 60° drop angle, when the crush strain is slightly over the limit (76%).

However, the method of calculation uses the following conservatisms:

1. The input assumptions are the maximum weight of the package, and the “weakest” foam.
2. The comparison of calculated and measured values in Table 2.12.1-7 demonstrates that for high angle drop test (80°), the crush is overestimated by approximately 40%.
3. Due to the geometry of the 60° drop angle, the foam area where the strain is close to the limit of 75% is small. Indeed, the strain value is the ratio of the crush thickness to the initial available foam thickness. As shown in Figure 2.12.1-15, the maximum strain calculated by the CASKDROP program is on a local area. The local effect of this high strain is negligible, compared to the total overall crush surface.

Due to the conservatisms noted above, the result that exceeds the 75% strain “lock up” limit by approximately 1% are negligible. Therefore, this condition will have no consequence on the package effectiveness.

2.12.1.7 Worst-Case Slapdown Angle

As discussed in Section 2.12.1.4, *Impact Analysis Method*, the SLAPDOWN program calculates position, angle, velocity and acceleration in both linear and rotational modes for a given slapdown orientation. The most damaging slapdown angle is defined as the angle that maximizes the acceleration.

Accelerations are extracted from the SLAPDOWN output files in Section 2.12.1.5, *Impact Analysis at Cold Temperature*, adding one calculation for the 30° configuration with primary impact on the lid end (all inputs utilized the values in Table 2.12.1-6).

The results demonstrate that the worst-case angle for the MFFP is 15°, regardless of which end impacts first. The slapdown analysis results are presented in Table 2.12.1-9 and shown in Figure 2.12.1-16.

Table 2.12.1-1 – Design Crush Strength of the Foam (psi)

Temperature	Strain	10 pcf Polyurethane Foam		11½ pcf Polyurethane Foam	
		Perpendicular ^①	Parallel ^①	Perpendicular ^①	Parallel ^①
Ambient ^②	10%	330 ^②	358 ^②	435 ^②	470 ^②
Ambient ^②	40%	398 ^②	416 ^②	540 ^②	555 ^②
Ambient ^②	70%	1,115 ^②	1,124 ^②	1,725 ^②	1,660 ^②
Cold (-20 °F)	10%	413.5	438.5	562.6	591.8
Cold (-20 °F)	40%	487.1	504.0	665.5	682.5
Cold (-20 °F)	70%	1,390.3	1,370.0	1,979.4	1,873.1
Hot (140 °F)	10%	246.0	261.0	346.3	361.3
Hot (140 °F)	40%	300.2	318.3	430.5	443.3
Hot (140 °F)	70%	805.8	818.8	1,248.2	1,205.7

Notes:

- ① Perpendicular-to-rise corresponds to a radial direction in the limiter (perpendicular to the main axis of the body). Parallel-to-rise corresponds to an axial direction in the limiter (parallel to the main axis of the body).
- ② Values at ambient temperature are taken from the nominal material properties as defined in Section 2.2, *Materials*, Tables 2.2-7 and 2.2-8.

Table 2.12.1-2 – Derivation of Shape Factors

Strain		Perpendicular to Rise		Parallel to Rise		Calculation Method
		Crush Stress, psi	Shape Factor	Crush Stress, psi	Shape Factor	
10%	σ_{10}	284	-	301	-	-
20%	σ_{20}	296	1.0423	302	1.0033	$= \sigma_{20} / \sigma_{10}$
30%	σ_{30}	327	0.9237	325	0.8978	$= \sigma_{30} / \sigma_{40}$
40%	σ_{40}	354	-	362	-	-
50%	σ_{50}	415	1.1723	435	1.2017	$= \sigma_{50} / \sigma_{40}$
60%	σ_{60}	593	1.6751	594	1.6409	$= \sigma_{60} / \sigma_{40}$
65%	σ_{65}	766	0.7213	747	0.7309	$= \sigma_{65} / \sigma_{70}$
70%	σ_{70}	1,062	-	1,022	-	-
75%	σ_{75}	1,604	1.5104	1,527	1.4941	$= \sigma_{75} / \sigma_{70}$
80%	σ_{80}	3,095	2.9143	2,853	2.7916	$= \sigma_{80} / \sigma_{70}$

Table 2.12.1-3 – Validation of Shape Factors

Strain	Crush Strength Data (psi) ^⓪		Computed Crush Strength (psi) ^⓪		Difference	
	Perp (⊥)	Par (//)	Perp (⊥)	Par (//)	Perp (⊥)	Par (//)
Foam density 10 pcf at cold temperature (-20 °F)						
10%	437	507	437	507	-	-
20%	447	497	455	509	2%	2%
30%	472	517	481	506	2%	-2%
40%	521	564	521	564	-	-
50%	621	655	611	678	-2%	4%
60%	850	877	873	925	3%	5%
65%	1,068	1,101	1016	1061	-5%	-4%
70%	1,409	1,451	1,409	1,451	-	-
75%	2,111	2,086	2128	2168	1%	4%
80%	3,635	3,474	4106	4051	13%	17%
Foam density 10 pcf at hot temperature(140 °F)						
10%	246	281	246	281	-	-
20%	256	276	256	282	0%	2%
30%	277	298	289	299	4%	0%
40%	313	333	313	333	-	-
50%	376	397	367	400	-2%	1%
60%	516	529	524	546	2%	3%
65%	655	682	638	670	-3%	-2%
70%	884	917	884	917	-	-
75%	1,313	1,371	1335	1370	2%	0%
80%	2,260	2,354	2576	2560	14%	9%
Foam density 12 pcf at ambient temperature						
10%	430	464	430	464	-	-
20%	448	466	448	466	0%	0%
30%	480	499	498	498	4%	0%
40%	539	555	539	555	-	-
50%	660	670	632	667	-4%	0%
60%	938	933	903	911	-4%	-2%
65%	1,226	1,191	1241	1202	1%	1%
70%	1,721	1,645	1,721	1,645	-	-
75%	2,566	2,472	2599	2458	1%	-1%
80%	4,432	4,419	5016	4592	13%	4%

Strain	Crush Strength Data (psi) ^①		Computed Crush Strength (psi) ^②		Difference	
	Perp (⊥)	Par (//)	Perp (⊥)	Par (//)	Perp (⊥)	Par (//)
Foam density 12 pcf at cold temperature (-20 °F)						
10%	614	676	614	676	-	-
20%	634	675	640	679	1%	1%
30%	671	709	689	705	3%	-1%
40%	746	785	746	785	-	-
50%	898	932	874	943	-3%	1%
60%	1,246	1,278	1249	1288	0%	1%
65%	1,572	1,620	1486	1562	-5%	-4%
70%	2,060	2,138	2,060	2,138	-	-
75%	3,110	3,098	3112	3194	0%	3%
80%	5,555	5,225	6005	5968	8%	14%
Foam density 12 pcf at hot temperature (140 °F)						
10%	342	371	342	371	-	-
20%	359	375	357	372	-1%	-1%
30%	390	407	409	413	5%	1%
40%	442	460	442	460	-	-
50%	538	557	518	553	-4%	-1%
60%	752	764	741	755	-1%	-1%
65%	964	993	950	990	-1%	0%
70%	1,317	1,355	1,317	1,355	-	-
75%	1,979	2,060	1990	2024	1%	-2%
80%	3,490	3,612	3839	3782	10%	5%

Notes:

- ① The “Crush strength data” column is taken from the General Plastics’ data.
- ② The “Computed Crush Strength” is the application of the shape factors on 10%/40%/70% strain values.

Table 2.12.1-4 – Determination of the Dynamic Crush Strength Curves (psi)

Strain	Crush Strength Curve [®]		Manufacturing Tolerance [®]		Dynamic Crush Strength	
	Perp (⊥)	Par (//)	Perp (⊥)	Par (//)	Perp (⊥)	Par (//)
Foam density 10 pcf at ambient temperature						
10%	330	358	330	358	452	492
20%	344	359	344	359	472	493
30%	368	373	368	373	506	513
40%	398	416	398	416	549	575
50%	467	500	467	500	649	698
60%	667	683	667	683	947	972
65%	804	822	804	822	1,158	1,186
70%	1,115	1,124	1,115	1,124	1,658	1,675
75%	1,684	1,681	1,684	1,681	2,648	2,643
80%	3,249	3,141	3,249	3,141	5,872	5,626
Foam density 10 pcf at cold temperature (-20 °F)						
10%	413.5	438.5	476	504	662	703
20%	431	440	496	506	692	706
30%	450	452	518	520	724	727
40%	487.1	504.0	560	580	786	816
50%	571	606	657	697	932	993
60%	816	827	938	951	1,370	1,391
65%	1,003	1,001	1,153	1,151	1,721	1,718
70%	1,390.3	1,370.0	1,599	1,576	2,494	2,453
75%	2,100	2,047	2,415	2,354	4,063	3,938
80%	4,052	3,824	4,660	4,398	9,409	8,707
Foam density 10 pcf at hot temperature(140 °F)						
10%	246.0	261.0	209	222	282	300
20%	256	262	218	223	295	302
30%	277	286	235	243	318	330
40%	300.2	318.3	255	271	346	369
50%	352	382	299	325	408	445
60%	503	522	428	444	592	616
65%	581	598	494	508	689	709
70%	805.8	818.8	685	696	975	991
75%	1,217	1,223	1,034	1,040	1,525	1,535
80%	2,348	2,286	1,996	1,943	3,232	3,131
Foam density 11½ pcf at ambient temperature						
10%	435	470	435	470	603	654
20%	453	472	453	472	629	656
30%	499	498	499	498	696	695
40%	540	555	540	555	757	779
50%	633	667	633	667	896	947
60%	905	911	905	911	1,317	1,327

Strain	Crush Strength Curve ^①		Manufacturing Tolerance ^②		Dynamic Crush Strength	
	Perp (⊥)	Par (//)	Perp (⊥)	Par (//)	Perp (⊥)	Par (//)
65%	1,244	1,213	1,244	1,213	1,874	1,822
70%	1,725	1,660	1,725	1,660	2,723	2,605
75%	2,605	2,480	2,605	2,480	4,457	4,196
80%	5,027	4,634	5,027	4,634	10,426	9,338
Foam density 11½ pcf at cold temperature (-20 °F)						
10%	562.6	591.8	647	681	917	968
20%	586	594	674	683	958	972
30%	615	613	707	705	1,008	1,005
40%	665.5	682.5	765	785	1,098	1,129
50%	780	820	897	943	1,305	1,378
60%	1,115	1,120	1,282	1,288	1,939	1,949
65%	1,428	1,369	1,642	1,574	2,572	2,449
70%	1,979.4	1,873.1	2,276	2,154	3,781	3,539
75%	2,990	2,799	3,439	3,219	6,313	5,803
80%	5,769	5,229	6,634	6,013	15,358	13,361
Foam density 11½ pcf at hot temperature (140 °F)						
10%	346.3	361.3	294	307	401	419
20%	361	363	307	309	419	422
30%	398	398	338	338	463	463
40%	430.5	443.3	366	377	503	519
50%	505	533	429	453	594	629
60%	721	727	613	618	866	873
65%	900	881	765	749	1,098	1,073
70%	1,248.2	1,205.7	1,061	1,025	1,569	1,511
75%	1,885	1,801	1,602	1,531	2,500	2,373
80%	3,638	3,366	3,092	2,861	5,516	5,004

Notes:

- ① The “Crush Strength Curve” is the application of the shape factors of Table 2.12.1-2 on the data from Table 2.12.1-1.
- ② The effect of manufacturing tolerance is held on data at ambient (nominal), cold (+15%), and hot (-15%) temperatures.

Table 2.12.1-5 – CASKDROP Program Input Data

Input data	Bottom End Limiter^①	Lid End Limiter^②
Impact Limiter Weight, pounds	1,000	1,400
Impact Limiter Outside Diameter, in.	60.0	60.0
Impact Limiter Overall Length, in.	35.0	35.0
Impact Limiter Conical Diameter, in.	36.0	36.0
Impact Limiter Conical Length, in.	15.0	15.0
Impact Limiter End Thickness, in.	15.0	15.0
Impact Limiter Hole Diameter, in.	20.0	20.0
Impact Limiter Hole Length, in.	8.0	8.0
Package and Payload Weight, pounds	13,600	13,600
Body Outside Diameter, in.	29.63	32.30
Body Overall Length, in.	171.3	171.3
Frictional Coefficient	0	0
Drop Height, feet	30.0	30.0
Variable crush stress	Variable ^③	Variable ^③
Drop Angle from Horizontal	Variable	Variable

Notes:

- ① The bottom end limiter is composed of 11½ pcf foam with a thin stainless steel shell (1/8-inch thick).
- ② The lid end limiter is composed of 10 pcf foam with a thick stainless steel shell (1/4-inch thick).
- ③ The complete dynamic crush strength curve as determined in Table 2.12.1-4 and combined with the drop angle.

Table 2.12.1-6 – SLAPDOWN Program Input Data

Input data	Cold temperature	Hot temperature
Length, Nose-to-C.G., in	85.665	85.665 in
Length, Tail-to-C.G. , in	85.665	85.665 in
Radius, Nose Limiter	Variable ^①	Variable ^①
Radius, Tail Limiter, in	30.0	30.0
Body mass, lb _m -s ² /in	34.59	36.61
Rotational moment of inertia ^② , lb _m -s ² /in	120,726	126,216
Drop Height, feet	30.0	30.0
Impact Angle (with Horizontal)	Variable	Variable
Force deflection curves ^③	Variable ^④	Variable ^④
Friction coefficient ^④	0.3 ^⑤	0.3 ^⑤

Notes:

- ① Variable based on the drop angle.
- ② Rotational moment of inertia about a perpendicular axis, through the center of gravity (see below).
- ③ The deflection curves of each impact limiter (Figure 2.12.1-1 through Figure 2.12.1-14). For the “Nose” impact limiter (first impact), the force-deflection curve is the one matching with the drop angle. For the “Tail” limiter (second impact), the force-deflection curve is always the one at 0° orientation.
- ④ For “slapdown” cases (drop angles from 15° to 30°).

Table 2.12.1-7 – Summary of Impact Limiter Deformations at Cold Temperature

Impact Angle wrt ^① Horizontal	Impact ^②	Test Measurements ^③ (inch)	Calculated Deflection (inch)	Calculated Maximum Strain ^④
0°	Both limiters	4.4	6.0	43%
15° ^⑤	First on lid	5.1	6.5	45%
	Second on bottom	4.2	6.9	46%
15° ^⑤	First on bottom	4.4	6.5	41%
	Second on lid	5.2	7.0	51%
30° ^⑤	First on lid	-	6.6	50%
45°	First on lid	-	6.5	49%
60°	First on lid	-	8.8	55%
80°	First on lid	6.1	8.7	56%

Notes:

- ① “With respect to” is abbreviated “wrt”.
- ② Maximum deformation occurs during the secondary slapdown impact of the 15° oblique drop event. All other maximum deformations occur in the primary event.
- ③ Results as measured after the free drop test performed on the CTU (see Appendix 2.12.3, *Certification Test Results*).
- ④ Maximum strain is calculated by the CASKDROP program.
- ⑤ Calculation performed with a friction factor on the “Nose” limiter of 0.3.

Table 2.12.1-8 – Summary of Impact Limiter Deformations at Hot Temperature

Impact Angle wrt ^① Horizontal	Impact ^②	Calculated Deflection (inch)	Calculated Maximum Strain ^③
0°	Both limiters	8.0	58%
15° ^④	First on lid	8.3	58%
	Second on bottom	10.5	69%
15° ^④	First on bottom	9.2	58%
	Second on lid	9.3	67%
30° ^④	First on lid	8.5	67%
45°	First on lid	8.6	68%
60°	First on lid	11.2	76%
80°	First on lid	11.2	73%

Notes:

- ① “With respect to” is abbreviated “wrt”.
- ② Maximum deformation occurs during the secondary slapdown impact of the 15° oblique drop event. All other maximum deformations occur in the primary event.
- ③ Maximum strain is calculated by the CASKDROP program.
- ④ Calculation performed with a friction factor on the “Nose” limiter of 0.3.

Table 2.12.1-9 – Summary of Impact Limiter Accelerations at Cold Temperature

Impact Angle wrt ^① Horizontal	Primary Impact Acceleration (g)	Secondary Impact Acceleration (g)
0°	108	108
-	On bottom	On lid
15° ^②	129	161
30° ^②	124	148
-	On lid	On bottom
15° ^②	128	158
30° ^②	123	146

Notes:

- ① “With respect to” is abbreviated “wrt”.
- ② Calculation performed with a friction factor on the “Nose” limiter of 0.3.

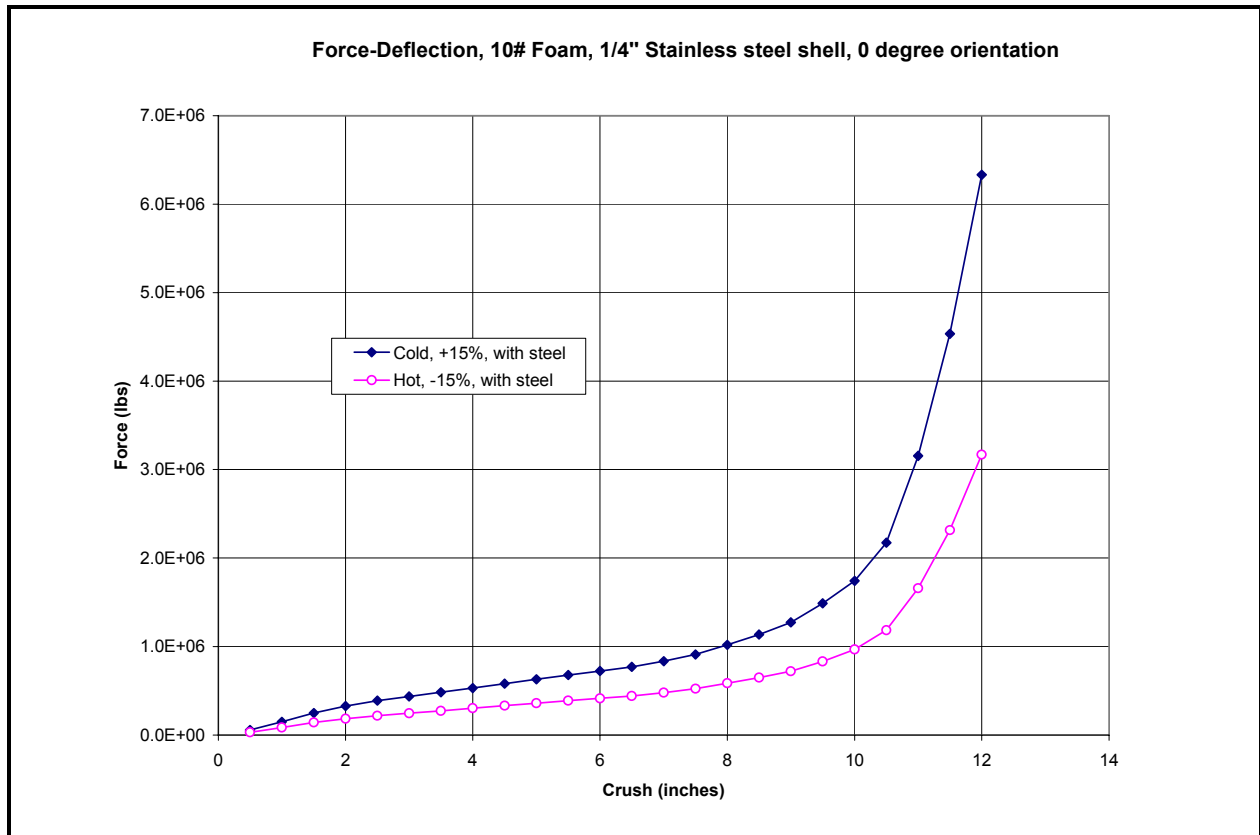


Figure 2.12.1-1 – Lid End Limiter, 0° Impact Angle, Force-Deflection Curve

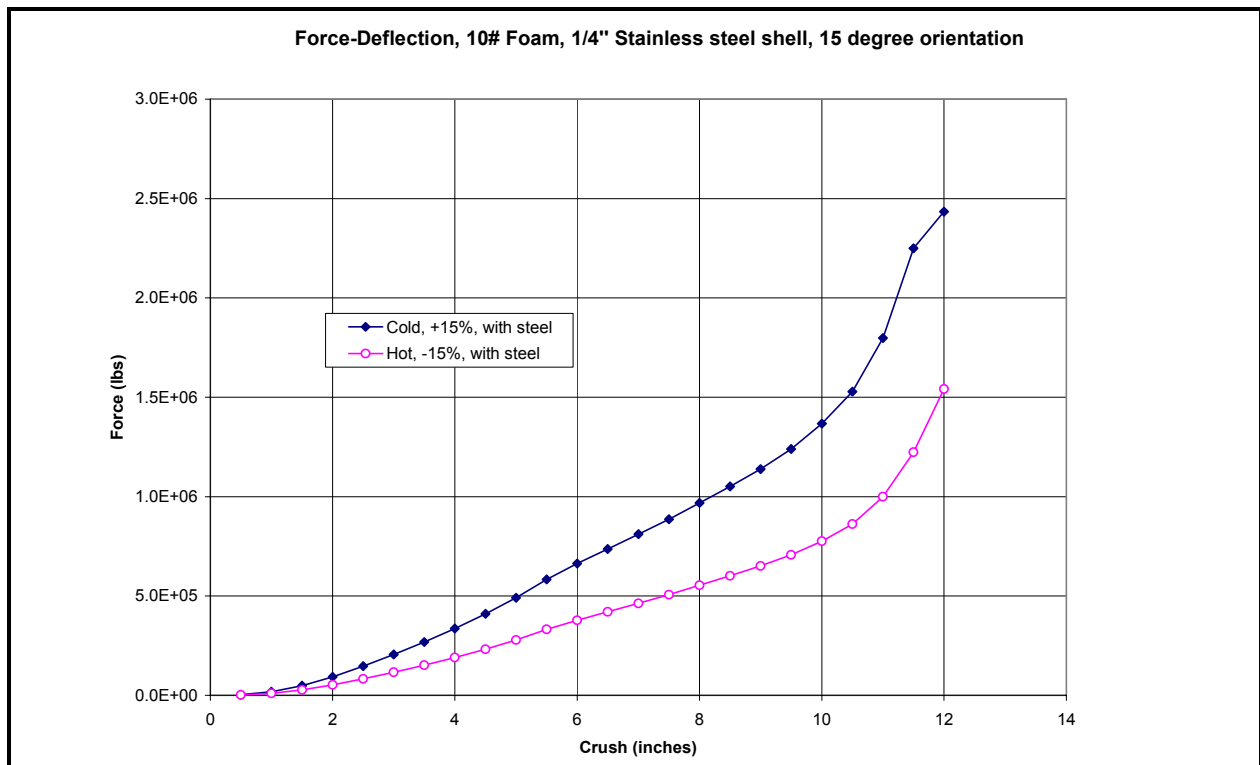


Figure 2.12.1-2 – Lid End Limiter, 15° Impact Angle, Force-Deflection Curve

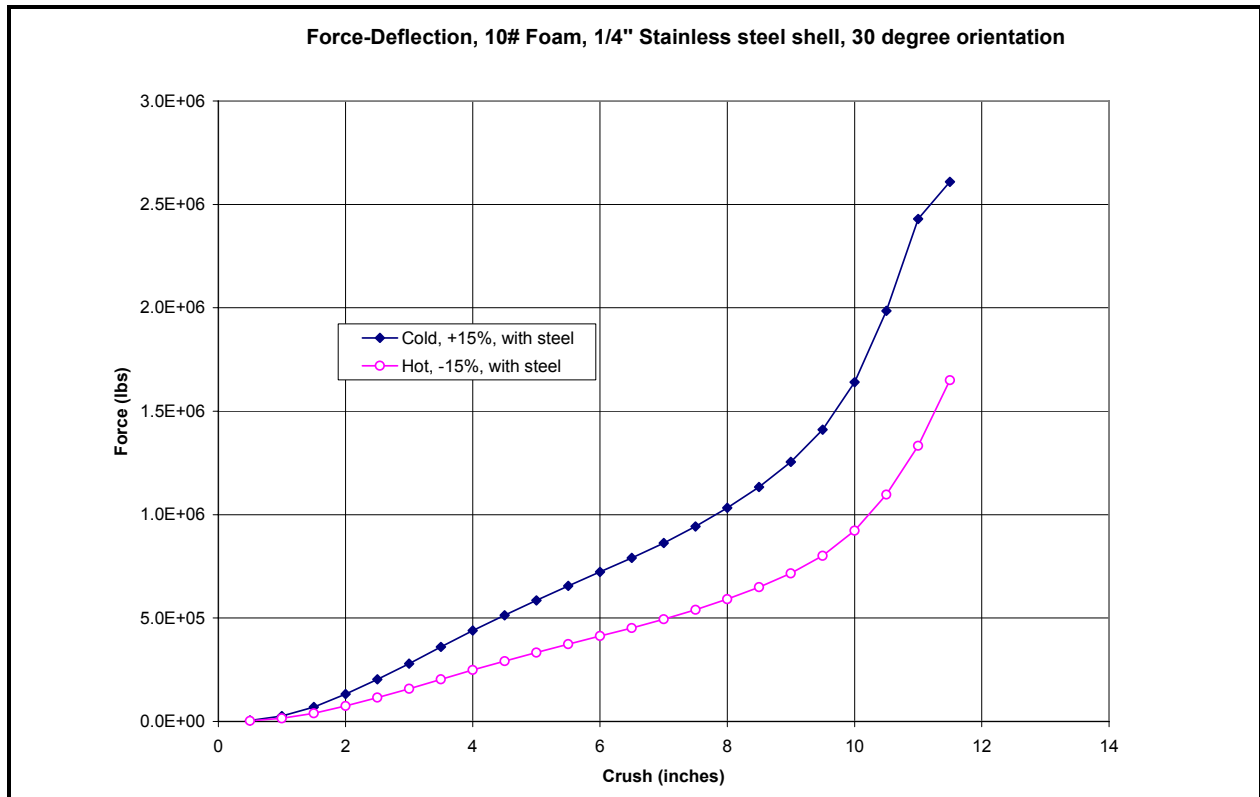


Figure 2.12.1-3 – Lid End Limiter, 30° Impact Angle, Force-Deflection Curve

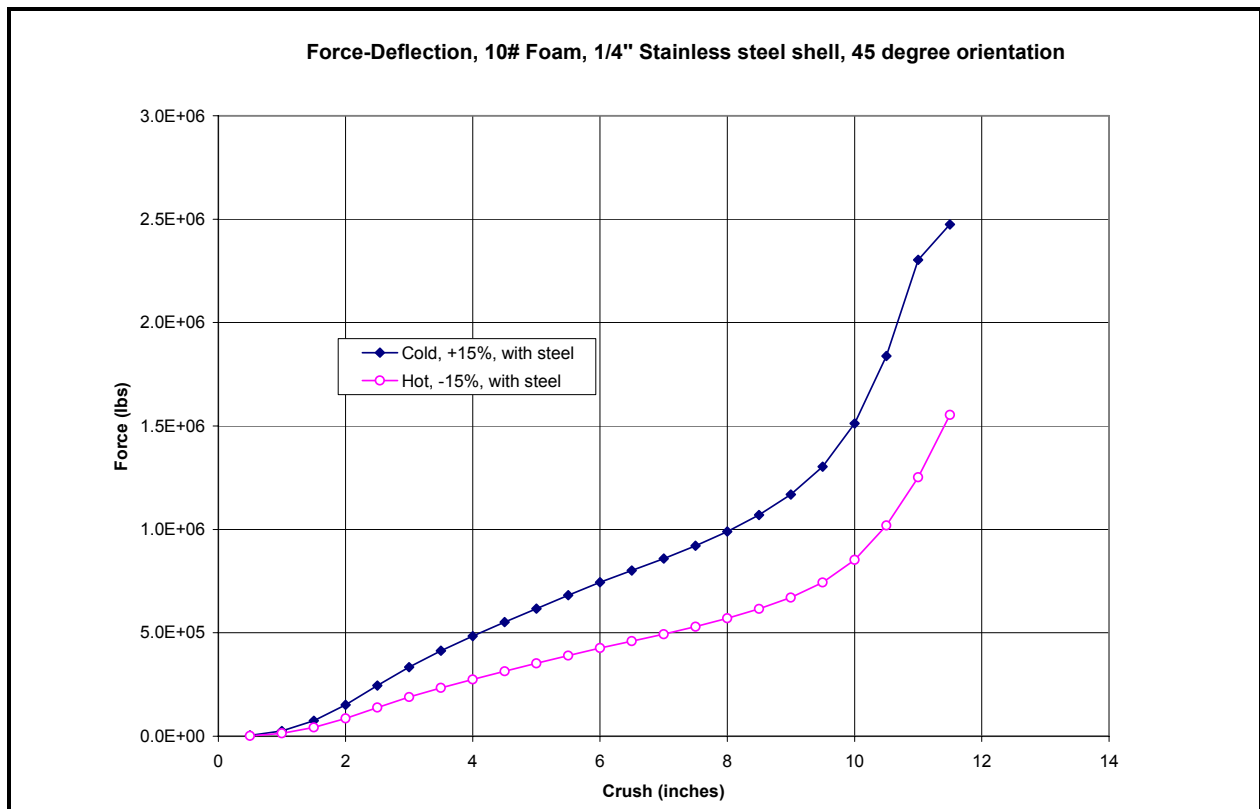


Figure 2.12.1-4 – Lid End Limiter, 45° Impact Angle, Force-Deflection Curve

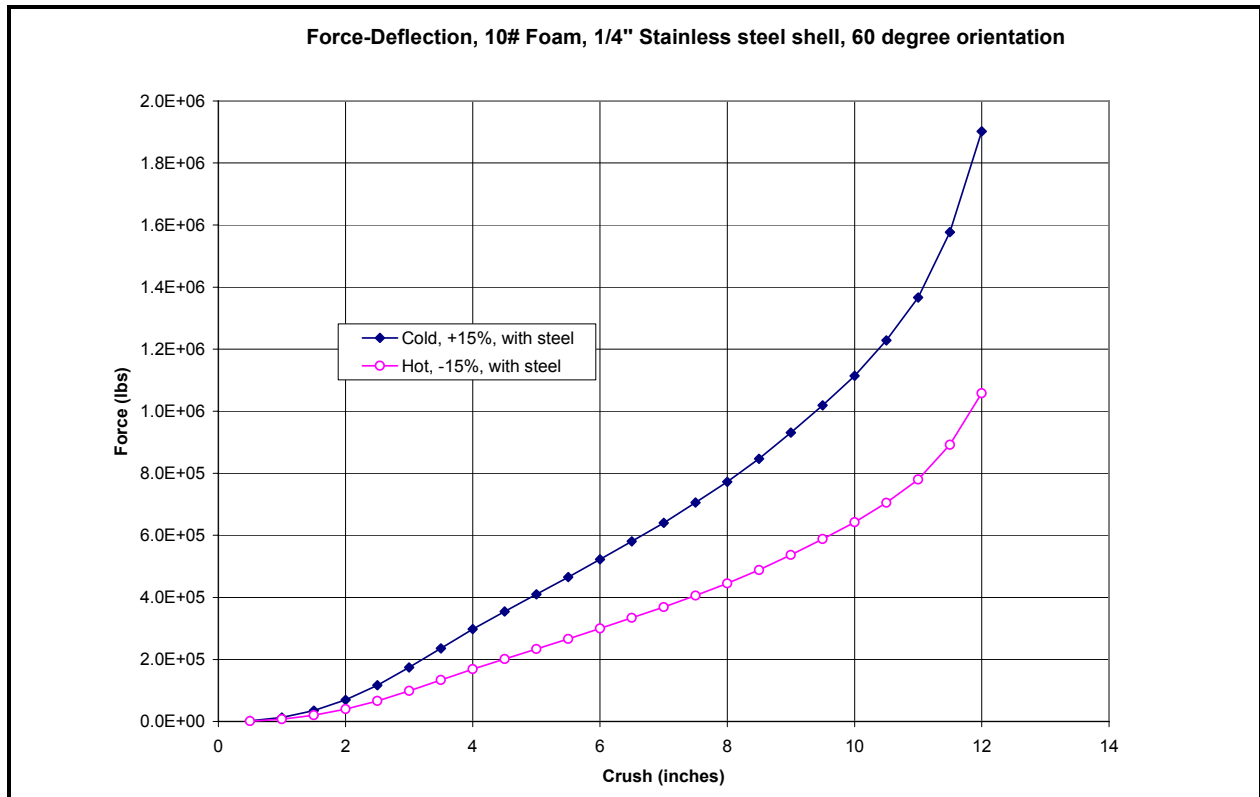


Figure 2.12.1-5 – Lid End Limiter, 60° Impact Angle, Force-Deflection Curve

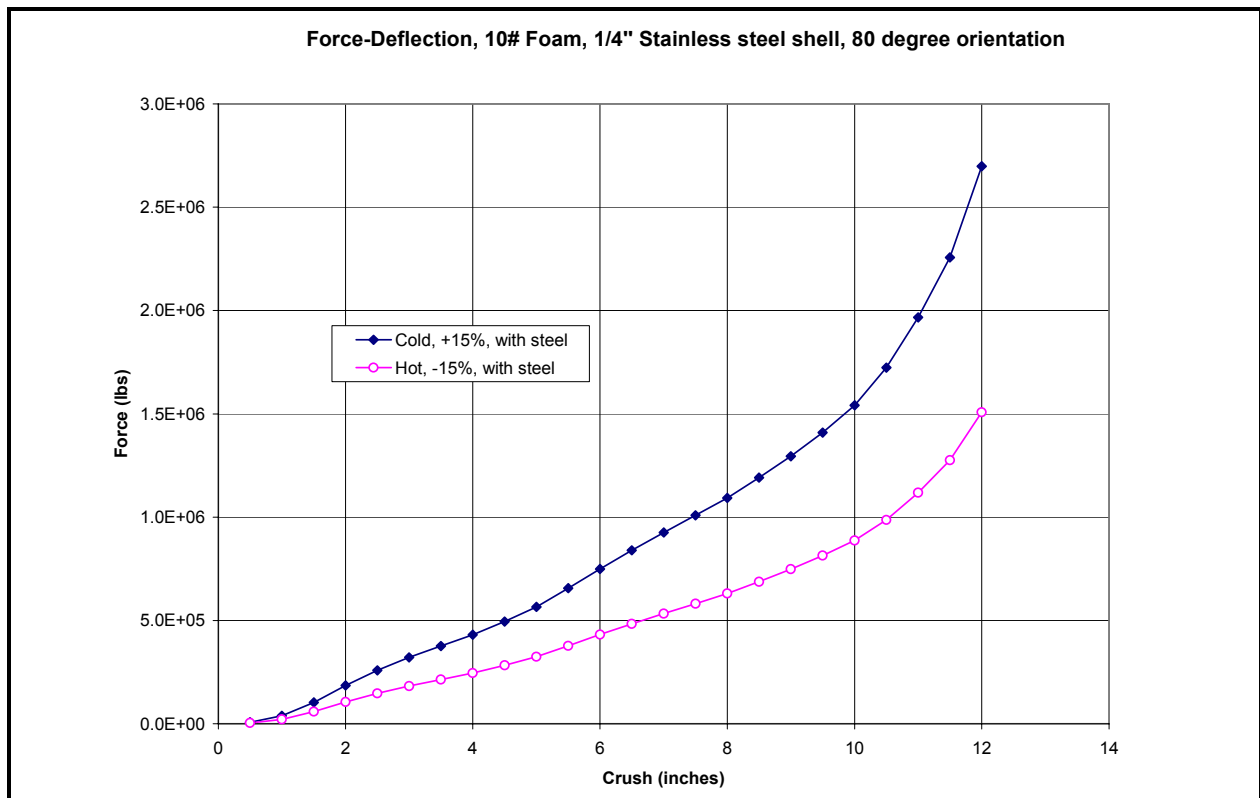


Figure 2.12.1-6 – Lid End Limiter, 80° Impact Angle, Force-Deflection Curve

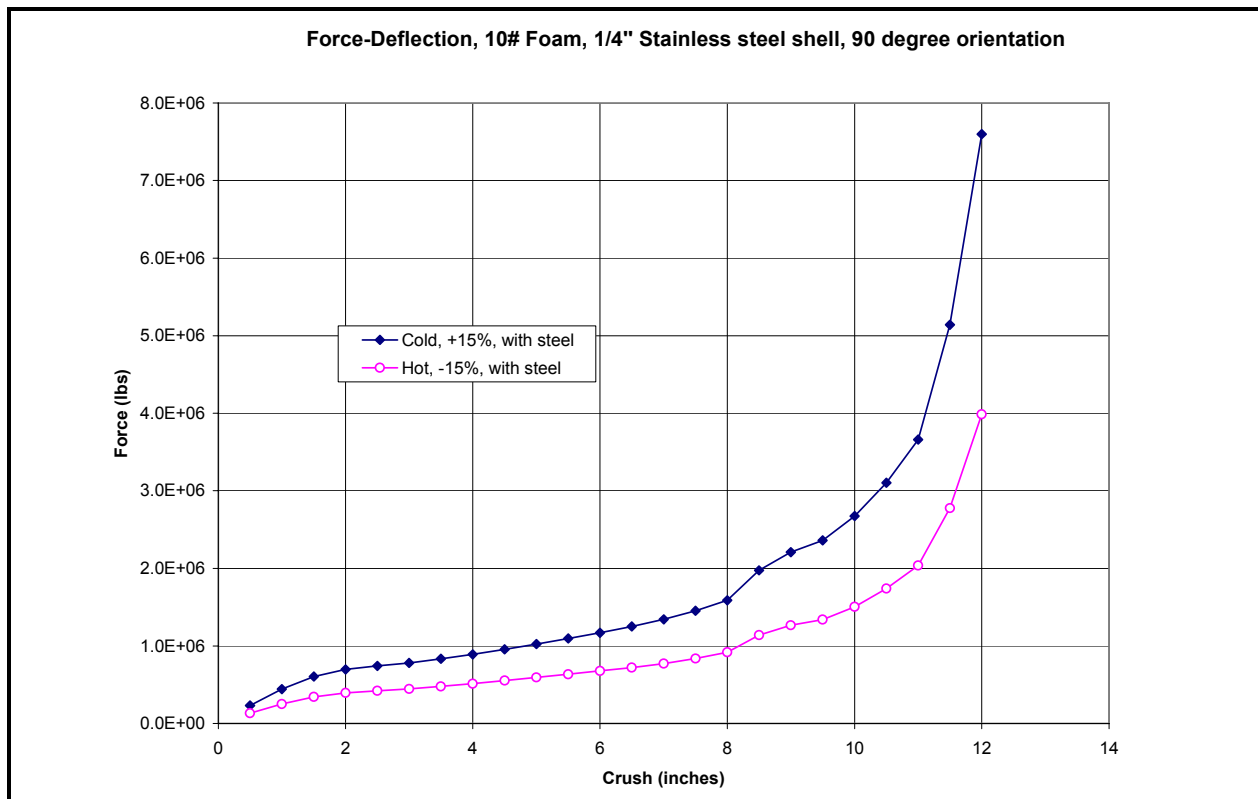


Figure 2.12.1-7 – Lid End Limiter, 90° Impact Angle, Force-Deflection Curve

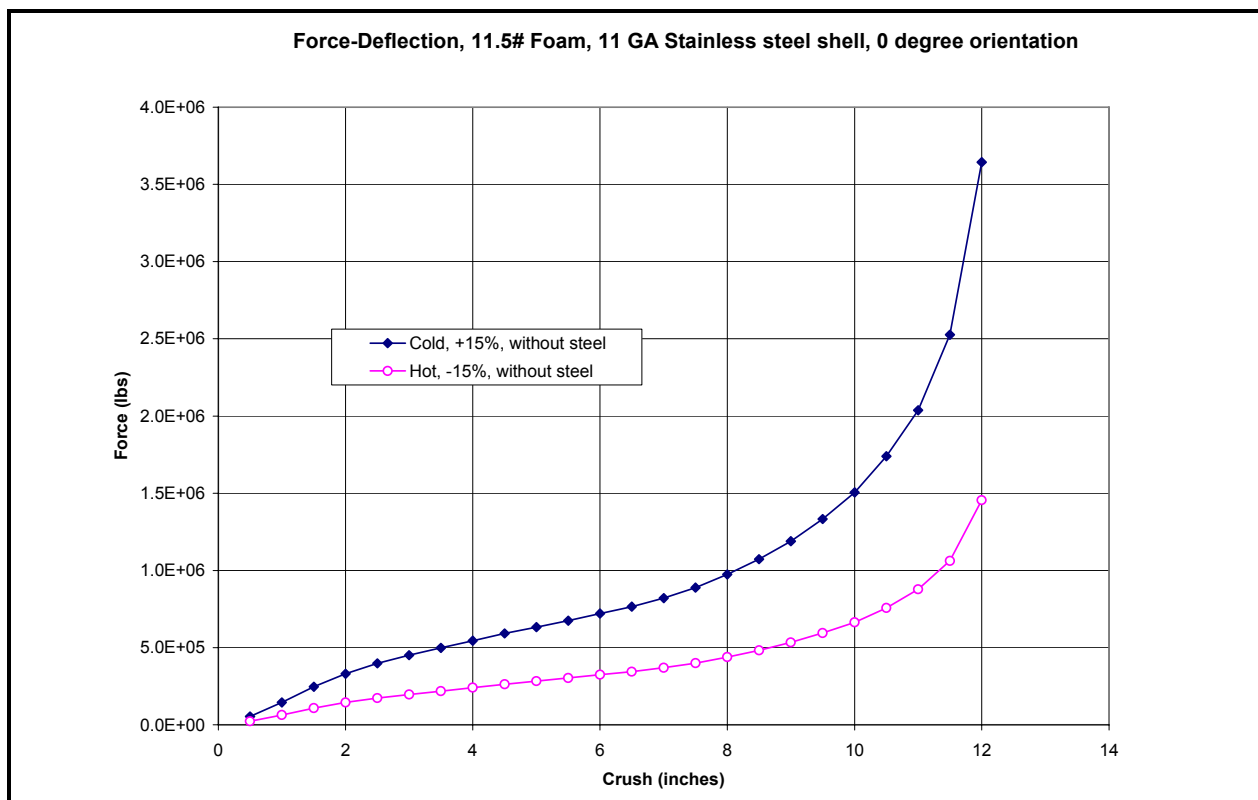


Figure 2.12.1-8 – Bottom End Limiter, 0° Impact Angle, Force-Deflection Curve

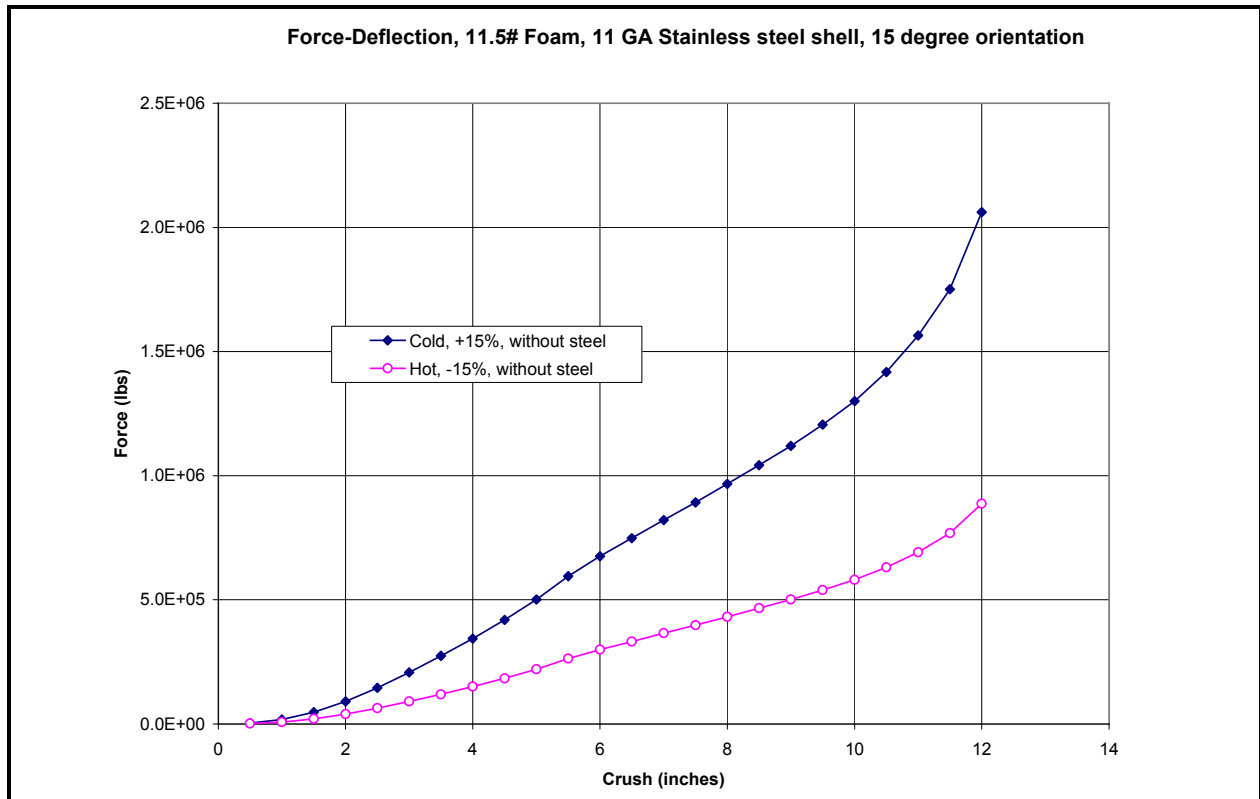


Figure 2.12.1-9 – Bottom End Limiter, 15° Impact Angle, Force-Deflection Curve

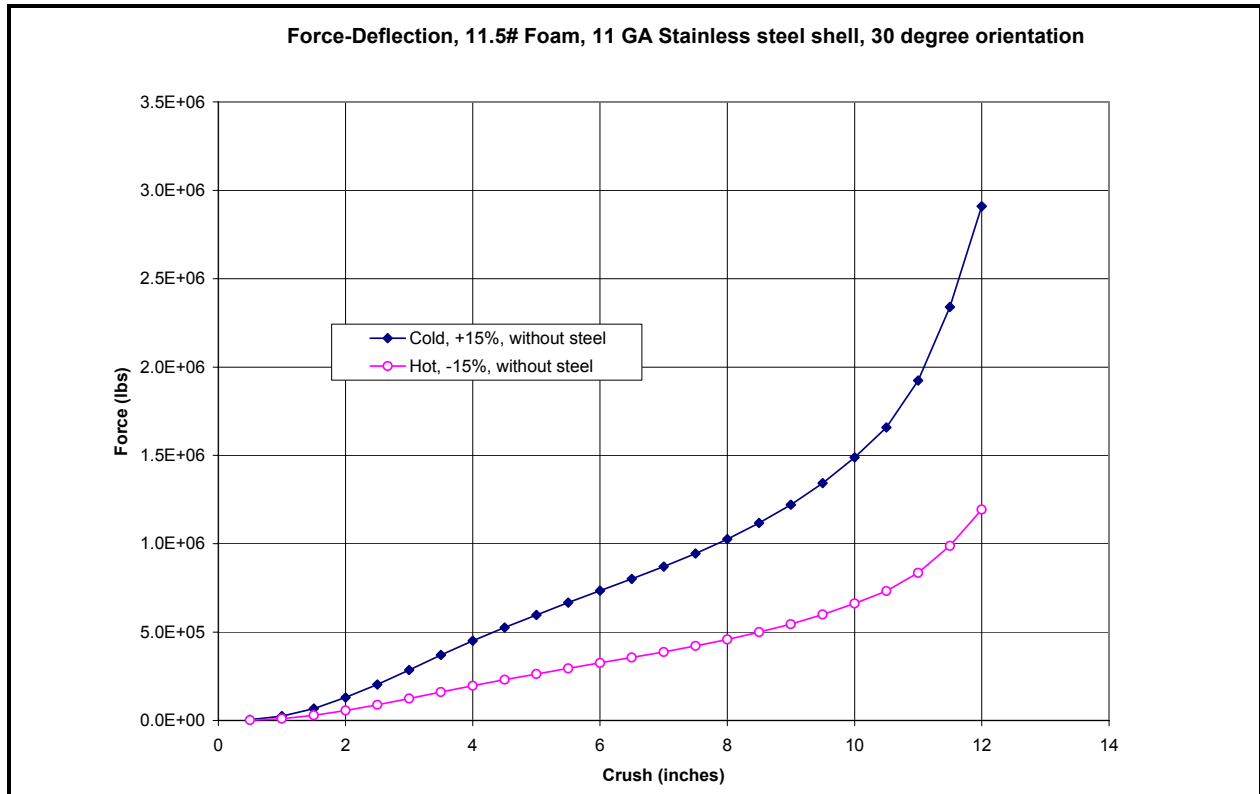


Figure 2.12.1-10 – Bottom End Limiter, 30° Impact Angle, Force-Deflection Curve

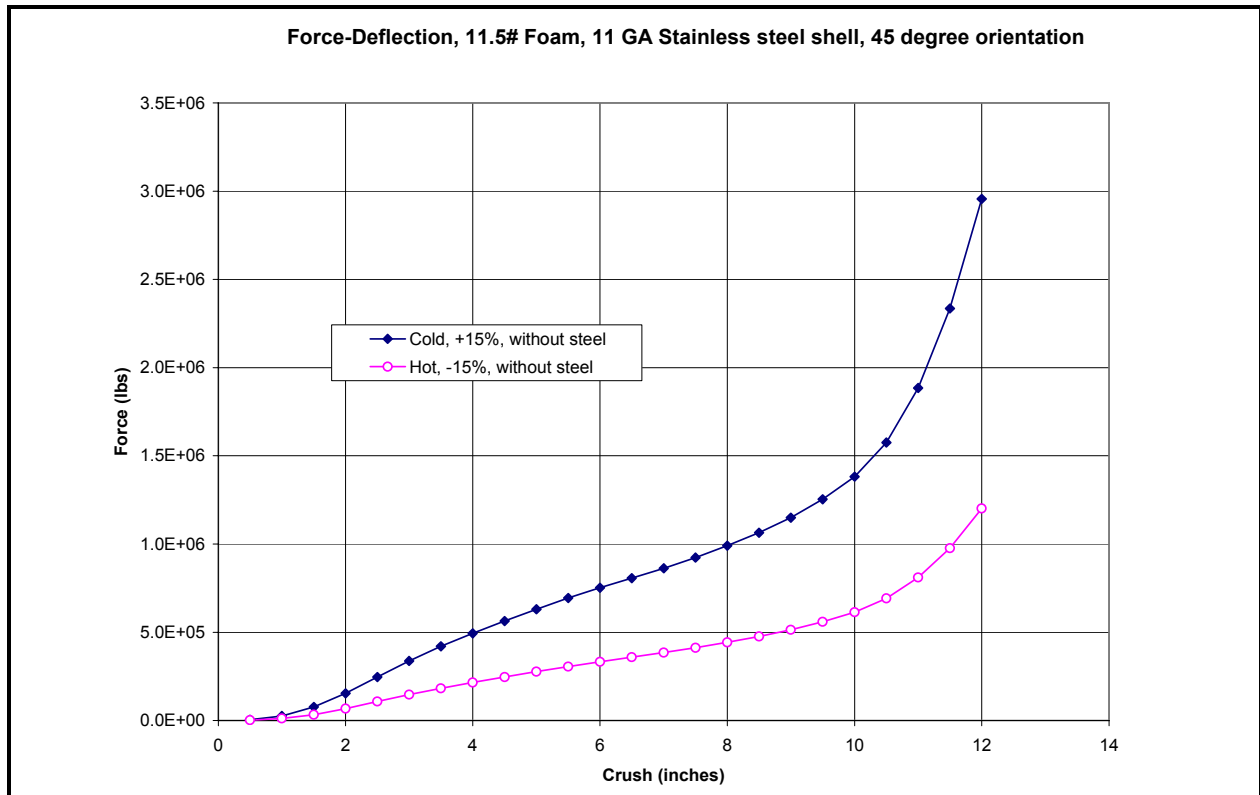


Figure 2.12.1-11 – Bottom End Limiter, 45° Impact Angle, Force-Deflection Curve

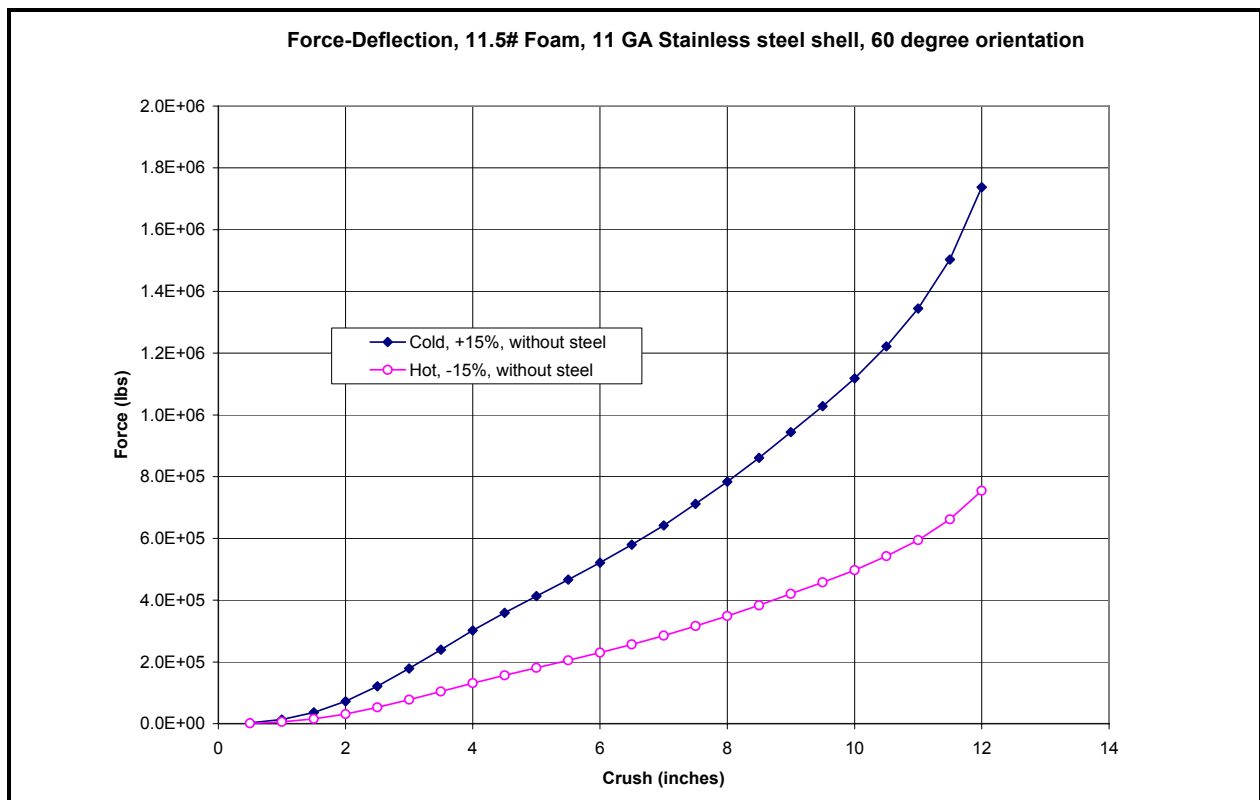


Figure 2.12.1-12 – Bottom End Limiter, 60° Impact Angle, Force-Deflection Curve

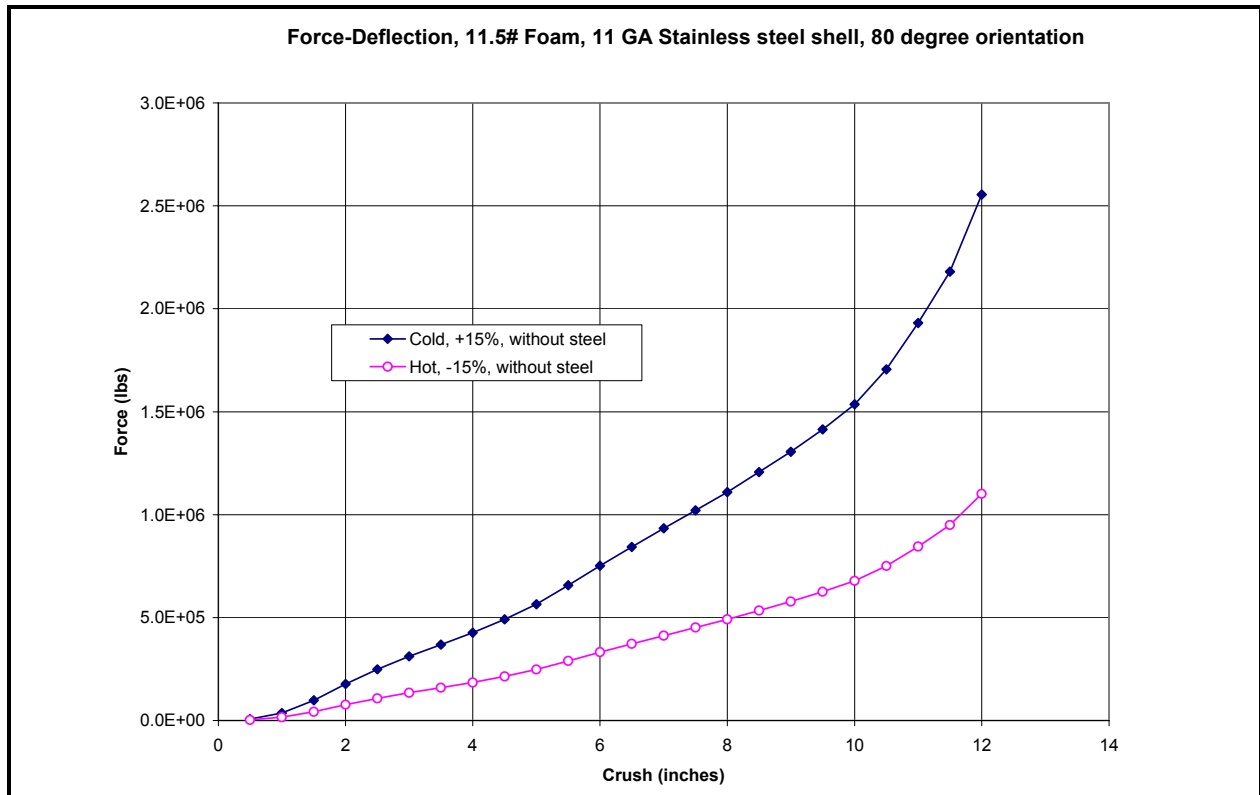


Figure 2.12.1-13 – Bottom End Limiter, 80° Impact Angle, Force-Deflection Curve

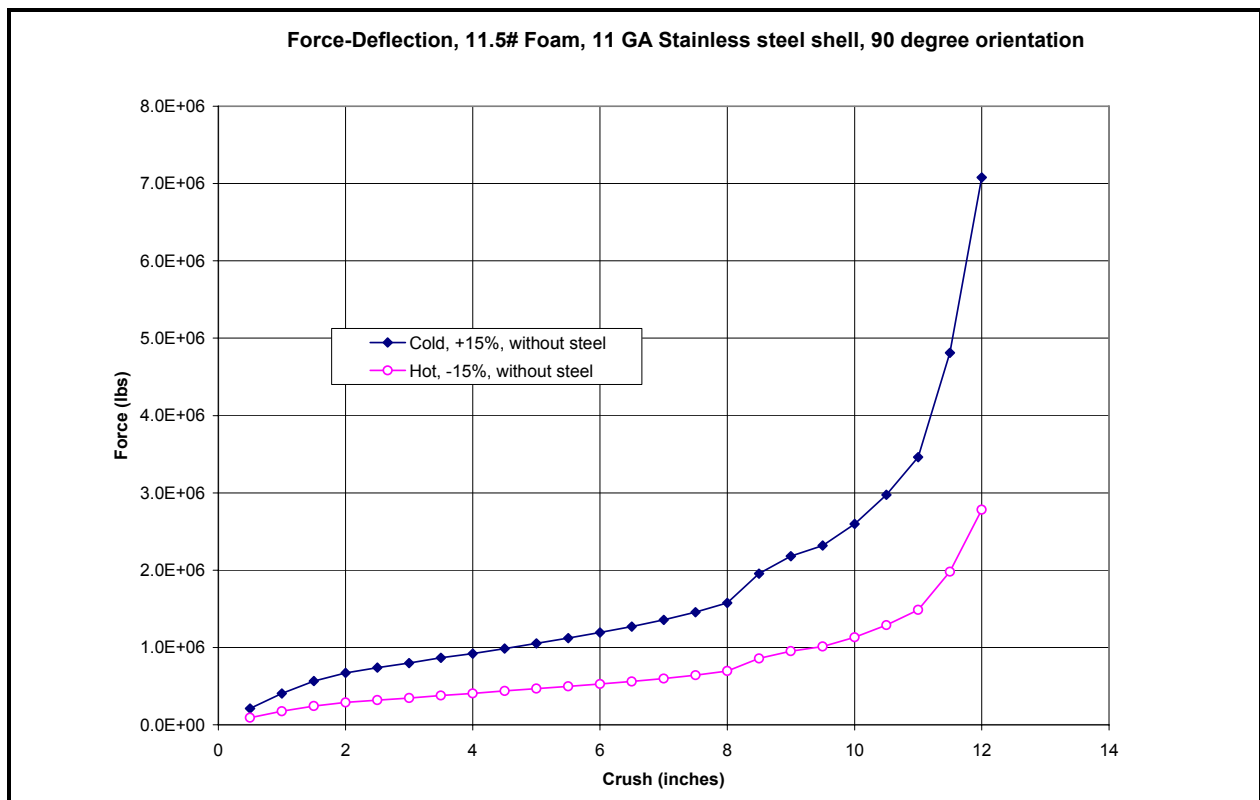


Figure 2.12.1-14 – Bottom End Limiter, 90° Impact Angle, Force-Deflection Curve

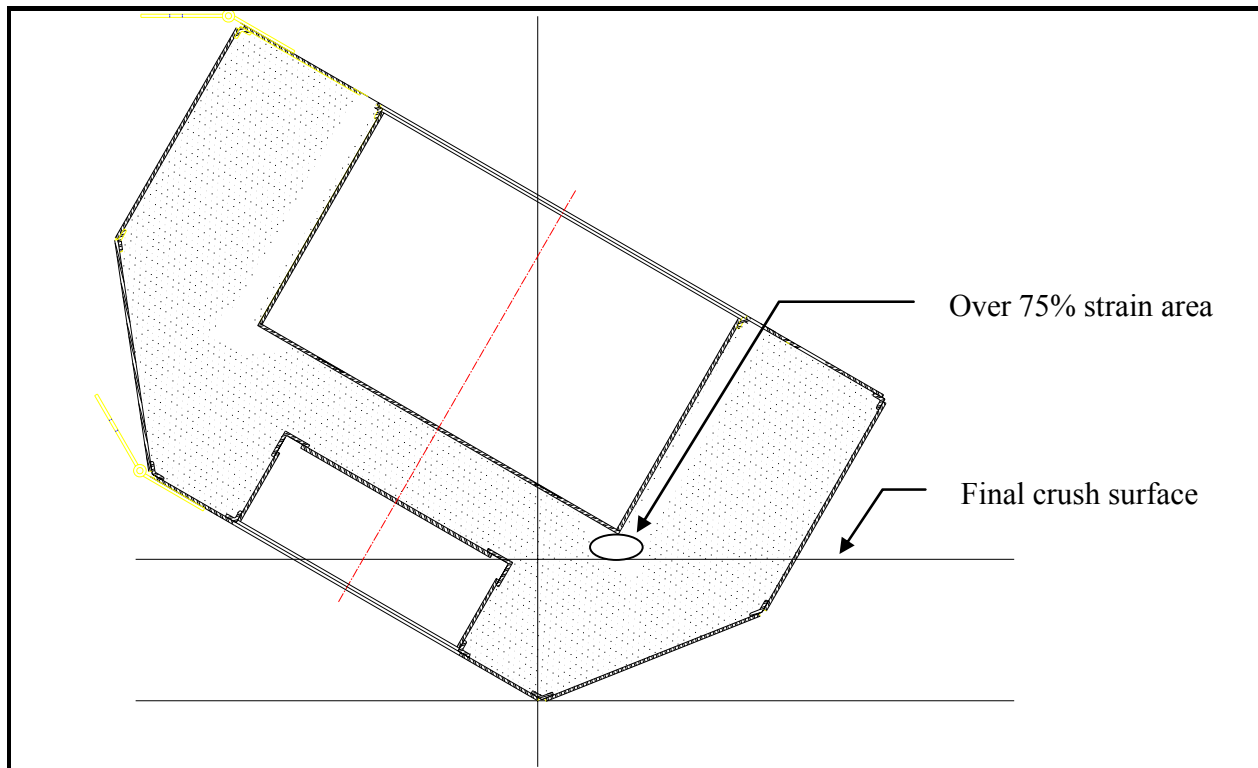


Figure 2.12.1-15 – Crush During Drop Test with Impact Angle > 45°

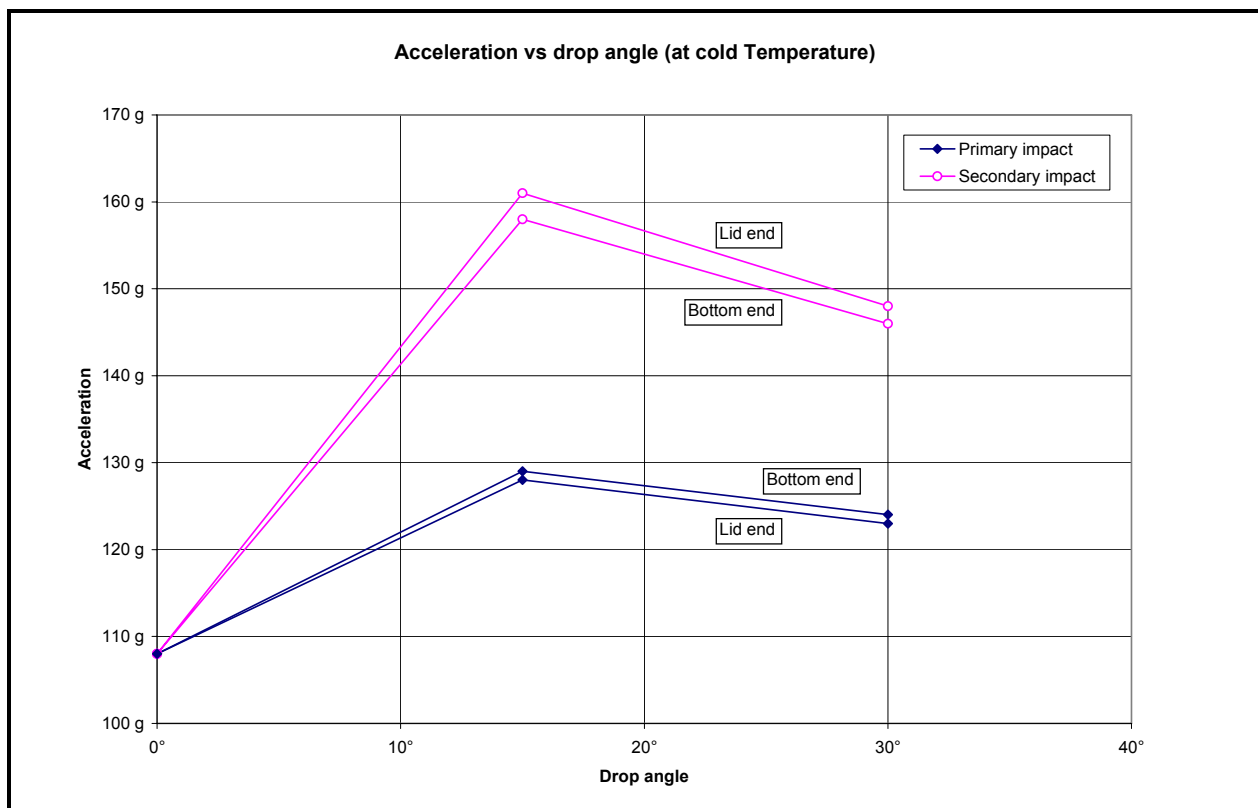


Figure 2.12.1-16 – Worst-Case Slapdown Angle

This page left intentionally blank.

2.12.2 Certification Test Plan

This appendix establishes the selected free drop and puncture drop test sequence for the MFFP certification test unit (CTU). Since the HAC thermal event of 10 CFR §71.73(c)(4)¹ will be evaluated by analysis, fire testing of the CTU will not be included in the certification tests.

As stated in Chapter 2.0, *Structural Evaluation*, the primary method of demonstration of compliance of the MFFP with the requirements of 10 CFR §71.73 in HAC free drop and puncture drop events is full-scale prototypic testing. The test program will address the following objectives:

1. To demonstrate a leaktight condition (leakage rate no greater than 1×10^{-7} ref-cc/sec, air, per ANSI N14.5²) after sequential 30-foot free drop and 40-inch puncture drop tests [10 CFR §71.73(c)(1) and 10 CFR §71.73(c)(3)]. Three different sequences of free drop followed by puncture drop tests are planned, and the containment boundary must be leaktight at the conclusion of each sequence.
2. To demonstrate that the payload remains subcritical after the free drop and puncture tests, and that no reconfiguration of the package or payload will cause the value of k_s to increase above the upper subcritical limit (USL) [10 CFR §71.55(e)].

Objective Number 1 will be demonstrated directly by leakage rate testing of the certification test unit (CTU) prior to and following the tests. Using deformation and/or reconfiguration data collected from the certification testing, Objective Number 2 will be evaluated in Chapter 6.0, *Criticality Evaluation*. In a similar manner, the effect of the HAC fire event on containment will be evaluated by analysis, using deformation data collected from the certification tests. The evaluation of the MFFP for water immersion per the requirements of 10 CFR §71.73(c)(6) will be demonstrated by analysis.

2.12.2.1 Initial Test Conditions

2.12.2.1.1 Internal Pressure

As shown in Section 2.6.1.1, *Summary of Pressures and Temperatures*, the MNOP of the MFFP is conservatively assumed to be 10 psig. The hoop stress in the containment shell that results from this pressure is less than 500 psi; therefore, it creates an insignificant contribution to the maximum containment shell stress in HAC free drop and puncture drop events. Consequently, no internal pressure will be used in the CTU during testing.

2.12.2.1.2 Temperature

Of greatest interest to the evaluation of containment integrity is the maximum impact acceleration. For the MFFP, this corresponds to the minimum temperature (-20 °F ambient) condition, due to the increase in crush strength of the foam with decreasing temperature. The maximum temperature condition (100 °F ambient) is of interest only if deformations of the impact limiter are so great that higher impact occurs through “bottoming” of the impact limiter structure. Otherwise, the minimum temperature condition governs. Consequently, the impact limiters are tested at a material temperature of -20 °F or less.

¹ Title 10, Code of Federal Regulations, Part 71 (10 CFR 71), *Packaging and Transportation of Radioactive Materials*, Final Rule, 01-26-04.

² ANSI N14.5-1997, *American National Standard for Radioactive Materials - Leakage Test on Packages for Shipment*, American National Standard Institute, Inc. (ANSI).

2.12.2.1.3 Maximum Impact Limiter Deformation

The analysis provided in Appendix 2.12.1, *Impact Limiter Evaluation*, demonstrates that the warm ambient temperature impacts do not result in excessive impact limiter deformations or “bottoming out”. Since maximum impact limiter deformation is not a concern for the certification tests, warm ambient tests will not be included in the test sequence.

2.12.2.2 Certification Test Unit (CTU)

Certification tests of the MFFP will utilize a full-scale CTU that is completely prototypic in design, materials, and fabrication. Consequently, the weight and center of gravity of the CTU will be prototypic. The CTU will include a prototypic strongback assembly for most tests. For some certification tests, the behavior of the strongback is not important and hence, can be conservatively simulated by the equivalent dead weight, as discussed in Section 2.12.2.2.1, *Mock Payload*. Multiple impact limiters will be used to prevent accumulation of damage for the selected test series, as appropriate.

Payload simulation will be accomplished by a combination of a prototypic FA and dummy FAs with the strongback, or a mock payload by itself. These simulated payloads are discussed in the following sections.

2.12.2.2.1 Mock Payload

The mock payload will be a bundle of approximately 800, 1/2-inch diameter steel bars, bringing the total weight of the mock payload to 7,500 pounds. This payload will be used to simulate the payload in the first test series where the free drop is primarily focused on buckling behavior of the shell. The use of the steel bar payload for this test is conservative, as explained below.

The buckling behavior of the body shell depends in part, on the distribution of the payload weight and the payload bending stiffness. The payload load results in a bending moment on the containment shell in the horizontal side drop. The more centrally the weight is applied to the interior, the greater the bending moment on the shell. Although the strongback is normally supported at its ends, the strongback will bend and contact the interior of the shell during the side free drop. The worst-case would be for a plastic hinge to form at the center of the strongback. For this case, the load at the center would be one-half of the total inertia load, neglecting any moment resistance of the strongback, leaving one quarter of the inertia load supported at each end (see Figure 2.12.2-1). Only the load at the center contributes to the bending moment. If F is the total inertia load of the strongback, the maximum moment in the simply supported shell of length L would be:

$$M_{\max} = \frac{(F/2)L}{4} = \frac{FL}{8}$$

If the load is distributed over the entire length L , as is the case for a bundle of steel bars, the maximum moment would be:

$$M_{\max} = \frac{FL}{8}$$

which is identical to the worst-case load for the strongback. This case is conservative because the strongback payload cannot apply half of its load at the center, since the nearest support disks

are located ± 10 inches from the center of the shell. In addition, the moment resistance of the strongback is neglected above, which increases the conservatism.

Note also that the bending moment of inertia of the steel bars is less than that of the strongback. The central structure of the strongback has a moment of inertia of approximately 275 in^4 . The moment of inertia of one steel bar is $\pi/64 \times (0.5)^4 = 0.00307 \text{ in}^4$. Since the bars lack shear continuity and will act independently, the mock payload has a total moment of inertia of $800 \times 0.00307 = 2.46 \text{ in}^4$, or less than one percent of the actual strongback. Therefore, use of the steel bars as a mock payload for the horizontal side drop, in which the worst-case bending moment in the shell is sought, is conservative.

2.12.2.2.2 Dummy Fuel Assembly

The dummy FAs used for certification testing will be designed to simulate the weight distribution and structural properties of an actual FA. To meet this requirement, each dummy assembly will consist of simulated end nozzles, guide sleeves, grids, and fuel rods. Each end of the dummy FA will include a simulated end nozzle. The end nozzles will be connected to each other by nine (9) 1/2-inch OD \times 3/8-inch ID guide sleeves made of aluminum. The fuel rods will be simulated by nominally 3/16-inch diameter solid steel rods, which are retained by simulated grid assemblies. The end nozzles and grid assemblies will be clamped by the strongback at the same locations and in the same way as an actual FA. The dummy fuel will have conservative weight properties compared to the real assembly. All of the dummy fuel assembly weights will be slightly more than the combined maximum weight of the upper bound FA weight of 1,580 pounds. The weight of all of the steel rods on a per inch basis will be 9.62 pounds or approximately 4.2% more than the unit length weight of all of the actual fuel rods.

The dummy FA will have less bending stiffness than the actual FA. Consequently, its mass will load the strongback with conservatively less favorable added stiffening when compared to an actual FA. Since the steel rods will be loosely contained by the grid assemblies, the elastic stiffness of the dummy FA results only from the moment of inertia of the array of nine simulated guide sleeves, having a total value of 2.03 in^4 , or, conservatively, 17.5% less than the moment of inertia of the array of 24 guide sleeves in the real fuel assembly. The frictional attachment of the real fuel rods to the grids provides somewhat more stiffness in the actual FA, which is conservatively not included in the dummy assembly. The dummy fuel assembly is depicted in Figure 2.12.2-2 and Figure 2.12.2-3.

2.12.2.2.3 Prototypic Fuel Assembly

The prototypic fuel assembly is an exact facsimile of the MK-BW/MOX1 FA without burnable poison rod assemblies (BPRAs), except that the fissile MOX fuel pellets are simulated using non-fissile tungsten carbide pellets. The prototypic FA will be utilized in those tests where the response of the FA is of primary interest.

2.12.2.3 Identification of Worst-Case Drop Tests

Two general categories of tests should be considered, based on the potential vulnerabilities of the MFFP to free drop and puncture damage:

1. Tests that evaluate the containment of the package, including buckling of the shell, performance of the lid bolts, distortion of the sealing area, and all other leaktight concerns. These tests are governed by the maximum (cold) impact loads.

In the same category are tests that evaluate the fire safety of the package. These tests are those which would cause thermally significant damage to, or loss of, the lid end impact limiter, since the only component of the package that is sensitive to HAC fire temperatures is the elastomer containment O-ring seal in the closure lid.

2. Tests which evaluate the criticality safety of the package, including the geometric stability of the strongback (i.e., maintaining an adequate spatial relationship between the FAs), the ability of the neutron poison plates to remain intact and in place, and the behavior of the fuel rods in key orientations. These tests should also assume the maximum impact loads.

These categories are now examined to identify specific areas of potential concern. According to 10 CFR §71.73, the package is to be tested in the orientation for which maximum damage is expected. In the discussions below, candidate tests are identified by matching package features, characteristics, and design goals with relevant tests in worst-case orientations. In all cases, the maximum impact is assumed as the governing case.

2.12.2.3.1 Tests of the Package Containment Performance

1. Buckling of the Package Shell: Since the MFFP is a relatively long and slender package, lateral buckling of the shell is of concern in both side and slapdown free drops. Using the methods of analysis of NUREG/CR-3966, the horizontal side drop case was determined to be governing over the slapdown based on bending moment in the shell. Containment shell buckling in the vertical free drop is also of concern. Therefore, these two orientations (horizontal and vertical) should be included in the certification test program.
2. Leakage Rate at Package Closure: The package closure must survive the governing drop impact forces in a leaktight condition. In the C.G.-over-corner drop (which, due to the proportions of the package, is a nearly vertical end drop), the maximum axial forces are applied to the closure bolts and to the closure lid structure. This response is because the axial component of impact force at the C.G.-over-corner (80° to the horizontal) is essentially equal to the pure vertical case. Conversely, in a slapdown free drop where the closure lid is at the secondary impact end of the package, the maximum lateral forces are applied to the closure lid and to the shell flange. Therefore, this orientation should be included in the certification test program.
3. Perforation of the Containment Boundary. The 9/16-inch thick containment shell is very resistant to perforation by the puncture bar. To fully demonstrate this resistance, experience has shown that the most likely orientation for perforation would be an oblique puncture through the package C.G. The most damaging angles have been determined to be between 25° – 40° (measured between the puncture bar axis normal to the package). The horizontal puncture through the package C.G. must also be considered, since, due to its greater stability, it might impart more deformation and material strain to the containment shell. Therefore, these puncture orientations should be included in the certification test program.
4. Puncture Perforation of the Lid End Impact Limiter Shell: The shell of the lid end impact limiter is designed to resist perforation by the puncture bar. This prevents concentrated puncture loads on the closure lid and seal flange, and, since there would be no loss of foam,

affords extra protection against elevated containment O-ring seal temperatures in the HAC fire event. As stated above, an oblique angle of between 25° and 40° (measured between the puncture bar axis normal to the impact limiter shell) is the most likely orientation to experience perforation of the steel shell. The most likely orientation of the package for perforation would therefore combine an oblique impact and a C.G. location as near as possible to the puncture bar axis. Since the elastomer containment O-ring seals are located solely in the closure lid, perforation of the bottom end limiter shell is of no consequence. Therefore, puncture drop tests of the lid end impact limiter should include this orientation.

5. Retention of the Lid End Impact Limiter: Because the presence of the lid end impact limiter is key to the thermal protection of the containment O-ring seals, loss of the impact limiter must not occur. Due to the tapered design of the limiters, the separation moments during free drop impacts are negligible, since the center of impact force is directed through the package, and cannot generate a separation moment. The tapered shape, the relatively long insertion length of the containment body into the limiter, and the energy-absorbing attachment bolt design all make loss of the limiter in free drops of no concern.

A direct attack by the puncture bar on the stiffer, outside edge of the limiter could potentially place a separation load on the limiter. The maximum puncture force would be generated when the puncture bar and package axes are nearly as parallel as physically possible. Therefore, a puncture drop for this orientation should be included in the certification test program.

2.12.2.3.2 Tests of the Package Criticality Performance

1. Geometric Stability of the Strongback: To maintain the fuel in a subcritical condition, the relative geometry of the FAs and the neutron poison plates must be kept within certain bounds. These bounds are defined in the criticality analysis given in Chapter 6.0, *Criticality Evaluation*, and are maintained during free drop and puncture drop events by the strongback. The greatest forces on the strongback result from the maximum lateral impact, which occurs at the secondary impact end of the package in the slapdown drop. From Section 2.12.1.7, *Worst-Case Slapdown Angle*, the worst-case secondary slapdown impact occurs for the shallow primary impact angle of 15° to the horizontal. Therefore, this orientation should be included in the certification test program.
2. Geometric Stability of the Fuel: Under free drop impacts, the fuel rods could bend or buckle. To maintain a subcritical state, the fuel rod pitch must remain within the bounds defined in Chapter 6.0, *Criticality Evaluation*. In the side orientation, the fuel rods experience lateral loads, which have the tendency to push the fuel rods together and decrease the pitch, a condition for which k_{eff} decreases. In the C.G.-over-corner (near-vertical) orientation, the relatively small lateral forces on the fuel are dominated by the axial forces, and fuel rod behavior is therefore less determinate, i.e., the pitch could increase or decrease. Therefore, the C.G.-over-corner (near vertical) orientation is of greatest concern for the geometric stability of the fuel and should be included in the certification test program.

2.12.2.3.3 Strongback Azimuth Orientation

As discussed above, the strongback should be tested to demonstrate its resistance to lateral impact in the slapdown free drop. The strongback is supported within the package by means of support disks, which consist of three clamp arms per disk. Since the structure of the support disks is not

uniform, the response to impact loading may vary depending on the rotational, or azimuth, orientation of the strongback relative to the axis of impact. Therefore, to fully characterize the structural performance of the strongback and support disks, a slapdown test in two azimuth orientations will be included in the certification test program, as shown in Figure 2.12.2-4.

2.12.2.4 Summary of Selected Certification Drop Tests

Based on the above discussions, four HAC, 30-ft free drop tests and up to six 40-inch puncture tests have been identified for inclusion in the certification test program. Although only a single worst-case free drop followed by a single worst-case puncture drop are required by 10 CFR §71.73, all of the tests listed below will be performed to ensure that each area of potential concern is subjected to worst-case conditions.

Because of the large number of tests to be performed, over-testing of some CTU features may become an issue. Of particular importance are the criticality performance tests, where FA or strongback deformations are of primary interest. If subject to over-testing, the deformations from one test may be invalidated by the deformations of the test which follows. Therefore, the selected tests will be conducted in three separate test series. As stated in 10 CFR §71.73(a), the puncture tests are to follow the free drop tests. Accordingly, each series of tests will consist of one to two free drop tests followed by one or more puncture drop tests. At the end of each series, the package will be opened and the strongback and FA deformations will be evaluated prior to proceeding to the next test series. Before opening the package, however, a leakage rate test will be performed to measure the leakage rate of all containment seals (closure lid and vent port penetrations). At the end of all tests, a leakage rate test of the entire containment boundary will be performed. The containment acceptance criteria is a leakage rate not exceeding 1×10^{-7} ref-cc/sec, air.

It is expected that a single containment boundary will suffice for all of the tests planned. The strongback, however, is likely to need some repair or perhaps replacement between test series. If repaired, the strongback will be restored to a prototypic condition for subsequent tests. Due to the accumulation of free drop and puncture damage on the impact limiters, at least two sets of limiters will be used to perform all of the tests.

2.12.2.4.1 Certification Test Series 1

Prior to beginning Test Series 1, a mock payload consisting of steel bars, as described in Section 2.12.2.2.1, *Mock Payload*, will be placed inside the package, and a pre-drop leakage rate test of all containment seals will be performed. Since this test series is focused on the response of the body, the mock payload will be utilized. The package will be chilled to at least -20 °F prior to the drop tests.

1. Horizontal, 30 ft Free Drop: Addresses lateral buckling of the package shell (see Figure 2.12.2-6).
2. Near-Vertical Puncture Drop on Lid End Impact Limiter Tapered Section, Axis of Package 75° from Vertical, Axis of Puncture Bar at 36.5° from a Normal to Tapered Surface: The package C.G. is directly over the puncture bar. Addresses perforation of the lid end impact limiter skin (see Figure 2.12.2-5).

3. Near-Vertical Puncture Drop on Lid End Impact Limiter Center Recessed Plate, Axis of Package at 65° from Vertical, Axis of Puncture Bar at 25° from a Normal to the Plate: Addresses perforation of the lid end impact limiter skin (see Figure 2.12.2-5).
4. Near vertical puncture drop on the outside edge of the lid end impact limiter. See Figure 2.12.2-5. The outside edge of the puncture bar will be nominally flush with the outside edge of the limiter. The lower limiter will be as close as practical to the puncture bar without touching it, so as to provide a nearly vertical package axis. Addresses impact limiter retention.

After each test, all package deformations will be fully evaluated and recorded. The impact limiters will then be removed, a leakage rate test of containment O-ring seals will be performed, the closure lid removed, and the mock payload removed.

2.12.2.4.2 Certification Test Series 2

A prototypic strongback payload will be utilized for this test series. The strongback will contain two dummy FAs and one prototypic FA. A pre-drop leakage rate test of all containment O-ring seals will be performed. A new pair of lid end and bottom end impact limiters will be installed. The package will be chilled to at least -20 °F prior to the free drop tests.

1. C.G.-Over-Corner (Near-Vertical, 80° Oblique), 30-ft Free Drop, Closure Lid Down: Addresses closure lid, closure bolt, and containment seal performance, and addresses prototypic fuel assembly behavior. Addresses axial buckling of the package shell (see Figure 2.12.2-7).
2. C.G.-Over-Corner Puncture Drop on Impact Damage from Test No. 1: Addresses the effect of puncture impact on prior free drop damage, and applies a puncture load to the closure area through the package C.G (see Figure 2.12.2-7).

After each test, all package deformations will be fully evaluated and recorded. Then, the lid end impact limiter will be removed, a leakage rate test of containment seals will be performed, the closure lid opened, and the strongback assembly removed. All deformations of the strongback and prototypic fuel assembly will be fully evaluated and recorded.

2.12.2.4.3 Certification Test Series 3

Prior to beginning Test Series 3, the prototypic fuel assembly will be removed from the strongback and a dummy fuel assembly installed in its place. The strongback will be repaired or replaced as necessary to ensure prototypic behavior in Test Series 3, and placed back in the CTU. After a pre-drop leakage rate test of all containment seals has been performed, a new lid end impact limiter will be installed. Just before testing, the package will be chilled to at least -20 °F.

1. Slapdown, 15° Oblique, 30-ft Free Drop, Closure Lid Primary Impact End: Package oriented to place strongback in azimuth no. 1 (see Figure 2.12.2-4). Addresses strongback under maximum lateral decelerations in one of its key azimuth orientations.
2. Slapdown, 15° Oblique, 30-ft Free Drop, Closure Lid Secondary Impact End: Package oriented to place strongback in azimuth no. 2. Addresses closure lid under maximum lateral decelerations and addresses strongback under maximum lateral decelerations in the other of its key orientations.

3. Puncture on Containment Shell, Package Horizontal, Bar Axis through C.G: Addresses perforation of the containment boundary from a perpendicular direction.
4. Puncture on Containment Shell, Package at 30° to Horizontal, Bar Axis through C.G: The package azimuth to be roughly opposite the azimuth of the proceeding puncture. Addresses perforation of the containment boundary from an oblique direction.

After each test, all package deformations will be fully evaluated and recorded. Then, both impact limiters will be removed and a leakage rate test of containment O-ring seals performed, followed by a leakage rate test of the entire containment boundary. The strongback will be removed and all deformations fully evaluated and recorded.

The selected certification test series are summarized in Table 2.12.2-1, and depicted in Figure 2.12.2-6, Figure 2.12.2-7, and Figure 2.12.2-8.

2.12.2.5 Acceptance Criteria

The following summarizes the acceptance criteria for all certification tests:

1. The containment boundary shall remain leaktight to a leakage rate not exceeding 1×10^{-7} ref-cc/sec, air. The containment O-ring seals shall be tested before they are disturbed (at the end of each test series), and the remainder of the metallic boundary shall be tested after the final test series.
2. In the horizontal drop, the containment shell shall remain stable and not buckle. Limited permanent deformation is acceptable.
3. Puncture drops on the lid end impact limiter shall not completely penetrate the limiter stainless steel shell. Partial tears (less than the full puncture bar circumference) and limited exposure of foam are acceptable.
4. The lid end impact limiter shall not become dislodged from the body. Depending on post-test configuration, breakage of one or more bolts is acceptable.
5. Deformations of the prototypic FA shall be bounded by the assumptions made in the criticality analysis of Chapter 6.0, *Criticality Evaluation*.
6. Deformations of the strongback and neutron poison plates shall be bounded by the assumptions made in the criticality analysis of Chapter 6.0, *Criticality Evaluation*.

Table 2.12.2-1 – Certification Test Series Summary

No.	Test Description	Addresses
Series No. 1		
1	Horizontal 30-ft free drop	Containment shell buckling
2	Oblique puncture on tapered skin	Perforation of lid end impact limiter skin
3	Oblique puncture on bottom disk	Perforation of lid end impact limiter skin
4	Puncture axial to limiter	Impact limiter retention
Series No. 2		
1	C.G.-over-corner (near-vertical) 30-ft free drop	Closure lid integrity; prototypic fuel integrity
2	C.G.-over-corner puncture on free drop damage	Effect of puncture on prior damage; puncture load on closure region
Series No. 3		
1	15° Slapdown 30-ft free drop, lid primary	Strongback deformations
2	15° Slapdown 30-ft free drop, lid secondary	Strongback deformations, closure lid integrity
3	Horizontal puncture on containment shell	Containment shell leaktight integrity
4	Oblique puncture on containment shell	Containment shell leaktight integrity

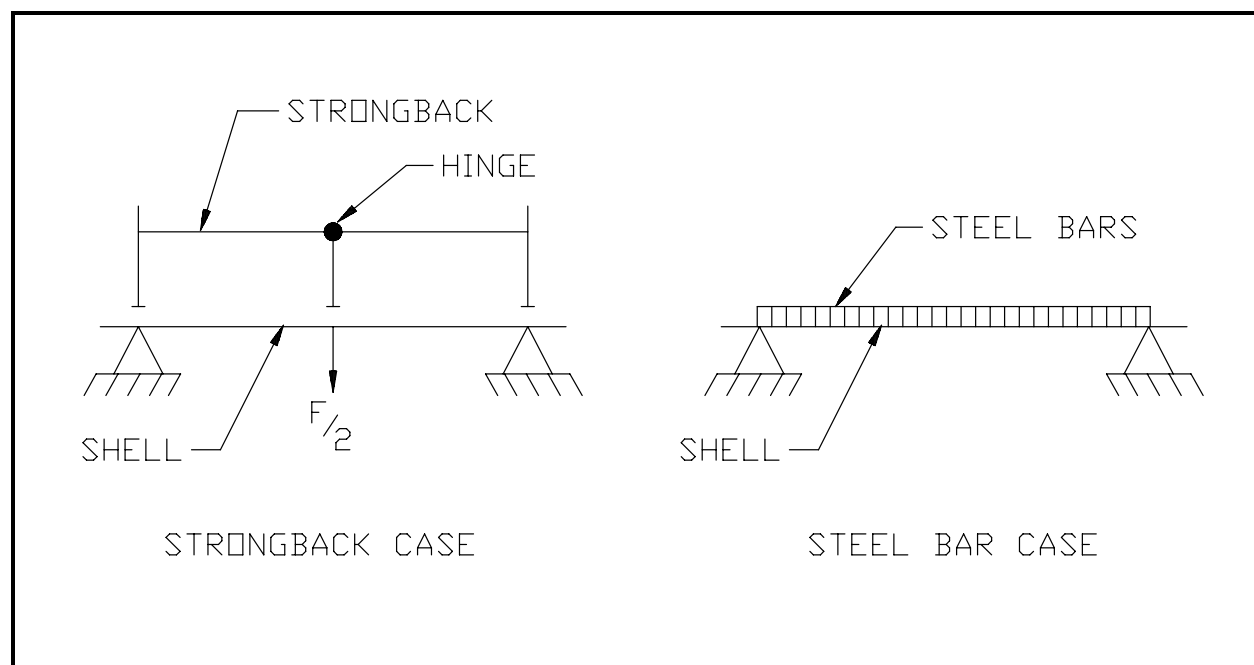


Figure 2.12.2-1 – Comparison of Strongback and Steel Rod Payloads in Bending

Security Related Information
Figure Withheld Under 10 CFR 2.390

Figure 2.12.2-2 – Dummy Fuel Assembly Cross Section

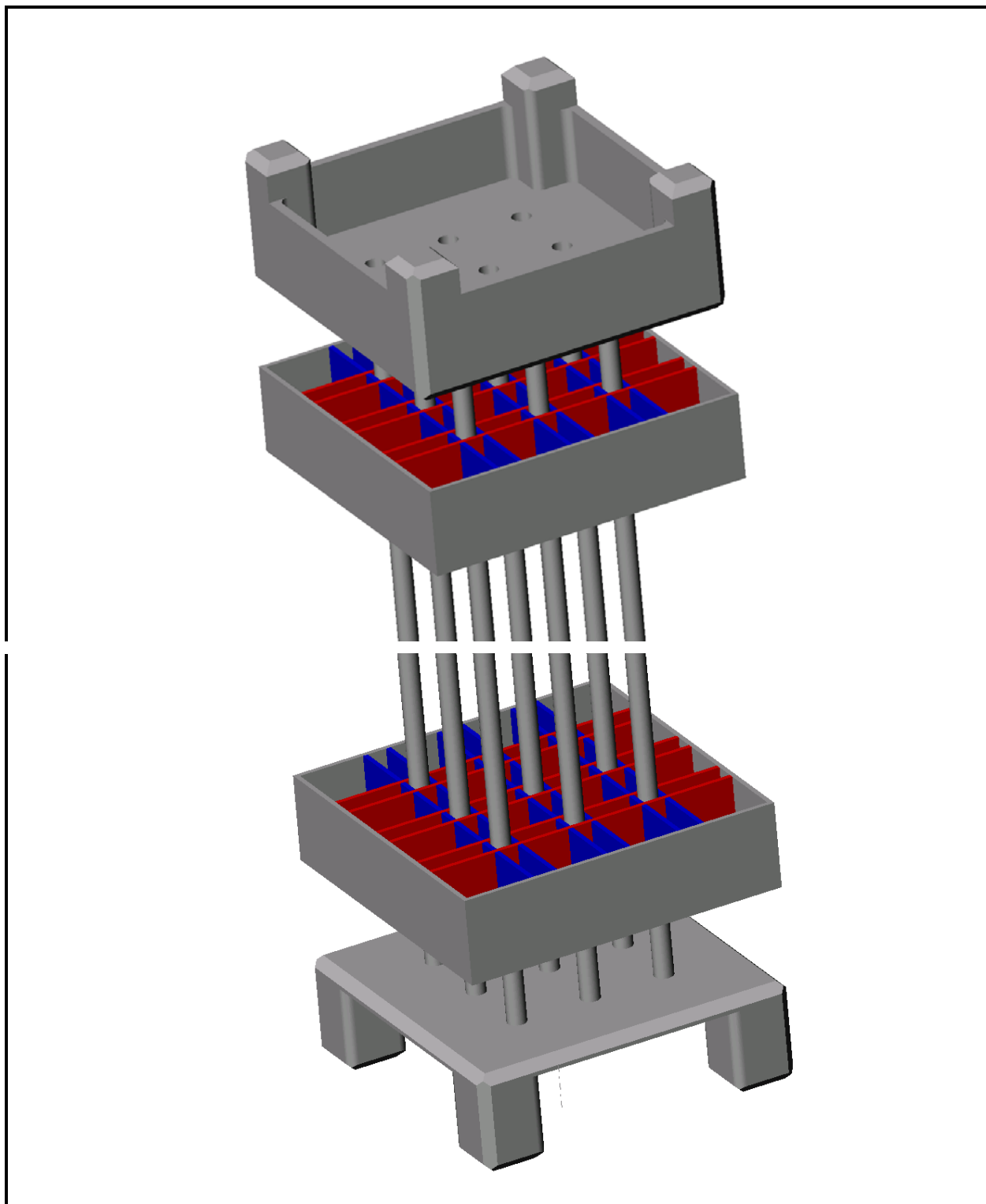


Figure 2.12.2-3 – Dummy Fuel Assembly (Fill Rods Removed for Clarity)

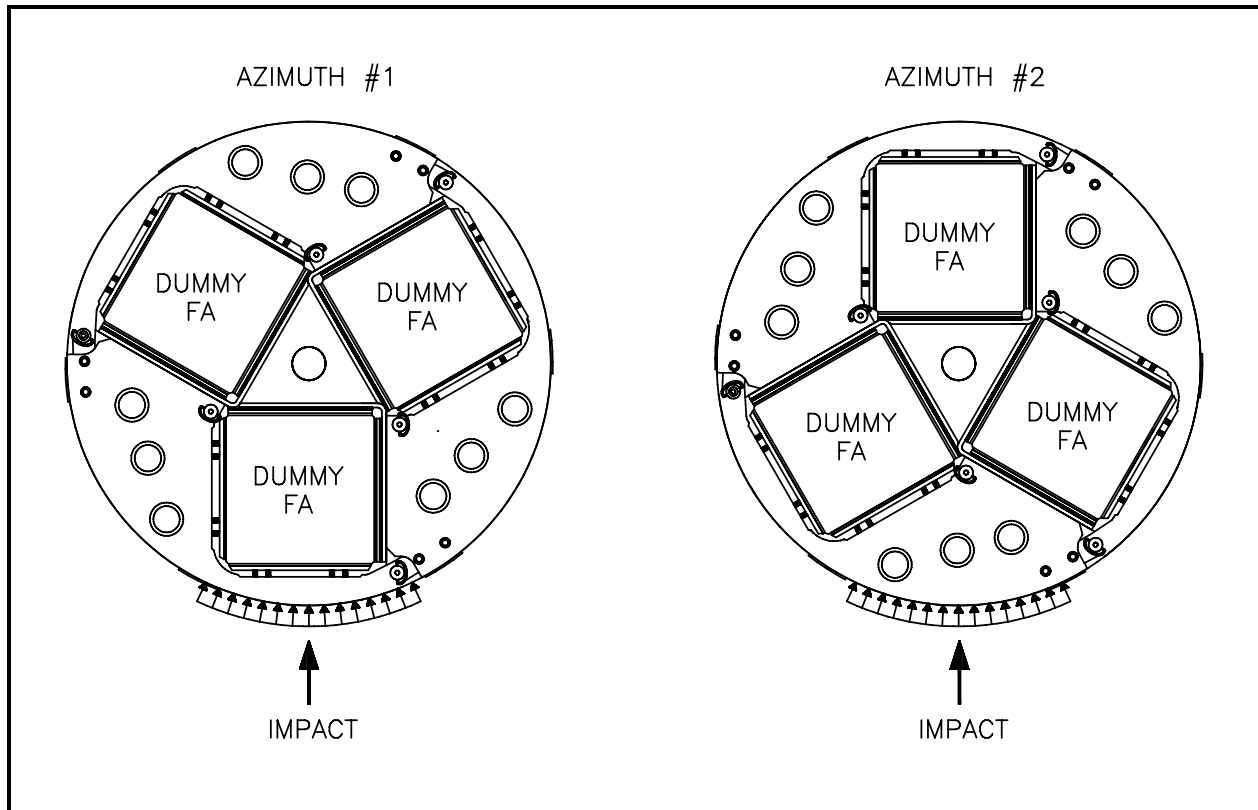


Figure 2.12.2-4 – Strongback Azimuth Orientations

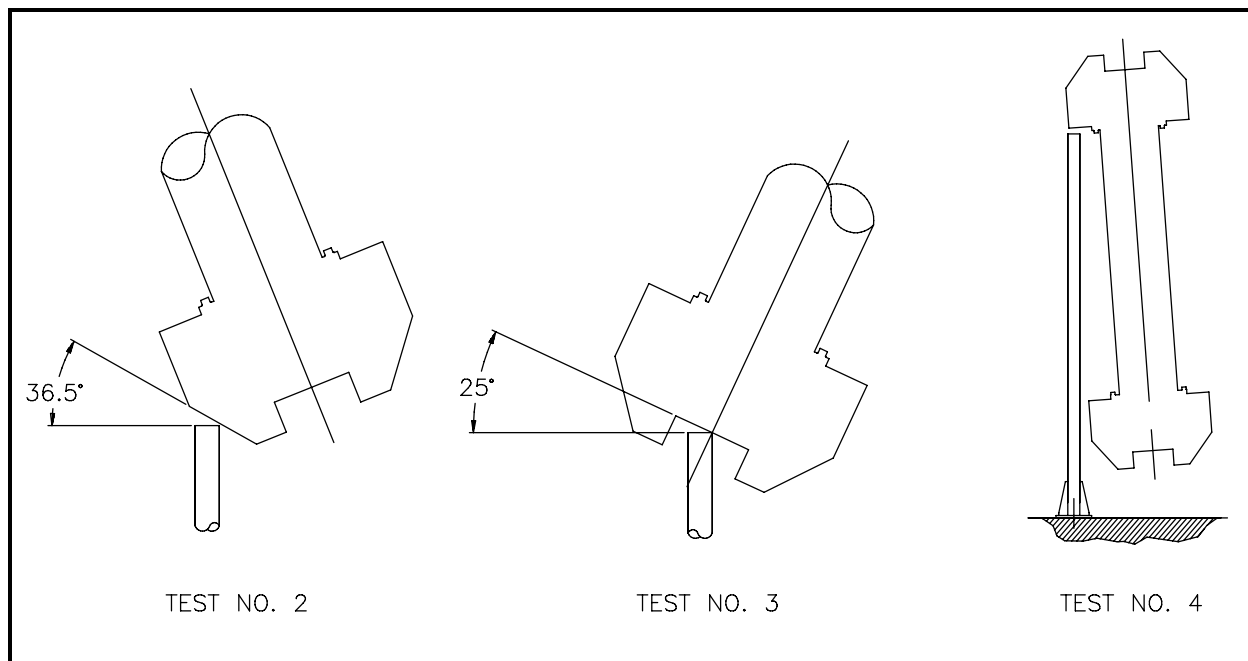


Figure 2.12.2-5 – Puncture Orientations for Test Series 1

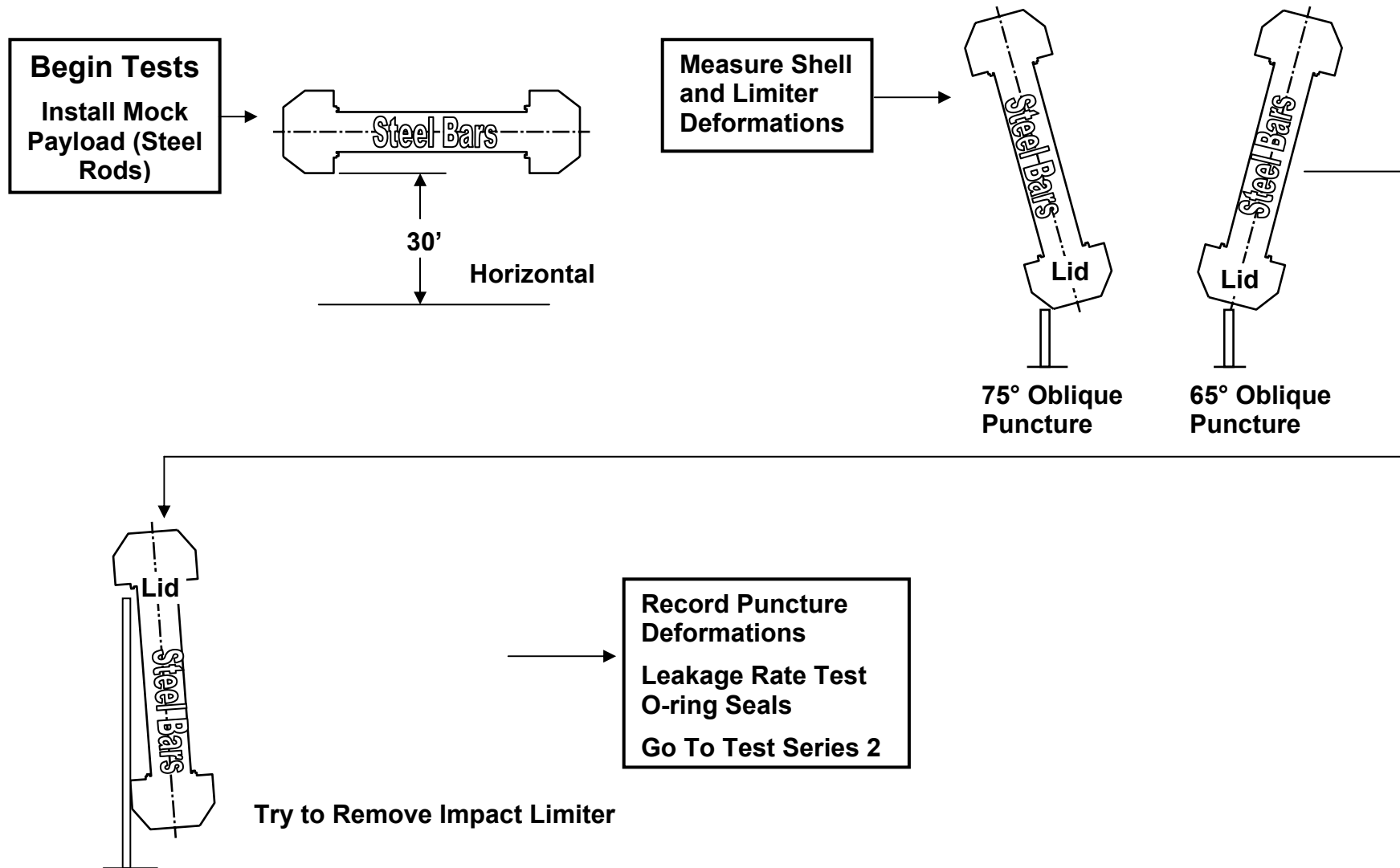


Figure 2.12.2-6 – Certification Test Series 1

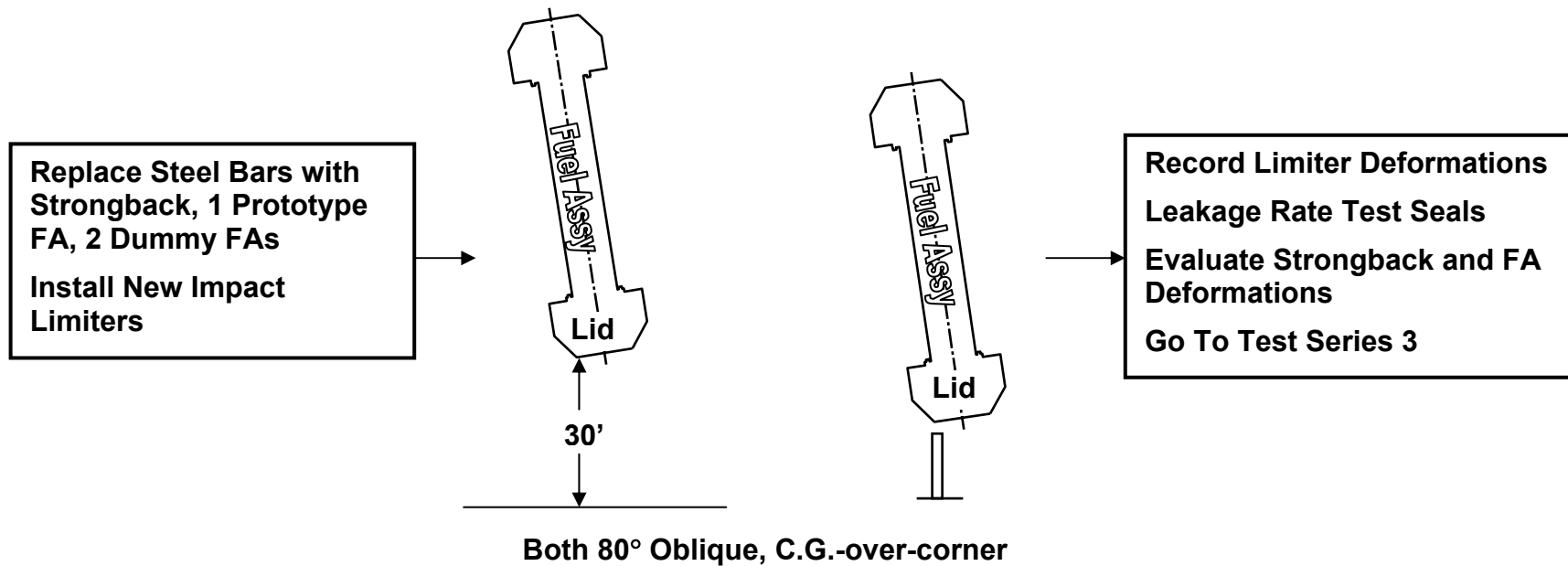


Figure 2.12.2-7 – Certification Test Series 2

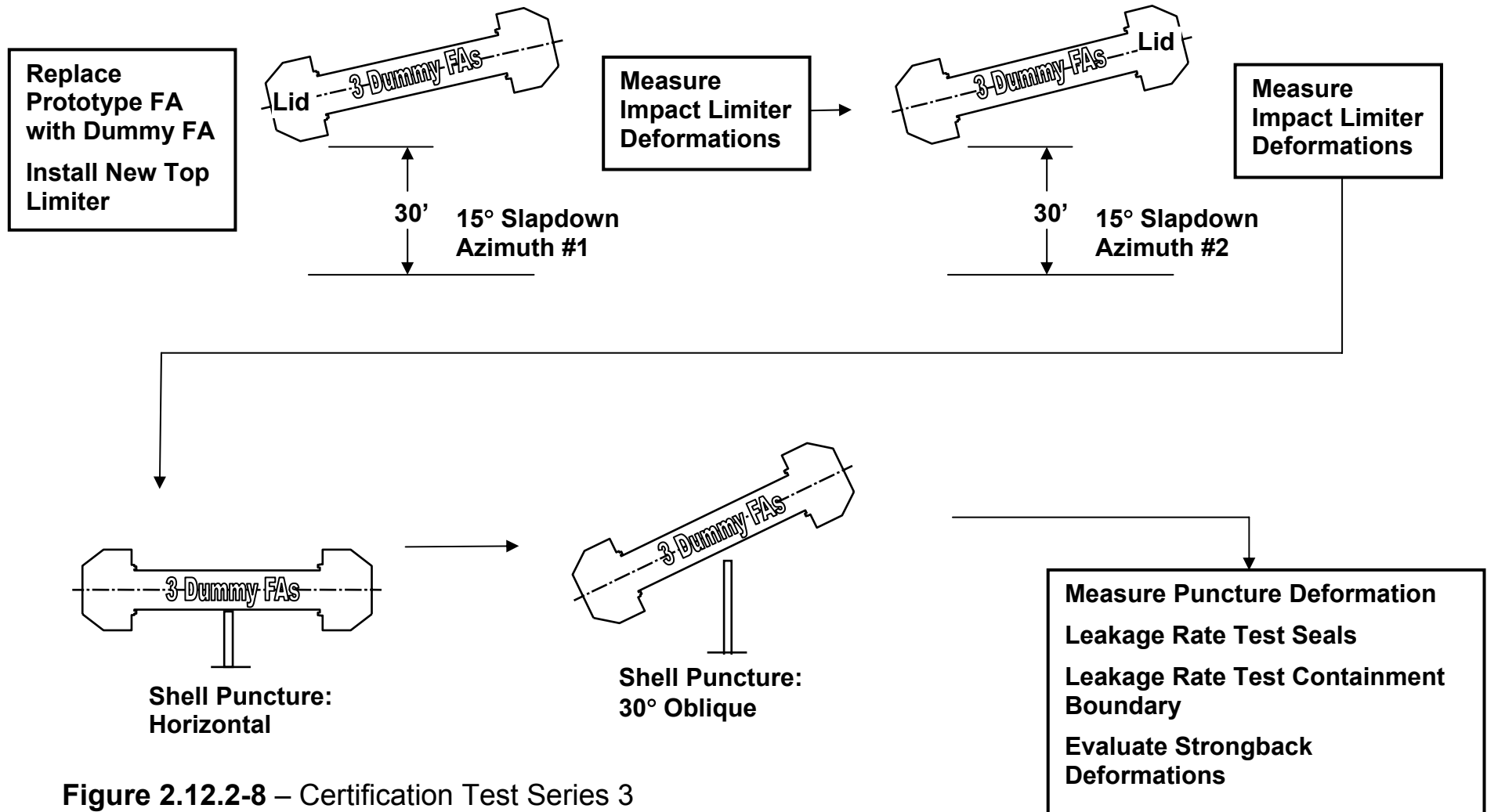


Figure 2.12.2-8 – Certification Test Series 3

This page left intentionally blank.

2.12.3 Certification Test Results

This appendix presents the results of hypothetical accident condition (HAC) tests that address the free drop and puncture test performance requirements of 10 CFR 71¹.

2.12.3.1 Introduction

The MFFP, when subjected to the sequence of hypothetical accident condition (HAC) tests specified in 10 CFR §71.73, subsequent to the free drop requirement of normal conditions of transport (NCT) tests specified in 10 CFR §71.71, is shown to meet the performance requirements specified in Subpart E of 10 CFR 71. Demonstration of compliance with the requirements is by a combination of full-scale testing and analysis. To support the free drop analysis activities, each of the free drops were recorded on high speed video, as discussed in Section 2.12.3.4.2, *Photometrics*, and following Series 2 with active instrumentation (accelerometers) to measure impact forces, as discussed in Section 2.12.3.4.1, *Accelerometers*. The HAC puncture tests were recorded with high speed video alone without active instrumentation. In particular, free drop and puncture testing of a MFFP CTU confirms that, after a worst-case HAC sequence, the containment boundary remains leaktight². Observations from testing of the CTU also confirm the conservative nature of impact limiter damage assumptions utilized in the thermal evaluation and strongback deformation used in criticality evaluations. Fuel assembly (FA) deformations were greater than expected and are discussed in detail below.

2.12.3.2 Summary

The MFFP certification tests were developed in a test plan (see Appendix 2.12.2, *Certification Test Plan*). Four 30-foot free drop tests and up to six 40-inch puncture drop tests were originally identified for inclusion in the certification test program. As described below, one of the free drop tests was repeated to gain additional information. Although only a single worst-case free drop followed by a single worst-case puncture drop is required by 10 CFR §71.73, additional tests performed were to ensure that each area of potential concern was subjected to worst-case conditions. A summary of all of the CTU test series is provided in Table 2.12.2-2 of Appendix 2.12.2, *Certification Test Plan*.

Because of the large number of tests performed, cumulative damage of CTU components was of some concern. Of particular importance are the performance tests of the criticality control structures, in which fuel assembly or strongback deformations are of primary interest. If subjected to over testing, the deformations from one test could invalidate the deformations of the following test. Therefore, the tests were conducted in three series. As required by 10 CFR §71.73(a), the puncture tests followed the free drop tests. Accordingly, each series of tests consisted of one or two 30-foot free drops followed by one or more puncture drop tests. At the end of each series, the package was evaluated before proceeding to the next test. Prior to opening the package, a leakage rate test was performed of all containment seals (closure lid and closure penetrations). At the end of all tests, a

¹ Title 10, Code of Federal Regulations, Part 71 (10 CFR 71), *Packaging and Transportation of Radioactive Material*, Final Rule, 01-26-04.

² “Leaktight” is a leakage rate not exceeding 1×10^{-7} reference - cubic centimeters per second (ref-cc/sec), air, as defined in ANSI N14.5-1997, *American National Standard for Radioactive Materials – Leakage Tests on Packages for Shipment*, American National Standards Institute, Inc. (ANSI).

leakage rate test of the entire containment boundary was performed. A leakage rate of less than or equal to 1×10^{-7} ref-cc/sec, air, was demonstrated following each test series.

A single containment boundary (body, closure lid and closure bolts) was utilized for all of the test series. The strongback and impact limiters were strategically replaced between test series, while the O-ring seals were replaced for each test series.

2.12.3.3 Test Facilities

Drop testing was performed at the Coyote Canyon Aerial Cable Facility of Sandia National Laboratories, in Albuquerque, New Mexico. The drop pad has a total weight of approximately two million pounds, which includes a 4-inch to 8-inch thick steel armor plate embedded in the top of the pad. The drop test facility has a 50,000 pound capacity for the regulatory defined, hypothetical accident condition 30-foot free drop. Therefore, the drop pad constituted an unyielding surface for the CTU, which had a maximum gross weight of approximately 13,800 pounds. The package was released by means of explosive cable cutters or a cargo release hook.

In accordance with the requirements of 10 CFR §71.73(c)(3), the puncture bars were fabricated from solid, 6-inch diameter mild steel. The puncture bars were welded perpendicularly to a 2-inch thick, mild steel plate having an outside square dimension of approximately 24 inches. The top edge of the puncture bar was finished with a maximum 1/4 inch radius. When utilized, the puncture bar was securely welded (mounted) to the impact surface, as shown in Figure 2.12.3-1.

2.12.3.4 Instrumentation

2.12.3.4.1 Accelerometers

Accelerometers were used to record data for selected 30-foot free drops. The number and placement of the accelerometers varied by drop and is described within each test description. The accelerometers were Endevco Model 7270A piezoresistive type. Data was recorded, conditioned, and reduced by the Sandia Mobile Instrumentation Data Acquisition System (MIDAS). A Fast Fourier Transform (FFT) of the raw data was performed to aid in the determination of the appropriate cutoff, or filtering frequency, for each drop orientation. The cutoff frequency was chosen to remove resonance and to find the rigid body response of the MFFP during a free drop.

2.12.3.4.2 Photometrics

With exception of two (2) puncture drops, all of the tests were recorded using high speed video. Generally four (4) cameras were set up; two (2) 1,000 frames per second (fps) digital cameras and two (2) 400 fps film cameras.

2.12.3.5 Initial Test Conditions

As shown in Section 2.12.2.1.1, *Internal Pressure*, the hoop stress in the containment shell that results from the internal pressure creates an insignificant contribution to the maximum containment shell stress in HAC free drop and puncture drop events. Consequently, no internal pressure was utilized in the CTU during testing.

To achieve maximum impact from the free drops, all of the test series began with the principal energy absorbing materials (crushable foam) below the minimum regulatory temperature of -20 °F. Only the impact limiters were chilled prior to each test series, except for Test Series 1, where the body was also chilled. For the remaining test series, chilled impact limiters were installed on the body, which was at ambient temperature. The results of these tests are therefore conservative, since the maximum cold impact forces were imposed on structures having slightly lower, ambient temperature strength.

No specific cooling was performed prior to the puncture drops. However, because the foam is highly thermally resistive, the temperature of the foam during the puncture drops was often considerably cooler than ambient conditions. All puncture drop tests on the body shell were performed with the shell at ambient temperatures.

Calibrated K-type thermocouples were installed in each of the impact limiters as shown in Figure 2.12.3-2. The thermocouple insertion depth was 10 to 15 inches.

2.12.3.6 Test Unit Description

The CTU was a prototypic, full-scale MFFP except as detailed below. A single prototypic body, closure lid, and set of closure lid bolts were used for all tests. A total of 5 impact limiters were used: 3 lid end and 2 bottom end impact limiters. Two (2) prototypic strongbacks were used. The simulated payload was varied for each test series, as described in Section 2.12.3.7, *CTU Payloads*.

The differences between the MFFP CTU and the MFFP packaging design depicted in Appendix 1.4.2, *Packaging General Arrangement Drawings*, are summarized as follows:

- Fuel Control Structures (FCSs): The FCSs were added to the strongback in response to the results of Test Series No. 2. Therefore, the CTU was tested without the FCSs installed. The FCSs are discussed in Section 2.7, *Hypothetical Accident Conditions*, and evaluated in Appendix 2.12.5, *Fuel Control Structure Evaluation*.
- Impact Limiter Closure Weld Joint: The final closure weld on the CTU lid end impact limiter consisted of a single-sided fillet between the corner angle and the 1/4-inch plate rather than the specified V-groove butt weld. The performance difference between these two weld joint designs is discussed in Section 2.12.7, *Impact Limiter Weld Joint Test Results*, which demonstrated that the packaging groove weld joint will preclude weld failure. Therefore, the use of the fillet weld joint design for the CTU testing is conservative.
- Closure Lid Bolt Preload: The CTU closure lid bolts were tightened to a maximum 250 lb_f-ft torque. The maximum specified tightening torque is 220 lb_f-ft. Since the difference in preload is small, the effect on the response of the closure lid to the free drops is minimal and may be neglected.
- Shortened Strongback Slots: To accommodate the addition of the 2 × 2 × 1/4 tube associated with the FCS, the slots on the longitudinal plates of the strongback were shortened from 2.00 inches to 1.00 inch for the CTU. The use of longer length slots had no effect on the response of the CTU strongback to the free drops.
- Seal Area Surface Finish: The surface finish on the CTU closure lid and seal flange was a 32 micro-inch finish rather than the specified 125 micro-inch finish. This smoother surface is conservative for sealing the butyl rubber material since the rougher surface finish will form a better seal than the smoother finish. The 125 micro-inch finish is the surface finish

recommended by Parker O-ring Handbook³. Therefore, this deviation had no effect on the O-ring seal performance of the CTU.

- **Location of Seal Test and Fill Ports:** The angle between the seal test port and the fill port was 30 degrees rather than the 120 degrees that is specified on Drawing 99008-20. Since the location of these ports have no effect on their performance, this variation had no effect on the structural response of the CTU to the free and puncture drop tests.
- **Closure Lid Bolt Hole Locations:** The closure lid bolt holes for the CTU were incorrectly drilled at a diameter of 30.07 inches rather than the specified diameter of 30.70 inches. To correct this error, new holes were drilled at the correct diameter by rotating the locations 7.5 degrees, which places the new holes halfway between the incorrect holes. The incorrectly drilled holes were then plugged with machined bar stock and welded in place using 1/8-inch groove welds. Since there are additional holes, this condition results in a weakened closure lid and was conservative for the free and puncture drop tests.
- **Impact Limiter Bolt Plating:** The CTU impact limiter bolts were not nickel plated. The lack of plating had no effect on the response of the impact limiter bolts to the free and puncture drop tests.
- **Test Instrumentation (e.g., thermocouples, accelerometers):** Active test instrumentation was used for the CTU. The addition of this instrumentation had no effect on the response of the CTU to the testing.
- **Handling Threaded Holes:** Tapped holes were added to the top surfaces of the MFFP CTU impact limiter lugs to facilitate lifting and handling the package during testing. The inclusion of these holes in the CTU is conservative.
- **Temporary Leakage Rate Test Port:** A temporary 1-inch NPT port was placed in the containment body to permit leakage rate testing dwell time determination. Following this determination, the hole was plugged and seal welded. The inclusion of this port in the CTU is conservative.
- **Strongback Retaining Bolts:** Following Series 1, the three 1/2-inch socket head cap screws (SHCS) that secure the strongback to the inside the body failed. The threaded portion of the SHCS within the lugs could not be removed. Therefore, the subsequent Test Series 3 and the Data Test (Test 11) were performed without these SHCS installed. Because very little force is required to fail these screws, the absence of the SHCS had no effect on the response of the CTU strongback to the free and puncture drop tests.
- **Gross Weight:** The lightest CTU configuration was in Test Series 3, at 13,217 pounds. This weight is somewhat lighter than the maximum MFFP gross weight of 14,260 pounds (see Section 2.1.3, *Weights and Center of Gravity*). However, since the lighter weight resulted in higher impact forces in the test, and since the maximum temperature effect is conservatively evaluated in Appendix 2.12.1, *Impact Limiter Evaluation*, the effect of the lighter weight CTU is fully evaluated.

The following table summarizes the major component weights of the CTU for each test series:

³ ORD 5700, *Parker O-ring Handbook*, 1992, Parker Hannifin Corporation, Cleveland, OH.

Packaging Component	Test Series 1	Test Series 2	Test Series 3
Empty Package			
• Body and Closure Lid/Bolts	3,775	3,775	3,775
• Strongback	N/A	2,102	2,100
• Lid End Impact Limiter	1,474	1,476	1,477
• Bottom End Impact Limiter	1,066	1,077	1,077
• Total	6,315	8,430	8,429
Payload			
• Mock Payload	7,500	N/A	N/A
• Fuel Assemblies	N/A	4,804	4,788
• Total	7,500	4,804	4,788
Total Loaded Package	13,815	13,234	13,217

2.12.3.7 CTU Payloads

2.12.3.7.1 Mock Payload

The mock payload consists of a bundle of approximately 800, 1/2-inch diameter steel bars, including end caps, having a total weight of 7,500 pounds. The mock payload is utilized in free drop orientations where the response of the strongback/fuel assemblies is not important (e.g., maximum bending forces on the body containment shell). A complete discussion of the mock payload is provided in Section 2.12.2.2.1, *Mock Payload*. The mock payload is shown in Figure 2.12.3-3.

2.12.3.7.2 Dummy Fuel Assembly

The dummy fuel assemblies used for certification testing were designed to simulate the weight, weight distribution, and structural properties of the real fuel assemblies, as discussed in Section 2.12.2.2.2, *Dummy Fuel Assembly*. The weights of the dummy assemblies were 1,592, 1,594, and 1,602 pounds, all slightly in excess of the MOX FA maximum weight of 1,580 pounds. The dummy fuel assembly is shown in Figure 2.12.3-4 and Figure 2.12.3-5.

2.12.3.7.3 Prototypic Fuel Assembly

A single prototypic FA was used for Test Series 2. As discussed in Section 2.12.2.2.3, *Prototypic Fuel Assembly*, the prototypic FA was an exact facsimile of the MOX FA, except that the fissile MOX fuel pellets were simulated using tungsten carbide pellets. The weight of the prototypic FA was 1,608 pounds, which was conservatively 28 pounds heavier than the maximum MK-BW/MOX1 FA weight of 1,580 pounds.

2.12.3.8 Test Results

The following sections report the results of free drop and puncture drop tests following the sequence provided in Appendix 2.12.2, *Certification Test Plan*.

Figure 2.12.3-6 through Figure 2.12.3-40 sequentially photo-document the certification testing process for the CTU.

2.12.3.8.1 Certification Test Series No. 1

2.12.3.8.1.1 Configuration

The package was assembled per drawings in Appendix 1.4.2, *Packaging General Arrangement Drawings*, except that the mock payload of steel bars replaced the strongback assembly. Prior to beginning all testing, the full containment boundary was leakage rate tested. Upon final closure prior to testing, the closure lid containment seals were successfully leakage rate tested.

2.12.3.8.1.2 Series 1, Test 1: 30-Foot Free Side Drop

The following list summarizes the test parameters:

- The CTU was oriented 0 degrees from horizontal (parallel to the target surface, as shown in Figure 2.12.3-6).
- The drop height was 30 feet.
- The lid end impact limiter foam temperature was -19 °F to -26 °F
- The bottom end impact limiter foam temperature was -22 °F to -24 °F
- The ambient temperature was 83 °F.
- Test conducted at 1:06 p.m. on Monday, 9/22/03.

A small rebound (bounce) occurred upon impact. The measured permanent deformation of the lid end impact limiter was approximately 24 inches (parallel to axis of the MFFP) × 28 inches and for the bottom end impact limiter, it was approximately 23 inches (parallel to axis of the MFFP) × 28 inches. The weld seam on the lid end impact limiter was split for a length of approximately 28 inches and less than 3 inches wide (see Figure 2.12.3-7). Based upon the width of the crushed impact limiters and the 400 frames per second (fps) video record, the depth of crush was approximately 4.4 inches and the approximate acceleration level was 140 g's. The final crush deformation was approximately 3½ inches. The body exhibited no signs of permanent deformation, without any bending along the body axis.

2.12.3.8.1.3 Series 1, Test 2: Near-Vertical HAC 40-Inch Puncture Drop

Originally, the near-vertical 40-inch puncture drop was planned to be the 4th test of Test Series 1. The drop order was changed so that the weld split caused by the 30-foot side drop could be immediately and directly challenged. The package was not re-chilled prior to the following puncture drop tests.

The following list summarizes the test parameters:

- The CTU was oriented 27 degrees from vertical (as shown in Figure 2.12.3-8). This orientation was chosen in order to expose the weakest part of the opening to the puncture bar.
- The drop height was 40 inches from the impact point to the top of the puncture bar. The impact point was the center of the damaged weld.
- The ambient temperature was 71 °F.
- Test conducted at 10:50 a.m. on Tuesday, 9/23/03.

The puncture bar struck the weld seam split directly and caused the split to open from 3 inches to approximately 5 inches. A few very small pieces of foam broke and fell from the impact limiters, but there was no bulk loss of foam (see Figure 2.12.3-9).

2.12.3.8.1.4 Series 1, Test 3: HAC 65-Degree Oblique 40-Inch Puncture Drop

The following list summarizes the test parameters:

- The CTU was oriented 66.5 degrees from horizontal (as shown in Figure 2.12.3-10).
- The puncture bar was aligned to strike the impact limiter end recessed plate.
- The drop height was 42 inches from the impact point to the top of the puncture bar.
- The ambient temperature was 80 °F.
- Test conducted at 2:26 p.m. on Tuesday, 9/23/03.

The puncture bar struck the lid end impact limiter end recessed plate causing a tear in the plate and resulted in an approximately 3-inch deep deformation. No foam was lost (see Figure 2.12.3-11).

2.12.3.8.1.5 Series 1, Test 4: HAC 75-Degree Oblique 40-Inch Puncture Drop

The following list summarizes the test parameters:

- The CTU was oriented 77 degrees from horizontal (as shown in Figure 2.12.3-12).
- The drop height was 40 inches from the impact point to the top of the puncture bar.
- The puncture bar was targeted to impact just below the ripple on the impact limiter from Test 1.
- The ambient temperature was 79 °F.
- Test conducted at 4:51 p.m. on Tuesday, 9/23/03.

The puncture bar struck the lid end impact limiter conical shell, resulting in a dent approximately 4 inches long. There was no puncture or tearing of the shell (see Figure 2.12.3-13).

2.12.3.8.1.6 Series 1 Test Results

Following the completion of the Series 1 drop tests, the CTU was removed from the drop site and taken to the shop facility. After removal of the impact limiters, a helium leakage rate test of the containment and vent port O-ring seals were successfully performed. Following the leakage rate test, the closure lid bolts and closure lid were removed. After removal of the mock payload, the interior of the body was cleaned and prepared for the next test series.

The Series 1 test results are summarized as:

- Test 1: 30-foot Side Drop
 - a. Containment shell did not buckle or plastically deform.
 - b. Lid end impact limiter shell weld at the outer diameter weld failed for approximate length of the crush zone (~28 inches). The maximum width of the split was less than 3 inches.
 - c. Impact deformation 4.4 inches, impact acceleration 140 g's.

- Test 2: Near-Vertical 40-inch Puncture Drop
 - a. The impact limiter was not removed by the puncture bar.
 - b. Impact limiter bolts did not stretch.
 - c. The width of the impact limiter shell split which originally occurred in Test 1 of this series was locally increased to ~5 inches. The overall length of the split did not increase.
- Test 3: 65-Degree Oblique 40-inch Puncture Drop

A 'crescent moon' tear of the top impact limiter end recessed plate resulting in a partial puncture of ~3 inches deep. No permanent deformation of the closure lid occurred.
- Test 4: 75-Degree Oblique 40-inch Puncture Drop

Conical shell of lid end impact limiter exhibited no sign of puncture or tearing of the shell.
- Conclusions of Test Series 1
 - a. Containment shell did not buckle.
 - b. Containment and vent port O-ring seals remained leaktight.
 - c. Impact limiters did not separate from body.
 - d. A majority of the closure lid bolt disassembly torques ranged from 160 lb_f-ft to 190 lb_f-ft. Two bolts had disassembly torques of 285 lb_f-ft and 350 lb_f-ft. None of the bolts appeared to be damaged.
 - e. As described above, the lid end impact limiter outer diameter corner weld joint failed along the crush zone. The puncture drop that directly attacked this damage increased the width of the joint, but did not remove or tear the impact limiter shell.

2.12.3.8.2 Certification Test Series No. 2

2.12.3.8.2.1 Configuration

The CTU was assembled per the drawings in Appendix 1.4.2, *Packaging General Arrangement Drawings*, using new, undamaged impact limiters. The payload consisted of the strongback, assembled with one (1) prototypic Fuel Assembly and two (2) Dummy Fuel Assemblies. Prior to testing a leakage rate test of the containment and vent port O-rings was performed successfully.

2.12.3.8.2.2 Series 2, Test 1: HAC 80-Degree Oblique C.G.-Over-Corner 30-Foot Drop

The following list summarizes the test parameters:

- The CTU was oriented 79 degrees from horizontal (as shown in Figure 2.12.3-14).
- The drop height was 30 feet.
- The lid end impact limiter foam temperature was -32 °F (primary impact end)
- The bottom end impact limiter foam temperature was -25 °F
- The ambient temperature was 77 °F.
- Test conducted at 11:47 a.m. on Monday, 9/29/03.

A rebound (bounce) of approximately 6 inches occurred and the duration of the impact, from first strike to rebound release was approximately 0.030 seconds. Based on the examination of the video metrics, the impact axial acceleration was approximately 100 g's. Figure 2.12.3-15 shows the resulting impact damage on the upper end impact limiter. Using the 1,000 fps video, the maximum crush, before rebound, is determined to be approximately 6.1 inches (see Figure 2.12.3-16). To gain additional information, this test was performed again with accelerometers (see Section 2.12.3.8.4, *Data Test (Test 11): Series 2, Test 1 Repeated With Accelerometers*). Also shown on Figure 2.12.3-16 are the results of the Data Test (Test #11) that essentially repeated this test and demonstrate the consistency of deformations. The repeated test deformation results are based on integration of accelerometer data.

2.12.3.8.2.3 Series 2, Test 2: HAC 80-Degree Oblique 40-inch Puncture Drop

The following list summarizes the test parameters:

- The CTU was oriented 80.1 degrees from horizontal (as shown in Figure 2.12.3-17).
- The drop height was 40 inches.
- The puncture bar was targeted to strike on the center of damage from Test 1 of this series.
- Impact limiters were not re-chilled prior to drop.
- The ambient temperature was 81 °F.
- Test conducted at 4:36 p.m. on Monday, 9/29/03.

The puncture bar struck the damage from Test 1 of this series. The puncture bar caused a small crack in the impact limiter shell, but did not perforate through the shell (see Figure 2.12.3-18).

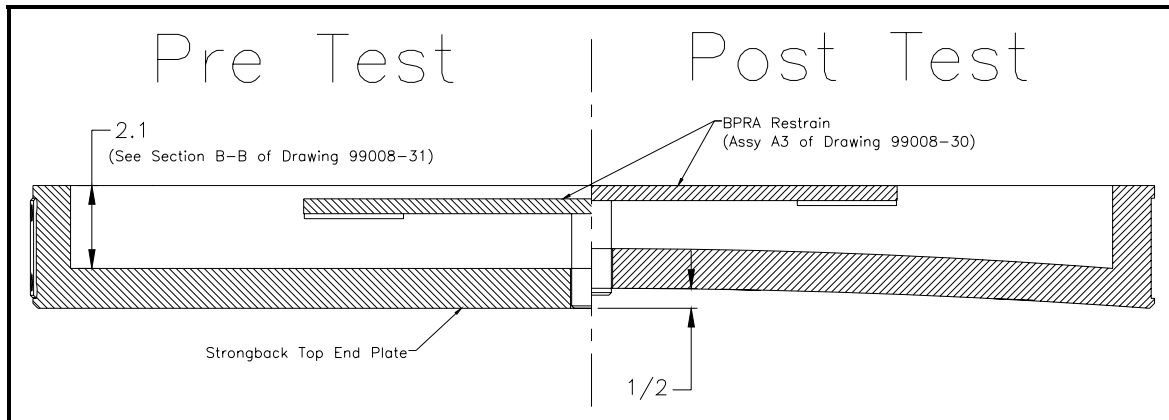
2.12.3.8.2.4 Series 2 Test Results

Following the Series 2 tests, the CTU was taken to the shop area for further inspection, leakage rate testing, and disassembly. The bottom end impact limiter was to be reused on the next series and was not removed. The lid end impact limiter was removed and stored. A helium leakage rate test of the containment and vent port O-ring seals was successfully performed after Series 2.

The Series 2 Test results are summarized as:

- Test 1: 80-Degree Oblique C.G.-Over-Corner 30-foot Drop
 - a. Containment shell did not buckle or plastically deform.
 - b. Impact deformation 6.1 inches, Impact acceleration 100 g's.
- Test 2: 80-Degree Oblique C.G.-Over-Corner Puncture Drop.
 - a. C.G.-over-corner puncture caused a very minor crack in the conical shell of the impact limiter.
 - b. Impact limiters were not removed.
 - c. The impact limiter shell was not penetrated, torn, or removed.
- Conclusions of Test Series 2
 - a. Containment O-ring seals remained leaktight.
 - b. The closure lid bolt disassembly torques ranged from 185 lb_r-ft to 225 lb_r-ft. None of the bolts appeared to be damaged.

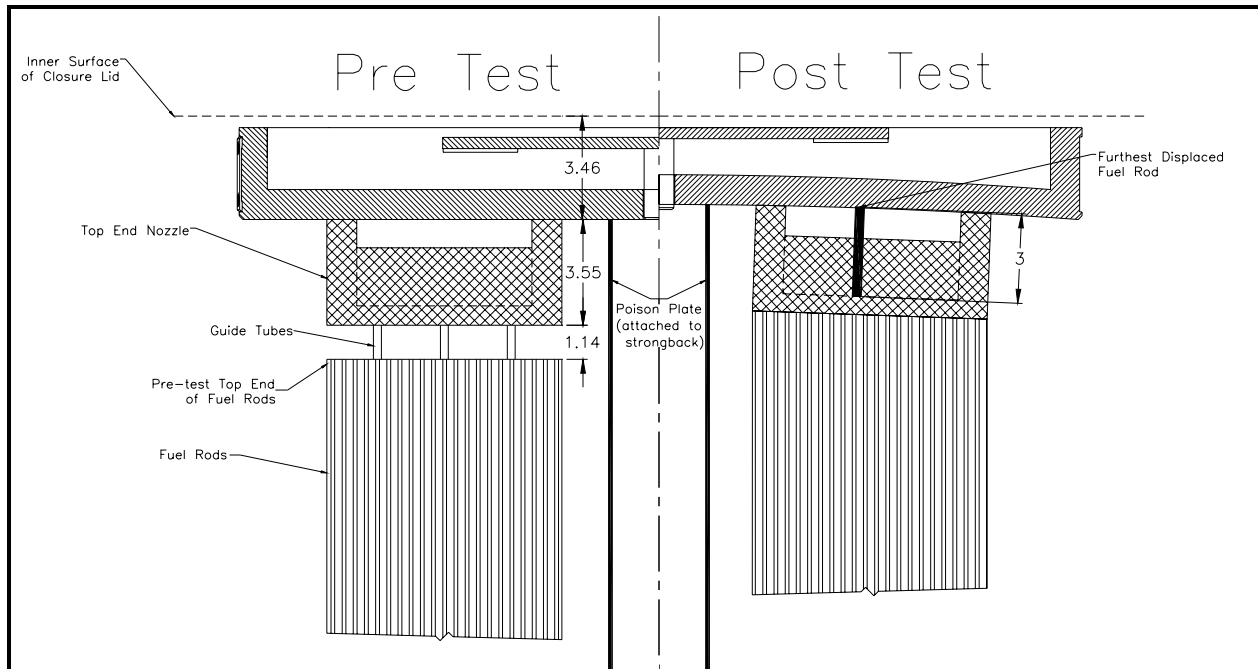
- c. One impact limiter bolt on the lid end impact limiter could not be removed using a wrench and was cut off.
- d. The top plate of the strongback was permanently deformed outwards (toward the lid) by approximately 1/2 inch. The top plate deformations described are the maximum, which occurs at the center to the strongback top plate. The design of the top plate is such that there is a 2.1 inch thick 'rim' at the outer diameter, which provides the central portion room to deform. See the schematic below which shows the type of deformation, and where the deformation measurement was taken.



Schematic of Strongback Top Plate Deformation

- e. The strongback retained its basic geometry with minor bending of the longitudinal plates at the top plate connection.
- f. The clamp arms remained in place and retained both the prototypic and dummy fuel assemblies in their global positions. Following the drops of this series, the clamp arms remained functional.
- g. The prototypic FA exhibited lateral deformations. The deformations caused the FA cross-section width to increase for the first 20 inches of fuel length (nearest the impact end). The post-test cross-section width, measure perpendicular to the axis of the containment body, is described graphically on Figure 2.12.3-19. The cross-section width measurements were taken every 6 inches. The maximum increase in cross-section width was approximately 1.1 inches. Figure 2.12.3-22 shows the location of maximum increase in cross-section width. This FA location was in the 'down' position during the drops. Figure 2.12.3-20 and Figure 2.12.3-21 provide additional views of the prototypic FA following the completion of the test series.
- h. Approximately eight (8) rods displaced through the top end nozzle by less than 3 inches. The flow plate of the top nozzle deformed outward. See Figure 2.12.3-23. The original distance from the top of the rods to the underside of the top end nozzle of the FA was 1.14 inches and the top end nozzle had a total depth of 3.55 inches. Schematically illustrated below are the pre- and post-test locations of several components of interest. The components are shown in a representative fashion, thus detail that is not essential to the discussion has been removed. Note that the poison plates coverage extend up to the underside of the strongback top plate. Because of the plenum, fissile material within the fuel rods starts approximately 7.3 inches below the top end of the fuel rod. Thus, even if

the fuel had displaced as far as the closure lid, the fissile material would be surrounded by the neutron poison plates.



Schematic of Strongback Top End Plate Deformation including Fuel Rod Displacement

- i. The neutron poison plates remained in position and had two minor cracks near the top nozzle of the prototypic fuel assembly. See Figure 2.12.3-24.
- j. Visual inspection revealed no fuel rod cladding rupture.

2.12.3.8.3 Certification Test Series No. 3

2.12.3.8.3.1 Configuration

The CTU was assembled per the drawings in Appendix 1.4.2, *Packaging General Arrangement Drawings*, using the bottom impact limiter from Test Series 2, and a new lid end impact limiter. A new (un-damaged) strongback was assembled with three (3) dummy fuel assemblies. A successful leakage rate test of the containment and vent port O-rings was performed. Four accelerometers were installed for the 30-foot drops of this test series. Two accelerometers were attached to the impact limiter doubler plates at each end of the CTU (23 inches from each end of the body). One accelerometer at each end recorded lateral g's (i.e., perpendicular to CTU longitudinal axis), and the second recorded axial g's (i.e., parallel to CTU longitudinal axis). Figure 2.12.3-25 illustrates the accelerometer locations.

2.12.3.8.3.2 Series 3, Test 1: HAC 15-Degree Slapdown 30-Foot Drop (Lid End Primary)

The following list summarizes the test parameters:

- The CTU was oriented 15 degrees from horizontal with the lid end of the CTU oriented for primary impact (as shown in Figure 2.12.3-26). Azimuth orientation #1 was used for this test. Figure 2.12.2-4 of Appendix 2.12.4 shows the definition of the azimuth orientations.
- The drop height was 30 feet.

- The lid end impact limiter foam temperature was -33 °F
- The bottom end impact limiter foam temperature was -35 °F
- Prior damage to the bottom end impact limiter was oriented 120 degrees from impact
- The ambient temperature was 73 °F.
- Test conducted at 12:20 p.m. on Thursday, 10/02/03.

Figure 2.12.3-27 through Figure 2.12.3-28 present the resultant lateral accelerations, filtered at 125 Hz. The primary impact resulted in a maximum lateral acceleration of 140 g's. The secondary impact resulted in a maximum lateral acceleration of 155 g's. The body exhibited no signs of permanent deformation. The secondary impact on the bottom end impact limiter resulted in a minor tear in the weld joint (see Figure 2.12.3-29). Similar to the lid end impact limiter weld in Series 1, Test 1, the weld joint failure length was approximately equal to the crush zone length.

2.12.3.8.3.3 Series 3, Test 2: HAC 15-Degree Slapdown 30-Foot Drop (Lid End Secondary)

The following list summarizes the test parameters:

- The CTU was oriented 15 degrees from horizontal with the closure lid end of the CTU oriented for secondary impact (as shown in Figure 2.12.3-30). Azimuth Orientation #2 was used for this test. Figure 2.12.2-4 in Appendix 2.12.2, *Certification Test Plan*, defines the azimuth orientations.
- The drop height was 30 feet.
- The CTU was rotated 180 degrees with respect to the containment boundary axis of revolution.
- The lid end impact limiter foam temperature was -26 °F
- The bottom end impact limiter foam temperature was -28 °F
- The ambient temperature was 76 °F.
- Test conducted at 3:50 p.m. on Thursday, 10/02/03.

The secondary impact on the lid end impact limiter caused a failure of the closure weld joint, nearly exactly as occurred on the Series 1, Test 1 30-foot side drop (see Figure 2.12.3-31). The accelerometers used in Test 1 of this series were used without modification for this test. Figure 2.12.3-32 and Figure 2.12.3-33 show the resultant lateral accelerations, filtered at 125 Hz. The primary impact resulted in a maximum lateral acceleration of 125 g's. The secondary impact resulted in a maximum lateral acceleration of 180 g's. The containment body exhibited no signs of permanent deformation.

2.12.3.8.3.4 Series 3, Test 3: HAC Horizontal Puncture Drop

The following list summarizes the test parameters:

- The CTU was oriented 0 degrees from horizontal (as shown in Figure 2.12.3-34). The puncture bar was aligned to strike a longitudinal weld of the middle body shell course.
- The drop height was 40 inches.
- The ambient temperature was 60 °F.
- Test conducted at 9:43 a.m. on Friday, 10/03/03.

The horizontal 40-inch puncture drop caused a dent approximately 2 1/8 inches deep (see Figure 2.12.3-35). Viewed externally, there was no indication of cracking or tearing of the body shell.

Because the strongback was not removable following this test, subsequent borescope viewing also revealed no indications of cracking or tearing of the body shell from the interior.

2.12.3.8.3.5 Series 3, Test 4: 30-Degree HAC 40-Inch Puncture Drop

The following list summarizes the test parameters:

- The CTU was oriented 30 degrees from horizontal (as shown in Figure 2.12.3-36).
- The drop height was 40 inches.
- The ambient temperature was 62 °F.
- Test conducted at 12:59 p.m. on Friday, 10/03/03.

The drop resulted in a dent approximately 1½ inches deep, as shown in Figure 2.12.3-37. Upon first contact, the CTU slid approximately 10-12 inches before ‘sticking’ and causing the indentation. The puncture bar was permanently bent approximately 3 degrees. Viewed externally, there was no indication of cracking or tearing of the body shell. Because the strongback was not removable following this test, an inspection was performed using a borescope viewing, which revealed no indications of cracking or tearing of the body shell from the interior.

2.12.3.8.3.6 Series 3 Test Results

Following the Series 3 tests, the CTU was taken to the shop area for further inspection, leakage rate testing, and disassembly. Both impact limiters were removed and stored. A helium leakage rate test of the containment and vent port O-ring seals was successfully performed.

The Series 3 test results are summarized as:

- Test 1: 15-Degree Slapdown 30-foot drop (lid end primary impact)
 - a. Primary impact deformation 5.1 inches, lateral acceleration 140 g’s.
 - b. Secondary impact deformation 4.2 inches, lateral acceleration 155 g’s.
 - c. Containment shell did not buckle or plastically deform.
- Test 2: 15-Degree Slapdown 30-foot drop (lid end secondary impact)
 - a. Primary impact deformation 4.4 inches, lateral acceleration 125 g’s.
 - b. Secondary impact deformation 5.2 inches, lateral acceleration 180 g’s.
 - c. Containment shell did not buckle or plastically deform.
 - d. Lid end impact limiter closure weld failed over the crush area.
- Test 3: Horizontal Puncture Drop
Horizontal puncture did not cause cracking of the containment shell.
- Test 4: 30-Degree Oblique Puncture Drop
The puncture drop did not cause cracking of the containment shell.
- Conclusions of Test Series 3
 - a. Containment and vent port O-ring seals remained leaktight.
 - b. Impact limiters were not removed.

- c. Borescope inspection of strongback revealed no significant re-configuration of the strongback axial plates or clamp arms. The borescope inspection was performed after all testing was completed. Also, refer to conclusion discussion in Section 2.12.3.8.4.3, *Data Test (Test 11) Results*, for more description of the interior.
- d. The inside surfaces of the puncture dents were viewed and showed no cracking or tearing of the containment shell material.
- e. The closure lid bolt disassembly torques ranged from 190 lb_f-ft to 230 lb_f-ft. None of the bolts appeared to be damaged.

2.12.3.8.4 Data Test (Test 11): Series 2, Test 1 Repeated With Accelerometers

2.12.3.8.4.1 Configuration

The CTU, subsequent to Test Series 3, and without removal of the contents, was reassembled with impact limiters having minimal damage. The impact zone on the lid end impact limiter was acceptable to absorb the test impact. The impact limiters were chilled to less than -20 °F prior to the test. A pre-test leakage rate test of the containment and vent port O-rings was successfully performed. Similar to Test Series 3, four accelerometers were installed for this 30-foot free drop test. Two accelerometers were attached to the impact limiter doubler plates at each end of the CTU (23 inches from each end of the body). One accelerometer at each end recorded lateral g's (i.e., perpendicular to CTU longitudinal axis), and the second recorded axial g's (i.e., parallel to CTU longitudinal axis). Figure 2.12.3-38 illustrates the accelerometer locations.

2.12.3.8.4.2 Data Test (Test 11): HAC 80 Degrees Oblique C.G.-Over-Corner 30-Foot Drop Repeated with Accelerometers

The following list summarizes the test parameters:

- The CTU was oriented 80 degrees from horizontal (as shown in Figure 2.12.3-14).
- The drop height was 30 feet.
- The lid end impact limiter foam temperature was -28 °F.
- The ambient temperature was 75 °F.
- Test conducted at 3:13 p.m. on Monday, 10/06/03.

Using the 1,000 fps video, the maximum crush, before rebound, is determined to be approximately 6.1 inches, as shown in Figure 2.12.3-40. A rebound (bounce) of approximately 6 inches occurred and the duration of the impact, from first strike to rebound release was approximately 0.030 seconds. The accelerometer data, filtered at 200 Hz, resulted in a maximum impact longitudinal acceleration of approximately 120 g's, as shown in Figure 2.12.3-39. The accelerometer trace shows 3 major peaks.

2.12.3.8.4.3 Data Test (Test 11) Results

Following the Data Test (Test 11), the CTU was transported to the shop area for further inspection, leakage rate testing, and disassembly. Both impact limiters were removed and stored. A leakage rate test of the containment seals was successfully performed.

The results for the Data Test (Test 11) are summarized as follows:

- a. Containment and vent port O-ring seals remained leaktight.

- b. The closure lid bolt disassembly torques ranged from 180 ft-lb_f to 205-lb_f. None of the bolts appeared to be damaged.
- c. Three impact limiter bolts on the lid end impact limiter could not be removed with standard tools and had to be cut-off.
- d. The containment body did not buckle due to longitudinal accelerations. Note that the containment body had two puncture dents resulting from Test Series 3.
- e. Because this test followed the puncture drop tests of Test Series 3, the strongback could not be removed from the body. The description of the strongback and containment boundary internal damage is based on what was visible with the closure lid removed and by the borescope inspection on the interior.
- f. The top plate of the strongback was permanently deformed outwards (towards the closure lid) by approximately 1/2 inch.
- g. The strongback retained its basic geometry with minor bending of the longitudinal plates where connected to the top plate.
- h. The clamp arms remained in place and retained the dummy fuel assemblies in their positions.
- i. The neutron poison plates remained in position and had two minor cracks near the top nozzle of the prototypic fuel assembly. The cracks were similar to those experienced in Test 1, Series 2, shown in Figure 2.12.3-24.

2.12.3.9 Pre-Test and Post-Test Leakage Rate Tests

Demonstration of containment vessel leak tightness was performed prior to and following each test series via a helium leakage rate test of each containment O-ring seal. In addition, a helium leakage rate test of the body structure was performed at the conclusion of the certification test series. Results of the successful mass spectrometer helium leakage rate testing are summarized below.

When accounting for the conversion between air leakage (per ANSI N14.5) and helium leakage, a 2.6 factor applies for standard temperatures and pressures. Thus, a reported helium leakage rate of 8.6×10^{-8} cc/s, helium, is equivalently 3.3×10^{-8} cc/s, air, a level well below the "leaktight" criterion of 1×10^{-7} cc/s, air, per ANSI N14.5.

Sealing Component	Maximum Detected Leakage Rate	Measurement for Test Condition
Main O-ring Seal	$<1.0 \times 10^{-8}$ cc/s, helium	All pre- and post-tests
Vent Port Plug O-ring Seal	2.0×10^{-9} cc/s, helium	All pre- and post-tests
Fill Port Plug O-ring Seal	8.6×10^{-8} cc/s, helium	Test Series 1 post-test
Body Structure	$<1.0 \times 10^{-8}$ cc/s, helium	Pre- and post-tests



Figure 2.12.3-1 – Attachment of Puncture Bar Assembly to Drop Pad

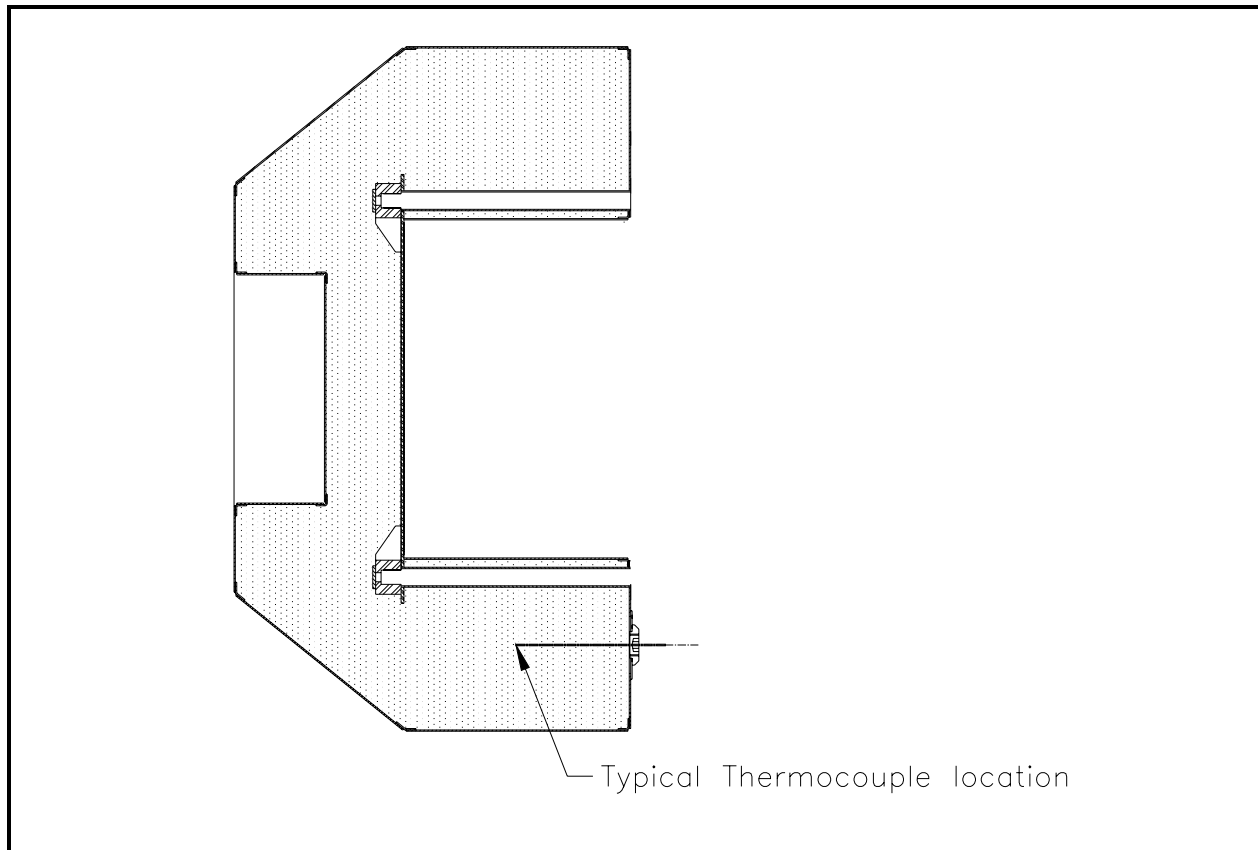


Figure 2.12.3-2 – Typical Location of Thermocouples



Figure 2.12.3-3 – Mock Payload (Shown Following Test Series 1)



Figure 2.12.3-4 – Dummy Fuel Assemblies (Supported on Fabrication Support Structures)



Figure 2.12.3-5 – Dummy Fuel Assembly (Loaded into Strongback)



Figure 2.12.3-6 – Series 1, Test 1: HAC 30-Foot Free Side Drop



Figure 2.12.3-7 – Series 1, Test 1: View of Lid End Impact Limiter Damage (~28" Length)



Figure 2.12.3-8 – Series 1, Test 2: HAC 40-inch Near Vertical Puncture Drop



Figure 2.12.3-9 – Series 1, Test 2: Close-up View of Puncture Damage



Figure 2.12.3-10 – Series 1, Test 3: HAC 65-Degree Oblique 40-Inch Puncture Drop



Figure 2.12.3-11 – Series 1, Test 3: Close-up View of Puncture Damage (~3" Deep)



Figure 2.12.3-12 – Series 1, Test 4: HAC 75-Degree Oblique 40-Inch Puncture Drop



Figure 2.12.3-13 – Series 1, Test 4: Close-up Views of Puncture Damage (~4" Length)



Figure 2.12.3-14 – Series 2, Test 1: HAC 80-Degree Oblique C.G.-Over-Corner 30-Foot Drop



Figure 2.12.3-15 – Series 2, Test 1: Overall View of Impact Limiter Damage

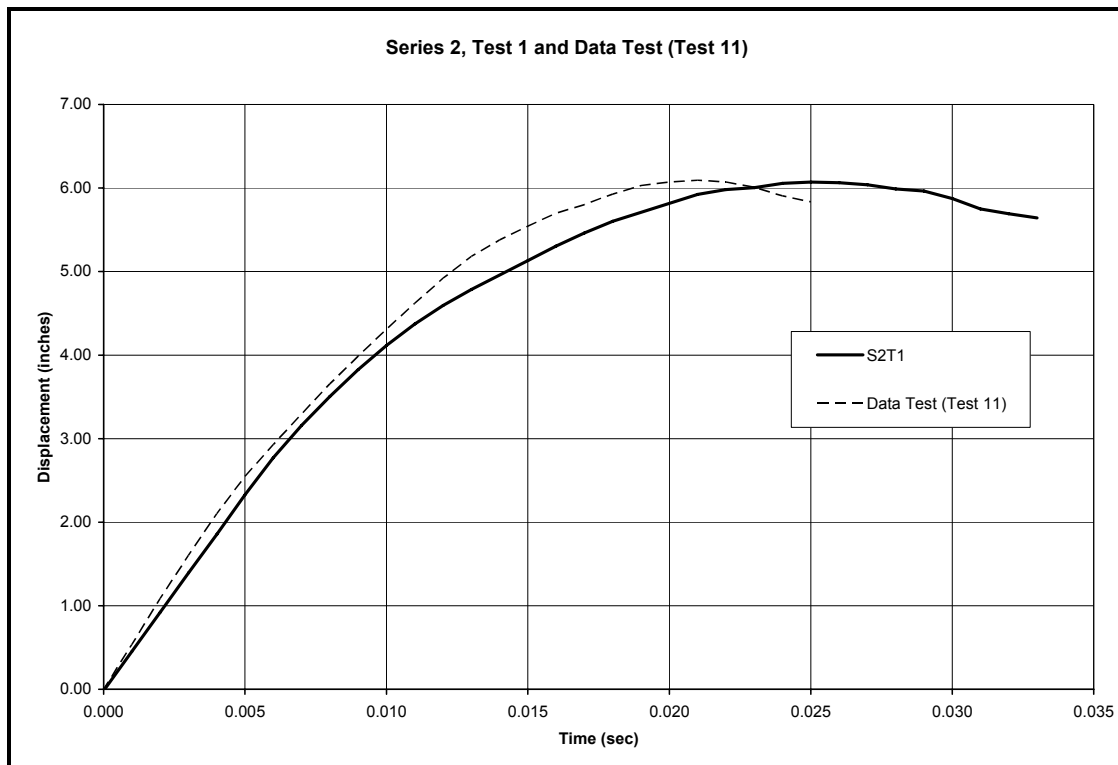


Figure 2.12.3-16 – Series 2, Test 1: Time-Displacement from 1,000 fps Video

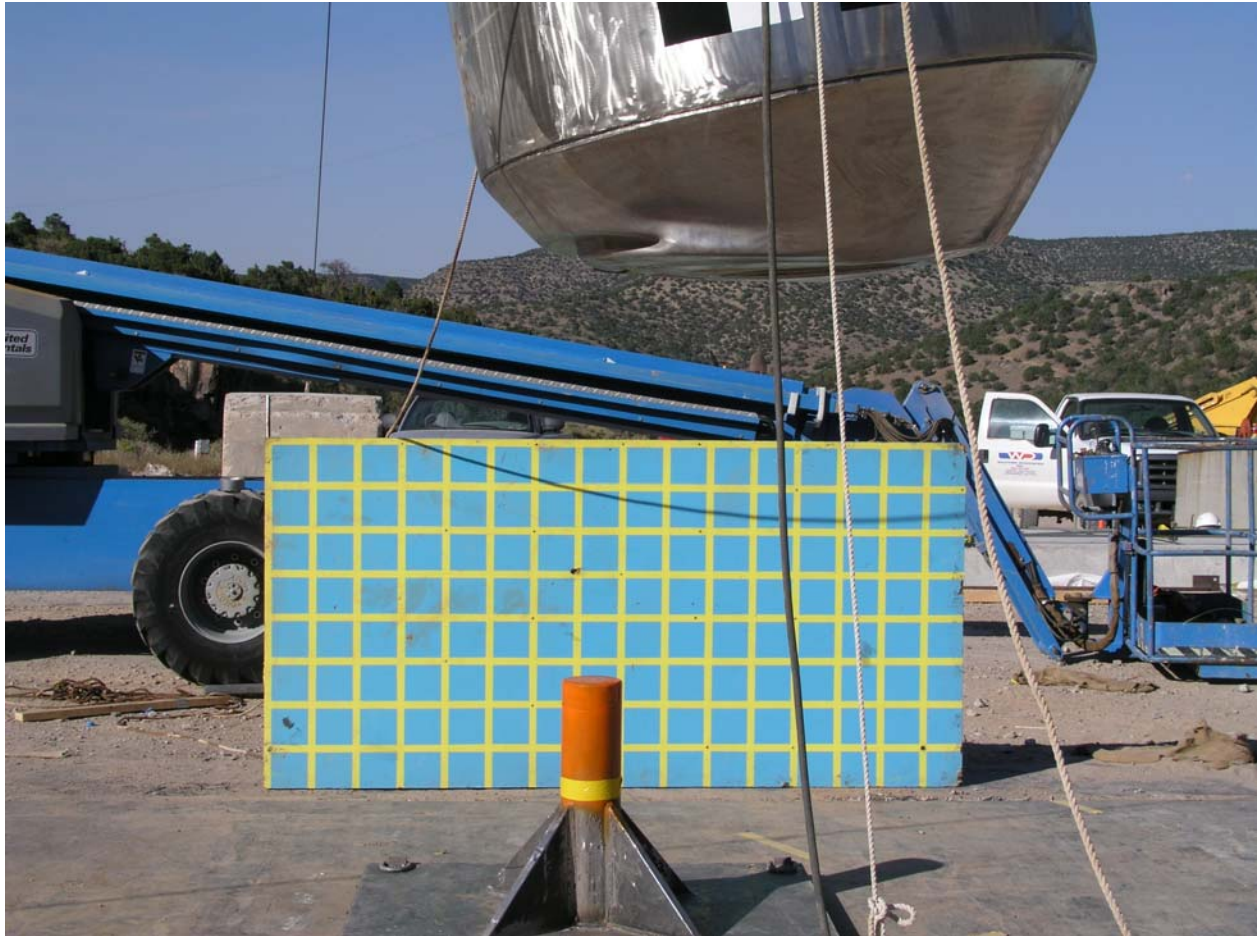


Figure 2.12.3-17 – Series 2, Test 2: HAC 80-Degree Oblique Puncture Drop



Figure 2.12.3-18 – Series 2, Test 2: Overall and Close-up Views of Damage (~1½" Deep)

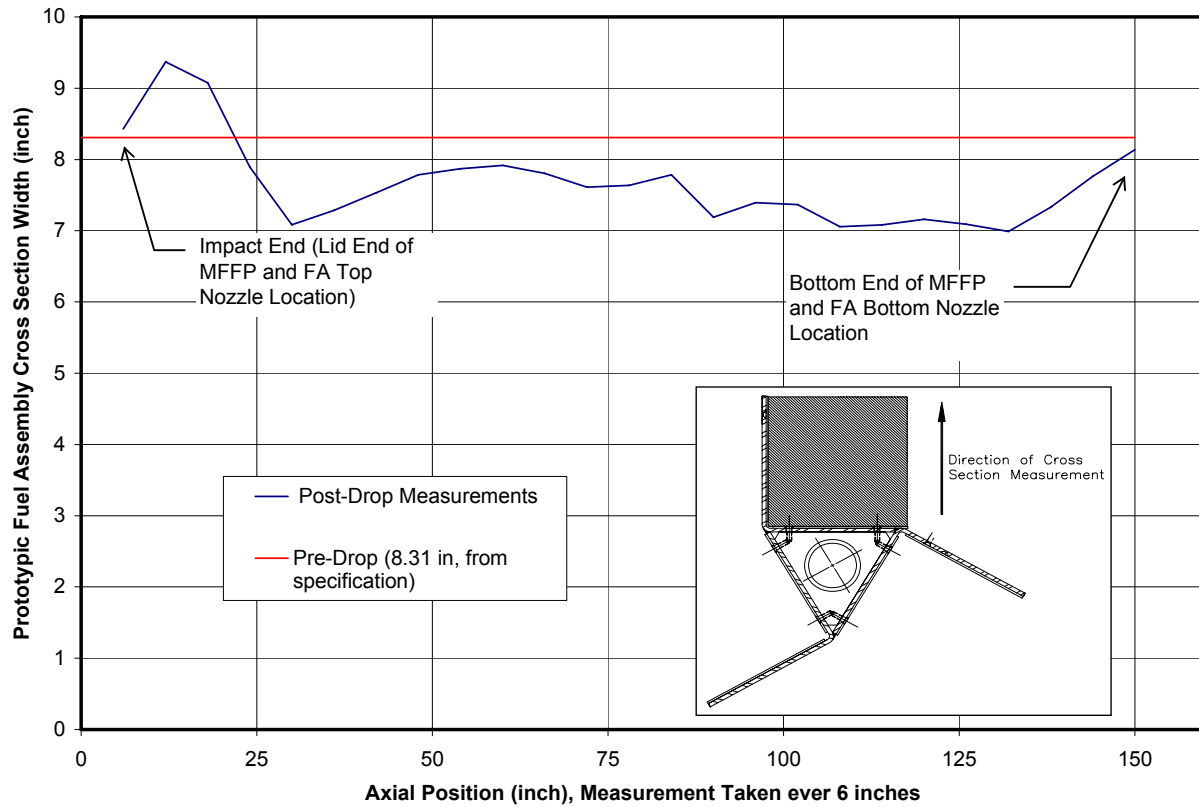


Figure 2.12.3-19 – Series 2: Post-test Cross-Sectional Width of the Prototypic Fuel Assembly



Figure 2.12.3-20 – Series 2: View from Top of Strongback (Clamp Arms Opened)



Figure 2.12.3-21 – Series 2: View from Bottom of Strongback (Clamp Arms Closed)

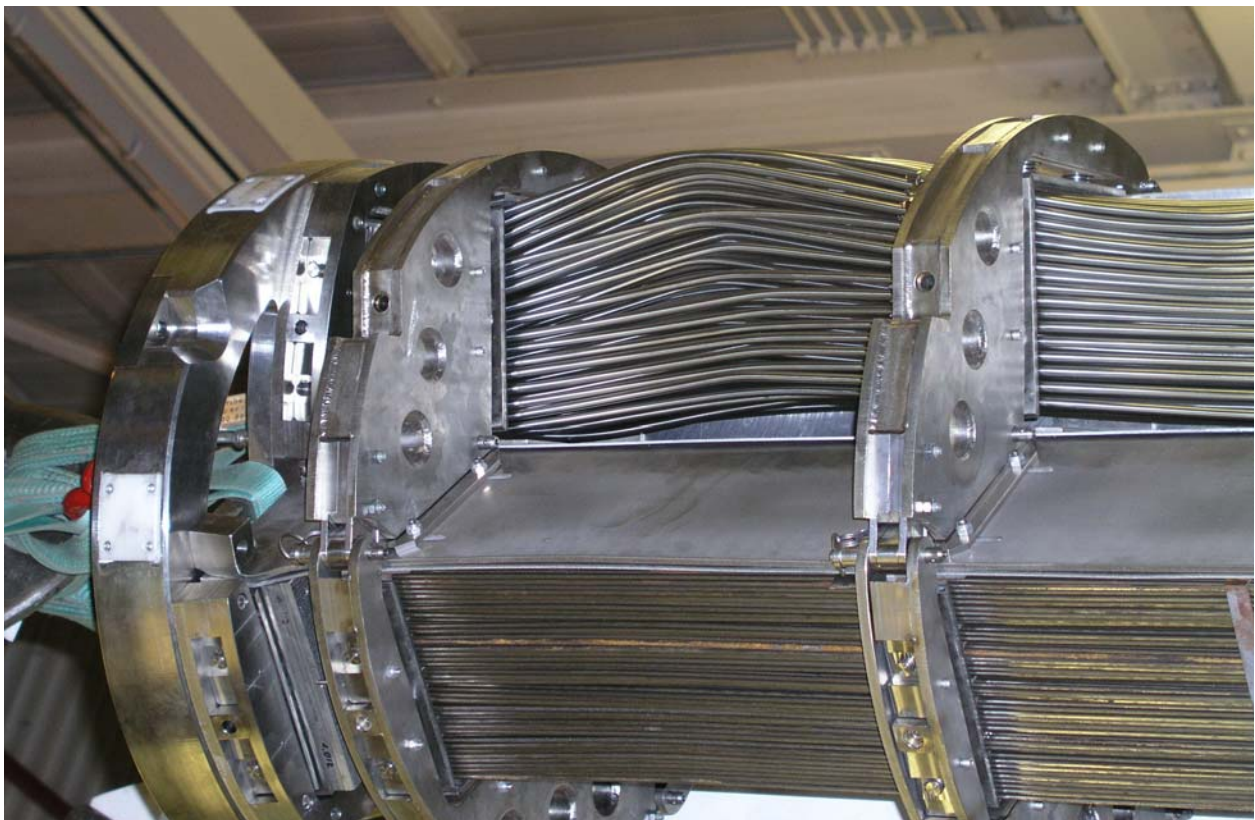


Figure 2.12.3-22 – Series 2: View of Worst Case Fuel Deformation (Nearest the Top Nozzle)



Figure 2.12.3-23 – Series 2: View of Top Nozzle Damage of the Prototypic Fuel Assembly

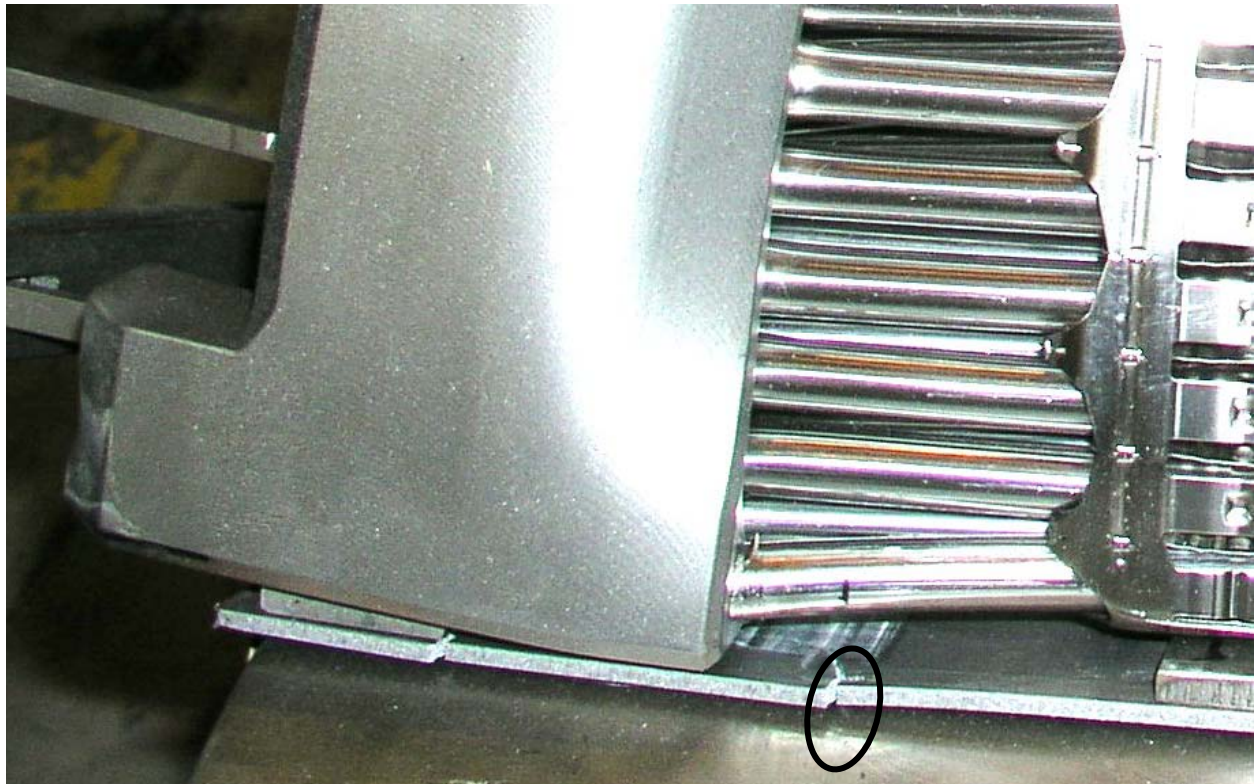


Figure 2.12.3-24 – Series 2: Worst-Case Neutron Poison Damage (Circled on Photo)

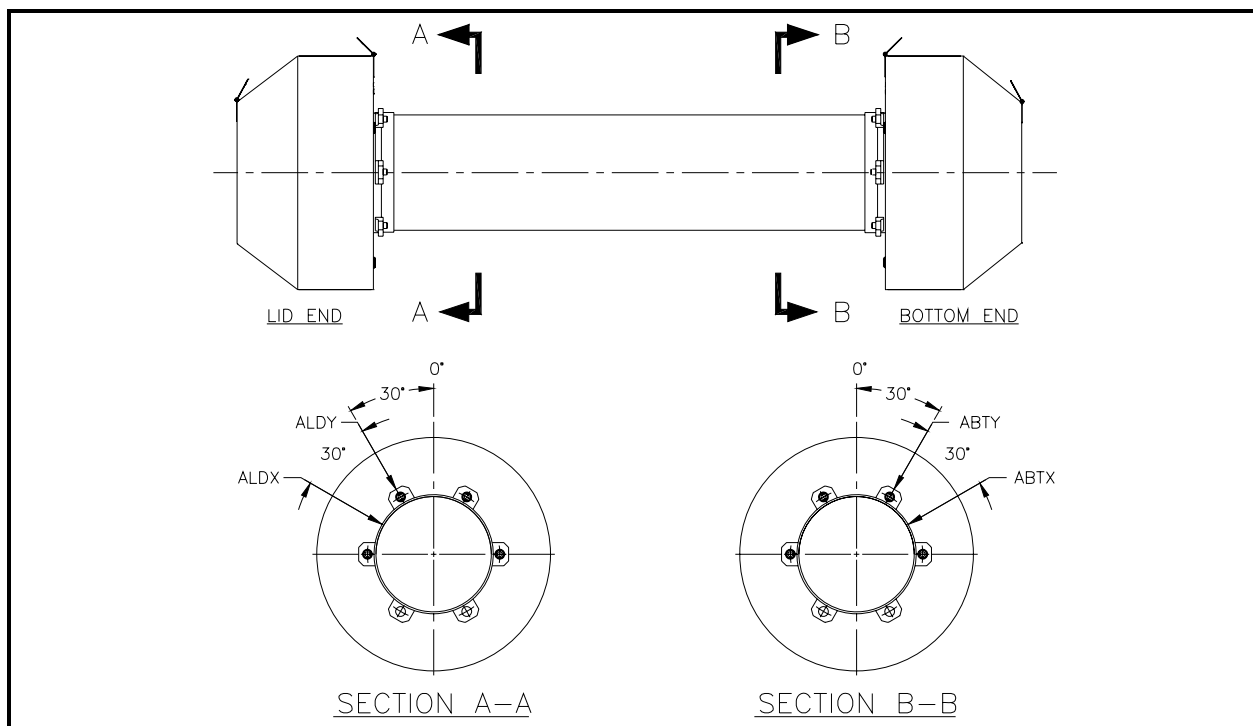


Figure 2.12.3-25 – Accelerometer Locations for Series 3, Test 1



Figure 2.12.3-26 – Series 3, Test 1: HAC 15-Degree Slapdown 30-Foot Drop (Lid End Primary)

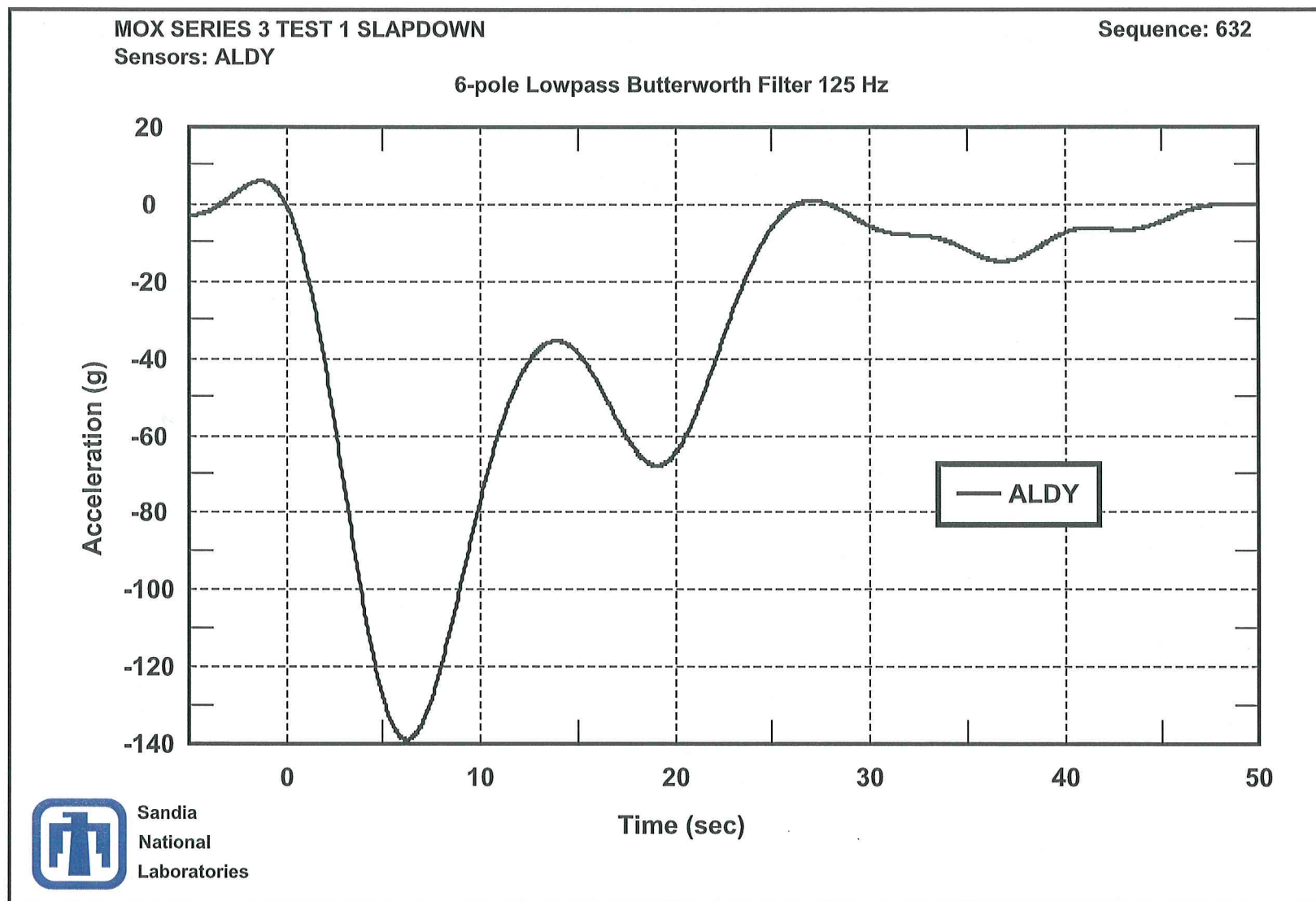


Figure 2.12.3-27 – Series 3, Test 1: Primary Impact Lateral Accelerations

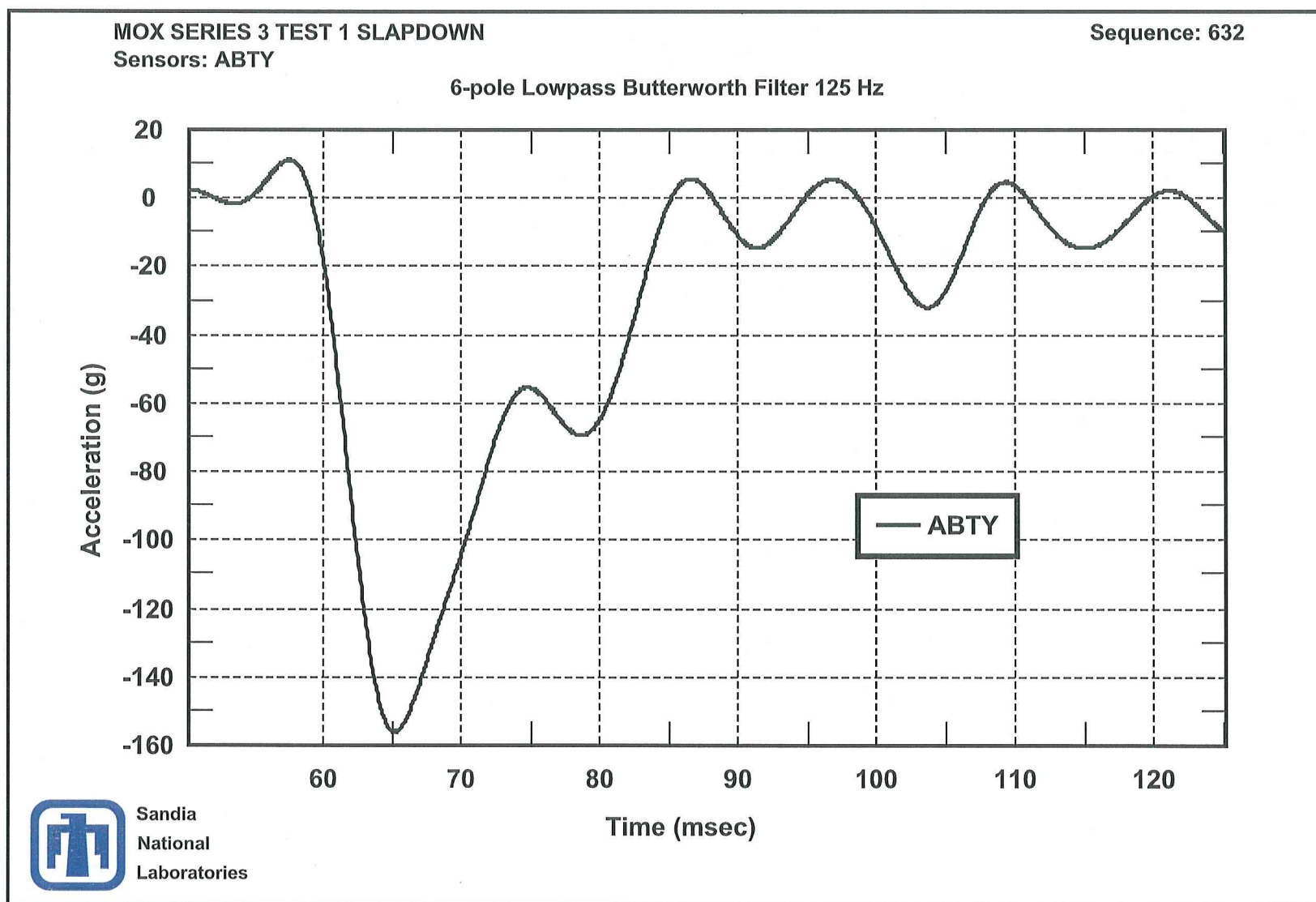


Figure 2.12.3-28 – Series 3, Test 1: Secondary Impact Lateral Accelerations



Figure 2.12.3-29 – Series 3, Test 1: Close-up View of Impact Limiter Damage (~21" Length)



Figure 2.12.3-30 – Series 3, Test 2: HAC 15-Degree Slapdown 30-Foot Drop (Lid End Secondary)



Figure 2.12.3-31 – Series 3, Test 2: Close-up View of Impact Limiter Damage (~31" Length)

This page left intentionally blank.

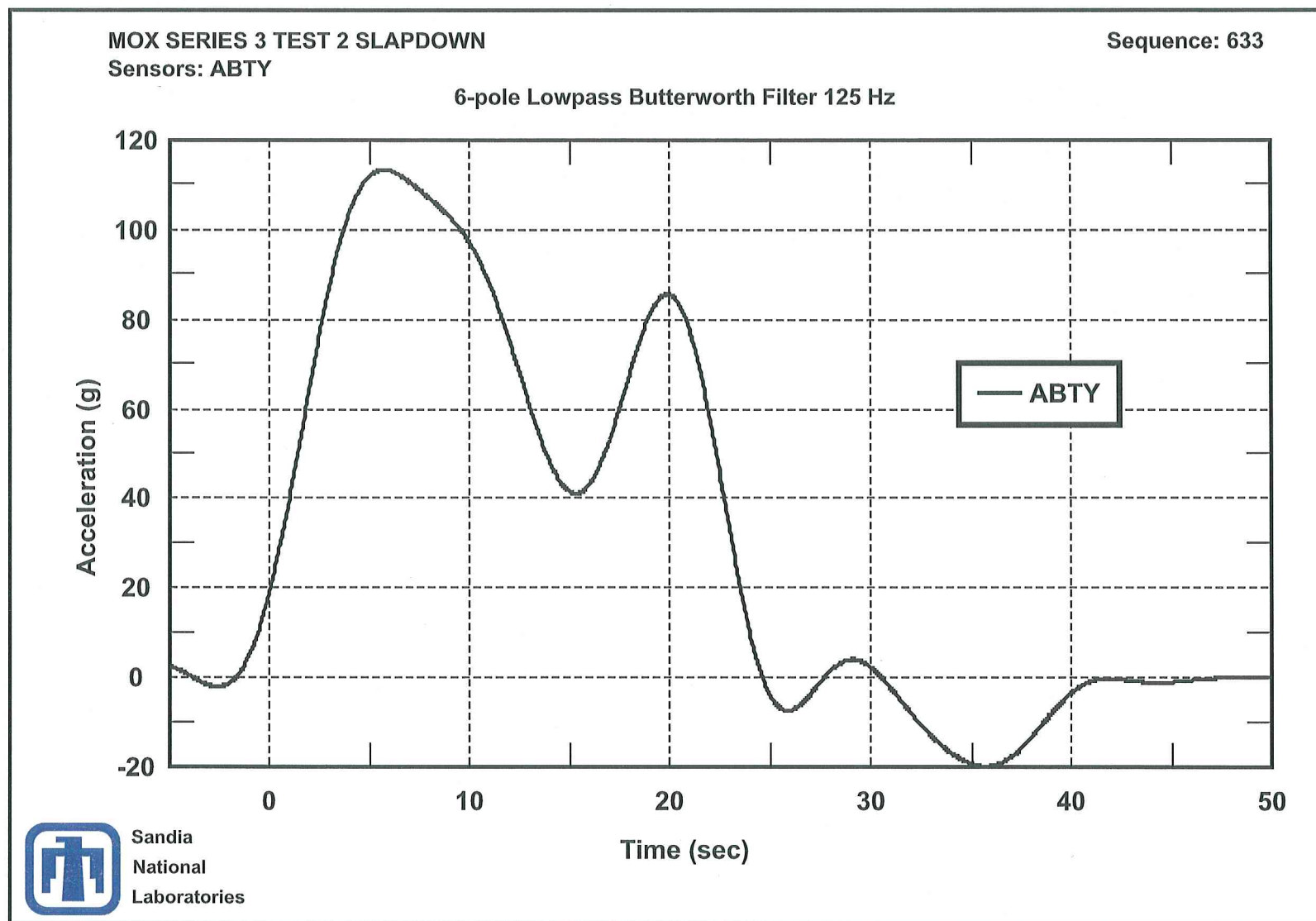


Figure 2.12.3-32 – Series 3, Test 2: Primary Impact Lateral Accelerations (Time scale is milliseconds)

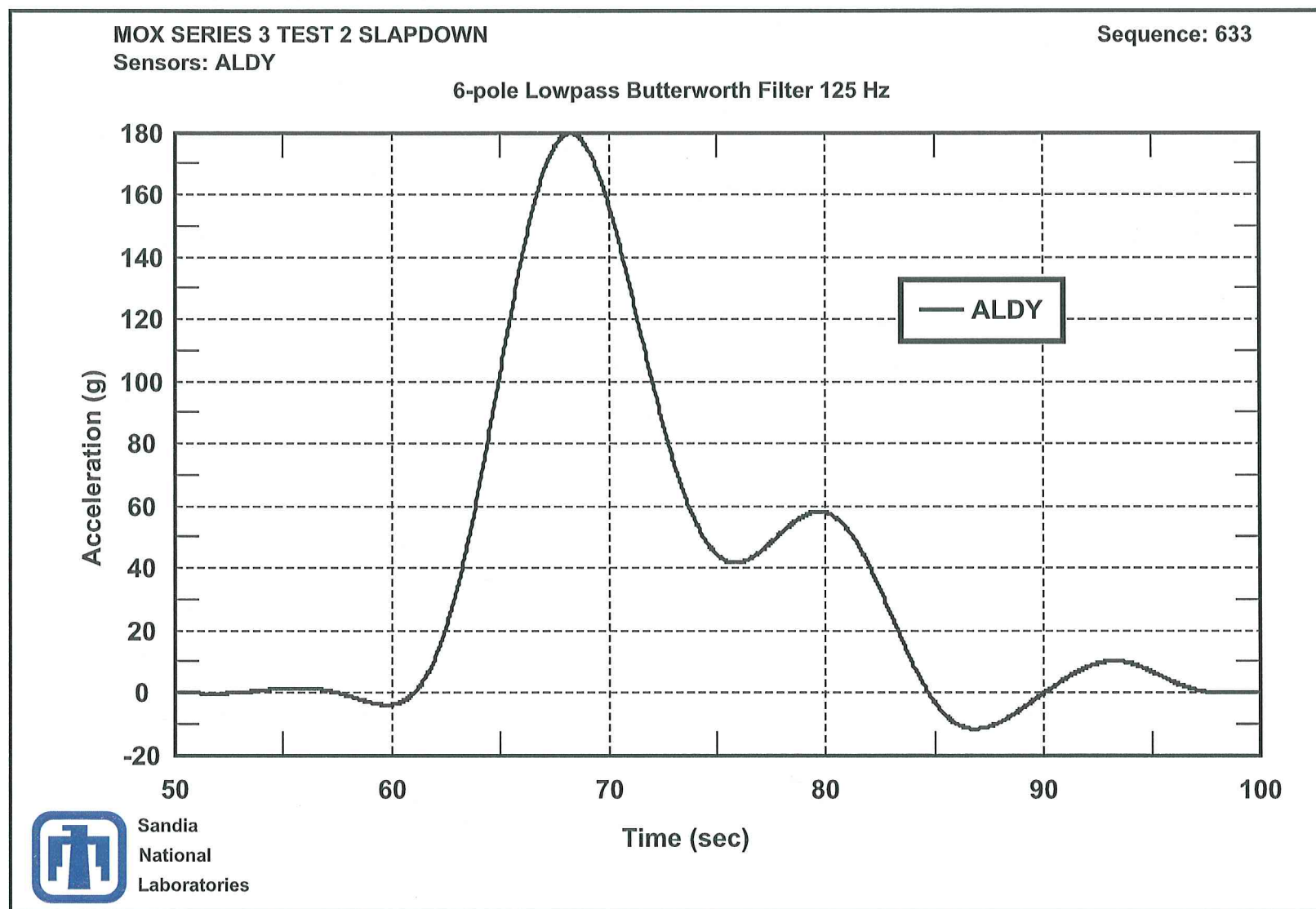


Figure 2.12.3-33 – Series 3, Test 2: Secondary Impact Lateral Accelerations (Time Scale is milliseconds)



Figure 2.12.3-34 – Series 3, Test 3: HAC Horizontal Puncture Drop



Figure 2.12.3-35 – Series 3, Test 3: Views of Shell Damage (~2 1/8" Deep)



Figure 2.12.3-36 – Series 3, Test 4: HAC 30-Degree Puncture Drop

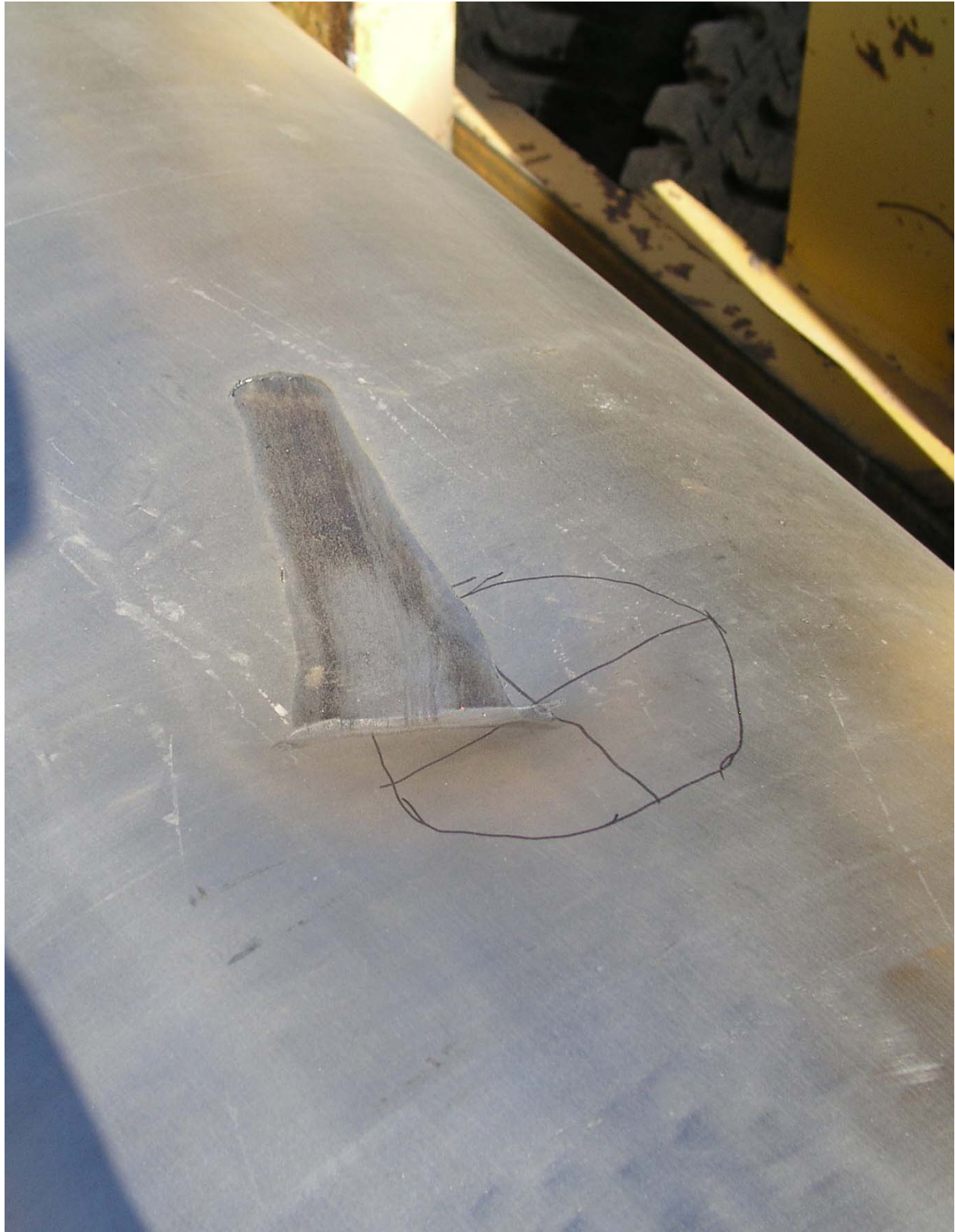


Figure 2.12.3-37 – Series 3, Test 4: HAC 30-Degree Oblique Puncture Drop Damage

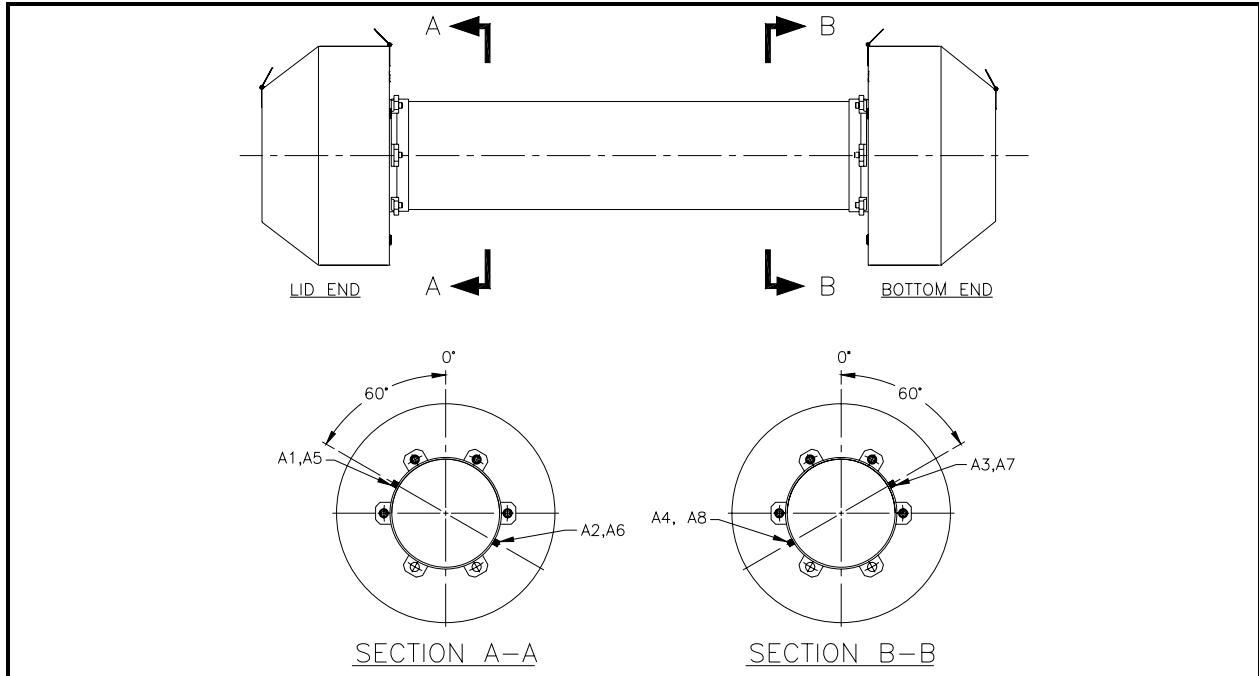


Figure 2.12.3-38 – Accelerometer Locations for Data Test (Test 11)

This page left intentionally blank.

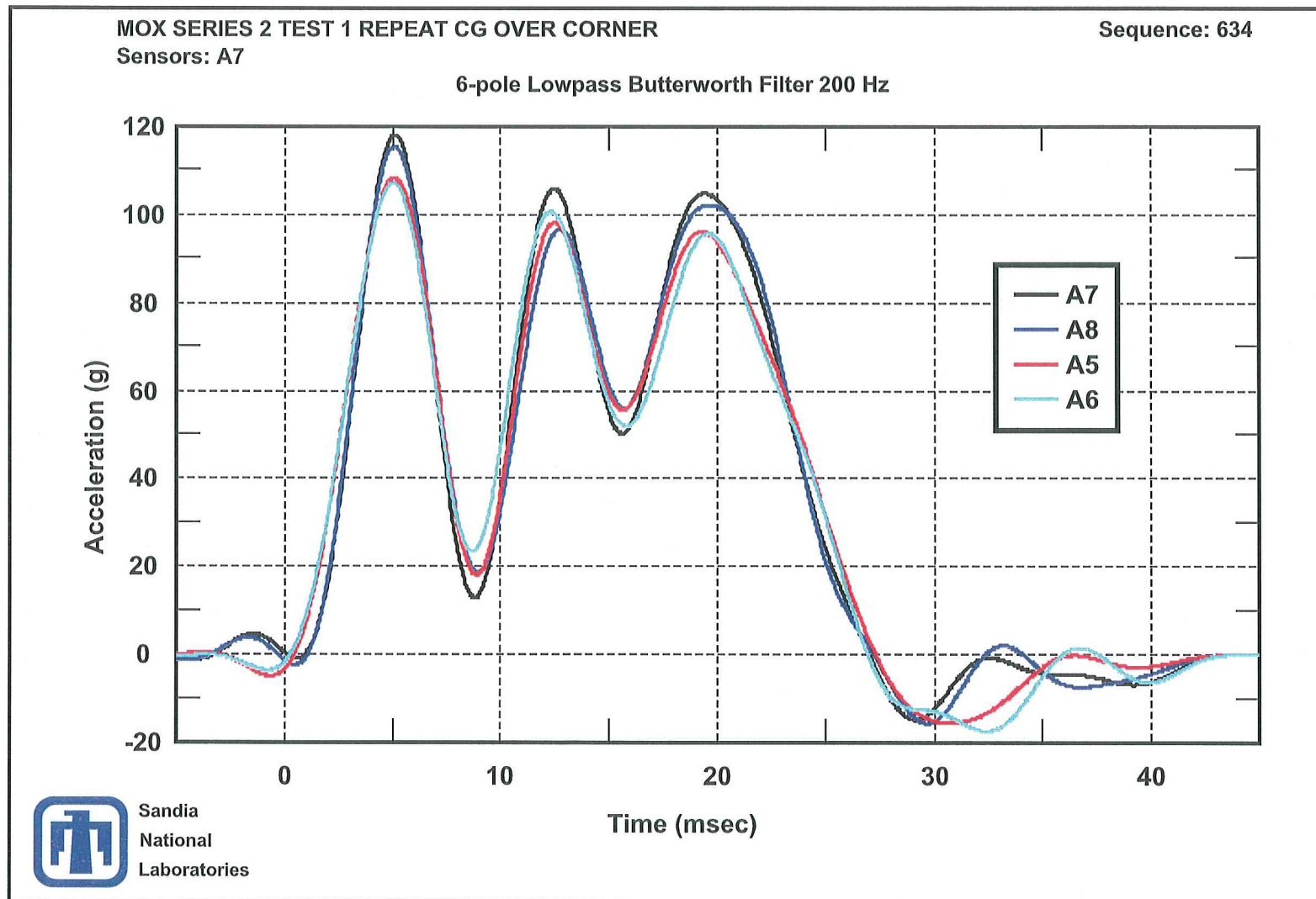


Figure 2.12.3-39 – Data Test (Test 11), Test 1: Impact Longitudinal Accelerations

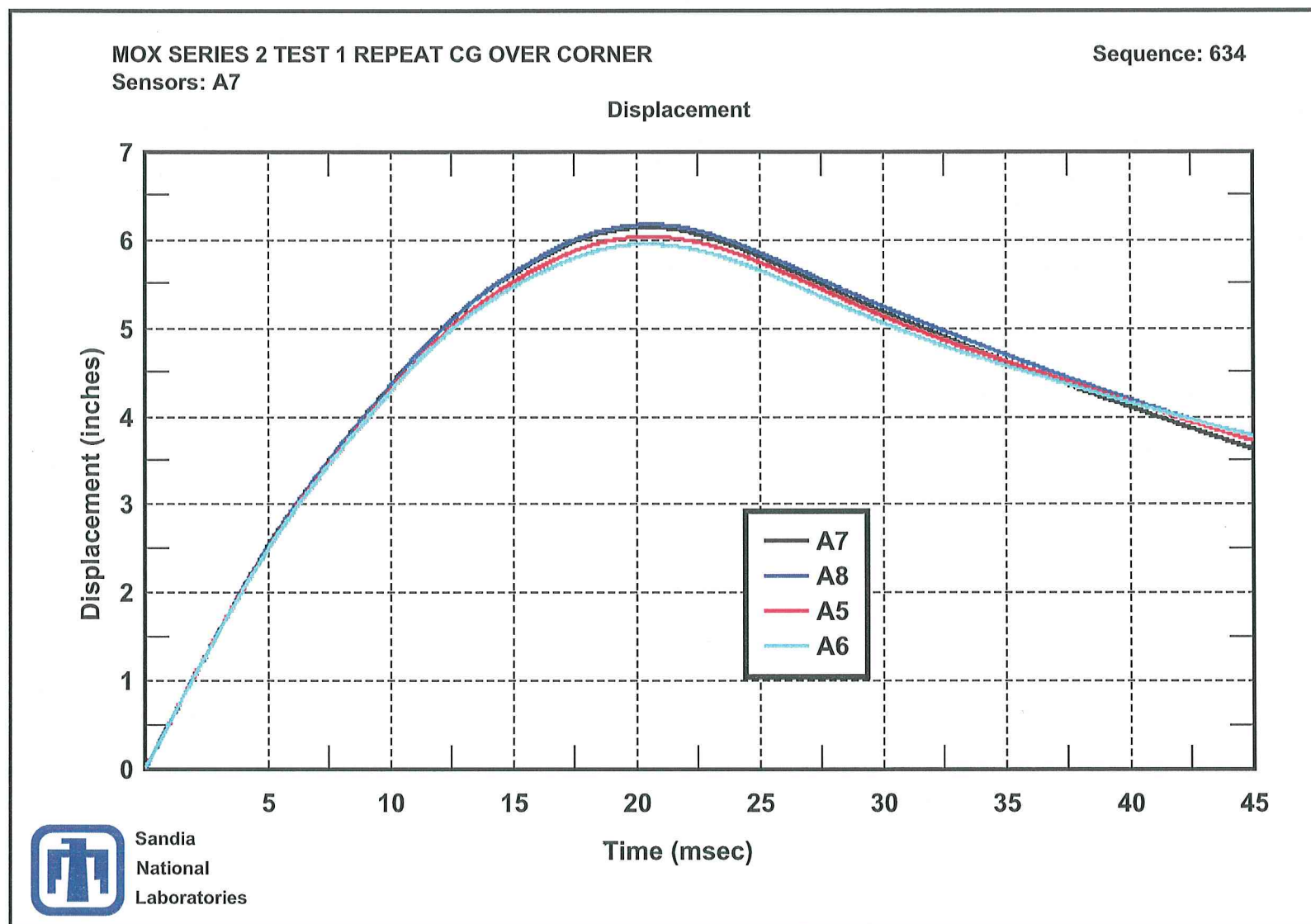


Figure 2.12.3-40 – Data Test (Test 11), Test 1: Longitudinal Displacement (Integrated from Accelerometer Signals)

2.12.4 Engineering Test Results

The engineering test unit (ETU) was built in half-scale, and incorporated only those features considered necessary for the evaluation of the planned tests. The primary purpose of the tests was to evaluate the puncture resistance of the package. The engineering test described herein addressed the following package design issues:

- *Resistance to Puncture.* While puncture on the body (including oblique orientation) was not expected to present any difficulty, puncture drop tests on or near the containment O-ring seal were of concern. The design of the lid end impact limiter includes an extra thickness shell to prevent perforation, thus completely protecting the seal area from puncture bar attack. Two different (half-scale) thicknesses were present on the ETU: 1/8-inch and 5/32-inch thick. The impact limiters were constructed using two thicknesses to allow for possible optimization of the design. The lesser thickness was tested first. If it had allowed perforation, the greater thickness would have been tested. However, the thinner shell prevented puncture, thus the thicker shell was not tested.
- *Containment Shell Stability.* Although non-linear FEA analyses show that the containment shell will not buckle during any of the NCT or HAC events, the ETU was fabricated using prototypic shell geometry.
- *Effect of thick shell on impact limiter behavior.* On a package of this size and weight, impact limiter shells of the proposed thickness will have a significant effect on impact force. Therefore, the test plan includes a 30-ft free drop to evaluate the impact limiter shell thickness effect.

Since the engineering tests were designed to evaluate specific performance parameters of the MFFP design, the regulatory test sequence stipulated by 10 CFR §71.73(c) was not adhered to. The certification testing, which is summarized in Appendix 2.12.3, *Certification Test Results*, was performed in accordance with the 10 CFR §71.73(c) regulatory test sequence as primary evidence of the MFFP robust design.

2.12.4.1 Engineering Test Unit Configuration

The ETU was a half-scale model of the MFFP and partially prototypic. The design features reproduced in the test unit were primarily those related to the structural behavior of either the seal area or of the impact limiters. The specific features of the test unit and their purpose were as follows:

1. The closure lid and shell flange regions were prototypic with regard to structural strength. The closure lid contained a single O-ring seal instead of three since leakage rate testing was performed by the pressure drop method rather than helium mass spectrometry. A pipe fitting was included in the package shell sidewall for pressurizing and monitoring the cavity (see Figure 2.12.4-1).
2. Only 12 closure bolts were used instead of the full quantity of 24 since the worst case load for the bolts (the inside-out impact of the contents in an end drop) was not being evaluated. The effect of fewer bolts on the seal area puncture deformation was not considered to be significant.
3. The package shell had a half-scale prototypic thickness of 9/32 inches (full-scale 9/16-inch thickness).

4. The impact limiters were retained by prototypic means, including six necked-down bolts, the shell bolt lugs, and the impact limiter internal attachments.
5. The impact limiter shells, shape, attachment means, and foam density of the impact limiters were essentially prototypic. For testing convenience, the thicker shells were used at the bottom end, and the thinner shells used at the lid end.
6. The limiter used at the bottom end of the package featured the thicker shells, which were made from Type 304 stainless steel in order to exactly model their resistance to perforation/tearing. All the flat shell sections and half the curved shells (cylindrical and tapered sections) were 11-gauge (0.120-inches) material. The other half of the curved shell was 5/32-inches thick. The limiter used at the lid (top) end of the package featured the thinner shell made from carbon steel, since no resistance to perforation was expected. All of the thin shell material of the top end limiter was 16-gauge (0.060-inches) material.
7. The foam in the thicker-shell limiter was nominally $10 \text{ lb}_m/\text{ft}^3$ and the thinner-shell limiter foam was nominally $11.5 \text{ lb}_m/\text{ft}^3$. These densities were analytically calculated to give essentially the same force deflection curve. Impact limiter crush performance in the free drop was expected to be similar.
8. The steel material used for the package shell and lid was ASTM A572 Grade 50. For modest strain levels this material will have a similar stress strain curve as the actual XM-19 steel based on a simple comparison of yield and tangent modulus. The minimum yield strengths are approximately the same (55 ksi for XM-19 and 50 ksi for A572). The ultimate strength and elongation for XM-19 and A572 are 100 ksi - 40%, and 65 ksi - 21%, respectively. The tangent moduli (calculated using engineering values) are therefore 112.5 ksi and 71.4 ksi, respectively. The test material has conservatively lower strain hardening, compared to the XM-19 material. The material report on the A572 shell material listed an yield strength of 52 ksi, which demonstrates the conservatism of using this material.
9. The strongback was not replicated in the ETU. The weight of the strongback and fuel assemblies was included as non-structural steel rods.

Although the engineering tests were not completely prototypic, the results are relevant in supporting the conclusions regarding the MFFP that: 1) the impact limiter shells, with exception of the recessed end plate, are puncture resistant, 2) the effect of puncture through the recessed end plate onto the closure lid is of little consequence, 3) the containment body shell is stable during a 30-foot side drop, and 4) the containment body shell is capable of sustaining direct puncture impact.

2.12.4.1.1 Interim Impact Limiter

During the testing of the thick shell sections, puncture impacts took place at the bottom end of the package and secondary impacts occurred at the lid end. To prevent damage to the thin shell limiter and the lid end from secondary impacts, an interim impact limiter was installed (refer to Figure 2.12.4-2).

2.12.4.1.2 Dummy Payload

A dummy payload was used to simulate the weight of the strongback and three fuel assemblies. The equivalent full-scale weight of the dummy payload is 6,616 pounds and essentially evenly distributed. In half-scale, the dummy payload weighed 827 pounds. A bundle of approximately

(181) 1/2-inch diameter round bars $\times 82 \pm 1/2$ inches long were used. This dummy payload arrangement had an approximate diameter of $7\frac{1}{2}$ inches. The bars were strapped together at each end. In this configuration, the dummy payload had little structural strength in bending. The axial clearance to the package cavity was approximately $3/4$ inches. The radial clearance was approximately $3\frac{1}{2}$ inches. Wooden blocks were strapped to the bundle at several locations along its length to maintain a gap between the bundle and the shell wall, which kept the payload from affording any puncture resistance (backing).

2.12.4.1.3 Test Facility

The tests were conducted using a drop pad consisting of 12-inches of reinforced concrete over 18-inches of packed gravel, topped by a 2-inch thick, 9×10 ft steel plate. The plate was connected to the concrete using high-strength grout. The combined weight of the steel and concrete was approximately 20,000 pounds. The weight of the half-scale model was 1,641 pounds (see Table 2.12.4-1), which is less than one-tenth of the weight of the drop pad.

Table 2.12.4-1 – Summary of Engineering Test Unit Component Weights

Component	Actual Half-Scale Weight, pounds	Full-Scale Weight = $8 \times$ [Half-Scale Weight], pounds
Bundle of Rebar (mock payload)	827	6,616
Containment Body	467	3,736
Stainless Impact Limiter	200	1,600
Carbon Steel Impact Limiter	147	1,176
Total Weight	1,641	13,128

The half-scale puncture bar was 3-inches in diameter and made from mild steel, having a maximum $1/8$ -inch radius. The bar was socket welded and gusseted to a $1\frac{1}{2}$ -inch thick baseplate, which was welded to the drop pad. The free length of bar was 16-inches, which was adequate to reach full depth before the outer surface of the impact limiter came in contact with the gussets.

2.12.4.2 Pre-Test Activities

Prior to free drop or puncture testing, the following activities were performed.

1. The quality assurance data package was reviewed to ensure that the ETU was adequate for the test requirements.
2. All ETU components were weighed. Separate weights were recorded for the package shell assembly, the package lid, each impact limiter, the interim impact limiter, and the dummy payload.

2.12.4.2.1 Leakage Rate Test Calibration

Damage to the seal area due to puncture drop testing was evaluated by means of a pressure drop test. It was assumed, for the purposes of this test program, that the seal would either perform adequately or it would exhibit a gross leak, and therefore sophisticated leakage rate test procedures were not required. The seal area was evaluated by pressurizing the package

internally, and monitoring the pressure over a brief time period. The arrangement of the leakage rate test components is shown in Figure 2.12.4-1.

1. *Pressure Integrity of Package.* Before testing, the pressure holding behavior of the package was confirmed. First, the closure lid was assembled by installing the O-ring seal and tightening the closure bolts according to the drawing. The package cavity was pressurized to 5 psig using regulated air to the package cavity through a shut-off valve. The pressure was monitored within the cavity, and when the pressure stabilized at 5 psig, the shut-off valve was closed. The pressure within the package was monitored for 45 minutes without variation of the internal pressure. Thus, the pressure integrity of the package was verified.
2. *Pressure Drop vs. Time.* Using a pipe plug with a 1/32-inch drilled hole, the package was re-pressurized and the pressure was monitored. The behavior of such a leak was characterized by noting the pressure drop vs. time. This information was used to establish an appropriate dwell time and pressure drop magnitude for use in later post-puncture leak testing.

2.12.4.3 Summary of Engineering Test Results

2.12.4.3.1 Test 1

Test 1 was an oblique puncture drop onto the conical portion of the 1/8-inch thick stainless steel impact limiter. The actual drop angle of the package axis with respect to horizontal was 69 degrees and the drop height was slightly greater than 40 inches, measured from the top of the puncture bar to the point of impact. The impact resulted in an indentation of 7/8 inches to 1 1/8 inches, depending on measurement method. There was no sign of cracking or tearing of the impact limiter shell. The planned drop orientation is shown in Figure 2.12.4-3. A photo record of the drop results is shown in Figure 2.12.4-4.

2.12.4.3.2 Test 2

Test 2 was an oblique puncture drop onto the cylindrical portion of the 1/8-inch thick stainless steel impact limiter. The actual drop angle of the package axis with respect to horizontal was 24 degrees and the drop height was slightly greater than 40 inches, measured from the top of the puncture bar to the point of impact. The impact resulted in an indentation of 3/4 inches. There was no sign of cracking or tearing of the impact limiter shell. The drop orientation is shown in Figure 2.12.4-5. A photo record of the drop results is shown in Figure 2.12.4-6.

2.12.4.3.3 Test 3

Test 3 was an oblique puncture drop onto the recessed end plate (1/8-inch thick) of the stainless steel impact limiter. The actual drop angle of the package axis with respect to horizontal was 64 degrees and the drop height was slightly greater than 40 inches, measured from the top of the puncture bar to the point of impact. The impact resulted in an indentation of 1 1/8 inches. There was a very small crescent tear over approximately 160 degrees of the puncture circle. The drop orientation is shown in Figure 2.12.4-7. A photo record of the drop results is shown in Figure 2.12.4-8.

2.12.4.3.4 Test 4

Test 4 was a side puncture drop onto containment body shell as near to the O-ring seal area as possible without contacting the impact limiter. The actual drop angle of the package axis with

respect to horizontal was 0 degrees and the drop height was slightly greater than 40 inches, measured from the top of the puncture bar to the point of impact. The impact resulted in a 3/8-inch indentation. There was no sign of cracking or tearing of the body shell. Following the test, a leakage rate check was performed. The actual internal pressure was 5.5 psi and held without change for 5 minutes. The drop orientation is shown in Figure 2.12.4-9. A photo record of the drop results is shown in Figure 2.12.4-10.

2.12.4.3.5 Test 5

Test 5 was an end puncture drop onto the thin shell (1/16-inch thick), carbon steel impact limiter. The actual drop angle of the package axis with respect to horizontal was 90 degrees and the drop height was slightly greater than 40 inches, measured from the top of the puncture bar to the point of impact. The impact resulted in a puncture of the shell of 2¾ inches. The package remained vertical for several seconds and slowly turned off the bar. The bar did not bend and there was very little ‘tearout’ damage. Following the test, a leakage rate check was performed. The actual internal pressure was 5.0 psi and held without change for 5 minutes. The drop orientation is shown in Figure 2.12.4-11. A photo record of the drop results is shown in Figure 2.12.4-12. Appearance of the photo notwithstanding, the puncture bar was still welded to the drop pad.

2.12.4.3.6 Test 6

Test 6 was a 30-foot side drop. The actual drop angle of the package axis with respect to horizontal was 0 degrees and the drop height was slightly greater than 30 feet. The impact caused no noticeable permanent deformation of the shell. The drop orientation is shown in Figure 2.12.4-13. A photo record of the drop results is shown in Figure 2.12.4-14. The small hollow tubes were aluminum crush gages used to measure crush distance.

2.12.4.3.7 Test 7

Test 7 was a side puncture drop onto the center of the containment body shell. The actual drop angle of the package axis with respect to horizontal was 0 degrees and the drop height was slightly greater than 40 inches, measured from the top of the puncture bar to the point of impact. The impact resulted in an indentation of 1⅞ inches maximum depth. The deformation gradually decreased to zero by approximately 18 inches from the impact point. At a distance of 3 inches from the point of impact, the deformation was approximately 1/2 inches, and at 6 inches distant, the deformation was approximately 5/32 inches. There was no sign of cracking or tearing of the containment body shell. The full scale dent depth would be twice the 1⅞ inches, or 2¼ inches. The drop orientation is shown in Figure 2.12.4-15. A photo record of the drop results is shown in Figure 2.12.4-16.

2.12.4.3.8 Test 8

Test 8 was an oblique puncture drop onto the conical portion of the 1/8-inch thick stainless steel impact limiter. This test was very similar to Test 1, except that the impact point was closer to the cylindrical-to-conical shell joint. The actual drop angle of the package axis with respect to horizontal was 77 degrees and the drop height was slightly greater than 40 inches, measured from the top of the puncture bar to the point of impact. The impact resulted in an indentation of approximately 2 inches. There was no sign of cracking or tearing of the impact limiter shell. Following the test a leakage rate check was performed. The actual internal pressure was 4.95 psi and held without change for 4 minutes. The planned drop orientation is shown in Figure 2.12.4-17. A photo record of the drop results is shown Figure 2.12.4-18.

2.12.4.3.9 Conclusions

Following the engineering tests, the test article was returned to the shop for final inspection of the O-ring seal area. No appreciable change of the seal region dimensions was noted. Based on the success of the 1/8-inch thick impact limiter shells in resisting perforation, the final design of the lid end impact limiter was determined to have 1/4-inch thick stainless steel shells (full-scale), and consequently, puncture bar impact on the seal region, and exposure of the seal region to HAC fire temperatures, is precluded. The engineering test also demonstrated the ability of the closure lid to resist puncture loads and remain sealed, although due to the perforation resistance of the impact limiter shells, this feature is not expected to be necessary. Because the recessed end plate did tear slightly, the plate thickness was increased from a full-scale thickness of 1/4 inches to 5/16 inches. Since no puncture resistance at the bottom end of the package is necessary (since there are no penetrations or elastomer seals located there), to minimize weight, the shell of the bottom end impact limiter was determined to have a full-scale thickness of 1/8-inch stainless steel.

Security Related Information
Figure Withheld Under 10 CFR 2.390

Figure 2.12.4-1 – ETU Leakage Rate Test Plumbing Schematic



Figure 2.12.4-2 – ETU Initial Configuration (with Interim Impact Limiter)

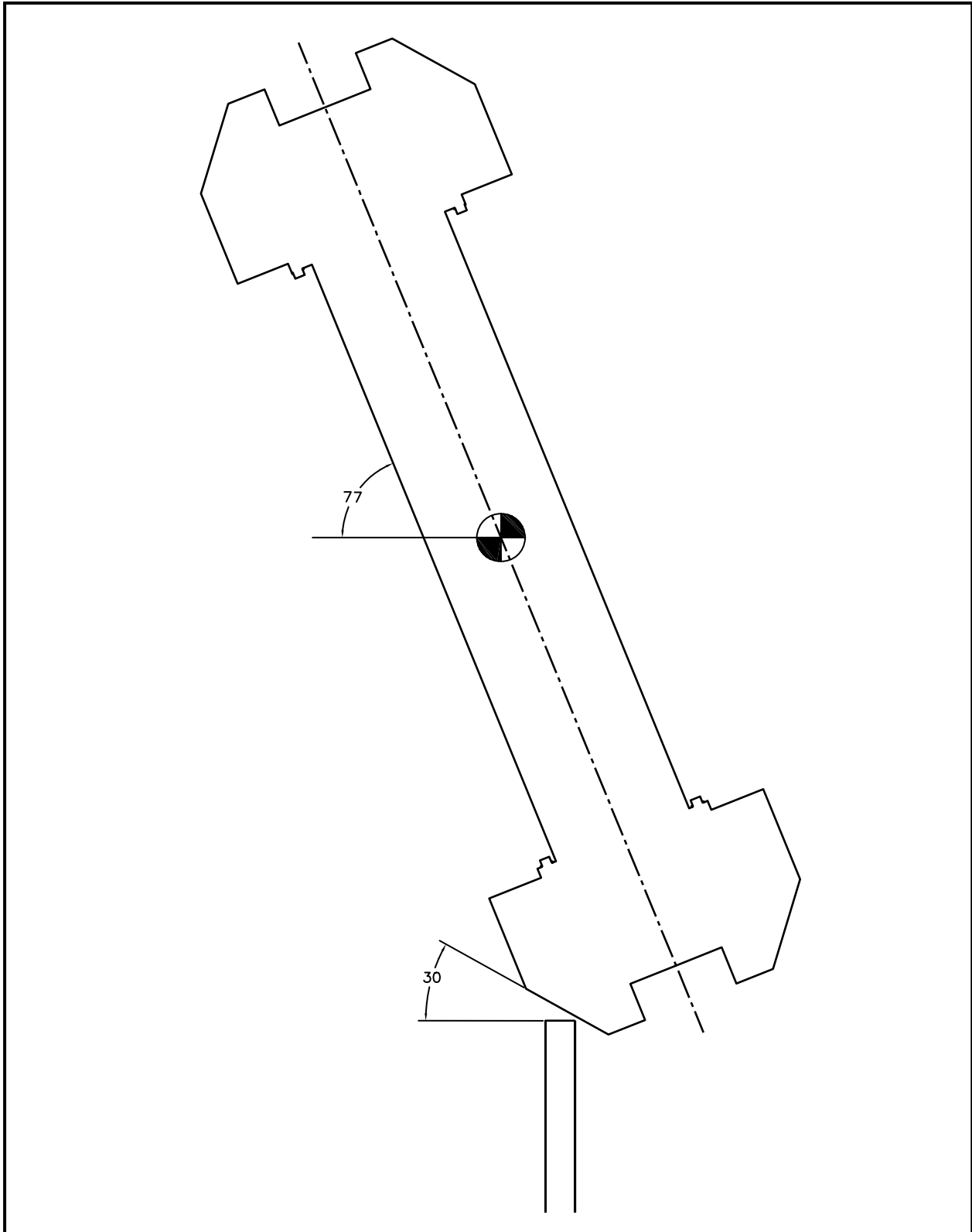


Figure 2.12.4-3 – ETU Test 1 Drop Orientation



Figure 2.12.4-4 – ETU Test 1: View of Puncture Damage; ~1" Deep

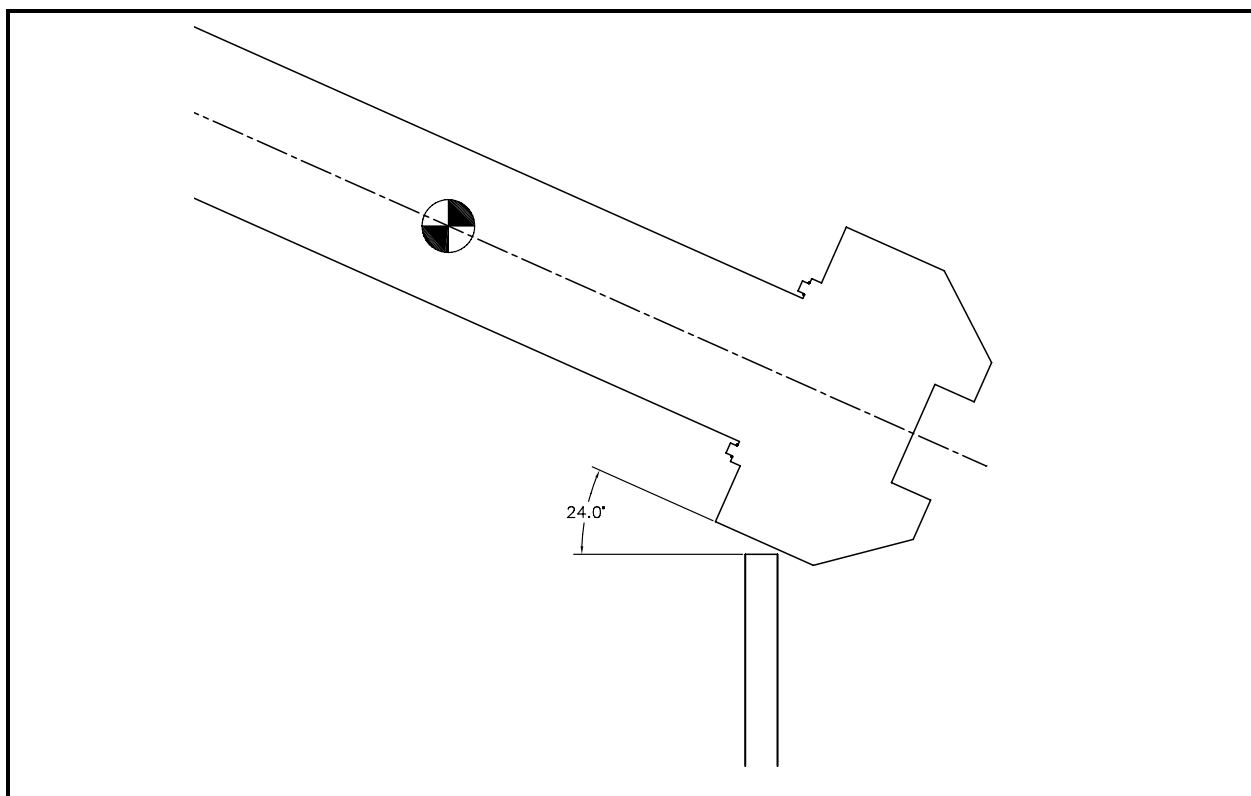


Figure 2.12.4-5 – ETU Test 2 Drop Orientation



Figure 2.12.4-6 – ETU Test 2: View of Puncture Damage; ~3/4" Deep

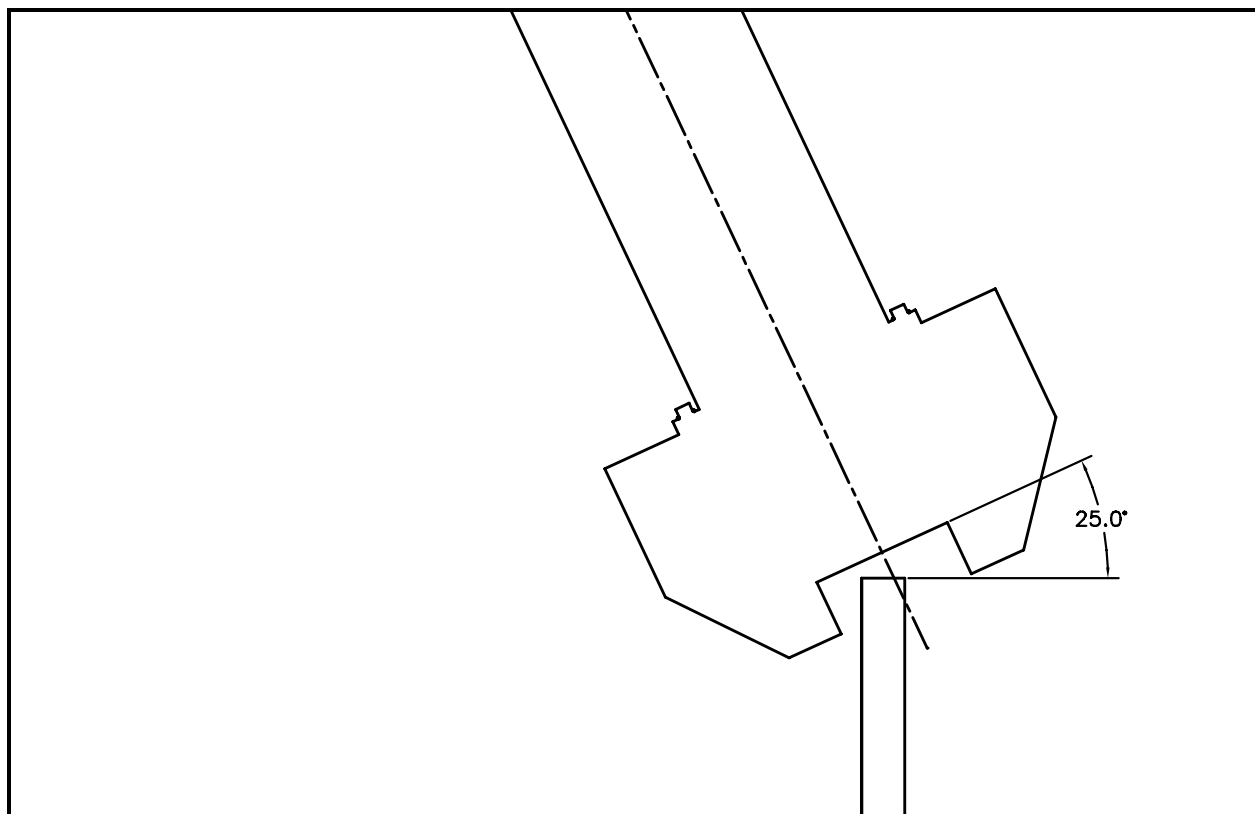


Figure 2.12.4-7 – ETU Test 3 Drop Orientation





Figure 2.12.4-10 – ETU Test 4: View of Puncture Damage; ~3/8" Deep

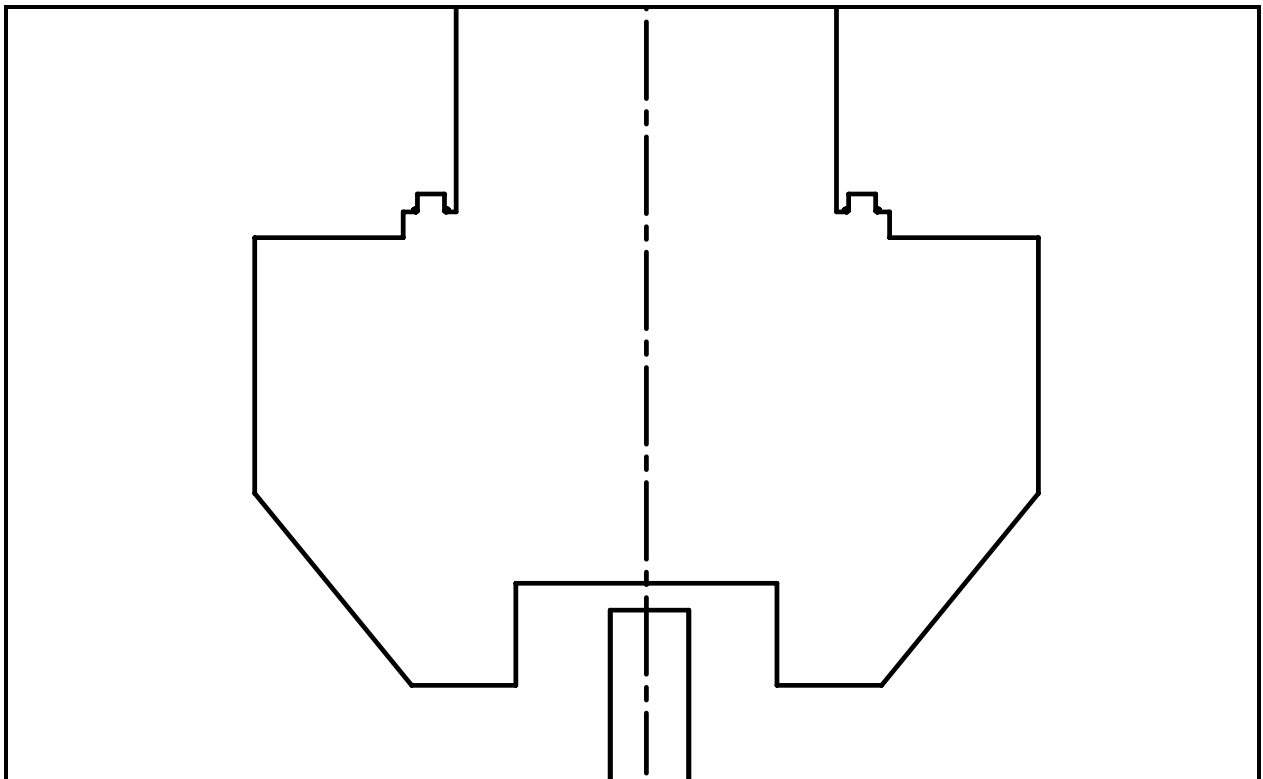


Figure 2.12.4-11 – ETU Test 5 Drop Orientation



Figure 2.12.4-12 – ETU Test 5: View of Puncture Damage; ~2³/₄" Deep



Figure 2.12.4-13 – ETU Test 6 Drop Orientation



Figure 2.12.4-14 – ETU Test 6: View of Free Drop Damage

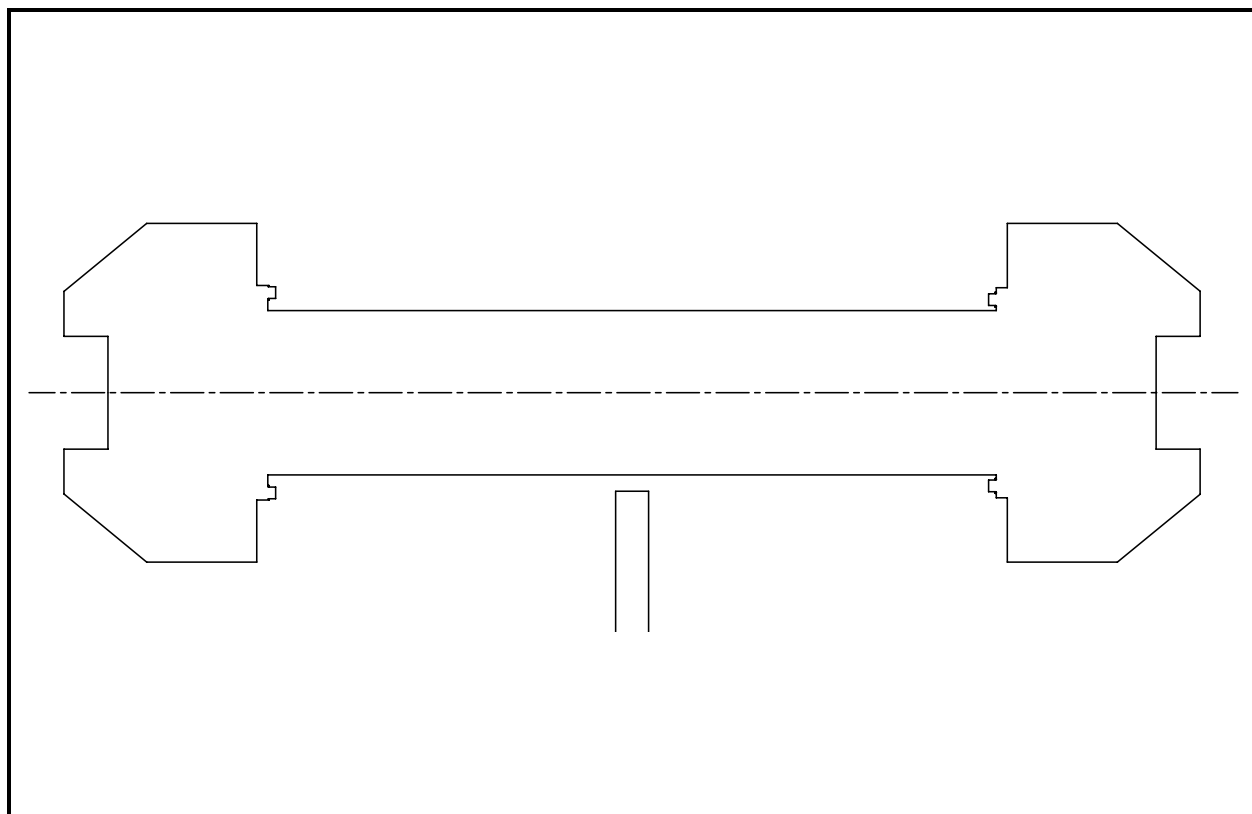


Figure 2.12.4-15 – ETU Test 7 Drop Orientation

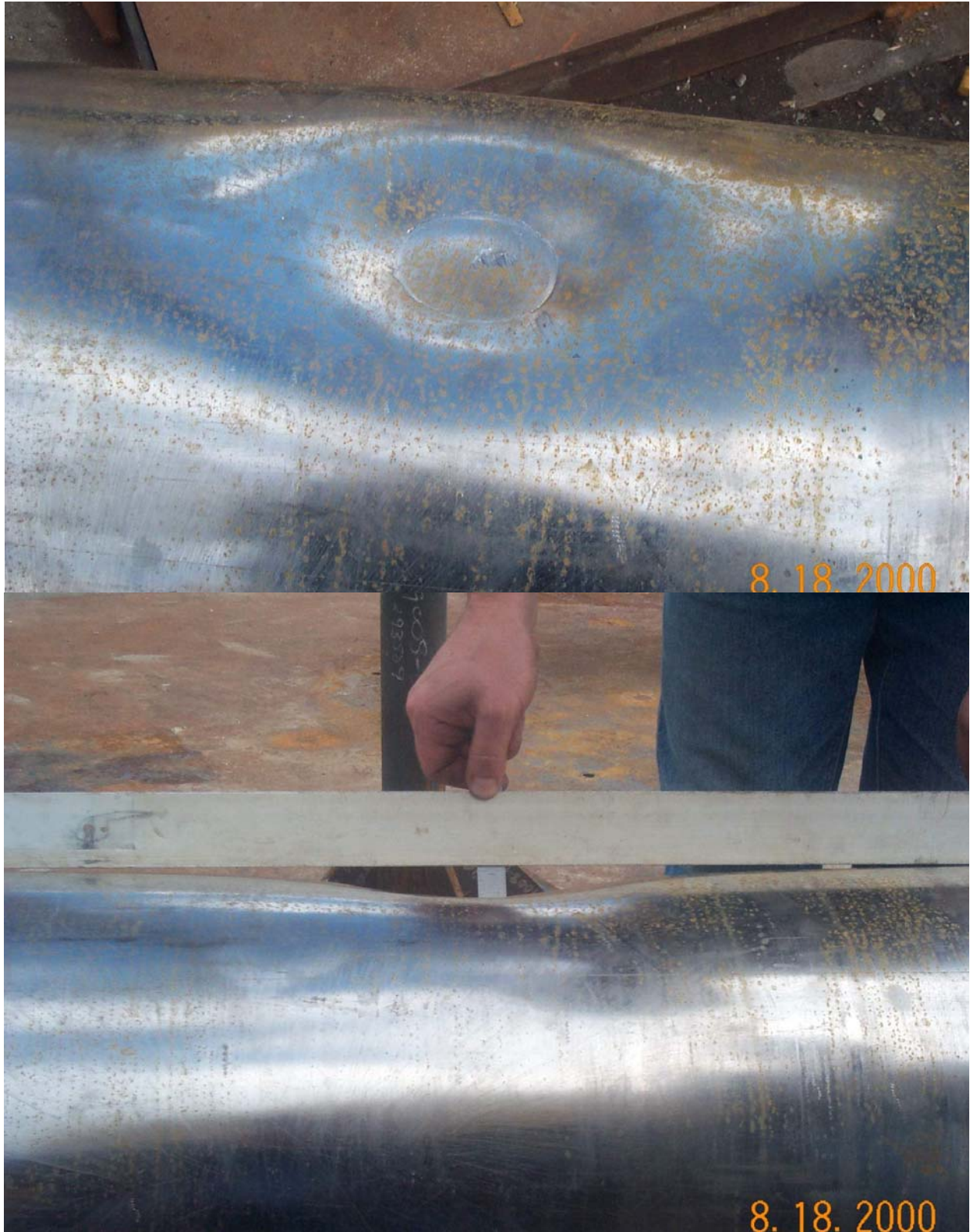


Figure 2.12.4-16 – ETU Test 7: View of Puncture Damage; ~1 $\frac{1}{8}$ " Deep

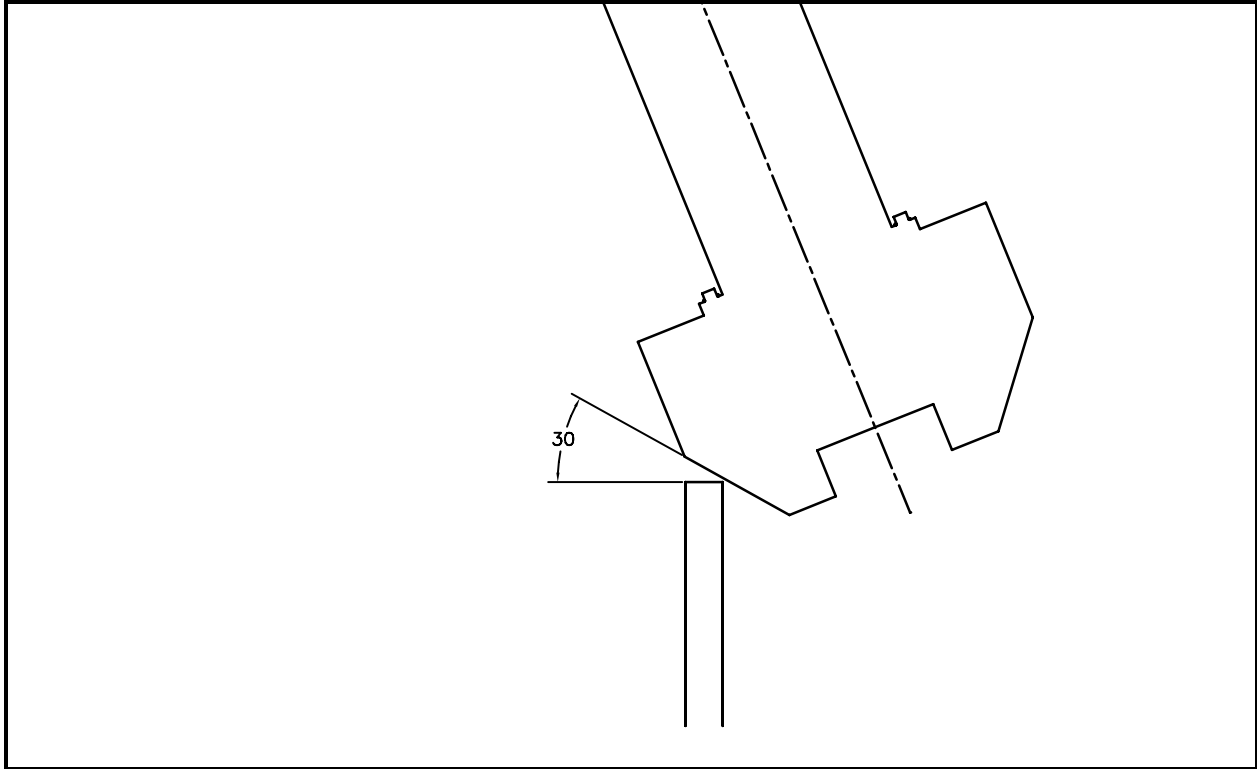


Figure 2.12.4-17 – ETU Test 8 Drop Orientation



Figure 2.12.4-18 – ETU Test 8: View of Puncture Damage; ~2" Deep

This page left intentionally blank.

2.12.5 Fuel Control Structure Evaluation

As discussed in Appendix 2.12.3, *Certification Test Results*, the 80 degrees-from-horizontal, 30-foot free drop resulted in lateral deformation of the fuel rods. The focus of this evaluation is the vertical or near-vertical free drop orientations. Geometric control of the fuel is required during the vertical or near-vertical orientations for criticality considerations, as discussed in Chapter 6.0, *Criticality Evaluation*. Horizontal orientations are considered in the evaluation of the strongback longitudinal structure. Although the fuel control structures (FCSs) are not specifically required to control the fuel for horizontal orientation impacts, the strongback longitudinal weldment provides separation of the fuel. This appendix demonstrates the FCS design satisfies all stability and stress requirements.

The FCS provides a fixed geometric boundary surrounding the fuel assembly (FA), preventing excessive pitch expansion and controlling lateral deformations of the fuel rods. Two primary design features of the FCS are important to the criticality evaluation.

1. The FCS provides a support structure for the neutron poison plates surrounding the exterior of the FA.
2. The FCS, with clamp arms, controls and limits the distortion of the fuel to a cross-section of 8.70 inches square, restricting an increase in the fuel rod pitch.

Since the FCSs were not included in the certification tests, the structural integrity for the hypothetical accident condition (HAC) free drops defined in 10 CFR §71.73(c)(1)¹ is demonstrated analytically in this appendix.

2.12.5.1 Summary of Results

The results of the evaluations contained in the following sections of this appendix demonstrate that:

- The fuel rod forces used to evaluate the FCS and strongback core are highly conservative and based on simple determination methods. Section 2.12.5.7, *Vertically Loaded Fuel Load Determination*, and Section 2.12.5.8, *Horizontally Loaded Fuel Load Determination*, present the fuel rod load derivations.
- The FCS structure provides significant geometric control of the MK-BW/MOX1 fuel assemblies as well as serving as a substrate to support additional neutron poison, thereby providing significant criticality margin. Section 2.12.5.6, *Stability Criteria*, through Section 2.12.5.13, *Lock Plate and Hinge Mounting Brackets*, provide the structural evaluation of the FCS.
- The structural integrity of the strongback is demonstrated in Section 2.12.5.14, *Strongback Global Stability*, through Section 2.12.5.20, *Strongback Stress Calculations - Horizontal Loads*, for the increased weight and effects of the FCS. These calculations included comprehensive checks of the stress and stability conditions.

¹ Title 10, Code of Federal Regulations, Part 71 (10 CFR 71), *Packaging and Transportation of Radioactive Materials*, Final Rule, 01-26-04.

2.12.5.2 Conditions Analyzed

The FCS is evaluated using four bounding loading conditions. Three of these conditions are comprised of maximum near vertical load plus a lateral loading applied by the FA rods. The fourth loading condition is comprised of maximum lateral loading only.

The loading cases are as follows:

1. LC1: 120g's vertical plus lateral loads applied by the FA rods on inside *pin block* box panel. Lateral loads are parallel to the local 'Y' axis (refer to Figure 2.12.5-5 for geometry).
2. LC2: 120g's vertical plus lateral loads applied by the FA rods on inside *hinge block* box panel. Lateral loads are parallel to the local 'X' axis (refer to Figure 2.12.5-5 for geometry).
3. LC3: 120g's vertical plus lateral loads applied by the FA rods on both hinge and pin block box panels.

The vertical g-loading in LC 1-3 is perpendicular to the lateral FA rod loading and is based on the 80 degrees from horizontal, 30-foot drops (Certification Test Series 2, Test 1 and Data Test 11) performed in the certification testing (Appendix 2.12.3, *Certification Test Results*). The lateral loads applied to the FCS by the FA rods are determined within this appendix.

The FCS is attached to the strongback and applies loads locally to the primary structure of the strongback. The worst-case reaction FCS load to the strongback results from a horizontal drop. Fuel buckling is not a concern during this horizontal drop. A fourth load case is performed to determine the worst-case FCS reaction forces on the strongback.

4. LC4: 180g's horizontal including inertia loads applied by the FA rods on inside hinge block box panel.

The hinge block of the FCS is mounted in close proximity to the strongback triangular core, while the pin block is mounted near the unsupported edge of the strongback angle plate, see Figure 2.12.5-5. Therefore, applying the acceleration and fuel support load perpendicular to the inside surface of the hinge block box panel causes loads to concentrate at the hinge, thus maximizing local loadings to the strongback.

2.12.5.3 FCS Geometry

The function of the FCSs is to control the geometry of the fuel assemblies to prevent excessive lateral displacement when subjected to a 120g vertical acceleration loading, including the lateral fuel loading.

The MFFP strongback is constructed as shown in Appendix 1.4.2, *Packaging General Arrangement Drawings*, Drawing 99008-30. The primary structural components are:

- The strongback core, which provides the longitudinal structure of the strongback.
- The top and bottom plates of the strongback, which interface with the ends of the FA and the containment body.
- The clamp arm assemblies, which provide the interface of the fuel to the strongback and restrain the fuel at the grid straps during all conditions of transport.
- The FCSs, which restrict the lateral movement of the fuel rods.

The MK-BW/MOX-1 FA physical characteristics important to this evaluation are geometry and weight. Table 2.12.5-1 and Figure 2.12.5-1 re-state the FA geometry and weight information from Section 1.2.3, *Contents of Packaging*.

The neutron poison plates and angle supports attached to the fuel segment angle are conservatively assumed to not provide any structural reinforcement, and therefore are not included in the FEA model. However, their mass is included with the angle component to account for their effect on the hinges and stiffeners associated with the drop acceleration load.

2.12.5.4 FCS Material Properties

The material properties used for the analyses herein are fully presented in Section 2.2, *Materials*, and are summarized in Table 2.12.5-2.

The FCS consists of four primary structural components; the box angle, channel stiffeners, hinge block, and pin block, see Figure 2.12.5-5. The material for the channel stiffeners, hinge block, and pin block is XM-19 stainless steel. These components are welded together (or machined as one) and subsequently bolted to the box angle. The pins used to connect the FCS to the strongback are ASTM A564 Grade 630 H1100 (17-4PH). The box angle is Type 304 stainless steel and the fasteners are ASTM F835 flat countersunk head cap screws. The chemical and mechanical requirements of F835² are similar to A574 (for regular socket head cap screws). The ASTM minimum tensile loads for both F835 and A574 are based on the same ultimate strength of 180 ksi. The primary difference between the two specifications is the product form; i.e. flat countersunk head cap screws versus regular socket head cap screws. Therefore, the material properties in Table 2.12.5-2 for A574 are considered to be applicable for determining the allowable stresses of F835 fasteners in the subsequent evaluations. The tangent modulus for XM-19 and Type 304 is determined below for use in the non-linear ANSYS[®] model.

The tangent modulus is defined as the slope of the true stress-strain curve between the material yield point and the ultimate breaking strength, given as:

$$E_{\text{TAN}} = \frac{(S_u - S_y)}{(\epsilon_u - 0.002)}$$

where S_u is the ultimate true stress, S_y is the yield true stress, and ϵ_u is the ultimate true strain, and the elongation or strain at the yield point is defined as 0.2%, or 0.002. Since the data is in the form of engineering stress-strain data, it must first be converted to true stress-strain data before use in the equation above for the tangent modulus. This conversion can be performed using the following relations³:

$$\sigma_{\text{true}} = \sigma_{\text{eng}} (1 + e_{\text{eng}})$$

$$\epsilon_{\text{true}} = \ln(1 + e_{\text{eng}})$$

² ASTM International, *Fasteners; Rolling Element Bearings*, Section 1, Volume 01.08, 2003

³ W. Johnson, P. B. Mellor, *Engineering Plasticity*, Halstead Press/Wiley and Sons, New York, 1983.

where σ_{eng} is the engineering stress value, and e_{eng} is the elongation (as a decimal value, percent divided by 100).

The data for XM-19 at 200 °F from Table 2.12.5-2 is first converted from engineering to true stress-strain and then used to calculate the tangent modulus. First, the true ultimate tensile strength is:

$$S_u = \sigma_{\text{eng}} (1 + e_{\text{eng}}) = 99,400 \times (1 + 0.35) = 134,190 \text{ psi}$$

where σ_{eng} is 99,400 psi and e_{eng} is 35.0% elongation⁴. Similarly, the true yield strength is

$$S_y = \sigma_{\text{eng}} (1 + e_{\text{eng}}) = 47,100 \times (1 + 0.002) = 47,194 \text{ psi}$$

where σ_{eng} is the stress at 0.2% strain of 47,100 psi. The true ultimate strain is:

$$\epsilon_u = \ln(1 + e_{\text{eng}}) = \ln(1 + 0.35) = 0.30$$

The tangent modulus for XM-19 at 200 °F is therefore:

$$E_{\text{TAN}} = \frac{(S_u - S_y)}{(\epsilon_u - 0.002)} = \frac{(134,190 - 47,194)}{(0.30 - 0.002)} = 291,933 \text{ psi}$$

The data for Type 304 at 200 °F from Table 2.12.5-2 is first converted from engineering to true stress-strain and then used to calculate the tangent modulus. First, the true ultimate tensile strength is:

$$S_u = \sigma_{\text{eng}} (1 + e_{\text{eng}}) = 71,000 \times (1 + 0.40) = 99,400 \text{ psi}$$

where σ_{eng} is 71,000 psi and e_{eng} is 40.0% elongation⁴. Similarly, the true yield strength is:

$$S_y = \sigma_{\text{eng}} (1 + e_{\text{eng}}) = 25,000 \times (1 + 0.002) = 25,050 \text{ psi}$$

where σ_{eng} is the stress at 0.2% strain of 25,000 psi. The true ultimate strain is:

$$\epsilon_u = \ln(1 + e_{\text{eng}}) = \ln(1 + 0.40) = 0.34$$

The tangent modulus for Type 304 at 200 °F is therefore:

$$E_{\text{TAN}} = \frac{(S_u - S_y)}{(\epsilon_u - 0.002)} = \frac{(99,400 - 25,050)}{(0.34 - 0.002)} = 219,970 \text{ psi}$$

2.12.5.5 FCS Stress Criteria

The stress criteria used for the analyses herein are fully presented in Section 2.1.2, *Design Criteria*, and are summarized in Table 2.12.5-3. The FCS is a criticality control structure component that is only required for HAC. Therefore, a combination of plastic and elastic analysis techniques from ASME Appendix F⁵ is utilized. The only sections that will use acceptance criteria from elastic

⁴ American Society of Mechanical Engineers (ASME) Boiler and Pressure Vessel Code, Section II, *Materials*, Part A, *Properties*, 2001 Edition with 2002 and 2003 Addenda.

⁵ American Society of Mechanical Engineers (ASME) Boiler and Pressure Vessel Code, Section III, *Rules for Construction of Nuclear Power Plant Components*, 2001 Edition with 2002 and 2003 addenda.

analysis are those related to the pinned connections in accordance with Appendix F, Section F-1336. All other evaluations utilize the plastic analysis acceptance criteria.

2.12.5.6 FCS Stability Criteria

The function of the strongback is to maintain the position of the neutron poison plates between the regions of "active" fuel. The structure is acceptable, provided global stability is maintained. HAC free drop loads and HAC criteria are used in this stability demonstration.

2.12.5.7 FCS Vertically Loaded Fuel Load Determination

This calculation evaluates the loads applied to the FCS during a near-vertical free drop in which the fuel rods buckle. The loads on the FCS are normal to the longitudinal axis and FCS panels, and are caused by restraining the lateral displacement of the fuel rods. The geometry and related data needed for this determination is given in Table 2.12.5-1. Since the fuel is in a 17×17 array with a 0.496-inch pitch and a single rod diameter of 0.374 inches, the bounds of the array are $16(0.496) + 0.374 = 8.31$ inches. The clearance between the FCS and the fuel rods is therefore $0.5(8.70 - 8.31) = 0.2$ inches. Some deflection of the FCS is expected to occur under loading from the fuel rods. Therefore, for purposes of calculation, the total clearance is increased by 0.05 inches to a total of 0.25 inches, to account for the full possible range of movement of the rods. This value bounds the worst-case calculated FCS deflections as shown in Figure 2.12.5-15. The buckling magnitude and buckling forces are the greatest in the space between clamp arms (hereafter called 'bay') which is nearest to the ground. The one long bay (length equal to 24.13 inches) is not governing, since the force applied by the fuel rods is proportional to the angle of deformation, and the angle is smaller in the longer bay than in the shorter ones. Thus, for analysis purposes, the free length of the rods is equal to the shorter distance between clamp arms of 20.5 inches.

The following assumptions govern this evaluation:

- The action of each fuel rod under the applied loading is Euler buckling caused by self weight under the impact loading. The resulting lateral deflection of the rods brings them into contact with the FCS, the strongback core, and with each other.
- Conservatively, all rods buckle in the same direction within a bay, and in opposite directions in adjacent bays. For example, if the rods deflect towards the FCS in the lowest bay, they deflect towards the strongback core in the next bay above it.
- Conservatively, those rods which are in contact stack up in perfect columns behind each other such that rod forces accumulate without loss. This assumption is conservative, since, as seen in Figure 2.12.5-2, the planes of deformation of the rods are not all perfectly parallel, and the rods, which are smooth, actually tend to slip past each other with only partial transfer of the lateral buckling load.
- The grid structures serve as points of inflection for the deflected rods. As shown in Figure 2.12.5-2 and in Figure 2.12.3-20, the spacing distances in the grid remain essentially unchanged. Also, it is noted that there is essentially no bending (and therefore zero moment) in the grids. Thus, the grids supply lateral support for the rods, but no moment support. Also, no axial friction support is assumed.

Since each rod deforms in a sine shape with inflection points at the grids, the deflection distance of any rod to the left and to the right is equal. In other words, the leftward deflection in the upper bay shown in Figure 2.12.5-3 is equal to the rightward deflection of the same rod in the lower bay. Given this fact, the magnitude of rod deflection is controlled by the first point of contact above or below the grid, whichever occurs first. For example (referring to Figure 2.12.5-3), row 1 deflects the least because it contacts the FCS after deflection through a distance equal to the gap of 0.25 inches between the rods and the FCS. Similarly, row 17 deflects the same amount, since it contacts the strongback core after deflecting through 0.25 inches in the adjacent bay. Note that the rods could deflect in the opposite direction, in which case the roles of the FCS and strongback core would be reversed in the above statements. Regardless of direction, the fuel has the strongback on one side and the FCS on the other. Other rows deflect through greater distances, owing to the clearance gaps between the rod rows. For example, the deflection of rows 2 and 16 is greater than for rows 1 and 17; the deflection of rows 3 and 15 is greater still; rows 4 and 14 greater still, and so on. The center row, row 9, deflects the most, and is the only row to contact other rods both above and below the grid.

Figure 2.12.5-4 depicts the free body diagram of a rod in a typical row (number 1 to 8) on the left of the figure, and a free body diagram of a rod in the central row (no. 9), on the right. Since rows 10 – 17 load the strongback core, they are not considered in this analysis.

For the general case, as discussed above, the segment is deflected equally at the top and bottom by the amount x_i . The force F_i represents the contact force of rod i with the rod to its left, or in the case where $i = 1$, with the FCS. The force F_{Gi} represents the force supplied by the grid in maintaining the row spacing. The force P is the buckling force along the rod axis, and the moment M_i is the bending moment in the rod. A free body diagram for a smaller segment is shown in the lower left of the figure. By symmetry, only half of the total contact force F_i is applied to the free body detail figure. Summing moments about the lower end, clockwise positive,

$$P(2x_i) - F_{Gi} \frac{L}{2} - 2M_i = 0$$

from which:

$$F_{Gi} = \frac{4(Px_i - M_i)}{L}$$

Summing forces in the horizontal direction, positive to the right, readily shows that $F_i = 2F_{Gi}$, so that the contact force is:

$$F_i = \frac{8(Px_i - M_i)}{L}$$

For the case of a rod in row 9, again summing moments about the lower end, clockwise positive,

$$P(2x_9) - \frac{1}{2}F_9L - 2M_9 = 0$$

By symmetry, the grid force is zero. The rod force is:

$$F_9 = \frac{4(Px_9 - M_9)}{L}$$

Before computing the rod forces, the parameters P , x_i , and M_i must be evaluated. In the following, any needed fuel assembly or cladding parameters are taken from Table 2.12.5-1.

The buckling force P, axial to the rod, is simply:

$$P = W_e g$$

where W_e is the effective weight of the rod, and g is the impact, which is bounded by 120 g. The weight of the rod which is above the bay where maximum buckling occurs is fully effective. The weight of the rod in the bay of interest is only 1/3 effective⁶. Since the rod is 152.4 inches long, and the length of the bay is $L = 20.5$ inches, the total effective weight of the rod is:

$$W_e = \left[\frac{(152.4 - 20.5)}{152.4} + \frac{20.5}{152.4} \left(\frac{1}{3} \right) \right] \times 5.33 = 4.85 \text{ lb}_f$$

where the weight of the entire rod is 5.33 lb_f. For purposes of analysis, the weight W_e will be applied in a lumped manner above the bay of interest. Note that W_e equals 91% of the total rod weight. The load P is therefore equal to $4.85 \times 120 = 582 \text{ lb}_f$ per rod.

The lateral deflections of the rods are:

$$x_i = C + (i - 1)G_r$$

where the clearance between the surface row (i.e., row 1) and the FCS is $C = 0.25$ inches, and the gap between rows, $G_r = 0.496 - 0.374 = 0.122$ inches, where 0.496 inches is the row pitch, and 0.374 inches is the rod diameter. Parameter i is the row number. For example, for the third row ($i = 3$):

$$x_3 = 0.250 + (3 - 1)0.122 = 0.494 \text{ inches}$$

The moment in the rod, M_i , can be evaluated from the common expression:

$$M = EI \frac{d^2 y}{dx^2}$$

where, for consistency with the nomenclature of most references, y is the lateral deflection of the rod, and x is the axial position along the rod, equal to zero at a point of inflection (in this case, at a grid). Since the equation of the elastic curve of an Euler column⁷ is:

$$y = A \sin \pi \frac{x}{L}$$

where A is the maximum lateral deflection, and L is the length of one half-wave, then the second derivative of the deflection, y , is:

$$\frac{d^2 y}{dx^2} = \left(\frac{\pi}{L} \right)^2 A \sin \pi \frac{x}{L}$$

and the maximum value, when $x = L/2$, is:

$$\frac{d^2 y}{dx^2}_{\text{MAX}} = \left(\frac{\pi}{L} \right)^2 A$$

⁶ This is by analogy to the case of a longitudinally vibrating rod with a mass at the free end. The solution to the vibration problem may be carried out assuming that 1/3 of the distributed mass of the rod is lumped in with the end mass. See Harris, Cyril M., *Shock and Vibration Handbook*, Third Edition, McGraw-Hill, 1988, Table 7.2.

⁷ Beer, Ferdinand P., and Johnson, E. Russell Jr., *Mechanics of Materials*, McGraw-Hill, 1981.

The moment in the rod is then:

$$M_{MAX} = EI \frac{d^2 y}{dx^2}_{MAX} = EI \left(\frac{\pi}{L} \right)^2 A$$

However, this elastic moment is limited by the plastic hinge moment, which can be found from the product of the shape factor and the yield moment. The shape factor⁸, SF, is:

$$SF = 1.698 \frac{R^4 - R_i^3 R}{R^4 - R_i^4} = 1.351$$

where the rod outer diameter, $R = 0.374/2 = 0.187$ inches, and the inner diameter, $R_i = R - t = 0.1645$ inches, where the wall thickness $t = 0.0225$ inches. The moment of inertia of the rod is:

$$I = \frac{\pi}{4} (R^4 - R_i^4) = 3.853(10^{-4}) \text{ in}^4$$

The yield strength of the rod cladding material at a bounding temperature of 200 °F is $S_y = 31,222$ psi. The bending moment for first yield of the cladding material is therefore:

$$M_y = \frac{S_y I}{R} = 64.3 \text{ in-lb}$$

Consequently the plastic hinge moment is:

$$M_p = (SF)M_y = 86.9 \text{ in-lb}$$

Since the elastic modulus, E , of the cladding material is $12.8(10^6)$ psi at 200 °F, the rod moment is equal to:

$$M_i = EI \left(\frac{\pi}{L} \right)^2 A = 115.8 x_i \text{ in-lb}, \leq 86.9 \text{ in-lb}$$

where x_i , substituted for A , is the maximum deflection of any rod from its neutral position, and L equals 20.5 inches.

The total force applied to the FCS can now be determined. The force of an individual rod is equal to F_i above. The total force of that row is equal to F_i multiplied times the number of active rods in the row (see Figure 2.12.5-1). Some rows have up to five inactive spaces (empty guide tubes) which, due to their stiffer cross section and low weight loading (tributary weight of one nozzle of less than one pound each), do not need to be included in the loading calculation. Finally, the total force is the sum of the force contributions of each row. The calculations are detailed in Table 2.12.5-4. Thus, the maximum force applied to the FCS from the buckled fuel rods is 17,452 pounds.

2.12.5.8 FCS Horizontal Fuel Load Determination

This section considers the loads applied to the FCS during a horizontal HAC free drop (including the secondary impact of a slapdown orientation). The loads on the FCS are normal to the fuel rod axis and FCS panels, and are the result of the fuel rod lateral displacements. The geometry

⁸Young, Warren C., *Roark's Formulas for Stress and Strain*, Sixth Edition, McGraw-Hill, 1989, Table 1, Case 15.

relevant to the determination of the fuel load on the FCS is free span between clamp arms. With exception to the bottom most set of clamp arms, the center-to-center distance is 20.50 inches. The bottom set has a center-to-center distance of 24.13 inches. The clamp pads are 2.25 inches wide.

Each fuel rod weighs 5.3 pounds and is 152.4 inches long. The unit weight of fuel rod is therefore $5.3/152.4 = 0.035$ lb_f/inch. The horizontal drop load is determined assuming the fuel rods load both the clamp arms and FCS channel. The fuel rod load tributary to the FCS channel is simply determined by multiplying the unit weight of the fuel rod by the tributary length of fuel rod. For the bottom set of FCSs, the tributary length is $(24.13 - 2.25)/2 = 10.94$ inches, assuming the FCS channel share the load equally with the clamp arms. There are 264 fuel rods per fuel assembly. Therefore, the maximum load which may be applied to the FCS channel supports at 1g of acceleration is: $0.035(10.94)(264) = 101.1$ pounds. For the 180 g horizontal acceleration, the horizontal load on the FCS attributed to a single fuel assembly is 18,198 pounds; however 19,000 pounds will conservatively be used.

2.12.5.9 Evaluation Assumptions and Methodology

ANSYS[®] Version 8.0 and Version 8.1 were utilized to perform finite element analysis on the FCS for the load cases stated in Section 2.12.5.2, *Conditions Analyzed*. The model includes the full geometry of each item, excluding clearance chamfers, and pin and bolt holes. Stresses for the pin hole sections are calculated manually in Section 2.12.5.19, *Evaluation of Strongback Response to FCS Loads*, using reaction forces extracted from the FEA runs. The FEA model uses coupled coincident nodes in the bolt locations. The component forces are collected at these locations and used to determine the bolt stresses in Section 2.12.5.12, *Fastener Analysis*.

The MOX strongback utilizes seven fuel control structures per fuel assembly. Therefore, there are a total of twenty one per strongback. Each FCS spans the length between two adjacent strongback clamp arms. The typical FCS span is 20.50 inches. The span between the bottom strongback endplate and adjacent clamp arm is 24.13 inches. The clamp pads are 2.25 inches wide. The bottom three FCSs are identical to the typical span versions, except the angle and neutron poison is slightly longer. The finite element analysis (FEA) model is adjusted to have a mass equivalent to that of the longer FCS, bounding stresses with respect to the vertical acceleration.

The fuel load determined in Section 2.12.5.7, *FCS Vertically Loaded Fuel Load Determination*, and Section 2.12.5.8, *FCS Horizontally Loaded Fuel Load Determination*, are applied as a pressure to the angle in the region backed by the stiffener. The maximum NCT hot temperature for the strongback structure, as determined in Section 3.4, *Thermal Evaluation for Normal Conditions of Transport*, is 178 °F. The structural evaluation of the FCS conservatively uses 200 °F. The stress acceptance criteria are determined using mechanical properties summarized in Table 2.12.5-2.

The model consists of SOLID45 3-D structural 4-node solid elements with CONTAC49 3-D point-to-surface contact elements between the primary bolted surfaces. Friction between the bolted surfaces is conservatively ignored. The material properties correspond to 200 °F and the tangent moduli for XM-19 and Type 304 used in the FEA model are calculated in Section 2.12.5.4 as 291,933 psi and 219,970 psi, respectively. Corresponding runs were made for load cases 1 through 3 with the tangent moduli set at 5% of the Modulus of Elasticity (i.e., 1,380,000 psi).

Table 2.12.5-5 provides summary results for comparison between the lower and higher tangent moduli. Results for the lower tangent moduli are taken from Table 2.12.5-7. The maximum

plastic strain is low (less than 3%) and the difference in plastic strain between the lower and higher tangent moduli is negligible. Stresses for both lower and higher tangent moduli runs are approximately the same, with only more redistribution of stress in the lower tangent modulus runs. The lower tangent modulus runs had slightly more net displacement or deflection as expected. Therefore, the lower tangent moduli calculated in Section 2.12.5.4 are considered conservative as the stresses are minimally affected and displacements are larger. Using the lower tangent moduli provides a more conservative evaluation of the FCS stability.

The FEA model has an approximately 0.31 inch longer channel on the hinge block side than the actual design. The hinge block side channel is a symmetry copy of the pin block side channel for model generation. The minor additional length is considered negligible in regard to the reaction loads and bounding with respect to weight and stresses. The bending stresses in the channel will be conservative because the load is applied over a slightly longer unsupported span. The pin block side of the channel is approximately 0.16 inches shorter than shown on the General Arrangement Drawing 99008-34. This difference is less than 2%, which is not significant considering the margins of safety shown in Table 2.12.5-6 and Table 2.12.5-7. The bending stress increases linearly with a set load and an increase in length. Therefore, the channel stress would increase by less than 2%, which is not a significant impact considering the lowest margin of safety for this part is 0.59.

The fuel lateral load is 17,452 pounds, however 18,000 pounds is conservatively used in load cases 1-3. The load is applied as a pressure to the angle in the region backed by the channel. This method is based on test results collected during certification testing. A prototypic fuel assembly was shown to undergo first mode Euler buckling, where it displaced perpendicular to its axis at the center of the span between clamp arms, see Figure 2.12.3-22 of Appendix 2.12.3, *Certification Test Results*.

2.12.5.10 FCS Finite Element Analysis (FEA)

Each component of the FCS is evaluated in the FEA model for general primary membrane stress intensity (P_m) and maximum primary membrane stress intensity (P_{max}). P_m is determined by looking at the stress intensity plots and plotting paths thru sections with high stress. The stress intensity is linearized across the path using the ANSYS® “prsect” and/or “plsect” command. P_{max} is conservatively taken as the maximum stress intensity from the component plots, which include peak stresses from geometrical discontinuities and local applications of boundary constraints. The plastic analysis acceptance criteria are per Table 2.12.5-3.

Table 2.12.5-6 and Table 2.12.5-7 demonstrate the FCS meets all the plastic analysis acceptance criteria. Margins of safety (MS) greater than or equal to zero are acceptable. Stress and displacement plots of the FEA are provided in Figure 2.12.5-11 through Figure 2.12.5-25, and Figure 2.12.5-36 through Figure 2.12.5-44.

During horizontal drop orientations in which the acceleration vector is primarily normal to the longitudinal axis of the fuel, fuel rod pitch is not of concern, and therefore the FCS geometry is not required to control the reactivity of the fuel. Because the FCS geometry is not required during horizontal drops, the FCS is not evaluated for LC4 (the horizontal load case). However, the connection points on the strongback longitudinal weldment are evaluated for LC4 to show that the side drop loads do not cause failure of non-FCS strongback components.

FEA Reaction and Bolt Loads

Contained in Table 2.12.5-8 through Table 2.12.5-11 are the reaction loads from the four analyzed conditions, as reported by the FEA model. Similarly, Table 2.12.5-12 through Table 2.12.5-14 contains the bolt loads from the three analyzed conditions. The reaction loads are used for the pinned connection elastic analysis and the bolt loads are used for the fastener analysis. Node reaction and bolt locations are shown in Figure 2.12.5-10.

2.12.5.11 Pinned Connection Elastic Analysis

The pinned sections of the FCS pin and hinge blocks are evaluated elastically according to the criteria in Table 2.12.5-3. The reaction loads from the FEA runs are used as the loads that act over the corresponding pinned section. The lug of the pin block and the bounding center lug of the hinge block are the pinned sections evaluated. The bounding reaction loads both come from Load Case 2 where the pressure load is applied to the hinge block side of the angle. The total reaction force perpendicular to the axis of the fuel assembly is the Square Root of the Sum of the Squares (SRSS) of the x and y direction reactions. The axial, z direction, reactions do not affect the pinned sections. Their related stresses are included in P_m and P_{max} in Section 2.12.5.10, *FCS Finite Element Analysis (FEA)*, for the plastic analysis.

The pin and hinge blocks are fabricated from Type XM-19 stainless steel. The stress allowable, based on the stress criteria in Table 2.12.5-3 and the material properties of Type XM-19 at 200 °F are summarized below.

Allowable Stresses	
Shear, S_τ (psi)	$S_\tau = 0.42S_u = 0.42(99,400) = 41,748$
Bearing, $S_{bearing}$ (psi)	$S_{bearing} = 2.1S_u = 2.1(99,400) = 208,740$
Pin Block Shear (See Figure 2.12.5-8)	
Net shear tear-out area, A_s (in ²)	$A_s = (\text{min. edge length})(\text{lug length})$ $= (0.22)(1.5) = 0.33$
Bounding reaction load, P (lb _f)	$P = 8,898$ (LC2, Table 2.12.5-9)
Shear Stress, τ (psi)	$\tau = P/2A_s = 8,898/(2(0.33)) = 13,482$
Margin of Safety	$MS = \frac{S_\tau}{\tau} - 1.0 = \frac{41,748}{13,482} - 1.0 = +2.10$
Pin Block Bearing (See Figure 2.12.5-8)	
Projected bearing area, A_b (in ²)	$A_b = (\text{pin dia})(\text{lug length}) = (0.375)(1.5) = 0.56$
Bounding reaction load, P (lb _f)	$P = 8,898$ (LC2, Table 2.12.5-9)
Bearing Stress, σ_b (psi)	$\sigma_b = P/A_b = 8,898/0.56 = 15,889$
Margin of Safety	$MS = \frac{S_{bearing}}{\sigma_b} - 1.0 = \frac{208,740}{15,889} - 1.0 = +12.14$

Hinge Block Center Lug Shear Stress	
Net shear tear-out area, A_s (in ²)	$A_s = (\text{min. edge length})(\text{lug length})$ $= (0.24)(1.5) = 0.36$
Bounding reaction load, P (lb _f)	$P = 7,590$ (LC2, Table 2.12.5-9)
Shear Stress, τ (psi)	$\tau = P/2A_s = 7,590/(2(0.36)) = 10,542$
Margin of Safety	$MS = \frac{S_{\tau}}{\tau} - 1.0 = \frac{41,748}{10,542} - 1.0 = +2.96$
Hinge Block Center Lug Bearing Stress	
Projected bearing area, A_b (in ²)	$A_b = (\text{pin dia})(\text{lug length}) = (0.375)(1.5) = 0.56$
Bounding reaction load, P (lb _f)	$P = 7,590$ (LC2, Table 2.12.5-9)
Bearing Stress, σ_b (psi)	$\sigma_b = P/A_b = 7,590/0.56 = 13,554$
Margin of Safety	$MS = \frac{S_{\text{bearing}}}{\sigma_b} - 1.0 = \frac{208,740}{13,554} - 1.0 = +14.40$
Hinge Block Outer Lug Shear Stress (See Figure 2.12.5-8)	
Net shear tear-out area, A_s (in ²)	$A_s = (\text{min. edge length})(\text{lug length})$ $= (0.24)(1.0) = 0.24$
Bounding reaction load, P (lb _f)	$P = 4,377$ (LC1, Table 2.12.5-8)
Shear Stress, τ (psi)	$\tau = P/2A_s = 4,377/[2(0.24)] = 9,119$
Margin of Safety	$MS = \frac{S_{\tau}}{\tau} - 1.0 = \frac{41,748}{9,119} - 1.0 = +3.58$
Hinge Block Outer Lug Bearing Stress	
Projected bearing area, A_b (in ²)	$A_b = (\text{pin dia})(\text{lug length}) = (0.375)(1.0) = 0.38$
Bounding reaction load, P (lb _f)	$P = 4,377$ (LC1, Table 2.12.5-8)
Bearing Stress, σ_b (psi)	$\sigma_b = P/A_b = 4,377/0.38 = 11,518$
Margin of Safety	$MS = \frac{S_{\text{bearing}}}{\sigma_b} - 1.0 = \frac{208,740}{11,518} - 1.0 = +17.12$

Quick-Release Pin Shear Load:

The quick-release pins used in conjunction with the FCS and strongback are Avibank (or equivalent) 3/8-inch diameter quick-release pins. The body and spindle are fabricated from corrosion resistant 17-4PH or PH15-7MO material. The calculated double shear strength per the manufacturer for this quick-release pin is 20,600 pounds.

Bounding reaction load (lb_f): $P = 5,078$ (LC2, Table 2.12.5-9) (single shear)

$$\begin{aligned} \text{Allowable Load (lb}_f\text{): } P_{\text{allow-DS}} &= 20,600 && \text{(double shear)} \\ P_{\text{allow-SS}} &= 20,600/2 = 10,300 && \text{(single shear)} \\ \text{Margin of Safety: } MS &= \frac{P_{\text{allow-SS}}}{P} - 1.0 = \frac{10,300}{5,078} - 1.0 = +1.03 \end{aligned}$$

Quick Release Pin Bearing Stress:

$$\begin{aligned} \text{Projected bearing area (in}^2\text{): } A_b &= (\text{pin dia})(\text{lug length}) = (0.375)(1.5) = 0.56 \text{ in}^2 \\ \text{Bounding reaction load (lb}_f\text{): } P &= 8,898 \quad (\text{LC2, Table 2.12.5-9}) \\ \text{Bearing Stress (psi): } \sigma_b &= P/A_b = 8,898/0.56 = 15,889 \\ \text{Allowable Stress (psi): } S_{\text{bearing}} &= 2.1S_u = 2.1(140,000) = 294,000 \\ \text{Margin of Safety: } MS &= \frac{S_{\text{bearing}}}{\sigma_b} - 1.0 = \frac{294,000}{15,889} - 1.0 = +17.50 \end{aligned}$$

2.12.5.12 Fastener Analysis

The welded hinge block/pin block/stiffener assembly is secured to the box angle with socket head screws, see Figure 2.12.5-9. The maximum tensile and shear loads are extracted from the FEA runs and used to check the screw stresses in accordance with Table 2.12.5-3.

The fasteners material is A574. The stress allowable, based on the stress criteria in Table 2.12.5-3 and the material properties of A574 at 200°F are summarized below.

Allowable Stresses	
Tensile, F_{tb} (psi)	$0.7S_u = 0.7(180,000) = 126,000$
Shear, F_{vb} (psi)	$0.42S_u = 0.42(180,000) = 75,600$
Bearing, S_{bearing} (psi)	$2.1S_u = 2.1(99,400) = 208,740$
Screw Tensile Stress	
Net tensile area, A_t (in ²)	$A_t = 0.0364$ (1/4–28 UNF Table 8-2 ⁹)
Bounding tensile load, P (lb _f)	$P = 240$ (LC1, Table 2.12.5-12)
Tensile Stress, f_t (psi)	$f_t = P/A_t = 240/0.0364 = 6,593$
Margin of Safety	$MS = \frac{F_{tb}}{f_t} - 1.0 = \frac{126,000}{6,593} - 1.0 = +18.11$

⁹ Shigley, J. E., Mischke, C. R., *Mechanical Engineering Design*, Fifth Edition, McGraw-Hill, 1989, New York, NY.

Screw Shear Stress	
Net shear area, A_s (in ²)	$A_s = 0.0326$ (1/4–28 UNF Table 8-2 ⁸)
Bounding reaction load, P (lb _f)	$P = 2,204$ (LC1, Table 2.12.5-12)
Shear Stress, f_v (psi)	$f_v = P / A_s = 2,204 / 0.0326 = 67,607$
Margin of Safety	$MS = \frac{F_{vb}}{f_v} - 1.0 = \frac{75,600}{67,607} - 1.0 = +0.12$
Bolt Tensile and Shear Stress Combination	
Bolt Tension + Shear Stress	$f_t^2/F_{tb}^2 + f_v^2/F_{vb}^2 \leq 1$
	$(6,593)^2/(126,000)^2 + (67,607)^2/(75,600)^2 = 0.80 < 1$
Allowable Stress	
The strongback longitudinal plate material is Type 304 stainless steel. The allowable stress, based on the stress criteria in Table 2.12.5-3 and the material properties of Type 304 at 200 °F, are summarized below.	
Ultimate Stress, S_u (psi)	71,000
Shear, S_τ (psi)	$0.42S_u = 0.42(71,000) = 29,820$
Minimum Edge Distance Check	
The minimum edge distance calculated is for the maximum square root, sum of the squares (SRSS) load from the screws near the edge of the angle.	
Projected screw angle area, A_p (in ²)	$A_p = (\text{screw head mean diameter})(\text{angle thickness})$ $= \frac{1}{2}(0.480 + 0.25)(0.125) = 0.37(0.125) = 0.046$
Bounding reaction load, P (lb _f)	$P = 1,380$ (LC1, Table 2.12.5-12)
Projected Area Stress, f_p (psi)	$f_p = P/A_p = 1,380/0.046 = 30,000$
Min. Angle Bolt Edge Distance	$L/d \geq [0.5 + 1.2(f_p/S_u)]$ $0.50/0.37 \geq [0.50 + 1.2(35,935/71,000)] \Rightarrow 1.35 \geq 1.01$
	$f_p/S_u \leq 2.1 \Rightarrow 30,000/71,000 \leq 2.1 \Rightarrow 0.42 < 2.1$
Tensile Pull-Out Shear Stress	
The angle is evaluated for tensile pull-out of the countersunk SHCS. The shear area of the angle is assumed to be the cylindrical area under the maximum countersunk head diameter (see Figure 2.12.5-9).	
Net axial shear area, A_s (in ²)	$A_s = \pi(t)(\text{head diameter}) = \pi(0.125)(0.480) = 0.188$
Bounding reaction load, P (lb _f)	$P = 240$ (LC1, Table 2.12.5-12)
Shear Stress, τ (psi)	$\tau = P/A_s = 240/0.188 = 1,277$
Margin of Safety	$MS = \frac{S_\tau}{\tau} - 1.0 = \frac{29,820}{1,277} - 1.0 = +22.35$

2.12.5.13 Lock Plate and Hinge Mounting Brackets

The lock plate and two hinge mounting brackets are reciprocal XM-19 components to the pin and hinge blocks that are bolted directly to the strongback angle plates. The lock plate is bolted near the outer edge of the strongback angle plate and is the component that the FCS pin block is pinned to. There are two identical hinge mounting brackets, for one FCS, that bolt to the strongback angle plate near the triangular core. The FCS hinge block is pinned to the hinge mounting brackets. See Figure 2.12.5-5 for the global orientation and coordinate system. Figure 2.12.5-27 and Figure 2.12.5-28 illustrate the details and coordinate systems for the lock plate and hinge mounting bracket evaluations. The coordinate systems in Figure 2.12.5-27 and Figure 2.12.5-28, correspond to that in Figure 2.12.5-5 and the FEA analysis.

2.12.5.13.1 Pinned Connection Elastic Analysis

The pinned sections of the lock plate and hinge mounting bracket are evaluated similarly to the pin and hinge blocks in Section 2.12.5.11, *Pinned Connection Elastic Analysis*. The stress criteria used are for elastic analysis from Table 2.12.5-3. The reaction loads from the FEA runs are used as the loads that act over the corresponding pinned section. The bounding reaction loads both come from Load Case 2 where the pressure load is applied to the hinge block side of the angle.

The pin and hinge blocks are fabricated from Type XM-19 stainless steel. The stress allowable, based on the stress criteria in Table 2.12.5-3 and the material properties of Type XM-19 at 200 °F are summarized below.

Allowable Stress	
Shear, S_τ (psi)	$0.42S_u = 0.42(99,400) = 41,748$
Bearing, $S_{bearing}$ (psi)	$2.1S_u = 2.1(99,400) = 208,740$
Lock Plate Shear Tear-Out	
Net shear tear-out area, A_s (in ²)	$A_s = (\text{min edge length})(\text{lug no})(\text{lug width} - \text{chamfer})$ $= (0.24)2(0.59 - 0.13) = 0.22$
Bounding reaction load, P (lb _f)	$P = 8,898$ (LC1, Table 2.12.5-8)
Shear Stress, τ (psi)	$\tau = \frac{P}{2A_s} = \frac{8,898}{2(0.22)} = 20,223$
Margin of Safety	$MS = \frac{S_\tau}{\tau} - 1.0 = \frac{41,748}{20,223} - 1.0 = +1.06$
Lock Plate Axial Shear	
The axial shear is evaluated for the lock plate, because it is not included in the FEA and the lug width and shear area are smaller than any of the other pinned components. The bounding axial load is from LC 1.	
Net axial shear area, A (in ²)	$A = (\text{lug width})(\text{plate thickness}) = (0.59)(0.67) = 0.40$
Bounding reaction load, P (lb _f)	$P = 1,126$ (LC2, Table 2.12.5-9)
Shear Stress, τ (psi)	$\tau = \frac{P}{A} = \frac{1,126}{0.40} = 2,815$

Margin of Safety	$MS = \frac{S_{\tau}}{\tau} - 1.0 = \frac{41,748}{2,815} - 1.0 = +13.83$
Lock Plate Bearing	
Projected bearing area, A_b (in ²)	$A_b = (\text{pin dia})(\text{lug no})(\text{lug width}) = (0.375)(2)(0.59) = 0.44$
Bounding reaction load, P (lb _f)	$P = 8,898$ (LC2, Table 2.12.5-9)
Bearing Stress, σ_b (psi)	$\sigma_b = \frac{P}{A_b} = \frac{8,898}{0.44} = 20,223$
Margin of Safety	$MS = \frac{S_{\text{bearing}}}{\sigma_b} - 1.0 = \frac{208,062}{20,223} - 1.0 = +9.32$
Hinge Mounting Bracket Axial Shear	
The axial shear is evaluated for the hinge mounting bracket, because it is not included in the FEA analysis. The bounding axial load is from Load Case 1.	
Net shear area, A (in ²)	$A = (\text{lug width})(\text{plate thickness}) = (2.44)(0.69) = 1.68$
Bounding reaction load, P (lb _f)	$P = 1,974$ (LC1, Table 2.12.5-8)
Shear Stress, τ (psi)	$\tau = \frac{P}{A} = \frac{1,974}{1.68} = 1,175$
Margin of Safety	$MS = \frac{S_{\tau}}{\tau} - 1.0 = \frac{41,748}{1,175} - 1.0 = +34.53$
Hinge Mounting Bracket Shear	
Net shear tear-out area, A_s (in ²)	$A_s = (\text{min edge length})(\text{width})$ $= (0.24)(2.44 - 2(0.13)) = 0.52$
Bounding reaction load, P (lb _f)	$P = 7,325$ (LC2, Table 2.12.5-9)
Shear Stress, τ (psi)	$\tau = \frac{P}{2A_s} = \frac{7,325}{2(0.52)} = 7,043$
Margin of Safety	$MS = \frac{S_{\tau}}{\tau} - 1.0 = \frac{41,748}{7,043} - 1.0 = +4.93$
Hinge Mounting Bracket Bearing	
Projected bearing area, A_b (in ²)	$A_b = (\text{pin dia})(\text{lug width}) = (0.375)(2.44) = 0.92$
Bounding reaction load, P (lb _f)	$P = 7,325$ (LC2, Table 2.12.5-9)
Bearing Stress, σ_b (psi)	$\sigma_b = \frac{P}{A_b} = \frac{7,325}{0.92} = 7,962$
Margin of Safety	$MS = \frac{S_{\text{bearing}}}{\sigma_b} - 1.0 = \frac{208,062}{7,962} - 1.0 = +25.22$

2.12.5.13.2 Fastener Analysis

Lock Plate Fasteners

The lock plate is used with the pin block and lock pin to hold the FCS in a closed position. The lock plate is fastened to the strongback angle plate with three, 3/8 – 16 UNC countersunk socket head cap screws (SHCS), $A_t = .078 \text{ in}^2$, in a triangular pattern as shown in Figure 2.12.5-27. The fastener loads and stresses are determined as follows.

The FEA analysis of the FCS calculates reaction loads at the lock pin. These reaction loads are applied to the lock plate to determine the loads on the lock plate fasteners. The three loads are F_x (out of the plane of the lock plate, creating tensile fastener loads from prying), and F_y and F_z (in plane, creating shear loads). The shear loads arise from direct shear loading as well as from a torsional moment created by the axial acceleration.

The parameters affecting the load calculations, as depicted on Figure 2.12.5-26 and Figure 2.12.5-27, are (inches):

$$y_{\text{bar}} = \frac{2 \times A_t \times L_3}{3 \times A_t} = \frac{2 \times 0.078 \times 0.62}{3 \times 0.078} = 0.41 \quad \text{fastener group centroid to the single fastener}$$

$$r = \sqrt{\left(\frac{w_1}{2}\right)^2 + (L_3 - y_{\text{bar}})^2}$$

$$= 0.78 \quad \text{fastener group centroid to one of the fasteners in the two-fastener row}$$

$$L_1 = 0.46 \quad \text{lock pin center to pivot edge}$$

$$L_2 = 0.73 \quad \text{pivot edge to single fastener}$$

$$L_3 = 0.62 \quad \text{single fastener row to two-fastener row}$$

$$w_1 = 1.5 \quad \text{width between fasteners in two-fastener row}$$

The total tensile load on the fastener group from prying about the strongback edge is:

$$F_{\text{xg}} = F_x \frac{-L_1}{L_2 + y_{\text{bar}}}$$

The tensile load per fastener is:

$$F_{\text{xb}} = F_{\text{xg}}/3$$

The direct shear load per fastener in the y-direction is:

$$F_{\text{yb}} = F_y/3$$

The direct shear load per fastener in the z-direction is:

$$F_{\text{zb}} = F_z/3$$

The shear force per fastener from the torsional moment about the x-axis is:

$$F' = -F_z \frac{L_1 + L_2 + y_{\text{bar}}}{3 \times y_{\text{bar}}}$$

The total shear, f_v , is the square root sum of the squares for the worst fastener, which is the front single fastener:

$$f_v = \sqrt{(F_{yb} + F'_y)^2 + (F_{ab} + F'_z)^2}$$

where F' is orthogonal to the bolt moment arm and may be decomposed into the coordinate system for combination. The total tensile load per fastener is $f_t = F_{xb}$. The tensile stress is $\sigma = f_t/A_t$ and the shear stress is $\tau = f_v/A_s$, where the tensile stress area, $A_t = 0.078 \text{ in}^2$, and the shear stress area, $A_s = 0.068 \text{ in}^2$, from Shigley¹⁰, Table 8.2. The margin of safety and interaction equations are calculated using the same allowable stresses and methods as in Section 2.12.5.12, *Fastener Analysis*. The results are given in Table 2.12.5-15. As shown, all of the lock plate fastener stresses are acceptable.

Hinge Mounting Bracket Fasteners

The top and bottom hinge mounting brackets are each bolted to the strongback angle plate with four 3/8–16UNC countersunk socket screws in a square pattern. The bolt loads and stresses for each load case are calculated using an excel spreadsheet, summarized in Table 2.12.5-16. All of the hinge mounting block bolt stresses are acceptable. The method and design information for finding the loads and stresses are as follows.

The reaction loads for the hinge block from the FEA runs are used (as equal and opposite) for the loads applied to the hinge mounting brackets. However, the reaction loads are first rotated thirty degrees to be perpendicular and parallel with the surface of the hinge mounting brackets. In Figure 2.12.5-5, the hinge mounting bracket (pinned to the hinge block) is at angle with the coordinate system. The strongback triangular core is an equilateral triangle, which has internal angles of sixty degrees. The attached angle plate has a ninety degree bend, therefore the hinge mounting brackets are at an angle of thirty degrees with the x-axis in Figure 2.12.5-5. The rotated x and y loads are in Table 2.12.5-16 as F_{xt} and F_{yt} . The hinge mounting brackets are supported by the strongback. The hinge mounting brackets are assumed to pivot about their back edge against the strongback angle plate creating tensile “prying” loads on the bolts. The bolts are also subjected to shear stresses in the two orthogonal directions perpendicular to the tensile load. The shear loads come directly from in-plane loads and a torsional moment created by the axial acceleration.

The parameters affecting the load calculations, as depicted on Figure 2.12.5-28 and Figure 2.12.5-29, are (inches):

w	$= 2.44$	width
l	$= 3.16$	length
b_e	$= 0.70$	bolt hole edge distance
b_s	$= 1.20$	bolt hole spread, square
p_e	$= 0.44$	pin edge distance
b_p	$= 0.82$	1st row bolt to pin spread
r	$= 0.85$	bolt pattern radius

The total tensile load per bolt from out-of-plane force component and “prying” about the back hinge mounting bracket edge is:

¹⁰ Shigley, J. E., Mischke, C. R., *Mechanical Engineering Design*, Fifth Edition, McGraw-Hill, 1989, New York, NY.

$$f_t = \frac{F_{\text{ryt}} \times (b_p + b_e + b_s)}{4 \times \left(b_e + \frac{b_s}{2}\right)}$$

The total shear, f_v , is F_{rxt} plus torsion about the y-axis from F_z , combined (SRSS) with for the worst bolt, which is one of the front bolts.

$$f_v = \sqrt{\left(\frac{F_{\text{rxt}}}{4} + \sin(45) \times F_z \times \frac{\left(b_p + \frac{b_s}{2}\right)}{(4 \times r)}\right)^2 + \left(\frac{F_z}{4} + \cos(45) \times F_z \times \frac{\left(b_p + \frac{b_s}{2}\right)}{(4 \times r)}\right)^2}$$

The results are presented in Table 2.12.5-16. In the referenced table, the tensile stress, sigma (σ), is simply f_t/A_t . The shear stress, tau (τ), is similarly f_v/A_s .

Minimum Edge Distance

The minimum edge distance calculated is for the single front bolt of the lock plate, which is the bolt nearest to the edge of the strongback angle plate. The load is conservatively assumed to be 'fv' from LC 1, Table 2.12.5-15. The load f_v includes the shear force in the direction of the plate edge combined with the shear force (that is not directed towards the plate edge) from the moment generated by the axial acceleration. See also, Figure 2.12.5-30.

$$\begin{aligned} \text{Projected bolt area on angle: } A_p &= (\text{bolt head mean diameter}^{11})(\text{angle plate thickness}) \\ &= 1/2(0.720 + 0.375)(0.25) = 0.55(0.25) = 0.14 \text{ in}^2 \end{aligned}$$

$$P = 3,343 \text{ lb}_f \quad (\text{from Table 2.12.5-15, LC1})$$

$$\text{Projected Area Stress: } f_p = P/A_p = 3,343/0.14 = 23,879 \text{ psi}$$

Check Angle Minimum Bolt Edge Distance:

$$L/d \geq [0.5 + 1.2(f_p/S_u)] \Rightarrow 0.73/0.55 \geq [0.5 + 1.2(23,879/71,000)] \Rightarrow 1.33 \geq 0.90$$

$$f_p/S_u \leq 2.1 \Rightarrow 23,879/71,000 \leq 2.1 \Rightarrow 0.34 \leq 2.1$$

Bolt Pull-Out:

The strongback angle plate is evaluated for pull-out of the countersunk socket heads. The shear area of the angle plate is assumed to be the cylindrical area under the countersunk head diameter. The maximum tensile bolt load is 'ft' from the top bracket, LC1 in Table 2.12.5-16.

$$\text{Net shear area: } A_s = \pi(t)(\text{head diameter}) = \pi(0.25)(0.720) = 0.57 \text{ in}^2$$

$$\text{Bounding reaction load: } P = 3,269 \text{ lb}_f \quad (\text{from Table 2.12.5-16, LC1})$$

$$\text{Shear Stress: } \tau = P/A_s = 3,269/0.57 = 5,735 \text{ psi}$$

$$\text{Allowable: } \tau_{\text{allow}} = 0.42S_u = 0.42(71,000) = 29,820 \text{ psi}$$

$$\text{Margin of Safety: } MS = (\tau_{\text{allow}}/\tau) - 1.0 = (29,820/5,735) - 1.0 = +4.20$$

¹¹ Industrial Fasteners Institute, *Manufacturers' Capability Guide*, 1986, Cleveland, Ohio

2.12.5.13.3 Net Section Bending Stress

The lock plate and hinge mounting brackets are subjected to bending stresses from the “prying” loads discussed in the fastener evaluation, Section 2.12.5.13.2, *Fastener Analysis*. The lock plate moment arm is assumed to be from the pin centerline to the edge of the strongback angle plate. The hinge mounting bracket moment arm is assumed to be from the pin centerline to the first row of bolts. The pin and hinge blocks are fabricated from Type XM-19 stainless steel. The allowable primary-plus-membrane stress (S_{m+b}) is $S_u = 99,400$ psi, based on the elastic analyses stress criteria in Table 2.12.5-3 and the material properties of Type XM-19 stainless steel at 200 °F. The analysis results and the resultant margin of safety (MS) are summarized below.

Lock Plate	
Net section, I_{net} (in ⁴)	$I_{net} = ((2 \times \text{lug width})(\text{lug height})^3)/12$ $= ((2 \times 0.59)(0.67)^3)/12 = 0.030$
Maximum load, P (lb _f)	$P = 8,893$ (LC2, Table 2.12.5-15)
Moment, M (in-lbs)	$M = P \times L = 8,893 \times 0.46 = 4,091$
Bending Stress, σ_b (psi)	$\sigma_b = \frac{Mc}{I_{net}} = \frac{4,091 \left(\frac{0.67}{2} \right)}{0.030} = 45,683$
Margin of Safety (MS)	$MS = \frac{S_{m+b}}{\sigma_b} - 1.0 = \frac{99,400}{45,683} - 1.0 = +1.18$
Hinge Mounting Bracket	
Net section, I_{net} (in ⁴)	$I_{net} = (\text{width} - 2(\text{hole OD}))[(\text{Height})^3/12]$ $= (2.44 - 2(0.41))[(0.69)^3/12] = 0.044$
Net Area, A_{net} (in ²)	$A_{net} = (\text{width} - 2(\text{Hole OD}))(\text{Height})$ $= (2.44 - 2(0.41))(0.69) = 1.12$
Maximum load (lb _f)	$P_y = 6,250$ (LC1, Table 2.12.5-16)
	$P_x = 3,816$ (LC1, Table 2.12.5-16)
Moment, M (in-lbs)	$M = P_y(L) = 6,250(0.82) = 5,125$
Bending Stress, σ_b (psi)	$\sigma_b = \frac{Mc}{I_{net}} = \frac{5,125(1/2(0.69))}{0.044} = 40,185$
Membrane Stress, σ_m (psi)	$\sigma_m = \frac{P_x}{A_{net}} = \frac{3,816}{1.12} = 3,407$
Membrane + Bending Stress, σ_{b+m} (psi)	$\sigma_{b+m} = \sigma_b + \sigma_m = 43,592$
Margin of Safety (MS)	$MS = \frac{S_{m+b}}{\sigma_{b+m}} - 1 = \frac{99,400}{43,592} - 1 = +1.28$

2.12.5.14 Strongback Global Stability

The strongback is constrained by the body such that, under axial loads, only very small lateral displacements are possible. Thus, it is not possible for the strongback to undergo a typical "lower order" elastic buckling mode failure. Stability is controlled by plastic stability of the structure. However, the following calculation is included to demonstrate the large margin against global elastic collapse.

The strongback longitudinal weldment ("core") is evaluated for axial stability under loads resulting from a postulated 120g end drop. The core is modeled as a bar with a uniformly distributed axial load with the base fixed and top end free, using closed form solutions from Article 2.12 of Timoshenko¹² (See Equation 'n' on p. 103):

$$(qL)_{CR} = \frac{7.837EI}{L^2}$$

L	Axial length of the core, use 160 inches																		
E	27.6×10^6 psi, Table TM-1 at 200 °F (Table 2.2-2).																		
A	<p>Cross sectional area of the three (3) plate angles which form the primary axial member in the Core.</p> <p>Calculated as 12.72 in^2 when neglecting the tube stiffeners on the free edges of the plate angles. See Figure 2.12.5-56.</p> <p>Considering the tube stiffeners, the area is:</p> $A_{\text{CORE}} = 12.72 \text{ in}^2 + (3 \text{ stiffeners})[(2.0 \text{ in})^2 - (1.5 \text{ in})^2]$ $= 12.72 \text{ in}^2 + 5.25 \text{ in}^2$ $= 17.97 \text{ in}^2$																		
I	274 in^4 , determined using ANSYS [®] for the three (3) plate angles that form the primary axial member in the core (see Figure 2.12.5-56)																		
q	<p>Unit weight/load of the strongback assembly and payload. From Table 2.1-3, Section 2.1.3, <i>Weights and Centers of Gravity</i>, the weights are (bold numbers):</p> <table> <tr> <th></th><th><u>Weight (pounds)</u></th></tr> <tr> <td>Top Endplate Assembly</td><td>190</td></tr> <tr> <td>Bottom Endplate Assembly</td><td>168</td></tr> <tr> <td>Fuel Control Structures</td><td>855</td></tr> <tr> <td>Total Strongback (w/o FCS, w/ endplates)</td><td>2,175</td></tr> <tr> <td>Total Strongback (w/ FCS, w/ endplates)</td><td>3,030</td></tr> <tr> <td><u>Payload</u></td><td>4,740</td></tr> <tr> <td>Strongback w/ FCS + Payload</td><td>7,770</td></tr> <tr> <td>Strongback w/o FCS + Payload:</td><td>6,915</td></tr> </table>		<u>Weight (pounds)</u>	Top Endplate Assembly	190	Bottom Endplate Assembly	168	Fuel Control Structures	855	Total Strongback (w/o FCS, w/ endplates)	2,175	Total Strongback (w/ FCS, w/ endplates)	3,030	<u>Payload</u>	4,740	Strongback w/ FCS + Payload	7,770	Strongback w/o FCS + Payload:	6,915
	<u>Weight (pounds)</u>																		
Top Endplate Assembly	190																		
Bottom Endplate Assembly	168																		
Fuel Control Structures	855																		
Total Strongback (w/o FCS, w/ endplates)	2,175																		
Total Strongback (w/ FCS, w/ endplates)	3,030																		
<u>Payload</u>	4,740																		
Strongback w/ FCS + Payload	7,770																		
Strongback w/o FCS + Payload:	6,915																		

¹² Timoshenko & Gere, *Theory of Elastic Stability*, Second Edition, McGraw-Hill Book Company, New York, 1961.

From the values above, addition of the FCSs increases the total load by $\approx 12\%$ or the structure load (less payload) by $\approx 40\%$. Using the length listed above, and conservatively including the fuel/payload weight, the (maximum) unit load is:

$$\begin{aligned}\frac{q}{L} &= \frac{7,770}{160} = 48.6 \text{ lb}_f @ (1 \text{ g}) \\ &= 5,828 \text{ lb}_f/\text{in} @ (120 \text{ g})\end{aligned}$$

Substituting into the stability equation:

$$(qL)_{CR} = \frac{7.837EI}{L^2} = \frac{7.837(27.6 \times 10^6)(274 \text{ in}^4)}{(160 \text{ in})^2} = 2.32 \times 10^6 \text{ lb}_f$$

And the critical distributed load is:

$$q_{CR} = \frac{2.32 \times 10^6}{L} = \frac{2.32 \times 10^6 \text{ lb}_f}{160 \text{ in}} = 14,470 \text{ lb}_f/\text{in}$$

Based on ASME B&PV Code, Appendix F, Subsection F-1331.5(a), the allowable load for free drop conditions is assumed to be 2/3 of the calculated critical value:

$$q'_{CR} = 2/3(14,470) = 9.65 \times 10^3 \text{ lb}_f/\text{in}$$

The margin of safety for the "applied load" to the postulated 120g axial free drop is:

$$MS = \frac{9.65 \times 10^3}{5.83 \times 10^3} - 1.0 = +0.66$$

Therefore, elastic stability criteria for the global structure are satisfied for the 120g end drop.

2.12.5.15 Strongback Local Stability

This section evaluates local stability of the "plate" section(s) extending from the central core using formulas for stability of plates from *Stress Analysis Manual*¹³:

$$\sigma_{CR} = \eta \bar{\eta} \frac{k\pi^2 E}{12(1-\nu^2)} \left(\frac{t}{b} \right)^2$$

where:

- Panel width is approximately 9 inches, use $b = 9$.
- Maximum panel height is the free span between clamp arm assemblies, considering the distance between the bolted connections and the "height" of the clamp arms, the free span is less than 18 inches for all locations except the bottom span which is less than 22 inches.
- η is a plasticity reduction factor. Because the applied stress is much less than the yield stress, η is assumed to be 1.0.

¹³ Air Force Flight Dynamics Laboratory, *Stress Analysis Manual*, Chapter 6 - Analysis of Plates, Wright Patterson AFB, Ohio, October 1986 (NTIS AD759199).

- $\bar{\eta}$ is a cladding reduction factor. The strongback is solid plate (no cladding), therefore $\bar{\eta}$ is 1.0.
- k is a function of aspect ratio (a/b), where a = length and b = width (see Figure 6-1 of Stress Analysis Manual provided as Figure 2.12.5-57 of this calculation).

Plates are stiffened by the clamp arms (and FCSs) which provide connections between the adjacent plates. In addition, the fuel is pressed against the plates by the clamp arms, which will restrict "out-of-plane" motion of the plates.

Span Length Reduced By FCS Stiffener

As described above, the bottom nominal span length between clamp arms is 22 inches. Since the FCS channel stiffener on the FCS provides significant restraint of the plate and thus the span length is reduced by a factor of 2. Therefore $a = 22/2 = 11$ and the constant, $k = 3.6$ (i.e., from curve D (dashed) at $a/b=1.2$, $k=3.6$ for 3 edges clamped and 1 edge free):

$$F_{CR} = \frac{3.6 \pi^2 (27,600 \text{ ksi})}{12(1-.3^2)} \left(\frac{0.25 \text{ in}}{9.0 \text{ in}} \right)^2 = 69.3 \text{ ksi}$$

This value is significantly above the minimum yield stress of the material.

"Free" Edge Pinned

The addition of the tube stiffener on the free edge of the strongback angles stiffens the plate angles. This added stiffness is evaluated by considering the "free" edge to be simply supported and ignoring the effect of the FCS channel stiffener. Therefore $a = 22$, $a/b = 2.4$, and the constant, $k = 5.6$ (i.e., from curve B at $a/b=2.2$, $k=5.6$, conservatively for simply supported on all edges):

$$F_{CR} = \frac{5.6 \pi^2 (27,600 \text{ ksi})}{12(1-.3^2)} \left(\frac{0.25 \text{ in}}{9.0 \text{ in}} \right)^2 \geq 100 \text{ ksi}$$

This value is significantly above the material yield stress.

Summary of Local Stability

Critical stresses are significantly greater than the yield stress. Therefore, elastic instability is not considered a viable failure mode.

Case	Critical Stress	Notes
$a = b = 9$: Considers restraint provided by the FCS stiffener assembly	69.3 ksi	Critical stress $\gg S_y$
$a = 22$, $b = 9$: Neglects restraint provided by the FCS stiffener/hinge assembly but considers free edge "simply supported" based on tube stiffener	> 100 ksi	Critical stress $\gg S_y$

2.12.5.16 Strongback Width-Thickness Ratio - Triangular Core

The sections comprising the triangular core are evaluated using the rules for flanges of box sections from ASME B&PV Code, Subsection NF-3322.2(d)(2)(b)(1):

$$\frac{238}{\sqrt{S_y}} = \frac{238}{\sqrt{25.0 \text{ ksi}}} = 47.6$$

Calculating the actual width/thickness ratio and comparing it to the allowable value:

$$\frac{b}{t} \approx \frac{8.3 \text{ in}}{0.25 \text{ in}} = 33.2 < 47.6$$

Therefore, the triangular core section is fully effective.

2.12.5.17 Strongback Width-Thickness Ratio - Plate Extensions

The plate sections extending from the triangular core are considered stiffened elements under compression (NF-3322.2(d)(2)), where the sections are stiffened on one side by the continuous connection to the triangular core and on the "free" edge by the 2 inches square tubes. The effective width is evaluated using NF-3322.2(d)(2)(b)(3):

$$\frac{253}{\sqrt{S_y}} = \frac{253}{\sqrt{25.0 \text{ ksi}}} = 50.6$$

The actual width/thickness ratio is:

$$\frac{b}{t} \approx \frac{9 \text{ in}}{0.25 \text{ in}} = 36 < 50.6$$

Therefore, when stiffened by the tube sections, the plate extensions of the strongback are fully effective in carrying compressive loads.

Although neglected here, the FCS stiffener assembly (stiffener, hinge, and latch) provide additional connections between the plates, reducing the unbraced span by a factor of ≈ 2 . This conservatism further ensures that the extensions are fully effective in transmitting axial (compressive) loads.

2.12.5.18 Strongback Axial Stress

Assuming that the FAs are supported by the endplate assembly and the end of the package, the strongback assembly supports only its own weight. The nominal axial stress, f_a , results from the weight of strongback assembly less the weight of the (impact end) endplate assembly, which will rest on the end of the package. Stresses are calculated with and without the FCS assemblies:

Excluding FCS assemblies:
$f_a = \frac{2175 - 168}{12.7} = 158 \text{ psi @ (1.0g)}$ $= 19.0 \text{ ksi @ (120g)}$

Including FCS and Tube Stiffeners
$f_a = \frac{3,030 - 168}{17.9} = 160 \text{ psi@}(1.0g)$ $= 19.2 \text{ ksi@}(120g)$

Comparing these impact stresses with the minimum yield stress of Type 304 stainless steel results in the following margins of safety:

Configuration	Calculated Stress (ksi)	Yield Stress (ksi)	M.S.
w/o FCSs	19.0	25.0	+0.32
w/ FCSs & tube stiffeners	19.2		+0.30

2.12.5.19 Evaluation of Strongback Response to FCS Loads

Under axial drop conditions, out-of-plane loads are imposed on the strongback core by the FCS. These loads are shown in Table 2.12.5-8 through Table 2.12.5-11, and are transmitted from the FCS by the hinges and the lock bar/pin block to their connecting points on the strongback longitudinal weldment.

A simple ANSYS® model using Shell43 elastic-plastic elements is used to estimate the impact of the pin block loads on the strongback longitudinal weldment.

FEA Model Geometry

The model includes the 1/4-inch thick plate angle and the 2-inch square × 1/4-inch thick tube stiffener at the "free" edge. The plate was modeled as 9 inches wide × 17 inches and 20.6 inches long (high). The tube area where the lock bar is attached is modeled as being identical (material and thickness) with the tube. This area is shown in Figure 2.12.5-32. The plate and stiffener tubes are modeled as Type 304 stainless steel.

Connections (contact element & couples)

Connections between the plate angle and stiffener tube are made as follows:

- The threaded fasteners used to connect the parts are modeled using a node coupled in the three translational directions. These are shown with green triangles in the geometry plots.
- Compressive connections between the parts are modeled by including Contac52 (point-to-point) contact elements between the plate and the tube (meshes are aligned such that the contact elements are oriented completely in the global 'X' direction). The contact elements are shown in Figure 2.12.5-33.

Boundary Conditions

As shown in Figure 2.12.5-31, the plate is assumed restrained (fixed in translation and rotation) at the upper and lower clamp arms and at the strongback "core". No boundary conditions are applied to the stiffener tube.

Applied Loads

As noted above, the area where the lock bar is attached is modeled with an increased thickness. The loads from Table 2.12.5-17 are distributed equally to all nodes within the lock bar (thicker) area (i.e., Force per node = Total Load/Number of Nodes). This simplification eliminates moments which might result from loads with opposite sign at the two ends of the pin (e.g., for case 1, the Fz load changes sign). However, the resulting stresses are expected to be small.

Stress Results

Stress results are summarized in Table 2.12.5-18. The table contains maximum stress intensities at the mid-thickness and top surface of the shell elements for the 1/4-inch thick plate angle and the 1/4-inch thick stiffener tube. Stresses are listed for the complete part and for the part with elements connected to the coupled nodes removed. Stress results are also shown in the following figures:

Load Case	Mid-thickness Stress Intensities	Top Surface Stress Intensities	Bottom Surface Stress Intensities
1	Figure 2.12.5-36	Figure 2.12.5-37	Figure 2.12.5-38
2	Figure 2.12.5-39	Figure 2.12.5-40	Figure 2.12.5-41
3	Figure 2.12.5-42	Figure 2.12.5-43	Figure 2.12.5-44
4	Figure 2.12.5-45	Figure 2.12.5-46	Figure 2.12.5-47

Strain Results

Stress results are described above. The tangent modulus used in the stress analyses is relatively small. Therefore, stresses will increase slowly after reaching the yield point, but strains may become large prior to stresses reaching their allowable values.

To ensure that results are reasonable, plastic strains are reviewed for the three axial drop load cases. The maximum strains occur as a result of the Load Step 3, and are 1.7% and 1.8% at the middle and outer fiber, respectively. Considering the magnitude and type of loading, these values are reasonable and will not result in loss of function. Therefore, the strongback and stiffener tube are acceptable. Note also that increases in yield under dynamic loading will decrease the plastic strains.

Fastener Loads

Load on the coupled nodes used to represent the fasteners are extracted from the ANSYS® analysis and are listed in Table 2.12.5-17. All fasteners are assumed to have a nominal size of 3/8 inch and the shear plane(s) are assumed to pass through the threaded part of the fasteners such that root areas are used for calculating shear stress.

Bearing

For each load condition, the bearing stress imposed by the fasteners on the connected members is calculated using the maximum shear load.

Load Condition 20.6-inch span	Max Shear (lb _f)	Bearing			Bearing Stress (ksi)
		Diameter (in)	Thickness (in)	Area (in ²)	
Condition 1 (Table 2.12.5-8)	2,267	0.375	0.25	0.0938	24.2
Condition 2 (Table 2.12.5-9)	3,513	0.375	0.25	0.0938	37.5
Condition 3 (Table 2.12.5-10)	2,760	0.375	0.25	0.0938	29.4
Condition 4 (Table 2.12.5-11)	3,634	0.375	0.25	0.0938	38.8
17.0-inch Span					
Condition 4 (Table 2.12.5-11)	4,095	0.375	0.25	0.0938	43.7

The ASME B&PV Code Level A allowable stress for bearing per NF-3322.1(f)(3), Equation (24b) or NF-3324.6(a)(5) is:

$$F_p = 1.5S_u = 1.5(71.0 \text{ ksi}) = 106.5 \text{ ksi}$$

Since all of the HAC bearing stresses are less than the NCT allowable stress, bearing is acceptable.

Edge Distance Check

Spacing along the row of fasteners is 1.5 inches. Minimum edge distance is approximately 1 inch (at the end of the tube stiffener). This distance exceeds the required edge distance per Table NF-3324.6(b)(1)-1 for 1/2-inch bolts (3/4-inch for cut edges). Therefore, edge distance is acceptable.

2.12.5.20 Strongback Stress Calculations – Horizontal Loads

Under horizontal (side) drop conditions, loads imposed on the strongback angle by the lock plate are provided by Table 2.12.5-11. The lock plate loads are summarized in Table 2.12.5-17 of this calculation.

Stress plots for the long FCS are included as Figure 2.12.5-45 through Figure 2.12.5-47 and for the standard FCS as Figure 2.12.5-48 and Figure 2.12.5-50 (for mid-thickness and surface stresses, respectively).

Component Stresses & Strains - Side Drop Loading

Side drop evaluations are provided for both long FCS and standard FCS spans. Stress results are summarized in Table 2.12.5-22 (long FCS) and Table 2.12.5-23 (standard FCS). The table contains maximum stress intensities at the mid-thickness and surface of the shell elements for the 1/4-inch thick plate angle and the 1/4-inch thick stiffener tube. Stresses are listed for the complete part, and for the part with elements connected to the coupled nodes removed. As shown by Table 2.12.5-23, all stresses in the 17.0-inch section are within the allowable values.

As shown by Table 2.12.5-22, all stresses in the long FCS are within the allowable values.

As noted previously, the tangent modulus used in this analysis is relatively small so strains may increase rapidly while stresses remain below the allowable values. Therefore, plastic strains are reviewed as listed in Table 2.12.5-26. The maximum calculated plastic strain intensity is approximately 14%. This value is much less than the ductility of Type 304 stainless steel. For example, the minimum specified elongation of annealed ASTM A-479/SA-479 Type 304 is 30%,

cold working which could decrease the available elongation will also provide significant increases in yield strength.

Based on the magnitude of the strains, additional side drop stress analyses are performed using a tangent modulus of .05E. This value is considered an upper bound for strains of the magnitude of those listed in Table 2.12.5-26. Using a large E_{tan} will result in larger calculated stresses. Stresses for these analyses are listed in Table 2.12.5-27 and Table 2.12.5-28.

As shown by Table 2.12.5-28, all stresses in the 17.0-inch span are within the allowable values.

As shown by Table 2.12.5-27, with the exception of 2 nodes in the stiffener tube, all stresses in the 20.6-span are within the allowable stress limits. Excluding the stresses at these nodes is acceptable as described below:

- The tubes perform their function (stiffening the free edge of the plate angle) by acting as beams. As such, the critical loading is beam bending. As shown by Figure 2.12.5-54 and Table 2.12.5-27, when the two nodes are removed, stresses in the beam are within the allowable stress limits.
- The large stresses at the single nodes are a result of concentrated loads being transmitted through the contact elements. Redistribution of these loads resulting from local yielding will not result in loss of support to the strongback plate.
- Since the tubes perform their stiffening function and will not fail from the isolated high stresses, the tubes are acceptable.

Therefore, the strongback is acceptable for side drop loads imposed by the Lock Plate.

Fastener Loads - Side Drop Loading

Fasteners are evaluated using the same methods as described in Section 2.12.5.13.2, *Fastener Analysis* (see Table 2.12.5-24 (long FCS) and Table 2.12.5-25 (standard FCS)). As shown, all stress ratios are less than 1. Therefore, the 3/8-inch fasteners (threads excluded from the shear plane) are acceptable.

Bearing and edge distance is included in the evaluation in Section 2.12.5.13.2, *Fastener Analysis*.

Table 2.12.5-1 – Fuel Assembly Physical Characteristics

Parameter	Mark-BW
Rod Array	17 × 17
Rods per Assembly	264
Guide Thimbles per Assembly	24
Instrument Sheaths per Assembly	1
Rod Pitch, inches	0.496
Rod Length, inches	152.4
Rod OD, inches	0.374
Fuel Rod Weight, pounds (each)	5.33
Cladding thickness, inches	0.0225
Cladding Yield Strength at 200 °F, psi	31,222
Cladding Modulus of Elasticity at 200 °F, psi	12.8(10 ⁶)

Table 2.12.5-2 – FCS Evaluation Material Properties Summary

Material Specification	Temperature, °F	Yield Strength (S_y), psi	Ultimate Strength (S_u), psi	Design Stress Intensity (S_m), psi	Elastic Modulus, ×10⁶ psi
XM-19 Stainless Steel	200	47,100	99,400	33,100	27.6
Type 304 Stainless Steel	200	25,000	71,000	20,000	27.6
A574 Grade 4037 or 4042	200	131,600	180,000	35,000	28.5
A564 Grade 630, H1100	200	106,300	140,000	28,000	28.5

Table 2.12.5-3 – Criticality Control Structure Allowable Stress Limits

Stress Category	HAC	
	Elastic Analyses	Plastic Analyses ^①
General Primary Membrane Stress Intensity	Lesser of: $2.4S_m$ $0.7S_u$	Greater of: $0.7S_u$ $S_y + 1/3(S_u - S_y)$
Local Primary Membrane Stress Intensity	Lesser of: $3.6S_m$ S_u	$0.9S_u$
Primary Membrane + Bending Stress Intensity	Lesser of: $3.6S_m$ S_u	$0.9S_u$
Range of Primary + Secondary Stress Intensity	Not Applicable	Not Applicable
Pure Shear Stress	$0.42S_u$	$0.42S_u$
Bearing Stress	$2.1S_u$	
Fatigue	Not Applicable	Not Applicable
Fastener HAC Allowable Stress Limits^{②③}		
Stress Category	Elastic Analyses ^④	Plastic Analyses ^①
Bolt Average Tensile Stress	Lesser of: $0.9S_y$ $2/3S_u$	Lesser of: S_y $0.7S_u$
Bolt Average Shear Stress	$0.6S_y$	Lesser of: $0.6S_y$ $0.42S_u$
Bolt Tension + Shear	$f_t^2/F_{tb}^2 + f_v^2/F_{vb}^2 \leq 1$	$f_t^2/F_{tb}^2 + f_v^2/F_{vb}^2 \leq 1$
Minimum Edge Distance	n/a	$L/d \geq [0.5 + 1.2(f_p/S_u)]$ $f_p/S_u \leq 2.1$

Notes:

- ① Plastic Analysis: ASME B&PV Code, Section III, Appendix F, F-1341.2.
- ② Bolt Joints: ASME B&PV Code, Section III, Appendix F, F-1335.
- ③ Bearing for Pinned Joints: ASME B&PV Code, Section III, Appendix F, F-1336.
- ④ Elastic Analysis for Pinned Joints: ASME B&PV Code, Section III, Appendix F, F-1331

Table 2.12.5-4 – FCS Force Calculations

Row No. (i) ^①	Rod Quan. (n) ^②	x_i (inches) ^③	M_i (in-lb _f) ^④	F_i per rod (lb _f) ^⑤	F, Row (lb _f) ^⑥	Cumulative Rows (lb _f)
1	17	0.250	23.2	45	773	773
2	17	0.372	37.3	68	1,151	1,924
3	14	0.494	51.4	90	1,258	3,182
4	15	0.616	65.5	112	1,681	4,863
5	17	0.738	79.7	134	2,283	7,146
6	12	0.860	86.9	161	1,937	9,083
7	17	0.982	86.9	189	3,215	12,298
8	17	1.104	86.9	217	3,686	15,985
9	12	1.226	86.9	122	1,467	17,452

Notes:

- ① Row 1 is on the outside of the assembly adjacent to the FCS; row 9 is the center row.
- ② See Figure 2.12.5-1.
- ③ Rod lateral deflection, $x_i = C + (i - 1)G_r$ where $C = 0.25$ inches and $G_r = 0.122$ inches.
- ④ Rod bending moment, $M_i = 115.8x_i$, up to a maximum of 86.9 in-lb_f.
- ⑤ Lateral force of a single rod, $F_i = 8(Px_i - M_i)/L$. In row 9, the force is half this value.
- ⑥ Equal to F_i times rod quantity n .

Table 2.12.5-5 – Low and High Tangent Modulus Results Comparison

Run	Component	Low Tangent Modulus ^①		High Tangent Modulus ^②	
		Max Stress, psi	Max Disp, in	Max Stress, psi	Max Disp, in
Load Case 1	Pin Block	54,162	0.0219	58,071	0.0211
	Hinge Block	54,590	0.0075	52,564	0.0072
	Stiffener	56,152	0.0264	54,404	0.0257
	Angle	36,598	0.0258	42,366	0.0251
Load Case 2	Pin Block	53,451	0.0098	52,970	0.0095
	Hinge Block	57,634	0.0187	66,770	0.0179
	Stiffener	55,168	0.0233	60,547	0.0225
	Angle	34,618	0.0246	37,847	0.0238
Load Case 3	Pin Block	47,153	0.0060	46,589	0.0060
	Hinge Block	52,521	0.0055	53,630	0.0054
	Stiffener	48,220	0.0077	48,480	0.0076
	Angle	29,814	0.0084	29,820	0.0084

Notes:

- ① Tangent modulus is calculated in Section 2.12.5.4 (291,933 psi for XM-19 and 219,970 psi for Type 304).
- ② Tangent modulus is assumed to be 5% of the Modulus of Elasticity at 200 °F (1,380,000 psi for both materials).

Table 2.12.5-6 – FCS General Primary Membrane Stress Intensity (P_m)

Run	Component	Material	Allowable Stress (psi)	Path	P_m (psi)	Margin of Safety
Load Case 1 (LC1)	Pin Block	XM-19	69,580	2	30,160	+1.31
	Hinge Block	XM-19	69,580	3B	26,340	+1.64
	Stiffener	XM-19	69,580	C2	39,350	+0.77
	Angle	304	49,700	14	9,847	+4.05
Load Case 2 (LC2)	Pin Block	XM-19	69,580	1	20,390	+2.41
	Hinge Block	XM-19	69,580	5	25,610	+1.72
	Stiffener	XM-19	69,580	13	27,390	+1.54
	Angle	304	49,700	15	9,274	+4.36
Load Case 3 (LC3)	Pin Block	XM-19	69,580	1	13,400	+4.19
	Hinge Block	XM-19	69,580	3B	18,030	+2.86
	Stiffener	XM-19	69,580	C1	15,570	+3.47
	Angle	304	49,700	14	8,053	+5.17

Table 2.12.5-7 – FCS Local Primary Membrane Stress Intensity

Run	Component	Material	Allowable Stress (psi)	Figure	P _{max} (psi)	Margin of Safety
Load Case 1 (LC1)	Pin Block	XM-19	89,460	2.12.5-11	54,162	+0.66
	Hinge Block	XM-19	89,460	2.12.5-12	54,590	+0.64
	Stiffener	XM-19	89,460	2.12.5-13	56,152	+0.59
	Angle	304	63,900	2.12.5-14	36,598	+0.75
Load Case 2 (LC2)	Pin Block	XM-19	89,460	2.12.5-16	53,451	+0.67
	Hinge Block	XM-19	89,460	2.12.5-17	57,634	+0.55
	Stiffener	XM-19	89,460	2.12.5-18	55,168	+0.62
	Angle	304	63,900	2.12.5-19	34,616	+0.85
Load Case 3 (LC3)	Pin Block	XM-19	89,460	2.12.5-21	47,153	+0.90
	Hinge Block	XM-19	89,460	2.12.5-22	52,521	+0.70
	Stiffener	XM-19	89,460	2.12.5-23	48,220	+0.86
	Angle	304	63,900	2.12.5-24	29,814	+1.14

Table 2.12.5-8 – Reactions for Load Condition 1 (lb_f)

Load Condition 1, Pressure Applied to Pin Block Side					
Component	NODE	F _x	F _y	SRSS (F _x &F _y)	F _z (Axial)
Pin Block	50000	1,522	4,367	4,625	0
	50006	-1,028	4,026	4,155	1,126
Pin Block Total				8,780	1,126
Hinge Block Top	50003	-201	4,372	4,377	741
Hinge Block Center	50004	-22	2,948	2,948	0
	50008	-261	1,868	1,886	1,974
Hinge Block Center Total				4,834	1,974
Hinge Block Bottom	50007	-54	155	164	0
Top Hinge Mounting Bracket	50003	-201	4,372	4,377	741
	50004	-22	2,948	2,948	0
Top Hinge Mounting Bracket Total				7,325	741
Bottom Hinge Mounting Bracket	50008	-261	1,868	1,886	1,974
	50007	-54	155	164	0
Bottom Hinge Mounting Bracket Total				2,050	1,974
Lock Plate (reciprocal to Pin Block Total)				8,780	1,126
Total Reactions (Sum of Nodes 50000 thru 50008)		0	17,736	17,736	3,840

Table 2.12.5-9 – Reactions for Load Condition 2 (lb_f)

Load Condition 1, Pressure Applied to Pin Block Side					
Component	NODE	F_x	F_y	SRSS (F_x&F_y)	F_z (Axial)
Pin Block	50000	5,076	165	5,078	
	50006	3,818	-138	3,820	1,022
Pin Block Total				8,898	1,022
Hinge Block Top	50003	733	1,308	1,500	1,616
Hinge Block Center	50004	3,615	1,250	3,825	
	50008	3,685	769	3,765	1,203
Hinge Block Center Total				7,590	1,203
Hinge Block Bottom	50007	809	-3,355	3,451	
Top Hinge Mounting Bracket	50003	733	1,308	1,500	1,616
	50004	3,615	1,250	3,825	
Top Hinge Mounting Bracket Total				5,325	1,616
Bottom Hinge Mounting Bracket	50008	3,685	769	3,765	1,203
	50007	809	-3,355	3,451	
Bottom Hinge Mounting Bracket Total				7,216	1,203
Lock Plate (Same as Pin Block Total)				8,898	1,022
Total Reactions (Sum of Nodes 50000 thru 50008)		17,736	0	17,736	3,840

Table 2.12.5-10 – Reactions for Load Condition 3 (lb_f)

Load Condition 1, Pressure Applied to Pin Block Side					
Component	NODE	F_x	F_y	SRSS (F_x&F_y)	F_z (Axial)
Pin Block	50000	3,554	2,272	4,219	
	50006	1,143	1,935	2,247	1,113
Pin Block Total				6,466	1,113
Hinge Block Top	50003	210	2,566	2,575	1,099
Hinge Block Center	50004	1,865	2,328	2,983	
	50008	1,780	1,516	2,338	1,629
Hinge Block Center Total				5,321	1,629
Hinge Block Bottom	50007	317	-1,750	1,779	
Top Hinge Mounting Bracket	50003	210	2,566	2,575	1,099
	50004	1,865	2,328	2,983	
Top Hinge Mounting Bracket Total				5,558	1,099
Bottom Hinge Mounting Bracket	50008	1,780	1,516	2,338	1,629
	50007	317	-1,750	1,779	
Bottom Hinge Mounting Bracket Total				4,117	1,629
Lock Plate (Same as Pin Block Total)				6,466	1,113
Total Reactions (Sum of Nodes 50000 thru 50008)		8,868	8,868	12,541	3,840

Table 2.12.5-11 – Reactions for Load Condition 4 (lb_f)

Load Condition 1, Pressure Applied to Pin Block Side					
Component	NODE	F_x	F_y	SRSS (F_x&F_y)	F_z (Axial)
Pin Block	50000	6,729	16	6,729	441
	50006	6,728	15	6,728	-441
Pin Block Total				13,457	0
Hinge Block Top	50003	1,488	-921	1,750	912
Hinge Block Center	50004	4,025	905	4,126	-262
	50008	4,024	907	4,125	262
Hinge Block Center Total				8,251	0
Hinge Block Bottom	50007	1,488	-922	1,751	-912
Top Hinge Mounting Bracket	50003	1,488	-921	1,750	912
	50004	4,025	905	4,126	-262
Top Hinge Mounting Bracket Total				5,876	650
Bottom Hinge Mounting Bracket	50008	4,024	907	4,125	262
	50007	1,488	-922	1,751	-912
Bottom Hinge Mounting Bracket Total				5,876	-650
Lock Plate (Same as Pin Block Total)				13,457	0
Total Reactions (Sum of Nodes 50000 thru 50008)		24,482	0	24,482	0

Table 2.12.5-12 – Bolt Loads for Load Condition 1 (lb_f)

Bolt Loads Pressure Applied to Pin Block Side							
Hinge Block	(x-axis is tensile load for bolt)						SRSS (Y & Z)
NODE	F _X	F _Y	F _Z	M _X (in-lb _f)	M _Y (in-lb _f)	M _Z (in-lb _f)	
744**	-217	1,161	122	0	0	0	1,167
6280‡	-152	794	278	0	0	0	841
8234‡	-203	1,080	68	0	0	0	1,182
8713	-55	913	549	0	0	0	1,065
8855	-76	1,054	412	0	0	0	1,132
17523‡	-85	391	49	0	0	0	394
19477‡	-13	25	-18	0	0	0	31
19956	-62	492	244	0	0	0	549
20098	-7	24	166	0	0	0	167
max	-217						1,167
Pin Block	(y-axis is tensile load for bolt)						SRSS (Y & Z)
NODE	F _X	F _Y	F _Z	M _X (in-lb _f)	M _Y (in-lb _f)	M _Z (in-lb _f)	
2605*	-1,653	77	43	0	0	0	1,654
5625‡	-1,306	-48	290	0	0	0	1,338
5698	-1,244	-226	199	0	0	0	1,260
16868‡	-1,379	-92	60	0	0	0	1,380
16941	-1,245	-240	95	0	0	0	1,249
max		-240					1,654
Stiffeners							SRSS (Y & Z)
pin block side	(y-axis is tensile load for bolt)						
3495*	1,653	-75	-43	0	0	0	1,654
3498	978	49	84	0	0	0	981
3870	2,202	236	-103	0	0	0	2,204
5303	1,940	96	-23	0	0	0	1,940
max		236					2,204
hinge block side	(x-axis is tensile load for bolt)						SRSS (Y & Z)
2509	-130	-1,801	-134	0	0	0	1,809
5883	-118	-580	211	0	0	0	617
5927**	217	-1,161	-122	0	0	0	1,167
6121	-213	-1,293	36	0	0	0	1,293
max	-213						1,809

Notes:

Starred nodes belong to same couple set between stiffener and hinge or pin block.

‡ nodes closest to angle sheet edge

Table 2.12.5-13 – Bolt Loads for Load Condition 2 (lb_f)

Bolt Loads Pressure Applied to Pin Block Side							
Hinge Block	(x-axis is tensile load for bolt)						SRSS (Y & Z)
NODE	F_X	F_Y	F_Z	M_X (in-lb_f)	M_Y (in-lb_f)	M_Z (in-lb_f)	
744**	56	-1,486	112	0	0	0	1,490
6280‡	-5	-715	-316	0	0	0	782
8234‡	-23	-56	-190	0	0	0	198
8713	-188	-674	241	0	0	0	716
8855	-106	87	101	0	0	0	133
17523‡	-7	-1,149	587	0	0	0	1,290
19477‡	-100	-1,187	318	0	0	0	1,229
19956	-228	-1,164	555	0	0	0	1,290
20098	-184	-991	498	0	0	0	1,108
max	-228						1,490
Pin Block	(y-axis is tensile load for bolt)						SRSS (X & Z)
NODE	F_X	F_Y	F_Z	M_X (in-lb_f)	M_Y (in-lb_f)	M_Z (in-lb_f)	
2605*	1,321	-205	72	0	0	0	1,323
5625‡	961	-197	58	0	0	0	962
5698	1,014	-101	4	0	0	0	1,014
16868‡	1,089	-206	326	0	0	0	1,137
16941	1,167	-128	191	0	0	0	1,183
max		-206					1,323
Stiffeners							
pin block side	(y-axis is tensile load for bolt)						SRSS (X & Z)
3495*	-1,321	205	-72	0	0	0	1,323
3498	-531	-86	91	0	0	0	538
3870	-1,762	-147	-25	0	0	0	1,762
5303	-1,285	-181	-67	0	0	0	1,287
max		-181					1,762
hinge block side	(x-axis is tensile load for bolt)						SRSS (Y & Z)
2509	238	2,059	-96	0	0	0	2,061
5883	84	842	207	0	0	0	867
5927**	-54	1,486	-112	0	0	0	1,490
6121	6	1,809	-22	0	0	0	1,809
max	238						2,061

Notes:

Starred nodes belong to same couple set between stiffener and hinge or pin block.

‡ nodes closest to angle sheet edge

Table 2.12.5-14 – Bolt Loads for Load Condition 3 (lb_f)

Bolt Loads Pressure Applied to Pin Block Side							
Hinge Block	(x-axis is tensile load for bolt)						SRSS (Y & Z)
NODE	F _X	F _Y	F _Z	M _X (in-lb _f)	M _Y (in-lb _f)	M _Z (in-lb _f)	
744**	40	-280	155	0	0	0	320
6280‡	-5	-13	-2	0	0	0	13
8234‡	-82	487	-34	0	0	0	489
8713	-43	58	366	0	0	0	371
8855	-30	503	257	0	0	0	565
17523‡	-1	-405	305	0	0	0	507
19477‡	-59	-619	121	0	0	0	630
19956	-91	-393	393	0	0	0	555
20098	-93	-498	326	0	0	0	595
Max	-93						630
Pin Block	(y-axis is tensile load for bolt)						SRSS (X & Z)
NODE	F _X	F _Y	F _Z	M _X (in-lb _f)	M _Y (in-lb _f)	M _Z (in-lb _f)	
2605*	-291	67	84	0	0	0	303
5625‡	-235	-8	166	0	0	0	288
5698	-237	-46	97	0	0	0	256
16868‡	-289	-18	177	0	0	0	339
16941	-236	-54	167	0	0	0	289
max		67					339
Stiffeners							
pin block side	(y-axis is tensile load for bolt)						SRSS (X & Z)
3495*	291	-67	-84	0	0	0	303
3498	-39	106	115	0	0	0	121
3870	1,157	65	-126	0	0	0	1,164
5303	500	44	-16	0	0	0	500
max		106					1,164
hinge block side	(x-axis is tensile load for bolt)						SRSS (Y & Z)
2509	60	960	-129	0	0	0	968
5883	37	-1	229	0	0	0	229
5927**	-40	280	-155	0	0	0	320
6121	61	550	47	0	0	0	552
max	61						968

Notes:

Starred nodes belong to same couple set between stiffener and hinge or pin block.

‡ nodes closest to angle sheet edge

Table 2.12.5-15 – Lock Plate Bolt Force Summary (lb_f)

Item	LC1	LC2	LC3	LC4
F _x	-494	-8,893	-4,697	-13,457
F _y	-8,393	-35	-4,207	-30
F _z	-1,126	-1,022	-1,113	0
F _{xg}	199	3,578	1,890	5,414
F _{xb}	66	1,193	630	1,805
F _{yb}	2,798	9	1,402	10
F _{zb}	375	341	371	0
F'	1,455	1,321	1,439	0
f _t	66	1,193	630	1,805
f _v	3,343	1,661	2,290	10
σ (psi)	850	15,291	8,076	23,138
τ (psi)	49,167	24,431	33,676	149
MS, σ	+147.29	+7.24	+14.60	+4.45
MS, τ	+0.54	+2.09	+1.24	+505
Interaction Check	0.42 < 1.0	0.12 < 1.0	0.20 < 1.0	0.03 < 1.0

Table 2.12.5-16 – Hinge Mounting Bracket Bolt Summary

Top Bracket									
Item	F _{rx} (lb _f)	F _{ry} (lb _f)	f _t (lb _f)	f _v (lb _f)	Σ (psi)	MS (on σ)	τ (psi)	MS (on τ)	Interac. Ratio
LC1	3,816	-6,250	-3,269	1,241	41,914	+2.01	18,247	+3.14	0.17
LC2	-2,487	-4,389	-2,296	-1,410	29,436	+3.28	20,732	+2.65	0.13
LC3	650	-5,276	-2,760	773	35,383	+2.56	11,365	+5.65	0.10
LC4	-4,783	-2,743	-1,435	1,433	18,392	+5.85	21,069	+2.59	0.10
Bottom Bracket									
Item	F _{rx} (lb _f)	F _{ry} (lb _f)	f _t (lb _f)	f _v (lb _f)	σ (psi)	MS (on σ)	τ (psi)	MS (on τ)	Interac. Ratio
LC1	1,284	-1,594	-834	1,407	10,690	+10.79	20,690	+2.65	0.08
LC2	-5,185	-8	-4	1,778	55	+2,292	26,141	+1.89	0.12
LC3	-1,932	-846	-442	1,312	5,671	+21.22	19,291	+2.92	0.07
LC4	-4,781	-2,744	-1,435	1,432	18,399	+5.85	21,062	+2.59	0.10

Table 2.12.5-17 – Loads on the Strongback from the Fuel Control Structures (lb_f)

Node	Out-Of-Plane F_x	In-Plane F_y	In-Plane/Axial F_z
Load Condition 1 From Table 2.12.5-8			
50000	1,522	4,367	--
50006	-1,028	4,026	1,126
Total	494	8,393	1,126
Applied	-500	-8,400	-1,150
Load Condition 2 From Table 2.12.5-9			
50000	5,076	165	--
50006	3,818	-138	1,022
Total	8,893	27	1,022
Applied	-8,900	-50	-1,050
Load Condition 3 From Table 2.12.5-10			
50000	3,554	2,272	--
50006	1,143	1,935	1,113
Total	4,697	4,207	1,113
Applied	-4,700	-4,250	-1,150
Load Condition 4 - Horizontal From Table 2.12.5-11			
50000	6,729	16	441
50006	6,728	15	-441
Total	13,457	31	0
Applied	-13,500	-50	50

Table 2.12.5-18 – Summary of Strongback Stress Results LC1-LC3

Load Case 1	Calculated Stress (ksi)		Margin of Safety ^①	
	P _m	P _m +P _b	P _m	P _m +P _b
Strongback Angle	19.0	19.1	+1.62	+2.35
Strongback Angle w/o ^② Bolt Nodes	13.4	13.5	+2.71	+3.73
Stiffener Tube	18.0	18.0	+1.76	+2.55
Stiffener Tube w/o Bolt Nodes	10.6	10.7	+3.69	+4.97
Load Case 2				
Strongback Angle	20.2	29.1	+1.46	+1.20
Strongback Angle w/o Bolt Nodes	20.6	29.1	+1.41	+1.20
Stiffener Tube	27.9	30.6	+0.78	+1.09
Stiffener Tube w/o Bolt Nodes	28.2	30.3	+0.76	+1.11
Load Case 3				
Strongback Angle	19.3	25.0	+1.58	+1.56
Strongback Angle w/o Bolt Nodes	17.4	25.0	+1.86	+1.56
Stiffener Tube	21.3	23.7	+1.33	+1.70
Stiffener Tube w/o Bolt Nodes	21.3	23.7	+1.33	+1.70

Notes:

- ① Allowable stresses are 49.7 ksi and 63.9 ksi for P_m and P_m + P_b, respectively
- ② "w/o" indicates that the coupled nodes (used at fastener locations) and connected elements are excluded from the listed results.

Table 2.12.5-19 – Fastener Evaluation for Lock Bar/Pin Block Loads

Load Case 1										
NODE	F _x	F _y	F _z	Axial, lb _f (F _y)	Shear, lb _f	f _t (ksi)	f _v (ksi)	f _t / F _{tb}	f _v / F _{vb}	Interaction
4573	10	136	250	10	284	0.13	2.58	0.00	0.03	0.00
4580	9	-32	132	9	136	0.11	1.23	0.00	0.02	0.00
4586	12	-87	66	12	109	0.16	0.99	0.00	0.01	0.00
4593	19	-222	2	19	222	0.24	2.02	0.00	0.03	0.00
4600	27	-756	-90	27	762	0.34	6.92	0.00	0.09	0.01
4798	23	-2,256	-140	23	2,260	0.29	20.55	0.00	0.27	0.07
4429	42	-1,723	-155	42	1,730	0.54	15.73	0.00	0.21	0.04
4804	23	-2,260	-179	23	2,267	0.30	20.61	0.00	0.27	0.07
4630	26	-749	-58	26	751	0.34	6.82	0.00	0.09	0.01
4637	19	-220	-102	19	243	0.24	2.21	0.00	0.03	0.00
4644	12	-86	-156	12	178	0.15	1.62	0.00	0.02	0.00
4650	8	-30	-242	8	244	0.11	2.22	0.00	0.03	0.00
4657	10	139	-443	10	464	0.13	4.22	0.00	0.06	0.00
Max:				42	2,267	Max:				0.07

Notes:

- ① Stresses based on fastener areas of 0.078 in² and 0.110 in² for tension and shear, respectively.
- ② Allowable stresses are 126.0 ksi and 75.6 ksi for tension and shear, respectively.
- ③ Shear load is: $(F_x^2 + F_z^2)^{1/2}$

Table 2.12.5-20 – Fastener Evaluation for Lock Bar/Pin Block Loads (lb_f)

Load Case 2										
NODE	F _x	F _y	F _z	Axial, lb _f (F _y)	Shear, lb _f	f _t (ksi)	f _v (ksi)	f _t / F _{tb}	f _v / F _{vb}	Interaction
4573	206	68	3,444	206	3,445	2.64	31.32	0.02	0.41	0.17
4580	194	-100	3,371	194	3,372	2.48	30.66	0.02	0.41	0.16
4586	151	-71	3,305	151	3,306	1.94	30.05	0.02	0.40	0.16
4593	274	49	3,259	274	3,259	3.51	29.63	0.03	0.39	0.15
4600	699	169	3,114	699	3,119	8.96	28.35	0.07	0.38	0.15
4798	94	-133	900	94	909	1.21	8.27	0.01	0.11	0.01
4429	692	-58	-112	692	126	8.87	1.15	0.07	0.02	0.01
4804	57	-116	-1,351	57	1,356	0.73	12.33	0.01	0.16	0.03
4630	686	177	-3,214	686	3,219	8.79	29.26	0.07	0.39	0.15
4637	280	57	-3,356	280	3,356	3.59	30.51	0.03	0.40	0.16
4644	155	-63	-3,404	155	3,405	1.98	30.95	0.02	0.41	0.17
4650	193	-91	-3,461	193	3,462	2.47	31.47	0.02	0.42	0.17
4657	202	64	-3,512	202	3,513	2.59	31.93	0.02	0.42	0.18
Max:				699	3,513	Max:				0.18

Notes:

- ① Stresses based on fastener areas of 0.078 in² and 0.110 in² for tension and shear, respectively.
- ② Allowable stresses are 126.0 ksi and 75.6 ksi for tension and shear, respectively.
- ③ Shear load is: $(F_x^2 + F_z^2)^{1/2}$

Table 2.12.5-21 – Fastener Evaluation for Lock Bar/Pin Block Loads

Load Case 3										
NODE	F_x	F_y	F_z	Axial, lb_f (F_y)	Shear, lb_f	f_t (ksi)	f_v (ksi)	f_t / F_{tb}	f_v / F_{vb}	Interaction
4573	110	117	2,621	110	2,624	1.42	23.85	0.01	0.32	0.10
4580	61	-64	1,843	61	1,844	0.78	16.76	0.01	0.22	0.05
4586	38	-75	1,487	38	1,489	0.48	13.54	0.00	0.18	0.03
4593	58	-112	1,277	58	1,282	0.75	11.65	0.01	0.15	0.02
4600	142	-357	1,047	142	1,106	1.82	10.05	0.01	0.13	0.02
4798	105	-1,143	228	105	1,165	1.35	10.60	0.01	0.14	0.02
4429	441	-870	-156	441	884	5.65	8.03	0.04	0.11	0.01
4804	107	-1,141	-552	107	1,267	1.37	11.52	0.01	0.15	0.02
4630	141	-349	-1,199	141	1,249	1.81	11.35	0.01	0.15	0.02
4637	57	-109	-1,384	57	1,388	0.73	12.62	0.01	0.17	0.03
4644	37	-74	-1,589	37	1,591	0.47	14.46	0.00	0.19	0.04
4650	62	-63	-1,976	62	1,977	0.79	17.97	0.01	0.24	0.06
4657	109	118	-2,757	109	2,760	1.40	25.09	0.01	0.33	0.11
Max:				441	2,760	Max:				0.11

Notes:

- ① Stresses based on fastener areas of 0.078 in² and 0.110 in² for tension and shear, respectively.
- ② Allowable stresses are 126.0 ksi and 75.6 ksi for tension and shear, respectively.
- ③ Shear load is: $(F_x^2 + F_z^2)^{1/2}$

Table 2.12.5-22 – Summary of Strongback Stress Results (20.6-inch model) LC4

Load Case 4	Allowable Stresses (ksi)		Margin of Safety^①	
	P_m	P_m+P_b	P_m	P_m+P_b
Strongback Angle	30.2	42.3	+0.65	+0.51
Strongback Angle w/o ^② Bolt Nodes	28.3	42.3	+0.76	+0.51
Stiffener Tube	44.6	45.7	+0.11	+0.40
Stiffener Tube w/o Bolt Nodes	44.6	45.7	+0.11	+0.40

Notes:

- ① Allowable stresses are 49.7 ksi and 63.9 ksi for P_m and P_m + P_b, respectively
- ② "w/o" indicates that the coupled nodes (used at fastener locations) and connected elements are excluded from the listed results.

Table 2.12.5-23 – Summary of Strongback Stress Results (17.0-inch model) LC4

Load Case 4	Allowable Stresses (ksi)		Stress Ratio ^①	
	P _m	P _m +P _b	P _m	P _m +P _b
Strongback Angle	25.8	35.1	+0.93	+0.82
Strongback Angle w/o ^② Bolt Nodes	25.3	35.1	+0.96	+0.82
Stiffener Tube	38.0	39.1	+0.31	+0.63
Stiffener Tube w/o Bolt Nodes	38.0	39.1	+0.31	+0.63

Notes:

- ① Allowable stresses are 49.7 ksi and 63.9 ksi for P_m and P_m + P_b, respectively
- ② "w/o" indicates that the coupled nodes (used at fastener locations) and connected elements are excluded from the listed results.

Table 2.12.5-24 – Fastener Evaluation for Lock Bar/Pin Block Loads – Side Free Drop on 20.6-inch Section

Load Case 4										
NODE	F _x	F _y	F _z	Axial, lb _f (F _y)	Shear, lb _f	f _t (ksi)	f _v (ksi)	f _t / F _{tb}	f _v / F _{vb}	Interaction
4573	230	-1,155	2,086	230	2,384	2.95	21.68	0.02	0.29	0.08
4580	398	608	3,539	398	3,591	5.10	32.64	0.04	0.43	0.19
4586	463	923	3,414	463	3,536	5.93	32.15	0.05	0.43	0.18
4593	795	536	3,594	795	3,634	10.19	33.03	0.08	0.44	0.20
4600	1,042	68	3,421	1,042	3,422	13.36	31.11	0.11	0.41	0.18
4798	248	-890	919	248	1,280	3.18	11.63	0.03	0.15	0.02
4429	1,000	-227	6	1,000	227	12.82	2.07	0.10	0.03	0.01
4804	247	-891	-904	247	1,269	3.17	11.54	0.03	0.15	0.02
4630	1,041	67	-3,416	1,041	3,417	13.35	31.06	0.11	0.41	0.18
4637	795	535	-3,591	795	3,631	10.19	33.01	0.08	0.44	0.20
4644	462	922	-3,409	462	3,532	5.93	32.10	0.05	0.42	0.18
4650	397	609	-3,535	397	3,587	5.09	32.61	0.04	0.43	0.19
4657	230	-1,154	-2,076	230	2,375	2.95	21.59	0.02	0.29	0.08
Max:				1,042	3,634	Max:				0.20

Notes:

- ① Stresses based on fastener areas of 0.078 in² and 0.110 in² for tension and shear, respectively.
- ② Allowable stresses are 126.0 ksi and 75.6 ksi for tension and shear, respectively.
- ③ Shear load is: $(F_x^2 + F_z^2)^{1/2}$

Table 2.12.5-25 – Fastener Evaluation for Lock Bar/Pin Block Loads – Side Free Drop on 17.0-inch Section

Load Case 4										
NODE	F _x	F _y	F _z	Axial, lb _f (F _y)	Shear, lb _f	f _t (ksi)	f _v (ksi)	f _t / F _{tb}	f _v / F _{vb}	Interaction
3805	169	-222	3,971	169	3,977	2.17	36.16	0.02	0.48	0.23
3811	424	72	4,094	424	4,095	5.44	37.22	0.04	0.49	0.24
3818	563	362	4,074	563	4,090	7.22	37.18	0.06	0.49	0.25
3825	980	363	3,788	980	3,805	12.57	34.59	0.10	0.46	0.22
3990	165	-624	1,006	165	1,184	2.12	10.76	0.02	0.14	0.02
3685	1,025	51	7	1,025	51	13.14	0.46	0.10	0.01	0.01
3996	164	-624	-985	164	1,166	2.11	10.60	0.02	0.14	0.02
3853	980	363	-3,782	980	3,799	12.57	34.54	0.10	0.46	0.22
3860	563	362	-4,069	563	4,085	7.22	37.14	0.06	0.49	0.24
3867	424	72	-4,090	424	4,091	5.44	37.19	0.04	0.49	0.24
3873	169	-223	-3,966	169	3,972	2.17	36.11	0.02	0.48	0.23
Max:				1,025	4,095	Max:				0.25

Notes:

- ① Stresses based on fastener areas of 0.078 in² and 0.110 in² for tension and shear, respectively.
- ② Allowable stresses are 126.0 ksi and 75.6 ksi for tension and shear, respectively.
- ③ Shear load is: $(F_x^2 + F_z^2)^{1/2}$

Table 2.12.5-26 – Side Drop Plastic Strain Intensity

Plastic Strain Intensity	E _{tan} ≈ .008E		E _{tan} = .05E	
	Middle Fiber	Extreme Fiber	Middle Fiber	Extreme Fiber
20.6-inch Span - Load Step 4 (Side Drop)				
Plate	5.5	9.8	1.04	1.48
Stiffener Tube	13.4	13.9	3.07	3.15
17.0-inch Span - Load Step 4 (Side Drop)				
	Middle Fiber	Extreme Fiber	Middle Fiber	Extreme Fiber
Plate	3.0	4.9	0.73	0.98
Stiffener Tube	8.8	9.2	2.05	2.23

Table 2.12.5-27 – Summary of Strongback Stress Results (20.6-inch model) LC4

Load Case 4 (High Tangent Modulus)	Allowable Stresses (ksi)		Margin of Safety ^①	
	P_m	$P_m + P_b$	P_m	$P_m + P_b$
Strongback Angle	30.3	42.0	+0.64	+0.52
Strongback Angle w/o ^② Bolt Nodes	30.3	42.0	+0.64	+0.52
Stiffener Tube	54.5	55.4	③	+0.15
Stiffener Tube w/o Bolt Nodes	54.5	55.4		+0.15
Stiffener Tube w/o 2 Nodes (Note 3)	46.4	N/A	+0.07	N/A

Notes:

- ① Allowable stresses are 49.7 ksi and 63.9 ksi for P_m and $P_m + P_b$, respectively
- ② "w/o" indicates that the coupled nodes (used at fastener locations) and connected elements are excluded from the listed results.
- ③ Nodes 5802 & 5803 at stiffener tube ends are peak stresses and excluded from comparison to allowable stresses. Conservatively, the outer surface stresses are compared to the membrane-plus-bending allowable stress. See Section 2.12.5.20, *Strongback Stress Calculations - Horizontal Loads*, for further discussion.

Table 2.12.5-28 – Summary of Strongback Stress Results (17.0-inch model) LC4

Load Case 4 (High Tangent Modulus)	Allowable Stresses (ksi)		Stress Ratio ^①	
	P_m	$P_m + P_b$	P_m	$P_m + P_b$
Strongback Angle	27.7	37.4	+0.79	+0.71
Strongback Angle w/o ^② Bolt Nodes	26.0	37.4	+0.91	+0.71
Stiffener Tube	44.8	46.7	+0.11	+0.37
Stiffener Tube w/o Bolt Nodes	44.8	46.7	+0.11	+0.37

Notes:

- ① Allowable stresses are 49.7 ksi and 63.9 ksi for P_m and $P_m + P_b$, respectively
- ② "w/o" indicates that the coupled nodes (used at fastener locations) and connected elements are excluded from the listed results.

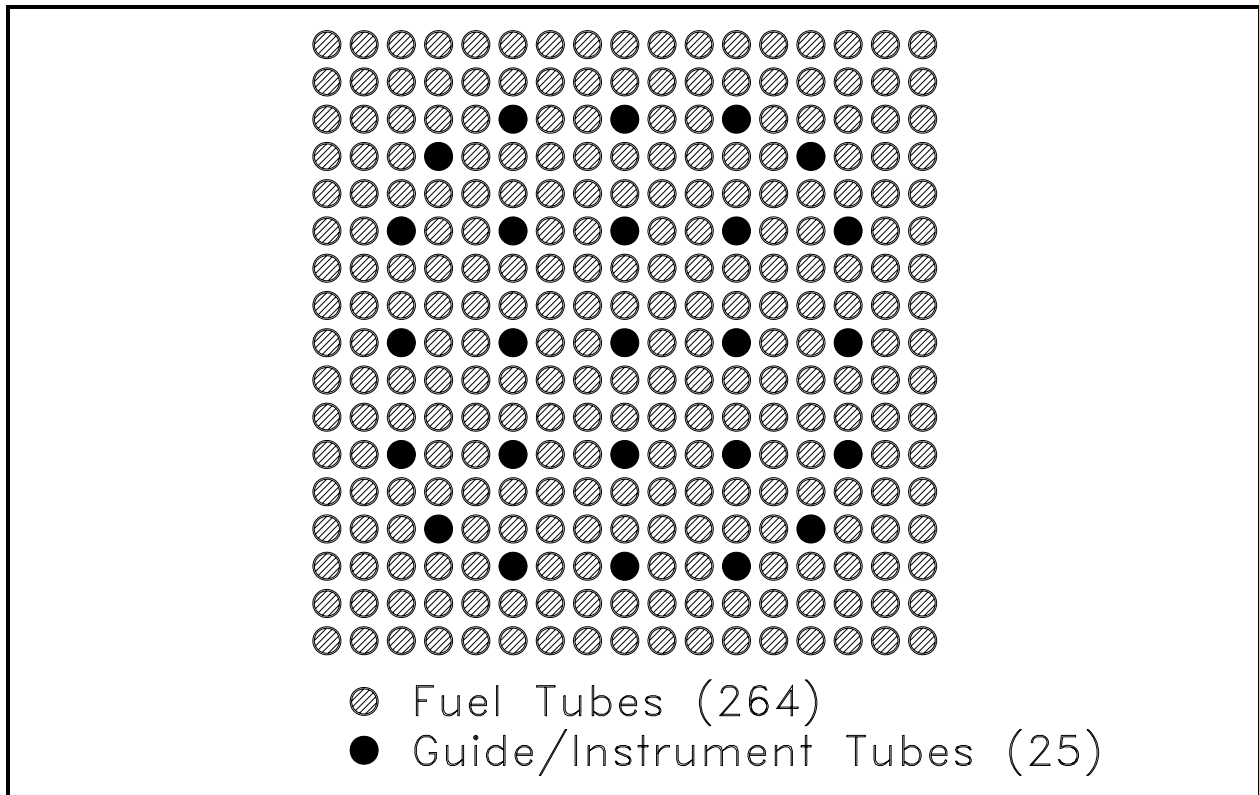


Figure 2.12.5-1 – MOX Fuel Assembly Rod Locations



Figure 2.12.5-2 – Buckled Shape of Fuel Rod from Certification Test

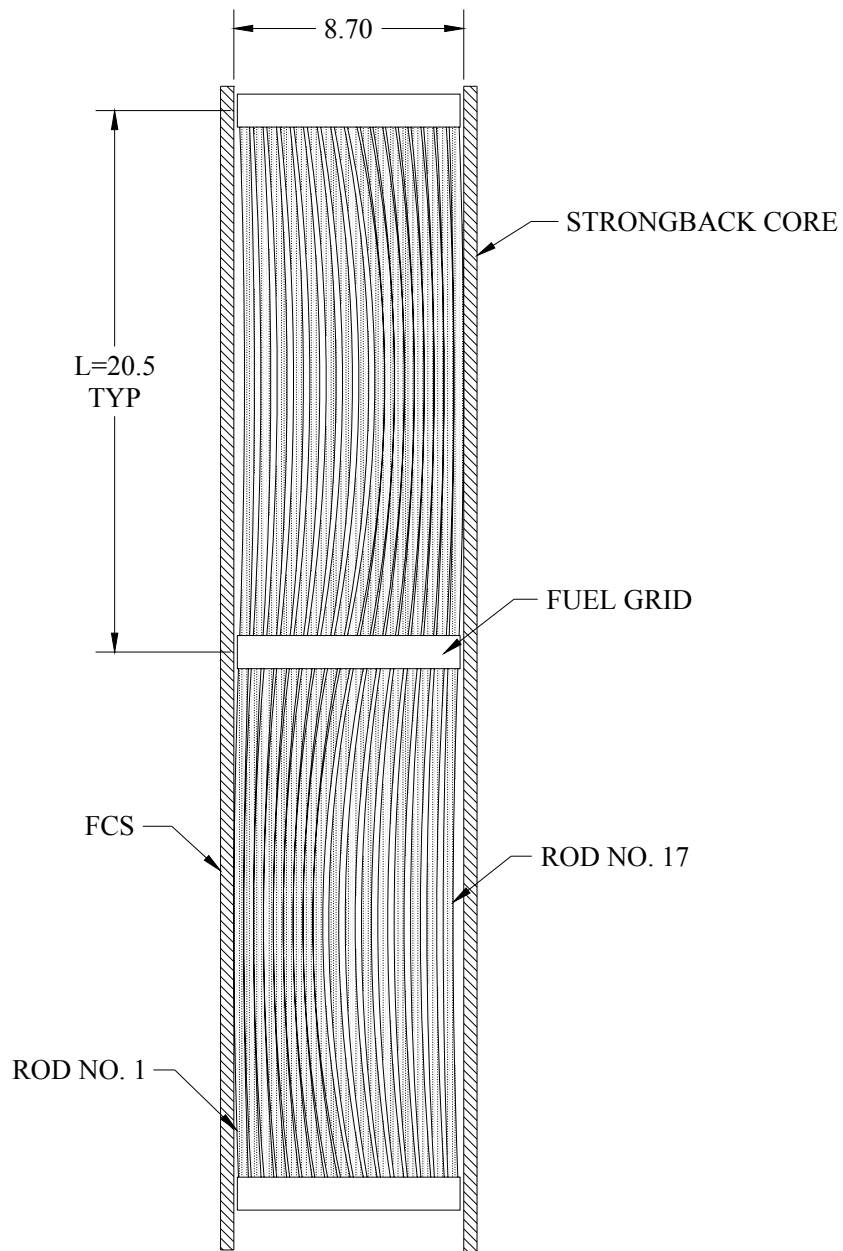


Figure 2.12.5-3 – Buckled Configuration of Fuel Rods

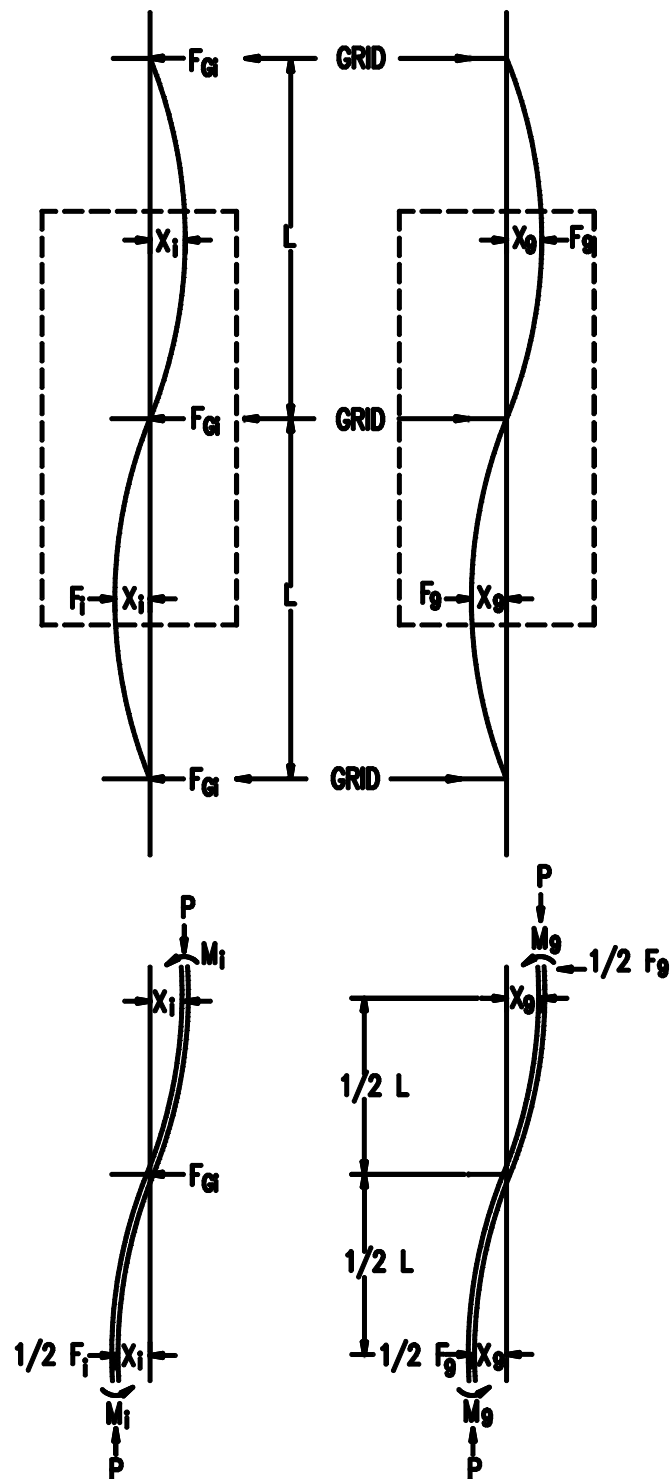


Figure 2.12.5-4 – Free Body Diagrams of Fuel Rods

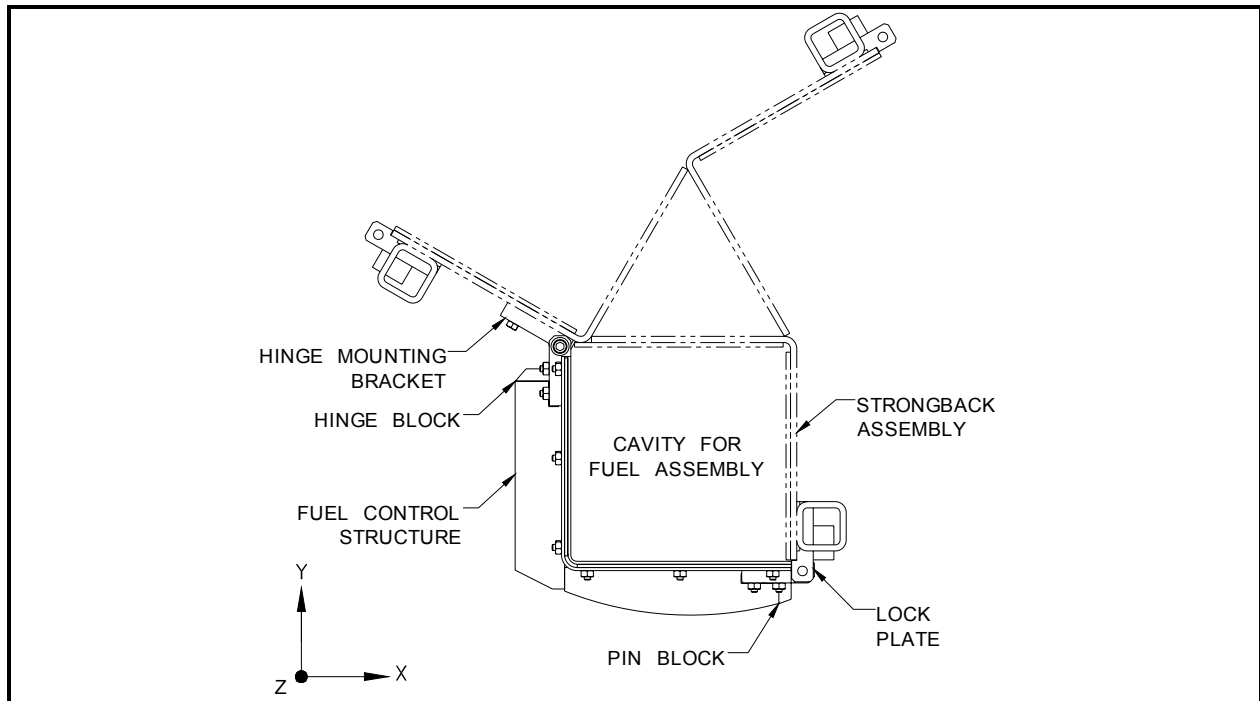


Figure 2.12.5-5 – FCS and Strongback Cross-Section

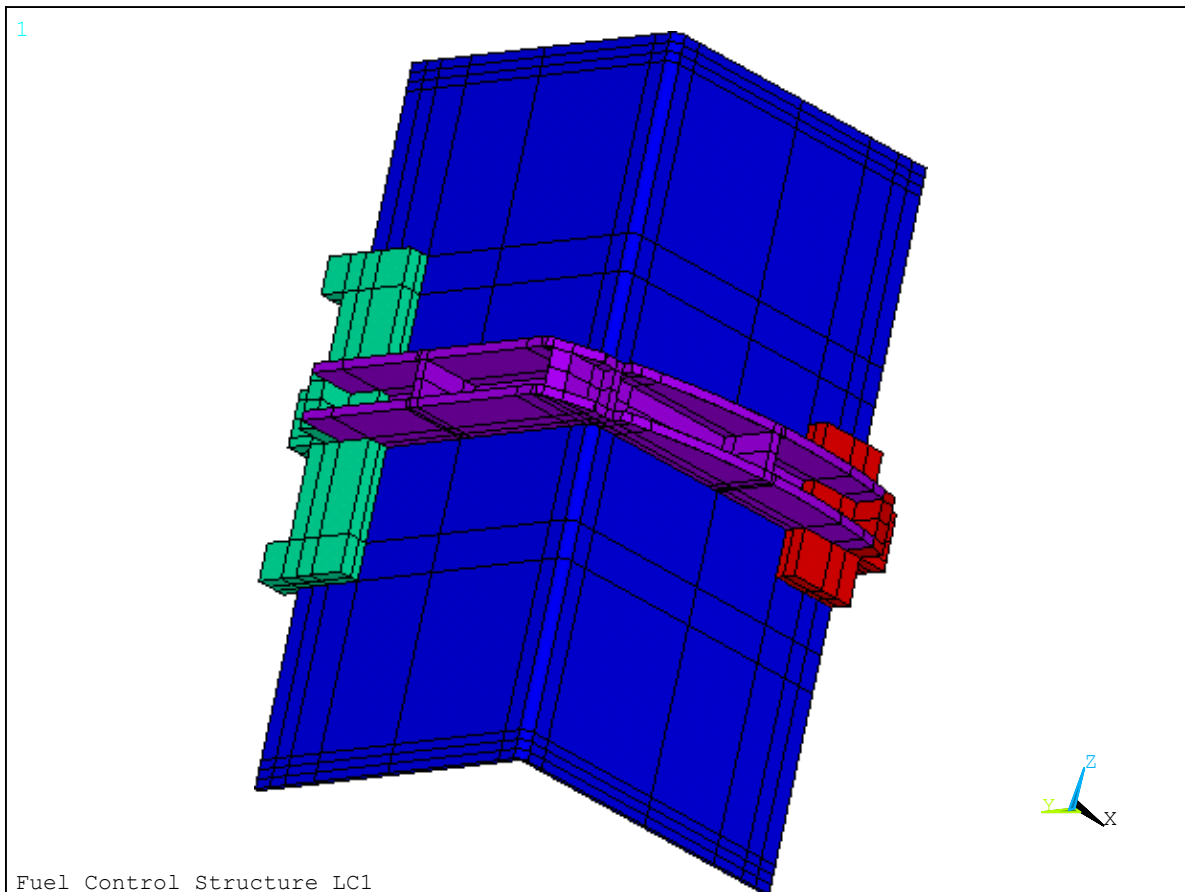


Figure 2.12.5-6 – FEA Volumes

1

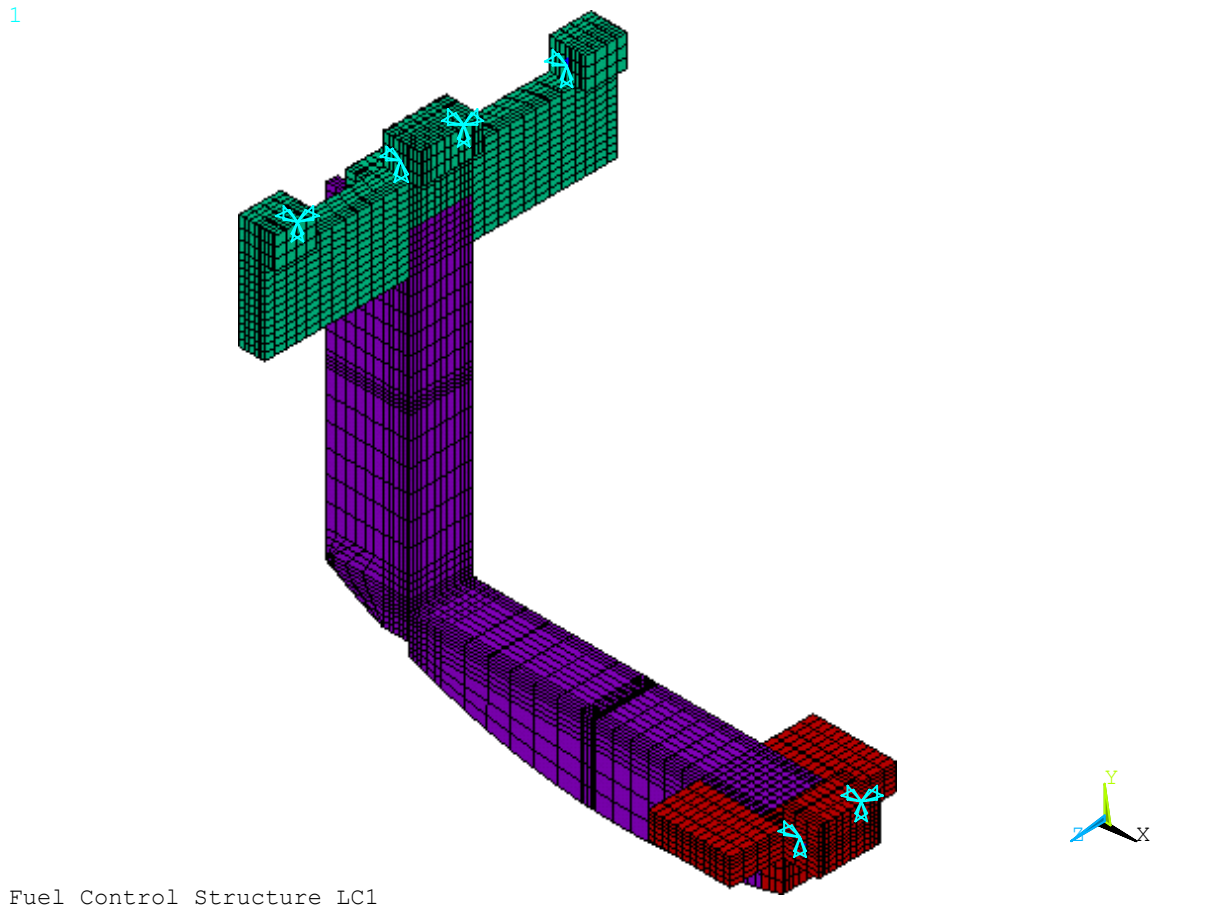


Figure 2.12.5-7 – Elements and Boundary Constraints (Shown without Angle)

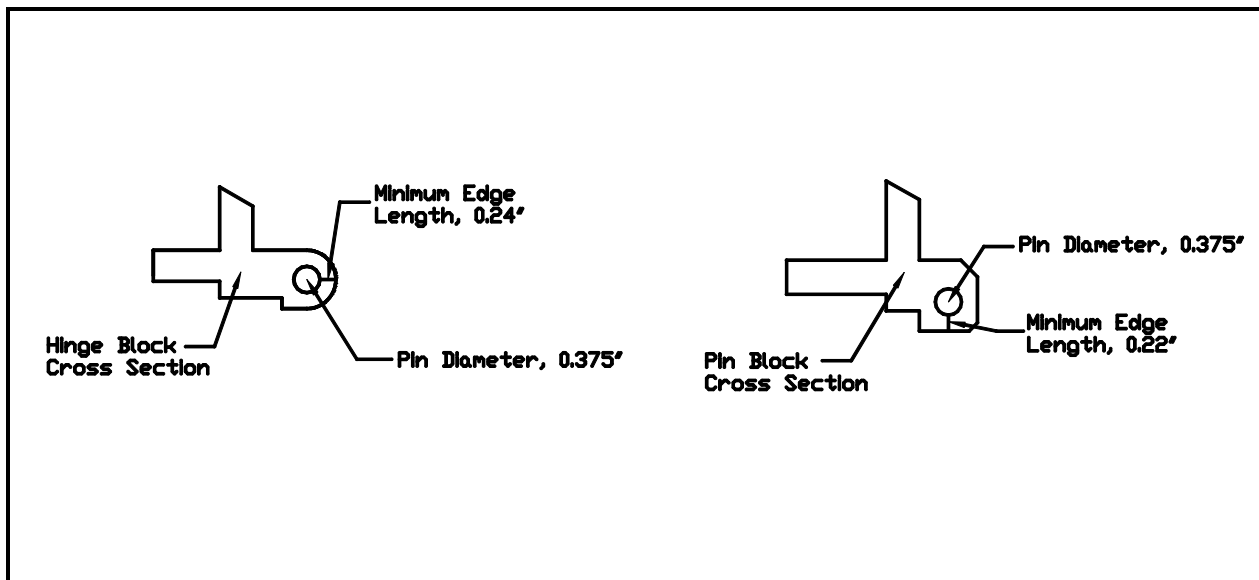


Figure 2.12.5-8 – Pin Diameters and Minimum Edge Lengths

Security Related Information
Figure Withheld Under 10 CFR 2.390

Figure 2.12.5-9 – Typical FCS Fastener Connection

Security Related Information
Figure Withheld Under 10 CFR 2.390

Figure 2.12.5-10 – Hinge and Pin Block Constraint and Bolt Locations

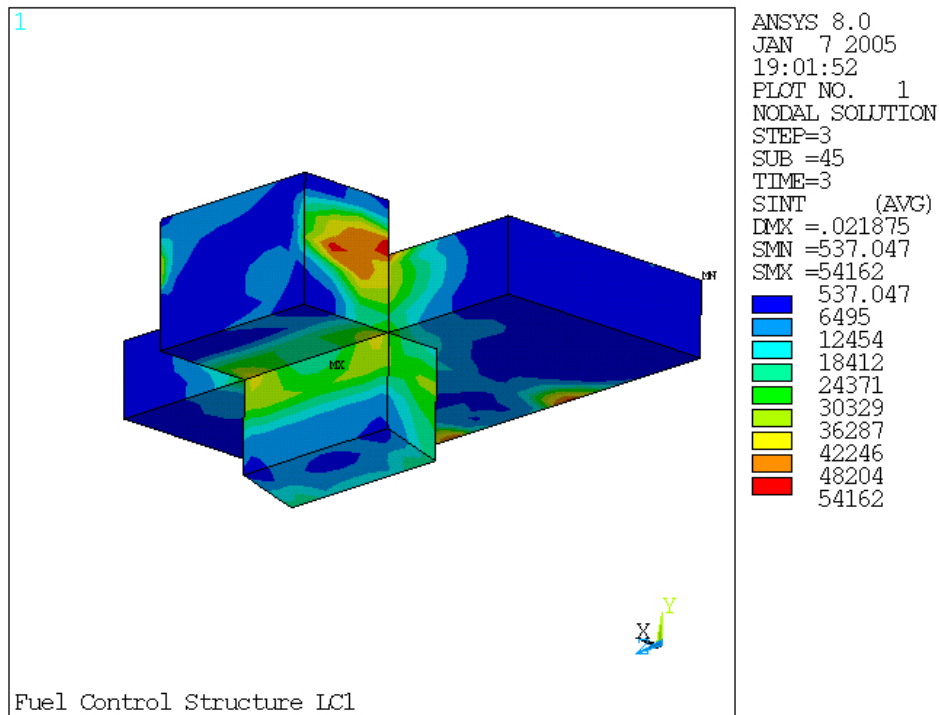


Figure 2.12.5-11 – LC1 Pin Block Stress Intensity

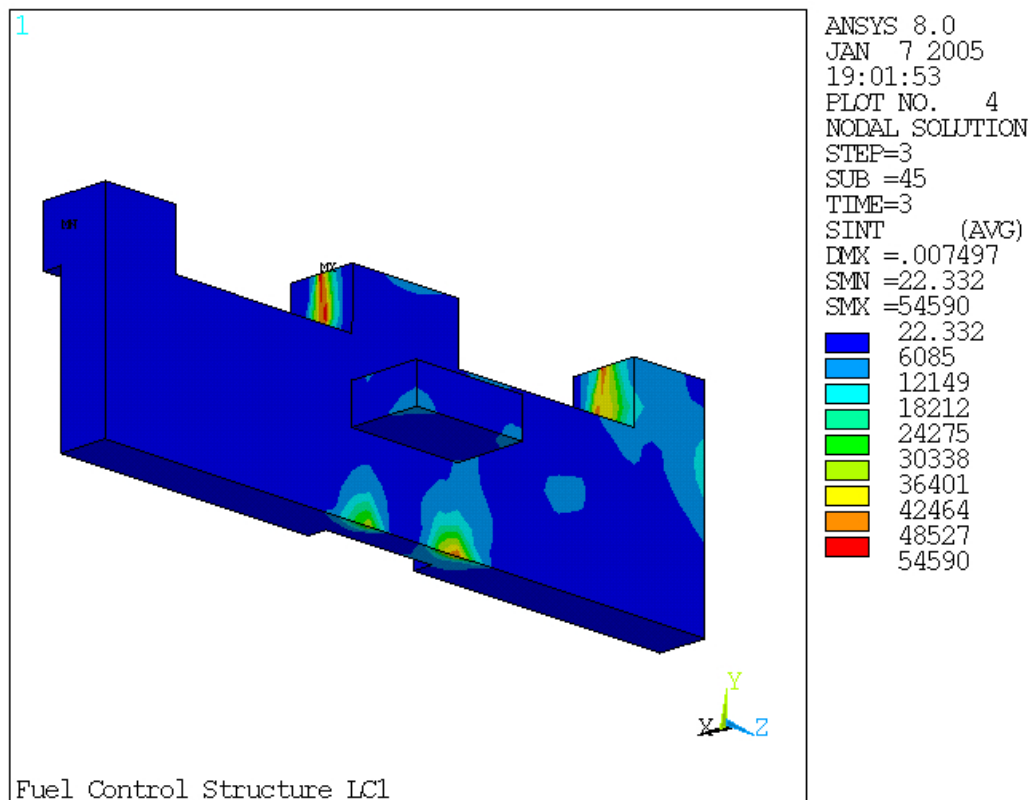


Figure 2.12.5-12 – LC1 Hinge Block Stress Intensity

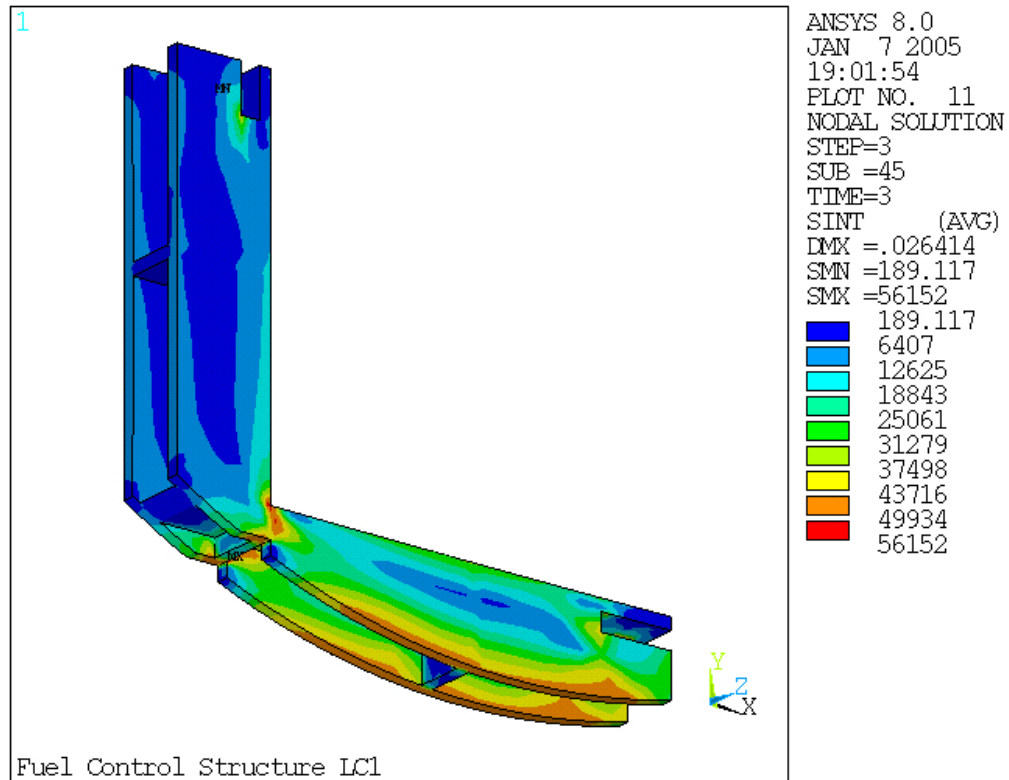


Figure 2.12.5-13 – LC1 Stiffener Stress Intensity

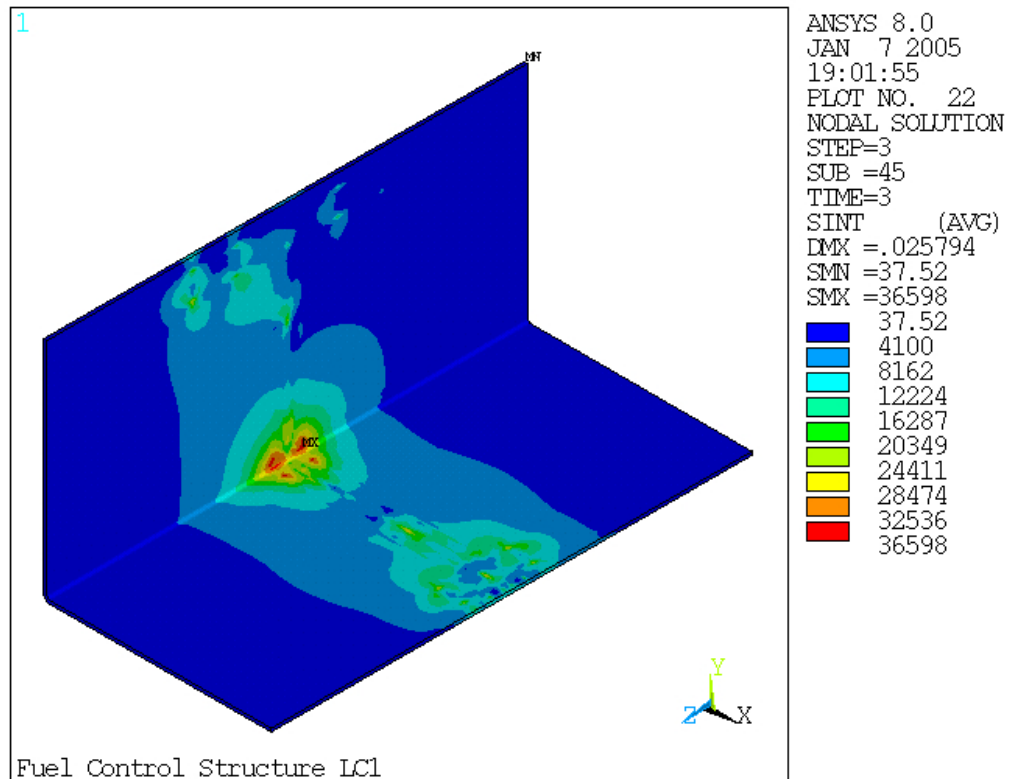


Figure 2.12.5-14 – LC1 Angle Stress Intensity

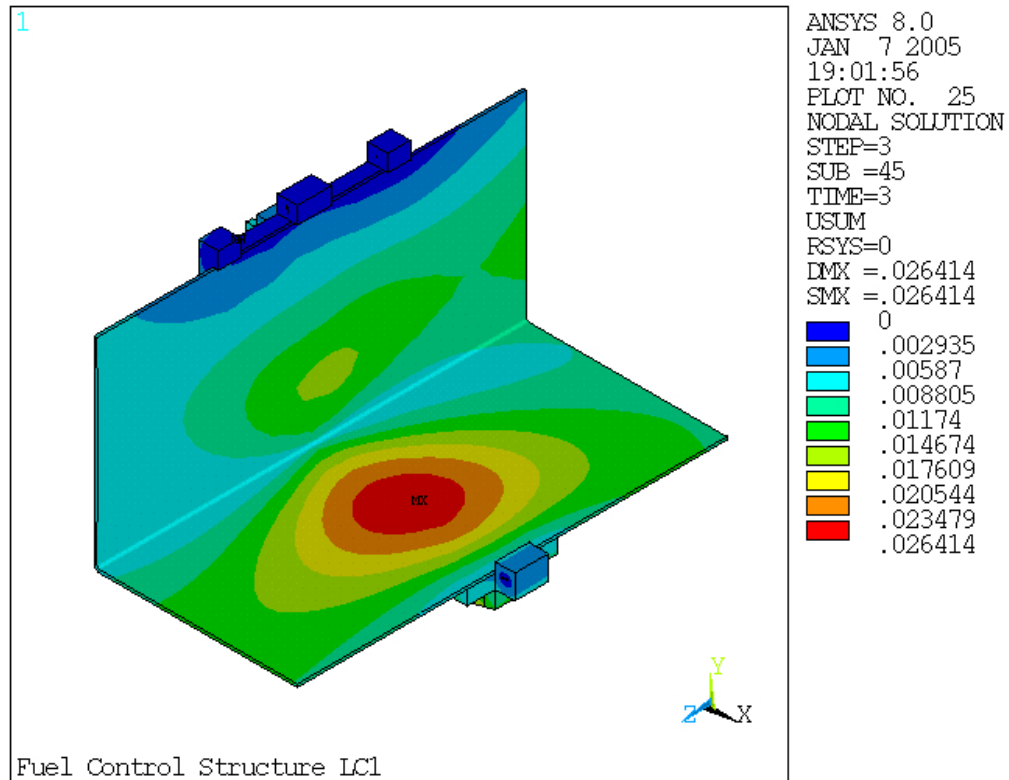


Figure 2.12.5-15 – LC1 Total Displacement

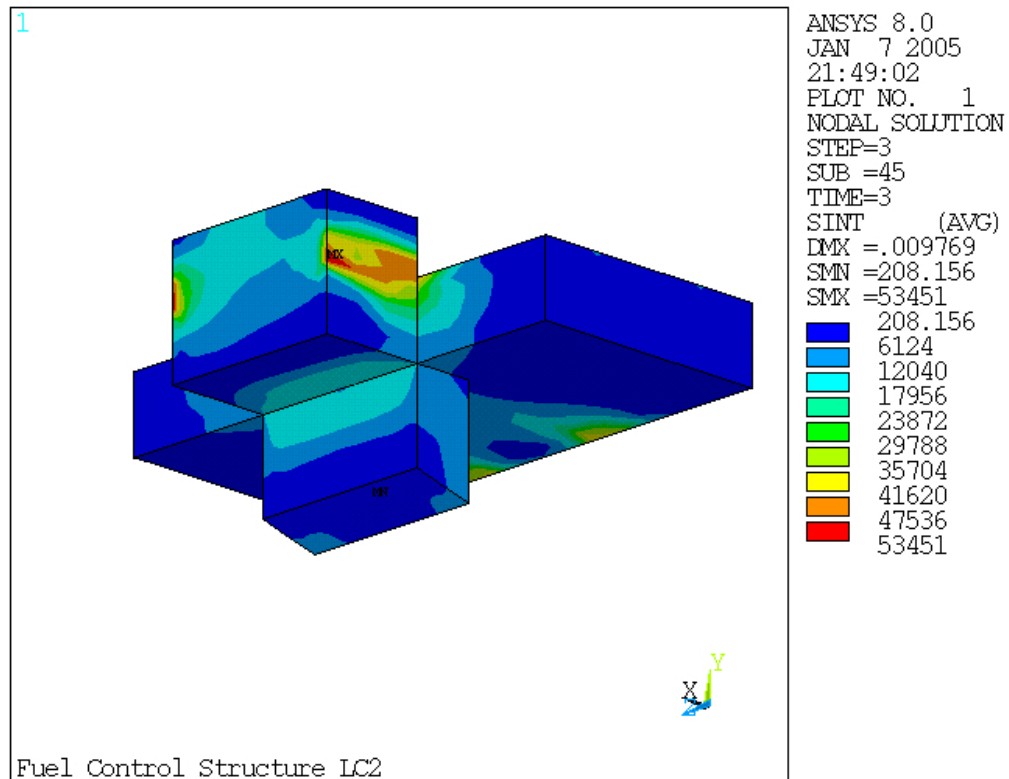


Figure 2.12.5-16 – LC2 Pin Block Stress Intensity

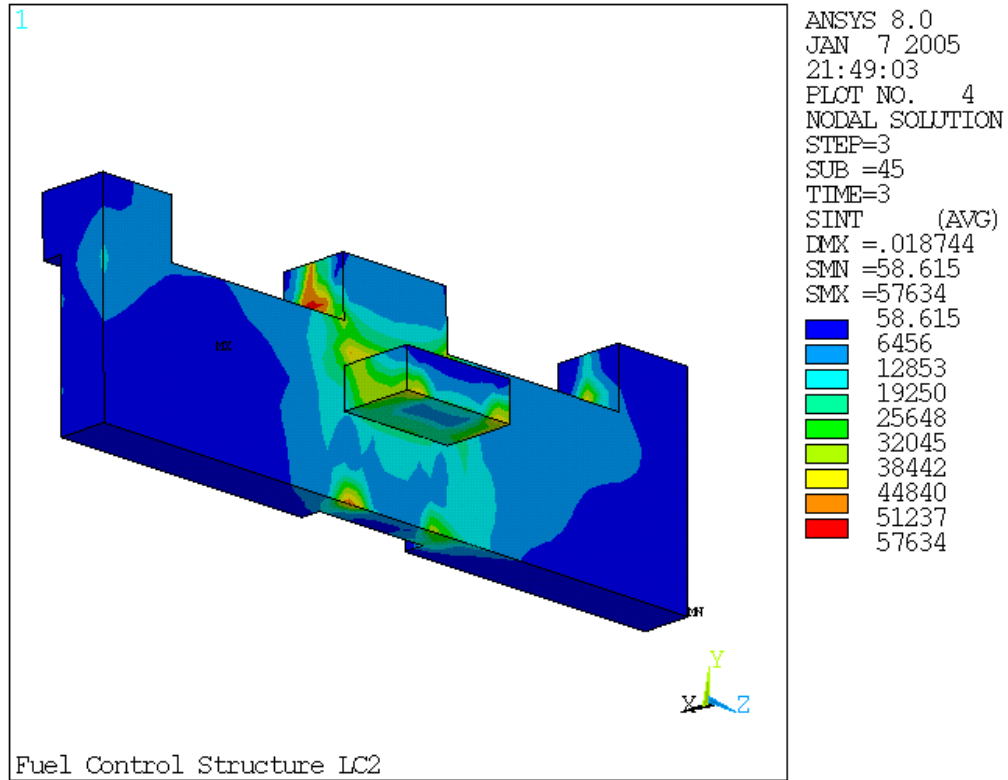


Figure 2.12.5-17 – LC2 Hinge Block Stress Intensity

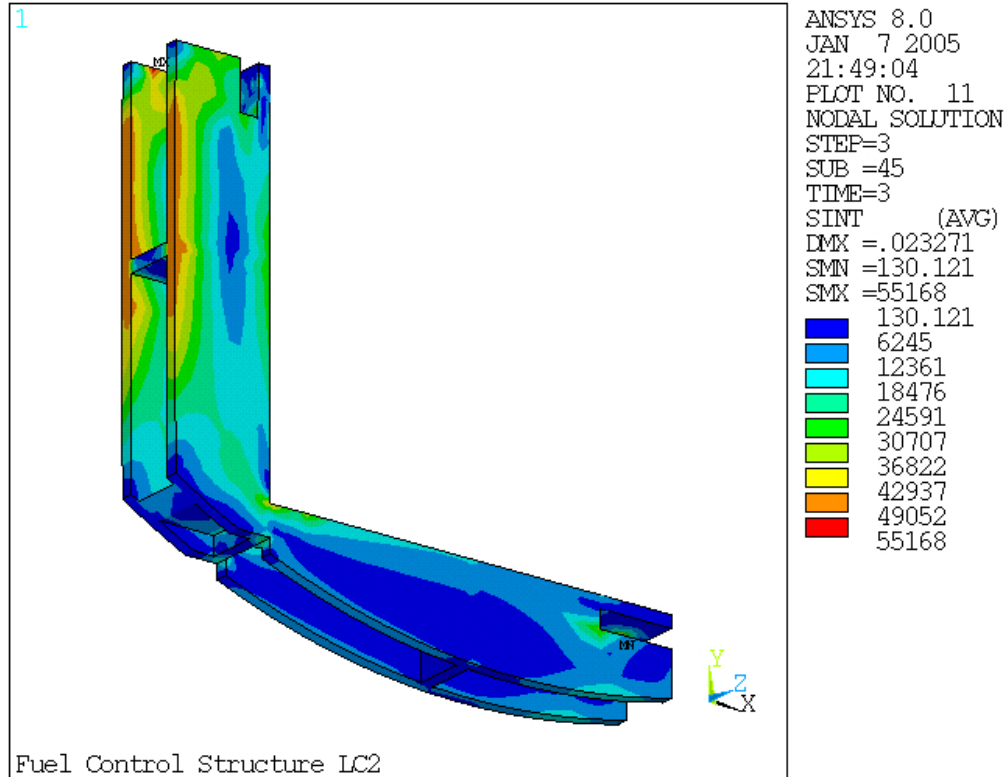


Figure 2.12.5-18 – LC2 Stiffener Stress Intensity

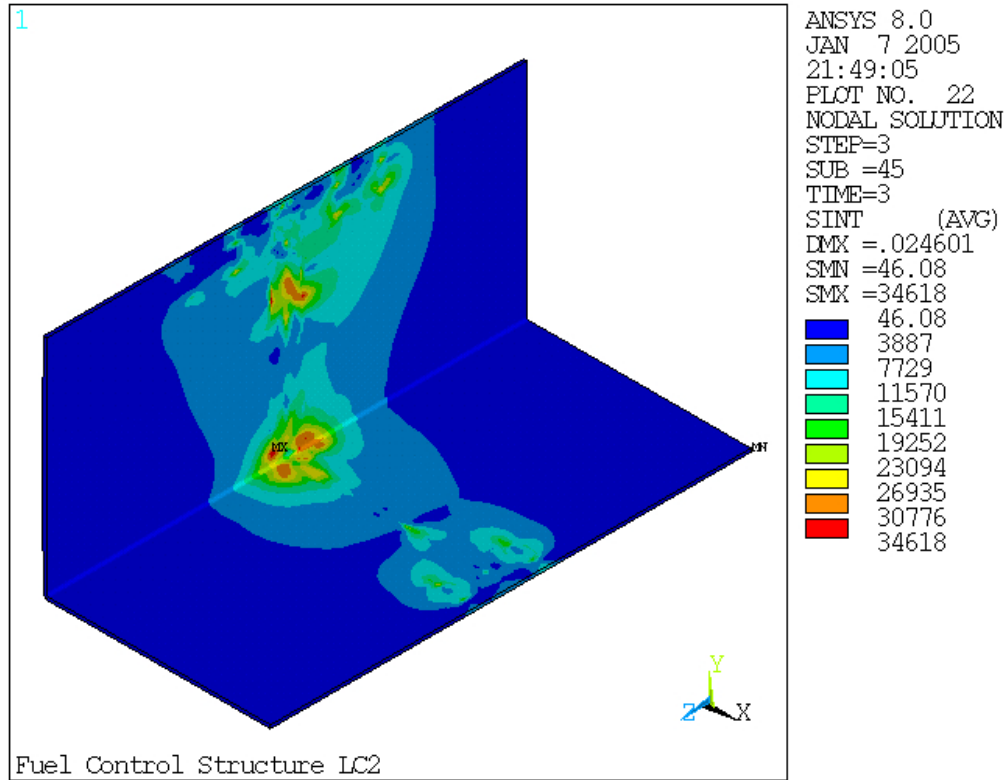


Figure 2.12.5-19 – LC2 Angle Stress Intensity

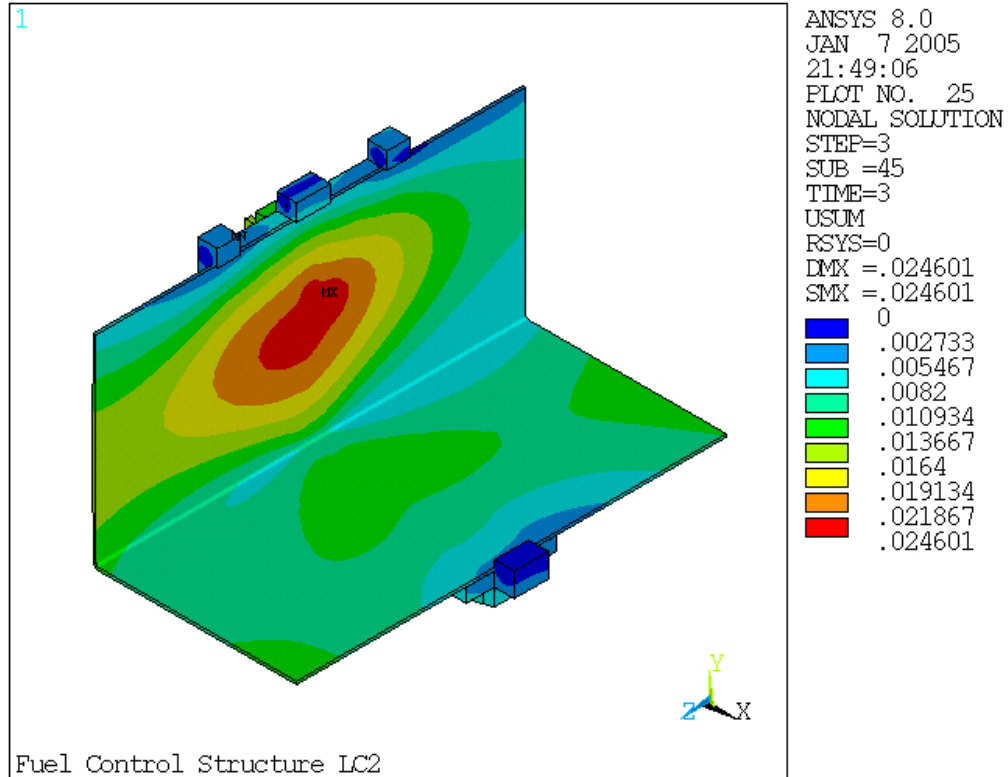


Figure 2.12.5-20 – LC2 Total Displacement

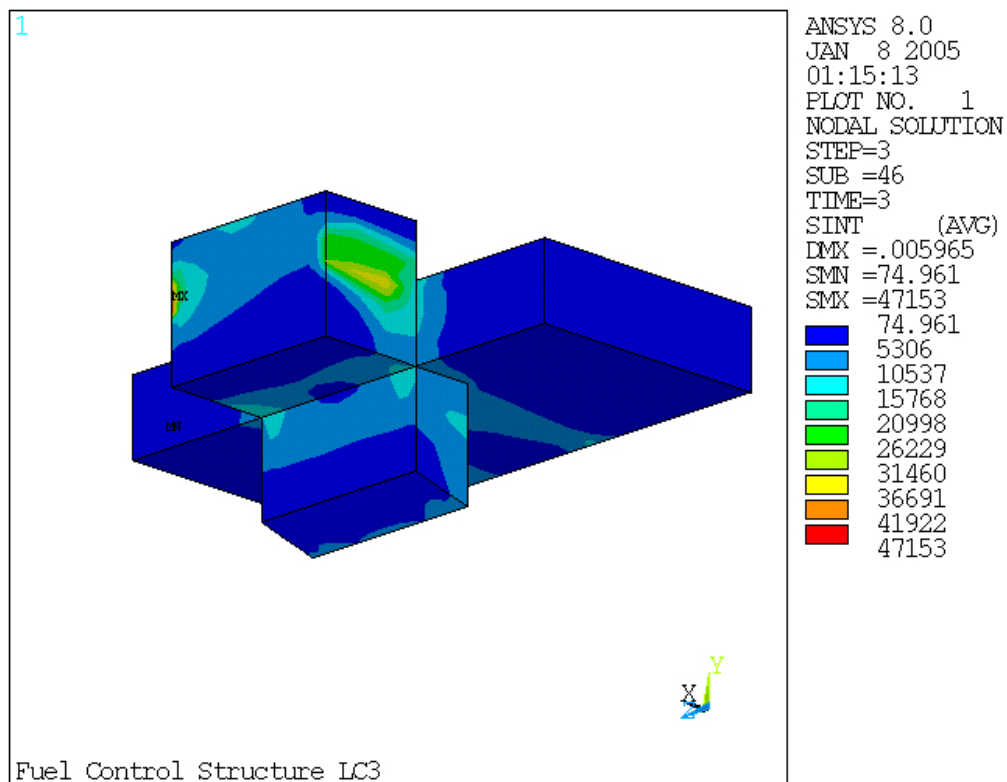


Figure 2.12.5-21 – LC3 Pin Block Stress Intensity

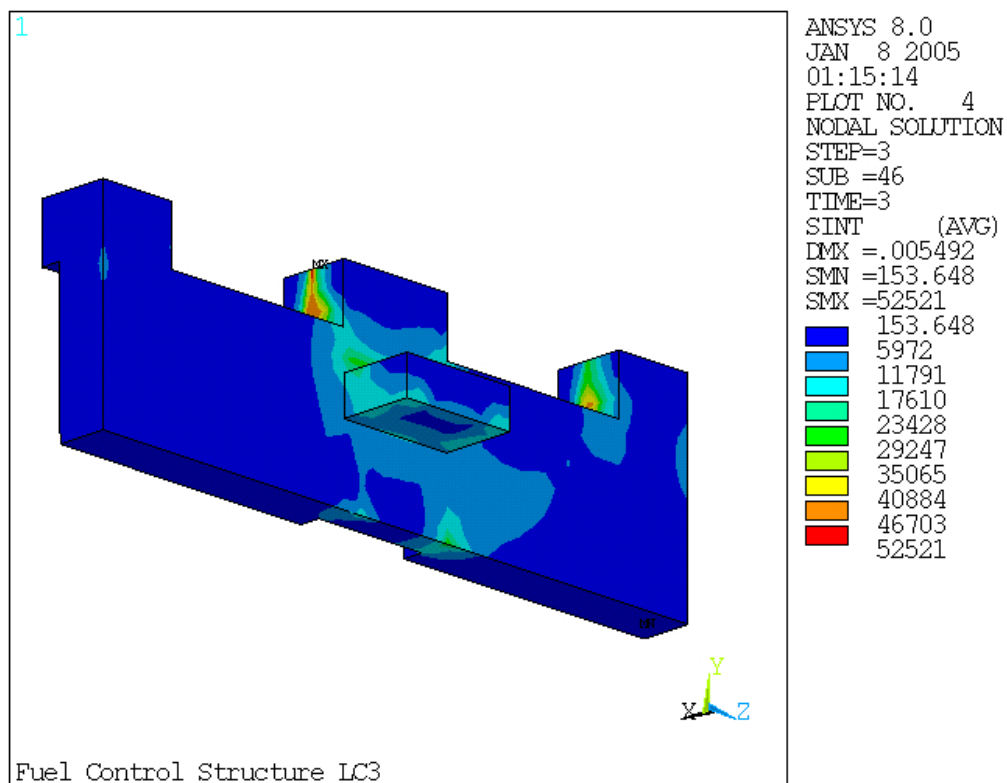


Figure 2.12.5-22 – LC3 Hinge Block Stress Intensity

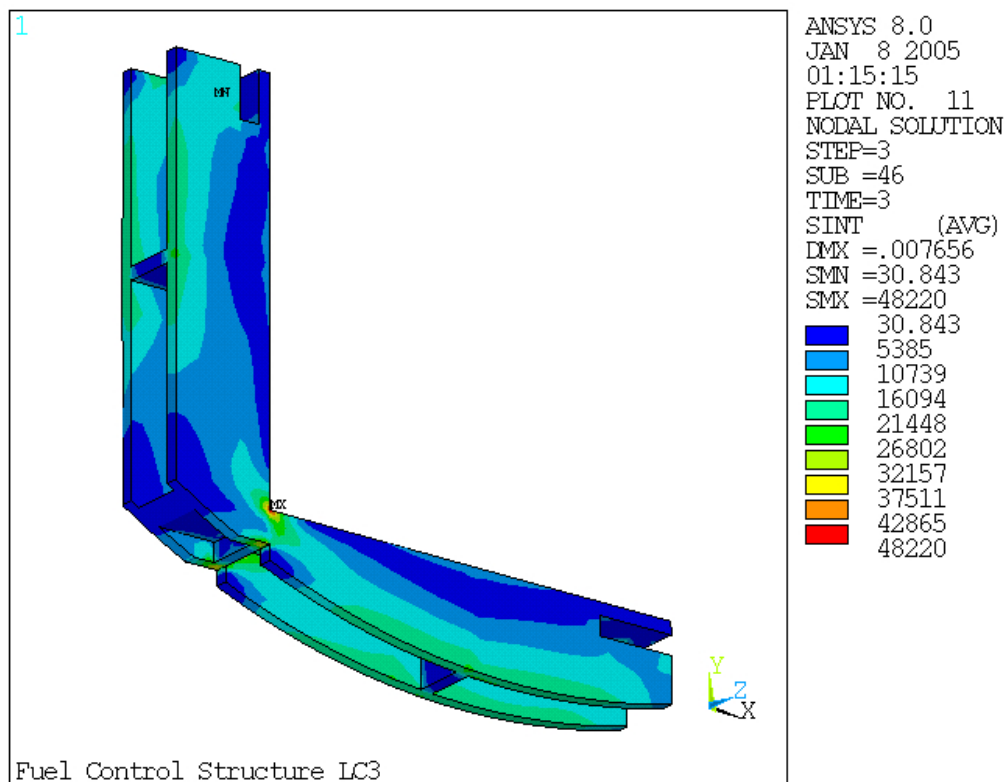


Figure 2.12.5-23 – LC3 Stiffener Stress Intensity

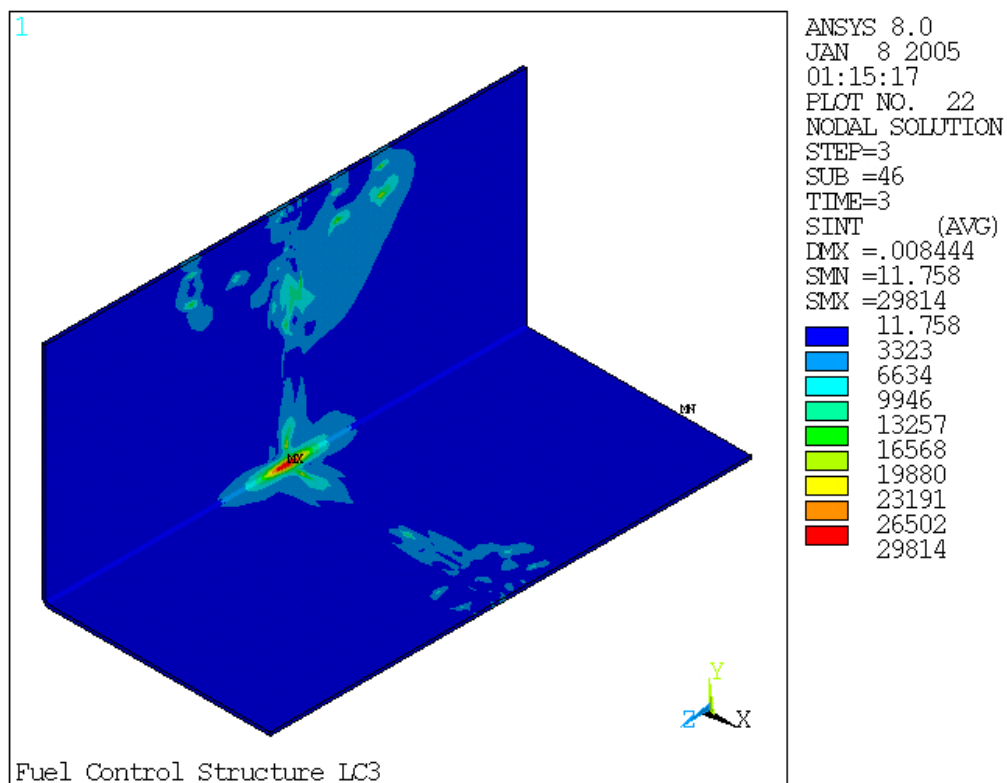


Figure 2.12.5-24 – LC3 Angle Stress Intensity

Security Related Information
Figure Withheld Under 10 CFR 2.390

Figure 2.12.5-9 – Typical FCS Fastener Connection

Security Related Information
Figure Withheld Under 10 CFR 2.390

Figure 2.12.5-10 – Hinge and Pin Block Constraint and Bolt Locations

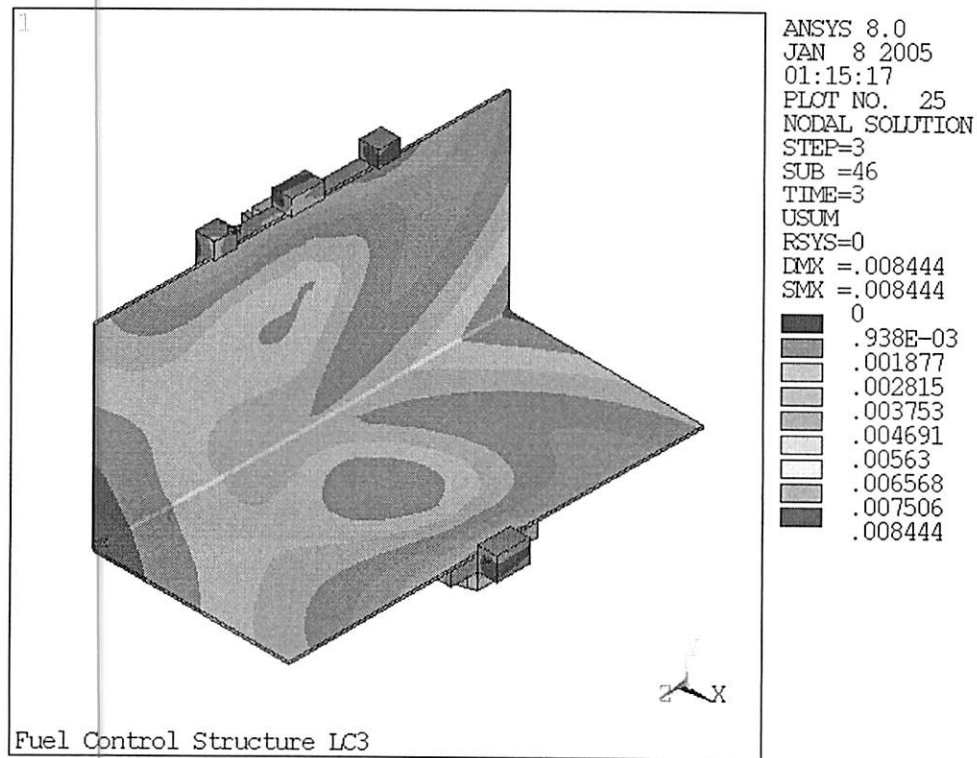


Figure 2.12.5-25 – LC3 Total Displacement

Security Related Information
Figure Withheld Under 10 CFR 2.390

Figure 2.12.5-26 – Lock Plate Details

Security Related Information
Figure Withheld Under 10 CFR 2.390

Figure 2.12.5-27 – Lock Plate (Refer to Figure 2.12.5-26 for Dimensions)

Security Related Information
Figure Withheld Under 10 CFR 2.390

Figure 2.12.5-28 – Hinge Mounting Bracket (Refer to Figure 2.12.5-29 for Dimensions)

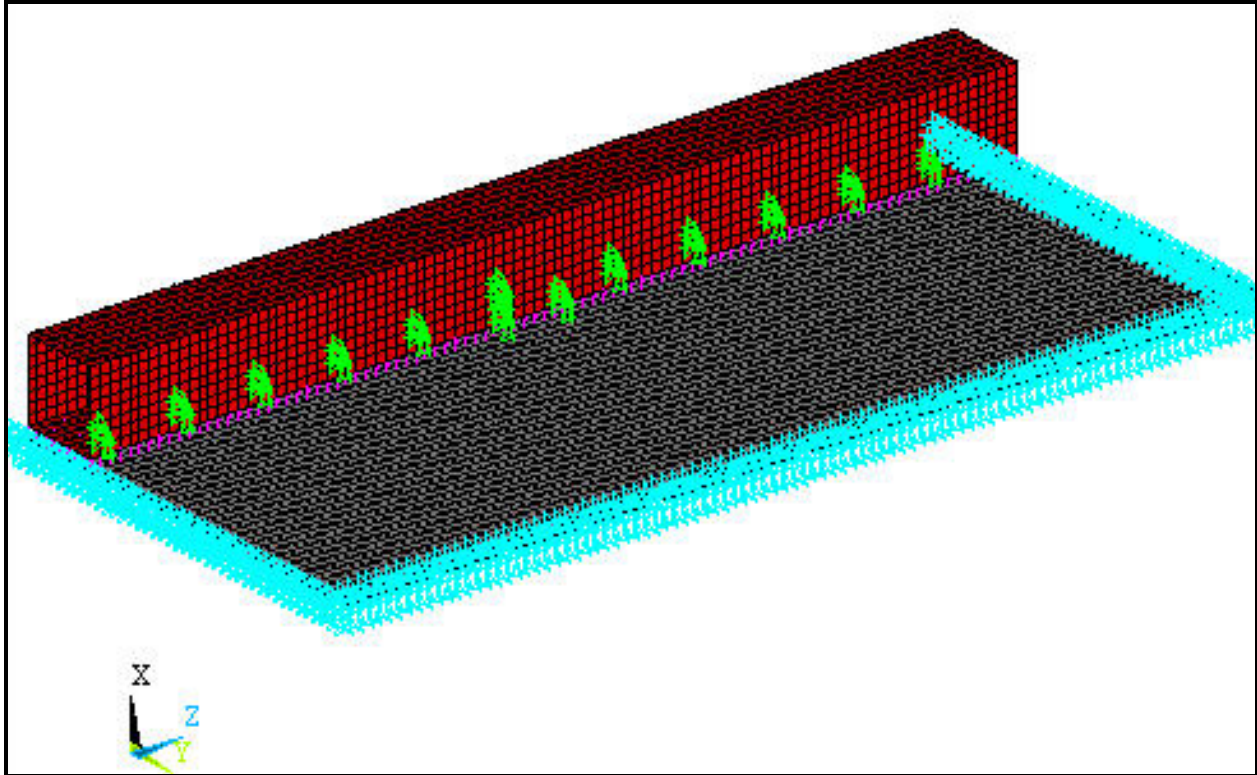


Figure 2.12.5-31 – Plate Angle Model for FCS Loads (w/ Boundary Conditions)

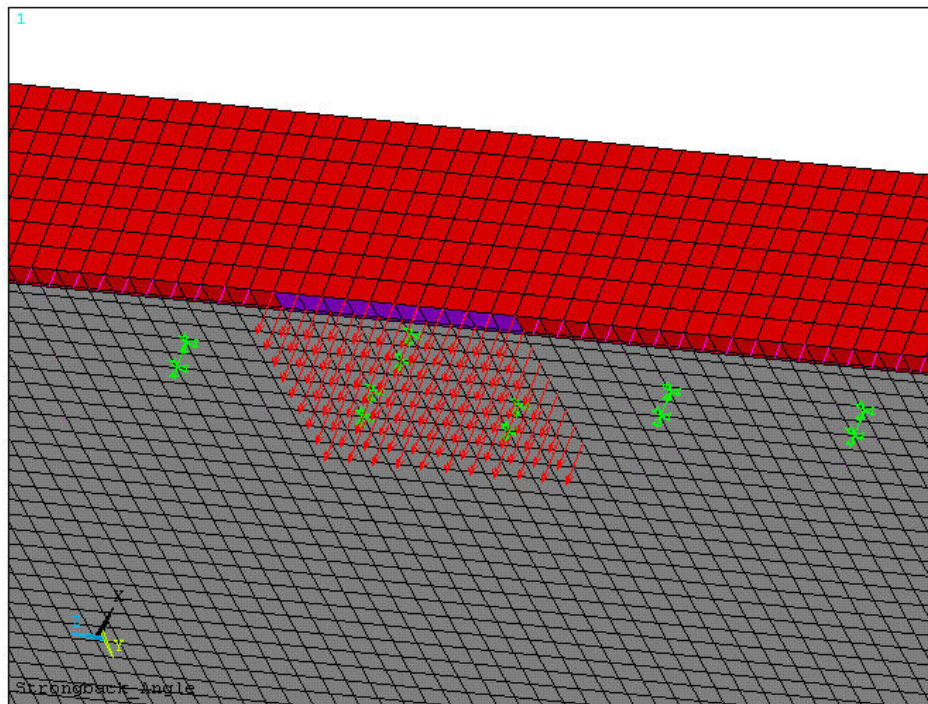


Figure 2.12.5-32 – Plate Angle Model for FCS Loads (Bottom View Showing “Thick” Section Where Loads Are Applied)

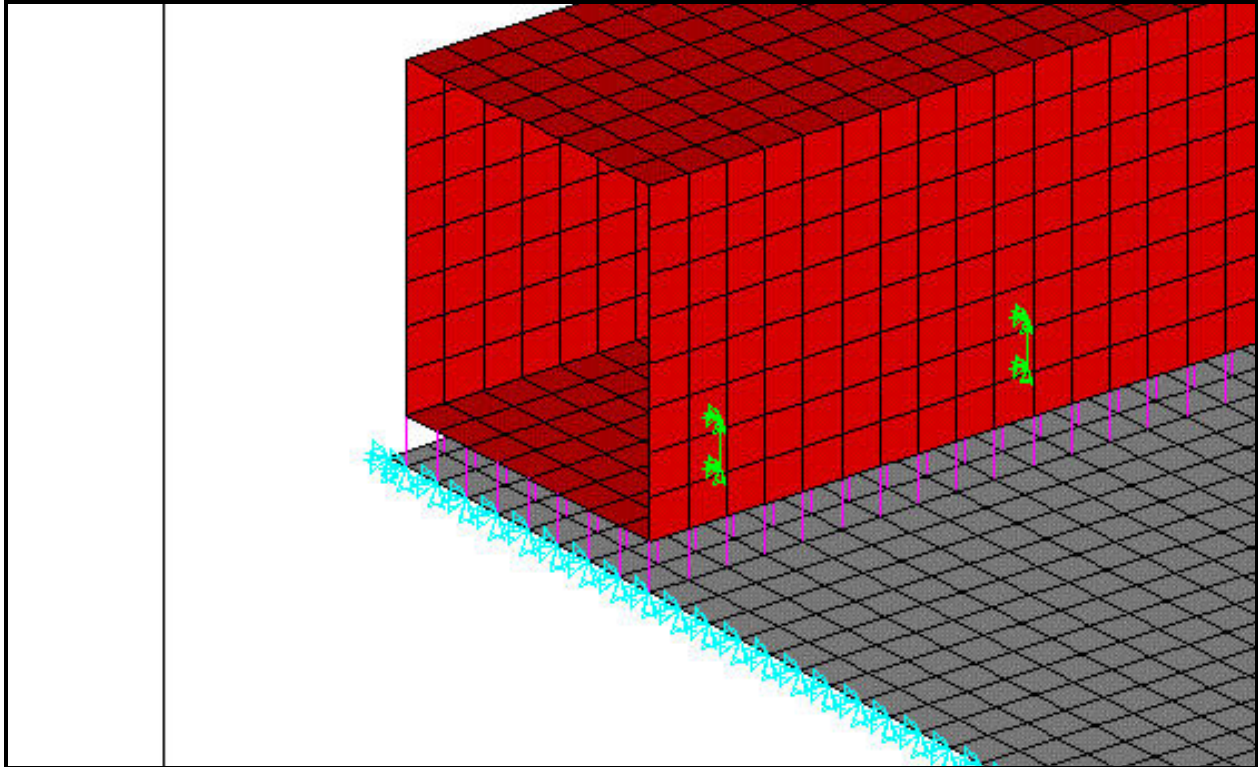


Figure 2.12.5-33 – Plate Angle Model for FCS Loads (Close-Up Showing Contac52 Elements Between Tube And Plate)

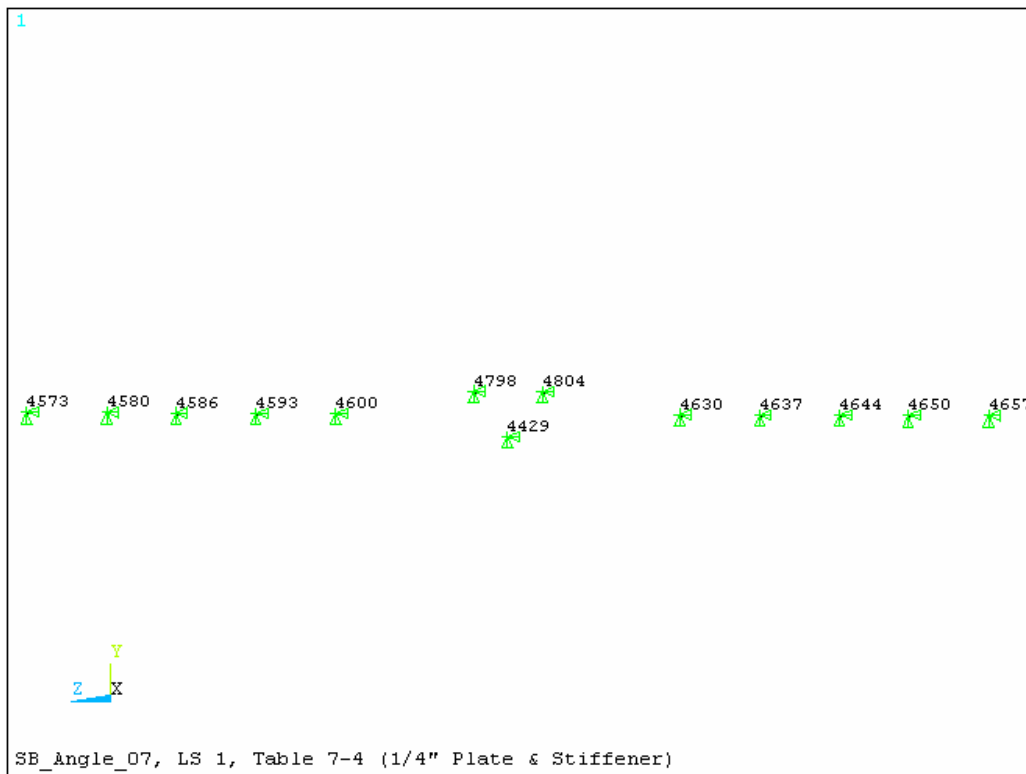


Figure 2.12.5-34 – Fastener Locations and Node Point IDs (Long FCS)

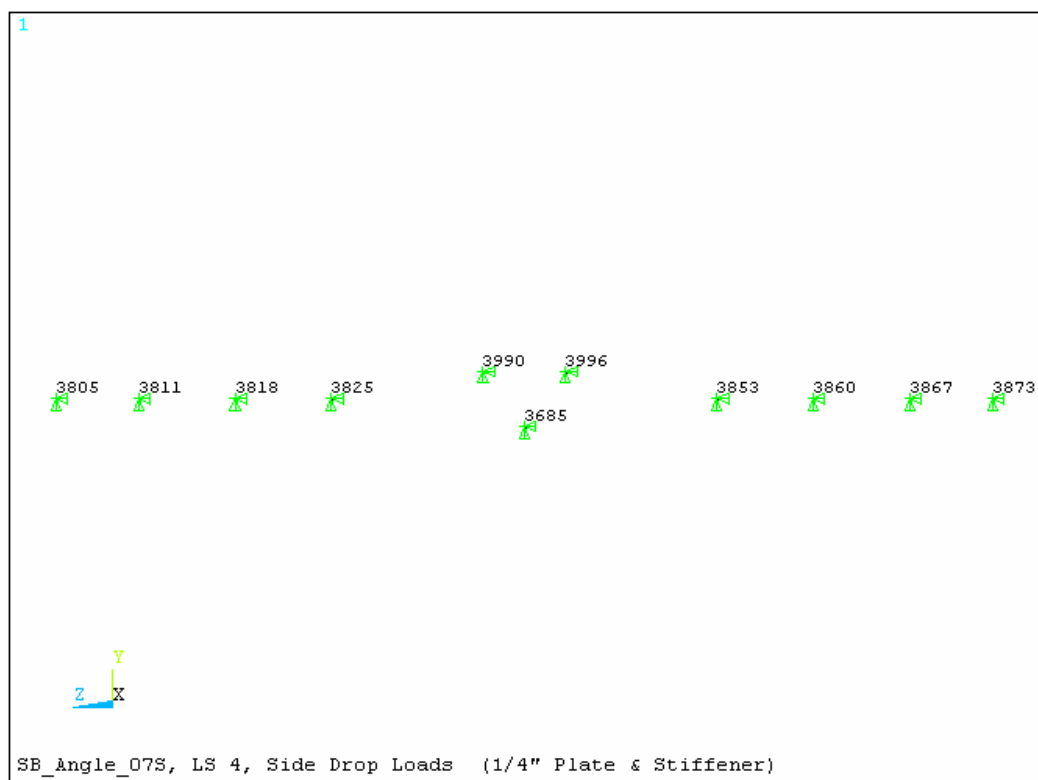


Figure 2.12.5-35 – Fastener Locations and Node Point IDs (Standard FCS)

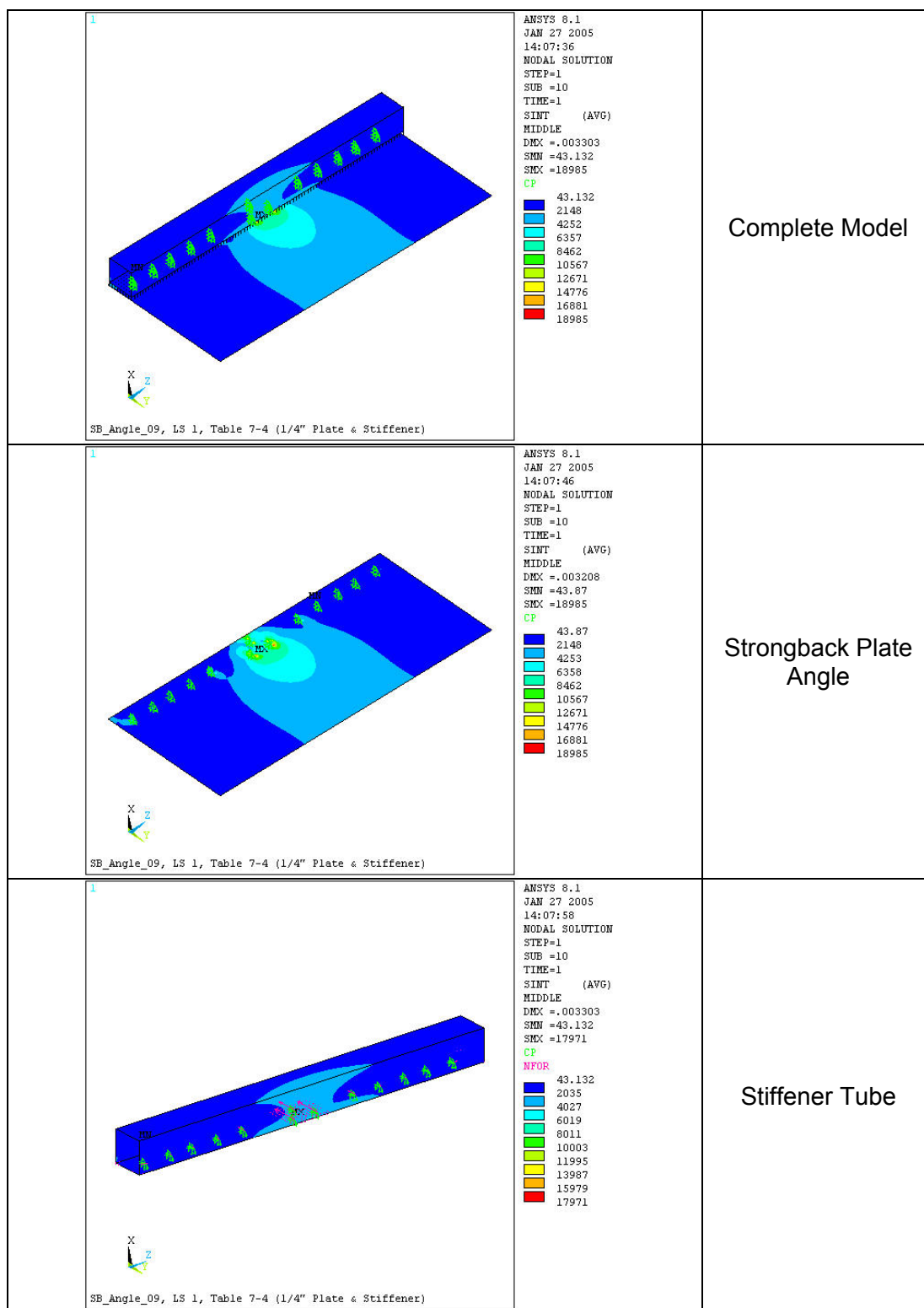


Figure 2.12.5-36 – Mid-thickness Stresses in Plate Angle Under Pin Block Load Case 1

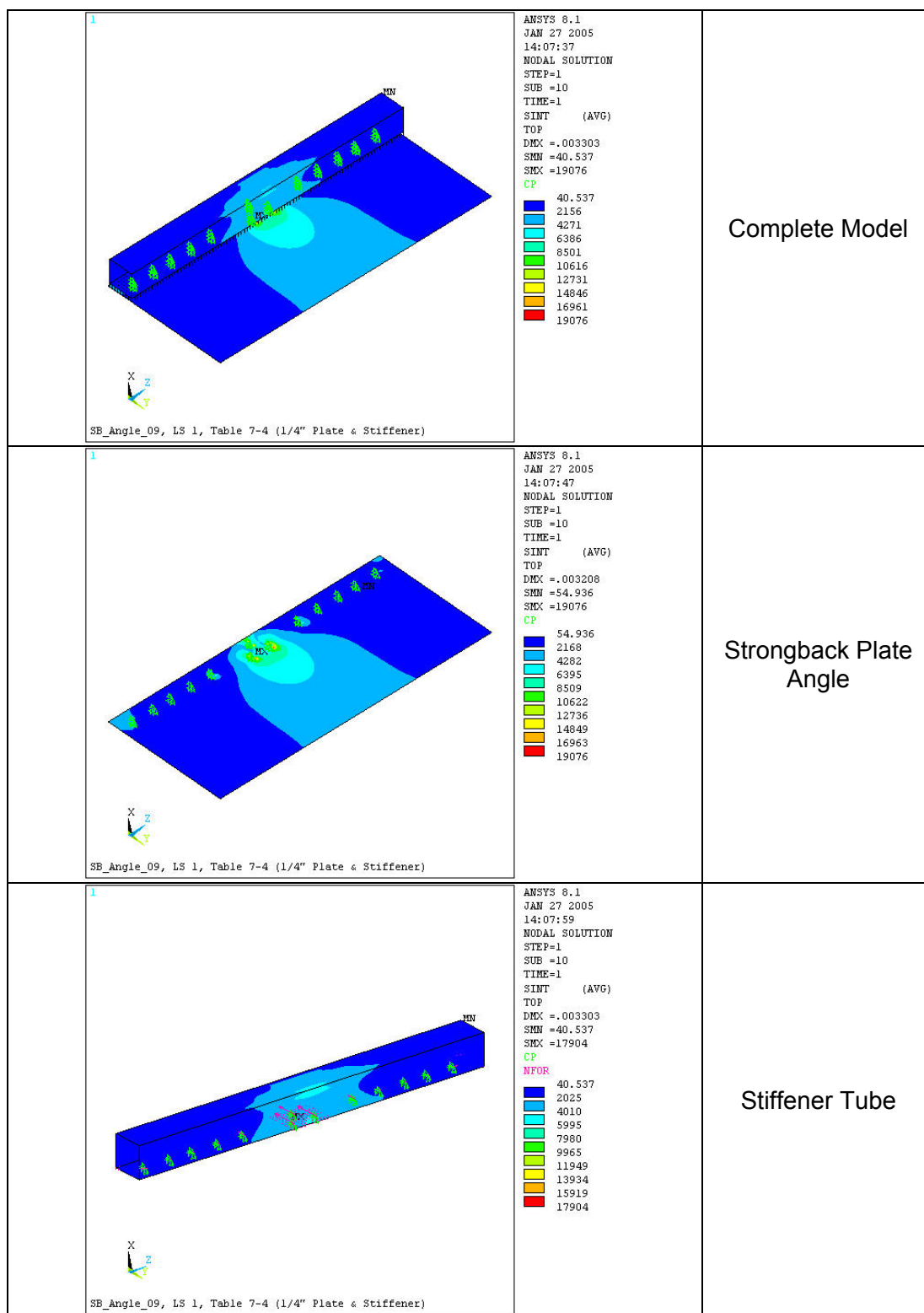


Figure 2.12.5-37 –Top Surface Stresses in Plate Angle Under Pin Block Load Case 1

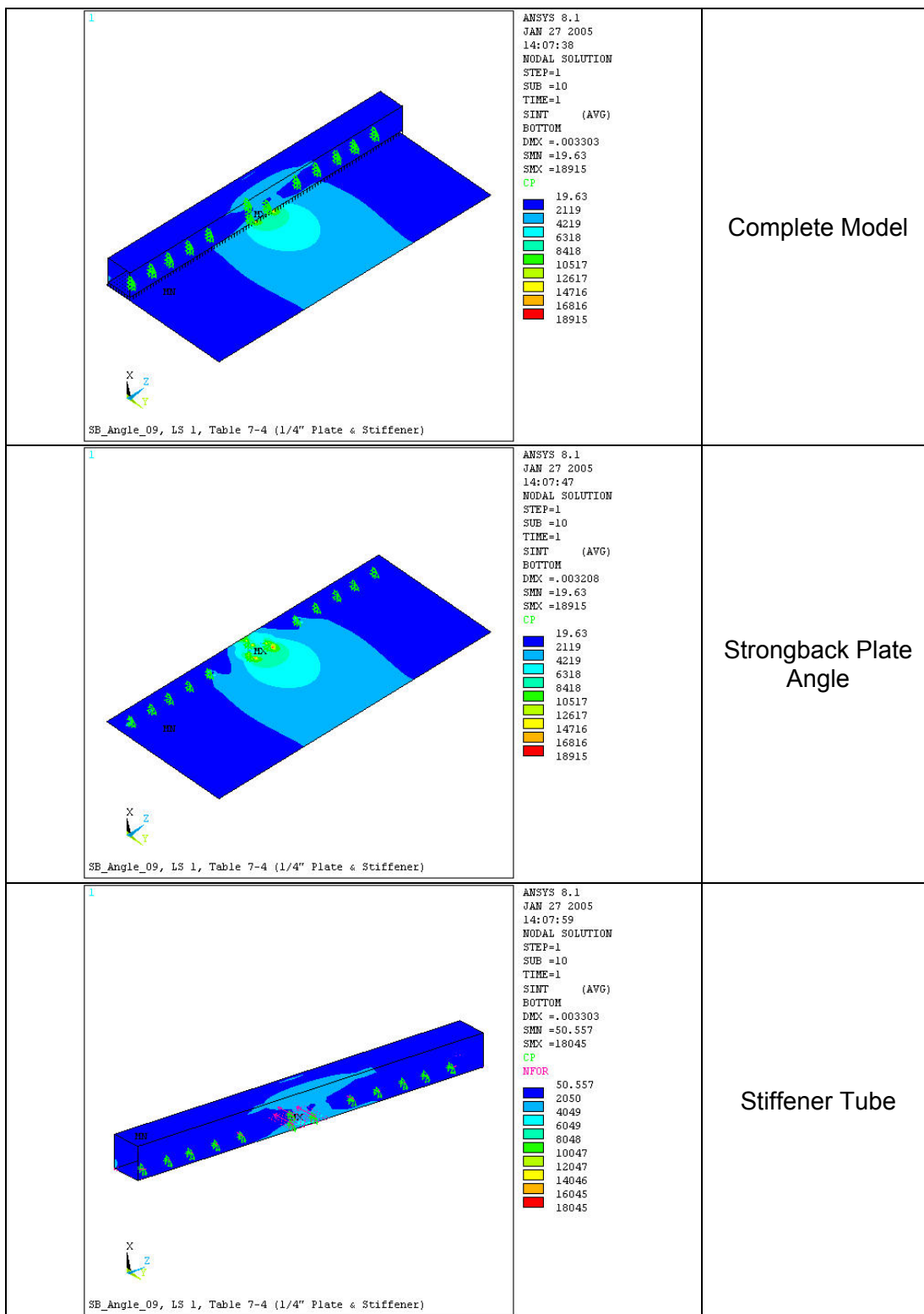


Figure 2.12.5-38 –Bottom Surface Stresses in Plate Angle Under Pin Block Load Case 1

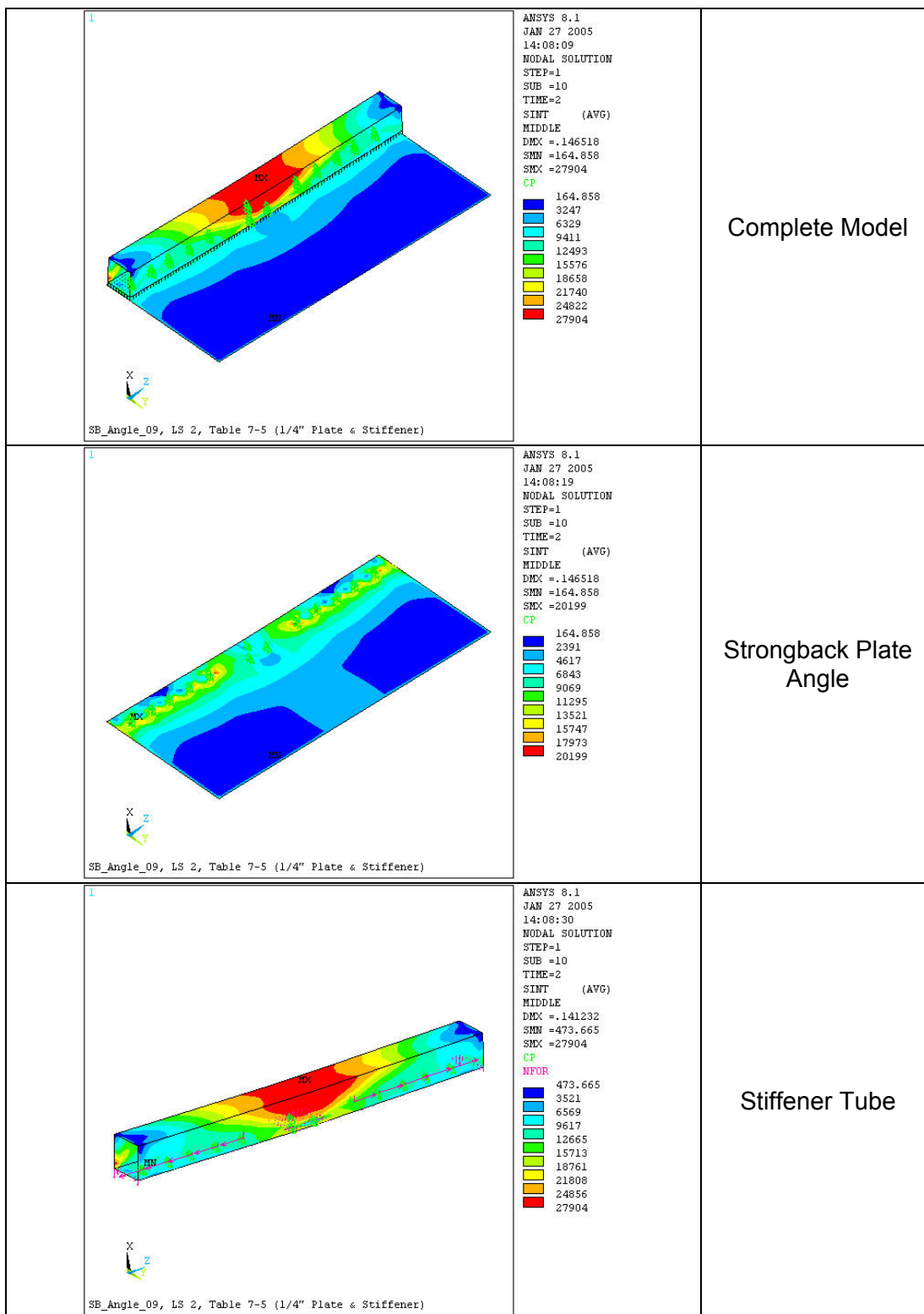


Figure 2.12.5-39 – Mid-thickness Stresses in Plate Angle Under Pin Block Load Case 2

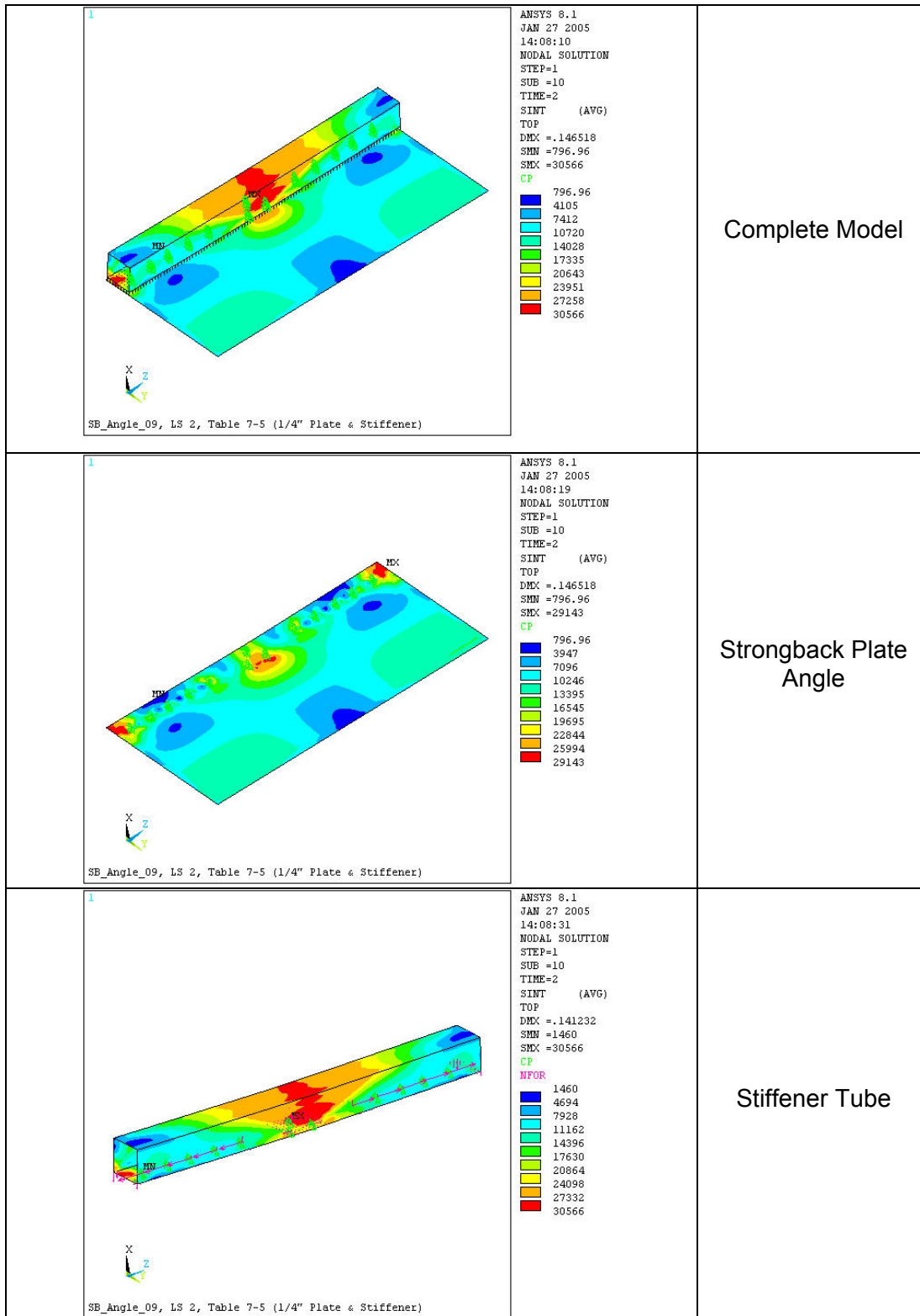


Figure 2.12.5-40 – Top Surface Stresses in Plate Angle Under Pin Block Load Case 2

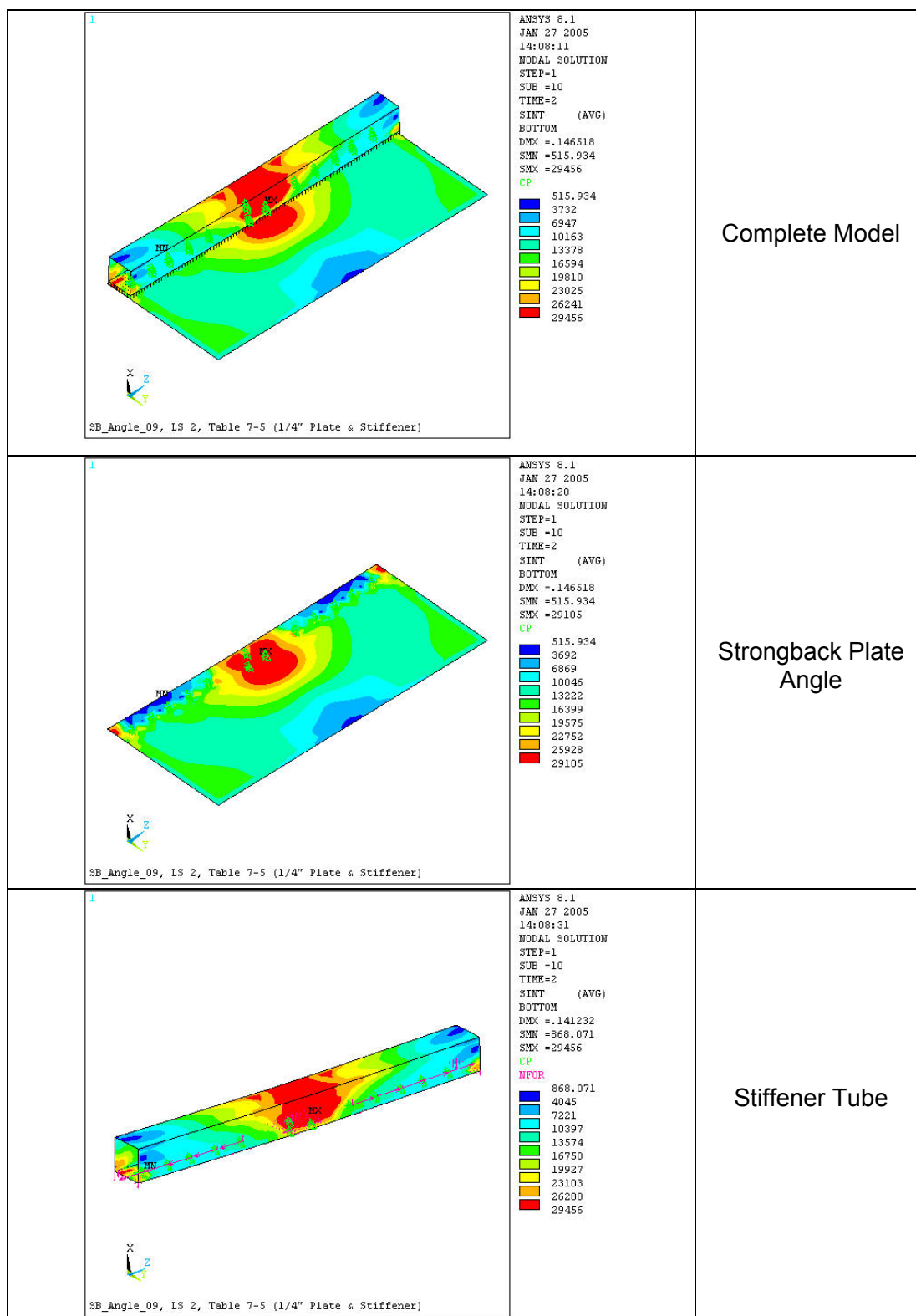


Figure 2.12.5-41 – Bottom Surface Stresses in Plate Angle Under Pin Block Load Case 2

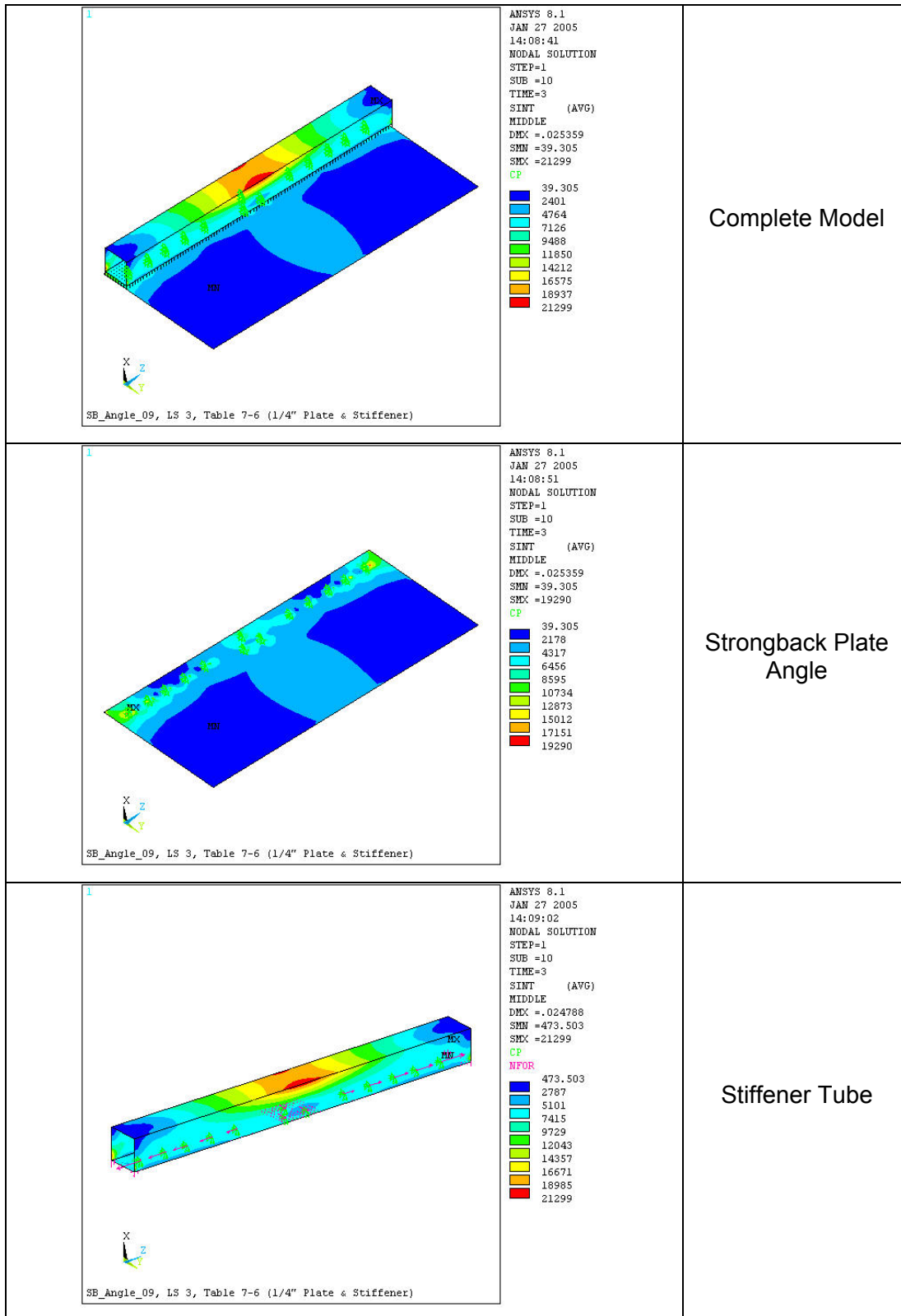


Figure 2.12.5-42 – Mid-thickness Stresses in Plate Angle Under Pin Block Load Case 3

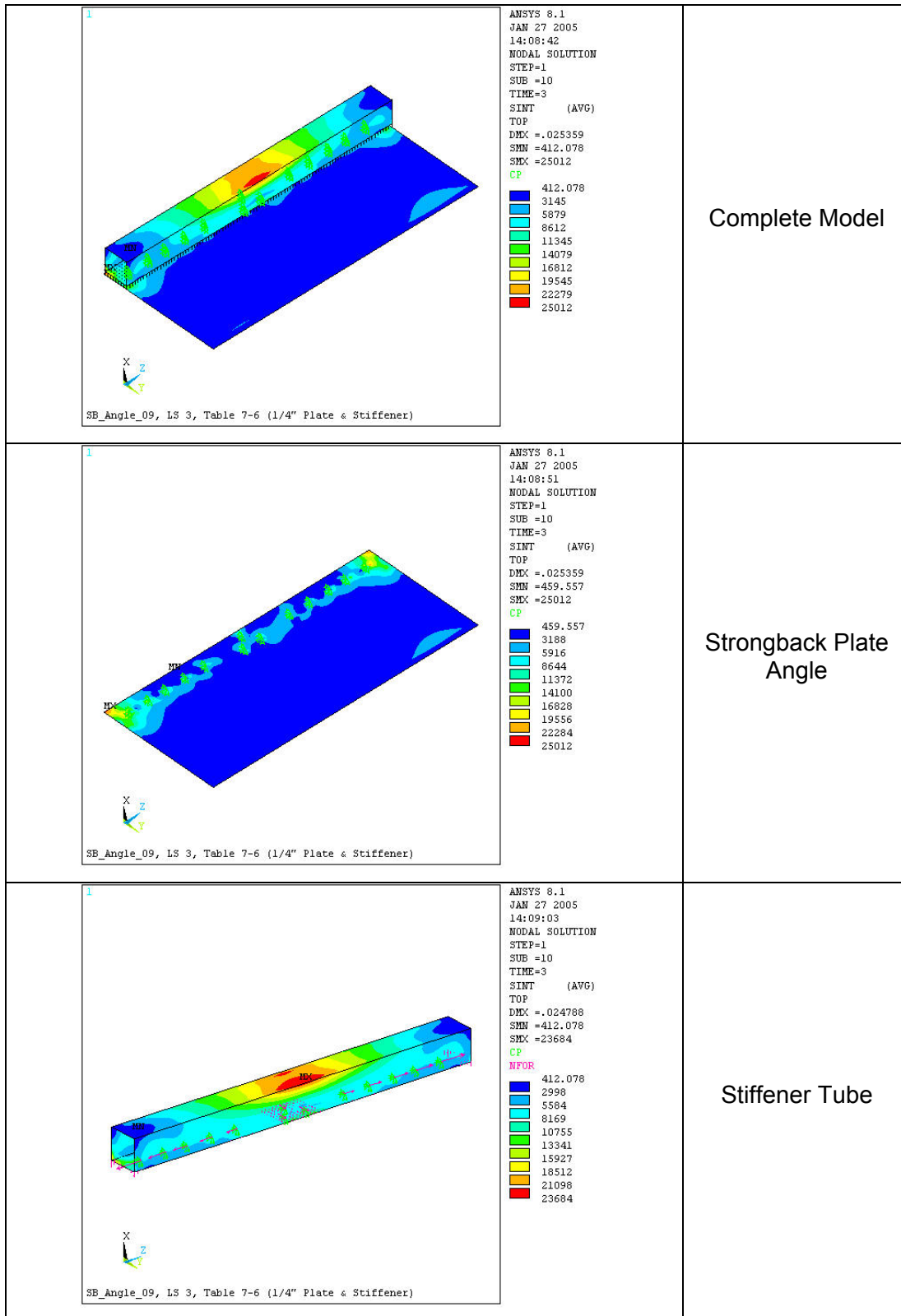


Figure 2.12.5-43 – Top Surface Stresses in Plate Angle Under Pin Block Load Case 3

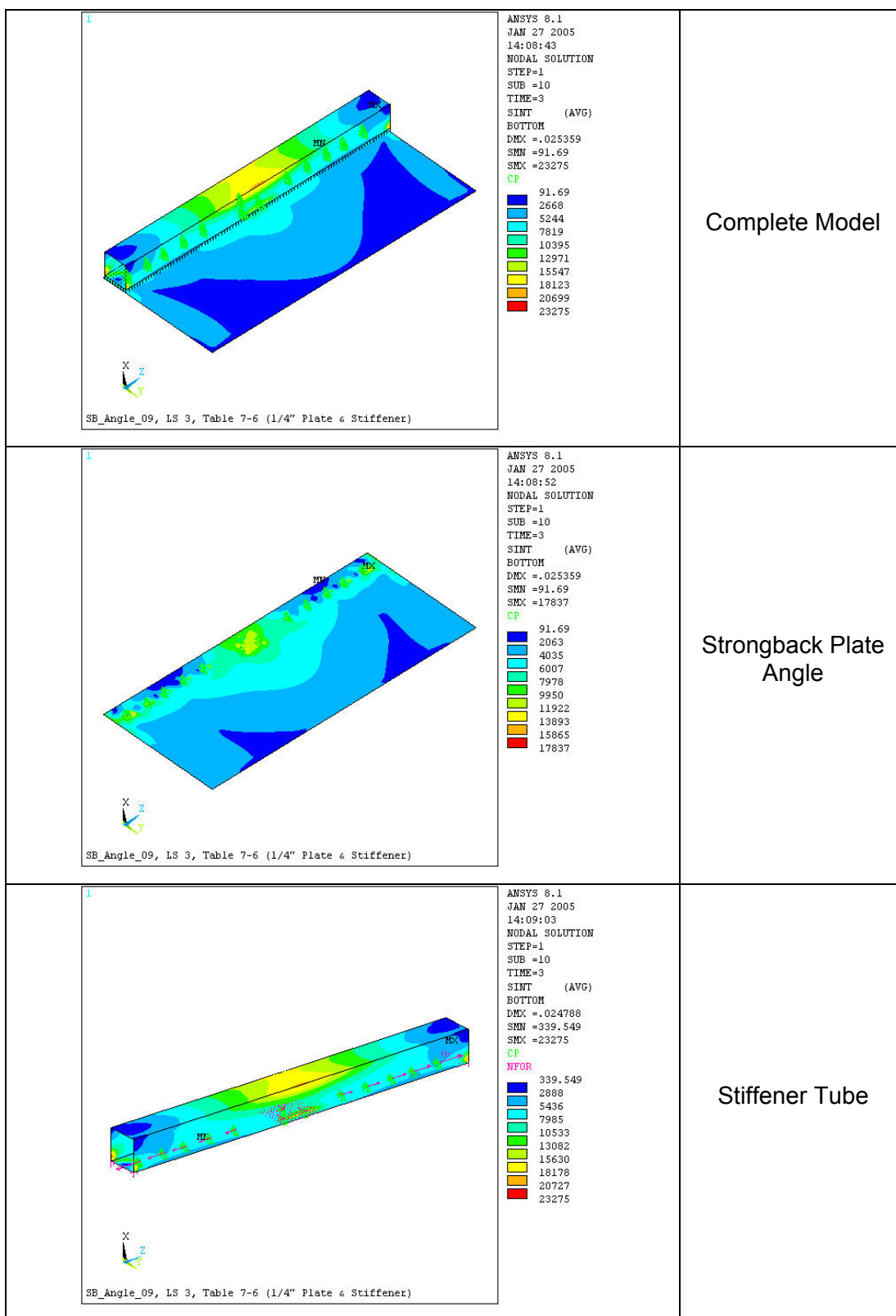


Figure 2.12.5-44 – Bottom Surface Stresses in Plate Angle Under Pin Block Load Case 3

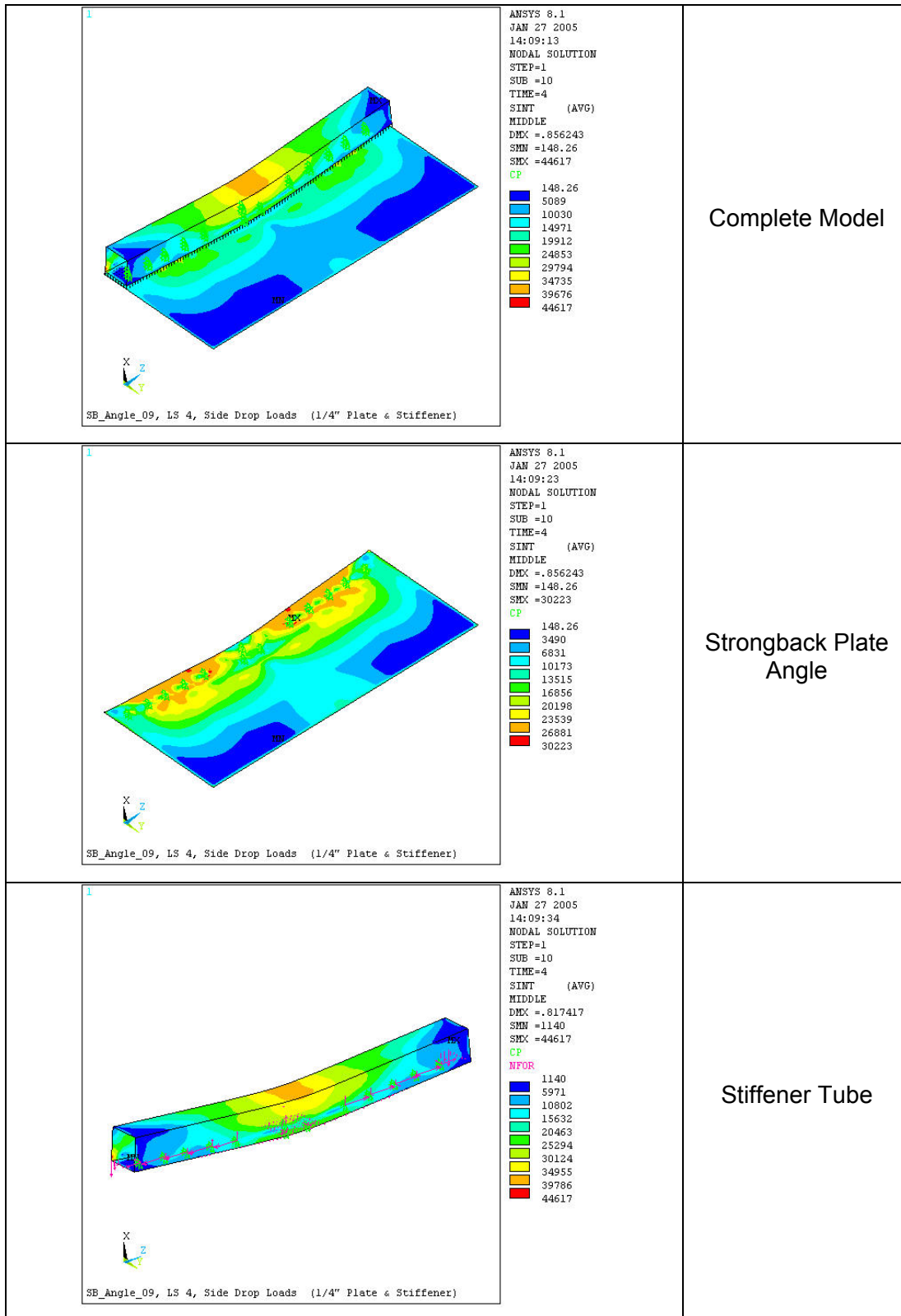


Figure 2.12.5-45 – Mid-thickness Stresses in Plate 20.6-inch Angle Under Pin Block Load Case 4

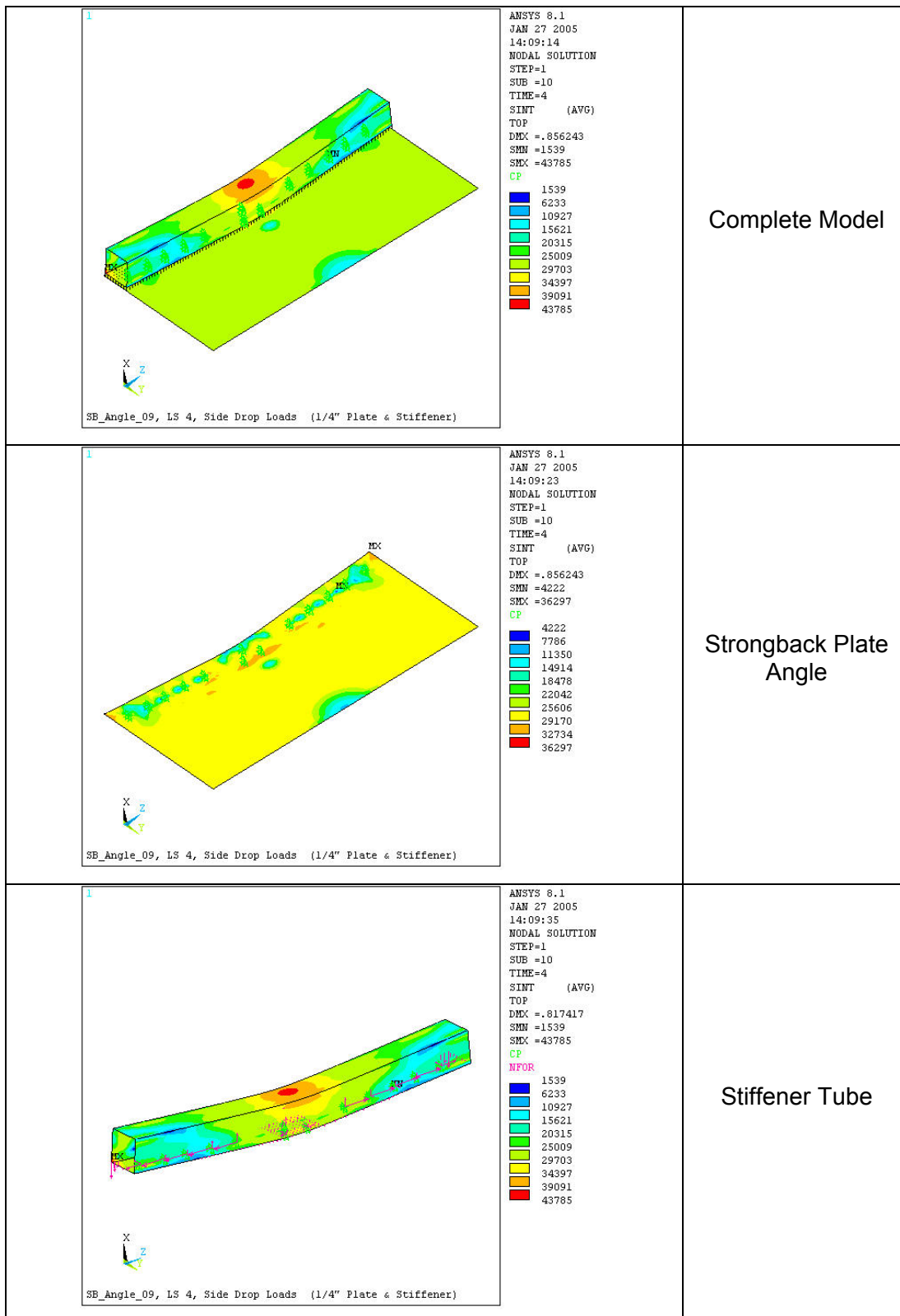


Figure 2.12.5-46 – Top Surface Stresses in 20.6-inch Plate Angle Under Pin Block Load Case 4

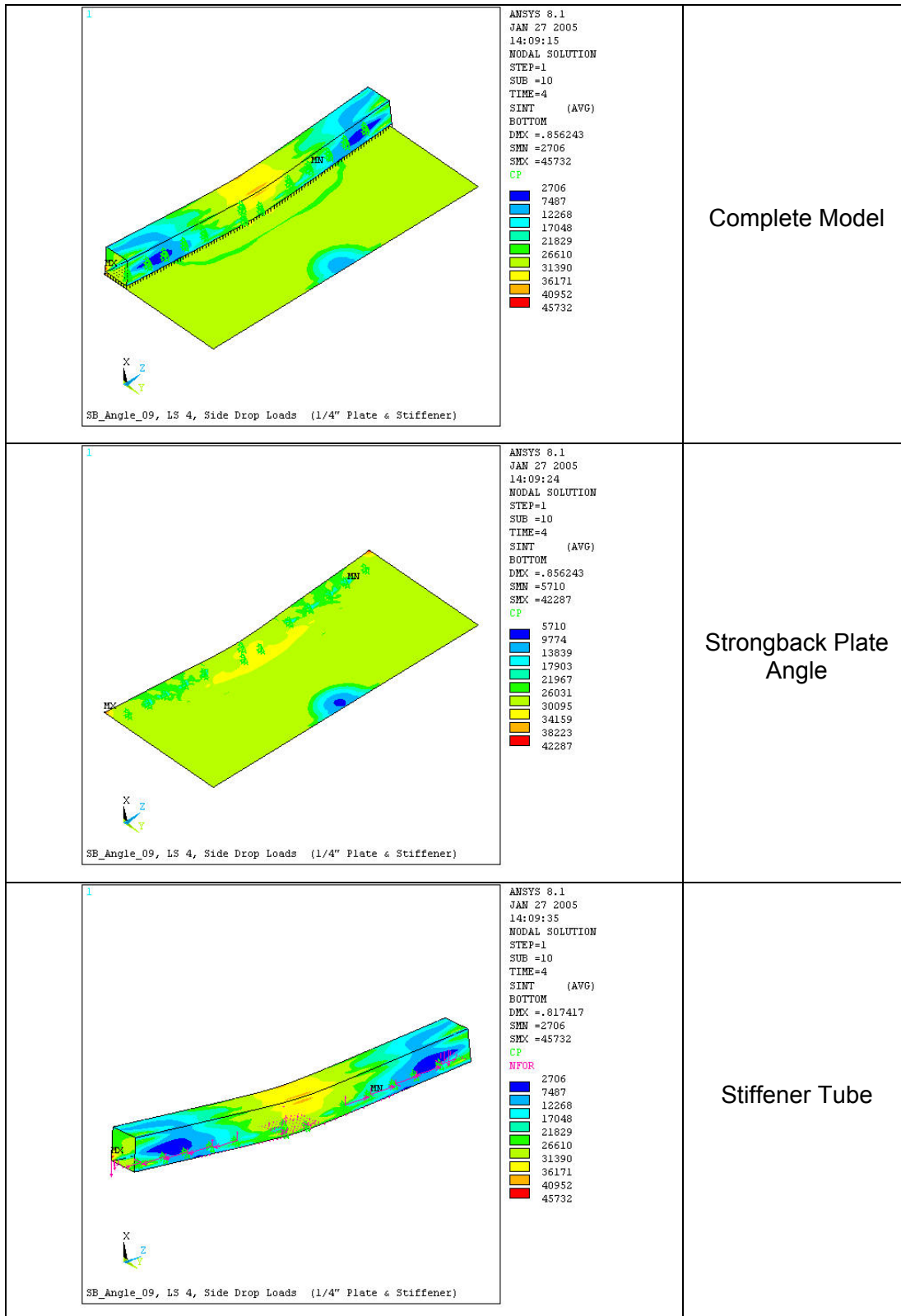


Figure 2.12.5-47 – Bottom Surface Stresses in 20.6-inch Plate Angle Under Pin Block Load Case 4

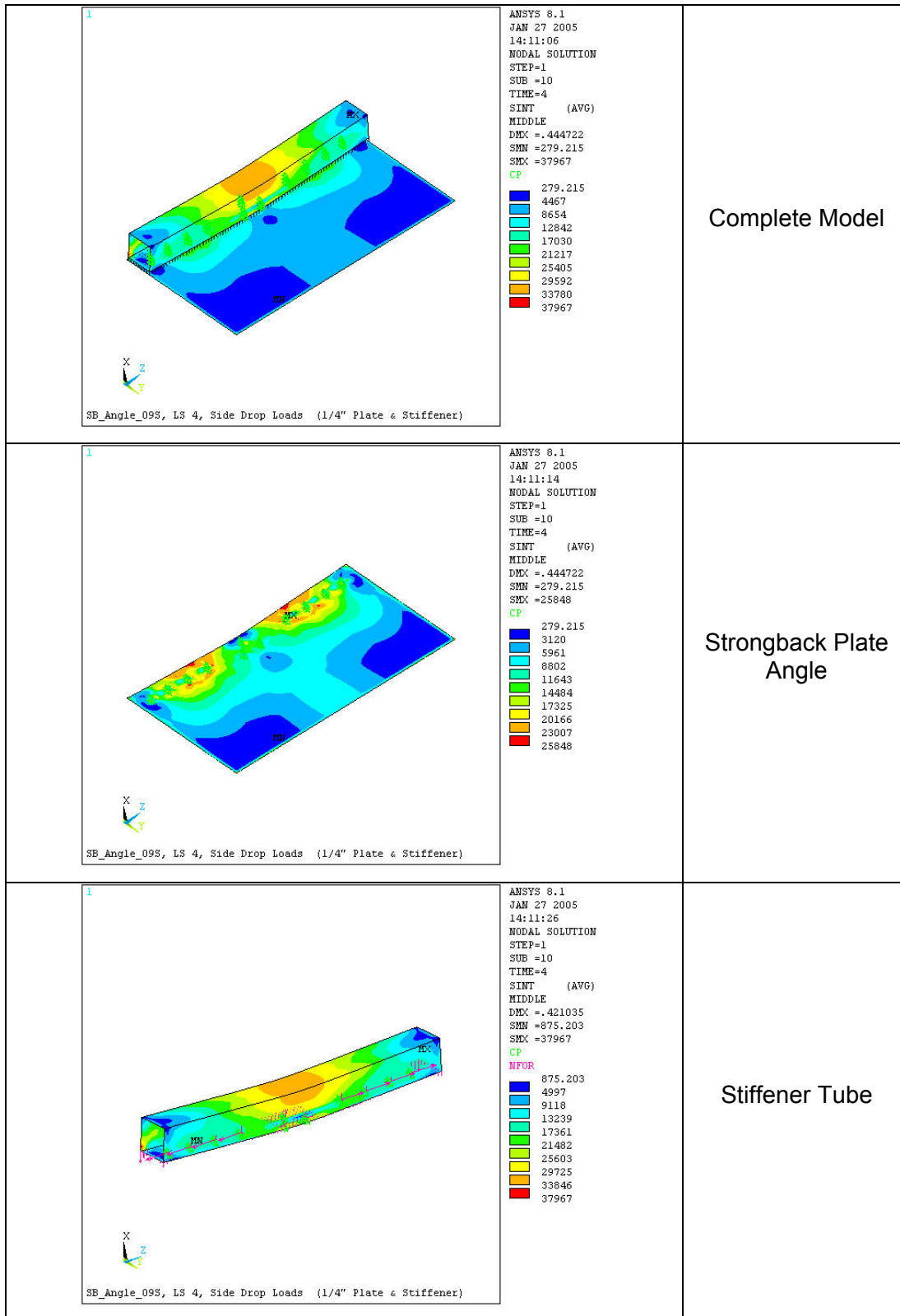


Figure 2.12.5-48 – Mid-thickness Stresses in Plate 17.0-inch Angle Under Pin Block Load Case 4

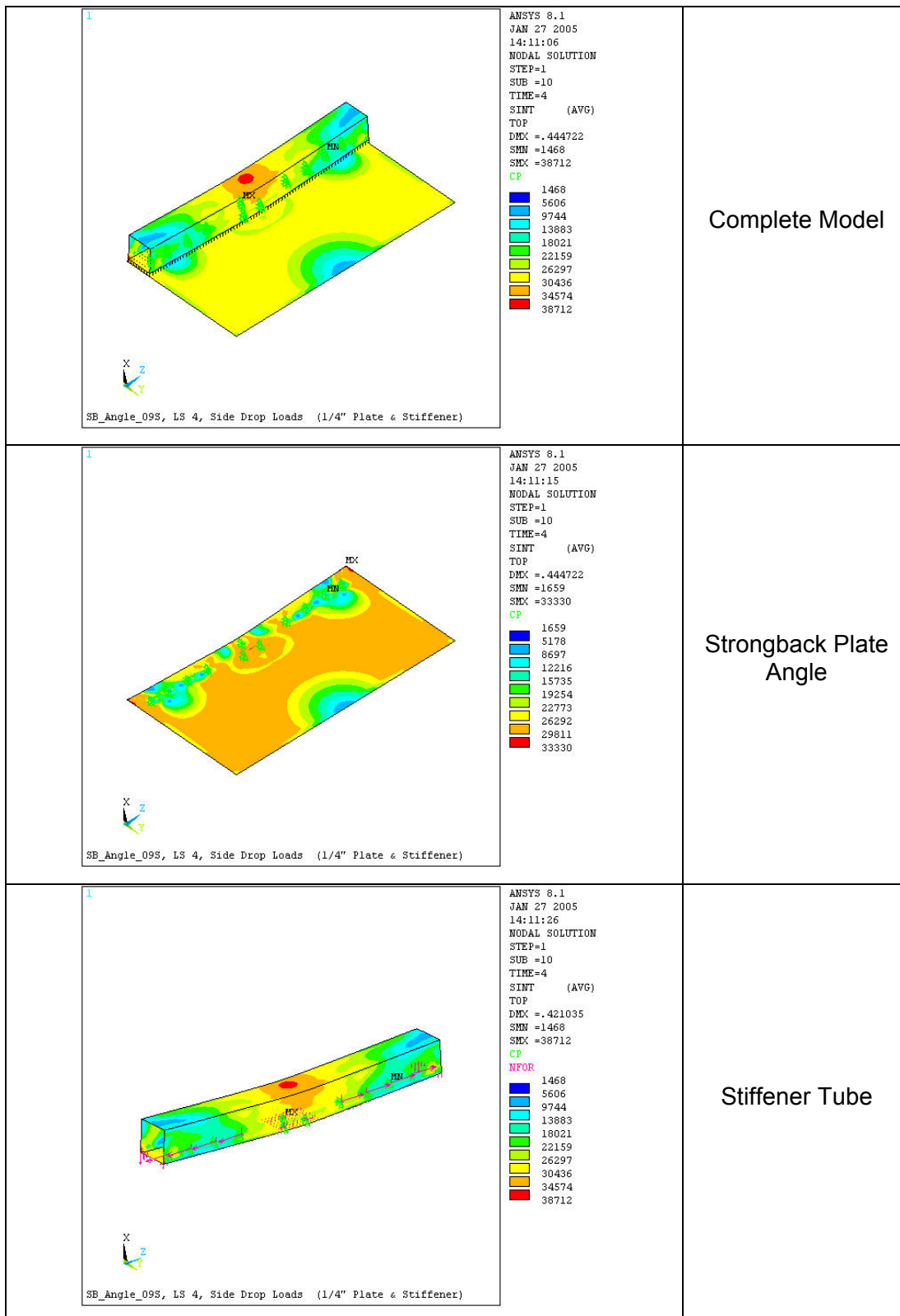


Figure 2.12.5-49 – Top Stresses in Plate 17.0-inch Angle Under Pin Block Load Case 4

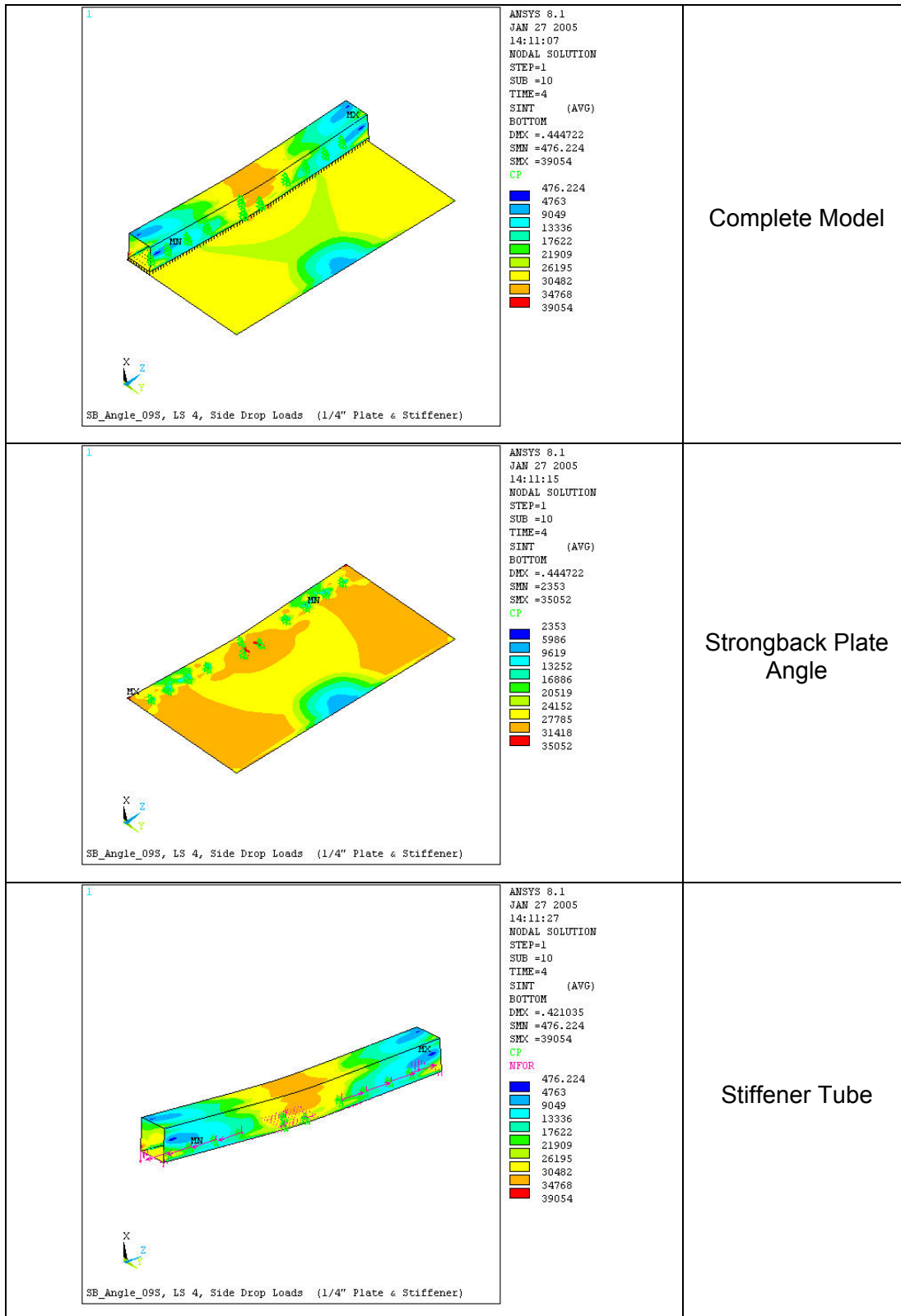


Figure 2.12.5-50 – Bottom Stresses in Plate 17.0-inch Angle Under Pin Block Load Case 4

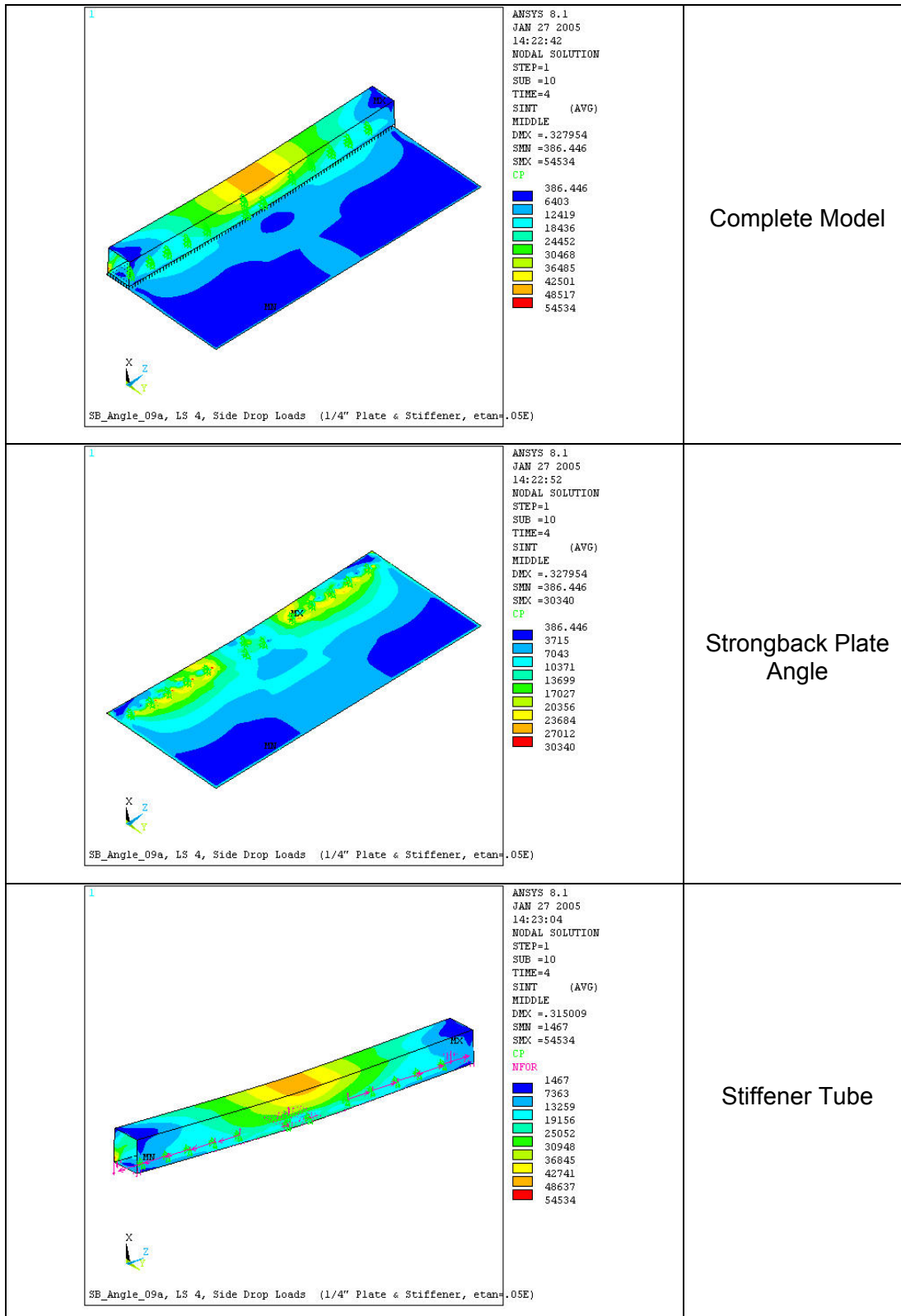


Figure 2.12.5-51 – Midthickness Stresses in 20.6-inch Angle w/ $E_{TAN}=.05E$ Under Pin Block Load Condition 4 (Side Drop)

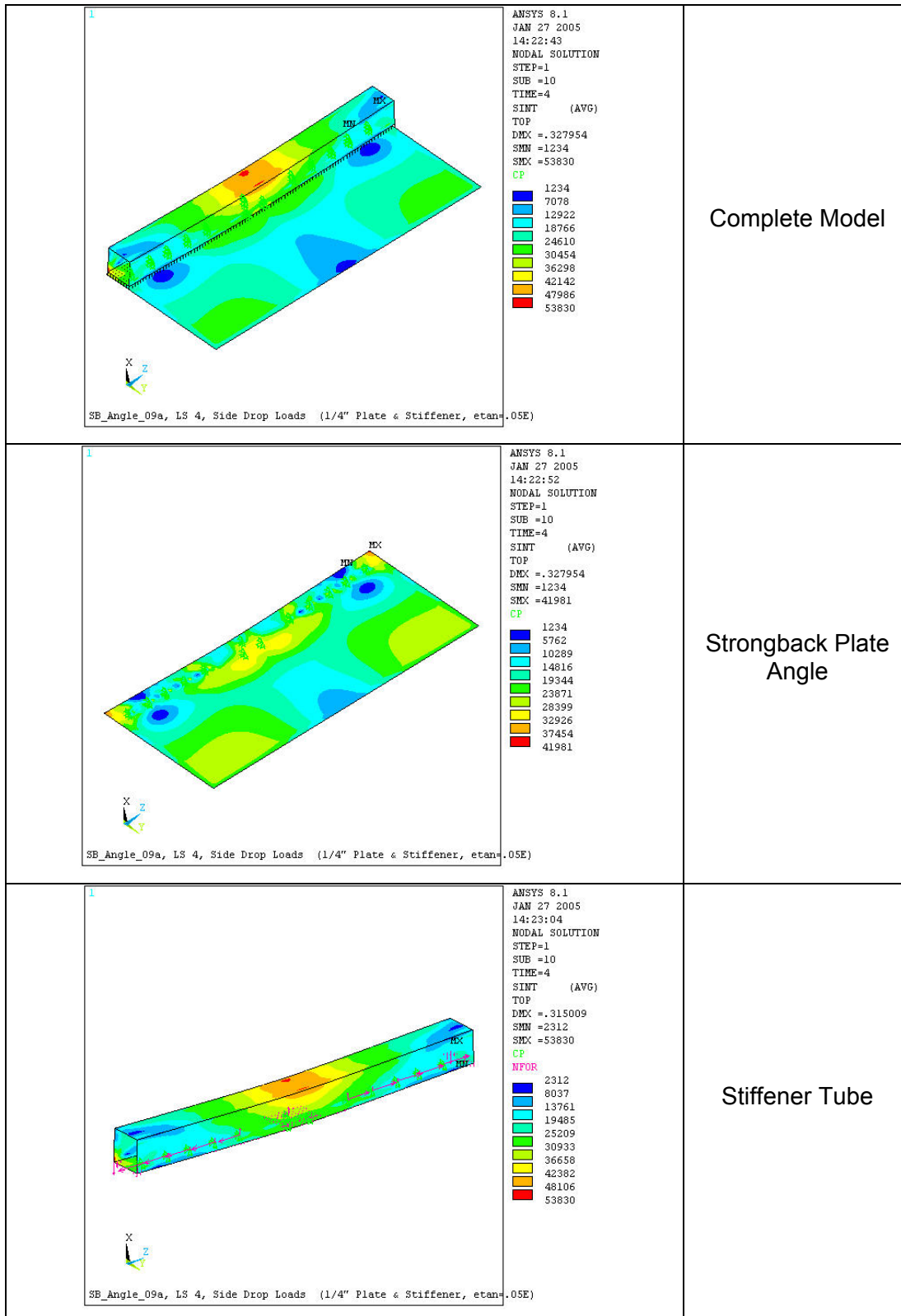


Figure 2.12.5-52 – Top Stresses in 20.6-inch Plate w/ $E_{Tan} = .05E$ Under Pin Block Load Condition 4 (Side Drop)

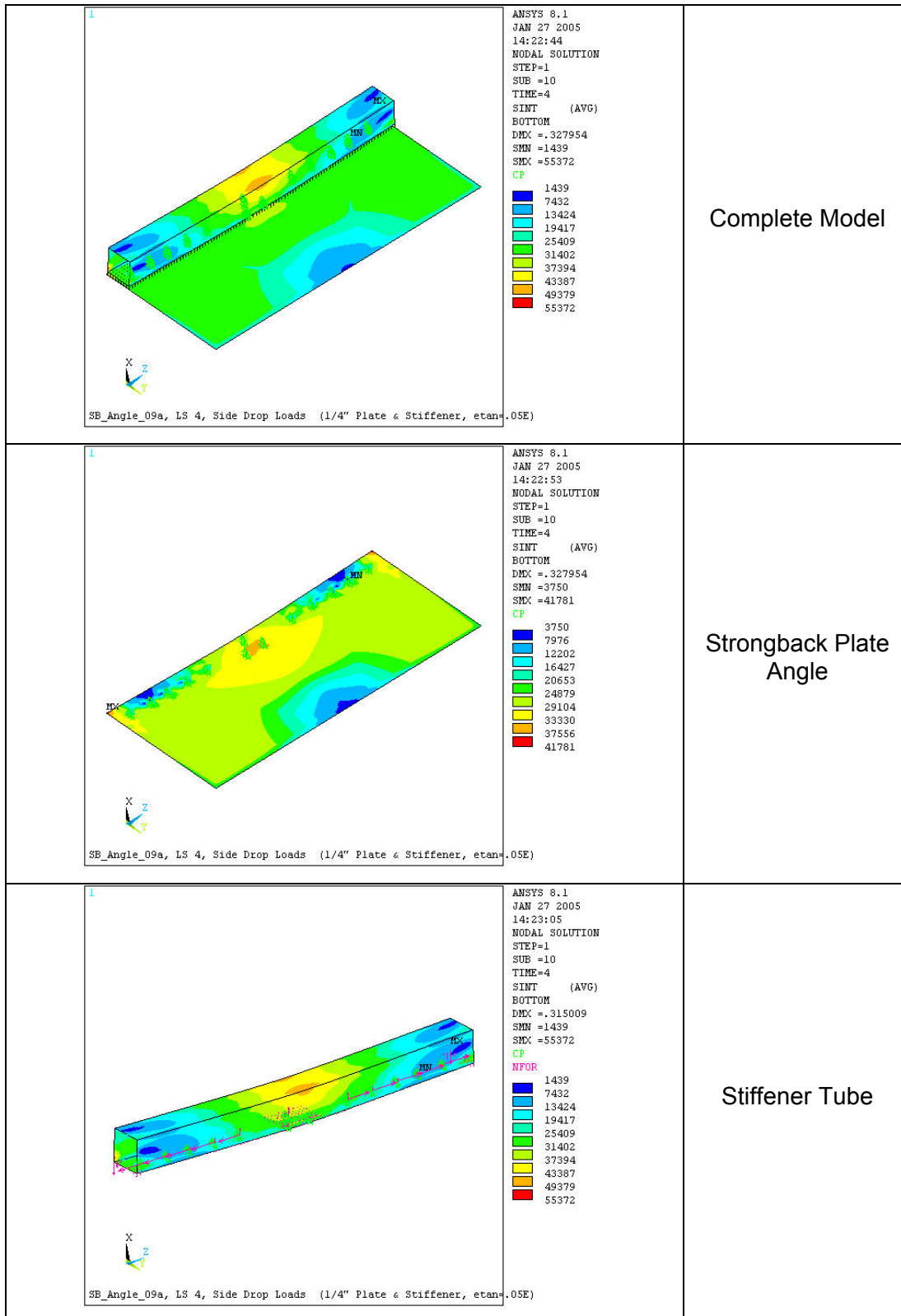


Figure 2.12.5-53 – Bottom Stresses in 20.6-inch Angle w/ $E_{Tan} = .05E$ Under Pin Block Load Condition 4 (Side Drop)

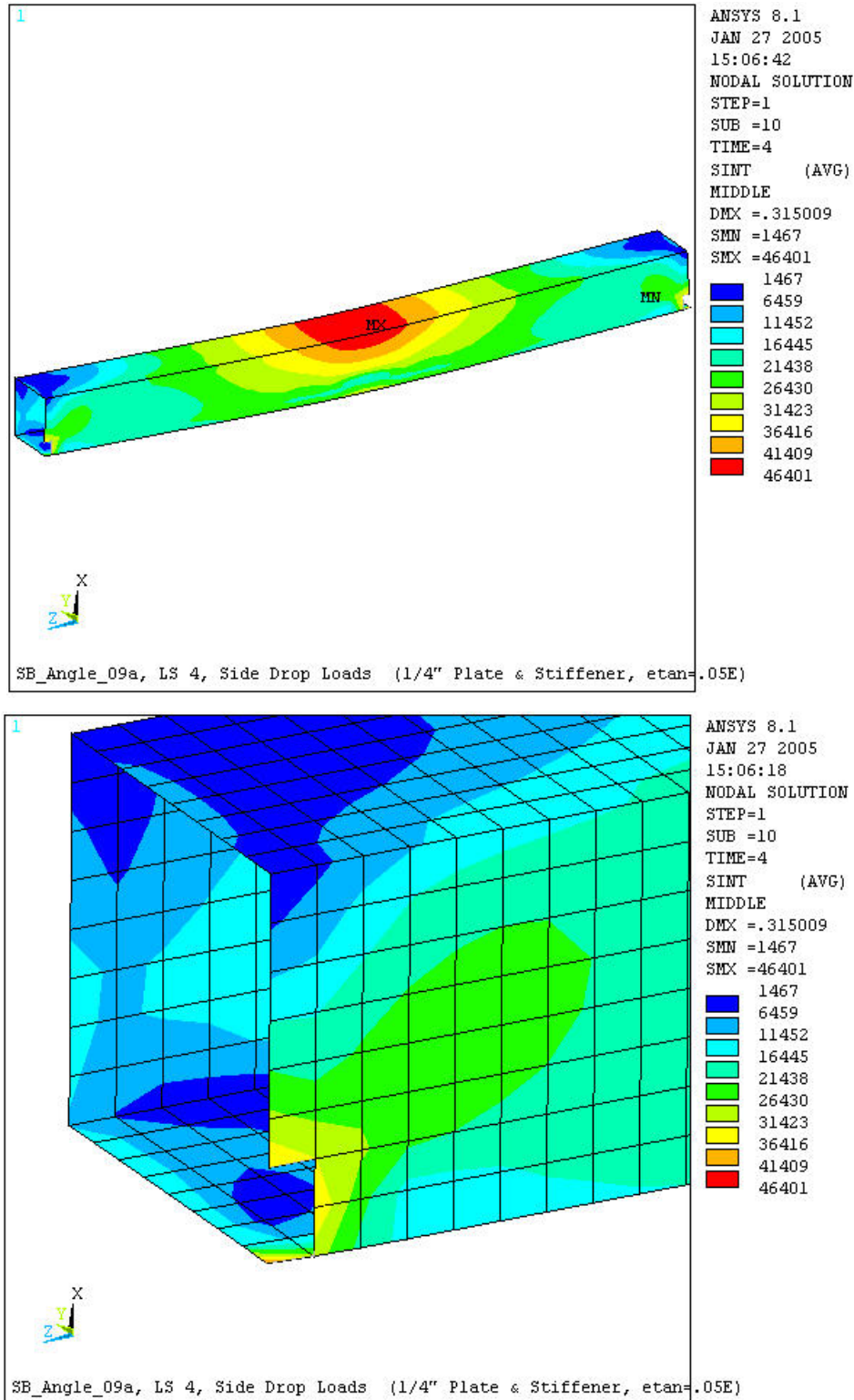


Figure 2.12.5-54 – Stiffener Tube Side Drop Midthickness Stress, 2 nodes Removed (Top) and Detail (Bottom), $E_{Tan} = .05E$

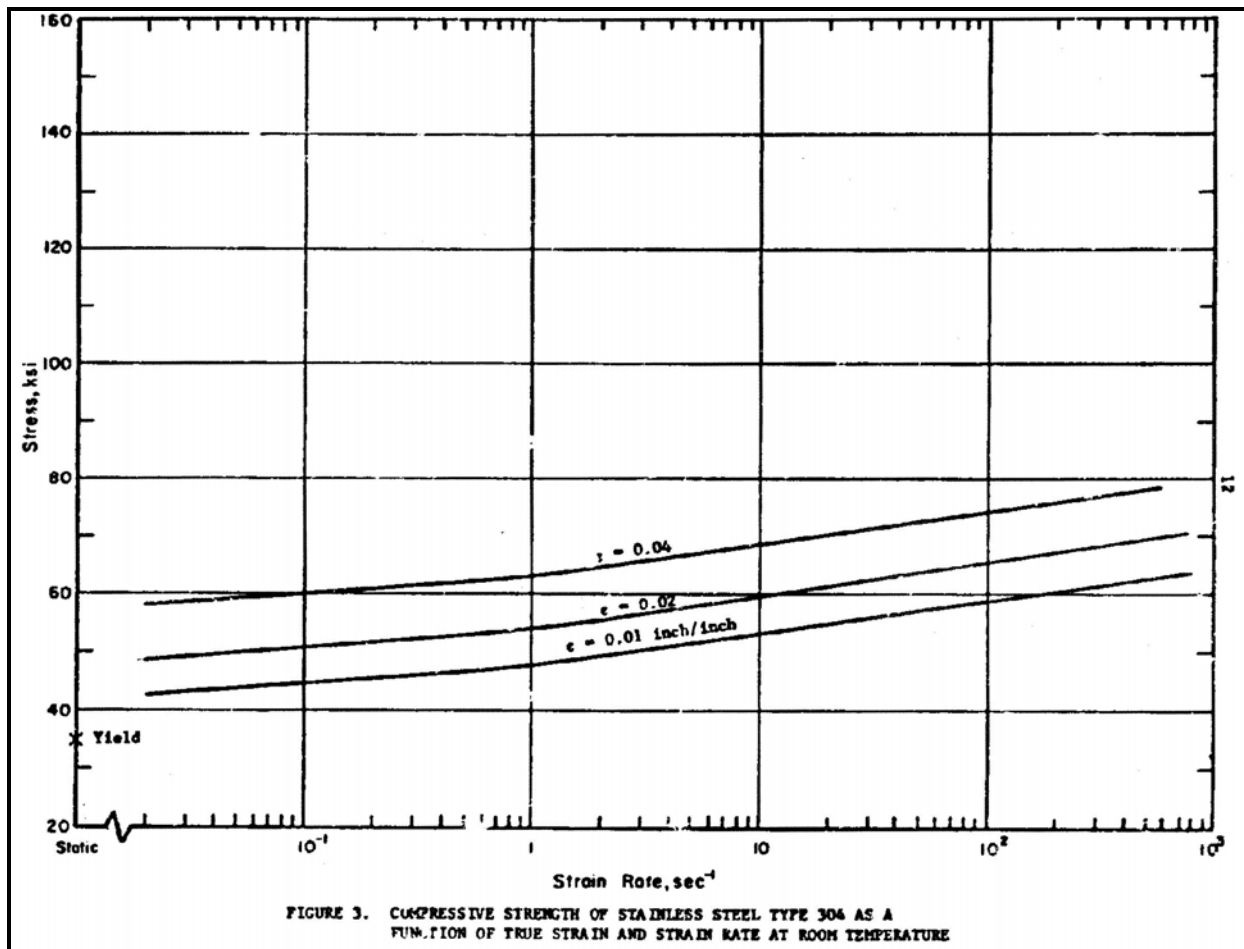


Figure 2.12.5-55 – Strain Rate Data for Type 304 Stainless Steel

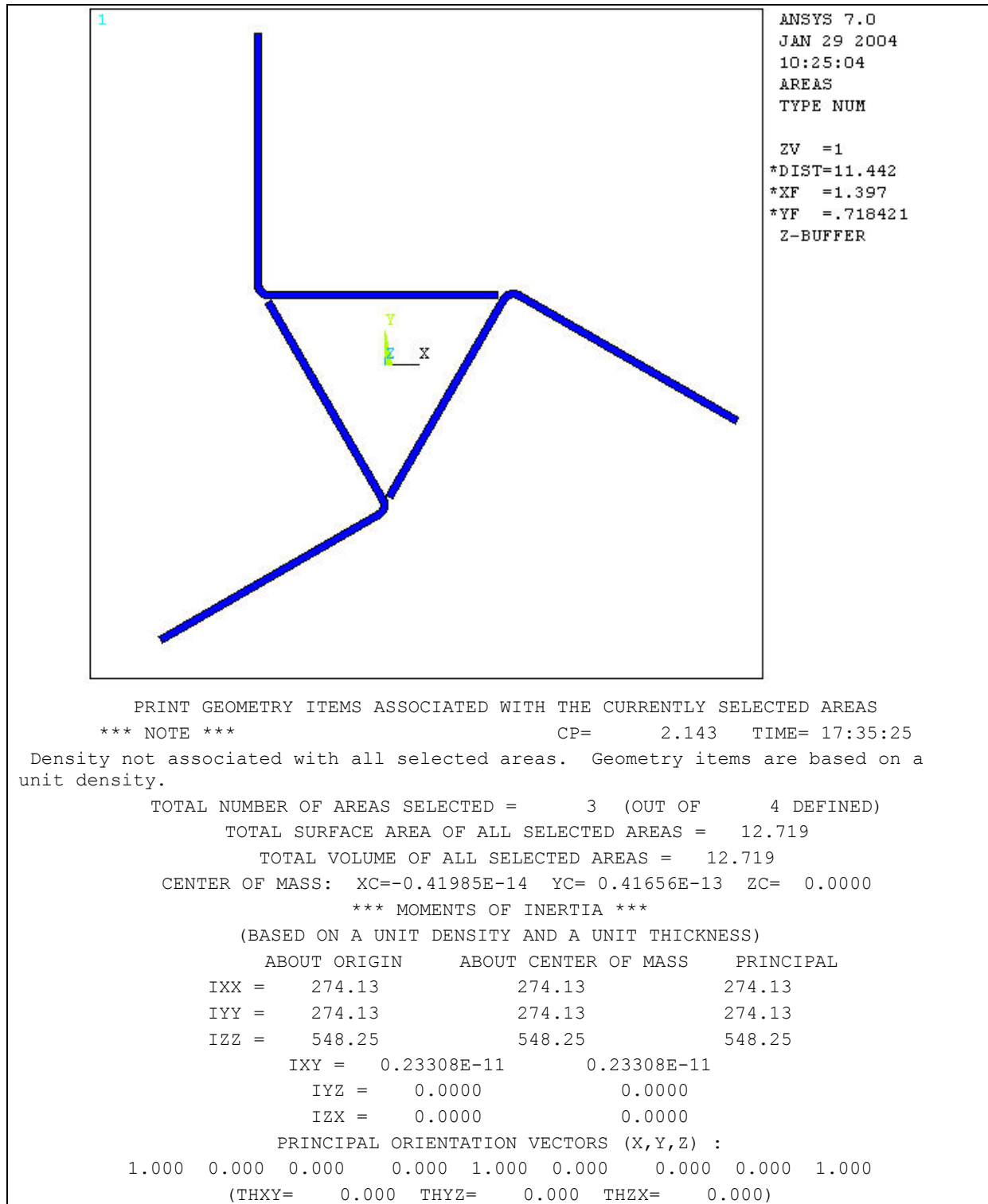


Figure 2.12.5-56 – Geometry Used to Determine Section Properties

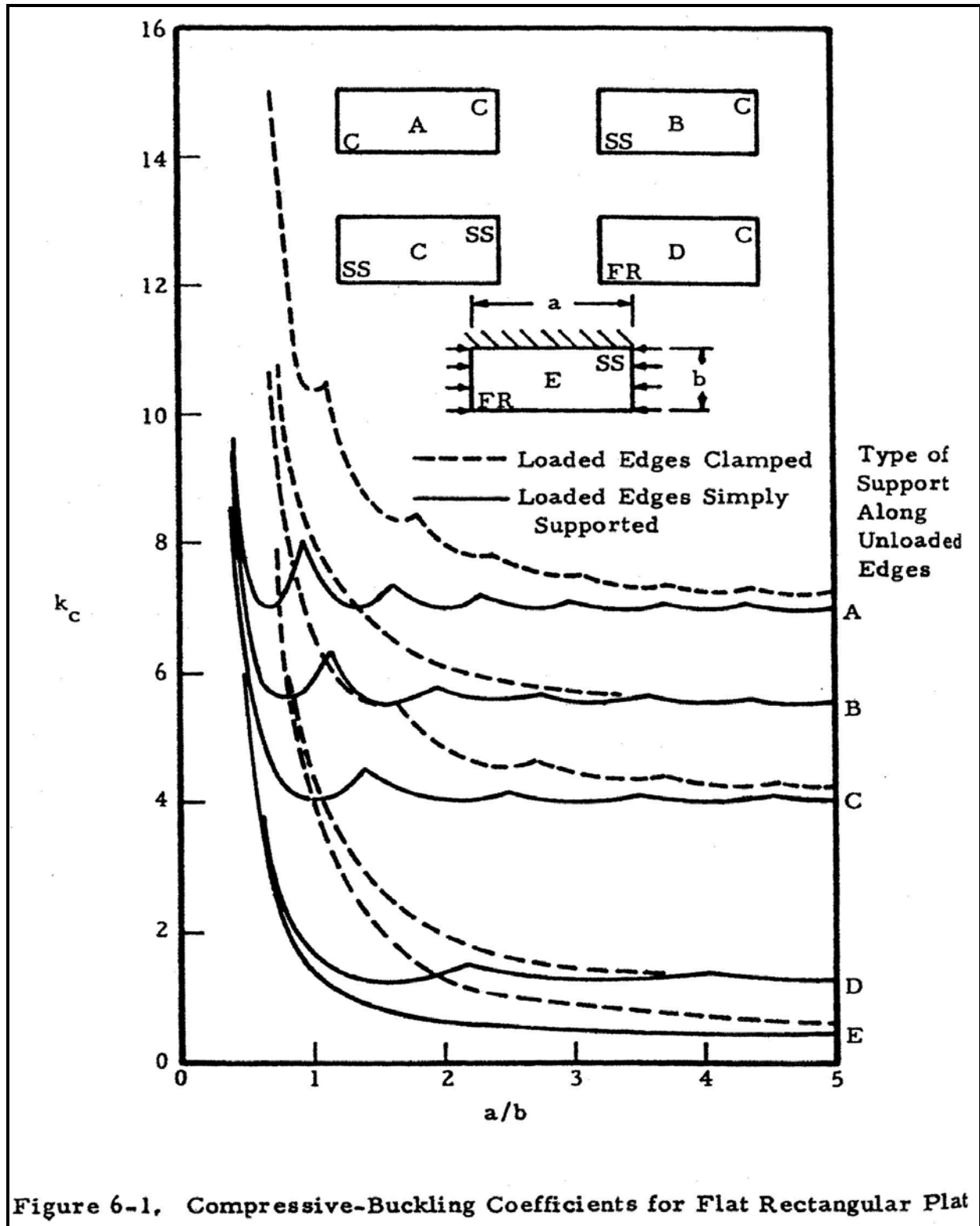


Figure 2.12.5-57 – Plate Stability Constants from *Stress Analysis Manual*

2.12.5.21 Representative ANSYS® Input Files

2.12.5.21.1 FCS Finite Element Model

This input file is representative of the FCS finite element analysis described in Section 2.12.5.10.

```

/prep7                                !Generate Box
!"Box"                                k,1,0,0,0
ET,1,SOLID45                          k,2,b_wid,0,0
nuxy,1,.29                           k,3,b_wid,b_thk,0
ex,1,27.6e6                          k,4,b_thk,b_thk,0
TB,kin,1,1,2,                        k,5,b_thk,b_wid,0
TBTEMP,0                             k,6,0,b_wid,0
TBDATA,,25000,219970                1,1,2
!"Stiffener"                        1,2,3
ET,2,SOLID45                        1,3,4
nuxy,2,.29                          1,4,5
dens,2,493/1728                    ! weight density 1,5,6
ex,2,27.6e6                        1,6,1
TB,kin,2,1,2,                      !FILLT,4,3,b_thk, ,
TBTEMP,0                          !FILLT,1,6,b_thk*2, ,
TBDATA,,47100, 291933              a,9,2,3,8
!"Gap Stiffness Value"             a,9,8,7,10
gstiff=4e6                         a,7,5,6,10
!"Contact for the stiffener"        vext,all,,,0,0,S_wid/2-s_thk
et,5,contac49                     asel,s,area,,4
!mp,mu,5,0.25                     asel,a,area,,9
r,5,gstiff                         asel,a,area,,13
keyopt,5,3,0                      vext,all,,,0,0,s_thk
keyopt,5,7,1                      asel,s,area,,17
!"Contact for the Pin Block"        asel,a,area,,22
et,7,contac49                     asel,a,area,,26
!mp,mu,7,0.25                     vext,all,,,0,0,z1-e_wid/2
r,7,gstiff                         asel,s,area,,30
keyopt,7,3,0                     asel,a,area,,35
keyopt,7,7,1                     asel,a,area,,39
!"Contact for the Hinge Block"      vext,all,,,0,0,e_wid/2
et,9,contac49                     asel,s,area,,43
!mp,mu,9,0.25                     asel,a,area,,48
r,9,gstiff                         asel,a,area,,52
keyopt,9,3,0                     vext,all,,,0,0,e_wid/2
keyopt,9,7,1                     asel,s,area,,56
!"Pin Block"                       asel,a,area,,61
ET,10,SOLID45                     asel,a,area,,65
nuxy,10,.29                       vext,all,,,0,0,b_len/2-z1-e_wid/2
dens,10,493/1728                  ! weight density alls
ex,10,27.6e6                      !Generate Stiffener
TB,kin,10,1,2,                    real,2
TBTEMP,0                          type,2
TBDATA,,47100, 291933            mat,2
!"Hinge Block"                    k,100,2*b_thk,0,0
ET,11,SOLID45                     k,101,2*b_thk,-s_thk,0
nuxy,11,.29                       k,103,b_wid,0,0
dens,11,493/1728                  ! weight density k,102,b_wid,-s_thk,0
ex,11,27.6e6                      a,100,101,102,103
TB,kin,11,1,2,                   vext,82,,,0,0,S_wid/2-s_thk
TBTEMP,0                         vext,83,,,0,0,s_thk
TBDATA,,47100, 291933            vext,90,,,0,-s_hgt+s_thk
ET,12,beam4                       asel,s,area,,84
R,12,10*0.05,10*0.000192,10*0.000192
!10*0.25,10*0.25                 asel,a,area,,89
nuxy,12,.29                       asel,a,area,,97
dens,12,0                         ! weight density vext,all,,,2*b_thk-s_hgt
ex,12,27.6e6                     local,11,0,0,0,1,45,0,
pi=3.1415926                     vsymm,y,19,24,1,500
!"Global Box"                     FLST,2,6,6,ORDE,4
b_len=17.5                       FITEM,2,22
b_wid=9.0 !box side length        FITEM,2,-24
b_thk=0.13                       FITEM,2,28
!"stiffener"                     FITEM,2,-30
s_wid=1.5 !stiffener width        VOV LAP, P51X
s_hgt=2.0 !stiffener height       FLST,5,15,6,ORDE,4
s_thk=0.25                       FITEM,5,2
thickness                         FITEM,5,5
!"End Piece"                     FITEM,5,31
e_wid=0.5                        !width        FITEM,5,-43
e_hgt=1.0                        !height       !Pin Block
e_thk=0.13                       !thickness  csys,0
!"Pin Block Piece"               k,1000,b_wid,-s_thk,0
p_wid=s_wid-s_thk*2              k,1001,b_wid-p_len,-s_thk,0
p_len=2.0                        !height      k,1002,b_wid-p_len,-s_thk-p_thk,0
p_thk=0.375                      !thickness k,1003,b_wid,-s_thk-p_thk,0
!"Hinge Block Piece"            a,1000,1001,1002,1003
h_wid=8.50/2                     vext,99,,,,,p_wid/2
h_len=2.0                        !width (z)    !Hinge Block
h_thk=0.375                      !height (y) k,2000,-s_thk,b_wid,0
!"Stiffener Locations"          k,2001,-s_thk,b_wid-h_len,0
z1=b_len/2-0.5 !center of 1st   k,2002,-s_thk-h_thk,b_wid-h_len,0
stiffener                       k,2003,-s_thk-h_thk,b_wid,0
z2=b_len/2 !center of 2nd stiffener
a,2000,2001,2002,2003
z3=b_len-5 !center of 3rd stiffener vext,106,,,,,s_wid/2-s_thk
vext,108,,,,,s_thk

vext,130,,,,,h_wid-s_wid/2
vext,137,,,,,s_thk
alls
!Devide things up by temporary Areas
!block,x1,x2,y1,y2,z1,z2
block,b_wid-0.5,-5,b_wid-0.5,-5,-5,b_len
vsel,u,volu,,30
VSBA,all, 197
VSBA,all, 199
alls
vdele,30,,,1
block,b_wid-1.0,-5,b_wid-1.0,-5,-5,b_len
vsel,u,volu,,1
VSBA,all, 7
VSBA,all, 18
alls
vdele,1,,,1
block,b_wid/2,-5,b_wid/2,-5,-5,b_len
vsel,u,volu,,1
VSBA,all, 7
VSBA,all, 18
alls
vdele,1,,,1
block,b_thk*2+0.5,-5,b_thk*2+0.5,-5,-5,b_len
vsel,u,volu,,1
VSBA,all, 7
VSBA,all, 18
alls
vdele,1,,,1
!Devide the where the pin block is
block,b_wid,b_wid-p_len,0.5,-s_hgt,-5,b_len
vsel,u,volu,,1
VSBA,all, 17
alls
vdele,1,,,1
block,b_wid,-s_hgt*2,0.5,-s_thk-p_thk,-5,b_len
vsel,u,volu,,1
VSBA,all, 5
alls
vdele,1,,,1
!Devide the where the hinge block is
block,1,-s_hgt*2,b_wid+1,b_wid-h_len,-5,b_len
vsel,u,volu,,1
VSBA,all, 5
alls
vdele,1,,,1
block,b_wid+1,-s_thk-h_thk,b_wid+1,-s_hgt*2,-5,b_wid
vsel,u,volu,,1
VSBA,all, 4
VSBA,all, 17
alls
vdele,1,,,1
block,b_wid+1,-s_thk-h_thk,b_wid+1,-s_hgt*2,-5,3.25 !2.5
hinge block key
vsel,u,volu,,1
VSBA,all, 4
alls
vdele,1,,,1
VSEL,S,loc,x,0,b_wid
VSEL,r,loc,y,0,b_wid
!Add mass of borai and end angles to main angle
vsum
*get,vangle,volu,all,volu
dplus=8/(2*vangle)
dtotal=dplus+(493/1728)
dens,1,dtotal
vatt,1,1,1
vsel,inve
vatt,2,2,2
vsel,s,volu,,66
vsel,a,volu,,76
vsel,a,volu,,99
vatt,10,10,10
vsel,s,volu,,20
vsel,a,volu,,77
vsel,a,volu,,86

```

```

vsel,a,volu,,90
vsel,a,volu,,63
vsel,a,volu,,65
vsel,a,volu,,125
vsel,a,volu,,158
vsel,a,volu,,162
vsel,a,volu,,189
vsel,a,volu,,191,199
vsel,u,volu,,195
vatt,11,11,11
vsel,s,volu,,49
vsel,a,volu,,68
vsel,a,volu,,185
vdele,all,,1
alls
!Add Pin Hole
vext,105,,,.875,,
vsel,s,volu,,1
vatt,10,10,10
alls
!Add Hinge Hole
vext,129,,,.75,
vsel,s,volu,,24
vatt,11,11,11
alls
vext,805,,,.75,
vsel,s,volu,,49
vatt,11,11,11
alls
!pin block mods
vext,5,,0,s_thk
vsel,s,volu,,67
vatt,10,10,10
alls
vsel,s,volu,,116
vsel,a,volu,,145
vsel,a,volu,,151
vatt,10,10,10
alls
asel,s,area,,619
asel,a,area,,627
asel,a,area,,647
vext,all,,0,0,2
alls
asel,s,area,,316
asel,a,area,,348
asel,a,area,,391
vext,all,,0,s_thk,0
alls
vsel,s,volu,,68,69,1
vsel,a,volu,,71,75,4
vsel,a,volu,,78,79,1
vatt,10,10,10
alls
vext,622,,0,0,-p_wid/2
vsel,s,volu,,91
vsel,a,volu,,144
vatt,10,10,10
alls
!hinge block stiffener
vext,362,,0,0,-p_wid/2
vsel,s,volu,,50
vsel,a,volu,,92
vatt,11,11,11
alls
!stiffener reinforcement mods
!hinge block side
vsel,s,volu,,8,10,2
vsel,a,volu,,15,18,3
vsel,a,volu,,42,43,1
vgen,2,all,,0,4.375,0
alls
vsbv,123,167,,dele,keep
vsbv,124,169,,dele,keep
vsbv,183,164,,dele,keep
vsbv,184,107,,dele,keep
vsel,s,volu,,123,124,1
vsel,a,volu,,172,173,1
vsel,a,volu,,175,178,3
vsel,a,volu,,183,185,2
vatt,2,2,2
alls
!pin block side
vsel,s,volu,,42,43,1
vsel,a,volu,,108,109,1
vsel,a,volu,,114,115,1
vgen,2,all,,4.375,0,0
alls
vsbv,132,184,,dele,keep
vsbv,133,216,,dele,keep
vsbv,149,220,,dele,keep
vsbv,150,218,,dele,keep
vsel,s,volu,,132,133,1
vsel,a,volu,,149
vsel,a,volu,,221,225,1

vatt,2,2,2
alls
!fix touching connected components
hinge
vdele,92,,1
vdele,50,,1
asel,s,area,,275
asel,a,area,,282
vext,all,,-s_hgt+h_thk+s_thk,0,0
vsel,s,volu,,50
vsel,a,volu,,92
vatt,11,11,11
alls
!fix touching connected components
pin
vdele,91,,1
vdele,144,,1
vdele,68,69,1
vdele,78,79,1
vdele,71,75,4,1
vdele,116,,1
vdele,145,,1
vdele,151,,1
asel,s,area,,7
asel,a,area,,293
asel,a,area,,328
asel,a,area,,399
asel,a,area,,426
vext,all,,0,0,s_thk
alls
asel,s,area,,392
asel,a,area,,330
vext,all,,0,-s_hgt+h_thk+s_thk,0
alls
asel,s,area,,431
asel,a,area,,438
asel,a,area,,352
vext,all,,0,0,1.25
alls
asel,s,area,,701
asel,a,area,,621
asel,a,area,,627
vext,all,,0,0,s_thk,0
alls
vsel,s,volu,,68,69,1
vsel,a,volu,,71,75,4
vsel,a,volu,,78,79,1
vsel,a,volu,,91,116,25
vsel,a,volu,,144,145,1
vsel,a,volu,,150,151,1
vsel,a,volu,,226
vatt,10,10,10
alls
!move hinge block web stiffener back
for clearance
vdele,82,,1
vdele,92,,1
vdele,50,,1
asel,s,area,,388
asel,a,area,,375
vext,all,,-
s_hgt+s_thk+h_thk+0.4583,0,0
vsel,s,volu,,50,82,32
vatt,11,11,11
alls
asel,s,area,,134
asel,a,area,,191
vext,all,,0,0.25,0,0
vsel,s,volu,,92
vsel,a,volu,,227
vatt,11,11,11
alls
!bring pin block down
asel,s,area,,288
asel,a,area,,348
vext,all,,0,0.435,0
vsel,s,volu,,228,229,1
vatt,10,10,10
alls
!bring hinge block down and over
asel,s,area,,578
asel,a,area,,974
vext,all,,0,0.25,0,0
vsel,s,volu,,230,231,1
vatt,11,11,11
alls
asel,s,area,,136
asel,a,area,,644
asel,a,area,,990
vext,all,,0,0,0.25
vsel,s,volu,,232,234,1
vatt,11,11,11
alls
asel,s,area,,274
asel,a,area,,281

asel,a,area,,374
asel,a,area,,387
vext,all,,0,0.25,0,0
vsel,s,volu,,235,238,1
vatt,11,11,11
alls
vsel,s,type,,11
alls,below,volume
nummrg,kp
alls
vdele,58,,1
vdele,60,,1
vdele,87,,1
vdele,88,,1
alls
!pin block/web mod
vdele,70,,1
vdele,72,,1
asel,s,area,,329
asel,a,area,,390
vext,all,,0,0.25,0
vsel,s,volu,,58,60,2
vatt,10,10,10
alls
vsel,s,type,,10
alls,below,volume
nummrg,kp
alls
!Cut Stiffener for interface with
cask
cyl4,5.175,11.819,0,,13.75,,2
vsba,all,264
vdele,70,,1
local,11,1,5.175,11.819,0
csys,11
vsel,s,loc,x,13.75,20
vdele,all,,1
csys,0
alls
vsel,s,,245,246
vatt,10,10,10
alls
vsel,u,type,,10
vsel,u,type,,11
vsel,u,type,,1
vatt,2,2,2
alls
vsel,s,,272
alls,below,volume
adrag,530,,618
vsba,272,32
vsel,s,,8,10,2
vatt,2,2,2
alls
accat,34,41
vdele,72,,1
!accat,306,1071
vdele,249,,1
vdele,250,,1
vdele,264,,1
!Set Up Mesh
LESIZE,121,,3,,1
LESIZE,125,,3,,1
LESIZE,137,,3,,1
LESIZE,140,,3,,1
LESIZE,167,,3,,1
LESIZE,183,,3,,1
LESIZE,186,,3,,1
LESIZE,740,,1,,0
LESIZE,1096,,8,,0
LESIZE,1183,,4,,0
LESIZE,992,,10,,0
LESIZE,82,,1,,0
LESIZE,100,,1,,0
LESIZE,118,,1,,0
LESIZE,28,,3,,0
LESIZE,1198,,4,,0
LESIZE,469,,6,,0
LESIZE,567,,6,,0
LESIZE,818,,6,,0
LESIZE,922,,6,,0
LESIZE,934,,6,,0
LESIZE,1039,,6,,0
LESIZE,1031,,3,,0
LESIZE,1364,,4,,0
LESIZE,1027,,4,,0
LESIZE,1375,,4,,0
LESIZE,434,,3,,0
LESIZE,686,,3,,0
LESIZE,426,,3,,0
LESIZE,1458,,3,,0
LESIZE,682,,3,,0
lsl,s,loc,x,b_wid-p_len+0.2,b_wid-
p_len+0.5
LESIZE,all,,6,,0

```

```

alls
lset,s,loc,y,b_wid-h_len+0.2,b_wid-
h_len+0.5
LESIZE,all,,,6,,,,,0
alls
lset,s,loc,x,b_wid-p_len-0.2,b_wid-
p_len-1.5
LESIZE,all,,,6,,,,,0
alls
lset,s,loc,y,b_wid-h_len-0.2,b_wid-
h_len-1.5
LESIZE,all,,,6,,,,,0
alls
lset,s,loc,x,1.0,3.0
LESIZE,all,,,6,,,,,0
alls
lset,s,loc,y,1.0,3.0
LESIZE,all,,,6,,,,,0
alls
lset,s,loc,x,b_thk/2
LESIZE,all,,,1,,,,,0
alls
lset,s,loc,y,b_thk/2
LESIZE,all,,,1,,,,,0
alls
vset,s,type,,11
alls,below,volume
lset,r,loc,x,-0.01,-0.24
LESIZE,all,,,3,,,,,0
alls
MSHAPE,0,3D
MSHKEY,1
VMESH,all
alls
!generate other symmetry half
vsymm,z,all,,,0,0
esel,s,type,,1
nsle,s
nummrg,node,0.001
alls
esel,s,type,,2
nsle,s
nummrg,node,0.001
alls
esel,s,type,,10
nsle,s
nummrg,node,0.001
alls
esel,s,type,,11
nsle,s
nummrg,node,0.001
alls
!Add Bolt couples
!pin block
nset,s,loc,x,b_wid-0.5
nset,r,loc,z,1.375
cpintf,ux,0.01
cpintf,uy,0.01
cpintf,uz,0.01
alls
nset,s,loc,x,b_wid-0.5
nset,r,loc,z,-1.375
cpintf,ux,0.01
cpintf,uy,0.01
cpintf,uz,0.01
alls
nset,s,loc,x,b_wid-1.5
nset,r,loc,z,1.375
cpintf,ux,0.01
cpintf,uy,0.01
cpintf,uz,0.01
alls
nset,s,loc,x,b_wid-1.5
nset,r,loc,z,-1.375
cpintf,ux,0.01
cpintf,uy,0.01
cpintf,uz,0.01
alls
!hinge block
nset,s,loc,y,b_wid-1.5
nset,r,loc,z,0
cpintf,ux,0.01
cpintf,uy,0.01
cpintf,uz,0.01
alls
nset,s,loc,y,b_wid-0.5
nset,r,loc,z,2.00
cpintf,ux,0.01
cpintf,uz,0.01
cpintf,uy,0.01
alls
nset,s,loc,y,b_wid-1.5
nset,r,loc,z,2.00
cpintf,ux,0.01
cpintf,uy,0.01
cpintf,uz,0.01
alls
nset,s,loc,y,b_wid-1.5
nset,r,loc,z,3.75
cpintf,ux,0.01
cpintf,uy,0.01
cpintf,uz,0.01
alls
nset,s,loc,y,b_wid-1.5
nset,r,loc,z,3.75
cpintf,ux,0.01
cpintf,uy,0.01
cpintf,uz,0.01
alls
nset,s,loc,y,b_wid-0.5
nset,r,loc,z,-2.00
cpintf,ux,0.01
cpintf,uy,0.01
cpintf,uz,0.01
alls
nset,s,loc,y,b_wid-1.5
nset,r,loc,z,-2.00
cpintf,ux,0.01
cpintf,uy,0.01
cpintf,uz,0.01
alls
nset,s,loc,y,b_wid-1.5
nset,r,loc,z,-3.75
cpintf,ux,0.01
cpintf,uy,0.01
cpintf,uz,0.01
alls
nset,s,loc,x,0.76
nset,r,loc,z,0
cpintf,ux,0.01
cpintf,uy,0.01
cpintf,uz,0.01
alls
nset,s,loc,x,0.76
nset,r,loc,z,0
cpintf,ux,0.01
cpintf,uy,0.01
cpintf,uz,0.01
alls
nset,s,loc,y,b_wid-4.0833
nset,r,loc,z,0
cpintf,ux,0.01
cpintf,uy,0.01
cpintf,uz,0.01
alls
type,12
real,12
mat,12
!Pin
n,50000,b_wid+0.875-0.437,-0.002,.75
e,50000,node(9.292,-0.083,0.75)
e,50000,node(9.583,-0.083,0.75)
e,50000,node(9.292,0.75)
e,50000,node(9.583,0.75)
e,50000,node(9.292,0.109,0.75)
e,50000,node(9.583,0.109,0.75)
n,50006,b_wid+0.875-0.437,-0.002,-
.75
e,50006,node(9.292,-0.083,-0.75)
e,50006,node(9.583,-0.083,-0.75)
e,50006,node(9.292,0,-0.75)
e,50006,node(9.583,0,-0.75)
e,50006,node(9.292,0.109,-0.75)
e,50006,node(9.583,0.109,-0.75)
!Hinge
n,50003,-.187,b_wid+0.75-0.437,3.25
e,50003,node(-0.167,9.25,3.25)
e,50003,node(-0.167,9.50,3.25)
e,50003,node(-.25,9.25,3.25)
e,50003,node(-.25,9.50,3.25)
n,50004,-.187,b_wid+0.75-0.437,0.75
e,50004,node(-0.167,9.25,0.750)
e,50004,node(-0.167,9.50,0.750)
e,50004,node(-.25,9.25,0.750)
e,50004,node(-.25,9.50,0.750)
!n,50005,-.187,b_wid+0.75-0.437,5
!e,50005,node(-0.167,9.25,5)
!e,50005,node(-0.167,9.50,5)
!e,50005,node(-.25,9.25,5)
!e,50005,node(-.25,9.50,5)
n,50007,-.187,b_wid+0.75-0.437,-3.25
e,50007,node(-0.167,9.25,-3.25)
e,50007,node(-0.167,9.50,-3.25)
e,50007,node(-.25,9.25,-3.25)
e,50007,node(-.25,9.50,-3.25)
n,50008,-.187,b_wid+0.75-0.437,-0.75
e,50008,node(-0.167,9.25,-0.750)
e,50008,node(-0.167,9.50,-0.750)
e,50008,node(-.25,9.25,-0.750)
e,50008,node(-.25,9.50,-0.750)
!n,50009,-.187,b_wid+0.75-0.437,-5
!e,50009,node(-0.167,9.25,-5)
!e,50009,node(-0.167,9.50,-5)
!e,50009,node(-.25,9.25,-5)
!e,50009,node(-.25,9.50,-5)
alls
!generate gaps
!box walls to stiffeners
!stiffeners are the 'target'
vset,s,type,,2
vset,a,type,,10
vset,a,type,,11
alls,below,volu
nset,r,loc,x,0
nset,r,loc,y,0,b_wid
nset,r,loc,z,-s_wid/2,s_wid/2
cm,stiff,node
alls,below,volu
nset,r,loc,y,0
nset,r,loc,x,0,b_wid
nset,r,loc,z,-s_wid/2,s_wid/2
cmset,a,stiff,node
cm,stiff,node
alls
!box walls are the 'Contact'
vset,s,type,,1
alls,below,volu
nset,r,loc,x,0
nset,r,loc,y,0,b_wid
nset,r,loc,z,-s_wid/2,s_wid/2
cm,box,node
alls,below,volu
nset,r,loc,y,0
nset,r,loc,x,0,b_wid
nset,r,loc,z,-s_wid/2,s_wid/2
cmset,a,box,node
cm,box,node
alls
type,5
mat,5
real,5
gcgen,box,stiff,2
alls
!pin block to stiffener and box
!pin block is 'target'
vset,s,type,,10
alls,below,volu
nset,r,loc,y,-s_thk
nset,r,loc,z,-s_wid/2,s_wid/2
cm,p_block,node
alls,below,volu
nset,r,loc,y,0
nset,r,loc,x,b_wid,b_wid-p_len
nset,r,loc,z,1.25+s_wid/2,s_wid/2
cmset,a,p_block,node
cm,p_block,node
alls,below,volu
nset,r,loc,y,0
nset,r,loc,x,b_wid,b_wid-p_len
nset,r,loc,z,-1.25-s_wid/2,-s_wid/2
cmset,a,p_block,node
cm,p_block,node
alls
!stiffener and box are 'contact'
vset,s,type,,2
alls,below,volu
nset,r,loc,y,-s_thk
nset,r,loc,x,b_wid-0.5,b_wid-p_len
nset,r,loc,z,-s_wid/2,s_wid/2
cm,parea,node
vset,a,type,,1
alls,below,volu
nset,r,loc,y,
nset,r,loc,x,b_wid,b_wid-p_len
nset,r,loc,z,1.25+s_wid/2,s_wid/2
cmset,a,parea,node

```

```

cm,parea,node
alls,below,volu
nset,r,loc,y,
nset,r,loc,x,b_wid,b_wid-p_len
nset,r,loc,z,-1.25-s_wid/2,-s_wid/2
cmset,a,parea,node
cm,parea,node
alls
type,7
mat,7
real,7
gcgen,parea,p_block,2
alls
!Hinge Block to stiffener and box
wall
!hinge block is 'target'
vset,s,type,,11
alls,below,volu
nset,r,loc,x,-s_thk
nset,r,loc,y,b_wid-1,b_wid-h_len
nset,r,loc,z,s_wid/2,-s_wid/2
cm,h_block,node
alls,below,volu
nset,r,loc,x,0
nset,r,loc,z,h_wid,s_wid/2
cmset,a,h_block,node
cm,h_block,node
alls,below,volu
nset,r,loc,x,0
nset,r,loc,z,-h_wid,-s_wid/2
cmset,a,h_block,node
cm,h_block,node
alls
!stiffener and box are 'contact'
vset,s,type,,2
alls,below,volu
nset,r,loc,x,-s_thk
nset,r,loc,y,b_wid-1,b_wid-h_len
cm,harea,node
vset,a,type,,1
alls,below,volu
nset,r,loc,x,
nset,r,loc,y,b_wid,b_wid-h_len
nset,r,loc,z,h_wid,s_wid/2
cmset,a,harea,node
cm,harea,node
alls,below,volu
nset,r,loc,x,
nset,r,loc,y,b_wid,b_wid-h_len
nset,r,loc,z,-h_wid,-s_wid/2
cmset,a,harea,node
cm,harea,node
alls
type,9
mat,9
real,9
gcgen,harea,h_block,2
alls
!Weld Pin Block to Stiffener
vset,s,type,,2
vset,a,type,,10
alls,below,volu
nset,r,loc,y,-s_thk-h_thk,-s_hgt
CPINTF,ALL,0.001,
alls
!Weld Hinge Block to Stiffener
vset,s,type,,2
vset,a,type,,11
alls,below,volu
nset,r,loc,x,-s_thk-h_thk,-s_hgt
CPINTF,ALL,0.001,
alls
!Pin Side
d,50000,Ux,
d,50000,Uy,
!d,50000,Uz,
d,50006,Ux,
d,50006,Uy,
d,50006,Uz,
!Hinge Side
d,50003,Ux,
d,50003,Uy,
d,50003,Uz,
d,50004,Ux,
d,50004,Uy,
!d,50004,Uz,
!d,50005,Ux,
!d,50005,Uy,
!d,50005,Uz,
d,50007,Ux,
d,50007,Uy,
!d,50007,Uz,
d,50008,Ux,
d,50008,Uy,
d,50008,Uz,
!d,50009,Ux,
!d,50009,Uy,
!d,50009,Uz,
alls
/solu
antype,static
solcontrol,on,on
autots,on
nropt,auto
!Load Step 1
!Apply g-Load
g=120
acel,0,0,g
NSUBST,10,25,1
lswrite,1
!Load Step 2
!Apply Initial Pressure
fp=18000/100/(b_wid-b_thk)/s_wid
eset,s,type,,1
nsle,s
nset,r,loc,y,b_thk
nset,r,loc,x,b_thk,b_wid
nset,r,loc,z,-s_wid/2,s_wid/2
sf,all,pres,fp
alls
NSUBST,10,25,1
lswrite,2
!Load Step 3
!Apply Full Pressure
fp=18000/(b_wid-b_thk)/s_wid
eset,s,type,,1
nsle,s
nset,r,loc,y,b_thk
nset,r,loc,x,b_thk,b_wid
nset,r,loc,z,-s_wid/2,s_wid/2
sf,all,pres,fp
alls
NSUBST,10,50,1
lswrite,3
lssolve,1,3,1
save
finish

```

2.12.5.21.2 Strongback Evaluation Finite Element Model

This input file is representative of the FCS finite element analysis described in Section 2.12.5.19.

```

/PREP7
/com Plate Dimensions
A_Plate=17.0
B=9
A2_Plate=A_Plate/2
tol=.001
T_Plate=0.25
/Com Stiffener Dimensions
H_Stiff=2.0
T_Stiff=0.25
/Com Loads
Fx_1=-500 $
Fy_1=-8400 $
Fz_1=-1150
Fx_2=-8900 $
Fy_2=-50 $
Fz_2=-1050
Fx_3=-4700 $
Fy_3=-4250 $
Fz_3=-1150
Fx_4=-13500 $
Fy_4=-50 $
Fz_4=50
et,1,shell43 $ r,1,T_Plate
et,2,shell43 $ r,2,T_Stiff
et,3,shell43 $ r,3,T_Stiff
et,52,contact52,,,1,0
keyopt,52,7,1
r,52,1.0e+06,,2,0
! initially closed & sliding
mu,52,0
/com Material 1 - Type 304
nuxy,1,0.3
mptemp,1,0,300
dens,1,493/1728
! weight density
mpdata,ex,1,1,27.6e+06,27.6e+06
pmo=0.05
tb,kin,1,2
tbtemp,0
tbdata,,25000,219970
! c1=sy, c2=tangent modulus
tbtemp,300
tbdata,,25000,219970
! c1=sy, c2=tangent modulus
/com Dimensions for Geometry
tempA=T_Stiff/2
tempB=H_Stiff-T_Stiff/2
temp1=(T_Plate+T_Stiff)/2
temp2=temp1+H_Stiff-T_Stiff
/com Define Plate
wprota,0,0,90 ! match 99008-20
coordinates
mat,1
real,1
type,1
rect,-A2_Plate,A2_Plate,0,B
rect,-A2_Plate,A2_Plate,0,B
rect,-A2_Plate,A2_Plate,TempA,TempB
aovlap,all
wpstyle
esize,0.22
amesh,all
cm,PlateA,area
cm,PlateL,line
cm,PlateK,kp
cm,PlateE,elem
cm,PlateN,node
cmgrp,Plate,PlateA,PlateL,PlateK,PlateE,PlateN
/com Define Stiffener.....
.
mat,1
real,3
type,3
block,-
A2_Plate,A2_Plate,tempA,tempB,temp1,
temp2
vdele,all
! delete vol, keep areas
ksel,s,loc,z,-A2_Plate-tol,-
A2_Plate+tol ! ends only
lslk,s,1
! line w/all kp
asll,s,1
! area w/all line
ksel,s,loc,z,+A2_Plate-
tol,+A2_Plate+tol ! ends only
lslk,s,1
! line w/all kp
! area w/all line
adele,all
! delete block ends
wpstyle
alls
cmsel,u,Plate
real,3
amesh,all
cm,StiffA,area
cm,StiffL,line
cm,StiffK,kp
cm,StiffE,elem
cm,StiffN,node
cmgrp,Stiff,StiffA,StiffL,StiffK,StiffE,StiffN
/com Pin Block Location (Welded Into Tube Stiffener)
cmsel,s,Stiff
nset,r,loc,z,-1.25,1.25
nset,r,loc,x,Temp1-tol,Temp1+tol
esln,s,1
cm,Pin_n,node
cm,Pin_e,elem
cmgrp,Pin,Pin_n,Pin_e
emodif,all,type,2 ! at Pin Block
emodif,all,real,2 ! at Pin Block
*get,iPin_n,node,0,count
alls
/com Connect Plate and Stiffener
nset,s,loc,Y,H_Stiff/2-
tol,H_Stiff/2+tol
nset,r,loc,X,0,H_Stiff/2
cm,TempN,node
cmsel,r,PlateN $ cm,TempP,node
cmsel,s,TempN
cmsel,r,StiffN $ cm,TempS,node
nset,node
cm,BoltN,node ! initialize group
for connected nodes
*do,i,-7.5,-3.0,1.5
cmsel,s,TempP
nodeP=node(0,T_Stiff/2,i)
cmsel,s,TempS
nodeS=node(0,T_Stiff/2,i)
nall
cp,next,ux,NodeS,NodeP
cp,next,uy,NodeS,NodeP
cp,next,uz,NodeS,NodeP
cmsel,s,BoltN ! add nodes
to group
nset,a,node,,NodeP
nset,a,node,,NodeS
cm,BoltN,node
*enddo
*do,i,3.0,7.5,1.5
cmsel,s,TempP
nodeP=node(0,T_Stiff/2,i)
cmsel,s,TempS
nodeS=node(0,T_Stiff/2,i)
nall
cp,next,ux,NodeS,NodeP
cp,next,uy,NodeS,NodeP
cp,next,uz,NodeS,NodeP
cmsel,s,BoltN ! add nodes
to group
nset,a,node,,NodeP
nset,a,node,,NodeS
cm,BoltN,node
*enddo
/com 3 Fasteners at Pin Block
cmsel,s,PlateN $ nodeP1=node(
0,1.37,-.75)
cmsel,s,StiffN $
nodeS1=node(T_Stiff,1.37,-.75)
nall
cp,next,ux,NodeS1,NodeP1
cp,next,uy,NodeS1,NodeP1
cp,next,uz,NodeS1,NodeP1
cmsel,s,PlateN $ nodeP2=node(
0,0.62,.00)
cmsel,s,StiffN $
nodeS2=node(T_Stiff,0.62,.00)
nall
cp,next,ux,NodeS2,NodeP2
cp,next,uy,NodeS2,NodeP2
cp,next,uz,NodeS2,NodeP2
cmsel,s,PlateN $ nodeP3=node(
0,1.37,+.75)
cmsel,s,StiffN $
nodeS3=node(T_Stiff,1.37,+.75)
nall
cp,next,ux,NodeS3,NodeP3
cp,next,uy,NodeS3,NodeP3
cp,next,uz,NodeS3,NodeP3
cmsel,s,BoltN ! add nodes
to group
nset,a,node,,NodeP1 $
nset,a,node,,NodeP2 $
nset,a,node,,NodeP3
nset,a,node,,NodeS1 $
nset,a,node,,NodeS2 $
nset,a,node,,NodeS3
cm,BoltN,node
/com Contact Elements
asel,s,area,,3
alls,below,area
cmsel,u,BoltN ! unselect
Bolted nodes
cm,TempP,node ! plate
nodes
cm,Temp,node
cmsel,s,Stiff
*get,Xmin,Node,0,MNLOC,X
nset,r,loc,X,Xmin-tol,Xmin+tol
cmsel,u,BoltN ! unselect
Bolted nodes
cm,TempS,node !
stiffener nodes
*get,HowMany,node,,count
esel,none
type,52
real,52
mat,52
model=0
*do,i,1,HowMany
cmsel,s,Temp
node1=ndnext(node1)
yloc=ny(node1)
zloc=nz(node1)
cmsel,s,TempS
node2=node(Xmin,yloc,zloc)
cmsel,a,TempP
e,node1,node2
*enddo
eplot
*get,N_Elem,elem,,count
*if,N_Elem,GT,HowMany,then
*msg,warn,N_Elem,HowMany
CONTACT GENERATION MAY BE
MESSUED UP, %I Elements from %I Nodes
*endif
alls
/com Groups for Boundary Conditions
cmsel,s,PlateN
nset,r,loc,y,0
nset,r,loc,z,-A2_Plate+tol,A2_Plate-
tol
cm,free_edge,node
cmsel,s,PlateN
nset,r,loc,y,B-tol,B+tol
cm,fix_edge,node
cmsel,s,PlateN
nset,r,loc,z,-A2_Plate-tol,-
A2_Plate+tol
cm,top_edge,node
cmsel,s,PlateN
nset,r,loc,z,+A2_Plate-
tol,+A2_Plate+tol
cm,bot_edge,node
alls
/com Apply Boundary Conditions
(Plate (not stiffener) Edges Only)
cmsel,s,top_edge
cmsel,a,bot_edge
cmsel,a,fix_edge
d,all,ux,0,,,uy,uz
alls
/com Load Step 1
/title,SB_Angle_07S, LS 1, Table 7-4
(1/4" Plate & Stiffener)
time,1

```



```
nlgeom,on
autots,on
nsubst,10,20,10,off
cnvtol,f,,.01,,10      !
modified convergence tolerance
neqit,100
nropt,auto
pred,on,,on
cmsel,s,Pin_n
f,all,fx, Fx_1/iPin_n
! out-of-plane
f,all,fz, Fz_1/iPin_n
! in-plane (axial)
f,all,fy, Fy_1/iPin_n
! in-plane
alls
lswrite
/com Load Step 2
fdelete,all,all
/title,SB_Angle_07S, LS 2, Table 7-5
(1/4" Plate & Stiffener)
time,2
nlgeom,on
autots,on
nsubst,10,20,10,off
cnvtol,f,,.01,,10      !
modified convergence tolerance
neqit,100
nropt,auto
pred,on,,on
cmsel,s,Pin_n
f,all,fx, Fx_2/iPin_n
! out-of-plane
f,all,fz, Fz_2/iPin_n
! in-plane (axial)
f,all,fy, Fy_2/iPin_n
! in-plane
alls
lswrite
/com Load Step 3
fdelete,all,all
(1/4" Plate & Stiffener)
time,3
nlgeom,on
autots,on
nsubst,10,20,10,off
cnvtol,f,,.01,,1      !
modified convergence tolerance
neqit,100
nropt,auto
pred,on,,on
cmsel,s,Pin_n
f,all,fx, Fx_3/iPin_n
! out-of-plane
f,all,fz, Fz_3/iPin_n
! in-plane (axial)
f,all,fy, Fy_3/iPin_n
! in-plane
alls
lswrite
! save,SB_Angle_07S-3,db      ! /com
Load Step 4
fdelete,all,all
/title,SB_Angle_07S, LS 4, Side Drop
Loads (1/4" Plate & Stiffener)
time,4
nlgeom,on
autots,on
nsubst,10,20,10,off
cnvtol,f,,.01,,1      !
modified convergence tolerance
neqit,100
nropt,auto
pred,on,,on
cmsel,s,Pin_n
! no axial force
f,all,fx, Fx_4/iPin_n
! out-of-plane
f,all,fz, Fz_4/iPin_n
! in-plane (axial)
f,all,fy, Fy_4/iPin_n
! in-plane
alls
lswrit
```

This page left intentionally blank.

2.12.6 CASKDROP Computer Program

This appendix briefly documents the methodology employed by the PacTec proprietary computer program CASKDROP. Used in conjunction with an appropriate packaging dynamic analysis computer code, such as SCANS¹ or SLAPDOWN², the computer program CASKDROP is used to demonstrate compliance of the package with 10 CFR §71.71(c)(7)³ and 10 CFR §71.73(c)(1) for normal conditions of transport (NCT) and hypothetical accident conditions (HAC) of transport free drop analyses, respectively.

A summary of the appendix subsections is as follows:

- describes the CASKDROP analysis methodology.
- provides an example problem with input and output.

2.12.6.1 Using CASKDROP to Determine Impact Limiter Deformation Behavior

The package is protected by polyurethane foam-filled, energy absorbing end buffers, called impact limiters. For purposes of the regulatory free drop analyses using the CASKDROP computer program, the impact limiters are assumed to absorb, in plastic deformation of the polyurethane foam, all of the potential energy of the drop event. In other words, the drop analyses assume that none of the potential energy of the free drop event is transferred to kinetic or strain energy of the target (i.e., the “unyielding” surface assumption of 10 CFR 71), nor strain energy in the package body itself.

CASKDROP evaluates all angles of drop from 0° (horizontal) to 90° (vertical) by performing a quasi-static analysis that ignores rotational effects. At orientations where rotational effects are important, use of a dynamic analysis computer program such as SCANS or SLAPDOWN is required utilizing the force-deflection data developed by CASKDROP. Three orientations where rotational motions (or pitch) play no role in the evaluation of the free drop analyses are:

- *END DROP* on the circular end surface of the impact limiter,
- *SIDE DROP* on the cylindrical side surfaces of the impact limiters, and
- *CORNER DROP* with the package center of gravity directly over the impact limiter corner.

For all orientations of impact, the prediction of impact limiter deformation behavior can be approached from straightforward energy balance principles:

$$E = W(h + \delta) = \int_0^{\delta} F_x dx$$

¹ *SCANS (Shipping Cask ANalysis System), A Microcomputer Based Analysis System for Shipping Cask Design Review*, NUREG/CR-4554 (UCID-20674), Lawrence Livermore National Laboratory.

² G. D. Sjaardema, G. W. Wellman, *Numerical and Analytical Methods for Approximating the Eccentric Impact Response (Slapdown) of Deformable Bodies*, SAND88-0616 (UC-71), Sandia National Laboratories.

³ Title 10, Code of Federal Regulations, Part 71 (10 CFR 71), *Packaging and Transportation of Radioactive Materials*, Final Rule, 01-26-04.

where W is the package gross weight, h is the drop height, δ is the maximum impact limiter deformation, and F_x is the force imposed on target at an impact limiter deformation of x . The left-hand term represents the potential energy of the free drop. The right-hand term represents the strain energy of the deformed impact limiter(s).

Given a specific drop angle, θ , and impact limiter deformation, δ , as illustrated in Figure 2.12.6-1, the result is an impact limiter crush plane “footprint.” Integration of the impact limiter crush plane yields a total crush force and centroidal distance of:

$$F = \iint \sigma\{\varepsilon\} dA \quad \text{and} \quad \bar{X} = \left(\frac{1}{F}\right) \iint \bar{x} \sigma\{\varepsilon\} dA$$

respectively, where F is the total integrated force, $\sigma\{\varepsilon\}$ is the differential stress as a function of strain, dA is the differential area (i.e., dA is a function of the “ x ” and “ y ” directions, or dx and dy), \bar{X} is the total integrated centroidal distance from the package center of gravity, and \bar{x} is the differential centroidal distance from the package center of gravity.

With reference to Figure 2.12.6-1, the geometric calculations for the impact surface (crush plane) and the associated strains are carried out using a translating X' - Y' - Z' coordinate system, with the X' - Y' plane corresponding to the crush plane. Due to the cylindrical nature of the problem, the overall crush plane is comprised of a segment of an ellipse corresponding to the outside surface of the impact limiter. The optional end hole requires removal of its associated elliptical segment. Similarly, the optional conical surface is an elliptical, parabolic, or hyperbolic segment depending on both the drop angle, θ , and angle of the cone.

Calculation of the differential strain is somewhat more complex. As illustrated in Figure 2.12.6-2, the differential strain, $\varepsilon\{x,y\}$, is calculated at the center of the differential area, dA . The differential strain is determined by calculating the amount of vertical deformation at the (x, y) location on the crush plane. The vertical distance from point (x, y) on the impact surface to the package or upper impact limiter surface is found and denoted z_{TOP} . Similarly, the vertical distance from point (x, y) on the impact surface to the undeformed lower impact limiter surface is found and denoted z_{BOT} . In equation format the differential strain at location (x, y) is simply:

$$\varepsilon = \frac{z_{BOT}}{z_{BOT} + z_{TOP}}$$

This strain is used to determine the corresponding crush stress from an implicit tabular definition of the crushable media stress-strain characteristics. For each differential area, dA , the differential force, dF , is found. The total force, F , is therefore the summation of the differential forces. Similarly, the centroidal distance, \bar{X} , is the summation of the moments, $\bar{x} \times dF$, divided by the total force.

Unbacked regions are defined as having an (x, y) location where z_{TOP} is calculated to occur outside the package’s “shadow” (i.e., or backing, occurring on the impact limiter surface). Unbacked regions usually utilize the nominal crush strength of the crushable media (typically 10% for polyurethane foam material) for integrated force purposes. The crush strength for unbacked regions is user-definable in the program CASKDROP.

For most drop angles, θ , and impact limiter deformations, δ , the impact limiter crush force, F , is transmitted to the package body in direct compression. Hence, the forces transmitted to the circumferential impact limiter attachments are essentially zero. However, for nearly vertical or

horizontal orientations at small deformations where the crush force occurs beyond the edge of the package, the forces transmitted to the impact limiter attachments can be substantially large. It is important to note that only the nearly vertical or nearly horizontal orientations are required to produce the prying motion; all other orientations will always compress the impact limiter onto the package body. Figure 2.12.6-3 illustrates the near vertical and near horizontal orientations producing impact limiter separation forces.

For the near vertical orientation, the moment about point “a” determines whether a separation force exists at the impact limiter attachments. Assuming for this case that a counterclockwise moment is positive (i.e., will tend to “pry” the impact limiter off the package), the equation for the moment about point “a,” M_a , is:

$$M_a = Fx_F + F_{IL}x_{IL}$$

Similarly, for the near horizontal orientation, the moment about point “b” determines whether a separation force exists at the impact limiter attachments. Assuming for this case that a clockwise moment is positive (i.e., will tend to “pry” the impact limiter off the package), the equation for the moment about point “b,” M_b , is:

$$M_b = Fx_F - F_{IL}x_{IL}$$

If M_a or M_b are positive, a separation force will occur at the impact limiter attachments whereas if M_a or M_b are zero or negative, a separation force will not occur. Note that use of a conically shaped impact limiter typically eliminates the impact limiter separation force by causing the crush force, F , to almost always occur between points “a” and “b.”

2.12.6.2 An Example Problem for the CASKDROP Program

An example problem is illustrated in Figure 2.12.6-4. The CASKDROP program utilizes a variety of physical input data to determine package and impact limiter geometry. In all cases, the package and impact limiter are assumed axisymmetric. The package is cylindrical, as is the impact limiter. Two fundamental variations in the basic cylindrical shape of the impact limiter are an optional end hole and optional conical end. The end hole may extend part or all of the way from the outside surface of the impact limiter to the package end. The conical end may be a truncated or fully developed cone, defined by a cone diameter and a cone length at the outside surface of the impact limiter. By varying the impact limiter dimensions the result is a wide variety of possible impact limiter shapes, from a totally enclosing “overpack” to pointed end-only buffers.

The CASKDROP program was primarily developed as an impact limiter design tool. Geometry and analysis control input to the CASKDROP program is fully interactive allowing changes “on the fly.” Figure 2.12.6-5 illustrates the CASKDROP screen for data entry into the *Input Window*.

The CASKDROP program allows for three types of crushable media definition:

1. **CONSTANT:** a constant crush stress independent of calculated strain.
2. **VARIABLE:** a variable, user-defined stress-strain definition.
3. **POLYFOAM:** a built-in polyurethane foam database providing accurate stress-strain definition for 5 to 25 pound per cubic foot (pcf) density and temperatures of -20 °F to +300 °F based on extensive sample testing.

The example problem assumes 20 pcf polyurethane foam at a temperature of -20 °F. A +60% bias is applied to the temperature-corrected stress-strain data to account for dynamic strain rate effects for the example problem. Figure 2.12.6-6 illustrates the CASKDROP input screen for the polyurethane foam crush media for the example problem.

For the example problem, the CASKDROP program utilizes polyurethane foam where “parallel to rise” foam curing occurs in the axial direction and “perpendicular to rise” foam curing occurs in the radial direction, although the difference between these two directions is small. The user may optionally select the “parallel-to-rise” or “perpendicular-to-rise” properties to be reversed or global for all drop orientations. For orientations other than axial (end drop) and radial (side drop), the CASKDROP program interpolates foam properties using an ellipse function. For the case where crush stress “parallel-to-rise” is in the axial direction, σ_{PAR} , and crush stress “perpendicular-to-rise” is in the radial direction, σ_{PER} , the interpolation equation at drop angle, θ , is:

$$\sigma_{\theta} = \sqrt{\frac{1}{\left(\frac{\sin \theta}{\sigma_{PAR}}\right)^2 + \left(\frac{\cos \theta}{\sigma_{PER}}\right)^2}}$$

Similarly, for the case where crush stress “perpendicular-to-rise” is in the axial direction, σ_{PER} , and crush stress “parallel-to-rise” is in the radial direction, σ_{PAR} , the interpolation equation is:

$$\sigma_{\theta} = \sqrt{\frac{1}{\left(\frac{\sin \theta}{\sigma_{PER}}\right)^2 + \left(\frac{\cos \theta}{\sigma_{PAR}}\right)^2}}$$

The *Control Window* allows the user to specify various analysis and output controls. The *Control Window* is separated into *Analysis*, *Crush*, *Angle*, *Static*, *Dynamic*, *Print*, and *File*.

Three *Analysis* options are available: dXY defines the number of integration elements in the crush plane, 25 for the example problem; Sln defines the analysis methodology (Global versus Local Strain Theory), *Global* for the example problem; ϵ/σ defines the strain (or crush stress) value to be utilized in unbacked regions (e.g., if a value is specified between 0 and 1, it is assumed a strain value and the corresponding crush stress at that strain is used; if a value is specified greater than 1, it is assumed to be a crush stress), 0.1 for the example problem corresponding to a crush stress at 10% strain from the polyurethane foam database.

The *Crush* options define the incremental deformations to be analyzed. The example problem specifies analyzing for crush deformations from 0.25 inch to 20 inch in 0.25 inch increments. Specifying a *Max* value greater than the actual maximum available crush depth (as determined geometrically) flags the CASKDROP program to not exceed the maximum available crush depth.

Similarly, the *Angle* options define the incremental angular orientations to be analyzed. The example problem specifies analyzing for drop angles from 0° to 90° in 15° increments.

The *Static* options allow the user to specify quasi-static analyses providing *Full* display output, *Smry* (summary) output, or *Both*. The example problem specifies *Full* output to the display only. Similarly, the *Dynamic* options allow the user to specify dynamic analyses providing *Full* display output, *Smry* (summary) output, or *Both*. The example problem does not specify a dynamic analysis as that module is not completed in the CASKDROP program.

The *Print* and *File* options allow the user to specify *Full* display output, *Smry* (summary) output, or *Both* to the printer or a file. The example problem specifies *Full* output to an output file only.

The *Output Window* provides the location for *Static* and *Dynamic* display output. A quasi-static solution is achieved when the strain energy of the crushable media (SE) is equal to the free-falling kinetic energy of the package (KE), or $SE/KE = 1$. The following tables provide a sample file output at 0° (side drop), at 45° , and at 90° (end drop).

This page left intentionally blank.



MFFP Safety Analysis Report

Docket No. 71-9295
Revision 0, June 2004

Side Drop
05-16-1995, 15:38:39

*** PACKAGING TECHNOLOGY ***

CASKDROP, v2.21
Jul 01, 1994

SAMPLE PROBLEM FOR QUALITY ASSURANCE CHECK (AREAS AND VOLUMES)			
Impact Limiter Weight (each) -	1,000 lbs	Cask and Payload Weight -	10,000 lbs
Impact Limiter Outside Diameter -	60.0000 in	Cask Outside Diameter -	40.0000 in
Impact Limiter Overall Length -	24.0000 in	Cask Overall Length -	48.0000 in
Impact Limiter Conical Diameter -	48.0000 in	Dynamic Unloading Modulus -	1.000E+07 lbs/in
Impact Limiter Conical Length -	10.0000 in	Rad Mass Moment of Inertia -	12,235 lb-in-s ²
Impact Limiter End Thickness -	12.0000 in	Frictional Coefficient -	0.0000
Impact Limiter Hole Diameter -	20.0000 in	Drop Height -	30.0000 ft
Impact Limiter Hole Length -	8.0000 in	Drop Angle from Horizontal -	0.0000°
Unbacked Area Threshold Strain -	0.1000 in/in	Crush Analysis Theory -	Global
Unbacked Area Crush Stress -	2,675 psi	Number of Integration Incs -	25

POLYFOAM CRUSH STRESS (Axial: " " to rise)	
Density = 20.000 pcf	
Temp = -20.000 F	
σ-yield = 2,552.3 psi	
Bias = 60.000%	
ε (in/in)	σ (psi)
0.000	0.0
0.100	2,552.3
0.200	2,687.0
0.300	2,868.8
0.400	3,302.9
0.500	4,115.1
0.600	6,074.3
0.650	7,942.0
0.700	10,925.0
0.750	15,001.8
0.800	26,829.5

POLYFOAM CRUSH STRESS (Radial: "⊥" to rise)	
Density = 20.000 pcf	
Temp = -20.000 F	
σ-yield = 2,675.0 psi	
Bias = 60.000%	
ε (in/in)	σ (psi)
0.000	0.0
0.100	2,675.0
0.200	2,785.4
0.300	2,959.9
0.400	3,345.9
0.500	4,147.7
0.600	6,062.8
0.650	7,868.8
0.700	10,180.0
0.750	15,554.4
0.800	29,704.8

POLYFOAM CRUSH STRESS (Actual Data @ 0.0°)	
Density = 20.000 pcf	
Temp = -20.000 F	
σ-yield = 2,675.0 psi	
Bias = 60.000%	
ε (in/in)	σ (psi)
0.000	0.0
0.100	2,675.0
0.200	2,785.4
0.300	2,959.9
0.400	3,345.9
0.500	4,147.7
0.600	6,062.8
0.650	7,868.8
0.700	10,180.0
0.750	15,554.4
0.800	29,704.8

DEFL (in)	MAX ε (%)	AREA (in ²)	VOLUME (in ³)	XBAR (in)	IMPACT FORCE (lbs)	ACCEL (g's)	I/L MOMENT (in-lbs)	STRAIN ENERGY (in-lbs)	KINETIC ENERGY (in-lbs)	SE/KE RATIO
0.250	2.50	221	37	0.00	106,881	8.9	0	13,360	4,323,000	0.00
0.500	5.00	318	105	0.00	289,508	24.1	0	62,909	4,326,000	0.01
0.750	7.50	396	194	0.00	518,875	43.2	0	163,957	4,329,000	0.04
1.000	10.00	465	302	0.00	733,200	61.1	0	320,466	4,332,000	0.07



MFFP Safety Analysis Report

Docket No. 71-9295
Revision 0, June 2004

Side Drop
05-16-1995, 15:38:39

*** PACKAGING TECHNOLOGY ***
(continued...)

CASKDROP, v2.21
Jul 01, 1994

DEFL (in)	MAX ϵ (%)	AREA (in ²)	VOLUME (in ³)	XBAR (in)	IMPACT FORCE (lbs)	ACCEL (g's)	I/L MOMENT (in-lbs)	STRAIN ENERGY (in-lbs)	KINETIC ENERGY (in-lbs)	SE/KE RATIO
1.250	12.49	528	425	0.00	955,009	79.6	0	531,492	4,335,000	0.12
1.500	14.99	587	565	0.00	1,107,366	92.3	0	789,289	4,338,000	0.18
1.750	17.49	644	719	0.00	1,270,225	105.9	0	1,086,488	4,341,000	0.25
2.000	19.99	699	886	0.00	1,371,441	114.3	0	1,416,697	4,344,000	0.33
2.250	22.49	752	1,068	0.00	1,509,207	125.8	0	1,776,778	4,347,000	0.41
2.500	24.99	804	1,262	0.00	1,668,937	139.1	0	2,174,046	4,350,000	0.50
2.750	27.49	855	1,469	0.00	1,761,221	146.8	0	2,602,815	4,353,000	0.60
3.000	29.99	906	1,690	0.00	1,946,101	162.2	0	3,066,230	4,356,000	0.70
3.250	32.49	955	1,921	0.00	2,044,813	170.4	0	3,565,095	4,359,000	0.82
3.500	34.98	1,005	2,167	0.00	2,249,052	187.4	0	4,101,828	4,362,000	0.94
3.614	36.13	1,027	2,285	0.00	2,326,676	193.9	0	4,363,372	4,363,372	1.00
3.750	37.48	1,053	2,424	0.00	2,419,003	201.6	0	4,956,582	4,365,000	1.14
4.000	39.98	1,101	2,692	0.00	2,640,297	220.0	0	5,588,994	4,368,000	1.28
4.250	42.48	1,149	2,975	0.00	2,759,520	230.0	0	6,263,971	4,371,000	1.43
4.500	44.98	1,197	3,267	0.00	2,956,003	246.3	0	6,978,412	4,374,000	1.60
4.750	47.48	1,244	3,571	0.00	3,208,534	267.4	0	7,748,979	4,377,000	1.77
5.000	49.98	1,292	3,889	0.00	3,357,376	279.8	0	8,569,718	4,380,000	1.96
5.250	52.48	1,339	4,219	0.00	3,603,141	300.3	0	9,439,782	4,383,000	2.15
5.500	54.97	1,385	4,556	0.00	3,906,997	325.6	0	10,378,550	4,386,000	2.37
5.750	57.47	1,432	4,909	0.00	4,215,273	351.3	0	11,393,833	4,389,000	2.60
6.000	59.97	1,479	5,275	0.00	4,573,066	381.1	0	12,492,376	4,392,000	2.84
6.250	62.47	1,520	5,650	0.00	4,961,100	413.4	0	13,684,147	4,395,000	3.11
6.500	64.97	1,559	6,035	0.00	5,404,072	450.3	0	14,979,793	4,398,000	3.41
6.750	67.47	1,597	6,430	0.00	5,893,283	491.1	0	16,391,963	4,401,000	3.72
7.000	69.97	1,632	6,834	0.00	6,440,254	536.7	0	17,933,655	4,404,000	4.07
7.250	72.47	1,666	7,246	0.00	7,087,717	590.6	0	19,624,651	4,407,000	4.45
7.500	74.96	1,698	7,667	0.00	8,001,352	666.8	0	21,510,785	4,410,000	4.88
7.750	77.46	1,730	8,095	0.00	9,446,226	787.2	0	23,691,732	4,413,000	5.37
8.000	79.96	1,760	8,532	0.00	11,484,412	957.0	0	26,308,062	4,416,000	5.96
8.250	82.46	1,790	8,976	0.00	13,964,555	1,163.7	0	29,489,183	4,419,000	6.67
8.500	84.96	1,818	9,427	0.00	16,801,077	1,400.1	0	33,334,887	4,422,000	7.54
8.750	87.46	1,846	9,885	0.00	19,931,256	1,660.9	0	37,926,428	4,425,000	8.57
9.000	89.96	1,873	10,350	0.00	23,276,639	1,939.7	0	43,327,415	4,428,000	9.78
9.250	92.45	1,899	10,822	0.00	26,896,391	2,241.4	0	49,599,044	4,431,000	11.19
9.500	94.95	1,925	11,300	0.00	30,724,250	2,560.4	0	56,801,624	4,434,000	12.81
9.750	97.45	1,950	11,784	0.00	34,740,688	2,895.1	0	64,984,741	4,437,000	14.65
10.000	99.95	1,974	12,275	0.00	38,887,797	3,240.6	0	74,188,302	4,440,000	16.71



MFFP Safety Analysis Report

Docket No. 71-9295
Revision 0, June 2004

Corner Drop
05-16-1995, 15:38:39

*** PACKAGING TECHNOLOGY ***

CASKDROP, v2.21
Jul 01, 1994

SAMPLE PROBLEM FOR QUALITY ASSURANCE CHECK (AREAS AND VOLUMES)			
Impact Limiter Weight (each) -	1,000 lbs	Cask and Payload Weight -	10,000 lbs
Impact Limiter Outside Diameter -	60.0000 in	Cask Outside Diameter -	40.0000 in
Impact Limiter Overall Length -	24.0000 in	Cask Overall Length -	48.0000 in
Impact Limiter Conical Diameter -	48.0000 in	Dynamic Unloading Modulus -	1.000E+07 lbs/in
Impact Limiter Conical Length -	10.0000 in	Rad Mass Moment of Inertia -	12,235 lb-in-s ²
Impact Limiter End Thickness -	12.0000 in	Frictional Coefficient -	0.0000
Impact Limiter Hole Diameter -	20.0000 in	Drop Height -	30.0000 ft
Impact Limiter Hole Length -	8.0000 in	Drop Angle from Horizontal -	45.0000°
Unbacked Area Threshold Strain -	0.1000 in/in	Crush Analysis Theory -	Global
Unbacked Area Crush Stress -	2,611 psi	Number of Integration Incs -	25

POLYFOAM CRUSH STRESS (Axial: "1" to rise)	
Density = 20.000 pcf	
Temp = -20.000 F	
σ -yield = 2,552.3 psi	
Bias = 60.000%	
ϵ (in/in)	σ (psi)
0.000	0.0
0.100	2,552.3
0.200	2,687.0
0.300	2,868.8
0.400	3,302.9
0.500	4,115.1
0.600	6,074.3
0.650	7,942.0
0.700	10,925.0
0.750	15,001.8
0.800	26,829.5

POLYFOAM CRUSH STRESS (Radial: "1" to rise)	
Density = 20.000 pcf	
Temp = -20.000 F	
σ -yield = 2,675.0 psi	
Bias = 60.000%	
ϵ (in/in)	σ (psi)
0.000	0.0
0.100	2,675.0
0.200	2,785.4
0.300	2,959.9
0.400	3,345.9
0.500	4,147.7
0.600	6,062.8
0.650	7,868.8
0.700	10,180.0
0.750	15,554.4
0.800	29,704.8

POLYFOAM CRUSH STRESS (Actual Data @ 45.0°)	
Density = 20.000 pcf	
Temp = -20.000 F	
σ -yield = 2,611.5 psi	
Bias = 60.000%	
ϵ (in/in)	σ (psi)
0.000	0.0
0.100	2,611.5
0.200	2,734.9
0.300	2,913.3
0.400	3,324.2
0.500	4,131.3
0.600	6,068.5
0.650	7,905.2
0.700	10,532.8
0.750	15,270.6
0.800	28,157.6

DEFL (in)	MAX ϵ (%)	AREA (in ²)	VOLUME (in ³)	XBAR (in)	IMPACT FORCE (lbs)	ACCEL (g's)	I/L MOMENT (in-lbs)	STRAIN ENERGY (in-lbs)	KINETIC ENERGY (in-lbs)	SE/KE RATIO
0.250	1.44	7	1	-8.30	1,351	0.1	0	169	4,323,000	0.00
0.500	2.88	20	4	-8.11	7,756	0.6	0	1,307	4,326,000	0.00
0.750	4.33	36	11	-7.90	21,631	1.8	0	4,981	4,329,000	0.00
1.000	5.79	55	22	-7.68	44,807	3.7	0	13,286	4,332,000	0.00
1.250	7.25	78	39	-7.44	78,737	6.6	0	28,729	4,335,000	0.01
1.500	8.71	102	61	-7.19	124,483	10.4	0	54,131	4,338,000	0.01
1.750	10.18	129	90	-6.92	182,320	15.2	0	92,481	4,341,000	0.02



MFFP Safety Analysis Report

Docket No. 71-9295
Revision 0, June 2004

Corner Drop
05-16-1995, 15:38:39

*** PACKAGING TECHNOLOGY ***
(continued...)

CASKDROP, v2.21
Jul 01, 1994

DEFL (in)	MAX ϵ (%)	AREA (in ²)	VOLUME (in ³)	XBAR (in)	IMPACT FORCE (lbs)	ACCEL (g's)	I/L MOMENT (in-lbs)	STRAIN ENERGY (in-lbs)	KINETIC ENERGY (in-lbs)	SE/KE RATIO
2.000	11.66	158	126	-6.65	250,919	20.9	0	146,636	4,344,000	0.03
2.250	13.14	189	169	-6.39	327,791	27.3	0	218,975	4,347,000	0.05
2.500	14.63	222	221	-6.15	409,985	34.2	0	311,197	4,350,000	0.07
2.750	16.12	256	280	-5.92	495,229	41.3	0	424,349	4,353,000	0.10
3.000	17.64	290	349	-5.70	581,988	48.5	0	559,001	4,356,000	0.13
3.250	19.14	321	425	-5.53	666,955	55.6	0	715,119	4,359,000	0.16
3.500	21.04	350	509	-5.39	750,161	62.5	0	892,258	4,362,000	0.20
3.750	23.53	379	600	-5.30	832,241	69.4	0	1,090,058	4,365,000	0.25
4.000	26.04	407	698	-5.24	913,114	76.1	0	1,308,228	4,368,000	0.30
4.250	28.58	435	804	-5.21	993,967	82.8	0	1,546,613	4,371,000	0.35
4.500	31.14	462	916	-5.20	1,075,026	89.6	0	1,805,237	4,374,000	0.41
4.750	33.55	490	1,035	-5.22	1,157,389	96.4	0	2,084,289	4,377,000	0.48
5.000	35.86	517	1,161	-5.24	1,240,678	103.4	0	2,384,048	4,380,000	0.54
5.250	38.16	545	1,293	-5.27	1,325,202	110.4	0	2,704,783	4,383,000	0.62
5.500	40.44	573	1,433	-5.30	1,413,119	117.8	0	3,047,073	4,386,000	0.69
5.750	42.71	600	1,579	-5.33	1,503,231	125.3	0	3,411,616	4,389,000	0.78
6.000	44.96	628	1,733	-5.37	1,596,230	133.0	0	3,799,049	4,392,000	0.86
6.250	47.21	656	1,894	-5.40	1,692,397	141.0	0	4,210,127	4,395,000	0.96
6.359	48.17	668	1,966	-5.41	1,735,814	144.7	0	4,396,303	4,396,303	1.00
6.500	49.43	684	2,061	-5.42	1,792,981	149.4	0	4,837,403	4,398,000	1.10
6.750	51.75	711	2,236	-5.44	1,897,584	158.1	0	5,298,723	4,401,000	1.20
7.000	54.19	739	2,417	-5.46	2,009,560	167.5	0	5,787,116	4,404,000	1.31
7.250	56.65	767	2,605	-5.47	2,128,316	177.4	0	6,304,351	4,407,000	1.43
7.500	59.12	795	2,800	-5.48	2,255,709	188.0	0	6,852,354	4,410,000	1.55
7.750	61.60	824	3,002	-5.48	2,392,365	199.4	0	7,433,363	4,413,000	1.68
8.000	64.10	852	3,212	-5.47	2,538,941	211.6	0	8,049,776	4,416,000	1.82
8.250	66.60	881	3,429	-5.47	2,701,943	225.2	0	8,704,887	4,419,000	1.97
8.500	69.12	909	3,652	-5.45	2,882,629	240.2	0	9,402,959	4,422,000	2.13
8.750	71.65	938	3,883	-5.43	3,079,002	256.6	0	10,148,162	4,425,000	2.29
9.000	74.19	967	4,121	-5.38	3,300,885	275.1	0	10,945,648	4,428,000	2.47
9.250	76.75	995	4,367	-5.32	3,573,055	297.8	0	11,804,891	4,431,000	2.66
9.500	79.31	1,024	4,619	-5.26	3,901,592	325.1	0	12,739,222	4,434,000	2.87
9.750	81.89	1,053	4,879	-5.17	4,292,510	357.7	0	13,763,484	4,437,000	3.10
10.000	84.49	1,082	5,146	-5.06	4,763,070	396.9	0	14,895,432	4,440,000	3.35
10.250	87.09	1,109	5,419	-4.95	5,316,128	443.0	0	16,155,332	4,443,000	3.64
10.500	89.71	1,134	5,698	-4.83	5,947,562	495.6	0	17,563,293	4,446,000	3.95
10.750	92.34	1,161	5,985	-4.74	6,665,548	555.5	0	19,139,932	4,449,000	4.30
11.000	94.98	1,184	6,270	-4.63	7,465,195	622.1	0	20,906,275	4,452,000	4.70
11.250	97.64	1,206	6,563	-4.54	8,360,345	696.7	0	22,884,467	4,455,000	5.14



MFFP Safety Analysis Report

Docket No. 71-9295
Revision 0, June 2004

End Drop
05-16-1995, 15:38:39

*** PACKAGING TECHNOLOGY ***

CASKDROP, v2.21
Jul 01, 1994

SAMPLE PROBLEM FOR QUALITY ASSURANCE CHECK (AREAS AND VOLUMES)			
Impact Limiter Weight (each) -	1,000 lbs	Cask and Payload Weight -	10,000 lbs
Impact Limiter Outside Diameter -	60.0000 in	Cask Outside Diameter -	40.0000 in
Impact Limiter Overall Length -	24.0000 in	Cask Overall Length -	48.0000 in
Impact Limiter Conical Diameter -	48.0000 in	Dynamic Unloading Modulus -	1.000E+07 lbs/in
Impact Limiter Conical Length -	10.0000 in	Rad Mass Moment of Inertia -	12,235 lb-in-s ²
Impact Limiter End Thickness -	12.0000 in	Frictional Coefficient -	0.0000
Impact Limiter Hole Diameter -	20.0000 in	Drop Height -	30.0000 ft
Impact Limiter Hole Length -	8.0000 in	Drop Angle from Horizontal -	90.0000°
Unbacked Area Threshold Strain -	0.1000 in/in	Crush Analysis Theory -	Global
Unbacked Area Crush Stress -	2,552 psi	Number of Integration Incs -	25

POLYFOAM CRUSH STRESS (Axial: " " to rise)	
Density = 20.000 pcf	
Temp = -20.000 F	
σ -yield = 2,552.3 psi	
Bias = 60.000%	
ϵ (in/in)	σ (psi)
0.000	0.0
0.100	2,552.3
0.200	2,687.0
0.300	2,868.8
0.400	3,302.9
0.500	4,115.1
0.600	6,074.3
0.650	7,942.0
0.700	10,925.0
0.750	15,001.8
0.800	26,829.5

POLYFOAM CRUSH STRESS (Radial: "⊥" to rise)	
Density = 20.000 pcf	
Temp = -20.000 F	
σ -yield = 2,675.0 psi	
Bias = 60.000%	
ϵ (in/in)	σ (psi)
0.000	0.0
0.100	2,675.0
0.200	2,785.4
0.300	2,959.9
0.400	3,345.9
0.500	4,147.7
0.600	6,062.8
0.650	7,868.8
0.700	10,180.0
0.750	15,554.4
0.800	29,704.8

POLYFOAM CRUSH STRESS (Actual Data @ 90.0°)	
Density = 20.000 pcf	
Temp = -20.000 F	
σ -yield = 2,552.3 psi	
Bias = 60.000%	
ϵ (in/in)	σ (psi)
0.000	0.0
0.100	2,552.3
0.200	2,687.0
0.300	2,868.8
0.400	3,302.9
0.500	4,115.1
0.600	6,074.3
0.650	7,942.0
0.700	10,925.0
0.750	15,001.8
0.800	26,829.5

DEFL (in)	MAX ϵ (%)	AREA (in ²)	VOLUME (in ³)	XBAR (in)	IMPACT FORCE (lbs)	ACCEL (g's)	I/L MOMENT (in-lbs)	STRAIN ENERGY (in-lbs)	KINETIC ENERGY (in-lbs)	SE/KE RATIO
0.250	2.08	1,518	377	0.00	810,360	67.5	0	101,295	4,323,000	0.02
0.500	4.17	1,541	759	0.00	1,592,808	132.7	0	401,691	4,326,000	0.09
0.750	6.25	1,564	1,147	0.00	2,311,804	192.7	0	889,768	4,329,000	0.21
1.000	8.33	1,587	1,541	0.00	2,931,701	244.3	0	1,545,206	4,332,000	0.36
1.250	10.42	1,610	1,941	0.00	3,416,844	284.7	0	2,338,774	4,335,000	0.54
1.500	12.50	1,634	2,346	0.00	3,752,646	312.7	0	3,234,960	4,338,000	0.75
1.750	14.58	1,657	2,758	0.00	3,971,661	331.0	0	4,200,498	4,341,000	0.97



MFFP Safety Analysis Report

Docket No. 71-9295
Revision 0, June 2004

End Drop
05-16-1995, 15:38:39

*** PACKAGING TECHNOLOGY ***
(continued...)

CASKDROP, v2.21
Jul 01, 1994

DEFL (in)	MAX ϵ (%)	AREA (in ²)	VOLUME (in ³)	XBAR (in)	IMPACT FORCE (lbs)	ACCEL (g's)	I/L MOMENT (in-lbs)	STRAIN ENERGY (in-lbs)	KINETIC ENERGY (in-lbs)	SE/KE RATIO
1.785	14.88	1,661	2,816	0.00	3,995,461	333.0	0	4,341,425	4,341,425	1.00
2.000	16.67	1,681	3,175	0.00	4,112,712	342.7	0	5,354,946	4,344,000	1.23
2.250	18.75	1,705	3,598	0.00	4,214,497	351.2	0	6,395,847	4,347,000	1.47
2.500	20.83	1,729	4,027	0.00	4,287,704	357.3	0	7,458,622	4,350,000	1.71
2.750	22.92	1,753	4,462	0.00	4,351,294	362.6	0	8,538,497	4,353,000	1.96
3.000	25.00	1,777	4,904	0.00	4,445,683	370.5	0	9,638,119	4,356,000	2.21
3.250	27.08	1,801	5,351	0.00	4,562,636	380.2	0	10,764,159	4,359,000	2.47
3.500	29.17	1,826	5,804	0.00	4,693,990	391.2	0	11,921,237	4,362,000	2.73
3.750	31.25	1,851	6,264	0.00	4,831,784	402.6	0	13,111,959	4,365,000	3.00
4.000	33.33	1,875	6,730	0.00	4,973,522	414.5	0	14,337,622	4,368,000	3.28
4.250	35.42	1,900	7,202	0.00	5,120,673	426.7	0	15,599,396	4,371,000	3.57
4.500	37.50	1,925	7,680	0.00	5,274,868	439.6	0	16,898,839	4,374,000	3.86
4.750	39.58	1,951	8,164	0.00	5,437,800	453.2	0	18,237,922	4,377,000	4.17
5.000	41.67	1,976	8,655	0.00	5,611,685	467.6	0	19,619,108	4,380,000	4.48
5.250	43.75	2,002	9,152	0.00	5,802,397	483.5	0	21,045,868	4,383,000	4.80
5.500	45.83	2,027	9,656	0.00	6,018,789	501.6	0	22,523,516	4,386,000	5.14
5.750	47.92	2,053	10,166	0.00	6,268,472	522.4	0	24,059,424	4,389,000	5.48
6.000	50.00	2,079	10,682	0.00	6,560,063	546.7	0	25,662,991	4,392,000	5.84
6.250	52.08	2,105	11,205	0.00	6,900,740	575.1	0	27,345,591	4,395,000	6.22
6.500	54.17	2,131	11,735	0.00	7,296,837	608.1	0	29,120,288	4,398,000	6.62
6.750	56.25	2,158	12,271	0.00	7,751,903	646.0	0	31,001,381	4,401,000	7.04
7.000	58.33	2,184	12,814	0.00	8,272,373	689.4	0	33,004,415	4,404,000	7.49
7.250	60.42	2,211	13,363	0.00	8,862,880	738.6	0	35,146,322	4,407,000	7.98
7.500	62.50	2,238	13,919	0.00	9,556,877	796.4	0	37,448,792	4,410,000	8.49
7.750	64.58	2,265	14,482	0.00	10,454,871	871.2	0	39,950,260	4,413,000	9.05
8.000	66.67	2,606	15,051	0.00	11,632,851	969.4	0	42,711,226	4,416,000	9.67
8.250	68.75	2,633	15,706	0.00	13,506,993	1,125.6	0	45,853,706	4,419,000	10.38
8.500	70.83	2,660	16,368	0.00	14,954,954	1,246.2	0	49,411,449	4,422,000	11.17
8.750	72.92	2,688	17,037	0.00	16,218,008	1,351.5	0	53,308,070	4,425,000	12.05
9.000	75.00	2,715	17,712	0.00	18,519,890	1,543.3	0	57,650,307	4,428,000	13.02
9.250	77.08	2,743	18,394	0.00	22,571,268	1,880.9	0	62,786,702	4,431,000	14.17
9.500	79.17	2,771	19,084	0.00	27,794,818	2,316.2	0	69,082,462	4,434,000	15.58
9.750	81.25	2,799	19,780	0.00	33,405,583	2,783.8	0	76,732,513	4,437,000	17.29
10.000	83.33	2,827	20,483	0.00	39,286,171	3,273.8	0	85,818,982	4,440,000	19.33
10.250	85.42	2,827	21,190	0.00	45,050,964	3,754.2	0	96,361,124	4,443,000	21.69
10.500	87.50	2,827	21,897	0.00	51,018,884	4,251.6	0	108,369,855	4,446,000	24.37
10.750	89.58	2,827	22,604	0.00	57,507,705	4,792.3	0	121,935,678	4,449,000	27.41
11.000	91.67	2,827	23,311	0.00	64,451,479	5,371.0	0	137,180,576	4,452,000	30.81
11.250	93.75	2,827	24,017	0.00	74,690,773	6,224.2	0	154,573,358	4,455,000	34.70
11.500	95.83	2,827	24,724	0.00	85,563,336	7,130.3	0	174,605,121	4,458,000	39.17
11.750	97.92	2,827	25,431	0.00	96,435,898	8,036.3	0	197,355,026	4,461,000	44.24
12.000	100.00	2,827	26,138	0.00	107,308,461	8,942.4	0	222,823,071	4,464,000	49.92

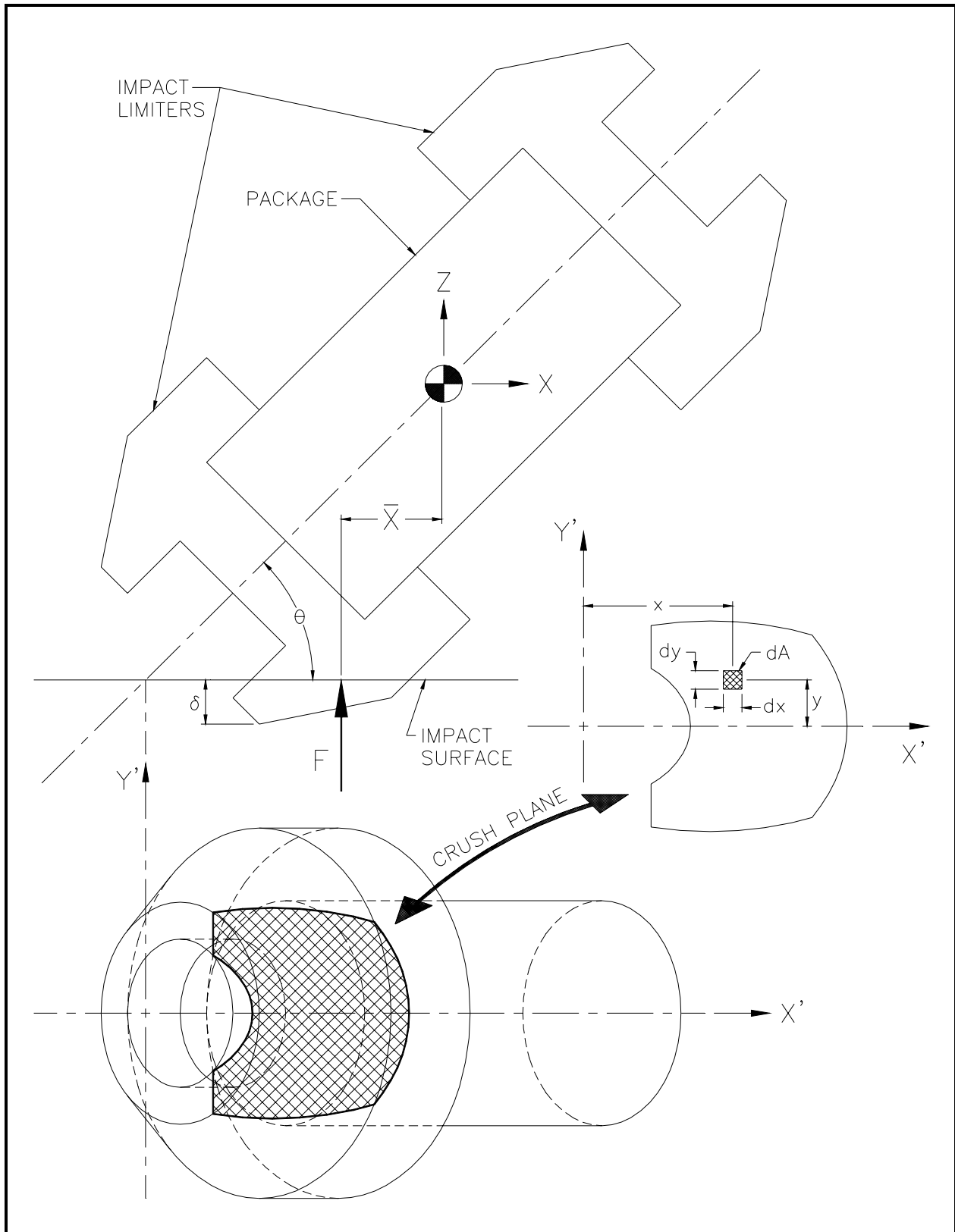


FIGURE 2.12.6-1 – Impact Limiter Force and Centroid Development

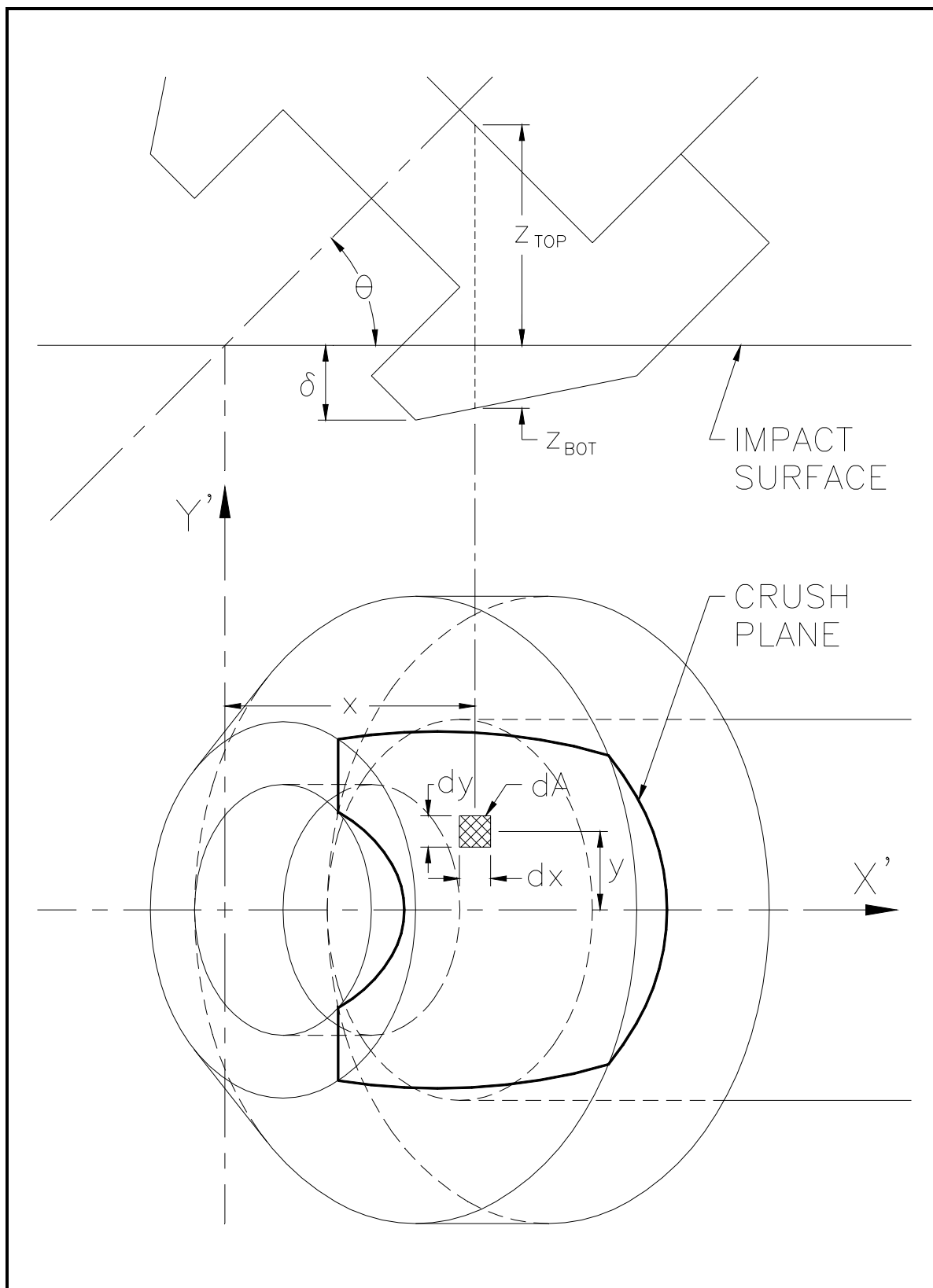


FIGURE 2.12.6-2 – Strain Determination

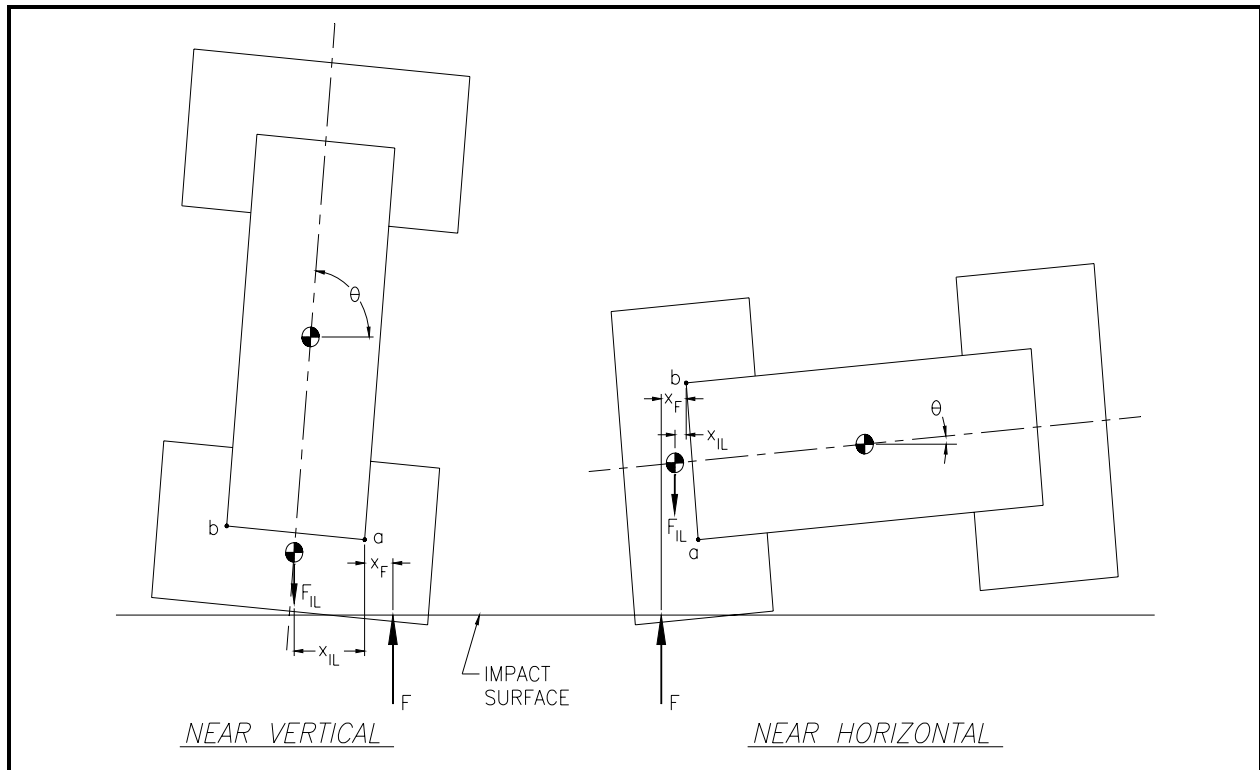


FIGURE 2.12.6-3 – Determination of Impact Limiter Separation Moments

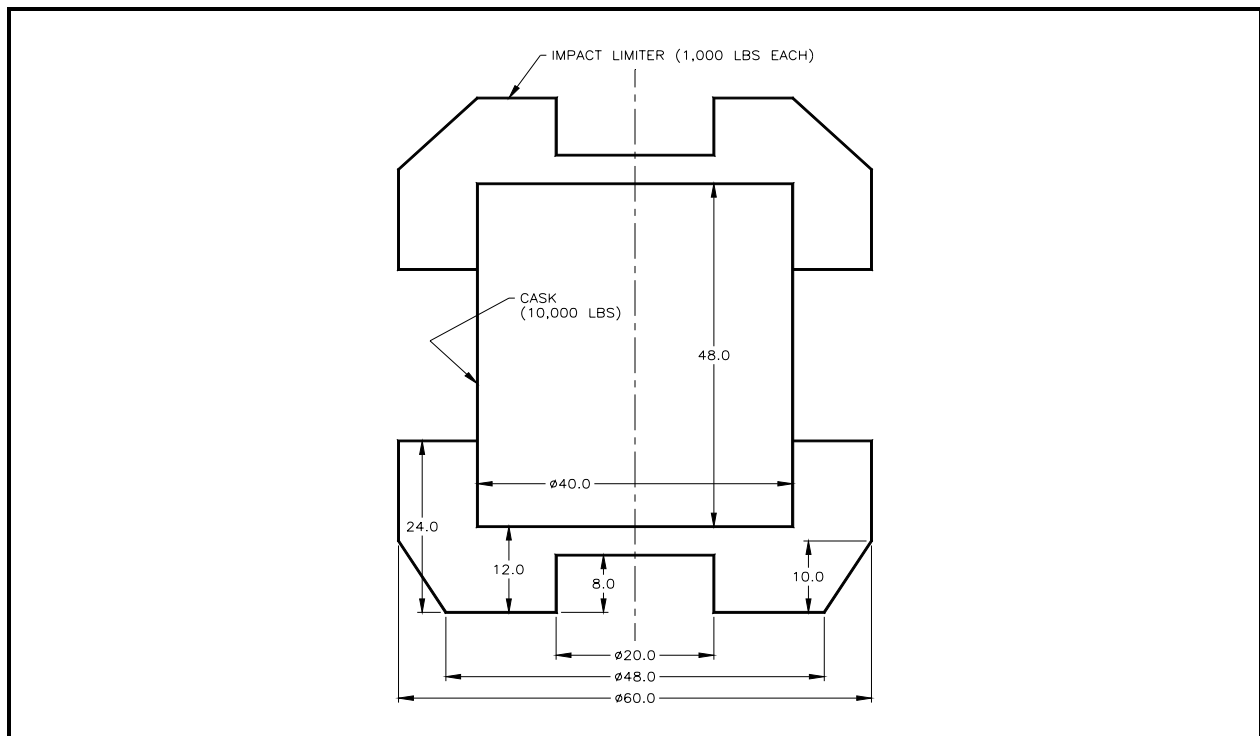


FIGURE 2.12.6-4 – Example Problem for CASKDROP

Packaging Technology's Cask Drop Analysis Program, v2.21						
Tuesday, May 16, 1995			9:38:19 pm			
[Input Window]						
Title: SAMPLE PROBLEM FOR QUALITY ASSURANCE CHECK (AREAS AND VOLUMES)						
IL Weight (each, lbs): 1000	Cask/Payload Weight (lbs): 10000					
IL Outside Diameter (in): 60	Cask Outside Diameter (in): 40					
IL Overall Length (in): 24	Cask Overall Length (in): 48					
IL Conical Diameter (in): 48	Free Drop Height (ft): 30					
IL Conical Length (in): 10	Radial Mass MI (lb-in-s ²): 12235.16					
IL End Thickness (in): 12	Frictional Coefficient (μ): 0					
IL End Hole Diameter (in): 20	Unloading Modulus (lbs/in): 10000000					
IL End Hole Length (in): 8	Crush Media Specification: PolyFoam					
[Control Window]						
Analysis	Crush (in)	Angle (°)	Static	Dynamic	Print	File
dXY: 25	Min: 0.25	Min: 0	Full <input checked="" type="checkbox"/>	Full <input type="checkbox"/>	Full <input type="checkbox"/>	Full <input checked="" type="checkbox"/>
Sln: Global	Max: 20	Max: 90	Smry <input type="checkbox"/>	Smry <input type="checkbox"/>	Smry <input type="checkbox"/>	Smry <input type="checkbox"/>
E/ σ : 0.1	Inc: 0.25	Inc: 45	Both <input type="checkbox"/>	Both <input type="checkbox"/>	Both <input type="checkbox"/>	Both <input type="checkbox"/>
[Output Window]						
[PgUp]/[PgDn] keys toggle active window; [F10] exits program						

FIGURE 2.12.6-5 – The CASKDROP Program *Input Window*

Packaging Technology's Cask Drop Analysis Program, v2.21					
Tuesday, May 16, 1995			9:38:29 pm		
[Input Window]					
Title: SAMPLE PROBLEM FOR QUALITY ASSURANCE CHECK (AREAS AND VOLUMES)					
IL Weight (each, lbs): 1000	Cask/Payload Weight (lbs): 10000				
IL Outside Di	[Polyurethane Foam Database]				
IL Overall	D (pcf): 20.0000		T (°F): -20.00		r (in): 40
IL Conical Di	σ (psi): 2552.3		Bias (%): 60		h (in): 48
IL Conical	t (ft): 30				
IL End Thi	in-s ²): 12235.16				
IL End Hole Di	nt (μ): 0				
IL End Hole	be/in): 10000000				
					cation: PolyFoam
[Control Window]					
Analysis	Cr	Orientation: Axial		Orientation: Radial	
dXY: 25	Mi				
Sln: Global	Ma				
E/ σ : 0.1	In				
[Output Window]					
[F2] calculates stress data and [F3] toggles orientation; [F10] exits...					

FIGURE 2.12.6-6 – The CASKDROP Program *Polyurethane Foam Window*

2.12.7 Impact Limiter Weld Joint Test Results

This appendix documents the results of bench tests of MFFP impact limiter weld joint designs. As shown in Figure 2.12.3-7 of Appendix 2.12.3, *Certification Test Results*, the closure weld (top outer corner angle) of the certification test unit (CTU) lid end impact limiter failed due to the 30-foot side free drop. Although the damage was assessed in Chapter 3.0, *Thermal Evaluation*, and determined to preserve O-ring seal temperatures within acceptable limits, maintaining the structural integrity of the weld joint is desirable.

Two 12-inch × 12-inch × 18-inch long L-shaped test specimens were fabricated to demonstrate weld joint integrity. The first test specimen (TS-1) utilized the weld joint for the impact limiter closure weld, as shown in the packaging drawings in Appendix 1.4.2, *Packaging General Arrangement Drawings*. The second test specimen (TS-2) was prototypic of the weld joint utilized for the CTU impact limiter. Both specimens were fabricated using Type 304 stainless steel material, which was the same material used for the CTU impact limiters. The two weld joint designs are shown in Figure 2.12.7-1.

2.12.7.1 Packaging Weld Joint Design

The packaging closure weld joint design utilizes a V-groove butt weld between the steel top plate and the corner angle. Since both the plate and the angle are joined through their full thickness, full-strength of the material is developed as the joint is deformed. The polyurethane foam is then fully encased in the steel shell of the impact limiter. Without direct exposure, the polyurethane foam will not experience any significant damage for the subsequent puncture drop and thermal event of 10 CFR §71.73¹.

2.12.7.2 Certification Test Unit Weld Joint Design

The closure weld of the CTU impact limiter consisted of a single-sided fillet weld between the corner angle and the 1/4-inch thick steel top plate, which included 1/2-inch deep slots at 5.2 inch spacing. Because the access to the inside of the plate and angle was not possible, the fillet weld was the only structural weld between the corner angle and the steel plate around the circumference of the impact limiter. During free drop impact, the plate/angle joint has to deform as a unit in order to maintain closure. However, the single-sided fillet weld is not adequate to cause the leg of the angle to deform with the plate. As the plate buckles and rotates due to compression of the impact, cracks develop in the fillet weld, which then leads to weld failure and separation between the angle and the 1/4-inch thick steel plate.

2.12.7.3 Bench Test Results

Each test specimen was placed in a hydraulic press so that the outside root of the angle was contacted by the hydraulic ram. The 1/4-inch plates were oriented at approximately 45 degrees with respect to the axis of the press. The test set-up is shown in Figure 2.12.7-2.

¹ Title 10, Code of Federal Regulations, Part 71 (10 CFR 71), *Packaging and Transportation of Radioactive Material*, Final Rule, 01-26-04.

Test Specimen 1 (TS-1) reflected the packaging weld joint design while Test Specimen 2 (TS-2) used the CTU weld joint design. Deforming TS-1 to nearly a flat condition resulted in no cracks developing in the welds. The fully deformed shape of TS-1 is shown in Figure 2.12.7-3. As shown in Figure 2.12.7-4, no cracks developed in the V-groove butt weld joint.

As TS-2 was deformed, cracks in the fillet welds initiated in the 1/2-inch slots. The cracks propagated beyond the slots into the straight section of the fillet weld as the specimen was further deformed. With continued deformation, the crack propagated until the fillet weld failed over its entire length. The plate was then separate from the angle leg, which did not bend. This behavior replicated the exact failure of the closure weld in the CTU impact limiters from the 30-foot side free drop. The TS-2 weld failure is shown in Figure 2.12.7-5 and Figure 2.12.7-6

2.12.7.4 Conclusions

Based on the comparable testing of the two different weld joint designs, it has been demonstrated that the design shown in the packaging drawings in Appendix 1.4.2, *Packaging General Arrangement Drawings*, is capable of large deformation without failure of the weld joint, and hence, preventing exposure of the polyurethane foam.

Security Related Information
Figure Withheld Under 10 CFR 2.390

FIGURE 2.12.7-1 – Weld Joint Designs for Test Specimens



FIGURE 2.12.7-2 – Bench Test Set-Up (TS-2 Shown)

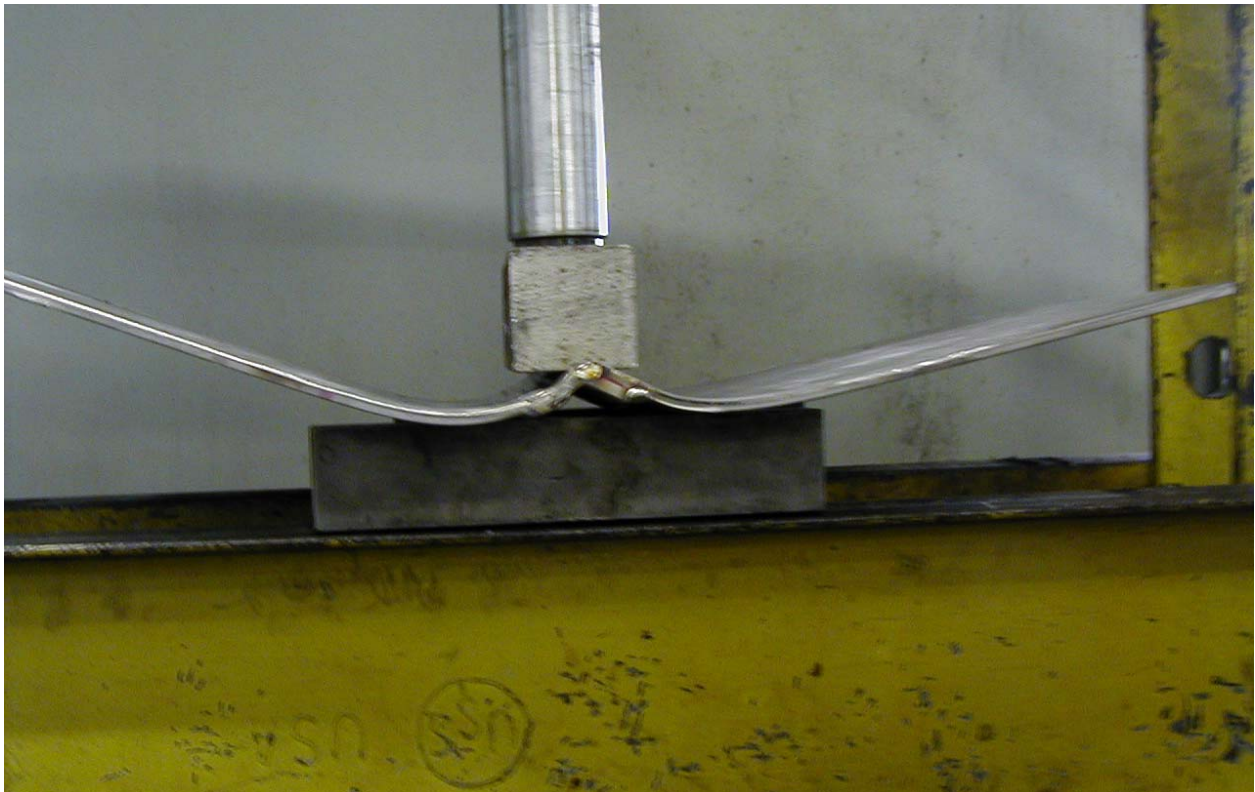


FIGURE 2.12.7-3 – TS-1 Fully Deformed



FIGURE 2.12.7-4 – View of V-Groove Weld of TS-1 (No weld cracks)

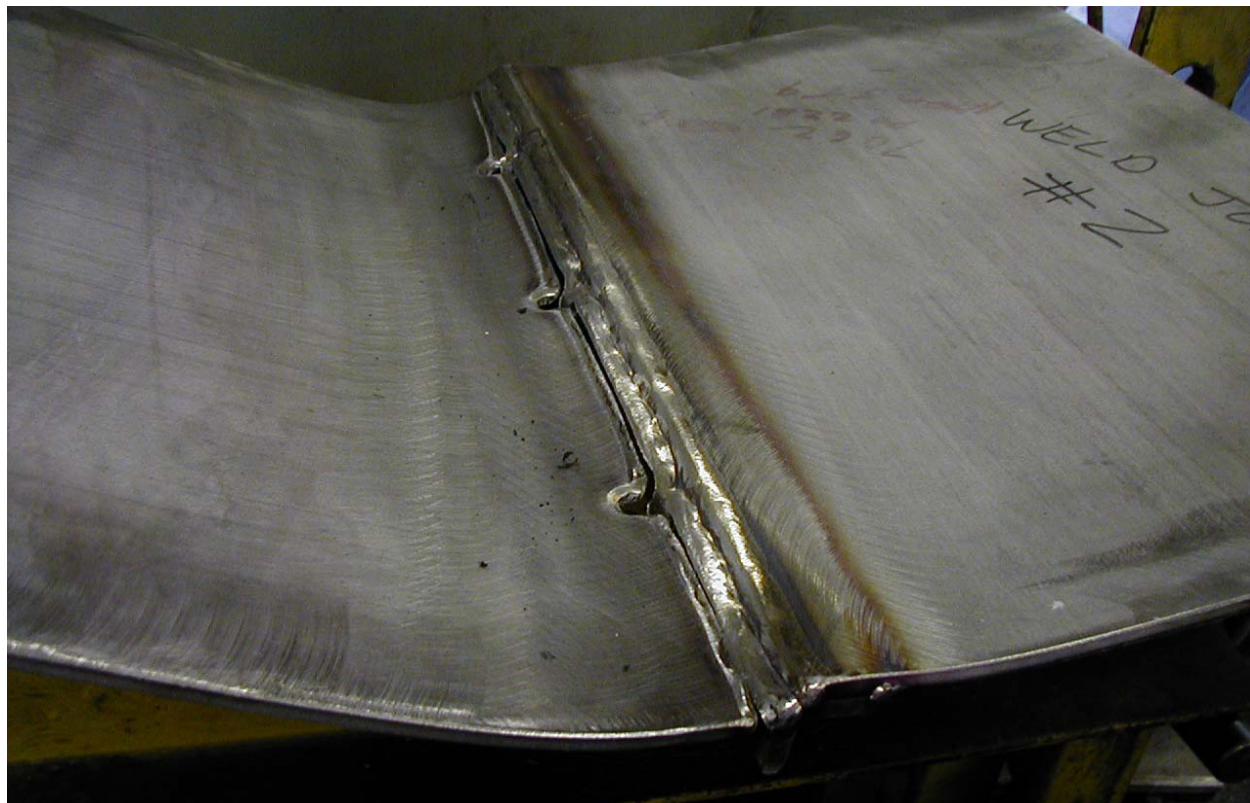


FIGURE 2.12.7-5 – View of Fillet Weld Failure of TS-2



FIGURE 2.12.7-6 – Close-up View of TS-2 Failed Fillet Weld Joint

2.12.8 Effect of Bounding Weight on Package Structural Responses

The free drop and puncture drop testing documented in Appendix 2.12.3, *Certification Test Results*, was performed without the presence of the fuel control structures (FCSs). Since the FCSs are integral with the strongback, they represent an additional contents weight that was not accounted for by the certification testing. Note that “contents” in this context refers to the fissile material contents (fuel assemblies) plus the strongback. This appendix documents the MFFP structural responses that would result from the increased weight of the contents consistent with the addition of the FCS.

2.12.8.1 Component Weights

As shown in Section 2.1.3, *Weights and Center of Gravity*, the maximum gross weight of the MFFP is 14,260 pounds, and the weight of the contents (including the FCS) is equal to the sum of the strongback (3,030 pounds) and three fuel assemblies (4,740 pounds), or 7,770 pounds. The certification test was performed in three series. The maximum gross weight and the weights of the certification test series are compared in Table 2.12.8-1 (Certification test weight data is extracted from Section 2.12.3.6, *Test Unit Description*).

2.12.8.2 Evaluations

The certification test series summary is given in Table 2.12.2-1. Each test is examined in the following paragraphs for the effect of the increased weight on the test results. Each evaluation focuses on the behavior of the package containment structure or impact limiters. The effect of the addition of the FCS on the strongback and fuel assembly behavior is evaluated separately in Appendix 2.12.5, *Fuel Control Structure Evaluation*. A buckling evaluation for the body shell is not needed since the increased weight, which is primarily associated with the contents, does not affect buckling response. The effect of maximum gross weight on the maximum impact limiter deformation in the warm condition is evaluated in Appendix 2.12.1, *Impact Limiter Evaluation*. The maximum deformations reported in Table 2.12.1-8 are evaluated using the maximum licensed package weight of 14,260 pounds (or 36.61 lb_m-s²/in, as shown in Table 2.12.1-6). Impact limiter maximum crush responses are not further evaluated in this appendix.

2.12.8.2.1 Test Series 1

The first test in Series 1 was a 30-ft horizontal free drop. The purpose of this test was to demonstrate that the containment shell would not experience excessive deformation or buckling from the lateral inertia forces. The payload of steel bars weighed 7,500 pounds, or 270 pounds less than the licensed contents weight. In reality, the weight of the containment shell itself contributes to the potential bending of the containment shell during the horizontal free drop. Therefore, taking into account the containment shell weight of 2,482 lbs, the additional weight of 270 lbs is only 2.6% of the licensed contents weight plus the shell weight. In the test, the containment shell did not experience any visible permanent deformation from the side drop impact. For this reason, the small increase of 270 pounds in contents weight will have no effect on the containment shell. Furthermore, as discussed in Section 2.12.2.2.1, *Mock Payload*, the steel bars together have a much smaller bending stiffness than the actual strongback used, and

consequently would exert somewhat less self-support than would the strongback, thus diminishing or even eliminating any possible effect due to the extra weight.

The next three tests in Series 1 were puncture bar attacks on various locations of the impact limiters. The weight of the certification test unit, 13,815 pounds, was 445 pounds (i.e., 3.1%) less than the maximum licensed weight of the MFFP of 14,260 lbs. Since the damage due to these impacts was minimal, as described in Section 2.12.3.8.1, *Certification Test Series No. 1*, it is reasonable to assume that an increase of only 3.1% in available puncture energy would have no effect. Thus, the extra contents weight would have little or no effect on the results from Test Series 1.

2.12.8.2.2 Test Series 2

The first test in Series 2 was a 30-ft, C.G.-over-corner (near vertical) free drop. The purpose of this test was to demonstrate that the closure system could withstand the inertia loading of the contents, and to test fuel assembly integrity. The prototypic strongback, prototypic fuel assembly, and two dummy fuel assemblies together weighed 6,906 pounds, or 864 pounds (i.e., 11.1%) less than the licensed contents weight. Although small, this difference could cause an increase in the loading on the closure system, which is evaluated as follows.

The effect on the closure lid structure is evaluated in two ways:

- Gross bending of the closure lid
- Puncture shear of the closure lid

The effect on the closure bolts is also evaluated.

Gross bending of the closure lid. The MFFP closure lid is a weldment consisting of two plates (3/4-inch thick outer plate and a 5/8-inch thick inner plate), which are connected by an array of radial and ring-shaped stiffeners. The total thickness of the lid weldment is 4.38 inches. During an end impact, the inertia load of the contents is applied to the inner surface of the lid as a pressure. The applied pressure is:

$$q = \frac{(w_{\text{contents}} + w_{\text{lid}})g}{(\pi/4)D_i^2} + p = 1,575 \text{ psi}$$

where: w_{contents} = 7,770 pounds (licensed weight of contents)

w_{lid} = 468 pounds (weight of closure lid)

D_i = 28.5 inches (inner diameter of package/closure lid)

g = 120g (end impact magnitude, from Section 2.12.5.2)

p = 25 psi (design pressure from Section 2.6.1.3.1)

For a simply supported circular plate of radius a , the maximum moment per unit width is at the center of the plate. From Roark¹, Table 24, Case 10a, the moment is:

¹ Young, W. C., *Roark's Formulas for Stress and Strain*, Sixth Edition, McGraw-Hill, 1989.

$$M_c = \frac{qa^2(3 + \nu)}{16} = 76,541 \text{ lb} \cdot \text{in/in}$$

where $\nu = 0.3$ and the radius a is conservatively based on the bolt circle diameter of the lid of 30.7 inches. In order to determine the bending stress in the closure lid, its moment of inertia per unit width (I_{total}) is determined by ignoring the stiffeners and taking credit only for the inner and outer lid plates. The vertical centroid, measured from the inner face of the inner plate is:

$$\bar{y} = \frac{\sum Ay}{\sum A} = \frac{(0.75)(4.00) + (0.625)(0.312)}{0.75 + 0.625} = 2.32 \text{ in}$$

The moment of inertia per inch of circumference is:

$$I_{\text{total}} = \sum (I + Ad^2) = \frac{1}{12}(0.75^3 + 0.625^3) + 0.75(4.00 - 2.32)^2 + 0.625(0.312 - 2.32)^2 = 4.69 \text{ in}^4 / \text{in}$$

The bending stress at the center of the plate is then given by:

$$\sigma_c = \frac{M_c \bar{y}}{I_{\text{total}}} = 37,863 \text{ psi}$$

The yield strength of the lid material at a bounding temperature of 200 °F is 47,100 psi from Table 2.2-1. The margin of safety against yield stress is:

$$MS = \frac{47,100}{37,863} - 1.0 = +0.24$$

Therefore, the closure lid remains elastic with the full contents weight when conservatively combining the cold, -20 °F impact to the warm, 200 °F material allowable.

Puncture shear of the closure lid. To evaluate puncture shear, a detailed evaluation of the load paths into and through the lid is made. During an end impact, the inertia load of the contents is sequentially supported as various parts of the strongback structure come into contact with the closure lid. Refer to Figure 2.12.8-1, which is a schematic representation of the structures which participate in the contact between the MFFP contents and the closure lid (the figure is to scale, but represents a composite cross section in order to show all of the elements in a single view). In the progress of the end impact, the first point of contact with the lid inner plate is at the outer rim of the top plate, as shown by the symbol ① in Figure 2.12.8-1. After undergoing approximately 0.3 inches of diaphragm deformation of the top plate, the BPRA Restraint Weldment comes in contact with the center portion of the lid, as shown by the symbol ②. All of the weight of the strongback and FCS is supported by either the top plate outer rim or the BPRA Restraint Weldment. A final contact can occur between the lid and the fuel assembly axial adjustment screws. As shown in Figure 2.12.8-1, these screws are located in the top plate and support the fuel assembly. Once the BPRA Restraint Weldment has come to rest against the closure lid, the fuel assemblies can cause further diaphragm deformation of the top plate by breaking the three, 1/2-13 UNC socket head cap screws which attach the top plate to the strongback (represented by a single bolt labeled 'B' in Figure 2.12.8-1). Note that the contact between the lid and the axial adjustment screws is driven solely by the weight of the fuel. The weight of the strongback and FCS continues to be carried into the closure lid by the top plate outer rim and the BPRA restraint weldment.

The structures of the closure lid which support the impact forces described above are also shown in Figure 2.12.8-1. The outer rim of the top plate is supported by the outer forging of the lid. The BPRA restraint weldment consists of three, 1-inch diameter hollow bars through which the bolts ('A' in the figure) pass. The three bars are placed on a 6.38-inch bolt circle, which are supported by the stiffening ring (7-inch diameter OD, 6-inch diameter ID) of the closure lid. The fuel assembly axial adjustment screws are supported by the inner plate of the closure lid.

The increase in contents weight from 6,906 pounds to 7,770 pounds arises from the following:

- Addition of 73 pounds to account for the maximum possible manufactured weight of the strongback.
- Addition of the FCS weight of 855 pounds.
- Reduction of 64 pounds since the simulated fuel weighed slightly more than the FA weight (including BPRA) of 4,740 pounds total.

As seen from this breakdown, all of the increase in weight is either part of the strongback structure, or, in the case of the FCS, is fully carried by the strongback. Consequently, in an end drop, the added weight will be carried into the closure lid by the same paths as was the weight of the strongback in the Series 2 free drop, namely, through the top plate outer rim and through the BPRA Restraint Weldment. Since these two pathways are well supported by internal closure lid structure, the added weight does not create a risk of puncture shear in the closure lid inner plate. The only source of load path into the closure lid that is not fully supported by internal structure is the fuel assembly axial adjustment screws. However, the licensed weight of the MOX FA is slightly less than the weight of the simulated fuel assembly actually tested. For this reason, no risk of puncture shear of the closure lid is presented by the increased contents weight.

Closure bolts. As for the normal conditions of transport bolt analysis given in Section 2.6.1.3.4, *Closure Bolt Evaluation*, NUREG/CR-6007² will be used to evaluate the closure bolts. The analysis makes the following assumptions:

- From Section 2.6.1.3.4, *Closure Bolt Evaluation*, the maximum force due to pre-load ($F_{a_{max}}$) is equal to 22,420 pounds. Differential thermal expansion ($F_{a_{therm}}$) is not applicable for HAC. Therefore, $F_{a_{pt}}$ as discussed in Table 4.9 of NUREG/CR-6007 is equal to 22,420 pounds.
- The sum of the tensile forces for the remaining loads ($F_{a_{al}}$) is equal to the sum of the forces resulting from the internal pressure load ($F_{a_{pressure}} = 687$ pounds) as calculated in Section 2.6.1.3.4, *Closure Bolt Evaluation*, and the vertical component of the impact load ($F_{a_{impact}}$) calculated below.
- In Appendix V of NUREG/CR-6007, $F_{a_{impact}}$ is calculated based on the very conservative assumption that the package is supported only at the impact corner of the package, and ignores any support provided by the impact limiter. The following analysis assumes some support is provided by the impact limiter. A modified derivation of $F_{a_{impact}}$ follows below.
- The closure lid has a step located at the bolt circle diameter that precludes prying forces.

² G.C. Mok, L.E. Fischer, S.T. Hsu, *Stress Analysis of Closure Bolts for Shipping Casks*, NUREG/CR-6007, UCRL-ED-110637, U.S. Nuclear Regulatory Commission, April 1992.

- There are no applied shear stresses from the horizontal component of the impact force since the shear load is carried by the closure lid.
- Per Table 6.3 of NUREG/CR-6007, the “tension plus shear plus bending plus residual torsion” stress limit is not evaluated for HAC. Therefore, the residual torsion stress is not considered in the calculation.

The maximum bolt impact force is now determined. Because of the cold conditions, the impact limiter crush zone has a minimum possible volume, resulting in the smallest possible crush foot print. Moreover, the regulatory test articles weighed slightly less than the maximum MFFP weight, which also results in a smaller crush volume. Consequently, the crush zone resulting from the regulatory drop predicts a conservative minimum backing of the closure bolts by the impact limiter.

The shape of the impact limiter crush zone is a wedge shape due to the impact angle as illustrated in Figure 2.12.8-2. The maximum depth of the deformation is measured as 6.1 inches as stated in Section 2.12.3.8.2.2, *Series 2, Test 1: HAC 80-Degree Oblique C.G.-Over-Corner 30-foot Drop*. Given this crush depth, the impact footprint extends nearly to the edge of the impact limiter’s 36 inch diameter face, as shown in Figure 2.12.8-2. The impact limiter has a 20-inch diameter hole on its end having a depth of 8 inches. Conservatively, no support is assumed for the area of the 20-inch diameter hole.

At a minimum, the impact limiter will provide support to the closure lid over the vertical projection of the footprint area onto the lid. Rather than assuming that the zone extends to the edge of the impact limiter’s 36 inch diameter face, it is conservatively assumed that the zone will extend only to the edge of the 20 inch hole. The force distribution will be a maximum at the impact corner of the closure lid, and will linearly decrease to zero at the opposite edge of the supported zone. Figure 2.12.8-2 illustrates the force distribution.

Using the nomenclature from NUREG/CR-6007 for the impact gs (a_i) and the drop angle (π_i), the total reaction force provided by the impact limiter equals the vertical component of the weight supported by the impact limiter multiplied by the impact gs and is given by:

$$R_{IL,y} = (W_{TOTAL-IL} \sin(\pi_i)) \times a_i$$

Because of the shape and distribution of the reaction force, the center of pressure of the distributed reaction force acts at location 8.28 inches from the impact corner of the closure lid as determined by 3D computer-aided design (CAD) software, and shown in Figure 2.12.8-2. This arm length is referred to as (y_f).

As shown on the free body diagram V.1 in Appendix V of NUREG/CR-6007, the vertical component of the load applied by the lid (W_l) and payload (W_c) during impact is equal to L , or:

$$L = ((W_l + W_c) \sin(\pi_i)) \times a_i$$

Taking into consideration the support force $R_{IL,y}$, the summation of moments about the impact point (Appendix V, equation V.1) becomes:

$$\sum fb \ y_b = L \ (y_L) - R_{IL,y} \ (y_f)$$

where (y_L) is the distance from the impact point to the center of the applied load (L), which equals the outside radius of the lid (R_{lo}). Following the derivation in Appendix V, the maximum bolt force, $(fb)_{max}$, for a bolt pattern having a total number of bolts (N_b) becomes:

$$(fb)_{\max} = \frac{4}{3} \frac{L(yL) - R_{IL,y}(yf)}{(Rlo)(Nb)}$$

In summary, the moment in the direction of opening the lid is $L(yL)$, the moment of the impact limiter in resisting that moment is $R_{IL,y}(yf)$, and the balance is resisted by the closure bolt forces.

Substituting the above equation into the equation for the axial force in Table 4.5 of NUREG/CR-6007 for an unprotected closure lid gives the following equation:

$$Fa_{\text{impact}} = \frac{1.34(ai)\sin(\pi i)[(Wl + Wc)Rlo - W_{\text{TOTAL-IL}}(yf)]}{Nb(Rlo)} = 11,157 \text{ lb}_m$$

where:

- Wl = 468 pounds (weight of closure lid)
- Wc = 7,770 pounds (licensed weight of contents)
- $W_{\text{TOTAL-IL}}$ = 12,770 pounds (MFFP weight (14,260 lb_m) - lower limiter weight (1,490 lb_m))
- Rlo = 16.15 inches (outer radius of closure lid)
- yf = 8.28 inches (location of reaction force centroid from lid edge)
- πi = 80° (package orientation)
- ai = 120g (impact magnitude)
- Nb = 24 (number of bolts)

The combined maximum tensile bolt forces are equal to:

$$Fa_{\text{al}} = Fa_{\text{pressure}} + Fa_{\text{impact}} = 687 + 11,157 = 11,844 \text{ lb}$$

A comparison of Fa_{pt} with Fa_{al} per Table 4.9, Step 1.4 of NUREG/CR-6007, shows that Fa_{pt} , equal to 22,420 pounds, is greater than Fa_{al} . Therefore, calculation of the average bolt stress (S_{ba}) is based on the pre-load, not the impact loads:

$$S_{ba} = (1.2732) \frac{Fa_{\text{pt}}}{Db a^2} = 66,943 \text{ psi}$$

where $Db a = 0.653$ inches from Section 2.6.1.3.4. From Table 2.1-1, the HAC allowable average tensile stress is the lesser of S_y (equal to 106,300 psi) or $0.7S_u$ (equal to $0.7 \times 140,000 = 98,000$ psi), with material properties taken from Table 2.2-5 at 200 °F. The corresponding margin of safety on average tensile stress, S_{ba} , is:

$$MS = \frac{98,000}{66,943} - 1.0 = +0.46$$

Since the calculated stress is less than the material yield strength of 106,300 psi, there is no plastic deformation in the closure lid or seal region. Because there is no resulting shear stress, the “Average Shear Stress” and the “Average Tensile + Average Shear” criteria are met.

The second test in Series 2 was a puncture drop test on the impact damage from the prior free drop. The weight of the certification test unit, 13,234 pounds, was 1026 pounds (i.e., 7.2%) less than the maximum licensed weight of the MFFP. However, based on the very minimal damage done to the impact limiter as a result of this test (see Figure 2.12.3-18), an increase in available

puncture energy of 7.2% will have a negligible effect. Thus, the extra contents weight would have little or no effect on the results from Test Series 2.

2.12.8.2.3 Test Series 3

The first two tests in Test Series 3 were 30-ft free drops in a slapdown orientation, one with the closure lid end striking first, and one with the closure lid end striking second. Each test also featured a different azimuth orientation of the strongback. As stated in Table 2.12.2-1, these two drops were planned to test the strongback and the closure system in the lateral direction. The effect of the added FCS weight on the strongback structure is evaluated in Appendix 2.12.5, *Fuel Control Structure Evaluation*. The added contents weight will have no effect on the behavior of the closure system in a slapdown orientation, since the secondary impact orientation was essentially horizontal.

The second two tests were puncture attacks on the containment boundary shell. The weight of the certification test unit, 13,217 pounds, was 1043 pounds (i.e., 7.3%) less than the maximum licensed weight of the MFFP. The governing case was Test 3, which was oriented perpendicular to the surface and directed through the package C.G. As stated in Section 2.12.3.8.3.4, *Series 3, Test 3: HAC Horizontal Puncture Drop*, the damage consisted of an indentation of approximately 2.13 inches deep. As shown in Figure 2.12.3-35, the deformation was not severe, and no cracking or loss of leaktight condition was noted from the test. An additional available puncture energy of 7.3% could produce an additional deformation of $0.073 \times 2.13 = 0.16$ inches. This modest increase in deformation would not cause containment boundary failure or loss of a leaktight condition. Thus, the extra contents weight would have little or no effect on the results from Test Series 3.

2.12.8.3 Conclusions

As shown in the foregoing calculations, the additional weight of the MFFP, up to the maximum licensed weight, will have little or no effect on the results obtained from full-scale certification testing.

Table 2.12.8-1 – Summary of Certification Test Unit Weights (pounds)

Component	Licensed	Test Series 1	Test Series 2	Test Series 3
Strongback	3,030	N/A	2,102	2,100
Fuel Assemblies	4,740	7,500*	4,804	4,788
<i>Contents Sum</i>	7,770	7,500	6,906	6,888
Empty Package**	6,490	6,315	6,328	6,329
<i>Gross Package</i>	14,260	13,815	13,234	13,217

*Mock payload composed of small steel rods.

**Empty package, without strongback.

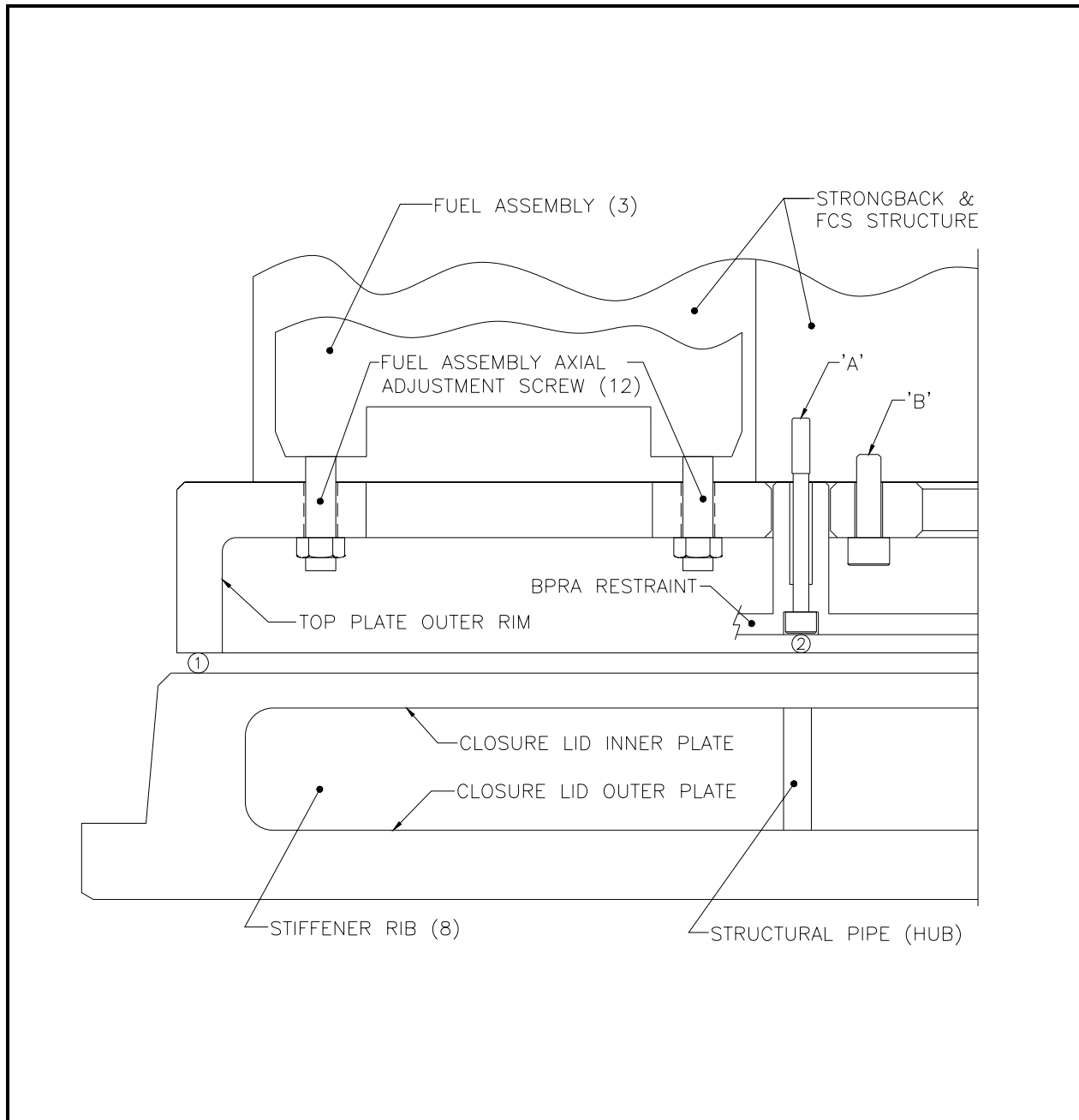


FIGURE 2.12.8-1 – Impact Conditions at the Top Plate – Closure Lid Interface

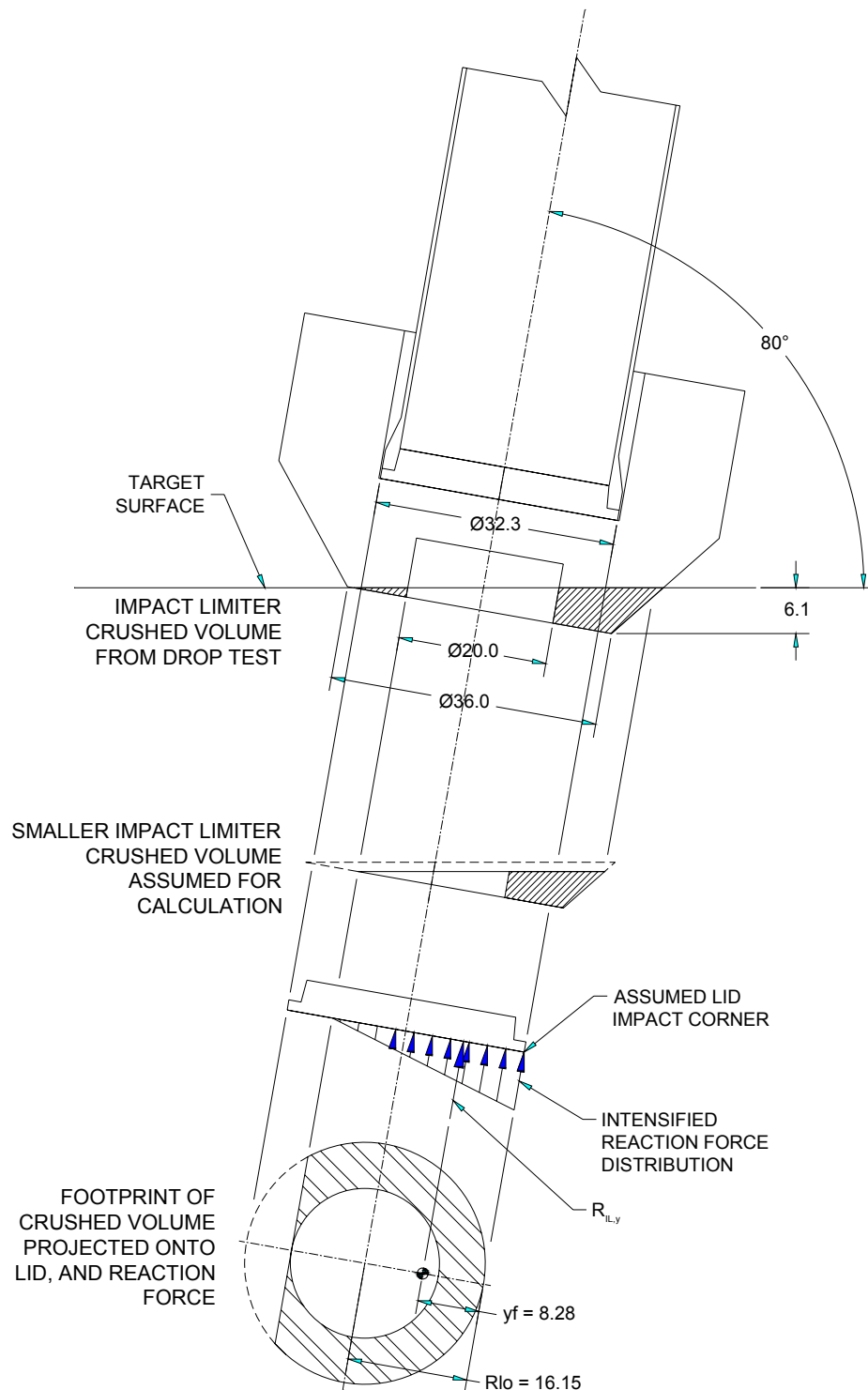


FIGURE 2.12.8-2 – Support Provided by the Impact Limiter

This page left intentionally blank.

3.0 THERMAL EVALUATION

3.1 Description of Thermal Design

This section identifies and describes the principal thermal design aspects of the MFFP. Further, this chapter demonstrates the thermal safety of the system and compliance with the thermal requirements of 10 CFR 71¹ when transporting a payload of up to three (3) mixed oxide fuel assemblies (MOX FAs) generating a maximum of 240 watts of decay heat. Specifically, all package components are shown to remain within their respective temperature limits under the normal conditions of transport (NCT). Further, per 10 CFR §71.43(g), the maximum accessible package surface temperature is demonstrated to be less than 122 °F for the maximum decay heat loading, an ambient temperature of 100 °F, and no insolation. The bulk temperature of the impact absorbing foam is shown to be less than 150 °F, based on NCT maximum temperature conditions. Therefore, the foam will retain sufficient structural integrity to protect the payload during the subsequent hypothetical accident condition (HAC) free drop scenarios described in Chapter 2.0, *Structural Evaluation*. Finally, the package is demonstrated to structurally withstand the damage arising from the HAC free drop scenarios and retain sufficient thermal protection to maintain all package component temperatures within their respective short term limits during the regulatory fire event and subsequent package cool-down.

3.1.1 Design Features

The MFFP packaging is designed to be a totally passive thermal system for transporting up to three (3) mixed oxide fuel assemblies (MOX FAs), with or without burnable poison assemblies installed. As described in Section 1.1, *Introduction*, the MFFP consists of a strongback assembly that provides support for three (3) fresh MOX PWR FAs, a stainless steel cylindrical vessel that provides leaktight containment, and energy absorbing impact limiters.

3.1.1.1 Body

The package body serves as a single containment boundary for the payload of MOX FAs. The components that form the containment boundary are the cylindrical shell, the bottom plate, the seal flange, the inner plate and seal ring of the closure lid, the vent port plug and elastomeric seal, the fill port plug and elastomeric seal, and the closure lid containment elastomeric O-ring. The cylindrical cavity formed by these components is 28½ inches in diameter and 165.45 inches in length.

The 9/16-inch thick body shell is fabricated from ASTM SA-240, XM-19 austenitic stainless steel. A circumferentially continuous doubler plate is used near each end of the shell to interface between the six impact limiter attachment lugs and the shell. The doubler plate also serves to provide an interface with the transportation skid for longitudinal restraint. The lid end of the body is locally thicker than the body shell to accommodate the closure lid sealing area and the closure bolt threaded holes. The wall thickness transition is a 3:1 minimum taper. The bottom end closure is fabricated from a 1½ inch thick forging. There are no containment penetrations located at the bottom end of the body.

¹ Title 10, Code of Federal Regulations, Part 71 (10 CFR 71), *Packaging and Transportation of Radioactive Material*, Final Rule, 01-26-04.

The closure lid is a weldment constructed of XM-19, and has a construction that provides significant strength and stiffness while also being weight efficient. The closure lid is constructed of a 3/4-inch thick outer plate and 5/8-inch thick inner plate, stiffened with eight, 1/2-inch thick radial ribs that are three inches deep. A 1/2-inch thick, 6-inch inner diameter cylinder forms a hub at the inner end of the radial ribs. The ribs are welded on all four edges to the adjacent structure. Each rib has a projection that passes through a slot in the outer plate, and the ribs and outer plate are securely welded together using 1/2-inch groove welds. The closure lid inner plate is welded to the outer ring using a full-penetration weld. The seal flange of the closure lid has a minimum thickness of one inch, and provides locations for three closure O-ring seals for leakage rate testing, as well as providing a location for the vent, fill, and test ports. The closure lid is attached to the body using twenty four (24) 3/4-10UNC ASTM A564, Grade 630 (H1100) socket head cap screws (SHCS).

Package closure is sealed using a single 3/8-inch cross-section diameter bore-type O-ring seal made from butyl rubber. O-rings of similar construction are located on either side of the containment O-ring to facilitate leakage rate testing. The inner O-ring creates a cavity, which is backfilled with helium during leakage rate tests. The outer O-ring is utilized to create a cavity for leakage rate testing. The body cavity is filled with atmospheric air during transport operations.

3.1.1.2 Impact Limiters

Impact limiters are installed at each end of the MFFP to provide thermal and impact protection under all regulatory conditions. The impact limiters are comprised of cylindrical and conical sections, with a maximum outer diameter of 60 inches. A recessed region at the bottom of the limiter is designed to reduce end drop impact forces. This recess has a diameter of 20 inches and a depth of eight inches. The impact limiter shells are constructed of ASTM A240, Type 304 stainless steel. The lid end impact limiter has 1/4-inch thick shells (5/16-inch thick for the recessed end plate) to resist perforation in the HAC puncture drop event, and to protect the closure lid and sealing area from damage due to the HAC puncture drop and thermal events. The bottom impact limiter has 11-gauge (0.12-inch thick) shells. Within the impact limiter shells is closed cell, rigid polyurethane foam. The polyurethane foam provides the majority of the energy absorption during the HAC free drop events, and thermal protection of the O-ring seals during the HAC fire event. Each impact limiter is secured to the body using six, relatively long, 1-8 UNC, ASTM A320, Grade L43 socket head cap screws (SHCS), with a majority of the shank length reduced to a diameter of 0.805 inches.

3.1.1.3 Strongback

The strongback assembly is fabricated primarily of ASTM A240, Type 304 stainless steel. The strongback longitudinal weldment is 1/4-inch thick plate, and provides support for the neutron poison plates and for the MOX FAs. Eight support disk assemblies, each of which are composed of three clamp arm assemblies, are attached to the strongback longitudinal weldment at each fuel assembly grid location. Between the clamp arm assemblies, the fuel control structures (FCSs) are attached to the strongback. The clamp arm assemblies are hinged to allow loading of the fuel assemblies. The clamp arms are designed with clamping mechanisms to securely clamp the fuel assemblies onto the strongback. Each clamp arm is constructed of two 3/8-inch thick plates, separated by the fuel clamping mechanism and stiffened to provide in-plane stability.

The FCS assemblies are constructed of a 1/8-inch thick angle plate constructed of Type 304 austenitic stainless steel. In the center of the longitudinal span of each FCS is a stiffener, constructed of 1/4-inch thick Type XM-19 austenitic stainless steel. Each FCS assembly is hinged to assist FA loading and unloading.

The top and bottom end plates clamp the top and bottom fuel assembly nozzles in the same way that the grids are clamped, and provide axial restraint to the fuel assembly. The loaded strongback is slid into and out of the body horizontally, aided by anti-friction plastic pads located in the top and bottom end disks. The top and bottom plate assemblies support the strongback such that the smaller support disks have no contact with the body shell.

When installed in the body, the inner end of the strongback is supported on a 2¼ inch diameter trunnion, which is bolted to the center of the inside of the bottom end closure. The upper end is supported by the contact between the top plate assembly and the body, and is secured to prevent axial motion of the strongback under normal over-the-road transportation forces using three removable SHCS that engage three lugs machined into the body weldment.

3.1.1.4 Neutron Moderation and Absorption

Criticality control is provided in the MFFP by the geometric spacing of the fuel assemblies and by borated neutron poison plates contained on the strongback assembly and the FCSs. The strongback weldment, clamp arm assemblies, and FCSs maintain the geometric spacing for the FAs. The borated neutron poison plates are secured to the strongback weldment by cover pads at ten locations corresponding to the fuel assembly clamping locations. On the FCSs, the neutron poison plates are secured with flat head machine screws. The neutron poison plates do not support any structural loading except their own weight.

3.1.1.5 Receptacles, Valves, Testing and Sample Ports

The package design includes a seal test port, a fill port, and a vent port. The seal test port accesses the cavity between the middle (containment) and upper O-ring bore seals on the closure lid, thereby allowing leaktight verification prior to shipping the loaded package. The fill port allows helium to be placed on the inner side of the containment O-ring seal for leaktight verification. The vent port permits venting of the internal cavity during loading and unloading of the package. Each port is an integral, recessed part of the closure lid, which protects the ports. There are no receptacles or valves utilized on this package.

3.1.2 Content's Decay Heat

The MFFP packaging is designed to transport up to three (3) MOX FAs, with or without burnable poison rod assemblies (BPRAs). As described in Section 1.2.3, *Contents of Packaging*, the MOX FAs are 17 × 17 un-irradiated, PWR commercial reactor fuel assemblies with 264 fuel rods, 24 guide tubes, and 1 instrument tube. A decay heat loading of 80 watts per assembly, evenly distributed over the 144 inch active fuel length, is utilized for the thermal evaluation.

3.1.3 Summary of Temperatures

The maximum temperatures for the MFFP under NCT and HAC conditions are summarized in Table 3.4-1 and Table 3.5-1, respectively.

3.1.4 Summary of Maximum Pressures

The maximum normal operating pressure (MNOP) for the MFFP resulting from the NCT Hot condition and conservative assumptions is 10 psig. The NCT internal pressures are presented in Table 3.4-2. Further details of these analyses are presented in Section 3.4.2, *Maximum Normal Operating Pressure*.

The maximum peak pressure generated within the package cavity under HAC conditions is estimated to be 138.2 psia (123.5 psig) at the end of the fire when the peak cavity gas temperature is reached. The pressure will then decrease as the package cools, reaching 76.5 psia (61.8 psig) 9.5 hours after the end of the fire. The HAC internal pressures are presented in Table 3.5-2. Further details of the analyses are presented in Section 3.5.3, *Maximum Temperatures and Pressures*.

3.2 Material Properties and Component Specifications

3.2.1 Material Properties

The thermally significant materials used in the fabrication of the MFFP include the following:

- XM-19 stainless steel used for the body shell, bottom, and closure lid
- Type 304 stainless steel used for the strongback structure and the impact limiter shells
- ASTM A320 Type L43 alloy steel used for the impact limiter attachment bolts
- ASTM A564, Grade 630 used in the closure lid bolts
- Polyurethane foam (nominal density of 10 lb_m/ft³) used in the lid end impact limiter
- Polyurethane foam (nominal density of 30 lb_m/ft³) used to provide thermal protection around the collar of the body.

This section presents the thermal properties used in the heat transfer model and the references from which they are obtained.

Table 3.2-1 presents the thermal properties for the A240, Type 304 stainless steel and the XM-19 austenitic stainless steel. The density of Type 304 stainless steel is 495.9 lb_m/ft³, while the density of XM-19 stainless steel is 492.5 lb_m/ft³.

Table 3.2-2 presents the material properties for the neutron absorbing material (i.e., boral). The boral material is a composite of a core material (chemical composition 69% aluminum, 24% boron, 6% carbon, 0.5% iron, and 0.1% silicon, titanium, copper, and zinc) sandwiched in a protective aluminum clad layer. The thermal conductivity is listed as bi-directional since the composite material exhibits a different thermal conductivity across the layers than along the layers. The combined material properties for the composite panel are computed as a function of thicknesses of the clad and core matrix materials. These parameters, in turn, are a function of the desired boron loading (i.e., 0.035 g/cm²) and temperature. The manufacturer's procedure for calculating the thermal conductivity, specific heat, and density are used to arrive at the specific values presented in Table 3.2-2.

Table 3.2-3 presents thermal properties for the A320, Grade L43 material used for the impact limiter attachment bolts and the A564, Grade 630 material used for the closure lid bolts. The density of the ASTM A320, Grade L43 material is 489.0 lb_m/ft³, while the density of the ASTM A564, Grade 630 material is 486.9 lb_m/ft³.

The heat transfer within the MOX FA is a combination of conduction and radiation heat transfer within and between the individual rods of the fuel assembly. Rather than include the details of the fuel geometry in the thermal model, the fuel assemblies and the surrounding space between the edges of the FAs and the surrounding surfaces of the strongback structure are represented as homogenous solid region with anisotropic thermal properties. The thermal properties are based on a detailed model of the FA geometry (see Appendix 3.6.2.2, *Effective Thermal Conductivity of MOX Fuel Assemblies*). The model accounts for conduction and radiation heat transfer between the individual rods and across the space between the edges of the FA and the strongback surfaces. The results of this detailed modeling are used to compute an 'effective thermal conductivity' for the radial and the axial directions. The same thermal properties can be conservatively applied to both the vertical and horizontal orientations of the fuel assembly. Table 3.2-4 presents the effective, anisotropic thermal properties for the homogenized fuel

region. Appendix 3.6.2, *Thermal Model Details*, presents the details of the methodology used to compute the various values.

Table 3.2-5 presents the thermal properties for the miscellaneous materials used in the thermal model. Material properties for the 11½ pcf polyurethane foam used in the lower impact limiter are not required since the 1/4-symmetry thermal model used for this safety calculation does not include the lower impact limiter. Specific thermal properties for the neoprene rubber and Delrin[®] plastic used for padding and bearing surfaces are not needed since the thermal model ignores the relatively small effect that these components have on the overall package conductivity. The impact of these materials on gas generation and maximum operating temperatures are considered. Table 3.2-6 presents the thermal conductivity of air. Because the thermal conductivity of air varies significantly with temperature, the computer model calculates the thermal conductivity as a function of the mean film temperature. The void spaces within the package are to be filled with air at one atmosphere.

Table 3.2-7 presents the important parameters in radiative heat transfer, emissivity (ϵ) for each radiating surface and solar absorptivity (α) value for the exterior surfaces. Under NCT conditions, the machined surfaces of the XM-19 stainless steel used for the body shell will have an emissivity of approximately 0.30 and a solar absorptivity of approximately 0.5. The surfaces of the XM-19 stainless steel used for the closure lid use a slightly lower emissivity of 0.25 to account for the high surface finish typically used for mating surfaces. In contrast, the ‘as-rolled’ and un-painted Type 304 stainless steel used for the shells of the impact limiter will yield a slightly higher emissivity of approximately 0.4. The solar absorptivity for the impact limiter surfaces will also be approximately 0.5.

The Type 304 stainless steel utilized for the strongback structure is assumed to have a conservatively low emissivity of 0.2, indicative of a bright finish. The surfaces of the boral neutron absorbing material use a nominal emissivity of 0.15.

3.2.2 Component Specifications

The materials that are considered temperature sensitive are the butyl rubber O-ring seals used for the closure lid and the vent/fill ports, the polyurethane foam used in the impact limiter, the neoprene rubber pads, and the Delrin[®] plastic.

The butyl rubber O-ring seals used for the containment seals are fabricated from Rainier Rubber compound RR0405-70, or equivalent material meeting the requirements of ASTM D2000 M4AA710 A13 B13 F17 F48 Z Trace Element. The butyl rubber sealing material has a working temperature range of -65 °F to 225 °F², and a short duration (8 hours) temperature range of 400 °F. Developmental O-ring seal testing, documented in the TRUPACT-II SAR³, investigated the butyl rubber O-ring seal’s performance at reduced and elevated temperatures. Further developmental O-ring seal testing was conducted as part of the Radioisotope Thermoelectric Generator (RTG) Transportation System Packaging⁴ design effort. This testing demonstrated that this specific butyl rubber compound has a

² Rainier Rubber Company, Company Standard Compounds, <http://www.rainierrubber.com>, Seattle, WA.

³ U. S. Department of Energy (DOE), *Safety Analysis Report for the TRUPACT-II Shipping Package*, USNRC Certificate of Compliance 71-9218, U.S Department of Energy, Carlsbad Field Office, Carlsbad, New Mexico.

⁴ DOE Docket No. 94-6-9904, *Radioisotope Thermoelectric Generator Transportation System Safety Analysis Report for Packaging*, WHC-SD-RTG-SARP-001, prepared for the U.S. Department of Energy Office of Nuclear Energy under Contract No. DE-AC06-87RL10930 by Westinghouse Hanford Company, Richland, WA. Per Appendix 2.10.6, elevated temperature tests were performed on Rainier Rubber Company butyl rubber compound No. RR-0405-70 O-ring seals with

peak temperature rating of 430 °F for durations of 1 hour or less, 400 °F for 8 hours or less, 375 °F for 24 hours or less, 350 °F for 168 hours or less, and 285 °F or less for the long-term (1 year) transportation duration. For conservatism, a long-term limit of 225 °F, a short-term limit of 400 °F for 8 hours or less, and a lower temperature limit of -40 °F are assumed for this analysis.

The NCT temperature range for the polyurethane foam material is -40 °F to 300 °F, per the foam manufacturer's recommendations⁵. Polyurethane foam is not subject to degradation with age when encased within the stainless steel shells.

The recommended maximum operating temperature for Delrin[®] plastic is 180 °F for continuous operation in air, with intermittent operation (based on the deflection temperature) up to 250 °F permitted⁶. Delrin[®] plastic has a minimum melting point of 347 °F. Except for material strength considerations, no limit exists for the minimum allowable operating temperature. The maximum operating temperature for the neoprene rubber is 180 °F for continuous operation in air, with intermittent use up to 250 °F⁶. A minimum allowable operating temperature -22 °F is recommended, primarily due to the potential loss of flexibility.

The other primary packaging materials are the Type 304 and XM-19 stainless steels and the aluminum material used in the boral. Stainless steel exhibits material property variations within the operating temperature range of the transportation package. In compliance with the ASME B&PV Code⁷, the maximum allowable temperature of stainless steel used for structural purposes is 800 °F for NCT conditions. The Type 304 and XM-19 stainless steels have a melting point above 2,500 °F, which is utilized as the upper bound temperature limit for HAC conditions. The minimum allowable temperature for stainless steel is below the -40 °F considered in this analysis.

The maximum operating temperature for boral⁸ is 850 °F for continuous operation under dry conditions and 1,000 °F for non-continuous operation under dry conditions. No limit exists for the minimum allowable operating temperature.

From Section 1.2.3, *Contents of Packaging*, the MOX FAs have an allowable cladding temperature limit of 392 °F for NCT conditions⁹ and 1,337 °F for HAC conditions¹⁰.

seal compressions as low as 10%. The specific time-temperature test parameters evaluated were 380 °F for 24 hours followed by 350 °F for 144 hours, for a total of 168 hours (1 week). At these temperatures, all elastomeric compounds are susceptible to relatively high helium permeability; thus, helium leakage rate testing was not performed. Instead, a hard vacuum of less than 0.15 torr was maintained on the test O-ring seals with no measurable pressure loss that would indicate leakage. At the end of the entire test sequence, the test O-ring seals were stabilized at -20 °F and shown, via helium leakage rate testing, to be leaktight (i.e., a leakage rate less than 1×10^{-7} standard -cubic centimeters per second (std-cc/s), air leakage).

⁵ *LAST-A-FOAM FR-3700 for Crash and Fire Protection of Nuclear Material Shipping Containers*, General Plastics Manufacturing Company, Tacoma, WA.

⁶ Mat Web On-Line Material Property Data (DuPont Delrin[®] Acetal, homopolymer, unfilled, extruded), www.matls.com.

⁷ American Society of Mechanical Engineers (ASME) Boiler & Pressure Vessel Code, Section III, *Rules for Construction of Nuclear Facility Components*, Division 1, Subsection NB, *Class 1 Components*, & Subsection NG, *Core Support Structures*, 2001 Edition, 2002 and 2003 Addenda.

⁸ AAR, *Standard Specification for Boral Composite Sheet*, AAR Advanced Structures.

⁹ Temperature provided by fuel vendor.

¹⁰ Sanders, et al, *A Method for Determining the Spent-Fuel Contribution to Transport Cask Containment Requirements*, Sandia National Laboratories, Albuquerque, NM, SAND90-2406, November 1992.

Table 3.2-1 – Properties of Stainless Steels

Material	Temperature (°F)	Density (lb _m /ft ³)	Thermal Conductivity (Btu/hr-ft-°F)	Specific Heat (Btu/lb _m -°F)
Stainless Steel ^① Type 304	-40	495.9	8.23	0.1127
	70		8.6	0.1148
	100		8.7	0.1154
	200		9.3	0.1202
	300		9.8	0.1235
	400		10.4	0.1271
	500		10.9	0.1293
	600		11.3	0.1309
	700		11.8	0.1329
	800		12.2	0.1337
	1000		13.2	0.1372
	1200		14.0	0.1391
	1400		14.9	0.1417
	1500		15.3	0.1428
Stainless Steel ^② XM-19	-40	492.5	5.67	0.1037
	70		6.4	0.1130
	100		6.6	0.1155
	200		7.1	0.1191
	300		7.7	0.1241
	400		8.2	0.1261
	500		8.8	0.1295
	600		9.3	0.1321
	700		9.9	0.1349
	800		10.4	0.1362
	1000		11.4	0.1386
	1200		12.5	0.1426
	1400		13.5	0.1458
	1500		14	0.1488

Notes:

- ① American Society of Mechanical Engineers (ASME) Boiler and Pressure Vessel Code, Section II, *Materials, Part D – Properties*, Table TCD, Material Group J, 2001 Edition, 2002 Addenda, New York.
- ② American Society of Mechanical Engineers (ASME) Boiler and Pressure Vessel Code, Section II, *Materials, Part D – Properties*, Table TCD, Material Group E, 2001 Edition, 2002 and 2003 Addenda.

Table 3.2-2 – Thermal Properties of Boral

Material	Temperature (°F)	Thermal Conductivity (Btu/hr-in-°F)		Specific Heat (Btu/lb _m -°F)	Density (lb _m /in ³)
		Through	Axial & 'Along'		
0.035 g/cc B10 loading, 0.118-inch total thickness ^①	-40	4.796	5.022	0.190	0.0917
	77	4.704	5.051	0.217	
	122	4.670	5.060	0.228	
	167	4.637	5.070	0.238	
	212	4.598	5.080	0.247	
	257	4.603	5.104	0.256	
	302	4.608	5.128	0.263	
	347	4.617	5.147	0.269	
	392	4.622	5.171	0.274	
	482	4.598	5.186	0.284	
	572	4.579	5.200	0.292	
	662	4.540	5.186	0.297	
	752	4.507	5.171	0.303	
	842	4.420	5.094	0.309	
	932	4.333	5.017	0.313	
	1472	3.823	4.565	0.336	

Notes:

- ① Based on mean of manufacturer's suggested values, AAR, *Standard Specification for Boral Composite Sheet*, AAR Advanced Structures.

Table 3.2-3 – Properties of Bolt Materials

Material	Temperature (°F)	Density (lb _m /ft ³)	Thermal Conductivity (Btu/hr-ft-°F)	Specific Heat (Btu/lb _m -°F)
Impact Limiter Bolt Material, A320, Gr L43 ^①	-40	489.0	17.8	0.0936
	70		19.3	0.1047
	100		19.7	0.1077
	200		20.6	0.1170
	300		21.2	0.1249
	400		21.4	0.1314
	500		21.4	0.1372
	600		21.2	0.1426
	700		20.9	0.1484
	800		20.5	0.1553
	1000		19.4	0.1710
	1200		18.0	0.2000
	1400		15.0	0.1723
	1500		15.0	0.1511
Closure Lid Bolt Material, A564, Gr 630 ^②	-40	486.9	9.2	0.1023
	70		9.9	0.1081
	100		10.1	0.1097
	200		10.6	0.1152
	300		11.2	0.1211
	400		11.7	0.1258
	500		12.2	0.1319
	600		12.7	0.1373
	700		13.2	0.1457
	800		13.5	0.1540
	1000		13.8	0.1771
	1200		14.2	0.2261
	1400		15.0	0.1665
	1500		15.4	0.1573

Notes:

- ① American Society of Mechanical Engineers (ASME) Boiler and Pressure Vessel Code, Section II, *Materials, Part D – Properties*, Table TCD, 2Ni-3/4Cr-1/3Mo, 1998 Edition.
- ② American Society of Mechanical Engineers (ASME) Boiler and Pressure Vessel Code, Section II, *Materials, Part D – Properties*, Table TCD, Material Group I, 2001 Edition, 2002 and 2003 Addenda.

Table 3.2-4 – Effective Thermal Properties for Homogenized Fuel Region

Material	Temperature (°F)	Thermal Conductivity (Btu/hr-in-°F) ^①		Specific Heat (Btu/lb _m -°F)	Density (lb _m /in ³)
		Axial	Radial		
Homogenized MOX Fuel Region	46	0.02125	--	0.0638	0.1246
	80	0.02120	--		
	260	0.01873	--		
	440	0.01683	--		
	620	0.01533	--		
	800	0.01420	--		
	980	0.01352	--		
	1160	0.01326	--		
	-20	--	0.00232		
	50	--	0.00269		
	150	--	0.00321		
	275	--	0.00390		
	425	--	0.00479		
	575	--	0.00579		
	725	--	0.00694		
	800	--	0.00754		

Notes:

- ① Homogenized fuel region is assumed to extend between the inner surfaces of the ‘fuel boxes’ on the strongback structure. See Appendix 3.6.2, *Thermal Model Details*, for development of the homogenized fuel region thermal properties.

Table 3.2-5 – Properties of Miscellaneous Solids

Material	Temperature (°F)	Density (lb _m /ft ³)	Thermal Conductivity (Btu/hr-ft-°F)	Specific Heat (Btu/lb _m -°F)
Polyurethane Foam ^①	---	10	0.01975	0.353
Polyurethane Foam ^①	---	30	0.04	0.353
Neoprene Rubber ^②	---	89	--	--
Delrin [®] plastic ^②	---	88	0.208	--

Notes:

- ① Thermal conductivity and specific heat for 10 and 30 lb_m/ft³ (pcf) polyurethane foam taken from product data sheet for *LAST-A-FOAM FR-3700 for Crash and Fire Protection of Nuclear Material Shipping Containers*, General Plastics Manufacturing Company, Tacoma, WA.
- ② Impact of neoprene rubber and Delrin[®] plastic components not considered thermally significant. Data per Mat Web On-Line Material Property Data, www.matls.com.

Table 3.2-6 – Properties of Air

Temperature (°F)	Density (lb _m /ft ³)	Specific Heat (Btu/lb _m -°F)	Dynamic Viscosity (lb _m /ft-hr)	Thermal Conductivity (Btu/hr-ft-°F)	Prandtl No.	Coef. Of Thermal Exp. (°F ⁻¹)
-40	Use Ideal Gas Law w/ M = 28.966	0.240	0.0367	0.0121	Compute as Pr = c _p μ / k	Compute as β = 1/(°F+459.67)
0		0.240	0.0395	0.0131		
50		0.240	0.0429	0.0143		
100		0.241	0.0461	0.0155		
200		0.242	0.0521	0.0178		
300		0.243	0.0576	0.0199		
400		0.245	0.0629	0.0220		
500		0.248	0.0678	0.0240		
600		0.251	0.0724	0.0259		
700		0.253	0.0768	0.0278		
800		0.256	0.0810	0.0297		
900		0.259	0.0850	0.0315		
1000		0.262	0.0889	0.0333		
1200		0.269	0.0962	0.0366		
1400		0.274	0.1031	0.0397		
1500		0.277	0.1063	0.0412		

Note: Properties based on curve fits in Rohsenow, Hartnett, and Choi, *Handbook of Heat Transfer*, 3rd edition, McGraw-Hill Publishers, 1998.

Table 3.2-7 – Emissivities and Absorptivities for NCT

Surface	Material And Assumed Condition	Emissivity (ϵ)	Solar Absorptivity (α)
Interior and exterior surfaces of body shell	Type XM-19 stainless steel ^① , slightly oxidized	0.30	0.50
Impact Limiter Shell	Type 304 Stainless Steel ^② , weathered	0.40	0.50
Strongback surfaces	Type 304 Stainless Steel ^③ , unoxidized	0.20	N/A
Poison Surfaces	Aluminum ^④ , bright	0.15	N/A
Closure lid/collar interface surfaces	Type XM-19 stainless steel ^⑤ , clean	0.25	N/A
Ambient Environment	--	1.00	N/A

Notes:

- ① Optical properties assumed similar to those for Type 304 stainless steel. Listed properties based on the values for ‘as-received’ surface finish values in Frank, R. C., and W. L. Plagemann, *Emissivity Testing of Metal Specimens*, Boeing Analytical Engineering coordination sheet No. 2-3623-2-RF-C86-349, August 21, 1986.
- ② Assumes a weathered, ‘as-received’ surface finish, Gubareff, G. G., J. E. Janssen, and R. H. Torborg, *Thermal Radiation Properties Survey*, 2nd Edition, Honeywell Research Center, 1960.
- ③ Based on representative values for a unoxidized, ‘bright’ surface from Gubareff, G. G., J. E. Janssen, and R. H. Torborg, *Thermal Radiation Properties Survey*, 2nd Edition, Honeywell Research Center, 1960 and Wood, W. D., *Thermal Radiative Properties of Selective Materials - Volume I*, Battelle Memorial Institute, Report No. AD 294-345, 1962.
- ④ Based on mean of manufacturer’s suggested values, AAR, *Standard Specification for Boral Composite Sheet*, AAR Advanced Structures.
- ⑤ Optical properties assumed similar to those for Type 304 stainless steel. Listed properties based on the lower values for ‘as-received’ surface finish values in Frank, R. C., and W. L. Plagemann, *Emissivity Testing of Metal Specimens*, Boeing Analytical Engineering coordination sheet No. 2-3623-2-RF-C86-349, August 21, 1986 and clean, un-oxidized surfaces from Gubareff, G. G., J. E. Janssen, and R. H. Torborg, *Thermal Radiation Properties Survey*, 2nd Edition, Honeywell Research Center, 1960 and Wood, W. D., *Thermal Radiative Properties Of Selective Materials - Volume I*, Battelle Memorial Institute, Report No. AD 294-345, 1962.

This page left intentionally blank.

3.3 General Considerations

3.3.1 Evaluation by Analysis

The MFFP is analytically evaluated in accordance with 10 CFR 71¹ and Regulatory Guide 7.8² for all applicable NCT and HAC thermal loads. Table 3.3-1 summarizes the design basis conditions considered in these evaluations. The load conditions are defined as follows:

- *NCT Hot*: An ambient temperature of 100 °F is used to evaluate the maximum temperatures within the package with maximum decay heat and 10 CFR §71.71(c)(1) prescribed insolation (see Table 3.3-2).
- *NCT Hot (no solar)*: Same as NCT Hot, but without insolation. This case serves as the basis for evaluation of the maximum temperature at the accessible surfaces of the package in accordance with 10 CFR §71.43(g). 10 CFR §71.43(g) stipulates that for non-exclusive use packages, the maximum accessible surface temperature must not exceed 122 °F for this condition. This case is also used as an initial condition for the HAC fire (hot) condition.
- *NCT Cold*: An ambient temperature of -20 °F is used to evaluate the temperatures within the package with maximum decay heat and no insolation. The steady-state results are used as initial conditions for the HAC fire (cold) described below.
- *NCT Cold (no heat)*: A -40 °F steady-state ambient temperature without decay heat. This is an analytically trivial case in that no analysis is required to determine that the package and its contents will reach -40 °F under steady-state conditions. The case addresses the minimum material temperatures that may occur.
- *HAC Fire (hot)*: Thermal conditions are evaluated as a steady-state ambient temperature of 100 °F with maximum decay heat and zero insolation prior to the event, followed by a thirty-minute transient with an ambient temperature of 1,475 °F with maximum decay heat and zero insolation, and then back to a steady-state ambient temperature of 100 °F with maximum decay heat and maximum insolation per 10 CFR §71.71(c)(1). This load case evaluates the peak temperature achieved for the various packaging components under the HAC fire event and the associated thermal stresses.
- *HAC Fire (cold)*: The evaluation involves a steady-state initial condition with an ambient temperature of -20 °F with maximum decay heat and zero insolation, followed by a 30-minute transient with an ambient temperature of 1,475 °F with maximum decay heat, and then back to a steady-state ambient temperature of -20 °F with maximum decay heat and zero insolation. This thermal condition may be evaluated either as an alternative to, or in addition to, the HAC fire (hot) condition above.

The primary heat transfer mechanisms utilized in the thermal analyses are conduction, convection, and radiation within the MFFP packaging, and convection and radiation from the exterior of the packaging

¹ Title 10, Code of Federal Regulations, Part 71 (10 CFR 71), *Packaging and Transportation of Radioactive Material*, Final Rule, 01-26-04.

² Regulatory Guide 7.8, *Load Combinations for the Structural Analysis of Shipping Casks for Radioactive Material*, Revision 1, U. S. Nuclear Regulatory Commission, March 1989.

to the ambient environment. The steady-state and transient heat transfer analyses are performed using the thermal network analyzer computer programs SINDA/FLUINT³ with Thermal Desktop^{®4}.

3.3.1.1 NCT Analytical Model

The NCT analytical thermal model of the MFFP is developed for use with the Thermal Desktop[®] and SINDA/FLUINT computer programs. These programs are designed to function together to build, exercise, and post-process a thermal model. The Thermal Desktop[®] computer program is used to provide graphical input and output display function, as well as computing the radiation exchange conductors for the defined geometry and optical properties. Thermal Desktop[®] is designed to run as an AutoCAD[®] application. As such, all of the CAD tools available for generating geometry within AutoCAD[®] can be used for generating a thermal model. In addition, the use of the AutoCAD[®] layers tool presents a convenient means of segregating the thermal model into its various elements.

The SINDA/FLUINT computer program is a general purpose code suitable for either finite difference or finite-element models. The code can be used to compute the steady-state and transient behavior of the modeled system. SINDA/FLUINT has been validated for simulating the thermal response of spent fuel packages and has been used in the safety analysis of numerous packages for both spent nuclear fuel and nuclear material.

The thermal model of the MFFP represents a 180° model of the package between the closure end of the package and the mid-point of the body cavity (i.e., a 1/4-symmetry model). Symmetry planes are assumed along the package's vertical axis and at the mid-point in the body cavity. This level of modeling is acceptable since symmetry conditions will exist across the vertical axis of the normally horizontal package and since the upper and lower impact limiters are essentially identical. Given that the closure lid end of the package contains the thermally sensitive butyl rubber O-rings, it was chosen for modeling. While in actual practice the active length of the MOX FAs will be located closer to the lower end of the package, this modeling conservatively assumes that the active length of the FAs are centered about the mid-plane of the body cavity. This modeling approach conserves the 1/4-symmetry in the decay heat loading and yields conservative temperatures for the O-ring containment seals, and closure lid end of the model.

Figure 3.3-1 presents a 'solid' view of the general layout of the thermal model used to simulate the thermal performance of the MFFP under NCT conditions. As seen, the thermal model provides an accurate representation of the geometry of the package and its internal structure. Specific modeling is included for the structure internal to the closure lid, the doubler and at the attachment lugs for the impact limiter, and the clamp arm structures used to secure the MOX FAs to the strongback structure.

Figure 3.3-2 presents a 'solid' view of the backside for the thermal model. The accurate representation of the impact limiter attachment lugs and bolts can be seen. Approximately 6,800 thermal nodes, 4,050 planar elements, 40 surfaces, and 3,060 solids are used to represent the various components of the MFFP and its MOX FAs. The model assumes temperature dependant thermal properties for all of the package's steel and aluminum (e.g., boral) components, as well as

³ SINDA/FLUINT, *Systems Improved Numerical Differencing Analyzer and Fluid Integrator*, Version 4.5, Cullimore & Ring Technologies, Inc., Littleton, CO, 2001.

⁴ Thermal Desktop[®], Version 4.5, Cullimore & Ring Technologies, Inc., Littleton, CO, 2003.

the air within the package cavity. Given that the polyurethane foam material properties change little over the NCT temperature range of interest, constant thermal property values are used for the polyurethane foam used in the impact limiter and the body collar.

Figure 3.3-3 illustrates the solids model of the body shell, the body collar, the doubler plate, impact limiter lugs, and the impact limiter attachment bolts. Approximately 700 nodes and 300 solids are used to provide geometric and thermal resolution over the 180° thermal representation of body shell.

Figure 3.3-4 and Figure 3.3-5 illustrate the solids model of the closure lid. As seen, the interior structure of the lid is accurately captured. Approximately 520 nodes, 230 solids, and 16 plate type elements are used to provide the geometric and thermal resolution over the 180° thermal representation of the closure lid. Heat transfer within the lid structure is modeled as a combination of conduction through the solids and radiation and closed-cell convection across the void spaces.

Figure 3.3-6 illustrates the thermal modeling of the 1/4-inch thick angles of the strongback structure, the 1/8-inch thick enclosing surfaces of the fuel control structures (FCSs), and the attachment blocks used to attach the strongback angle plates. The hinges and channel stiffening members of the FCS are omitted from the thermal model. Approximately 700 nodes, 300 solids, and 540 plate type elements are used to provide the geometric and thermal resolution over the 180° thermal representation of the strongback structure.

Figure 3.3-7 illustrates the thermal modeling of the 11-gauge (0.12-inch) thick boral plates used to provide neutron absorption along the surfaces of the strongback and the FCSs. Approximately 400 nodes and 7 plate type elements are used to provide the geometric and thermal resolution. The layout of the thermal modeling for the boral plates is similar to that used for the associated strongback structure. Heat transfer between the boral plates and the strongback plates is assumed to be via conduction and radiation across a nominal 0.02 inch air gap. This modeling approach conservatively bounds the thermal resistance between the two surfaces which, due to variations in flatness and contact pressure, may not be in direct contact over their entire surface area.

Figure 3.3-8 illustrates a combined view of the strongback structure, clamp arm, and top plate. Each clamp arm structure has been simplified to two (2) 3/8-inch thick plates for the purposes of the thermal modeling. This modeling approach captures the principal heat transfer paths and the ‘blocking’ effect that the clamp arms provide for radiation exchange along the length of the body cavity. While the ‘push blocks’ have not specifically been modeled, contact conductance is included between the clamp arms and the outer surfaces of the FCSs.

Figure 3.3-9 illustrates the solid elements used to simulate the MOX FAs and the surrounding air space between the edges of the FAs and the inner surfaces of the FCSs. As explained in Section 3.2, *Material Properties and Component Specifications*, rather than include the details of the fuel geometry in the thermal model, the entire region within each FCS is represented as homogenous solid with a uniform volumetric heat load and anisotropic thermal properties. The thermal properties are based on a detailed model of the fuel assembly geometry (see Appendix 3.6.2, *Thermal Model Details*). A volumetric heat load is applied to the solids based on a volume representing an 8.887 inch × 8.887 inch area within the inner surfaces of the FCSs and the 144-inch active length of the fuel. The 8.887 inch dimension, based on a preliminary design of the FCS, is 3/16 inches larger than the actual 8.7 inch inside dimension of the FCS. The additional thermal resistance within the FAs associated with the assumed larger dimension is insignificant, but conservatively bounds (i.e., is higher than) the value associated with the actual 8.7 inch dimension. Further, in the actual design, the start of the active length of the fuel will rest closer to

the bottom end of the package than the distance between the end of the active fuel region and the closure end of the package. However, for conservatism, this analysis assumes that half of the active fuel length (i.e., 72 inches) is within the modeled section. This assumption places the heat generating region of the FAs closer to the closure seals than will occur in the actual package. The remaining 7.145 inches of fuel length required to raise the top of each FA to within approximately 3.8 inches of the inner surface of the closure lid (i.e., the same distance as the actual FA is expected to reach) is assumed to be 'inactive' fuel. The same thermal conductivity properties are applied over this 'inactive' length, but the volumetric heating is set to zero. Table 3.2-4 presents the effective, anisotropic thermal properties for the homogenized fuel region.

Due to the non-uniform composition and geometry of the boron/aluminum composite plates and the FAs with direction, anisotropic thermal conductivity properties are used for these materials. Material orientators are used within the model to specify which thermal properties are associated with each direction of heat flow.

Figure 3.3-10 illustrates the solid model used for the impact limiter shell and polyurethane foam. Approximately 1,750 nodes, 1,030 solids, and 660 plate type elements are used to provide the geometric and thermal resolution over the 180° thermal representation of the impact limiter.

3.3.1.2 HAC Analytical Model

The analytical thermal model of the MFFP used for HAC conditions is a modified version of the NCT model described in Section 3.3.1.1, *NCT Analytical Model*. The primary modifications to the model consist of the following:

- Simulated the worst-case HAC free and puncture drop damage consisting of a 30-foot side drop on the closure lid end and subsequent puncture damage to the impact limiter outer sheet,
- Increased the emissivity of all external surfaces of the body shell and the impact limiters to 0.8 to account for possible soot accumulation on the surfaces during the HAC event,
- Increased the emissivity of the inner surfaces of the body shell and the impact limiter to 0.6 to account for possible oxidation of the XM-19 and Type 304 stainless steels during the HAC event,
- Simulated the charring and ablation of the polyurethane surfaces that may occur (see Section 3.5.2.2, *Performance of Rigid Polyurethane Foam Under HAC Fire Conditions*),
- Application of convection heat transfer coefficients between the package and the ambient that are appropriate for gas velocities of 32 to 50 ft/sec (10 to 15 m/sec)^{5,6} during the 30-minute fire event,
- Used convection coefficients based on still air are assumed following the 30-minute fire event,

⁵ Schneider, M.E and Kent, L.A., *Measurements of Gas Velocities And Temperatures In A Large Open Pool Fire, Heat and Mass Transfer in Fire* - HTD Vol. 73, 1987, ASME, New York, NY.

⁶ Advisory Material For The IAEA Regulations For The Safe Transport Of Radioactive Material, Safety Series No. 37, Third Edition, Amended 1990, International Atomic Energy Agency, Vienna, 1990.

- Used variable ambient conditions to simulate the elevated temperature of the fire for convective and radiation heat transfer and then re-set to the pre-fire ambient condition, with the addition of ambient heating due to insolation.

Discussion of the HAC thermal analysis is provided in Section 3.5, *Thermal Evaluation Under Hypothetical Accident Conditions*.

3.3.2 Evaluation by Test

This section is not applicable since evaluation by test was not performed for the MFFP.

3.3.3 Margins of Safety

A summary of the maximum temperatures, with their respective temperature margins, for both NCT and HAC are provided in Table 3.3-3. As shown by this table, the minimum temperature margin is 61 °F for the closure lid O-ring seal under HAC. From Section 3.1.4, *Summary of Maximum Pressures*, the maximum normal operating pressure (MNOP) is 10 psig. Therefore, the margin of safety (MS) for the 25-psig design pressure is:

$$MS = \frac{25}{10} - 1.0 = +1.50$$

From Section 3.1.4, *Summary of Maximum Pressures*, the maximum pressure for HAC is 123.5 psig. Structural evaluation of the MFFP for this maximum pressure at temperature is provided in Section 2.7.4.3, *Stress Calculations*. As shown in that section, the margin of safety (MS) for the 123.5-psig pressure is +2.15.

Thermally-induced stresses in the MFFP are discussed in Section 3.4.3, *Maximum Thermal Stresses* for NCT.

Table 3.3-1 – MFFP Package Design Basis Thermal Load Conditions

Condition	Description	Applicable Conditions				
		Ambient Temperature (°F)	Insolation		Decay Heat	
			Max. ⁽¹⁾	Zero	Max.	Zero
1	NCT Hot ⁽²⁾	100	✗		✗	
2	NCT Hot (no solar) ^(2,3,6)	100		✗	✗	
3	NCT Cold ^(2,3)	-20		✗	✗	
4	NCT Cold Environment (no heat) ^(4,5)	-40		✗		✗
5	HAC Fire (hot) ⁽³⁾	100 / 1475 / 100	- / - / ✗	✗ / ✗ / -	✗	
6	HAC Fire (cold) ⁽³⁾	-20 / 1475 / -20		✗	✗	

Notes:

- (1) Insolation in accordance with 10 CFR §71.71(c)(1).
- (2) Thermal conditions used to evaluate thermal acceptance criteria and for structural load combinations.
- (3) For the HAC fire event, a transient consisting of an initial steady-state initial condition (i.e., case 2 or case 3), followed by a 30-minute fire event, and concluded with a post-fire transient analysis to establish the peak temperatures. Insolation can be ignored prior to and during the fire, but must be included following the fire.
- (4) NCT Cold Environment load condition is evaluated without decay heat to establish minimum material temperatures for material compatibility.
- (5) NCT Cold Environment condition evaluated with maximum decay heat to establish the worst-case thermal gradients.
- (6) NCT Hot (no solar) used to assure compliance with 10 CFR §71.43(g) criteria for accessible surface temperature.

Table 3.3-2 – Insolation Data per 10 CFR §71.71(c)(1)

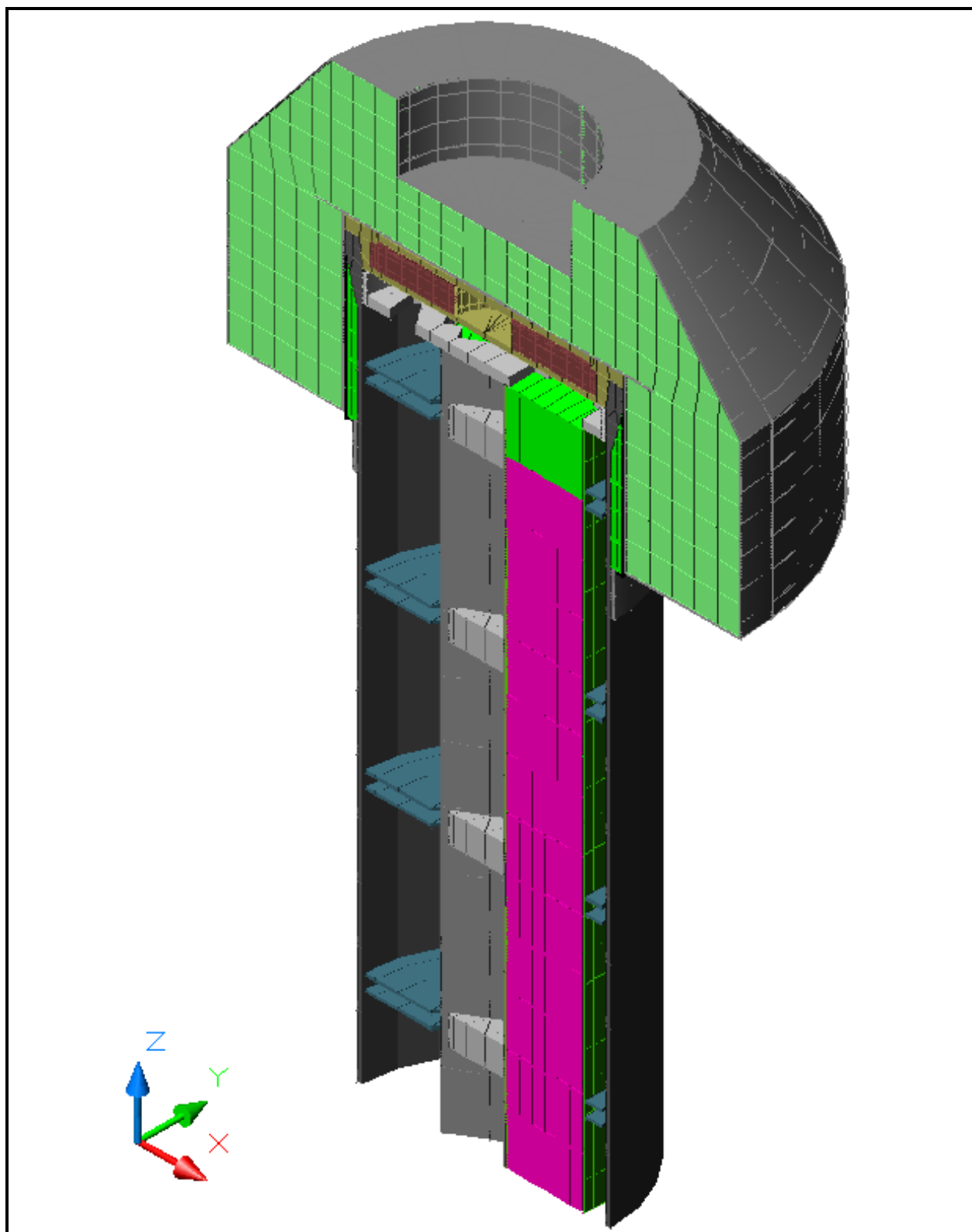
Form and Location of Surface	Total Insolation for a 12-hour Period (g cal/cm ²) ⁽¹⁾
Flat surfaces transported horizontally; base surface	None
Flat surfaces transported horizontally; all other surfaces	800
Flat surfaces not transported horizontally	200
Curved surfaces	400

- Notes:** (1) The 12-hour period covers the daylight hours. Insolation for the remaining 12 hours (nights) is zero. The total insolation values are averaged over a 12-hour period vs. 24 hours for evaluation of package temperatures since the relatively low thermal mass of the package will lead to faster response to the daily variation in insolation levels.

Table 3.3-3 –Summary of Thermal Margins for NCT and HAC Thermal Analyses (°F)

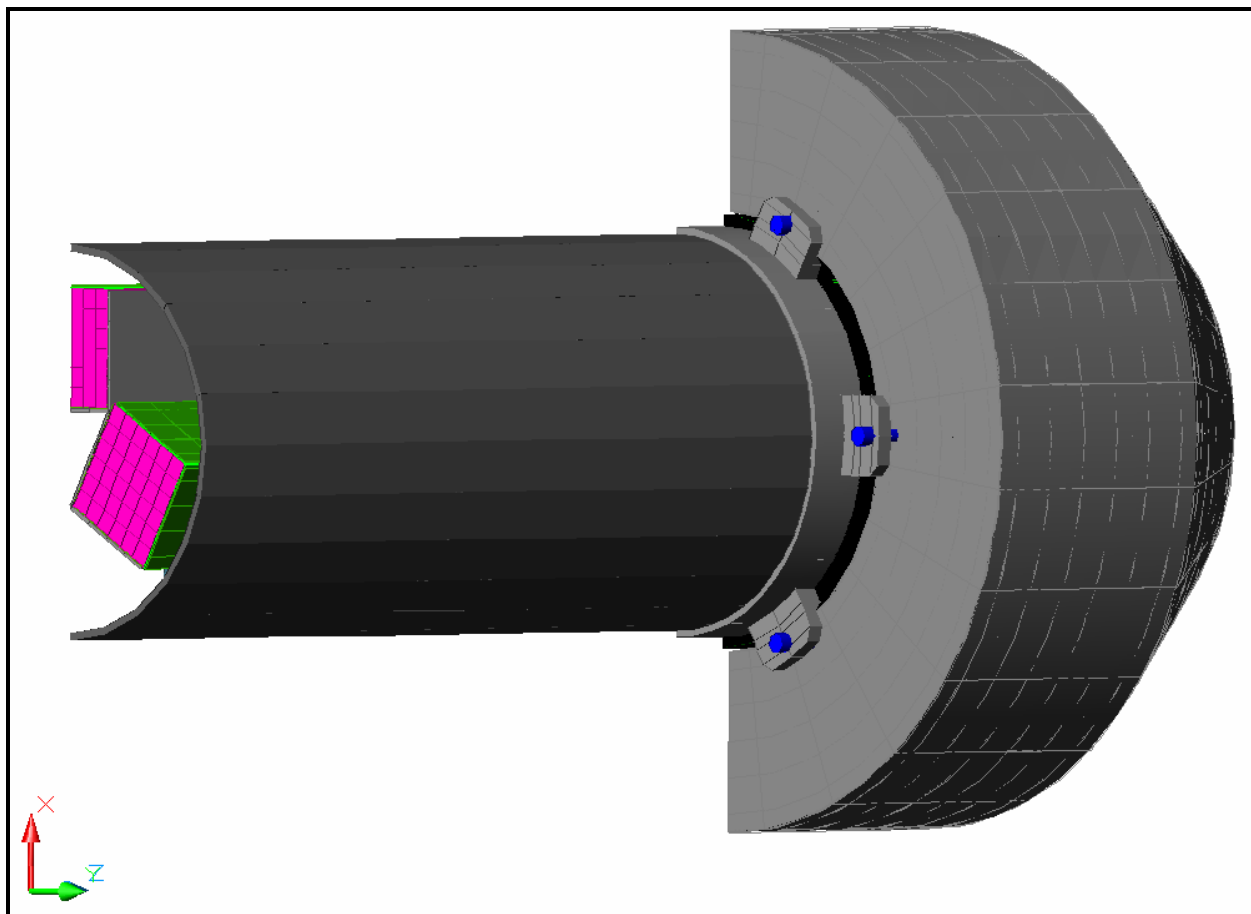
Item	Hot NCT	Peak HAC	Maximum Allowable		Minimum Temperature Margin ⁽¹⁾
			NCT	HAC	
Peak MOX FA	221	518	392	1,337	171
Avg. MOX FA	190	310	392	1,337	202
Poison On Strongback	178	494	850	1,000	506
Poison On FCS	177	652	850	1,000	348
Strongback Structure	178	599	800	800	201
Body Shell	159	1,361	800	2,500	641
Body Collar	149	414	800	1,000	586
Closure Lid	147	301	800	1,000	653
Impact Limiter Lugs	154	1,282	800	2,500	646
Impact Limiter					
• Max. Foam	149	N/A	300	N/A	151
• Bulk Avg. Foam	145	N/A	300	N/A	155
• Skin	149	1,429	800	2,500	651
Impact Limiter Bolts					
• Bolt Head	154	1,283	800	2,500	646
• Bolt Shaft	144	1,006	800	2,500	656
• Bolt Threads	144	295	800	2,500	656
O-ring Seals					
• Closure Lid	159	339	225	400	61 °F
• Vent/Sampling Port	146	295	225	400	79 °F

Note: (1) Minimum temperature margin based on **bold** temperatures.



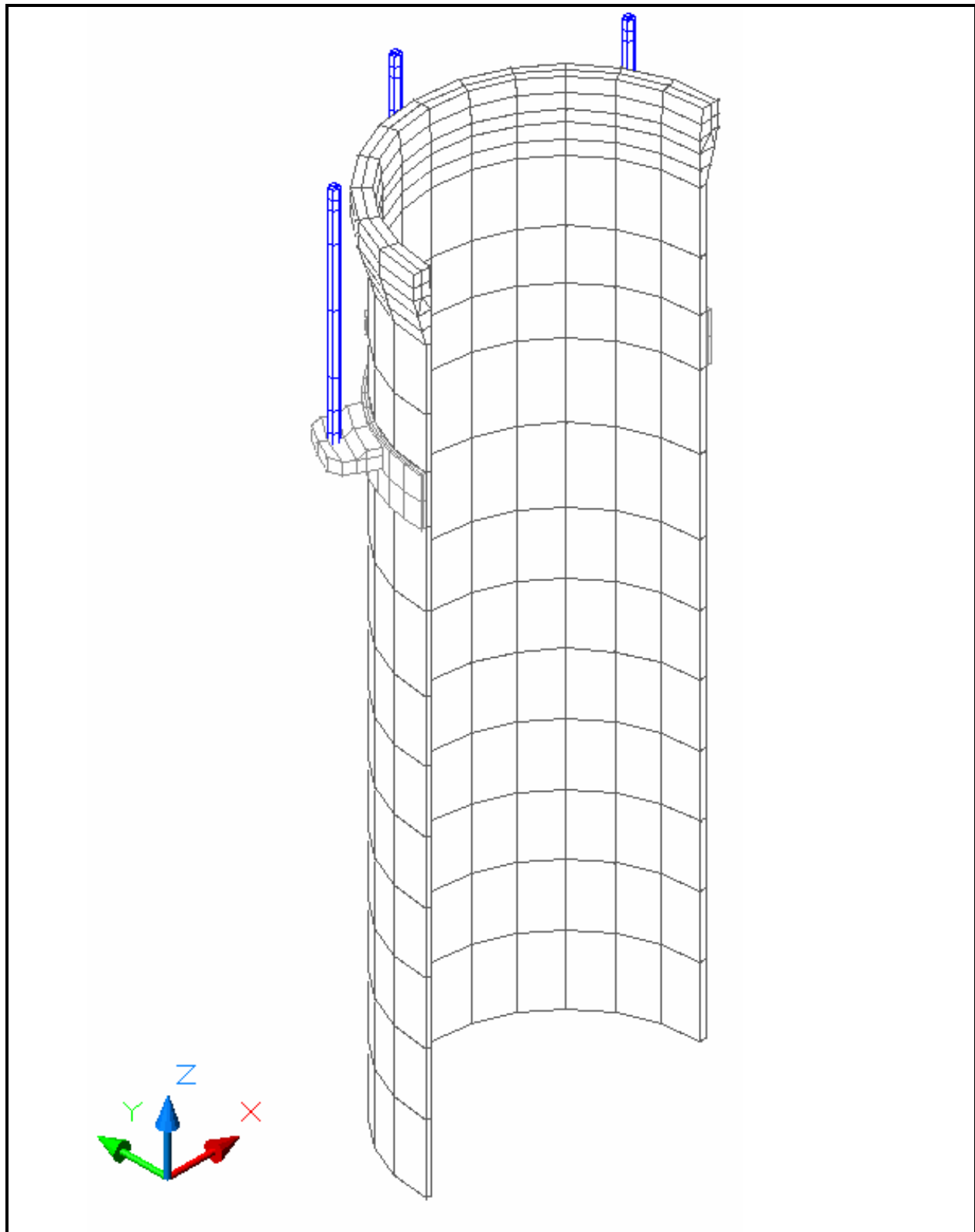
(Note: the positive z-axis is oriented the length of the package and the positive x-axis towards the bottom of the normally horizontal package)

Figure 3.3-1 – Solid View of NCT Thermal Model



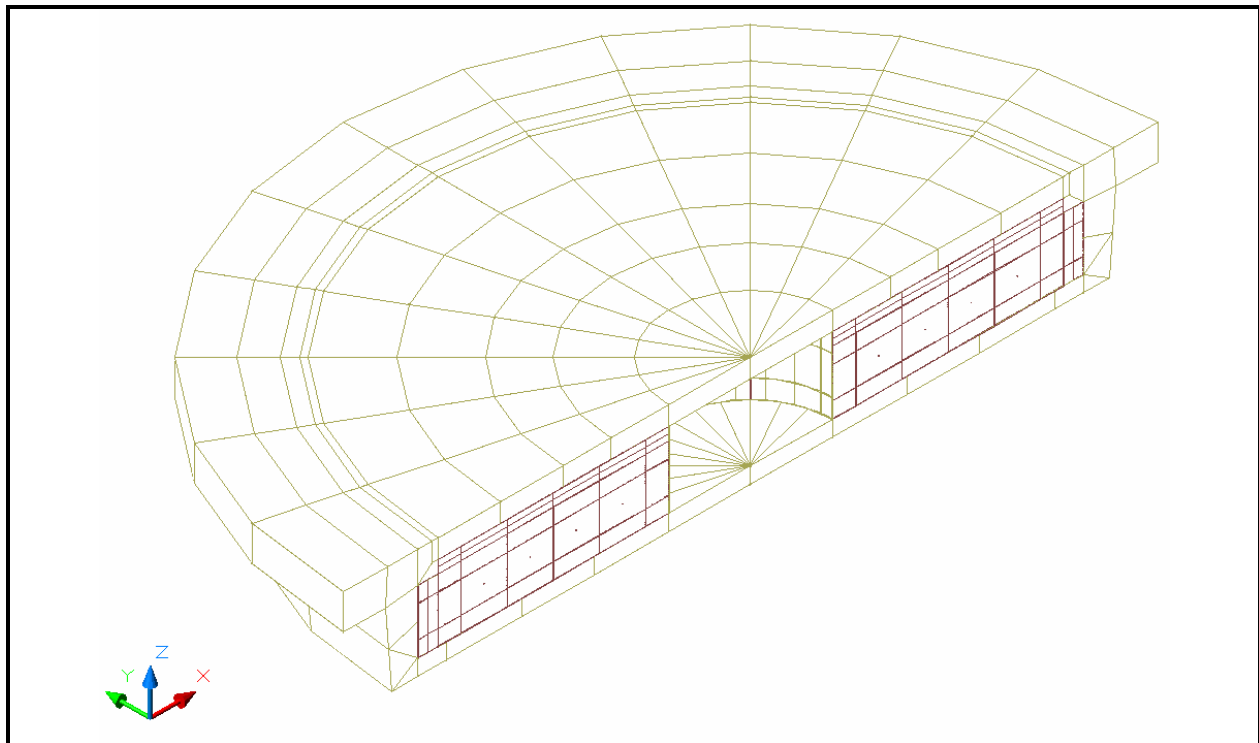
(Note: the positive z-axis is oriented the length of the package and the positive x-axis towards the bottom of the normally horizontal package)

Figure 3.3-2 – Solid View of ‘Backside’ of NCT Thermal Model



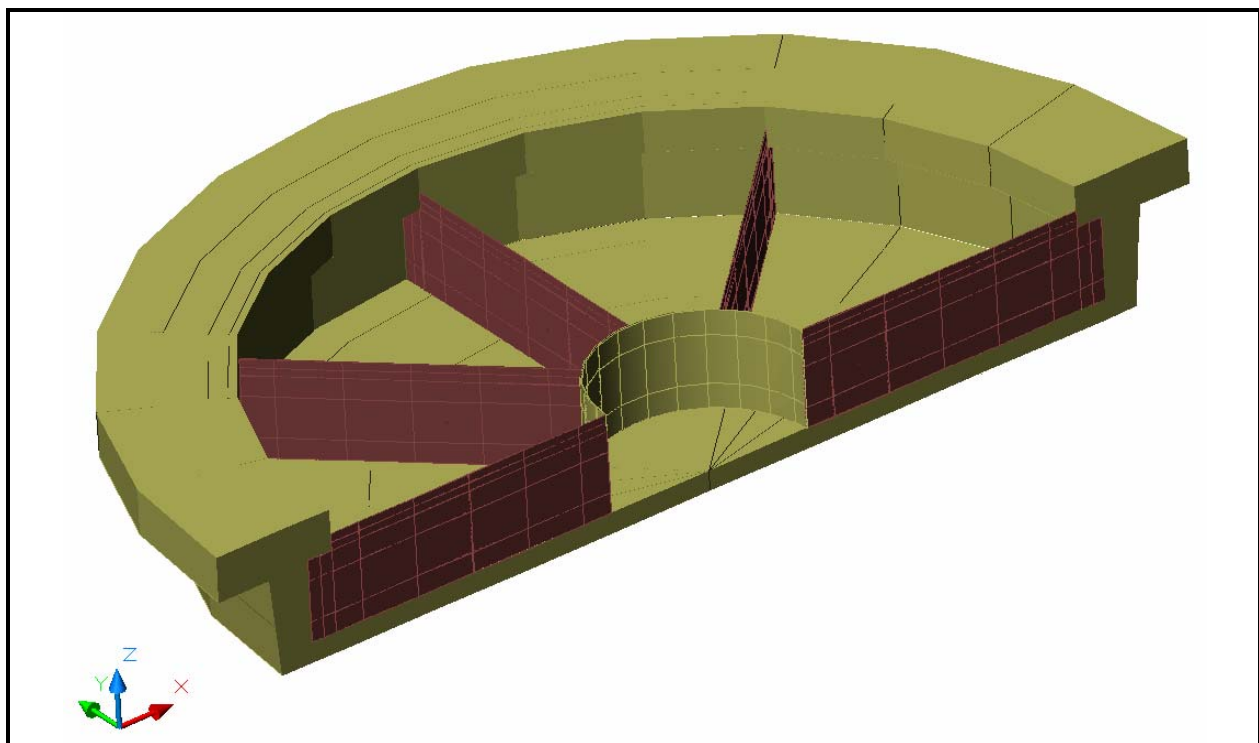
(Note: the positive z-axis is oriented the length of the package and the positive x-axis towards the bottom of the normally horizontal package)

Figure 3.3-3 – Perspective View of Solid Model for Body Shell



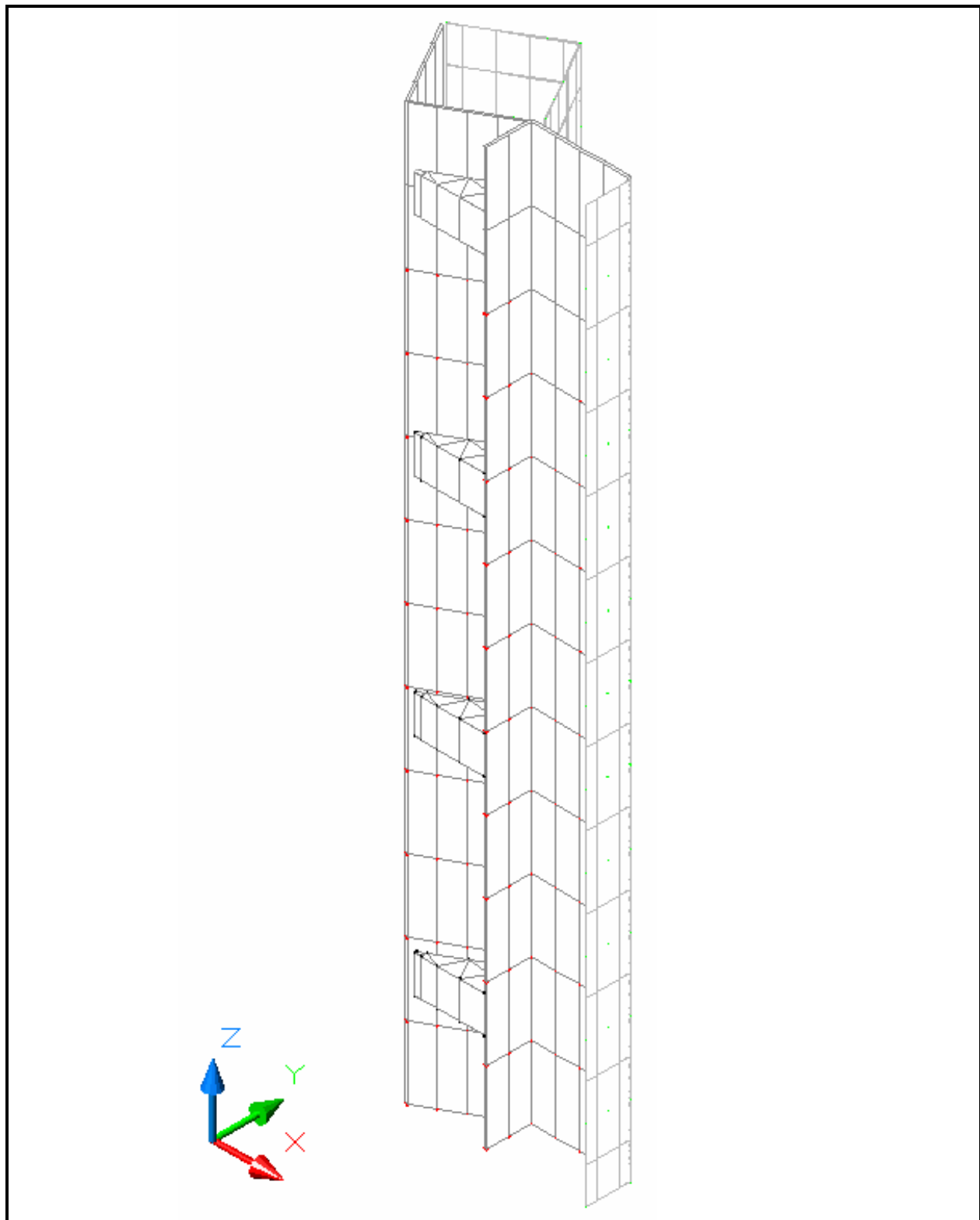
(Note: the positive z-axis is oriented the length of the package and the positive x-axis towards the bottom of the normally horizontal package)

Figure 3.3-4 – Perspective View of Solid Model for Closure Lid



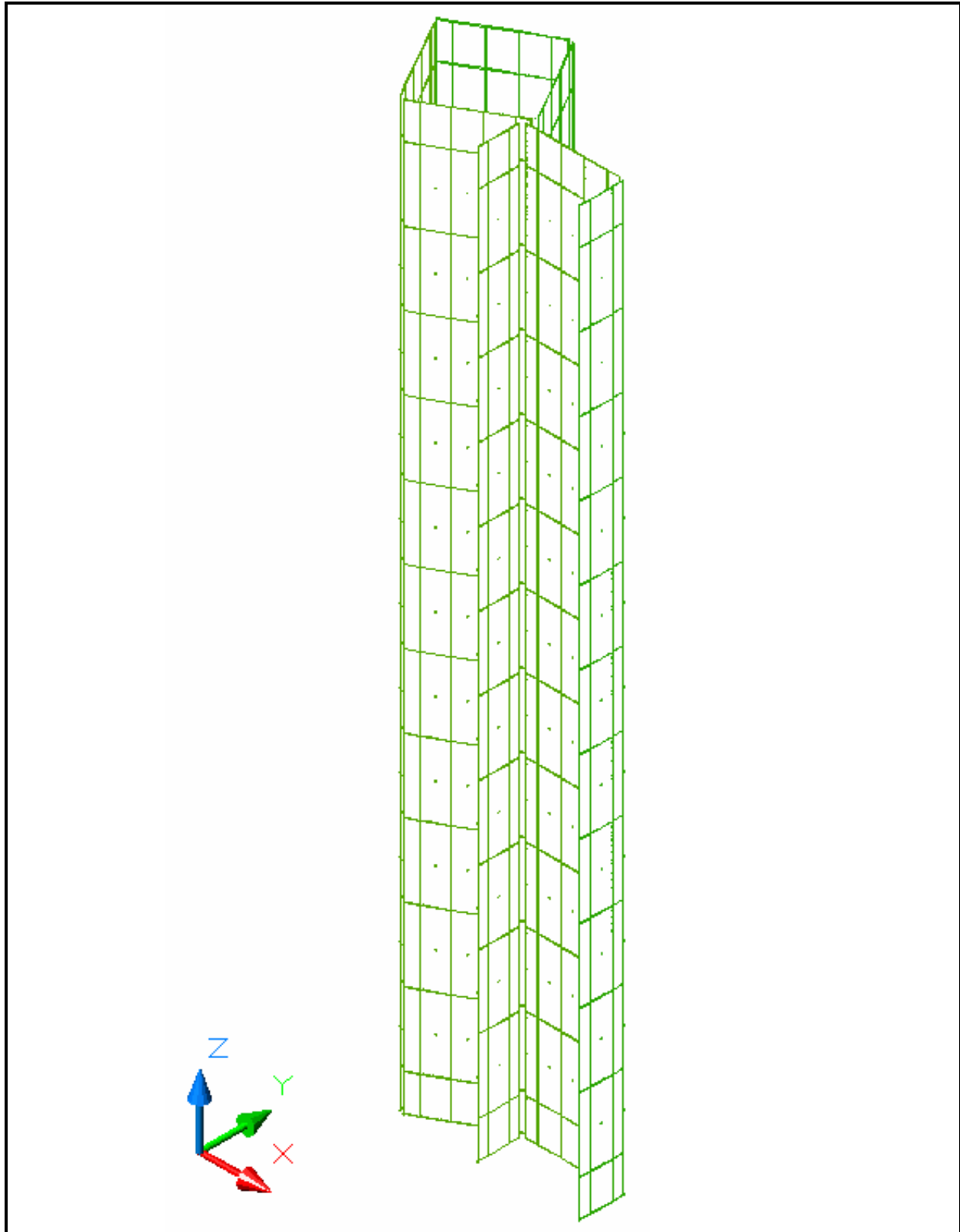
(Note: the positive z-axis is oriented the length of the package and the positive x-axis towards the bottom of the normally horizontal package)

Figure 3.3-5 – Perspective View of Solid Closure Lid Model (Top Cover not shown for Clarity)



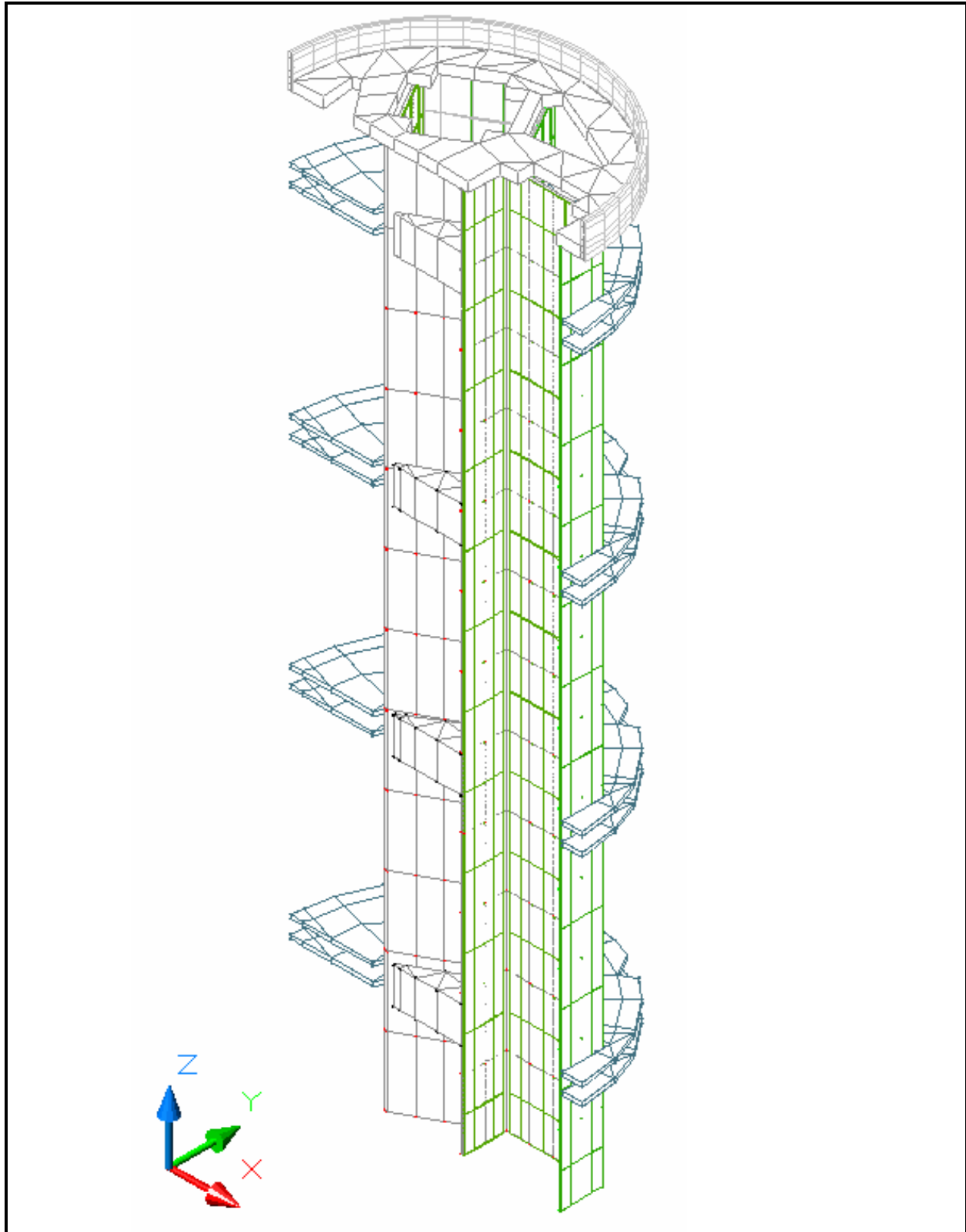
(Note: the positive z-axis is oriented the length of the package and the positive x-axis towards the bottom of the normally horizontal package)

Figure 3.3-6 – Solid View of Strongback Structure



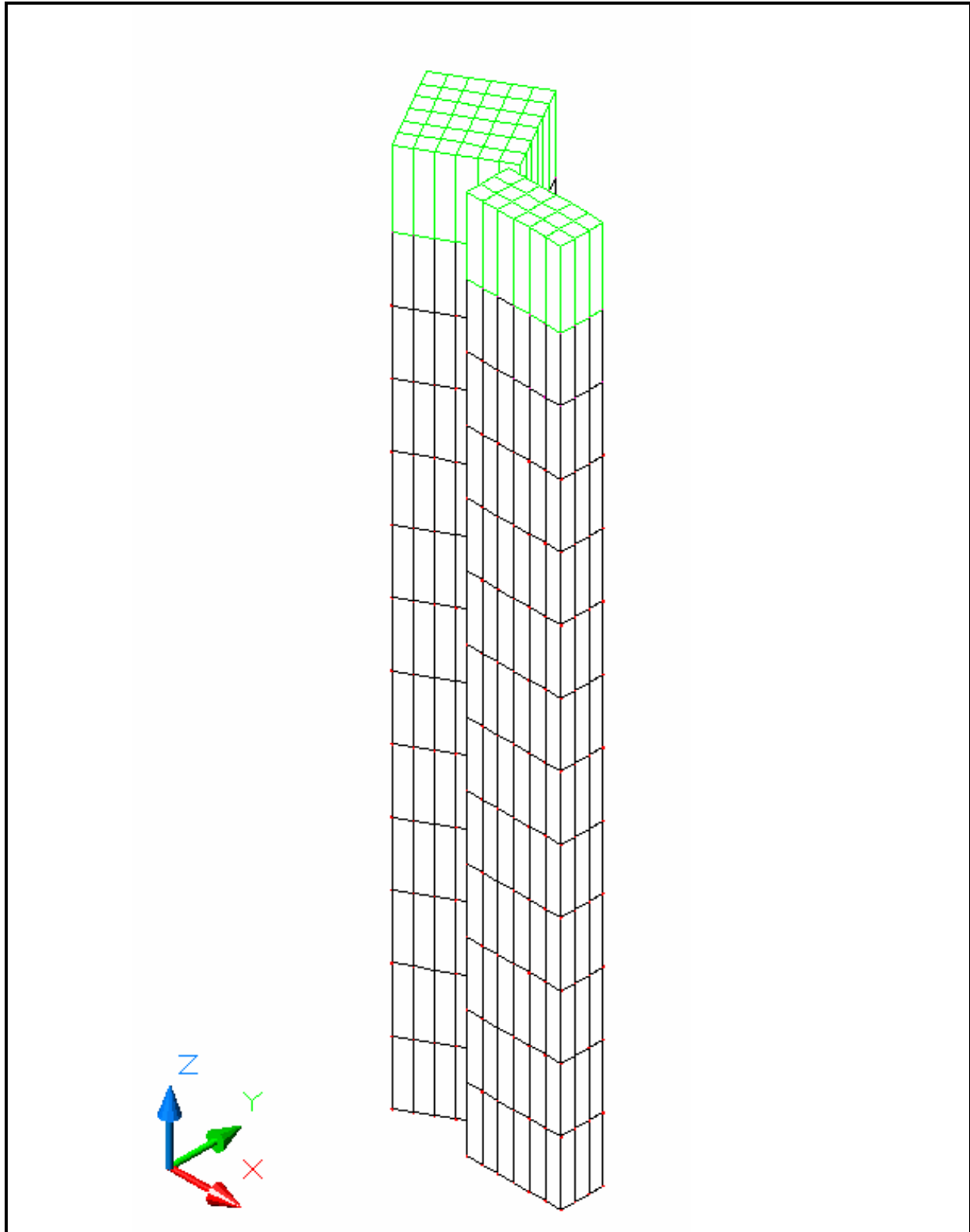
(Note: the positive z-axis is oriented the length of the package and the positive x-axis towards the bottom of the normally horizontal package)

Figure 3.3-7 – Solid View of Boral Neutron Absorber Plates



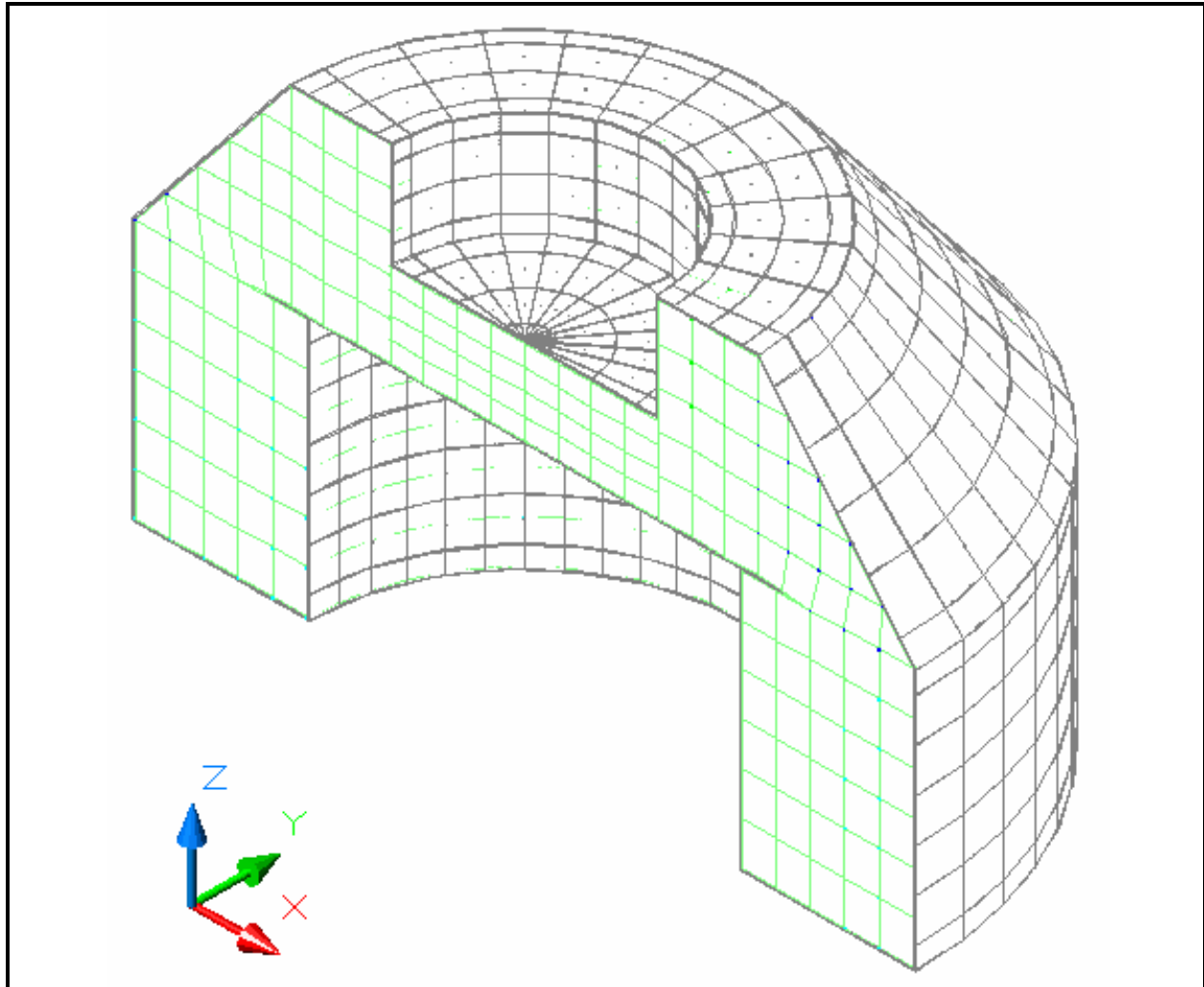
(Note: the positive z-axis is oriented the length of the package and the positive x-axis towards the bottom of the normally horizontal package)

Figure 3.3-8 – Solid View of Strongback Structure



(Note: the positive z-axis is oriented the length of the package and the positive x-axis towards the bottom of the normally horizontal package)

Figure 3.3-9 – Solid View of ‘Homogenized’ Regions Representing MOX FAs



(Note: the positive z-axis is oriented the length of the package and the positive x-axis towards the bottom of the normally horizontal package)

Figure 3.3-10 – Solid View of Impact Limiter Model

3.4 Thermal Evaluation for Normal Conditions of Transport

This section presents the thermal analysis methodology and the evaluation of the thermal performance for the Mixed Oxide Fresh Fuel Package (MFFP) under NCT conditions to demonstrate compliance with the requirements of 10 CFR §71.43(g)¹ and §71.71. The thermal evaluations are performed using conservative analytical techniques to assure that all materials are maintained within their applicable minimum and maximum allowable temperature during all modes of operation.

The thermal loading on the MFFP during NCT arises from insolation on the outer surfaces of the package and from the decay heat of the payload. The thermal conditions that are considered for NCT are those specified in 10 CFR §71.71(c)(1). Accordingly, an ambient temperature of 100 °F with the following insolation values are used for heat input to the exterior package surfaces. Note that since the package is normally transported horizontally, the ends of the impact limiter are treated as ‘flat surfaces not transported horizontally’ with an insolation value of 200 gcal/cm².

Form and Location of Surface	Total Insolation for a 12-Hour Period (gcal/cm2)
Flat surfaces transported horizontally:	
• Base	None
• Other surfaces	800
Flat surfaces not transported horizontally	200
Curved surfaces	400

These values represent the total insolation over a 12-hour period. The NCT evaluations applied these insolation values averaged over a 12-hour period as a steady-state heat loading on the package surfaces.

3.4.1 Heat and Cold

3.4.1.1 Heat

Table 3.4-1 presents a summary of the temperatures determined for the major components of the MFFP packaging normal conditions of transportation (NCT). The steady-state thermal analysis results demonstrate that the MOX FA, strongback structure, body shell, containment O-ring seals, and impact limiter components of the MFFP are all within their respective allowable material temperatures under the evaluated NCT conditions and for the design decay heat loading. Additionally, the minimum material temperatures under the NCT cold condition with zero decay heat also comply with the material specifications. The analysis also demonstrates that all accessible package surfaces remain below 122 °F when transported in an ambient temperature of 100 °F and without insolation, as stipulated by 10 CFR §71.43(g).

The maximum temperatures for the MFFP are determined for operation in a constant 100 °F ambient air temperature with and without the regulatory insolation. These NCT thermal load cases are

¹ Title 10, Code of Federal Regulations, Part 71 (10 CFR 71), *Packaging and Transportation of Radioactive Material*, Final Rule, 01-26-04.

described in Section 3.3.1, *Evaluation by Analysis*, (i.e., Load Conditions 1 and 2). As seen from the summary of the temperature results presented in Table 3.4-1, the peak temperatures determined for the MFFP components and the MOX FAs are well within their allowable temperature limits, as established in Section 3.2, *Material Properties and Components Specifications*.

Delrin[®] plastic is used as a bearing surface between the body shell and the strongback assembly at the circumference of the top and base plates. At this location the Delrin[®] plastic will reach a temperature level that is between that of the top plate and the body shell in the same location. Examination of the temperature distributions in Figure 3.4-2 and Figure 3.4-5 indicates this temperature level to be between 150 and 164 °F. As such, the Delrin[®] plastic is shown to remain within its continuous operational temperature limit of 180 °F and well below the allowable 250 °F limit for intermittent operation.

Neoprene pads are used throughout the strongback structure to cushion the interface between various components. As such, the peak temperature reached by the neoprene pads will be equivalent to the peak temperature of the strongback structure. The peak temperature of 178.4 °F level achieved for the poison surfaces on the strongback structure under the NCT Hot condition is within the allowable maximum service temperature of 180 °F established for the neoprene rubber in Section 3.2, *Material Properties and Components Specifications*.

In compliance with 10 CFR §71.43(g), the maximum temperature of any accessible outer surface is limited to 122 °F or less under NCT conditions when insolation is not present. Since, as demonstrated in Table 3.4-1, the maximum temperature of the accessible surfaces under load Case 2 (i.e., 100 °F and no insolation) is 110 °F or lower, compliance with 10 CFR §71.43(g) is demonstrated.

Figure 3.4-1 through Figure 3.4-5 illustrate the temperature distribution within the MFFP for the NCT Hot condition. The overall temperature distribution within the MFFP is illustrated in Figure 3.4-1. As expected from the low decay heat loading applicable to this design, only a relatively small temperature differential exists within the package. The distribution of the active fuel length within the model can be noted from the figure.

Figure 3.4-2 illustrates the temperature distribution within the body shell. Again, only a relatively small temperature differential exists along the length of the shell, with the minimum temperature occurring at the closure lid. Figure 3.4-3 and Figure 3.4-4 present the associated temperature distributions within the closure lid and the impact limiter, respectively. The temperature distribution within the impact limiter illustrated in Figure 3.4-4 reflects the conservative assumptions of a 12-hour average insolation loading applied to the entire surface of the impact limiter. In reality, due to the insulation quality of the polyurethane foam, the temperature distribution within the limiter would be more accurately a function of a 24-hour average insolation loading. Further, self shading will limit the insolation loading on the lower surfaces of the impact limiter. As such, the actual peak temperatures to be expected within the impact limiter are conservatively bounded by this analysis.

Figure 3.4-5 presents the predicted temperature distribution within the strongback structure. As seen from the figure, the relatively high thermal conductivity of the boral neutron poison plates, combined with the low decay heat loading and its uniform distribution over the active fuel length, results in uniform temperature levels over much of the strongback structure.

3.4.1.2 Cold

The minimum temperature distribution for the MFFP packaging occurs with a zero decay heat load and an ambient air temperature of -40 °F per 10 CFR §71.71(c)(2). The steady-state analysis of this condition represents a trivial case that requires no thermal calculations be performed. Instead, it is assumed that all package components achieve the -40 °F temperature under steady-state conditions. As discussed in Section 3.2.2, *Component Specifications*, the -40 °F temperature is within the allowable range of all of the MFFP packaging components.

As a potential initial condition for all normal or accident events, a minimum uniform temperature of -20 °F and no insolation must be considered per 10 CFR §71.71(b) and §71.73(b) (i.e., Load Condition 3, Table 3.3-1). Table 3.4-1 presents a summary of the resulting temperatures with the design MOX FA decay heat load. All of the assumed conditions for minimum temperatures yield component temperature levels that are within the allowable temperature limits.

Figure 3.4-6 illustrates the temperature distribution within the MFFP packaging for the NCT Cold condition of -20 °F and no insolation.

3.4.2 Maximum Normal Operating Pressure

The maximum normal operating pressure (MNOP) for NCT is presented in Table 3.4-2. The MNOP is based on an initial cavity backfill of air at atmospheric pressure at 70 °F (294 K), an assumed failure rate of 3% of the fuel rods¹, and heat up of the gases in internal cavity under the design decay heat loading and the respective ambient condition. For the purpose of rod pressure determination, the only significant gas contributor is the initial helium backfill as no fission products will exist within the un-irradiated FAs.

The bulk average gas temperature for each condition is determined by the SINDA/FLUINT thermal model. The body cavity is assumed to have a free volume of approximately 80,073 cubic inches. The free volume in the body cavity is based on a cavity 28.5 inches in diameter and 165.25² inches long, a displacement volume of 4,685 cubic inches for each FA, and a displacement volume of 11,292 cubic inches for the strongback assembly. The strongback displacement is computed based on a total weight of 2,900 pounds, of which 160 pounds is from the neutron poison plates (density = 0.0917 lb_m/in³, per Table 3.2-2) and the remaining 2,740 pounds is assumed to be Type 304 stainless steel (density = 0.287 lb_m/in³, per Table 3.2-1).

The total moles of helium fill gas within each fuel assembly depend on the assembly specific fuel rod total free volume and the fill gas pressure. Since the rods are backfilled during fabrication and prior to irradiation or exposure to elevated temperatures, the nominal rod dimensions are used. The ideal gas law applies for determination of fuel rod fill gas moles:

$$N_{\text{Rod}} = \frac{P_{\text{Fill}} V_{\text{rod}}}{RT}$$

¹ U. S. Nuclear Regulatory Commission, NUREG-1617, Table 4-1, *Standard Review Plan for Transportation Packages for Spent Fuel*, March 2000.

² Correct value is 165.45 inches; value used is conservative.

where:

$$\begin{aligned} P_{\text{Fill}} &= \text{Rod fill gas pressure (atm)} \\ V_{\text{rod}} &= \text{Fuel assembly rod internal free volume (liters)} \\ R &= \text{Ideal Gas Constant} = 0.0821 \text{ atm-liter/gmole-K} \\ T &= \text{Temperature at rod backfill} = 294 \text{ K (70 } ^\circ\text{F)} \end{aligned}$$

There are 264 fuel rods in a 17×17 MOX FA, and 24 burnable poison assembly rods (BPRAs). Each fuel rod and BPRA has an initial helium fill pressure between 200 to 300 psig, and 400 to 600 psig, respectively. For conservatism, the initial helium fill pressure will be assumed to be 300 psig for the fuel rods and 600 psig for the BPRAs. The free volume for a fuel rod or BPRA is 1.67 in^3 (0.0274 liters). Based on the equation above, there would be 7.55 g-moles of helium fill gas in each MOX FA, or a total of $N_{\text{MOX Fill Gas}} = 22.64$ g-moles for three assemblies.

The initial gas in the internal cavity at the time of closure is calculated as follows:

$$N_{\text{fill}} = \frac{1 \text{ atm} \times V_{\text{free}}}{R \times T_{\text{fill}}}$$

The maximum NCT pressure is then calculated as follows:

$$P_{\text{NCT Max}} = \frac{N_{\text{package}} RT_{\text{NCT}}}{V_{\text{free}}}$$

$$N_{\text{package}} = N_{\text{fill}} + \text{Rod Failure Rate} \times N_{\text{MOX fill gas}} + N_{\text{outgassing}}$$

where:

$$\begin{aligned} N_{\text{package}} &= \text{total moles of gas in internal cavity} \\ N_{\text{fill}} &= \text{moles air within internal cavity at time of package closure} \end{aligned}$$

Rod Failure Rate = assumed number of failed rods within each MOX FA. A 3% failure rate, which matches the regulatory failure rate for NCT of spent nuclear fuel, will conservatively bound the expected failure rate for a fresh FA.

$$\begin{aligned} N_{\text{MOX fill gas}} &= \text{moles of rod fill gas within package cavity} \\ N_{\text{outgassing}} &= \text{moles gas generated by outgassing from component material within package cavity} \\ &= 0 \text{ (NCT temperatures are within long-term temperature limits for the materials)} \\ R &= \text{Ideal gas constant (0.0821 atm-liter/gmole-K)} \\ V_{\text{free}} &= \text{Internal cavity free volume} \\ &= \text{Gross cavity volume minus displacement volumes for FAs and strongback} \\ &= 105,420 - [(3 \times 4,685) + 11,292], \text{ in}^3 = 80,073 \text{ in}^3 (1,312 \text{ liters}) \\ T_{\text{NCT}} &= \text{Bulk average gas temperature within package (K) at the specific condition} \end{aligned}$$

The computed maximum NCT pressure from Table 3.4-2 is seen to be 17.6 psia (2.9 psig). For conservatism, the MNOP is assumed to be 24.7 psia (10 psig). Significant margin exists between the MNOP and the MFFP's design pressure limit of 39.7 psia (25 psig).

3.4.3 Maximum Thermal Stresses

Maximum thermal stresses for NCT are determined using the temperature results from Section 3.4.1.1, *Heat*, and Section 3.4.1.2, *Cold*. NCT thermal stresses are discussed in Section 2.6.1, *Heat*, and Section 2.6.2, *Cold*.

3.4.4 Evaluation of Package Performance for Normal Conditions of Transport

The steady-state thermal analysis results demonstrate that the MOX FA, strongback structure, body shell, containment seals, and impact limiter components of the MFFP are all within their respective allowable material temperatures under the evaluated NCT conditions and for the design decay heat loading. Additionally, the minimum material temperatures under the NCT cold condition with zero decay heat also comply with the material specifications. The analysis also demonstrates that all accessible package surfaces remain below 122 °F when transported in an ambient temperature of 100 °F and without insolation, as stipulated by 10 CFR §71.43(g).

The MNOP resulting from the NCT Hot condition and conservative assumptions is within the package's maximum design pressure limit.

Therefore, the MFFP is found to comply with all of the thermal requirements specified in 10 CFR §71.71.

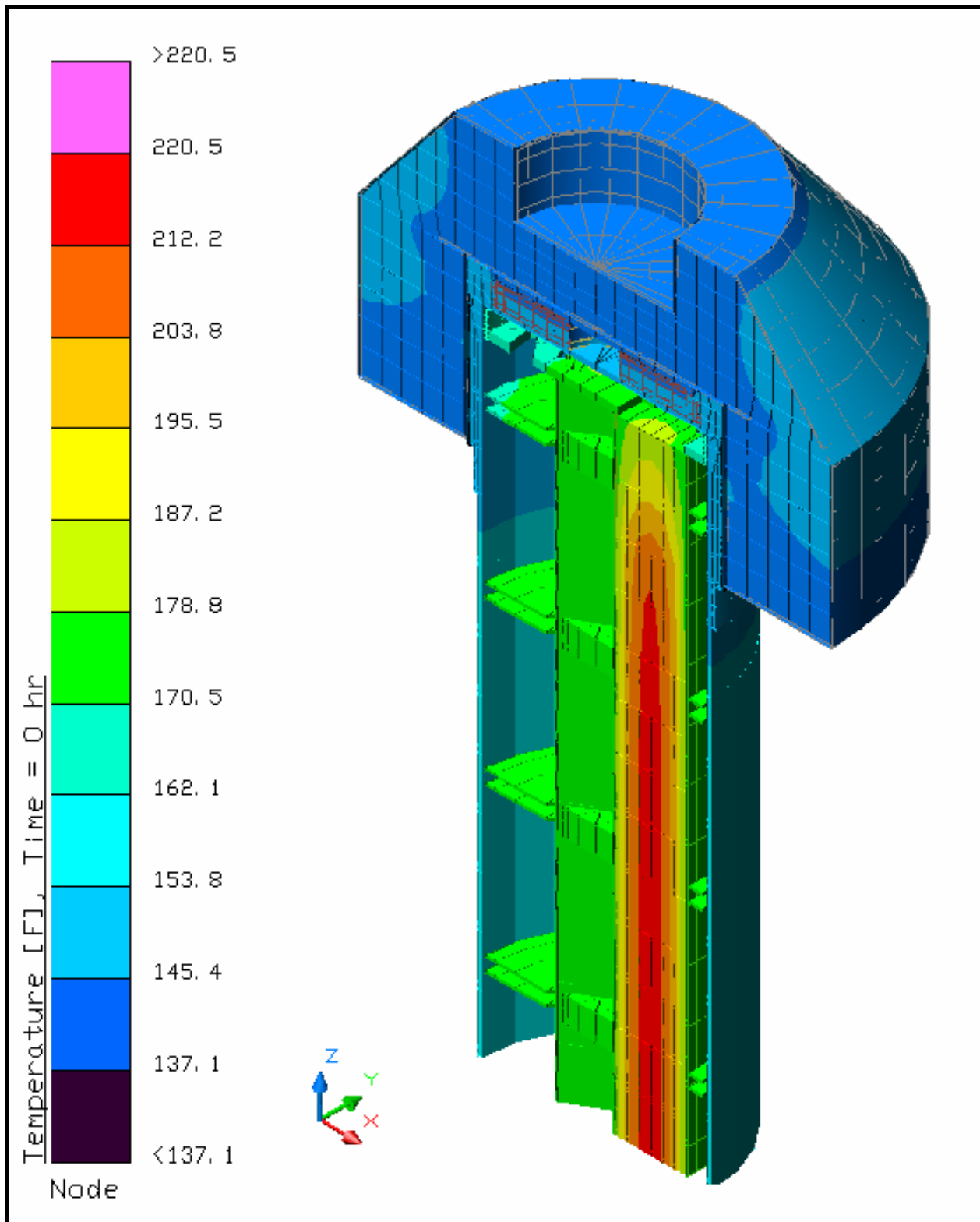
Table 3.4-1 – NCT Temperatures

Location	Temperature (°F)			
	NCT Hot	NCT Hot w/o Solar	NCT Cold	Maximum Allowable ⁽¹⁾
Peak MOX FA	221	179	77	392
Avg. MOX FA	190	130	37	392
Poison On Strongback	178	134	22	850
Poison On Fuel Box Enclosure	177	133	21	850
Strongback Structure	178	134	22	800
Body Shell	159	110	-9	800
Body Collar	149	109	-9	800
Closure Lid	147	109	-9	800
Impact Limiter Lugs	154	108	-10	800
Impact Limiter				
• Max. Foam	149	107	-11	300
• Bulk Avg. Foam	145	101	-11	300
• Skin	149	107	-11	800
Impact Limiter Bolts				
• Bolt Head	154	107	-12	800
• Bolt Shaft	144	106	-13	800
• Bolt Threads	144	107	-11	800
Seals				
• Closure Seal	159	110	-10	225
• Vent/Sampling Port	146	108	-10	225
Bulk Avg. Fill Gas	166	121	5	--

Notes: (1) See Section 3.2, *Material Properties and Component Specifications* for basis for ‘Maximum Allowable’ temperatures.

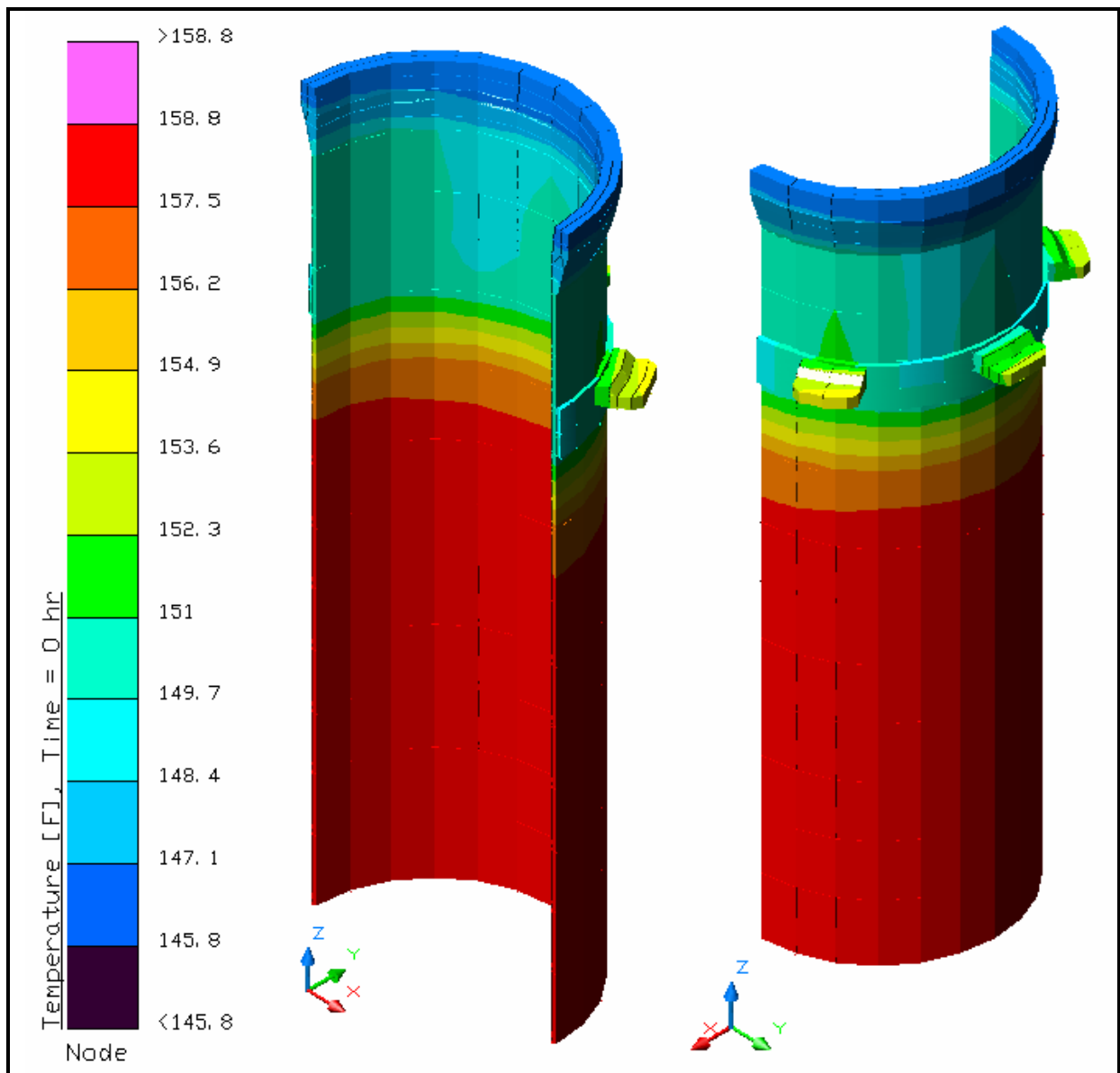
Table 3.4-2 – Package NCT Internal Pressures

Parameter	NCT Hot	NCT Hot w/o Solar	NCT Cold
Bulk Avg. Fill Gas Temperature	166 °F	121 °F	5 °F
Quantity of Package Fill Gas	54.3 g-moles	54.3 g-moles	54.3 g-moles
Gas From Failed FA Rods	0.68 g-moles	0.68 g-moles	0.68 g-moles
Gas From Component Outgassing	0 g-moles	0 g-moles	0 g-moles
Internal Cavity Pressure	17.6 psia (2.9 psig)	16.3 psia (1.6 psig)	13.1 psia (-1.6 psig)



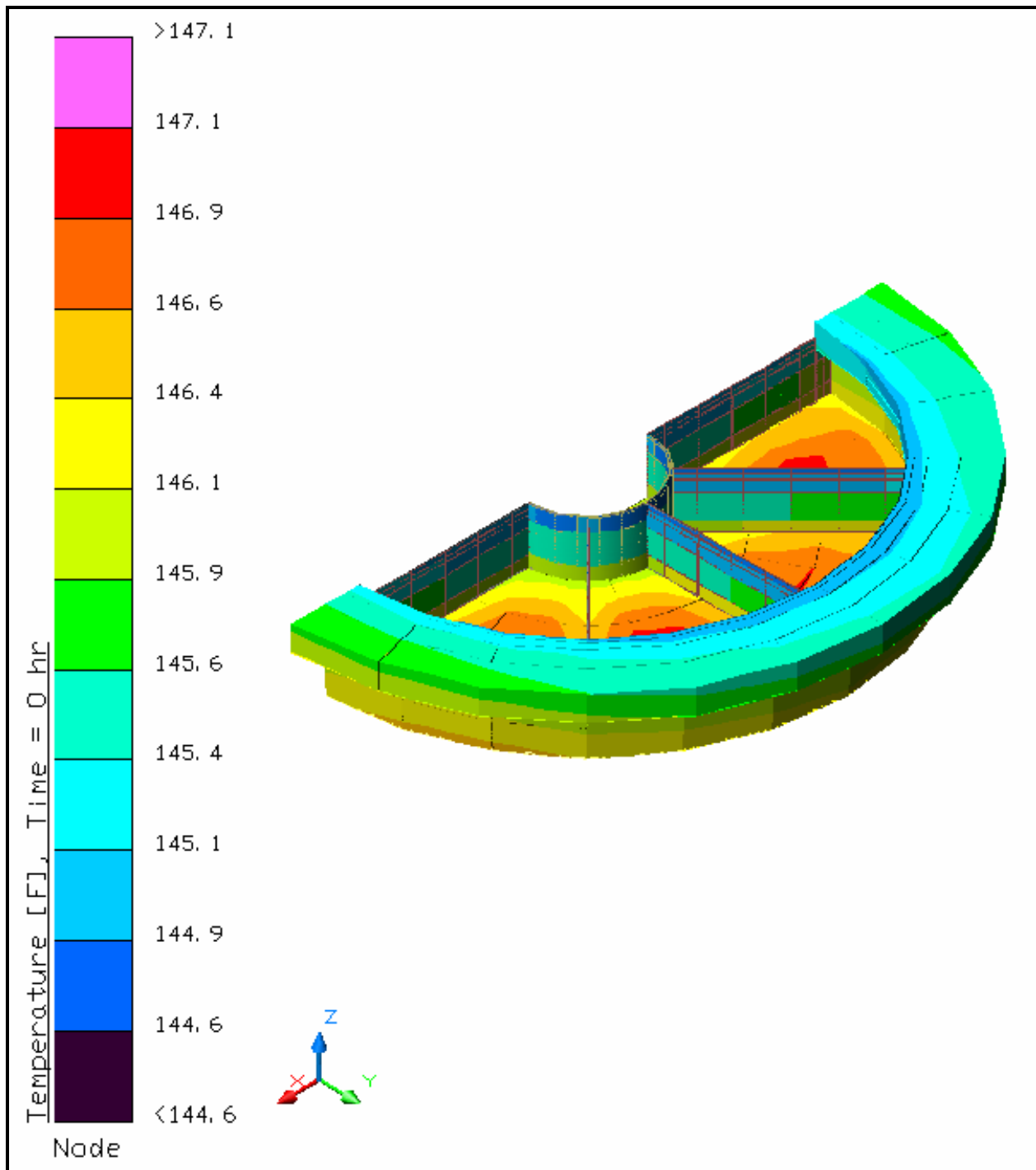
(Note: the positive z-axis is oriented the length of the package and the positive x-axis towards the bottom of the normally horizontal package)

Figure 3.4-1 – Temperature Distribution within MFFP for NCT Hot Condition



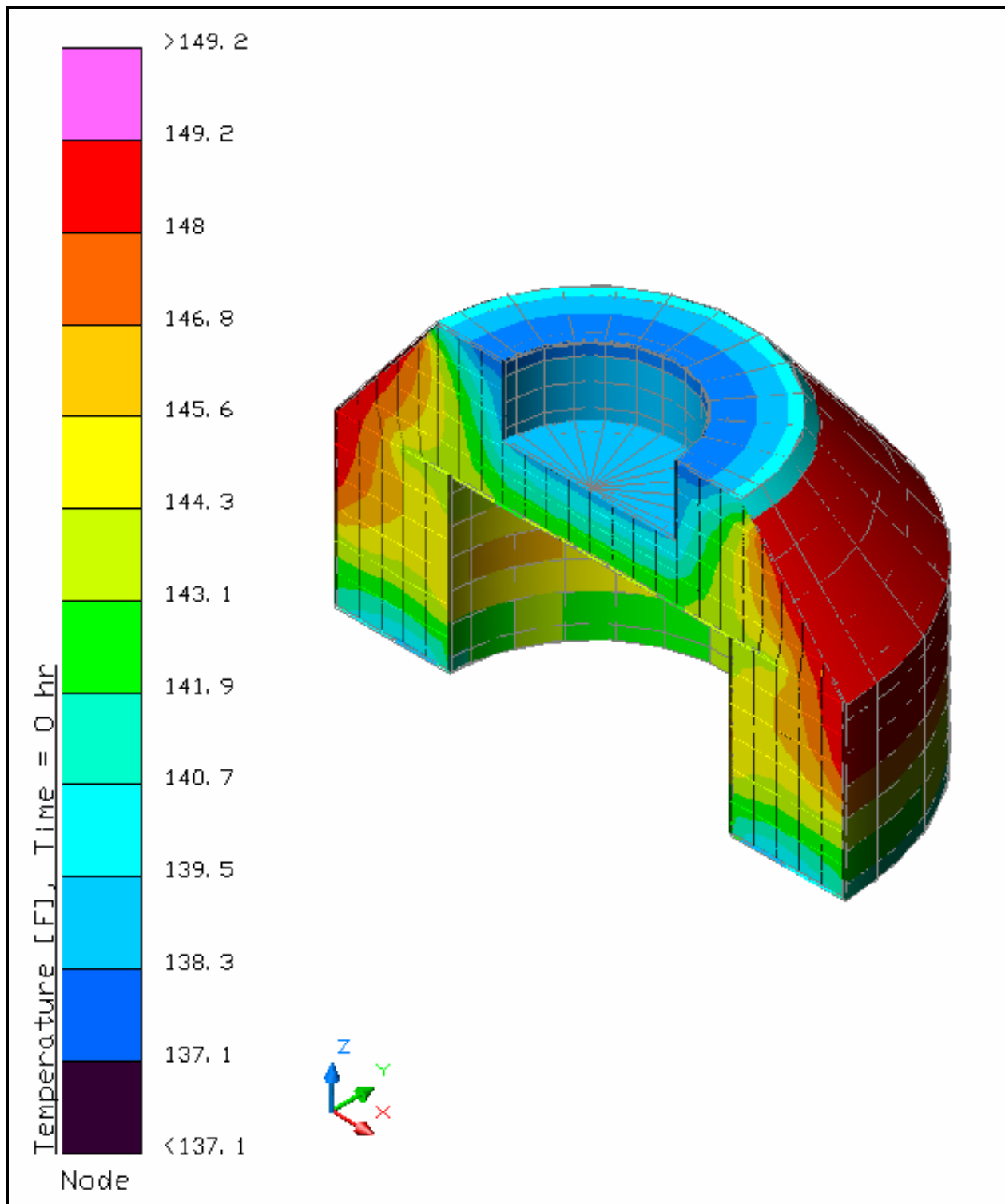
(Note: the positive z-axis is oriented the length of the package and the positive x-axis towards the bottom of the normally horizontal package)

Figure 3.4-2 – Temperature Distribution within Body Shell for NCT Hot Condition



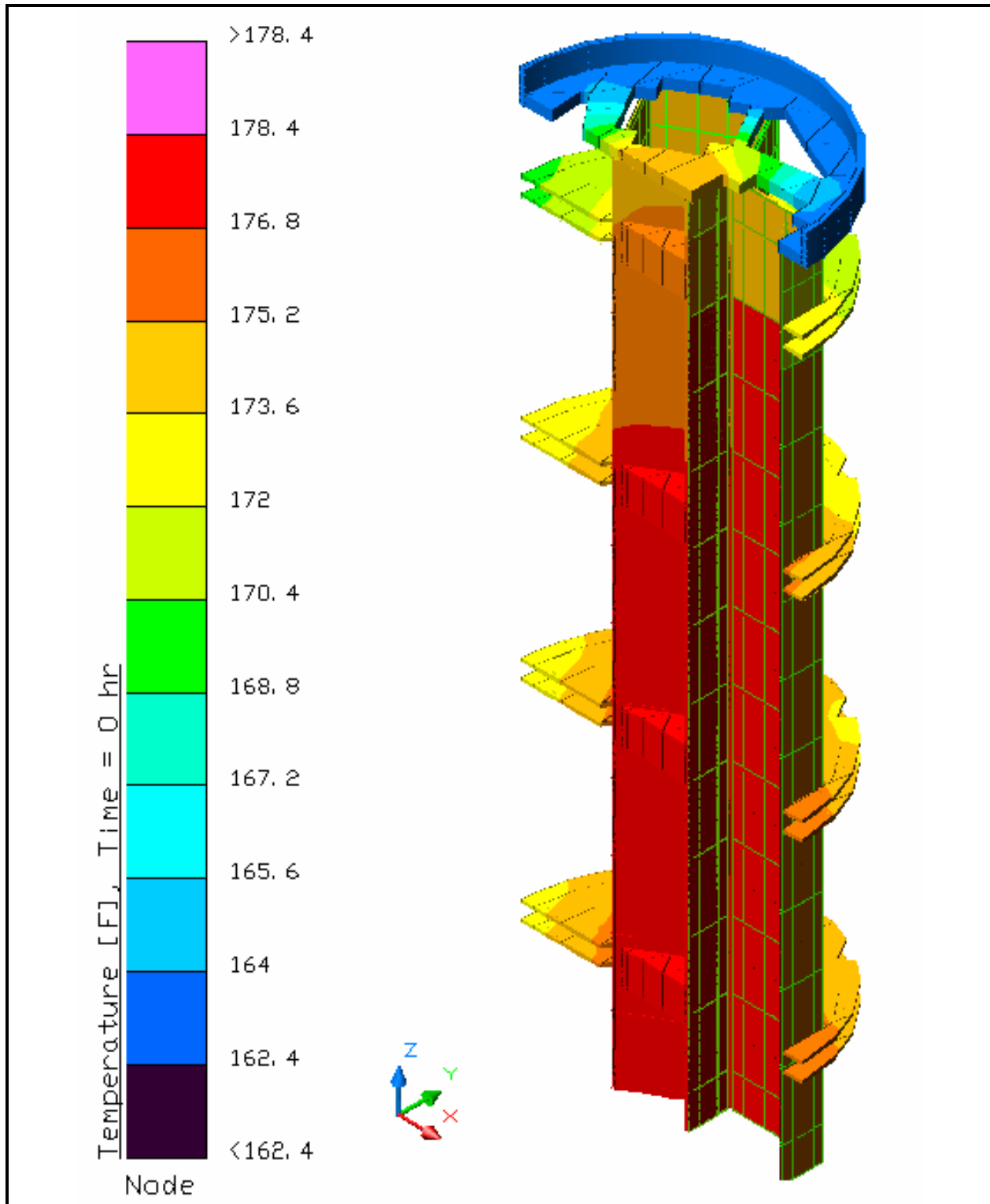
(Note: the positive z-axis is oriented the length of the package and the positive x-axis towards the bottom of the normally horizontal package)

Figure 3.4-3 – Temperature Distribution within Closure Lid for NCT Hot Condition



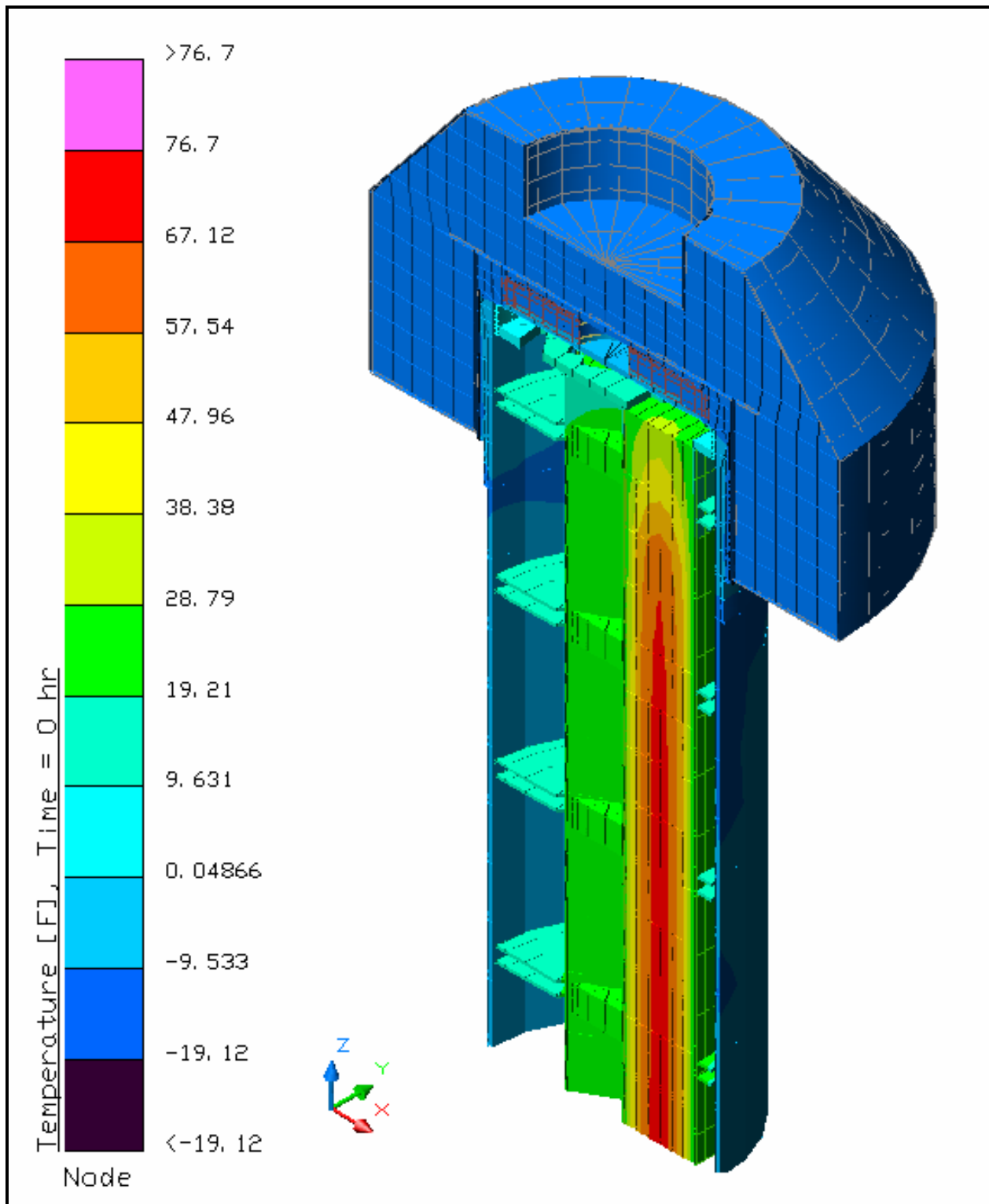
(Note: the positive z-axis is oriented the length of the package and the positive x-axis towards the bottom of the normally horizontal package)

Figure 3.4-4 – Temperature Distribution within Impact Limiter for NCT Hot Condition



(Note: the positive z-axis is oriented the length of the package and the positive x-axis towards the bottom of the normally horizontal package)

Figure 3.4-5 – Temperature Distribution within Strongback Structure for NCT Hot Condition



(Note: the positive z-axis is oriented the length of the package and the positive x-axis towards the bottom of the normally horizontal package)

Figure 3.4-6 – Temperature Distribution within MFFP for NCT Cold Condition

3.5 Thermal Evaluation Under Hypothetical Accident Conditions

This section presents the results of the MFFP thermal analysis for the hypothetical accident condition (HAC) specified in 10 CFR §71.73(c)(4)¹.

3.5.1 Initial Conditions

The initial temperature distribution in the package prior to the HAC fire event is taken from the steady state conditions determined in Section 3.4.1.1, *Heat*, with 100 °F, the design decay heat loading, and no insolation. The absence of insolation prior to the HAC event is consistent with the *Summary and Resolution of Public Comments* relating to §71.73, which states, “...the effects of solar radiation may be neglected before and during the thermal test...”. Insolation is included after the end of the 30 minute fire for computing the thermal response of the package during cool down.

To determine the effect of a HAC fire event, the damaged MFFP described in Section 3.3.1.2, *HAC Analytical Model*, is exposed to a convective and radiative heat flux associated with a fully engulfing fire with a flame temperature of 1,475 °F and an effective emissivity of 0.90. The duration of the HAC fire event is 30 minutes, after which time the thermal boundary conditions are returned to the original ambient temperature of 100 °F. Following the end of the HAC fire event, the thermal transient analysis is continued for a sufficient time to determine the maximum temperatures for all components. Consistent with the requirements of 10 CFR §71.73(c)(4), the surface absorptivity of all external surfaces is set to 0.8.

3.5.2 Fire Test Conditions

3.5.2.1 Analytical Model

The analytical model used for the evaluation of the thermal performance of the MFFP design under HAC conditions is the same as that described in Section 3.3.1.1, *NCT Analytical Model*, for all but the impact limiters. The presence of the impact limiters provides significant thermal protection to the MFFP, even after accounting for the potential damage arising from the free drop and puncture drop accidents. However, due to the potential free drop and puncture drop damage and the potential degradation of the polyurethane foam under the elevated temperatures resulting from the HAC fire, both the geometry and the thermal properties of the impact limiter components will be significantly different from those used to compute the NCT performance. The following paragraphs address the modeling changes to the impact limiter to account for the free drop damage, the physical changes occurring in the foam material exposed to elevated temperatures, and the potential damage related to the puncture drop.

To bound the potential damage to the MFFP from the pre-fire accidents, the results from a series of free drop tests on a full-scale prototypic certification test unit (CTU) were examined for potential damage affects on the package. The drop tests covered a range of hypothetical drop orientations (i.e., side drop, C.G.-over-corner, and slapdown free drop tests, plus a series of puncture drop tests). Of the evaluated drop scenarios, the side free drop with a subsequent

¹ Title 10, Code of Federal Regulations, Part 71 (10 CFR 71), *Packaging and Transportation of Radioactive Material*, Final Rule, 01-26-04.

puncture bar attack to the impact limiter at the same damaged area is determined to have the potential for inflicting the most damage to the thermally sensitive area of the package (i.e., the closure and/or vent/sampling port seals).

Appendix 2.12.3, *Certification Test Results*, describes the setup and damage resulting from a side free drop test on the CTU and presents photos that illustrate the level of damage incurred (see Figure 3.5-1). An approximate inward crush of 4.4 inches was observed during the free drop with a resultant final crush depth of approximately 3.5 inches after springback. In addition to the inward crush, the weld joint on the outer edge of the lid end impact limiter was split for an approximate length of 28 inches, as shown in Appendix 2.12.3, *Certification Test Results*. No other weld joint failure was noted on the remainder of the impact limiter. The actual weld joint design for the MFFP impact limiter will not fail, as discussed in Appendix 2.12.7, *Impact Limiter Weld Joint Test Results*. However, the CTU weld joint damage is included in the thermal evaluation to provide additional conservatism in the thermal model for the HAC condition.

Since the drop tests were conducted for simulated cold weather operations, the extent of damage needed to be extrapolated to the higher temperature levels within the polyurethane foam under NCT hot conditions. Figure 3.5-2 illustrates the differences in the predicted crushed depths, with the depth of the crush doubling from approximately 3.5 inches to approximately 7 inches for operations under NCT hot conditions. The foam crush is modeled explicitly by modifying the geometry of the impact limiter prior to the initiation of the HAC event to capture the extent of foam compaction associated with the flattening of the limiter. Figure 3.5-3 illustrates the revised geometry of the thermal model for the impact limiter shell to simulate the side free drop hot damage. The increase in apparent foam density in the damaged region is conservatively ignored and the thermal conductivity of the foam changes only slightly with density.

Although this assumed crush for the NCT hot condition is less than the maximum dynamic crush deflection identified in Table 2.12.1-8 of Appendix 2.12.1, *Impact Limiter Evaluation*, the assumed damage plus the additional foam loss due to the assumed weld joint failure bounds the potential increased crush distance identified in Table 2.12.1-8 of Appendix 2.12.1, *Impact Limiter Evaluation*, without weld joint failure.

The second area in which the thermal model of the impact limiter was modified addressed the physical change to the outer layer of the foam material when exposed to the elevated temperatures of the HAC event. As discussed in Section 3.5.2.2, *Performance of Rigid Polyurethane Foam Under HAC Fire Conditions*, the LAST-A-FOAM® FR-3700 material undergoes a non-linear thermal response when exposed to elevated temperatures. Little or no decomposition occurs at temperatures below 400 °F, but decomposition increases non-linearly with temperature until only about 5% of the original mass is left when a temperature of 1,500 °F is reached. However, despite this weight loss, the material does not typically ‘burn away’, but instead develops a char layer that has a similar thickness and which acts thermally like a layer of still gas with multiple layers of radiation planes. By modeling this layer as a pseudo ‘void’ space, the thermal model not only captures the thermal conductivity of the layer, it conservatively estimates the level of radiation heat transfer occurring across the depth of the char layer. This modeling approach also conservatively accounts for possibility that, under limited situations, a portion of the foam material may be carried outside of the impact limiter skin by the force of the outgas flow. Since the modeled ‘void’ space is actually filled with char material, neither free nor forced convection will occur.

To bound the extent of the foam material impacted by the elevated temperatures and the potential loss due to ablation of the char layer, the modeling assumes that the outer 4-inch layer of foam at the circumference of the impact limiter and a 3-inch layer of foam at the flat faces of the impact limiter are lost at the beginning of the HAC event. Figure 3.5-4 illustrates the changes to the geometry of the polyurethane foam within the impact limiter to simulate both the side free drop damage and the potential degradation of the foam under the elevated temperatures from the HAC fire event. See the discussion in Section 3.5.2.2, *Performance of Rigid Polyurethane Foam Under HAC Fire Conditions*, for additional information regarding the basis for this modeling approach..

The third type of modeling change made to the impact limiter thermal model for the HAC event captured the potential damage due to the puncture bar drop. The puncture bar drop tests demonstrated that no serious damage to the impact limiter would occur from any of the drop orientations, except for the puncture bar attack on the recessed end of the limiter (see Figure 2.12.3-11) where a tear in the plate was noted. In the event that this puncture bar damage was combined with the weld split noted from the side drop, there would be the potential for developing a ‘chimney’ flow of hot gases through the impact limiter during the HAC fire event. Such a scenario would further require an orientation of the impact limiter during the fire event to be such that the weld split and puncture bar tear were vertically aligned. Further, the two damaged regions would need to be located in approximately the same circumferential location on the limiter. While such a scenario is highly improbable, the thermal modeling for the HAC event evaluated the potential impact on the thermal performance of the MFFP by simulating a local region of foam lost due to ablation in the region of the ‘chimney flow’. This ‘chimney flow’ region is simulated as an additional loss of foam over a semi-circular shaped region in the vicinity of the side impact damage (see right side of Figure 3.5-2) which leaves only approximately 1 inch of foam remaining at its apex. While in reality, this damaged area will develop over the duration of the 30-minute fire, the thermal model conservatively assumes it forms instantaneously when the fire event commences.

The scenarios for developing a chimney flow within the impact limiter with the package in the horizontal orientation were evaluated and dismissed as not being credible events. The puncture drop tests demonstrated that the puncture bar would not cause a failure in the side weld joint (see Figure 2.12.3-13) or would tear a hole in the side of the impact limiter. The opening of the meltable plugs during the fire is not sufficient to create a chimney flow based on full-scale burn tests of other NRC-licensed packages. As such, the modeling addressed the only scenario deemed plausible which would create the upper/lower openings required to initiate the formation of a chimney. Again, it should be noted that the type of weld joint failure conservatively assumed for this thermal modeling will not occur for the actual weld joint design for the MFFP impact limiter, as discussed in Appendix 2.12.7, *Impact Limiter Weld Joint Test Results*.

3.5.2.2 Performance of Rigid Polyurethane Foam Under HAC Fire Conditions

The General Plastics LAST-A-FOAM® FR-3700 polyurethane foam used in the impact limiters has been used in more than 25 radioactive materials (RAM) packages over the last 20 years. The FR-3700 formulation is specially designed to allow predictable impact-absorption performance under dynamic loading, while also providing an intumescent char layer that insulates and protects hazardous materials, even when exposed to pool-fire conditions. Upon exposure of this proprietary rigid polyurethane foam to fire temperatures, the foam degrades into an intumescent char that swells and tends to fill voids or gaps in the impact limiters created by free drop or puncture bar damage. The resultant char layer is structurally strong and will shield the underlying undamaged foam from further direct exposure to the

external high temperatures. This behavior has been observed in full-scale fire tests of other RAM packages, such as TRUPACT-II² and HalfPACT³ packages.

Since the degradation of the foam under elevated temperatures is an endothermic process, the foam is self-extinguishing and will not support a flame once the external fire is removed. However, the gases generated by the degradation process are combustible and will burn under piloted conditions. Further, a portion of these generated gases could remain trapped within the charred layer of the foam for a period after the cessation of the HAC fire event and would be available to support further combustion, but at a much reduced level, until sufficient time has passed for their depletion from the cell structure.

Since the mechanisms behind the observed variations in the thermal properties and behavior of the FR-3700 foam at elevated temperatures are varied and complex, and because only a limited amount of research has occurred in this area, no definitive analytical model of the foam properties under HAC conditions exists. As such, a combination of empirical data and modeling conservatism is used to simulate the thermal performance of the LAST-A-FOAM[®] FR-3700 polyurethane foam for this application.

The FR-3700 product literature⁴ describes the setup and results of a series of fire tests conducted on a series of 5-gallon paint cans filled with FR-3700 foam at densities from 8 to 24 pounds per cubic foot. One end of the test articles (i.e., the “hot face” surface) was subjected to an open diesel fueled burner flame at temperatures of 1,800 to 2,200 °F for 45 minutes. This flame duration is 15 minutes longer than the 30 minute HAC fire event required by 10 CFR §71.73(c)(3). A thermal shield prevented direct exposure to the burner flame by any surface of the test article other than the hot face. Each of the three test articles was instrumented with nine thermocouples. In addition, samples of the foam were subjected to thermal decomposition testing in a radiant oven. The exposure temperatures for the tests varied from 70 to 1,500 °F, and were conducted in both air and nitrogen atmospheres. A thermogravimetric analysis (TGA) was conducted to evaluate the sample weight loss as a function of temperature. These test results indicate that the following steps occur in the thermal breakdown of the foam during the HAC fire event:

- Below 500 °F, the variation in foam thermal properties with temperature are slight and reversible. As such, fixed values for specific heat and thermal conductivity are appropriate.
- Irreversible thermal degradation of the foam begins as the temperature rises above 500 °F and increases non-linearly with temperature. This degradation is accompanied by vigorous out-gassing from the foam and an indeterminate amount of internal heat generation. The internal heat generation arises from the gases generated by the degradation process that are combustible under piloted conditions. However, since the decomposition process is exothermic, the foam will not support combustion indefinitely and further, the out-gassing process removes a significant amount of heat itself via mass transport.

² U.S Department of Energy (DOE), *Safety Analysis Report for the TRUPACT-II Shipping Package*, USNRC Docket No. 71-9218, U.S. Department of Energy, Carlsbad Field Office, Carlsbad, New Mexico.

³ U.S Department of Energy (DOE), *Safety Analysis Report for the HalfPACT Shipping Package*, USNRC Docket No. 71-9279, U.S. Department of Energy, Carlsbad Field Office, Carlsbad, New Mexico.

⁴ *LAST-A-FOAM FR-3700 for Crash and Fire Protection of Nuclear Material Shipping Containers*, General Plastics Manufacturing Company, Tacoma, WA.

- The weight loss due to out-gassing not only has direct affect on the heat flux into the remaining virgin foam, but changes the composition of the resulting foam char since the foam constituents are lost at different rates. This change in composition affects both the specific heat and the thermal conductivity of the foam char layer.
- As temperature continues to rise, the developing char layer begins to take on the characteristics of a gas-filled cellular structure where radiative interchange from one cell surface to another becomes a significant portion of the overall heat transfer mechanism. This change in the dominant heat transfer mechanism causes the apparent heat conductivity to take on a highly non-linear relationship with temperature.
- Finally, at temperatures above 1,250 °F, the thermal breakdown of the foam is essentially completed and only about 5 to 10% of the original mass is left. In the absence of direct exposure to a flame or erosion by the channeling of the outgas products through the foam, the char layer will be the same or slightly thicker than the original foam depth. This char layer will continue to provide radiative shielding to the underlying foam material.

Given the observed non-linear variations in the thermal properties and behavior of the FR-3700 foam at elevated temperatures, a thermal modeling method was devised to conservatively simulate the decomposition behavior of the foam during the HAC fire event. As discussed above, the foam begins an irreversible decomposition process at approximately 500 °F, and reaches a stable char at temperatures in excess of 1,250 °F. The decomposition wave front begins at the outer layer and progresses inward with time. The final depth of the char is a function of the foam density and the fire temperature and duration. This decomposition process is conservatively modeled by transforming a thickness of foam equal to the expected final char depth into still air at the beginning of the fire and simulating conduction and radiation across this air-filled ‘void’ from the hot impact limiter shell to the remaining foam surface. Since the char material would normally completely fill this void and severely restrict the radiative heat transfer mode (the dominant mode at fire temperatures), this approach is conservative.

The depth of the final char thickness which can be expected for the 10 lb_m/ft³ density foam used in the top end impact limiter is estimated from a table provided in the FR-3700 product literature⁴, under the section entitled *Fire Protection*, which lists the temperatures obtained from laboratory fire tests. The test specimen was a 5-gallon metal pail filled with the foam material at various densities, and instrumented with thermocouples at specified depths from the top surface. The pail was completely filled with foam and fitted with a metal lid and a burner flame was applied to the lid end of the pail (i.e., the *hot face* or H.F.). The top three rows of the table lists the temperatures achieved at various depths in the foam for 8, 16, and 24 lb_m/ft³ density after an elapsed time of 30 minutes⁵, and the maximum temperature reached at each depth. As can be noted from the temperatures achieved at the hot face, the flame temperatures in the tests are considerably hotter than the regulatory fire temperature of 1,475 °F. Therefore, in order to render the data in the table consistent with a regulatory flame temperature of 1,475 °F, the test results were proportionately reduced as a function of depth and an assumed hot face temperature of 1,475 °F. For example, for 8 lb_m/ft³ foam at zero depth (i.e., the hot face), the temperature was reduced to 1,475 °F, while at the 1-inch depth the temperature after 30 minutes was reduced to

⁵ The lower three rows present data for foam with a cover layer of ceramic fiber insulation which is not used in this application and, therefore, not included this discussion.

960 °F. Repeating this process at increasing depths, the temperature was reduced by lesser amounts, until at a depth of 6 inches (where there was no temperature response after 30 minutes) the correction is zero.

The resulting predicted thermal response of the foam for regulatory fire conditions is illustrated in Figure 3.5-5. The figure illustrates the estimated corrected curves for the regulatory flame temperature of 1,475 °F for 8 and 16 lb_m/ft³ density foam. Curves for 10, 12, and 14 lb_m/ft³ density foams are found by linear interpolation. It should also be noted that this procedure conservatively ignores the non-linear effect of radiation heat transfer wherein the rate of heat transfer to the hot face from the flame would not scale linearly as assumed here, but would scale with the absolute temperature to the fourth power. As such, had this effect been properly accounted for, the actual foam temperatures would be even lower since the heat available to decompose the foam would be significantly lower than assumed by this approach.

Based on the results presented in Figure 3.5-5, the 10 lb_m/ft³ foam is predicted to reach approximately 500 °F at a depth of 3 inches after 30 minutes and that the foam temperature at a depth of approximately 4.5 inches would not have responded at all. Given that a temperature of 500 °F represents the point where irreversible foam decomposition occurs, the result indicates that the char depth for 10 lb_m/ft³ foam would be 3 inches after 30 minutes of exposure to a 1,475 °F regulatory fire.

Therefore, the performance of the LAST-A-FOAM® FR-3700 during the HAC event is analytically simulated for this application by reducing the depth of foam at each location to conservatively bound the potential loss of the foam from any of the various mechanisms described above. The heat transfer across the resultant void space is then computed based on conduction and radiation across an equivalent air space, despite the fact that the affected foam will typically be simply decomposed to a char layer as opposed to being lost altogether. By removing the foam at the start of the HAC fire transient and by treating the affected foam as a void space for the purposes of computing the radiation heat transfer across the char layer, the modeling conservatively bounds the temperature response of the package to the transient loss of the foam over the time period of the HAC event and the potential loss of a portion of the char layer due to ablation. Specifically, the modeling assumes that the outer 4-inch layer of foam at the circumference of the impact limiter and a 3-inch layer of foam at the flat faces of the impact limiter are lost at the beginning of the HAC event.

3.5.3 Maximum Temperatures and Pressures

3.5.3.1 Maximum Temperatures

Table 3.5-1 provides a summary of pre-fire, steady-state temperatures, the temperatures at the end of the 30-minute fire event, and the peak temperatures achieved during the subsequent package cooldown. Figure 3.5-6 illustrates the associated temperature distribution within the MFFP at the end of the 30-minute fire. As noted from Table 3.5-1, the peak temperatures for the critical components (e.g., closure and vent port O-ring seals, peak MOX FAs, boral, etc.) are all within their respective allowable limits.

The peak MOX FA temperature achieved during the HAC event is over 800 °F below the allowable short-term limit of 1,337 °F. The strongback and the FCSs effectively shield the FAs from direct exposure to the hot surfaces of the body shell. The peak temperature of 652 °F noted for the boral neutron absorbing material is well below the allowable short-term limit of 1,000 °F.

Although the body shell temperature reaches a peak temperature of approximately 1,360 °F during the HAC event, the time at temperature levels over 1,000 °F is less than 30 minutes (see Figure 3.5-9). As such, no significant permanent loss in material structural properties is expected. In contrast, the body collar and closure lid, which are shielded by the impact limiter structure despite the assumed damage conditions, remain below 500 °F throughout the HAC transient. Figure 3.5-7 illustrates the temperature distribution in the body shell at the end of the 30-minute fire when the peak shell temperature is achieved, while Figure 3.5-8 illustrates the temperature distribution in the shell approximately 2 hours after the end of the 30-minute fire when the peak temperatures at the closure lid bolts is reached.

The peak butyl O-ring seal temperature of 339 °F seen for the closure seal is below the conservatively established short-term limit of 400 °F for exposures of 8 hours or less. The peak vent/sampling port O-ring temperatures are predicted to be approximately 295 °F. As the temperature trends presented in Figure 3.5-10 illustrates, not only are the peak O-ring seal temperatures below the allowable short-term limit of 400 °F, but the transient O-ring seal temperatures demonstrate that the temperature trend for the material complies with the time at temperature limitations defined in Section 3.2, *Material Properties and Component Specifications*.

Figure 3.5-9 and Figure 3.5-10 illustrate the transient temperature response during the simulated HAC event for selected package components.

3.5.3.2 Maximum Pressures

With the exception of the consideration for potential out-gassing from components within the body cavity and an assumed 100% failure rate⁶ for the MOX fuel rods, the maximum pressure attained for HAC conditions is determined in the same manner as described in Section 3.4.2, *Maximum Normal Operating Pressure*. While the MFFP is designed to protect the MOX FA from catastrophic failure during the pre-fire free and puncture drops and the subsequent 30-minute fire event, this analysis conservatively assumes that the cladding boundary on all fuel rods and poison rods within the MOX FA have been breached. As determined in Section 3.4.2, *Maximum Normal Operating Pressure*, a total of 22.64 g-moles of helium gas exists within the fuel rods of the three (3) MOX FAs within the package.

Further, it is conservatively assumed that the entire mass of the neoprene rubber and the Delrin[®] plastic pads have been volatilized under the elevated temperatures reached within the body cavity during the HAC event. There are approximately 7 pounds of neoprene rubber and 2.3 pounds of Delrin[®] plastic in the body cavity. Volatizing this entire mass would create approximately 143.1 g-moles of gas within the cavity.

Table 3.5-2 presents the predicted pressure within the body cavity prior to the HAC fire, at the end of the 30-minute fire, and 9.5 hours after the end of the fire. As seen, the peak pressure generated within the package cavity is estimated to be 138.2 psia at the end of the fire when the peak cavity gas temperature is reached. The pressure will then decrease as the package cools, reaching 76.5 psia 9.5 hours after the end of the fire.

⁶ U. S. Nuclear Regulatory Commission, NUREG-1617, Table 4-1, *Standard Review Plan for Transportation Packages for Spent Fuel*, March 2000.

3.5.4 Accident Conditions for Fissile Material Packages for Air Transport

This section does not apply for the MFFP, since air transport is not claimed.

3.5.5 Evaluation of Package Performance for Accident Conditions of Transport

The evaluation of the package performance under HAC conditions demonstrates that the packaging will have sufficient thermal protection remaining after the hypothetical drop and puncture bar damage to protect the thermally sensitive areas of the packaging. All package components are seen as remaining within their associated maximum temperature limits.

Table 3.5-1 - HAC Temperatures

Location	Temperature (°F)			
	Pre-fire Steady-state	End Of 30 Minute Fire	HAC Peaks	Maximum Allowable
Peak MOX FA	179	436	518	1,337
Avg. MOX FA	130	240	310	1,337
Poison On Strongback	134	408	494	1,000
Poison On Fuel Box Enclosure	133	652	652	1,000
Strongback Structure	134	569	599	800
Body Shell	110	1,361	1,361	2,500
Body Collar	109	325	414	1,000
Closure Lid	109	179	301	1,000
Impact Limiter Lugs	108	1,282	1,282	2,500
Impact Limiter				
• Max. Foam	107	N/A	N/A	N/A
• Bulk Avg. Foam	101	N/A	N/A	N/A
• Skin	107	1,429	1,429	2,500
Impact Limiter Bolts				
• Bolt Head	107	1,283	1,283	2,500
• Bolt Shaft	106	1,006	1,006	2,500
• Bolt Threads	107	233	295	2,500
O-ring Seals				
• Closure Lid	110	200	339	400
• Vent/Sampling Port	108	148	295	400
Bulk Avg. Fill Gas	121	770	770	--

Notes:

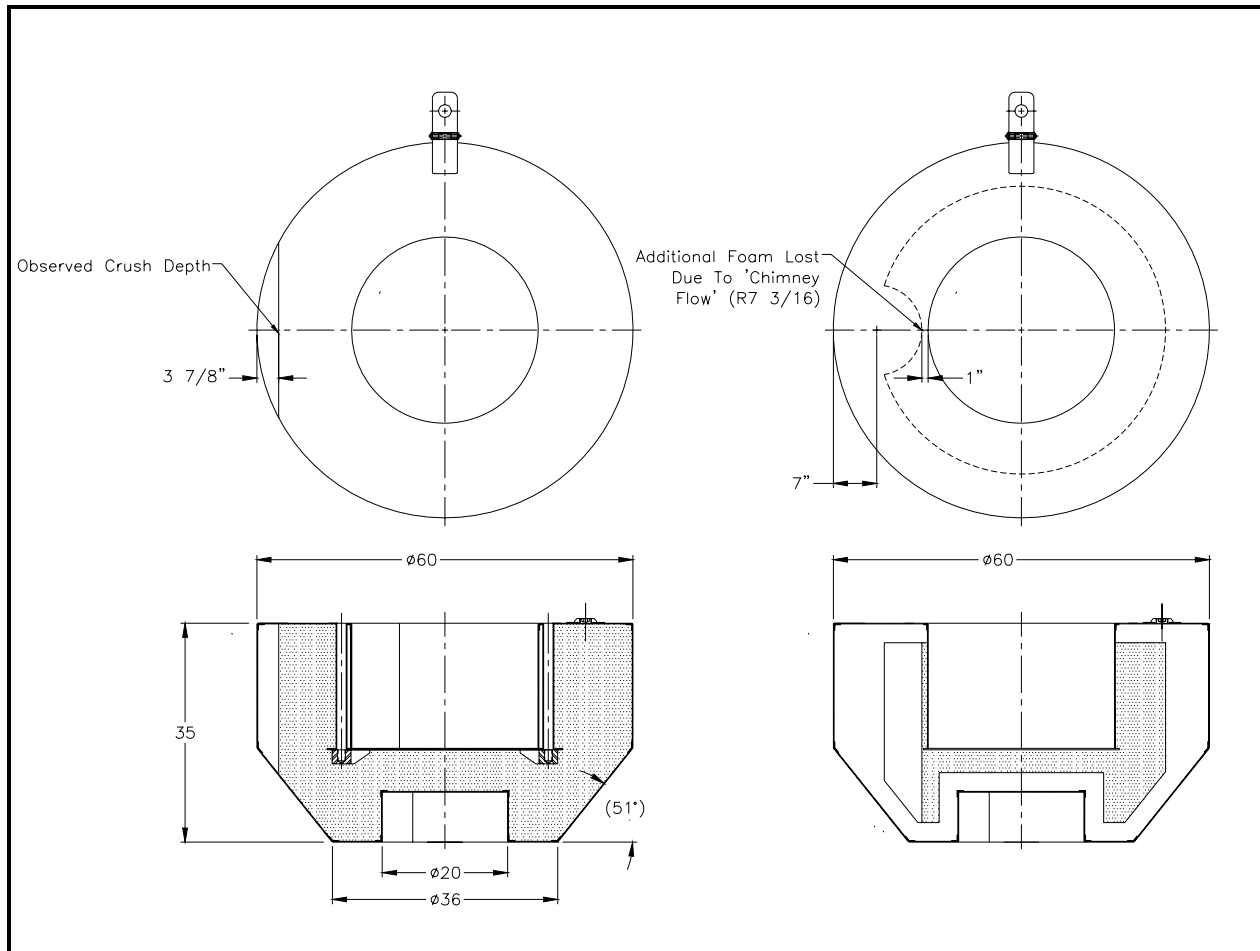
- ① Pre-fire steady-state conditions taken from Table 3.4-1 for 'NCT Hot without Insolation'.
- ② See Section 3.2, *Material Properties and Component Specifications*, for basis for 'Maximum Allowable' temperatures.

Table 3.5-2 – Package HAC Internal Pressures

Parameter	Pre-fire Steady-State	End Of 30-Minute Fire	9.5 Hours After Fire
Bulk Avg. Fill Gas Temperature	121 °F	770 °F	221 °F
Quantity of Package Fill Gas	54.3 g-moles	54.3 g-moles	54.3 g-moles
Gas From Failed FA Rods	0.68 g-moles	22.64 g-moles	22.64 g-moles
Gas From Component Outgassing	0 g-moles	143.1 g-moles	143.1 g-moles
Internal Cavity Pressure	16.3 psia (1.6 psig)	138.2 psia (123.5 psig)	76.5 psia (61.8 psig)

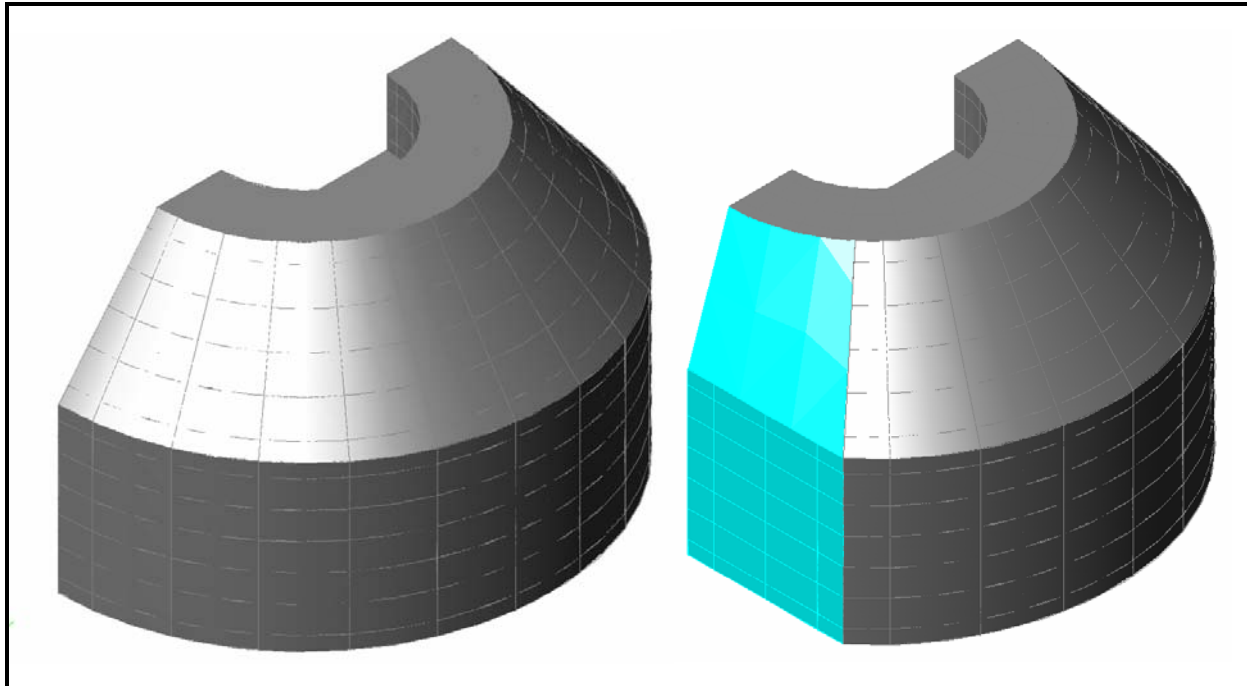


Figure 3.5-1 – CTU Impact Limiter Damage from Full-Scale Side 30-ft Free Drop Test



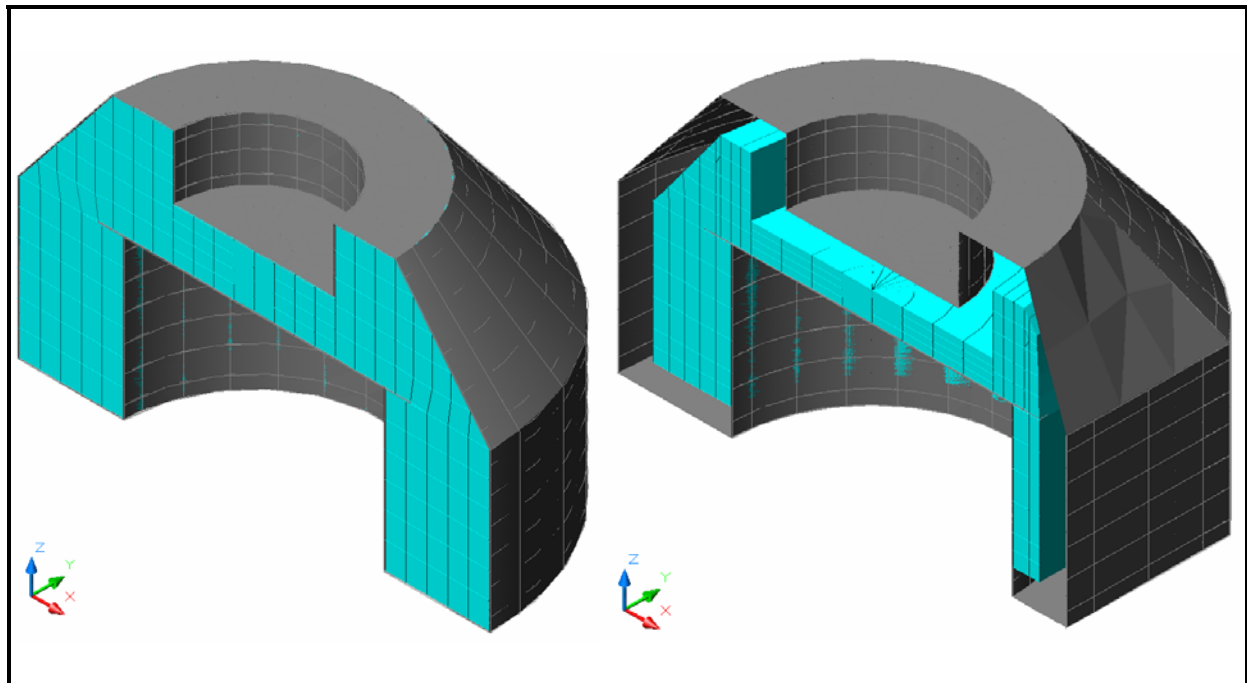
(Note: Observed impact limiter damage from drop test on left and simulated damaged impact limiter for warm weather conditions on right)

Figure 3.5-2 – Projected Side Drop Damage to Impact Limiter



(Note: Undamaged impact limiter from NCT model on left and simulated damaged impact limiter for HAC modeling on right)

Figure 3.5-3 – Illustration of Modification to Impact Limiter Geometry to Reflect Side Drop Damage



(Note: Undamaged foam geometry from NCT model on left and simulated damaged foam geometry for HAC modeling on right)

Figure 3.5-4 – Illustration of Foam Geometry Modification to Reflect Potential Loss During HAC Event

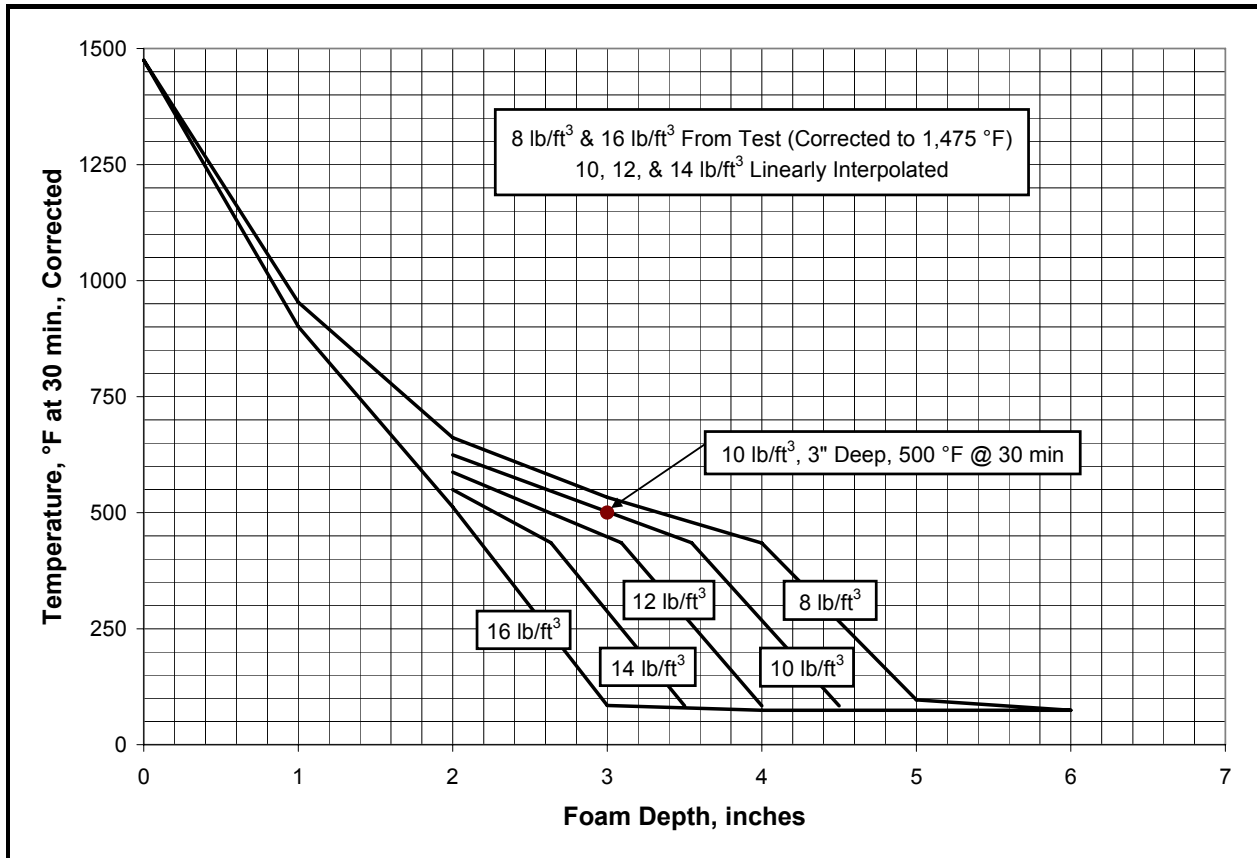


Figure 3.5-5 – Predicted Foam Temperature Response to Regulatory Fire After 30 Minutes

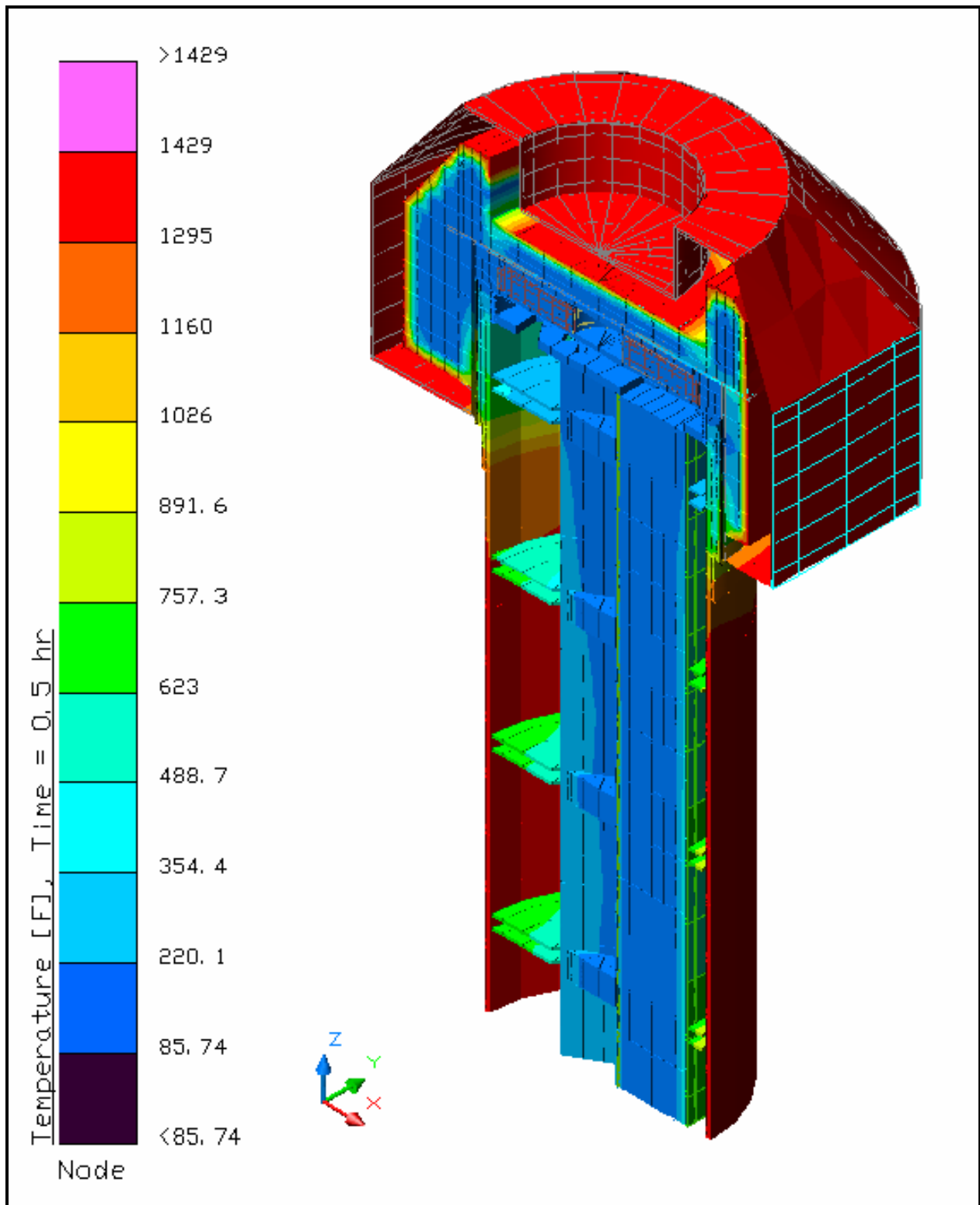


Figure 3.5-6 – Temperature Distribution within MFFP at End of 30-Minute Fire Event

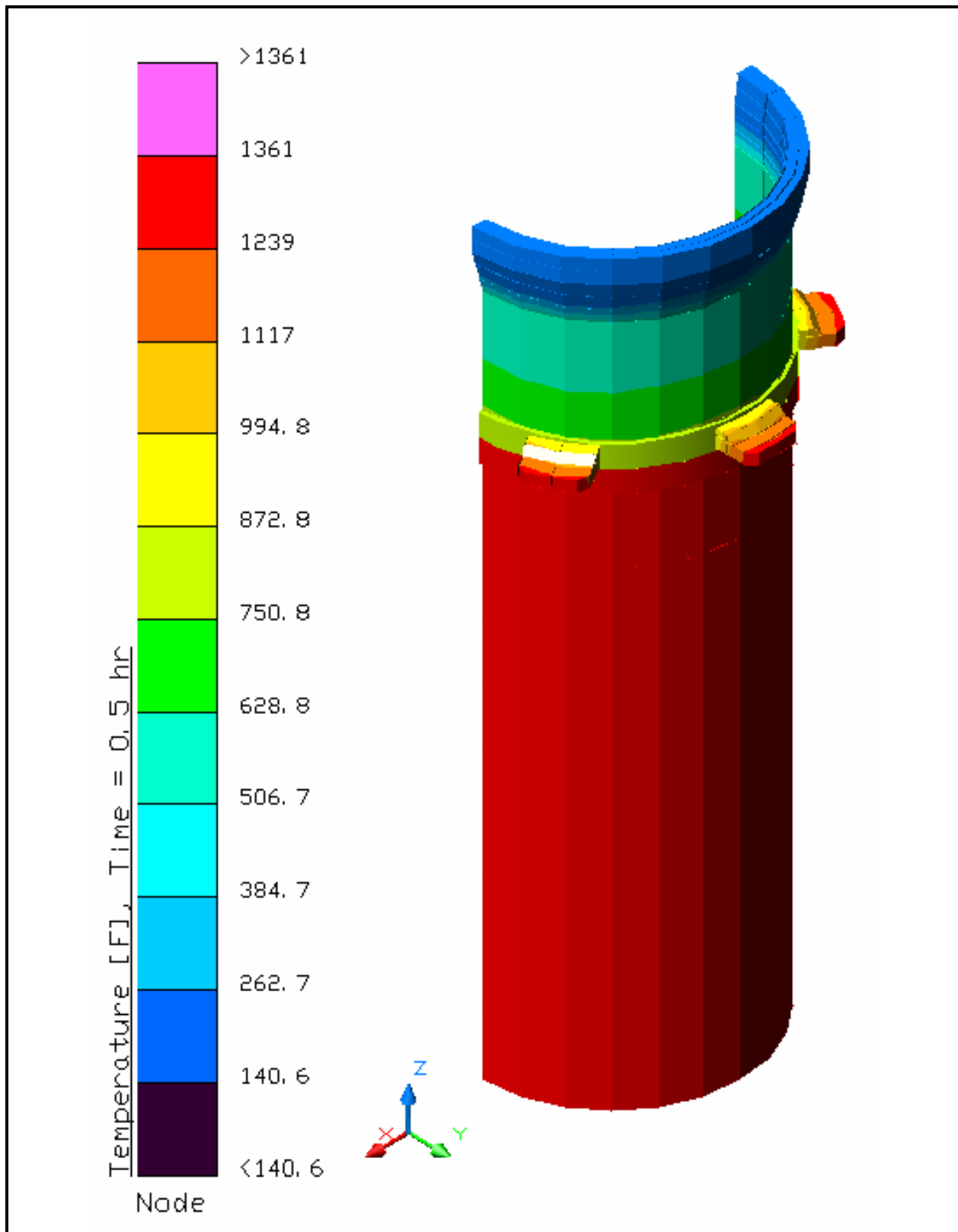


Figure 3.5-7 – Body Shell Temperature Distribution at End of 30-Minute Fire Event

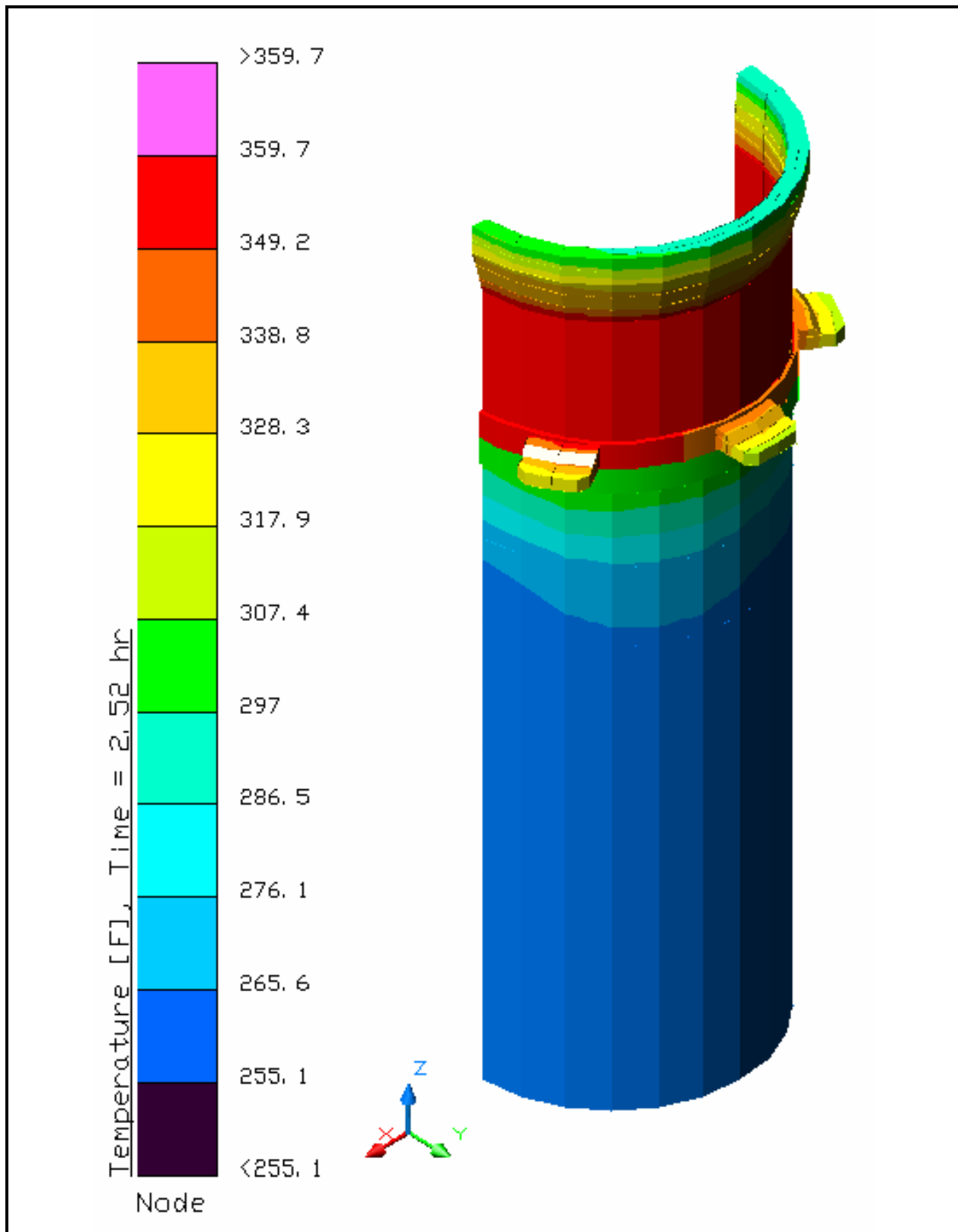


Figure 3.5-8 – Body Shell Temperature Distribution 2 Hours After End of Fire Event

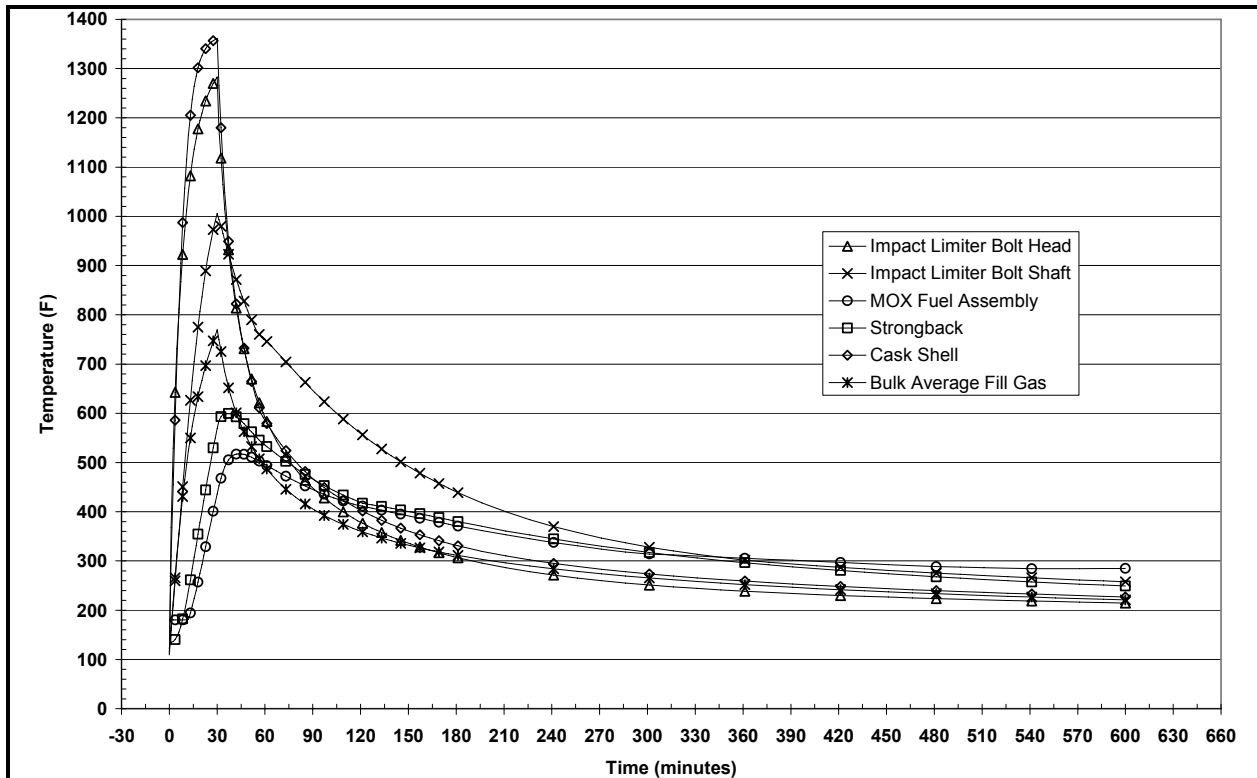


Figure 3.5-9 – HAC Temperature Transient for Selected MFFP Components

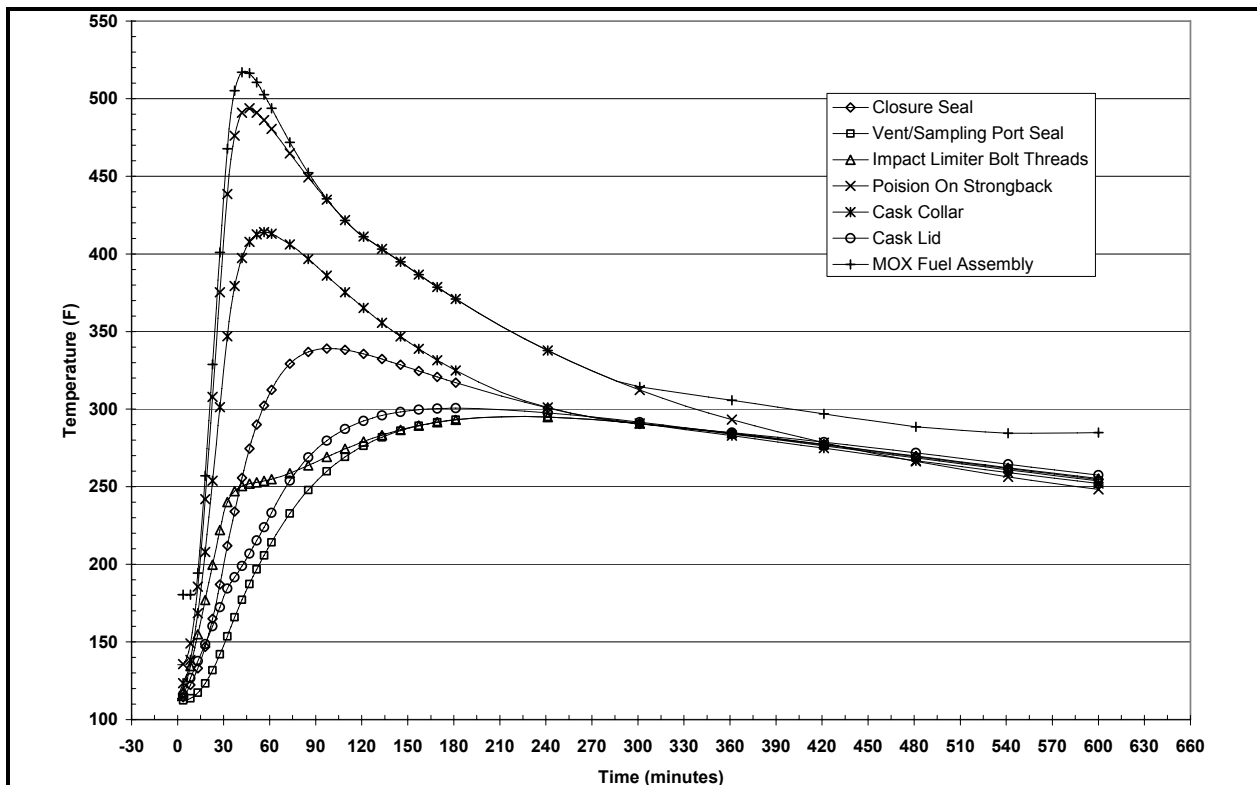


Figure 3.5-10 – HAC Temperature Transient for Additional MFFP Components

3.6 Appendices

3.6.1 Computer Analysis Results

3.6.2 Thermal Model Details

This page intentionally left blank.

3.6.1 Computer Analysis Results

Due to the size and number of the output files associated with each analyzed condition, results from the computer analysis are provided on a CD-ROM.

This page left intentionally blank.

3.6.2 Thermal Model Details

3.6.2.1 Convection Coefficient Calculation

The evaluation of the thermal performance of the MFFP over the wide range of potential operating conditions encountered during NCT and HAC conditions is based on semi-empirical relationships for convection heat transfer. The convective heat transfer coefficient, h_c , has a form of:

$$h_c = Nu \frac{k}{L}$$

where k is the thermal conductivity of the gas at the mean film temperature and L is the characteristic length of the vertical or horizontal surface. These semi-empirical relationships are chosen to account for the variation in convection heat transfer rates between laminar and turbulent operating conditions and for the shape and orientation of the specific surface experiencing convective heat transfer. The specific relationships used for this analysis are discussed below.

Natural convection from vertical surfaces is computed using Equations 6-39 to 6-42 of Rohsenow, et. al.²⁴, where the characteristic length is the height of the surface. These equations, which are applicable over the range of Rayleigh number (Ra) between 1 and 10^{12} , are as follows:

$$Nu^T = \bar{C}_L Ra^{1/4}$$

$$\bar{C}_L = \frac{4}{3} \left[\frac{0.503}{\left(1 + (0.492/Pr)^{9/16}\right)^{4/9}} \right]$$

$$Nu_L = \frac{2.8}{\ln(1 + 2.8/Nu^T)}$$

$$Nu_t = C_t^V Ra^{1/3}$$

$$C_t^V = \frac{0.13 Pr^{0.22}}{(1 + 0.61 Pr^{0.81})^{0.42}}$$

$$Nu = \frac{h_c L}{k} = \left[(Nu_L)^6 + (Nu_t)^6 \right]^{1/6}$$

$$Ra_L = \frac{\rho^2 g_c \beta L^3 \Delta T}{\mu^2} \times Pr$$

where:

h_c = convection coefficient

Nu = Nusselt number

g_c = gravitational acceleration

β = coefficient of thermal expansion

²⁴ Rohsenow, Hartnett, and Ganic, *Handbook of Heat Transfer Fundamentals*, 2nd edition, McGraw-Hill Publishers, 1973.

ΔT = temperature difference

μ = dynamic viscosity

L = characteristic length

Ra = Rayleigh number

ρ = density of air at the film temperature

Pr = Prandtl number

k = thermal conductivity of air at the mean film temperature

h_c = convection coefficient

Note that k , c_p , and μ are each a function of air temperature as taken from Table 3.2-6. Values for ρ are computed using the ideal gas law, β for an ideal gas is simply the inverse of the absolute temperature of the gas, and Pr is computed using the values for k , c_p , and μ from Table 3.2-6. Unit conversion factors are used as required to reconcile the units for the various properties used.

Calculation of the convection coefficient between horizontal, cylinders (i.e., the body shell and portions of the impact limiter) and the ambient environment is computed using Equation 3-43, Chapter 1, from Guyer²⁵. The characteristic length, D , is the outer diameter of the cylinder. This equation, applicable for $10^{-5} < Ra < 10^{12}$, is as follows:

$$Nu = \frac{h_c D}{k} = \left\{ 0.60 + \frac{0.387 Ra_D^{1/6}}{\left[1 + (0.559/Pr)^{9/16} \right]^{8/27}} \right\}^2$$

Natural convection from horizontal surfaces is computed from Equations 4.39 and 4.40 of Rohsenow, et. al.²⁶ where the characteristic dimension (L) is equal to the plate surface area divided by the plate perimeter. For a heated surface facing upwards or a cooled surface facing downwards and $Ra > 1$:

$$Nu = \frac{h_c L}{k} = \left[(Nu_L)^{10} + (Nu_t)^{10} \right]^{1/10}$$

$$Nu_L = \frac{1.4}{\ln \left(1 + 1.677 / (\overline{C}_L Ra^{1/4}) \right)}$$

$$\overline{C}_L = \frac{0.671}{\left[1 + (0.492/Pr)^{9/16} \right]^{4/9}}$$

$$Nu_t = 0.14 Ra^{1/3}$$

For a heated surface facing downwards or a cooled surface facing upwards and $10^3 < Ra < 10^{10}$, the correlation is as follows:

$$Nu = Nu_L = \frac{2.5}{\ln(1 + 2.5/Nu^T)}$$

$$Nu^T = \frac{0.527}{\left(1 + (1.9/Pr)^{9/10} \right)^{2/9}} Ra^{1/5}$$

²⁵ Guyer, E.C., *Handbook of Applied Thermal Design*, McGraw-Hill, Inc., 1989.

²⁶ Rohsenow, Hartnett, and Choi, *Handbook of Heat Transfer*, 3rd edition, McGraw-Hill Publishers, 1998.

3.6.2.2 Effective Thermal Conductivity of MOX Fuel Assemblies

3.6.2.2.1 Purpose

The thermal analysis of the MFFP presented in Sections 3.4, *Thermal Evaluation for Normal Conditions of Transport*, and 3.5, *Thermal Evaluation Under Hypothetical Accident Conditions* models the zirconium alloy clad fuel assemblies as homogeneous solid regions with uniform internal heat generation. In order to accurately predict the temperature rise from the enclosing walls of the strongback assembly to the peak rod location within each fuel assembly using this type of modeling the effective thermal conductivity of the homogeneous solid region must be determined. The effective thermal conductivity calculation accounts for the actual geometry of the fuel assembly and the fact that the heat generation occurs only within the fuel rods.

3.6.2.2.2 Assumptions

1. Table 3.6-1 presents a summary of the relevant design information for the MOX FAs, including portions extracted from Table 1.2-1 of Section 1.2.3, *Contents of Packaging*, and Table 6.2-1 and Table 6.2-3 of Section 6.2, *Fissile Material Contents*.
2. The fuel assemblies are centered within each strongback enclosure.
3. The zirconium alloy cladding is assumed to have a conservatively low emissivity value²⁷ of 0.16.
4. Per Section 3.2, *Material Properties and Component Specifications*, the boron surfaces within fuel control structures (FCSs) around the fuel assemblies have an emissivity of 0.15, while the stainless steel surfaces have an emissivity of 0.2.
5. A decay heat loading of 80 watts is uniformly distributed over the 144-inch active fuel length.
6. Heat transfer from the assembly to the guide sleeve is via radiation and conduction only.
7. The dimension between the inner surfaces of the FCSs is assumed to be 8.887 inch dimension, based on a preliminary design of the FCS. Although this dimension is 3/16 inches larger than the actual 8.7 inch inside dimension of the FCS, the additional thermal resistance within the FAs associated with the larger dimension is insignificant, but conservatively bounds (i.e., is higher than) the value associated with the actual 8.7-inch dimension.

3.6.2.2.3 Methodology

The analysis methodology used for this calculation is based on the calculation approach outlined in Section 3.2.2 of Report BBA000000-01717-5705-00010²⁸. One quarter of the MOX FA and the surrounding strongback walls are modeled. The boundaries formed by the strongback enclosure

²⁷ Murphy, E. V. and Havelock, F., *Emissivity of Zirconium Alloys In Air In The Temperature Range 100-400 °C*, Journal of Nuclear Materials, Volume 60, 1976, pp. 167-176.

²⁸ “*Spent Nuclear Fuel Effective Thermal Conductivity Report*”, prepared TRW Environmental Safety Systems, Inc. for DOE Civilian Radioactive Waste Management System (CRWMS), Report BBA000000-01717-5705-00010, Rev. 0, July 1996.

are set to specified temperature levels for the purposes of this calculation, while symmetry conditions are assumed at the remaining two boundaries. The Thermal Desktop^{®29} and SINDA/FLUINT³⁰ computer programs were used to develop and exercise this detailed thermal model of the fuel assembly. Figure 3.6-1 presents a perspective view of the modeled fuel assembly and strongback wall segment, while Figure 3.6-2 illustrates the finite element modeling used.

The interior of the MFFP is to be filled with air with heat transfer across the interior void volume of the MOX FA via radiation and conduction. Heat transfer across the interiors of the various fuel rods is via conduction through the MOX pellet. While a gap may exist between the cladding and the fuel pellet, the associated ΔT is assumed to be negligible since the size of the gap is small and since the level of decay heat is also low. Further, other analyses have shown the resistance due to this gap has an insignificant effect on the radial heat transfer within the fuel assembly.

Table 3.6-2 presents the component thermal conductivity values assumed for the thermal modeling. Since the analysis is conducted using a series of steady-state simulations, values for density and specific heat are not required.

The design volumetric heat loading used for the MOX FA is as follows:

$$\text{Design volumetric heat load} = \left[\frac{(\text{Decay Heat per Assembly}) \times (\text{Peaking Factor})}{(\text{No. of fuel rods}) \times (\text{Volume per rod})} \right]$$

$$\begin{aligned} \text{Volume per rod} &= \text{Active Fuel Length} \times \pi \times (\text{Fuel rod OD} - 2 \times \text{Cladding Thickness})^2 / 4 \\ &= 144" \times \pi \times (0.374 - 2 \times 0.0225)^2 / 4 \\ &= 12.241769 \text{ in}^3 \end{aligned}$$

$$\begin{aligned} \text{Design volumetric heat load w/ 80 W} &= \left[\frac{(80 \text{ watts}) \times (1.00)}{(264) \times (12.241769 \text{ in}^3)} \right] \\ &= 0.0247538 \text{ watts/in}^3 \end{aligned}$$

3.6.2.2.4 Effective Thermal Conductivity Calculations

The thermal model described above was exercised for boundary temperature levels (i.e., -40, 0, 50, 100, 150, 200, 275, 350, 425, 500, 575, 650, and 725°F). Figure 3.6-3 presents a representative illustration of the computed temperature distribution within the MOX FA, with the illustrated case being for a boundary temperature of 150 °F. The resulting peak temperatures computed for the fuel assembly are presented in Table 3.6-3. In accordance with the development of the equation for effective conductivity of the SAND90-2406 report³¹ (i.e., see page II-127 and equation 6.1-5), the effective thermal conductivity is computed as:

²⁹ Thermal Desktop[®], Version 4.5, Cullimore & Ring Technologies, Inc., Littleton, CO, 2003.

³⁰ SINDA/FLUINT, Systems Improved Numerical Differencing Analyzer and Fluid Integrator, Version 4.5, Cullimore & Ring Technologies, Inc., Littleton, CO, 2001.

³¹ SAND90-2406, Sanders, T. L., et al., *A Method for Determining the Spent-Fuel Contribution to Transport Cask Containment Requirements*, TTC-1019, UC-820, November 1992.

$$k_{\text{effective}} = \left[\frac{0.29468 \times \text{Volumetric Heat Generation Based On Assembly Width} \times \left(\frac{\text{Assembly Width}}{2} \right)^2}{(T_{\text{peak}} - T_{\text{sleeve}})} \right]$$

This equation can be restated as:

$$k_{\text{effective}} = \left[\frac{0.29468 \times \text{Decay Heat Loading For Modeled Section} \times 4}{4 \times \text{Length of Modeled Segment} \times (T_{\text{peak}} - T_{\text{sleeve}})} \right]$$

The decay heat loading computed from the model, the length of the modeled segment (i.e., 1.0 inches high), and the noted peak temperature and boundary sleeve temperature are substituted to yield the computed effective thermal conductivity. Table 3.6-3 presents the computed effective thermal conductivity for the MOX FA heat load and boundary temperature. As expected, the Report BBA000000-01717-5705-00010 values, which assume a fuel cladding emissivity of 0.8, are close to those predicted for the MOX FA at low temperatures where conduction dominates, but diverge from the computed MOX effective conductivity values at high temperatures where heat transfer via radiation dominates.

For use in finite element modeling, Section 6.2.2 of Report BBA000000-01717-5705-00010²⁸ recommends that the effective thermal conductivity values be made a function of the mean assembly temperature, or $(T_{\text{peak}} - T_{\text{sleeve}})/2$. Figure 3.6-4 illustrates the correlation between the computed effective thermal conductivity and the median assembly temperature.

The axial heat transfer within the fuel assembly is assumed to be limited to that which will occur within the cladding of the fuel rods only. This approach is based on the conservative assumption that gaps between the individual fuel pellets will limit the axial heat transfer rate between the individual pellets. The axial thermal conductivity values presented in Table 3.2-4 use the fuel rod geometry and number of fuel rods for MOX FA and the cross-sectional area of the fuel region to account for the fact that the fuel assemblies are treated as homogenized regions within this modeling. For example, at a temperature of 260 °F, the effective axial conductivity is computed as:

$$k_{\text{axial direction}} = 264 \text{ pins} \times \frac{\pi}{4} \left(0.374''^2 - (0.374'' - 2 \times 0.0225'')^2 \right) \times 0.2255 \frac{\text{Btu}}{\text{hr} - \text{in} - ^\circ\text{F}} \div (8.887'' \times 8.887'')$$

$$k_{\text{axial direction}} = 0.01873 \frac{\text{Btu}}{\text{hr} - \text{in} - ^\circ\text{F}} @ 260^\circ\text{F}$$

Table 3.6-1 – Summary of Design Data for MOX FA

Parameter	Value
Number of fuel rods	264
Number of guide tubes	24
Number of instrument tubes	1
Parameter	Inches
Pellet diameter	0.3225
Active fuel length	144
Cladding thickness	0.023
Fuel rod OD	0.374
Fuel rod pitch	0.496
Poison rod tube OD	0.381
Poison rod tube thickness	0.0255
Guide tube OD	0.482
Guide tube thickness	0.016

Table 3.6-2 – Thermal Properties for Effective Fuel Conductivity Calculation

Temperature (°F)	Conductivity (BTU/hr-in-°F)
Zirconium Alloy Cladding ^{32,33,34}	
32	0.8442
100	0.8404
200	0.8373
300	0.8380
400	0.8421
500	0.8500
600	0.8609
700	0.8756
800	0.8940
1000	0.9407
MOX Pellet ³⁵	
46	0.2559
80	0.2552
260	0.2255
440	0.2027
620	0.1846
800	0.1709
980	0.1628
1160	0.1597
Type 304 Stainless Steel - See Table 3.2-1	
Air - See Table 3.2-6	

³² Peletsky V. E. and Musayeva, Z. A., *Effect Of Oxidation On Transport Properties of Zirconium - 1% Niobium Alloy*, International Journal Of Thermophysics, Vol. 16, Number 6, 1995, pp 1481 –1487.

³³ Peletsky V. E. and Petrova, I. L., *Investigation Of The Thermophysical Properties of The Alloy Zr - 1% Nb By A Subsecond Pulse Heating Technique*, High Temperatures - High Pressures, 1997, Volume 29, pp 373 –378.

³⁴ Lusternik, V. E., Peletsky V. E., and Petrova, I. L., *High Temperature Calorimetric Measurements of Zr - 1% Nb Alloy At Various Rates Of Heating*, High Temperatures - High Pressures, 1993, Volume 25, pp 539 –543.

³⁵ Van Craeynest, J. C. and Stora, J. P. *Effet del la porosite' sur la variation de la conductibilite' thermique de bioxyde d'uranium en foncitionde la temperature*, Journal of Nuclear Materials, Volume 37, 1970, pp. 153-158.

Table 3.6-3 – Computed MOX Effective Thermal Conductivity

Decay Heat (W)	Sleeve Temperature (°F)	Peak Temperature (°F)	Medium Assembly Temperature (°F)	Effective Thermal Conductivity (Btu/hr-in-°F)
80	-40	17.5	-11.3	0.00237
	0	53.1	26.6	0.00256
	50	98.4	74.2	0.00281
	100	144.5	122.3	0.00306
	150	191	170.5	0.00332
	200	238	219.0	0.00358
	275	309.1	292.1	0.00399
	350	380.8	365.4	0.00442
	425	452.9	439.0	0.00488
	575	598.2	586.6	0.00587
	650	671.2	660.6	0.00642
	725	744.4	734.7	0.00701

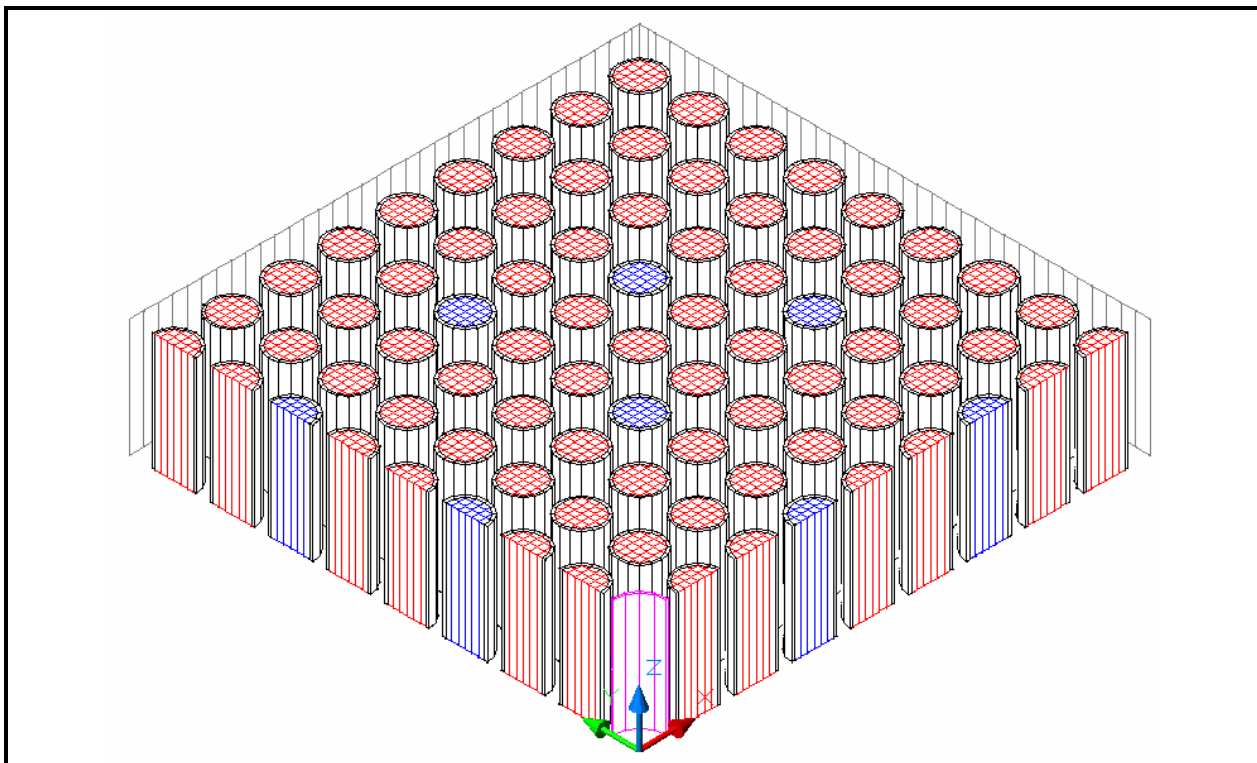


Figure 3.6-1 – Perspective View of MOX Thermal Model (1/4-Segment)

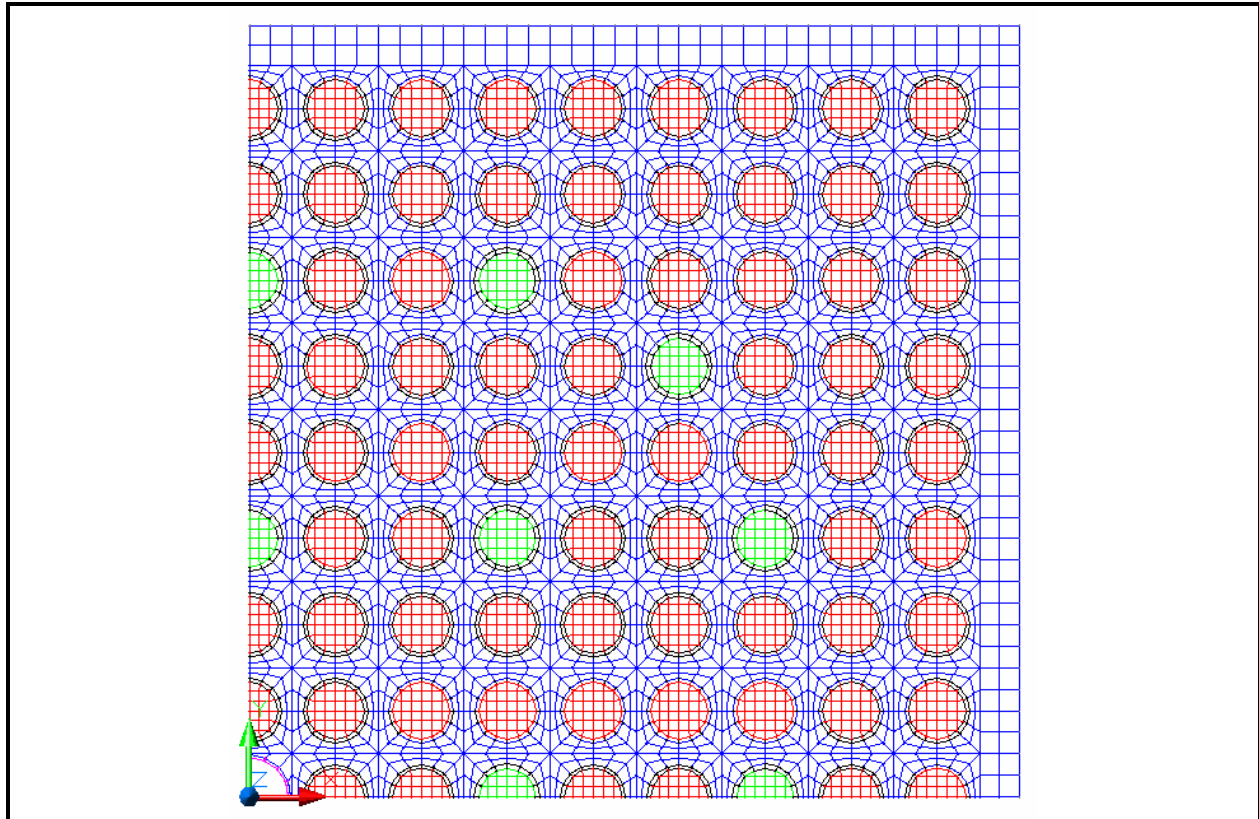


Figure 3.6-2 – Finite Element Modeling of 1/4-Segment MOX Assembly

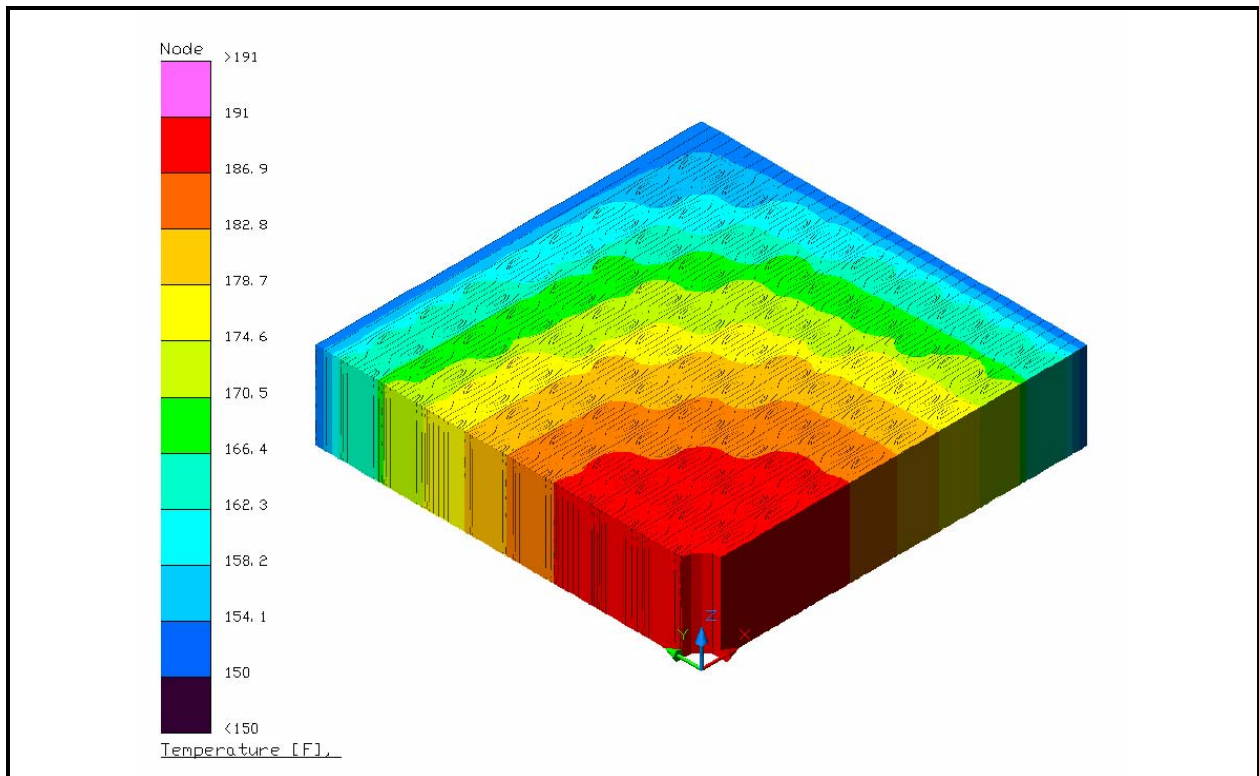


Figure 3.6-3 – Representative Temperature Distribution within 1/4-Segment MOX Assembly

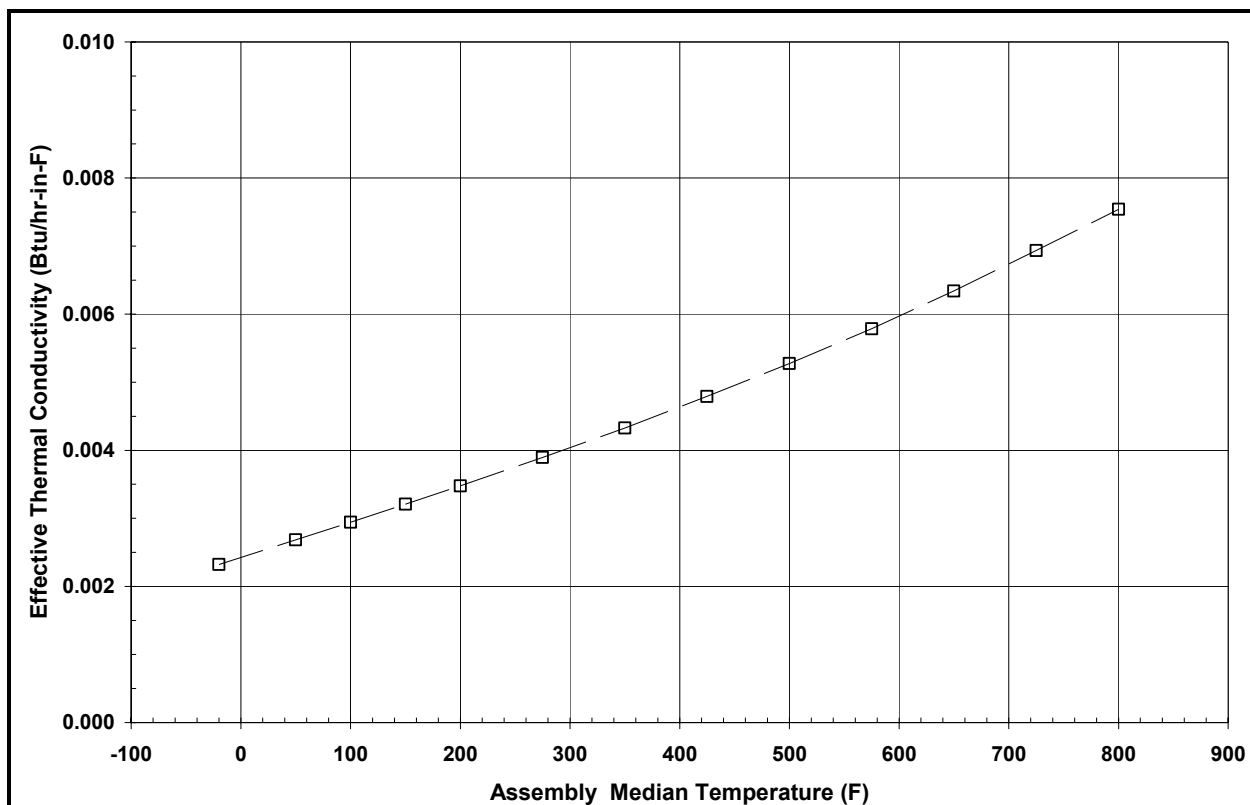


Figure 3.6-4 – Effective Radial Thermal Conductivity for MOX FAs

4.0 CONTAINMENT

4.1 Description of the Containment System

4.1.1 Containment Boundary

A single level of containment is provided for the fresh MOX fuel payload by the MFFP. In general, all containment components are fabricated from Type XM-19 austenitic stainless steel, with exceptions noted in the following detailed description.

The containment boundary for the MFFP consists of the 9/16-inch thick cylindrical shell, the 1½-inch thick bottom plate, the 5/8-inch inner closure lid plate, the closure lid seal forging, and the upper forging on the body. The non-stainless steel components included in the containment boundary are the center butyl O-ring seal for the closure lid, the ASTM A564, 630 (H1100), nickel plated alloy steel closure bolts, the ASTM B16 brass vent and fill port plugs, and their associated butyl rubber sealing elements.

4.1.1.1 Containment Penetrations

The only penetrations into the containment boundary are the vent port, fill port, and closure lid. Each penetration is designed to demonstrate “leaktight” sealing integrity, i.e., a leakage rate not to exceed 1×10^{-7} standard cubic centimeters per second (scc/s), air, per ANSI N14.5¹.

4.1.1.2 Closure

With reference to Figure 1.1-2 in Chapter 1.0, *General Information*, the closure lid is secured to the body via twenty-four (24), 3/4-inch × 3-inch long socket head cap screws (SHCS). The installation of the closure lid consists of four main steps:

1. As an option, lightly lubricate the O-ring seals with vacuum grease; install the O-ring seals into their respective O-ring seal grooves located in the closure lid.
2. Align the closure lid with the body.
3. Install the closure lid.
4. Install twenty-four (24), 3/4-inch SHCS through the closure lid and into the lid end forging on the body.

4.1.1.3 Seals

The elastomeric portion of the containment boundary is comprised of a nominally 3/8-inch diameter, O-ring bore seal in the center groove of the closure lid, and stat-o-seal sealing elements (an O-ring integrated with a stainless steel washer) for the vent and fill port plugs.

The elastomeric containment O-ring seals and stat-o-seals are fabricated of a butyl compound, suitable for normal conditions of transport (NCT) ranging from a low temperature of -65 °F to a high

¹ ANSI N14.5-1997, *American National Standard for Radioactive Materials - Leakage Test on Packages for Shipment*, American National Standard Institute, Inc. (ANSI).

temperature of 225 °F for long durations. Further, the butyl compound is capable of a hypothetical accident condition (HAC) high temperature of 400 °F for a short duration (8 hours). Details of the containment vessel and associated penetrations are provided in the drawings in Section 1.4.2, *Packaging General Arrangement Drawings*. Further discussion of the thermal performance capabilities of the butyl rubber O-ring seals is provided in Section 3.2.2, *Component Specifications*.

Three nearly identical O-ring seals are provided on the outer diameter of the closure lid. The center O-ring seal comprises the containment seal, whereas the outer O-ring seal serves to create an annular test cavity for verification of the center seal integrity via leakage rate testing. The inner O-ring seal serves to create a fill cavity for the test gas. For leakage rate testing of the closure lid containment O-ring seal using a helium mass spectrometer leak detector (MSLD) or other leak test equipment, the fill cavity is purged and backfilled with helium gas, and the seal test cavity is evacuated and tested using a MSLD (or other leak test equipment). Upon successfully performing the closure lid main O-ring seal leakage rate test, the MSLD (or other leak test equipment) is moved to the vent and fill ports to verify sealing integrity, since these penetrations form part of the package's containment boundary.

4.1.1.4 Welds

All containment vessel body welds are full penetration welds that have been radiographed to ensure structural and containment integrity. Non-radiographed, safety related welds, such as those that attach the impact limiter mounting lugs to the cylindrical shell, are examined using liquid penetrant testing on the final pass or both the root and final passes, as applicable. All containment boundary welds are confirmed to be leaktight as delineated in Section 8.1.4, *Fabrication Leakage Rate Tests*.

4.1.2 Special Requirements for Plutonium

The MFFP is designed to contain and transport payloads in excess of 20 Ci of plutonium in solid form (i.e., fuel assemblies). Therefore, the requirements of 10 CFR §71.63² are satisfied.

² Title 10, Code of Federal Regulations, Part 71 (10 CFR 71), *Packaging and Transportation of Radioactive Material*, Final Rule, 01-26-04.

4.2 General Considerations

4.2.1 Type A Fissile Package

This section does not apply for the MFFP, since the package is a Type B fissile package.

4.2.2 Type B Packages

The MFFP is designed with a “leaktight” containment boundary, as defined by ANSI N14.5¹, to contain the MOX FA payload. Leak tightness of the containment boundary has been demonstrated by full-scale structural testing, as presented in Appendix 2.12.3, *Certification Test Results*, that demonstrated no release of radioactive materials per the “leaktight” definition of ANSI N14.5 under any of the normal conditions of transport tests and the hypothetical accident condition tests described in 10 CFR §71.71² and §71.73, respectively. The full-scale structural tests included leakage rate tests of the containment metallic boundary and elastomeric seals. These leakage rate tests are specified for the MFFP in Section 8.1.4, *Fabrication Leakage Rate Tests*.

¹ ANSI N14.5-1997, *American National Standard for Radioactive Materials – Leakage Tests on Packages for Shipment*, American National Standards Institute, Inc. (ANSI).

² Title 10, Code of Federal Regulations, Part 71 (10 CFR 71), *Packaging and Transportation of Radioactive Material*, Final Rule, 01-26-04.

This page left intentionally blank.

4.3 Containment Requirements for Normal Conditions of Transport

4.3.1 Containment of Radioactive Material

The results of the normal conditions of transport (NCT) structural and thermal evaluations presented in Sections 2.6, *Normal Conditions of Transport*, and 3.4, *Thermal Evaluation Under Normal Conditions of Transport*, respectively, and the results of the full-scale structural testing presented in Appendix 2.12.3, *Certification Test Results*, demonstrate that there is no release of radioactive materials per the “leaktight” definition of ANSI N14.5¹ under any of the normal conditions of transport tests described in 10 CFR §71.71².

4.3.2 Pressurization of the Containment Vessel

The maximum normal operating pressure (MNOP) of the MFFP is 10 psig per Section 3.4.2, *Maximum Normal Operating Pressure*. The design pressure of the MFFP is 25 psig. Based on the structural analyses presented in Section 2.0, *Structural Evaluation*, pressure increases to 25 psig will not reduce the effectiveness of the MFFP in maintaining containment integrity per Section 4.3.1, *Containment of Radioactive Material*.

4.3.3 Containment Criterion

At the completion of fabrication, the MFFP shall be leakage rate tested as described in Section 4.5.1, *Fabrication Leakage Rate Tests*. For annual maintenance, the MFFP shall be leakage rate tested as described in Section 4.5.2, *Maintenance/Periodic Leakage Rate Tests*. In addition, at the time of seal replacement if other than during routine maintenance (e.g., if damage during assembly necessitates seal replacement), maintenance/periodic leakage rate testing shall be performed for that seal. For verification of proper assembly prior to shipment, the MFFP shall be leakage rate tested as described in Section 4.5.3, *Preshipment Leakage Rate Tests*.

¹ ANSI N14.5-1997, *American National Standard for Radioactive Materials – Leakage Tests on Packages for Shipment*, American National Standards Institute, Inc. (ANSI).

² Title 10, Code of Federal Regulations, Part 71 (10 CFR 71), *Packaging and Transportation of Radioactive Material*, Final Rule, 01-26-04.

This page left intentionally blank.

4.4 Containment Requirements for Hypothetical Accident Conditions

4.4.1 Fission Gas Products

Although there are no fission gas products in the MOX FAs, the pressures for hypothetical accident conditions (HAC) are calculated assuming 100% of fill gas is released from all of the fuel rods in the three fuel assemblies inside the package, as presented in Section 3.5.3, *Maximum Temperatures and Pressures*.

4.4.2 Containment of Radioactive Material

The results of the hypothetical accident condition (HAC) structural and thermal evaluations performed in Sections 2.7, *Hypothetical Accident Conditions*, and 3.5, *Thermal Evaluation Under Hypothetical Accident Conditions*, respectively, and the results of the full-scale structural testing presented in Appendix 2.12.3, *Certification Test Results*, demonstrate that there is no release of radioactive materials per the “leaktight” definition of ANSI N14.5¹ under any of the hypothetical accident condition tests described in 10 CFR §71.73².

4.4.3 Containment Criteria

The MFFP is leakage rate tested as described in Section 4.1.1.3, *Seals*, to demonstrate the leaktight containment criterion of ANSI N14.5.

¹ ANSI N14.5-1997, *American National Standard for Radioactive Materials – Leakage Tests on Packages for Shipment*, American National Standards Institute, Inc. (ANSI).

² Title 10, Code of Federal Regulations, Part 71 (10 CFR 71), *Packaging and Transportation of Radioactive Materials*, United States Nuclear Regulatory Commission (USNRC), Final Rule, 01-26-04.

This page left intentionally blank.

4.5 Leakage Rate Tests for Type B Packages

The MFFP is designed with a “leaktight” containment boundary, as defined in ANSI N14.5¹, to transport the MOX FAs. Demonstration of the leaktight capabilities of the MFFP are accomplished by performing leakage rate tests of the metallic and elastomeric containment boundary. A summary of these leakage rate tests prior to first use, during routine maintenance, and upon assembly for transport is described in the following sections.

4.5.1 Fabrication Leakage Rate Tests

During fabrication and following the pressure testing per Section 8.1.3.2, *Pressure Testing*, the containment boundary is tested per the leakage rate test delineated in Section 8.1.4, *Fabrication Leakage Rate Tests*. The fabrication leakage rate tests are consistent with the guidelines of Section 7.3 of ANSI N14.5. These leakage rate tests verify the containment integrity of each penetration and the metallic boundary of the MFFP to a leakage rate not to exceed 1×10^{-7} scc/s, air, following fabrication of the package.

4.5.2 Maintenance/Periodic Leakage Rate Tests

Annually, or at the time of damaged containment seal replacement or sealing surface repair, the O-ring seals shall be leakage rate tested as delineated in Section 8.2.2, *Maintenance/Periodic Leakage Rate Tests*. The maintenance/periodic leakage rate tests are consistent with the guidelines of Sections 7.4 and 7.5 of ANSI N14.5. This test verifies the integrity of each O-ring seal to a leakage rate not to exceed 1×10^{-7} scc/s, air.

4.5.3 Preshipment Leakage Rate Tests

Prior to shipment of a loaded MFFP, the center O-ring seal, the vent port stat-o-seal and the fill port stat-o-seal shall be leak tested per Section 7.4, *Preshipment Leakage Rate Tests*. The preshipment leakage rate tests are consistent with the guidelines of Section 7.6 of ANSI N14.5. This test verifies the sealing integrity of the closure lid, vent port, and fill port seals to a leakage rate sensitivity of 1×10^{-3} scc/s, air.

The maintenance/periodic leakage rate tests, delineated in Section 8.2.2, *Maintenance/Periodic Leakage Rate Tests*, may be performed as an option, in lieu of the preshipment leakage rate tests.

¹ ANSI N14.5-1997, *American National Standard for Radioactive Materials – Leakage Tests on Packages for Shipment*, American National Standards Institute, Inc. (ANSI).

This page left intentionally blank.

5.0 SHIELDING EVALUATION

The compliance of the MFFP packaging with respect to the dose rate limits established by 10 CFR §71.47¹ for normal conditions of transport (NCT) or 10 CFR §71.51(a)(2) for hypothetical accident conditions (HAC) are satisfied when limiting the MFFP package to three (3) Mixed Oxide (MOX) fresh fuel assemblies (FAs) having a radioisotope content listed in Table 1.2-2.

Under these conditions, the maximum surface dose rate will be less than the limit of 200 mrem/hr for NCT and verified by measurement. This dose rate limit is for payload packages prior to addition of any lead, steel or other shielding material for *as-low-as-reasonably-achievable* (ALARA) dose reduction purposes during non-transport handling operations.

Prior to transport, the MFFP package shall be monitored for both gamma and neutron radiation to demonstrate compliance with 10 CFR §71.47. As noted in Section 2.6.7, *Free Drop*, the MFFP package is not significantly deformed under NCT free drop conditions. Therefore, the package will meet the dose rate limits for NCT if the measurements demonstrate compliance with the allowable dose rate levels in 10 CFR §71.47 (200 mrem/hr). The transport index, as defined in 10 CFR §71.4, will be determined by measuring the dose rate a distance of one meter from the package surface per the requirements of 49 CFR §173.403².

Shielding materials are not specifically provided by the MFFP package, and none are permitted within the package to meet the dose rate limits of 10 CFR §71.47 for NCT. Since significant fuel deformation or package deformation does not occur under HAC, the HAC surface dose rates and 1-meter dose rates will not be significantly different from the NCT dose rates. This result ensures that the post-HAC, allowable dose rate of 1 rem/hr a distance of one meter from the package surface per 10 CFR §71.51(a)(2) will be met because the surface dose rate will remain below the 200 mrem/hr limit.

¹ Title 10, Code of Federal Regulations, Part 71 (10 CFR 71), *Packaging and Transportation of Radioactive Material*, Final Rule, 01-26-04.

² Title 49, Code of Federal Regulations, Part 173 (49 CFR 173), *Shippers - General Requirements for Shipments and Packagings*, Final Rule, 01-26-04.

This page left intentionally blank.

6.0 CRITICALITY EVALUATION

The following analyses demonstrate that the MFFP complies with the requirements of 10 CFR §71.55¹ and §71.59. The analyses presented herein show that the criticality requirements are satisfied when limiting the MFFP package to a maximum of three pressurized water reactor (PWR) mixed-oxide (MOX) fresh fuel assemblies (FAs) as described in Section 1.2.3, *Contents of Packaging*.

6.1 Description of Criticality Design

6.1.1 Design Features Important for Criticality

A comprehensive description of the MFFP package is provided in Section 1.2, *Packaging Description*, and in the drawings in Appendix 1.4.2, *Packaging General Arrangement Drawings*. This section summarizes those design features important for criticality.

The primary design feature used to ensure criticality safety is the use of neutron poison plates (boral) with a minimum B-10 areal density of 0.035 g/cm². The neutron poison plates surround each fuel assembly on all four sides. Neutron poison plates that span the active fuel length are fastened to the radial and tangential strongback angles. The remaining two sides of each assembly are constrained by fuel control structures (FCSs), which are hinged angles placed between the clamp arms. Neutron poison plates (boral) are bolted to the exterior surface of each FCS.

Criticality safety is also ensured by the structural design of the MFFP. The stainless steel strongback angles and clamp arms firmly secure the FAs to the package. The FCS provides additional support in the event of an accident and prevents unrestrained pitch expansion of the fuel. Finally, the stainless steel shell of the package itself provides separation from adjacent packages and provides a leaktight containment boundary that excludes water from the package.

6.1.2 Summary Table of Criticality Evaluation

The upper subcritical limit (USL) for ensuring that the MFFP (package or package array) is acceptably subcritical, as determined in Section 6.8, *Benchmark Evaluations*, is:

$$\text{USL} = 0.9288$$

The package is considered to be acceptably subcritical if the computed k_{safe} (k_s), which is defined as $k_{\text{effective}}$ (k_{eff}) plus twice the statistical uncertainty (σ), is less than the USL, or:

$$k_s = k_{\text{eff}} + 2\sigma < \text{USL}$$

The USL is determined on the basis of a benchmark analysis and incorporates the combined effects of code computational bias, the uncertainty in the bias based on both benchmark-model and computational uncertainties, and an administrative margin. The results of the benchmark analyses indicate that the USL is adequate to ensure subcriticality of the MFFP.

¹ Title 10, Code of Federal Regulations, Part 71 (10 CFR 71), *Packaging and Transportation of Radioactive Material*, Final Rule, 01-26-04.

The results of the criticality calculations are summarized in Table 6.1-1. The maximum calculated k_s is 0.9037 which occurs for the HAC infinite array case with fully moderated internal region and void external region. Under NCT, the maximum calculated k_s is 0.6039 for the array case.

The NCT cases assume no moderation. This assumption is credible because of the leaktight performance of the MFFP under both NCT and HAC. Consequently, NCT reactivities are negligibly low.

For HAC, water is assumed to be present in the containment system. Reactivity increases monotonically as water density is increased to a maximum of 100% water density. For the HAC cases, the pitch is also allowed to expand to the maximum possible extent allowed by the FCS to simulate possible fuel assembly damage. Reactivity is a maximum when the pitch is the maximum allowed by the FCS, indicating that the system is undermoderated.

6.1.3 Criticality Safety Index

For both NCT and HAC, an infinite number of MFFPs are evaluated in a close-packed hexagonal array. Therefore, “N” is infinite, and in accordance with 10 CFR §71.59 the criticality safety index (CSI) is $50/N = 0$.

Table 6.1-1 – Summary of Criticality Analysis Results

Normal Conditions of Transport (NCT)			
Case	k_{eff}	σ	k_s
Single Unit Maximum k_s	0.2858	0.0008	0.2874
Infinite Array Maximum k_s	0.6027	0.0006	0.6039
Hypothetical Accident Conditions (HAC)			
Case	k_{eff}	σ	k_s
Single Unit Maximum k_s	0.8981	0.0010	0.9001
Infinite Array Maximum k_s	0.9017	0.0010	0.9037
USL	0.9288		

6.2 Fissile Material Contents

The payload cavity of an MFFP can accommodate one triangular strongback assembly containing up to three mixed-oxide (MOX) fresh fuel assemblies (FAs). The overall arrangement of the fuel within the package is provided in Figure 6.3-1. Because MCNP utilizes metric inputs, metric values are also specified here and in other tables in this chapter. The physical design parameters of a MOX FA are given in Table 6.2-1 and Table 6.2-2. The nucleonic MOX FA design parameters are given in Table 6.2-3.

As discussed in Table 6.2-3, the actual MOX FAs may contain zoned fuel regions, although in the criticality analysis all fuel pins are conservatively assumed to be at the maximum Pu loading. In addition, the fuel assemblies may contain burnable poison rods, although in the criticality analysis burnable poison rods are conservatively ignored.

Table 6.2-1 – MOX PWR Fuel Assembly Physical Design Parameters

Parameter	English Value	Metric Value
Configuration	17 × 17	
Number of Fuel Rods	264	
Number of Guide Tubes	24	
Number of Instrument Tubes	1	
Length (top of leaf spring to bottom nozzle)	161.61 inches	410.49 cm
Width, top nozzle	8.406 inches	21.351 cm
Width, bottom nozzle	8.425 inches	21.400 cm
Width, overall assembly	8.565 inches maximum	21.755 cm maximum
Weight of UO ₂ /PuO ₂ per assembly (95% theoretical density)	1,157 pounds	525 kg
Weight of Heavy Metals per assembly (95% theoretical density)	1,020 pounds	463 kg
Fuel Rod Pitch	0.496 ± 0.006 inches	1.2598 ± 0.015 cm
Guide Thimble OD	0.482 inches	1.224 cm
Guide Thimble ID	0.450 inches	1.143 cm

Table 6.2-2 – MOX Fuel Rod Physical Parameters

Parameter	English Value	Metric Value
Cladding Material	Zirconium-Based M5 Alloy	
Outside Diameter	0.374 inches	0.950cm
Inside Diameter	0.329 inches	0.836 cm
Overall Length	152.4 inches	387.1 cm
Active Fuel Length	144.00 inches	365.76 cm
Weight	5.33 pounds	2.42 kg
Weight of UO ₂ /PuO ₂	4.384 pounds	1.989 kg
Upper End Cap Length	0.515 inches	1.308 cm
Lower End Cap Length	0.575 inches	1.461 cm

Table 6.2-3 – Nucleonic Design Parameters

Parameter	English Value	Metric Value
Pellet Diameter	0.3225 inches	0.8192 cm
Pellet Density	--	10.44 g/cc (95% theoretical density) 10.99 g/cc (100% theoretical density)
Effective Pellet Density (homogenized pellet stack accounting for dish and chamfer, used in MCNP models)	--	10.31 g/cc (95% theoretical density) 10.85 g/cc (100% theoretical density)
Concentration Ranges* (^w %) (average per assembly) * The maximum Pu loading of 6.0% applies to both the assembly average and individual fuel rods. The rods may either vary (such as the use of high, medium, and low enriched zones within the assembly), or be constant.	<u>Total Uranium 94.0^w% or greater of which:</u> ²³⁴ U: 0 to 0.05 ^w % ²³⁵ U: 0 to 0.30 ^w % ²³⁸ U: 99.65 to 100 ^w % <u>Total Plutonium up to 6.0^w% of which:</u> ²³⁸ Pu: 0 to 0.05 ^w % ²³⁹ Pu: 90 to 95 ^w % ²⁴⁰ Pu: 5 to 9 ^w % ²⁴¹ Pu: 0 to 1 ^w % ²⁴² Pu: 0 to 0.1 ^w %	

6.3 General Considerations

Criticality calculations for the MFFP package are performed using the three-dimensional Monte Carlo computer code MCNP5¹. Descriptions of the fuel assembly geometric models are given in Section 6.3.1, *Model Configuration*. The material properties for all materials used in the models are provided in Section 6.3.2, *Material Properties*. The computer code and cross section libraries used are provided in Section 6.3.3, *Computer Codes and Cross-Section Libraries*. Finally, the most reactive configuration for each case is provided in Section 6.3.4, *Demonstration of Maximum Reactivity*.

6.3.1 Model Configuration

6.3.1.1 Contents Model

The MFFP contents are represented by a conservative model of the MOX fresh fuel assembly. The model contains fuel loading that exceeds the designs currently being considered. In addition, the fuel assembly model conservatively:

- Neglects fuel rod zoning
- Assumes the maximum fuel loading, including fissile isotope distribution, possible
- Ignores any effect of burnable poison fuel assemblies, even if present.

Table 6.2-1, Table 6.2-2, and Table 6.2-3 contain the significant parameters used in the contents model. The contents model uses nominal dimensions with the exception of the pitch, which is optimized to maximize reactivity.

Each fuel pin is modeled explicitly, including the top and bottom end plugs, plenum, and pellet/cladding gap. The 24 empty guide thimbles are modeled explicitly, and the center instrument tube is assumed to be the same as a guide thimble. The grid straps are conservatively ignored, as well as the top and bottom nozzles, which are modeled as variable density water. The fuel pin pellet-cladding gap is also filled with variable density water to match the moderation assumed in the package cavity. The HAC models also consider the reactivity effects of the fuel pins shifting axially.

6.3.1.2 Packaging Model

A comprehensive description of the MFFP packaging is provided in Section 1.2, *Packaging Description*, and in the packaging drawings in Appendix 1.4.2, *Packaging General Arrangement Drawings*. The packaging includes a containment vessel, an internal strongback assembly, and impact limiters. The impact limiters cover each end of the body and are steel shells filled with polyurethane foam.

The packaging is lightweight due to the weight constraints built into the design. For modeling simplicity, the impact limiters are neglected for both NCT and HAC models. Ignoring the impact limiters conservatively:

¹ MCNP5, "MCNP – A General Monte Carlo N-Particle Transport Code, Version 5; Volume II: User's Guide," LA-CP-03-0245, Los Alamos National Laboratory, April, 2003.

- Allows for greater reflection in the single package cases (because the reflector is closer to the contents).
- Accounts for any HAC damage to the limiters (due to crush during impact).
- Conservatively places packages closer together for the array calculations (because the impact limiters would provide additional spacing and reduce moderation or reflection).

Because the containment shell sustains only localized puncture damage during HAC (refer to Figure 2.12.3-35 for puncture damage) and because minor variations in the package dimensions have little effect on the criticality calculations, nominal packaging dimensions are used for both the basic NCT and HAC models.

Details of the packaging model are provided in the following figures. Figures are presented to scale and are generated from the MCNP input files. The packaging model represents geometrically significant structural and poison materials. Key dimensions used in the MCNP models are provided in Table 6.3-1. Notations are made in the table when the model dimensions differ from the final design. The model is more conservative than the final design because the FCS poison plates as modeled are smaller than actual size.

Figure 6.3-1 shows the model geometry through a planar slice of the package for the NCT case. The strongback is modeled as a simplified triangular shaped structure. Because the design allows for easy water migration through the strongback, any water moderation is modeled to completely fill all void spaces. Water reflector (12 inches) surrounds the package on all sides. Figure 6.3-2 shows an axial view of the NCT geometry.

Figure 6.3-3 and Figure 6.3-4 present a close-up view of the lower fuel assembly at different axial elevations with labels on all major components. Each fuel assembly is completely surrounded on all four sides to restrict movement. As shown in Figure 6.3-3, the top and right boundary of the assembly is bounded by the strongback. Borated aluminum (boral) neutron poison plates are bolted to the strongback between the strongback and neutron poison cover plates.

The strongback and strongback boral are continuous pieces, while the neutron poison cover plates are segmented and are located only opposite each clamp arm. Steel bolts are explicitly modeled in the strongback boral to reduce the boron loading. As shown in Figure 6.3-3, the left and bottom boundary of each assembly is supported by eight clamp arms and seven fuel control structures (FCSs). Each FCS segment has neutron poison plates attached on the outer surface of the FCS. For simplicity, the clamp arms and strongback support triangles are not explicitly modeled, although the seven steel segments that form the FCS are modeled as one continuous piece because the steel clamp arms will be present between the segments. The impact of including the clamp arms and strongback triangles is assessed in additional calculations in which these components are homogenized into the water region.

The FCS neutron poison plates are modeled as discrete segments. The FCS neutron poison plates are not modeled with bolt holes as with the strongback boral, although the FCS neutron poison plates are modeled conservatively short to minimize the amount of boral.

Figure 6.3-5 shows a close-up view of the model corner. Note that the neutron poison plate is explicitly modeled as a B₄C-Al matrix clad on each side by aluminum.

Figure 6.3-6 and Figure 6.3-7 show the top and bottom of the package. Note that the top and bottom nozzles are modeled as variable density water. Also, these figures explicitly show the

fuel pin end caps and plenum regions. Figure 6.3-8 and Figure 6.3-9 show the strongback and FCS poison plates and the extent to which they overlap the active fuel region.

6.3.2 Material Properties

All material compositions used in the models are representative of the actual materials used in the MFFP. The compositions and densities of all packaging materials as input to MCNP are provided in Table 6.3-2 through Table 6.3-6. Note that most materials (Type 304, XM-19, fuel) are input with weight fractions on the material card and gram density on the cell card. The boral is input with number densities on the material card and total number density on the cell card.

As fuel isotopics are provided as ranges in Table 6.2-3, the fuel isotopics selected for the criticality model are chosen to maximize reactivity. As Pu-241 is more reactive than Pu-239 for moderated systems (which are the most reactive cases for the MFFP), the Pu-241 content is maximized. As Pu-240 acts as a poison, the Pu-240 content is minimized. The balance of Pu is assumed to be Pu-239. The U-235 content is conservatively assumed to be at the maximum value. The fuel isotopics utilized are provided in Table 6.3-2.

The effective density of the fuel is computed to be 10.31 g/cm^3 based on the mass of fuel in a pin (95% theoretical density), pellet diameter, and active fuel length, as shown in Table 6.3-2. The fuel density assuming 100% theoretical density is 10.85 g/cm^3 .

Type 304 stainless steel is used for the strongback angles and poison cover plates; its composition and density are provided in Table 6.3-3.

Most of the models used in the analysis assume M5 fuel cladding, end caps, and thimble tubes; M5 composition and density are provided in Table 6.3-4. Final runs were made with a more generic zirconium-based material with niobium in the range 0 to 3%.

Type XM-19 stainless steel is used for the MFFP structural shell; its composition and density are provided in Table 6.3-5.

The neutron poison plates have a minimum B-10 areal density of 0.035 g/cm^2 . Only 75% credit is taken for the B-10 number density. The number densities of the B₄C-Al boral matrix are provided in Table 6.3-6. The boral is clad with aluminum assumed to be pure and with a density of 2.713 g/cm^3 .

Water used in the models is assumed to be pure; density is case dependent.

6.3.3 Computer Codes and Cross-Section Libraries

The Monte Carlo computer program MCNP5 is used for this criticality analysis and has been verified for proper operation on the machine(s) on which it is installed. MCNP5 and its predecessor codes (MCNP4C, MCNP4B, etc.) have been an industry standard for neutron transport and criticality analysis for several decades.

MCNP5 primarily uses continuous energy ENDF/B-VI cross sections at room temperature, although ENDF/B-V cross sections are used when ENDF/B-VI cross sections are not available (i.e., iron, chromium, and nickel). A summary of the neutron cross sections utilized are provided in Table 6.3-7. Note that these cross sections are the default cross sections utilized by the program when no particular cross section set is specified. The S(α,β) card [LWTR.01t] is used to simulate hydrogen in room temperature water.

The NCT cases are run with 500 generations and 1,000 particles per generation. These files converge quickly because of the absence of moderating material. The HAC cases are run with 500 generations and 2,000 particles per generation. All cases use the SDEF card to distribute the starting neutrons over the length of every fuel pin. This ensures a uniform starting distribution and stable convergence. A 1- σ standard deviation of approximately 0.001 is considered acceptable for the results.

6.3.4 Demonstration of Maximum Reactivity

6.3.4.1 Single Package

The most reactive single package model is for the HAC case max_hac_single_sul. To ensure this is the most reactive case, the following parameters have been investigated:

- The internal moderation is varied from 0 to 1.0 g/cm³. The water in the pellet-cladding gap is also assumed to vary with the internal moderation. The most reactive condition is for full-density water.
- The pitch is varied from the “nominal-minus-tolerance” value to the maximum pitch such that the fuel assembly completely fills the space constrained by the FCS. The pitch is expanded uniformly over all three assemblies. Note that in the fully expanded position, the steel neutron poison cover plates that hold the borated aluminum to the strongback are artificially removed from the package model to allow room for this expansion. The case with a maximum pitch is the most reactive.
- The package is reflected with steel, which is shown to be slightly more reactive than either water or lead reflectors.
- Miscellaneous minor steel components in the package are homogenized into the water region for the most reactive case. This addition of steel further raises the reactivity slightly.
- The zirconium based alloy cladding has no niobium content, which is shown to be slightly more reactive than with niobium present.
- The fuel pellets are assumed to be 100% dense.
- The most reactive number of fuel pins are allowed to shift either up or down to the maximum possible extent.
- The most reactive single package therefore has full density moderator inside the package and the pellet-cladding gap, maximum pitch, steel reflector, homogenized minor steel components, pure-zirconium cladding, 100% dense fuel pellets, and axially shifted fuel pins.

6.3.4.2 Arrays of Undamaged Packages

The most reactive NCT array case is max_nct_array. An infinite hexagonal array is assumed. Because the MFFP is leaktight under NCT conditions, the package cavity is assumed to be dry. In the absence of moderation, the reactivity is very low and only one pitch is investigated. The only parameter investigated is the external water density, which is allowed to vary over the range 0 to 1.0 g/cm³. The fuel pellets are assumed to be 100% dense and the zirconium based alloy cladding has no niobium content. Maximum reactivity is obtained with no water between the packages.

6.3.4.3 Arrays of Damaged Packages

The most reactive HAC array case is max_hac_array_sd2. An infinite hexagonal array is assumed. To ensure this is the most reactive case, the following parameters have been investigated:

- The internal moderation is varied from 0 to 1.0 g/cm³. The water in the pellet-cladding gap is also assumed to vary with the internal moderation. The most reactive condition is for full-density water.
- The external moderation is varied from 0 to 1.0 g/cm³. The most reactive condition is for no external moderation.
- The pitch is varied from the “nominal minus tolerance” value to the maximum pitch such that the fuel assembly completely fills the space constrained by the FCS. The pitch is expanded uniformly over all three assemblies. Note that in the fully expanded position, the steel neutron poison cover plates that hold the borated aluminum to the strongback are artificially removed from the package model to allow room for this expansion. The case with a maximum pitch is the most reactive.
- Miscellaneous minor steel components in the package are homogenized into the water region for the most reactive case. This addition of steel further raises the reactivity slightly.
- The zirconium based alloy cladding has no niobium content, which is shown to be slightly more reactive than with niobium present.
- The fuel pellets are assumed to be 100% dense.
- The most reactive number of fuel pins are allowed to shift either up or down to the maximum possible extent.
- The most reactive package array therefore has full density moderator inside the package and the pellet-cladding gap, no external moderation, maximum pitch, homogenized minor steel components, pure-zirconium cladding, 100% dense fuel pellets, and axially shifted fuel pins.

Table 6.3-1 – Key Packaging Model Dimensions

Description	English Value (in)	Metric Value (cm)
Total package length	171.3	435.2
Body shell OD	29.625	75.248
Body shell ID	28.50	72.39
Bottom end thickness	1.50	3.81
Closure lid thickness (total)	4.38	11.13
Closure lid upper plate thickness	0.75	1.91
Closure lid lower plate thickness	0.63	1.60
Length of “tangential” strongback angle	8.30	21.08
Length of “radial” strongback angle	9.07	23.04
Strongback thickness	0.25	0.64
Strongback length (excluding top/bottom plate assemblies)	160.11	406.68
Radial poison plate hole diameter (same as tangential) (0.4 inches on SAR drawing, negligible impact on results)	0.375	0.953
Radial poison plate hole axial location (same as tangential)	Refer to drawings in §1.4.2	Refer to drawings in §1.4.2
Radial poison plate width (same as tangential)	8.43	21.41
Radial poison plate, radial distance between bolt holes (used for all pairs) (4.7 inches on SAR drawing, negligible impact on results)	4.352	11.054
Radial poison plate, axial distance between bolt holes (used for all pairs, same as tangential) (2.8 inches on SAR drawing, negligible impact on results)	2.848	7.234
Radial poison plate, distance from inner hole to edge of plate (2.2 inches on SAR drawing, negligible impact on results)	2.12	5.39
Tangential poison plate, radial distance between bolt holes (used for all pairs)	5.50	13.97
Tangential poison plate, distance from inner hole to edge of plate (1.0 inches on SAR drawing, negligible impact on results)	0.97	2.46
Poison cover plate thickness	0.1874 (7-gauge)	0.4760
Poison cover plate width	8.43	21.41
Poison cover plate height (Note: used for both radial and tangential)	4.25	10.80
End poison cover plate height (Note: modeled as 1.25 inches at the top for simplicity)	1.0	2.54
Middle triangle base length (also used for upper triangle)	7.36	18.69

Table 6.3-1 – Key Packaging Model Dimensions (con't)

Description	English Value (in)	Metric Value (cm)
Middle triangle height (also used for upper triangle)	6.38	16.21
Middle triangle plate thickness	0.50	1.27
Middle triangle, 3-in. Sch 40 pipe OD	3.50	8.89
Middle triangle, 3-in. Sch 40 pipe ID	3.068	7.793
Middle triangle pipe height	2.85	7.24
Upper triangle height	2.00	5.08
Upper triangle hole ID (minimum)	2.032	5.161
Maximum Al cladding thickness for boral	0.017	0.043
Maximum boral thickness	0.085	0.216
Thickness of FCS steel (0.125 inches on SAR drawing, negligible impact on results)	0.187	0.475
Width of radial FCS arm (assumed, value not on SAR drawing)	8.63	21.92
Width of tangential FCS arm (assumed, value not on SAR drawing)	8.88	22.56
Width of radial FCS Boral® (8.14 inches on SAR drawing, model is conservative)	7.75	19.69
Width of tangential FCS Boral® (8.56 inches on SAR drawing, model is conservative)	8.00	20.32
Distance from surface of strongback boral to inner surface of FCS (maximum area for FA expansion) (8.7 inches on SAR drawing, model is conservative)	8.8	22.4
Height of bottom FCS Boral® segment (21.12 inches on SAR drawing, model is conservative)	20.30	51.56
Height of standard length FCS Boral® segments (17.5 inches on SAR drawing, model is conservative)	17.0	43.18

Table 6.3-2 – Fuel Composition

Component	Wt.% in U or Pu	Wt.% in U or Pu Assumed for Models	Wt.% in Total Mixture
Total U/(U+Pu) = 94.0 wt.%			
U-234	≤ 0.05	0	0
U-235	≤ 0.3	0.3	0.249
U-238	99.65 - 100	99.7	82.615
Total Pu/(U+Pu) = 6.0 wt.%			
Pu-238	≤ 0.05	0	0
Pu-239	90.0 – 95.0	94	4.972
Pu-240	5.0 – 9.0	5	0.264
Pu-241	≤ 1.0	1	0.053
Pu-242	≤ 0.1	0	0
O	--	--	11.847
Total	--	--	100.0

Table 6.3-3 – Type 304 Stainless Steel Composition

Component	Wt.%
C	0.08
Si	1.0
P	0.045
Cr	19.0
Mn	2.0
Fe	68.375
Ni	9.5
Density = 7.94 g/cm ³	

Table 6.3-4 – Zirconium- M5 Alloy Composition

Component	Wt.%
Zr	Balance
Nb	1.2
Density = 6.50 g/cm ³	

Table 6.3-5 – XM-19 Austenitic Stainless Steel Composition

Component	Wt. %
C	0.06
N	0.4
Si	0.75
P	0.04
S	0.03
V	0.3
Cr	23.5
Mn	6.0
Ni	13.5
Nb	0.3
Mo	3.0
Fe	52.12
Density = 7.94 g/cm ³	

Note: Maximum values used, balance is Fe.

Table 6.3-6 – Boral Composition (0.035 g/cm² B-10)

Component	Number Density (atoms/b-cm)
B-10	7.3123E-03
B-11	3.9244E-02
C	1.2248E-02
Al	3.3439E-02
Total	9.2244E-02

Note: Boral thickness is 0.085 inches. The number density of B-10 has been reduced to 75% of the minimum value corresponding to an areal density of 0.035 g/cm²; remaining elements unchanged. Neutron poison plates consist of B₄C mixed with aluminum; B₄C theoretical density is 2.51 g/cm³.

Table 6.3-7 – MCNP5 Neutron Cross Sections

Isotope/Element	Cross Section Label
1001.62c	1-h-1 at 293.6K from endf-vi.8 njoy99.50
7014.62c	7-n-14 at 293.6K from endf-vi.8 njoy99.50
8016.62c	8-o-16 at 293.6K from endf-vi.8 njoy99.50
13027.62c	13-al-27 at 293.6K from endf-vi.8 njoy99.50
16032.62c	16-s-32 at 293.6K from endf/b-vi.8 njoy99.50
23000.62c	23-v-0 at 293.6K from endf/b-vi.8 njoy99.50
25055.62c	25-mn-55 at 293.6K from endf/b-vi.8 njoy99.50
5010.66c	5-b-10 at 293.6K from endf-vi.1 njoy99.50
5011.66c	5-b-11 at 293.6K from endf-vi.0 (MOD) njoy99.50
6000.66c	6-c-0 at 293.6K from endf-vi.6 njoy99.50
15031.66c	15-p-31 at 293.6K from endf-vi.6 njoy99.50
14000.60c	14-si-nat from endf/b-vi
24000.50c	njoy
26000.55c	njoy
28000.50c	njoy
40000.66c	40-zr-0 at 293.6K from endf-vi.1 njoy99.50
41093.66c	41-nb-93 at 293.6K from endf-vi.6 njoy99.50
42000.66c	42-mo-0 at 293.6K from endf-vi.0 njoy99.50
92235.66c	92-u-235 at 293.6K from endf-vi.5 njoy99.50
92238.66c	92-u-238 at 293.6K from endf-vi.5 njoy99.50
94239.66c	94-pu-239 at 293.6K from endf-vi.5 njoy99.50
94240.66c	94-pu-240 at 293.6K from endf-vi.2 njoy99.50
94241.66c	94-pu-241 at 293.6K from endf-vi.3 njoy99.50

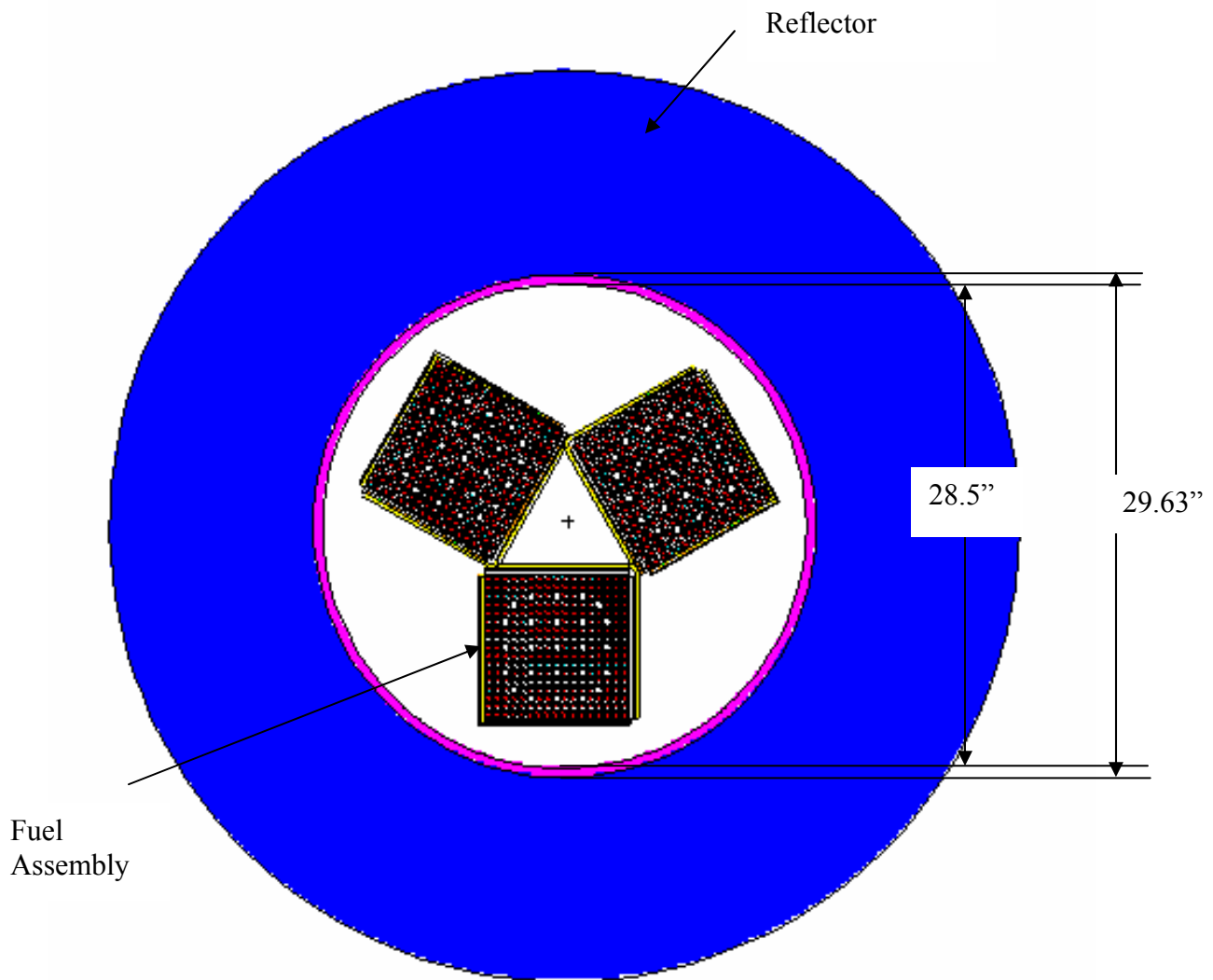


Figure 6.3-1 – NCT Model Geometry, Planar View

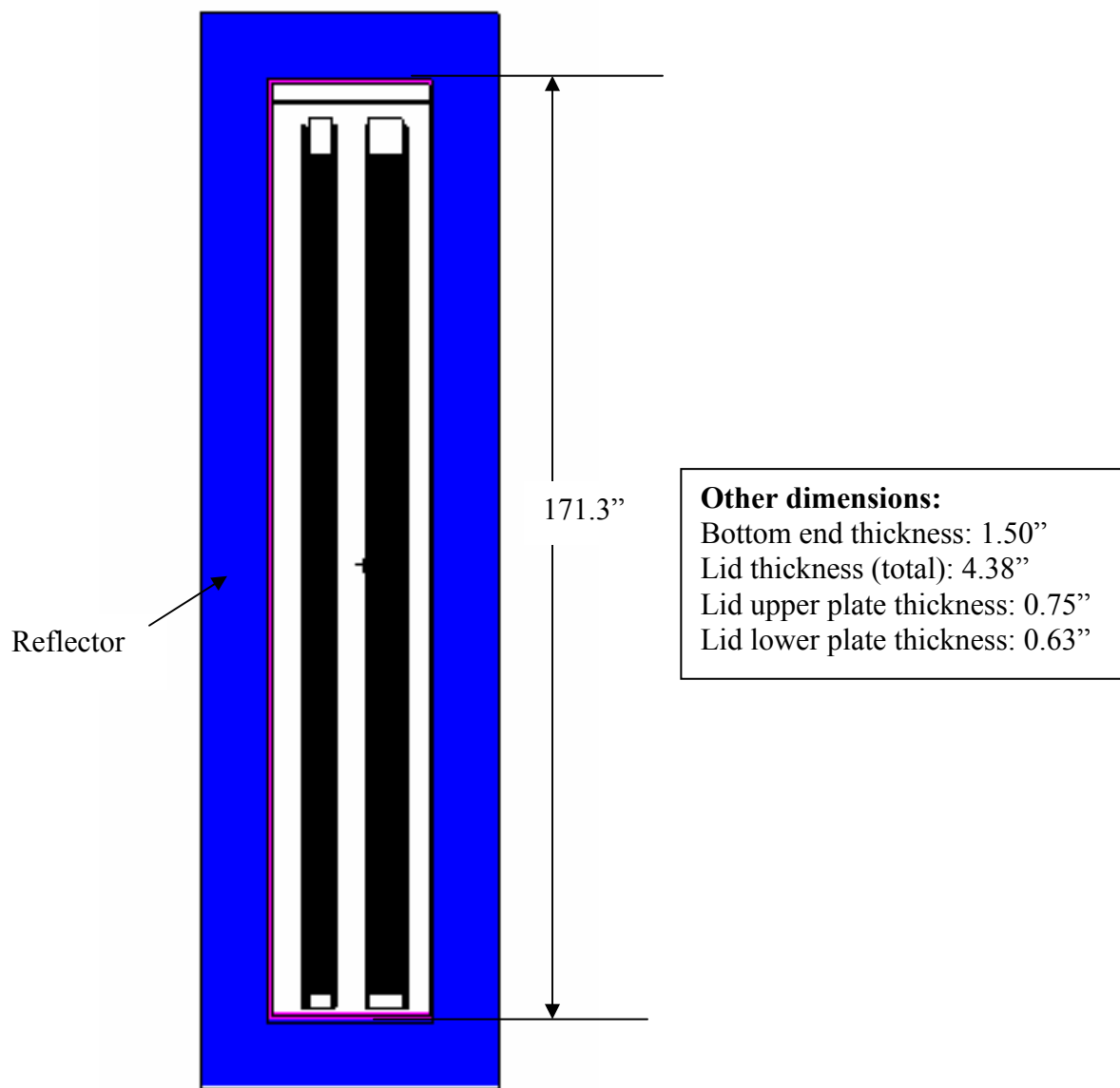
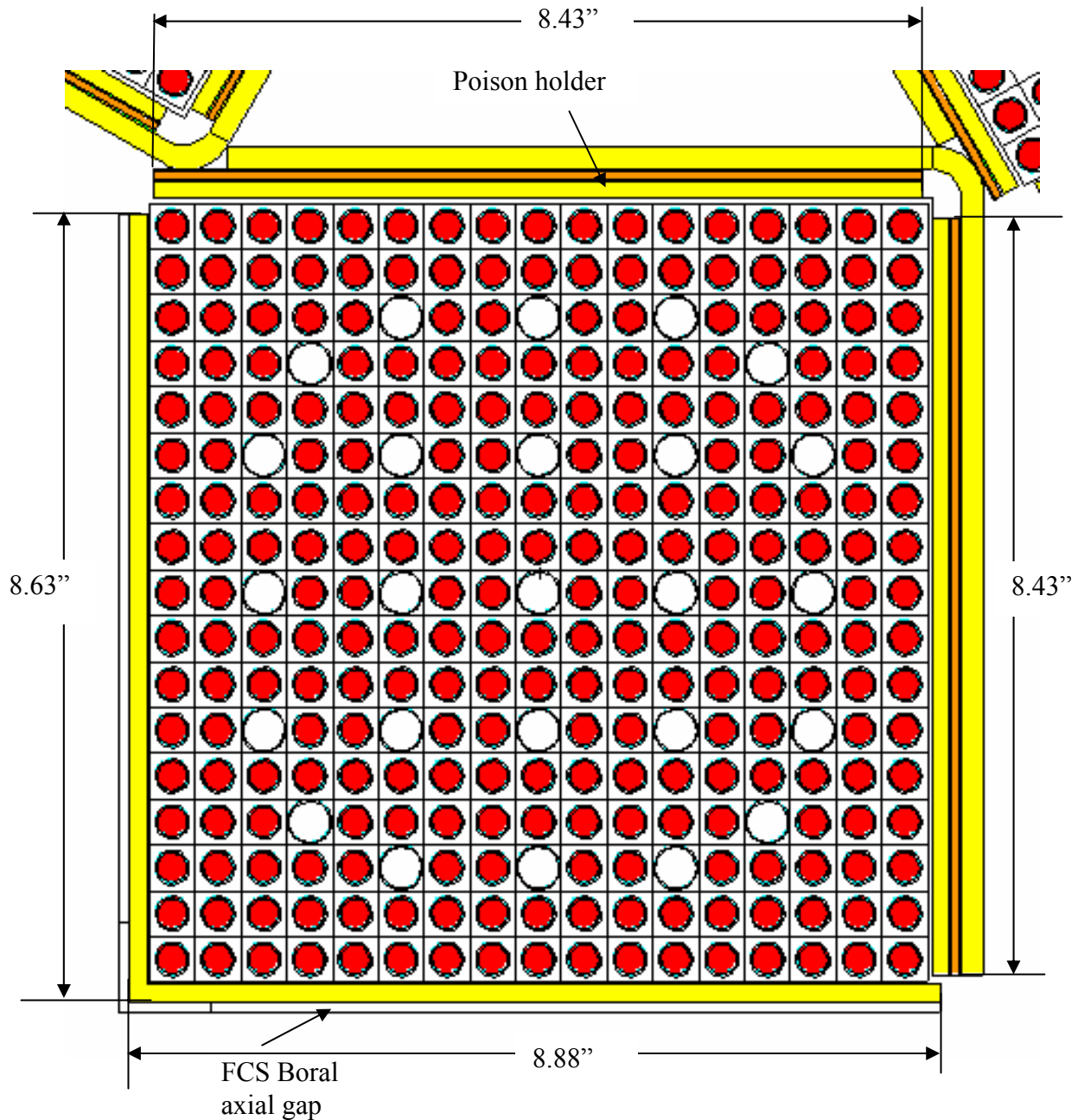


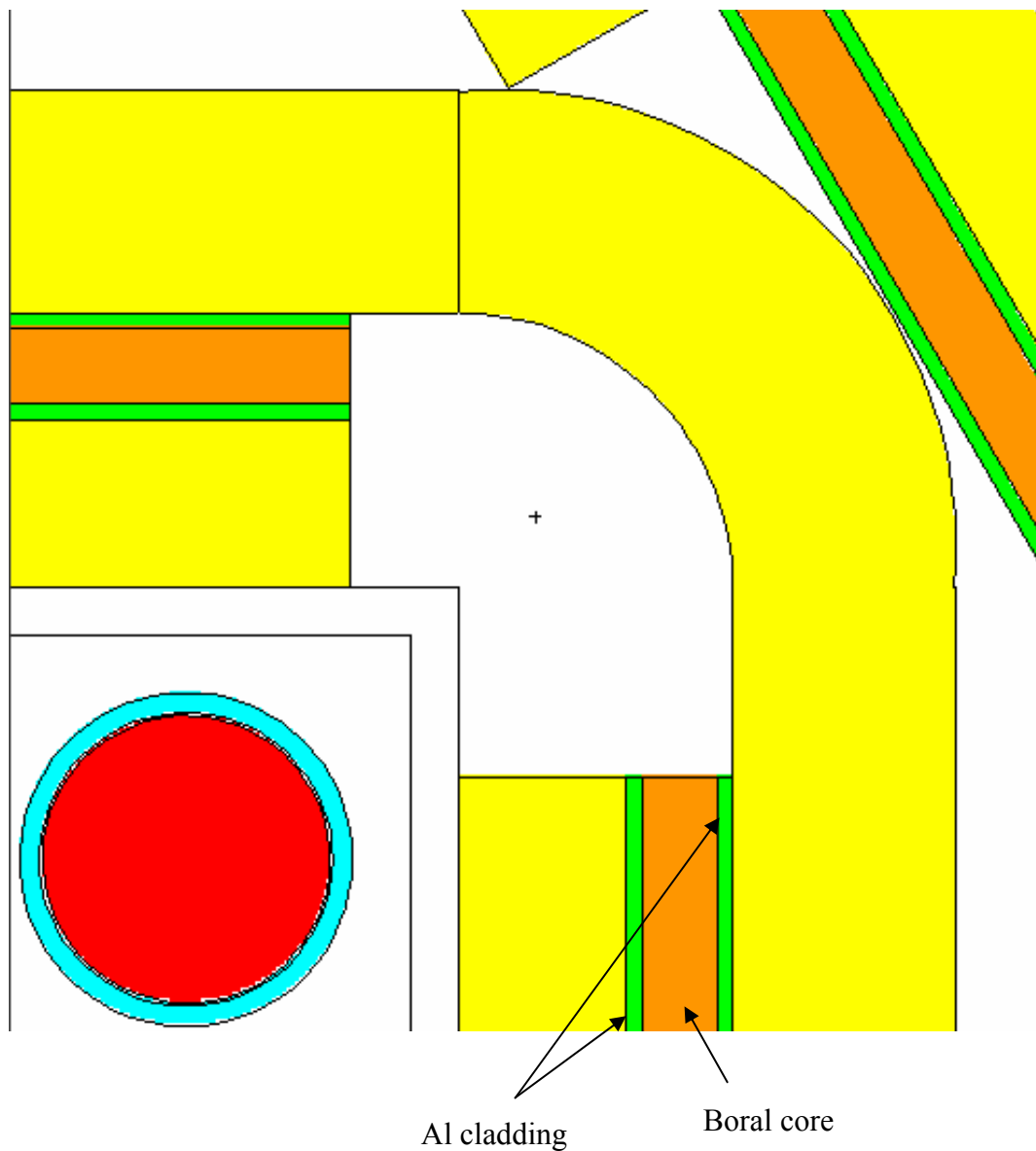
Figure 6.3-2 – NCT Model Geometry, Axial View



Other dimensions:

Thickness of FCS Sheet: 0.1874"
Poison holder height (except end): 4.25"
End poison holder height: 1.25"
Poison holder thickness: 0.1874"
Guide thimble OD: 0.482"
Guide thimble ID: 0.450"

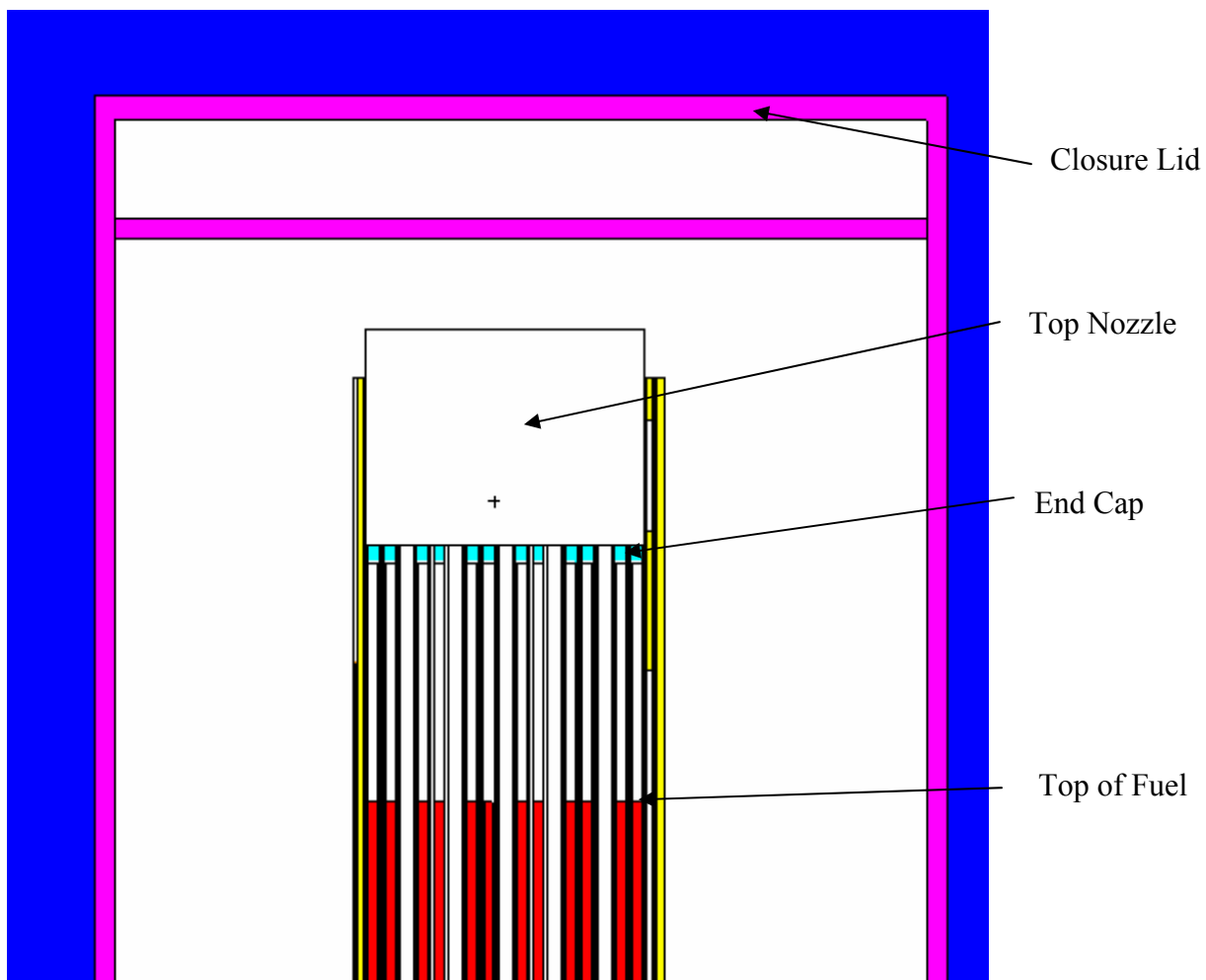
Figure 6.3-4 – NCT Model Geometry (Close-up through Neutron Poison Cover Plate)



Other dimensions:

Fuel pellet OD: 0.3225"
Cladding OD: 0.374"
Cladding ID: 0.329"
Boral cladding thickness: 0.017"
Boral thickness: 0.085"
Strongback thickness: 0.25"
Strongback length: 160.11"

Figure 6.3-5 – NCT Model Geometry (Close-up of Corner)



Other dimensions:

Overall fuel assembly length: 161.61"

Overall fuel rod length: 152.4"

Active fuel length: 144.0"

Figure 6.3-6 – NCT Model Geometry (Axial Close-up of Top)

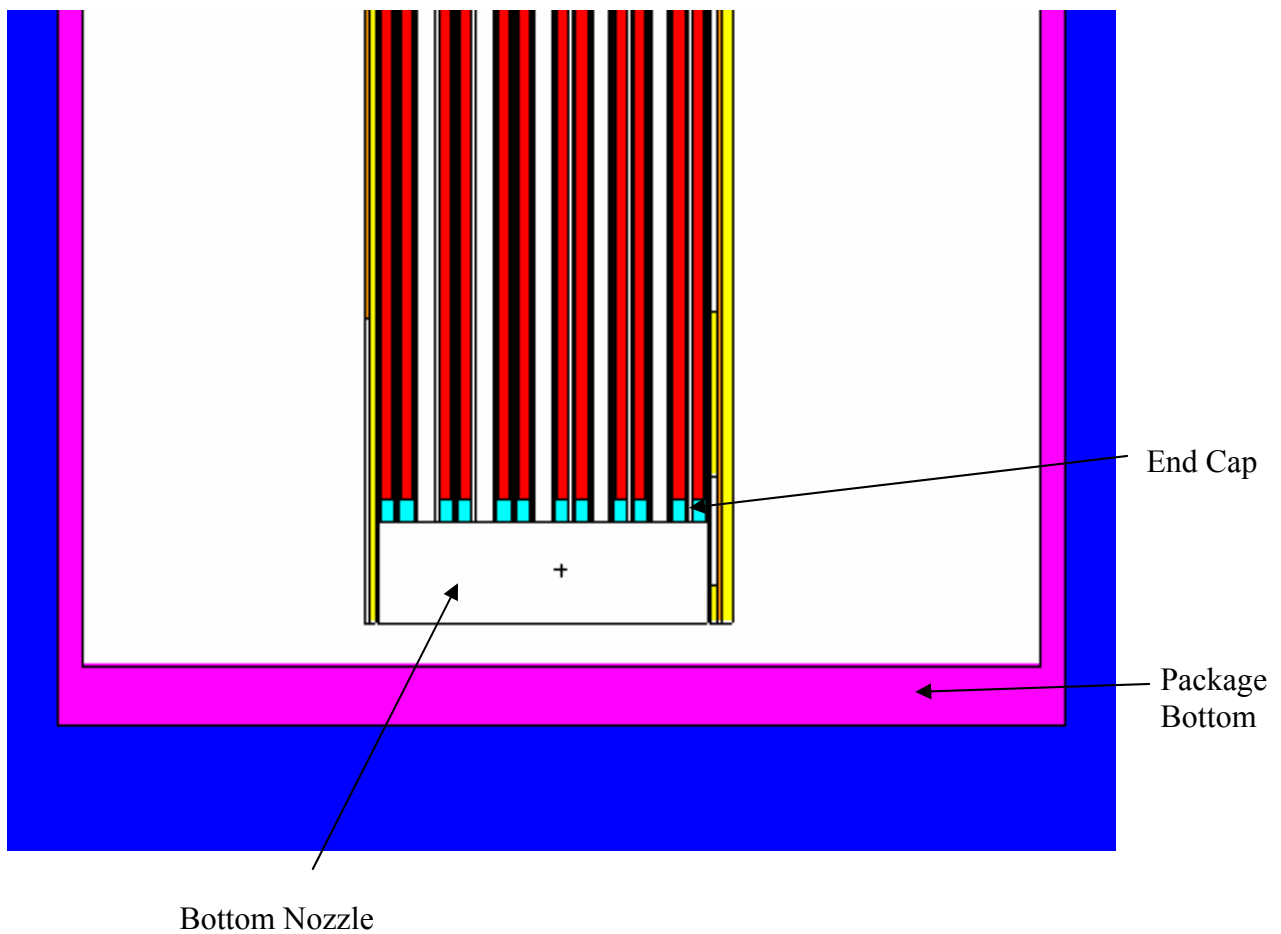


Figure 6.3-7 – NCT Model Geometry (Axial Close-up of Bottom)

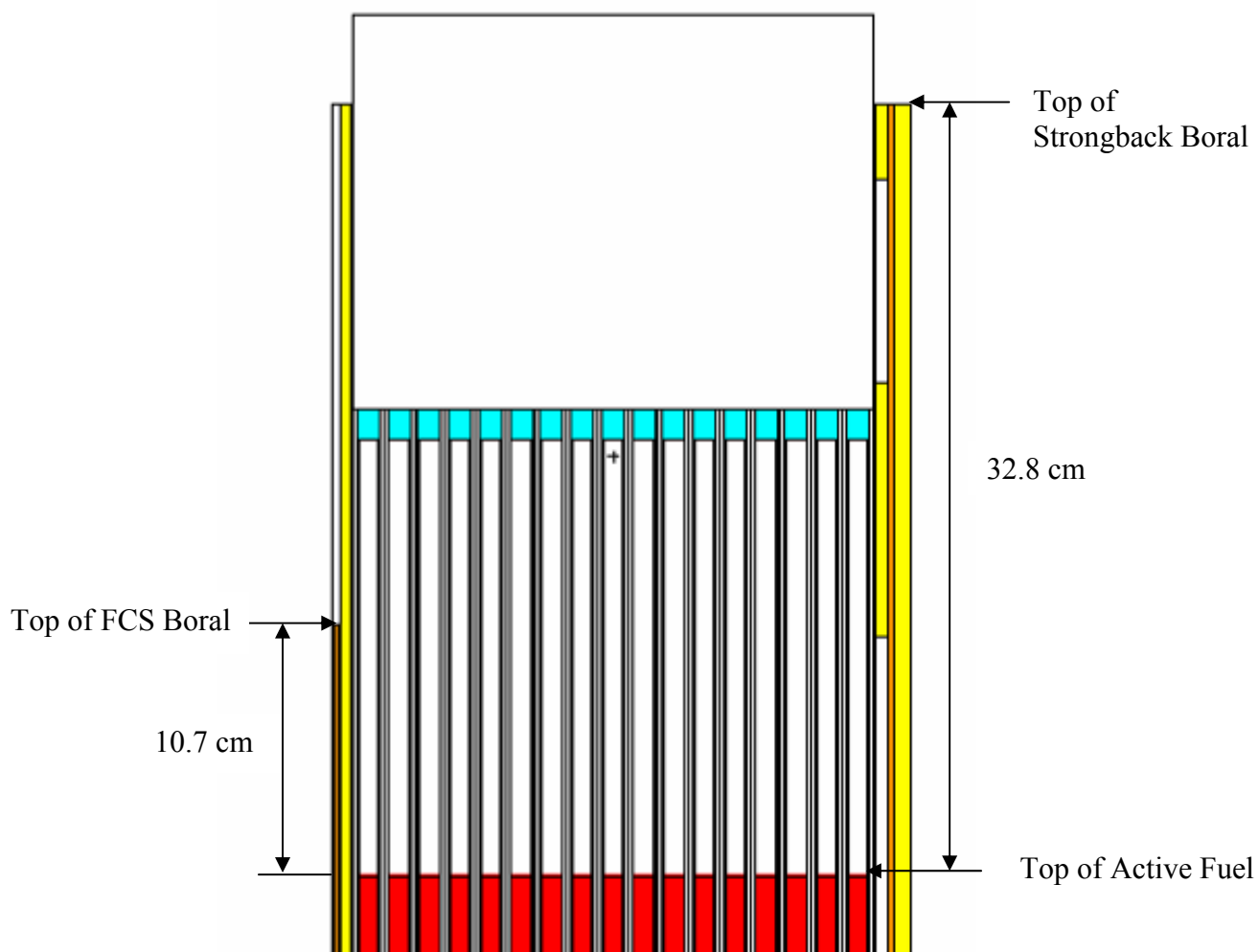


Figure 6.3-8 – NCT Model Geometry (Top Poison Coverage)

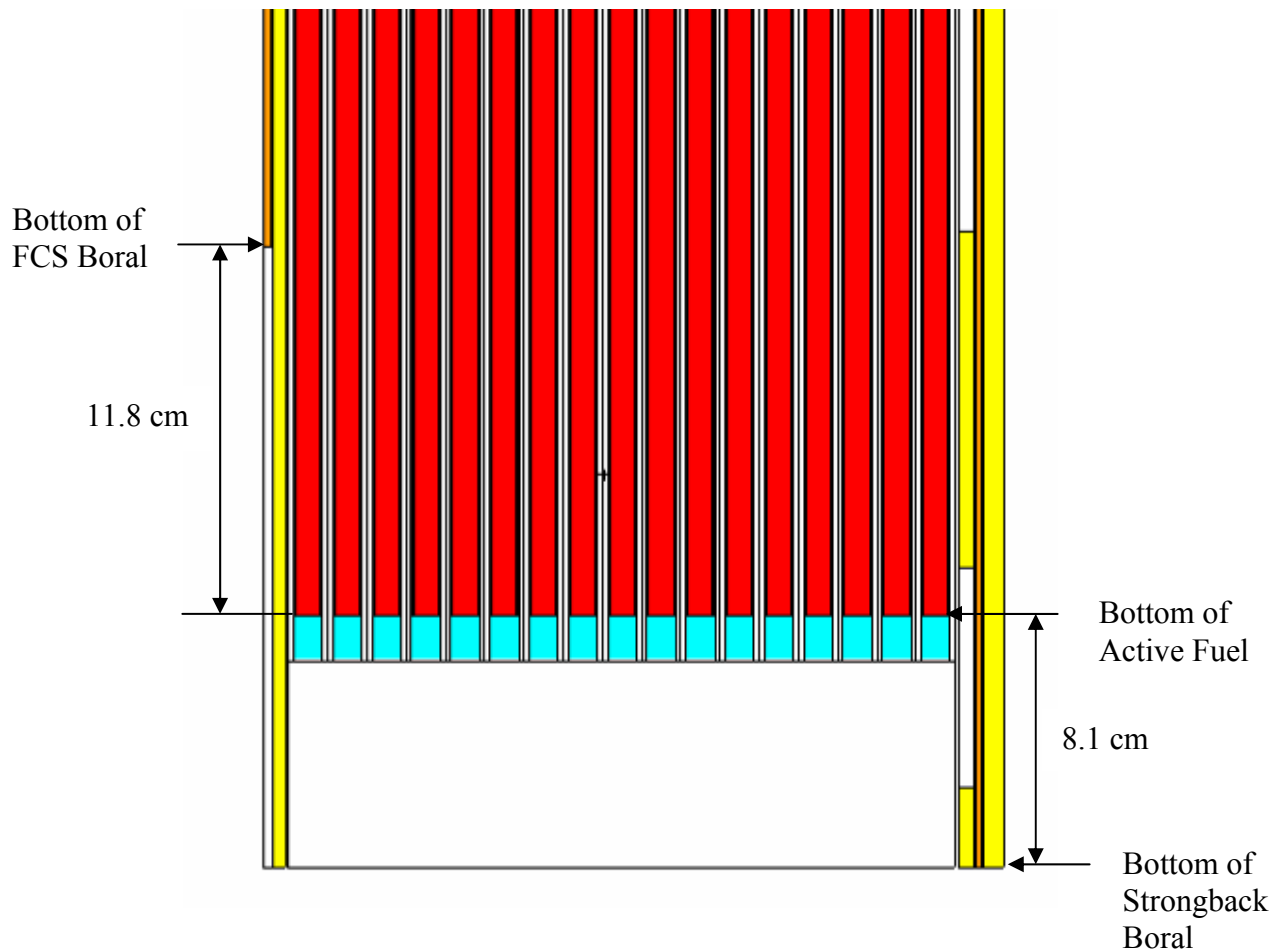


Figure 6.3-9 – NCT Model Geometry (Bottom Poison Coverage)

This page left intentionally blank.

6.4 Single Package Evaluation

Compliance with the requirements of 10 CFR §71.55 is demonstrated by analyzing optimally moderated damaged and undamaged, single-unit MFFP packages. The figures and descriptions provided in Section 6.3.1, *Model Configuration*, describe the basic geometry of the single-unit models.

6.4.1 Single Package Configuration

Because the engineering drop tests show no measurable change in the package external dimensions but expansion of the assembly pitch, the NCT and HAC models are the same, except (1) optimized internal water (within voids inside containment) is included in the HAC calculations, (2) the HAC cases allow for pitch expansion up to the maximum allowed extent, and (3) the HAC cases consider axial shifting of the fuel pins.

Each of the three FAs are radially symmetric about the origin. The model is constructed by building the lower assembly in the correct geometrical location using the MCNP LATTICE feature and then simply rotating copies of this assembly counterclockwise to build the other two assemblies. To simplify model preparation, the strongback assembly and outer FCS are modeled in separate MCNP “universes” and then inserted into the primary universe by use of the MCNP FILL command. This allows for simple rotation of these components to generate the complete model.

6.4.1.1 NCT Configuration

The largest allowable pin pitch in the undamaged condition is assumed (0.502 inches, 1.2751 cm). The package is reflected on all sides with 12 inches of three common reflectors: water, steel, and lead (cases nct_single_b35pnomplustol, nct_single_b35pnomplustol_Rsteel, nct_single_b35pnomplustol_Rlead). The lead reflector case is the most reactive of the three reflectors analyzed. Other reflectors might yield slightly higher results, although in the absence of internal moderation, the reactivity is extremely low (<0.3) and no further analysis is warranted. Because no water is present within the package for the NCT cases and the reactivity is low, parametric studies on the pitch are not warranted.

All cases except the final maximum case (max_nct_single) are run with a pellet density of 10.31 g/cm^3 and M5 cladding. To bound possible future fluctuations in the pellet density and cladding composition, the lead reflector case is run with a pellet density of 10.85 g/cm^3 and pure-zirconium cladding. It is shown in Section 6.6.3, *Impact of Niobium Content in the Cladding*, that pure zirconium cladding is slightly more reactive than cladding containing niobium.

6.4.1.2 HAC Configuration

The FCS limits the expansion of the fuel assemblies to a maximum of 8.8 inches. This dimension of 8.8 inches is defined from the surface of the strongback boral to the inner surface of the FCS, see Figure 6.4-1. In the HAC single package models, the pitch is allowed to range from a minimum value of nominal minus tolerance (0.490 inches) to a maximum value such that the OD of the outer fuel pins fill a region 8.8 inches square (0.5266 inches). In the MCNP models, the steel poison cover plates are “sliced off” to allow for this pin expansion. The various pitches used in the analysis, along with the nomenclature utilized, are provided in Table 6.4-1.

For the HAC single package model, it is assumed that water has completely flooded the package internals, including the pellet-cladding gap. The package is reflected with 12 inches of water on all sides. Note that reactivity increases with increasing pitch, indicating that the system is under moderated. The maximum reactivity is calculated for the maximum pitch expansion.

Using this model with maximum pitch and 12 inches water reflector, a further series of cases are run to investigate the effects of reduced internal moderation by reducing the internal water density. Because water is free to flow throughout the internals of the package, it is assumed that all internal water densities are uniformly reduced. As expected for an under moderated system, the reactivity decreases with decreasing water density.

The worst-case pitch geometry is also run with full-water moderation and both steel and lead reflectors. The increase in k_s with these reflectors is small (only a few mk), and the system is most reactive with a steel reflector. Because the difference in k_s between the three reflectors studied is small (~ 3 mk), analysis of other reflectors is not warranted.

Because the high-density steel and lead reflector cases (cases hac_single_b35pmax2_Rsteel, hac_single_b35pmax2_Rlead) are slightly more reactive than the water reflectors, additional cases (denoted with _hsteel in case name) are run to investigate the effect of including minor steel components that have been ignored in the model, namely, the clamp arms and the strongback triangles. The clamp arms are steel structures that weigh approximately 36 pounds each and secure the fuel assembly to the strongback. The strongback triangles fit into the triangular region between the strongbacks and provide support. The top and bottom triangles are primarily solid steel, while the triangle pieces in the central regions are fabricated from 1/2-inch thick steel plate and are mostly void.

For simplicity, this additional steel is not modeled explicitly but is homogenized into the water surrounding the assemblies. Water between the fuel pins remains unchanged and does not contain the homogenized steel. The triangle steel represents approximately 5.8% (by volume) of the region between the strongbacks, while the clamp arm steel represents approximately 3.2% (by volume) of the region between the fuel and the body shell wall. To maximize the amount of steel within the model, 5.8% steel is assumed for both regions. The reactivity for this case is slightly higher than the case without the homogenized steel, although the increase is within the statistical uncertainty of the calculations.

All cases except the final maximum cases (beginning max_hac_single) are run with a pellet density of 10.31 g/cm^3 and M5 cladding. To bound possible future fluctuations in the pellet density and cladding composition, the case with a steel reflector and homogenized minor steel components is run with a pellet density of 10.85 g/cm^3 and pure-zirconium cladding. It is shown in Section 6.6.3, *Impact of Niobium Content in the Cladding*, that pure zirconium cladding is slightly more reactive than cladding containing niobium.

The last set of calculations allows axial shifting of the fuel pins. These models use a pellet density of 10.85 g/cm^3 and pure-zirconium cladding. Approximately 8 fuel pins shifted upward through the holes in the top nozzle during the drop tests. In order to bound any potential axial displacement of the fuel pins, models are developed in which pins are allowed to shift up to the top lid or down to the bottom of the package. Models are developed with 8, 24, 60, and 116 pins shifted either up or down in a regular pattern, see Figure 6.4-2. Pins are shifted every other row to increase moderation between pins at the ends. To approximate the actual test results, models are also developed with only 10 or 20 randomly selected rods shifting either up or down. Cases are also developed in which all of the rods displace either up or down.

Pins are assumed to shift either up or down within a model, as the direction of shift will be dependent upon the package orientation upon impact. It is not possible for the some pins to shift up and other pins to shift down as a result of the same accident.

The relation of fuel to the top and bottom of the strongback for the nominal (unshifted) geometry is shown in Figure 6.3-6 and Figure 6.3-7, respectively. Fuel pins shifted up and down are shown in Figure 6.4-3 and Figure 6.4-4, respectively. Note that the top and bottom nozzles, as well as elements of the strongback, are necessarily ignored to allow the pins to shift in this fashion. Such extreme shifting would likely be incredible and was not observed in the drop tests.

6.4.2 Single Package Results

Criticality results for the NCT single package analysis is provided in Table 6.4-2. For the NCT case, the maximum $k_s = 0.2874$ is below the USL and is obtained for the case with a lead reflector, a pellet density of 10.85 g/cm^3 , and pure zirconium cladding.

Criticality results for the HAC single package analysis without and with axially shifted fuel pins are provided in Table 6.4-3 and Table 6.4-4, respectively. For the HAC case, the maximum $k_s = 0.9001$ is below the USL and is obtained for the case with full-density water (with homogenized minor steel components) in the package cavity, maximum pin pitch, a steel reflector, a pellet density of 10.85 g/cm^3 , pure zirconium cladding, and shifted fuel pins. The maximum $k_s = 0.9001$ occurs for two different cases, 20 fuel pins randomly shifted down, and 8 fuel pins shifted up. Allowing various combinations of fuel pins to shift axially has a small, positive effect on the reactivity, although the effect is in typically within the uncertainty of the Monte Carlo method.

NCT cases are run with 1,000 particles per generation, 530 generations, with 30 generations skipped. HAC cases are run with 2,000 particles per generation, 530 generations, with 30 generations skipped. MCNP5 performs statistical checks on k-collision, k-absorption, and k-track length. These cycle values should be normally distributed at the 99% confidence level or below. All of the reported results meet this convergence criteria. Convergence plots for the limiting NCT and HAC cases are provided in Figure 6.4-5 and Figure 6.4-6, respectively.

This page left intentionally blank.

Table 6.4-1 – Summary of Fuel Pin Pitch Nomenclature and Dimensions

Fuel Pin Pitch	Case label abbreviation	Pin Pitch (cm)	Pin Pitch (inches)
Nominal minus the tolerance	pnomminustol	1.2446	0.4900
Nominal	pnom	1.2598	0.4960
Nominal plus the tolerance	pnomplustol	1.2751	0.5020
Mid-point value	pmid	1.2952	0.5099
Maximum	pmax	1.3150	0.5177
Maximum with removal of poison cover plates	pmax2	1.3376	0.5266

Table 6.4-2 – Criticality Results for NCT Single Package

Case Identifier	Internal Water Density (g/cm ³)	EALF (MeV)	H/ (²³⁹ Pu+ ²³⁵ U)	V ^m /V ^f	²³⁹ Pu/ (U+Pu)	k _{eff}	σ	k _s (k _{eff} +2σ)
max_nct_single	0	3.62E-01	0	1.740	0.056	0.2858	0.0008	0.2874
nct_single_b35pnomplustol_Rsteel	0	2.66E-01	0	1.740	0.056	0.2627	0.0008	0.2642
nct_single_b35pnomplustol_Rlead	0	3.52E-01	0	1.740	0.056	0.2766	0.0008	0.2781
nct_single_b35pnomplustol	0	1.03E-01	0	1.740	0.056	0.2076	0.0005	0.2086

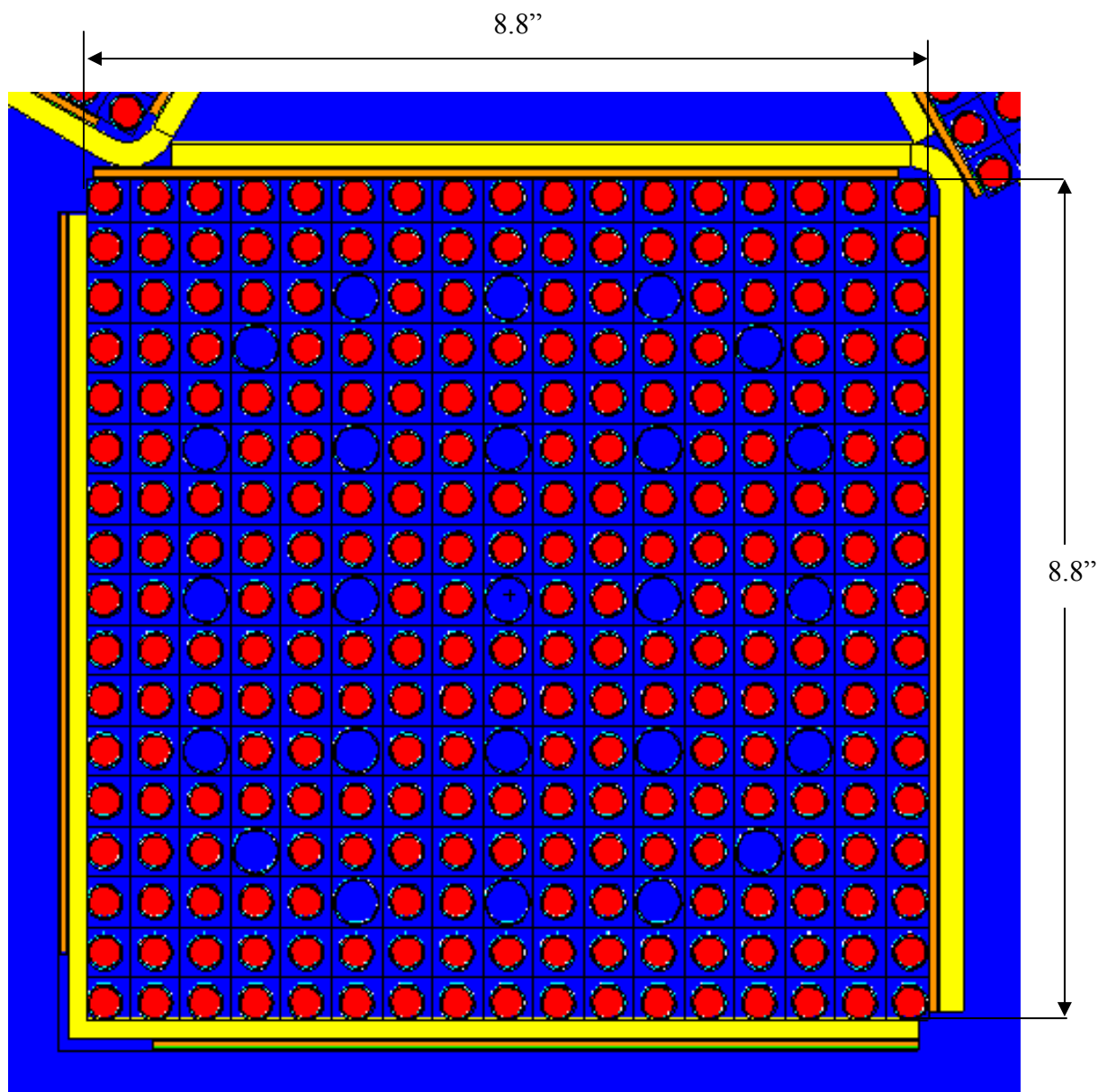
Table 6.4-3 – Criticality Results for HAC Single Package (no shifted pins)

Case Identifier	Internal Water Density (g/cm ³)	EALF (MeV)	H/ (²³⁹ Pu+ ²³⁵ U)	V ^m /V ^f	²³⁹ Pu/ (U+Pu)	k _{eff}	σ	k _s (k _{eff} +2σ)
max_hac_single_0Nb	1	7.32E-7	96.044	2.050	0.056	0.8958	0.0009	0.8976
hac_single_b35pmax2_Rsteel_hsteel	1	6.59E-07	101.074	2.050	0.056	0.8910	0.0010	0.8930
hac_single_b35pmax2_Rlead_hsteel	1	6.66E-07	101.074	2.050	0.056	0.8902	0.0010	0.8921
hac_single_b35pmax2_Rsteel	1	6.53E-07	101.074	2.050	0.056	0.8880	0.0010	0.8900
hac_single_b35pmax2_Rlead	1	6.68E-07	101.074	2.050	0.056	0.8860	0.0009	0.8879
hac_single_b35pmax2	1	6.60E-07	101.074	2.050	0.056	0.8854	0.0009	0.8872
hac_single_b35pmax	1	7.23E-07	95.466	1.936	0.056	0.8752	0.0010	0.8771
hac_single_b35pmid	1	7.82E-07	90.631	1.838	0.056	0.8626	0.0010	0.8646
hac_single_b35pnomplustol	1	8.45E-07	85.793	1.740	0.056	0.8511	0.0010	0.8532
hac_single_b35pnom	1	9.11E-07	82.179	1.667	0.056	0.8448	0.0010	0.8468
hac_single_b35pnomminustol	1	9.76E-07	78.609	1.594	0.056	0.8335	0.0010	0.8354
hac_single_b35pmax2_i95	0.95	7.49E-07	96.021	2.050	0.056	0.8621	0.0009	0.8640
hac_single_b35pmax2_i90	0.9	8.61E-07	90.967	2.050	0.056	0.8347	0.0010	0.8367
hac_single_b35pmax2_i75	0.75	1.41E-06	75.806	2.050	0.056	0.7527	0.0009	0.7546
hac_single_b35pmax2_i50	0.5	5.51E-06	50.537	2.050	0.056	0.5873	0.0008	0.5890
hac_single_b35pmax2_i25	0.25	9.77E-05	25.269	2.050	0.056	0.3993	0.0007	0.4007
hac_single_b35pmax2_i10	0.1	3.04E-03	10.107	2.050	0.056	0.2838	0.0005	0.2847
hac_single_b35pmax2_i0	0	9.90E-02	0.000	2.050	0.056	0.2064	0.0004	0.2071

Table 6.4-4 – Criticality Results for HAC Single Package (with shifted pins)

Case Identifier	Internal Water Density (g/cm ³)	Shifted Pins	EALF (MeV)	H/ (²³⁹ Pu+ ²³⁵ U)	V ^m /V ^f	²³⁹ Pu/ (U+Pu)	k _{eff}	σ	k _s (k _{eff} +2σ)
max_hac_single_srnddn10	1	10 down random	7.28E-07	96.044	2.050	0.056	0.8970	0.0009	0.8988
max_hac_single_srnddn20	1	20 down random	7.15E-07	96.044	2.050	0.056	0.8983	0.0009	0.9001
max_hac_single_sd1	1	8 down	7.22E-07	96.044	2.050	0.056	0.8957	0.0010	0.8976
max_hac_single_sd2	1	24 down	7.19E-07	96.044	2.050	0.056	0.8958	0.0010	0.8977
max_hac_single_sd3	1	60 down	7.17E-07	96.044	2.050	0.056	0.8960	0.0009	0.8978
max_hac_single_sd4	1	116 down	7.22E-07	96.044	2.050	0.056	0.8956	0.0010	0.8976
max_hac_single_salldn	1	All down	7.30E-07	96.044	2.050	0.056	0.8963	0.0010	0.8983
max_hac_single_srndup10	1	10 up random	7.14E-07	96.044	2.050	0.056	0.8968	0.0010	0.8987
max_hac_single_srndup20	1	20 up random	7.26E-07	96.044	2.050	0.056	0.8964	0.0010	0.8983
max_hac_single_su1	1	8 up	7.24E-07	96.044	2.050	0.056	0.8981	0.0010	0.9001
max_hac_single_su2	1	24 up	7.25E-07	96.044	2.050	0.056	0.8958	0.0010	0.8979
max_hac_single_su3	1	60 up	7.08E-07	96.044	2.050	0.056	0.8962	0.0009	0.8981
max_hac_single_su4	1	116 up	7.13E-07	96.044	2.050	0.056	0.8964	0.0010	0.8985
max_hac_single_sallup	1	All up	7.26E-07	96.044	2.050	0.056	0.8953	0.0009	0.8972

This page left intentionally blank.



Note that the pitch has expanded to the maximum possible extent (8.8-inch square) and that the poison holders have been "sliced off" to allow for this expansion.

Figure 6.4-1 – HAC Model Geometry, Worst-Case Pitch

10 randomly shifted pins															
1	1	1	1	1	1	1	1	1	1	1	1	1	1	1	1
1	1	1	1	1	1	1	1	1	1	1	1	1	1	1	1
1	1	1	1	1	4	1	1	4	1	1	4	1	1	1	1
1	1	1	4	1	3	1	1	1	1	1	1	1	4	1	1
1	1	1	1	1	1	1	1	1	1	1	3	1	1	1	1
1	1	4	1	1	4	1	1	4	1	1	4	1	1	4	1
1	1	1	3	1	1	3	1	1	1	1	1	1	1	1	1
1	1	1	1	1	1	1	1	1	1	1	1	1	3	1	1
1	1	4	1	1	4	1	1	4	1	3	4	1	1	4	1
1	1	1	1	1	1	3	1	1	1	1	1	1	1	1	1
1	1	1	1	1	1	1	1	1	1	1	1	1	3	1	1
1	1	4	1	1	4	1	1	4	1	1	4	1	1	4	1
1	1	1	1	1	1	1	1	1	1	3	1	1	1	1	1
1	1	1	4	1	1	3	1	1	1	1	1	1	4	1	1
1	1	1	1	1	4	1	1	4	1	1	4	1	1	1	1
1	1	1	1	1	1	1	1	1	1	1	1	1	1	1	1
1	1	1	1	1	1	1	1	1	1	1	1	1	1	1	1
20 randomly shifted pins															
1	1	1	1	1	1	1	1	1	1	1	1	1	1	1	1
1	1	1	1	1	1	1	1	1	1	1	1	1	1	1	1
1	1	1	1	1	4	1	1	4	1	1	4	1	1	1	1
1	1	1	4	1	3	1	1	1	1	1	1	1	4	1	1
1	1	1	1	1	1	1	3	1	1	1	3	1	1	1	1
1	1	4	1	1	4	1	1	4	1	1	4	1	1	4	1
1	1	1	3	1	1	3	1	1	1	3	1	1	1	1	1
1	1	1	1	1	1	1	3	1	1	1	1	1	3	1	1
1	1	4	1	1	4	1	1	4	1	3	4	1	1	4	1
1	1	1	3	1	1	3	1	1	3	1	1	1	1	1	1
1	1	1	1	1	1	1	1	1	1	3	1	1	3	1	1
1	1	4	3	1	4	1	3	4	1	1	4	1	1	4	1
1	1	1	1	1	1	1	1	1	1	3	1	1	1	1	1
1	1	1	4	1	1	3	1	1	3	1	1	3	4	1	1
1	1	1	1	1	4	1	1	4	1	1	4	1	1	1	1
1	1	1	1	1	1	1	1	1	1	1	1	1	1	1	1
1	1	1	1	1	1	1	1	1	1	1	1	1	1	1	1
1 is a fuel pin in the standard axial position															
3 is a shifted fuel pin (either up or down)															
4 is a guide thimble															

Figure 6.4-2 – Fuel Pin Loading Patterns for Axially Shifted Fuel

8 shifted pins															
1	1	1	1	1	1	1	1	1	1	1	1	1	1	1	1
1	1	1	1	1	1	1	1	1	1	1	1	1	1	1	1
1	1	1	1	1	4	1	1	4	1	1	4	1	1	1	1
1	1	1	4	1	1	1	1	1	1	1	1	1	4	1	1
1	1	1	1	1	1	1	1	1	1	1	1	1	1	1	1
1	1	4	1	1	4	1	1	4	1	1	4	1	1	4	1
1	1	1	1	1	1	1	1	1	1	1	1	1	1	1	1
1	1	1	1	1	1	1	3	3	3	1	1	1	1	1	1
1	1	4	1	1	4	1	3	4	3	1	4	1	1	4	1
1	1	1	1	1	1	1	3	3	3	1	1	1	1	1	1
1	1	1	1	1	1	1	1	1	1	1	1	1	1	1	1
1	1	4	1	1	4	1	1	4	1	1	4	1	1	4	1
1	1	1	1	1	1	1	1	1	1	1	1	1	1	1	1
1	1	1	4	1	1	1	1	1	1	1	1	1	4	1	1
1	1	1	1	1	4	1	1	4	1	1	4	1	1	1	1
1	1	1	1	1	1	1	1	1	1	1	1	1	1	1	1
1	1	1	1	1	1	1	1	1	1	1	1	1	1	1	1
24 shifted pins															
1	1	1	1	1	1	1	1	1	1	1	1	1	1	1	1
1	1	1	1	1	1	1	1	1	1	1	1	1	1	1	1
1	1	1	1	1	4	1	1	4	1	1	4	1	1	1	1
1	1	1	4	1	1	1	1	1	1	1	1	1	4	1	1
1	1	1	1	1	1	1	1	1	1	1	1	1	1	1	1
1	1	4	1	1	4	3	3	4	3	3	4	1	1	4	1
1	1	1	1	1	3	1	1	1	1	1	3	1	1	1	1
1	1	1	1	1	3	1	3	3	3	1	3	1	1	1	1
1	1	4	1	1	4	1	3	4	3	1	4	1	1	4	1
1	1	1	1	1	3	1	3	3	3	1	3	1	1	1	1
1	1	1	1	1	3	1	1	1	1	1	3	1	1	1	1
1	1	4	1	1	4	3	3	4	3	3	4	1	1	4	1
1	1	1	1	1	1	1	1	1	1	1	1	1	1	1	1
1	1	1	4	1	1	1	1	1	1	1	1	1	4	1	1
1	1	1	1	1	4	1	1	4	1	1	4	1	1	1	1
1	1	1	1	1	1	1	1	1	1	1	1	1	1	1	1
1	1	1	1	1	1	1	1	1	1	1	1	1	1	1	1
1 is a fuel pin in the standard axial position															
3 is a shifted fuel pin (either up or down)															
4 is a guide thimble															

Figure 6.4-2 – Fuel Pin Loading Patterns for Axially Shifted Fuel (2/3)

60 shifted pins																
1	1	1	1	1	1	1	1	1	1	1	1	1	1	1	1	1
1	1	1	1	1	1	1	1	1	1	1	1	1	1	1	1	1
1	1	1	1	1	4	1	1	4	1	1	4	1	1	1	1	1
1	1	1	4	3	3	3	3	3	3	3	3	3	4	1	1	1
1	1	1	3	1	1	1	1	1	1	1	1	1	3	1	1	1
1	1	4	3	1	4	3	3	4	3	3	4	1	3	4	1	1
1	1	1	3	1	3	1	1	1	1	1	3	1	3	1	1	1
1	1	1	3	1	3	1	3	3	3	1	3	1	3	1	1	1
1	1	4	3	1	4	1	3	4	3	1	4	1	3	4	1	1
1	1	1	3	1	3	1	3	3	3	1	3	1	3	1	1	1
1	1	1	3	1	3	1	1	1	1	1	3	1	3	1	1	1
1	1	4	3	1	4	3	3	4	3	3	4	1	3	4	1	1
1	1	1	3	1	1	1	1	1	1	1	1	1	3	1	1	1
1	1	1	4	3	3	3	3	3	3	3	3	3	4	1	1	1
1	1	1	1	1	4	1	1	4	1	1	4	1	1	1	1	1
1	1	1	1	1	1	1	1	1	1	1	1	1	1	1	1	1
1	1	1	1	1	1	1	1	1	1	1	1	1	1	1	1	1
116 shifted pins																
1	1	1	1	1	1	1	1	1	1	1	1	1	1	1	1	1
1	3	3	3	3	3	3	3	3	3	3	3	3	3	3	3	1
1	3	1	1	1	4	1	1	4	1	1	4	1	1	1	3	1
1	3	1	4	3	3	3	3	3	3	3	3	3	4	1	3	1
1	3	1	3	1	1	1	1	1	1	1	1	1	3	1	3	1
1	3	4	3	1	4	3	3	4	3	3	4	1	3	4	3	1
1	3	1	3	1	3	1	1	1	1	1	3	1	3	1	3	1
1	3	1	3	1	3	1	3	3	3	1	3	1	3	1	3	1
1	3	4	3	1	4	1	3	4	3	1	4	1	3	4	3	1
1	3	1	3	1	3	1	3	3	3	1	3	1	3	1	3	1
1	3	1	3	1	3	1	1	1	1	1	3	1	3	1	3	1
1	3	4	3	1	4	3	3	4	3	3	4	1	3	4	3	1
1	3	1	3	1	1	1	1	1	1	1	1	1	3	1	3	1
1	3	1	4	3	3	3	3	3	3	3	3	3	4	1	3	1
1	3	1	1	1	4	1	1	4	1	1	4	1	1	1	3	1
1	3	3	3	3	3	3	3	3	3	3	3	3	3	3	3	1
1	1	1	1	1	1	1	1	1	1	1	1	1	1	1	1	1
1 is a fuel pin in the standard axial position																
3 is a shifted fuel pin (either up or down)																
4 is a guide thimble																

Figure 6.4-2 – Fuel Pin Loading Patterns for Axially Shifted Fuel (3/3)

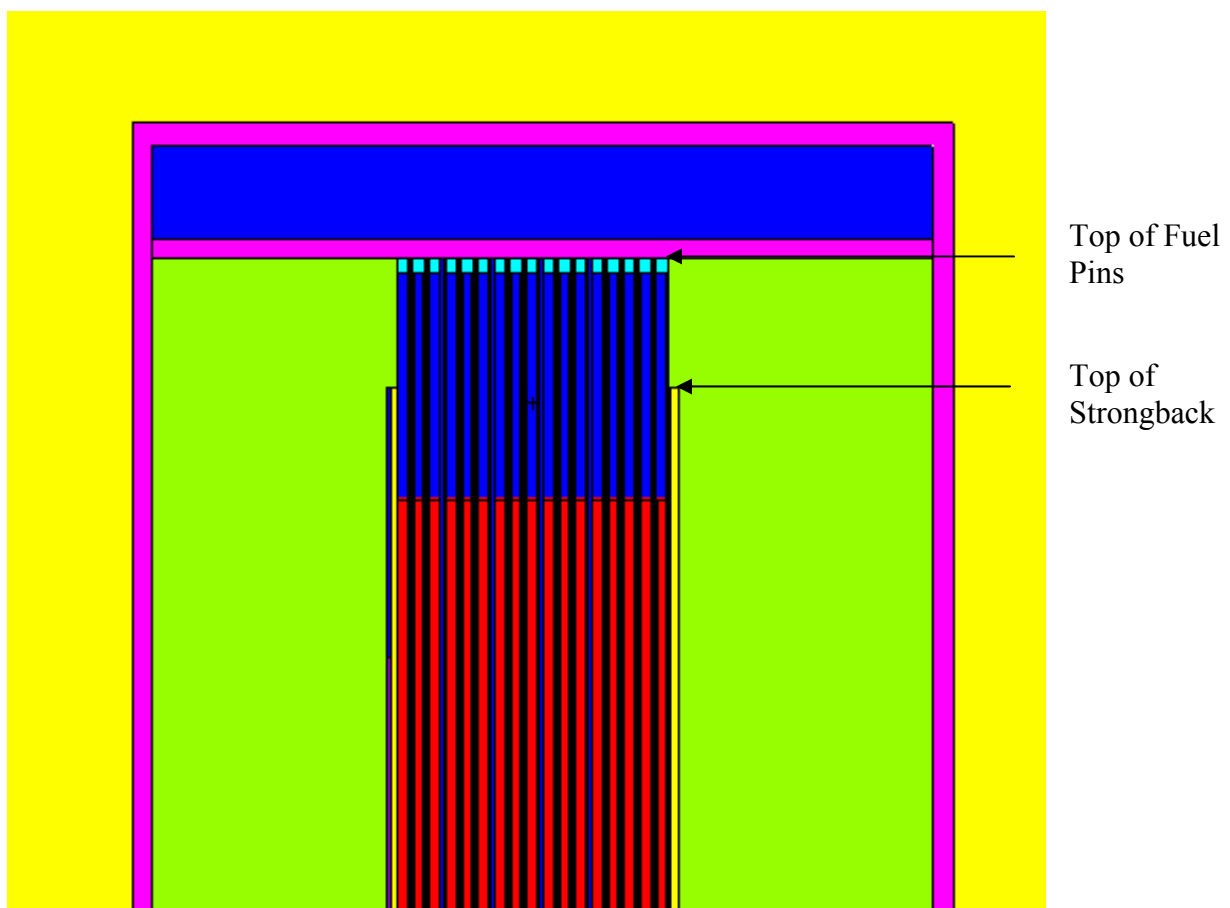


Figure 6.4-3 – HAC Model Geometry, Pins Shifted Up

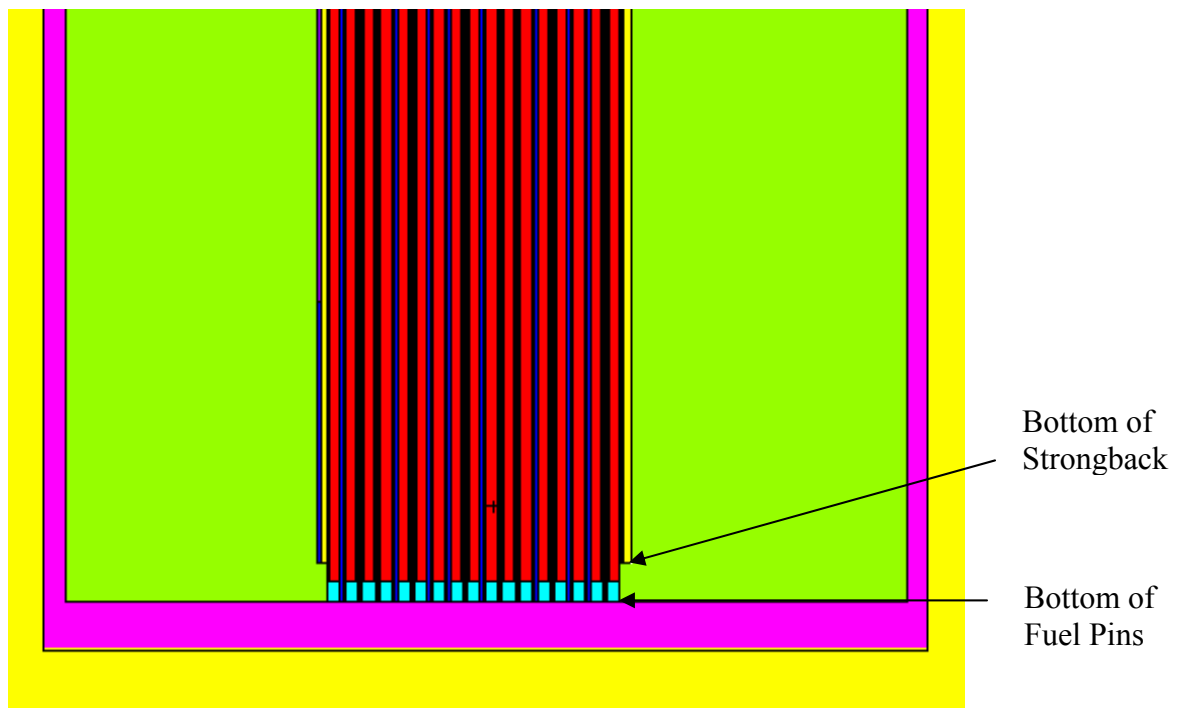


Figure 6.4-4 – HAC Model Geometry, Pins Shifted Down

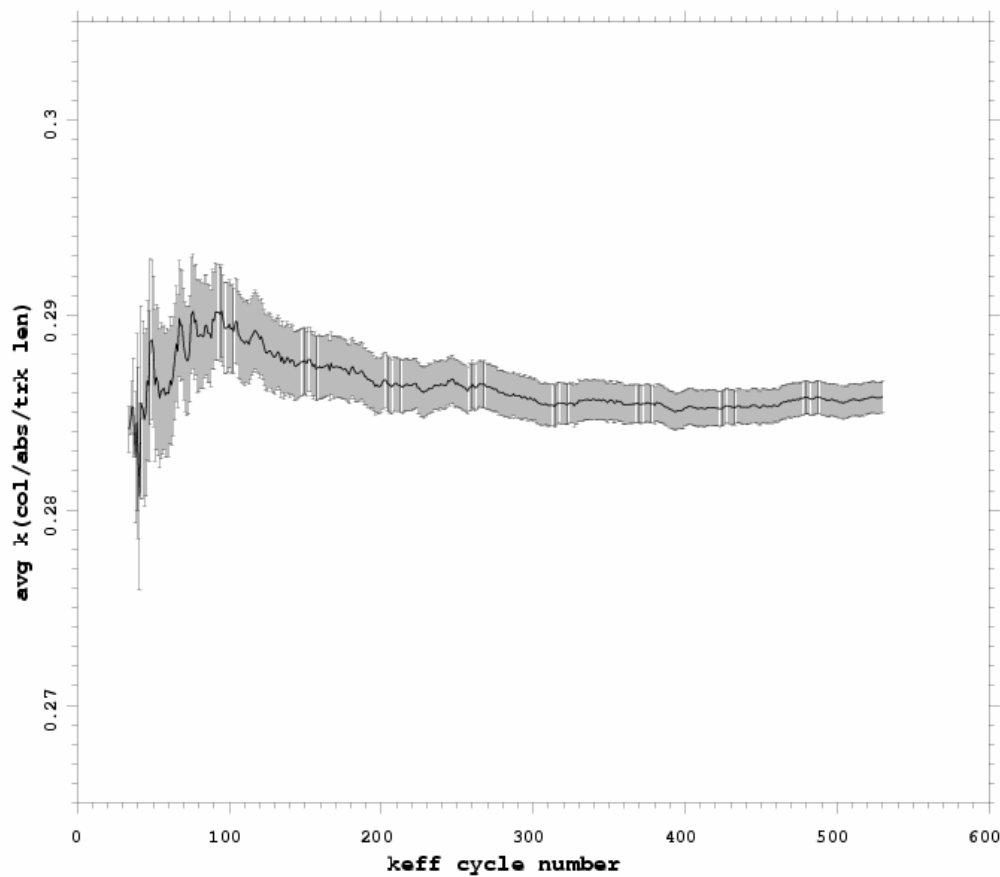


Figure 6.4-5 – Convergence of Maximum NCT Single Case (max_nct_single)

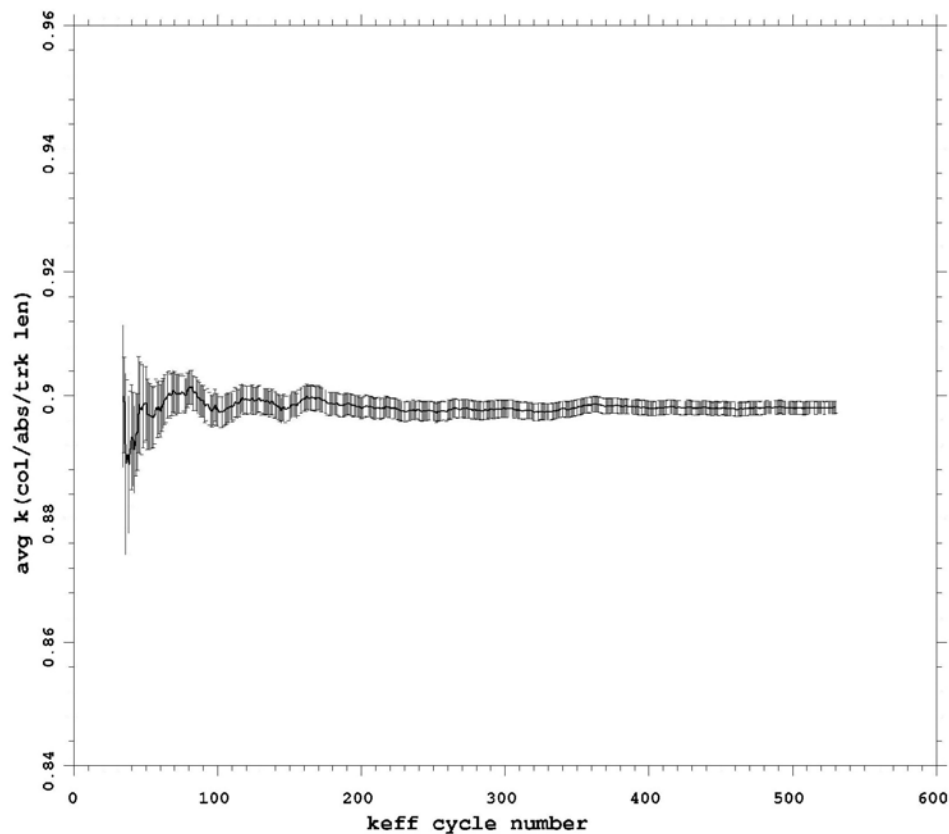


Figure 6.4-6 – Convergence of Maximum HAC Single Case (max_hac_single_su1)

6.5 Evaluation of Package Arrays Under Normal Conditions of Transport

6.5.1 NCT Array Configuration

The NCT array model is developed by assuming an infinite close-packed hexagonal array, see Figure 6.5-1. No water is assumed inside the package and the clamp arms and strongback triangles are ignored. Outside the package, water is assumed to vary between 0.0 and 1.0 g/cm³. The worst-case is obtained for no water between the packages.

All cases except the final maximum case (max_nct_array) are run with a pellet density of 10.31 g/cm³ and M5 cladding. To bound possible future fluctuations in the pellet density and cladding composition, the case with no external moderator is run with a pellet density of 10.85 g/cm³ and pure-zirconium cladding. It is shown in Section 6.6.3, *Impact of Niobium Content in the Cladding*, that pure zirconium cladding is slightly more reactive than cladding containing niobium.

6.5.2 NCT Array Results

The maximum $k_s = 0.6039$ is below the USL and is obtained for the case with no external moderation, a pellet density of 10.85 g/cm³, and a pure zirconium cladding. Criticality results for the NCT array cases are provided in Table 6.5-1.

Cases are run with 1,000 particles per generation, 530 generations, with 30 generations skipped. Convergence is well-behaved and the convergence plot as a function of generation for the limiting case is provided in Figure 6.5-2.

This page left intentionally blank.

Table 6.5-1 – Criticality Results for an Infinite Array of NCT Packages

Case Identifier	Water Density (g/cm ³)		EALF (MeV)	H/ (²³⁹ Pu+ ²³⁵ U)	V ^m /V ^f	²³⁹ Pu/ (U+Pu)	k _{eff}	σ	k _s (k _{eff} +2σ)
	Internal	External							
Max_nct_array	0	0	0.0977	0	1.740	0.056	0.6027	0.0006	0.6039
nct_array_b35pnomplustol_o100	0	1.0	0.0273	0	1.740	0.056	0.3225	0.0006	0.3237
nct_array_b35pnomplustol_o95	0	0.95	0.0262	0	1.740	0.056	0.3273	0.0006	0.3285
nct_array_b35pnomplustol_o90	0	0.90	0.0255	0	1.740	0.056	0.3309	0.0006	0.3321
nct_array_b35pnomplustol_o75	0	0.75	0.0237	0	1.740	0.056	0.3464	0.0006	0.3476
nct_array_b35pnomplustol_o50	0	0.50	0.0199	0	1.740	0.056	0.3805	0.0007	0.3818
nct_array_b35pnomplustol_o25	0	0.25	0.0189	0	1.740	0.056	0.4523	0.0007	0.4536
nct_array_b35pnomplustol_o10	0	0.1	0.0262	0	1.740	0.056	0.5311	0.0007	0.5325
nct_array_b35pnomplustol_o05	0	0.05	0.0385	0	1.740	0.056	0.5664	0.0006	0.5677
nct_array_b35pnomplustol_o001	0	0.001	0.0947	0	1.740	0.056	0.5882	0.0006	0.5895
nct_array_b35pnomplustol_o0	0	0	0.0955	0	1.740	0.056	0.5887	0.0006	0.5898

This page left intentionally blank.

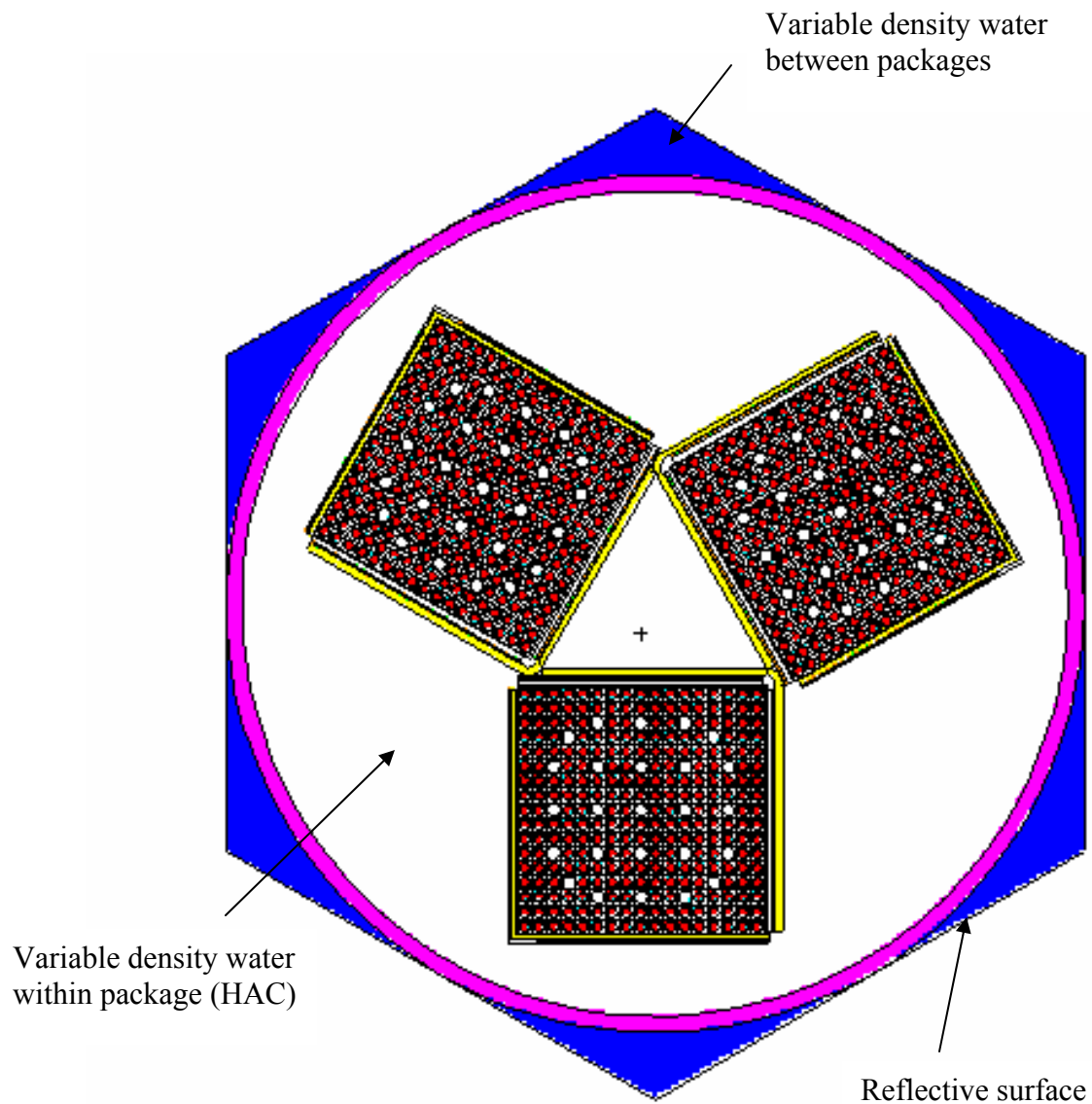


Figure 6.5-1 – Model Geometry, Infinite Array

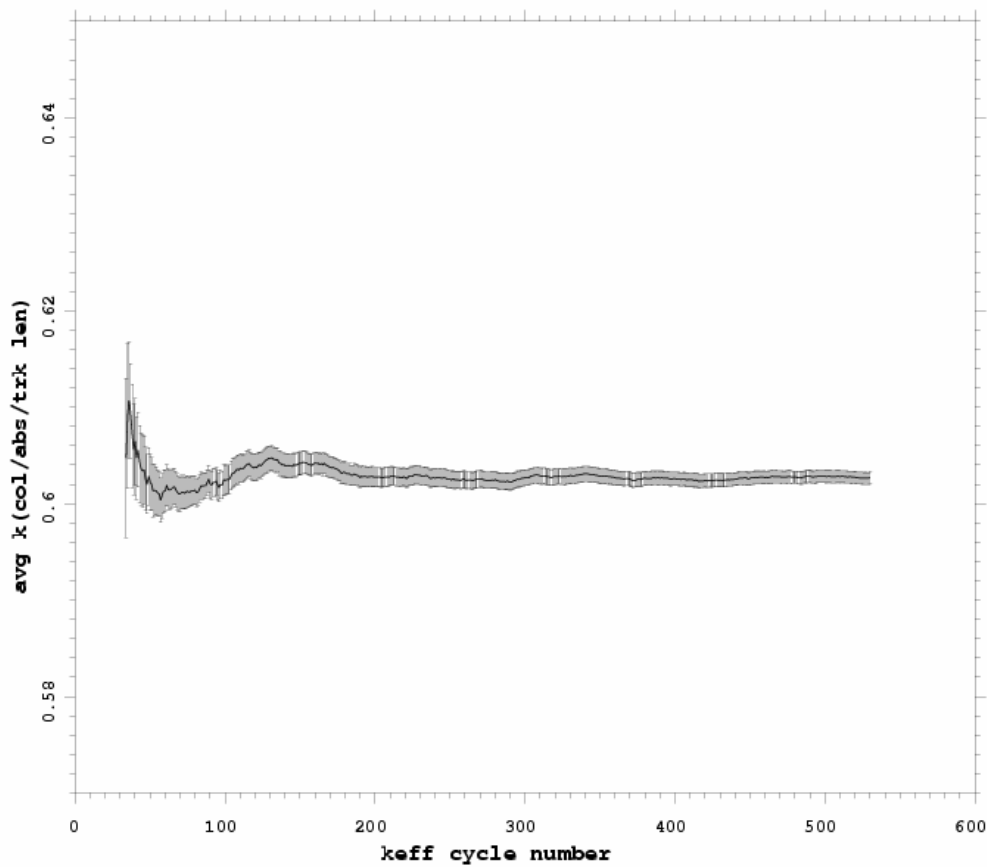


Figure 6.5-2 – Convergence of Maximum NCT Array Case (max_nct_array)

6.6 Package Arrays Under Hypothetical Accident Conditions

6.6.1 HAC Array Configuration

The HAC array models are developed in the same manner as the NCT array models. The worst-case pitch from the single package HAC case (0.5266 inches) is assumed for all models. Internal and external water densities are varied independently to obtain the most reactive configuration. Because water is free to flow throughout the internals of the package, it is assumed that all internal water densities are uniformly reduced. Initially, the clamp arms and strongback angles are ignored. The maximum reactivity for the cases without clamp arms or strongback angles is obtained for the case with full internal moderation and no moderation between packages.

Although full-density internal water results in the worst-case reactivity, water also serves to isolate the fuel assemblies from one another. Therefore, ignoring the minor steel components, such as the clamp arms and strongback triangles, is a small non-conservative assumption because neutrons pass easily through steel and thus steel within the package will increase reactivity. As with the HAC single package models, the effect of ignoring small amounts of steel (i.e., the clamp arms and strongback angles) is quantified by assuming 5.8% (by volume) steel is homogenized within the body (case hac_array_b35pmax2_i100o0_hsteel). The reactivity increase when including the homogenized steel is insignificant and is within the uncertainty of this calculation.

All cases except the final maximum cases (beginning max_hac_array) are run with a pellet density of 10.31 g/cm³ and M5 cladding. To bound possible future fluctuations in the pellet density and cladding composition, the case with no external moderator, 100% internal moderator, and homogenized minor steel components is run with a pellet density of 10.85 g/cm³ and pure-zirconium cladding. It is shown in Section 6.6.3, *Impact of Niobium Content in the Cladding*, that pure zirconium cladding is slightly more reactive than cladding containing niobium.

A final set of cases is run that allow the fuel pins to shift axially, as described in Section 6.4.1.2. These cases have a pellet density of 10.85 g/cm³ and pure-zirconium cladding.

Because the MFFP may transport either one or two assemblies instead of the maximum of three, dummy assemblies are used to balance the package weight. These dummy assemblies are fabricated out of steel. To examine the impact on reactivity of the dummy assemblies, reference HAC array models are run with both one and two fuel assemblies and dummy “assemblies” of void, water, and steel. The reactivity drops in all cases, indicating that any dummy fuel assembly design is acceptable.

6.6.2 HAC Array Results

The maximum $k_s = 0.9037$ is below the USL and is obtained for full internal moderation, no moderation between packages, a homogenized steel/water mixture surrounding the assemblies, a pellet density of 10.85 g/cm³, pure-zirconium cladding, and 24 fuel pins shifted down. This value is only ~4 mk higher than the single package HAC result, indicating that communication between the packages is minimal. Note that allowing various combinations of fuel pins to shift axially has a small, positive effect on the reactivity, although the effect is in typically within the uncertainty of the Monte Carlo method. The detailed results for a full (3 assembly) package

without and with shifted fuel pins are provided in Table 6.6-1 and Table 6.6-2, respectively. The detailed results for a partially filled package are provided in Table 6.6-3.

Cases are run with 2,000 particles per generation, 530 generations, with 30 generations skipped. Convergence is well-behaved and the convergence plot as a function of generation for the limiting case is provided in Figure 6.6-1.

6.6.3 Impact of Niobium Content in the Cladding

The importance of the niobium content in the fuel assembly cladding is evaluated for 0 and 3% niobium by weight. Niobium perturbation calculations (using the MCNP perturbation feature) for single and array HAC cases are evaluated to identify the most reactive niobium content in the cladding under flooded conditions. Both cases indicate that 0 wt% niobium is more reactive than the 3 wt% niobium in the cladding. The difference in the reactivity is on the order of 0.001, which is also the approximate magnitude of the convergence of the remaining calculations. Thus, ignoring the niobium in the cladding for the maximum criticality calculations will be a small conservatism.

For the HAC array case (max_hac_array_pertNb) the removal of the niobium (3% by weight) results in a 0.00110 ± 0.00025 increase in the reactivity. The second order contribution of the perturbation is calculated as 0.00010 ± 0.00004 . The HAC single package case (max_hac_single_pertNb) gives an increase in the reactivity of 0.00065 ± 0.00024 (with a second order term of 0.00004 ± 0.00003) for the removal of 3% by weight niobium from the cladding. The perturbation reactivity values are not directly used for comparison to the USL and are used simply to identify the most reactive case to be evaluated. Due to the small change in k , statistical fluctuations can randomly exceed the effect seen from the niobium content variation.

Table 6.6-1 – Criticality Results for an Infinite Array of HAC Packages (no shifted pins)

Case Identifier	Water Density (g/cm ³)		EALF (MeV)	H/ (²³⁹ Pu+ ²³⁵ U)	V ^m /V ^f	²³⁹ Pu/ (U+Pu)	k _{eff}	σ	k _s (k _{eff} +2σ)
	Internal	External							
max_hac_array_rho_0Nb	1	0	7.26E-7	96.044	2.050	0.056	0.8996	0.0010	0.9016
hac_array_b35pmax2_i100o0_hsteel	1	0	6.61E-07	101.074	2.050	0.056	0.8951	0.0010	0.8971
hac_array_b35pmax2_i100o100	1	1.0	6.67E-07	101.074	2.050	0.056	0.8883	0.0010	0.8903
hac_array_b35pmax2_i100o50	1	0.5	6.60E-07	101.074	2.050	0.056	0.8893	0.0010	0.8913
hac_array_b35pmax2_i100o10	1	0.10	6.48E-07	101.074	2.050	0.056	0.8930	0.0009	0.8948
hac_array_b35pmax2_i100o05	1	0.05	6.57E-07	101.074	2.050	0.056	0.8909	0.0010	0.8929
hac_array_b35pmax2_i100o01	1	0.01	6.51E-07	101.074	2.050	0.056	0.8932	0.0010	0.8952
hac_array_b35pmax2_i100o001	1	0.001	6.55E-07	101.074	2.050	0.056	0.8919	0.0010	0.8938
hac_array_b35pmax2_i100o0	1	0	6.60E-07	101.074	2.050	0.056	0.8912	0.0010	0.8931
hac_array_b35pmax2_i95o0	0.95	0	7.43E-07	96.021	2.050	0.056	0.8683	0.0010	0.8702
hac_array_b35pmax2_i90o0	0.9	0	8.55E-07	90.967	2.050	0.056	0.8470	0.0010	0.8489
hac_array_b35pmax2_i75o0	0.75	0	1.39E-06	75.806	2.050	0.056	0.7662	0.0010	0.7682
hac_array_b35pmax2_i50o0	0.5	0	4.90E-06	50.537	2.050	0.056	0.6221	0.0009	0.6238
hac_array_b35pmax2_i25o0	0.25	0	5.19E-05	25.269	2.050	0.056	0.4926	0.0007	0.4940
hac_array_b35pmax2_i10o0	0.1	0	6.08E-04	10.107	2.050	0.056	0.4849	0.0006	0.4862
hac_array_b35pmax2_i0o100	0	1.0	2.47E-02	0	2.050	0.056	0.3270	0.0004	0.3278
hac_array_b35pmax2_i0o90	0	0.9	2.27E-02	0	2.050	0.056	0.3342	0.0005	0.3351
hac_array_b35pmax2_i0o50	0	0.5	1.82E-02	0	2.050	0.056	0.3847	0.0005	0.3856
hac_array_b35pmax2_i0o10	0	0.10	2.51E-02	0	2.050	0.056	0.5343	0.0005	0.5352
hac_array_b35pmax2_i0o01	0	0.01	7.55E-02	0	2.050	0.056	0.5880	0.0005	0.5889
hac_array_b35pmax2_i0o001	0	0.001	9.35E-02	0	2.050	0.056	0.5905	0.0004	0.5913
hac_array_b35pmax2_i0o0	0	0	9.76E-02	0	2.050	0.056	0.5917	0.0004	0.5926

Table 6.6-2 – Criticality Results for an Infinite Array of HAC Packages (with shifted pins)

Case Identifier	Water Density (g/cm ³)		Shifted Pins	EALF (MeV)	H/ (²³⁹ Pu+ ²³⁵ U)	V ^m /V ^f	²³⁹ Pu/ (U+Pu)	k _{eff}	σ	k _s (k _{eff} +2σ)
	Internal	External								
max_hac_array_srnddn10	1	0	10 down random	7.18E-07	96.044	2.050	0.056	0.9004	0.0010	0.9025
max_hac_array_srnddn20	1	0	20 down random	7.23E-07	96.044	2.050	0.056	0.9002	0.0011	0.9023
max_hac_array_sd1	1	0	8 down	7.20E-07	96.044	2.050	0.056	0.9001	0.0010	0.9020
max_hac_array_sd2	1	0	24 down	7.36E-07	96.044	2.050	0.056	0.9017	0.0010	0.9037
max_hac_array_sd3	1	0	60 down	7.27E-07	96.044	2.050	0.056	0.8992	0.0010	0.9012
max_hac_array_sd4	1	0	116 down	7.02E-07	96.044	2.050	0.056	0.9008	0.0009	0.9026
max_hac_array_salldn	1	0	All down	7.21E-07	96.044	2.050	0.056	0.9001	0.0010	0.9020
max_hac_array_srndup10	1	0	10 up random	7.33E-07	96.044	2.050	0.056	0.8991	0.0009	0.9010
max_hac_array_srndup20	1	0	20 up random	7.14E-07	96.044	2.050	0.056	0.8998	0.0009	0.9016
max_hac_array_su1	1	0	8 up	7.30E-07	96.044	2.050	0.056	0.9004	0.0009	0.9023
max_hac_array_su2	1	0	24 up	7.10E-07	96.044	2.050	0.056	0.8999	0.0010	0.9020
max_hac_array_su3	1	0	60 up	7.13E-07	96.044	2.050	0.056	0.9003	0.0010	0.9022
max_hac_array_su4	1	0	116 up	7.01E-07	96.044	2.050	0.056	0.8979	0.0010	0.8998
max_hac_array_sallup	1	0	All up	7.30E-07	96.044	2.050	0.056	0.8997	0.0010	0.9016

Table 6.6-3 – Criticality Results for an Infinite Array of HAC Partially Filled Packages (no shifted pins)

Case Identifier	Number of Assemblies	Dummy Assembly Material	EALF (MeV)	H/ (²³⁹ Pu+ ²³⁵ U)	V ^m /V ^f	²³⁹ Pu/ (U+Pu)	k _{eff}	σ	k _s (k _{eff} +2σ)
hac_array_b35pmax2_i100o0_hsteel	3	null	6.61E-07	101.074	2.050	0.056	0.8951	0.0010	0.8971
hac_array_b35pmax2_i100o0_hsteel_1asss	1	Steel	6.61E-07	101.074	2.050	0.056	0.8577	0.0010	0.8596
hac_array_b35pmax2_i100o0_hsteel_1assv	1	Void	6.70E-07	101.074	2.050	0.056	0.8548	0.0010	0.8568
hac_array_b35pmax2_i100o0_hsteel_1assw	1	Water	6.68E-07	101.074	2.050	0.056	0.8568	0.0010	0.8588
hac_array_b35pmax2_i100o0_hsteel_2asss	2	Steel	6.56E-07	101.074	2.050	0.056	0.8772	0.0009	0.8791
hac_array_b35pmax2_i100o0_hsteel_2assv	2	Void	6.73E-07	101.074	2.050	0.056	0.8753	0.0009	0.8771
hac_array_b35pmax2_i100o0_hsteel_2assw	2	Water	6.65E-07	101.074	2.050	0.056	0.8741	0.0010	0.8761

This page left intentionally blank.

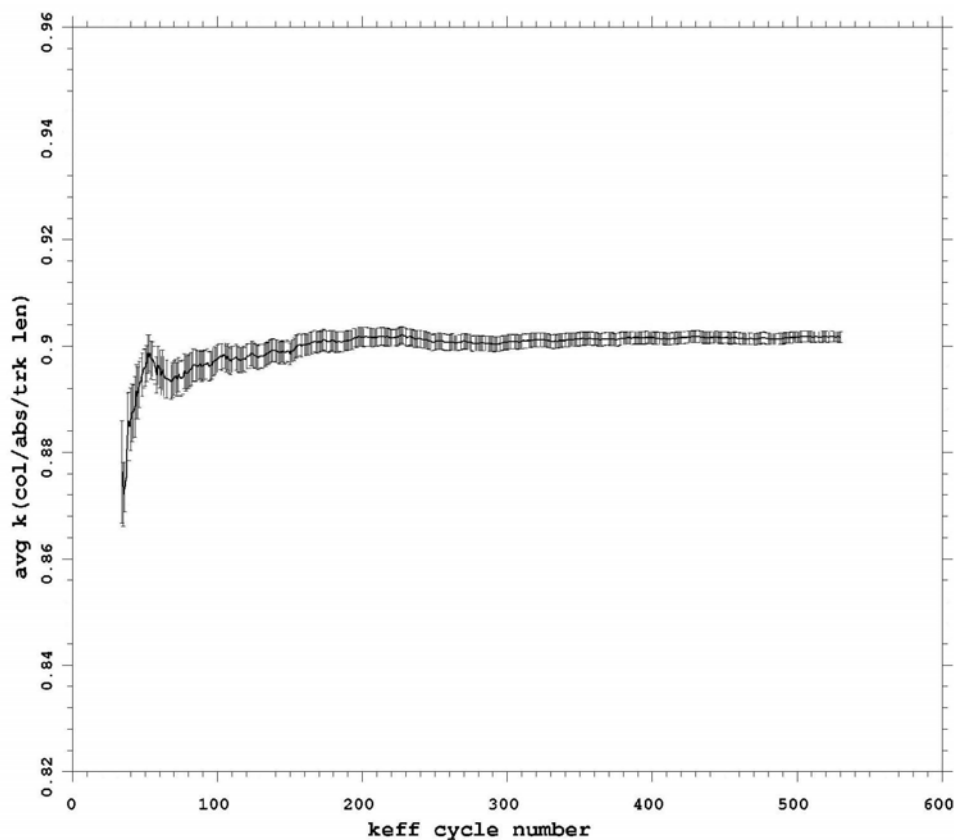


Figure 6.6-1 – Convergence of Maximum HAC Array Case (max_hac_array_sd2)

This page left intentionally blank.

6.7 Fissile Material Packages for Air Transport

This section does not apply for the MFFP, since air transport is not claimed.

This page left intentionally blank.

6.8 Benchmark Evaluations

The MCNP, Version 5, Monte Carlo computer code¹ with point-wise ENDF/B-V and -VI cross sections has been used extensively in criticality evaluations. This section justifies the validity of this computation tool and data library combination for application to the MFFP package criticality analysis and a bias factor is obtained from these calculations of the critical experiments.

The MCNP code uses room temperature continuous-energy (point-wise) cross sections that are thoroughly documented in Appendix G of the manual. These cross sections are defined with a high-energy resolution that describes each resolved cross section resonance for the isotope. All of the cross-sections used for these analyses were generated from the U.S. Evaluated Nuclear Data Files (ENDF/B).

The validation of the point-wise cross sections is conducted using 84 experimental criticality benchmarks applicable to the MFFP. The statistical analysis of the benchmark experiments results in a USL of 0.9288.

6.8.1 Applicability of Benchmark Experiments

The experimental benchmarks are taken from the OECD Nuclear Energy Agency's *International Handbook of Evaluated Criticality Safety Benchmark Experiments*². This Handbook discusses each experiment in detail. It includes estimates of the uncertainty in the measurements, detailed information regarding dimensions and material compositions, comparisons between the multiplication factor calculated by various computer codes, and a list of input files that were used in their calculations. The only changes made to the input files involve changing to a consistent set of cross section libraries, as needed.

The critical experiment benchmarks are selected for use in this USL determination based upon their similarity to the MOX fresh fuel assembly. The important constituents of the MOX assembly are: mixed oxide fuel (plutonium with depleted uranium), borated absorber plates and a steel container and components. The nominal pin cell moderator volume to fuel volume ratio is 1.60 for MFFP fuel. Cases are selected based on plutonium being the dominant fissile material in a solid form (i.e., solutions were excluded). This first selection criteria identified critical experiments with composite mixed oxide fuel rods with uranium enrichments of less than 2%, greater than 1% Pu/(U+Pu) and moderator to fuel ratios of less than 20. This set of 145 experiments is filtered to remove those cases that contained cadmium and hafnium absorber materials which are not present in this analysis (leaving only boron as the accepted absorber material). The remaining 77 experiments have mixed plutonium/uranium fuel in a lattice with a thermal spectrum, similar to MOX fuel.

To provide benchmarks with harder neutron spectra, a second selection is performed over the metal fuel experiments with the same criteria. From this second search, 7 more critical benchmark experiments are identified. These later experiments use metal fuel in a graphite moderator/reflector.

¹ MCNP5, "MCNP – A General Monte Carlo N-Particle Transport Code, Version 5; Volume II: User's Guide," LA-CP-03-0245, Los Alamos National Laboratory, April, 2003.

² OECD Nuclear Energy Agency, *International Handbook of Evaluated Criticality Safety Benchmark Experiments*, NEA/NSC/DOC(95)03, September, 2003.

The overall selection of cases is weighted to the thermal spectra where calculated MOX assembly reactivity is highest. The critical experiments selected are listed in Table 6.8-1.

6.8.2 Bias Determination

The ORNL USLSTATS code³, described in Appendix C of NUREG/CR-6361⁴, is used to establish an upper subcritical limit (USL) for the analysis. Computed multiplication factors, k_{eff} , for the MOX package are deemed to be adequately subcritical if the computed value of k_{eff} plus two standard deviations is below the USL as follows:

$$k_s = k_{\text{eff}} + 2\sigma < \text{USL}$$

The USL includes the combined effects of code bias, uncertainty in the benchmark experiments, uncertainty in the computational evaluation of the benchmark experiments, and an administrative margin of subcriticality. The USL is determined using the confidence band with administrative margin technique (USLSTATS Method 1).

USLSTATS takes as input the k_{eff} as calculated by MCNP5, the total 1- σ uncertainty (combined benchmark and computational uncertainties), and a trending parameter. For the current analysis, four trending parameters have been selected (1) moderator to fuel volume ratio (v^m/v^f), (2) H/(Pu239+U235) ratio, (3) Pu239/(Pu+U), and (4) Energy of the Average Lethargy causing Fission (EALF). Parameters (1) and (2) are applied to only to the first 77 benchmarks because these parameters are not directly applicable to dry, non-lattice benchmarks. Parameters (3) and (4) are applied to all 84 benchmarks. The USL is computed by trending upon these variables and selecting the lowest USL.

The uncertainty value, σ_{tot} , assigned to each case is a combination of the benchmark-model uncertainty for each experiment, σ_{bench} , and the Monte Carlo uncertainty associated with the particular computational evaluation of the case, σ_{comp} , or:

$$\sigma_{\text{tot}} = (\sigma_{\text{bench}}^2 + \sigma_{\text{comp}}^2)^{1/2}$$

These values are input into the USLSTATS program in addition to the following parameters, which are the values suggested by the USLSTATS user's manual:

- P, proportion of population falling above lower tolerance level = 0.995
- $1-\gamma$, confidence on fit = 0.95
- α , confidence on proportion P = 0.95
- Δk_m , administrative margin used to ensure subcriticality = 0.05.

³ USLSTATS, "USLSTATS: A Utility To Calculate Upper Subcritical Limits For Criticality Safety Applications," Version 1.3.6, Oak Ridge National Laboratory, December 15, 1998.

⁴ J. J. Lichtenwalter, S. M. Bowman, M. D. DeHart, C. M. Hopper, *Criticality Benchmark Guide for Light-Water-Reactor Fuel in Transportation and Storage Packages*, NUREG/CR-6361, ORNL/TM-13211, March 1997.

This data is followed by triplets of trending parameter value, computed k_{eff} , and uncertainty for each case. The USL Method 1 performs a confidence band analysis on the data for the trending parameter. All benchmark data used as input to USLSTATS are reported in Table 6.8-2.

Note that USLSTATS assumes that all benchmark experiments have a $k_{\text{eff}} = 1.000$. However, some of the benchmark k_{eff} are greater or less than 1.000. The most accurate value for the model reactivity is used and the k_{eff} input into USLSTATS is normalized by dividing by the benchmark k_{eff} . The benchmark-model reactivity may be different than 1.000 due to experiments that were not exactly critical or due to model simplifications. For example, for experiments with fixed rod patterns, the addition of one more rod may bring the experiment from sub-critical to super-critical without the possibility of being exactly critical. Other known model assumptions may be evaluated with the experiment and may be included in the benchmark reactivity. Corrections may be based on analytical evaluation or measurements and the uncertainties in these adjustments are included in the benchmark's overall uncertainty. Typically the combined corrections are small and benchmark-model k_{eff} are close to 1.000.

The USL generated for each of the three trending parameters utilized is provided below.

Trending parameter	USL equation	Range of Applicability
v^m/v^f	USL1 = $0.9289 + (4.0398\text{E-}04) * X$	$1.1112 \leq X \leq 17.5$
H/ (Pu239+U235)	USL1 = $0.9309 + (1.4706\text{E-}06) * X$	$51.000 \leq X \leq 1145.$
Pu239/(U+Pu)	USL1 = $0.9297 + (1.0963\text{E-}02) * X$ ($X < 0.709$) = 0.9374 ($X \geq 0.709$)	$0.014 \leq X \leq 0.95$
EALF	USL1 = $0.9288 + (3.6369\text{E-}02) * X$ ($X < 0.20144$) = 0.9362 ($X \geq 0.201$)	$8.07\text{E-}8 \leq X \leq 0.40$ MeV

All of the trending parameters show little correlation, thus the use of a constant USL is appropriate. The MCNP results show an average negative bias (under prediction) in the reactivity for the selected benchmarks of about 0.007 ± 0.006 . The minimum USL value of 0.9288 is used which includes the bias, trend corrections, administrative margin (0.05) and the 95% confidence band width of the data.

Results for v^m/v^f

The volume ratio is equivalent to trending by pin pitch and was used as a selection criteria for the 77 lattice benchmark cases. The volume fractions are used to better represent the mixture of hexagonal and square lattice geometries used in the benchmarks. The USL1 value is a minimum at the minimum moderator to fuel volume ratio. As shown in Figure 6.8-1 there is little correlation with this variable and the calculated benchmark reactivity. The calculations for the MOX package have v^m/v^f ratios from about 1.6 to 2 with full density water. Not adjusting for the water density provides a trending that will be similar to trending on fuel pin pitch. The possible influence with water density is covered with the H/Pu+U ratio below.

Results for H/(Pu239+U235)

This parameter is utilized with the 77 lattice benchmark cases. Reactivity trend with respect to the ratio of the primary moderator (H) to the primary fissile isotopes (Pu239 and U235) within the pin cell was not significant. The smeared atom densities in the pin cells are used. For the

MOX package analyses, the H/(Pu239+U235) ratio ranges from 0 to 101. As shown on Figure 6.8-2, the benchmark data for low H/(Pu239+U235) ratios is sparse and variable. However, for this analysis the higher reactivity and more important cases occur with the larger H/(Pu239+U235) values (around 100) and in this range there is adequate benchmark data. The more important MFFP cases occur with more moderation which is also apparent in the EALF trending as discussed below.

Results for Pu239/(U+Pu)

This parameter is utilized with all 84 benchmark cases. The Pu239/(U+Pu) trending parameter was selected to identify any bias resulting from the selection of benchmark cases with different plutonium and uranium concentrations. The MOX package has a Pu239/(U+Pu) ratio of 0.056, which is within the range of applicability for the benchmark data as shown in Figure 6.8-3.

Results for EALF

This parameter is utilized with all 84 benchmark cases. The EALF comparison provides a means to observe neutron spectral dependencies or trends. The USL1 for the EALF parameter has a negligible increase with increasing EALF as shown in Figure 6.8-4 for the benchmark cases. The MOX analyses have EALF values from 6.5E-7 to 0.35 MeV. As shown in Figure 6.8-5 cases with a high EALF have a lower calculated reactivity. The MOX case with the peak reactivity has an EALF of 7.36E-7 MeV which is well represented by the benchmarks. Additional refinement of the benchmarks for high EALF values is not warranted due to the low calculated reactivity in this range, and thus large margin for safety.

Table 6.8-1 – Experimental Benchmarks

Used Y/N	Identification	Solid poison	EALF (eV)	Pu/(U+Pu) ratio	Pitch type	Pitch size (cm)
Y	MIX-COMP-THERM-001-001	null	1.07	0.2237	Square	0.9525
Y	MIX-COMP-THERM-001-002	null	0.292	0.2237	Square	1.258
Y	MIX-COMP-THERM-001-003	null	0.174	0.2237	Square	1.5342
Y	MIX-COMP-THERM-001-004	null	0.12	0.2237	Square	1.905
Y	MIX-COMP-THERM-002-001	null	0.581	0.0204	Square	1.778
Y	MIX-COMP-THERM-002-002	null	0.769	0.0204	Square	1.778
Y	MIX-COMP-THERM-002-003	null	0.197	0.0204	Square	2.20914
Y	MIX-COMP-THERM-002-004	null	0.288	0.0204	Square	2.20914
Y	MIX-COMP-THERM-002-005	null	0.142	0.0204	Square	2.51447
Y	MIX-COMP-THERM-002-006	null	0.188	0.0204	Square	2.51447
Y	MIX-COMP-THERM-003-001	null	0.922	0.0659	Square	1.3208
Y	MIX-COMP-THERM-003-002	null	0.559	0.0659	Square	1.4224
Y	MIX-COMP-THERM-003-003	null	0.663	0.0659	Square	1.4224
Y	MIX-COMP-THERM-003-004	null	0.192	0.0659	Square	1.8679
Y	MIX-COMP-THERM-003-005	null	0.159	0.0659	Square	2.01158
Y	MIX-COMP-THERM-003-006	null	0.103	0.0659	Square	2.6416
Y	MIX-COMP-THERM-004-001	null	0.149	0.03	Square	1.825
Y	MIX-COMP-THERM-004-002	null	0.148	0.0299	Square	1.825
Y	MIX-COMP-THERM-004-003	null	0.147	0.028	Square	1.825
Y	MIX-COMP-THERM-004-004	null	0.123	0.03	Square	1.956
Y	MIX-COMP-THERM-004-005	null	0.122	0.0299	Square	1.956
Y	MIX-COMP-THERM-004-006	null	0.121	0.0298	Square	1.956

Used Y/N	Identification	Solid poison	EALF (eV)	Pu/(U+Pu) ratio	Pitch type	Pitch size (cm)
Y	MIX-COMP-THERM-004-007	null	0.0951	0.03	Square	2.225
Y	MIX-COMP-THERM-004-008	null	0.0948	0.0299	Square	2.225
Y	MIX-COMP-THERM-004-009	null	0.0944	0.0298	Square	2.225
Y	MIX-COMP-THERM-004-010	null	0.082	0.03	Square	2.474
Y	MIX-COMP-THERM-004-011	null	0.0916	0.0299	Square	2.474
Y	MIX-COMP-THERM-005-001	null	0.399	0.0399	Hexagonal	2.159
Y	MIX-COMP-THERM-005-002	null	0.263	0.0399	Hexagonal	2.3622
Y	MIX-COMP-THERM-005-003	null	0.18	0.0399	Hexagonal	2.667
Y	MIX-COMP-THERM-005-004	null	0.15	0.0399	Hexagonal	2.90322
Y	MIX-COMP-THERM-005-005	null	0.111	0.0399	Hexagonal	3.52044
Y	MIX-COMP-THERM-005-006	null	0.0956	0.0399	Hexagonal	4.064
Y	MIX-COMP-THERM-005-007	null	0.0912	0.0399	Hexagonal	4.318
Y	MIX-COMP-THERM-006-001	null	0.383	0.0204	Hexagonal	2.032
Y	MIX-COMP-THERM-006-002	null	0.2	0.0204	Hexagonal	2.3622
Y	MIX-COMP-THERM-006-003	null	0.145	0.0204	Hexagonal	2.667
Y	MIX-COMP-THERM-006-004	null	0.123	0.0204	Hexagonal	2.90322
Y	MIX-COMP-THERM-006-005	null	0.101	0.0204	Hexagonal	3.3528
Y	MIX-COMP-THERM-006-006	null	0.0954	0.0204	Hexagonal	3.52044
Y	MIX-COMP-THERM-006-007	null	0.144	0.0204	Hexagonal	2.667
N	MIX-COMP-THERM-006-008	Hf	0.145	0.0204	Hexagonal	2.667
N	MIX-COMP-THERM-006-009	Hf	0.145	0.0204	Hexagonal	2.667
N	MIX-COMP-THERM-006-010	Hf	0.145	0.0204	Hexagonal	2.667
N	MIX-COMP-THERM-006-011	Hf	0.145	0.0204	Hexagonal	2.667
N	MIX-COMP-THERM-006-012	Hf	0.146	0.0204	Hexagonal	2.667
Y	MIX-COMP-THERM-006-013	Boron	0.145	0.0204	Hexagonal	2.667
Y	MIX-COMP-THERM-006-014	Boron	0.145	0.0204	Hexagonal	2.667
Y	MIX-COMP-THERM-006-015	Boron	0.145	0.0204	Hexagonal	2.667
Y	MIX-COMP-THERM-006-016	Boron	0.146	0.0204	Hexagonal	2.667
N	MIX-COMP-THERM-006-017	Cd	0.147	0.0204	Hexagonal	2.667
N	MIX-COMP-THERM-006-018	Cd + Hf	0.147	0.0204	Hexagonal	2.667
N	MIX-COMP-THERM-006-019	Cd + Hf	0.146	0.0204	Hexagonal	2.667
N	MIX-COMP-THERM-006-020	Cd + Hf	0.147	0.0204	Hexagonal	2.667
N	MIX-COMP-THERM-006-021	Cd + Hf	0.146	0.0204	Hexagonal	2.667
N	MIX-COMP-THERM-006-022	Cd + Hf	0.146	0.0204	Hexagonal	2.667
N	MIX-COMP-THERM-006-023	B + Cd	0.146	0.0204	Hexagonal	2.667
N	MIX-COMP-THERM-006-024	B + Cd	0.146	0.0204	Hexagonal	2.667
N	MIX-COMP-THERM-006-025	B + Cd	0.146	0.0204	Hexagonal	2.667
N	MIX-COMP-THERM-006-026	B + Cd	0.147	0.0204	Hexagonal	2.667
N	MIX-COMP-THERM-006-027	Cd	0.146	0.0204	Hexagonal	2.667
N	MIX-COMP-THERM-006-028	Cd	0.147	0.0204	Hexagonal	2.667
Y	MIX-COMP-THERM-006-029	null	0.101	0.0204	Hexagonal	3.3528
N	MIX-COMP-THERM-006-030	Hf	0.101	0.0204	Hexagonal	3.3528
N	MIX-COMP-THERM-006-031	Hf	0.101	0.0204	Hexagonal	3.3528
N	MIX-COMP-THERM-006-032	Hf	0.101	0.0204	Hexagonal	3.3528
N	MIX-COMP-THERM-006-033	Hf	0.101	0.0204	Hexagonal	3.3528
N	MIX-COMP-THERM-006-034	Hf	0.101	0.0204	Hexagonal	3.3528
Y	MIX-COMP-THERM-006-035	Boron	0.1	0.0204	Hexagonal	3.3528
Y	MIX-COMP-THERM-006-036	Boron	0.101	0.0204	Hexagonal	3.3528
Y	MIX-COMP-THERM-006-037	Boron	0.101	0.0204	Hexagonal	3.3528
Y	MIX-COMP-THERM-006-038	Boron	0.101	0.0204	Hexagonal	3.3528
N	MIX-COMP-THERM-006-039	Cd	0.101	0.0204	Hexagonal	3.3528

Used Y/N	Identification	Solid poison	EALF (eV)	Pu/(U+Pu) ratio	Pitch type	Pitch size (cm)
N	MIX-COMP-THERM-006-040	Cd + Hf	0.101	0.0204	Hexagonal	3.3528
N	MIX-COMP-THERM-006-041	Cd + Hf	0.101	0.0204	Hexagonal	3.3528
N	MIX-COMP-THERM-006-042	Cd + Hf	0.101	0.0204	Hexagonal	3.3528
N	MIX-COMP-THERM-006-043	Cd + Hf	0.101	0.0204	Hexagonal	3.3528
N	MIX-COMP-THERM-006-044	Cd + Hf	0.101	0.0204	Hexagonal	3.3528
N	MIX-COMP-THERM-006-045	B + Cd	0.101	0.0204	Hexagonal	3.3528
N	MIX-COMP-THERM-006-046	B + Cd	0.101	0.0204	Hexagonal	3.3528
N	MIX-COMP-THERM-006-047	B + Cd	0.101	0.0204	Hexagonal	3.3528
N	MIX-COMP-THERM-006-048	B + Cd	0.101	0.0204	Hexagonal	3.3528
N	MIX-COMP-THERM-006-049	Cd	0.101	0.0204	Hexagonal	3.3528
N	MIX-COMP-THERM-006-050	Cd	0.101	0.0204	Hexagonal	3.3528
Y	MIX-COMP-THERM-007-001	null	0.203	0.0199	Hexagonal	2.3622
Y	MIX-COMP-THERM-007-002	null	0.146	0.0199	Hexagonal	2.667
Y	MIX-COMP-THERM-007-003	null	0.123	0.0199	Hexagonal	2.9032
Y	MIX-COMP-THERM-007-004	null	0.1	0.0199	Hexagonal	3.3528
Y	MIX-COMP-THERM-007-005	null	0.0954	0.0199	Hexagonal	3.5204
Y	MIX-COMP-THERM-007-006	null	0.145	0.0199	Hexagonal	2.667
Y	MIX-COMP-THERM-007-007	Boron	0.146	0.0199	Hexagonal	2.667
Y	MIX-COMP-THERM-007-008	Boron	0.146	0.0199	Hexagonal	2.667
Y	MIX-COMP-THERM-007-009	Boron	0.146	0.0199	Hexagonal	2.667
Y	MIX-COMP-THERM-007-010	Boron	0.145	0.0199	Hexagonal	2.667
N	MIX-COMP-THERM-007-011	Hf	0.146	0.0199	Hexagonal	2.667
N	MIX-COMP-THERM-007-012	Hf	0.146	0.0199	Hexagonal	2.667
N	MIX-COMP-THERM-007-013	Hf	0.146	0.0199	Hexagonal	2.667
N	MIX-COMP-THERM-007-014	Hf	0.146	0.0199	Hexagonal	2.667
N	MIX-COMP-THERM-007-015	Hf	0.145	0.0199	Hexagonal	2.667
N	MIX-COMP-THERM-007-016	Cd	0.147	0.0199	Hexagonal	2.667
N	MIX-COMP-THERM-007-017	B + Cd	0.147	0.0199	Hexagonal	2.667
N	MIX-COMP-THERM-007-018	B + Cd	0.147	0.0199	Hexagonal	2.667
N	MIX-COMP-THERM-007-019	B + Cd	0.147	0.0199	Hexagonal	2.667
N	MIX-COMP-THERM-007-020	B + Cd	0.147	0.0199	Hexagonal	2.667
N	MIX-COMP-THERM-007-021	Cd + Hf	0.147	0.0199	Hexagonal	2.667
N	MIX-COMP-THERM-007-022	Cd + Hf	0.147	0.0199	Hexagonal	2.667
N	MIX-COMP-THERM-007-023	Cd + Hf	0.147	0.0199	Hexagonal	2.667
N	MIX-COMP-THERM-007-024	Cd + Hf	0.147	0.0199	Hexagonal	2.667
N	MIX-COMP-THERM-007-025	Cd + Hf	0.147	0.0199	Hexagonal	2.667
N	MIX-COMP-THERM-007-026	Cd	0.146	0.0199	Hexagonal	2.667
N	MIX-COMP-THERM-007-027	Cd	0.147	0.0199	Hexagonal	2.667
Y	MIX-COMP-THERM-008-001	null	0.408	0.02	Hexagonal	2.032
Y	MIX-COMP-THERM-008-002	null	0.205	0.02	Hexagonal	2.3622
Y	MIX-COMP-THERM-008-003	null	0.147	0.02	Hexagonal	2.667
Y	MIX-COMP-THERM-008-004	null	0.124	0.02	Hexagonal	2.9032
Y	MIX-COMP-THERM-008-005	null	0.101	0.02	Hexagonal	3.3528
Y	MIX-COMP-THERM-008-006	null	0.0952	0.02	Hexagonal	3.5204
Y	MIX-COMP-THERM-008-007	null	0.146	0.02	Hexagonal	2.667
N	MIX-COMP-THERM-008-008	Hf	0.146	0.02	Hexagonal	2.667
N	MIX-COMP-THERM-008-009	Hf	0.147	0.02	Hexagonal	2.667
N	MIX-COMP-THERM-008-010	Hf	0.147	0.02	Hexagonal	2.667
N	MIX-COMP-THERM-008-011	Hf	0.147	0.02	Hexagonal	2.667
N	MIX-COMP-THERM-008-012	Hf	0.147	0.02	Hexagonal	2.667
Y	MIX-COMP-THERM-008-013	Boron	0.146	0.02	Hexagonal	2.667

Used Y/N	Identification	Solid poison	EALF (eV)	Pu/(U+Pu) ratio	Pitch type	Pitch size (cm)
Y	MIX-COMP-THERM-008-014	Boron	0.147	0.02	Hexagonal	2.667
Y	MIX-COMP-THERM-008-015	Boron	0.147	0.02	Hexagonal	2.667
Y	MIX-COMP-THERM-008-016	Boron	0.147	0.02	Hexagonal	2.667
N	MIX-COMP-THERM-008-017	Cd	0.148	0.02	Hexagonal	2.667
N	MIX-COMP-THERM-008-018	Cd + Hf	0.147	0.02	Hexagonal	2.667
N	MIX-COMP-THERM-008-019	Cd + Hf	0.148	0.02	Hexagonal	2.667
N	MIX-COMP-THERM-008-020	Cd + Hf	0.148	0.02	Hexagonal	2.667
N	MIX-COMP-THERM-008-021	Cd + Hf	0.148	0.02	Hexagonal	2.667
N	MIX-COMP-THERM-008-022	Cd + Hf	0.148	0.02	Hexagonal	2.667
N	MIX-COMP-THERM-008-023	B + Cd	0.147	0.02	Hexagonal	2.667
N	MIX-COMP-THERM-008-024	B + Cd	0.148	0.02	Hexagonal	2.667
N	MIX-COMP-THERM-008-025	B + Cd	0.148	0.02	Hexagonal	2.667
N	MIX-COMP-THERM-008-026	B + Cd	0.148	0.02	Hexagonal	2.667
N	MIX-COMP-THERM-008-027	Cd	0.148	0.02	Hexagonal	2.667
N	MIX-COMP-THERM-008-028	Cd	0.148	0.02	Hexagonal	2.667
Y	MIX-COMP-THERM-009-001	null	0.537	0.015	Hexagonal	1.397
Y	MIX-COMP-THERM-009-002	null	0.304	0.015	Hexagonal	1.524
Y	MIX-COMP-THERM-009-003	null	0.158	0.015	Hexagonal	1.8034
Y	MIX-COMP-THERM-009-004	null	0.119	0.015	Hexagonal	2.032
Y	MIX-COMP-THERM-009-005	null	0.0972	0.015	Hexagonal	2.286
Y	MIX-COMP-THERM-009-006	null	0.093	0.015	Hexagonal	2.3622
Y	MIX-MET-INTER-001-001	null	36800	0.4525	null	null
Y	MIX-MET-FAST-008-002	null	347000	0.4525	null	null
Y	MIX-MET-FAST-008-003	null	83400	0.4525	null	null
Y	MIX-MET-FAST-008-004	null	186000	0.4525	null	null
Y	MIX-MET-FAST-008-005	null	285000	0.4525	null	null
Y	MIX-MET-INTER-001-006	null	26600	0.191	null	null
Y	PU-MET-FAST-033-001	null	422000	0.5255	null	null

This page left intentionally blank.

Table 6.8-2 – Benchmark k_{eff} Results

Case Name	EALF (MeV)	v_m/v_f	$\frac{^{239}\text{Pu}}{(\text{U}+\text{Pu})}$	H/ ($^{239}\text{Pu} + ^{235}\text{U}$)	k_{ben}	σ_{bench}	k_{MCNP}	σ_{MCNP}	k_{MCNP} (normalized)	σ_{tot}
MIXCT1\mixct-001-c1	1.002E-06	3.335	0.193	51	1	0.0025	0.9919	0.0007	0.9919	0.0026
MIXCT1\mixct-001-c2	2.802E-07	6.868	0.193	106	1	0.0026	0.9931	0.0007	0.9931	0.0027
MIXCT1\mixct-001-c3	1.683E-07	10.881	0.193	168	1	0.0032	0.9908	0.0007	0.9908	0.0033
MIXCT1\mixct-001-c4	1.175E-07	17.534	0.193	271	1	0.0039	0.9944	0.0007	0.9944	0.0040
MIXCT2\mixct-002-pnl30	5.853E-07	1.195	0.019	147	1.001	0.0059	0.9926	0.0008	0.9916	0.0060
MIXCT2\mixct-002-pnl31	7.786E-07	1.195	0.019	147	1.0009	0.0045	0.9965	0.0009	0.9956	0.0046
MIXCT2\mixct-002-pnl32	1.962E-07	2.525	0.019	310	1.0024	0.0029	0.9959	0.0008	0.9936	0.0030
MIXCT2\mixct-002-pnl33	2.866E-07	2.525	0.019	310	1.0024	0.0021	1.0028	0.0008	1.0004	0.0023
MIXCT2\mixct-002-pnl34	1.407E-07	3.641	0.019	447	1.0038	0.0022	0.9978	0.0008	0.9940	0.0023
MIXCT2\mixct-002-pnl35	1.859E-07	3.641	0.019	447	1.0029	0.0024	1.0055	0.0008	1.0026	0.0025
MIXCT3\mixct-003-c1	8.994E-07	1.681	0.060	74	1	0.0071	0.9932	0.0009	0.9932	0.0072
MIXCT3\mixct-003-c2	5.499E-07	2.165	0.060	96	1	0.0057	0.9919	0.0009	0.9919	0.0058
MIXCT3\mixct-003-c3	6.544E-07	2.165	0.060	96	1	0.0052	0.9944	0.0009	0.9944	0.0053
MIXCT3\mixct-003-c4	1.898E-07	4.706	0.060	208	1	0.0028	0.9947	0.0009	0.9947	0.0029
MIXCT3\mixct-003-c5	1.571E-07	5.672	0.060	252	1	0.0024	0.9944	0.0009	0.9944	0.0026
MIXCT3\mixct-003-c6	1.017E-07	10.754	0.060	477	1	0.002	1.0000	0.0008	1.0000	0.0022
MIXCT4\mixct-004-c01	1.471E-07	2.420	0.021	438	1	0.0046	0.9909	0.0007	0.9909	0.0047
MIXCT4\mixct-004-c02	1.462E-07	2.420	0.021	438	1	0.0046	0.9929	0.0007	0.9929	0.0047
MIXCT4\mixct-004-c03	1.461E-07	2.420	0.021	438	1	0.0046	0.9924	0.0007	0.9924	0.0047
MIXCT4\mixct-004-c04	1.216E-07	2.976	0.021	538	1	0.0039	0.9934	0.0007	0.9934	0.0040
MIXCT4\mixct-004-c05	1.203E-07	2.976	0.021	538	1	0.0039	0.9883	0.0007	0.9883	0.0040
MIXCT4\mixct-004-c06	1.199E-07	2.976	0.021	538	1	0.0039	0.9949	0.0007	0.9949	0.0040
MIXCT4\mixct-004-c07	9.415E-08	4.239	0.021	767	1	0.004	0.9938	0.0007	0.9938	0.0041
MIXCT4\mixct-004-c08	9.387E-08	4.239	0.021	767	1	0.004	0.9948	0.0007	0.9948	0.0041



MFFP Safety Analysis Report

Docket No. 71-9295
Revision 1, January 2005

Case Name	EALF (MeV)	v_m/v_f	$\frac{^{239}\text{Pu}}{(\text{U}+\text{Pu})}$	$\frac{\text{H}}{(^{239}\text{Pu} + ^{235}\text{U})}$	k_{ben}	σ_{bench}	k_{MCNP}	σ_{MCNP}	k_{MCNP} (normalized)	σ_{tot}
MIXCT4\mixct-004-c09	9.37E-08	4.239	0.021	767	1	0.004	0.9957	0.0007	0.9957	0.0041
MIXCT4\mixct-004-c10	8.083E-08	5.552	0.021	1005	1	0.0051	0.9952	0.0007	0.9952	0.0051
MIXCT4\mixct-004-c11	8.067E-08	5.552	0.021	1005	1	0.0051	0.9968	0.0007	0.9968	0.0051
MIXCT5\mixct-005-c1	3.957E-07	1.931	0.030	166	1.0008	0.0022	0.9936	0.0006	0.9928	0.0023
MIXCT5\mixct-005-c2	2.601E-07	2.566	0.030	220	1.0011	0.0026	0.9932	0.0006	0.9921	0.0027
MIXCT5\mixct-005-c3	1.787E-07	3.624	0.030	311	1.0016	0.0029	0.9995	0.0006	0.9979	0.0030
MIXCT5\mixct-005-c4	1.48E-07	4.533	0.030	389	1.0021	0.0028	0.9976	0.0006	0.9955	0.0029
MIXCT5\mixct-005-c5	1.092E-07	7.270	0.030	624	1.0026	0.0036	1.0024	0.0005	0.9998	0.0036
MIXCT5\mixct-005-c6	9.453E-08	10.117	0.030	868	1.0033	0.0042	1.0017	0.0005	0.9984	0.0042
MIXCT5\mixct-005-c7	9.029E-08	11.587	0.030	994	1.0035	0.0042	1.0034	0.0004	0.9999	0.0042
MIXCT6\mixct-006-c01	3.81E-07	1.515	0.019	186	1.0016	0.0051	0.9897	0.0006	0.9881	0.0051
MIXCT6\mixct-006-c02	1.98E-07	2.488	0.019	305	1.0017	0.0036	0.9951	0.0006	0.9934	0.0037
MIXCT6\mixct-006-c03	1.44E-07	3.515	0.019	431	1.0026	0.0036	0.9920	0.0006	0.9894	0.0037
MIXCT6\mixct-006-c04	1.22E-07	4.397	0.019	540	1.0051	0.0044	0.9985	0.0006	0.9934	0.0044
MIXCT6\mixct-006-c05	9.97E-08	6.282	0.019	771	1.004	0.0054	1.0008	0.0005	0.9968	0.0054
MIXCT6\mixct-006-c06	9.41E-08	7.054	0.019	866	1.0055	0.0051	0.9988	0.0005	0.9933	0.0051
MIXCT6\mixct-006-c07	1.43E-07	3.515	0.019	431	1.0024	0.0045	0.9899	0.0006	0.9875	0.0045
MIXCT6\mixct-006-c13	1.43E-07	3.515	0.019	431	1.0021	0.0044	0.9879	0.0006	0.9858	0.0044
MIXCT6\mixct-006-c14	1.44E-07	3.515	0.019	431	1.0026	0.0044	0.9869	0.0006	0.9843	0.0044
MIXCT6\mixct-006-c15	1.44E-07	3.515	0.019	431	1.0033	0.0044	0.9877	0.0006	0.9844	0.0044
MIXCT6\mixct-006-c16	1.44E-07	3.515	0.019	431	1.0035	0.0045	0.9868	0.0006	0.9833	0.0045
MIXCT6\mixct-006-c29	9.91E-08	6.282	0.019	771	1.004	0.0087	0.9948	0.0005	0.9908	0.0087
MIXCT6\mixct-006-c35	9.96E-08	6.282	0.019	771	1.0044	0.0087	0.9926	0.0005	0.9882	0.0087
MIXCT6\mixct-006-c36	9.95E-08	6.282	0.019	771	1.0036	0.0087	0.9929	0.0005	0.9893	0.0087
MIXCT6\mixct-006-c37	9.96E-08	6.282	0.019	771	1.0041	0.0087	0.9921	0.0005	0.9880	0.0087



MFFP Safety Analysis Report

Docket No. 71-9295
Revision 1, January 2005

Case Name	EALF (MeV)	v_m/v_f	$\frac{^{239}\text{Pu}}{(\text{U}+\text{Pu})}$	$\frac{\text{H}}{(^{239}\text{Pu} + ^{235}\text{U})}$	k_{ben}	σ_{bench}	k_{MCNP}	σ_{MCNP}	k_{MCNP} (normalized)	σ_{tot}
MIXCT6\mixct-006-c38	9.98E-08	6.282	0.019	771	1.0044	0.0087	0.9915	0.0005	0.9872	0.0087
MIXCT7\mixct-007-c1	1.96E-07	2.488	0.016	337	1.0023	0.0035	0.9981	0.0005	0.9958	0.0035
MIXCT7\mixct-007-c2	1.418E-07	3.515	0.016	476	1.0024	0.0039	0.9949	0.0005	0.9926	0.0039
MIXCT7\mixct-007-c3	1.195E-07	4.397	0.016	596	1.0036	0.0046	0.9975	0.0005	0.9940	0.0046
MIXCT7\mixct-007-c4	9.755E-08	6.282	0.016	850	1.0037	0.0057	0.9973	0.0004	0.9936	0.0057
MIXCT7\mixct-007-c5	9.255E-08	7.054	0.016	955	1.0044	0.0061	0.9970	0.0004	0.9927	0.0061
MIXCT7\mixct-007-ca1	1.404E-07	3.515	0.016	476	1.0024	0.0045	0.9934	0.0005	0.9911	0.0045
MIXCT7\mixct-007-cb1	1.417E-07	3.515	0.016	476	1.0024	0.0044	0.9898	0.0005	0.9874	0.0044
MIXCT7\mixct-007-cb2	1.419E-07	3.515	0.016	476	1.0026	0.0044	0.9910	0.0005	0.9884	0.0044
MIXCT7\mixct-007-cb3	1.414E-07	3.515	0.016	476	1.0027	0.0044	0.9919	0.0005	0.9892	0.0044
MIXCT7\mixct-007-cb4	1.41E-07	3.515	0.016	476	1.0025	0.0044	0.9932	0.0005	0.9907	0.0044
MIXCT8\mixct-008-c1	4.028E-07	1.515	0.014	223	0.9997	0.0032	0.9909	0.0006	0.9912	0.0033
MIXCT8\mixct-008-c2	2.009E-07	2.488	0.014	366	1.0008	0.003	0.9938	0.0006	0.9930	0.0031
MIXCT8\mixct-008-c3	1.442E-07	3.515	0.014	517	1.0023	0.0038	0.9946	0.0006	0.9923	0.0038
MIXCT8\mixct-008-c4	1.211E-07	4.397	0.014	647	1.0015	0.0047	0.9979	0.0005	0.9964	0.0047
MIXCT8\mixct-008-c5	9.875E-08	6.282	0.014	924	1.0022	0.0056	0.9995	0.0005	0.9973	0.0056
MIXCT8\mixct-008-c6	9.344E-08	7.054	0.014	1038	1.0028	0.0065	0.9992	0.0005	0.9964	0.0065
MIXCT8\mixct-008-ca1	1.434E-07	3.515	0.014	517	1.0023	0.0039	0.9933	0.0006	0.9910	0.0039
MIXCT8\mixct-008-cb1	1.447E-07	3.515	0.014	517	1.0023	0.0039	0.9911	0.0005	0.9889	0.0039
MIXCT8\mixct-008-cb2	1.448E-07	3.515	0.014	517	1.0023	0.0039	0.9923	0.0006	0.9901	0.0039
MIXCT8\mixct-008-cb3	1.439E-07	3.515	0.014	517	1.0023	0.0039	0.9925	0.0006	0.9902	0.0039
MIXCT8\mixct-008-cb4	1.435E-07	3.515	0.014	517	1.0023	0.0039	0.9921	0.0006	0.9898	0.0039
MIXCT9\mixct-009-c1	5.586E-07	1.111	0.014	228	1.0003	0.0054	0.9938	0.0006	0.9935	0.0054
MIXCT9\mixct-009-c2	3.131E-07	1.569	0.014	321	1.002	0.0049	0.9904	0.0006	0.9884	0.0049
MIXCT9\mixct-009-c3	1.602E-07	2.718	0.014	556	1.0035	0.005	0.9923	0.0006	0.9888	0.0050

Case Name	EALF (MeV)	v_m/v_f	$\frac{^{239}\text{Pu}}{(\text{U}+\text{Pu})}$	$\frac{\text{H}}{(^{239}\text{Pu} + ^{235}\text{U})}$	k_{ben}	σ_{bench}	k_{MCNP}	σ_{MCNP}	k_{MCNP} (normalized)	σ_{tot}
MIXCT9\mixct-009-c4	1.203E-07	3.800	0.014	778	1.0046	0.0062	0.9929	0.0005	0.9883	0.0062
MIXCT9\mixct-009-c5	9.804E-08	5.155	0.014	1055	1.0059	0.0074	0.9961	0.0005	0.9902	0.0074
MIXCT9\mixct-009-c6	9.336E-08	5.593	0.014	1145	1.0067	0.008	0.9974	0.0005	0.9908	0.0080
MIXFAST\mixmf-008-c1	0.03351	na	0.951	0	0.992	0.0063	1.0023	0.0011	1.0104	0.0064
MIXFAST\mixmf-008-c2	0.32584	na	0.951	0	1.001	0.0023	1.0147	0.0010	1.0137	0.0025
MIXFAST\mixmf-008-c3	0.084968	na	0.951	0	0.986	0.0044	0.9682	0.0010	0.9819	0.0045
MIXFAST\mixmf-008-c4	0.17542	na	0.951	0	0.973	0.0045	0.9830	0.0009	1.0103	0.0046
MIXFAST\mixmf-008-c5	0.27435	na	0.951	0	1.006	0.0069	0.9989	0.0009	0.9929	0.0070
MIXFAST\mixmf-008-c6	0.027577	na	0.223	0	0.971	0.0042	0.9744	0.0009	1.0035	0.0043
MIXFAST\pumf-033-c1	0.40279	na	0.493	0	0.9967	0.0026	0.9992	0.0005	1.0025	0.0026

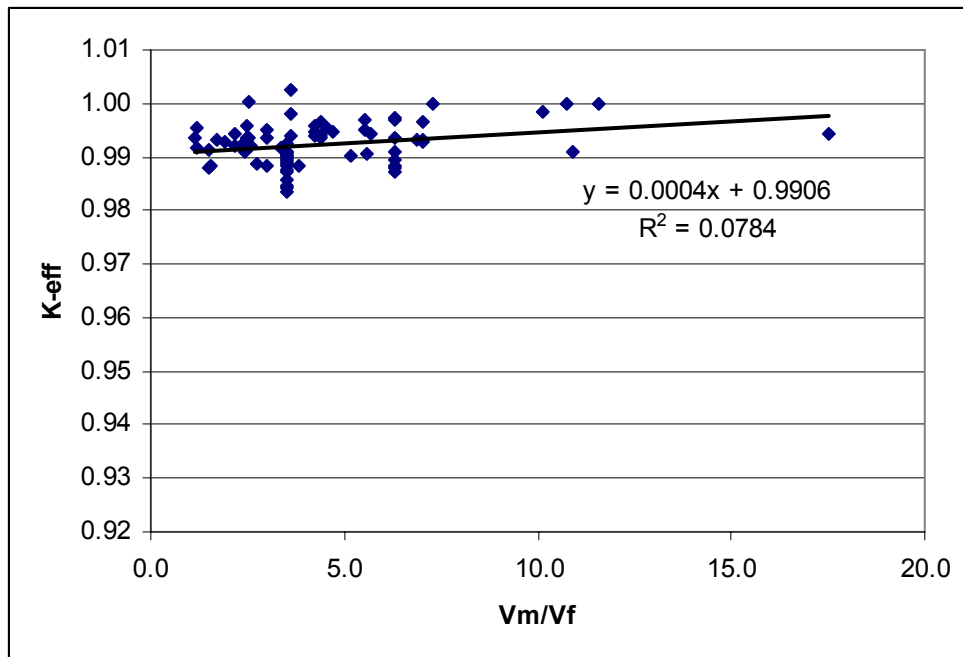


Figure 6.8-1 – Benchmark Data Trend for V_m/V_f

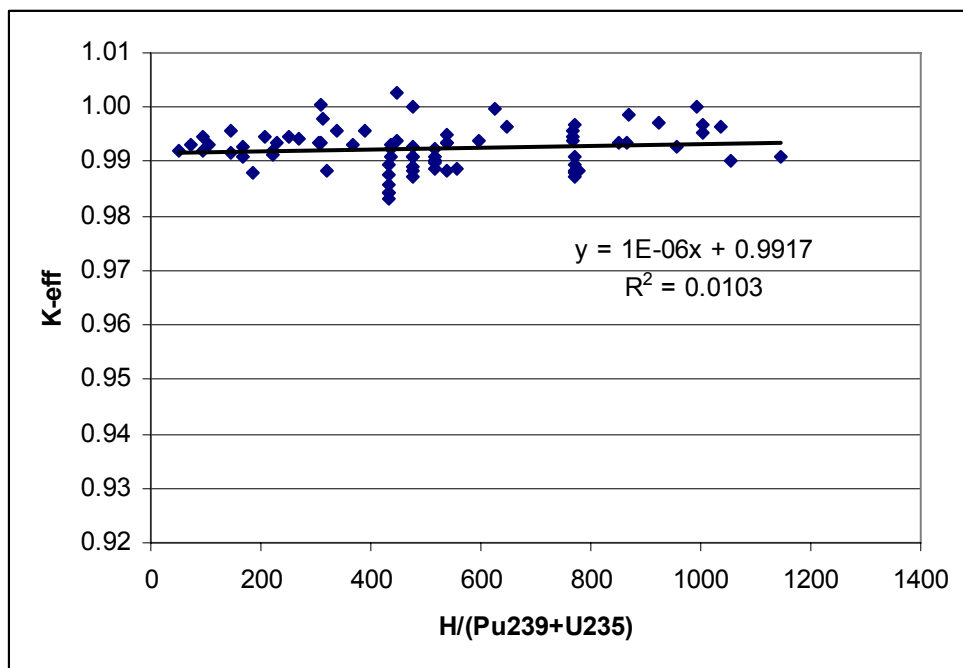


Figure 6.8-2 – Benchmark Data Trend for $H/(\text{Pu-239}+\text{U-235})$

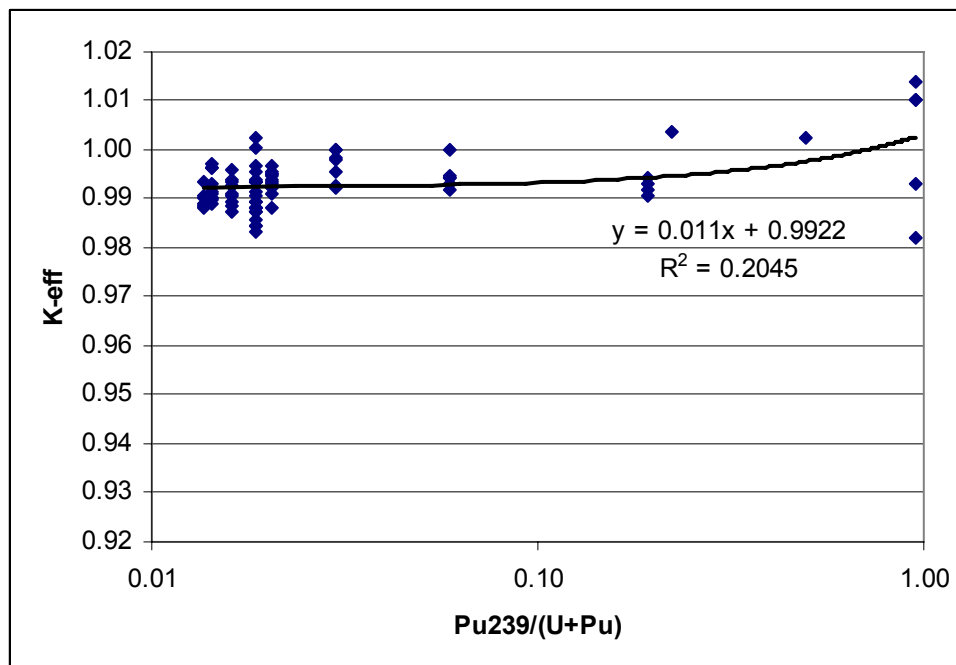


Figure 6.8-3 – Benchmark Data Trend for Pu-239/(U+Pu)

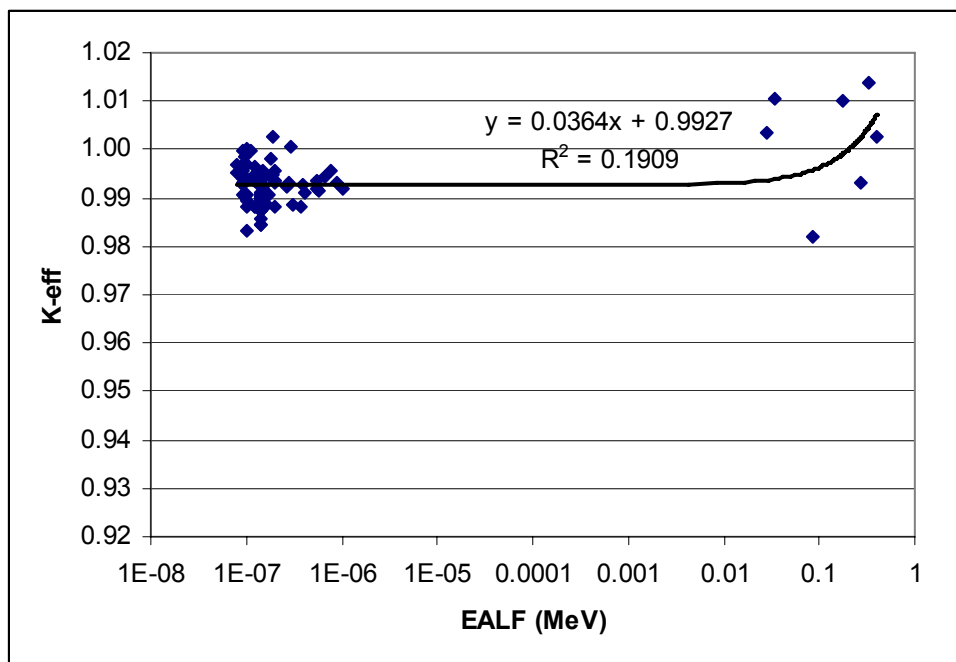


Figure 6.8-4 – Benchmark Data Trend for EALF

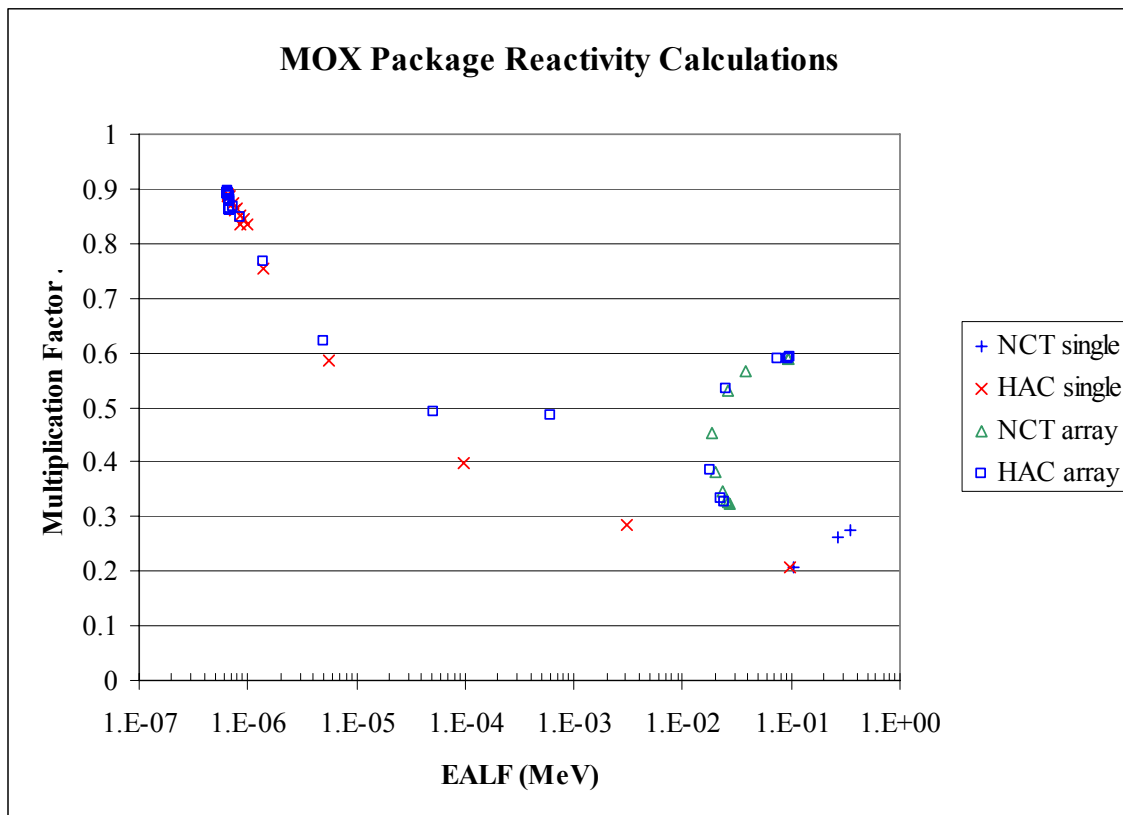


Figure 6.8-5 – Correlation of the MFFP Reactivity to EALF

This page left intentionally blank.

6.9 Appendices

Representative MCNP models are included in the following appendices:

6.9.1 Single Package Model

6.9.2 Infinite Array Model

This page left intentionally blank.

6.9.1 Single Package Model

This file is for the worst-case HAC model (max_hac_single_sul). Other files may be generated by adjusting the water density in the desired cells and modifying the pin pitch to the desired value.

```

MOX package max single conditions with 10.85 g/cc Fuel no Nb
c
c *****Fuel Assembly*****
c cells 1 to 3 transform the 3 assemblies to their locations
c 1 4 -1.0 -21 22 -23 24 -25 6 imp:n=1 $ top nozzle, void
c 2 4 -1.0 -21 22 -23 24 -7 26 imp:n=1 $ bottom nozzle, void
c 7 0 -21 22 -23 24 126 -25 fill=20 imp:n=1 $ pins
c
c 201 like 1 but trcl=53 $ assembly 2
c 202 like 2 but trcl=53
c 207 like 7 but trcl=53
c 220 like 1 but trcl=54 $ assembly 3
c 221 like 2 but trcl=54
c 222 like 7 but trcl=54
c
c -- "box" around fuel
c
c 301 0 (302 -303 300 -304 -906 26):
c (303 -305 300 -301 -906 26) fill=30 imp:n=1 $ "box" cutout
c 302 like 301 but trcl=53
c 303 like 301 but trcl=54
c
c perimeter containing strongback #1 in -y
c 50 0 (26 -906 902 -909 904 -910):
c (26 -906 909 -912 904 -901):
c (26 -906 912 904 -908):
c (26 -906 911 905 -904 -908):
c (26 -906 905 -900 903 -911) fill=7 imp:n=1
c perimeter containing strongback #2
c 51 like 50 but trcl=53
c perimeter containing strongback #3
c 52 like 50 but trcl=54
c
c *****water beyond three units*****
c 131 9 -1.4 -61 -69 64 #7 #50 #51 #52 #301 #302 #303
c #207 #222 imp:n=1
c
c *****containment*****
c 141 5 -7.94 -62 -66 63 (61:65:-64) imp:n=1 $ outer steel
c 143 5 -7.94 -61 -70 69 imp:n=1 $ upper inner steel
c 145 4 -1.0 -61 -65 70 imp:n=1 $ upper void
c
c *****beyond containment*****
c 195 6 -7.94 -72 -76 73 (62:66:-63) imp:n=0.25 $ one foot refl
c 199 0 (72:76:-73) imp:n=0 $ outside world
c
c Universe 20: Fuel Lattice
c
c 200 4 -1.0 -12 11 -14 13 u=20 lat=1 trcl=30 fill=0:16 0:16 0:0
c 1 1 1 1 1 1 1 1 1 1 1 1 1 1 1 1 $ row 17
c 1 1 1 1 1 1 1 1 1 1 1 1 1 1 1 1 $ row 16
c 1 1 1 1 1 4 1 1 4 1 1 4 1 1 1 1 $ row 15
c 1 1 1 4 1 1 1 1 1 1 1 1 4 1 1 1 $ row 14
c 1 1 1 1 1 1 1 1 1 1 1 1 1 1 1 1 $ row 13
c 1 1 4 1 1 4 1 1 4 1 1 4 1 1 4 1 $ row 12
c 1 1 1 1 1 1 1 1 1 1 1 1 1 1 1 1 $ row 11
c 1 1 1 1 1 1 1 2 2 2 1 1 1 1 1 1 $ row 10
c 1 1 4 1 1 4 1 2 4 2 1 4 1 1 4 1 $ row 9
c 1 1 1 1 1 1 1 2 2 2 1 1 1 1 1 1 $ row 8
c 1 1 1 1 1 1 1 1 1 1 1 1 1 1 1 1 $ row 7
c 1 1 4 1 1 4 1 1 4 1 1 4 1 1 4 1 $ row 6
c 1 1 1 1 1 1 1 1 1 1 1 1 1 1 1 1 $ row 5
c 1 1 4 1 1 1 1 1 1 1 1 1 4 1 1 1 $ row 4
c 1 1 1 1 1 4 1 1 4 1 1 4 1 1 1 1 $ row 3
c 1 1 1 1 1 1 1 1 1 1 1 1 1 1 1 1 $ row 2
c 1 1 1 1 1 1 1 1 1 1 1 1 1 1 1 1 imp:n=1 $ row 1 (top)
c
c Universe 1: Fuel pin in normal position

```

```

c
10 1 -10.85 -1 -4 5 u=1 imp:n=1 $ fuel
11 4 -1.0 -2 1 -4 5 u=1 imp:n=1 $ radial gap
12 7 -6.5 -3 2 -8 5 u=1 imp:n=1 $ clad
13 4 -1.0 3 7 -6 u=1 imp:n=1 $ radially beyond pin
14 4 -1.0 -2 -8 4 u=1 imp:n=1 $ above fuel void
15 7 -6.5 -3 -6 8 u=1 imp:n=1 $ top of fuel cap
16 7 -6.5 -3 -5 7 u=1 imp:n=1 $ bottom of fuel cap
17 4 -1.0 6 u=1 imp:n=1 $ top water to infinity
18 4 -1.0 -7 u=1 imp:n=1 $ bottom water to infinity
c
c Universe 2: Fuel pin shifted up
c
410 1 -10.85 -1 -4 5 trcl=(0 0 23.7109) u=2 imp:n=1 $ fuel
411 4 -1.0 -2 1 -4 5 trcl=(0 0 23.7109) u=2 imp:n=1 $ radial gap
412 7 -6.5 -3 2 -8 5 trcl=(0 0 23.7109) u=2 imp:n=1 $ clad
413 4 -1.0 3 7 -6 trcl=(0 0 23.7109) u=2 imp:n=1 $ radially beyond pin
414 4 -1.0 -2 -8 4 trcl=(0 0 23.7109) u=2 imp:n=1 $ above fuel void
415 7 -6.5 -3 -6 8 trcl=(0 0 23.7109) u=2 imp:n=1 $ top of fuel cap
416 7 -6.5 -3 -5 7 trcl=(0 0 23.7109) u=2 imp:n=1 $ bottom of fuel cap
417 4 -1.0 6 trcl=(0 0 23.7109) u=2 imp:n=1 $ top water to infinity
418 4 -1.0 -7 trcl=(0 0 23.7109) u=2 imp:n=1 $ bottom water to
infinity
c
c Universe 3: Fuel pin shifted down
c
420 1 -10.85 -1 -4 5 trcl=(0 0 -9.4361) u=3 imp:n=1 $ fuel
421 4 -1.0 -2 1 -4 5 trcl=(0 0 -9.4361) u=3 imp:n=1 $ radial gap
422 7 -6.5 -3 2 -8 5 trcl=(0 0 -9.4361) u=3 imp:n=1 $ clad
423 4 -1.0 3 7 -6 trcl=(0 0 -9.4361) u=3 imp:n=1 $ radially beyond pin
424 4 -1.0 -2 -8 4 trcl=(0 0 -9.4361) u=3 imp:n=1 $ above fuel void
425 7 -6.5 -3 -6 8 trcl=(0 0 -9.4361) u=3 imp:n=1 $ top of fuel cap
426 7 -6.5 -3 -5 7 trcl=(0 0 -9.4361) u=3 imp:n=1 $ bottom of fuel cap
427 4 -1.0 6 trcl=(0 0 -9.4361) u=3 imp:n=1 $ top water to infinity
428 4 -1.0 -7 trcl=(0 0 -9.4361) u=3 imp:n=1 $ bottom water to infinity
c
c Universe 4: Instrument/guide tube
c
41 4 -1.0 -18 5 -8 u=4 imp:n=1 $ inside
42 7 -6.5 -19 18 5 -8 u=4 imp:n=1 $ tube
43 4 -1.0 19 5 -8 u=4 imp:n=1 $ beyond tube
44 4 -1.0 8 u=4 imp:n=1
45 4 -1.0 -5 u=4 imp:n=1
c
c Universe 14: Water only
c
46 4 -1.0 -998 u=14 imp:n=1
47 4 -1.0 998 u=14 imp:n=1
c
c Universe 7: Strongback
c
700 6 -7.94 715 -710 u=7 imp:n=1 $ tangential strongback
701 6 -7.94 (710 711 718):(-711 713) u=7 imp:n=1 $ radial strongback+bend
702 2 -2.713 714 -719 -716 u=7 imp:n=1 $ tan Al clad
703 21 9.2244E-02 719 -720 -716
730 731 732 733 734 735 736 737 738
739 740 741 742 743 744 745 746 747
750 751 752 753 754 755 756 757 758
759 760 761 762 763 764 765 766 767 u=7 imp:n=1 $ tangential boron
704 2 -2.713 720 -715 -716 u=7 imp:n=1 $ tan Al clad
706 2 -2.713 712 -722 -717 u=7 imp:n=1 $ rad Al clad
707 21 9.2244E-02 722 -723 -717
770 771 772 773 774 775 776 777 778
779 780 781 782 783 784 785 786 787
790 791 792 793 794 795 796 797 798
799 800 801 802 803 804 805 806 807 u=7 imp:n=1 $ radial boron
708 2 -2.713 723 -713 -717 u=7 imp:n=1 $ rad Al
710 4 -1.0 (710 711 -718):(-716 -710 717 -715):
(710 -713 717 -711) u=7 imp:n=1
719 6 -7.94 ((-717 -712):(-716 -714 717)) -809 u=7 imp:n=1 $ poison holder
720 4 -1.0 ((-717 -712):(-716 -714 717)) 809 -810 u=7 imp:n=1
721 6 -7.94 ((-717 -712):(-716 -714 717)) 810 -811 u=7 imp:n=1
722 4 -1.0 ((-717 -712):(-716 -714 717)) 811 -812 u=7 imp:n=1
723 6 -7.94 ((-717 -712):(-716 -714 717)) 812 -813 u=7 imp:n=1
724 4 -1.0 ((-717 -712):(-716 -714 717)) 813 -814 u=7 imp:n=1

```


725	6	-7.94	((-717 -712):(-716 -714 717))	814 -815	u=7	imp:n=1	
726	4	-1.0	((-717 -712):(-716 -714 717))	815 -816	u=7	imp:n=1	
727	6	-7.94	((-717 -712):(-716 -714 717))	816 -817	u=7	imp:n=1	
728	4	-1.0	((-717 -712):(-716 -714 717))	817 -818	u=7	imp:n=1	
729	6	-7.94	((-717 -712):(-716 -714 717))	818 -819	u=7	imp:n=1	
730	4	-1.0	((-717 -712):(-716 -714 717))	819 -820	u=7	imp:n=1	
731	6	-7.94	((-717 -712):(-716 -714 717))	820 -821	u=7	imp:n=1	
732	4	-1.0	((-717 -712):(-716 -714 717))	821 -822	u=7	imp:n=1	
733	6	-7.94	((-717 -712):(-716 -714 717))	822 -823	u=7	imp:n=1	
734	4	-1.0	((-717 -712):(-716 -714 717))	823 -824	u=7	imp:n=1	
735	6	-7.94	((-717 -712):(-716 -714 717))	824 -825	u=7	imp:n=1	
736	4	-1.0	((-717 -712):(-716 -714 717))	825 -826	u=7	imp:n=1	
737	6	-7.94	((-717 -712):(-716 -714 717))	826	u=7	imp:n=1	
c							
750	6	-7.94	719 -720 -750		u=7	imp:n=1	\$ screws in boral
751	6	-7.94	719 -720 -751		u=7	imp:n=1	
752	6	-7.94	719 -720 -752		u=7	imp:n=1	
753	6	-7.94	719 -720 -753		u=7	imp:n=1	
754	6	-7.94	719 -720 -754		u=7	imp:n=1	
755	6	-7.94	719 -720 -755		u=7	imp:n=1	
756	6	-7.94	719 -720 -756		u=7	imp:n=1	
757	6	-7.94	719 -720 -757		u=7	imp:n=1	
758	6	-7.94	719 -720 -758		u=7	imp:n=1	
759	6	-7.94	719 -720 -759		u=7	imp:n=1	
760	6	-7.94	719 -720 -760		u=7	imp:n=1	
761	6	-7.94	719 -720 -761		u=7	imp:n=1	
762	6	-7.94	719 -720 -762		u=7	imp:n=1	
763	6	-7.94	719 -720 -763		u=7	imp:n=1	
764	6	-7.94	719 -720 -764		u=7	imp:n=1	
765	6	-7.94	719 -720 -765		u=7	imp:n=1	
766	6	-7.94	719 -720 -766		u=7	imp:n=1	
767	6	-7.94	719 -720 -767		u=7	imp:n=1	
c							
770	6	-7.94	722 -723 -770		u=7	imp:n=1	
771	6	-7.94	722 -723 -771		u=7	imp:n=1	
772	6	-7.94	722 -723 -772		u=7	imp:n=1	
773	6	-7.94	722 -723 -773		u=7	imp:n=1	
774	6	-7.94	722 -723 -774		u=7	imp:n=1	
775	6	-7.94	722 -723 -775		u=7	imp:n=1	
776	6	-7.94	722 -723 -776		u=7	imp:n=1	
777	6	-7.94	722 -723 -777		u=7	imp:n=1	
778	6	-7.94	722 -723 -778		u=7	imp:n=1	
779	6	-7.94	722 -723 -779		u=7	imp:n=1	
780	6	-7.94	722 -723 -780		u=7	imp:n=1	
781	6	-7.94	722 -723 -781		u=7	imp:n=1	
782	6	-7.94	722 -723 -782		u=7	imp:n=1	
783	6	-7.94	722 -723 -783		u=7	imp:n=1	
784	6	-7.94	722 -723 -784		u=7	imp:n=1	
785	6	-7.94	722 -723 -785		u=7	imp:n=1	
786	6	-7.94	722 -723 -786		u=7	imp:n=1	
787	6	-7.94	722 -723 -787		u=7	imp:n=1	
c							
790	6	-7.94	722 -723 -790		u=7	imp:n=1	
791	6	-7.94	722 -723 -791		u=7	imp:n=1	
792	6	-7.94	722 -723 -792		u=7	imp:n=1	
793	6	-7.94	722 -723 -793		u=7	imp:n=1	
794	6	-7.94	722 -723 -794		u=7	imp:n=1	
795	6	-7.94	722 -723 -795		u=7	imp:n=1	
796	6	-7.94	722 -723 -796		u=7	imp:n=1	
797	6	-7.94	722 -723 -797		u=7	imp:n=1	
798	6	-7.94	722 -723 -798		u=7	imp:n=1	
799	6	-7.94	722 -723 -799		u=7	imp:n=1	
800	6	-7.94	722 -723 -800		u=7	imp:n=1	
801	6	-7.94	722 -723 -801		u=7	imp:n=1	
802	6	-7.94	722 -723 -802		u=7	imp:n=1	
803	6	-7.94	722 -723 -803		u=7	imp:n=1	
804	6	-7.94	722 -723 -804		u=7	imp:n=1	
805	6	-7.94	722 -723 -805		u=7	imp:n=1	
806	6	-7.94	722 -723 -806		u=7	imp:n=1	
807	6	-7.94	722 -723 -807		u=7	imp:n=1	
c							
810	6	-7.94	719 -720 -730		u=7	imp:n=1	
811	6	-7.94	719 -720 -731		u=7	imp:n=1	
812	6	-7.94	719 -720 -732		u=7	imp:n=1	
813	6	-7.94	719 -720 -733		u=7	imp:n=1	

```

814      6  -7.94      719 -720 -734      u=7  imp:n=1
815      6  -7.94      719 -720 -735      u=7  imp:n=1
816      6  -7.94      719 -720 -736      u=7  imp:n=1
817      6  -7.94      719 -720 -737      u=7  imp:n=1
818      6  -7.94      719 -720 -738      u=7  imp:n=1
819      6  -7.94      719 -720 -739      u=7  imp:n=1
820      6  -7.94      719 -720 -740      u=7  imp:n=1
821      6  -7.94      719 -720 -741      u=7  imp:n=1
822      6  -7.94      719 -720 -742      u=7  imp:n=1
823      6  -7.94      719 -720 -743      u=7  imp:n=1
824      6  -7.94      719 -720 -744      u=7  imp:n=1
825      6  -7.94      719 -720 -745      u=7  imp:n=1
826      6  -7.94      719 -720 -746      u=7  imp:n=1
827      6  -7.94      719 -720 -747      u=7  imp:n=1
c
c      Universe 30:  "box" around fuel
c
c 310      2  -2.713      -313 317      u=30 imp:n=1 $ radial left
c 311      2  -2.713      316 -310      u=30 imp:n=1 $ tangential bot
c 312      2  -2.713      314 -315 317 u=30 imp:n=1 $ radial right
c 315      2  -2.713      311 -312 316 u=30 imp:n=1 $ tangential top
316      6  -7.94      315 312      u=30 imp:n=1
317      4  -1.0      (312 -317 -315):(-316 -312) u=30 imp:n=1
c
320      4  -1.0      -315 317 -320      u=30 imp:n=1 $ radial water gap
321      21  9.2244E-02 313 -314 317 320 -321 u=30 imp:n=1 $ radial boral
322      4  -1.0      -315 317 321 -322 u=30 imp:n=1
323      21  9.2244E-02 313 -314 317 322 -323 u=30 imp:n=1
324      4  -1.0      -315 317 323 -324 u=30 imp:n=1
325      21  9.2244E-02 313 -314 317 324 -325 u=30 imp:n=1
326      4  -1.0      -315 317 325 -326 u=30 imp:n=1
327      21  9.2244E-02 313 -314 317 326 -327 u=30 imp:n=1
328      4  -1.0      -315 317 327 -328 u=30 imp:n=1
329      21  9.2244E-02 313 -314 317 328 -329 u=30 imp:n=1
330      4  -1.0      -315 317 329 -330 u=30 imp:n=1
331      21  9.2244E-02 313 -314 317 330 -331 u=30 imp:n=1
332      4  -1.0      -315 317 331 -332 u=30 imp:n=1
333      21  9.2244E-02 313 -314 317 332 -333 u=30 imp:n=1
334      4  -1.0      -315 317 333      u=30 imp:n=1
c
340      2  -2.713      -313 317 320 -321 u=30 imp:n=1 $ radial Al cladding
341      2  -2.713      -313 317 322 -323 u=30 imp:n=1
342      2  -2.713      -313 317 324 -325 u=30 imp:n=1
343      2  -2.713      -313 317 326 -327 u=30 imp:n=1
344      2  -2.713      -313 317 328 -329 u=30 imp:n=1
345      2  -2.713      -313 317 330 -331 u=30 imp:n=1
346      2  -2.713      -313 317 332 -333 u=30 imp:n=1
c
347      2  -2.713      314 -315 317 320 -321 u=30 imp:n=1 $ radial Al cladding
348      2  -2.713      314 -315 317 322 -323 u=30 imp:n=1
349      2  -2.713      314 -315 317 324 -325 u=30 imp:n=1
350      2  -2.713      314 -315 317 326 -327 u=30 imp:n=1
351      2  -2.713      314 -315 317 328 -329 u=30 imp:n=1
352      2  -2.713      314 -315 317 330 -331 u=30 imp:n=1
353      2  -2.713      314 -315 317 332 -333 u=30 imp:n=1
c
360      4  -1.0      -312 316 -320      u=30 imp:n=1 $ tangential water gap
361      21  9.2244E-02 310 -311 316 320 -321 u=30 imp:n=1 $ tangential boral
362      4  -1.0      -312 316 321 -322 u=30 imp:n=1
363      21  9.2244E-02 310 -311 316 322 -323 u=30 imp:n=1
364      4  -1.0      -312 316 323 -324 u=30 imp:n=1
365      21  9.2244E-02 310 -311 316 324 -325 u=30 imp:n=1
366      4  -1.0      -312 316 325 -326 u=30 imp:n=1
367      21  9.2244E-02 310 -311 316 326 -327 u=30 imp:n=1
368      4  -1.0      -312 316 327 -328 u=30 imp:n=1
369      21  9.2244E-02 310 -311 316 328 -329 u=30 imp:n=1
370      4  -1.0      -312 316 329 -330 u=30 imp:n=1
371      21  9.2244E-02 310 -311 316 330 -331 u=30 imp:n=1
372      4  -1.0      -312 316 331 -332 u=30 imp:n=1
373      21  9.2244E-02 310 -311 316 332 -333 u=30 imp:n=1
374      4  -1.0      -312 316 333      u=30 imp:n=1
c
380      2  -2.713      316 311 -312 320 -321 u=30 imp:n=1 $ horizontal Al cladding
381      2  -2.713      316 311 -312 322 -323 u=30 imp:n=1
382      2  -2.713      316 311 -312 324 -325 u=30 imp:n=1

```

```

383      2      -2.713      316 311 -312 326 -327 u=30 imp:n=1
384      2      -2.713      316 311 -312 328 -329 u=30 imp:n=1
385      2      -2.713      316 311 -312 330 -331 u=30 imp:n=1
386      2      -2.713      316 311 -312 332 -333 u=30 imp:n=1
c
387      2      -2.713      316 -310 320 -321 u=30 imp:n=1 $ horizontal Al cladding
388      2      -2.713      316 -310 322 -323 u=30 imp:n=1
389      2      -2.713      316 -310 324 -325 u=30 imp:n=1
390      2      -2.713      316 -310 326 -327 u=30 imp:n=1
391      2      -2.713      316 -310 328 -329 u=30 imp:n=1
392      2      -2.713      316 -310 330 -331 u=30 imp:n=1
393      2      -2.713      316 -310 332 -333 u=30 imp:n=1
c
c      Universe 51:  Dummy universe containing fuel
c
c      999      1 -10.31 -999 u=51      imp:n=1  $ for diagnostics only, not used
c      1000     1 -10.31  999 u=51      imp:n=1  $ for diagnostics only, not used
c
c      *****Fuel Assembly*****
c      fuel pin
1      cz      0.409575      $ fuel radius
2      cz      0.41783      $ radius inside clad
3      cz      0.47498      $ radius outside clad
4      pz      182.88      $ top of fuel
5      pz -182.88      $ bottom of fuel
6      pz      202.7555      $ top of fuel pin
7      pz -184.3405      $ bottom of fuel pin
8      pz      201.4474      $ bottom of top cap
11     px      -0.6688      $ lattice definition
12     px      0.6688
13     py      -0.6688
14     py      0.6688
c      200      pz      -119.38
c      guide tube
18     cz      0.57150
19     cz      0.61214
c      perimeter of fuel assembly
21     px      10.2391 $ offset from surface 905
22     px      -12.1116 $
23     py      -6.6593 $ offset from surface 904
24     py      -29.0113 $
25     pz      226.466
26     pz      -190.95720
126    pz      -193.776
c      *****containment*****
61     cz      36.1950
62     cz      37.6174
63     pz      -197.5866 $ 1.5" thick
64     pz      -193.7766 $ 1.11" below bottom of fuel (strongback bottom not modeled)
65     pz      235.6866
66     pz      237.5916
c      67     pz      -203.0222
c      68     pz      -201.1172
69     pz      226.4664
70     pz      228.0666
c      *****outside of water refl****
72     cz      68.0974
73     pz      -228.0666 $ 1' water from 63
76     pz      268.0716 $ 1' water from 66
c
c      -- "box"
c
300    py -29.7925 $ defining box in u=0
301    py -29.0114
302    px -12.8928
303    px -12.1117
304    py -7.5675
305    px  9.9672
c
310    25 py 0.04445
311    25 py 0.2604
312    25 py 0.3048
313    25 px 0.04445
314    25 px 0.2604
315    25 px 0.3048

```

```

316      25 px 2.54
317      25 py 2.54
c
320      pz -171.049
321      pz -119.532
322      pz -109.758
323      pz -67.412
324      pz -57.638
325      pz -15.316
326      pz -5.542
327      pz 36.855
328      pz 46.629
329      pz 89.002
330      pz 98.776
331      pz 141.097
332      pz 150.871
333      pz 193.548
c
c      strongback surfaces
c
710      22 px 0
711      22 py 0
712      22 px 0.476
713      22 px 0.7808
714      22 py 0.476
715      22 py 0.7808
716      22 px -0.3114 $ 0.43" less than surface 713
717      22 py -0.54
718      22 cz 0.7808
719      22 py 0.5205
720      22 py 0.7364
722      22 px 0.5205
723      22 px 0.7364
c
730      22 c/y -2.7752 -189.6872 0.47625
731      22 c/y -2.7752 -179.5526 0.47625
732      22 c/y -2.7752 -172.3187 0.47625
733      22 c/y -2.7752 -118.2624 0.47625
734      22 c/y -2.7752 -111.0285 0.47625
735      22 c/y -2.7752 -66.1416 0.47625
736      22 c/y -2.7752 -58.9077 0.47625
737      22 c/y -2.7752 -14.0462 0.47625
738      22 c/y -2.7752 -6.8123 0.47625
739      22 c/y -2.7752 38.1254 0.47625
740      22 c/y -2.7752 45.3593 0.47625
741      22 c/y -2.7752 90.2716 0.47625
742      22 c/y -2.7752 97.5055 0.47625
743      22 c/y -2.7752 142.3670 0.47625
744      22 c/y -2.7752 149.6009 0.47625
745      22 c/y -2.7752 194.8180 0.47625
746      22 c/y -2.7752 202.0519 0.47625
747      22 c/y -2.7752 213.8172 0.47625
c
750      22 c/y -16.7452 -189.6872 0.47625
751      22 c/y -16.7452 -179.5526 0.47625
752      22 c/y -16.7452 -172.3187 0.47625
753      22 c/y -16.7452 -118.2624 0.47625
754      22 c/y -16.7452 -111.0285 0.47625
755      22 c/y -16.7452 -66.1416 0.47625
756      22 c/y -16.7452 -58.9077 0.47625
757      22 c/y -16.7452 -14.0462 0.47625
758      22 c/y -16.7452 -6.8123 0.47625
759      22 c/y -16.7452 38.1254 0.47625
760      22 c/y -16.7452 45.3593 0.47625
761      22 c/y -16.7452 90.2716 0.47625
762      22 c/y -16.7452 97.5055 0.47625
763      22 c/y -16.7452 142.3670 0.47625
764      22 c/y -16.7452 149.6009 0.47625
765      22 c/y -16.7452 194.8180 0.47625
766      22 c/y -16.7452 202.0519 0.47625
767      22 c/y -16.7452 213.8172 0.47625
c
770      22 c/x -5.9248 -189.6872 0.47625
771      22 c/x -5.9248 -179.5526 0.47625
772      22 c/x -5.9248 -172.3187 0.47625

```

```

773 22 c/x -5.9248 -118.2624 0.47625
774 22 c/x -5.9248 -111.0285 0.47625
775 22 c/x -5.9248 -66.1416 0.47625
776 22 c/x -5.9248 -58.9077 0.47625
777 22 c/x -5.9248 -14.0462 0.47625
778 22 c/x -5.9248 -6.8123 0.47625
779 22 c/x -5.9248 38.1254 0.47625
780 22 c/x -5.9248 45.3593 0.47625
781 22 c/x -5.9248 90.2716 0.47625
782 22 c/x -5.9248 97.5055 0.47625
783 22 c/x -5.9248 142.3670 0.47625
784 22 c/x -5.9248 149.6009 0.47625
785 22 c/x -5.9248 194.8180 0.47625
786 22 c/x -5.9248 202.0519 0.47625
787 22 c/x -5.9248 213.8172 0.47625
c
790 22 c/x -16.9789 -189.6872 0.47625
791 22 c/x -16.9789 -179.5526 0.47625
792 22 c/x -16.9789 -172.3187 0.47625
793 22 c/x -16.9789 -118.2624 0.47625
794 22 c/x -16.9789 -111.0285 0.47625
795 22 c/x -16.9789 -66.1416 0.47625
796 22 c/x -16.9789 -58.9077 0.47625
797 22 c/x -16.9789 -14.0462 0.47625
798 22 c/x -16.9789 -6.8123 0.47625
799 22 c/x -16.9789 38.1254 0.47625
800 22 c/x -16.9789 45.3593 0.47625
801 22 c/x -16.9789 90.2716 0.47625
802 22 c/x -16.9789 97.5055 0.47625
803 22 c/x -16.9789 142.3670 0.47625
804 22 c/x -16.9789 149.6009 0.47625
805 22 c/x -16.9789 194.8180 0.47625
806 22 c/x -16.9789 202.0519 0.47625
807 22 c/x -16.9789 213.8172 0.47625
c
809 pz -188.417
810 pz -181.331 $ PH 1 (bottom)
811 pz -170.541 $ PH 1
812 pz -120.040 $ PH 2
813 pz -109.250
814 pz -67.920 $ PH 3
815 pz -57.130
816 pz -15.824 $ PH 4
817 pz -5.034
818 pz 36.347 $ PH 5
819 pz 47.137
820 pz 88.494 $ PH 6
821 pz 99.284
822 pz 140.589 $ PH 7
823 pz 151.379
824 pz 193.040 $ PH 8
825 pz 203.830 $ PH 8
826 pz 212.547
c
900 px 11.18006 $ FIXED for strongbacks touching
901 py -5.71956 $ FIXED for strongbacks touching
902 px -11.9593
903 py -28.7574 $ surface 901 minus 9.07"
c
c 904 is -7.1354 and 905 is 9.7633 for nominal case (with poison holders).
c they are shifted to cut off poison holders to allow for
c expansion for damaged cases.
c
c To completely "slice off" the poison holders, set
c 904 to -6.6593 and 905 to 10.2392.
c
904 py -6.6593 $ tangential strongback lower bound, surface 901 minus total thickness
905 px 10.2392 $ radial strongback left bound, surface 901 minus total thickness
906 pz 215.7222
908 c/z 9.87856 -7.02106 1.3015
909 px -9.9019
910 py -6.35448
911 py -7.1344 $ fixed
912 px 9.7653 $ fixed
c

```

```

998      so  10000
999      pz  345.5565

mode     n
c        print
kcode    2000  1 30  530
ksrc      -16.08  10.4  0
           17.82   7.67  0
           0.55 -17.81  0
cut:n     j j 0 0
c
c        Materials
c
m1      92235      -0.249    $ fuel pellet
        92238      -82.615
        94239      -4.972
        94240      -0.264
        94241      -0.053
        8016      -11.847
m2      13027      1.0      $ aluminum cladding for BORAL
m4      1001       2        $ water
        8016       1
mt4     lwtr.01t
m5      6000      -0.06     $ XM-19
        7014      -0.4
        14000     -0.75
        15031     -0.04
        16032     -0.03
        23000     -0.3
        24000     -23.5
        25055     -6
        28000     -13.5
        41093     -0.3
        42000     -3
        26000     -52.12
m6      6000      -0.08     $ SS-304
        14000     -1.0
        15031     -0.045
        24000     -19.0
        25055     -2.0
        26000     -68.375
        28000     -9.5
m7      40000     -1.0     $ Cladding
c        41093     -0.030
m8      82000      1.0      $ lead
m9      6000      -25.1     $ water/steel mix, 5.8% steel by volume
        14000     -313.9
        15031     -14.1
        24000     -5964.9
        25055     -627.9
        26000     -21465.8
        28000     -2982.5
        1001      -7240.1
        8016      -57462.7
mt9     lwtr.01t
m21     5010      7.3123E-03 $ 35 mg/cm2 B-10, 75% credit
        5011      3.9244E-02
        6000      1.2248E-02
        13027     3.3439E-02
c        total 9.2244E-02
c
c        Translations
c
c        tr22 is the intersection of planes 904 and 905
c        when the poison holders are present (904 and 905 shift when it is
c        desired to "slice off" the poison holders).
c        Note that the origin of Universe 7 corresponds to the intersection
c        of these planes.
c
*tr22    9.7643 -7.1354 0.0
c
c        tr25 is the intersection of planes 300 and 302. The origin of Universe 30
c        corresponds to the intersection of these planes.
c
*tr25   -12.8928 -29.7925 0.0

```

```
c
c      tr30 is computed by taking the coordinates of the intersection of planes
c      22 and 24 and adding half the pitch (note: can't be exact or else planes will
c      overlap, causing program termination.)
c
*tr30  -11.6368 -28.5365 0.0
c
c      tr53 and tr54 rotate the bottom assembly to create assemblies 2 and 3
c
*tr53  0 0 0           120 30 90   150 120 90   90 90 0 $ +x+y
*tr54  0 0 0           120 150 90   30 120 90   90 90 0 $ -x-y
```


This page left intentionally blank.

6.9.2 Infinite Array Model

The infinite array models are geometrically the same as the single package models, although small changes have been made to the outer boundary to simulate the infinite array. Additional cells and surfaces are listed below.

```

195      0      -881 882 -886 885 -883 884 -66 63 62  imp:n=1 $ w between packages
199      0      (881:-882:886:-885:883:-884:66:-63)  imp:n=0 $ outside world

c      hexagonal boundary of one unit lattice cell, close packed
*881    px      37.6184
*882    px     -37.6184
*883    p     -0.5000000      0.866025404      0.0000000      37.6184
*884    p     -0.5000000      0.866025404      0.0000000     -37.6184
*885    p      0.5000000      0.866025404      0.0000000     -37.6184
*886    p      0.5000000      0.866025404      0.0000000      37.6184

```

This page left intentionally blank.

7.0 PACKAGE OPERATIONS

This chapter delineates the procedures for loading a payload into the MOX Fresh Fuel Package (MFFP), and leakage rate testing of the containment boundary O-ring seals. The MFFP is designed such that both lid insertion/removal and strongback insertion/removal may be performed either horizontally or vertically. The operational steps provided in this chapter address both loading/unloading options.

A variety of auxiliary equipment is utilized in the loading and unloading operations. While this equipment is not included in the transportation license for the package, a listing of the equipment and its function is provided below for clarity.

Air Pallet – Device used to move the MFFP when attached to the skid.

Package Connection Collar – Locating collar on the base of the insertion/extraction station. Package is aligned with and attached to the connection collar. (Used only for horizontal operations.)

Handling Lift Equipment – Equipment used to lift the MFFP (with attached transport skid).

Insertion/Extraction Station – Device used to insert and remove the strongback from the package. (Used only for horizontal operations.)

Lid Handling Fixture – Fixture that bolts to the package lid to assist in lid attachment/removal operations. (Used only for horizontal operations.)

Load/Unload Station – Device into which the strongback is installed when being loaded/unloaded with a fuel assembly.

Sealing Surface Protector – Device that attaches to the seal flange and protects the sealing surface during strongback loading/unloading operations.

Strongback Lift Tool – Tool that attaches to the top of the strongback for vertical transfer.

Top Plate Lifting Assembly – Lifting equipment used to remove the strongback top plate assembly.

Upending Frame – Device used to transfer the MFFP (with attached transport skid) between horizontal and vertical orientations. (Used only for vertical operations.)

Wall Mount Fixture – Fixture to which the upending frame attaches when the MFFP (with attached transport skid) is in the vertical orientation. (Used only for vertical operations.)

7.1 Package Loading

This section delineates the procedures for loading a payload into the MFFP. Hereafter, reference to specific MFFP components may be found in Appendix 1.4.2, *Packaging General Arrangement Drawings*. Note that the steps provided in the following sections may be performed in any logical sequence.

The loading operation shall be performed in a dry environment. If precipitation enters the cavity, the free-standing water shall be removed prior to loading the payload.

7.1.1 Preparation for Loading

7.1.1.1 Removal of MFFP from the Transport Conveyance

1. Disengage the tie-down devices from the shipping skid and the transport conveyance.
CAUTION: Failure to disengage the tie-down devices may result in damage to the packaging, shipping skid, and/or the transport conveyance.
2. Using an air pallet or other lifting equipment, remove the MFFP/shipping skid from the transport conveyance and move to the loading area.
3. Remove the air pallet or other lifting equipment

7.1.1.2 Removal of the Closure Lid

7.1.1.2.1 Horizontal Operations

1. Remove the six (6) 1-inch socket head cap screws (SHCS) from the lid end impact limiter.
2. Utilizing appropriate lifting equipment, carefully lift and remove the lid end impact limiter and place in a secure area.
3. If necessary, repeat Steps 1 and 2 for the bottom end impact limiter.
4. Vent the interior of the MFFP through the lid end vent plug.
5. Loosen and / or remove the twenty-four (24) 3/4-inch SHCS attaching the lid to the package body. Ensure the lid remains in place on the body.
6. Utilizing four (4) 1/2-inch hex bolts, secure the lid handling fixture to the closure lid. Tighten the hex bolts to snug tight condition. Ensure any of the lid attachment fasteners that are covered by the lid handling fixture are removed prior to installing the lid handling fixture.
7. Connect appropriate lifting equipment to the lid handling fixture.
8. Remove any of the twenty-four (24) 3/4-inch SHCS not already removed in Steps 5 or 6 and carefully remove the closure lid with the lifting equipment and lid handling fixture. If necessary, the three T-handle assemblies on the lid handling fixture or three (3) 1/2-inch-13 x 2-inch bolts may be utilized in the three equally-spaced holes marked "for lid handling only" to assist in breaking the seal of the closure lid. Care shall be taken to not damage the MFFP containment seal surfaces.
9. Store the closure lid in a manner such that potential damage to the O-ring seals and sealing surfaces is minimized.

7.1.1.2.2 Vertical Operations

1. Attach the handling lift equipment, using the shackles on the support skid, in preparation for lifting the MFFP. Ensure the handling lift equipment "Lid End" is oriented toward the lid end of the MFFP.
2. Lift and place the MFFP with attached transport skid into the upending frame.
3. Secure the MFFP to the upending frame with both the ball lock pins and the tie-down straps.
4. Remove the six (6) 1-inch socket head cap screws (SHCS) from the lid end impact limiter.

5. Utilizing appropriate lifting equipment, carefully lift and remove the lid end impact limiter and place in a secure area.
6. Vent the interior of the MFFP through the lid end vent plug.
7. Loosen the twenty-four (24), 3/4-inch SHCS attaching the lid to the package body. This step may also be performed following Step 8.
8. Ensure the upending frame lift arm is positioned with the lift point aligned with the approximate MFFP centerline and that attachment fasteners are snug tight. Using appropriate lifting equipment, rotate the upending frame with attached MFFP and skid to the vertical orientation. Transfer the upending frame to the location of the wall mount fixture and secure in place.
9. Rotate or remove the upending frame lift arm from the lifting position to the unloading (vertical) position.
10. Remove the twenty-four (24), 3/4-inch SHCS loosened in Step 7. If necessary, three (3) 1/2-inch-13 x 2 inch bolts may be utilized in the three equally-spaced holes marked "for lid handling only" to assist in breaking the seal of the closure lid.
11. Install three (3) swivel hoist rings with 1/2-inch-13 threads and rated load of at least 170 lb_f into the three (3) equally spaced threaded holes labeled "For Lid Handling Only". Carefully remove the closure lid with the appropriate lifting equipment.
12. Store the closure lid in a manner such that potential damage to the O-ring seals and sealing surfaces is minimized.

7.1.1.3 Removal of the Strongback from the MFFP

7.1.1.3.1 Horizontal Operations

1. Install the sealing surface protector on the MFFP seal flange.
NOTE: The sealing surface protector orientation is labeled along the edge. Correct orientation is required for correct interfacing with the insertion/extraction station.
2. Align the MFFP body and connect to the insertion/extraction station.
3. Insert the attachment bar of the insertion/extraction station into the center hole on the top plate of the strongback.
4. Remove the three (3) 1/2-inch SHCS that secure the strongback to the body.
5. Remove the strongback from the body using the insertion/extraction station. Care shall be taken to not damage the MFFP containment sealing surfaces.
6. Disconnect the MFFP body from the insertion/extraction station and move the MFFP body away from the insertion/extraction station.
7. Visually inspect the following components for wear or damage that could impair their function and, if necessary, replace or repair per the requirements of the drawings in Appendix 1.4.2, *Packaging General Arrangement Drawings*.
 - a. Strongback
 - b. Fuel control structures (FCSs)

- c. Neutron absorber plates on strongback and FCSs
- 8. Ensure the strongback restraint arms on the insertion/extraction station are closed and latched. Connect appropriate lifting equipment to the uprighting attachment point.
- 9. Upend the strongback and insertion/extraction station. After uprighting, fix the insertion/extraction station in the upright position using the installed struts.
- 10. Lower the strongback and disconnect the insertion/extraction attachment bar from the strongback. Install the strongback lift tool into the center hole on the top plate of the strongback.
- 11. Connect appropriate lifting equipment to the strongback lift tool, unlatch the strongback restraint arms and swing into their full-open position. Lift and transport the strongback to the load/unload station.

7.1.1.3.2 Vertical Operations

- 1. Optional: Install the sealing surface protector on the MFFP seal flange.
- 2. Remove the three (3) 1/2-inch SHCS that secure the strongback to the body.
- 3. Attach the strongback lift tool to the center hole in the top plate assembly of the strongback.
- 4. Connect appropriate lifting equipment to the strongback lift tool. Lift and transport the strongback to the load/unload station.
- 5. Visually inspect the following components for wear or damage that could impair their function and, if necessary, replace or repair per the requirements of the drawings in Appendix 1.4.2, *Packaging General Arrangement Drawings*.
 - a. Strongback
 - b. Fuel control structures (FCSs)
 - c. Neutron absorber plates on strongback and FCSs

7.1.2 Loading of Contents

7.1.2.1 Loading of Fuel Assemblies into Strongback

- 1. Close and latch the side restraints on the load/unload station and remove the strongback lift tool.
- 2. Remove the three (3) 3/8-inch SHCS attaching the BPRA restraint weldment to the top plate and remove the BPRA restraint weldment. Remove the three (3) 1/2-inch and three (3) 3/4-inch SHCS attaching the top plate to the strongback. Connect the top plate lifting assembly to the top plate. Lift the top plate clear of the strongback and place in a secure area.
- 3. Rotate the load/unload station top restraint into position and engage the strongback with the restraint pin.
- 4. Unlatch the load/unload station side restraints and swing into their full-open position.
- 5. Verify that the MOX fuel assemblies (FAs) to be loaded meet the payload requirements and limitations of the MFFP license.

6. Unlatch the eight (8) strongback clamp arms and the seven (7) fuel control structures (FCSs) for one of the strongback FA carrier sections by removing the appropriate quick-release pins and rotate each into the full-open position.
7. Ensure that the two fixed clamp pads on the bottom end plate are in their full open positions.
8. Utilizing appropriate lifting equipment, carefully place the FA, still vertically oriented, into the open section of the strongback.
9. Close each of the eight (8) clamp arms and the seven (7) FCSs. Secure each clamp arm and FCS in their closed position with the respective quick-release pin.
10. Using a manual or powered socket wrench, rotate the two tensioning SHCS located at each clamp arm and the bottom end plate clockwise to apply the clamping force to the FA grids. Once all control arms and FCSs are secured, disconnect and remove the lifting equipment from the FA.
11. Rotate the strongback approximately 120 degrees so that the next empty FA section in the strongback is accessible for loading.
12. Repeat Steps 6 through 11 for the second and third FAs (or dummy FAs), as necessary.
13. After the strongback is fully loaded with FAs, close and latch the load/unload station side restraints, and remove the load/unload station top restraint. Ensure the clamp pads on the top plate are fully retracted, and install the top end plate assembly.
14. Install the three (3) outer 3/4-inch SHCS that secure the top plate to the strongback. Tighten to 80 – 90 lb_r-ft torque, lubricated.
15. Install the three (3) inner 1/2-inch SHCS that secure the top plate to the strongback. Tighten to 23 – 27 lb_r-ft torque, lubricated.
16. Install the three (3) 3/8-inch SHCS that secure the BPRA restraint weldment to the strongback. Tighten to 23 – 27 lb_r-ft torque, lubricated.
17. Using a manual or powered socket wrench, rotate the two adjustment screws located at each top plate clamp pad clockwise to apply the clamping force to the FA top nozzle.
18. Tighten the four (4) 3/4-inch swivel clamp pads on the top plate until the screw pad contacts the FA top nozzle. Lock each swivel clamp pad in place with a hex nut.
19. Repeat Step 18 for the second and third FAs (or dummy FAs).

7.1.2.2 Loading of the Strongback into the MFFP

7.1.2.2.1 Horizontal Operations

1. Install the strongback lift tool into the receptacle in the center of the top plate of the strongback and connect appropriate lifting equipment. Unlatch the load/unload station side restraints and swing into their full-open position.
2. Lift and transport the strongback from the load/unload station to the insertion/extraction station. Place the strongback on the insertion/extraction station.

CAUTION: The strongback must be properly oriented for the insertion operation before the strongback is placed on the insertion/extraction station.

3. Close and latch the strongback restraint arms on the insertion/extraction station. Disconnect from the lifting equipment and remove the strongback lift tool.
4. Connect the insertion/extraction attachment bar by engaging the receptacle in the center of the top plate and raise the strongback.
5. Attach appropriate lifting equipment to the upper attachment point on the insertion/extraction station in preparation for returning the strongback to a horizontal orientation.
6. Detach the installed struts. Lower the insertion/extraction station to a horizontal orientation.
7. Ensure that the MFFP interior is free of debris and/or damage that could prevent proper loading of the strongback.
8. If not already in position, install the sealing surface protector on the MFFP seal flange.
NOTE: The sealing surface protector orientation is labeled along the edge. Correct orientation is required for correct interfacing with the insertion/extraction station.
9. Move and align the MFFP with the package connection collar on the insertion/extraction station.
NOTE: Ensure that the azimuth orientation of the strongback and the lugs integral to the MFFP body are correctly aligned so that strongback insertion can be accomplished without interference.
10. Insert the strongback into the MFFP using the insertion/extraction station. Care shall be taken not to damage the MFFP containment seal surfaces.
11. Install the three (3) 1/2-inch SHCS that secure the strongback to the body. Tighten to 70 – 75 lbf-ft torque, lubricated.
12. Disconnect the insertion/extraction station from the strongback.
13. Disconnect and move the MFFP body away from the insertion/extraction station.
14. Remove the sealing surface protector from the MFFP seal flange.

7.1.2.2.2 Vertical Operations

1. Install the strongback lift tool into the receptacle in the center of the top plate of the strongback and connect appropriate lifting equipment. Unlatch the load/unload station side restraints and swing into their full-open position.
2. Ensure that the MFFP interior is free of debris and/or damage that could prevent proper loading of the strongback.
3. Lift and transport the strongback from the load/unload station and lower into the MFFP. Care shall be taken not to damage the MFFP containment seal surfaces.
NOTE: Ensure that the azimuth orientation of the strongback and the lugs integral to the MFFP body are correctly aligned so that strongback insertion can be accomplished without interference and be removed later using the insertion/extraction station, if desired.
4. Install the three (3) 1/2-inch SHCS that secure the strongback to the body. Tighten to 70 – 75 lbf-ft torque, lubricated.

5. Disconnect and remove the strongback lift tool from the strongback.
6. Remove the sealing surface protector from the MFFP seal flange.

7.1.2.3 Closure Lid Installation

7.1.2.3.1 Horizontal Operations

1. Visually inspect the following components for wear or damage that could impair their function and, if necessary, replace or repair per the requirements of the drawings in Appendix 1.4.2, *Packaging General Arrangement Drawings*.
 - a. Vent port plug and accompanying O-ring seal
 - b. Seal test port plug and accompanying O-ring seal
 - c. Fill port plug and accompanying O-ring seal
 - d. Closure lid bolts
 - e. Impact limiters
 - f. Impact limiter SHCS
2. Visually inspect the closure lid O-ring seals. If necessary, remove the O-ring seal(s) and clean the seal(s) and the sealing surface(s) on the closure lid and body to remove contamination. If, during the visual examination, it is determined that damage to the O-ring seal(s) and/or sealing surface(s) is sufficient to impair containment integrity, replace the damaged seal(s) and/or repair the damaged sealing surface(s) per Section 8.2.3.2.1, *Seal Area Routine Inspection and Repair*.
3. As an option, sparingly apply vacuum grease to the O-ring seals and install into the appropriate O-ring seal grooves in the closure lid, the vent port plug, the seal test port plug, and the fill port plug.
4. If the closure lid was removed from the lid handling fixture following removal from the package, secure the lid handling fixture to the closure lid utilizing four (4) 1/2-inch hex bolts. Tighten the hex bolts to snug tight condition. Ensure the vent port is open by loosening the vent port plug.
5. Install the closure lid on the MFFP body. Care shall be taken not to damage the sealing surfaces.
6. Remove the four (4) 1/2-inch hex bolts and the lid handling fixture. Ensure the lid remains in place on the body.
7. Install the twenty-four (24) 3/4-inch SHCS. Using a crossing pattern, tighten the SHCS to 175 – 220 lb_f-ft torque, lubricated.
8. Tighten the vent port, seal test port, and fill port plugs to 8 – 10 lb_f-ft torque.
9. Leakage rate test the vent port and closure lid containment O-ring seal in accordance with Section 7.4, *Preshipment Leakage Rate Test*.
10. Carefully lift and install the lid end impact limiter on the MFFP.
11. Install the six (6), 1-inch SHCS and tighten to 180 – 220 lb_f-ft torque, lubricated.
12. If not previously installed, install the bottom end impact limiter on the MFFP per Steps 10 and 11.
13. If previously installed, inspect the bottom end impact limiter to verify it is properly installed.

14. Install the tamper-indicating device on the appropriate lid end impact limiter bolts.

7.1.2.3.2 Vertical Operations

1. Visually inspect the following components for wear or damage that could impair their function and, if necessary, replace or repair per the requirements of the drawings in Appendix 1.4.2, *Packaging General Arrangement Drawings*.
 - a. Vent port plug and accompanying O-ring seal
 - b. Seal test port plug and accompanying O-ring seal
 - c. Fill port plug and accompanying O-ring seal
 - d. Closure lid bolts
 - e. Impact limiters
 - f. Impact limiter SHCS
2. Visually inspect the closure lid O-ring seals. If necessary, remove the O-ring seal(s) and clean the seal(s) and the sealing surface(s) on the closure lid and body to remove contamination. If, during the visual examination, it is determined that damage to the O-ring seal(s) and/or sealing surface(s) is sufficient to impair containment integrity, replace the damaged seal(s) and/or repair the damaged sealing surface(s) per Section 8.2.3.2.1, *Seal Area Routine Inspection and Repair*.
3. As an option, sparingly apply vacuum grease to the O-ring seals and install into the appropriate O-ring seal grooves in the closure lid, the vent port plug, the seal test port plug, and the fill port plug.
4. If not already installed, install three (3) swivel hoist rings with 1/2 inch-13 threads and rated load of at least 170 lb_f into the three (3) equally spaced threaded holes labeled "For Lid Handling Only". Ensure the vent port is open by loosening the vent port plug.
5. Install the closure lid on the MFFP body. Care shall be taken not to damage the sealing surfaces.

NOTE: Ensure the lid is installed in the correct orientation, allowing the lid to be removed later in a horizontal orientation, if desired.
6. Remove the lifting equipment and three (3) swivel hoist rings.
7. Install the twenty-four (24), 3/4-inch SHCS. Using a crossing pattern, tighten the SHCS to 175 – 220 lb_f-ft torque, lubricated.
8. Tighten the vent port, seal test port, and fill port plugs to 8 – 10 lb_f-ft torque.
9. Leakage rate test the vent port and closure lid containment O-ring seal in accordance with Section 7.4, *Preshipment Leakage Rate Test*.
10. Position the upending fixture lift arm such that the lifting point is over the center of the MFFP.
11. Attach the appropriate lifting equipment to the upending frame and disconnect the upending frame from the wall mount fixture.
12. Lift and move the upending frame with the MFFP to a position appropriate for transitioning to the horizontal orientation.

13. Transition the upending frame with attached MFFP to the horizontal orientation.
14. Carefully lift and install the lid end impact limiter on the MFFP.
15. Install the six (6), 1-inch SHCS and tighten to 180 – 220 lb_r-ft torque, lubricated.
16. Inspect the bottom end impact limiter to verify it is properly installed.
17. Install the tamper-indicating device on the appropriate lid end impact limiter bolts.

7.1.3 Preparation for Transport (Loaded)

1. Using an air pallet or other lifting equipment, load the MFFP/shipping skid into the transport conveyance.
2. Remove the air pallet or other lifting equipment.
3. Install the tie-down devices to the shipping skid and the transport conveyance to secure the MFFP.
4. Set the shock indicators affixed to the package shell.
5. Monitor external radiation for each loaded MFFP per the guidelines of 49 CFR §173.441¹.
6. Determine that surface contamination levels for each loaded MFFP is per the guidelines of 49 CFR §173.443.
7. Determine the transport index for each loaded MFFP per the guidelines of 49 CFR §173.403.
8. Complete all necessary shipping papers in accordance with Subpart C of 49 CFR 172².
9. MFFP marking shall be in accordance with 10 CFR §71.85(c)³ and Subpart D of 49 CFR 172. Package labeling shall be in accordance with Subpart E of 49 CFR 172. Package placarding shall be in accordance with Subpart F of 49 CFR 172.

¹ Title 49, Code of Federal Regulations, Part 173 (49 CFR 173), *Shippers—General Requirements for Shipments and Packagings*, Final Rule, 01-26-04.

² Title 49, Code of Federal Regulations, Part 172 (49 CFR 172), *Hazardous Materials Tables and Hazardous Communications Regulations*, Final Rule, 01-26-04.

³ Title 10, Code of Federal Regulations, Part 71 (10 CFR 71), *Packaging and Transportation of Radioactive Material*, Final Rule, 01-26-04.

This page left intentionally blank.

7.2 Package Unloading

This section delineates the procedures for unloading a strongback from the MFFP. Hereafter, reference to specific MFFP components may be found in Appendix 1.4.2, *Packaging General Arrangement Drawings*. Note that the steps provided in the following sections may be performed in any logical sequence.

The unloading operation shall be performed in a dry environment. If precipitation enters the cavity, the free-standing water shall be removed prior to installing the closure lid.

7.2.1 Receipt of Package from Carrier

Prior to performing any unloading operations, the external surfaces of the MFFP shall be surveyed for potential radioactive contamination per the requirements of 10 CFR §20.1906¹. In addition, inspect the tamper-indicating device on the lid end impact limiter bolts to verify that no unauthorized opening of the MFFP has occurred, and record the condition of the shock indicators.

7.2.2 Removal of Contents

7.2.2.1 Removal of MFFP from the Transport Conveyance

1. Disengage the tie-down devices from the shipping skid and the transport conveyance.

CAUTION: Failure to disengage the tie-down devices may result in damage to the packaging, shipping skid, and/or the transport conveyance.

2. Using an air pallet or other lifting equipment, remove the MFFP/shipping skid from the transport conveyance and move to the loading area.
3. Remove the air pallet or other lifting equipment.

7.2.2.2 Removal of the Closure Lid

7.2.2.2.1 Horizontal Operations

1. Remove the tamper indicating device located between two of the lid end impact limiter bolts.
2. Remove the six (6) 1-inch socket head cap screws (SHCS) from the lid end impact limiter.
3. Utilizing appropriate lifting equipment, carefully lift and remove the lid end impact limiter and place in a secure area.
4. If necessary, repeat Steps 2 and 3 for the bottom end impact limiter.
5. Vent the interior of the MFFP through the lid end vent plug.
6. Loosen and / or remove the twenty-four (24), 3/4-inch SHCS attaching the lid to the package body. Ensure the lid remains in place on the body.

¹ Title 10, Code of Federal Regulations, Part 20 (10 CFR 20), *Standards for Protection of Radiation*, 01-01-03 Edition.

7. Utilizing four (4) 1/2-inch hex bolts, secure the lid handling fixture to the closure lid. Tighten the hex bolts to snug tight condition. Ensure any of the lid attachment fasteners that are covered by the lid handling fixture are removed prior to installing the lid handling fixture.
8. Connect appropriate lifting equipment to the lid handling fixture.
9. Remove any of the twenty-four (24), 3/4-inch SHCS not already removed in Steps 6 or 7 and carefully remove the closure lid with the lifting equipment and lid handling fixture. If necessary, the three T-handle assemblies on the lid handling fixture or three (3) 1/2-inch-13 x 2-inch bolts may be utilized in the three equally-spaced holes marked “for lid handling only” to assist in breaking the seal of the closure lid. Care shall be taken to not damage the MFFP containment seal surfaces.
10. Store the closure lid in a manner such that potential damage to the O-ring seals and sealing surfaces is minimized.

7.2.2.2 Vertical Operations

1. Remove the tamper indicating device located between two of the lid end impact limiter bolts.
2. Attach the handling lift equipment, using the shackles on the support skid, in preparation for lifting the MFFP. Ensure the handling lift equipment “Lid End” is oriented toward the lid end of the MFFP.
3. Lift and place the MFFP with attached transport skid into the upending frame.
4. Secure the MFFP to the upending frame with both the ball lock pins and the tie-down straps.
5. Remove the six (6) 1-inch socket head cap screws (SHCS) from the lid end impact limiter.
6. Utilizing appropriate lifting equipment, carefully lift and remove the lid end impact limiter and place in a secure area.
7. Vent the interior of the MFFP through the lid end vent plug.
8. Loosen the twenty-four (24), 3/4-inch SHCS securing the closure lid. This step may also be performed following Step 10.
9. Ensure the upending frame lift arm is positioned with the lift point aligned with the approximate MFFP centerline and that attachment fasteners are snug tight. Using appropriate lifting equipment, rotate the upending frame with attached MFFP and skid to the vertical orientation. Transfer the upending frame to the location of the wall mount fixture and secure in place.
10. Rotate or remove the upending frame lift arm from the lifting position to the unloading position.
11. Remove the twenty-four (24), 3/4-inch SHCS loosened in Step 8. If necessary, three (3) 1/2-inch-13 x 2-inch bolts may be utilized in the three equally-spaced holes marked “for lid handling only” to assist in breaking the seal of the closure lid.
12. Install three (3) swivel hoist rings with 1/2-inch-13 threads and rated load of at least 170 lb_f into the three (3) equally spaced threaded holes labeled “For Lid Handling Only”. Carefully remove the closure lid with the appropriate lifting equipment.

13. Store the closure lid in a manner such that potential damage to the O-ring seals and sealing surfaces is minimized.

7.2.2.3 Removal of the Strongback from the MFFP

7.2.2.3.1 Horizontal Operations

1. Install the sealing surface protector on the MFFP seal flange.
NOTE: The sealing surface protector orientation is labeled along the edge. Correct orientation is required for correct interfacing with the insertion/extraction station.
2. Align the MFFP body and connect to the insertion/extraction station.
3. Insert the attachment bar of the insertion/extraction station into the center hole on the top plate of the strongback.
4. Remove the three (3) 1/2-inch SHCS that secure the strongback to the body.
5. Remove the strongback from the body using the insertion/extraction station. Care shall be taken to not damage the MFFP containment sealing surfaces.
6. Disconnect the MFFP body from the insertion/extraction station and move the MFFP body away from the insertion/extraction station.
7. Ensure the strongback restraint arms on the insertion/extraction station are closed and latched. Connect appropriate lifting equipment to the uprighting attachment point.
8. Upend the strongback and insertion/extraction station. After uprighting, fix the insertion/extraction station in the upright position using the installed struts.
9. Lower the strongback and disconnect the insertion/extraction attachment bar from the strongback. Install the strongback lift tool into the center hole on the top plate of the strongback.
10. Connect appropriate lifting equipment to the strongback lift tool, unlatch the strongback restraint arms and swing into their full-open position. Lift and transport the strongback to the load/unload station.

7.2.2.3.2 Vertical Operations

1. Optional: Install the sealing surface protector on the MFFP seal flange.
2. Remove the three (3) 1/2-inch SHCS that secure the strongback to the body.
3. Attach the strongback lift tool to the center hole in the top plate assembly of the strongback.
4. Connect appropriate lifting equipment to the strongback lift tool. Lift and transport the strongback to the load/unload station.

7.2.2.4 Unloading of Fuel Assemblies from the Strongback

1. Close and latch the side restraints on the load/unload station and remove the strongback lift tool.

2. Remove the three (3) 3/8-inch SHCS attaching the BPRA restraint weldment to the top plate and remove the BPRA restraint weldment. Remove the three (3) 1/2-inch and three (3) 3/4-inch SHCS attaching the top plate to the strongback. Ensure that the two fixed clamp pads on the top plate are in their full open positions. Connect the top plate lifting assembly to the top plate. Lift the top plate clear of the strongback and place in a secure area.
3. Rotate the load/unload station top restraint into position and engage the strongback with the restraint pin.
4. Unlatch the load/unload station side restraints and swing into their full-open position.
5. Utilizing appropriate lifting equipment, attach the FA lifting equipment to the FA.
6. Using a manual or powered socket wrench, rotate the two adjustment screws located at each clamp arm counterclockwise to release the clamping force on the FA grids.
7. Unlatch the eight (8) strongback clamp arms and the seven (7) fuel control structures (FCSs) for one of the FA carrier sections by removing the appropriate quick-release pin and rotate each into the full-open position.
8. Ensure that the two fixed clamp pads on the bottom end plate are in their full open positions.
9. Utilizing appropriate lifting equipment, carefully remove the FA from the strongback.
10. Close each of the eight (8) clamp arms and the seven (7) FCSs. Secure each clamp arm and FCS in their closed position with the respective quick-release pin.
11. Rotate the strongback approximately 120 degrees so that the next FA is accessible for unloading.
12. Repeat Steps 5 through 11 for the second and third FAs (or dummy FAs, if removed).
13. After the strongback is fully unloaded, close and latch the load/unload station side restraints, and remove the load/unload station top restraint. Install the top plate assembly.
14. Install the three (3) outer 3/4-inch SHCS that secure the top plate to the strongback. Tighten to 80 – 90 lb_f-ft torque, lubricated.
15. Install the three (3) inner 1/2-inch SHCS that secure the top plate to the strongback. Tighten to 23 – 27 lb_f-ft torque, lubricated.
16. Install the three (3) 3/8-inch SHCS that secure the BPRA restraint weldment to the strongback. Tighten to 23 – 27 lb_f-ft torque, lubricated.

7.2.2.5 Loading of the Empty Strongback into the MFFP

7.2.2.5.1 Horizontal Operations

1. Install the strongback lift tool into the receptacle in the center of the top plate of the strongback and connect appropriate lifting equipment. Unlatch the load/unload station side restraints and swing into their full-open position.
2. Lift and transport the strongback from the load/unload station to the insertion/extraction station. Place the strongback on the insertion/extraction station.

CAUTION: The strongback must be properly oriented for the insertion operation before the strongback is placed on the insertion/extraction station.

3. Close and latch the strongback restraint arms on the insertion/extraction station. Disconnect from the lifting equipment and remove the strongback lift tool.
4. Connect the insertion/extraction attachment bar by engaging the receptacle in the center of the top plate and raise the strongback.
5. Attach appropriate lifting equipment to the upper attachment point on the insertion/extraction station in preparation for returning the strongback to a horizontal orientation.
6. Detach the installed struts. Lower the insertion/extraction station to a horizontal orientation.
7. Ensure that the MFFP interior is free of debris and/or damage that could prevent proper loading of the strongback.
8. If not already in position, install the sealing surface protector on the MFFP seal flange.

NOTE: The sealing surface protector orientation is labeled along the edge. Correct orientation is required for correct interfacing with the insertion/extraction station.

9. Align the MFFP body and connect to the insertion/extraction station.

NOTE: Ensure that the azimuth orientation of the strongback and the lugs integral to the MFFP body are correctly aligned so that strongback insertion can be accomplished without interference.

10. Insert the strongback into the MFFP using the insertion/extraction station. Care shall be taken to not damage the MFFP containment seal surfaces.
11. Install the three (3) 1/2-inch SHCS that secure the strongback to the body. Tighten to 70 – 75 lb_f-ft torque, lubricated.
12. Disconnect the insertion/extraction station from the strongback.
13. Disconnect and move the MFFP body away from the insertion/extraction station.
14. Remove the sealing surface protector from the MFFP seal flange.

7.2.2.5.2 Vertical Operations

1. Install the strongback lift tool into the receptacle in the center of the top plate of the strongback and connect appropriate lifting equipment. Unlatch the load/unload station side restraints and swing into their full-open position.
2. Ensure that the MFFP interior is free of debris and/or damage that could prevent proper loading of the strongback.
3. Optional: Install the sealing surface protector on the MFFP seal flange.
4. Lift and transport the strongback from the load/unload station and lower into the MFFP.

NOTE: Ensure that the azimuth orientation of the strongback and the lugs integral to the MFFP body are correctly aligned so that strongback insertion can be accomplished without interference and be removed later using the insertion/extraction station, if desired.

5. Install the three (3) 1/2-inch SHCS that secure the strongback to the body. Tighten to 70 – 75 lb_f-ft torque, lubricated.
6. Disconnect from the lifting equipment and remove the strongback lift tool.
7. Remove the sealing surface protector from the MFFP seal flange.

7.2.2.6 Closure Lid Installation

7.2.2.6.1 Horizontal Operations

1. Visually inspect the following components for wear or damage that could impair their function and, if necessary, replace or repair per the requirements of the drawings in Appendix 1.4.2, *Packaging General Arrangement Drawings*.
 - a. Vent port plug and accompanying O-ring seal
 - b. Seal test port plug and accompanying O-ring seal
 - c. Fill port plug and accompanying O-ring seal
 - d. Closure lid bolts
 - e. Impact limiters
 - f. Impact limiters SHCS
2. Visually inspect the closure lid O-ring seals. If necessary, remove the O-ring seal(s) and clean the seal(s) and the sealing surface(s) on the closure lid and body to remove contamination. If, during the visual examination, it is determined that damage to the O-ring seal(s) and/or sealing surface(s) is sufficient to impair containment integrity, replace the damaged seal(s) and/or repair the damaged sealing surface(s) per Section 8.2.3.2.1, *Seal Area Routine Inspection and Repair*.
3. As an option, sparingly apply vacuum grease to the O-ring seals and install into the appropriate O-ring seal grooves in the closure lid, the vent port plug, the seal test port plug, and the fill port plug.
4. If the closure lid was removed from the lid handling fixture following removal, secure the lid handling fixture to the closure lid utilizing four (4) 1/2 hex bolts. Tighten the hex bolts to snug tight condition. Ensure the vent port is open by loosening the vent port plug.
5. Install the closure lid on the MFFP body. Care shall be taken to not damage the sealing surfaces.
6. Remove the four (4) 1/2-inch hex bolts and the lid handling fixture. Ensure the lid remains in place on the body.
7. Install the twenty-four (24), 3/4-inch SHCS. Using a crossing pattern, tighten the SHCS to 175 – 220 lb_f-ft torque, lubricated.
8. Tighten the vent port, seal test port, and fill port plugs to 8 – 10 lb_f-ft torque.
9. Carefully lift and install the lid end impact limiter on the MFFP.
10. Install the six (6), 1-inch SHCS and tighten to 180 – 220 lb_f-ft torque, lubricated.
11. If not previously installed, install the bottom end impact limiter on the MFFP per Steps 9 and 10.

12. If previously installed, inspect the bottom end impact limiter to verify it is properly installed.

7.2.2.6.2 Vertical Operations

1. Visually inspect the following components for wear or damage that could impair their function and, if necessary, replace or repair per the requirements of the drawings in Appendix 1.4.2, *Packaging General Arrangement Drawings*.
 - a. Vent port plug and accompanying O-ring seal
 - b. Seal test port plug and accompanying O-ring seal
 - c. Fill port plug and accompanying O-ring seal
 - d. Closure lid bolts
 - e. Impact limiters
 - f. Impact limiters SHCS
2. Visually inspect the closure lid O-ring seals. If necessary, remove the O-ring seal(s) and clean the seal(s) and the sealing surface(s) on the closure lid and body to remove contamination. If, during the visual examination, it is determined that damage to the O-ring seal(s) and/or sealing surface(s) is sufficient to impair containment integrity, replace the damaged seal(s) and/or repair the damaged sealing surface(s) per Section 8.2.3.2.1, *Seal Area Routine Inspection and Repair*.
3. As an option, sparingly apply vacuum grease to the O-ring seals and install into the appropriate O-ring seal grooves in the closure lid, the vent port plug, the seal test port plug, and the fill port plug.
4. If not already installed, install three (3) swivel hoist rings with 1/2 inch-13 threads and rated load of at least 170 lb_f into the three (3) equally spaced threaded holes labeled "For Lid Handling Only". Ensure the vent port is open by loosening the vent port plug.
5. Using appropriate lifting equipment, lift and install the closure lid on the MFFP body. Care shall be taken to not damage the sealing surfaces.

NOTE: Ensure the lid is installed in the correct orientation, allowing the lid to be removed later in a horizontal orientation, if desired.

6. Remove the lifting equipment and three (3) swivel hoist rings.
7. Install the twenty-four (24), 3/4-inch SHCS. Using a crossing pattern, tighten the SHCS to 175 – 220 lb_f-ft torque, lubricated .
8. Tighten the vent port, seal test port, and fill port plugs to 8 – 10 lb_f-ft torque.
9. Position the upending fixture lift arm such that the lifting point is over the center of the MFFP.
10. Attach the appropriate lifting equipment to the upending frame and disconnect the upending frame from the wall mount fixture.
11. Lift and move the upending frame with the MFFP to a position appropriate for transitioning to the horizontal orientation.
12. Transition the upending frame with attached MFFP to the horizontal orientation.
13. Carefully lift and install the lid end impact limiter on the MFFP.

14. Install the six (6), 1-inch SHCS and tighten to 180 – 220 lb_f-ft torque, lubricated .
15. Inspect the bottom end impact limiter to verify it is properly installed.

7.2.2.7 Final Package Preparations for Transport (Unloaded)

1. Using an air pallet or other lifting equipment, load the MFFP into the transport conveyance.
2. Remove the air pallet or other lifting equipment.
3. Install the tie-down devices to the shipping skid and the transport conveyance to secure the MFFP.
4. Transport the MFFP in accordance with Section 7.3, *Preparation of an Empty Package for Transport*.

7.3 Preparation of an Empty Package for Transport

Previously used and empty MFFPs shall be prepared and transported per the requirements of 49 CFR §173.428¹.

¹ Title 49, Code of Federal Regulations, Part 173 (49 CFR 173), *Shippers—General Requirements for Shipments and Packagings*, Final Rule, 01-26-04.

This page left intentionally blank.

7.4 Preshipment Leakage Rate Test

After the MFFP is assembled and prior to shipment, leakage rate testing shall be performed to confirm proper assembly of the package following the guidelines of Section 7.6, *Preshipment Leakage Rate Test*, and Appendix A.5.2, *Gas Pressure Rise*, of ANSI N14.5¹.

7.4.1 Gas Pressure Rise Leakage Rate Test Acceptance Criteria

In order to demonstrate containment integrity in preparation for shipment, no leakage shall be detected when tested to a sensitivity of 1×10^{-3} reference cubic centimeters per second (scc/sec) air, or less, per Section 7.6, *Preshipment Leakage Rate Test*, of ANSI N14.5.

7.4.2 Determining the Test Volume and Test Time

1. Assemble a leakage rate test apparatus that consists of, at a minimum, the components illustrated in Figure 7.4-1, using a calibrated volume with a range of 100 – 500 cubic centimeters, and a calibrated pressure transducer with a minimum sensitivity of 100 millitorr. Connect the test apparatus to the test volume (i.e., the seal test port, or the vent port, as appropriate).
2. Set the indicated sensitivity on the digital readout of the calibrated pressure transducer, ΔP , to, at a minimum, the resolution (i.e., sensitivity) of the calibrated pressure transducer (e.g., $\Delta P = 1, 10, \text{ or } 100$ millitorr sensitivity).
3. Open all valves (i.e., the vent valve, calibration valve, and vacuum pump isolation valve), and record ambient atmospheric pressure, P_{atm} .
4. Isolate the calibrated volume by closing the vent and calibration valves.
5. Evacuate the test volume to a pressure less than the indicated sensitivity on the digital readout of the calibrated pressure transducer or 0.76 torr, whichever is less.
6. Isolate the vacuum pump from the test volume by closing the vacuum pump isolation valve. Allow the test volume pressure to stabilize and record the test volume pressure, P_{test} (e.g., $P_{\text{test}} < 1$ millitorr for an indicated sensitivity of 1 millitorr).
7. Open the calibration valve and, after allowing the system to stabilize, record the total volume pressure, P_{total} .
8. Knowing the calibrated volume, V_c , calculate and record the test volume, V_t , using the following equation:

$$V_t = V_c \left(\frac{P_{\text{atm}} - P_{\text{total}}}{P_{\text{total}} - P_{\text{test}}} \right)$$

9. Knowing the indicated sensitivity on the digital readout of the calibrated pressure transducer, ΔP , calculate and record the test time, t , using the following equation (based on Equation B.14 of ANSI N14.5-1997):

$$t = \Delta P(1.32)V_t$$

¹ ANSI N14.5-1997, *American National Standard for Radioactive Materials - Leakage Tests on Packages for Shipment*, American National Standards Institute, Inc. (ANSI).

7.4.3 Performing the Gas Pressure Rise Leakage Rate Test

1. Isolate the calibrated volume by closing the calibration valve.
2. Open the vacuum pump isolation valve and evacuate the test volume to a pressure less than the test volume pressure, P_{test} , determined in Step 6 of Section 7.4.2, *Determining the Test Volume and Test Time*.
3. Isolate the vacuum pump from the test volume by closing the vacuum pump isolation valve. Allow the test volume pressure to stabilize and record the beginning test pressure, P_1 . After a period of time equal to " t " seconds, determined in Step 9 of Section 7.4.2, *Determining the Test Volume and Test Time*, record the ending test pressure, P_2 . To be acceptable, there shall be no difference between the final and initial pressures such that the requirements of Section 7.4.1, *Gas Pressure Rise Leakage Rate Test Acceptance Criteria*, are met.
4. If, after repeated attempts, the O-ring seal fails to pass the leakage rate test, replace the damaged seal and/or repair the damaged sealing surfaces per Section 8.2.3.2.1, *Sealing Area Routine Inspection and Repair*. Perform verification leakage rate test per the applicable procedure delineated in Section 8.2.2, *Maintenance/Periodic Leakage Rate Tests*.

7.4.4 Optional Preshipment Leakage Rate

As an option to Section 7.4.3, *Performing the Gas Pressure Rise Leakage Rate Test*, Section 8.2.2, *Maintenance/Periodic Leakage Rate Tests*, may be performed.

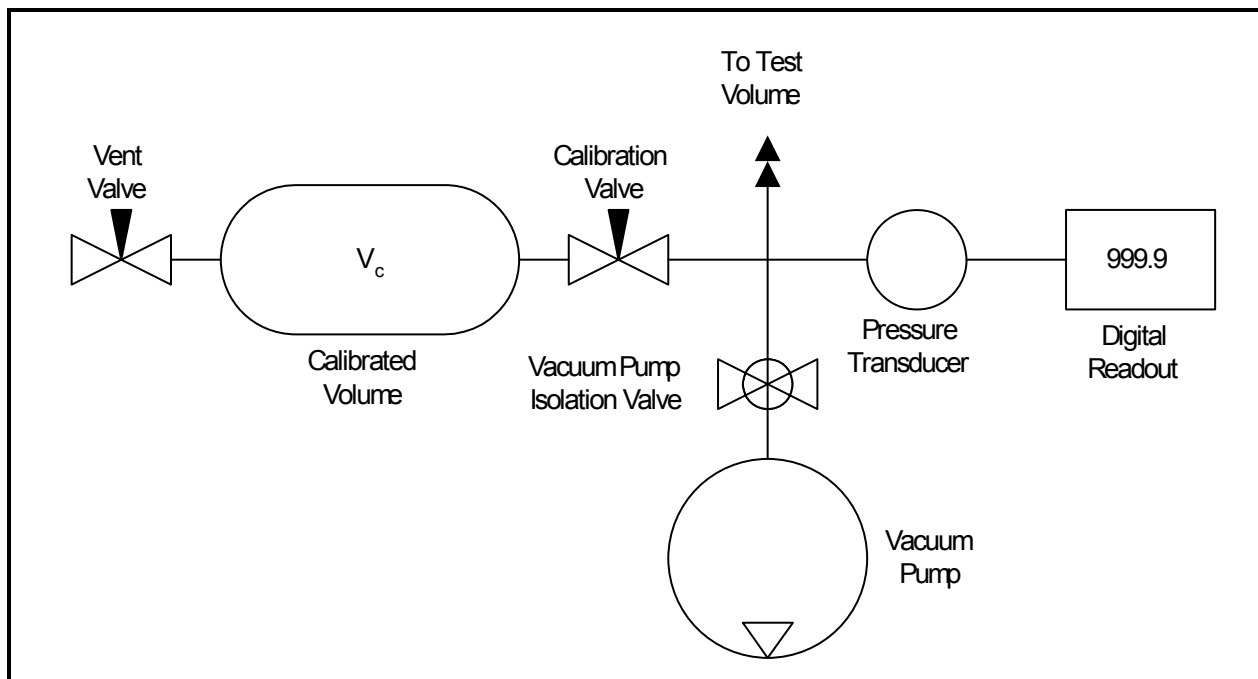


Figure 7.4-1 – Pressure Rise Leakage Rate Test Schematic

8.0 ACCEPTANCE TESTS AND MAINTENANCE PROGRAM

8.1 Acceptance Tests

Per the requirements of 10 CFR §71.85¹, this section discusses the inspections and tests to be performed prior to first use of the MFFP.

8.1.1 Visual Inspection and Measurements

All MFFP materials of construction and welds shall be examined in accordance with requirements delineated on the drawings in Appendix 1.4.2, *Packaging General Arrangement Drawings*, per the requirements of 10 CFR §71.85(a). Furthermore, the inspections of Section 8.2.3.2, *Seal Areas and Grooves*, shall be performed prior to pressure and leakage rate testing.

8.1.2 Weld Examinations

All welds are inspected per the requirements delineated on the drawings in Appendix 1.4.2, *Packaging General Arrangement Drawings*.

8.1.3 Structural and Pressure Tests

8.1.3.1 Lifting Device Load Testing

The MFFP does not contain any lifting devices requiring load testing.

8.1.3.2 Pressure Testing

Per the requirements of 10 CFR §71.85(b), the MFFP containment boundary shall be pressure tested to 150% of the maximum normal operating pressure (MNOP) to verify structural integrity. The MNOP of the MFFP is 10 psig. Thus, the MFFP containment vessel shall be pressure tested to $10 \times 1.5 = 15$ psig minimum.

Following pressure testing of the containment boundary, accessible base material and welds directly related to the pressure testing of the containment vessel shall be visually inspected for plastic deformation or cracking in accordance with AWS D.1.6², and liquid penetrant inspected per ASME Boiler and Pressure Vessel Code, Section V³, Article 6, and ASME Boiler and Pressure Vessel Code, Section III⁴, Division 1, Subsection NB, Article NB-5000, as delineated on the drawings in Appendix 1.4.2, *Packaging General Arrangement Drawings*. Indications of

¹ Title 10, Code of Federal Regulations, Part 71 (10 CFR 71), *Packaging and Transportation of Radioactive Material*, Final Rule, 01-26-04.

² ANSI/AWS D1.6:1999, *Structural Welding Code – Stainless Steel*, American Welding Society (AWS).

³ American Society of Mechanical Engineers (ASME) Boiler and Pressure Vessel Code, Section V, *Nondestructive Examination*, 2001 Edition, 2002 and 2003 Addenda.

⁴ American Society of Mechanical Engineers (ASME) Boiler and Pressure Vessel Code, Section III, *Rules for Construction of Nuclear Power Plant Components*, 2001 Edition, 2002 and 2003 Addenda.

cracking or distortion shall be recorded on a nonconformance report and dispositioned prior to final acceptance in accordance with the cognizant quality assurance program.

Leak testing per Section 8.1.4, *Fabrication Leakage Rate Tests*, shall be performed after completion of pressure testing to verify package configuration and performance to design criteria.

8.1.4 Fabrication Leakage Rate Tests

This section provides the generalized procedure for fabrication leakage rate testing of the containment vessel boundaries and penetrations following the completion of fabrication. Fabrication leakage rate testing shall follow the guidelines of Section 7.3, *Fabrication Leakage Rate Test*, of ANSI N14.5⁵.

Prior to leakage rate testing, internal components that are not permanently affixed to the containment boundary, such as the strongback, shall be removed. For ease of leakage rate testing, the interior surfaces of the containment boundary should be thoroughly cleaned.

Fabrication leakage rate testing shall be performed on the containment boundary. Three separate tests comprise the series. Each test shall meet the acceptance criteria delineated in Section 8.1.4.1, *Fabrication Leakage Rate Test Acceptance Criteria*.

8.1.4.1 Fabrication Leakage Rate Test Acceptance Criteria

1. To be acceptable, each leakage rate test shall demonstrate a “leaktight” leakage rate of 1×10^{-7} reference cubic centimeters per second (scc/s), air, or less, per Section 6.3, *Application of Reference Air Leakage Rate (L_R)*, of ANSI N14.5.
2. In order to demonstrate the leaktight leakage rate, the sensitivity of the leakage rate test procedure shall be 5×10^{-8} cm³/s, air, or less, per Section 8.4, *Sensitivity*, of ANSI N14.5.

8.1.4.2 Helium Leakage Rate Testing the Containment Structure Integrity

1. The fabrication leakage rate test of the MFFP cask shall be performed following the guidelines of Section A.5.3, *Gas Filled Envelope – Gas Detector*, of ANSI N14.5.
2. Assemble the MFFP with all three O-ring seals installed on the closure lid. Dunnage may be installed in the containment cavity for volume reduction. Assembly is as shown on the MFFP drawings in Appendix 1.4.2, *Packaging General Arrangement Drawings*.
3. Loosen and remove the vent port plug to allow gas flow from the cavity and install a test port tool.
4. Install a helium mass spectrometer leak detector (MSLD) to the test port tool. Evacuate through the vent port until the vacuum is sufficient to operate the MSLD.
5. Surround the assembled MFFP with an envelope filled with helium gas of 99% purity or better to a pressure slightly greater than atmospheric pressure.
6. Perform the helium leakage rate test to the requirements of Section 8.1.4.1, *Fabrication Leakage Rate Test Acceptance Criteria*. If, after repeated attempts, the containment structure

⁵ ANSI N14.5-1997, *American National Standard for Radioactive Materials – Leakage Tests on Packages for Shipment*, American National Standards Institute, Inc. (ANSI).

fails to pass the leakage rate test, isolate the leak path and, prior to repairing the leak path and repeating the leakage rate test, record on a nonconformance report and disposition prior to final acceptance in accordance with the cognizant quality assurance program.

7. Remove the test port tool and re-install the vent port plug. Tighten to 8 – 10 lb-ft torque.

8.1.4.3 Helium Leakage Rate Testing the Main O-ring Seal

1. The fabrication leakage rate test of the MFFP containment O-ring seal integrity shall be performed following the guidelines of Section A.5.4, *Evacuated Envelope – Gas Detector*, of ANSI N14.5.
2. Assemble the MFFP with the three O-ring seals installed in the closure lid. Ensure the vent, seal test, and fill ports are installed with their associated O-ring seals. Assembly is as shown on the drawings in Appendix 1.4.2, *Packaging General Arrangement Drawings*.
3. Utilizing a test port tool, attach a vacuum pump and a source of helium gas, in parallel, to the fill port.
4. Close the valve to the source of helium gas and open the valve to the vacuum pump.
5. Utilizing a test port tool, rotate the fill port closure bolt to the open position.
6. Evacuate the system to a 90% vacuum or better ($\leq 10\%$ ambient atmospheric pressure). Isolate the vacuum pump from the system.
7. Provide a helium atmosphere inside the evacuated cavity by backfilling with helium gas (99% purity or better) to ambient atmospheric pressure (+1 psi, -0 psi).
8. Utilizing the test port tool, rotate the fill port plug to the closed position, and remove the helium-contaminated test port tool from the fill port.
9. Install a clean (helium-free) test port tool into the seal test port.
10. Utilizing appropriate fittings, attach a helium MSLD to the test port tool.
11. Utilizing the test port tool, rotate the seal test port closure bolt to the open position.
12. Evacuate the cavity above the lid containment O-ring seal until the vacuum is sufficient to operate the leak detector per the manufacturer's recommendations.
13. Perform the helium leakage rate test to the requirements of Section 8.1.4.1, *Fabrication Leakage Rate Test Acceptance Criteria*. If, after repeated attempts, the MFFP containment O-ring seal fails to pass the leak test, isolate the leak path and, prior to repairing the leak path and repeating the leak test, record on a nonconformance report and disposition prior to final acceptance in accordance with the cognizant quality assurance program.

8.1.4.4 Helium Leakage Rate Testing the Vent Port Plug O-ring Seal

1. The fabrication leakage rate test of the MFFP vent port plug O-ring containment seal integrity shall be performed following the guidelines of ANSI N14.5, Section A.5.4, *Evacuated Envelope – Gas Detector*.

2. The MFFP shall be assembled with all three O-ring seals installed on the closure lid. Ensure the vent, seal test, and fill port plugs are installed with their associated O-ring seals. Assembly is as shown on the MFFP drawings in Appendix 1.4.2, *Packaging General Arrangement Drawings*.
3. Verify the presence of a helium atmosphere below the vent port plug O-ring containment seal, as specified above in Steps 3 – 8 of Section 8.1.4.3, *Helium Leakage Rate Testing the Main O-ring Seal*.
4. Install a test port tool into the vent port.
5. Utilizing appropriate fittings, attach a helium MSLD to the test port tool.
6. Evacuate the cavity above the vent port plug O-ring containment seal until the vacuum is sufficient to operate the leak detector per the manufacturer's recommendations.
7. Perform the helium leakage rate test to the requirements of Section 8.1.4.1, *Fabrication Leakage Rate Test Acceptance Criteria*. If, after repeated attempts, the vent port plug O-ring containment seal fails to pass the leak test, isolate the leak path and, prior to repairing the leak path and repeating the leak test, record on a nonconformance report and disposition prior to final acceptance in accordance with the cognizant quality assurance program.

8.1.4.5 Helium Leakage Rate Testing the Fill Port Plug O-ring Seal

1. The fabrication leakage rate test of the MFFP fill port plug O-ring containment seal integrity shall be performed following the guidelines of Section A.5.4, *Evacuated Envelope – Gas Detector*, of ANSI N14.5.
2. The MFFP shall be assembled with all three O-ring seals installed on the closure lid. Ensure the vent, seal test, and fill port plugs are installed with their associated O-ring seals. Assembly is as shown on the MFFP drawings in Appendix 1.4.2, *Packaging General Arrangement Drawings*.
3. Verify the presence of a helium atmosphere below the fill port plug O-ring containment seal, as specified above in Steps 3 – 8 of Section 8.1.4.3, *Helium Leakage Rate Testing the Main O-ring Seal*.
4. Install a test port tool into the fill port.
5. Utilizing appropriate fittings, attach a helium MSLD to the test port tool.
6. Evacuate the cavity above the fill port plug O-ring containment seal until the vacuum is sufficient to operate the leak detector per the manufacturer's recommendations.
7. Perform the helium leakage rate test to the requirements of Section 8.1.4.1, *Fabrication Leakage Rate Test Acceptance Criteria*. If, after repeated attempts, the fill port plug O-ring containment seal fails to pass the leak test, isolate the leak path and, prior to repairing the leak path and repeating the leak test, record on a nonconformance report and disposition prior to final acceptance in accordance with the cognizant quality assurance program.

8.1.5 Component and Material Tests

8.1.5.1 Polyurethane Foam

This section establishes the requirements and acceptance criteria for installation, inspection, and testing of rigid, closed-cell, polyurethane foam utilized within the MFFP.

8.1.5.1.1 Introduction and General Requirements

The polyurethane foam used within the MFFP impact limiters is comprised of a specific “formulation” of foam constituents (i.e., mix of chemical constituents) that defines the foam’s physical characteristics such as density, compressive stress, and specific heat. Based on the foam’s physical requirements, chemical constituents are combined into batches containing multiple parts (e.g., parts A and B) for easier handling. Therefore, a foam “batch” is defined as mixing into vats a specific foam formulation for each part. Based on the foam’s physical requirements, portions from each batch part are combined to produce the liquid foam material for pouring into the component to be foamed. Thus, a foam “pour” is defined as apportioning the batch parts into a desired quantity of liquid foam material for subsequent installation (pouring).

The following sections describe the general requirements for chemical composition, constituent storage, foamed component preparation, foam material installation, and foam pour and test data records.

8.1.5.1.1.1 Polyurethane Foam Chemical Composition

The foam supplier shall certify that the chemical composition of the polyurethane foam is as delineated below, with the chemical component weight percents falling within the specified ranges. In addition, the foam supplier shall certify that the finished (cured) polyurethane foam does not contain halogen-type flame retardants or trichloromonofluoromethane (Freon 11).

Carbon.....	50% - 70%	Phosphorus.....	≤ 2%
Oxygen.....	14% - 34%	Silicon.....	< 1%
Nitrogen.....	4% - 12%	Chlorides.....	< 1%
Hydrogen.....	4% - 10%	Other.....	< 1%

8.1.5.1.1.2 Polyurethane Foam Constituent Storage

The foam supplier shall certify that the polyurethane foam constituents have been properly stored prior to use, and that the polyurethane foam constituents have been used within their shelf life.

8.1.5.1.1.3 Foamed Component Preparation

Prior to polyurethane foam installation, the foam supplier shall verify that an anti-bond agent, such as automotive wax, has been applied to all of the component shell interior surfaces. In addition, due to the internal pressures generated during the foam pouring/curing process, the foam supplier shall visually verify that adequate bracing/shoring of the component shells is provided to maintain the dimensional configuration throughout the foam pouring/curing process.

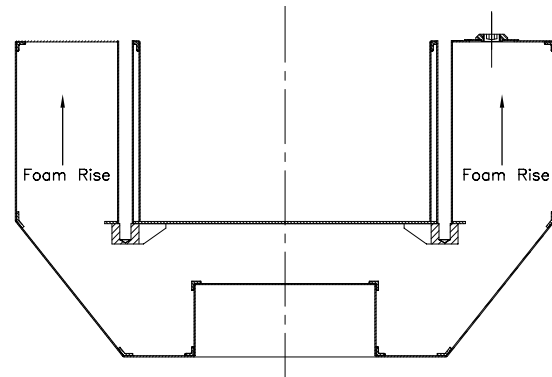
8.1.5.1.1.4 Polyurethane Foam Installation

The direction of foam rise shall be vertically aligned with the impact limiter longitudinal axis. The surrounding walls of the component shell where the liquid foam material is to be installed shall be between 55 °F and 95 °F prior to foam installation. Measure and record the component shell temperature to an accuracy of ± 2 °F prior to foam installation.

In the case of multiple pours into a single foamed component, the cured level of each pour shall be measured and recorded to an accuracy of ± 1 inch.

Measure and record the weight of liquid foam material installed during each pour to an accuracy of ± 10 pounds.

All test samples shall be poured into disposable containers at the same time as the actual pour it represents, clearly marking the test sample container with the pour date and a unique pour identification number. All test samples shall be cut from a larger block to obtain freshly cut faces. Prior to physical testing, each test sample shall be cleaned of superfluous foam dust.



8.1.5.1.1.5 Polyurethane Foam Pour and Test Data Records

A production pour and testing record shall be compiled by the foam supplier during the foam pouring operation and subsequent physical testing. Upon completion of production and testing, the foam supplier shall issue certification referencing the production record data and test data pertaining to each foamed component. At a minimum, relevant pour and test data shall include:

- formulation, batch, and pour numbers, with foam material traceability, and pour date,
- foamed component description, part number, and serial number,
- instrumentation description, serial number, and calibration due date,
- pour and test data (e.g., date, temperature, dimensional, and/or weight measurements, compressive modulus, thermal conductivity, compressive stress, etc., as applicable), and
- technician and Quality Assurance/Quality Control (QA/QC) sign-off.

8.1.5.1.2 Physical Characteristics

The following subsections define the required physical characteristics of the polyurethane foam material used for the MFFP impact limiter designs.

Testing for the various polyurethane foam physical characteristics is based on a “formulation”, “batch”, or “pour”, as appropriate, as defined in Section 8.1.5.1.1, *Introduction and General Requirements*. The physical characteristics determined for a specific foam formulation are relatively insensitive to small variations in chemical constituents and/or environmental conditions, and therefore include physical testing for compressive modulus, Poisson’s ratio, thermal expansion coefficient, thermal conductivity, specific heat, and leachable chlorides. Similarly, the physical characteristics determined for a batch are only slightly sensitive to small changes in formulation and/or environmental conditions during batch mixing, and therefore

include physical testing for flame retardancy, intumescence, and leachable chlorides. Finally, the physical characteristics determined for a pour are also only slightly sensitive to small changes in formulation and slightly more sensitive to variations in environmental conditions during pour mixing, and therefore include physical testing for density and compressive stress.

8.1.5.1.2.1 Physical Characteristics Determined for a Foam Formulation

Foam material physical characteristics for the following parameters shall be determined once for a particular foam formulation. If multiple components are to be foamed utilizing a specific foam formulation, then additional physical testing, as defined below, need not be performed.

8.1.5.1.2.1.1 Thermal Conductivity

1. The thermal conductivity test shall be performed using a heat flow meter (HFM) apparatus. The HFM establishes steady state unidirectional heat flux through a test specimen between two parallel plates at constant but different temperatures. By measurement of the plate temperatures and plate separation, Fourier's law of heat conduction is used by the HFM to automatically calculate thermal conductivity. Description of a typical HFM is provided in ASTM C518⁶. The HFM shall be calibrated against a traceable reference specimen per the HFM manufacturer's operating instructions.
2. Three (3) test samples shall be taken from the sample pour. Each test sample shall be of sufficient size to enable testing per the HFM manufacturer's operating instructions.
3. Place the test samples in a room (ambient) temperature environment (i.e., 65 °F to 85 °F) for sufficient time to thermally stabilize the test samples.
4. Measure and record the necessary test sample parameters as input data to the HFM per the HFM manufacturer's operating instructions.
5. Perform thermal conductivity testing and record the measured thermal conductivity for each test sample following the HFM manufacturer's operating instructions.
6. Determine and record the average thermal conductivity of the three test samples. The numerically averaged thermal conductivity of the three test samples shall nominally be 0.24 Btu-in/hr-ft²-°F ±20% (i.e., within the range of 0.19 to 0.29 Btu-in/hr-ft²-°F) for 10 pounds per cubic foot (pcf) density foam and 0.26 Btu-in/hr-ft²-°F ±20% (i.e., within the range of 0.21 to 0.31 Btu-in/hr-ft²-°F) for 11½ pcf density foam.

8.1.5.1.2.1.2 Specific Heat

1. The specific heat test shall be performed using a differential scanning calorimeter (DSC) apparatus. The DSC establishes a constant heating rate and measures the differential heat flow into both a test specimen and a reference specimen. Description of a typical DSC is

⁶ ASTM C518, *Standard Test Method for Steady-State Heat Flux Measurements and Thermal Transmission Properties by Means of the Heat Flux Meter Apparatus*, American Society of Testing and Materials (ASTM).

provided in ASTM E1269⁷. The DSC shall be calibrated against a traceable reference specimen per the DSC manufacturer's operating instructions.

2. Three (3) test samples shall be taken from the sample pour. Each test sample shall be of sufficient size to enable testing per the DSC manufacturer's operating instructions.
3. Place the test samples in a room (ambient) temperature environment (i.e., 65 °F to 85 °F) for sufficient time to thermally stabilize the test samples.
4. Measure and record the necessary test sample parameters as input data to the DSC per the DSC manufacturer's operating instructions.
5. Perform specific heat testing and record the measured specific heat for each test sample following the DSC manufacturer's operating instructions.
6. Determine and record the average specific heat of the three test specimens. The numerically averaged specific heat at 75 °F of the three test samples shall be 0.35 Btu/lb_m-°F ±20% (i.e., within the range of 0.28 to 0.42 Btu/lb_m-°F).

8.1.5.1.2.1.3 Leachable Chlorides

1. The leachable chlorides test shall be performed using an ion chromatograph (IC) apparatus. The IC measures inorganic anions of interest (i.e., chlorides) in water. Description of a typical IC is provided in EPA Method 300.0⁸. The IC shall be calibrated against a traceable reference specimen per the IC manufacturer's operating instructions.
2. One (1) test sample shall be taken from a pour from each foam batch. The test sample shall be a cube with dimensions of 2.00 ±0.03 inches.
3. Place the test sample in a room (ambient) temperature environment (i.e., 65 °F to 85 °F) for sufficient time to thermally stabilize the test sample. Measure and record the room temperature to an accuracy of ±2 °F.
4. Obtain a minimum of 550 ml of distilled or de-ionized water for testing. The test water shall be from a single source to ensure consistent anionic properties for testing control.
5. Obtain a 400 ml, or larger, contaminant free container that is capable of being sealed. Fill the container with 262 ±3 ml of test water. Fully immerse the test sample inside the container for a duration of 72 ±3 hours. If necessary, use an inert standoff to ensure the test sample is completely immersed for the full test duration. Seal the container.
6. Obtain a second, identical container to use as a "control". Fill the control container with 262 ±3 ml of the same test water. Seal the control container.
7. At the end of the test period, measure and record the leachable chlorides in the test water per the IC manufacturer's operating instructions. The leachable chlorides in the test water shall not exceed one part per million (1 ppm).

⁷ ASTM E1269, *Standard Test Method for Determining Specific Heat Capacity by Differential Scanning Calorimetry*, American Society of Testing and Materials (ASTM).

⁸ EPA Method 300.0, *Determination of Inorganic Anions in Water by Ion Chromatography*, U.S. Environmental Protection Agency.

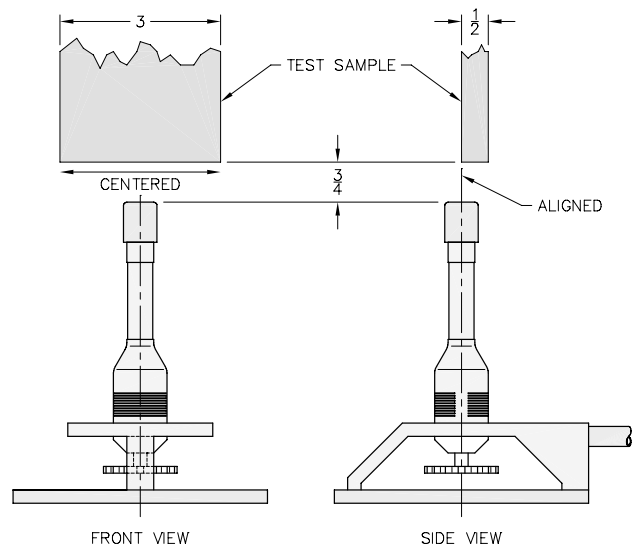
8. Should leachable chlorides in the test water exceed 1 ppm, measure and record the leachable chlorides in the test water from the “control” container. The difference in leachable chlorides from the test water and “control” water sample shall not exceed 1 ppm.

8.1.5.1.2.2 Physical Characteristics Determined for a Foam Batch

Foam material physical characteristics for the following parameters shall be determined once for a particular foam batch based on the formulation defined in Section 8.1.5.1.2.1, *Physical Characteristics Determined for a Foam Formulation*. If a single or multiple components are to be poured utilizing a single foam batch, then additional physical testing, as defined below, need not be performed for each foam pour. Foam used for the upper flange collar does not need to conform with this subsection.

8.1.5.1.2.2.1 Flame Retardancy

1. Three (3) test samples shall be taken from a pour from each foam batch. Each test sample shall be a rectangular prism with nominal dimensions of 0.5 inches thick, 3.0 inches wide, and a minimum length of 8.0 inches.
2. Place the test samples in a room (ambient) temperature environment (i.e., 65 °F to 85 °F) for sufficient time to thermally stabilize the test samples. Measure and record the room temperature to an accuracy of ± 2 °F.
3. Install a $\varnothing 3/8$ inches, or larger, Bunsen or Tirrill burner inside an enclosure of sufficient size to perform flame retardancy testing. Adjust the burner flame height to $1\frac{1}{2} \pm 1/8$ inches. Verify that the burner flame temperature is 1,550 °F, minimum.
4. Support the test sample with the long axis oriented vertically within the enclosure such that the test sample's bottom edge will be $3/4 \pm 1/16$ inches above the top edge of the burner.
5. Move the burner flame under the test sample for an elapsed time of 60 ± 2 seconds. As illustrated, align the burner flame with the front edge of the test sample thickness and the center of the test sample width.
6. Immediately after removal of the test sample from the burner flame, measure and record the following data:
 - a. Measure and record, to the nearest second, the elapsed time until flames from the test sample extinguish.
 - b. Measure and record, to the nearest second, the elapsed time until drips from the test sample extinguish.
 - c. Measure and record, to the nearest second, the burn length following cessation of all visible burning and smoking.
7. Flame retardancy testing acceptance is based on the following criteria:



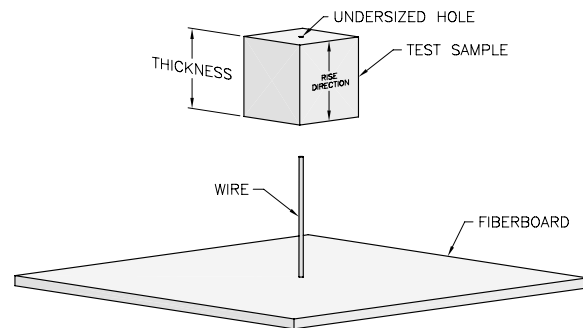
- a. The numerically averaged flame extinguishment time of each of the three test samples shall not exceed fifteen (15) seconds.
- b. The numerically averaged flame extinguishment time of drips from each of the three test samples shall not exceed three (3) seconds.
- c. The numerically averaged burn length of each of the three test samples shall not exceed six (6) inches.

8.1.5.1.2.2.2 Intumescence

1. Three (3) test samples shall be taken from a pour from each foam batch. Each test sample shall be a cube with nominal dimensions of 2.0 inches.
2. Place the test samples in a room (ambient) temperature environment (i.e., 65 °F to 85 °F) for sufficient time to thermally stabilize the test samples. Measure and record the room temperature to an accuracy of ± 2 °F.
3. Preheat a furnace to 1,475 °F ± 18 °F.
4. Identify two opposite faces on each test sample as the thickness direction. Measure and record the initial thickness (t_i) of each test sample to an accuracy of ± 0.01 inches.
5. Mount a test sample onto a fire resistant fiberboard, with one face of the thickness direction contacting to the board. The direction of foam rise shall be normal to the fiberboard face. As illustrated above, the test samples may be mounted by installing onto a 12 to 16 gauge wire ($\varnothing 0.105$ to $\varnothing 0.063$ inches, respectively) of sufficient length, oriented perpendicular to the fiberboard face. The test samples may be pre-drilled with an undersized hole to allow installation onto the wire.
6. Locate the test sample/fiberboard assembly over the opening of the pre-heated furnace for a 90 ± 3 second duration. After removal of the test sample/fiberboard assembly from the furnace, gently extinguish any remaining flames and allow the test sample to cool.
7. Remove the test sample from the fiberboard. Measure and record the final thickness (t_f) of the test sample to an accuracy of ± 0.1 inches.
8. For each sample tested, determine and record the intumescence, I , as a percentage of the original sample length as follows:

$$I = \left(\frac{t_f - t_i}{t_i} \right) \times 100$$

9. Determine and record the average intumescence of the three test samples. The numerically averaged intumescence of the three test samples shall be a minimum of 50%.



8.1.5.1.2.3 Physical Characteristics Determined for a Foam Pour

Foam material physical characteristics for the following parameters shall be determined for each foam pour based on the formulation defined in Section 8.1.5.1.2.1, *Physical Characteristics Determined for a Foam Formulation*.

8.1.5.1.2.3.1 Density

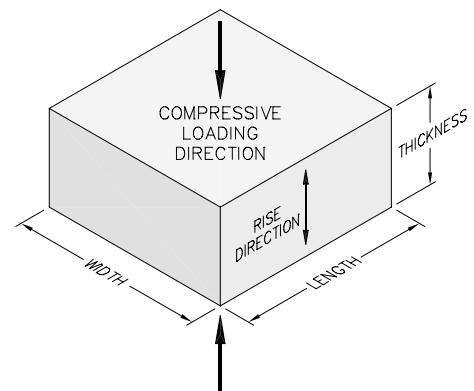
1. Three (3) test samples shall be taken from the foam pour. Each test sample shall be a rectangular prism with nominal dimensions of 1.0 inch thick (T), minimum, × 2.0 inches wide (W) × 2.0 inches long (L).
2. Place the test samples in a room (ambient) temperature environment (i.e., 65 °F to 85 °F) for sufficient time to thermally stabilize the test samples. Measure and record the room temperature to an accuracy of ±2 °F.
3. Measure and record the weight of each test sample to an accuracy of ±0.01 grams.
4. Measure and record the thickness, width, and length of each test sample to an accuracy of ±0.001 inches.
5. Determine and record the room temperature density of each test sample utilizing the following formula:

$$\rho_{\text{foam}} = \frac{\text{Weight, g}}{453.6 \text{ g/lb}_m} \times \frac{1,728 \text{ in}^3/\text{ft}^3}{T \times W \times L \text{ in}^3}, \text{pcf}$$

6. Determine and record the average density of the three test samples. The numerically averaged density of the three test samples shall nominally be within ±15% (i.e., within the range of 8.5 to 11.5 pcf for the nominal 10 pcf foam and 9.8 to 13.2 pcf for nominal 11½ pcf foam).

8.1.5.1.2.3.2 Parallel-to-Rise Compressive Stress

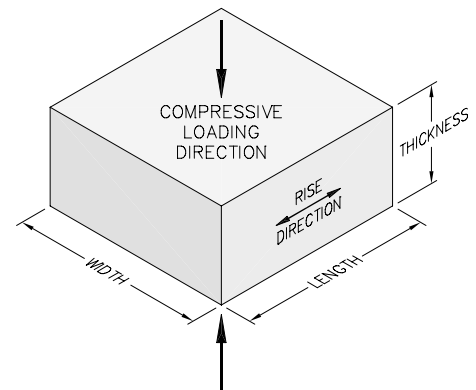
1. Three (3) test samples shall be taken from the foam pour. Each test sample shall be a rectangular prism with nominal dimensions of 1.0 inch thick (T) × 2.0 inches wide (W) × 2.0 inches long (L). The thickness dimension shall be the parallel-to-rise direction.
2. Place the test samples in a room (ambient) temperature environment (i.e., 65 °F to 85 °F) for sufficient time to thermally stabilize the test samples. Measure and record the room temperature to an accuracy of ±2 °F.
3. Measure and record the thickness, width, and length of each test sample to an accuracy of ±0.001 inches.
4. Compute and record the surface area of each test sample by multiplying the width by the length (i.e., W × L).
5. Place a test sample in a Universal Testing Machine. Lower the machine's crosshead until it touches the test sample. Set the machine's parameters for the thickness of the test sample.



6. Apply a compressive load to each test sample at a rate of 0.10 ± 0.05 inches/minute until a strain of 70%, or greater, is achieved. For each test sample, plot the compressive stress versus strain and record the compressive stress at strains of 10%, 40%, and 70%.
7. Determine and record the average parallel-to-rise compressive stress of the three test samples from each batch pour. As delineated in Table 8.1-1, the average parallel-to-rise compressive stress for each batch pour shall be the nominal compressive stress $\pm 20\%$ at strains of 10%, 40%, and 70%.
8. Determine and record the average parallel-to-rise compressive stress of all test samples from each foamed component. As delineated in Table 8.1-1, the average parallel-to-rise compressive stress for a foamed component shall be the nominal compressive stress $\pm 15\%$ at strains of 10%, 40%, and 70%.

8.1.5.1.2.3.3 Perpendicular-to-Rise Compressive Stress

1. Three (3) test samples shall be taken from the foam pour. Each test sample shall be a rectangular prism with nominal dimensions of 1.0 inch thick (T) \times 2.0 inches wide (W) \times 2.0 inches long (L). The thickness dimension shall be the perpendicular-to-rise direction.
2. Place the test samples in a room (ambient) temperature environment (i.e., 65 °F to 85 °F) for sufficient time to thermally stabilize the test samples. Measure and record the room temperature to an accuracy of ± 2 °F.
3. Measure and record the thickness, width, and length of each test sample to an accuracy of ± 0.001 inches.
4. Compute and record the surface area of each test sample by multiplying the width by the length (i.e., $W \times L$).
5. Place a test sample in a Universal Testing Machine. Lower the machine's crosshead until it touches the test sample. Set the machine's parameters for the thickness of the test sample.
6. Apply a compressive load to each test sample at a rate of 0.10 ± 0.05 inches/minute until a strain of 70%, or greater, is achieved. For each test sample, plot the compressive stress versus strain and record the compressive stress at strains of 10%, 40%, and 70%.
7. Determine and record the average perpendicular-to-rise compressive stress of the three test samples from each batch pour. As delineated in Table 8.1-1, the average perpendicular-to-rise compressive stress for each batch pour shall be the nominal compressive stress $\pm 20\%$ at strains of 10%, 40%, and 70%.
8. Determine and record the average perpendicular-to-rise compressive stress of all test samples from each foamed component. As delineated in Table 8.1-1, the average perpendicular-to-rise compressive stress for a foamed component shall be the nominal compressive stress $\pm 15\%$ at strains of 10%, 40%, and 70%.



8.1.5.2 Neutron Poison Plates

8.1.5.2.1 Visual Examinations

The neutron poison plates specified on the drawings in Appendix 1.4.2, *Packaging General Arrangement Drawings* shall be visually examined for defects and cracks prior to being installed on the strongback.

8.1.5.2.2 Dimensional Inspections

The neutron poison plates shall be verified to meet the dimensional requirements specified on the drawings in Appendix 1.4.2, *Packaging General Arrangement Drawings* prior to being installed on the strongback.

8.1.5.2.3 Boron Areal Density

The neutron poison plates (i.e., boron) specified on the drawings in Appendix 1.4.2, *Packaging General Arrangement Drawings* shall be verified to have a minimum total boron per unit area of the sandwiched material. Samples from each sheet portion of the neutron absorber are to be retained for testing and record purposes. The boron-10 (^{10}B) areal density within a panel shall be verified by wet chemical analysis and/or neutron attenuation testing to be 0.035 gram/cm² or greater. The acceptance standards shall be controlled by statistical data to ensure the minimum requirements are achieved with a 95% probability at a 95% confidence level. The maximum variations in the manufacturing processes (statistical tolerance interval) over a significantly large sample size shall be the basis of the acceptance criteria. All material certifications, lot control records, and test records are to be maintained to ensure material traceability.

Table 8.1-1 – Acceptable Compressive Stress Ranges for Foam (psi)

Sample Range	Parallel-to-Rise at Strain, $\epsilon_{ }$						Perpendicular-to-Rise at Strain, ϵ_{\perp}					
	$\epsilon = 10\%$		$\epsilon = 40\%$		$\epsilon = 70\%$		$\epsilon = 10\%$		$\epsilon = 40\%$		$\epsilon = 70\%$	
Foam Density (pcf)	10	11½	10	11½	10	11½	10	11½	10	11½	10	11½
Nominal -20%	286	376	333	444	899	1328	264	348	318	432	892	1380
Nominal -15%	304	400	354	472	955	1411	281	370	338	459	948	1466
Nominal	358	470	416	555	1124	1660	330	435	398	540	1115	1725
Nominal +15%	412	541	478	638	1293	1909	380	500	458	621	1282	1984
Nominal +20%	430	564	499	666	1349	1992	396	522	478	648	1338	2070

8.1.6 Shielding Tests

The MFFP does not contain any biological shielding.

8.1.7 Thermal Tests

Material properties utilized in Chapter 3.0, *Thermal Evaluation*, are consistently conservative for the normal conditions of transport (NCT) and hypothetical accident condition (HAC) thermal analyses performed. As such, with the exception of the tests required for polyurethane foam, as shown in Section 8.1.5, *Component and Material Tests*, specific acceptance tests for material thermal properties are not performed.

This page left intentionally blank.

8.2 Maintenance Program

This section describes the maintenance program used to ensure continued performance of the MFFP.

8.2.1 Structural and Pressure Tests

Perform structural pressure testing on the MFFP containment vessel per the requirements of Section 8.1.3.2, *Pressure Testing*, once every five years. Upon completing the structural pressure test, perform leakage rate testing per the requirements of Section 8.1.4, *Fabrication Leakage Rate Tests*.

8.2.2 Maintenance/Periodic Leakage Rate Tests

This section provides the generalized procedure for maintenance and periodic leakage rate testing of the containment vessel penetrations during routine maintenance, or at the time of seal replacement or seal area repair. Verification leakage rate testing shall follow the guidelines of Section 7.4, *Maintenance Leakage Rate Test*, and Section 7.5, *Periodic Leakage Rate Test*, of ANSI N14.5¹.

Maintenance and periodic leakage rate testing shall be performed on the main O-ring seal, vent port seal, and fill port seal in accordance with Section 8.2.2.2, *Helium Leakage Rate Testing the Main O-ring Seal*, Section 8.2.2.3, *Helium Leak Testing the Vent Port Plug O-ring Seal*, and Section 8.2.2.4, *Helium Leakage Rate Testing the Fill Port Plug O-ring Seal*, respectively.

8.2.2.1 Maintenance/Periodic Verification Leakage Rate Test Acceptance Criteria

Maintenance and periodic verification leak testing acceptance criteria are identical to the criteria delineated in Section 8.1.4.1, *Fabrication Leakage Rate Test Acceptance Criteria*.

8.2.2.2 Helium Leakage Rate Testing the Main O-ring Seal

1. The maintenance/periodic verification leak test of the MFFP containment O-ring seal integrity shall be performed following the guidelines of Section A.5.4, *Evacuated Envelope – Gas Detector*, of ANSI N14.5.
2. Assemble the MFFP with the three O-ring seals installed in the closure lid. Ensure the vent, seal test, and fill port plugs are installed with their associated O-ring seals. Assembly is as shown on the drawings in Appendix 1.4.2, *Packaging General Arrangement Drawings*.
3. Utilizing a test port tool, attach a vacuum pump and a source of helium gas, in parallel, to the fill port.
4. Close the valve to the source of helium gas and open the valve to the vacuum pump.
5. Utilizing a test port tool, rotate the fill port plug to the open position.
6. Evacuate the system to a 90% vacuum or better ($\leq 10\%$ ambient atmospheric pressure). Isolate the vacuum pump from the system.

¹ ANSI N14.5-1997, *American National Standard for Radioactive Materials – Leakage Tests on Packages for Shipment*, American National Standards Institute, Inc. (ANSI).

7. Provide a helium atmosphere inside the evacuated cavity by backfilling with helium gas (99% purity or better) to ambient atmospheric pressure (+1 psi, -0 psi).
8. Utilizing a test port tool, rotate the fill port plug to the closed position, and remove the helium-contaminated test port tool from the fill port.
9. Install a clean (helium-free) test port tool into the seal test port.
10. Utilizing appropriate fittings, attach a helium mass spectrometer leak detector (MSLD) to the test port tool.
11. Utilizing the test port tool, rotate the seal test port plug to the open position.
12. Evacuate the cavity above the lid containment O-ring seal until the vacuum is sufficient to operate the leak detector per the manufacturer's recommendations.
13. Perform the helium leakage rate test to the requirements of Section 8.2.2.1, *Maintenance/Periodic Leakage Rate Test Acceptance Criteria*. If, after repeated attempts, the MFFP containment O-ring seal fails to pass the leak test, isolate the leak path and, prior to repairing the leak path and repeating the leak test, record on a nonconformance report and disposition prior to final acceptance in accordance with the cognizant quality assurance program.

8.2.2.3 Helium Leakage Rate Testing the Vent Port Plug O-ring Seal

1. The maintenance/periodic verification leak test of the MFFP vent port plug O-ring containment seal integrity shall be performed following the guidelines of ANSI N14.5, Section A.5.4, *Evacuated Envelope – Gas Detector*.
2. The MFFP shall be assembled with all three O-ring seals installed on the closure lid. Ensure the vent, seal test, and fill port plugs are installed with their associated O-ring seals. Assembly is as shown on the MFFP drawings in Appendix 1.4.2, *Packaging General Arrangement Drawings*.
3. Verify the presence of a helium atmosphere below the vent port plug O-ring containment seal, as specified above in Steps 3 – 8 of Section 8.2.2.2, *Helium Leakage Rate Testing the Main O-ring Seal*.
4. Install a test port tool into the vent port.
5. Utilizing appropriate fittings, attach a helium MSLD to the test port tool.
6. Evacuate the cavity above the vent port plug O-ring containment seal until the vacuum is sufficient to operate the leak detector per the manufacturer's recommendations.
7. Perform the helium leakage rate test to the requirements of Section 8.2.2.1, *Maintenance/Periodic Leakage Rate Test Acceptance Criteria*. If, after repeated attempts, the vent port plug O-ring containment seal fails to pass the leak test, isolate the leak path and, prior to repairing the leak path and repeating the leak test, record on a nonconformance report and disposition prior to final acceptance in accordance with the cognizant quality assurance program.

8.2.2.4 Helium Leakage Rate Testing the Fill Port Plug O-ring Seal

1. The maintenance/periodic verification leak test of the MFFP fill port closure bolt O-ring containment seal integrity shall be performed following the guidelines of Section A.5.4, *Evacuated Envelope – Gas Detector*, of ANSI N14.5.
2. The MFFP shall be assembled with all three O-ring seals installed on the lid. Ensure the vent, seal test, and fill ports are installed with their associated O-ring seals. Assembly is as shown on the MFFP drawings in Appendix 1.4.2, *Packaging General Arrangement Drawings*.
3. Verify the presence of a helium atmosphere below the fill port plug O-ring containment seal, as specified above in Steps 3 – 8 of Section 8.2.2.2, *Helium Leakage Rate Testing the Main O-ring Seal*.
4. Install a test port tool into the fill port.
5. Utilizing appropriate fittings, attach a helium MSLD to the test port tool.
6. Evacuate the cavity above the fill port closure bolt O-ring containment seal until the vacuum is sufficient to operate the leak detector per the manufacturer's recommendations.
7. Perform the helium leakage rate test to the requirements of Section 8.2.2.1, *Maintenance/Periodic Leakage Rate Test Acceptance Criteria*. If, after repeated attempts, the MFFP fill port closure bolt O-ring containment seal fails to pass the leak test, isolate the leak path and, prior to repairing the leak path and repeating the leak test, record on a nonconformance report and disposition prior to final acceptance in accordance with the cognizant quality assurance program.

8.2.3 Component and Material Tests

8.2.3.1 Fasteners

All threaded components shall be visually inspected annually for deformed or stripped threads. Damaged threaded components shall be repaired or replaced prior to further use. The threaded components to be visually inspected include the containment lid bolts, vent port closure bolt, fill port closure bolt, seal test port closure bolt, strongback/neutron plate fasteners, fuel channel support fasteners, and impact limiter bolts.

All quick-release pins shall be visually inspected annually for proper operation and damage. Inoperable or damaged pins shall be repaired or replaced prior to further use.

8.2.3.2 Seal Areas and Grooves

8.2.3.2.1 Seal Area Routine Inspection and Repair

Before each use and at the time of seal replacement, the sealing surfaces on the closure lid and body shall be visually inspected for damage that could impair the sealing capabilities of the MFFP. Perform surface finish inspections for the body upper forging, and the O-ring grooves and sealing surfaces on the closure lid. Damage shall be repaired prior to further use (e.g., using emery cloth or other surface finishing techniques) to restore the sealing surfaces to the surface finish specified in Section 8.2.3.2.2, *Surface Finish of Sealing Areas*.

Upon completion of containment seal area repairs, perform a leakage rate test per the applicable section of Section 8.2.2, *Maintenance/Periodic Leakage Rate Tests*.

8.2.3.2.2 Surface Finish of Sealing Areas

The surface finish for the main O-ring sealing regions shall be a 125 micro-inch finish, or better, to maintain package configuration and performance to design criteria. If the surface condition is determined to exceed 125 micro-inch, repair the surface per the requirements of Section 8.2.3.2.1, *Seal Area Routine Inspection and Repair*.

8.2.3.3 Impact Limiters

Before each use, the impact limiters shall be inspected for tears or perforations in the stainless steel sheets, and for the presence of the fire-consumable plastic plugs. Any damage shall be repaired prior to further use.

8.2.3.4 Strongback

Before each use, the strongback (including neutron poison plates) shall be inspected for missing or damaged components. Any damage shall be repaired prior to further use.

8.2.3.5 Fuel Control Structures

Before each use, the fuel control structures (FCSs), including neutron poison plates, shall be inspected for missing or damaged components. Any damage shall be repaired prior to further use.

8.2.3.6 Seals

All containment O-ring seals shall be replaced annually (or when damaged) per the specifications as delineated on the drawings in Appendix 1.4.2, *Packaging General Arrangement Drawings*. Following seal replacement and prior to a loaded shipment, the seal(s) shall be leakage rate tested to the requirements of Section 8.2.2, *Maintenance/Periodic Verification Leak Tests*.

8.2.4 Thermal Tests

No thermal tests are necessary to ensure continued performance of the MFFP.

8.2.5 Miscellaneous Tests

No miscellaneous tests are necessary to ensure continued performance of the MFFP.



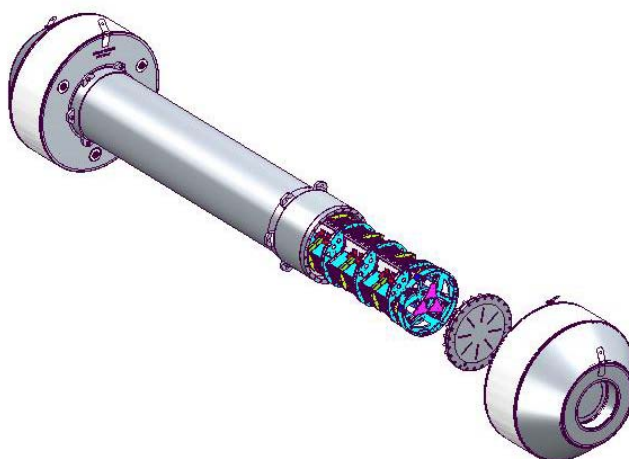
DOCKET 71-9295

Mixed Oxide Fresh Fuel Package

Appendix A: ARB-17

**Appendix B: AFS-B with 175 MOX rods and
Excess Material Assembly**

Appendix C: AFS-C with TA-18 MOX Rods



Safety Analysis Report

Volume 2
Revision 7
July 2008

This page left intentionally blank.

A1.0 GENERAL INFORMATION

Appendix A of the MOX Fresh Fuel Package (MFFP) Safety Analysis Report (SAR) supports the addition of the Areva Rod Box-17 (ARB-17) as an allowable content of the MFFP. The ARB-17 is a rod container designed to transport up to 17 MOX fuel rods. The rod type is identical to the rods comprising the standard MOX fuel assembly described in Chapter 1.0, *General Information*. The ARB-17 is described in more detail in the following sections.

In this SAR Appendix, reference is made to the main SAR for information that has not changed. Referenced tables, figures, and sections that do not contain the letter “A” (e.g., Table 1.2-1, Figure 3.5-1, Section 6.1.1) refer to items in the main SAR. Referenced tables, figures, and sections that contain the letter “A” (e.g., Table A6.4-1, Figure A1.2-1, Section A6.1.1) refer to items in Appendix A.

A1.1 Introduction

The Mixed Oxide Fresh Fuel Package, Model: **MFFP**, is designed to transport fresh MOX pressurized water reactor (PWR) fuel assemblies. The ARB-17 MOX fuel rod container has been designed with outer dimensions consistent with a standard fuel assembly so that it will interface properly with the strongback and clamp arms.

A full-scale, prototypic certification test unit (CTU) was subjected to a series of hypothetical accident condition (HAC) free and puncture drop tests as part of the original SAR submittal. The results of this testing program are directly applicable to the ARB-17 payload because the loaded ARB-17 payload weight (approximately 1,525 pounds) is bounded by the weight of a fuel assembly (1,580 pounds), and also because the ARB-17 itself does not perform a structural function. A detailed discussion of the CTU and certification tests is provided in Appendix 2.12.3, *Certification Test Results*. These tests, coupled with supplementary analytical evaluations in Chapter A2.0, *Structural Evaluation*, conclusively demonstrates the leaktight¹ containment boundary integrity and structural performance of the MFFP with a payload containing one or more ARB-17 containers.

The thermal analysis for the ARB-17 payload is provided in Chapter A3.0, *Thermal Evaluation*. Because an ARB-17 contains significantly less decay heat than a fuel assembly, MFFP strongback and shell temperatures are bounded by those reported in Chapter 3.0, *Thermal Evaluation*. However, due primarily to the simplistic analytical method employed, under HAC the maximum fuel rod temperature for rods within the ARB-17 is computed to be higher than the maximum temperature computed for a fuel assembly. This temperature is well within the HAC temperature limit for a fuel rod. The HAC internal pressure also increases somewhat when using an ARB-17 due to the increased mass of combustibles within this item.

Based on the shielding and criticality assessments provided in Chapter A5.0, *Shielding Evaluation*, and Chapter A6.0, *Criticality Evaluation*, the Criticality Safety Index (CSI) for the MFFP is zero (0.0), and the Transport Index (TI) is determined at the time of shipment.

¹ Leaktight is defined as 1×10^{-7} standard cubic centimeters per second (scc/s), or less, air leakage per ANSI N14.5-1997, *American National Standard for Radioactive Materials – Leakage Tests on Packages for Shipment*, American National Standards Institute, (ANSI), Inc

Authorization is sought for shipment of the MFFP with the ARB-17 payload by all modes of conveyance, except for aircraft, as a Type B(U)F package per the definitions delineated in 10 CFR §71.4.

A1.2 Package Description

General arrangement drawings of the packaging are provided in Section 1.4.2, *Packaging General Arrangement Drawings*. The addition of the ARB-17 does not alter these packaging drawings because the ARB-17 is included with the contents.

A1.2.1 Packaging

The packaging description is unchanged from the description provided in Section 1.2.1, *Packaging*.

A1.2.2 Containment System

The containment system description is unchanged from the description provided in Section 1.2.2, *Containment System*.

A1.2.3 Contents of Packaging

The MFFP may carry up to three (3) ARB-17 containers. The ARB-17 itself is part of the contents and not part of the packaging. For shipping less than a total of three fuel assemblies and ARB-17 containers, non-fuel dummy fuel assemblies are utilized in the unoccupied strongback locations to balance the weight. Any combination of ARB-17, standard fuel assembly, and dummy fuel assembly is acceptable (e.g., 1 ARB-17 and 2 fuel assemblies; 1 ARB-17, 1 fuel assembly, and 1 dummy fuel assembly; 3 ARB-17s, etc.). The physical size and weight of the dummy fuel assemblies are nominally the same as the MK-BW/MOX1 17 × 17 design. The physical fuel rod parameters provided in Table 1.2-1 and nuclear design parameters provided in Table 1.2-2 are applicable to fuel rods in the ARB-17.

A sketch of the ARB-17 is provided in Figure A1.2-1. The exterior enclosure of the ARB-17 consists of 0.75 inch thick stainless steel side walls with a 1.5 inch thick stainless steel top end closure plate and a 0.75 inch thick stainless steel bottom end closure plate. The outside envelope of the ARB-17 is 8.43 inches square by 159.85 inches long (not including the swivel hoist ring). A swivel hoist ring is mounted to the top of the ARB-17 to facilitate vertical handling.

Each ARB-17 may contain up to 17 MOX fuel rods, which may be either undamaged, slightly damaged, or a combination of both (e.g., 9 undamaged and 8 slightly damaged). Slightly damaged fuel rods may be bent, scratched, or dented, but under no circumstances may exhibit cladding breach. A 2-inch, Schedule 40 pipe mounted with pipe clamps against one wall of the ARB-17 is used to transport both undamaged or slightly damaged fuel rods. Slightly damaged fuel rods may be transported within this pipe only if the bending in the fuel rod is minor. Examples of allowable ARB-17 loading are illustrated in Figure A1.2-2.

A Buna-N rubber pad is used at the top of the fuel support pipe to cushion the ends of the fuel rods. To limit movement of the fuel rods during shipment, stainless steel dunnage rods are used as needed to fill the remaining void within the fuel support pipe (the pipe component may fit a maximum of 22 fuel and dunnage rods). Each undamaged fuel rod is inserted into a polypropylene sleeve that is 0.004 inches thick and ≤ 2 inches in circumference (diameter ≤ 0.637 inches) to prevent scratching of the cladding.

Slightly damaged fuel rods with bending that precludes shipment in the fuel support pipe are clamped in the C-channel within the ARB-17. Any unused space is filled with stainless steel dunnage rods, as needed. Fuel rods exhibiting cladding breach are not acceptable for transportation in an ARB-17. Use of polypropylene sleeves for the slightly damaged rods is optional.

A1.2.3.1 Radionuclide Inventory

The nuclear parameters for the ARB-17 rods are unchanged from those provided in Table 1.2-2.

A1.2.3.2 Maximum Payload Weight

A conservative weight of approximately 1,525 pounds may be determined for the ARB-17 by assuming 17 slightly damaged fuel rods in the C-channel and 22 stainless steel dunnage rods in the pipe component. This weight is bounded by the 1,580 pound weight of a fuel assembly (including a BPRA). The maximum MFFP payload weight for a payload containing an ARB-17 (i.e., two fuel assemblies and one ARB-17) is 4,685 pounds. Therefore, the maximum payload weight is bounded by the value of 4,740 pounds provided in Section 1.2.3.2, *Maximum Payload Weight*.

A1.2.3.3 Maximum Decay Heat

The maximum decay heat of an ARB-17 is $17/264 \times 80 = 5.15$ watts, which is bounded by the 80 watt decay heat of a standard fuel assembly. The maximum MFFP decay heat for a payload containing an ARB-17 (i.e., two fuel assemblies and one ARB-17) is 165 watts. This maximum heat load is bounded by the 240 watts provided in Section 1.2.3.3, *Maximum Decay Heat*.

A1.2.3.4 Maximum Pressure Buildup

The maximum normal operating pressure (MNOP) of the MFFP transporting one or more ARB-17 rod containers is bounded by the 10 psig value provided in Section 1.2.3.4, *Maximum Pressure Buildup*.

A1.2.4 Operational Features

Operating procedures and instructions for loading, unloading, and preparing an empty MFFP for transport with the ARB-17 are provided in Chapter A7.0, *Package Operations*.

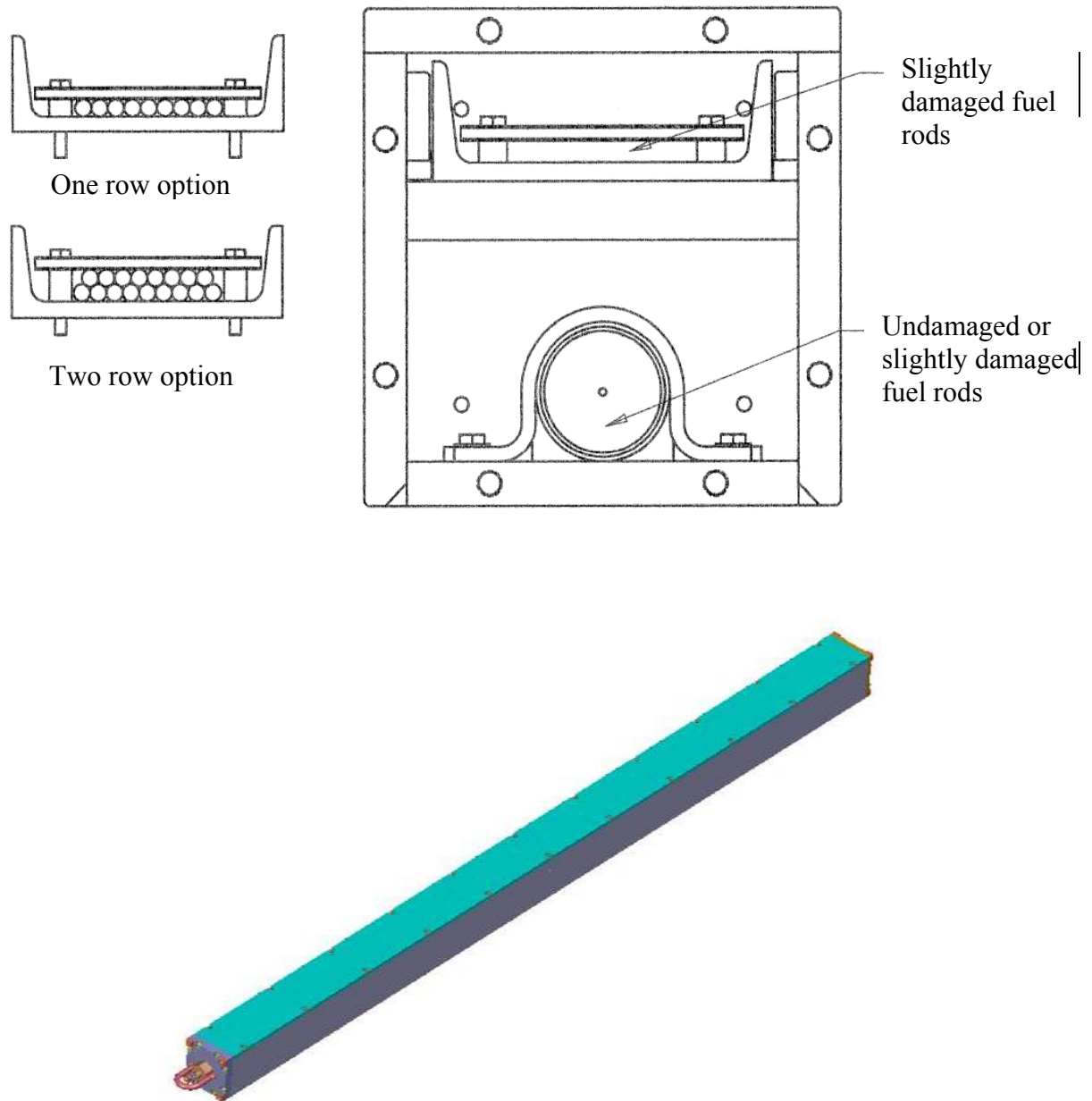
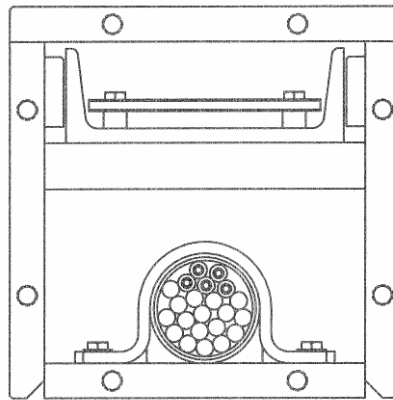
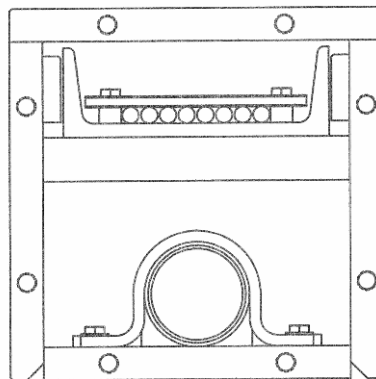


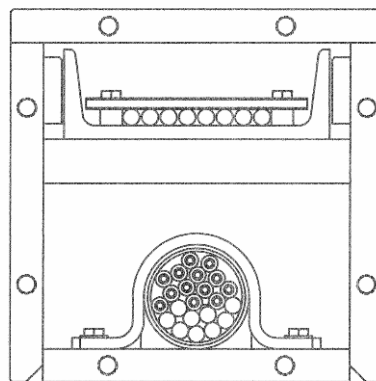
Figure A1.2-1 – ARB-17 Sketches



Example 1: 17 fresh fuel rods and 5 dunnage rods, empty C-channel



Example 2: 8 slightly damaged fuel rods in C-channel, empty pipe component



Example 3: 8 slightly damaged rods in C-channel, 9 fresh fuel rods and 13 dunnage rods in pipe component

Figure A1.2-2 – ARB-17 Sample Loadings

A1.3 General Requirements for All Packages

The ARB-17 has no effect on the way in which the MFFP meets the general requirements for packaging.

This page left intentionally blank.

A1.4 Appendices

A1.4.1 Nomenclature

The nomenclature list from Section 1.4.1, *Nomenclature*, is applicable. Additional nomenclature listed below.

ARB-17 – Container used to transport up to 17 standard MOX fuel rods, which may be either undamaged or exhibit minor damage.

A1.4.2 Packaging General Arrangement Drawings

The general arrangement drawings are unchanged from those provided in Section 1.4.2, *Packaging General Arrangement Drawings*. Because the ARB-17 is included with the contents and not the packaging, packaging drawings are not necessary for this component.

This page left intentionally blank.

A2.0 STRUCTURAL EVALUATION

This chapter of Appendix A provides a structural evaluation of the MFFP when transporting the ARB-17 fuel rod container. Inclusion of a maximum of three (3) ARB-17 containers is evaluated. A payload of three (3) ARB-17 containers results in the highest HAC internal pressure and bounds the cases in which one (1) or two (2) ARB-17 containers are transported, with the remaining positions in the strongback loaded with dummy fuel assemblies or standard MOX fuel assemblies.

A2.1 Structural Design

A2.1.1 Discussion

A comprehensive discussion of the MFFP design and standard configuration is provided in Section 1.2, *Package Description*. The MFFP drawings show the detailed geometry of the package, as well as the dimension, tolerances, materials, and fabrication requirements, and are provided in Appendix 1.4.2, *Packaging General Arrangement Drawings*. A physical description of the ARB-17 is provided in Section A1.2.3, *Contents of Packaging*. The following discussion is limited to the ARB-17.

Because the ARB-17 is a payload container and not a packaging component, and its presence is not required to meet criticality limits, no structural analysis is performed for the ARB-17 in support of the MFFP license.

The overall dimensions allow the ARB-17 to occupy no more space within the strongback than a MOX fuel assembly. The structural evaluations and testing performed as part of the original license activities adequately characterize the performance of the MFFP with this payload in all cases except HAC pressure, as described in section A2.7.4, *Thermal*.

A2.1.2 Design Criteria

The MFFP design criteria are unchanged from those provided in Section 2.1.2, *Design Criteria*. Because the ARB-17 is not a packaging component, no licensing design criteria are applicable for this component. The ARB-17 is not a criticality control structure, and no credit for the ARB-17 is taken in the criticality analysis presented in Chapter A6.0, *Criticality Evaluation*.

A2.1.3 Weights and Center of Gravity

The loaded weight of the ARB-17, conservatively assuming 17 fuel rods and 22 stainless steel dunnage rods, is 1,525 pounds, which is 3.5% less than the gross weight of 1,580 pounds for a fuel assembly or dummy fuel assembly. Therefore, the weight of the MFFP when transporting one or more ARB-17 containers is bounded by the weights given in Section 2.1.3, *Weights and Center of Gravity*, for transport of MOX fuel assemblies.

The longitudinal center of gravity (CG) of the package is essentially unchanged from the CG when package contains three (3) fuel assemblies, or 103.7 inches from the bottom end impact limiter.

A2.2 Materials

The ARB-17 is constructed primarily of stainless steel plate, with a Buna-N rubber bumper to tightly secure the fuel rods. Stainless steel is already used in the MFFP, and the Buna-N material is similar to butyl rubber used in the O-rings. These materials do not result in any chemical or galvanic reactions, and are not significantly affected by radiation.

No structural function is credited for the ARB-17; therefore, no additional structural properties are included in this Appendix.

A2.3 Fabrication and Examination

Because the ARB-17 is not a packaging component, a discussion of fabrication and examination is not applicable.

A2.4 Lifting and Tie-down Standards for All Packages

Because the gross weight of the MFFP is lower when transporting the ARB-17 container, this section is unchanged from Section 2.4, *Lifting and Tie-down Standards for All Packages*.

A2.5 General Considerations

The results and conclusions of this section remain unchanged from Section 2.5, *General Considerations*.

A2.6 Normal Conditions of Transport

A2.6.1 Heat

It is demonstrated in Section A3.4, *Thermal Evaluation for Normal Conditions of Transport*, that under NCT the MFFP strongback and shell temperatures associated with the ARB-17 payload are bounded by the standard three (3) fuel assembly payload. Therefore, all associated pressure and thermal stresses are bounded by the values presented in Section 2.6.1, *Heat*.

A2.6.2 Cold

This section is unchanged from Section 2.6.2, *Cold*.

A2.6.3 Reduced External Pressure

This section is unchanged from Section 2.6.3, *Reduced External Pressure*.

A2.6.4 Increased External Pressure

This section is unchanged from Section 2.6.4, *Increased External Pressure*.

A2.6.5 Vibration and Shock

Because the ARB-17 is stiffer and more robust than a fuel assembly, the presence of an ARB-17 would help stiffen the strongback structure and further dampen any vibrations. Therefore, the results in Section A.2.6.5, *Vibration and Shock*, remain bounding.

A2.6.6 Water Spray

This section is unchanged from Section 2.6.6, *Water Spray*.

A2.6.7 Free Drop

Because a loaded ARB-17 is slightly lighter than a fuel assembly (including BPRA), the response of the MFFP to a free drop would be essentially the same when compared to the standard payload.

A2.6.8 Corner Drop

This section is unchanged from Section 2.6.8, *Corner Drop*.

A2.6.9 Compression

This section is unchanged from Section 2.6.9, *Compression*.

A2.6.10 Penetration

This section is unchanged from Section 2.6.10, *Penetration*.

A2.7 Hypothetical Accident Conditions

A2.7.1 Free Drop

The weight of the MFFP containing one or more ARB-17 containers is bounded by the weight of the MFFP with a payload of three (3) standard fuel assemblies. Because the ARB-17 is stiffer than the standard fuel assembly, it will provide more of its own support, particularly the case of lateral loading (e.g., the side or slapdown orientations). Therefore, the system response to a free drop is bounded by the discussion presented in Section 2.7.1, *Free Drop*.

A2.7.2 Crush

This section is unchanged from Section 2.7.2, *Crush*.

A2.7.3 Puncture

The weight of the MFFP containing one or more ARB-17 containers is bounded by the weight of the MFFP with a payload of three (3) standard fuel assemblies. Therefore, the system response to a puncture is bounded by the discussion presented in Section 2.7.3, *Puncture*.

A2.7.4 Thermal

A2.7.4.1 Summary of Pressures and Temperatures

Package pressures and temperatures due to the HAC thermal event are presented in Section A3.5.3, *Maximum Temperatures and Pressures*. MFFP strongback and shell temperatures under HAC associated with the ARB-17 payload are bounded by the standard three (3) fuel assembly payload. From Table A3.5-1, the maximum internal pressure during the HAC thermal event is 146.0 psig (160.7 psia), with the package initially at atmospheric pressure. This pressure exceeds the true pressure under HAC, as little combustion/pyrolysis of the polymer materials is expected, and most fuel rods will not rupture. For stress analysis purposes, a pressure of 150 psig is used, which conservatively bounds the maximum internal pressure. This value is 20 psig higher than the maximum pressure used in the standard payload analysis (130 psig). The reason for the increase is the larger amount of combustibles in the ARB-17 compared to a fuel assembly (i.e., rubber bumper and polypropylene sleeves for the fuel rods).

A2.7.4.2 Differential Thermal Expansion

This section is unchanged from Section 2.7.4.2, *Differential Thermal Expansion*, as the temperatures are bounded by the standard payload temperatures.

A2.7.4.3 Stress Calculations

As discussed in Section A2.7.4.1, *Summary of Pressures and Temperatures*, a conservative maximum internal pressure of 150 psig is assumed under HAC. Shell stresses due to the design pressure of 25 psig are calculated in Section 2.6.1, *Heat*. Therefore, the stress in the shell due to the HAC maximum pressure is found from:

$$\sigma_{HAC} = \frac{150}{25} \sigma_{NCT}$$

The results of this scaling for the shell, bottom end closure, and closure lid are shown in Table A2.7-1. For simplicity, the bottom end and closure lid stresses used in the scaling are peak values, but allowable stresses for membrane-only stress (the lesser of $2.4S_m$ or $0.7S_u$) are conservatively used. As shown, the minimum margin of safety is +1.73.

A2.7.5 Immersion – Fissile Material

This section is unchanged from Section 2.7.5, *Immersion – Fissile Material*.

A2.7.6 Immersion – All Packages

This section is unchanged from Section 2.7.6, *Immersion – All Packages*.

A2.7.7 Deep Water Immersion Test (for Type B Packages Containing More than 10^5 A₂)

This section is unchanged from Section 2.7.7, *Deep Water Immersion Test*.

A2.7.8 Summary of Damage

The ARB-17 is acceptable for use as a payload container. The response of the MFFP to drop and puncture accidents is bounded when using the ARB-17. Temperatures and thermal stresses of the packaging are also bounded when using the standard payload. The only non-conservative change when comparing against the standard payload is an increase in thermal pressure stresses as a result of assumed combustion of plastics within the ARB-17. However, the minimum margin of safety of +1.73 is acceptable with considerable margin.

Table A2.7-1 – HAC Thermal Pressure Stresses and Margins of Safety

Component	Stress at 25 psia Internal Pressure (psi)	Stress at 150 psia Internal Pressure (psi)	Allowable Stress (psi)^①	Margin of Safety
Shell	674	4,044	11,055	+1.73
Closure Lid	1,510	9,060	65,940	+6.28
Bottom End Closure	2,904	17,424	65,940	+2.78

Notes:

① See Section 2.7.4.3, *Stress Calculations*, for derivation of these allowable stress values.

A2.8 Accident Conditions for Air Transport of Plutonium

This section does not apply for the MFFP, since air transport is not claimed.

A2.9 Accident Conditions for Fissile Material Packages for Air Transport

This section does not apply for the MFFP, since air transport is not claimed.

A2.10 Special Form

This section does not apply for the MFFP, since special form is not claimed.

A2.11 Fuel Rods

This section does not apply for the MFFP, since containment by the fuel rod cladding is not claimed.

A2.12 Appendices

There are no appendices to Chapter A2.0. The applicability of the appendices to Chapter 2, *Structural Evaluation*, is given in Table A2.12-1.

Table A2.12-1 – Applicability of Section 2.12 Appendices to the ARB-17 Payload

Appendix	Applicability
2.12.1, Impact Limiter Evaluation	As the weight of the ARB-17 is bounded by the weight of a fuel assembly, the impact limiter evaluation from Section 2.12.1 remains bounding.
2.12.2, Certification Test Plan	Unchanged from Section 2.12.2
2.12.3, Certification Test Results	Unchanged from Section 2.12.3
2.12.4, Engineering Test Results	Unchanged from Section 2.12.4
2.12.5, Fuel Control Structural Evaluation	As the weight of the ARB-17 is bounded by the weight of a fuel assembly, and because it is more structurally robust than a fuel assembly, the fuel control structural evaluation from Section 2.12.5 remains bounding.
2.12.6, CASKDROP Computer Program	Unchanged from Section 2.12.6
2.12.7, Impact Limiter Weld Joint Test Results	Unchanged from Section 2.12.7
2.12.8, Effect of Bounding Weight on Package Structural Responses	As the weight of the ARB-17 is bounded by the weight of a fuel assembly, the package structural responses evaluation from Section 2.12.8 remains bounding.

A3.0 THERMAL EVALUATION

A3.1 Description of Thermal Design

This section identifies and describes the principal thermal design aspects of the MOX Fresh Fuel Package (MFFP) containing ARB-17 container(s). The results presented in this chapter demonstrate the thermal safety of the system and compliance with the thermal requirements of 10 CFR 71¹ when transporting up to three (3) ARB-17 containers.

The analysis demonstrates that the addition of the ARB-17 does not impact the packaging temperatures, and the temperatures for these items reported in Chapter 3.0, *Thermal Evaluation*, remain bounding. However, the peak HAC fuel cladding temperature estimated for the fuel rods in an ARB-17 is higher than the peak temperature computed for a fuel assembly, largely due to the simplified method employed, although the HAC fuel temperature limit is not approached. Also, due to the increased quantities of combustibles in the ARB-17 (the ARB-17 utilizes a Buna-N rubber bumper and polypropylene sleeves for the fuel rods), the peak HAC pressure with an ARB-17 payload exceeds the peak HAC pressure with three (3) fuel assemblies. The package is demonstrated to structurally withstand this increased pressure.

A3.1.1 Design Features

The principal thermal design features of the MFFP are described in Section 3.1.1, *Design Features*, while the principal features of the ARB-17 are described in Section A1.2.3, *Contents of Packaging*.

A3.1.2 Content's Decay Heat

The payload for the MFFP under this amendment consists of up to three (3) ARB-17 containers. If less than 3 ARB-17 containers are loaded, the other positions in the strongback will be occupied by a combination of MOX fuel assemblies and/or dummy fuel assemblies. A maximum decay heat of 80 watts is conservatively assumed for each MOX fuel assembly, and an intact MOX fuel assembly has 264 fuel rods. Therefore, the proportional maximum decay heat for each ARB-17, based on a maximum loading of 17 fuel rods, is approximately 5.15 watts.

A3.1.3 Summary of Temperatures

The maximum temperatures for the MFFP under NCT and HAC are summarized in Table 3.4-1 and Table 3.5-1, respectively. While these packaging temperatures are associated with the transportation of three (3) MOX fuel assemblies, they are bounding for the MFFP temperatures arising from the transportation of the ARB-17 payload. The peak temperature of fuel rods within the ARB-17 under NCT conditions is 194 °F (see Section A3.4, *Thermal Evaluation for Normal Conditions of Transport*) while the peak temperature achieved under HAC is 615 °F (see Section A3.5, *Thermal Evaluation under Hypothetical Accident Conditions*).

¹ Title 10, Code of Federal Regulations, Part 71 (10 CFR 71), *Packaging and Transportation of Radioactive Material*, 01-01-06 Edition.

A3.1.4 Summary of Maximum Pressures

The maximum normal operating pressure (MNOP) for the MFFP with the ARB-17 payload resulting from the NCT Hot condition and conservative assumptions is 2.8 psig. This value is bounded by the value of 10 psig for the standard payload. The NCT internal pressures are presented in Table A3.4-1 and Table A3.4-2 for each payload combination considered. Further details of the pressure analysis are presented in Section A3.4.2, *Maximum Normal Operating Pressure*.

The peak pressure generated within the package cavity under HAC is conservatively estimated assuming that the entire inventory of organic material within the strongback and ARB-17 containers is totally combusted/pyrolyzed. The associated maximum pressure generated is estimated to be 146.0 psig (160.7 psia) at the end of the fire when the peak cavity gas temperature is reached. The pressure will then decrease as the package cools. The HAC internal pressures for each payload combination considered are presented in Tables A3.5-1 and A3.5-2. Further details of the analyses are presented in Section A3.5.3, *Maximum Temperatures and Pressures*.

A3.2 Material Properties and Component Specifications

A3.2.1 Material Properties

The ARB-17 and the dummy fuel assemblies are fabricated of stainless steel. The thermal properties of stainless steel are described in Section 3.2.1, *Material Properties*.

A3.2.2 Component Specifications

In addition to the materials listed in Section 3.2.2, *Component Specifications*, the materials associated with the ARB-17 that are considered temperature sensitive are the Buna-N (nitrile) rubber bumper used for cushioning the undamaged fuel rods during loading and the polypropylene sleeve used to prevent scratching of the cladding.

The Buna-N rubber material has a working temperature range of -65 °F to 225 °F ¹, and a short duration (30 minutes or less) temperature range of up to 360 °F, and a maximum temperature capability of 550 to 625 °F. The polypropylene sleeve material has a melting point between 273 and 329 °F and a thermal degradation temperature in excess of 428 °F ². Because the polypropylene sleeve serves no structural purpose, a service temperature of 275 °F is assumed.

¹ Parker O Ring Handbook, ORD 5700/USA, 2001.

² Matweb, Online Material Data Sheets, www.matweb.com.

This page left intentionally blank.

A3.3 General Considerations

A3.3.1 Evaluations by Analysis

The MFFP with the ARB-17 payload is analytically evaluated in accordance with 10 CFR 71¹ and Regulatory Guide 7.8² for the bounding NCT and HAC thermal loads. Section 3.3.1, *Evaluation by Analysis*, summarizes the design basis conditions considered in these evaluations.

A3.3.1.1 NCT Analytical Model

The NCT analytical thermal model of the MFFP is based on the Thermal Desktop[®] 3 and SINDA/FLUINT⁴ computer programs. Details of these programs, together with a description of the thermal model for the MFFP, are described in Section 3.3.1.1, *NCT Analytical Model*.

Given that the ARB-17 is designed to fit within the strongback assembly of the MFFP, and given that the maximum heat within an ARB-17 is less than 7% of the decay heat of a MOX fuel assembly, the methodology used to evaluate the thermal performance of the ARB-17 within the MFFP is conservatively based on use of the maximum strongback temperature achieved for the transportation of the three (3) MOX fuel assemblies as a boundary condition for a 1-dimensional heat transfer analysis within the ARB-17. The thermal model conservatively assumes the 17 MOX fuel rods are centered within the ARB-17 and ignores any conductance between the fuel support pipe and the sidewall of the box. In addition, the contribution of radiation heat transfer within the ARB-17 is ignored, as is any potential heat transfer via convection.

Figure A3.3-1 illustrates the thermal resistance elements considered by the 1-dimensional thermal model of the ARB-17. The modeling simulates the cross section of the ARB-17 as a series of concentric cylinders with equivalent separation distances. The area occupied by the fuel pellets and the airspace between the fuel rods is lumped into a composite, porous fuel region at the center of the assembly. The decay heat loading is modeled as a uniform volumetric heat source. The effective thermal conductivity of this composite fuel region is computed based on area weighting of the conductivity for the fuel and air. The temperature rise from the edge of the composite fuel region to its center is computed using the standard equation for a cylinder with a uniform volumetric heat source. The remaining temperature rise from the edge of the ARB-17 to the edge of the composite fuel region is computed using the standard equation for radial heat transfer through a cylinder and the associated material properties and geometry for each resistance element in the 1-D model (see Figure A3.3-1).

¹ Title 10, Code of Federal Regulations, Part 71 (10 CFR 71), *Packaging and Transportation of Radioactive Material*, 01-01-06 Edition.

² Regulatory Guide 7.8, *Load Combinations for the Structural Analysis of Shipping Casks for Radioactive Material*, Revision 1, U. S. Nuclear Regulatory Commission, March 1989.

³ Thermal Desktop[®], Version 4.5, Cullimore & Ring Technologies, Inc., Littleton, CO, 2003.

⁴ SINDA/FLUINT, *Systems Improved Numerical Differencing Analyzer and Fluid Integrator*, Version 4.5, Cullimore & Ring Technologies, Inc., Littleton, CO, 2001.

A3.3.1.2 HAC Analytical Model

The analytical thermal model of the MFFP with the ARB-17 under HAC uses the same methodology used for the NCT evaluation. The peak strongback temperature presented in Section 3.5, *Thermal Evaluation under Hypothetical Accident Conditions*, is used as a steady-state boundary temperature for the 1-D thermal model of the ARB-17 described above.

A3.3.2 Evaluation by Test

This section is not applicable because evaluation by test was not performed for the MFFP with the ARB-17 box assembly.

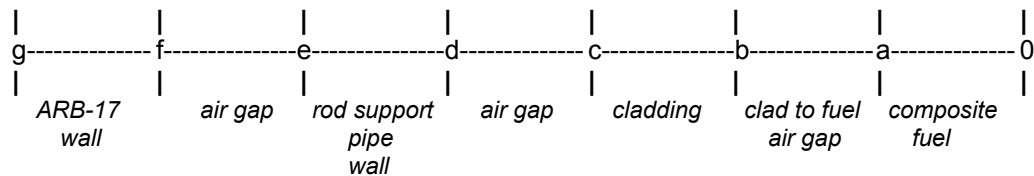
A3.3.3 Margins of Safety

A summary of the maximum temperatures for the MFFP, with their respective temperature margins, for both NCT and HAC are provided in Table 3.3-3. Because the integrity of the ARB-17 is not important to this safety analysis, the margin of safety related to it is not applicable.

From Section A3.1.4, *Summary of Maximum Pressures*, the maximum normal operating pressure (MNOP) is 2.8 psig, which is bounded by the calculated MNOP of 2.9 psig for the standard payload of three (3) fuel assemblies. (Note that the reported MNOP for the package is 10 psig, which is obtained by rounding up the 2.9 psig value.) Therefore, the margin of safety (MS) for the 25-psig design pressure is:

$$MS = \frac{25}{2.8} - 1.0 = +7.9$$

From Section A3.1.4, *Summary of Maximum Pressures*, the maximum pressure for HAC is 146 psig. Structural evaluation of the MFFP for this maximum pressure (rounded up to 150 psig) at temperature is provided in Section A2.7.4.3, *Stress Calculations*. As shown in that section, the minimum MS for the HAC pressure is +1.73.



0 = center of composite fuel rod (0-in)
a = outer radius of composite fuel pellet (0.7942-in)
b = inner radius of composite fuel rod cladding (0.8663-in)
c = outer radius of composite fuel rod (0.9634-in)
d = fuel rod support pipe inner radius (1.0335-in)
e = fuel rod support pipe outer radius (1.1875-in)
f = ARB-17 inner wall radius (3.5797-in)
g = ARB-17 outer wall radius (4.3297-in)

Figure A3.3-1 – Overview of 1-Dimensional Thermal Model for ARB-17

This page left intentionally blank.

A3.4 Thermal Evaluation for Normal Conditions of Transport

A3.4.1 Heat and Cold

A3.4.1.1 Heat

The maximum temperature for the ARB-17 is determined assuming the peak temperature of 178 °F for the strongback assembly obtained from Section 3.4.1.1, *Heat*, for the NCT Hot condition. Since this temperature is associated with a decay heat loading of 240 watts, it conservatively bounds the strongback temperatures associated with the transport of any number of ARB-17 containers. Note that even with a payload of two (2) fuel assemblies and one (1) ARB-17, the heat loading drops to $2 \times 80 + 5.15 \sim 165$ watts, which is significantly less than 240 watts. Adding more ARB-17s would cause the total heat load to drop even further.

Based on the 1-dimensional thermal model described above and a decay heat load of 5.15 watts for the maximum payload configuration of 17 fuel rods, an estimated temperature rise of approximately 16 °F will occur between the outside edge of the ARB-17 and the center of the composite fuel region. When combined with the assumed boundary condition of 178 °F for the strongback, the computed temperature rise within the ARB-17 yields a predicted maximum temperature of 194 °F for the NCT Hot condition. This predicted peak temperature is bounding whether the other positions in the strongback are occupied by other ARB-17 containers, MOX fuel assemblies, or dummy fuel assemblies. Further, based on the maximum temperature of 194 °F, none of the organic material within the ARB-17 or the strongback assembly will experience any thermal decomposition and out-gassing under NCT conditions.

The results presented in Section 3.4.1.1, *Heat*, for the MFFP remain valid and bounding for the MFFP temperatures associated with the transport of the ARB-17 payload. Specifically, the closure seals and the impact limiter foam temperatures remain below their associated temperature limits. Additionally, the MFFP analysis demonstrated that the accessible package surfaces remain below 122 °F when transported in an ambient temperature of 100 °F and without insolation, as stipulated by 10 CFR §71.43(g).

A3.4.1.2 Cold

The minimum temperature distribution for the MFFP with the ARB-17 occurs with a zero decay heat load and an ambient air temperature of -40 °F per 10 CFR §71.71(c)(2). The steady-state analysis of this condition represents a trivial case that requires no thermal calculations be performed. Instead, it is assumed that all package components achieve the -40 °F temperature under steady-state conditions. The -40 °F temperature is within the allowable range of all of the packaging components. The package temperatures for the NCT Cold condition of -20 °F and no insolation are bounded by those presented in Section 3.4.1.2, *Cold*, for the MFFP.

A3.4.2 Maximum Normal Operating Pressure

The maximum normal operating pressure (MNOP) for NCT are presented in Tables A3.4-1 and A3.4-2 for the various combinations of potential payloads. Six potential payload combinations involving the ARB-17, fuel assemblies, and dummy fuel assemblies are considered:

1. 3 ARB-17 containers
2. 2 ARB-17 containers and 1 dummy fuel assembly
3. 1 ARB-17 container and 2 dummy fuel assembly
4. 1 ARB-17 container, 1 fuel assembly, and 1 dummy fuel assembly
5. 2 ARB-17 containers, 1 fuel assembly
6. 1 ARB-17 container, 2 fuel assemblies

The MNOP is based on an initial package backfill of air at atmospheric pressure at 70 °F (294 K), an assumed failure rate of 3% of the MOX fuel and control rods, and heat up of the gases in the package cavity based on the transport of three (3) MOX fuel assemblies and the respective ambient condition. For the purpose of rod pressure determination, the only significant gas contributor is the initial helium backfill as no fission products exist within the un-irradiated fuel assemblies.

The bulk average gas temperature from Section 3.4.1.1, *Heat*, for the MFFP under the NCT Hot condition is used as the basis for the MNOP calculation with the ARB-17. Since the decay heat loading assumed for the MFFP bounds the heat dissipation associated with any of the potential ARB-17 payload configurations, the associated bulk average gas temperature will also be bounding. The package cavity has a gross free volume of approximately 105,547 cubic inches, based on a package cavity OD of 28.5 inches and a length of 165.45 inches. The displacement volume for each MOX fuel assembly is 4,685 in³, while a displacement volume of 11,292 in³ is assumed for the strongback assembly (see Section 3.4.2, *Maximum Normal Operating Pressure*). The solid volume for the ARB-17 is 4,984 in³, while the solid volume for the dummy fuel assemblies is approximately 5,366 in³.

The amount of helium fill gas within each MOX fuel assembly fuel rod and poison rod was determined in Section 3.4.2, *Maximum Normal Operating Pressure*, to be 0.0243 and 0.0475 g-moles, respectively. Given that there are 264 fuel rods and 24 burnable poison rods (from the BPRA) in each 17x17 MOX fuel assembly, the total helium content within an intact MOX fuel assembly is 7.55 g-moles.

The initial gas in the package cavity at the time of sealing is calculated as follows:

$$N_{\text{fill}} = \frac{1 \text{ atm} \times V_{\text{free}}}{R \times T_{\text{fill}}}$$

where:

- T_{fill} = temperature of air within package cavity at time of package closure
- R = Ideal gas constant (0.08206 atm-liter/gmole-°K)
- V_{free} = Package cavity free volume
- = Gross cavity volume minus displacement volumes for the ARB-17 containers, dummy fuel assemblies, MOX fuel assemblies, and the strongback

= 79,303 in³ (1,299.5 liters) for bounding payload of three (3) ARB-17 box assemblies

The MNOP is then calculated as follows:

$$MNOP = \frac{N_{\text{cask}} RT_{\text{NCT}}}{V_{\text{free}}}$$

$$N_{\text{cask}} = N_{\text{fill}} + \text{Rod Failure Rate} \times N_{\text{MOX fill gas}} + N_{\text{outgassing}}$$

where:

N_{cask} = total moles of gas in package cavity

N_{fill} = moles air within package cavity at time of package closure

Rod Failure Rate = assumed percentage of failed rods within each MOX fuel assembly and ARB-17. A 3% failure rate, which matches the regulatory failure rate for normal conditions of transport of spent fuel assemblies, will bound the expected failure rate for fresh fuel.

$N_{\text{MOX fill gas}}$ = moles of rod fill gas within package cavity

$N_{\text{outgassing}}$ = moles gas generated by out-gassing from component material within package cavity

T_{NCT} = Bulk average gas temperature within package (K) at the specific condition

Table A3.4-1 lists the computed package pressure under NCT conditions for the transport of ARB-17 containers and dummy fuel assemblies. Table A3.4-2 lists the computed package pressure for the transport of ARB-17 containers and MOX fuel assemblies. The peak pressure developed is similar for the various combinations of payloads examined with the MNOP of 17.5 psia (2.8 psig) arising from the transport of 1 ARB-17 box assembly and 2 MOX fuel assemblies. A significant margin exists between this calculated MNOP and the package's NCT design pressure limit of 39.7 psia (25 psig).

No hydrogen or other flammable gases will be generated as result of the thermal or radiation-induced decomposition of the organic material within the package. This conclusion is based on the relatively low temperatures achieved under NCT conditions and the low radioactivity of the un-irradiated MOX fuel rods.

A3.4.3 Maximum Thermal Stresses

The maximum thermal stresses for NCT are bounded by those determined for the MFFP package with the MOX fuel assembly payload. See the discussion in Section 2.6.1, *Heat*, and Section 2.6.2, *Cold*.

A3.4.4 Evaluation of Package Performance for Normal Conditions of Transport

The steady-state thermal analysis presented in Section 3.4, *Thermal Evaluation for Normal Conditions of Transport*, demonstrated that the components of the MFFP with the MOX fuel assembly payload are within their respective allowable temperature limits. That evaluation is valid and bounding for the MFFP with the ARB-17.

The MNOP resulting from the NCT Hot condition and conservative assumptions is within the package's maximum design pressure limit.

Therefore, the MFFP with the ARB-17 is found to comply with all of the thermal requirements specified in 10 CFR §71.71.

Table A3.4-1 – NCT Internal Pressures w/o MOX Fuel Assemblies

Parameter	3 ARB-17s	2 ARB-17s and 1 Dummy FA	1 ARB-17 and 2 Dummy FA
Bulk Avg. Fill Gas Temperature	165.6 °F	165.6 °F	165.6 °F
Package Void Volume	1299.5 liters	1293.3 liters	1287.0 liters
Quantity Of Package Fill Gas	53.82 g-moles	53.56 g-moles	53.30 g-moles
Gas From Failed Fuel Assembly Rods	0.04 g-moles	0.02 g-moles	0.01 g-moles
Gas From Organic Component Out-gassing	0 g-moles	0 g-moles	0 g-moles
Package Cavity Pressure	17.4 psia (2.7 psig)	17.4 psia (2.7 psig)	17.4 psia (2.7 psig)

Table A3.4-2 – NCT Internal Pressures w/ MOX Fuel Assemblies

Parameter	1 ARB-17, 1 MOX FA, 1 Dummy FA	2 ARB-17s and 1 MOX FA	1 ARB-17 and 2 MOX FAs
Bulk Avg. Fill Gas Temperature	165.6 °F	165.6 °F	165.6 °F
Package Void Volume	1298.2 liters	1304.4 liters	1309.3 liters
Quantity Of Package Fill Gas	53.76 g-moles	54.02 g-moles	54.22 g-moles
Gas From Failed Fuel Assembly Rods	0.24 g-moles	0.25 g-moles	0.47 g-moles
Gas From Organic Component Out-gassing	0 g-moles	0 g-moles	0 g-moles
Package Cavity Pressure	17.4 psia (2.7 psig)	17.4 psia (2.7 psig)	17.5 psia (2.8 psig)

A3.5 Thermal Evaluation under Hypothetical Accident Conditions

This section presents the results of the thermal evaluation of the MFFP with the ARB-17 under the hypothetical accident conditions (HAC) specified in 10 CFR §71.73(c)(4)¹.

A3.5.1 Initial Conditions

The initial conditions assumed for the MFFP are presented in Section 3.5, *Thermal Evaluation under Hypothetical Accident Conditions*. No damage is assumed to have occurred to the ARB-17 or the dummy fuel assemblies as a result of the drop events that precede the HAC fire event.

A3.5.2 Fire Test Conditions

No fire tests were performed for the MFFP with the ARB-17.

A3.5.2.1 Analytical Model

The analytical model of the MFFP under HAC is described in Section 3.5.2.1, *Analytical Model*, and Section 3.5.2.2, *Performance of Rigid Polyurethane Foam Under HAC Fire Conditions*. The peak temperature for the ARB-17 under HAC is estimated using the 1-dimensional thermal model of the ARB-17 described in Section A3.3.1.1, *NCT Analytical Model*.

A3.5.3 Maximum Temperatures and Pressures

A3.5.3.1 Maximum Temperatures

The maximum temperatures attained in the MFFP components under HAC with the ARB-17 payload are bounded by those presented in Section 3.5.3.1, *Maximum Temperatures*. The peak strongback assembly temperature predicted from the evaluation of the MFFP is 599 °F. Adding the estimated ΔT between the strongback and the center of the fuel region within the ARB-17 of approximately 16 °F, as determined in Section A3.4.1.1, *Heat*, yields a peak temperature of 615 °F within the ARB-17. This temperature level is within the short-term thermal limits for the fuel rods and all metallic components of the ARB-17.

While both the peak temperature and the duration of the elevated temperatures within the package are seen as insufficient to cause serious thermal decomposition of the organic material within the strongback and ARB-17 assemblies, this evaluation conservatively assumes that the material fully decomposes to the extent that the available oxygen permits.

A3.5.3.2 Maximum Pressures

With the exception of the consideration for potential out-gassing from organic components within the package cavity and an assumed 100% failure rate for the MOX fuel assembly rods, the maximum pressure attained under HAC is determined in the same manner as described in Section A3.4.2, *Maximum Normal Operating Pressure*. While the MFFP is designed to protect

¹ Title 10, Code of Federal Regulations, Part 71 (10 CFR 71), *Packaging and Transportation of Radioactive Material*, 01-01-06 Edition.

the MOX fuel assemblies and the MOX fuel rods from catastrophic failure during the pre-fire free and puncture bar drops and the subsequent 30-minute fire event, this analysis conservatively assumes that the cladding on all fuel and burnable poison rods (if present) have been breached. As stated in Section A3.4.2, *Maximum Normal Operating Pressure*, the amount of helium fill gas within each MOX fuel assembly fuel rod and poison rod is 0.0243 and 0.0475 g-moles, respectively, and the total helium content within an intact MOX fuel assembly is 7.55 g-moles. No significant change in the package cavity free volume is expected as a result of the HAC drop event.

Approximately 7 pounds of neoprene rubber $(C_4H_5Cl)_n$ and 2.3 pounds of Delrin[®] plastic $(C_6H_{14}O_2)_n$ are used in the strongback assembly. Approximately 0.28 pounds of Buna-N rubber $(C_7H_9N)_n$ and 0.94 pounds of polypropylene $(C_3H_6)_n$ material are used within each ARB-17. The breakdown of these organic materials under HAC is limited by the fact that the peak cavity temperature and its duration under HAC are too low to permit complete pyrolysis (i.e., the process of breaking up a substance into other molecules as a result of heating in an inert atmosphere).

This combustion/pyrolyzation of the entire mass of neoprene rubber and Delrin[®] plastic would create approximately 143.1 g-moles of additional gas within the cavity, while pyrolyzation of the entire mass of Buna-N rubber and polypropylene in the ARB-17 could create approximately 18.4 g-moles of additional gas for each ARB-17 assembly. The quantity of gas generated from the organics contained in the ARB-17 assembly is limited by the assumption that the thermal decomposition of the strongback organic material occurs first. However, in reality, since insufficient oxygen content and temperature level exists within the package cavity to completely decompose all of the organic material, the total additional gas will be limited regardless of which organic decomposes first, and it is expected that a majority of the organic material will remain in its original solid form.

Table A3.5-1 lists the computed package pressure under HAC for the transport of ARB-17 and dummy fuel assemblies. Table A3.5-2 lists the computed package pressure for the transport of ARB-17 containers and MOX fuel assemblies. The peak pressure generated within the package cavity is estimated to be 160.7 psia (146.0 psig) at the end of the fire when the peak cavity gas temperature is reached. The pressure will then decrease as the package cools.

The predicted peak pressures presented in Tables A3.5-1 and A3.5-2 are considered to have a high degree of conservatism. This conclusion is based on the fact that there is an insufficient amount of oxygen within the package cavity to permit the full decomposition of the organic material, that the Buna-N rubber and polypropylene in the ARB-17 is isolated within the fuel support pipe (thus making it even more unlikely that the material can decompose), and because both the relatively low peak temperature and the relatively short duration of the elevated temperatures will prevent any significant thermal decomposition from occurring in the absence of active combustion of the material.

A3.5.4 Accident Conditions for Fissile Material Packages for Air Transport

This section does not apply for the MFFP because air transport will not be utilized.

A3.5.5 Evaluation of Package Performance for Accident Conditions of Transport

The evaluation of the MFFP package with the ARB-17 under HAC demonstrates that the packaging has sufficient thermal protection remaining after the hypothetical drop and puncture bar damage to protect the thermally sensitive areas of the packaging. All package components are seen as remaining within their associated maximum temperature limits.

Table A3.5-1 –HAC Internal Pressures w/o MOX Fuel Assemblies

Parameter	3 ARB-17s	2 ARB-17s and 1 Dummy FA	1 ARB-17 and 2 Dummy FAs
Bulk Avg. Fill Gas Temperature	769.5 °F	769.5 °F	769.5 °F
Package Void Volume	1299.5 liters	1293.3 liters	1287.0 liters
Quantity Of Package Fill Gas	53.82 g-moles	53.56 g-moles	53.30 g-moles
Gas From Failed Fuel Assembly Rods	1.24 g-moles	0.83 g-moles	0.41 g-moles
Gas From Organic Component Out-gassing	198.5 g-moles	179.9 g-moles	161.2 g-moles
Package Cavity Pressure	160.7 psia (146.0 psig)	149.2 psia (134.5 psig)	137.6 psia (122.9 psig)

Table A3.5-2 –HAC Internal Pressures w/ MOX Fuel Assemblies

Parameter	1 ARB-17, 1 MOX FA, 1 Dummy FA	2 ARB-17s and 1 MOX FA	1 ARB-17 and 2 MOX FAs
Bulk Avg. Fill Gas Temperature	769.5 °F	769.5 °F	769.5 °F
Package Void Volume	1298.2 liters	1304.4 liters	1309.3 liters
Quantity Of Package Fill Gas	53.76 g-moles	54.02 g-moles	54.22 g-moles
Gas From Failed Fuel Assembly Rods	7.96 g-moles	8.37 g-moles	15.51 g-moles
Gas From Organic Component Out-gassing	161.4 g-moles	180.1 g-moles	161.6 g-moles
Package Cavity Pressure	141.6 psia (126.9 psig)	153.1 psia (138.4 psig)	145.5 psia (130.8 psig)

A3.6 Appendices

A3.6.1 Computer Analysis Results

Since the safety evaluations are based on hand calculations, there are no sample computer input and output files to be provided.

This page left intentionally blank.

A4.0 CONTAINMENT

The ARB-17 does not provide containment. Therefore, package containment is unchanged from the description provided in Chapter 4.0, *Containment*.

This page left intentionally blank.

A5.0 SHIELDING EVALUATION

The compliance of the MFFP packaging with respect to the dose rate limits established by 10 CFR §71.47¹ for normal conditions of transport (NCT) or 10 CFR §71.51(a)(2) for hypothetical accident conditions (HAC) are satisfied when limiting the MFFP package to three (3) Mixed Oxide (MOX) fresh fuel assemblies (FAs) having a radioisotope content listed in Table 1.2-2. Replacing FAs with any number of ARB-17s would reduce the dose rates, because the ARB-17 contains only 17 fuel rods, compared to the 264 fuel rods in a standard FA.

Under these conditions, the maximum surface dose rate will be less than the limit of 200 mrem/hr for NCT and verified by measurement. This dose rate limit is for payload packages prior to addition of any lead, steel or other shielding material for *as-low-as-reasonably-achievable* (ALARA) dose reduction purposes during non-transport handling operations.

Prior to transport, the MFFP package shall be monitored for both gamma and neutron radiation to demonstrate compliance with 10 CFR §71.47. As noted in Section 2.6.7, *Free Drop*, the MFFP package is not significantly deformed under NCT free drop conditions. Therefore, the package will meet the dose rate limits for NCT if the measurements demonstrate compliance with the allowable dose rate levels in 10 CFR §71.47 (200 mrem/hr). The transport index, as defined in 10 CFR §71.4, will be determined by measuring the dose rate a distance of one meter from the package surface per the requirements of 49 CFR §173.403².

Shielding materials are not specifically provided by the MFFP package, and none are permitted within the package to meet the dose rate limits of 10 CFR §71.47 for NCT. Because significant fuel deformation or package deformation does not occur under HAC, the HAC surface dose rates and 1-meter dose rates will not be significantly different from the NCT dose rates. This result ensures that the post-HAC, allowable dose rate of 1 rem/hr a distance of one meter from the package surface per 10 CFR §71.51(a)(2) will be met because the surface dose rate will remain below the 200 mrem/hr limit.

¹ Title 10, Code of Federal Regulations, Part 71 (10 CFR 71), *Packaging and Transportation of Radioactive Material*, 01-01-06 Edition.

² Title 49, Code of Federal Regulations, Part 173 (49 CFR 173), *Shippers - General Requirements for Shipments and Packagings*, 10-01-06 Edition.

This page left intentionally blank.

A6.0 CRITICALITY EVALUATION

The following analyses demonstrate that the MFFP complies with the requirements of 10 CFR §71.55¹ and §71.59. The analyses presented herein show that the criticality requirements are satisfied when any number of PWR MOX fuel assemblies are replaced with ARB-17 containers containing up to 17 standard MOX fuel rods.

A6.1 Description of Criticality Design

A6.1.1 Design Features Important for Criticality

No structural credit is taken for the ARB-17 in this criticality analysis. The design features of the MFFP important to criticality are discussed in Section 6.1.1, *Design Features Important for Criticality*.

A6.1.2 Summary Table of Criticality Evaluation

Replacing a standard fuel assembly with an ARB-17 containing 17 fuel rods reduces the reactivity. Therefore, the limiting values provided in Table 6.1-1 remain bounding.

A6.1.3 Criticality Safety Index

An infinite number of MFFPs are evaluated in a close-packed hexagonal array. Therefore, “N” is infinite, and in accordance with 10 CFR §71.59 the criticality safety index (CSI) is $50/N = 0$.

¹ Title 10, Code of Federal Regulations, Part 71 (10 CFR 71), *Packaging and Transportation of Radioactive Material*, 01-01-06 Edition.

This page left intentionally blank.

A6.2 Fissile Material Contents

The content of an ARB-17 is up to 17 MOX fuel rods. The fuel rod parameters are unchanged from the standard MOX fuel rod and are provided in Section 6.2, *Fissile Material Contents*.

The MFFP may contain up to three ARB-17 boxes, although the most likely configuration is one ARB-17 and two dummy fuel assemblies. Other configurations, such as 1 fuel assembly and 2 ARB-17 boxes, or 2 fuel assemblies and 1 ARB-17 box, are acceptable.

Fuel rods may be either undamaged or lightly damaged. These “damaged” rods may be bent, scratched, or nicked, but under no circumstances would exhibit cladding breach.

This page left intentionally blank.

A6.3 General Considerations

Criticality calculations for the MFFP are performed using the three-dimensional Monte Carlo computer code MCNP5¹.

A6.3.1 Model Configuration

A6.3.1.1 Contents Model

The ARB-17 is not modeled in the criticality evaluation. Because the ARB-17 is not modeled, the fuel rods are assumed to arrange themselves in the most reactive configuration within the cavity formed between the strongback and FCS. To add conservatism and maintain model symmetry, 25 rods are modeled, which results in a 5x5 square array. A variety of pitches are examined in order to maximize reactivity, as well as radial and axial shifting of the rods.

Each undamaged fuel rod is placed inside a plastic sleeve to prevent scratching during transportation. The amount of plastic is insignificant and is not modeled in MCNP.

A6.3.1.2 Packaging Model

The packaging model is unchanged from the description provided in Section 6.3.1.2, *Packaging Model*.

A6.3.2 Material Properties

The material properties are unchanged from the descriptions provided in Section 6.3.2, *Material Properties*.

A6.3.3 Computer Codes and Cross-Section Libraries

The computer codes and cross section libraries are unchanged from the descriptions provided in Section 6.3.3, *Computer Codes and Cross-Section Libraries*.

A6.3.4 Demonstration of Maximum Reactivity

The reactivity of a package containing one, two, or three ARB-17 boxes is bounded by the three fuel assembly evaluation. The most reactive cases described in Section 6.3.4, *Demonstration of Maximum Reactivity*, remain bounding.

¹ MCNP5, "MCNP – A General Monte Carlo N-Particle Transport Code, Version 5; Volume II: User's Guide," LA-CP-03-0245, Los Alamos National Laboratory, April, 2003.

This page left intentionally blank.

A6.4 Single Package Evaluation

Compliance with the requirements of 10 CFR §71.55 is demonstrated by analyzing optimally moderated single-unit MFFP packages. The figures and descriptions provided in Section 6.3.1, *Model Configuration*, describe the basic geometry of the single-unit models, although the contents are different.

A6.4.1 Single Package Configuration

A6.4.1.1 NCT Configuration

No MCNP models are developed for the NCT configuration with an ARB-17 payload. Under NCT, in the absence of moderation the reactivity will be bounded by the standard three fuel assembly analysis of Section 6.4.1.1, *NCT Configuration*, because the reactivity for the dry condition is governed by the fissile mass in the package. As an ARB-17 contains significantly less fissile mass than a standard fuel assembly, the NCT reactivity for the fully loaded ARB-17 is bounded by a standard fuel assembly. Therefore, no NCT models for configurations containing the ARB-17 are required.

A6.4.1.2 HAC Configuration

Under HAC, explicit models are required because it is assumed the rods in an ARB-17 reach optimum moderation, while expansion of a standard fuel assembly is limited by the FCS and strongback. The approach is to conservatively model the contents of three ARB-17 boxes within the MFFP. No standard fuel assemblies are included in the models, although if the reactivity of three ARB-17 boxes is significantly less than the reactivity of three standard fuel assemblies, it may be inferred that a loaded ARB-17 can be less reactive than a standard fuel assembly.

Because the ARB-17 reactivity is expected to be very low, no credit is taken for the structure of the ARB-17, and rods are allowed to arrange themselves in a regular pitch within the strongback/FCS cavity. Twenty-five (25) rods are modeled rather than the maximum value of 17 simply to maintain symmetry in the model and add conservatism. The most reactive HAC single package model (max_hac_single_su1) from the standard three fuel assembly analysis is used as the base case for this analysis, with each standard fuel assembly replaced by 25 rods.

The standard 17x17 fuel assembly lattice is used to vary the rod pitch and location of the ARB-17 rod cluster by simply moving the rods throughout the lattice and filling the empty lattice locations with water. Using this simple method, the only difference between models is the arrangement of rods in the lattice.

A variety of rod pitches and cluster locations are utilized to calculate the maximum reactivity. A description of the HAC single package ARB-17 models is provided in Table A6.4-1. Each 5x5 cluster of rods is modeled in one of six X-Y locations: (1) top center, (2) top right, (3) top left, (4) center, (5) bottom left, and (6) bottom right. The rod pitch is also allowed to vary differently in the X and Y directions. Figure A6.4-1 through Figure A6.4-3 shows the model geometry for many of the configurations; the geometry of the remaining configurations may be inferred.

For convenience, for all but two cases, the fuel rods are assumed to be in the same axial location as a standard MOX fuel assembly. As axial shifting can result in a fuel rod that is extended beyond the poison plates, cases are also developed where the fuel rods are assumed to shift either up or down. Case `hs_arb_3d_up` has all rods shifted axially up, and case `hs_arb_3d_dn` has all rods shifted axially down. Axial shifting of rods up or down is shown in Figure 6.4-3 and Figure 6.4-4, respectively, for the standard MOX fuel assembly. Axial shifting for the ARB-17 fuel rods is performed in the same manner.

Results for the HAC single package are provided in Table A6.4-2. The most reactive configuration is `hs_arb_3d_up`, which has a regular pitch of 2.6751 cm and is centered between the strongback and the FCS. The multiplication factor is 0.62838, which is far below the USL of 0.9288. Because the reactivity of the most reactive case is low, further refining the critical pitch search to include pitches between the coarse pitches selected is not warranted. This case also has all rods shifted axially upward, although the effect of axial shifting on the reactivity is quite small and may be a result of statistical fluctuation. Note that reactivity decreases as the 5x5 clusters are brought closer together (the “top center” cases). The reason for this effect is that bringing the clusters closer together also brings them closer to the poison plates.

A6.4.2 Single Package Results

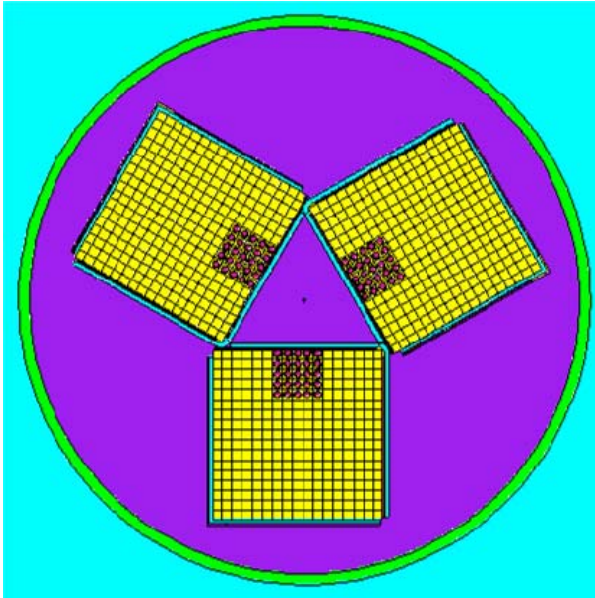
Results for the HAC single package are provided in Table A6.4-2. The most reactive case is listed in boldface.

Table A6.4-1 – HAC Single Package ARB-17 Case Descriptions

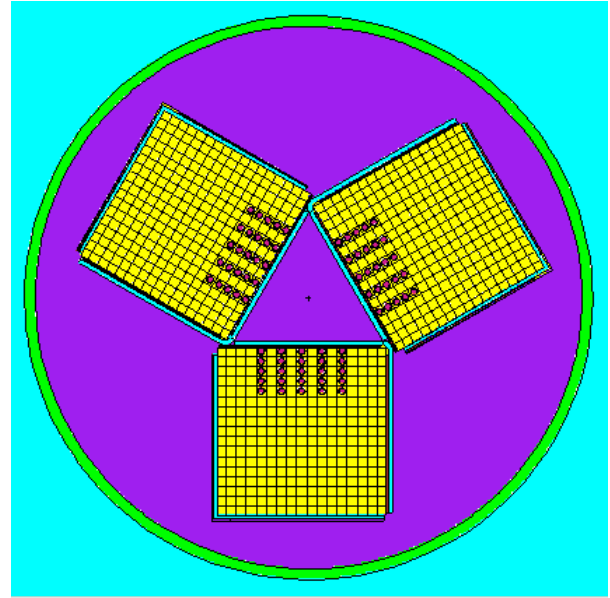
Case	X-Pitch (cm)	Y-Pitch (cm)	Cluster Location (X-Y)	Figure
hs_arb_1	1.3376	1.3376	Top Center	Figure A6.4-1
hs_arb_1d	1.3376	1.3376	Center	--
hs_arb_2	2.6751	1.3376	Top Center	Figure A6.4-1
hs_arb_2d	2.6751	1.3376	Center	--
hs_arb_3	2.6751	2.6751	Top Center	Figure A6.4-1
hs_arb_3b	2.6751	2.6751	Top Right	Figure A6.4-1
hs_arb_3c	2.6751	2.6751	Top Left	Figure A6.4-2
hs_arb_3d	2.6751	2.6751	Center	Figure A6.4-2
hs_arb_3d up	2.6751	2.6751	Center	Figure A6.4-2
hs_arb_3d dn	2.6751	2.6751	Center	Figure A6.4-2
hs_arb_3e	2.6751	2.6751	Bottom Left	Figure A6.4-2
hs_arb_3f	2.6751	2.6751	Bottom Right	Figure A6.4-2
hs_arb_4	4.0127	2.6751	Top Center	Figure A6.4-3
hs_arb_4d	4.0127	2.6751	Center	--
hs_arb_5	4.0127	4.0127	Top Center	Figure A6.4-3
hs_arb_5d	4.0127	4.0127	Center	--
hs_arb_6	5.3503	4.0127	Top Center	Figure A6.4-3
hs_arb_6d	5.3503	4.0127	Center	--
hs_arb_7	5.3503	5.3503	Center	Figure A6.4-3

Table A6.4-2 – Criticality Results for HAC Single Package

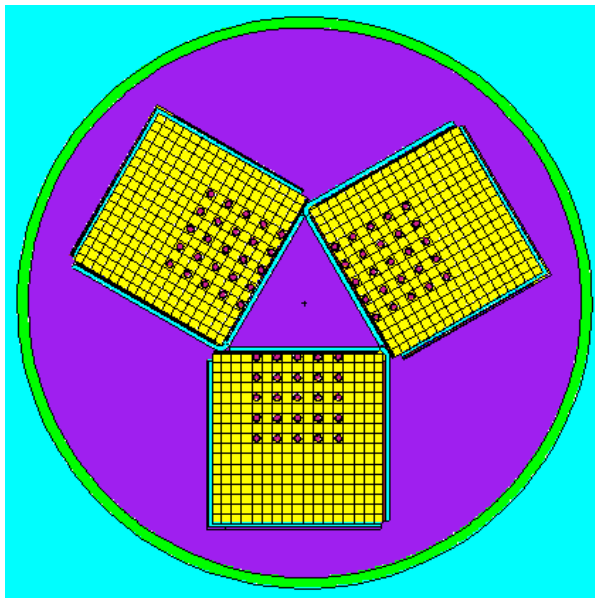
Case	Cluster Location (X-Y)	Figure	k_{eff}	σ	$k_s (k+2\sigma)$
hs_arb_1	Top Center	Figure A6.4-1	0.37799	0.00074	0.37947
hs_arb_1d	Center	--	0.44393	0.00080	0.44553
hs_arb_2	Top Center	Figure A6.4-1	0.47320	0.00083	0.47486
hs_arb_2d	Center	--	0.54358	0.00089	0.54536
hs_arb_3	Top Center	Figure A6.4-1	0.59163	0.00083	0.59329
hs_arb_3b	Top Right	Figure A6.4-1	0.53386	0.00090	0.53566
hs_arb_3c	Top Left	Figure A6.4-2	0.54095	0.00085	0.54265
hs_arb_3d	Center	Figure A6.4-2	0.62561	0.00091	0.62743
hs_arb_3d_up	Center	Figure A6.4-2	0.62650	0.00094	0.62838
hs_arb_3d_dn	Center	Figure A6.4-2	0.62651	0.00088	0.62827
hs_arb_3e	Bottom Left	Figure A6.4-2	0.54081	0.00085	0.54251
hs_arb_3f	Bottom Right	Figure A6.4-2	0.52784	0.00084	0.52952
hs_arb_4	Top Center	Figure A6.4-3	0.56296	0.00083	0.56462
hs_arb_4d	Center	--	0.59569	0.00092	0.59753
hs_arb_5	Top Center	Figure A6.4-3	0.54075	0.00084	0.54243
hs_arb_5d	Center	--	0.55350	0.00092	0.55534
hs_arb_6	Top Center	Figure A6.4-3	0.45303	0.00085	0.45473
hs_arb_6d	Center	--	0.46585	0.00082	0.46749
hs_arb_7	Center	Figure A6.4-3	0.38717	0.00077	0.38871



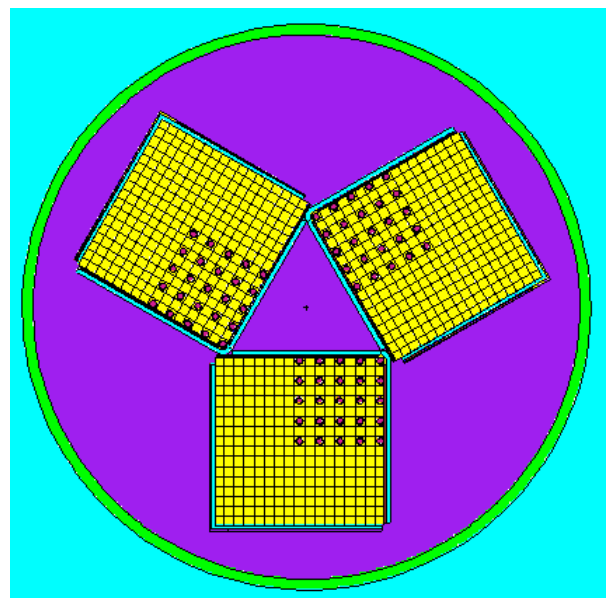
Case 1 “top center”



Case 2 “top center”



Case 3 “top center”



Case 3B “top right”

Figure A6.4-1 – Cases HS_ARB_1, 2, 3, and 3B

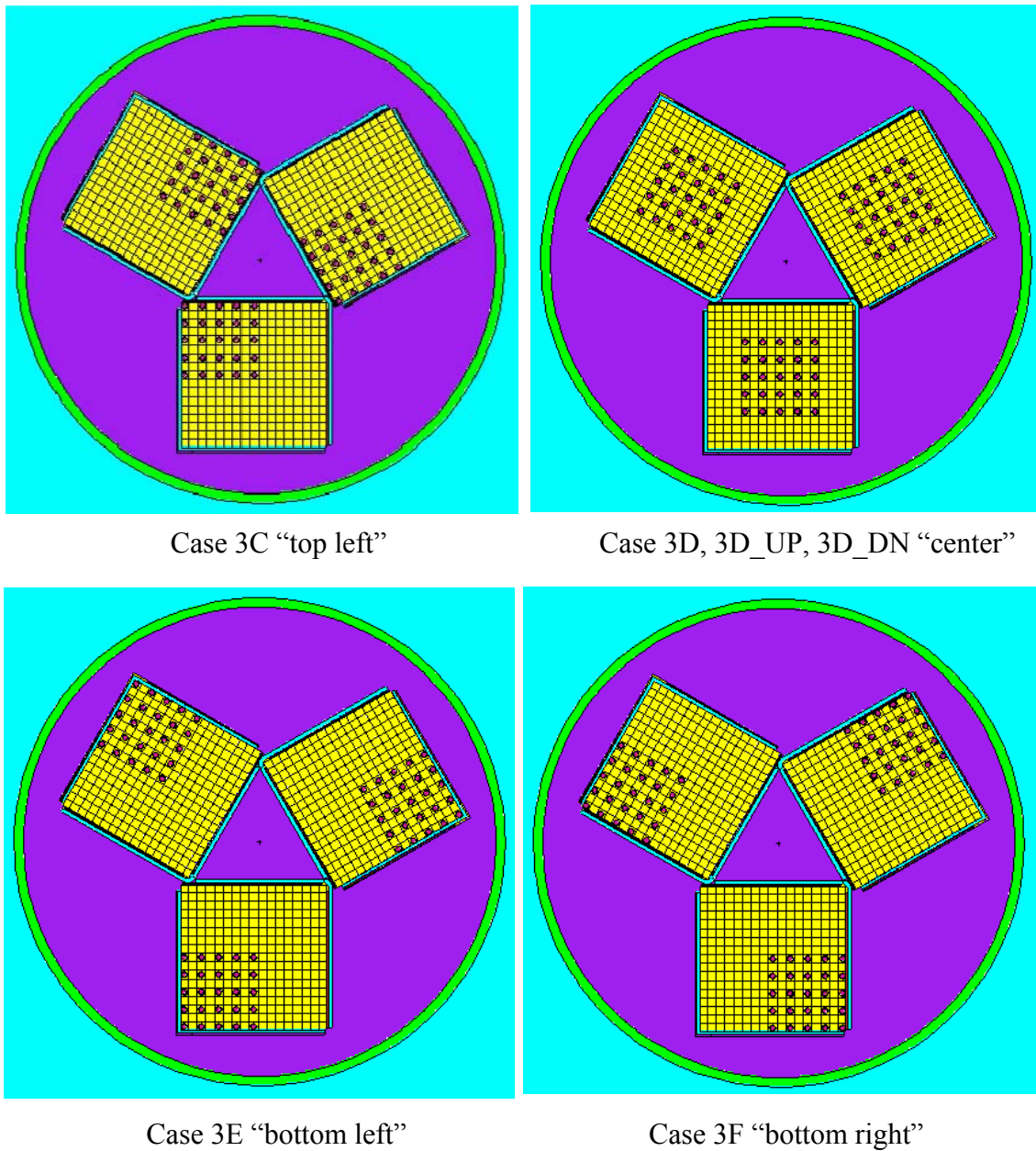
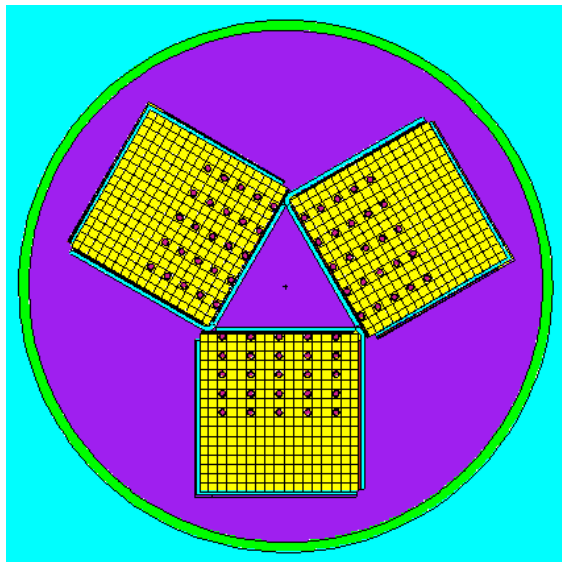
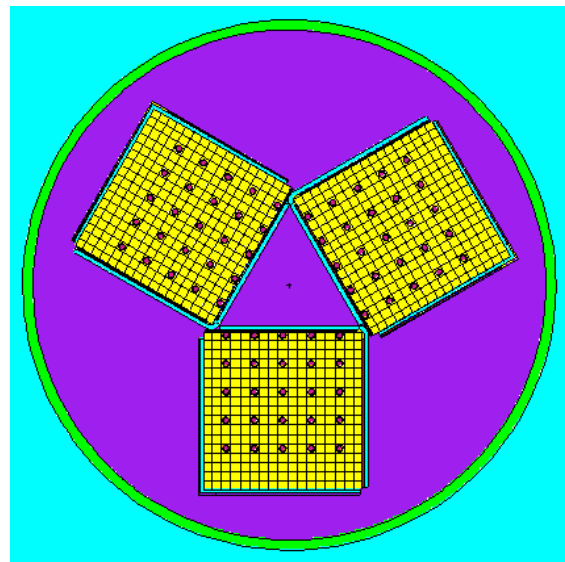


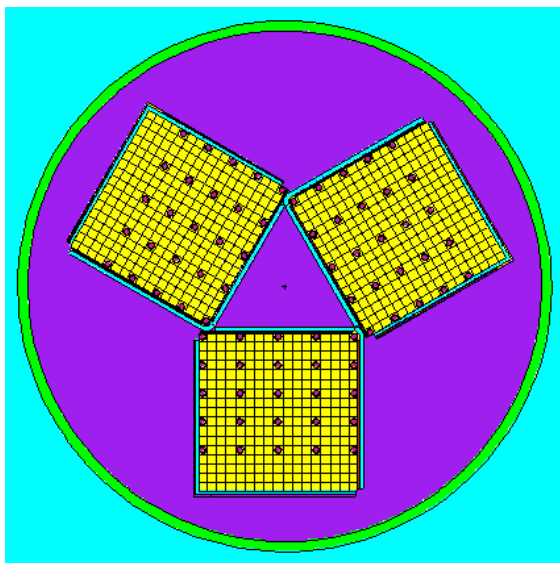
Figure A6.4-2 – Cases HS_ARB_3C, 3D, 3E, and 3F



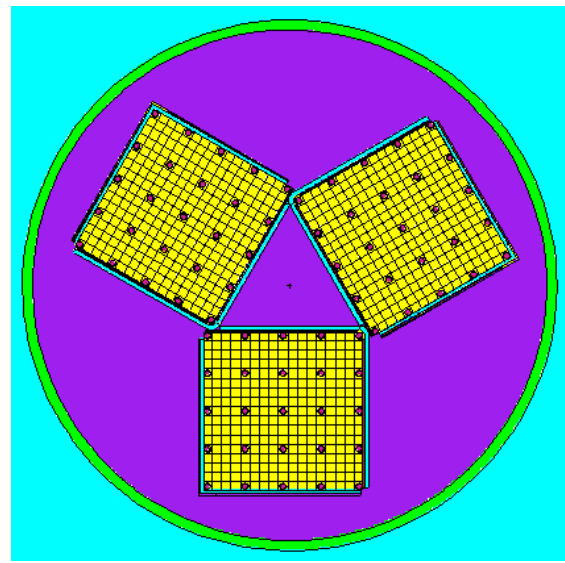
Case 4 “top center”



Case 5 “top center”



Case 6 “top center”



Case 7 “center”

Figure A6.4-3 – Cases HS_ARB_4, 5, 6, and 7

This page left intentionally blank.

A6.5 Evaluation of Package Arrays Under Normal Conditions of Transport

No MCNP models are developed for the NCT array configuration with an ARB-17 payload. Under NCT, in the absence of moderation the reactivity will be bounded by the standard three fuel assembly analysis of Section 6.5, *Evaluation of Package Arrays Under Normal Condition of Transport*, because the reactivity for the dry condition is governed by the fissile mass in the package. As an ARB-17 contains significantly less fissile mass than a standard fuel assembly, the NCT reactivity for the fully loaded ARB-17 is bounded by a standard fuel assembly. Therefore, no NCT array models for configurations containing the ARB-17 are required.

This page left intentionally blank.

A6.6 Package Arrays Under Hypothetical Accident Conditions

A6.6.1 HAC Array Configuration

Only a limited number of HAC infinite array cases are run for the ARB-17 because it has already been established for this package that the single package and infinite array HAC reactivities are nearly identical (see Table 6.1-1). Neutronic communication between packages is small because the package is large and heavily poisoned. The most reactive single package ARB-17 cases are run in the infinite array configuration. “Bottom left” and “bottom right” cases are also run, as this configuration minimizes the distance to fuel in neighboring packages. Infinite array results are provided in Table A6.6-1. As expected, k_s values for the infinite array cases are similar to the single package results, indicating little communication between packages. The most reactive case is ha_arb_3d_up, with $k_s = 0.62920$, which is less than the USL of 0.9288.

From both the single package and infinite array results for the ARB-17, it may be concluded that a payload of 3 ARB-17 cans is significantly less reactive than a payload of 3 fuel assemblies. In fact, comparing the ARB-17 can results with the results in Table 6.3-3, a package with a single fuel assembly and two dummies is more reactive than a package with 3 ARB-17 cans. Therefore, a fully loaded ARB-17 is much less reactive than a single MOX fuel assembly, and any combination of fuel assemblies, ARB-17, and dummy assemblies is acceptable for transportation.

A6.6.2 HAC Array Results

Results for the HAC single package are provided in Table A6.6-1. The most reactive case is listed in boldface.

Table A6.6-1 – Criticality Results for an Infinite Array of HAC Packages

Case	k_{eff}	σ	$k_s (k+2\sigma)$
ha_arb_3d	0.62526	0.00090	0.62706
ha_arb_3d_up	0.62732	0.00094	0.62920
ha_arb_3d_dn	0.62715	0.00090	0.62895
ha_arb_3e	0.54228	0.00092	0.54412
ha_arb_3f	0.52969	0.00090	0.53149

A6.7 Fissile Material Packages for Air Transport

This section does not apply for the MFFP, because air transport is not claimed.

This page left intentionally blank.

A6.8 Benchmark Evaluations

The benchmark evaluation is provided in Section 6.8, *Benchmark Evaluations*. A USL of 0.9288 is justified.

This page left intentionally blank.

A6.9 Appendices

Representative MCNP models are included in the following appendices:

A6.9.1 Single Package Model

A6.9.2 Infinite Array Model

This page left intentionally blank.

A6.9.1 Single Package Model

This file is for the worst-case HAC model (hs_arb_3d_up).

```

MOX package max single conditions with 10.85 g/cc Fuel no Nb
c
c *****Fuel Assembly*****
c cells 1 to 3 transform the 3 assemblies to their locations
c 1 4 -1.0 -21 22 -23 24 -25 6 imp:n=1 $ top nozzle, void
c 2 4 -1.0 -21 22 -23 24 -7 26 imp:n=1 $ bottom nozzle, void
c 7 0 -21 22 -23 24 126 -25 fill=20 imp:n=1 $ pins
c
c 201 like 1 but trcl=53 $ assembly 2
c 202 like 2 but trcl=53
c 207 like 7 but trcl=53
c 220 like 1 but trcl=54 $ assembly 3
c 221 like 2 but trcl=54
c 222 like 7 but trcl=54
c
c -- "box" around fuel
c
c 301 0 (302 -303 300 -304 -906 26):
c (303 -305 300 -301 -906 26) fill=30 imp:n=1 $ "box" cutout
c 302 like 301 but trcl=53
c 303 like 301 but trcl=54
c
c perimeter containing strongback #1 in -y
c 50 0 (26 -906 902 -909 904 -910):
c (26 -906 909 -912 904 -901):
c (26 -906 912 904 -908):
c (26 -906 911 905 -904 -908):
c (26 -906 905 -900 903 -911) fill=7 imp:n=1
c perimeter containing strongback #2
c 51 like 50 but trcl=53
c perimeter containing strongback #3
c 52 like 50 but trcl=54
c
c *****water beyond three units*****
c 131 9 -1.4 -61 -69 64 #7 #50 #51 #52 #301 #302 #303
c #207 #222 imp:n=1
c
c *****containment*****
c 141 5 -7.94 -62 -66 63 (61:65:-64) imp:n=1 $ outer steel
c 143 5 -7.94 -61 -70 69 imp:n=1 $ upper inner steel
c 145 4 -1.0 -61 -65 70 imp:n=1 $ upper void
c
c *****beyond containment*****
c 195 6 -7.94 -72 -76 73 (62:66:-63) imp:n=0.25 $ one foot refl
c 199 0 (72:76:-73) imp:n=0 $ outside world
c
c Universe 20: Fuel Lattice
c
c 200 4 -1.0 -12 11 -14 13 u=20 lat=1 trcl=30 fill=0:16 0:16 0:0
c 5 5 5 5 5 5 5 5 5 5 5 5 5 5 5 5 $ row 17
c 5 5 5 5 5 5 5 5 5 5 5 5 5 5 5 5 $ row 16
c 5 5 5 5 5 5 5 5 5 5 5 5 5 5 5 5 $ row 15
c 5 5 5 5 5 5 5 5 5 5 5 5 5 5 5 5 $ row 14
c 5 5 5 5 2 5 2 5 2 5 2 5 2 5 5 5 $ row 13
c 5 5 5 5 5 5 5 5 5 5 5 5 5 5 5 5 $ row 12
c 5 5 5 5 2 5 2 5 2 5 2 5 2 5 5 5 $ row 11
c 5 5 5 5 5 5 5 5 5 5 5 5 5 5 5 5 $ row 10
c 5 5 5 5 2 5 2 5 2 5 2 5 2 5 5 5 $ row 9
c 5 5 5 5 5 5 5 5 5 5 5 5 5 5 5 5 $ row 8
c 5 5 5 5 2 5 2 5 2 5 2 5 2 5 5 5 $ row 7
c 5 5 5 5 5 5 5 5 5 5 5 5 5 5 5 5 $ row 6
c 5 5 5 5 2 5 2 5 2 5 2 5 2 5 5 5 $ row 5
c 5 5 5 5 5 5 5 5 5 5 5 5 5 5 5 5 $ row 4
c 5 5 5 5 5 5 5 5 5 5 5 5 5 5 5 5 $ row 3
c 5 5 5 5 5 5 5 5 5 5 5 5 5 5 5 5 $ row 2
c 5 5 5 5 5 5 5 5 5 5 5 5 5 5 5 5 imp:n=1 $ row 1 (top)
c
c Universe 1: Fuel pin in normal position
c
c 10 1 -10.85 -1 -4 5 u=1 imp:n=1 $ fuel
c 11 4 -1.0 -2 1 -4 5 u=1 imp:n=1 $ radial gap

```

```

12      7 -6.5      -3      2 -8      5      u=1      imp:n=1      $ clad
13      4 -1.0      -2      3      7 -6      u=1      imp:n=1      $ radially beyond pin
14      4 -1.0      -2      -8      4      u=1      imp:n=1      $ above fuel void
15      7 -6.5      -3      -6      8      u=1      imp:n=1      $ top of fuel cap
16      7 -6.5      -3      -5      7      u=1      imp:n=1      $ bottom of fuel cap
17      4 -1.0      -2      6      u=1      imp:n=1      $ top water to infinity
18      4 -1.0      -2      -7      u=1      imp:n=1      $ bottom water to infinity
c
c      Universe 2: Fuel pin shifted up
c
410      1 -10.85      -1      -4      5      trcl=(0 0 23.7109) u=2      imp:n=1      $ fuel
411      4 -1.0      -2      1 -4      5      trcl=(0 0 23.7109) u=2      imp:n=1      $ radial gap
412      7 -6.5      -3      2 -8      5      trcl=(0 0 23.7109) u=2      imp:n=1      $ clad
413      4 -1.0      -2      3      7 -6      trcl=(0 0 23.7109) u=2      imp:n=1      $ radially beyond pin
414      4 -1.0      -2      -8      4      trcl=(0 0 23.7109) u=2      imp:n=1      $ above fuel void
415      7 -6.5      -3      -6      8      trcl=(0 0 23.7109) u=2      imp:n=1      $ top of fuel cap
416      7 -6.5      -3      -5      7      trcl=(0 0 23.7109) u=2      imp:n=1      $ bottom of fuel cap
417      4 -1.0      -2      6      u=2      imp:n=1      $ top water to infinity
418      4 -1.0      -2      -7      trcl=(0 0 23.7109) u=2      imp:n=1      $ bottom water to
infinity
c
c      Universe 3: Fuel pin shifted down
c
420      1 -10.85      -1      -4      5      trcl=(0 0 -9.4361) u=3      imp:n=1      $ fuel
421      4 -1.0      -2      1 -4      5      trcl=(0 0 -9.4361) u=3      imp:n=1      $ radial gap
422      7 -6.5      -3      2 -8      5      trcl=(0 0 -9.4361) u=3      imp:n=1      $ clad
423      4 -1.0      -2      3      7 -6      trcl=(0 0 -9.4361) u=3      imp:n=1      $ radially beyond pin
424      4 -1.0      -2      -8      4      trcl=(0 0 -9.4361) u=3      imp:n=1      $ above fuel void
425      7 -6.5      -3      -6      8      trcl=(0 0 -9.4361) u=3      imp:n=1      $ top of fuel cap
426      7 -6.5      -3      -5      7      trcl=(0 0 -9.4361) u=3      imp:n=1      $ bottom of fuel cap
427      4 -1.0      -2      6      u=3      imp:n=1      $ top water to infinity
428      4 -1.0      -2      -7      trcl=(0 0 -9.4361) u=3      imp:n=1      $ bottom water to infinity
c
c      Universe 4: Instrument/guide tube
c
41      4 -1.0      -18      5 -8      u=4      imp:n=1      $ inside
42      7 -6.5      -19      18 5 -8      u=4      imp:n=1      $ tube
43      4 -1.0      19      5 -8      u=4      imp:n=1      $ beyond tube
44      4 -1.0      8      u=4      imp:n=1
45      4 -1.0      -5      u=4      imp:n=1
c
c      Universe 5: Water only
c
46      4 -1.0      -998      u=5      imp:n=1
47      4 -1.0      998      u=5      imp:n=1
c
c      Universe 7: Strongback
c
700      6 -7.94      715 -710      u=7      imp:n=1      $ tangential strongback
701      6 -7.94      (710 711 718):(-711 713) u=7      imp:n=1      $ radial strongback+bend
702      2 -2.713      714 -719 -716      u=7      imp:n=1      $ tan Al clad
703      21 9.2244E-02 719 -720 -716
          730 731 732 733 734 735 736 737 738
          739 740 741 742 743 744 745 746 747
          750 751 752 753 754 755 756 757 758
          759 760 761 762 763 764 765 766 767 u=7      imp:n=1 $ tangential borol
704      2 -2.713      720 -715 -716      u=7      imp:n=1      $ tan Al clad
706      2 -2.713      712 -722 -717      u=7      imp:n=1      $ rad Al clad
707      21 9.2244E-02 722 -723 -717
          770 771 772 773 774 775 776 777 778
          779 780 781 782 783 784 785 786 787
          790 791 792 793 794 795 796 797 798
          799 800 801 802 803 804 805 806 807 u=7      imp:n=1 $ radial borol
708      2 -2.713      723 -713 -717      u=7      imp:n=1      $ rad Al
710      4 -1.0      (710 711 -718):(-710 717 -715):
          (710 -713 717 -711)      u=7      imp:n=1
719      6 -7.94      ((-717 -712):(-716 -714 717)) -809 u=7      imp:n=1 $ poison holder
720      4 -1.0      ((-717 -712):(-716 -714 717)) 809 -810 u=7      imp:n=1
721      6 -7.94      ((-717 -712):(-716 -714 717)) 810 -811 u=7      imp:n=1
722      4 -1.0      ((-717 -712):(-716 -714 717)) 811 -812 u=7      imp:n=1
723      6 -7.94      ((-717 -712):(-716 -714 717)) 812 -813 u=7      imp:n=1
724      4 -1.0      ((-717 -712):(-716 -714 717)) 813 -814 u=7      imp:n=1
725      6 -7.94      ((-717 -712):(-716 -714 717)) 814 -815 u=7      imp:n=1
726      4 -1.0      ((-717 -712):(-716 -714 717)) 815 -816 u=7      imp:n=1
727      6 -7.94      ((-717 -712):(-716 -714 717)) 816 -817 u=7      imp:n=1

```

728	4	-1.0	((-717 -712):(-716 -714 717))	817 -818	u=7	imp:n=1	
729	6	-7.94	((-717 -712):(-716 -714 717))	818 -819	u=7	imp:n=1	
730	4	-1.0	((-717 -712):(-716 -714 717))	819 -820	u=7	imp:n=1	
731	6	-7.94	((-717 -712):(-716 -714 717))	820 -821	u=7	imp:n=1	
732	4	-1.0	((-717 -712):(-716 -714 717))	821 -822	u=7	imp:n=1	
733	6	-7.94	((-717 -712):(-716 -714 717))	822 -823	u=7	imp:n=1	
734	4	-1.0	((-717 -712):(-716 -714 717))	823 -824	u=7	imp:n=1	
735	6	-7.94	((-717 -712):(-716 -714 717))	824 -825	u=7	imp:n=1	
736	4	-1.0	((-717 -712):(-716 -714 717))	825 -826	u=7	imp:n=1	
737	6	-7.94	((-717 -712):(-716 -714 717))	826	u=7	imp:n=1	
c							
750	6	-7.94	719 -720 -750		u=7	imp:n=1	\$ screws in boral
751	6	-7.94	719 -720 -751		u=7	imp:n=1	
752	6	-7.94	719 -720 -752		u=7	imp:n=1	
753	6	-7.94	719 -720 -753		u=7	imp:n=1	
754	6	-7.94	719 -720 -754		u=7	imp:n=1	
755	6	-7.94	719 -720 -755		u=7	imp:n=1	
756	6	-7.94	719 -720 -756		u=7	imp:n=1	
757	6	-7.94	719 -720 -757		u=7	imp:n=1	
758	6	-7.94	719 -720 -758		u=7	imp:n=1	
759	6	-7.94	719 -720 -759		u=7	imp:n=1	
760	6	-7.94	719 -720 -760		u=7	imp:n=1	
761	6	-7.94	719 -720 -761		u=7	imp:n=1	
762	6	-7.94	719 -720 -762		u=7	imp:n=1	
763	6	-7.94	719 -720 -763		u=7	imp:n=1	
764	6	-7.94	719 -720 -764		u=7	imp:n=1	
765	6	-7.94	719 -720 -765		u=7	imp:n=1	
766	6	-7.94	719 -720 -766		u=7	imp:n=1	
767	6	-7.94	719 -720 -767		u=7	imp:n=1	
c							
770	6	-7.94	722 -723 -770		u=7	imp:n=1	
771	6	-7.94	722 -723 -771		u=7	imp:n=1	
772	6	-7.94	722 -723 -772		u=7	imp:n=1	
773	6	-7.94	722 -723 -773		u=7	imp:n=1	
774	6	-7.94	722 -723 -774		u=7	imp:n=1	
775	6	-7.94	722 -723 -775		u=7	imp:n=1	
776	6	-7.94	722 -723 -776		u=7	imp:n=1	
777	6	-7.94	722 -723 -777		u=7	imp:n=1	
778	6	-7.94	722 -723 -778		u=7	imp:n=1	
779	6	-7.94	722 -723 -779		u=7	imp:n=1	
780	6	-7.94	722 -723 -780		u=7	imp:n=1	
781	6	-7.94	722 -723 -781		u=7	imp:n=1	
782	6	-7.94	722 -723 -782		u=7	imp:n=1	
783	6	-7.94	722 -723 -783		u=7	imp:n=1	
784	6	-7.94	722 -723 -784		u=7	imp:n=1	
785	6	-7.94	722 -723 -785		u=7	imp:n=1	
786	6	-7.94	722 -723 -786		u=7	imp:n=1	
787	6	-7.94	722 -723 -787		u=7	imp:n=1	
c							
790	6	-7.94	722 -723 -790		u=7	imp:n=1	
791	6	-7.94	722 -723 -791		u=7	imp:n=1	
792	6	-7.94	722 -723 -792		u=7	imp:n=1	
793	6	-7.94	722 -723 -793		u=7	imp:n=1	
794	6	-7.94	722 -723 -794		u=7	imp:n=1	
795	6	-7.94	722 -723 -795		u=7	imp:n=1	
796	6	-7.94	722 -723 -796		u=7	imp:n=1	
797	6	-7.94	722 -723 -797		u=7	imp:n=1	
798	6	-7.94	722 -723 -798		u=7	imp:n=1	
799	6	-7.94	722 -723 -799		u=7	imp:n=1	
800	6	-7.94	722 -723 -800		u=7	imp:n=1	
801	6	-7.94	722 -723 -801		u=7	imp:n=1	
802	6	-7.94	722 -723 -802		u=7	imp:n=1	
803	6	-7.94	722 -723 -803		u=7	imp:n=1	
804	6	-7.94	722 -723 -804		u=7	imp:n=1	
805	6	-7.94	722 -723 -805		u=7	imp:n=1	
806	6	-7.94	722 -723 -806		u=7	imp:n=1	
807	6	-7.94	722 -723 -807		u=7	imp:n=1	
c							
810	6	-7.94	719 -720 -730		u=7	imp:n=1	
811	6	-7.94	719 -720 -731		u=7	imp:n=1	
812	6	-7.94	719 -720 -732		u=7	imp:n=1	
813	6	-7.94	719 -720 -733		u=7	imp:n=1	
814	6	-7.94	719 -720 -734		u=7	imp:n=1	
815	6	-7.94	719 -720 -735		u=7	imp:n=1	
816	6	-7.94	719 -720 -736		u=7	imp:n=1	

```

817      6  -7.94      719 -720 -737      u=7  imp:n=1
818      6  -7.94      719 -720 -738      u=7  imp:n=1
819      6  -7.94      719 -720 -739      u=7  imp:n=1
820      6  -7.94      719 -720 -740      u=7  imp:n=1
821      6  -7.94      719 -720 -741      u=7  imp:n=1
822      6  -7.94      719 -720 -742      u=7  imp:n=1
823      6  -7.94      719 -720 -743      u=7  imp:n=1
824      6  -7.94      719 -720 -744      u=7  imp:n=1
825      6  -7.94      719 -720 -745      u=7  imp:n=1
826      6  -7.94      719 -720 -746      u=7  imp:n=1
827      6  -7.94      719 -720 -747      u=7  imp:n=1
c
c      Universe 30:  "box" around fuel
c
c 310      2  -2.713      -313 317      u=30 imp:n=1 $ radial left
c 311      2  -2.713      316 -310      u=30 imp:n=1 $ tangential bot
c 312      2  -2.713      314 -315 317 u=30 imp:n=1 $ radial right
c 315      2  -2.713      311 -312 316 u=30 imp:n=1 $ tangential top
316      6  -7.94      315 312      u=30 imp:n=1
317      4  -1.0      (312 -317 -315):(-316 -312) u=30 imp:n=1
c
320      4  -1.0      -315 317 -320      u=30 imp:n=1 $ radial water gap
321      21  9.2244E-02 313 -314 317 320 -321 u=30 imp:n=1 $ radial boral
322      4  -1.0      -315 317 321 -322 u=30 imp:n=1
323      21  9.2244E-02 313 -314 317 322 -323 u=30 imp:n=1
324      4  -1.0      -315 317 323 -324 u=30 imp:n=1
325      21  9.2244E-02 313 -314 317 324 -325 u=30 imp:n=1
326      4  -1.0      -315 317 325 -326 u=30 imp:n=1
327      21  9.2244E-02 313 -314 317 326 -327 u=30 imp:n=1
328      4  -1.0      -315 317 327 -328 u=30 imp:n=1
329      21  9.2244E-02 313 -314 317 328 -329 u=30 imp:n=1
330      4  -1.0      -315 317 329 -330 u=30 imp:n=1
331      21  9.2244E-02 313 -314 317 330 -331 u=30 imp:n=1
332      4  -1.0      -315 317 331 -332 u=30 imp:n=1
333      21  9.2244E-02 313 -314 317 332 -333 u=30 imp:n=1
334      4  -1.0      -315 317 333      u=30 imp:n=1
c
340      2  -2.713      -313 317 320 -321 u=30 imp:n=1 $ radial Al cladding
341      2  -2.713      -313 317 322 -323 u=30 imp:n=1
342      2  -2.713      -313 317 324 -325 u=30 imp:n=1
343      2  -2.713      -313 317 326 -327 u=30 imp:n=1
344      2  -2.713      -313 317 328 -329 u=30 imp:n=1
345      2  -2.713      -313 317 330 -331 u=30 imp:n=1
346      2  -2.713      -313 317 332 -333 u=30 imp:n=1
c
347      2  -2.713      314 -315 317 320 -321 u=30 imp:n=1 $ radial Al cladding
348      2  -2.713      314 -315 317 322 -323 u=30 imp:n=1
349      2  -2.713      314 -315 317 324 -325 u=30 imp:n=1
350      2  -2.713      314 -315 317 326 -327 u=30 imp:n=1
351      2  -2.713      314 -315 317 328 -329 u=30 imp:n=1
352      2  -2.713      314 -315 317 330 -331 u=30 imp:n=1
353      2  -2.713      314 -315 317 332 -333 u=30 imp:n=1
c
360      4  -1.0      -312 316 -320      u=30 imp:n=1 $ tangential water gap
361      21  9.2244E-02 310 -311 316 320 -321 u=30 imp:n=1 $ tangential boral
362      4  -1.0      -312 316 321 -322 u=30 imp:n=1
363      21  9.2244E-02 310 -311 316 322 -323 u=30 imp:n=1
364      4  -1.0      -312 316 323 -324 u=30 imp:n=1
365      21  9.2244E-02 310 -311 316 324 -325 u=30 imp:n=1
366      4  -1.0      -312 316 325 -326 u=30 imp:n=1
367      21  9.2244E-02 310 -311 316 326 -327 u=30 imp:n=1
368      4  -1.0      -312 316 327 -328 u=30 imp:n=1
369      21  9.2244E-02 310 -311 316 328 -329 u=30 imp:n=1
370      4  -1.0      -312 316 329 -330 u=30 imp:n=1
371      21  9.2244E-02 310 -311 316 330 -331 u=30 imp:n=1
372      4  -1.0      -312 316 331 -332 u=30 imp:n=1
373      21  9.2244E-02 310 -311 316 332 -333 u=30 imp:n=1
374      4  -1.0      -312 316 333      u=30 imp:n=1
c
380      2  -2.713      316 311 -312 320 -321 u=30 imp:n=1 $ horizontal Al cladding
381      2  -2.713      316 311 -312 322 -323 u=30 imp:n=1
382      2  -2.713      316 311 -312 324 -325 u=30 imp:n=1
383      2  -2.713      316 311 -312 326 -327 u=30 imp:n=1
384      2  -2.713      316 311 -312 328 -329 u=30 imp:n=1
385      2  -2.713      316 311 -312 330 -331 u=30 imp:n=1

```

```

386      2   -2.713      316 311 -312 332 -333 u=30 imp:n=1
c
387      2   -2.713      316 -310 320 -321 u=30 imp:n=1 $ horizontal Al cladding
388      2   -2.713      316 -310 322 -323 u=30 imp:n=1
389      2   -2.713      316 -310 324 -325 u=30 imp:n=1
390      2   -2.713      316 -310 326 -327 u=30 imp:n=1
391      2   -2.713      316 -310 328 -329 u=30 imp:n=1
392      2   -2.713      316 -310 330 -331 u=30 imp:n=1
393      2   -2.713      316 -310 332 -333 u=30 imp:n=1
c
c      Universe 51:  Dummy universe containing fuel
c
c      999      1 -10.31 -999 u=51      imp:n=1  $ for diagnostics only, not used
c      1000     1 -10.31  999 u=51      imp:n=1  $ for diagnostics only, not used

c      *****Fuel Assembly*****
c      fuel pin
1      cz      0.409575                      $ fuel radius
2      cz      0.41783                      $ radius inside clad
3      cz      0.47498                      $ radius outside clad
4      pz      182.88                      $ top of fuel
5      pz     -182.88                      $ bottom of fuel
6      pz      202.7555                    $ top of fuel pin
7      pz     -184.3405                    $ bottom of fuel pin
8      pz      201.4474                    $ bottom of top cap
11     px      -0.6688                    $ lattice definition
12     px       0.6688
13     py      -0.6688
14     py       0.6688
c      200      pz     -119.38
c      guide tube
18     cz       0.57150
19     cz       0.61214
c      perimeter of fuel assembly
21     px      10.2391 $ offset from surface 905
22     px     -12.1116 $
23     py     -6.6593 $ offset from surface 904
24     py     -29.0113 $
25     pz      226.466
26     pz     -190.95720
126    pz     -193.776
c      *****containment*****
61     cz      36.1950
62     cz      37.6174
63     pz     -197.5866 $ 1.5" thick
64     pz     -193.7766 $ 1.11" below bottom of fuel (strongback bottom not modeled)
65     pz      235.6866
66     pz      237.5916
c      67      pz     -203.0222
c      68      pz     -201.1172
69     pz      226.4664
70     pz      228.0666
c      *****outside of water refl****
72     cz      68.0974
73     pz     -228.0666 $ 1' water from 63
76     pz      268.0716 $ 1' water from 66
c
c      -- "box"
c
300     py     -29.7925  $ defining box in u=0
301     py     -29.0114
302     px     -12.8928
303     px     -12.1117
304     py     -7.5675
305     px       9.9672
c
310     25 py      0.04445
311     25 py      0.2604
312     25 py      0.3048
313     25 px      0.04445
314     25 px      0.2604
315     25 px      0.3048
316     25 px       2.54
317     25 py       2.54
c

```



```

320      pz -171.049
321      pz -119.532
322      pz -109.758
323      pz -67.412
324      pz -57.638
325      pz -15.316
326      pz -5.542
327      pz 36.855
328      pz 46.629
329      pz 89.002
330      pz 98.776
331      pz 141.097
332      pz 150.871
333      pz 193.548
c
c      strongback surfaces
c
710      22 px 0
711      22 py 0
712      22 px 0.476
713      22 px 0.7808
714      22 py 0.476
715      22 py 0.7808
716      22 px -0.3114    $ 0.43" less than surface 713
717      22 py -0.54
718      22 cz 0.7808
719      22 py 0.5205
720      22 py 0.7364
722      22 px 0.5205
723      22 px 0.7364
c
730      22 c/y -2.7752 -189.6872 0.47625
731      22 c/y -2.7752 -179.5526 0.47625
732      22 c/y -2.7752 -172.3187 0.47625
733      22 c/y -2.7752 -118.2624 0.47625
734      22 c/y -2.7752 -111.0285 0.47625
735      22 c/y -2.7752 -66.1416 0.47625
736      22 c/y -2.7752 -58.9077 0.47625
737      22 c/y -2.7752 -14.0462 0.47625
738      22 c/y -2.7752 -6.8123 0.47625
739      22 c/y -2.7752 38.1254 0.47625
740      22 c/y -2.7752 45.3593 0.47625
741      22 c/y -2.7752 90.2716 0.47625
742      22 c/y -2.7752 97.5055 0.47625
743      22 c/y -2.7752 142.3670 0.47625
744      22 c/y -2.7752 149.6009 0.47625
745      22 c/y -2.7752 194.8180 0.47625
746      22 c/y -2.7752 202.0519 0.47625
747      22 c/y -2.7752 213.8172 0.47625
c
750      22 c/y -16.7452 -189.6872 0.47625
751      22 c/y -16.7452 -179.5526 0.47625
752      22 c/y -16.7452 -172.3187 0.47625
753      22 c/y -16.7452 -118.2624 0.47625
754      22 c/y -16.7452 -111.0285 0.47625
755      22 c/y -16.7452 -66.1416 0.47625
756      22 c/y -16.7452 -58.9077 0.47625
757      22 c/y -16.7452 -14.0462 0.47625
758      22 c/y -16.7452 -6.8123 0.47625
759      22 c/y -16.7452 38.1254 0.47625
760      22 c/y -16.7452 45.3593 0.47625
761      22 c/y -16.7452 90.2716 0.47625
762      22 c/y -16.7452 97.5055 0.47625
763      22 c/y -16.7452 142.3670 0.47625
764      22 c/y -16.7452 149.6009 0.47625
765      22 c/y -16.7452 194.8180 0.47625
766      22 c/y -16.7452 202.0519 0.47625
767      22 c/y -16.7452 213.8172 0.47625
c
770      22 c/x -5.9248 -189.6872 0.47625
771      22 c/x -5.9248 -179.5526 0.47625
772      22 c/x -5.9248 -172.3187 0.47625
773      22 c/x -5.9248 -118.2624 0.47625
774      22 c/x -5.9248 -111.0285 0.47625
775      22 c/x -5.9248 -66.1416 0.47625

```

```

776 22 c/x -5.9248 -58.9077 0.47625
777 22 c/x -5.9248 -14.0462 0.47625
778 22 c/x -5.9248 -6.8123 0.47625
779 22 c/x -5.9248 38.1254 0.47625
780 22 c/x -5.9248 45.3593 0.47625
781 22 c/x -5.9248 90.2716 0.47625
782 22 c/x -5.9248 97.5055 0.47625
783 22 c/x -5.9248 142.3670 0.47625
784 22 c/x -5.9248 149.6009 0.47625
785 22 c/x -5.9248 194.8180 0.47625
786 22 c/x -5.9248 202.0519 0.47625
787 22 c/x -5.9248 213.8172 0.47625
c
790 22 c/x -16.9789 -189.6872 0.47625
791 22 c/x -16.9789 -179.5526 0.47625
792 22 c/x -16.9789 -172.3187 0.47625
793 22 c/x -16.9789 -118.2624 0.47625
794 22 c/x -16.9789 -111.0285 0.47625
795 22 c/x -16.9789 -66.1416 0.47625
796 22 c/x -16.9789 -58.9077 0.47625
797 22 c/x -16.9789 -14.0462 0.47625
798 22 c/x -16.9789 -6.8123 0.47625
799 22 c/x -16.9789 38.1254 0.47625
800 22 c/x -16.9789 45.3593 0.47625
801 22 c/x -16.9789 90.2716 0.47625
802 22 c/x -16.9789 97.5055 0.47625
803 22 c/x -16.9789 142.3670 0.47625
804 22 c/x -16.9789 149.6009 0.47625
805 22 c/x -16.9789 194.8180 0.47625
806 22 c/x -16.9789 202.0519 0.47625
807 22 c/x -16.9789 213.8172 0.47625
c
809 pz -188.417
810 pz -181.331 $ PH 1 (bottom)
811 pz -170.541 $ PH 1
812 pz -120.040 $ PH 2
813 pz -109.250
814 pz -67.920 $ PH 3
815 pz -57.130
816 pz -15.824 $ PH 4
817 pz -5.034
818 pz 36.347 $ PH 5
819 pz 47.137
820 pz 88.494 $ PH 6
821 pz 99.284
822 pz 140.589 $ PH 7
823 pz 151.379
824 pz 193.040 $ PH 8
825 pz 203.830 $ PH 8
826 pz 212.547
c
900 px 11.18006 $ FIXED for strongbacks touching
901 py -5.71956 $ FIXED for strongbacks touching
902 px -11.9593
903 py -28.7574 $ surface 901 minus 9.07"
c
c 904 is -7.1354 and 905 is 9.7633 for nominal case (with poison holders).
c they are shifted to cut off poison holders to allow for
c expansion for damaged cases.
c
c To completely "slice off" the poison holders, set
c 904 to -6.6593 and 905 to 10.2392.
c
904 py -6.6593 $ tangential strongback lower bound, surface 901 minus total thickness
905 px 10.2392 $ radial strongback left bound, surface 901 minus total thickness
906 pz 215.7222
908 c/z 9.87856 -7.02106 1.3015
909 px -9.9019
910 py -6.35448
911 py -7.1344 $ fixed
912 px 9.7653 $ fixed
c
998 so 10000
999 pz 345.5565

```

```

mode      n
c          print
kcode     2000 1 30 530
sdef      cell=d1 pos=0 0 0 rad=d3 ext=d4 axs=0 0 1
sil       1 7:200:410 207:200:410 222:200:410
spl       1 1 1
si3       0.409575
si4       182.88
cut:n     j j 0 0
c
c          Materials
c
m1        92235      -0.249    $ fuel pellet
          92238      -82.615
          94239      -4.972
          94240      -0.264
          94241      -0.053
          8016       -11.847
m2        13027      1.0      $ aluminum cladding for BORAL
m4        1001       2        $ water
          8016       1
mt4       lwtr.01t
m5        6000      -0.06     $ XM-19
          7014      -0.4
          14000     -0.75
          15031     -0.04
          16032     -0.03
          23000     -0.3
          24000     -23.5
          25055     -6
          28000     -13.5
          41093     -0.3
          42000     -3
          26000     -52.12
m6        6000      -0.08     $ SS-304
          14000     -1.0
          15031     -0.045
          24000     -19.0
          25055     -2.0
          26000     -68.375
          28000     -9.5
m7        40000     -1.0     $ Cladding
c         41093     -0.030
m8        82000      1.0      $ lead
m9        6000      -25.1     $ water/steel mix, 5.8% steel by volume
          14000     -313.9
          15031     -14.1
          24000     -5964.9
          25055     -627.9
          26000     -21465.8
          28000     -2982.5
          1001      -7240.1
          8016      -57462.7
mt9       lwtr.01t
m21       5010      7.3123E-03 $ 35 mg/cm2 B-10, 75% credit
          5011      3.9244E-02
          6000      1.2248E-02
          13027     3.3439E-02
c          total 9.2244E-02
c
c          Translations
c
c          tr22 is the intersection of planes 904 and 905
c          when the poison holders are present (904 and 905 shift when it is
c          desired to "slice off" the poison holders).
c          Note that the origin of Universe 7 corresponds to the intersection
c          of these planes.
c
*tr22     9.7643 -7.1354 0.0
c
c          tr25 is the intersection of planes 300 and 302. The origin of Universe 30
c          corresponds to the intersection of these planes.
c
*tr25     -12.8928 -29.7925 0.0
c

```

```
c      tr30 is computed by taking the coordinates of the intersection of planes
c      22 and 24 and adding half the pitch (note: can't be exact or else planes will
c      overlap, causing program termination.)
c
*tr30  -11.6368 -28.5365 0.0
c
c      tr53 and tr54 rotate the bottom assembly to create assemblies 2 and 3
c
*tr53  0 0 0          120 30 90    150 120 90    90 90 0 $ +x+y
*tr54  0 0 0          120 150 90    30 120 90    90 90 0 $ -x-y
```

This page left intentionally blank.

A6.9.2 Infinite Array Model

The infinite array models are geometrically the same as the single package models, although small changes have been made to the outer boundary to simulate the infinite array. Additional cells and surfaces are listed below.

```

195      0      -881 882 -886 885 -883 884 -66 63 62  imp:n=1 $ w between packages
199      0      (881:-882:886:-885:883:-884:66:-63)  imp:n=0 $ outside world

c      hexagonal boundary of one unit lattice cell, close packed
*881    px      37.6184
*882    px     -37.6184
*883    p     -0.5000000      0.866025404      0.0000000      37.6184
*884    p     -0.5000000      0.866025404      0.0000000     -37.6184
*885    p      0.5000000      0.866025404      0.0000000     -37.6184
*886    p      0.5000000      0.866025404      0.0000000      37.6184

```

This page left intentionally blank.

A7.0 PACKAGE OPERATIONS

A7.1 Package Loading

The package loading operations are the same as the operations for fuel assembly loading described in Chapter 7.1, *Package Loading*. The ARB-17 is handled in the same manner as a fuel assembly.

The ARB-17 may contain fuel rods that are slightly damaged. These damaged rods may be bent, scratched, or nicked, but under no circumstances shall exhibit cladding breach. The structural integrity of these fuel rods must be confirmed by visual inspection prior to loading in the ARB-17.

A7.2 Package Unloading

The package unloading operations are the same as the operations for fuel assembly unloading described in Chapter 7.2, *Package Unloading*. The ARB-17 is handled in the same manner as a fuel assembly.

A7.3 Preparation of an Empty Package for Transport

Previously used and empty MFFPs shall be prepared and transported per the requirements of 49 CFR §173.428¹.

A7.4 Preshipment Leakage Rate Test

The preshipment leakage rate test is the same as described in Section 7.4, *Preshipment Leakage Rate Test*.

¹ Title 49, Code of Federal Regulations, Part 173 (49 CFR 173), *Shippers—General Requirements for Shipments and Packagings*, 10-01-06 Edition.

This page left intentionally blank.

A8.0 ACCEPTANCE TESTS AND MAINTENANCE PROGRAM

A8.1 Acceptance Tests

Per the requirements of 10 CFR §71.85¹, this section discusses the inspections and tests to be performed prior to first use of the ARB-17 rod container.

A8.1.1 Visual Inspections and Measurements

Each ARB-17 rod container shall be examined in accordance with the requirements delineated on the applicable fabrication drawing.

A8.1.2 Weld Inspections

All welds shall be inspected to the requirements delineated on the applicable fabrication drawing.

A8.1.3 Structural and Pressure Tests

The ARB-17 rod container does not require any lifting device load tests or pressure tests.

A8.1.4 Fabrication Leakage Rate Tests

The ARB-17 rod container does not require any leakage rate tests.

A8.1.5 Component and Material Tests

The ARB-17 rod container does not require any component or material tests.

A8.1.6 Shielding Tests

The ARB-17 rod container does not require any shielding tests.

A8.1.7 Thermal Tests

The ARB-17 rod container does not require any thermal tests.

¹ Title 10, Code of Federal Regulations, Part 71 (10 CFR 71), *Packaging and Transportation of Radioactive Material*, 01-01-06 Edition.

A8.2 Maintenance Program

The ARB-17 rod container does not require a scheduled maintenance program. The parts which are routinely handled during use (the body, the lid, and the lid fasteners) are visually inspected prior to use. Damaged components shall be repaired or replaced prior to use.

B1.0 GENERAL INFORMATION

Appendix B of the MOX Fresh Fuel Package (MFFP) Safety Analysis Report (SAR) supports the addition of one (1) AFS-B rod container and one (1) Excess Material Assembly (EMA) as allowable contents of the MFFP. As these items fill only two of the three available strongback locations, the third strongback location is filled with a dummy fuel assembly. Alternately, the AFS-B may be transported separately with two dummy fuel assemblies per strongback, and the EMA may be transported in lieu of a standard fuel assembly.

The AFS-B is a rod container that may transport up to 175 MOX fuel rods. The fuel rod type is identical to the rods comprising the standard MOX fuel assembly described in Chapter 1.0, *General Information*. The EMA is a fuel assembly comprised of MOX fuel rods that do not meet all of the performance requirements of a standard MOX fuel rod, primarily pellet OD and Pu-238 isotopic composition. These out-of-tolerance values have no impact on the licensing analyses.

In this SAR Appendix, reference is made to the main SAR for information that has not changed. Referenced tables, figures, and sections that do not contain the letter “B” (e.g., Table 1.2-1, Figure 3.5-1, Section 6.1.1) refer to items in the main SAR. Referenced tables, figures, and sections that contain the letter “B” (e.g., Table B6.4-1, Figure B1.2-1, Section B6.1.1) refer to items in Appendix B.

B1.1 Introduction

The Mixed Oxide Fresh Fuel Package, Model: **MFFP**, is designed to transport fresh MOX pressurized water reactor (PWR) reactor fuel assemblies. The AFS-B fuel rod container has outer dimensions consistent with those of a standard fuel assembly and interfaces with the strongback and clamp arms in the same way. The EMA has the same outer dimensions, appearance, and number of fuel rods/guide tubes as a standard MOX fuel assembly.

A full-scale, prototypic certification test unit (CTU) was subjected to a series of hypothetical accident condition (HAC) free and puncture drop tests as part of the original SAR submittal. The results of this testing program are directly applicable to the AFS-B/EMA payload because the loaded AFS-B and EMA weight is bounded by the weight of a fuel assembly (including a BPRA). A detailed discussion of the CTU and certification tests is provided in Appendix 2.12.3, *Certification Test Results*. These tests, coupled with supplementary analytical evaluations, conclusively demonstrated the leaktight¹ containment boundary integrity and criticality control performance of the MFFP.

The thermal analysis for the AFS-B payload is provided in Chapter B3.0, *Thermal Evaluation*. Because an MFFP loaded with an AFS-B and EMA contains significantly less decay heat than three fuel assemblies, MFFP strongback and shell temperatures are bounded by those reported in Chapter 3.0, *Thermal Evaluation*. However, due primarily to the simplistic analytical method employed, for HAC only, the maximum fuel rod temperatures for rods within the AFS-B are computed to be higher than the maximum temperature computed for a fuel assembly. These

¹ Leaktight is defined as 1×10^{-7} standard cubic centimeters per second (scc/s), or less, air leakage per ANSI N14.5-1997, *American National Standard for Radioactive Materials – Leakage Tests on Packages for Shipment*, American National Standards Institute, (ANSI), Inc

temperatures are well below the respective temperature limits for a fuel rod. The internal pressure under NCT and HAC with the AFS-B/EMA payload is bounded by the pressure with three fuel assemblies.

Based on the shielding and criticality assessments provided in Chapter B5.0, *Shielding Evaluation*, and Chapter B6.0, *Criticality Evaluation*, the Criticality Safety Index (CSI) for the MFFP is zero (0.0), and the Transport Index (TI) is determined at the time of shipment.

Authorization is sought for shipment of the MFFP containing an AFS-B and/or EMA by all modes of conveyance, except for aircraft, as a Type B(U)F package per the definitions delineated in 10 CFR §71.4.

B1.2 Package Description

General arrangement drawings of the packaging are provided in Section 1.4.2, *Packaging General Arrangement Drawings*. The addition of the AFS-B and EMA does not alter these packaging drawings. A drawing of the AFS-B rod container is given in Section B1.4.2, *Packaging General Arrangement Drawings*.

B1.2.1 Packaging

The MFFP packaging description is unchanged from the description provided in Section 1.2.1, *Packaging*. The AFS-B rod container is designed to hold up to 175 MOX fuel rods of the type used in the MOX fuel assemblies. The container has outer cross sectional dimensions of 8.4 inches square, a length from bottom to top of 159.9 inches, and an overall length (to the lift ring bolt head) of 161.2 inches. The primary material of construction of the container is ASTM 6061-T651 aluminum alloy. The two side walls, the bottom plate, and the lid are all $\frac{3}{4}$ inches thick. The side plates are attached to the bottom plate with two longitudinal, 3/8-inch groove welds. The lid is attached with twenty-two (22) zinc-plated, 3/8-16 UNC, SAE J429 Grade 8, hex head cap screws. The two square end pieces are made of solid aluminum alloy, and each are attached to the container with eight (8) zinc-plated SAE J429 3/8-16 UNC hex head cap screws made of Grade 8 alloy steel. The lower square end piece is 2.4 inches thick and the upper square end piece is 3.0 inches thick. Each bolt is secured in place using a thin stainless steel lock tab. Two of the eight bolts on each end go horizontally into the lid, in addition to the 22 cap screws on the top of the lid.

Inside the container is a $\frac{1}{2}$ -inch thick shelf, made of the same aluminum alloy, which fits into $\frac{1}{4}$ -inch deep grooves in each side wall. The shelf is supported by $\frac{1}{4}$ -inch thick aluminum support plates on 15.3-inch centers. The region between the shelf and the lid is the rod cavity, which is 6.9 inches wide, 3.4 inches deep, and 153.5 inches long. The support plates and the shelf are located with intermittent 1/8-inch fillet welds, none of which are load bearing. Along the inside of the two side plates are two, 2.1-inch wide grooves, 0.4 inches deep. These grooves accommodate the bulkheads used in the AFS-C rod container, but they have no function in the AFS-B container. The components of the AFS-B feature numerous small holes that ensure the AFS-B will not hold pressure.

The lid is lifted by means of two, $\frac{1}{4}$ -20 UNC threaded holes in the lid. The holes are located such that at least half of the hole is blocked by the top of the sidewall, which prevents an overly-long lifting bolt from possibly damaging any fuel rods. The container is lifted from its top end using a swivel hoist ring. All threaded holes may optionally be fitted with helical-coil thread inserts. The label 'AFS-B' is painted prominently on both sides of the container. The AFS-B is finished with a clear anodize treatment.

An external view of the AFS-B rod container is given in Figure B1.2-1. An internal cross sectional view is given in Figure B2.7-1.

B1.2.2 Containment System

The containment system description is unchanged from the description provided in Section 1.2.2, *Containment System*.

B1.2.3 Contents of Packaging

The MFFP may simultaneously transport one (1) AFS-B containing up to 175 standard MOX fuel rods, and one (1) EMA. The 175 fuel rod limit is a geometrical limit based on the size of the cavity, assuming the fuel rods are packed in a hexagonal lattice. If necessary, for a payload of fewer than 175 rods, aluminum or stainless steel dunnage rods are used to take up the remaining space. A non-fuel dummy assembly is utilized in the unoccupied strongback location. The physical size and weight of the non-fuel dummy assemblies are nominally the same as the MK-BW/MOX1 17 × 17 design. Alternately, the AFS-B may be transported separately with two dummy fuel assemblies per strongback, and the EMA may be transported in lieu of a standard fuel assembly.

Because the AFS-B with 175 fuel rods is more reactive than a MOX fuel assembly, it is not acceptable to transport more than one (1) AFS-B per MFFP. Also, the AFS-B cannot be combined in a shipment with more than (1) EMA or standard fuel assembly. For transportation purposes, an EMA and a standard MOX fuel assembly may be considered interchangeable. Examples of acceptable and unacceptable loading configurations are summarized below:

Acceptable Loading Configurations	Unacceptable Loading Configurations
1 AFS-B, 1 EMA/fuel assembly, 1 dummy	1 AFS-B, 2 EMAs/fuel assemblies
1 AFS-B, 2 dummies	2 AFS-Bs, 1 dummy
Any combination of fuel assemblies, EMAs, and dummy fuel assemblies	3 AFS-Bs

The physical parameters for a fuel rod provided in Table 1.2-1 and nuclear design parameters provided in Table 1.2-2 are applicable to rods in the AFS-B. These parameters are also applicable to the EMA, with the exceptions that the OD of the fuel pellets may be out of tolerance (nominal pellet diameter = 0.323 inch), and the weight percent Pu-238 exceeds the 0.05 wt.% limit specified in Table 1.2-2 (EMA fuel rods have Pu-238/Pu as high as 0.19 wt.%). Pu-238 is a neutronic poison and is neglected in the criticality analysis, so there is no safety concern associated with this value being outside of the tolerance. Minor fluctuations of the fuel pellet OD are also negligible.

B1.2.3.1 Radionuclide Inventory

The nuclear parameters for the AFS-B rods are unchanged from those provided in Table 1.2-2. As noted above, the rods in the EMA do not meet the performance specifications of a standard fuel rod, although the differences are minor and without safety significance.

B1.2.3.2 Maximum Payload Weight

The loaded AFS-B has a payload weight of approximately 1,500 pounds. The EMA, which weighs approximately the same as a standard MOX fuel assembly and will not be loaded with a burnable poison rod assembly (BPRA), weighs less than the 1,580 pound design weight of a fuel assembly loaded with a BPRA. The combined payload weight of the AFS-B, EMA, and dummy fuel assembly is therefore bounded by the value of 4,740 pounds provided in Section 1.2.3.2, *Maximum Payload Weight*.

B1.2.3.3 Maximum Decay Heat

Assuming that the EMA has a maximum decay heat of 80 watts, and the loaded AFS-B has a maximum decay heat of $175/264 \times 80 = 53$ watts, the maximum decay heat for this payload is 133 watts. This maximum heat load is bounded by the 240 watts provided in Section 1.2.3.3, *Maximum Decay Heat*.

B1.2.3.4 Maximum Pressure Buildup

The maximum normal operating pressure (MNOP) is bounded by the 10 psig value provided in Section 1.2.3.4, *Maximum Pressure Buildup*. The design pressure of 25 psig is also unchanged.

B1.2.4 Operational Features

Operating procedures and instructions for loading, unloading, and preparing an empty MFFP for transport with the AFS-B and EMA are provided in Chapter B7.0, *Package Operations*.

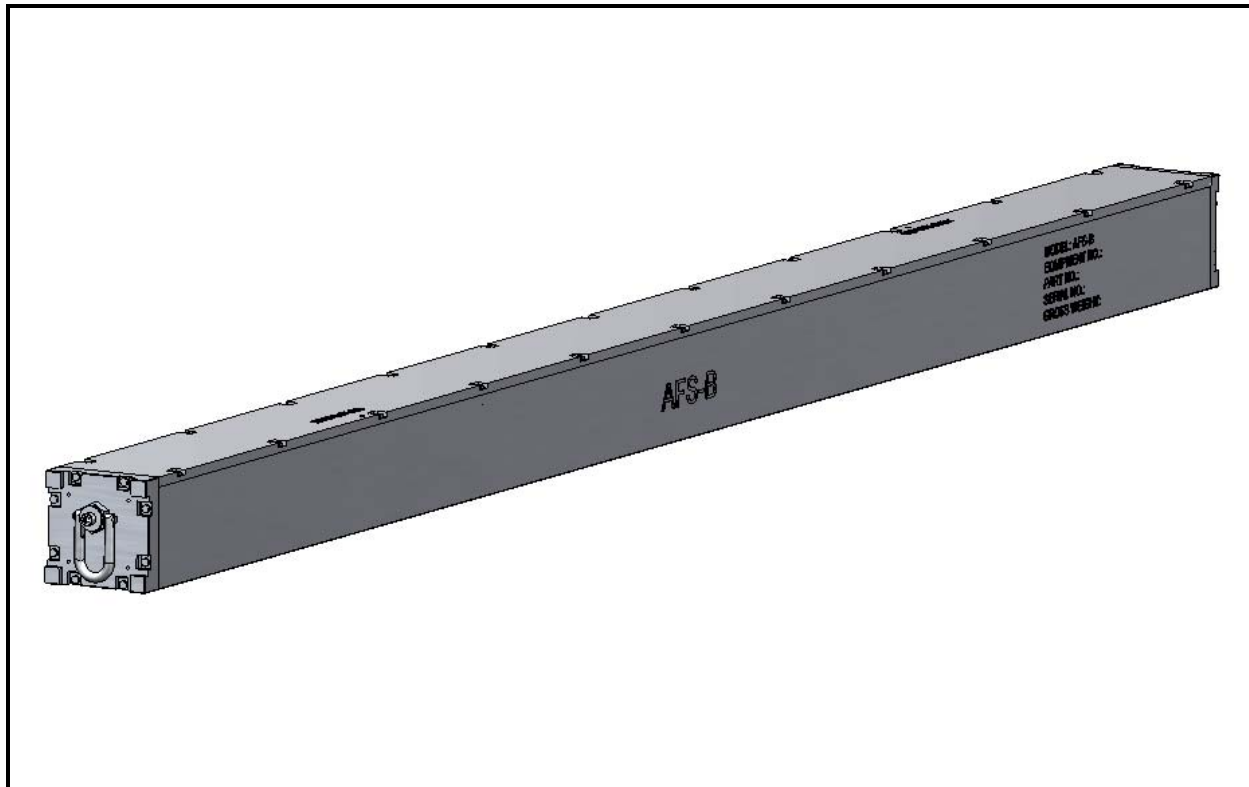


Figure B1.2-1 – AFS-B Rod Container

This page left intentionally blank.

B1.3 General Requirements for All Packages

The AFS-B and EMA have no effect on the way in which the MFFP meets the general requirements for packaging. |

This page left intentionally blank.

B1.4 Appendices

B1.4.1 Nomenclature

The nomenclature list from Section 1.4.1, *Nomenclature*, is applicable. Additional nomenclature listed below.

AFS-B – Container used to transport up to 175 standard MOX fuel rods. The AFS-B interfaces with the strongback in the same manner as a fuel assembly.

Excess Material Assembly (EMA) – Fuel assembly comprised of 264 fuel rods that do not necessarily meet the performance requirements of a standard MOX fuel rod. An EMA has the same outer dimensions and visual appearance of a standard fuel assembly.

B1.4.2 Packaging General Arrangement Drawings


The general arrangement drawings of the body, strongback, and impact limiters are unchanged from those provided in Section 1.4.2, *Packaging General Arrangement Drawings*. The following AFS-B drawing is included in this section:

- 99008-60, Rev. 1, 2 sheets, *AFS-B Assembly*

This page left intentionally blank.

Security Related Information
Figure Withheld Under 10 CFR 2.390

DWG NO 99008-60 SH 1 REV 1 1

1	SEE DCR NO.: 99008-56	BIT	7/24/08
REV.	DESCRIPTION	REL	DATE
REVISION HISTORY			
 AREVA Federal Services LLC Packaging Projects Tacoma, WA 98402			
AFS-B ASSEMBLY SAR DRAWING			
SCALE: 1:5		WT. - LBS	
REV: 1		SHEET 1 OF 2	
DWG NO	99008-60		
SIZE	D		
CADFILE	9900801.DWG		
DWG-3290248			

Security Related Information
Figure Withheld Under 10 CFR 2.390

DWG NO. 99008-60 SH 2 REV 1

REV: 1 SHEET 2 OF 2
DWG NO. 99008-60

B2.0 STRUCTURAL EVALUATION

This chapter of Appendix B provides a structural evaluation of the MFFP when transporting one (1) AFS-B rod container and one (1) Excess Material Assembly (EMA). As these items fill only two of the three available strongback locations, the third strongback location is filled with a dummy fuel assembly. Alternately, the AFS-B may be transported separately with two dummy fuel assemblies per strongback, and the EMA may be transported in lieu of a standard fuel assembly. It is demonstrated that all quantities of interest are bounded by the analyses presented in Chapter 2.0, *Structural Evaluation*.

B2.1 Structural Design

B2.1.1 Discussion

A comprehensive discussion of the MFFP design and standard configuration is provided in Section 1.2, *Package Description*. The MFFP drawings show the detailed geometry of the package, as well as the dimensions, tolerances, materials, and fabrication requirements, and are provided in Appendix 1.4.2, *Packaging General Arrangement Drawings*.

A physical description of the AFS-B rod container is provided in Section B1.2.3, *Contents of Packaging*, and is shown in the drawings in Appendix B1.4.2, *Packaging General Arrangement Drawings*. The AFS-B container is a robust box designed to provide confinement of individual fuel rods under all conditions of transport. The AFS-B container has the same external boundary dimensions as a standard MOX fuel assembly, and thus is loaded, mounted, and unloaded from the strongback in the same manner as a fuel assembly. The structural evaluations and testing performed as part of the original license activities adequately characterize the performance of the MFFP with this payload.

The EMA is structurally identical to a MOX fuel assembly, and its structural response will be the same as a MOX fuel assembly described in Chapter 2.0, *Structural Evaluation*. Therefore, no additional structural evaluations are necessary for this item.

B2.1.2 Design Criteria

The MFFP design criteria are unchanged from those provided in Section 2.1.2, *Design Criteria*. The design criteria for the AFS-B rod container are based on the functional requirement that the rod container confine the rods inside the container boundary under all NCT and HAC. Because the AFS-B rod container is transported within the MFFP strongback, it is protected from gross distortion by the fuel control structure (FCS). As shown in Section 2.12.5, *Fuel Control Structure Evaluation*, the FCS provides a limit to any reconfiguration of the fuel assembly which could occur as a result of the worst case HAC event. The MOX fuel assembly consists of a larger number of rods (264) than is contained in the AFS-B rod container (175). In addition, the rods in the MOX fuel assembly are unconfined by any structure other than the FCS, whereas fuel rods in the AFS-B rod container are confined within a container having significant structure. Therefore, gross distortion of the fuel rods or of the AFS-B container, or escape of the fuel rods from the container, will not occur.

To enhance criticality safety by preventing the potential for damage to the fuel rods in the HAC free drop impact event, the AFS-B rod container is designed to minimize the relative motion of the rods under impact conditions. To accomplish this, the AFS-B rod container is designed to limit the “rattle space” of the fuel rods (including any dummy rods as necessary) to less than approximately one half rod diameter.

The only component of the AFS-B container which is not supported externally by the strongback or FCS is the internal shelf. To ensure that the “rattle space” available to the rods cannot increase as a result of the free drop impact event, the internal shelf is designed to have a primary bending stress less than the yield point of the shelf material at NCT maximum temperature.

B2.1.3 Weights and Center of Gravity

The loaded weight of the AFS-B, conservatively assuming 175 fuel rods, is bounded by 1,500 pounds, which is 5% less than the gross weight of 1,580 pounds for a fuel assembly or dummy fuel assembly. Because the EMA will not contain a burnable poison rod assembly (BPRA), the EMA weight is bounded by the 1,580 pound design weight of the combined fuel assembly and BPRA. Therefore, the weight of the MFFP when transporting one (1) AFS-B, one (1) EMA, and one (1) dummy fuel assembly is bounded by the weights given in Section 2.1.3, *Weights and Center of Gravity*, for transport of MOX fuel assemblies.

The longitudinal center of gravity (CG) of the package is essentially unchanged from that reported in Section 2.1.3, *Weights and Center of Gravity*, or 103.7 inches from the bottom end impact limiter.

B2.2 Materials

The AFS-B is constructed primarily of ASTM B209, 6061-T651 aluminum plate material. The lid and ends are attached with SAE J429 zinc-plated hex head cap screws made from Grade 8 material. A stainless steel swivel hoist ring is included for lifting. No non-metallic materials are used in the AFS-B. These materials do not result in any chemical or galvanic reactions, and are not significantly affected by radiation. The material properties for the aluminum material at 70 and 200 °F needed for calculations are given in Table B2.2-1, and are taken from the ASME B&PV Code,¹ as noted. Note that although there is limited welding of the 6061 material, welding is not used in regions where the material properties of unwelded material are used in stress analysis.

¹ American Society of Mechanical Engineers (ASME) Boiler and Pressure Vessel Code, Section II, Materials, Part D, Properties, 2001 Edition, 2002 and 2003 Addenda.

Table B2.2-1 - Material Properties of ASTM B209 6061-T651 Aluminum Alloy

Temperature, °F	Yield Strength, psi	Ultimate Strength, psi	Coefficient of Thermal Expansion, 10 ⁻⁶ in/in/°F
70	35,000 ^①	42,000 ^①	-
200	33,700 ^②	-	13.0 ^③

Notes:

①Yield and ultimate strength at 70 °F from ASME B&PV Code, Section II, Part B, SB-209.

②Yield strength at 200 °F from ASME B&PV Code, Section II, Part D, Table Y-1.

③Coefficient of thermal expansion from ASME B&PV Code, Section II, Part D, Table TE-2.

B2.3 Fabrication and Examination

The AFS-B rod container is fabricated to the requirements of the drawing shown in Appendix B1.4.2, *Packaging General Arrangement Drawings*. The materials of construction are specified to either ASTM or SAE standards. The rod container is inspected to the dimensional requirements of the drawing. Welds are visually inspected to the AWS D1.2² welding code.

B2.4 Lifting and Tie-down Standards for All Packages

Because the gross weight of the MFFP is lower when transporting the AFS-B rod container and EMA compared to three (3) fuel assemblies, this section is unchanged from Section 2.4, *Lifting and Tie-down Standards for All Packages*, in regards to the package itself.

The AFS-B uses a 5/8-11 UNC swivel hoist ring for handling. The thread depth for this swivel hoist ring bolt is 1.28-in. The minimum required thread depth may be computed by the following equation:

$$L_i = \frac{A_t \times S_t}{A_i \times S_i}, \text{ where}$$

A_t is the tensile stress area of the 5/8-11 UNC bolt (0.2201 in²)

S_t is the allowable ultimate tensile strength for the 5/8-11 UNC bolt (170,000/5 = 34,000 psi)³

A_i is the internal aluminum thread stripping area per inch length (1.4255 in²/in-length)

S_i is the governing allowable shear strength of the aluminum thread (0.6 x 42,000/5 = 5,040 psi using ultimate strength). Note that this value bounds the value obtained using the yield strength (0.6 x 35,000/3 = 7,000 psi). Material properties are at 70 °F.

The minimum length of aluminum thread to develop the full tensile strength of the external thread is then:

² ANSI/AWS D1.2, *Structural Welding Code – Aluminum*, American Welding Society (AWS).

³ Conservatively high tensile strength obtained from ASTM A574, *Standard Specification for Alloy Steel Socket-Head Cap Screws*. Actual tensile strength of swivel hoist ring bolt will be equal to or less than this value.

$$L_i = \frac{(0.2201)(34,000)}{(1.4255)(5,040)} = 1.0416 \text{ in}$$

As this length is less than the 1.28-in thread depth of the swivel hoist ring bolt, tear out of the aluminum threads is not a concern. The governing factor is therefore the swivel hoist ring bolt, and the performance of this item is ensured by the rated capacity of the swivel hoist ring. Note that an optional 300 series insert may also be used, which would further increase the conservatism.

B2.5 General Considerations

The AFS-B rod container is evaluated by reasoned argument and by analysis in the following sections. In addition, the results and conclusions of Section 2.5, *General Considerations*, remain unchanged.

B2.6 Normal Conditions of Transport

B2.6.1 Heat

It is demonstrated in Section B3.4, *Thermal Evaluation for Normal Conditions of Transport*, that under NCT, all MFFP component temperatures associated with the AFS-B payload are bounded by the standard three (3) fuel assembly payload. Therefore, all associated pressure and thermal stresses are bounded by the values presented in Section 2.6.1, *Heat*. For the AFS-B rod container, the bounding temperature of the sidewalls and the internal shelf is 200 °F. Since the AFS-B is vented, it cannot retain pressure.

B2.6.1.1 Differential Thermal Expansion

The evaluation of differential thermal expansion given in Section 2.6.1.2, *Differential Thermal Expansion*, is not affected by use of the AFS-B rod container. An additional evaluation of the differential thermal expansion between the strongback and the AFS-B container will now be made.

From Section 2.6.1.2, *Differential Thermal Expansion*, the design temperature of the strongback is $T_{SB} = 180$ °F, and the coefficient of thermal expansion for the strongback material is $\alpha_{SB} = 8.8 \times 10^{-6}$ in/in/°F. As stated above, the bounding temperature for the AFS-B container is $T_{AFS-B} = 200$ °F, and from Table B2.2-1, the coefficient of thermal expansion is $\alpha_{AFS-B} = 13.0 \times 10^{-6}$ in/in/°F. The overall length of the container is $L = 159.9$ inches. The reference temperature is 70 °F. The differential thermal growth of the rod container and the strongback is:

$$\delta = \alpha_{AFS-B}(L)(T_{AFS-B} - 70) - \alpha_{SB}(L)(T_{SB} - 70) = 0.115 \text{ inches}$$

This calculation conservatively assumes that the entire length of the two components is at the respective peak temperatures, and thus overestimates the relative thermal expansion. To prevent axial interference of the AFS-B container with the strongback, the clamp pads will be set with a clearance to the end of the AFS-B container. As stated in Section B7.1, *Package Loading*, the 3/4-10 clamp pad screw will be backed out a minimum of one turn from the position of contact,

ensuring a minimum axial clearance between the AFS-B container and the strongback of 0.1 inches at the reference temperature. This is adequate to ensure that the thermal expansion force is negligible or non-existent considering the conservatism of the evaluation above.

B2.6.2 Cold

This section is unchanged from Section 2.6.2, *Cold*.

B2.6.3 Reduced External Pressure

This section is unchanged from Section 2.6.3, *Reduced External Pressure*.

B2.6.4 Increased External Pressure

This section is unchanged from Section 2.6.4, *Increased External Pressure*.

B2.6.5 Vibration and Shock

The vibration normally incident to transportation will have no effect on the AFS-B rod container. The AFS-B container is installed and retained in the same manner as a MOX fuel assembly. The spring loaded clamp arms which hold the container in place will significantly dampen any vibrational loads which could come from the cask body. Furthermore, any fatigue cracks which might occur from vibration, which are too small to be noted during a visual inspection, would have no effect on the ability of the AFS-B to perform its function of confining the rods in a HAC free drop impact. Therefore, vibration and shock are not of concern for the AFS-B rod container.

B2.6.6 Water Spray

This section is unchanged from Section 2.6.6, *Water Spray*.

B2.6.7 Free Drop

Because a loaded AFS-B is slightly lighter than a fuel assembly (including BPRA), the response of the MFFP to a free drop would be essentially the same when compared to the standard payload.

Since the AFS-B rod container is shown to confine the fuel rods in a HAC free drop impact (see Section B2.7.1), its performance will be acceptable for the NCT free drop event.

B2.6.8 Corner Drop

This section is unchanged from Section 2.6.8, *Corner Drop*.

B2.6.9 Compression

This section is unchanged from Section 2.6.9, *Compression*.

B2.6.10 Penetration

This section is unchanged from Section 2.6.10, *Penetration*.

B2.7 Hypothetical Accident Conditions

B2.7.1 Free Drop

The functional criteria of the AFS-B rod container is to confine the fuel rods in the worst-case HAC free drop event. As an additional enhancement to criticality safety, the container should also restrict the relative movement of the rods to minimize the potential for damage to the fuel rods.

The MFFP strongback, including the fuel control structure (FCS), is designed to maintain a complete MOX fuel assembly in a subcritical configuration during the governing free drop event. Using physical test (see Appendix 2.12.3, *Certification Test Results*) and calculations (see Appendix 2.12.5, *Fuel Control Structure Evaluation*), it has been demonstrated that *a*) the fuel rods do not break or fragment, and *b*) the strongback and FCS are capable of confining the rods within a defined geometry. As stated in Section B1.2, *Package Description*, the AFS-B rod container consists of a completely enclosed structure made of 6061-T651 aluminum plates of $\frac{3}{4}$ -inch nominal thickness. The lid of the container is attached using 22, $\frac{3}{8}$ -inch diameter bolts. The container has the same boundary dimensions as the MOX fuel assembly, and is mounted in the strongback in the same manner. As such, the AFS-B container represents an added level of confinement for the fuel rods, beyond that provided by the strongback and FCS. For this reason, confinement of the fuel rods by the AFS-B container is ensured. Table B2.7-1 presents added detail which supports this conclusion. As stated in Section B2.1.2, *Design Criteria*, the rod movement in an impact is restricted to a maximum of approximately one-half of a rod diameter.

The rod cavity inside the AFS-B container is formed by the $\frac{3}{4}$ -inch thick lid plate, the two $\frac{3}{4}$ -inch thick side plates, thick end plates (minimum thickness of 2.4 inches), and a $\frac{1}{2}$ -inch thick shelf plate. The shelf plate is located in longitudinal, $\frac{1}{4}$ -inch deep grooves on the inside face of each $\frac{3}{4}$ -inch thick side plate, and supported against the bottom plate by support plates at 15.3-inch intervals. Note that each weld between the shelf and the side plates is only 2-inches long, centered on each support plate, as shown in Section B of drawing 99008-60. This weld is not structural, and serves only to compensate for any weld distortion which might occur from the two groove welds. As such, a strength reduction does not need to be considered, since the longer, unsupported length between support plates is far from any heat affected zone. Figure B2.7-1 shows a cross section of the AFS-B container. To demonstrate that the rod cavity maintains its internal geometric integrity in the worst-case free drop impact, the following evaluation is performed. The internal geometric integrity assures that the “rattle space” inside the container is minimized to prevent any possible damage to the rods. However, any loss of the rod container contents is precluded by the rod container primary structure, as discussed above. In the following, it is assumed that the impact occurs with the shelf oriented horizontally with the container lid side up. This orientation governs over all others where some component of the rod load is directed toward the thick sidewalls of the container.

In this evaluation, any support from the support plates beneath the shelf will be conservatively neglected. The shelf is then a plate, simply supported on its two long sides, and free on its two short sides. A governing impact of 180g is taken from Section 2.12.5.2, *Conditions Analyzed*, for

the maximum slapdown impact. From Table 2.12.5-1, the fuel rod weight is 5.33 lb each, and the length is $L_r = 152.4$ inches. From Figure B2.7-1, the internal width of the cavity is $b = 6.9$ inches. For 175 rods, the total weight of rods is therefore $W = 175 \times 5.33 = 933$ lb. Since the rods rest on an area bounded by the rod length and the cavity width, the impact pressure on the shelf is:

$$q = \frac{Wg}{L_r b} = 159.7 \text{ psi}$$

A formula from Roark,⁴ Table 26, Case 1a, is used. Even though this formula assumes simple support on the narrow ends as well as the sides, the maximum stress at the center of the plate, which is more than 10 plate-widths distant from the ends, will not be materially affected. The length of the shelf is $L_s = 153.5$ inches. The ratio a/b is $153.5/6.9 = 22.2$, from which $\beta = 0.75$. The maximum stress at the center of the plate is found from:

$$\sigma = \frac{\beta q b^2}{t^2} = 22,810 \text{ psi}$$

where $t = 0.5$ inches, and the other quantities are as defined above. From Table B2.2-1, the yield strength of the shelf material at the bounding temperature of 200 °F is 33,700 psi. The margin of safety against yield of the shelf is:

$$MS = \frac{33,700}{22,810} - 1 = +0.48$$

Since the shelf does not yield, the “rattle space” available for the rods does not increase as a result of the slapdown free drop event. Other impact orientations would place lower loadings on the shelf. Thus, the AFS-B rod container supports the geometry assumptions made in the criticality analysis of Chapter 6, *Criticality Evaluation*.

⁴ Young, W. C., *Roark's Formulas for Stress and Strain*, Sixth Edition, McGraw-Hill, 1989.

Table B2.7-1 – Comparison of the MOX Fuel Assembly and the AFS-B Rod Container in the MFFP Strongback

MOX Fuel Assembly	AFS-B Rod Container	Conclusion
Strongback clamps on fuel grids	Strongback clamps on container	AFS-B lid is both bolted in place and clamped in place by the strongback
Max weight of 1,580 lb	Max weight of 1,500 lb	AFS-B applies lower inertia loads to the strongback in free drop impact events
264 rods	175 rods	Lighter payload in AFS-B
Rods self-supporting over span between clamp arms	Rods fully supported by thick walls and bolted lid of container	AFS-B eliminates rod bending loads
Rods can move axially a limited amount	Rods are confined by thick, bolted end structures	AFS-B confines rods axially
Rod lateral buckling is controlled by strongback and FCS	Rod lateral buckling is controlled by strongback and FCS, plus: 1. restricted free space inside container 2. rods supported by thick walls of container	AFS-B adds a significant layer of rod support to that existing in the basic strongback/FCS

Security Related Information

Figure Withheld Under 10 CFR 2.390

Figure B2.7-1 – AFS-B Rod Container Cross Section View

B2.7.2 Crush

This section is unchanged from Section 2.7.2, *Crush*.

B2.7.3 Puncture

The weight of the MFFP containing an AFS-B rod container and EMA is bounded by the weight of the MFFP with a payload of three (3) standard fuel assemblies. Therefore, the system response to a puncture is bounded by the discussion presented in Section 2.7.3, *Puncture*.

B2.7.4 Thermal

B2.7.4.1 Summary of Pressures and Temperatures

Package pressures and temperatures due to the HAC thermal event are presented in Section B3.5.3, *Maximum Temperatures and Pressures*. MFFP strongback and shell temperatures under HAC associated with the AFS-B payload are bounded by the standard three (3) fuel assembly payload. From Section B3.5.3.2, *Maximum Pressures*, the maximum internal pressure during the HAC thermal event is 117.1 psig. This pressure is bounded by the 130 psig pressure used in Section 2.7.4, *Thermal*.

B2.7.4.2 Differential Thermal Expansion

This section is unchanged from Section 2.7.4.2, *Differential Thermal Expansion*, as the MFFP strongback and shell temperatures under HAC associated with the AFS-B payload are bounded by the standard three (3) fuel assembly payload.

B2.7.4.3 Stress Calculations

As discussed in Section B2.7.4.1, *Summary of Pressures and Temperatures*, a conservative maximum internal pressure of 117.1 psig is calculated for the HAC thermal event. This pressure is lower than the 130 psig pressure used in Section 2.7.4.3, *Stress Calculations*. Therefore, the stresses calculated in Section 2.7.4.3 conservatively bound the stresses resulting from the payload evaluated in this Appendix.

B2.7.5 Immersion – Fissile Material

This section is unchanged from Section 2.7.5, *Immersion – Fissile Material*. In addition, since each separate cavity of the AFS-B container is vented, full flooding of all cavities by water in the immersion test is assured.

B2.7.6 Immersion – All Packages

This section is unchanged from Section 2.7.6, *Immersion – All Packages*.

B2.7.7 Deep Water Immersion Test (for Type B Packages Containing More than 10^5 A₂)

This section is unchanged from Section 2.7.7, *Deep Water Immersion Test*.

B2.7.8 Summary of Damage

The AFS-B rod container maintains its structural integrity and functionality in the worst-case HAC free drop event, which bounds the loadings of all other HAC events on the container. Since the AFS-B rod container is mounted in the same way as a MOX fuel assembly but weighs less, the response of the MFFP to drop and puncture accidents is unchanged when using the AFS-B. Therefore, the AFS-B is acceptable for use as a payload container.

B2.8 Accident Conditions for Air Transport of Plutonium

This section does not apply for the MFFP, since air transport is not claimed.

B2.9 Accident Conditions for Fissile Material Packages for Air Transport

This section does not apply for the MFFP, since air transport is not claimed.

B2.10 Special Form

This section does not apply for the MFFP, since special form is not claimed.

B2.11 Fuel Rods

This section does not apply for the MFFP, since containment by the fuel rod cladding is not claimed.

B2.12 Appendices

There are no appendices to Chapter B2.0. The applicability of the appendices to Chapter 2, *Structural Evaluation*, is given in Table B2.12-1.

Table B2.12-1 – Applicability of Section 2.12 Appendices to the AFS-B Payload

Appendix	Applicability
2.12.1, Impact Limiter Evaluation	As the weight of the AFS-B is bounded by the weight of a fuel assembly, the impact limiter evaluation from Section 2.12.1 remains bounding.
2.12.2, Certification Test Plan	Unchanged from Section 2.12.2
2.12.3, Certification Test Results	Unchanged from Section 2.12.3
2.12.4, Engineering Test Results	Unchanged from Section 2.12.4
2.12.5, Fuel Control Structural Evaluation	As the weight of the AFS-B is bounded by the weight of a fuel assembly, and because it is more structurally robust than a fuel assembly, the fuel control structural evaluation from Section 2.12.5 remains bounding.
2.12.6, CASKDROP Computer Program	Unchanged from Section 2.12.6
2.12.7, Impact Limiter Weld Joint Test Results	Unchanged from Section 2.12.7
2.12.8, Effect of Bounding Weight on Package Structural Responses	As the weight of the AFS-B is bounded by the weight of a fuel assembly, the package structural responses evaluation from Section 2.12.8 remains bounding.

This page left intentionally blank.

B3.0 THERMAL EVALUATION

B3.1 Description of Thermal Design

This section identifies and describes the principal thermal design aspects of the MOX Fresh Fuel Package (MFFP) for the transportation of the AFS-B rod container and the Excess Material Assembly (EMA) payload. The results presented in this chapter demonstrate the thermal safety of the package and compliance with the thermal requirements of 10 CFR 71¹ and supports the addition of the AFS-B rod container and the EMA as allowable contents of the MFFP.

The analysis demonstrates that the addition of the AFS-B rod container and EMA does not impact the packaging temperatures, and the temperatures for these items reported in Chapter 3.0, *Thermal Evaluation*, remain bounding. However, the peak HAC fuel cladding temperatures estimated for the fuel rods in an AFS-B are higher than the peak temperature computed for a fuel assembly, largely due to the simplified method employed. Nevertheless, the maximum allowable fuel temperature limits are not approached. The internal pressure of the package under HAC is bounded by the pressure resulting from the transportation of three (3) intact MOX fuel assemblies.

B3.1.1 Design Features

The principal thermal design features of the MFFP are described in Section 3.1.1, *Design Features*, while the principal features of the AFS-B rod container and the EMA are described in Section B1.2.3, *Contents of Packaging*.

B3.1.2 Content's Decay Heat

The payload configuration for the MFFP in this Appendix consists of one (1) AFS-B rod container, one (1) EMA, and one (1) dummy fuel assembly. Alternatively, a single AFS-B container or a single EMA can be loaded with two (2) dummy fuel assemblies. The design maximum decay heat for the AFS-B container is 53 watts, based on a maximum loading of 175 MOX fuel rods and the fact that a standard MOX fuel assembly has 264 fuel rods and a design decay heat loading of 80 watts. However, for conservatism, a decay heat loading of 80 watts is assumed for both the AFS-B rod container and the EMA.

B3.1.3 Summary of Temperatures

The maximum temperatures for the MFFP under NCT and HAC are summarized in Table B3.1-1. The packaging temperatures are taken from Table 3.4-1 and Table 3.5-1, respectively. While these packaging temperatures are associated with the transportation of three (3) MOX fuel assemblies, they are bounding for the MFFP temperatures arising from the transportation of a payload consisting of one (1) AFS-B rod container and one (1) EMA. Table B3.1-1 also presents the NCT and HAC temperatures for the AFS-B rod container and its payload of fuel rods. The peak temperature within the AFS-B rod container under NCT conditions is 206 °F (see Section

¹ Title 10, Code of Federal Regulations, Part 71 (10 CFR 71), *Packaging and Transportation of Radioactive Material*, 01-01-06 Edition.

B3.4, *Thermal Evaluation for Normal Conditions of Transport*), while the peak temperature achieved under HAC is predicted to be 613 °F (see Section B3.5, *Thermal Evaluation under Hypothetical Accident Conditions*). The peak temperature within the EMA is bounded by the temperatures predicted for the MOX fuel assembly.

B3.1.4 Summary of Maximum Pressures

The maximum normal operating pressure (MNOP) for the MFFP with the AFS-B rod container and EMA payload resulting from the NCT Hot condition and conservative assumptions is 2.8 psig. This pressure is bounded by the standard package MNOP of 10 psig. Further details of the pressure analysis are presented in Section B3.4.2, *Maximum Normal Operating Pressure*.

The peak pressure generated within the package cavity under HAC is conservatively estimated assuming that the entire inventory of organic material integral to the strongback assembly is totally combusted/pyrolyzed. No organic material is used in the AFS-B rod container.

The maximum pressure under HAC is estimated to be 117.1 psig (131.8 psia) at the end of the fire when the peak cavity gas temperature is reached. The pressure will then decrease as the package cools. Further details of the analysis are presented in Section B3.5.3, *Maximum Temperatures and Pressures*.

Table B3.1-1 –Summary of Temperatures for NCT and HAC (°F)

Item	Hot NCT	Peak HAC	Maximum Allowable		Minimum Temperature Margin ⁽¹⁾
			NCT	HAC	
Peak AFS-B Fuel Rod	206	613	392	1,337	186
Peak EMA Fuel Rod	221	518	392	1,337	171
Peak AFS-B Container	183	602	1,100	1,100	498
Avg. AFS-B Container	182	601	-	-	NA
<i>Temperatures for MFFP Package from Table 3.4-1 and Table 3.5-1</i>					
<i>Strongback Structure</i>	<i>178</i>	599	<i>800</i>	800	<i>201</i>
<i>Body Shell</i>	159	<i>1,361</i>	800	<i>2,500</i>	<i>641</i>
<i>Body Collar</i>	<i>149</i>	414	<i>800</i>	1,000	<i>586</i>
<i>Closure Lid</i>	147	<i>301</i>	800	<i>1,000</i>	<i>653</i>
<i>Impact Limiter Lugs</i>	154	<i>1,282</i>	800	<i>2,500</i>	<i>646</i>
<i>Impact Limiter</i>					
• <i>Max. Foam</i>	<i>149</i>	<i>N/A</i>	300	<i>N/A</i>	<i>151</i>
• <i>Bulk Avg. Foam</i>	<i>145</i>	<i>N/A</i>	300	<i>N/A</i>	<i>155</i>
• <i>Skin</i>	149	<i>1,429</i>	800	<i>2,500</i>	<i>651</i>
<i>Impact Limiter Bolts</i>					
• <i>Bolt Head</i>	154	<i>1,283</i>	800	<i>2,500</i>	<i>646</i>
• <i>Bolt Shaft</i>	144	<i>1,006</i>	800	<i>2,500</i>	<i>656</i>
• <i>Bolt Threads</i>	144	<i>295</i>	800	<i>2,500</i>	<i>656</i>
<i>O-ring Seals</i>					
• <i>Closure Lid</i>	<i>159</i>	339	<i>225</i>	400	<i>61</i>
• <i>Vent/Sampling Port</i>	146	<i>295</i>	225	<i>400</i>	<i>79</i>

Note: (1) Minimum temperature margin based on **bold** temperatures.

This page left intentionally blank.

B3.2 Material Properties and Component Specifications

B3.2.1 Material Properties

The material specifications for the MFFP package are defined in Section 3.2.1, *Material Properties*. The AFS-B rod container is fabricated primarily of clear anodized 6061-T6 aluminum. For the purposes of this calculation the material properties of the aluminum is characterized by a single thermal conductivity point of 96 Btu/hr-ft-°F¹ with an emissivity of 0.76². The EMA materials are the same as those for a standard MOX fuel assembly.

B3.2.2 Component Specifications

For thermal analysis purposes, the components of the EMA have the same specifications as those for the standard MOX fuel assembly. In addition to the materials listed in Section 3.2.2, *Component Specifications*, the only material associated with the AFS-B rod container that is considered temperature sensitive is the aluminum. 6061 aluminum has a melting temperature of approximately 1,100 °F¹.

No organic material is used in the AFS-B rod container. The characteristics of the organic material within the MFFP package are defined Section 3.2.2, *Component Specifications*.

¹ American Society of Mechanical Engineers (ASME) Boiler and Pressure Vessel Code, Section II, *Materials, Part D – Properties*, 2001 Edition, with 2002 and 2003 Addenda, New York.

² Gilmore, D. G., Editor, *Satellite Thermal Control Handbook*, The Aerospace Corporation Press, El Segundo, CA, 1994, pp A-8.

This page left intentionally blank.

B3.3 General Considerations

B3.3.1 Evaluations by Analysis

The MFFP with the AFS-B rod container and the EMA is analytically evaluated in accordance with 10 CFR 71 and Regulatory Guide 7.8¹ for the bounding NCT and HAC thermal loads. Section 3.3.1, *Evaluation by Analysis*, summarizes the design basis conditions considered in these evaluations.

B3.3.1.1 NCT Analytical Model

The NCT analytical thermal model of the MFFP is based on the Thermal Desktop[®]² and SINDA/FLUINT³ computer programs. Details of these programs, together with a description of the thermal model for the MFFP, are described in Section 3.3.1.1, *NCT Analytical Model*. That analysis demonstrated that a significant thermal margin exists for all package components.

Given that the AFS-B rod container has outer dimensions similar to a standard fuel assembly and interfaces with the strongback and clamp arms of the MFFP in a similar manner, and given that the maximum decay heat of the 175 fuel rods is less than 70% of that for a 264 rod MOX fuel assembly, the methodology used to evaluate the thermal performance of the AFS-B rod container within the MFFP is conservatively based on use of the maximum strongback temperature achieved for the transportation of the three (3) MOX fuel assemblies as a boundary condition for a 1-dimensional heat transfer analysis within the AFS-B rod container. The thermal performance of the EMA is bounded by that predicted for the MOX fuel assembly.

Figure B3.3-1 illustrates a cross-section through a loaded AFS-B rod container. As seen, the 175 fuel rods are expected to be arranged in a consolidated bundle consisting of 10 layers of 17 to 18 rods each. The temperature rise between the strongback and the center fuel rod in the consolidated bundle is computed using the 1-dimensional thermal model of the loaded AFS-B rod container illustrated in Figure B3.3-2.

Temperature of AFS-B rod container

The heat transfer between the AFS-B rod container and the strongback (i.e., c-to-h and g-to-h in Figure B3.3-2) is computed as a combination of radiation and conduction across an air gap based on the conservative assumption that the AFS-B container is centered within the fuel control structure (FCS) of the strongback assembly. Given the inside dimension for the FCS of 8.7-in, and an outside dimension of 8.4-in for the AFS-B container, the resulting uniform gap is 0.15-in. The heat transfer between the AFS-B container and the FCS is computed as:

¹ Regulatory Guide 7.8, *Load Combinations for the Structural Analysis of Shipping Casks for Radioactive Material*, Revision 1, U. S. Nuclear Regulatory Commission, March 1989.

² Thermal Desktop[®], Version 4.5, Cullimore & Ring Technologies, Inc., Littleton, CO, 2003.

³ SINDA/FLUINT, *Systems Improved Numerical Differencing Analyzer and Fluid Integrator*, Version 4.5, Cullimore & Ring Technologies, Inc., Littleton, CO, 2001.

$$q' = A \left[\frac{1}{(\epsilon_c^{-1} - 1) + \frac{1}{F_{c-h}} + (\epsilon_h^{-1} - 1)} \sigma (T_c^4 - T_h^4) + \frac{k}{x} (T_c - T_h) \right] \quad (\text{Eqn. 1})$$

where:

q' = heat transfer rate, Btu/hr

A = heat transfer area, in²

ϵ_c = emissivity of AFS-B rod container = 0.76

ϵ_h = emissivity of FCS surfaces = 0.20⁴

F_{c-h} = view factor between AFS-B container and FCS surfaces = 1.

σ = Stefan-Boltzmann constant = 1.190278×10^{-11} Btu/hr-in²-R⁴

T_c = temperature of AFS-B container, °R

T_h = temperature of FCS surfaces, = 178°F or 638°R at the NCT Hot condition⁵

k = thermal conductivity of air, Btu/hr-in²-R⁶

x = gap distance between AFS-B and FCS surfaces = 0.15-in

The temperature rise between the center shelf of the AFS-B container and the sidewalls (i.e., e-to-c in Figure B3.3-2) is insignificant due to the combination of the limited heat load and the use of aluminum. Even assuming all 80 watts of decay heat passed between the center shelf and the container sidewalls and that this heat load was limited to the 144-inch active fuel length of the MOX fuel rods, the ΔT required to transfer this heat load is estimated via:

$$\Delta T = \frac{\text{Heat Load}}{\text{Area} \frac{\text{conductivity of aluminum}}{\text{average distance for heat to travel}}}$$

$$\Delta T = \frac{80 \text{ watts} \times 3.412 \text{ Btu/watt}}{(0.5 \text{ inches} \times 144 \text{ inches} \times 2 \text{ paths}) \frac{96/12 \text{ Btu/hr - inch - F}}{(8.4 \text{ inches}/4)}}$$

$$\Delta T = 0.5^\circ \text{F}$$

The ΔT required at the joint between the shelf and the container sidewalls (assuming all heat transfers via the intermittent welds) is estimated via:

$$\Delta T = \frac{80 \text{ watts} \times 3.412 \text{ Btu/watt}}{(0.125 \text{ inches} \times 7 \text{ inches} \times 144 \text{ inches}/15.3 \text{ inches} \times 2 \text{ paths}) \frac{96/12 \text{ Btu/hr - inch}}{(0.25 \text{ inches})}}$$

$$\Delta T = 0.5^\circ \text{F}$$

⁴ Section 3.2.1, *Material Properties*.

⁵ Table 3.4-1, *NCT Temperatures*

⁶ Table 3.2-6, *Properties of Air*

Finally, the temperature difference to distribute the heat from the joint with the center shelf equally over the sidewalls is estimated via:

$$\Delta T = \frac{80 \text{ watts} \times 3.412 \text{ Btu/watt}}{(0.75 \text{ inches} \times 144 \text{ inches} \times 4 \text{ paths}) \frac{96/12 \text{ Btu/hr} \cdot \text{inch}}{(8.4 \text{ inches}/4)}}$$

$$\Delta T = 0.17^\circ \text{F}$$

Therefore, the center shelf is conservatively predicted to be within 1.2°F of the sidewall temperatures. As such, the estimation of the temperature rise within the consolidated fuel bundle can be computed assuming uniform temperatures on all sides of the AFS-B container.

Temperature of outer edges of fuel bundle

The heat transfer between the AFS-B rod container and the consolidated fuel rod bundle (i.e., b-to-c, d-to-e, and f-to-g in Figure B3.3-2) is computed as a combination of radiation and conduction across an air gap based on the conservative assumption that the consolidated fuel bundle is centered within the AFS-B container. The inside dimension of the AFS-B container is 6.9-in wide and 3.4-in high. The height and average width of the fuel rod stack within the rod container (see Figure B3.3-1) is equal to:

$$\begin{aligned} \text{Height} &= \text{fuel rod diameter}^7 \times (1 \text{ row} + 9 \text{ rows} \times \sin 60^\circ) \\ &= 0.374\text{-in} \times (1 + 7.7942) \\ &= 3.29\text{-in} \end{aligned}$$

$$\begin{aligned} \text{Width} &= \text{fuel rod diameter} \times (18 \text{ rods} + 17 \text{ rods})/2. \\ &= 0.374\text{-in} \times (18 + 17)/2. \\ &= 6.55\text{-in} \end{aligned}$$

Therefore, the average gap between the top and bottom of the consolidated fuel rod bundle and the AFS-B rod container is $(3.4\text{-in} - 3.29\text{-in})/2 + \frac{1}{4}$ of the rod diameter of 0.374-in, or 0.15-in. The gap between the sides of consolidated fuel rod bundle and the AFS-B rod container is $(6.9\text{-in} - 6.55\text{-in})/2 + \frac{1}{4}$ of the rod diameter, or 0.27-in. The average gap is computed as $(6.9\text{-in} \times 0.15\text{-in} + 3.4\text{-in} \times 0.27\text{-in})/(6.9\text{-in} + 3.4\text{-in}) = 0.19\text{-in}$.

The heat transfer between the AFS-B container and the outer edges of the consolidated fuel rod bundle is computed as:

$$q' = A \left[\frac{1}{(\epsilon_b^{-1} - 1) + \frac{1}{F_{b-c}} + (\epsilon_c^{-1} - 1)} \sigma (T_b^4 - T_c^4) + \frac{k}{x} (T_b - T_c) \right] \quad (\text{Eqn. 2})$$

where:

q' = heat transfer rate, Btu/hr

A = heat transfer area, in²

ϵ_c = emissivity of AFS-B rod container = 0.76

⁷ Table 3.6-1, *Summary of Design Data for MOX FA*

ϵ_b = emissivity of fuel rod surfaces = 0.20
 F_{b-c} = view factor between fuel bundle edges and AFS-B container = 1.
 σ = Stefan-Boltzmann constant = 1.190278×10^{-11} Btu/hr-in²-R⁴
 T_c = temperature of AFS-B container, °R
 T_b = avg. temperature of outer edges of fuel rod surfaces, °R
 k = thermal conductivity of air, Btu/hr-in²-R
 x = avg. gap distance between AFS-B and fuel rod surfaces

Temperature of hottest fuel rod

The heat transfer within the consolidated fuel bundle is computed by conservatively assuming the individual rods are separated by a finite distance from each of its neighbors and are not in direct contact. As such, the heat transfer between the rods is computed as radiation and conduction across the air gap separating the individual fuel rods. Since the ΔT across the width of the individual fuel rods is insignificant in comparison, it is ignored for the purposes of this calculation. Figure B3.3-3 illustrates the idealized configuration assumed for the fuel bundle for the purposes of estimating the temperature rise within it.

As idealized, the fuel bundle is treated as a series of concentric layers of fuel rods with the temperature in each layer being the same. With the exception of the center rod, the heat transfer via radiation from layer 'n-1' to layer 'n' for $n \geq 2$ is computed as:

$$q'_{\text{rad}} = \text{Area} \times \left[\frac{1}{(\epsilon_{n-1}^{-1} - 1) + \frac{1}{F_{n-1 \text{ to } n}} + \frac{\text{Area}_{n-1}}{\text{Area}_n} (\epsilon_n^{-1} - 1)} \sigma (T_{n-1}^4 - T_n^4) \right]$$

$$q'_{\text{rad}} = 2\pi \times r \times L \times 6(n-1) \times \left[\frac{1}{(0.2^{-1} - 1) + \frac{1}{F_{n-1 \text{ to } n}} + \frac{n-1}{n} (0.2^{-1} - 1)} \sigma (T_{n-1}^4 - T_n^4) \right] \quad (\text{Eqn. 3})$$

where:

q'_{rad} = radiation heat transfer rate fuel layer 'n-1' to layer 'n', Btu/hr
 r = radius of fuel rod, = 0.187-in
 L = active length of fuel rod = 144-in
 n = number of the rod layer, with the center rod at $n = 0$
 ϵ_{n-1} & ϵ_n = emissivity of fuel rod surfaces = 0.20
 $F_{n-1 \text{ to } n}$ = view factor from fuel layer 'n-1' to layer 'n' = $(2n-1)/(6(n-1))$
 σ = Stefan-Boltzmann constant = 1.190278×10^{-11} Btu/hr-in²-R⁴
 T_{n-1} = temperature of fuel rods in layer 'n-1', °R
 T_n = temperature of fuel rods in layer 'n', °R

For the radiation heat transfer from the center rod to the next layer (i.e., $n=1$), the heat transfer is computed as:

$$q'_{\text{rad}} = 2\pi \times r \times L \times \left[\frac{1}{(0.2^{-1} - 1) + \frac{1}{1} + \frac{1}{3}(0.2^{-1} - 1)} \sigma (T_0^4 - T_{n=1}^4) \right] \quad (\text{Eqn. 4})$$

Since no credit is taken for direct contact between the fuel rods, the conduction heat transfer between the rods will be via conduction across the intervening air gap. Each fuel rod will conductively exchange heat with six adjacent rods. Of these conduction points, $6(2n-1)$ will be between rods in layer 'n-1' to those in rod layer 'n'. The surface area associated with each conduction point is $2\pi \cdot r \cdot L/6$, while a conservative separation distance between the surfaces of $2 \cdot r \cdot (1 - \sin 60^\circ)$ is used. The conduction heat transfer from rod layer 'n-1' to layer 'n' for $n \geq 1$ is computed as:

$$q'_{\text{cond}} = \frac{2\pi \times r \times L/6 \times 6(2n-1) \times k \times (T_{n-1} - T_n)}{2 \times r \times (1 - \sin 60^\circ)}$$

$$q'_{\text{cond}} = \frac{\pi \times L \times (2n-1) \times k \times (T_{n-1} - T_n)}{(1 - \sin 60^\circ)} \quad (\text{Eqn. 5})$$

where:

q'_{cond} = conduction heat transfer rate fuel layer 'n-1' to layer 'n', Btu/hr

L = active length of fuel rod = 144-in

n = number of the rod layer, with the center rod at $n = 0$

k = thermal conductivity of air, Btu/hr-in²-R

T_{n-1} = temperature of fuel rods in layer 'n-1', °R

T_n = temperature of fuel rods in layer 'n', °R

B3.3.1.2 HAC Analytical Model

The analytical thermal model of the MFFP with the AFS-B rod container under HAC uses the same methodology used for the NCT evaluation. Since the NCT methodology is based on steady-state conditions and it ignores the effects of thermal mass and transient heating, the predicted HAC temperatures are conservative. The peak strongback temperature presented in Section 3.5, *Thermal Evaluation under Hypothetical Accident Conditions*, is used as a steady-state boundary temperature for the 1-D thermal model of the AFS-B rod container described above.

B3.3.2 Evaluation by Test

This section is not applicable since evaluation by test was not performed for the MFFP with the AFS-B rod container and EMA.

B3.3.3 Margins of Safety

A summary of the maximum temperatures for the MFFP, with their respective temperature margins, for both NCT and HAC are provided in Table 3.3-3.

From Section B3.1.4, *Summary of Maximum Pressures*, the maximum normal operating pressure (MNOP) is 2.8 psig, which is bounded by the calculated MNOP of 2.9 psig for the standard payload of three (3) fuel assemblies. (Note that the reported MNOP for the package is 10 psig, which is obtained by rounding up the 2.9 psig value.) Therefore, the margin of safety (MS) for the 25-psig design pressure is:

$$MS = \frac{25}{2.8} - 1.0 = +7.9$$

From Section B3.1.4, *Summary of Maximum Pressures*, the maximum pressure for HAC is 117.1 psig. This pressure is bounded by the 123.5 psig pressure for the standard three (3) fuel assembly payload. Therefore, the MS of +2.15 reported in Section 3.3.3, *Margins of Safety*, is bounding.

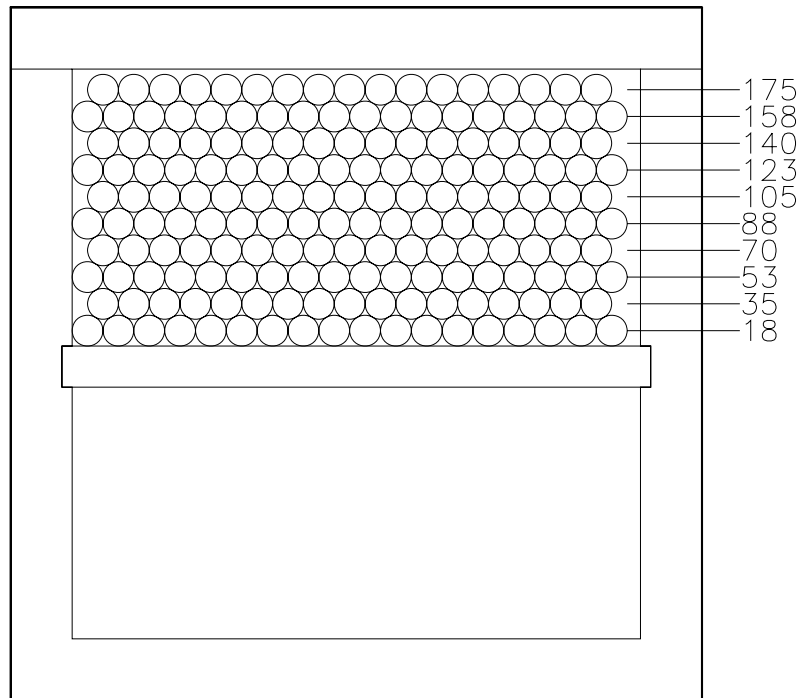
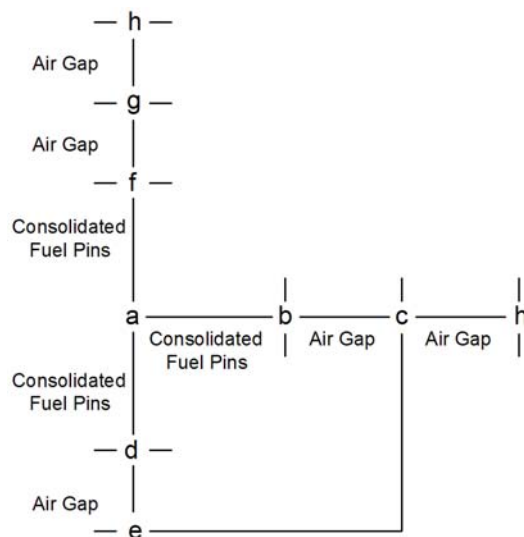


Figure B3.3-1 - Consolidated Fuel Rod Bundle within AFS-B Rod Container



a = center of the consolidated fuel rod bundle
 b = side edge of the consolidated fuel rod bundle
 c = side of AFS-B rod container
 d = bottom side of the consolidate fuel rod bundle
 e = center shelf of AFS-B rod container
 f = top edge of the consolidated fuel rod bundle
 g = top of AFS-B rod container
 h = strongback assembly of MFFP Package

Figure B3.3-2 - 1-D Thermal Model of AFS-B Rod Box Container

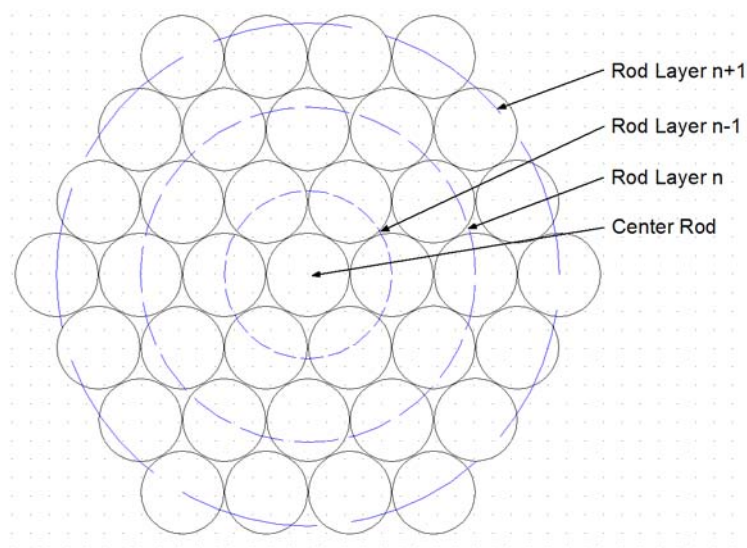


Figure B3.3-3 - Consolidated Fuel Rod Bundle Modeling

B3.4 Thermal Evaluation for Normal Conditions of Transport

B3.4.1 Heat and Cold

B3.4.1.1 Heat

The maximum temperatures for the AFS-B rod container and EMA are determined assuming the peak temperature of 178 °F for the strongback assembly obtained from Section 3.4.1.1, *Heat*, for the NCT Hot condition. Since this temperature is associated with a decay heat loading of 240 watts, it conservatively bounds the strongback temperatures associated with the transport of one (1) AFS-B rod container and one (1) EMA with a combined total decay heat loading of 133 watts. For conservatism, the peak temperatures are determined for a total decay heat loading of 160 watts, divided equally between the AFS-B rod container and the EMA.

Based on the 1-dimensional thermal model described above, a conservative decay heat load of 80 watts for the maximum payload configuration of 175 fuel rods, and an iterative solution of equation #1 from Section B3.3.1.1, *NCT Analytical Model*, the peak temperature for the AFS-B rod container is 183°F for the NCT Hot condition. Adding the 1.2°F ΔT determined in Section B3.3.1.1 for the temperature difference between the center shelf and the sidewall, yields a peak AFS-B temperature of 184°F. The average sidewall temperature is 182°F.

The associated peak fuel rod temperature within the AFS-B rod container is computed by iterative solution of equations #3 to #5. Since the fuel bundle is 10 rod layers high and 17 to 18 rod layers wide, the peak temperature of the center fuel rod is conservatively predicted by assuming the fuel bundle extends 8 layers in all directions from the center rod. Based on this assumption, the predicted peak fuel rod temperature within the AFS-B rod container is 206 °F for the NCT Hot condition. This predicted peak temperature is bounding whether the other positions in the strongback are occupied by one EMA and a dummy fuel assembly, or by two dummy fuel assemblies.

The maximum temperature for the EMA is bounded by the predicted maximum temperature for the MOX fuel assembly obtained from Section 3.4.1.1, *Heat*, of 221 °F.

The results presented in Section 3.4.1.1, *Heat*, for the MFFP remain valid and bounding for the MFFP temperatures associated with the transport of the AFS-B rod container and EMA. Specifically, the closure seals and the impact limiter foam temperatures remain below their associated temperature limits. Additionally, the MFFP analysis demonstrated that the accessible package surfaces remain below 122 °F when transported in an ambient temperature of 100 °F and without insolation, as stipulated by 10 CFR §71.43(g).

B3.4.1.2 Cold

The minimum temperature distribution for the MFFP with the AFS-B rod container and EMA occurs with a zero decay heat load and an ambient air temperature of -40 °F per 10 CFR §71.71(c)(2). The steady-state analysis of this condition represents a trivial case that requires no thermal calculations be performed. Instead, it is assumed that all package components achieve the -40 °F temperature under steady-state conditions. The -40 °F temperature is within the allowable range of all of the packaging components. The package temperatures for the NCT

Cold condition of -20 °F and no insulation are bounded by those presented in Section 3.4.1.2, *Cold*, for the MFFP.

B3.4.2 Maximum Normal Operating Pressure

The maximum normal operating pressure (MNOP) for NCT is based on an initial package backfill of air at atmospheric pressure at 70 °F (294 K) and an assumed failure rate of 3% of the MOX fuel rods. For conservatism, the heat up of the gases in the package cavity is assumed to be the same as that determined for the transport of three (3) MOX fuel assemblies for the respective ambient condition. For the purpose of rod pressure determination, the only significant gas contributor is the initial helium backfill as no fission products will exist within the un-irradiated fuel assemblies.

The bulk average gas temperature from Section 3.4.1.1, *Heat*, for the MFFP under the NCT Hot condition is used as the basis for the MNOP calculation with the AFS-B rod container and EMA. Since the decay heat loading assumed for the MFFP bounds the heat dissipation associated with the AFS-B rod container and EMA, the associated bulk average gas temperature will also be bounding. The package cavity has a gross free volume of approximately 105,547 in³, based on a package cavity OD of 28.5 inches and a length of 165.45 inches. The displacement volume for the EMA is approximately 4,685 in³, while a displacement volume for the strongback assembly is 11,292 in³ (see Section 3.4.2, *Maximum Normal Operating Pressure*). The displacement volume for an unloaded AFS-B rod container is 4,592 in³ based on an approximate weight of 450 lbs and a density of 0.098 lbs/in³. The volume of the 175 fuel rods is 2,941 in³ based on a rod diameter of 0.374 in. and a length of 153 in. The solid volume for the dummy fuel assembly is approximately 5,366 in³.

The amount of helium fill gas within each MOX fuel assembly fuel rod and poison rod was determined in Section 3.4.2, *Maximum Normal Operating Pressure*, to be 0.0243 and 0.0475 g-moles, respectively. The total helium volume within a MOX fuel assembly is 7.55 g-moles. This helium content bounds that for the EMA. Given that there are a maximum of 175 fuel rods in the AFS-B rod container, the total helium content is 4.25 g-moles.

The initial gas in the package cavity at the time of sealing is calculated as follows:

$$N_{\text{fill}} = \frac{1 \text{ atm} \times V_{\text{free}}}{R \times T_{\text{fill}}}$$

where:

- T_{fill} = temperature of air within package cavity at time of package closure
- R = Ideal gas constant (0.08206 atm-liter/gmole-K)
- V_{free} = Package cavity free volume
- = Gross cavity volume minus displacement volumes for the loaded AFS-B rod container, the dummy fuel assembly, the EMA, and the strongback
- = 76,671 in³ (1,256 liters)

The MNOP is then calculated as follows:

$$\text{MNOP} = \frac{N_{\text{cask}} RT_{\text{NCT}}}{V_{\text{free}}}$$

$$N_{\text{cask}} = N_{\text{fill}} + \text{Rod Failure Rate} \times N_{\text{MOX fill gas}} + N_{\text{outgassing}}$$

where:

N_{cask} = total moles of gas in package cavity

N_{fill} = moles air within package cavity at time of package closure

Rod Failure Rate = assumed percentage of failed fuel rods within the AFS-B rod container and the EMA. A 3% failure rate, which matches the regulatory failure rate for normal conditions of transport of spent fuel assemblies, will bound the expected failure rate for fresh fuel.

$N_{\text{MOX fill gas}}$ = moles of rod fill gas within package cavity

$N_{\text{outgassing}}$ = moles gas generated by out-gassing from component material in cask cavity

T_{NCT} = Bulk average gas temperature within package (K) at the specific condition

= 166°F or 347 K¹

Based on the above relationships and assumptions, the MNOP for the bounding payload combination of one (1) AFS-B rod container with 175 fuel rods, one (1) EMA, and one (1) dummy fuel assembly is 17.5 psia (2.8 psig). A significant margin exists between this calculated MNOP and the package's NCT design pressure limit of 39.7 psia (25 psig).

No hydrogen or other combustible gases will be generated as result of the thermal or radiation-induced decomposition of the organic material within the package. This conclusion is based on the low peak temperature achieved under NCT transport conditions and the low radioactivity associated with the un-irradiated MOX fuel rods.

B3.4.3 Maximum Thermal Stresses

The maximum thermal stresses for NCT are bounded by those determined for the MFFP with the MOX fuel assembly payload. See the discussion in Section 2.6.1, *Heat*, and Section 2.6.2, *Cold*.

B3.4.4 Evaluation of Package Performance for Normal Conditions of Transport

The steady-state thermal analysis presented in Section 3.4, *Thermal Evaluation for Normal Conditions of Transport*, demonstrates that the components of the MFFP with the MOX fuel assembly payload are within their respective allowable temperature limits. That evaluation is valid and bounding for the MFFP with the AFS-B rod container and the EMA.

¹ Table 3.4-1, *NCT Temperatures*

The MNOP resulting from the NCT Hot condition and conservative assumptions is within the package's maximum design pressure limit.

Therefore, the MFFP with the AFS-B rod container and the EMA is found to comply with all of the thermal requirements specified in 10 CFR §71.71. |

B3.5 Thermal Evaluation under Hypothetical Accident Conditions

This section presents the results of the thermal evaluation of the MFFP with the AFS-B rod container and EMA under the hypothetical accident conditions (HAC) specified in 10 CFR §71.73(c)(4)¹.

B3.5.1 Initial Conditions

The initial conditions assumed for the MFFP are presented in Section 3.5, *Thermal Evaluation under Hypothetical Accident Conditions*. Due to their robust design, no significant damage is assumed to have occurred to the AFS-B rod container, the EMA, and the dummy fuel assemblies as a result of the drop events that precede the HAC fire event. Even if damaged, the integrity of these components is not important to the thermal safety of the MFFP package.

B3.5.2 Fire Test Conditions

No fire tests were performed for the MFFP with the AFS-B rod container and EMA.

B3.5.2.1 Analytical Model

The analytical model of the MFFP under HAC is described in Section 3.5.2.1, *Analytical Model*, and Section 3.5.2.2, *Performance of Rigid Polyurethane Foam Under HAC Fire Conditions*. The peak temperature for the AFS-B rod container under HAC is estimated using the methodology and 1-dimensional thermal model described in Section B3.3.1.1, *NCT Analytical Model*.

The thermal performance of the EMA under HAC is bounded by the results for the MOX fuel assembly.

B3.5.3 Maximum Temperatures and Pressures

B3.5.3.1 Maximum Temperatures

The maximum temperatures attained in the MFFP components under HAC with the AFS-B rod container and EMA assembly are bounded by those presented in Section 3.5.3.1, *Maximum Temperatures*. The peak strongback assembly temperature predicted from the evaluation of the MFFP is 599 °F and the transient analysis demonstrates that the peak temperature condition lasts for less than 15 minutes.

Based on a decay heat load of 80 watts for the maximum payload configuration of 175 fuel rods and an iterative solution of equation #1 from Section B3.3.1.1, the estimated peak temperature for the AFS-B rod container under HAC conditions is 601°F, while the peak center shelf temperature is estimated to be 602°F. In a similar fashion, based on equation #2 from Section B3.3.1.1, the temperature of the outer surface of the fuel bundle within the AFS-B rod container is predicted to be 606°F. The associated peak fuel rod temperature, computed by iterative solution of equations #3 to #5, is estimated to be 613°F.

¹ Title 10, Code of Federal Regulations, Part 71 (10 CFR 71), *Packaging and Transportation of Radioactive Material*, 01-01-06 Edition.

The peak temperature within the EMA is bounded by the temperatures predicted for the intact MOX fuel assembly in Section 3.5.3.1, *Maximum Temperatures*.

Although both the peak temperature and the duration of the elevated temperatures within the package are seen as insufficient to cause significant thermal decomposition of the organic material integral to the strongback assembly, it is conservatively assumed that 100% of the organic material fully decomposes to the extent that the available oxygen permits.

B3.5.3.2 Maximum Pressures

With the exception of the consideration for potential out-gassing from organic components within the package cavity and an assumed 100% failure rate for the fuel rods, the maximum pressure attained under HAC is determined in the same manner as described in Section B3.4.2, *Maximum Normal Operating Pressure*. While the MFFP is designed to protect the enclosed fuel rods from catastrophic failure during the pre-fire free and puncture bar drops and the subsequent 30-minute fire event, this analysis conservatively assumes that the cladding on all fuel rods are breached. As stated in Section B3.4.2, *Maximum Normal Operating Pressure*, the amount of helium fill gas within the EMA is 7.55 g-moles and the total helium content of the AFS-B rod container with 175 fuel rods is 4.25 g-moles. No significant change in the package cavity free volume is expected as a result of the HAC drop event.

Per Section 3.5.3.2, *Maximum Pressures*, approximately 7 pounds of neoprene rubber (C_4H_5Cl)_n and 2.3 pounds of Delrin[®] plastic ($C_6H_{14}O_2$)_n are used in the strongback assembly. The breakdown of these organic materials under HAC is limited by the facts that a limited amount of oxygen exists in the cask cavity and the peak cavity temperature and its duration under HAC are too low to permit complete pyrolysis (i.e., the process of breaking up a substance into other molecules as a result of heating in an inert atmosphere). For this evaluation, it is assumed that 75% of the oxygen is consumed generating carbon monoxide and only 25% is used in the generation of carbon dioxide gas. A larger ratio of carbon dioxide generation will result in a lower cask pressure. Under this conservative assumption, volatilizing the entire mass of neoprene rubber and Delrin[®] plastic would generate approximately 137.3 g-moles of additional gas within the cavity.

The peak pressure generated within the package cavity is estimated to be 131.8 psia (117.1 psig) at the end of the 30 minute fire event when the peak cavity gas temperature is reached. This pressure is bounded by the pressure from a payload of three fuel assemblies (138.2 psia). The pressure will then decrease as the package cools. The predicted peak pressure is considered to have a high degree of conservatism since there is insufficient oxygen within the package cavity to permit the full decomposition of the organic material and because both the relatively low peak temperature and the relatively short duration of the elevated temperatures will prevent any significant decomposition from occurring in the absence of active combustion of the material. It is expected that a majority of the organic material will remain in its original, solid form.

B3.5.4 Accident Conditions for Fissile Material Packages for Air Transport

This section does not apply for the MFFP since air transport will not be utilized.

B3.5.5 Evaluation of Package Performance for Accident Conditions of Transport

The evaluation of the MFFP with the AFS-B rod container and EMA under HAC demonstrates that the packaging has sufficient thermal protection remaining after the hypothetical drop and puncture bar damage to protect the thermally sensitive areas of the packaging. All package components are seen as remaining within their associated maximum temperature limits.

This page left intentionally blank.

B3.6.1 Computer Analysis Results

The safety evaluations are based on hand calculations. The following are reproduction of the spreadsheet pages used to compute the temperatures within the AFS-B rod container.

PEAK MOX ROD TEMPERATURES

This page left intentionally blank.

B4.0 CONTAINMENT

The AFS-B does not provide containment. Therefore, package containment is unchanged from the description provided in Chapter 4.0, *Containment*.

This page left intentionally blank.

B5.0 SHIELDING EVALUATION

The compliance of the MFFP packaging with respect to the dose rate limits established by 10 CFR §71.47¹ for normal conditions of transport (NCT) or 10 CFR §71.51(a)(2) for hypothetical accident conditions (HAC) are satisfied when limiting the MFFP package to three (3) Mixed Oxide (MOX) fresh fuel assemblies (FAs) having a radioisotope content listed in Table 1.2-2. Replacing 3 FAs with one (1) EMA and one (1) AFS-B containing up to 175 fuel rods would reduce the dose rates, because in this configuration the MFFP would contain no more than 439 fuel rods, compared to the 792 fuel rods for three standard FAs.

Under these conditions, the maximum surface dose rate will be less than the limit of 200 mrem/hr for NCT and verified by measurement. This dose rate limit is for payload packages prior to addition of any lead, steel or other shielding material for *as-low-as-reasonably-achievable* (ALARA) dose reduction purposes during non-transport handling operations.

Prior to transport, the MFFP package shall be monitored for both gamma and neutron radiation to demonstrate compliance with 10 CFR §71.47. As noted in Section 2.6.7, *Free Drop*, the MFFP package is not significantly deformed under NCT free drop conditions. Therefore, the package will meet the dose rate limits for NCT if the measurements demonstrate compliance with the allowable dose rate levels in 10 CFR §71.47 (200 mrem/hr). The transport index, as defined in 10 CFR §71.4, will be determined by measuring the dose rate a distance of one meter from the package surface per the requirements of 49 CFR §173.403².

Shielding materials are not specifically provided by the MFFP package, and none are permitted within the package to meet the dose rate limits of 10 CFR §71.47 for NCT. Because significant fuel deformation or package deformation does not occur under HAC, the HAC surface dose rates and 1-meter dose rates will not be significantly different from the NCT dose rates. This result ensures that the post-HAC, allowable dose rate of 1 rem/hr a distance of one meter from the package surface per 10 CFR §71.51(a)(2) will be met because the surface dose rate will remain below the 200 mrem/hr limit.

¹ Title 10, Code of Federal Regulations, Part 71 (10 CFR 71), *Packaging and Transportation of Radioactive Material*, 01-01-06 Edition.

² Title 49, Code of Federal Regulations, Part 173 (49 CFR 173), *Shippers - General Requirements for Shipments and Packagings*, 10-01-06 Edition.

This page left intentionally blank.

B6.0 CRITICALITY EVALUATION

The following analyses demonstrate that the MFFP complies with the requirements of 10 CFR §71.55¹ and §71.59. The analyses presented herein show that the criticality requirements are satisfied when one (1) excess material assembly (EMA), one (1) AFS-B rod container holding up to 175 MOX fuel rods, and one (1) dummy fuel assembly are transported in an MFFP.

B6.1 Description of Criticality Design

B6.1.1 Design Features Important for Criticality

The AFS-B is conservatively ignored in this criticality analysis. However, as noted in Section B2.0, *Structural Evaluation*, the AFS-B sufficiently protects the fuel rods so that damage to the fuel rods will not occur. Therefore, there are no specific design features of the AFS-B important for criticality. The design features of the MFFP important to criticality are discussed in Section 6.1.1, *Design Features Important for Criticality*.

B6.1.2 Summary Table of Criticality Evaluation

The results of the criticality calculations are summarized in Table B6.1-1. The NCT results are bounded by the three fuel assembly results reported in Table 6.1-1, and those results are simply reproduced in the table below. The HAC analysis results are more reactive than the standard three fuel assembly analysis because the 175 AFS-B rods are conservatively allowed to expand to fill the cavity formed between the strongback and FCS. The maximum calculated k_s is 0.9240, which occurs for the HAC infinite array case with fully moderated internal region and void external region. The maximum k_s is below the USL of 0.9288.

Note that the results in Table B6.1-1 are artificially high because no credit is taken for the AFS-B, allowing the fuel rods to arrange in the most reactive pitch. In actuality, if the analysis were repeated taking credit for the AFS-B, the reactivity would drop considerably because there is very little space available inside the AFS-B for moderation, as all available void space is filled with dunnage rods.

¹ Title 10, Code of Federal Regulations, Part 71 (10 CFR 71), *Packaging and Transportation of Radioactive Material*, 01-01-06 Edition.

Table B6.1-1 – Summary of Criticality Analysis Results

Normal Conditions of Transport (NCT)			
Case	k_{eff}	σ	k_s
Single Unit Maximum k_s	0.2858	0.0008	0.2874
Infinite Array Maximum k_s	0.6027	0.0006	0.6039
Hypothetical Accident Conditions (HAC)			
Case	k_{eff}	σ	k_s
Single Unit Maximum k_s	0.9186	0.0010	0.9207
Infinite Array Maximum k_s	0.9219	0.0010	0.9240
USL	0.9288		

B6.1.3 Criticality Safety Index

An infinite number of MFFPs are evaluated in a close-packed hexagonal array. Therefore, “N” is infinite, and in accordance with 10 CFR §71.59 the criticality safety index (CSI) is $50/N = 0$.

B6.2 Fissile Material Contents

The contents are one (1) EMA and one (1) AFS-B containing up to 175 standard MOX fuel rods. The third strongback location is loaded with a dummy fuel assembly, as defined in Section B1.2.3, *Contents of Packaging*. The fuel rod parameters for the rods in the AFS-B are unchanged from the standard MOX fuel rod and are provided in Section 6.2, *Fissile Material Contents*.

The EMA is a one-of-a-kind MOX fuel assembly composed of fuel rods that do not meet all of the performance requirements of a standard fuel rod. The EMA is composed of 264 MOX fuel rods in the same arrangement as a standard MOX fuel assembly. Some EMA fuel pellets do not meet the dimensional tolerances of a standard fuel pellet. In addition, the Pu-238 weight percent is out of tolerance for some of the rods. However, the total EMA fissile Pu mass is significantly less than the Pu mass analyzed for the standard bounding assembly in Chapter 6.0, *Criticality Evaluation*.

The maximum Pu/(U+Pu) for any rod in the EMA is 5.01%, while the average Pu/(U+Pu) for the EMA is only 3.41%. For the standard assembly, each rod is modeled at the maximum value of 6.0% Pu/(U+Pu). Therefore, the EMA has significantly less plutonium than a standard assembly and will be less reactive.

The maximum rod Pu-238 wt.% in the EMA is 0.19%, and the average Pu-238 wt.% is 0.086%. Both of these values exceed the current SAR limit of 0.05% for Pu-238 listed in Table 6.2-3. However, Pu-238 acts as a poison for criticality and is not modeled in the standard assembly. Therefore, the higher Pu-238 content will further lower the EMA reactivity when compared to a standard assembly. The remaining isotopic values are within the ranges provided in Table 6.2-3.

This page left intentionally blank.

B6.3 General Considerations

Criticality calculations for the MFFP are performed using the three-dimensional Monte Carlo computer code MCNP5¹.

B6.3.1 Model Configuration

B6.3.1.1 Contents Model

The AFS-B is not modeled in the criticality evaluation. Because the AFS-B is not modeled, the fuel rods are assumed to arrange themselves in the most reactive configuration within the cavity formed between the strongback and FCS. To maintain model symmetry, a variety of regular square arrangements are modeled, including 14x14, 13x13, 12x13, 12x12, 11x11, and 10x10. (Note that the 14x14 arrangement (196 rods) is not physically possible due to the 175 rod limit of the AFS-B cavity.) A limited number of non-regular pitch cases are also developed.

Stainless steel or aluminum dunnage rods are used in the AFS-B to prevent lateral movement of the fuel rods. These dunnage rods are ignored in the criticality models.

The rod arrangements of the contents represents an extremely conservative and incredible arrangement, as the AFS-B, even if damaged in an accident, would displace a large volume and would not allow the rod arrangements assumed in this analysis.

B6.3.1.2 Packaging Model

The packaging model is unchanged from the description provided in Section 6.3.1.2, *Packaging Model*.

B6.3.2 Material Properties

The material properties are unchanged from the descriptions provided in Section 6.3.2, *Material Properties*.

B6.3.3 Computer Codes and Cross-Section Libraries

The computer codes and cross section libraries are unchanged from the descriptions provided in Section 6.3.3, *Computer Codes and Cross-Section Libraries*.

B6.3.4 Demonstration of Maximum Reactivity

The most reactive single package model is for the HAC case hs_11x11_ema_161. The parameters of the most reactive case are:

¹ MCNP5, "MCNP – A General Monte Carlo N-Particle Transport Code, Version 5; Volume II: User's Guide," LA-CP-03-0245, Los Alamos National Laboratory, April, 2003.

- 161 fuel rods in an 11x11 lattice to represent the rods in an AFS-B, with two rods in each of the outer lattice locations.
- The EMA modeled as a standard fuel assembly with 6.0% Pu/(Pu+U) and fully expanded fuel rods to maximize reactivity.
- Fully moderated with water, including the pellet to cladding gap.
- Steel reflection, which bounds reflection by water.
- 100% theoretically dense pellets to maximize the plutonium mass.
- Miscellaneous minor steel components in the package are homogenized into the water region inside the package.

The most reactive HAC array model uses the most reactive HAC single package model as a base case. Properties of the most reactive HAC array model are:

- Infinite hexagonal reflection.
- Void between packages.
- Dummy fuel assembly modeled as steel to increase neutron transmission between packages.

B6.4 Single Package Evaluation

Compliance with the requirements of 10 CFR §71.55 is demonstrated by analyzing an optimally moderated single-unit MFFP. The figures and descriptions provided in Section 6.3.1, *Model Configuration*, describe the basic geometry of the single-unit models, although the contents are different.

B6.4.1 Single Package Configuration

B6.4.1.1 NCT Configuration

No MCNP models are developed for the NCT configuration with a payload of 1 EMA and 1 AFS-B containing 175 rods. Under NCT, in the absence of moderation the reactivity will be bounded by the standard three fuel assembly analysis of Section 6.4.1.1, *NCT Configuration*, because the reactivity for the dry condition is governed by the fissile mass in the package. Under the assumed configuration with 1 AFS-B and 1 EMA, the MFFP would contain no more than $175 + 264 = 439$ fuel rods. The standard three fuel assembly models contain $264 \times 3 = 792$ fuel rods. Therefore, the NCT results for three fuel assemblies bound the AFS-B/EMA configuration. Therefore, no NCT models for the AFS-B/EMA configuration are required.

B6.4.1.2 HAC Configuration

Under HAC, explicit models are required because it is assumed the rods in the AFS-B reach optimum moderation, while expansion of a standard fuel assembly is limited by the FCS and strongback. The approach is to conservatively model the contents of an AFS-B within the MFFP.

The package is assumed to be flooded. Because the AFS-B is not modeled, it is assumed that the rods are free to arrange themselves into the most reactive configuration. As a point of interest, the most reactive rod pitch is first determined by simply modeling an arbitrary number of rods (13×13) in a square array reflected by water, see Figure B6.4-2. Note that the packaging, including the poison plates, are ignored. The pitch is varied until the maximum reactivity is obtained. The results in Table B6.4-1 indicate that the most reactive rod pitch is 2.4 cm. As the inner dimensions of the cavity is 8.8", the number of rods that will fit at the optimum pitch is only $[(8.8)(2.54)/2.4]^2 \sim 87$. A pitch of 2.2 cm is nearly as reactive, with a corresponding ~ 103 rods. 103 rods may be approximately modeled as a 10×10 array.

Because the optimum pitch results in a reduced number of rods that may fit in the cavity, there is a reactivity tradeoff between the pitch and the fissile mass, because these quantities cannot be optimized simultaneously. If a regular pitch is assumed, the optimum pitch will have a greatly reduced number of rods. Conversely, if the maximum 175 rods are modeled, the pitch will not be optimized for all rods.

Through non-regular modeling of the rod arrangements, it is possible to create scenarios in which the pitch is nearly optimized throughout most of the cavity, but clusters of rods are added to other regions of the cavity to bring the total number of rods to a larger value, up to 175. In

this manner, a larger number rods may be modeled, although the pitch is not optimized in all regions of the model.

The worst-case single package model for three fuel assemblies from Section 6.4, *Single Package Evaluation* (case max_hac_single_srddn20), is used as the base packaging model for these cases, although all rods are initially positioned at the axial height of a rod in the standard MOX fuel assembly. The AFS-B/EMA model geometry is shown in Figure B6.4-3. Note that all cases use steel as the external reflector rather than water because a steel reflector is shown in Section 6.4 to be slightly more reactive than water. The EMA is conservatively modeled as a standard fuel assembly with the pitch expanded to the maximum extent, consistent with the most reactive assembly configuration from Section 6.4.1.2, *HAC Configuration*. The dummy fuel assembly is simply modeled as water. Results are provided in Table B6.4-2 and are discussed in the following paragraphs.

In the following cases, the number of rods does not sum to the limit of 175 and are evenly distributed throughout the cavity: 14x14, 13x13, 12x13, 12x12, 11x11, and 10x10. (Note that the 14x14 arrangement (196 rods) is not physically possible due to the 175 rod limit of the AFS-B cavity.) These cases are termed “standard pitch” cases, and the outer rows of rods do not touch the poison plates. In the “expanded pitch” cases, the rods are further expanded to the poison plates, see Figure B6.4-4. Comparing these “regular pitch” cases, the 12x13 expanded pitch case (156 rods) is the most reactive, although the 10x10 case (100 rods) is much closer to the optimum pitch. Clearly, the fissile mass is so greatly reduced when the optimum pitch is modeled that the most reactive case is for a non-optimum pitch with a higher fissile mass.

A limited number of cases are developed that model non-regular rod pitches. The 12x13 standard pitch, 12x13 expanded pitch, 12x12, 11x11, and 10x10 standard pitch cases are modified to add additional rods to the lattice to increase the number of rods up to the limit of 175. These various configurations are shown in Figure B6.4-5 through Figure B6.4-7. The most reactive case is hs_11x11_ema_161, which has two rods in each of the outer array locations, for a total of 161 rods. Note that the reactivity of this case is statistically equivalent to the reactivity of the 12x13 expanded pitch case with a regular pitch.

It must be stressed that none of the proposed rod scenarios (either regular or non-regular) are credible because the AFS-B, even if severely damaged, would displace most of the volume available for rod expansion and would preclude such rod arrangements from forming (see Figure B6.4-1 for a cross sectional sketch of the AFS-B with 175 rods). Ignoring the AFS-B is conservative for modeling purposes, but should not be viewed as a credible or likely scenario. It is also demonstrated in Chapter B2.0, *Structural Evaluation*, that the AFS-B will maintain its design function of protecting the fuel rods in an accident.

For the previous cases, no axial shifting is assumed. Consistent with the three fuel assembly models, the most reactive case determined above (hs_11x11_ema_161) is further analyzed for axial shifting of the both the AFS-B and EMA rods.

In case hs_11x11_ema2n, the EMA rods are allowed to shift downward in the same pattern that resulted in the most reactive condition for the three fuel assembly model (max_hac_single_srddn20). The multiplication factor actually dropped slightly, indicating that this change is within the statistical uncertainty of the Monte Carlo method. Therefore, the remaining models use the EMA in the standard configuration.

Four rod shifting scenarios are considered for the AFS-B rods: (1) all rods shifted down (maxdn), (2) all rods shifted up (maxup), (3) rods alternately shifted up or down (mix), and (4) rods shifted up or down in a checkerboard pattern (mix2). No AFS-B rod shifting scenario results in a reactivity increase, and the observed differences are likely the result of statistical fluctuation.

The most reactive condition is case hs_11x11_ema_161, with a $k_s = 0.92067$, which is below the USL of 0.9288. Note that this reactivity is artificially high because the geometry control provided by the AFS-B was conservatively neglected.

B6.4.2 Single Package Results

The optimum pitch search results are provided in Table B6.4-1. The multiplication factors are high because no poison plates are modeled. Results for the HAC single package are provided in Table B6.4-2. The most reactive case in each table is listed in boldface.

Table B6.4-1 – Most Reactive Rod Pitch

Case	Pitch (cm)	k_{eff}	σ	k_s ($k+2\sigma$)
13x13_p09	1.8	1.03880	0.00099	1.04078
13x13_p1	2	1.07919	0.00099	1.08117
13x13_p11	2.2	1.09440	0.00106	1.09652
13x13_p12	2.4	1.10038	0.00098	1.10234
13x13_p13	2.6	1.09115	0.00093	1.09301
13x13_p14	2.8	1.07248	0.00099	1.07446

Table B6.4-2 – Criticality Results for HAC Single Package

Case	AFS-B X-pitch (cm)	AFS-B Y-pitch (cm)	Number of Rods in AFS-B	k_{eff}	σ	k_s ($k+2\sigma$)
No axial shifting						
hs_14x14_ema	1.5966	1.5966	196	0.90106	0.00104	0.90314
hs_13x13_ema	1.7194	1.7194	169	0.91139	0.00102	0.91343
hs_12x13_ema	1.8628	1.7194	156	0.91179	0.00099	0.91377
hs_12x13_ema_175	1.8628	1.7194	175	0.91679	0.00101	0.91881
hs_12x13max_ema	1.9458	1.7836	156	0.91716	0.00099	0.91914
hs_12x13max_ema_175	1.9458	1.7836	175	0.89781	0.00095	0.89971
hs_12x13max_ema_175r	1.9458	1.7836	175	0.91022	0.00102	0.91226
hs_12x12_ema	1.8628	1.8628	144	0.91102	0.00101	0.91304
hs_12x12_ema_175	1.8628	1.8628	175	0.91640	0.00099	0.91838
hs_11x11_ema	2.0360	2.0360	121	0.90243	0.00098	0.90439
hs_11x11_ema_161	2.0360	2.0360	161	0.91859	0.00104	0.92067
hs_11x11_ema_175	2.0360	2.0360	175	0.91742	0.00097	0.91936
hs_10x10_ema	2.2354	2.2354	100	0.88423	0.00098	0.88619
hs_10x10_ema_136	2.2354	2.2354	136	0.90474	0.00097	0.90668
hs_10x10_ema_164	2.2354	2.2354	164	0.90752	0.00102	0.90956
hs_10x10_ema_175	2.2354	2.2354	175	0.90513	0.00098	0.90709
With axial shifting						
hs_11x11_ema _{dn} _161	2.0360	2.0360	161	0.91614	0.00102	0.91818
hs_11x11 _{dn} _ema_161	2.0360	2.0360	161	0.91660	0.00096	0.91852
hs_11x11 _{up} _ema_161	2.0360	2.0360	161	0.91707	0.00096	0.91899
hs_11x11 _{mix} _ema_161	2.0360	2.0360	161	0.91768	0.00098	0.91964
hs_11x11 _{mix2} _ema_161	2.0360	2.0360	161	0.91363	0.00102	0.91567

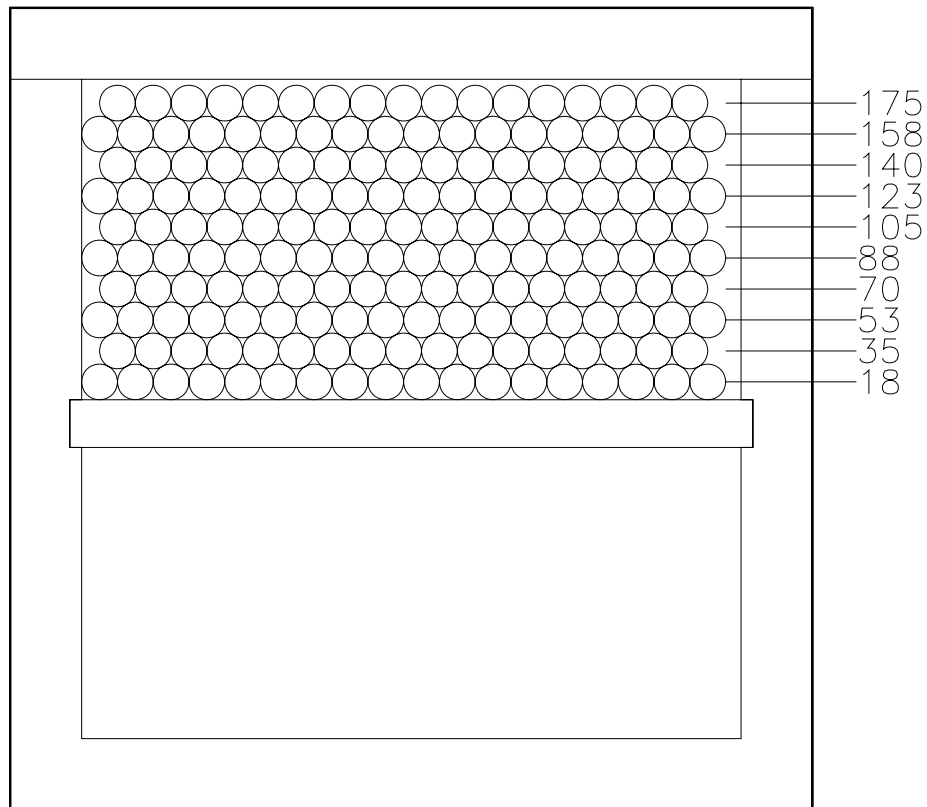
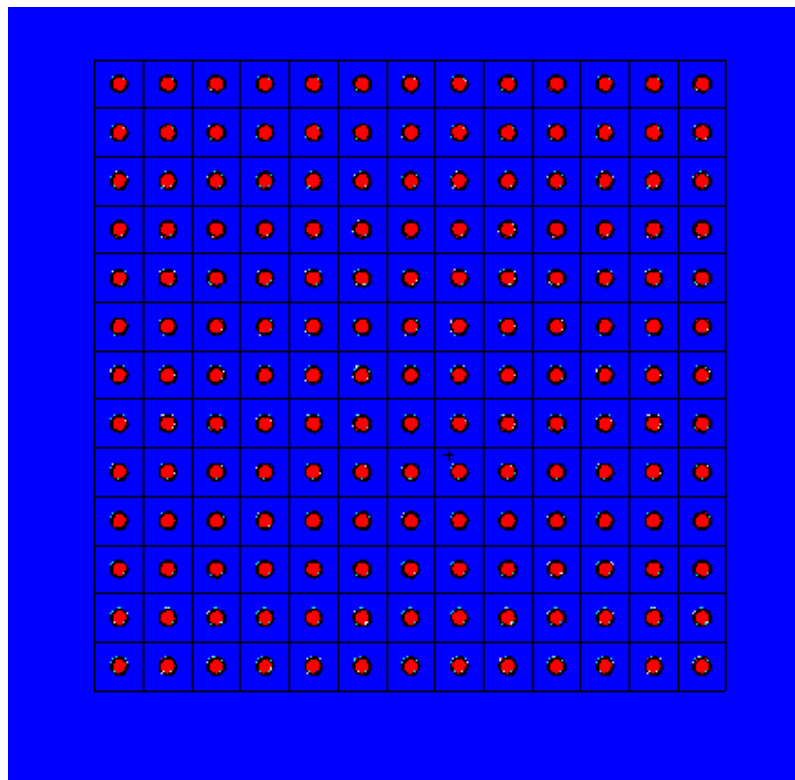


Figure B6.4-1 – AFS-B with 175 MOX Rods



Single array, water reflected, no poison

Figure B6.4-2 – Optimum Pitch Model

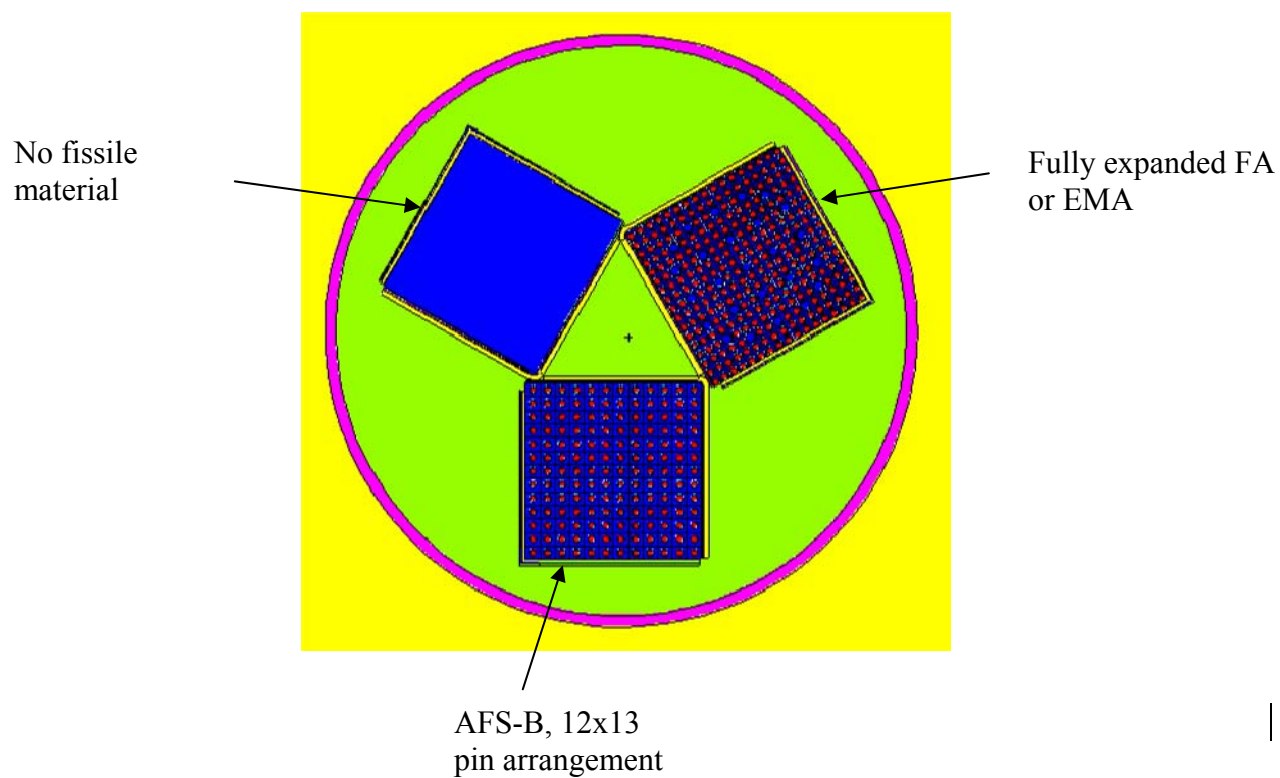


Figure B6.4-3 – AFS-B(12x13)/EMA HAC Single Package Model

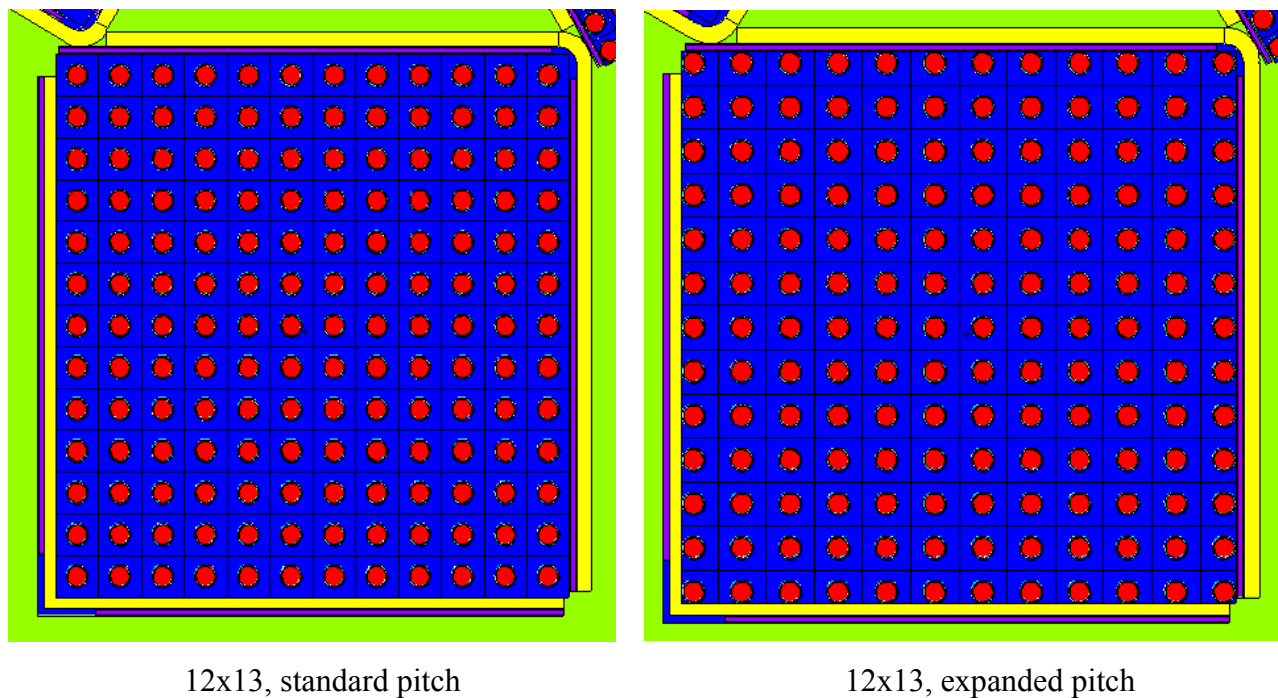
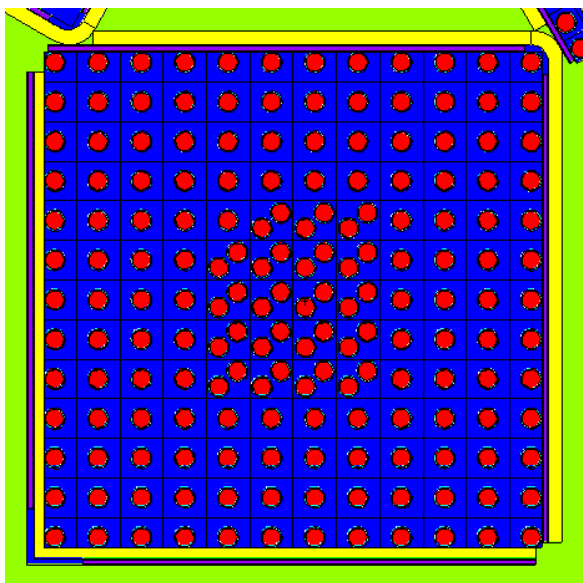
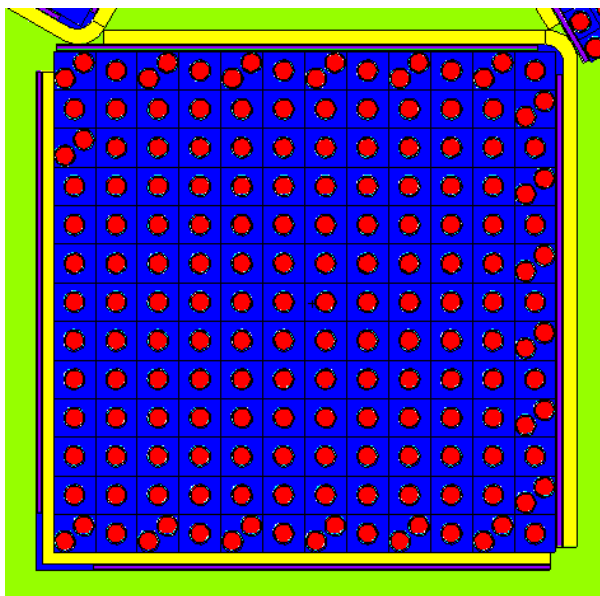


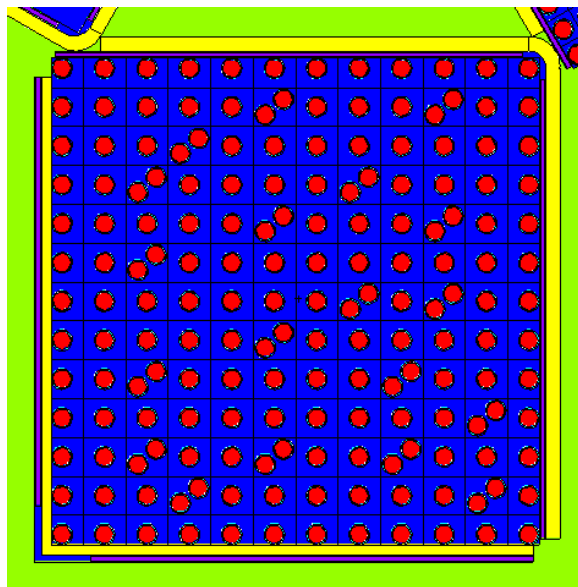
Figure B6.4-4 – Standard and Expanded Pitch Comparison



hs_12x13max_ema_175

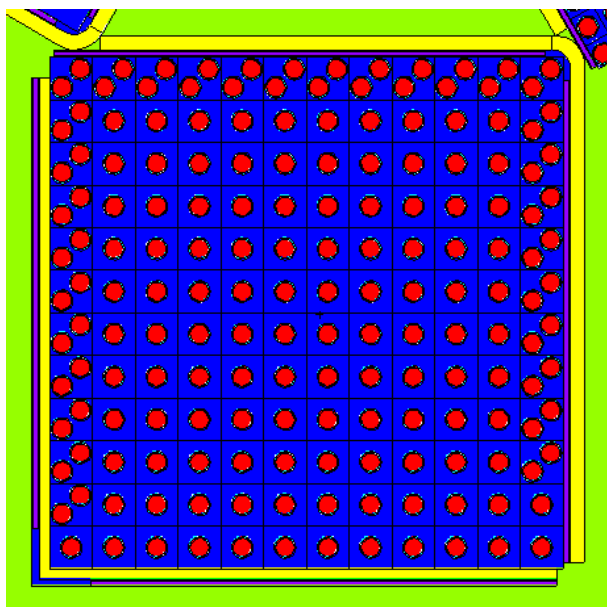


hs_12x13_ema_175

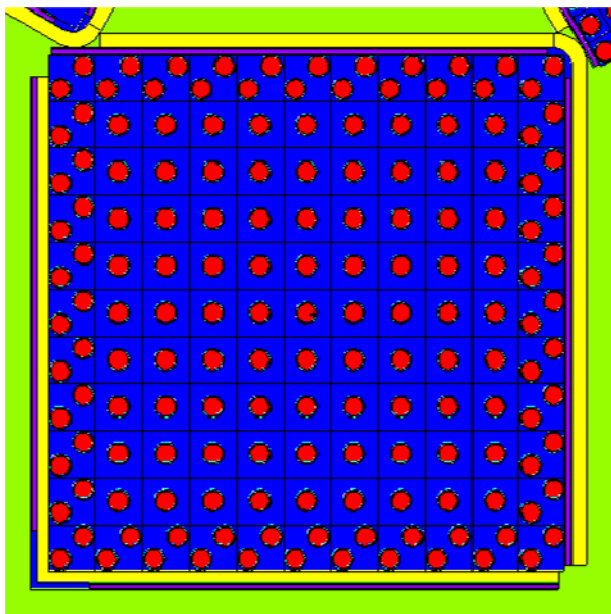


hs_12x13max_ema_175r

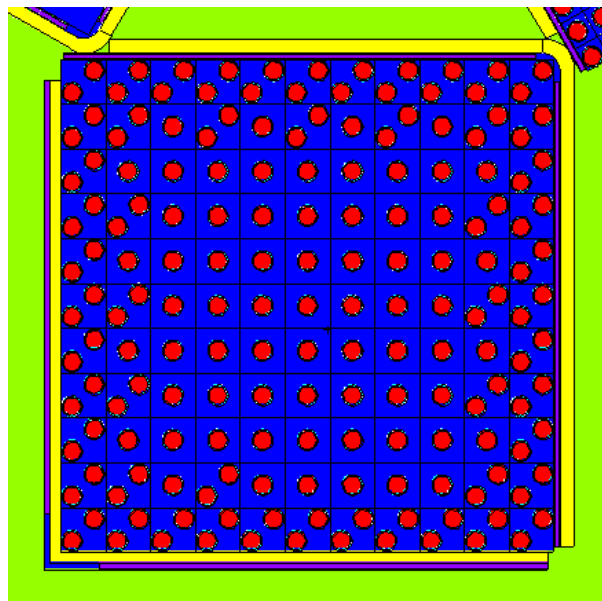
Figure B6.4-5 – 12x13 Non-Regular Rod Patterns



hs_12x12_ema_175

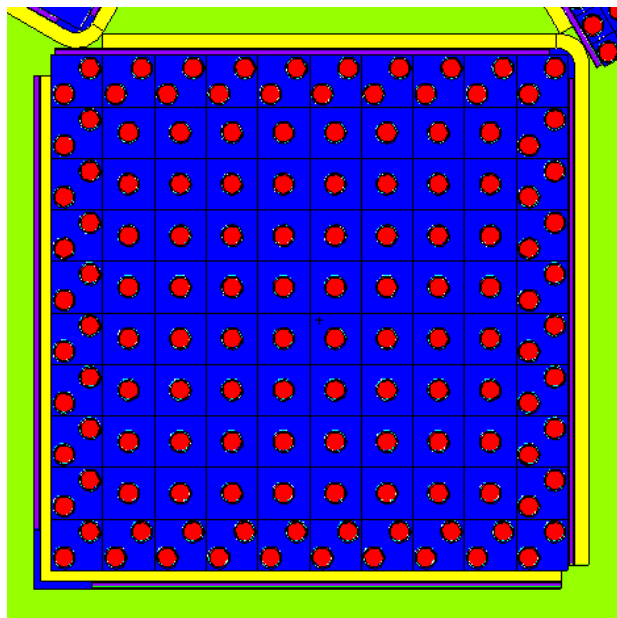


hs_11x11_ema_161

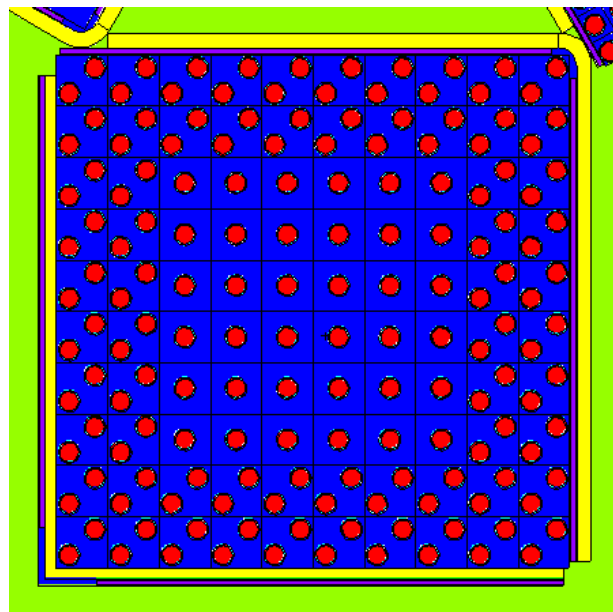


hs_11x11_ema_175

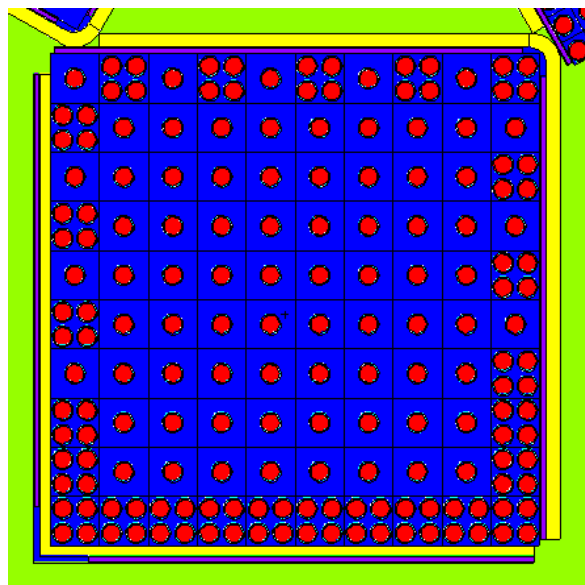
Figure B6.4-6 – 12x12 and 11x11 Non-Regular Rod Patterns



hs_10x10_ema_136



hs_10x10_ema_164



hs_10x10_ema_175

Figure B6.4-7 – 10x10 Non-Regular Rod Patterns

B6.5 Evaluation of Package Arrays Under Normal Conditions of Transport

No MCNP array models are developed for the NCT configuration with a payload of 1 EMA and 1 AFS-B containing 175 rods. Under NCT, in the absence of moderation the reactivity will be bounded by the standard three fuel assembly analysis of Section 6.5, *Evaluation of Package Arrays Under Normal Conditions of Transport*, because the reactivity for the dry condition is governed by the fissile mass in the package. Under the assumed configuration with 1 AFS-B and 1 EMA, the MFFP would contain no more than $175 + 264 = 439$ fuel rods. The standard three fuel assembly models contain $264 * 3 = 792$ fuel rods. Therefore, the NCT results for three fuel assemblies bound the AFS-B/EMA configuration. Therefore, no NCT array models for the AFS-B/EMA configuration are required.

This page left intentionally blank.

B6.6 Package Arrays Under Hypothetical Accident Conditions

B6.6.1 HAC Array Configuration

Only a limited number of HAC infinite array cases are run for the AFS-B/EMA because it has already been established for this package that the single package and infinite array HAC reactivities are nearly identical (see Table 6.1-1). Neutronic communication between packages is small because the package is large and heavily poisoned. Therefore, the most reactive single package case is run in the infinite array configuration.

For the HAC array, it has been established from the original three fuel assembly analysis (Section 6.6, *Package Arrays Under Hypothetical Accident Conditions*) that the most reactive condition is for full moderation within the packages. For low water density ($\leq 0.1 \text{ g/cm}^3$) between packages, reactivity is maximized and the reactivity fluctuation for different low water densities is statistical in nature. Consequently, void is modeled between the packages. Because the fuel is the same as the standard three fuel assembly analysis, these modeling parameters will also result in the most reactive condition for AFS-B/EMA configuration. Also, axial shifting of rods has been shown in Section B6.4.1.2, *HAC Configuration*, to have little effect on system reactivity other than statistical fluctuation. Therefore, for the HAC array, it is sufficient to infinitely reflect the most reactive single package case from Table B6.4-2.

In this case (ha_11x11_ema_161) it is assumed that the dummy fuel location is modeled as water. In actuality, the dummy fuel assembly is a large steel box with void on the inside that approximates the weight of a fuel assembly. As the neutron transmission is greater through either void or steel compared to water, modeling the dummy fuel assembly could slightly increase the reactivity for the array condition. Therefore, two additional cases are run in which the water in the empty location is replaced with steel or void. The results for these cases are provided in Table B6.6-1. The most reactive case has steel in the empty location, although the three results are statistically equivalent, and the multiplication factor of 0.92400 is less than the USL of 0.9288.

While the maximum k_s is approaching to the USL, the assumption that the AFS-B provides no constraint to the rods is not realistic, as there is no scenario in which the postulated rod expansion could be realized in actual practice. The AFS-B, even if severely damaged in an accident, would occupy space and preclude the postulated rod expansion

B6.6.2 HAC Array Results

Results for the HAC single package are provided in Table B6.6-1. The most reactive case is listed in boldface.

Table B6.6-1 – Criticality Results for an Infinite Array of HAC Packages

Case	Dummy Assembly	k_{eff}	σ	$k_s (k+2\sigma)$
ha_11x11_ema_161	Water	0.92101	0.00099	0.92299
ha_11x11_ema_161_st	Steel	0.92192	0.00104	0.92400
ha_11x11_ema_161_vd	Void	0.92131	0.00098	0.92327

B6.7 Fissile Material Packages for Air Transport

This section does not apply for the MFFP, because air transport is not claimed.

This page left intentionally blank.

B6.8 Benchmark Evaluations

The benchmark evaluation is provided in Section 6.8, *Benchmark Evaluations*. A USL of 0.9288 is justified.

This page left intentionally blank.

B6.9 Appendices

Representative MCNP models are included in the following appendices:

B6.9.1 Single Package Model

B6.9.2 Infinite Array Model

This page left intentionally blank.

B6.9.1 Single Package Model

This file is for the worst-case HAC model (hs_11x11_ema_161).

```

175 pin max with 10.85 g/cc Fuel no Nb
c
c *****Fuel Assembly*****
c cells 1 to 3 transform the 3 assemblies to their locations
c 1 4 -1.0 -21 22 -23 24 -25 6 imp:n=1 $ top nozzle, void
c 2 4 -1.0 -21 22 -23 24 -7 26 imp:n=1 $ bottom nozzle, void
c 7 0 -21 22 -23 24 126 -25 fill=20 imp:n=1 $ pins
c
c 201 like 1 but trcl=53 $ assembly 2
c 202 like 2 but trcl=53
c 207 like 7 but fill=21 trcl=53
c 220 like 1 but trcl=54 $ assembly 3
c 221 like 2 but trcl=54
c 222 like 7 but fill=5 trcl=54
c
c -- "box" around fuel
c
c 301 0 (302 -303 300 -304 -906 26):
c (303 -305 300 -301 -906 26) fill=30 imp:n=1 $ "box" cutout
c 302 like 301 but trcl=53
c 303 like 301 but trcl=54
c
c perimeter containing strongback #1 in -y
c 50 0 (26 -906 902 -909 904 -910):
c (26 -906 909 -912 904 -901):
c (26 -906 912 904 -908):
c (26 -906 911 905 -904 -908):
c (26 -906 905 -900 903 -911) fill=7 imp:n=1
c perimeter containing strongback #2
c 51 like 50 but trcl=53
c perimeter containing strongback #3
c 52 like 50 but trcl=54
c
c *****water beyond three units*****
c 131 9 -1.4 -61 -69 64 #7 #50 #51 #52 #301 #302 #303
c #207 #222 imp:n=1
c
c *****containment*****
c 141 5 -7.94 -62 -66 63 (61:65:-64) imp:n=1 $ outer steel
c 143 5 -7.94 -61 -70 69 imp:n=1 $ upper inner steel
c 145 4 -1.0 -61 -65 70 imp:n=1 $ upper void
c
c *****beyond containment*****
c 195 0 -881 882 -886 885 -883 884 -66 63 62 imp:n=1 $ w between packages
c 199 0 (881:-882:886:-885:883:-884:66:-63) imp:n=0 $ outside world
c
c Universe 20: Fuel Lattice
c
c 200 4 -1.0 -12 11 -14 13 u=20 lat=1 trcl=30 fill=0:10 0:10 0:0
c 6 6 6 6 6 6 6 6 6 6 6 $ row 11
c 6 1 1 1 1 1 1 1 1 1 6 $ row 10
c 6 1 1 1 1 1 1 1 1 1 6 $ row 9
c 6 1 1 1 1 1 1 1 1 1 6 $ row 8
c 6 1 1 1 1 1 1 1 1 1 6 $ row 7
c 6 1 1 1 1 1 1 1 1 1 6 $ row 6
c 6 1 1 1 1 1 1 1 1 1 6 $ row 5
c 6 1 1 1 1 1 1 1 1 1 6 $ row 4
c 6 1 1 1 1 1 1 1 1 1 6 $ row 3
c 6 1 1 1 1 1 1 1 1 1 6 $ row 2
c 6 6 6 6 6 6 6 6 6 6 6 imp:n=1 $ row 1 (top)
c
c Universe 21: EMA
c
c 201 4 -1.0 -212 211 -214 213 u=21 lat=1 trcl=31 fill=0:16 0:16 0:0
c 1 1 1 1 1 1 1 1 1 1 1 1 1 1 1 1 $ row 17
c 1 1 1 1 1 1 1 1 1 1 1 1 1 1 1 1 $ row 16
c 1 1 1 1 1 4 1 1 4 1 1 4 1 1 1 1 $ row 15
c 1 1 1 4 1 1 1 1 1 1 1 1 4 1 1 1 $ row 14
c 1 1 1 1 1 1 1 1 1 1 1 1 1 1 1 1 $ row 13
c 1 1 4 1 1 4 1 1 4 1 1 4 1 1 1 1 $ row 12
c 1 1 1 1 1 1 1 1 1 1 1 1 1 1 1 1 $ row 11

```

```

1 1 1 1 1 1 1 1 1 1 1 1 1 1 1 1 1 $ row 10
1 1 4 1 1 4 1 1 4 1 1 4 1 1 1 1 1 $ row 9
1 1 1 1 1 1 1 1 1 1 1 1 1 1 1 1 1 $ row 8
1 1 1 1 1 1 1 1 1 1 1 1 1 1 1 1 1 $ row 7
1 1 4 1 1 4 1 1 4 1 1 4 1 1 1 1 1 $ row 6
1 1 1 1 1 1 1 1 1 1 1 1 1 1 1 1 1 $ row 5
1 1 1 4 1 1 1 1 1 1 1 1 1 4 1 1 1 $ row 4
1 1 1 1 1 4 1 1 4 1 1 4 1 1 1 1 1 $ row 3
1 1 1 1 1 1 1 1 1 1 1 1 1 1 1 1 1 $ row 2
1 1 1 1 1 1 1 1 1 1 1 1 1 1 1 1 1 imp:n=1 $ row 1 (top)
c
c Universe 1: Fuel pin in normal position
c
10 1 -10.85 -1 -4 5 u=1 imp:n=1 $ fuel
11 4 -1.0 -2 1 -4 5 u=1 imp:n=1 $ radial gap
12 7 -6.5 -3 2 -8 5 u=1 imp:n=1 $ clad
13 4 -1.0 3 7 -6 u=1 imp:n=1 $ radially beyond pin
14 4 -1.0 -2 -8 4 u=1 imp:n=1 $ above fuel void
15 7 -6.5 -3 -6 8 u=1 imp:n=1 $ top of fuel cap
16 7 -6.5 -3 -5 7 u=1 imp:n=1 $ bottom of fuel cap
17 4 -1.0 6 u=1 imp:n=1 $ top water to infinity
18 4 -1.0 -7 u=1 imp:n=1 $ bottom water to infinity
c
c Universe 2: Fuel pin shifted up
c
410 1 -10.85 -1 -4 5 trcl=(0 0 23.7109) u=2 imp:n=1 $ fuel
411 4 -1.0 -2 1 -4 5 trcl=(0 0 23.7109) u=2 imp:n=1 $ radial gap
412 7 -6.5 -3 2 -8 5 trcl=(0 0 23.7109) u=2 imp:n=1 $ clad
413 4 -1.0 3 7 -6 trcl=(0 0 23.7109) u=2 imp:n=1 $ radially beyond pin
414 4 -1.0 -2 -8 4 trcl=(0 0 23.7109) u=2 imp:n=1 $ above fuel void
415 7 -6.5 -3 -6 8 trcl=(0 0 23.7109) u=2 imp:n=1 $ top of fuel cap
416 7 -6.5 -3 -5 7 trcl=(0 0 23.7109) u=2 imp:n=1 $ bottom of fuel cap
417 4 -1.0 6 trcl=(0 0 23.7109) u=2 imp:n=1 $ top water to infinity
418 4 -1.0 -7 trcl=(0 0 23.7109) u=2 imp:n=1 $ bottom water to
infinity
c
c Universe 3: Fuel pin shifted down
c
420 1 -10.85 -1 -4 5 trcl=(0 0 -9.4361) u=3 imp:n=1 $ fuel
421 4 -1.0 -2 1 -4 5 trcl=(0 0 -9.4361) u=3 imp:n=1 $ radial gap
422 7 -6.5 -3 2 -8 5 trcl=(0 0 -9.4361) u=3 imp:n=1 $ clad
423 4 -1.0 3 7 -6 trcl=(0 0 -9.4361) u=3 imp:n=1 $ radially beyond pin
424 4 -1.0 -2 -8 4 trcl=(0 0 -9.4361) u=3 imp:n=1 $ above fuel void
425 7 -6.5 -3 -6 8 trcl=(0 0 -9.4361) u=3 imp:n=1 $ top of fuel cap
426 7 -6.5 -3 -5 7 trcl=(0 0 -9.4361) u=3 imp:n=1 $ bottom of fuel cap
427 4 -1.0 6 trcl=(0 0 -9.4361) u=3 imp:n=1 $ top water to infinity
428 4 -1.0 -7 trcl=(0 0 -9.4361) u=3 imp:n=1 $ bottom water to infinity
c
c Universe 4: Instrument/guide tube
c
41 4 -1.0 -18 5 -8 u=4 imp:n=1 $ inside
42 7 -6.5 -19 18 5 -8 u=4 imp:n=1 $ tube
43 4 -1.0 19 5 -8 u=4 imp:n=1 $ beyond tube
44 4 -1.0 8 u=4 imp:n=1
45 4 -1.0 -5 u=4 imp:n=1
c
c Universe 5: Water only
c
46 4 -1.0 -998 u=5 imp:n=1
47 4 -1.0 998 u=5 imp:n=1
c
c Universe 8: Steel only
c
48 6 -7.94 -998 u=8 imp:n=1
49 6 -7.94 998 u=8 imp:n=1
c
c Universe 6: Two fuel pins
c
600 4 -1.0 #601 #602 u=6 imp:n=1
601 0 -600 fill=1(0.5 0.5 0) u=6 imp:n=1
602 0 -603 fill=1(-0.5 -0.5 0) u=6 imp:n=1
c
c Universe 7: Strongback
c
700 6 -7.94 715 -710 u=7 imp:n=1 $ tangential strongback

```

```

701 6 -7.94 (710 711 718):(-711 713) u=7 imp:n=1 $ radial strongback+bend
702 2 -2.713 714 -719 -716 u=7 imp:n=1 $ tan Al clad
703 21 9.2244E-02 719 -720 -716
      730 731 732 733 734 735 736 737 738
      739 740 741 742 743 744 745 746 747
      750 751 752 753 754 755 756 757 758
      759 760 761 762 763 764 765 766 767 u=7 imp:n=1 $ tangential boral
704 2 -2.713 720 -715 -716 u=7 imp:n=1 $ tan Al clad
706 2 -2.713 712 -722 -717 u=7 imp:n=1 $ rad Al clad
707 21 9.2244E-02 722 -723 -717
      770 771 772 773 774 775 776 777 778
      779 780 781 782 783 784 785 786 787
      790 791 792 793 794 795 796 797 798
      799 800 801 802 803 804 805 806 807 u=7 imp:n=1 $ radial boral
708 2 -2.713 723 -713 -717 u=7 imp:n=1 $ rad Al
710 4 -1.0 (710 711 -718): (716 -710 717 -715):
      (710 -713 717 -711) u=7 imp:n=1
719 6 -7.94 ((-717 -712):(-716 -714 717)) -809 u=7 imp:n=1 $ poison holder
720 4 -1.0 ((-717 -712):(-716 -714 717)) 809 -810 u=7 imp:n=1
721 6 -7.94 ((-717 -712):(-716 -714 717)) 810 -811 u=7 imp:n=1
722 4 -1.0 ((-717 -712):(-716 -714 717)) 811 -812 u=7 imp:n=1
723 6 -7.94 ((-717 -712):(-716 -714 717)) 812 -813 u=7 imp:n=1
724 4 -1.0 ((-717 -712):(-716 -714 717)) 813 -814 u=7 imp:n=1
725 6 -7.94 ((-717 -712):(-716 -714 717)) 814 -815 u=7 imp:n=1
726 4 -1.0 ((-717 -712):(-716 -714 717)) 815 -816 u=7 imp:n=1
727 6 -7.94 ((-717 -712):(-716 -714 717)) 816 -817 u=7 imp:n=1
728 4 -1.0 ((-717 -712):(-716 -714 717)) 817 -818 u=7 imp:n=1
729 6 -7.94 ((-717 -712):(-716 -714 717)) 818 -819 u=7 imp:n=1
730 4 -1.0 ((-717 -712):(-716 -714 717)) 819 -820 u=7 imp:n=1
731 6 -7.94 ((-717 -712):(-716 -714 717)) 820 -821 u=7 imp:n=1
732 4 -1.0 ((-717 -712):(-716 -714 717)) 821 -822 u=7 imp:n=1
733 6 -7.94 ((-717 -712):(-716 -714 717)) 822 -823 u=7 imp:n=1
734 4 -1.0 ((-717 -712):(-716 -714 717)) 823 -824 u=7 imp:n=1
735 6 -7.94 ((-717 -712):(-716 -714 717)) 824 -825 u=7 imp:n=1
736 4 -1.0 ((-717 -712):(-716 -714 717)) 825 -826 u=7 imp:n=1
737 6 -7.94 ((-717 -712):(-716 -714 717)) 826 u=7 imp:n=1
c
750 6 -7.94 719 -720 -750 u=7 imp:n=1 $ screws in boral
751 6 -7.94 719 -720 -751 u=7 imp:n=1
752 6 -7.94 719 -720 -752 u=7 imp:n=1
753 6 -7.94 719 -720 -753 u=7 imp:n=1
754 6 -7.94 719 -720 -754 u=7 imp:n=1
755 6 -7.94 719 -720 -755 u=7 imp:n=1
756 6 -7.94 719 -720 -756 u=7 imp:n=1
757 6 -7.94 719 -720 -757 u=7 imp:n=1
758 6 -7.94 719 -720 -758 u=7 imp:n=1
759 6 -7.94 719 -720 -759 u=7 imp:n=1
760 6 -7.94 719 -720 -760 u=7 imp:n=1
761 6 -7.94 719 -720 -761 u=7 imp:n=1
762 6 -7.94 719 -720 -762 u=7 imp:n=1
763 6 -7.94 719 -720 -763 u=7 imp:n=1
764 6 -7.94 719 -720 -764 u=7 imp:n=1
765 6 -7.94 719 -720 -765 u=7 imp:n=1
766 6 -7.94 719 -720 -766 u=7 imp:n=1
767 6 -7.94 719 -720 -767 u=7 imp:n=1
c
770 6 -7.94 722 -723 -770 u=7 imp:n=1
771 6 -7.94 722 -723 -771 u=7 imp:n=1
772 6 -7.94 722 -723 -772 u=7 imp:n=1
773 6 -7.94 722 -723 -773 u=7 imp:n=1
774 6 -7.94 722 -723 -774 u=7 imp:n=1
775 6 -7.94 722 -723 -775 u=7 imp:n=1
776 6 -7.94 722 -723 -776 u=7 imp:n=1
777 6 -7.94 722 -723 -777 u=7 imp:n=1
778 6 -7.94 722 -723 -778 u=7 imp:n=1
779 6 -7.94 722 -723 -779 u=7 imp:n=1
780 6 -7.94 722 -723 -780 u=7 imp:n=1
781 6 -7.94 722 -723 -781 u=7 imp:n=1
782 6 -7.94 722 -723 -782 u=7 imp:n=1
783 6 -7.94 722 -723 -783 u=7 imp:n=1
784 6 -7.94 722 -723 -784 u=7 imp:n=1
785 6 -7.94 722 -723 -785 u=7 imp:n=1
786 6 -7.94 722 -723 -786 u=7 imp:n=1
787 6 -7.94 722 -723 -787 u=7 imp:n=1
c

```

```

790      6  -7.94      722 -723 -790      u=7  imp:n=1
791      6  -7.94      722 -723 -791      u=7  imp:n=1
792      6  -7.94      722 -723 -792      u=7  imp:n=1
793      6  -7.94      722 -723 -793      u=7  imp:n=1
794      6  -7.94      722 -723 -794      u=7  imp:n=1
795      6  -7.94      722 -723 -795      u=7  imp:n=1
796      6  -7.94      722 -723 -796      u=7  imp:n=1
797      6  -7.94      722 -723 -797      u=7  imp:n=1
798      6  -7.94      722 -723 -798      u=7  imp:n=1
799      6  -7.94      722 -723 -799      u=7  imp:n=1
800      6  -7.94      722 -723 -800      u=7  imp:n=1
801      6  -7.94      722 -723 -801      u=7  imp:n=1
802      6  -7.94      722 -723 -802      u=7  imp:n=1
803      6  -7.94      722 -723 -803      u=7  imp:n=1
804      6  -7.94      722 -723 -804      u=7  imp:n=1
805      6  -7.94      722 -723 -805      u=7  imp:n=1
806      6  -7.94      722 -723 -806      u=7  imp:n=1
807      6  -7.94      722 -723 -807      u=7  imp:n=1
c
810      6  -7.94      719 -720 -730      u=7  imp:n=1
811      6  -7.94      719 -720 -731      u=7  imp:n=1
812      6  -7.94      719 -720 -732      u=7  imp:n=1
813      6  -7.94      719 -720 -733      u=7  imp:n=1
814      6  -7.94      719 -720 -734      u=7  imp:n=1
815      6  -7.94      719 -720 -735      u=7  imp:n=1
816      6  -7.94      719 -720 -736      u=7  imp:n=1
817      6  -7.94      719 -720 -737      u=7  imp:n=1
818      6  -7.94      719 -720 -738      u=7  imp:n=1
819      6  -7.94      719 -720 -739      u=7  imp:n=1
820      6  -7.94      719 -720 -740      u=7  imp:n=1
821      6  -7.94      719 -720 -741      u=7  imp:n=1
822      6  -7.94      719 -720 -742      u=7  imp:n=1
823      6  -7.94      719 -720 -743      u=7  imp:n=1
824      6  -7.94      719 -720 -744      u=7  imp:n=1
825      6  -7.94      719 -720 -745      u=7  imp:n=1
826      6  -7.94      719 -720 -746      u=7  imp:n=1
827      6  -7.94      719 -720 -747      u=7  imp:n=1
c
c      Universe 30:  "box" around fuel
c
c 310      2  -2.713      -313 317      u=30 imp:n=1 $ radial left
c 311      2  -2.713      316 -310      u=30 imp:n=1 $ tangential bot
c 312      2  -2.713      314 -315 317 u=30 imp:n=1 $ radial right
c 315      2  -2.713      311 -312 316 u=30 imp:n=1 $ tangential top
316      6  -7.94      315 312      u=30 imp:n=1
317      4  -1.0      (312 -317 -315):(-316 -312) u=30 imp:n=1
c
320      4  -1.0      -315 317 -320      u=30 imp:n=1 $ radial water gap
321      21  9.2244E-02 313 -314 317 320 -321 u=30 imp:n=1 $ radial borat
322      4  -1.0      -315 317 321 -322 u=30 imp:n=1
323      21  9.2244E-02 313 -314 317 322 -323 u=30 imp:n=1
324      4  -1.0      -315 317 323 -324 u=30 imp:n=1
325      21  9.2244E-02 313 -314 317 324 -325 u=30 imp:n=1
326      4  -1.0      -315 317 325 -326 u=30 imp:n=1
327      21  9.2244E-02 313 -314 317 326 -327 u=30 imp:n=1
328      4  -1.0      -315 317 327 -328 u=30 imp:n=1
329      21  9.2244E-02 313 -314 317 328 -329 u=30 imp:n=1
330      4  -1.0      -315 317 329 -330 u=30 imp:n=1
331      21  9.2244E-02 313 -314 317 330 -331 u=30 imp:n=1
332      4  -1.0      -315 317 331 -332 u=30 imp:n=1
333      21  9.2244E-02 313 -314 317 332 -333 u=30 imp:n=1
334      4  -1.0      -315 317 333      u=30 imp:n=1
c
340      2  -2.713      -313 317 320 -321 u=30 imp:n=1 $ radial Al cladding
341      2  -2.713      -313 317 322 -323 u=30 imp:n=1
342      2  -2.713      -313 317 324 -325 u=30 imp:n=1
343      2  -2.713      -313 317 326 -327 u=30 imp:n=1
344      2  -2.713      -313 317 328 -329 u=30 imp:n=1
345      2  -2.713      -313 317 330 -331 u=30 imp:n=1
346      2  -2.713      -313 317 332 -333 u=30 imp:n=1
c
347      2  -2.713      314 -315 317 320 -321 u=30 imp:n=1 $ radial Al cladding
348      2  -2.713      314 -315 317 322 -323 u=30 imp:n=1
349      2  -2.713      314 -315 317 324 -325 u=30 imp:n=1
350      2  -2.713      314 -315 317 326 -327 u=30 imp:n=1

```

```

351      2      -2.713      314 -315 317 328 -329 u=30 imp:n=1
352      2      -2.713      314 -315 317 330 -331 u=30 imp:n=1
353      2      -2.713      314 -315 317 332 -333 u=30 imp:n=1
c
360      4      -1.0          -312 316 -320          u=30 imp:n=1 $ tangential water gap
361     21  9.2244E-02 310 -311 316 320 -321 u=30 imp:n=1 $ tangential boron
362      4      -1.0          -312 316 321 -322 u=30 imp:n=1
363     21  9.2244E-02 310 -311 316 322 -323 u=30 imp:n=1
364      4      -1.0          -312 316 323 -324 u=30 imp:n=1
365     21  9.2244E-02 310 -311 316 324 -325 u=30 imp:n=1
366      4      -1.0          -312 316 325 -326 u=30 imp:n=1
367     21  9.2244E-02 310 -311 316 326 -327 u=30 imp:n=1
368      4      -1.0          -312 316 327 -328 u=30 imp:n=1
369     21  9.2244E-02 310 -311 316 328 -329 u=30 imp:n=1
370      4      -1.0          -312 316 329 -330 u=30 imp:n=1
371     21  9.2244E-02 310 -311 316 330 -331 u=30 imp:n=1
372      4      -1.0          -312 316 331 -332 u=30 imp:n=1
373     21  9.2244E-02 310 -311 316 332 -333 u=30 imp:n=1
374      4      -1.0          -312 316 333          u=30 imp:n=1
c
380      2      -2.713      316 311 -312 320 -321 u=30 imp:n=1 $ horizontal Al cladding
381      2      -2.713      316 311 -312 322 -323 u=30 imp:n=1
382      2      -2.713      316 311 -312 324 -325 u=30 imp:n=1
383      2      -2.713      316 311 -312 326 -327 u=30 imp:n=1
384      2      -2.713      316 311 -312 328 -329 u=30 imp:n=1
385      2      -2.713      316 311 -312 330 -331 u=30 imp:n=1
386      2      -2.713      316 311 -312 332 -333 u=30 imp:n=1
c
387      2      -2.713      316 -310 320 -321 u=30 imp:n=1 $ horizontal Al cladding
388      2      -2.713      316 -310 322 -323 u=30 imp:n=1
389      2      -2.713      316 -310 324 -325 u=30 imp:n=1
390      2      -2.713      316 -310 326 -327 u=30 imp:n=1
391      2      -2.713      316 -310 328 -329 u=30 imp:n=1
392      2      -2.713      316 -310 330 -331 u=30 imp:n=1
393      2      -2.713      316 -310 332 -333 u=30 imp:n=1
c
c      Universe 51: Dummy universe containing fuel
c
c      999      1 -10.31 -999 u=51      imp:n=1 $ for diagnostics only, not used
c      1000     1 -10.31  999 u=51      imp:n=1 $ for diagnostics only, not used
c
c      *****Fuel Assembly*****
c      fuel pin
1      cz      0.409575          $ fuel radius
2      cz      0.41783          $ radius inside clad
3      cz      0.47498          $ radius outside clad
4      pz      182.88          $ top of fuel
5      pz      -182.88         $ bottom of fuel
6      pz      202.7555         $ top of fuel pin
7      pz      -184.3405         $ bottom of fuel pin
8      pz      201.4474         $ bottom of top cap
11     px      -1.018          $ lattice definition
12     px      1.018
13     py      -1.018
14     py      1.018
c
211    px      -0.6688          $ EMA lattice definition
212    px      0.6688
213    py      -0.6688
214    py      0.6688
c      200      pz      -119.38
c      guide tube
18     cz      0.57150
19     cz      0.61214
c      perimeter of fuel assembly
21     px      10.2391 $ offset from surface 905
22     px      -12.1116 $
23     py      -6.6593 $ offset from surface 904
24     py      -29.0113 $
25     pz      226.466
26     pz      -190.95720
126    pz      -193.776
c      *****containment*****
61     cz      36.1950
62     cz      37.6174

```

```

*63      pz  -197.5866  $ 1.5" thick
64      pz  -193.7766  $ 1.11" below bottom of fuel (strongback bottom not modeled)
65      pz  235.6866
*66      pz  237.5916
c 67      pz  -203.0222
c 68      pz  -201.1172
69      pz  226.4664
70      pz  228.0666
c  *****outside of water refl****
72      cz  68.0974
73      pz  -228.0666  $ 1' water from 63
76      pz  268.0716  $ 1' water from 66
c
c  -- "box"
c
300      py -29.7925  $ defining box in u=0
301      py -29.0114
302      px -12.8928
303      px -12.1117
304      py -7.5675
305      px  9.9672
c
310      25 py 0.04445
311      25 py 0.2604
312      25 py 0.3048
313      25 px 0.04445
314      25 px 0.2604
315      25 px 0.3048
316      25 px 2.54
317      25 py 2.54
c
320      pz -171.049
321      pz -119.532
322      pz -109.758
323      pz -67.412
324      pz -57.638
325      pz -15.316
326      pz -5.542
327      pz 36.855
328      pz 46.629
329      pz 89.002
330      pz 98.776
331      pz 141.097
332      pz 150.871
333      pz 193.548
c
c  extra pins
c
600      c/z 0.5 0.5 0.475
601      c/z -0.5 0.5 0.475
602      c/z 0.5 -0.5 0.475
603      c/z -0.5 -0.5 0.475
c
c  strongback surfaces
c
710      22 px 0
711      22 py 0
712      22 px 0.476
713      22 px 0.7808
714      22 py 0.476
715      22 py 0.7808
716      22 px -0.3114  $ 0.43" less than surface 713
717      22 py -0.54
718      22 cz 0.7808
719      22 py 0.5205
720      22 py 0.7364
722      22 px 0.5205
723      22 px 0.7364
c
730      22 c/y -2.7752 -189.6872 0.47625
731      22 c/y -2.7752 -179.5526 0.47625
732      22 c/y -2.7752 -172.3187 0.47625
733      22 c/y -2.7752 -118.2624 0.47625
734      22 c/y -2.7752 -111.0285 0.47625
735      22 c/y -2.7752 -66.1416 0.47625

```

736 22 c/y -2.7752 -58.9077 0.47625
737 22 c/y -2.7752 -14.0462 0.47625
738 22 c/y -2.7752 -6.8123 0.47625
739 22 c/y -2.7752 38.1254 0.47625
740 22 c/y -2.7752 45.3593 0.47625
741 22 c/y -2.7752 90.2716 0.47625
742 22 c/y -2.7752 97.5055 0.47625
743 22 c/y -2.7752 142.3670 0.47625
744 22 c/y -2.7752 149.6009 0.47625
745 22 c/y -2.7752 194.8180 0.47625
746 22 c/y -2.7752 202.0519 0.47625
747 22 c/y -2.7752 213.8172 0.47625
c
750 22 c/y -16.7452 -189.6872 0.47625
751 22 c/y -16.7452 -179.5526 0.47625
752 22 c/y -16.7452 -172.3187 0.47625
753 22 c/y -16.7452 -118.2624 0.47625
754 22 c/y -16.7452 -111.0285 0.47625
755 22 c/y -16.7452 -66.1416 0.47625
756 22 c/y -16.7452 -58.9077 0.47625
757 22 c/y -16.7452 -14.0462 0.47625
758 22 c/y -16.7452 -6.8123 0.47625
759 22 c/y -16.7452 38.1254 0.47625
760 22 c/y -16.7452 45.3593 0.47625
761 22 c/y -16.7452 90.2716 0.47625
762 22 c/y -16.7452 97.5055 0.47625
763 22 c/y -16.7452 142.3670 0.47625
764 22 c/y -16.7452 149.6009 0.47625
765 22 c/y -16.7452 194.8180 0.47625
766 22 c/y -16.7452 202.0519 0.47625
767 22 c/y -16.7452 213.8172 0.47625
c
770 22 c/x -5.9248 -189.6872 0.47625
771 22 c/x -5.9248 -179.5526 0.47625
772 22 c/x -5.9248 -172.3187 0.47625
773 22 c/x -5.9248 -118.2624 0.47625
774 22 c/x -5.9248 -111.0285 0.47625
775 22 c/x -5.9248 -66.1416 0.47625
776 22 c/x -5.9248 -58.9077 0.47625
777 22 c/x -5.9248 -14.0462 0.47625
778 22 c/x -5.9248 -6.8123 0.47625
779 22 c/x -5.9248 38.1254 0.47625
780 22 c/x -5.9248 45.3593 0.47625
781 22 c/x -5.9248 90.2716 0.47625
782 22 c/x -5.9248 97.5055 0.47625
783 22 c/x -5.9248 142.3670 0.47625
784 22 c/x -5.9248 149.6009 0.47625
785 22 c/x -5.9248 194.8180 0.47625
786 22 c/x -5.9248 202.0519 0.47625
787 22 c/x -5.9248 213.8172 0.47625
c
790 22 c/x -16.9789 -189.6872 0.47625
791 22 c/x -16.9789 -179.5526 0.47625
792 22 c/x -16.9789 -172.3187 0.47625
793 22 c/x -16.9789 -118.2624 0.47625
794 22 c/x -16.9789 -111.0285 0.47625
795 22 c/x -16.9789 -66.1416 0.47625
796 22 c/x -16.9789 -58.9077 0.47625
797 22 c/x -16.9789 -14.0462 0.47625
798 22 c/x -16.9789 -6.8123 0.47625
799 22 c/x -16.9789 38.1254 0.47625
800 22 c/x -16.9789 45.3593 0.47625
801 22 c/x -16.9789 90.2716 0.47625
802 22 c/x -16.9789 97.5055 0.47625
803 22 c/x -16.9789 142.3670 0.47625
804 22 c/x -16.9789 149.6009 0.47625
805 22 c/x -16.9789 194.8180 0.47625
806 22 c/x -16.9789 202.0519 0.47625
807 22 c/x -16.9789 213.8172 0.47625
c
809 pz -188.417
810 pz -181.331 \$ PH 1 (bottom)
811 pz -170.541 \$ PH 1
812 pz -120.040 \$ PH 2
813 pz -109.250


```

814 pz -67.920 $ PH 3
815 pz -57.130
816 pz -15.824 $ PH 4
817 pz -5.034
818 pz 36.347 $ PH 5
819 pz 47.137
820 pz 88.494 $ PH 6
821 pz 99.284
822 pz 140.589 $ PH 7
823 pz 151.379
824 pz 193.040 $ PH 8
825 pz 203.830 $ PH 8
826 pz 212.547
c
c hexagonal boundary of one unit lattice cell, close packed
*881 px 37.6184
*882 px -37.6184
*883 p -0.5000000 0.866025404 0.0000000 37.6184
*884 p -0.5000000 0.866025404 0.0000000 -37.6184
*885 p 0.5000000 0.866025404 0.0000000 -37.6184
*886 p 0.5000000 0.866025404 0.0000000 37.6184
c
900 px 11.18006 $ FIXED for strongbacks touching
901 py -5.71956 $ FIXED for strongbacks touching
902 px -11.9593
903 py -28.7574 $ surface 901 minus 9.07"
c
c 904 is -7.1354 and 905 is 9.7633 for nominal case (with poison holders).
c they are shifted to cut off poison holders to allow for
c expansion for damaged cases.
c
c To completely "slice off" the poison holders, set
c 904 to -6.6593 and 905 to 10.2392.
c
904 py -6.6593 $ tangential strongback lower bound, surface 901 minus total thickness
905 px 10.2392 $ radial strongback left bound, surface 901 minus total thickness
906 pz 215.7222
908 c/z 9.87856 -7.02106 1.3015
909 px -9.9019
910 py -6.35448
911 py -7.1344 $ fixed
912 px 9.7653 $ fixed
c
998 so 10000
999 pz 345.5565

mode n
c print
kcode 2000 0.9 30 530
sdef cell=d1 pos=0 0 0 rad=d3 ext=d4 axs=0 0 1
sil 1 7:200:10 207:201:10
spl 1 1
si3 0.409575
si4 182.88
cut:n j j 0 0
c
c Materials
c
m1 92235 -0.249 $ fuel pellet
92238 -82.615
94239 -4.972
94240 -0.264
94241 -0.053
8016 -11.847
m2 13027 1.0 $ aluminum cladding for BORAL
m4 1001 2 $ water
8016 1
mt4 lwtr.01t
m5 6000 -0.06 $ XM-19
7014 -0.4
14000 -0.75
15031 -0.04
16032 -0.03
23000 -0.3
24000 -23.5

```

```

25055      -6
28000      -13.5
41093      -0.3
42000      -3
26000      -52.12
m6         6000      -0.08      $ SS-304
14000      -1.0
15031      -0.045
24000      -19.0
25055      -2.0
26000      -68.375
28000      -9.5
m7         40000     -1.0      $ Cladding
c          41093     -0.030
m8         82000      1.0      $ lead
m9         6000      -25.1      $ water/steel mix, 5.8% steel by volume
14000      -313.9
15031      -14.1
24000      -5964.9
25055      -627.9
26000      -21465.8
28000      -2982.5
1001       -7240.1
8016       -57462.7
mt9        lwtr.01t
m21        5010      7.3123E-03 $ 35 mg/cm2 B-10, 75% credit
          5011      3.9244E-02
          6000      1.2248E-02
          13027     3.3439E-02
c          total 9.2244E-02
c
c          Translations
c
c          tr22 is the intersection of planes 904 and 905
c          when the poison holders are present (904 and 905 shift when it is
c          desired to "slice off" the poison holders).
c          Note that the origin of Universe 7 corresponds to the intersection
c          of these planes.
c
*tr22      9.7643 -7.1354 0.0
c
c          tr25 is the intersection of planes 300 and 302. The origin of Universe 30
c          corresponds to the intersection of these planes.
c
*tr25      -12.8928 -29.7925 0.0
c
c          tr30 is computed by taking the coordinates of the intersection of planes
c          22 and 24 and adding half the pitch (note: can't be exact or else planes will
c          overlap, causing program termination.)
c
*tr30      -11.0956 -27.9953 0.0
*tr31      -11.6368 -28.5365 0.0
c
c          tr53 and tr54 rotate the bottom assembly to create assemblies 2 and 3
c
*tr53      0 0 0          120 30 90    150 120 90    90 90 0 $ +x+y
*tr54      0 0 0          120 150 90    30 120 90    90 90 0 $ -x-y

```

This page left intentionally blank.

B6.9.2 Infinite Array Model

The infinite array models are geometrically the same as the single package models, although small changes have been made to the outer boundary to simulate the infinite array. Additional cells and surfaces are listed below.

```
195      0      -881 882 -886 885 -883 884 -66 63 62  imp:n=1 $ w between packages
199      0      (881:-882:886:-885:883:-884:66:-63)  imp:n=0 $ outside world

c      hexagonal boundary of one unit lattice cell, close packed
*881    px      37.6184
*882    px     -37.6184
*883    p     -0.5000000      0.866025404      0.0000000      37.6184
*884    p     -0.5000000      0.866025404      0.0000000     -37.6184
*885    p      0.5000000      0.866025404      0.0000000     -37.6184
*886    p      0.5000000      0.866025404      0.0000000      37.6184
```

This page left intentionally blank.

B7.0 PACKAGE OPERATIONS

B7.1 Package Loading

The AFS-B contents are loaded in the following manner:

1. Remove the 22 bolts that attach the lid of the AFS-B. Remove the AFS-B lid.
2. Load up to 175 standard MOX fuel rods. If less than 175 rods are placed into the box, add steel or aluminum dunnage rods until all space is filled.
3. Place the AFS-B lid on the body. Tighten the 22 bolts to the torque value specified on *Packaging General Arrangement Drawing 99008-60*. For each bolt, bend lock tab against bolt flat.

Once the AFS-B has been loaded, the package loading operations are essentially the same as the operations for fuel assembly loading described in Chapter 7.1, *Package Loading*. The AFS-B and EMA and handled in the same manner as a fuel assembly.

The only difference is the tightening of the swivel clamp pads. Because the AFS-B is constructed of aluminum, a thermal expansion gap is provided. Therefore, modify Step 18 of Section 7.1.2.1, *Loading of Fuel Assemblies into Strongback*, as follows:

- 7.1.2.1, Step 18: Tighten the four (4) 3/4-inch swivel clamp pads on the top plate until the screw pad contacts the AFS-B top. Then loosen each swivel clamp pad 1 – 1½ turns, and lock in place with a hex nut.

B7.2 Package Unloading

The package unloading operations are the same as the operations for fuel assembly unloading described in Chapter 7.2, *Package Unloading*. The AFS-B and EMA and handled in the same manner as a fuel assembly.

The AFS-B contents are unloaded in the following manner:

1. Remove the 22 bolts that attach the lid of the AFS-B. Remove the AFS-B lid.
2. Unload the fuel and dunnage rods present.
3. Place the AFS-B lid on the body. Tighten the 22 bolts to the torque value specified on *Packaging General Arrangement Drawing 99008-60*. For each bolt, bend lock tab against bolt flat.

B7.3 Preparation of an Empty Package for Transport

Previously used and empty MFFPs shall be prepared and transported per the requirements of 49 CFR §173.428¹.

¹ Title 49, Code of Federal Regulations, Part 173 (49 CFR 173), *Shippers—General Requirements for Shipments and Packagings*, 10-01-06 Edition.

B7.4 Preshipment Leakage Rate Test

The preshipment leakage rate test is the same as described in Section 7.4, *Preshipment Leakage Rate Test*.

B8.0 ACCEPTANCE TESTS AND MAINTENANCE PROGRAM

B8.1 Acceptance Tests

Per the requirements of 10 CFR §71.85¹, this section discusses the inspections and tests to be performed prior to first use of the AFS-B rod container.

B8.1.1 Visual Inspections and Measurements

Each AFS-B rod container shall be examined in accordance with the requirements delineated on the drawings in Appendix B1.4.2, *Packaging General Arrangement Drawings*, prior to use.

B8.1.2 Weld Inspections

All welds shall be inspected to the requirements delineated on the drawings in Appendix B1.4.2, *Packaging General Arrangement Drawings*.

B8.1.3 Structural and Pressure Tests

The AFS-B rod container does not require any lifting device load tests or pressure tests.

B8.1.4 Fabrication Leakage Rate Tests

The AFS-B rod container does not require any leakage rate tests.

B8.1.5 Component and Material Tests

The AFS-B rod container does not require any component or material tests.

B8.1.6 Shielding Tests

The AFS-B rod container does not require any shielding tests.

B8.1.7 Thermal Tests

The AFS-B rod container does not require any thermal tests.

¹ Title 10, Code of Federal Regulations, Part 71 (10 CFR 71), *Packaging and Transportation of Radioactive Material*, 01-01-06 Edition.

B8.2 Maintenance Program

The AFS-B rod container does not require a scheduled maintenance program. The parts which are routinely handled during use (the body, the lid, and the lid fasteners) are visually inspected prior to use. Damaged components shall be repaired or replaced prior to use.

C1.0 GENERAL INFORMATION

Appendix C of the MOX Fresh Fuel Package (MFFP) Safety Analysis Report (SAR) supports the addition of up to three (3) AFS-C rod containers containing Los Alamos Technical Area 18 (TA-18) MOX fuel rods. Two types of TA-18 fuel rods are available, Exxon Nuclear (Exxon) and Pacific Northwest Laboratory (PNL). Because these rods have different outer diameters and lengths, they will be separated within the AFS-C cavity. The AFS-C may transport up to 116 Exxon rods and 69 PNL rods. The maximum number of rods is limited by the cavity size of the AFS-C.

In this SAR Appendix, reference is made to the main SAR for information that has not changed. Referenced tables, figures, and sections that do not contain the letter “C” (e.g., Table 1.2-1, Figure 3.5-1, Section 6.1.1) refer to items in the main SAR. Referenced tables, figures, and sections that contain the letter “C” (e.g., Table C6.4-1, Figure C1.2-1, Section C6.1.1) refer to items in Appendix C.

C1.1 Introduction

The Mixed Oxide Fresh Fuel Package, Model: **MFFP**, is designed to transport fresh MOX pressurized water reactor (PWR) reactor fuel assemblies. The AFS-C fuel rod container has outer dimensions that are consistent with those of a standard fuel assembly and interfaces with the strongback and clamp arms in the same way.

A full-scale, prototypic certification test unit (CTU) was subjected to a series of hypothetical accident condition (HAC) free and puncture drop tests as part of the original SAR submittal. The results of this testing program are directly applicable to the AFS-C payload because the loaded AFS-C payload weight is bounded by the weight of a fuel assembly (including a BPRA). A detailed discussion of the CTU and certification tests is provided in Appendix 2.12.3, *Certification Test Results*. These tests, coupled with supplementary analytical evaluations, conclusively demonstrated the leaktight¹ containment boundary integrity and criticality control performance of the MFFP.

The thermal analysis for the AFS-C payload is provided in Chapter C3.0, *Thermal Evaluation*. Because an MFFP loaded with three (3) AFS-C containers holding TA-18 rods has the same decay heat as three fuel assemblies, MFFP strongback and shell temperatures are the same as those reported in Chapter 3.0, *Thermal Evaluation*. However, due primarily to the simplistic analytical method employed, both the NCT and HAC maximum fuel rod temperatures for rods within the AFS-C are computed to be higher than the maximum temperature computed for a fuel assembly. These temperatures are well below the respective temperature limits for a fuel rod. The internal pressure under NCT and HAC with the AFS-C payload is bounded by the pressure with three fuel assemblies.

¹ Leaktight is defined as 1×10^{-7} standard cubic centimeters per second (scc/s), or less, air leakage per ANSI N14.5-1997, *American National Standard for Radioactive Materials – Leakage Tests on Packages for Shipment*, American National Standards Institute, (ANSI), Inc

Based on the shielding and criticality assessments provided in Chapter C5.0, *Shielding Evaluation*, and Chapter C6.0, *Criticality Evaluation*, the Criticality Safety Index (CSI) for the MFFP is zero (0.0), and the Transport Index (TI) is determined at the time of shipment.

Authorization is sought for shipment of the MFFP containing up to three (3) AFS-C containers with TA-18 MOX rods by all modes of conveyance, except for aircraft, as a Type B(U)F package per the definitions delineated in 10 CFR §71.4.

C1.2 Package Description

General arrangement drawings of the packaging are provided in Section 1.4.2, *Packaging General Arrangement Drawings*. The addition of the AFS-C does not alter these packaging drawings. A drawing of the AFS-C rod container is given in Section C1.4.2, *Packaging General Arrangement Drawings*.

C1.2.1 Packaging

The MFFP packaging description is unchanged from the description provided in Section 1.2.1, *Packaging*. The AFS-C rod container is designed to hold up to 116 Exxon fuel rods, up to 69 PNL fuel rods, or both quantities together. The container has outer cross sectional dimensions of 8.4 inches square, a length from bottom to top of 159.9 inches, and an overall length (to the lift ring bolt head) of 161.2 inches. The primary material of construction of the container is ASTM 6061-T651 aluminum alloy. The two side walls, the bottom plate, and the lid are all $\frac{3}{4}$ inches thick. The side plates are attached to the bottom plate with two longitudinal, 3/8-inch groove welds. The lid is attached with twenty-two (22) zinc-plated, 3/8-16 UNC, SAE J429 Grade 8, hex head cap screws. The two square end pieces are made of solid aluminum alloy, and each are attached to the container with eight (8) zinc-plated SAE J429 3/8-16 UNC hex head cap screws made of Grade 8 alloy steel. The lower square end piece is 2.4 inches thick and the upper square end piece is 3.0 inches thick. Each bolt is secured in place using a thin stainless steel lock tab. Two of the eight bolts on each end go horizontally into the lid, in addition to the 22 cap screws on the top of the lid.

Inside the container is a $\frac{1}{2}$ -inch thick shelf, made of the same aluminum alloy, which fits into $\frac{1}{4}$ -inch deep grooves in each side wall. The shelf is supported by $\frac{1}{4}$ -inch thick aluminum support plates on 15.3-inch centers. The support plates and the shelf are located with intermittent 1/8-inch fillet welds, none of which are load bearing. Along the inside of the two side plates are two, 2.1-inch wide grooves, 0.4 inches deep. Each groove holds a 2-inch thick plate of the same aluminum alloy, which serve as bulkheads. The two bulkheads form rod cavities on each end of the container: a 78.3-inch long cavity for Exxon rods at the lower end and a 37.7-inch long cavity for the PNL rods at the top end. The cavity located between the two bulkheads is empty. Both rod cavities are 6.9 inches wide and 3.4 inches deep. The components of the AFS-C feature numerous small holes that ensure flooding or draining of water from its various cavities.

The lid is lifted by means of two, $\frac{1}{4}$ -20 UNC threaded holes in the lid. The holes are located such that at least half of the hole is blocked by the top of the sidewall, which prevents an overly-long lifting bolt from possibly damaging any fuel rods. The container is lifted from its top end using a swivel hoist ring. All threaded holes may optionally be fitted with helical-coil thread inserts. The label 'AFS-C' is painted prominently on both sides of the container. The AFS-C is finished with a clear anodize treatment.

An external view of the AFS-C rod container is given in Figure C1.2-1. An internal cross sectional view is given in Figure C2.7-1, and views of a typical bulkhead in Figure C2.7-2.

C1.2.2 Containment System

The containment system description is unchanged from the description provided in Section 1.2.2, *Containment System*.

C1.2.3 Contents of Packaging

The MFFP may transport up to three (3) AFS-C rod containers, each containing up to 116 Exxon rods, up to 69 PNL rods, or both quantities together. These limits are based upon the number of rods that will fit within the AFS-C inner cavity, although less rods may be necessary in order to meet the decay heat limit for the package. The actual quantity of rods transported will be limited by either the physical space (i.e., the quantities listed above), or by the decay heat limit of 240 Watts total in the MFFP (see Section C1.2.3.3, *Maximum Decay Heat*.) If necessary, for a payload of fewer than the maximum quantities of rods, aluminum or stainless steel dunnage rods are used to take up the remaining space. For shipping less than a total of three (3) AFS-C containers, non-fuel dummy assemblies are utilized in the unoccupied strongback locations. The physical size and weight of the non-fuel dummy assemblies are nominally the same as the MK-BW/MOX1 17 × 17 design.

The physical parameters for the Exxon and PNL fuel rods are provided in Table C1.2-1. The Exxon rods are well characterized. However, known data for the PNL rods are limited to rod OD, rod length, average plutonium mass, and average plutonium isotopics. No records are available for a number of other PNL rod characteristics, such as pellet OD, active fuel height, and maximum plutonium mass. Data listed as “assumed” in Table C1.2-1 represent the most reactive estimated values determined in Chapter C6.0, *Criticality Analysis*, and are considered bounding. In the criticality analysis, the Exxon rods are conservatively limited to 65 g Pu per rod, and the PNL rods are conservatively limited to 42 g Pu per rod.

C1.2.3.1 Radionuclide Inventory

The average fuel rod isotopics for the Exxon and PNL rods as of 1980 are provided in Table C1.2-2. As these values are averages, these values are not necessarily bounding for criticality purposes. The bounding isotopics used for criticality are discussed in detail in Chapter C6.0, *Criticality Analysis*. Because the values in Table C1.2-2 are 1980 vintage, and Pu-241 has a half life of 14.35 years, the Pu-241 content of the actual rods will be less than the values provided here because most of the Pu-241 will have decayed to Am-241.

C1.2.3.2 Maximum Payload Weight

The weight of a single loaded AFS-C containing 116 Exxon and 69 PNL rods is approximately 1,230 pounds. This weight is bounded by the 1,580 pound weight of a standard fuel assembly (with BPRA). Three loaded AFS-C containers would weigh approximately 3,690 pounds. Therefore, the maximum payload weight is bounded by the value of 4,740 pounds provided in Section 1.2.3.2, *Maximum Payload Weight*.

C1.2.3.3 Maximum Decay Heat

The maximum heat load for the package is unchanged from the value of 240 watts provided in Section 1.2.3.3, *Maximum Decay Heat*. In addition, each AFS-C is limited to a maximum heat load of 80 watts (i.e., combined heat load of the Exxon and PNL rods), the Exxon cavity is limited to a maximum heat load of 80 watts, and the PNL cavity is limited to a maximum heat load of 30 watts.

C1.2.3.4 Maximum Pressure Buildup

The maximum normal operating pressure (MNOP) is bounded by the 10 psig value provided in Section 1.2.3.4, *Maximum Pressure Buildup*. The design pressure of 25 psig is also unchanged.

C1.2.4 Operational Features

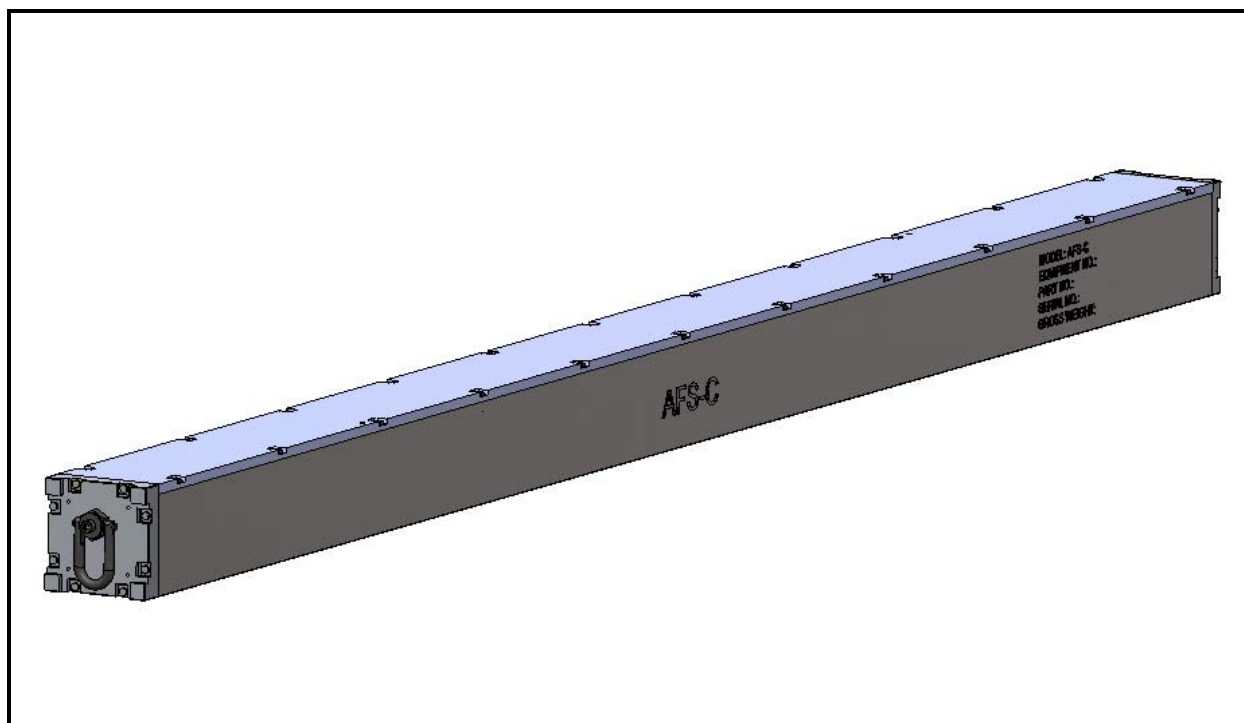
Operating procedures and instructions for loading, unloading, and preparing an empty MFFP for transport with the AFS-C are provided in Chapter C7.0, *Package Operations*.

Table C1.2-1 – Fuel Rod Data

	Exxon		PNL	
Parameter	English Value	Metric Value	English Value	Metric Value
Cladding Material	Zircaloy		Zircaloy	
Overall Length	77.26 in	196.24 cm	36.6 in	92.96 cm
Weight per rod	4.0 lb	---	3.3 lb	---
Active Fuel Length	70 in	177.8 cm	28 in (assumed)	71.12 cm (assumed)
Cladding OD	0.451 in	1.1455 cm	0.565 in	1.4351 cm
Cladding ID	0.381 in	0.9677 cm	0.520 in (assumed)	1.3208 cm (assumed)
Pellet OD	0.3716 in	0.9439 cm	0.5135 in (assumed)	1.3043 cm (assumed)
Effective Pellet Density	--	10.85 g/cm ³ (assumed)	--	10.85 g/cm ³ (assumed)
Pu mass (average)	--	58.3 g	--	37.4 g
Pu mass (maximum)	--	65 g (assumed)	--	42 g (assumed)

Table C1.2-2 – Average Fuel Rod Isotopics

Isotope	Exxon wt. % (1980 average)	PNL wt. % (1980 average)
U-235	0.71	0.71
U-238	99.29	99.29
Total U	100	100
Pu-238	0.745	0.28
Pu-239	75.13	75.38
Pu-240	17.26	18.10
Pu-241	5.23	5.08
Pu-242	1.55	1.15
Total Pu	100	100

**Figure C1.2-1 – AFS-C Rod Container**

C1.3 General Requirements for All Packages

The AFS-C has no effect on the way in which the MFFP meets the general requirements for packaging.

This page left intentionally blank.

C1.4 Appendices

C1.4.1 Nomenclature

The nomenclature list from Section 1.4.1, *Nomenclature*, is applicable. Additional nomenclature listed below.

AFS-C – Container used to transport up to 116 Exxon rods and 69 PNL rods. The AFS-C interfaces with the strongback in the same manner as a fuel assembly.

Exxon Rod – A type of MOX fuel rod with a length of approximately 77.3-in.

Pacific Northwest Laboratory (PNL) Rod – A type of MOX fuel rod with a length of approximately 36.6-in.

Los Alamos Technical Area 18 (TA-18) – Building at Los Alamos National Laboratory that currently stores the Exxon and PNL rods.

C1.4.2 Packaging General Arrangement Drawings

The general arrangement drawings of the body, strongback, and impact limiters are unchanged from those provided in Section 1.4.2, *Packaging General Arrangement Drawings*. The following AFS-C drawing is included in this section:

- 99008-61, Rev. 1, 2 sheets, *AFS-C Assembly*

This page left intentionally blank.

8

7

6

5

4

3

DWG NO 99008-61

REV 1

REV 1

1

D

D

Security Related Information
Figure Withheld Under 10 CFR 2.390

C

C

B

B

A

A

8

7

6


5

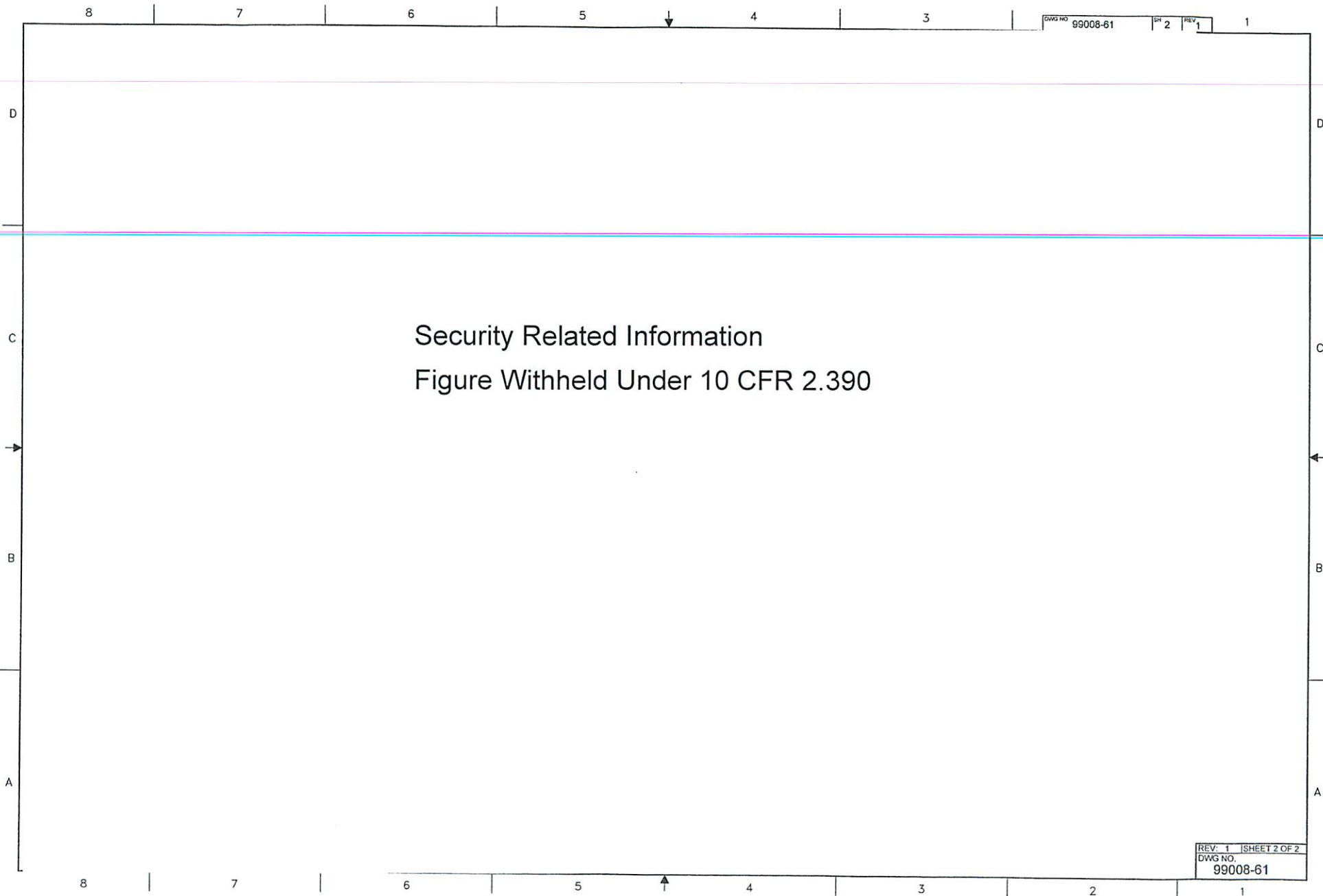
4

3

2

1

1	SEE DCR NO: 99008-58	REL	7-24-08
REV.	DESCRIPTION	REL	DATE
REVISION HISTORY			
 AREVA Federal Services LLC Packaging Projects Tacoma, WA 98402			
AFS-C ASSEMBLY SAR DRAWING			
SCALE: 1:3		WT - LBS	
REV: 1		SHEET 1 OF 2	
DWG NO.		DWG NO.	
D		99008-61	
CAD FILE: 99008111.BLDG.DWG		DWG-3000247	



C2.0 STRUCTURAL EVALUATION

This chapter of Appendix C provides a structural evaluation of the MFFP when transporting up to three (3) AFS-C rod containers containing Los Alamos Technical Area 18 (TA-18) MOX fuel rods. Two types of TA-18 fuel rods are available, Exxon Nuclear (Exxon) and Pacific Northwest Laboratory (PNL). Because these rods have different outer diameters and lengths, they will be segregated longitudinally within the AFS-C cavity. The AFS-C may transport up to 116 Exxon rods and 69 PNL rods. The maximum number of rods is limited by the cavity size of the AFS-C. It is demonstrated that all quantities of interest are bounded by the analyses presented in Chapter 2.0, *Structural Evaluation*.

C2.1 Structural Design

C2.1.1 Discussion

A comprehensive discussion of the MFFP design and standard configuration is provided in Section 1.2, *Package Description*. The MFFP drawings show the detailed geometry of the package, as well as the dimension, tolerances, materials, and fabrication requirements, and are provided in Appendix 1.4.2, *Packaging General Arrangement Drawings*. A physical description of the AFS-C is provided in Section B1.2.3, *Contents of Packaging*. The following discussion is limited to the AFS-C.

A physical description of the AFS-C rod container is provided in Section C1.2.3, *Contents of Packaging*, and is shown in the drawings in Appendix C1.4.2, *Packaging General Arrangement Drawings*. The AFS-C container is a robust box designed to provide confinement of the fuel rods under all conditions of transport. The AFS-C container has the same external boundary dimensions as a standard MOX fuel assembly, and thus is loaded, mounted, and unloaded from the strongback in the same manner as a fuel assembly. The structural evaluations and testing performed as part of the original license activities adequately characterize the performance of the MFFP with this payload.

C2.1.2 Design Criteria

The MFFP design criteria are unchanged from those provided in Section 2.1.2, *Design Criteria*. The design criteria for the AFS-C rod container are based on the functional requirement that the rod container confine the rods inside the container boundary under all NCT and HAC. Because the AFS-C rod container is transported within the MFFP strongback, it is protected from gross distortion by the fuel control structure (FCS). As shown in Section 2.12.5, *Fuel Control Structure Evaluation*, the FCS provides a limit to any reconfiguration of the fuel assembly which could occur as a result of the worst case HAC event. The MOX fuel assembly consists of a larger number of rods (264) than is contained in the AFS-C rod container (up to 116 Exxon rods and 69 PNL rods). In addition, the rods in the MOX fuel assembly are unconfined by any structure other than the FCS, whereas fuel rods in the AFS-C rod container are confined within a container having significant structure. Therefore, gross distortion of the fuel rods or of the AFS-C container, or escape of the fuel rods or fuel rod fragments from the container, are not of concern.

To enhance criticality safety by preventing the potential for damage to the fuel rods in the HAC free drop impact event, the AFS-C rod container is designed to minimize the relative motion of the rods under impact conditions. To accomplish this, the AFS-C rod container is designed to limit the “rattle space” of the fuel rods (including any dummy rods as necessary) to less than approximately one half rod diameter.

The only components of the AFS-C container which are not supported externally by the strongback or FCS are the internal shelf and rod cavity bulkheads. To ensure that the “rattle space” available to the rods cannot increase as a result of the free drop impact event, these components are designed to have a primary bending stress less than the yield point of their material at NCT maximum temperature.

C2.1.3 Weights and Center of Gravity

The loaded weight of the AFS-C, conservatively assuming 116 Exxon and 69 PNL rods, is bounded by 1,230 pounds, which is 22% less than the gross weight of 1,580 pounds for a fuel assembly (including a BPRA). Therefore, the weight of the MFFP when transporting one or more AFS-C containers is bounded by the weights given in Section 2.1.3, *Weights and Center of Gravity*, for transport of MOX fuel assemblies.

When transporting both Exxon and PNL fuel rods, the weight is nearly balanced in the AFS-C container, and the center of gravity of the overall MFFP is essentially unchanged from the case of the standard MOX fuel assembly payload, where it is located 103.7 inches from the end of the bottom impact limiter. When transporting AFS-C containers with only Exxon rods, the center of gravity of the MFFP will be shifted approximately 3 inches toward the closed end, compared to the standard MOX fuel payload. When transporting AFS-C containers with only PNL rods, the center of gravity of the MFFP will be shifted approximately 1.5 inches toward the lid end, compared to the standard MOX payload. These shifts of c.g. are small relative to the overall length of the MFFP of approximately 200 inches, and will not have a significant effect on lifting, tiedown, or HAC response of the package.

C2.2 Materials

The AFS-C is constructed primarily of ASTM B209, 6061-T651 aluminum plate material. The lid and ends are attached with bolts made from SAE J429 Grade 8 material. A stainless steel swivel hoist ring is included for lifting. No non-metallic materials are used in the AFS-C. These materials do not result in any chemical or galvanic reactions, and are not significantly affected by radiation. The material properties for the aluminum material at 70 and 200 °F needed for calculations are given in Table C2.2-1, and were taken from the ASME B&PV Code,¹ as noted. Note that although there is limited welding of the 6061 material, welding is not used in regions where the material properties are used in stress analysis.

¹ American Society of Mechanical Engineers (ASME) Boiler and Pressure Vessel Code, Section II, Materials, Part D, Properties, 2001 Edition, 2002 and 2003 Addenda.

Table C2.2-1 - Material Properties of ASTM B209 6061-T651 Aluminum Alloy

Temperature, °F	Yield Strength, psi	Ultimate Strength, psi	Coefficient of Thermal Expansion, 10 ⁻⁶ in/in/°F
70	35,000 ^①	42,000 ^①	-
200	33,700 ^②	-	13.0 ^③

Notes:

①Yield and ultimate strength at 70 °F from ASME B&PV Code, Section II, Part B, SB-209.

②Yield strength at 200 °F from ASME B&PV Code, Section II, Part D, Table Y-1.

③Coefficient of thermal expansion from ASME B&PV Code, Section II, Part D, Table TE-2.

C2.3 Fabrication and Examination

The AFS-C rod container is fabricated to the requirements of the drawings shown in Appendix C1.4.2, *Packaging General Arrangement Drawings*. The materials of construction are specified to either ASTM or SAE standards. The rod container is inspected to the dimensional requirements of the drawing. Welds are visually inspected to the AWS D1.2² welding code.

C2.4 Lifting and Tie-down Standards for All Packages

Because the gross weight of the MFFP is lower when transporting an AFS-C rod container, this section is unchanged from Section 2.4, *Lifting and Tie-down Standards for All Packages*, in regards to the package itself.

The AFS-B uses a 5/8-11 UNC swivel hoist ring for handling. The thread depth for this swivel hoist ring bolt is 1.28-in. The minimum required thread depth may be computed by the following equation:

$$L_i = \frac{A_t \times S_t}{A_i \times S_i}, \text{ where}$$

A_t is the tensile stress area of the 5/8-11 UNC bolt (0.2201 in²)

S_t is the allowable ultimate tensile strength for the 5/8-11 UNC bolt (170,000/5 = 34,000 psi)³

A_i is the internal aluminum thread stripping area per inch length (1.4255 in²/in-length)

S_i is the governing allowable shear strength of the aluminum thread (0.6 x 42,000/5 = 5,040 psi using ultimate strength). Note that this value bounds the value obtained using the yield strength (0.6 x 35,000/3 = 7,000 psi). Material properties are at 70 °F.

The minimum length of aluminum thread to develop the full tensile strength of the external thread is then:

² ANSI/AWS D1.2, *Structural Welding Code – Aluminum*, American Welding Society (AWS).

³ Conservatively high tensile strength obtained from ASTM A574, *Standard Specification for Alloy Steel Socket-Head Cap Screws*. Actual tensile strength of swivel hoist ring bolt will be equal to or less than this value.

$$L_i = \frac{(0.2201)(34,000)}{(1.4255)(5,040)} = 1.0416 \text{ in}$$

As this length is less than the 1.28-in thread depth of the swivel hoist ring bolt, tear out of the aluminum threads is not a concern. The governing factor is therefore the swivel hoist ring bolt, and the performance of this item is ensured by the rated capacity of the swivel hoist ring. Note that an optional 300 series insert may also be used, which would further increase the conservatism.

C2.5 General Considerations

The AFS-C rod container is evaluated by reasoned argument and by analysis in the following sections. In addition, the results and conclusions of Section 2.5, *General Considerations*, remain unchanged.

C2.6 Normal Conditions of Transport

C2.6.1 Heat

It is demonstrated in Section C3.4, *Thermal Evaluation for Normal Conditions of Transport*, that under NCT the MFFP strongback and shell temperatures associated with the AFS-C payload are bounded by the standard three (3) fuel assembly payload. Therefore, all associated pressure and thermal stresses are bounded by the values presented in Section 2.6.1, *Heat*. For the AFS-C rod container, the bounding temperature of the sidewalls and the internal shelf is 200 °F. Since the AFS-C is vented, it cannot retain pressure.

C2.6.1.1 Differential Thermal Expansion

The evaluation of differential thermal expansion given in Section 2.6.1.2, *Differential Thermal Expansion*, is not affected by use of the AFS-C rod container. An additional evaluation of the differential thermal expansion between the strongback and the AFS-C container will now be made.

From Section 2.6.1.2, *Differential Thermal Expansion*, the design temperature of the strongback is $T_{SB} = 180$ °F, and the coefficient of thermal expansion for the strongback material is $\alpha_{SB} = 8.8 \times 10^{-6}$ in/in/°F. As stated above, the bounding temperature for the AFS-C container is $T_{AFS-C} = 200$ °F, and from Table C2.2-1, the coefficient of thermal expansion is $\alpha_{AFS-C} = 13.0 \times 10^{-6}$ in/in/°F. The overall length of the container is $L = 159.9$ inches. The reference temperature is 70 °F. The differential thermal growth of the rod container and the strongback is:

$$\delta = \alpha_{AFS-C}(L)(T_{AFS-C} - 70) - \alpha_{SB}(L)(T_{SB} - 70) = 0.115 \text{ inches}$$

This calculation conservatively assumes that the entire length of the two components is at the respective peak temperatures, and thus overestimates the relative thermal expansion. To prevent axial interference of the AFS-C container with the strongback, the clamp pads will be set with a clearance to the end of the AFS-C container. As stated in Section C7.1, *Package Loading*, the 3/4-10 clamp pad screw will be backed out a minimum of one turn from the position of contact, ensuring a minimum axial clearance between the AFS-C container and the strongback of 0.1

inches at the reference temperature. This is adequate to ensure that the thermal expansion force is negligible or non-existent considering the conservatism of the evaluation above.

C2.6.2 Cold

This section is unchanged from Section 2.6.2, *Cold*.

C2.6.3 Reduced External Pressure

This section is unchanged from Section 2.6.3, *Reduced External Pressure*.

C2.6.4 Increased External Pressure

This section is unchanged from Section 2.6.4, *Increased External Pressure*.

C2.6.5 Vibration and Shock

The vibration normally incident to transportation will have no effect on the AFS-C rod container. The AFS-C container is installed and retained in the same manner as a MOX fuel assembly. The spring loaded clamp arms which hold the container in place will significantly dampen any vibrational loads which could come from the cask body. Furthermore, any fatigue cracks which might occur from vibration, which are too small to be noted during a visual inspection, would have no effect on the ability of the AFS-C to perform its function of confining the rods in a HAC free drop impact. Therefore, vibration and shock are not of concern for the AFS-C rod container.

C2.6.6 Water Spray

This section is unchanged from Section 2.6.6, *Water Spray*.

C2.6.7 Free Drop

Because a loaded AFS-C is lighter than a fuel assembly (including BPRA), the response of the MFFP to a free drop would be essentially the same when compared to the standard payload.

Since the AFS-C rod container is shown to confine the fuel rods in a HAC free drop impact (see Section C2.7.1), its performance will be acceptable for the NCT free drop event.

C2.6.8 Corner Drop

This section is unchanged from Section 2.6.8, *Corner Drop*.

C2.6.9 Compression

This section is unchanged from Section 2.6.9, *Compression*.

C2.6.10 Penetration

This section is unchanged from Section 2.6.10, *Penetration*.

C2.7 Hypothetical Accident Conditions

C2.7.1 Free Drop

The functional criteria of the AFS-C rod container is to confine the Exxon and PNNL fuel rods in the worst-case HAC free drop event. As an additional enhancement to criticality safety, the container should also restrict the relative movement of the rods to minimize the potential for damage to the fuel rods.

The MFFP strongback, including the fuel control structure (FCS), is designed to maintain a complete MOX fuel assembly in a subcritical configuration during the governing free drop event. Using physical test (see Appendix 2.12.3, *Certification Test Results*) and calculations (see Appendix 2.12.5, *Fuel Control Structure Evaluation*), it has been demonstrated that *a*) the fuel rods do not break or fragment, and *b*) the strongback and FCS are capable of confining the rods within a defined geometry. As stated in Section C1.2, *Package Description*, the AFS-C rod container consists of a completely enclosed structure made of 6061-T651 aluminum plates of $\frac{3}{4}$ -inch nominal thickness. The lid of the container is attached using 22, $\frac{3}{8}$ -inch diameter bolts. The container has the same boundary dimensions as the MOX fuel assembly, and is mounted in the strongback in the same way. As such, the AFS-C container represents an added level of confinement for the fuel rods, beyond that provided by the strongback and FCS. For this reason, confinement of the fuel rods by the AFS-C container is ensured. Table C2.7-1 presents added detail which supports this conclusion. As stated in Section C2.1.2, *Design Criteria*, the movement of rods in an impact is restricted to a maximum of approximately one-half of a rod diameter.

The rod cavities inside the AFS-C container are formed by the $\frac{3}{4}$ -inch thick lid plate, the two $\frac{3}{4}$ -inch thick side plates, the $\frac{1}{2}$ -inch thick shelf plate, the thick end plates (minimum thickness of 2.4 inches), and the two, 2-inch thick bulkhead plates. The Exxon rod cavity is located at one end of the container and is 78.3 inches long, and the PNL rod cavity is located at the other end, and is 37.7 inches long. The shelf plate is located in longitudinal, $\frac{1}{4}$ -inch deep grooves on the inside face of each $\frac{3}{4}$ -inch thick side plate, and supported against the bottom plate by support plates at 15.3-inch intervals. Figure C2.7-1 shows a cross section of the AFS-C container. The bulkhead plates are located in 0.4-inch deep grooves on the inside face of each side plate. Figure C2.7-2 shows a typical cross section view of a bulkhead plate. The bulkhead plate spans the distance between the two side plates, and closes off one end of each rod cavity. To demonstrate that the rod cavity maintains its internal geometric integrity in the worst-case free drop impact, the following evaluations are performed. The internal geometric integrity assures that the "rattle space" inside the container is minimized to prevent any possible damage to the rods. However, any loss of the rod container contents is precluded by the rod container primary structure, as discussed above.

Shelf Evaluation. In the following, it is assumed that the impact occurs with the shelf oriented horizontally with the container lid side up. This orientation governs over all others where some component of the rod load is directed toward the thick sidewalls of the container. Any support from the support plates beneath the shelf is conservatively neglected. The shelf is then a plate, simply supported on its two long sides, and free on its two short sides. A governing impact of

180g is taken from Section 2.12.5.2, *Conditions Analyzed*, for the maximum slapdown impact. The loading from the weight of the fuel rods will be taken from the governing case of either the Exxon or PNL rods. Note that each weld between the shelf and the side plates is only 2-inches long, centered on each support plate, as shown in Section B of drawing 99008-61. This weld is not structural, and serves only to compensate for any weld distortion which might occur from the two groove welds. As such, a strength reduction does not need to be considered, since the longer, unsupported length between support plates is far from any heat affected zone.

From Table C1.2-1, the Exxon fuel rod weight is 4 lb each, and the length is $L_{Ex} = 77.3$ inches. From the same table, the PNL fuel rod weight is 3.3 lb each, and the length is $L_{PNL} = 36.6$ inches. From Figure C2.7-1, the internal width of the cavity is $b = 6.9$ inches. For 116 Exxon rods, the total weight is $W_{Ex} = 116 \times 4 = 464$ lb. The total weight of the PNL rods is $W_{PNL} = 69 \times 3.3 = 228$ lb. Since the rods rest on an area bounded by the rod length and the cavity width, the impact pressure on the shelf is:

$$q = \frac{W_{Ex}g}{L_{Ex}b} = 156.6 \text{ psi for Exxon rods}$$

$$q = \frac{W_{PNL}g}{L_{PNL}b} = 162.5 \text{ psi for PNL rods}$$

Therefore the governing load is $q = 162.5$ psi, which will conservatively be assumed to apply to the entire shelf, rather than just the area beneath the PNL rods. A formula from Roark,⁴ Table 26, Case 1a, is used. Even though this formula assumes simple support on the narrow ends as well as the sides, the maximum stress at the center of the plate, which is more than 10 plate-widths distant from the ends, will not be materially affected. The length of the shelf is $L_s = 153.5$ inches. The ratio a/b is $153.5/6.9 = 22.2$, from which $\beta = 0.75$. The maximum stress at the center of the plate is found from:

$$\sigma = \frac{\beta qb^2}{t^2} = 23,210 \text{ psi}$$

where $t = 0.5$ inches, and the other quantities are as defined above. From Table C2.2-1, the yield strength of the shelf material at the bounding temperature of 200 °F is 33,700 psi. The margin of safety against yield of the shelf is:

$$MS = \frac{33,700}{23,210} - 1 = +0.45$$

Since the shelf does not yield, the “rattle space” available for the rods does not increase as a result of the slapdown free drop event. Other impact orientations would place lower loadings on the shelf.

Bulkhead Evaluation. In this evaluation, stresses associated with the bulkhead are demonstrated to remain below the yield point of the aluminum alloy material in the worst case end drop impact of 120g, taken from Section 2.12.5.2, *Conditions Analyzed*. The governing weight is that of the Exxon fuel rods, having a maximum weight of $W_{Ex} = 464$ lb. The bulkhead is modeled as a beam, simply supported at each side plate, for a span of $L = 6.9$ inches, and a width (see Figure C2.7-2) of

⁴ Young, W. C., *Roark's Formulas for Stress and Strain*, Sixth Edition, McGraw-Hill, 1989.

b = 3.3 inches, assuming a 0.1-in total gap. (Note that the nomenclature has been partially redefined so as to be consistent with common textbook formulas.) The moment of inertia is:

$$I = \frac{bh^3}{12} = 2.2 \text{ in}^4$$

where h = 2 inches. The c-distance is h/2 = 1 inch. The loading per inch of length of the beam is:

$$w = \frac{W_{\text{Ex}}g}{L} = 8069.6 \text{ lb/in}$$

where g = 120 for the end drop impact. The bending moment is:

$$M = \frac{wL^2}{8} = 48,024 \text{ in-lb}$$

The bending stress is:

$$\sigma = \frac{Mc}{I} = 21,829 \text{ psi}$$

From Table C2.2-1, the yield strength of the bulkhead material at the bounding temperature of 200 °F is 33,700 psi. The margin of safety against bending yield of the bulkhead is:

$$MS = \frac{33,700}{21,829} - 1 = +0.54$$

The bearing stress on the two grooves in the side plates which support the bulkhead is equal to:

$$\sigma_b = \frac{F}{A} = \frac{W_{\text{Ex}}g}{2bt_g} = 27,214 \text{ psi}$$

where a value of $t_g = 5/16$ (0.31) inches is conservatively used for the 3/8 (0.4) inches deep groove in the side plate. Conservatively, this bearing stress will be compared to the tensile yield strength, even though bearing stress is commonly permitted to reach a much higher value. The margin of safety on bearing yield is:

$$MS = \frac{33,700}{26,953} - 1 = +0.25$$

The groove edge which supports the bulkhead is subject to a shearing load on a plane oriented at 45° to the plane of the bulkhead. The shear area per groove is:

$$A_s = t_g b \sqrt{2} = 1.45 \text{ in}^2$$

The shear stress is:

$$\tau = \frac{W_{\text{Ex}}g}{2A_s} = 19,200 \text{ psi}$$

The shear yield strength is equal to 0.6 times the tensile yield strength. The margin of safety is:

$$MS = \frac{(0.6)33,700}{19,200} - 1 = +0.05$$

Note that in all of these calculations, the yield point of the material is conservatively chosen as a stress criteria, even though the HAC event is classified as a Service Level D loading condition by Regulatory Guide 7.6.⁵ Since neither the shelf nor the bulkhead experience yield in the governing slapdown or end drop impacts, the “rattle space” available for the rods does not increase as a result of the worst case free drop event. Thus, the AFS-C rod container supports the geometry assumptions made in the criticality analysis of Chapter 6, *Criticality Evaluation*.

Table C2.7-1 Comparison of the MOX Fuel Assembly and the AFS-C Rod Container in the MFFP Strongback

MOX Fuel Assembly	AFS-C Rod Container	Conclusion
Strongback clamps on fuel grids	Strongback clamps on container	AFS-C lid is both bolted in place and clamped in place by the strongback
Max weight of 1,580 lb	Max weight of 1,230 lb	Lighter payload in AFS-C, which applies lower inertia loads to the strongback in free drop impact events
264 rods	116 Exxon plus 69 PNL (185) rods	Fewer rods in AFS-C
Rods self-supporting over span between clamp arms	Rods supported by thick walls and bolted lid of container	AFS-C eliminates rod bending loads
Rods can move axially a limited amount	Rods are confined by thick, bolted end structures	AFS-C confines rods axially
Rod lateral buckling is controlled by strongback and FCS	Rod lateral buckling is controlled by strongback and FCS, plus: <ol style="list-style-type: none"> 1. restricted free space inside container 2. rods supported by thick walls of container 3. rods are shorter than MOX rods 	AFS-C adds a significant layer of rod support to that existing in the basic strongback/FCS

⁵ U.S. Nuclear Regulatory Commission, Regulatory Guide 7.6, *Design Criteria for the Structural Analysis of Shipping Cask Containment Vessels*, Revision 1, March 1978.

Security Related Information
Figure Withheld Under 10 CFR 2.390

Figure C2.7-1 AFS-C Rod Container Cross Section View

Security Related Information
Figure Withheld Under 10 CFR 2.390

Figure C2.7-2 AFS-C Rod Container Bulkhead Views

C2.7.2 Crush

This section is unchanged from Section 2.7.2, *Crush*.

C2.7.3 Puncture

The weight of the MFFP containing up to three AFS-C rod containers is bounded by the weight of the MFFP with a payload of three (3) standard fuel assemblies. Therefore, the system response to a puncture is bounded by the discussion presented in Section 2.7.3, *Puncture*.

C2.7.4 Thermal

C2.7.4.1 Summary of Pressures and Temperatures

Package pressures and temperatures due to the HAC thermal event are presented in Section C3.5.3, *Maximum Temperatures and Pressures*. MFFP strongback and shell temperatures under HAC associated with the AFS-C payload are essentially the same as the standard three (3) fuel assembly payload. From Section C3.5.3.2, *Maximum Pressures*, the maximum internal pressure during the HAC thermal event is 121.4 psig, with the package initially at atmospheric pressure. This pressure is bounded by the 130 psig pressure used in Section 2.7.4, *Thermal*.

C2.7.4.2 Differential Thermal Expansion

This section is unchanged from Section 2.7.4.2, *Differential Thermal Expansion*, as the MFFP strongback and shell temperatures under HAC associated with the AFS-C payload are essentially the same as the standard three (3) fuel assembly payload.

C2.7.4.3 Stress Calculations

As discussed in Section C2.7.4.1, *Summary of Pressures and Temperatures*, a conservative maximum internal pressure of 121.4 psig is calculated for the HAC thermal event. This pressure is lower than the 130 psig pressure used in Section 2.7.4.3, *Stress Calculations*. Therefore, the stresses calculated in Section 2.7.4.3 conservatively bound the stresses resulting from the payload evaluated in this Appendix.

C2.7.5 Immersion – Fissile Material

This section is unchanged from Section 2.7.5, *Immersion – Fissile Material*.

C2.7.6 Immersion – All Packages

This section is unchanged from Section 2.7.6, *Immersion – All Packages*.

C2.7.7 Deep Water Immersion Test (for Type B Packages Containing More than 10^5 A₂)

This section is unchanged from Section 2.7.7, *Deep Water Immersion Test*.

C2.7.8 Summary of Damage

The AFS-C rod container maintains its structural integrity and functionality in the worst-case HAC free drop event, which bounds the loadings of all other HAC events on the container. Since the AFS-C rod container is mounted in the same way as a MOX fuel assembly but weighs less, the response of the MFFP to drop and puncture accidents is unchanged when using the AFS-C. Therefore, the AFS-C is acceptable for use as a payload container.

C2.8 Accident Conditions for Air Transport of Plutonium

This section does not apply for the MFFP, since air transport is not claimed.

C2.9 Accident Conditions for Fissile Material Packages for Air Transport

This section does not apply for the MFFP, since air transport is not claimed.

C2.10 Special Form

This section does not apply for the MFFP, since special form is not claimed.

C2.11 Fuel Rods

This section does not apply for the MFFP, since containment by the fuel rod cladding is not claimed.

C2.12 Appendices

There are no appendices to Chapter C2.0. The applicability of the appendices to Chapter 2, *Structural Evaluation*, is given in Table C2.12-1.

Table C2.12-1 – Applicability of Section 2.12 Appendices to the AFS-C Payload

Appendix	Applicability
2.12.1, Impact Limiter Evaluation	As the weight of the AFS-C is bounded by the weight of a fuel assembly, the impact limiter evaluation from Section 2.12.1 remains bounding.
2.12.2, Certification Test Plan	Unchanged from Section 2.12.2
2.12.3, Certification Test Results	Unchanged from Section 2.12.3
2.12.4, Engineering Test Results	Unchanged from Section 2.12.4
2.12.5, Fuel Control Structural Evaluation	As the weight of the AFS-C is bounded by the weight of a fuel assembly, and because it is more structurally robust than a fuel assembly, the fuel control structural evaluation from Section 2.12.5 remains bounding.
2.12.6, CASKDROP Computer Program	Unchanged from Section 2.12.6
2.12.7, Impact Limiter Weld Joint Test Results	Unchanged from Section 2.12.7
2.12.8, Effect of Bounding Weight on Package Structural Responses	As the weight of the AFS-C is bounded by the weight of a fuel assembly, the package structural responses evaluation from Section 2.12.8 remains bounding.

This page left intentionally blank.

C3.0 THERMAL EVALUATION

C3.1 Description of Thermal Design

This section identifies and describes the principal thermal design aspects of the MOX Fresh Fuel Package (MFFP) for the transportation of the AFS-C rod container loaded with the Los Alamos Technical Area 18 (TA-18) MOX fuel rods. The results presented in this chapter demonstrate the thermal safety of the package and compliance with the thermal requirements of 10 CFR 71¹ and supports the addition of up to three (3) AFS-C rod containers containing TA-18 fuel rods as allowable contents of the MFFP.

The analysis demonstrates that the addition of the AFS-C rod container does not impact the packaging temperatures and that the temperatures reported in Chapter 3.0, *Thermal Evaluation*, remain bounding. However, the peak NCT and HAC fuel cladding temperatures estimated for the fuel rods in an AFS-C rod container are higher than the peak temperature computed for an intact MOX fuel assembly, largely due to the simplified method employed. Nevertheless, the maximum allowable fuel temperature limits are not approached. The internal pressure of the package under HAC is bounded by the pressure resulting from the transportation of three (3) intact MOX fuel assemblies.

C3.1.1 Design Features

The principal thermal design features of the MFFP are described in Section 3.1.1, *Design Features*, while the principal features of the AFS-C rod container are described in Section C1.2.3, *Contents of Packaging*.

C3.1.2 Content's Decay Heat

The payload for the MFFP under this amendment consists of up to three (3) AFS-C rod containers. Each AFS-C may transport up to 116 Exxon rods and 69 PNL rods. A decay heat loading of 80 watts per AFS-C is assumed for the purposes of this thermal evaluation. A mixed payload of Exxon and PNL TA-18 fuel rods assumes a maximum decay heat of 30 watts within the PNL rods, thus leaving a maximum allowable decay heat load of 50 watts for the Exxon rods. If the PNL fuel rod payload dissipates less than 30 watts, the allowable decay heat load in the Exxon fuel rods can be increased accordingly so long as the maximum decay heat within the AFS-C rod container is 80 watts or less. Transportation of Exxon fuel rods alone assumes a total decay heat load of 80 watts.

The decay heat is assumed to be evenly distributed over the active fuel length of each payload. The Exxon rods have a total length of approximately 77.3 inches and an active fuel length of 70 inches. The PNL rods have a total length of approximately 36.6 inches and an assumed active length of 28 inches.

¹ Title 10, Code of Federal Regulations, Part 71 (10 CFR 71), *Packaging and Transportation of Radioactive Material*, 01-01-06 Edition.

C3.1.3 Summary of Temperatures

The maximum temperatures for the MFFP Packaging under NCT and HAC are summarized in Table C3.1-1. The packaging temperatures are taken from Table 3.4-1 and Table 3.5-1, respectively. While these packaging temperatures are associated with the transportation of three (3) MOX fuel assemblies, they are bounding for the MFFP temperatures arising from the transportation of a payload consisting of up to three (3) AFS-C rod containers loaded with TA-18 fuel rods. Table C3.1-1 also presents the NCT and HAC temperatures for the AFS-C rod container and its payload of fuel rods. The peak temperature within the AFS-C rod container under NCT conditions is 240 °F (see Section C3.4, *Thermal Evaluation for Normal Conditions of Transport*), while the peak temperature achieved under HAC is predicted to be 631 °F (see Section C3.5, *Thermal Evaluation under Hypothetical Accident Conditions*).

C3.1.4 Summary of Maximum Pressures

The maximum normal operating pressure (MNOP) for the MFFP with the AFS-C rod container loaded with TA-18 fuel rods resulting from the NCT Hot condition and conservative assumptions is 2.8 psig. Further details of the pressure analysis are presented in Section C3.4.2, *Maximum Normal Operating Pressure*.

The maximum peak pressure generated within the package cavity under HAC is conservatively estimated assuming that the entire inventory of organic material within the strongback assembly is totally combusted/pyrolyzed. No organic material is used in the AFS-C rod container.

The maximum pressure under HAC is 121.4 psig (136.1 psia) at the end of the fire when the peak cavity gas temperature is reached. The pressure will then decrease as the package cools. Further details of the analysis are presented in Section C3.5.3, *Maximum Temperatures and Pressures*.

Table C3.1-1 –Summary of Temperatures for NCT and HAC (°F)

Item	Hot NCT	Peak HAC	Maximum Allowable		Minimum Temperature Margin ⁽¹⁾
			NCT	HAC	
Peak Exxon Fuel Rod	240	631	392	1,337	152
Peak PNL Fuel Rod	238	627	392	1,337	154
Peak AFS-C Container	191	607	1,100	1,100	493
Avg. AFS-C Container	182	601	-	-	NA
<i>Temperatures for MFFP Package from Table 3.4-1 and Table 3.5-1</i>					
<i>Strongback Structure</i>	<i>178</i>	599	<i>800</i>	800	<i>201</i>
<i>Body Shell</i>	159	<i>1,361</i>	800	<i>2,500</i>	<i>641</i>
<i>Body Collar</i>	<i>149</i>	414	<i>800</i>	1,000	<i>586</i>
<i>Closure Lid</i>	147	<i>301</i>	800	<i>1,000</i>	<i>653</i>
<i>Impact Limiter Lugs</i>	154	<i>1,282</i>	800	<i>2,500</i>	<i>646</i>
<i>Impact Limiter</i>					
• <i>Max. Foam</i>	<i>149</i>	<i>N/A</i>	300	<i>N/A</i>	<i>151</i>
• <i>Bulk Avg. Foam</i>	<i>145</i>	<i>N/A</i>	300	<i>N/A</i>	<i>155</i>
• <i>Skin</i>	149	<i>1,429</i>	800	<i>2,500</i>	<i>651</i>
<i>Impact Limiter Bolts</i>					
• <i>Bolt Head</i>	154	<i>1,283</i>	800	<i>2,500</i>	<i>646</i>
• <i>Bolt Shaft</i>	144	<i>1,006</i>	800	<i>2,500</i>	<i>656</i>
• <i>Bolt Threads</i>	144	<i>295</i>	800	<i>2,500</i>	<i>656</i>
<i>O-ring Seals</i>					
• <i>Closure Lid</i>	<i>159</i>	339	<i>225</i>	400	<i>61</i>
• <i>Vent/Sampling Port</i>	146	<i>295</i>	225	<i>400</i>	<i>79</i>

Note: (1) Minimum temperature margin based on **bold** temperatures.

This page left intentionally blank.

C3.2 Material Properties and Component Specifications

C3.2.1 Material Properties

The material specifications for the MFFP package are defined in Section 3.2.1, *Material Properties*. The AFS-C rod container is fabricated primarily of clear anodized 6061-T6 aluminum. For the purposes of this calculation the material properties of the aluminum is characterized by a single thermal conductivity point of 96 Btu/hr-ft-°F¹ with an emissivity of 0.76².

The TA-18 MOX fuel rods are assumed to have similar material properties and specifications as those defined for the standard MOX fuel assemblies.

C3.2.2 Component Specifications

In addition to the materials listed in Section 3.2.2, *Component Specifications*, the only material associated with the AFS-C rod container that is considered temperature sensitive is the aluminum. 6061 aluminum has a melting temperature point of approximately 1,100 °F¹.

No organic material is used in the AFS-C rod container. The characteristics of the organic material within the MFFP package are defined in Section 3.2.2, *Component Specifications*.

¹ American Society of Mechanical Engineers (ASME) Boiler and Pressure Vessel Code, Section II, *Materials, Part D – Properties*, 2001 Edition, with 2002 and 2003 Addenda, New York

² Gilmore, D. G., Editor, *Satellite Thermal Control Handbook*, The Aerospace Corporation Press, El Segundo, CA, 1994, pp A-8.

This page left intentionally blank.

C3.3 General Considerations

C3.3.1 Evaluations by Analysis

The MFFP with the AFS-C rod container loaded with TA-18 fuel rods is analytically evaluated in accordance with 10 CFR 71 and Regulatory Guide 7.8¹ for the bounding NCT and HAC thermal loads. Section 3.3.1, *Evaluation by Analysis*, summarizes the design basis conditions considered in these evaluations.

C3.3.1.1 NCT Analytical Model

The NCT analytical thermal model of the MFFP is based on the Thermal Desktop[®]² and SINDA/FLUINT³ computer programs. Details of these programs, together with a description of the thermal model for the MFFP, are described in Section 3.3.1.1, *NCT Analytical Model*. That analysis demonstrated that a significant thermal margin exists for all package components.

The AFS-C rod container has outer dimensions similar to a standard fuel assembly and interfaces with the strongback and clamp arms assembly of the MFFP in a similar manner. Further, the maximum heat dissipation is the same as that of a standard MOX fuel assembly. As such, the methodology used to evaluate the thermal performance of the AFS-C rod container loaded with TA-18 fuel rods within the MFFP is conservatively based on use of the maximum strongback temperature achieved for the transportation of the three (3) MOX fuel assemblies as a boundary condition for a 1-dimensional heat transfer analysis within the AFS-C rod container.

Figure C3.3-1 illustrates a cross-section through the portion of the AFS-C rod container loaded with 116 Exxon fuel rods, while Figure C3.3-2 illustrates the cross-section through the portion of the AFS-C loaded with 69 PNL fuel rods. The Exxon fuel rods are expected to be arranged in a consolidated bundle consisting of 8 layers of 14 to 15 rods each and the PNL fuel rods are expected to be arranged in 6 layers of 11 to 12 rods each. The temperature rise between the strongback and the center fuel rod in the consolidated bundle is computed using the 1-dimensional thermal model of the loaded AFS-C rod container illustrated in Figure C3.3-3.

Temperature of AFS-C rod container

The heat transfer between the AFS-C rod container and the strongback (i.e., c-to-h and g-to-h in Figure C3.3-3) is computed as a combination of radiation and conduction across an air gap based on the conservative assumption that the AFS-C container is centered within the fuel control structure (FCS) of the strongback assembly. Given the inside dimension for the FCS of 8.7-in, and an outside dimension of 8.4-in for the AFS-C container, the resulting uniform gap is 0.15-in. The heat transfer between the AFS-C container and the FCS is computed as:

¹ Regulatory Guide 7.8, *Load Combinations for the Structural Analysis of Shipping Casks for Radioactive Material*, Revision 1, U. S. Nuclear Regulatory Commission, March 1989.

² Thermal Desktop[®], Version 4.5, Cullimore & Ring Technologies, Inc., Littleton, CO, 2003.

³ SINDA/FLUINT, *Systems Improved Numerical Differencing Analyzer and Fluid Integrator*, Version 4.5, Cullimore & Ring Technologies, Inc., Littleton, CO, 2001.

$$q' = A \left[\frac{1}{(\epsilon_c^{-1} - 1) + \frac{1}{F_{c-h}} + (\epsilon_h^{-1} - 1)} \sigma (T_c^4 - T_h^4) + \frac{k}{x} (T_c - T_h) \right] \quad (\text{Eqn. 1})$$

where:

q' = heat transfer rate, Btu/hr

A = heat transfer area, in²

ϵ_c = emissivity of AFS-C rod container = 0.76

ϵ_h = emissivity of FCS surfaces = 0.20⁴

F_{c-h} = view factor between AFS-C container and FCS surfaces = 1.

σ = Stefan-Boltzmann constant = 1.190278×10^{-11} Btu/hr-in²-R⁴

T_c = temperature of AFS-C container, °R

T_h = temperature of FCS surfaces, = 178°F or 638°R at the NCT Hot condition⁵

k = thermal conductivity of air, Btu/hr-in²-R⁶

x = gap distance between AFS-C and FCS surfaces = 0.15-in

The temperature rise between the center shelf of the AFS-C container and the sidewalls (i.e., e-to-c in Figure C3.3-3) is insignificant due to the combination of the limited heat load and the use of aluminum. Even assuming all 80 watts of decay heat passed between the center shelf and the container sidewalls and that this heat load is limited to the 70-inch active fuel length of the Exxon fuel rods, the ΔT required to transfer this heat load is estimated via:

$$\Delta T = \frac{\text{Heat Load}}{\text{Area} \frac{\text{conductivity of aluminum}}{\text{average distance for heat to travel}}}$$

$$\Delta T = \frac{80 \text{ watts} \times 3.412 \text{ Btu/h/watt}}{(0.5 \text{ inches} \times 70 \text{ inches} \times 2 \text{ paths}) \frac{96/12 \text{ Btu/hr - inch - F}}{(8.4 \text{ inches}/4)}}$$

$$\Delta T = 1^\circ \text{F}$$

The ΔT required at the joint between the shelf and the container sidewalls (assuming all heat transfers via the intermittent welds) is estimated via:

$$\Delta T = \frac{80 \text{ watts} \times 3.412 \text{ Btu/h/watt}}{(0.125 \text{ inches} \times 7 \text{ inches} \times 70 \text{ inches}/15.3 \text{ inches} \times 2 \text{ paths}) \frac{96/12 \text{ Btu/hr - inch}}{(0.25 \text{ inches})}}$$

$$\Delta T = 1.1^\circ \text{F}$$

⁴ Section 3.2.1, *Material Properties*.

⁵ Table 3.4-1, *NCT Temperatures*

⁶ Table 3.2-6, *Properties of Air*

Finally, the temperature difference to distribute the heat from the joint with the center shelf equally over the sidewalls is estimated via:

$$\Delta T = \frac{80 \text{ watts} \times 3.412 \text{ Btu/watt}}{(0.75 \text{ inches} \times 70 \text{ inches} \times 4 \text{ paths}) \frac{96/12 \text{ Btu/hr} \cdot \text{inch}}{(8.4 \text{ inches}/4)}}$$

$$\Delta T = 0.34^\circ \text{F}$$

Therefore, the center shelf is conservatively predicted to be within 2.5°F of the sidewall temperatures. As such, the estimation of the temperature rise within the consolidated fuel bundle can be computed assuming uniform temperatures on all sides of the AFS-C container.

Temperature of outer edges of fuel bundle

The heat transfer between the AFS-C rod container and the consolidated fuel rod bundle (i.e., b-to-c, d-to-e, and f-to-g in Figure C3.3-3) is computed as a combination of radiation and conduction across an air gap based on the conservative assumption that the consolidated fuel bundle is centered within the AFS-C container. The inside dimension of the AFS-C container is 6.9 inches wide and 3.4-inches high and the height and average width of the Exxon fuel rod stack within the rod container (see Figure C3.3-1) is equal to:

$$\begin{aligned} \text{Height} &= \text{fuel rod diameter} \times (1 \text{ row} + 7 \text{ rows} \times \sin 60^\circ) \\ &= 0.451\text{-inches} \times (1 + 6.06) \\ &= 3.18\text{-inches} \end{aligned}$$

$$\begin{aligned} \text{Width} &= \text{fuel rod diameter} \times (14 \text{ rods} + 15 \text{ rods})/2. \\ &= 0.451\text{-inches} \times (14 + 15)/2. \\ &= 6.54\text{-inches} \end{aligned}$$

The height and average width of the PNL fuel rod stack within the rod container (see Figure C3.3-2) is equal to:

$$\begin{aligned} \text{Height} &= \text{fuel rod diameter} \times (1 \text{ row} + 5 \text{ rows} \times \sin 60^\circ) \\ &= 0.565\text{-inches} \times (1 + 4.33) \\ &= 3.01\text{-inches} \end{aligned}$$

$$\begin{aligned} \text{Width} &= \text{fuel rod diameter} \times (11 \text{ rods} + 12 \text{ rods})/2. \\ &= 0.565\text{-inches} \times (11 + 12)/2. \\ &= 6.50\text{-inches} \end{aligned}$$

Therefore, the average gap between the consolidated Exxon fuel rod bundle and the AFS-C rod container is $(3.4 \text{ inches} - 3.18 \text{ inches})/2 + 1/4$ of the rod diameter, or 0.22-inches on the top and bottom and $(6.9 \text{ inches} - 6.54 \text{ inches})/2 + 1/4$ of the rod diameter, or 0.29 -inches on the sides. The average gap on all sides is computed as $(6.9 \text{ inches} \times 0.22 \text{ inches} + 3.4 \text{ inches} \times 0.29 \text{ inches})/(6.9 \text{ inches} + 3.4 \text{ inches}) = 0.24\text{-inches}$. In a similar fashion, the average gap on all sides for the PNL consolidated fuel bundle is 0.34-inches.

The heat transfer between the AFS-C container and the outer edges of the consolidated fuel rod bundle is computed as:

$$q' = A \left[\frac{1}{(\epsilon_b^{-1} - 1) + \frac{1}{F_{b-c}} + (\epsilon_c^{-1} - 1)} \sigma (T_b^4 - T_c^4) + \frac{k}{x} (T_b - T_c) \right] \quad (\text{Eqn. 2})$$

where:

q' = heat transfer rate, Btu/hr

A = heat transfer area, in²

ϵ_c = emissivity of AFS-C rod container = 0.76

ϵ_b = emissivity of fuel rod surfaces = 0.20

F_{b-c} = view factor between fuel bundle edges and AFS-C container = 1.

σ = Stefan-Boltzmann constant = 1.190278×10^{-11} Btu/hr-in²-R⁴

T_c = temperature of AFS-C container, °R

T_b = avg. temperature of outer edges of fuel rod surfaces, °R

k = thermal conductivity of air, Btu/hr-in²-R

x = avg. gap distance between AFS-C and fuel rod surfaces

Temperature of hottest fuel rod

The heat transfer within the consolidated fuel bundle is computed by conservatively assuming the individual rods are separated by a finite distance from each of its neighbors and are not in direct contact. As such, the heat transfer between the rods is computed as radiation and conduction across the air gap separating the individual fuel rods. Since the ΔT across the width of the individual fuel rods is insignificant in comparison, it is ignored for the purposes of this calculation. Figure C3.3-4 illustrates the idealized configuration assumed for the fuel bundle for the purposes of estimating the temperature rise within it.

As idealized, the fuel bundle is treated as a series of concentric layers of fuel rods with the temperature in each layer being the same. With the exception of the center rod, the heat transfer via radiation from layer 'n-1' to layer 'n' for $n \geq 2$ is computed as:

$$q'_{\text{rad}} = \text{Area} \times \left[\frac{1}{(\epsilon_{n-1}^{-1} - 1) + \frac{1}{F_{n-1 \text{ to } n}} + \frac{\text{Area}_{n-1}}{\text{Area}_n} (\epsilon_n^{-1} - 1)} \sigma (T_{n-1}^4 - T_n^4) \right]$$

$$q'_{\text{rad}} = 2\pi \times r \times L \times 6(n-1) \times \left[\frac{1}{(0.2^{-1} - 1) + \frac{1}{F_{n-1 \text{ to } n}} + \frac{n-1}{n} (0.2^{-1} - 1)} \sigma (T_{n-1}^4 - T_n^4) \right] \quad (\text{Eqn. 3})$$

where:

q'_{rad} = radiation heat transfer rate fuel layer 'n-1' to layer 'n', Btu/hr

r = radius of fuel rod, = 0.2255-in for Exxon fuel and 0.2825-in for PNL fuel

L = active length of fuel rod = 70-in for Exxon fuel and 28-in for PNL fuel

n = number of the rod layer, with the center rod at $n = 0$

ϵ_{n-1} & ϵ_n = emissivity of fuel rod surfaces = 0.20

$F_{n-1 \text{ to } n}$ = view factor from fuel layer 'n-1' to layer 'n' = $(2n-1)/(6(n-1))$

σ = Stefan-Boltzmann constant = 1.190278×10^{-11} Btu/hr-in²-R⁴

T_{n-1} = temperature of fuel rods in layer 'n-1', °R

T_n = temperature of fuel rods in layer 'n', °R

For the radiation heat transfer from the center rod to the next layer (i.e., n=1), the heat transfer is computed as:

$$q'_{\text{rad}} = 2\pi \times r \times L \times \left[\frac{1}{(0.2^{-1} - 1) + \frac{1}{1} + \frac{1}{3}(0.2^{-1} - 1)} \sigma (T_0^4 - T_{n=1}^4) \right] \quad (\text{Eqn. 4})$$

Since no credit is taken for direct contact between the fuel rods, the conduction heat transfer between the rods will be via conduction across the intervening air gap. Each fuel rod will conductively exchange heat with six adjacent rods. Of these conduction points, $6(2n-1)$ will be between rods in layer 'n-1' to those in rod layer 'n'. The surface area associated with each conduction point is $2\pi \cdot r \cdot L/6$, while a conservative separation distance between the surfaces of $2 \cdot r \cdot (1 - \sin 60^\circ)$ is used. The conduction heat transfer from rod layer 'n-1' to layer 'n' for $n \geq 1$ is computed as:

$$q'_{\text{cond}} = \frac{2\pi \times r \times L/6 \times 6(2n-1) \times k \times (T_{n-1} - T_n)}{2 \times r \times (1 - \sin 60^\circ)}$$

$$q'_{\text{cond}} = \frac{\pi \times L \times (2n-1) \times k \times (T_{n-1} - T_n)}{(1 - \sin 60^\circ)} \quad (\text{Eqn. 5})$$

where:

q'_{cond} = conduction heat transfer rate fuel layer 'n-1' to layer 'n', Btu/hr

L = active length of fuel rod

n = number of the rod layer, with the center rod at $n = 0$

k = thermal conductivity of air, Btu/hr-in²-R

T_{n-1} = temperature of fuel rods in layer 'n-1', °R

T_n = temperature of fuel rods in layer 'n', °R

C3.3.1.2 HAC Analytical Model

The analytical thermal model of the MFFP with the AFS-C rod container loaded with TA-18 fuel rods under HAC uses the same methodology used for the NCT evaluation. Since the NCT methodology is based on steady-state conditions and it ignores the effects of thermal mass and transient heating, the predicted HAC temperatures are conservative. The peak strongback temperature presented in Section 3.5, *Thermal Evaluation under Hypothetical Accident Conditions*, is used as a steady-state boundary temperature for the 1-D thermal model of the AFS-C rod container described above.

C3.3.2 Evaluation by Test

This section is not applicable since evaluation by test was not performed for the MFFP with the AFS-C rod container loaded with TA-18 fuel rods.

C3.3.3 Margins of Safety

A summary of the maximum temperatures for the MFFP, with their respective temperature margins, for both NCT and HAC are provided in Table 3.3-3.

From Section C3.1.4, *Summary of Maximum Pressures*, the maximum normal operating pressure (MNOP) is 2.8 psig, which is bounded by the calculated MNOP of 2.9 psig for the standard payload of three (3) fuel assemblies. (Note that the reported MNOP for the package is 10 psig, which is obtained by rounding up the 2.9 psig value.) Therefore, the margin of safety (MS) for the 25-psig design pressure is:

$$MS = \frac{25}{2.8} - 1.0 = +7.9$$

From Section C3.1.4, *Summary of Maximum Pressures*, the maximum pressure for HAC is 121.4 psig. This pressure is bounded by the 123.5 psig pressure for the standard three (3) fuel assembly payload. Therefore, the MS of +2.15 reported in Section 3.3.3, *Margins of Safety*, is bounding.

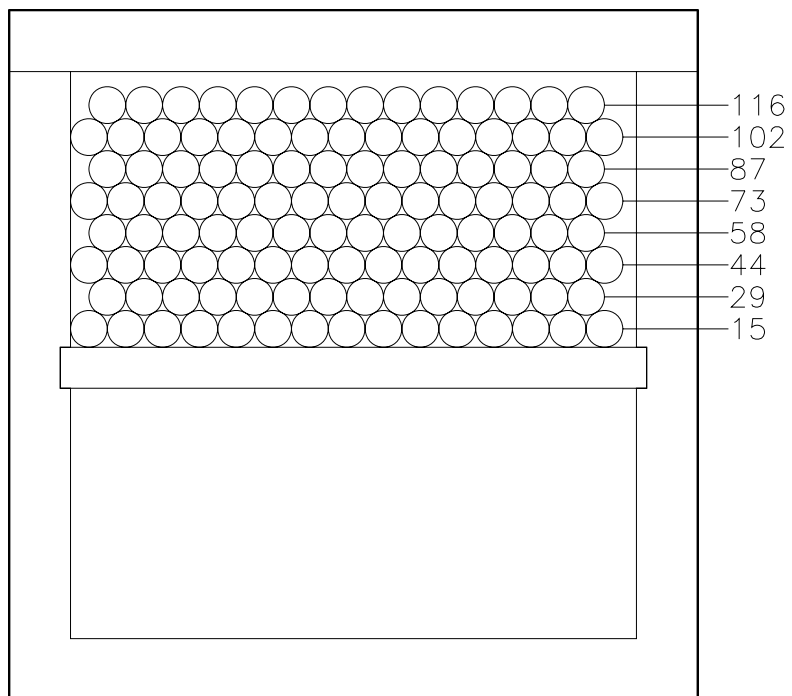


Figure C3.3-1 - Consolidated Exxon Fuel Rod Bundle within AFS-C Rod Container

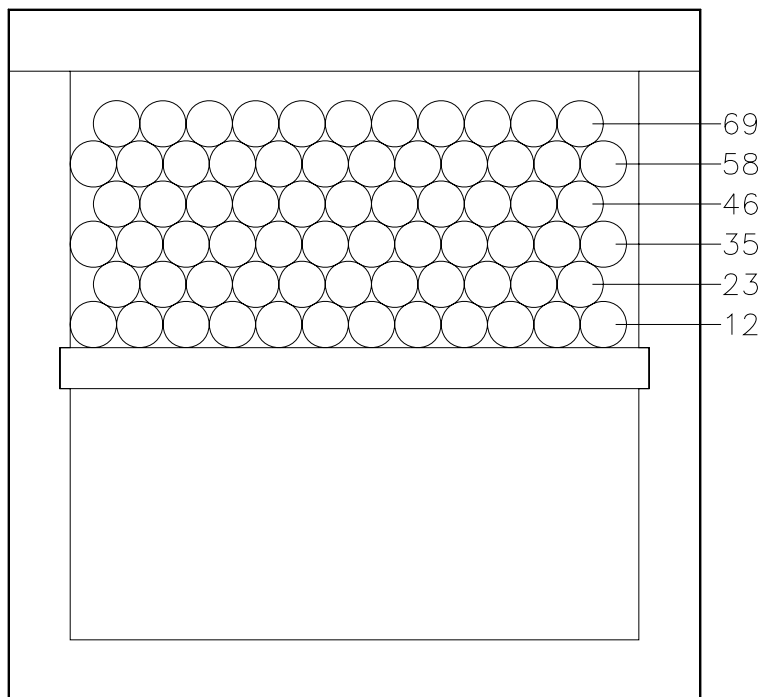
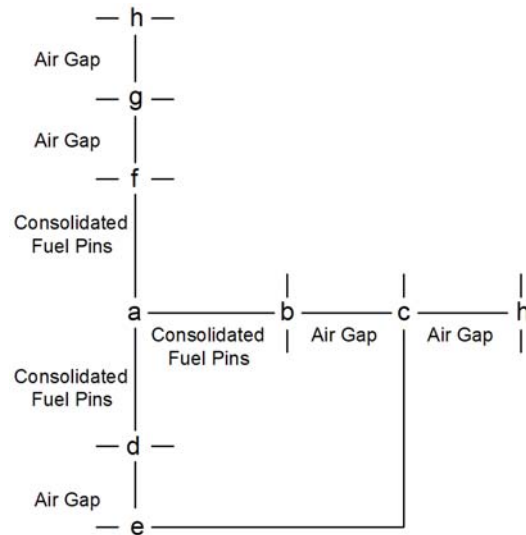


Figure C3.3-2 - Consolidated PNL Fuel Rod Bundle within AFS-C Rod Container



a = center of the consolidated fuel rod bundle
 b = side edge of the consolidated fuel rod bundle
 c = side of AFS-C rod container
 d = bottom side of the consolidate fuel rod bundle
 e = center shelf of AFS-C rod container
 f = top edge of the consolidated fuel rod bundle
 g = top of AFS-C rod container
 h = strongback assembly of MFFP Package

Figure C3.3-3 - 1-D Thermal Model of AFS-C Rod Box Container

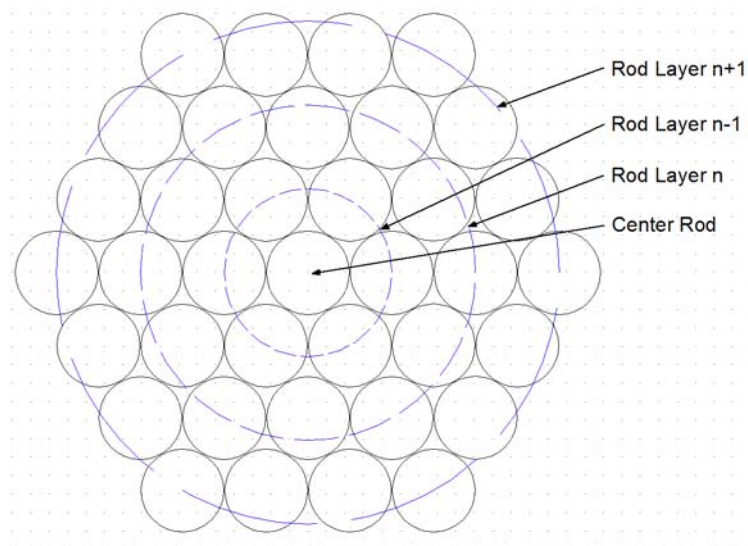


Figure C3.3-4 - Consolidated Fuel Rod Bundle Modeling

C3.4 Thermal Evaluation for Normal Conditions of Transport

C3.4.1 Heat and Cold

C3.4.1.1 Heat

The maximum temperatures for the AFS-C rod container loaded with TA-18 MOX fuel rods are determined assuming the peak temperature of 178 °F for the strongback assembly obtained from Section 3.4.1.1, *Heat*, for the NCT Hot condition. Since this temperature is associated with a decay heat loading of 240 watts, a similar strongback temperature will occur with the transport of up to three (3) AFS-C rod containers with the same total decay heat loading. While the TA-18 fuel rod payload may result in a higher heat flux on a per inch basis, the aluminum sidewalls and center shelf of the AFS-C container and the boral material in the strongback will effectively spread the heat load axially such that the local rise in the peak strongback temperature will be 3 °F or less. This conclusion is based on a sensitivity thermal analysis using the thermal model for the MFFP, described in Section 3.3.1.1, *NCT Analytical Model*. Given this relatively small temperature increase and since the sensitivity modeling does not include the axial spreading of the heat flux within the aluminum sidewalls of the AFS-C rod container, the use of the strongback temperature as a boundary condition for this calculation is an appropriate assumption for the purposes of this safety evaluation.

Based on the 1-dimensional thermal model described above and a decay heat load of 80 watts for the Exxon fuel rods, and an iterative solution of equation #1 from Section C3.3.1.1, *NCT Analytical Model*, the estimated peak sidewall temperature for the AFS-C rod container is 188°F for the section housing the Exxon TA-18 rods, while the average sidewall temperature is 182°F. Adding the 2.5°F ΔT determined in Section C3.3.1.1 for the temperature difference between the center shelf and the sidewall, yields a peak AFS-C temperature of 191°F for the NCT Hot condition.

Based on an iterative solution of equation #2 from Section C3.3.1.1, the temperature of the outer surface of the Exxon fuel bundle within the AFS-C rod container is predicted to be 209°F. The associated peak fuel rod temperature is computed by iterative solution of equations #3 to #5. Since the Exxon fuel bundle is 8 rod layers high and 14 to 15 rod layers wide, the peak temperature of the center fuel rod is conservatively predicted by assuming the fuel bundle extents 7 layers in all directions from the center rod. Based on this assumption, the associated peak fuel rod temperature within the AFS-C rod container under NCT Hot conditions is estimated to be 240°F.

Using the same modeling approach used for the Exxon fuel rods, but assuming a decay heat loading of 30 watts and an assumed active fuel length of 28 inches, the peak AFS-C rod container sidewall temperature for the section housing the PNL TA-18 fuel rods is determined to be 187°F, with a peak rod temperature of 238°F. In reality, the aluminum sidewalls of the AFS-C rod container will spread the decay heat in the axial direction, effectively lowering the decay heat loading per inch and resulting in lower temperature rises than those estimated above.

These predicted peak temperatures are bounding whether the other positions in the strongback are occupied by another AFS-C rod container or a dummy fuel assembly. Further, based on the

maximum temperature of 240 °F, none of the organic material within the strongback assembly will experience thermal decomposition and out-gassing under NCT conditions.

The results presented in Section 3.4.1.1, *Heat*, for the MFFP remain valid for the MFFP component temperatures associated with the transport of the AFS-C rod containers loaded with TA-18 fuel rods. Specifically, the closure seals and the impact limiter foam temperatures remain below their associated temperature limits. Additionally, the MFFP analysis demonstrated that the accessible package surfaces remain below 122 °F when transported in an ambient temperature of 100 °F and without insolation, as stipulated by 10 CFR §71.43(g).

C3.4.1.2 Cold

The minimum temperature distribution for the MFFP with the AFS-C rod containers occurs with a zero decay heat load and an ambient air temperature of -40 °F per 10 CFR §71.71(c)(2). The steady-state analysis of this condition represents a trivial analytical case that requires no thermal calculations be performed. Instead, it is assumed that all package components achieve the -40 °F temperature under steady-state conditions. The -40 °F temperature is within the allowable range of all of the packaging components. The package temperatures for the NCT Cold condition of -20 °F and no insolation are bounded by those presented in Section 3.4.1.2, *Cold*, for the MFFP.

C3.4.2 Maximum Normal Operating Pressure

The maximum normal operating pressure (MNOP) for NCT is based on an initial package backfill of air at atmospheric pressure at 70 °F (294 K) and an assumed failure rate of 3% of the TA-18 fuel rods. The heat up of the gases in package cavity is assumed to be the same as that determined for the transport of three (3) MOX fuel assemblies for the respective ambient condition. For the purpose of rod pressure determination, the only significant gas contributor is the initial gas backfill within the TA-18 fuel rods as no fission products will exist within the un-irradiated rods.

The bulk average gas temperature from Section 3.4.1.1, *Heat*, for the MFFP under the NCT Hot condition is used as the basis for the MNOP calculation with the AFS-C rod containers. Since the decay heat loading assumed for the MFFP is equal to the heat dissipation associated with the AFS-C rod containers loaded with TA-18 fuel rods, the associated bulk average gas temperature will also be similar. The package cavity has a gross free volume of approximately 105,547 in³, based on a package cavity OD of 28.5 inches and a length of 165.45 inches. The displacement volume for the strongback assembly is 11,292 in³ (see Section 3.4.2, *Maximum Normal Operating Pressure*). The solid volume for an unloaded AFS-C rod container is 4,694 in³ based on an approximate weight of 460 lbs and a density of 0.098 lbs/in³. The volume of 116 Exxon fuel rods is 1,432 in³ based on a rod diameter of 0.451-in. and a length of 77.26-in. and the volume of 69 PNL fuel rods is 633 in³ based on a rod diameter of 0.565-in. and a length of 36.6-in.

The solid volume for the dummy fuel assembly is approximately 5,366 in³. Since the dummy fuel assembly has a lower solid volume than a loaded AFS-C rod container and since it contains no fuel rods that could fail and release gas, the transport of three (3) AFS-C containers will bound the pressure generated for a payload containing a mix of AFS-C containers and dummy fuel assemblies.

The type and amount of fill gas within each TA-18 fuel rod is unknown. For the purposes of this safety evaluation, the gas quantities associated with the standard MOX fuel rod, as determined in

Section 3.4.2, *Maximum Normal Operating Pressure*, is conservatively used. Based on this assumption, the total gas volume within the maximum payload of 116 Exxon fuel rods and 69 PNL fuel rods is 4.49 g-moles.

The initial gas in the package cavity at the time of sealing is calculated as follows:

$$N_{\text{fill}} = \frac{1 \text{ atm} \times V_{\text{free}}}{R \times T_{\text{fill}}}$$

where:

- T_{fill} = temperature of air within package cavity at time of package closure
- R = Ideal gas constant (0.08206 atm-liter/gmole-°K)
- V_{free} = Package cavity free volume
= Gross cavity volume minus displacement volumes for the AFS-C rod container(s), the dummy fuel assembly(s), and the strongback
= 73,978 in³ (1,212 liters)

The MNOP is then calculated as follows:

$$\text{MNOP} = \frac{N_{\text{cask}} RT_{\text{NCT}}}{V_{\text{free}}}$$

$$N_{\text{cask}} = N_{\text{fill}} + \text{Rod Failure Rate} \times N_{\text{MOX fill gas}} + N_{\text{outgassing}}$$

where:

- N_{cask} = total moles of gas in package cavity
- N_{fill} = moles air within package cavity at time of package closure
- Rod Failure Rate = assumed percentage of failed rods. A 3% failure rate, which matches the regulatory failure rate for normal conditions of transport of spent fuel assemblies, will bound the expected failure rate for fresh fuel.
- $N_{\text{MOX fill gas}}$ = moles of rod fill gas within package cavity
- $N_{\text{outgassing}}$ = moles gas generated by out-gassing from component material in cask cavity
- T_{NCT} = Bulk average gas temperature within package (K) at the specific condition
= 166°F or 347 K¹

Based on the above relationships and assumptions, the MNOP for the bounding payload combination of three (3) AFS-C rod container loaded with 116 Exxon fuel rods and 69 PNL fuel

¹ Table 3.4-1, *NCT Temperatures*

rods is 17.5 psia (2.8 psig). A significant margin exists between this calculated MNOP and the package's NCT design pressure limit of 39.7 psia (25 psig).

No hydrogen or other combustible gases will be generated as result of the thermal or radiation-induced decomposition of the organic material within the package. This conclusion is based on the low peak temperature achieved under NCT transport conditions and the low radioactivity associated with the un-irradiated MOX fuel rods.

C3.4.3 Maximum Thermal Stresses

The maximum thermal stresses for NCT are bounded by those determined for the MFFP with the MOX fuel assembly payload. See the discussion in Section 2.6.1, *Heat*, and Section 2.6.2, *Cold*.

C3.4.4 Evaluation of Package Performance for Normal Conditions of Transport

The steady-state thermal analysis presented in Section 3.4, *Thermal Evaluation for Normal Conditions of Transport*, demonstrated that the components of the MFFP with the MOX fuel assembly payload are within their respective allowable temperature limits. That evaluation is valid and bounding for the MFFP with the AFS-C rod containers loaded with TA-18 MOX fuel rods. The MNOP resulting from the NCT Hot condition and conservative assumptions is within the maximum design pressure limit of the package.

Therefore, the MFFP with the AFS-C rod container is found to comply with all of the thermal requirements specified in 10 CFR §71.71.

C3.5 Thermal Evaluation under Hypothetical Accident Conditions

This section presents the results of the thermal evaluation of the MFFP with the AFS-C rod container loaded with TA-18 fuel rods under the hypothetical accident conditions (HAC) specified in 10 CFR §71.73(c)(4)¹.

C3.5.1 Initial Conditions

The initial conditions assumed for the MFFP are presented in Section 3.5, *Thermal Evaluation under Hypothetical Accident Conditions*. Due to its robust design, no significant damage is assumed to have occurred to the AFS-C rod container(s) and dummy fuel assemblies as a result of the drop events that precede the HAC fire event. Even if damaged, the integrity of these components are not important to the thermal safety of the MFFP package.

C3.5.2 Fire Test Conditions

No fire tests were performed for the MFFP with the AFS-C rod container loaded with TA-18 fuel rods.

C3.5.2.1 Analytical Model

The analytical model of the MFFP under HAC is described in Section 3.5.2.1, *Analytical Model*, and Section 3.5.2.2, *Performance of Rigid Polyurethane Foam Under HAC Fire Conditions*. The peak temperature for the AFS-C rod container loaded with TA-18 fuel rods under HAC is estimated using the methodology and 1-dimensional thermal model of the AFS-C rod container described in Section C3.3.1.1, *NCT Analytical Model*.

C3.5.3 Maximum Temperatures and Pressures

C3.5.3.1 Maximum Temperatures

The maximum temperatures attained in the MFFP components under HAC with the AFS-C rod container and TA-18 fuel rods are bounded by those presented in Section 3.5.3.1, *Maximum Temperatures*. The peak strongback assembly temperature predicted from the evaluation of the MFFP is 599 °F and the transient analysis demonstrates that the peak temperature condition lasts for less than 15 minutes.

Based on a decay heat load of 80 watts for the maximum payload configuration of 116 Exxon fuel rods and an iterative solution of equation #1 from Section C3.3.1.1, the peak sidewall temperature for the AFS-C rod container under HAC conditions is 604°F, while the peak center shelf temperature is 607°F. In a similar fashion, based on equation #2 from Section C3.3.1.1, the peak temperature on the outer surface of the fuel bundle is predicted to be 613°F.

The associated peak fuel rod temperature is computed by iterative solution of equations #3 to #5 in the same manner as it was under NCT conditions. The peak Exxon fuel rod temperature is

¹ Title 10, Code of Federal Regulations, Part 71 (10 CFR 71), *Packaging and Transportation of Radioactive Material*, 01-01-06 Edition.

computed to be 631°F, while the peak PNL fuel rod temperature is 627°F. These temperature levels are within the short-term thermal limits for the fuel rods and all metallic components of the AFS-C rod container.

Although both the peak temperature and the duration of the elevated temperatures within the package are seen as insufficient to cause serious thermal decomposition of the organic material within the strongback, it is conservatively assumed that the organic material on the strongback assembly fully decomposes to the extent that the available oxygen permits.

C3.5.3.2 Maximum Pressures

With the exception of the consideration for potential out-gassing from organic components within the package cavity and an assumed 100% failure rate for the fuel rods, the maximum pressure attained under HAC is determined in the same manner as described in Section C3.4.2, *Maximum Normal Operating Pressure*. While the MFFP is designed to protect the enclosed fuel rods from catastrophic failure during the pre-fire free and puncture bar drops and the subsequent 30-minute fire event, this analysis conservatively assumes that the cladding on all fuel rods have breached. As stated in Section C3.4.2, *Maximum Normal Operating Pressure*, the maximum amount of fill gas contained within an AFS-C rod container loaded with TA-18 fuel rods is conservatively estimated to be 4.49 g-moles. No significant change in the package cavity free volume is expected as a result of the HAC drop event.

Per Section 3.5.3.2, *Maximum Pressures*, approximately 7 pounds of neoprene rubber (C_4H_5Cl)_n and 2.3 pounds of Delrin[®] plastic ($C_6H_{14}O_2$)_n are used in the strongback assembly. The breakdown of these organic materials under HAC is limited by the facts that a limited amount of oxygen exists in the cask cavity and the peak cavity temperature and its duration under HAC are too low to permit complete pyrolysis (i.e., the process of breaking up a substance into other molecules as a result of heating in an inert atmosphere). For this evaluation, it is assumed that 75% of the oxygen is consumed generating carbon monoxide and only 25% is used in the generation of carbon dioxide gas. A larger ratio of carbon dioxide generation will result in a lower cask pressure. Under this conservative assumption, volatilizing the entire mass of neoprene rubber and Delrin[®] plastic would generate approximately 136.6 g-moles of additional gas within the cavity.

The peak pressure generated within the package cavity is estimated to be 136.1 psia (121.4 psig) at the end of the 30 minute fire event when the peak cavity gas temperature is reached. This pressure is bounded by the pressure from a payload of three fuel assemblies (138.2 psia). The pressure will then decrease as the package cools. The predicted peak pressure is considered to have a high degree of conservatism since there is insufficient oxygen within the package cavity to permit the full decomposition of the organic material and because both the relatively low peak temperature and the relatively short duration of the elevated temperatures will prevent any significant decomposition from occurring in the absence of active combustion of the material. It is expected that a majority of the organic material will remain in its original, solid form.

C3.5.4 Accident Conditions for Fissile Material Packages for Air Transport

This section does not apply for the MFFP since air transport will not be utilized.

C3.5.5 Evaluation of Package Performance for Accident Conditions of Transport

The evaluation of the MFFP with the AFS-C rod container loaded with TA-18 fuel rods under HAC demonstrates that the packaging has sufficient thermal protection remaining after the hypothetical drop and puncture bar damage to protect the thermally sensitive areas of the packaging. All package components are seen as remaining within their associated maximum temperature limits.

This page left intentionally blank.

PEAK EXXON & PNL ROD TEMPERATURES

NCT Conditions - Exxon Fuel

From Rod Layer	To Rod Layer	Inch Rod Dia.	Inch Rod Length	Btu/hr-in-F Air-k @ 220F	Rod emiss	Watt Rod Power	Watt Total Power	Inner Rod T F	Outer Rod T F	Watt Qrad	Watt Qconv	Watt Qtotal
6	7	0.451	70	0.00152	0.2	0.690	87.59	217.4	209.4	11.918	87.800	87.800
5	6	0.451	70	0.00152	0.2	0.690	62.76	224.2	217.4	8.842	54.577	63.419
4	5	0.451	70	0.00152	0.2	0.690	42.07	229.7	224.2	5.994	36.117	42.111
3	4	0.451	70	0.00152	0.2	0.690	25.52	234	229.7	3.701	21.962	25.663
2	3	0.451	70	0.00152	0.2	0.690	13.10	237.1	234	1.908	11.309	13.217
1	2	0.451	70	0.00152	0.2	0.690	4.83	239	237.1	0.670	4.159	4.829
0	1	0.451	70	0.00152	0.2	0.690	0.69	239.9	239	0.064	0.657	0.721

HAC Conditions - Exxon Fuel

From Rod Layer	To Rod Layer	Inch Rod Dia.	Inch Rod Length	Btu/hr-in-F Air-k @ 600F	Rod emiss	Watt Rod Power	Watt Total Power	Inner Rod T F	Outer Rod T F	Watt Qrad	Watt Qconv	Watt Qtotal
6	7	0.451	70	0.00216	0.2	0.690	87.59	617.7	613.2	27.322	60.742	88.064
5	6	0.451	70	0.00216	0.2	0.690	62.76	621.5	617.7	19.715	43.402	63.117
4	5	0.451	70	0.00216	0.2	0.690	42.07	624.6	621.5	13.246	28.989	42.215
3	4	0.451	70	0.00216	0.2	0.690	25.52	627	624.6	7.989	17.444	25.433
2	3	0.451	70	0.00216	0.2	0.690	13.10	628.8	627	4.241	9.345	13.586
1	2	0.451	70	0.00216	0.2	0.690	4.83	629.9	628.8	1.475	3.426	4.901
0	1	0.451	70	0.00216	0.2	0.690	0.69	630.5	629.9	0.161	0.623	0.784

NCT Conditions - PNL Fuel

From Rod Layer	To Rod Layer	Inch Rod Dia.	Inch Rod Length	Btu/hr-in-F Air-k @ 200F	Rod emiss	Watt Rod Power	Watt Total Power	Inner Rod T F	Outer Rod T F	Watt Qrad	Watt Qconv	Watt Qtotal
4	5	0.565	28	0.00148	0.2	0.435	26.52	221.8	213.2	4.505	22.093	26.598
3	4	0.565	28	0.00148	0.2	0.435	16.09	228.5	221.8	2.807	13.387	16.194
2	3	0.565	28	0.00148	0.2	0.435	8.26	233.3	228.5	1.451	6.951	8.302
1	2	0.565	28	0.00148	0.2	0.435	3.04	236.3	233.3	0.523	2.569	3.092
0	1	0.565	28	0.00148	0.2	0.435	0.43	237.7	236.3	0.049	0.400	0.449

HAC Conditions - PNL Fuel

From Rod Layer	To Rod Layer	Inch Rod Dia.	Inch Rod Length	Btu/hr-in-F Air-k @ 600F	Rod emiss	Watt Rod Power	Watt Total Power	Inner Rod T F	Outer Rod T F	Watt Qrad	Watt Qconv	Watt Qtotal
4	5	0.565	28	0.00216	0.2	0.435	26.52	618.3	613.7	9.658	17.195	26.853
3	4	0.565	28	0.00216	0.2	0.435	16.09	621.9	618.3	5.911	10.466	16.377
2	3	0.565	28	0.00216	0.2	0.435	8.26	624.5	621.9	3.030	5.399	8.430
1	2	0.565	28	0.00216	0.2	0.435	3.04	626.1	624.5	1.063	1.994	3.056
0	1	0.565	28	0.00216	0.2	0.435	0.43	626.9	626.1	0.107	0.332	0.439

Temperature Legend

- user input temperature
- temperature linked to other cells on spreadsheet
- temperature obtained from AFS-to-FCS worksheet

C4.0 CONTAINMENT

The AFS-C does not provide containment. Therefore, package containment is unchanged from the description provided in Chapter 4.0, *Containment*.

This page left intentionally blank.

C5.0 SHIELDING EVALUATION

The compliance of the MFFP with respect to the dose rate limits established by 10 CFR §71.47¹ for normal conditions of transport (NCT) or 10 CFR §71.51(a)(2) for hypothetical accident conditions (HAC) are satisfied when limiting the MFFP package to three (3) AFS-C rod containers, each containing up to 116 Exxon rods and 69 PNL rods having an average radioisotope content listed in Table C1.2-2.

Under these conditions, the maximum surface dose rate will be less than the limit of 200 mrem/hr for NCT and verified by measurement. This dose rate limit is for payload packages prior to addition of any lead, steel or other shielding material for *as-low-as-reasonably-achievable* (ALARA) dose reduction purposes during non-transport handling operations.

Prior to transport, the MFFP package shall be monitored for both gamma and neutron radiation to demonstrate compliance with 10 CFR §71.47. As noted in Section 2.6.7, *Free Drop*, the MFFP package is not significantly deformed under NCT free drop conditions. Therefore, the package will meet the dose rate limits for NCT if the measurements demonstrate compliance with the allowable dose rate levels in 10 CFR §71.47 (200 mrem/hr). The transport index, as defined in 10 CFR §71.4, will be determined by measuring the dose rate a distance of one meter from the package surface per the requirements of 49 CFR §173.403².

Shielding materials are not specifically provided by the MFFP package, and none are permitted within the package to meet the dose rate limits of 10 CFR §71.47 for NCT. Because significant fuel deformation or package deformation does not occur under HAC, the HAC surface dose rates and 1-meter dose rates will not be significantly different from the NCT dose rates. This result ensures that the post-HAC, allowable dose rate of 1 rem/hr a distance of one meter from the package surface per 10 CFR §71.51(a)(2) will be met because the surface dose rate will remain below the 200 mrem/hr limit.

¹ Title 10, Code of Federal Regulations, Part 71 (10 CFR 71), *Packaging and Transportation of Radioactive Material*, 01-01-06 Edition.

² Title 49, Code of Federal Regulations, Part 173 (49 CFR 173), *Shippers - General Requirements for Shipments and Packagings*, 10-01-06 Edition.

This page left intentionally blank.

C6.0 CRITICALITY EVALUATION

The following analyses demonstrate that the MFFP complies with the requirements of 10 CFR §71.55¹ and §71.59. The analyses presented herein demonstrate that the criticality requirements are satisfied when three AFS-C rod containers, each containing up to 116 Exxon rods and up to 69 PNL rods, are transported in an MFFP.

C6.1 Description of Criticality Design

C6.1.1 Design Features Important for Criticality

The AFS-C is conservatively ignored in this criticality analysis. However, as noted in Section C2.0, *Structural Evaluation*, the AFS-C sufficiently protects the fuel rods so that rod breach damage to the fuel rods will not occur. Therefore, there are no specific design features of the AFS-C important for criticality. The design features of the MFFP important to criticality are discussed in Section 6.1.1, *Design Features Important for Criticality*.

C6.1.2 Summary Table of Criticality Evaluation

The results of the criticality calculations are summarized in Table C6.1-1. The maximum calculated k_s (i.e., $k_{eff} + 2\sigma$) for each condition is compared to the upper subcritical limit (USL) of 0.9288. The maximum calculated k_s values are below the USL.

Note that the results in Table C6.1-1 are artificially high because no credit is taken for the AFS-C, allowing the fuel rods to arrange in the most reactive pitch. In actuality, if the analysis were repeated taking credit for the AFS-C, the reactivity would drop considerably because there is very little space available inside the AFS-C for moderation, as all available void space is filled with dunnage rods.

¹ Title 10, Code of Federal Regulations, Part 71 (10 CFR 71), *Packaging and Transportation of Radioactive Material*, 01-01-06 Edition.

Table C6.1-1 – Summary of Criticality Analysis Results

Normal Conditions of Transport (NCT)			
Case	k_{eff}	σ	k_s
Single Unit Maximum k_s	0.2383	0.0006	0.2396
Infinite Array Maximum k_s	0.4899	0.0005	0.4910
Hypothetical Accident Conditions (HAC)			
Case	k_{eff}	σ	k_s
Single Unit Maximum k_s	0.8929	0.0010	0.8948
Infinite Array Maximum k_s	0.8972	0.0010	0.8991
USL	0.9288		

C6.1.3 Criticality Safety Index

An infinite number of MFFPs are evaluated in a close-packed hexagonal array. Therefore, “N” is infinite, and in accordance with 10 CFR §71.59 the criticality safety index (CSI) is $50/N = 0$.

C6.2 Fissile Material Contents

The contents are three AFS-C rod containers, each containing up to 116 Exxon rods and up to 69 PNL rods. Physical data for the two rod types are summarized in Table C6.2-1. Because MCNP utilizes metric inputs but the drawings are in English units, both English and metric values for dimensional information are provided in this table.

The Exxon rods are well characterized. However, known data for the PNL rods are limited to rod OD, rod length, average plutonium mass, and average plutonium isotopics. No records are available for a number of other PNL rod characteristics, such as pellet OD, active fuel height, and maximum plutonium mass. When a PNL rod characterization value is not known, parametric criticality runs are performed for a range of reasonable values (the parametric analysis is discussed in Section C6.4.1.2.2, *HAC Single Package: PNL Rods Only*). The “assumed” PNL values reported in Table C6.2-1 are consistent with the most reactive case of this parametric analysis and are considered bounding.

The payload cavity of an MFFP can accommodate one triangular strongback assembly containing up to three AFS-C rod containers. The number of rods that may fit within each AFS-C has been determined based on the AFS-C cavity cross sectional area of 3.4-in x 6.9-in and the outer diameter of the fuel rods (provided in Table C6.2-1). The AFS-C may fit 116 Exxon rods (4 layers of 15 rods and 4 layers of 14 rods) and 69 PNL rods (3 layers of 12 rods and 3 layers of 11 rods) in a tightly-packed arrangement. The AFS-C contains separate compartments for Exxon and PNL rods. If less than the maximum number of rods is placed in an AFS-C, the excess planar volume is filled with stainless steel or aluminum dunnage rods. Note that neither the AFS-C nor dunnage rods are required for criticality control, although the presence of these items protects the rods from cladding breach in an accident.

The average isotopic composition of each rod type as of 1980 is reported in Table C6.2-2. However, the isotopic composition varies within the rods of each type. The isotopic composition and plutonium mass is known for each of the Exxon rods, although similar information for the PNL rods is not available. The isotopics selected for analysis bound the known isotopics of the Exxon rods by maximizing Pu-241 wt. %, minimizing Pu-240 wt. %, and setting the balance wt. % to be Pu-239. This assumption is highly conservative because no credit is taken for the decay of Pu-241, which has undergone nearly two half-lives of decay since 1980. The average PNL isotopics are similar to the average Exxon isotopics, so it may be inferred that this isotopic set is also bounding for the PNL rods.

Cladding for both rod types is modeled as pure zirconium, and both rod types utilize natural uranium in the fuel matrix. To be consistent with the MOX fuel assembly analysis in Chapter 6.0, *Criticality Evaluation*, it is assumed that the effective pellet density for each rod type is 10.85 g/cm³. The 10.85 g/cm³ density is very high and represents 100% theoretically dense MOX pellet material smeared over the pellet gaps and dish/chamfers.

The mass of Pu per rod drives the system reactivity and is modeled precisely, while the mass of natural uranium modeled in each fuel rod has a negligible effect on the reactivity and is selected to maintain an effective pellet density of 10.85 g/cm³. In most of the MCNP models, 60 g of Pu is modeled in the Exxon rods, and 40 g of Pu is modeled in the PNL rods. The maximum measured Pu mass in any Exxon rod is 60 g, while the 40 g Pu assumed for the PNL rods is chosen to

reasonably bound the average PNL value of 37.4 g Pu. After the criticality analysis was complete, it was decided to add additional conservatism by increasing the mass of Pu in each fuel rod. Rather than repeat the entire analysis, only the most reactive cases are run with 65 g Pu for the Exxon rods (a 5 g increase in Pu) and 42 g Pu in the PNL rods (a 2 g increase in Pu). For this reason, the data in Table C6.2-3 is presented for all the Pu masses utilized, and the columns marked “bounding” resulted in the highest reactivity.

Fuel pellet composition is input to MCNP as a weight percent for each isotope of interest. The Pu mass and effective pellet density (10.85 g/cm^3) are set as fixed quantities and uranium oxide is added as needed to obtain the desired density. Therefore, the mass of uranium is not conserved when comparing Exxon1 to Exxon2, or comparing PNL1, PNL2, PNL3, and PNL4, because conserving the mass of uranium would result in non-physical pellet densities. However, the bounding rod descriptions utilize maximum fissile masses, as shown in Table C6.2-3.

As the Exxon rods are well defined, only one set of dimensional inputs is required for this rod type. However, parametric studies are performed on the PNL rod active fuel length and pellet diameter because these quantities are not well defined, which causes the material specifications to vary in order to maintain the target Pu mass. All of the various PNL rod permutations are included in Table C6.2-3.

Note that the Pu/(Pu+U) values given in Table C6.2-3 are artificially selected to give the target density of 10.85 g/cm^3 and will not correspond precisely to the true values. Therefore, these values should not be considered limits. This approach is different than the MOX fuel assembly analysis in Chapter 6.0, *Criticality Evaluation*, for which a maximum Pu/(Pu+U) = 6.0% is stipulated, but a maximum plutonium mass per assembly is not explicitly treated as a limit.

Two values are selected for the PNL rod active fuel length, 36” and 28”. The 36” value represents almost no plenum, while the 28” value represents a plenum length comparable in size to the Exxon rod plenum length. Two different PNL pellet diameters are also investigated, 0.4856” and 0.5135”. The smaller pellet diameter is computed assuming that the Exxon and PNL rods have the same cladding and gap thickness: $0.4856'' = 0.565'' - (0.451'' - 0.3716'')$. The larger pellet diameter is computed assuming that the MFFP and PNL rods have the same cladding and gap thickness: $0.5135'' = 0.565'' - (0.374'' - 0.3225'')$. The MOX fuel rod data (rod OD = 0.374” and pellet OD = 0.3225”) are obtained from Table 6.2-2 and Table 6.2-3, respectively.

Table C6.2-1 – Fuel Rod Data

Parameter	Exxon		PNL	
	English Value	Metric Value	English Value	Metric Value
Cladding Material	Zircaloy-2		Zircaloy-2	
Overall Length	77.26 in	196.24 cm	36.6 in	92.96 cm
Active Fuel Length	70 in	177.8 cm	28 in (assumed)	71.12 cm (assumed)
Cladding OD	0.451 in	1.1455 cm	0.565 in	1.4351 cm
Cladding ID	0.381 in	0.9677 cm	0.520 in (assumed)	1.3208 cm (assumed)
Pellet OD	0.3716 in	0.9439 cm	0.5135 in (assumed)	1.3043 cm (assumed)
Effective Pellet Density	--	10.85 g/cm ³ (assumed)	--	10.85 g/cm ³ (assumed)
Pu mass (average)	--	58.3 g	--	37.4 g
Pu mass (maximum)	--	65 g (assumed)	--	42 g (assumed)

Table C6.2-2 – Fuel Rod Isotopics

Isotope	Exxon wt. % (1980 average)	PNL wt. % (1980 average)	MCNP wt. %
U-235	0.71	0.71	0.71
U-238	99.29	99.29	99.29
Total U	100	100	100
Pu-238	0.745	0.28	0
Pu-239	75.13	75.38	79.5
Pu-240	17.26	18.10	14
Pu-241	5.23	5.08	6.5
Pu-242	1.55	1.15	0
Total Pu	100	100	100

Table C6.2-3 – MCNP Fuel Rod Compositions Utilized

Isotope	Exxon1	Exxon2 (bounding)	PNL1	PNL2	PNL3	PNL4 (bounding)
Density (g/cm ³)	10.85	10.85	10.85	10.85	10.85	10.85
Active Fuel Height (in)	70	70	36	28	28	28
Pellet OD (in)	0.3716	0.3716	0.4856	0.4856	0.5135	0.5135
Pu mass (g)	60	65	40	40	40	42
Pu/(Pu+U)	5.041%	5.462%	3.829%	4.920%	4.400%	4.620%
U-235	0.594%	0.592%	0.602%	0.595%	0.598%	0.597%
U-238	83.115%	82.746%	84.175%	83.220%	83.675%	83.483%
Pu-239	3.533%	3.828%	2.683%	3.448%	3.084%	3.238%
Pu-240	0.622%	0.674%	0.473%	0.607%	0.543%	0.570%
Pu-241	0.289%	0.313%	0.219%	0.282%	0.252%	0.265%
O	11.847%	11.847%	11.848%	11.847%	11.848%	11.848%
Total	100%	100%	100%	100%	100%	100%
U-235 (g)	8.0	8.0	7.1	5.5	6.2	6.2
U-238 (g)	1121.9	1116.9	997.8	767.3	862.7	860.7
Pu-239 (g)	47.7	51.7	31.8	31.8	31.8	33.4
Pu-240 (g)	8.4	9.1	5.6	5.6	5.6	5.9
Pu-241 (g)	3.9	4.2	2.6	2.6	2.6	2.7
O (g)	159.9	159.9	140.5	109.2	122.2	122.1
Fissile (U235+Pu239+ Pu241) (g)	59.6	63.9	41.5	39.9	40.6	42.3

Note: The Pu/(Pu+U) values are not limiting values.

C6.3 General Considerations

Criticality calculations for the MFFP are performed using the three-dimensional Monte Carlo computer code MCNP5¹.

C6.3.1 Model Configuration

C6.3.1.1 Contents Model

The AFS-C and dunnage rods are not modeled in the criticality evaluation. Because the AFS-C is not modeled, the fuel rods are assumed to arrange themselves in the most reactive configuration within the cavity formed between the strongback and FCS. Models are developed for three scenarios: (1) only Exxon rods, (2) only PNL rods, and (3) with both rod types combined. To maintain model symmetry, a variety of regular square arrangements are modeled for the Exxon rods, including 11x11, 10x10, 9x9, and 8x8. For the PNL rods, 9x9, 8x8, and 7x7 arrangements are considered. (Note that the Exxon 11x11 arrangement (121 rods) is not physically possible due to the 116 rod limit of the AFS-C cavity, and the PNL 9x9 arrangement (81 rods) is not possible due to the 69 rod limit of the AFS-C cavity.) A limited number of non-regular pitch cases are also developed.

Stainless steel or aluminum dunnage rods are used in the AFS-C to prevent lateral movement of the fuel rods. These dunnage rods are ignored in the criticality models.

The rod arrangements of the contents represents an extremely conservative and incredible arrangement, as the AFS-C, even if damaged in an accident, would displace a large volume and would not allow the rod arrangements assumed in this analysis.

C6.3.1.2 Packaging Model

The packaging model is unchanged from the description provided in Section 6.3.1.2, *Packaging Model*.

C6.3.2 Material Properties

The material properties are unchanged from the descriptions provided in Section 6.3.2, *Material Properties*.

C6.3.3 Computer Codes and Cross-Section Libraries

The computer codes and cross section libraries are unchanged from the descriptions provided in Section 6.3.3, *Computer Codes and Cross-Section Libraries*.

¹ MCNP5, "MCNP – A General Monte Carlo N-Particle Transport Code, Version 5; Volume II: User's Guide," LA-CP-03-0245, Los Alamos National Laboratory, April, 2003.

C6.3.4 Demonstration of Maximum Reactivity

Reactivity of the NCT cases is negligible. The most reactive single package model is for the HAC Case G13 (see Table C6.4-7). The parameters of the most reactive single package model are:

- 11x11 array of Exxon rods (lower layer) and 9x9 array of PNL rods (upper layer) in each AFS-C.
- 65 g Pu per Exxon rod, and 42 g Pu per PNL rod.
- Fully moderated with water, including the pellet to cladding gap.
- Steel reflection, which bounds reflection by water.
- Miscellaneous minor steel components in the package are homogenized into the water region inside the package.

The most reactive HAC array model (Case J12, see Table C6.6-1) uses the most reactive HAC single package model as a base case. Properties of the most reactive HAC array model are:

- Infinite hexagonal reflection.
- Low density (0.1 g/cm^3) water between packages (note that this result is statistically equivalent to modeling void between packages).

C6.4 Single Package Evaluation

Compliance with the requirements of 10 CFR §71.55 is demonstrated by analyzing an optimally moderated single-unit MFFP. The figures and descriptions provided in Section 6.3.1, *Model Configuration*, describe the basic geometry of the single-unit models, although the contents are different.

C6.4.1 Single Package Configuration

C6.4.1.1 NCT Configuration

Under NCT conditions, the internals of the package are assumed to be dry. In the absence of internal moderation, reactivity will be a maximum for the maximum fuel mass. It has been established that the AFS-C will not contain more than 116 Exxon rods and 69 PNL rods. The total number of rods is conservatively bounded by assuming an 11x11 array of Exxon rods and a 9x9 array of PNL rods within each AFS-C.

In conjunction with the HAC single package models, parametric runs are performed on the PNL rods to determine the optimum values for the active fuel height, pellet OD, and cladding ID. The results of this analysis are used in the NCT models. For a discussion of the method used to determine the geometry of the PNL rod, see Section C6.4.1.2.2, *HAC Single Package: PNL Rods Only*.

For Cases A1 through A3, the fuel rods are modeled with the Exxon rods in a lower region and the PNL rods stacked on top of the Exxon rods in an upper region. (The internal geometry arrangement is the same as the HAC single package Case G1.) This configuration is run with three different reflector materials: water, steel, and lead. The results in Table C6.4-1 indicate that lead is the most reactive reflector for a dry system. In Case A4, the lead reflected case is further modified to place all of the fuel rods in a single 13x13 array, which is an axially tighter configuration. (The internal geometry arrangement is the same as the HAC single package Case G5.) Because internal moderation is not an issue for the NCT cases, this more axially compact arrangement is more reactive.

In Cases A1 through A4, the Exxon rods are modeled with 60 g Pu, and the PNL rods are modeled with 40 g Pu. To add conservatism, the most reactive case from above (Case A4) is rerun with 65 g Pu in the Exxon rods and 42 g Pu in the PNL rods (Case A5). Case A5 is the most reactive case, with $k_s = 0.23958$. This value is far below the USL of 0.9288.

C6.4.1.2 HAC Configuration

For the HAC single package analysis, water is present inside the package and the fuel rods are assumed to be arranged in the most reactive configuration. Consistent with the most reactive models from Section 6.4, *Single Package Evaluation*, all base cases are modeled with a steel reflector and steel hardware is homogenized into the water surrounding the FCS cavities (note that moderating water within the FCS cavities does not contain homogenized steel). The most reactive case is also run with a water reflector to confirm that the steel reflector is bounding.

The analysis is performed in three steps. First, only Exxon rods are present in the package. Second, only PNL rods are present in the package. Third, both types of rods are present in the package simultaneously.

C6.4.1.2.1 HAC Single Package: Exxon Rods Only

Each AFS-C is assumed to contain up to 121 Exxon rods but no PNL rods. As the AFS-C cannot contain more than 116 Exxon rods, this scenario represents an excess of 5 rods. 121 rods have been selected both to bound the total mass of Pu and to simplify model preparation, as 121 rods may be arranged in an 11x11 square lattice to fill the cavity formed by the strongback and FCS. No credit is taken for geometric control provided by the AFS-C for criticality purposes, although the geometric constraint provided by the AFS-C limits the maximum number of Exxon rods to 116.

The most reactive Exxon rod pitch is first determined by simply modeling an arbitrary number of Exxon rods (11x11) in a square array reflected by water. Only one cluster of rods is modeled, and the packaging is not modeled, as shown in Figure C6.4-1. In the absence of neutron poison, the reactivity is high. The pitch is varied and the array is free to expand until the maximum reactivity is obtained. The results in Table C6.4-2 indicate that the most reactive rod pitch is 2.6 cm (Case B4). As the inner dimension of the strongback/FCS cavity is 8.8", the number of rods that will fit at the optimum pitch is approximately $[(8.8)(2.54)/2.6]^2 \sim 74$.

Because the optimum pitch results in a reduced number of rods that may fit in the cavity, there is a reactivity tradeoff between the pitch and the fissile mass, because these quantities cannot be optimized simultaneously. If all rods are modeled at the optimum pitch, only ~74 rods will fit rather than the maximum of 121. Conversely, if 121 rods are modeled, the pitch will be below the optimum value and the system will be undermoderated. If a non-regular pitch is assumed, the optimum pitch may be maintained throughout a portion of the cavity while rods are allowed to cluster along the edges of the cavity. The criticality analysis considers all of these scenarios.

Because the AFS-C is not modeled, sufficient axial clearance is present in the model to allow double stacking of the Exxon rods. This fact is advantageous for modeling purposes because it is not necessary to omit any rods from the model as the pitch is expanded. A double stacking arrangement is assumed where a lower group rests on the bottom of the MFFP, and an upper group is stacked above the lower group. Therefore, as the pitch expands, the rods that no longer fit in the lower group are shifted to the upper group.

Initially, all 121 rods (11x11) are modeled in the lower group and the upper group is filled with water. When 100 rods are modeled in the lower group (10x10), the excess 21 rods are moved to the upper group. This pattern is continued until there are 64 rods in the bottom group and 57 rods in the upper group. The top group is always modeled at the optimum pitch of 2.6 cm. The axial stacking arrangement is shown in Figure C6.4-2 for Case C2. The planar views for this case are shown in Figure C6.4-3 for both the lower and upper groups.

Results are provided in Table C6.4-3 for a number of rod arrangements. Among the cases with a regular pitch for all rods (Cases C1 through C9), Case C1 (121 lower rods and no upper rods) is the most reactive. Although the rod arrangement is undermoderated, this arrangement is more reactive than cases where rods are split between the lower and upper groups.

The relative worth of the shifted rods is also investigated. Comparing Cases C3 and C4 (9x9 lower), the reactivity is statistically unchanged when the 40 upper rods are replaced with water, indicating that the reactivity contribution of the 40 rods in the upper group is negligible. A similar conclusion may be obtained when comparing Cases C5 and C6 (8x8 lower).

The optimum pitch of 2.6 cm may be confirmed by comparing Cases C5 and C7. In Case C7, the lower 8x8 array is fully expanded to the maximum extent (3.0294 cm), while in Case C5 the pitch of the lower array is fixed at 2.6 cm, leaving a gap of water around the 8x8 array, see Figure C6.4-4. The reactivity for the optimum pitch case is significantly higher than the reactivity for the overmoderated case. It is also interesting to note that when Case C7 is run with no lower rods (Case C8) and no upper rods (Case C9), it becomes apparent that the reactivity for Case C7 is dominated by the upper and not the lower rods. Therefore, for all cases examined, reactivity is dominated by either the lower or upper group of rods, and it does not appear that neutronic interaction between these groups plays a significant role in the reactivity.

In Cases C1 through C9, the lattice is assumed to be regular, and the most reactive case has 121 rods in the lower group. In cases C20 through C29, non-regular lattices are investigated. For Cases C20 through C23 (shown in Figure C6.4-5), the pitch is maintained at near optimum (9x9 lattice from Case C3) while extra rods are placed into the regions around the edges. For Cases C24 through C27 (shown in Figure C6.4-6), a tighter 10x10 lattice is used, which is more reactive. All cases are bounded by the regular lattice Case C1, although Cases C1 and C27 are statistically equivalent. The maximum $k_s = 0.88627$ is achieved for Case C1, which is below the USL of 0.9288.

C6.4.1.2.2 HAC Single Package: PNL Rods Only

The basic analysis methodology utilized on the Exxon rods is repeated for the PNL rods. However, initial parametric runs are needed because, unlike the Exxon rods, the PNL rods are not as well characterized. Three key pieces of information that are not known are the active fuel height, the cladding ID, and the pellet OD. The approach is to vary each of these parameters within a range of reasonable values to determine the most reactive condition. This fuel rod description is then used in the remainder of the models.

The overall length of a PNL fuel rod is 36.6". Therefore, it is assumed that the active fuel length may vary between the ranges of 36" to 28". For the parametric models in which the active fuel height is investigated (Cases D1 and D2), the cladding thickness (0.035") and pellet-to-cladding gap (0.0047") are assumed to be the same as the Exxon rods. These dimensions may be used to compute the pellet OD and cladding ID based upon the known rod OD. The rods are modeled in a 9x9 array reflected by water (similar to the Exxon array shown in Figure C6.4-1) with a fixed pitch of 3.2 cm. Because the internal rod geometry is not well characterized, minor details such as end caps are neglected and the rods are simply modeled as pellets and cladding.

Results are provided in Table C6.4-4. In Case D1, the active fuel height is 36", while for Case D2, the active fuel height is 28". The fuel pellet composition changes with active fuel height to maintain a constant pellet density of 10.85 g/cm³ and Pu mass of 40 g, as discussed in Section C6.2. Because Case D2 is more reactive than Case D1, it is concluded that a shorter active fuel height is more reactive. Therefore, the remaining parametric cases are performed with an active fuel height of 28".

In Case D3, the pellet OD is the same as Case D2, while the cladding thickness is consistent with the standard MOX fuel assembly. The MOX fuel assembly cladding thickness is 0.0225", which results in a large pellet-to-cladding gap for this case. In Case D4, both the cladding thickness and pellet-to-cladding gap are consistent with the standard MOX fuel assembly. As the MFFP pellet-to-cladding gap is 0.00325", the PNL pellet OD must expand accordingly. Case D4 is the most reactive, although the effects of cladding thickness, pellet-to-cladding gap, and pellet OD do not have a strong influence on the reactivity. Consistent with Case D4, subsequent PNL rod models have an active fuel height of 28", a pellet OD of 0.5135", and a cladding ID of 0.5200".

An optimum PNL rod pitch study is performed similar to the optimum rod pitch study performed for the Exxon rods, although a 9x9 array is assumed because a lesser number of PNL rods may fit in the AFS-C. The array geometry is similar to the Exxon model shown in Figure C6.4-1. The results provided in Table C6.4-5 indicate that maximum reactivity is reached at a pitch of 3.2 cm. Note that the optimum PNL rod pitch is larger than the optimum Exxon rod pitch of 2.6 cm.

The same technique utilized in the Exxon-only models is utilized in the PNL-only models. However, because the AFS-C cannot fit more than 69 PNL rods, a bounding 9x9 square array of rods is assumed, which represents an additional 12 rods. The rods are divided between lower and upper groups. As the pitch in the lower group increases, reducing the number of rods in the lower group, an equivalent number of rods is added to the upper group. The pitch for the upper group of rods is always set at the optimum value of 3.2 cm. For convenience, the z-position of the interface between the lower and upper groups is assumed to be at the same location as the Exxon rod models. This assumption will facilitate model preparation when the PNL and Exxon rods are combined (see Section C6.4.1.2.3, *HAC Single Package: Combined Exxon and PNL Rods*).

Results are provided in Table C6.4-6. The trends in the PNL results are the same as the Exxon results, although the system reactivity is lower. The most reactive condition (Case F1) occurs when all 81 rods are in the lower group. Rods that have been shifted to the upper group contribute little to the reactivity. The optimum moderation is reached when the bottom array is modeled with a 7x7 square lattice, which results in a pitch of 3.2 cm. However, in this scenario 32 rods have been shifted upward and the reactivity is significantly less than the case in which all 81 rods are in the lower group.

Because the most reactive configuration occurs when all the rods are in the lower group, in Cases F20 through F26 the lower rods are arranged in a non-regular pitch. In this manner, many of the rods may be moderated at or near the optimum value, although other rods must necessarily be undermoderated when these rods are clustered together. Various non-regular pitch models are developed, as shown in Figure C6.4-8 and Figure C6.4-9. As shown in Table C6.4-6, none of the non-regular pitch models are more reactive than the regular 9x9 pitch model. The maximum $k_s = 0.85551$ is achieved for Case F1, which is below the USL of 0.9288.

C6.4.1.2.3 HAC Single Package: Combined Exxon and PNL Rods

In Sections C6.4.1.2.1 and C6.4.1.2.2, the Exxon and PNL rods are addressed separately. In actuality, the rods may be stacked in a basket that is placed in the AFS-C cavity. In the current section, the two rod types are combined within the AFS-C.

The most reactive Exxon-only model (Case C1) and the most reactive PNL-only model (Case F1) are combined into an AFS-C. It is assumed that the Exxon rods comprise the lower group and the

PNL rods comprise the upper group, as shown in Figure C6.4-10. Note that in the actual loaded arrangement, the rods are loaded into separate compartments that are separated by approximately 37-in, although this separation is not credited in the analysis. The results shown in Table C6.4-7 indicate that the reactivity does not increase appreciably when the rods are combined within an AFS-C because the most reactive group (the Exxon rods in this case) dominates. This result is consistent with the results of the previous sections, as the reactivity of the Exxon-only and PNL-only models do not change appreciably when the upper rods are replaced with water.

No credit is taken for axial separation provided by the AFS-C, so additional cases are developed in which the Exxon and PNL rods are mixed within the lower group. Because the PNL rods are short and could conceivably double-stack upon each other, the active fuel length of the PNL rods that slide into the lower region is doubled (56") to more closely match the active fuel length of the Exxon rods. The PNL rods in the upper region are modeled with the standard active fuel length of 28" and most reactive PNL pitch of 3.2 cm.

Both 12x12 and 13x13 array cases are run with most or all of the rods in the lower group. Three configurations are developed for the 12x12 models (Cases G2 through G4), as shown in Figure C6.4-11. For a 12x12 array, there are $144 - 121 = 23$ locations available for PNL rods. As each location contains two PNL rods, $81 - 2 \times 23 = 35$ PNL rods remain in the upper region. The upper rods are modeled at the optimum PNL pitch of 3.2 cm.

Four configurations are developed for the 13x13 models (Cases G5 through G8), as shown in Figure C6.4-12. For a 13x13 array, there are $169 - 121 = 48$ locations available for PNL rods, which exceeds the number of PNL rods available ($48 \times 2 = 96 > 81$). Therefore, 41 double-length PNL rods are modeled in the lower region, as well as 7 water holes. In Cases G5 through G7, 121 Exxon rods and 82 PNL rods are modeled, while in Case G8, 114 Exxon rods and 68 PNL rods are modeled, which are similar to the number of rods that could actually be transported within the AFS-C (i.e., 116 Exxon rods and 69 PNL rods). All cases are less reactive than Case G1, in which the two rod types are axially separated.

In Cases G9 through G12, the limiting case (G1) is modified to confirm some of the initial base assumptions taken from the standard fuel assembly analysis in Section 6.4, *Single Package Evaluation*. In Case G9, the steel reflector is replaced with a water reflector. The reactivity drops slightly, as expected. It is assumed that a lead reflector would be statistically equivalent to the steel reflector, consistent with Section 6.4. In Case G10, the internal water, which has been homogenized with steel components, is modeled as ordinary water. The reactivity drops slightly, consistent with the behavior in Section 6.4. In Cases G11 and G12, the internal water density is modeled at reduced values of 0.95 g/cm^3 and 0.90 g/cm^3 , respectively. Reactivity drops as the internal water density drops, as expected. Note that Cases G11 and G12 should be compared against Case G10, because the homogenized steel has been omitted from these cases for convenience.

When comparing the Exxon-only cases (Case C1 through C29), the PNL-only cases (Cases F1 through F26), and the combined cases (Cases G1 through G12), the maximum reactivity is achieved for Case G1. In this case, 121 Exxon rods are modeled in the lower group, and 81 PNL rods are modeled in the upper group. Note that the reactivity is statistically equivalent to Case C1, in which no PNL rods are present. Therefore, it may be concluded that the PNL rods have a minor impact on the reactivity.

In all of the previous HAC single package cases, the Exxon rods are modeled with 60 g Pu, and the PNL rods are modeled with 40 g Pu. To add conservatism, the most reactive case from above (Case G1) is rerun with 65 g Pu in the Exxon rods and 42 g Pu in the PNL rods (Case G13). Case G13 is the most reactive case, with $k_s = 0.89475$. This value is below the USL of 0.9288.

C6.4.2 Single Package Results

The optimum pitch search results are provided in Table C6.4-2 and Table C6.4-5 for Exxon and PNL rods, respectively. (The multiplication factors are high because no poison plates are modeled.) The PNL rod parametric study results are provided in Table C6.4-4. The remaining tables present the single package results. The most reactive case in each table is listed in boldface.

Table C6.4-1 – Criticality Results for NCT Single Package

Case No.	Filename	Reflector	k_{eff}	σ	k_s ($k_{eff}+2\sigma$)
A1	nsc_pb	Lead	0.16738	0.00050	0.16838
A2	nsc_st	Steel	0.16521	0.00047	0.16615
A3	nsc_h2o	Water	0.13931	0.00044	0.14019
A4	nsc_pb2	Lead	0.23030	0.00059	0.23148
Case A5 is Case A4 with increased Pu mass in the fuel rods					
A5	nsc_pb2h	Lead	0.23834	0.00062	0.23958

Table C6.4-2 – Exxon Rod Optimum Pitch Study Results

Case No.	Filename	Pitch (cm)	k_{eff}	σ	k_s ($k_{eff}+2\sigma$)
B1	11x11_p1	2.0	0.94625	0.00099	0.94823
B2	11x11_p11	2.2	0.98556	0.00100	0.98756
B3	11x11_p12	2.4	1.00537	0.00099	1.00735
B4	11x11_p13	2.6	1.01493	0.00104	1.01701
B5	11x11_p14	2.8	1.00856	0.00100	1.01056
B6	11x11_p15	3.0	0.99715	0.00096	0.99907

Note: Scoping study; no poison plates.

Table C6.4-3 – HAC Single Package, Exxon Rods Only

Case No.	Filename	Bottom Pitch (cm)	Number in Lower Group	Number in Upper Group	k_{eff}	σ	k_s ($k_{eff}+2\sigma$)
Regular Lattice Cases							
C1	hse_b11x11_t0	2.1208	121	0	0.88443	0.00092	0.88627
C2	hse_b10x10_t21	2.3562	100	21	0.86949	0.00097	0.87143
C3	hse_b9x9_t40	2.6508	81	40	0.83604	0.00095	0.83794
C4	hse_b9x9_t0	2.6508	81	0	0.83645	0.00096	0.83837
C5	hse_b8x8_t57	2.6	64	57	0.80936	0.00100	0.81136
C6	hse_b8x8_t0	2.6	64	0	0.80948	0.00102	0.81152
C7	hse_b8x8e_t57	3.0294	64	57	0.78095	0.00097	0.78289
C8	hse_b0_t57	NA	0	57	0.78316	0.00092	0.78500
C9	hse_b8x8e_t0	3.0294	64	0	0.77597	0.00094	0.77785
Non-Regular Lattice Cases							
C20	hse_b9x9_105_t16	2.6508	105	16	0.86236	0.00099	0.86434
C21	hse_b9x9_109_t12	2.6508	109	12	0.86090	0.00096	0.86282
C22	hse_b9x9_113_t8	2.4836	113	8	0.87403	0.00098	0.87599
C23	hse_b9x9_121	2.6508	121	0	0.86975	0.00095	0.87165
C24	hse_b9x9_121c2	2.6508	121	0	0.84431	0.00095	0.84621
C25	hse_b10x10_121	2.3562	121	0	0.87573	0.00101	0.87775
C26	hse_b10x10_121c2	2.3562	121	0	0.87247	0.00097	0.87441
C27	hse_b10x10_121c3	2.3562	121	0	0.88399	0.00099	0.88597
C28	hse_b10x10_121c4	2.3562	121	0	0.87952	0.00094	0.88140
C29	hse_b10x10_121c5	2.2354	121	0	0.88203	0.00095	0.88393

Table C6.4-4 – PNL Rod Parametric Study Results

Case No.	Filename	Active Fuel Height (in)	Pellet OD (in)	Cladding ID (in)	k_{eff}	σ	k_s ($k_{eff}+2\sigma$)
D1	hsp_para1	36	0.4856	0.4950	0.95016	0.00092	0.95200
D2	hsp_para2	28	0.4856	0.4950	0.96743	0.00096	0.96935
D3	hsp_para3	28	0.4856	0.5200	0.96552	0.00100	0.96752
D4	hsp_para4	28	0.5135	0.5200	0.97171	0.00094	0.97359

Table C6.4-5 – PNL Rod Optimum Pitch Study Results

Case No.	Filename	Pitch (cm)	k_{eff}	σ	k_s ($k_{\text{eff}}+2\sigma$)
E1	9x9_p14	2.8	0.95817	0.00102	0.96021
E2	9x9_p15	3.0	0.97067	0.00097	0.97261
D4	hsp_para4	3.2	0.97171	0.00094	0.97359
E3	9x9_p17	3.4	0.96626	0.00096	0.96818
E4	9x9_p18	3.6	0.95506	0.00102	0.95710

Note: Scoping study, no poison plates.

Table C6.4-6 – HAC Single Package, PNL Rods Only

Case No.	Filename	Bottom Pitch (cm)	Number in Lower Group	Number in Upper Group	k_{eff}	σ	k_s ($k_{\text{eff}}+2\sigma$)
Regular Lattice Cases							
F1	hsp_b9x9_t0	2.6148	81	0	0.85357	0.00097	0.85551
F2	hsp_b8x8_t17	2.9880	64	17	0.83339	0.00098	0.83535
F3	hsp_b7x7e_t32	3.4862	49	32	0.78205	0.00099	0.78403
F4	hsp_b7x7_t32	3.2	49	32	0.80302	0.00096	0.80494
F5	hsp_b7x7_t0	3.2	49	0	0.79669	0.00099	0.79867
Non-Regular Lattice Cases							
F20	hsp_8x8_81	2.9880	81	0	0.84687	0.00096	0.84879
F21	hsp_8x8_81c2	2.9880	81	0	0.83939	0.00099	0.84137
F22	hsp_8x8_81c3	2.7960	81	0	0.84475	0.00095	0.84665
F23	hsp_8x8_81c4	2.7960	81	0	0.83525	0.00097	0.83719
F24	hsp_7x7_81	3.2	73	8	0.83204	0.00091	0.83386
F25	hsp_7x7_82	3.2	82	0	0.81319	0.00094	0.81507
F26	hsp_7x7_82c2	3.2	82	0	0.80830	0.00099	0.81028

Table C6.4-7 – HAC Single Package, Combined Exxon and PNL Rods

Case No.	Filename	Bottom Pitch (cm)	Number in Lower Group	Number in Upper Group	k_{eff}	σ	k_s ($k_{eff}+2\sigma$)
G1	hsc_b11x11_t9x9	2.1208	121 Exxon	81 PNL	0.88605	0.00092	0.88789
G2	hsc_b12x12_t35	1.8632	121 Exxon 46 PNL	35 PNL	0.86705	0.00101	0.86907
G3	hsc_b12x12_t35c2	1.8632	121 Exxon 46 PNL	35 PNL	0.87047	0.00097	0.87241
G4	hsc_b12x12_t35c3	1.9278	121 Exxon 46 PNL	35 PNL	0.86880	0.00097	0.87074
G5	hsc_b13x13_t0	1.7198	121 Exxon 82 PNL	0	0.84800	0.00102	0.85004
G6	hsc_b13x13_t0c2	1.7198	121 Exxon 82 PNL	0	0.85788	0.00096	0.85980
G7	hsc_b13x13_t0c3	1.7672	121 Exxon 82 PNL	0	0.84519	0.00097	0.84713
G8	hsc_e114_p68	1.7672	114 Exxon 68 PNL	0	0.85344	0.00098	0.85540
G9	hsc_b11x11_t9x9_h2o	2.1208	121 Exxon	81 PNL	0.88261	0.00095	0.88451
G10	hsc_b11x11_t9x9_ih2o	2.1208	121 Exxon	81 PNL	0.88220	0.00097	0.88414
G11	hsc_b11x11_t9x9_w95	2.1208	121 Exxon	81 PNL	0.86114	0.00098	0.86310
G12	hsc_b11x11_t9x9_w90	2.1208	121 Exxon	81 PNL	0.83769	0.00094	0.83957
Case G13 is Case G1 with increased Pu mass in the fuel rods							
G13	hsc_b11x11_t9x9h	2.1208	121 Exxon	81 PNL	0.89285	0.00095	0.89475

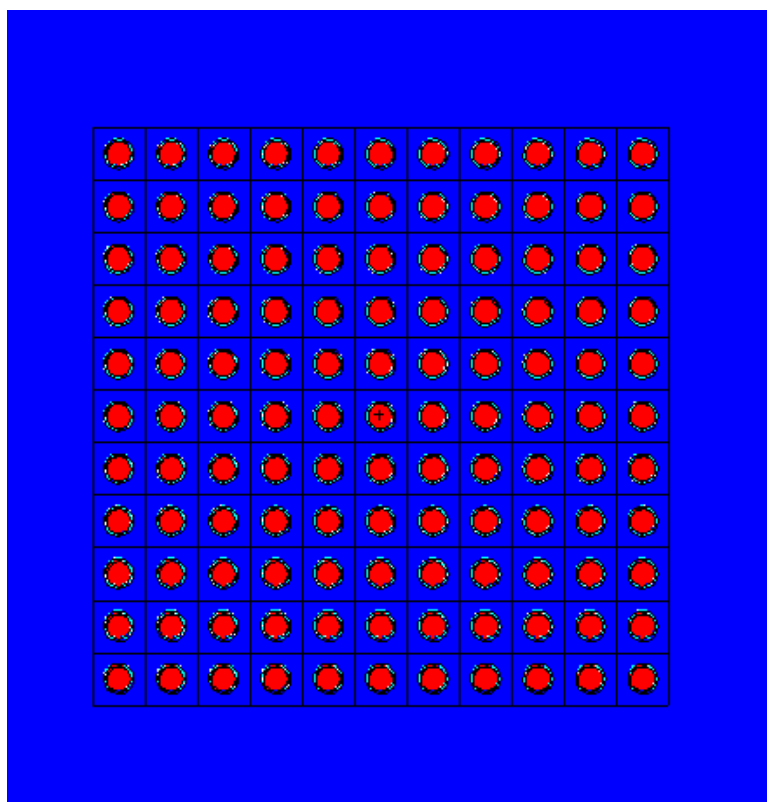


Figure C6.4-1 – Exxon Rod Optimum Pitch Study (Cases B1 through B6)

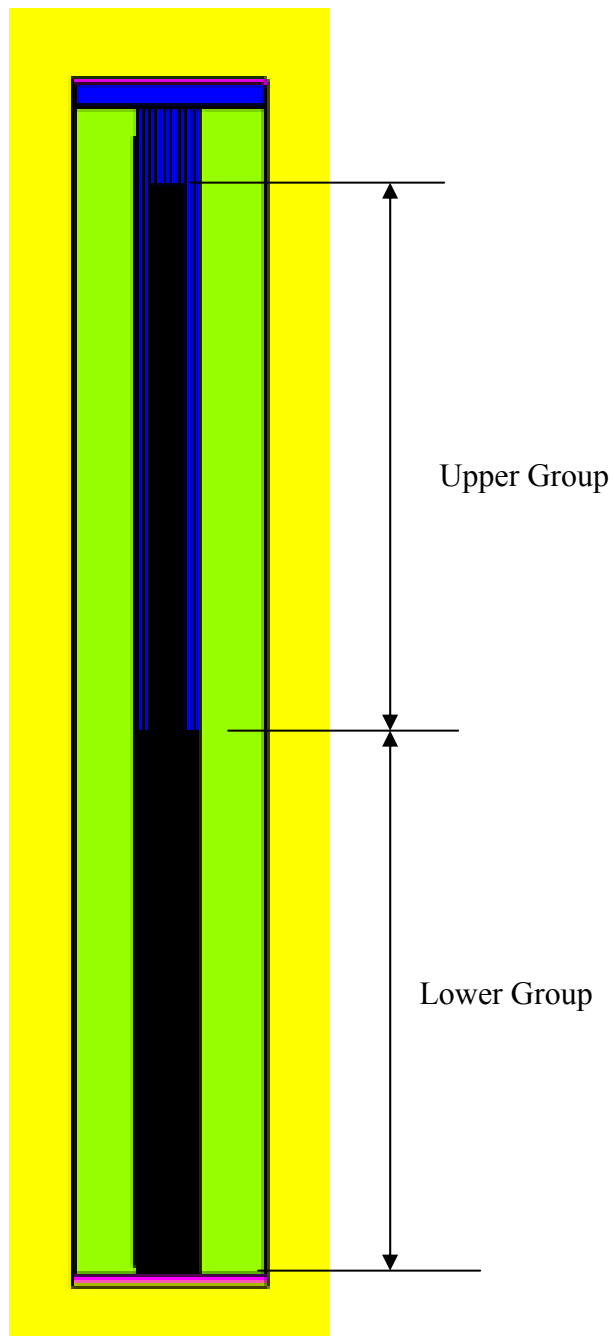
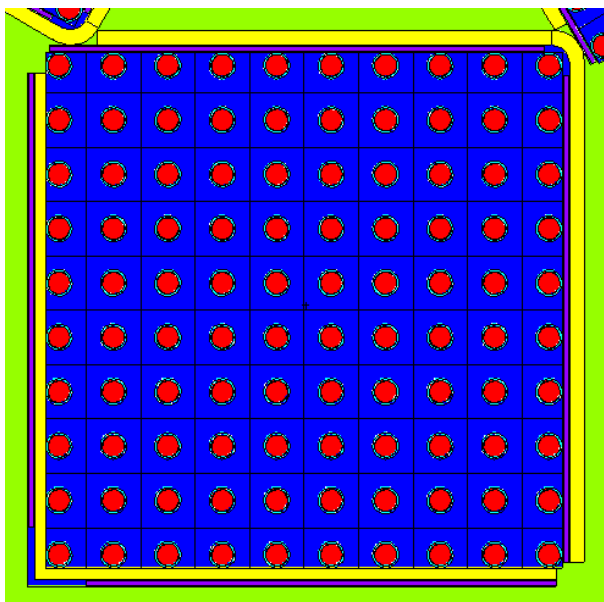
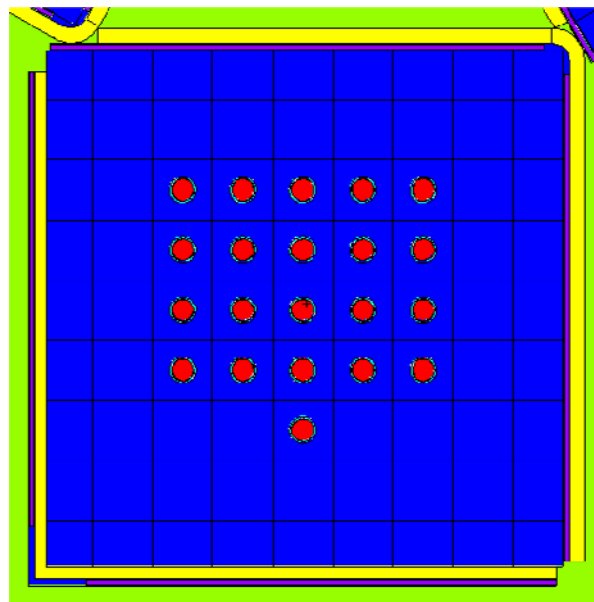


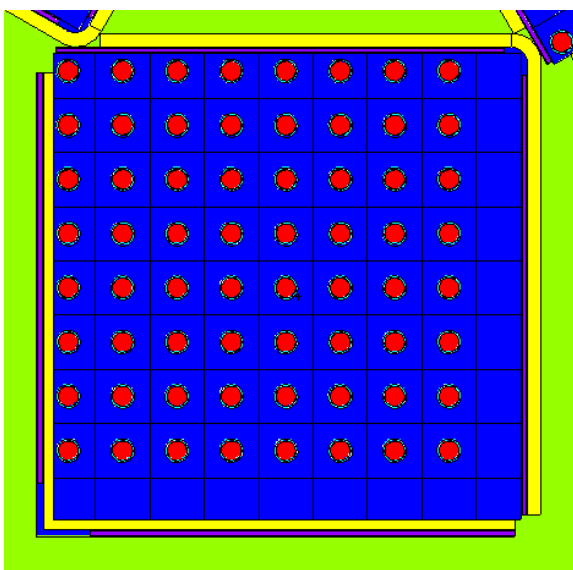
Figure C6.4-2 – Exxon Case C2 (side view)



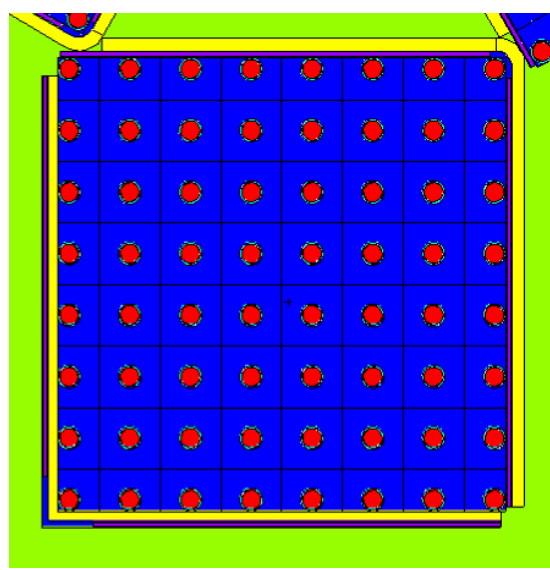
Lower Group (10x10)



Upper Group (21 rods)

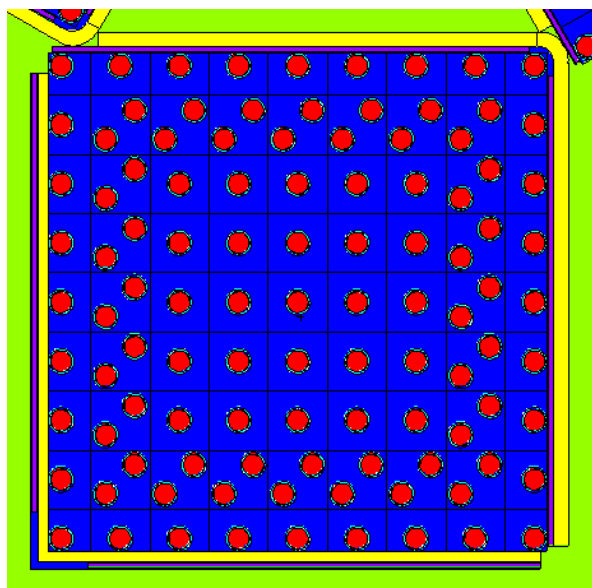
Figure C6.4-3 – Exxon Case C2 (planar view)

8x8 lower, optimum pitch (Case C5)

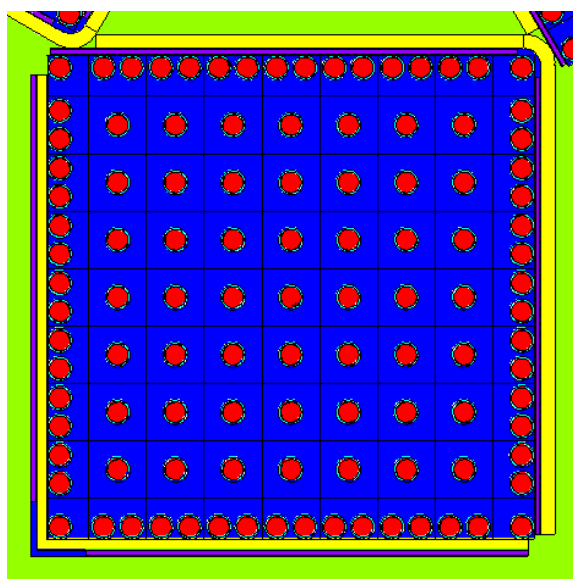


8x8 lower, maximum pitch (Case C7)

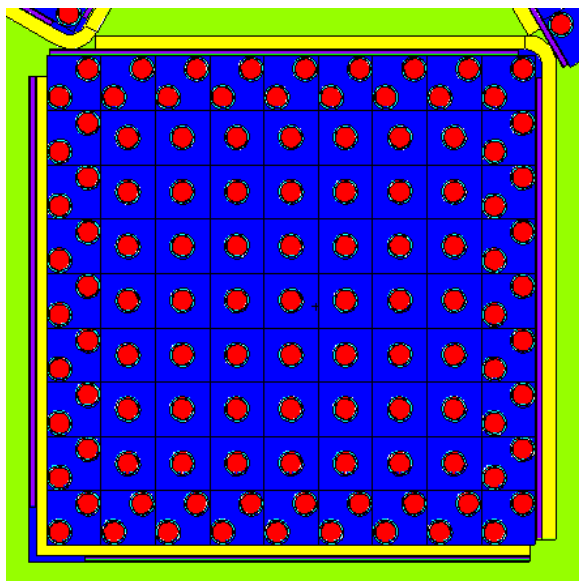
Figure C6.4-4 – Configurations for Exxon Cases C5 and C7



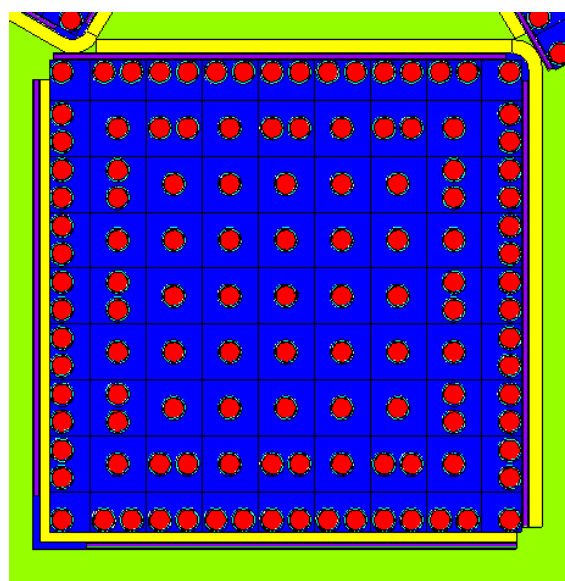
Case C20 (9x9, 105 lower, 16 upper)



Case C21 (9x9, 109 lower, 12 upper)

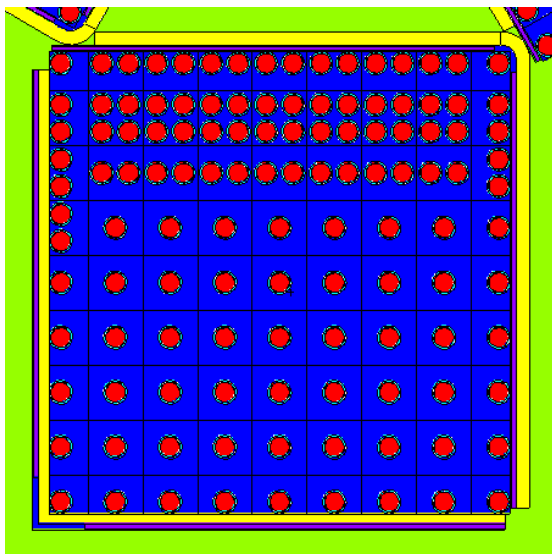


Case C22 (9x9, 113 lower, 8 upper)

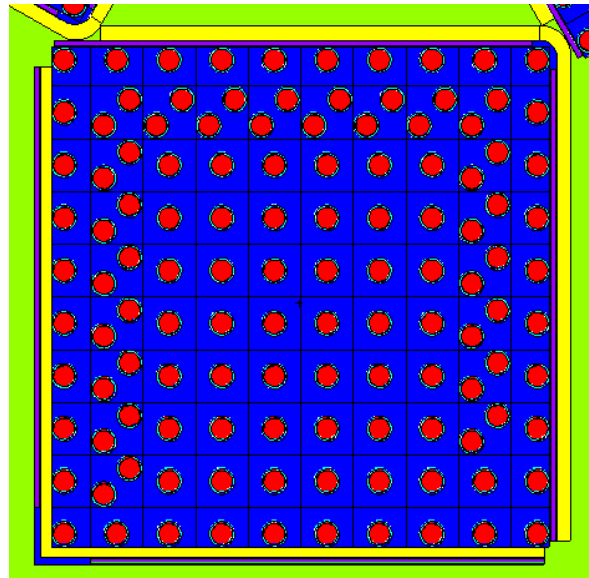


Case C23 (9x9, 121 lower, 0 upper)

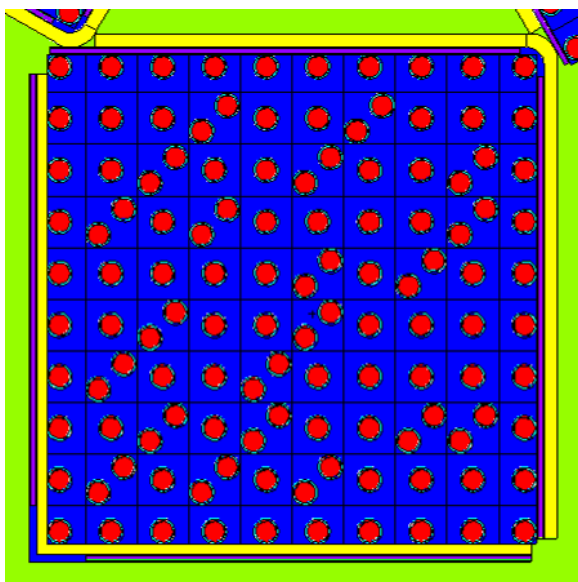
Figure C6.4-5 – Non-Regular Configurations for Cases C20 through C23



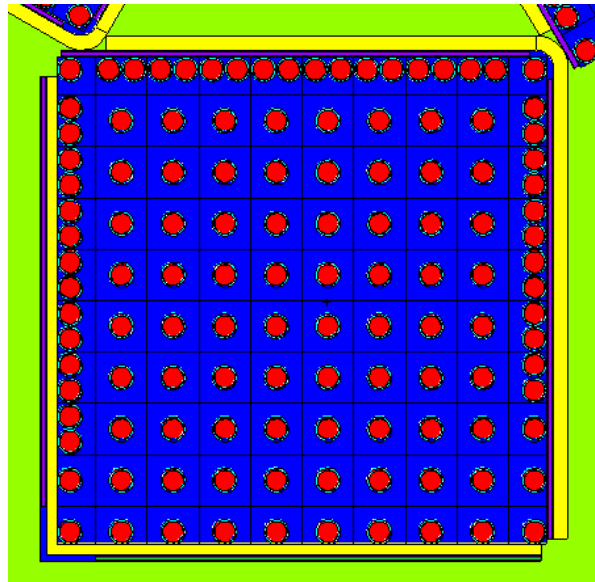
Case C24 (9x9, 121 lower, 0 upper)



Case C25 (10x10, 121 lower, 0 upper)

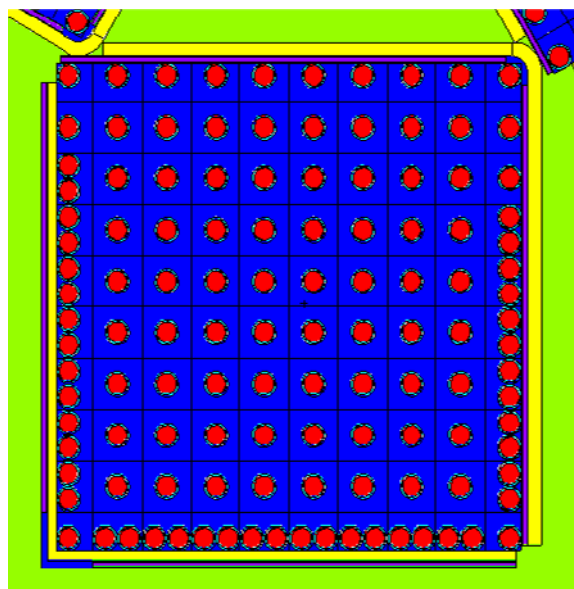


Case C26 (10x10, 121 lower, 0 upper)

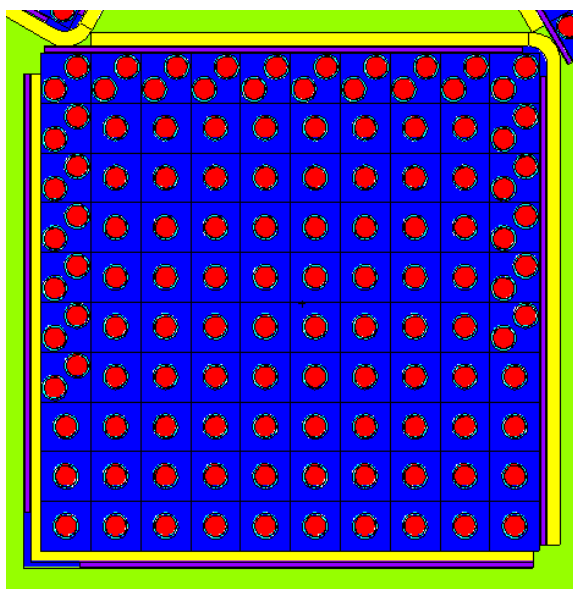


Case C27 (10x10, 121 lower, 0 upper)

Figure C6.4-6 – Non-Regular Configurations for Cases C24 through C27

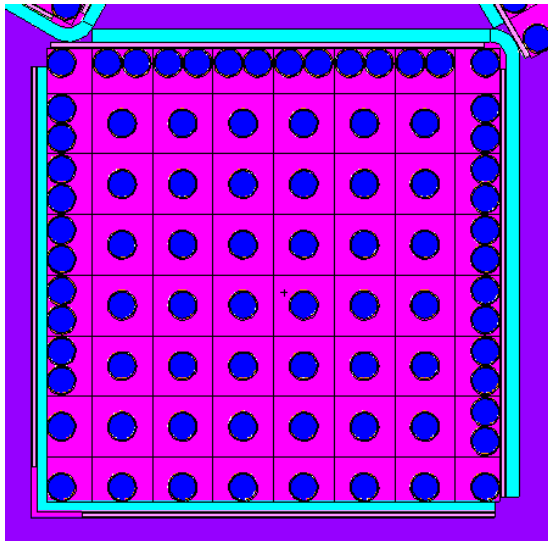


Case C28 (10x10, 121 lower, 0 upper)

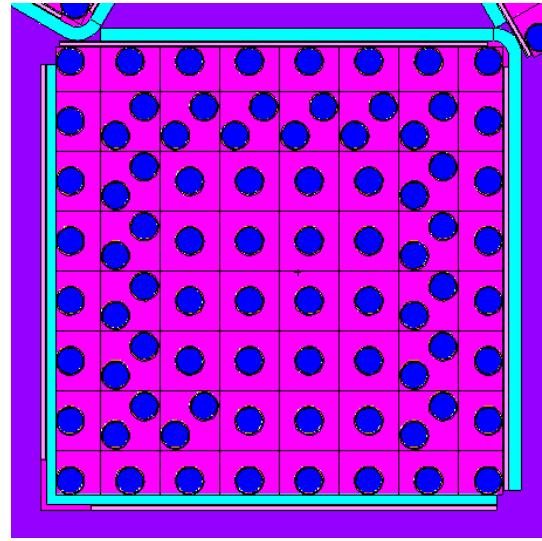


Case C29 (10x10, 121 lower, 0 upper)

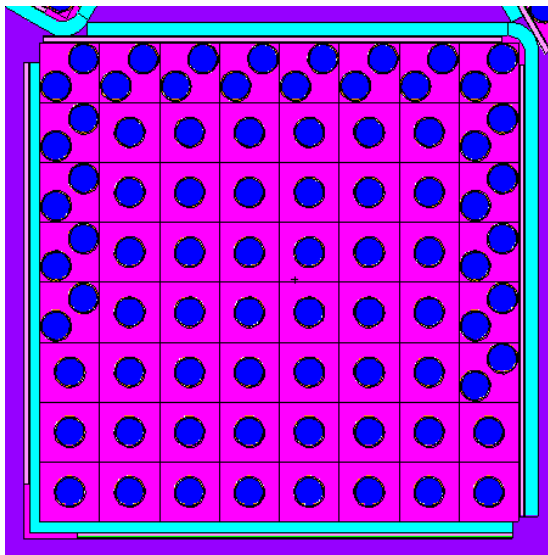
Figure C6.4-7 – Non-Regular Configurations for Cases C28 and C29



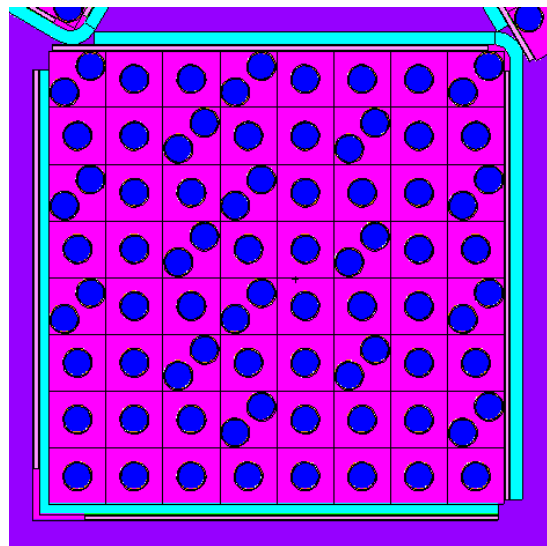
Case F20 (8x8, 81 lower, 0 upper)



Case F21 (8x8, 81 lower, 0 upper)

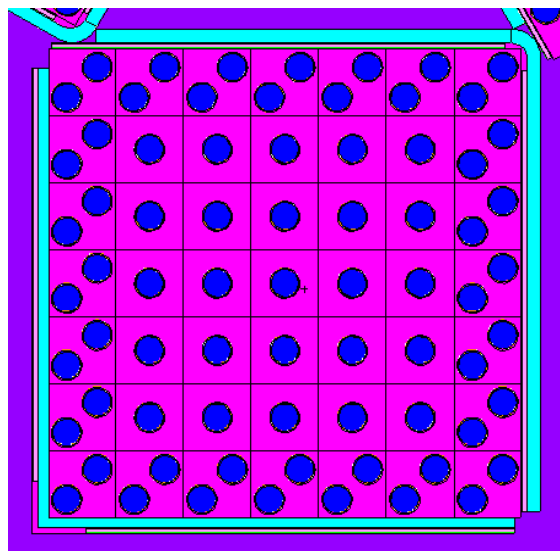


Case F22 (8x8, 81 lower, 0 upper)

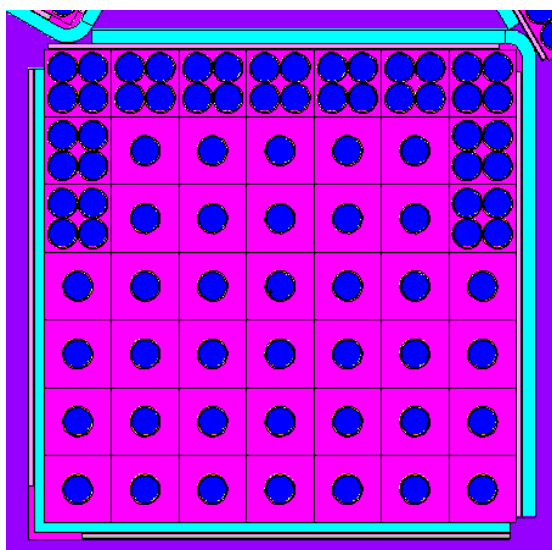


Case F23 (8x8, 81 lower, 0 upper)

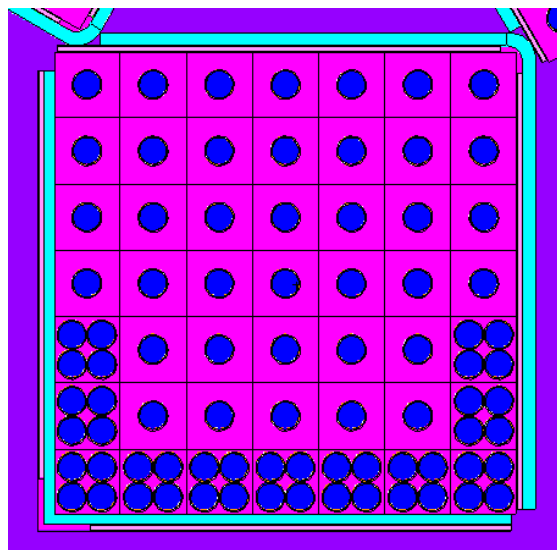
Figure C6.4-8 – Non-Regular Configurations for Cases F20 through F23



Case F24 (7x7, 73 lower, 8 upper)



Case F25 (7x7, 82 lower, 0 upper)



Case F26 (7x7, 82 lower, 0 upper)

Figure C6.4-9 – Non-Regular Configurations for Cases F24 through F26

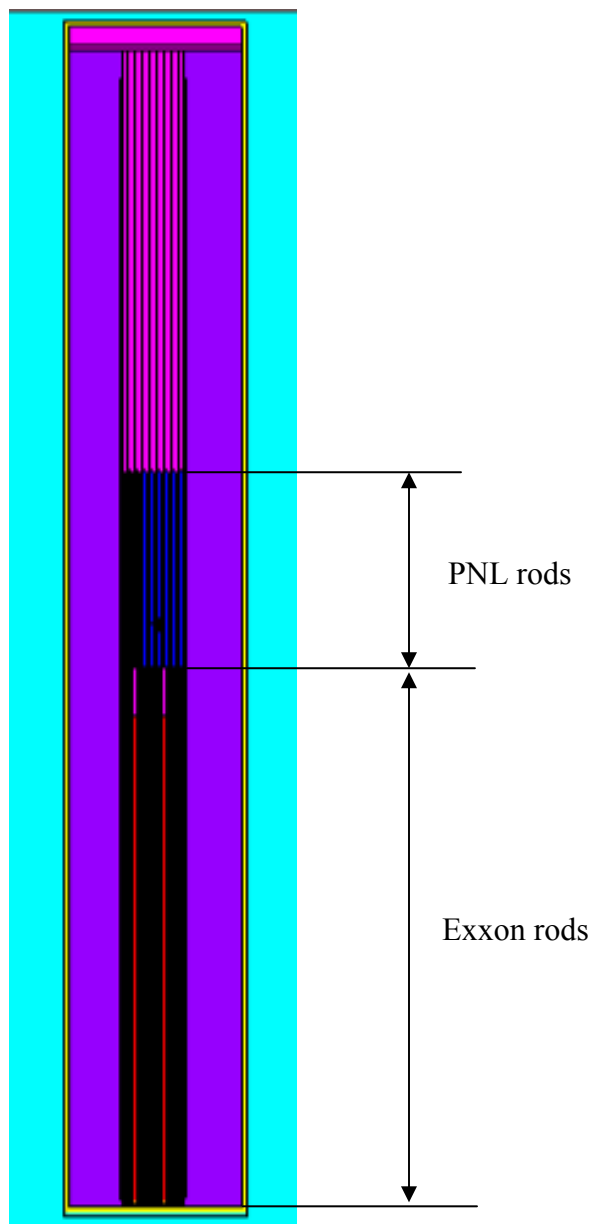
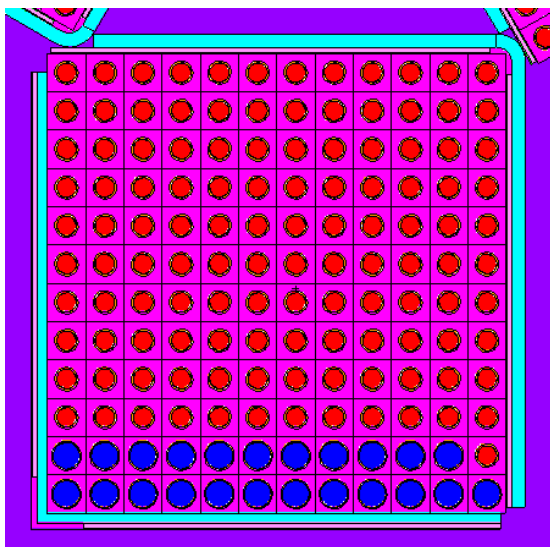
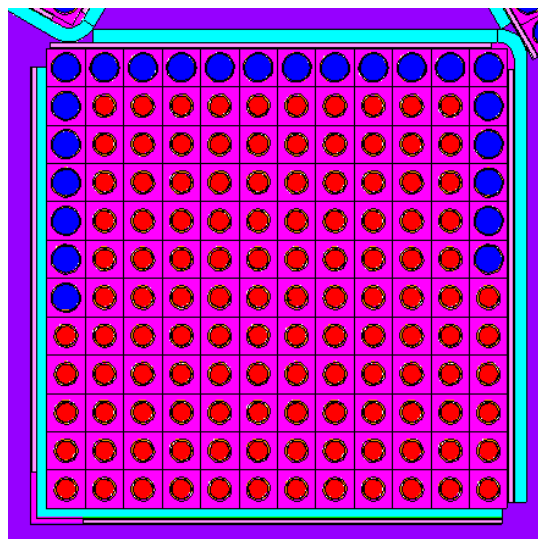


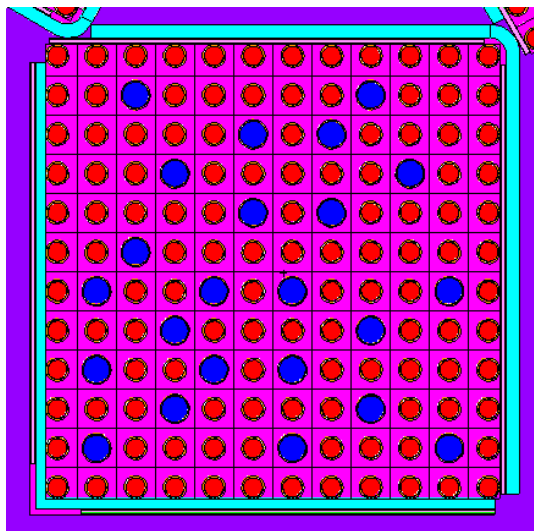
Figure C6.4-10 – Combined Exxon and PNL Rod Cases



Case G2 (12x12, Configuration 1)

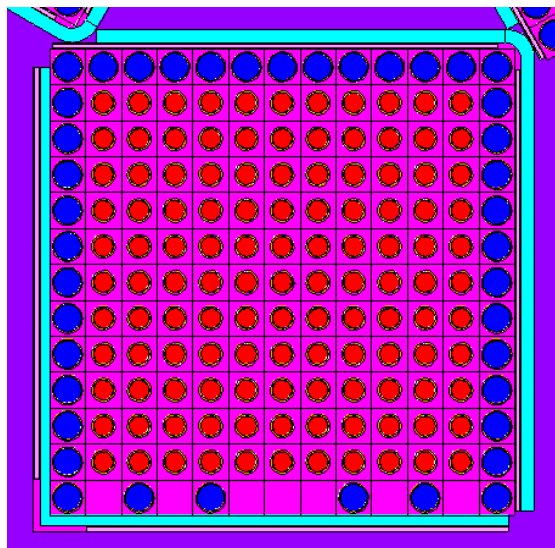


Case G3 (12x12, Configuration 2)

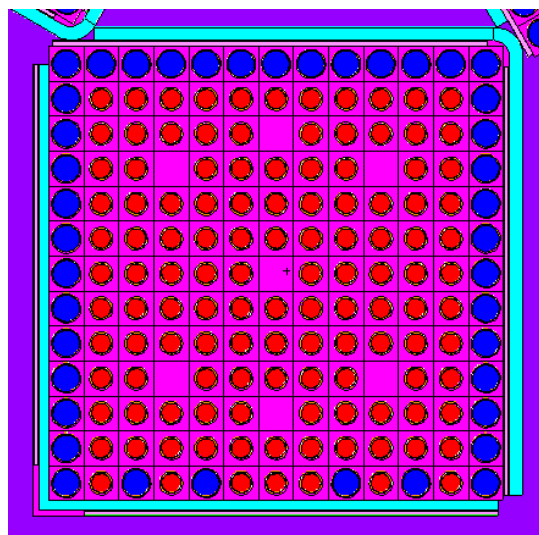


Case G4 (12x12, Configuration 3)

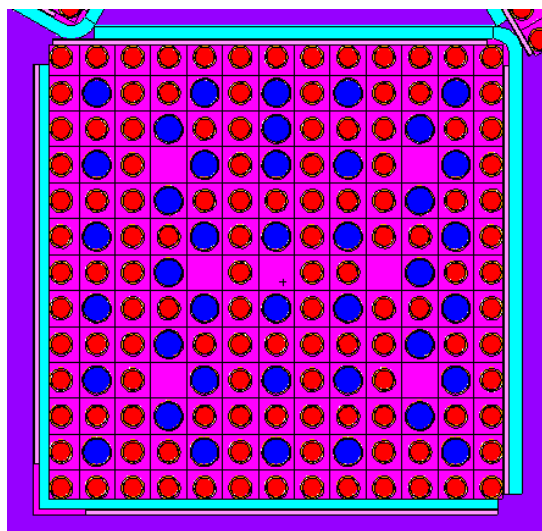
Figure C6.4-11 – Configurations for Combined Rod Cases G2 through G4



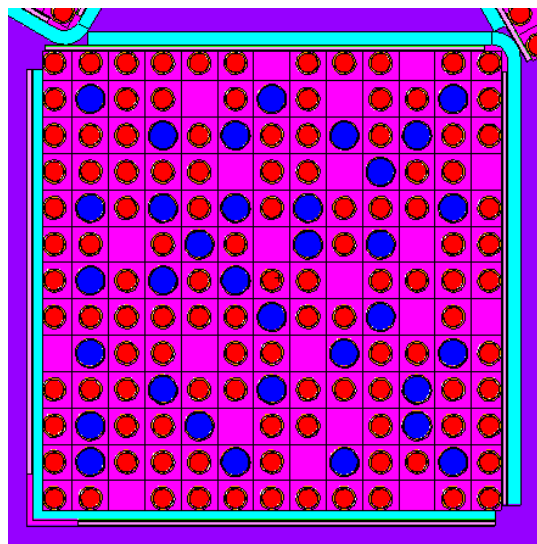
Case G5 (13x13, Configuration 1)



Case G6 (13x13, Configuration 2)



Case G7 (13x13, Configuration 3)



Case G8 (13x13, Configuration 4)

Figure C6.4-12 – Configurations for Combined Rod Cases G5 through G8

C6.5 Evaluation of Package Arrays Under Normal Conditions of Transport

C6.5.1 NCT Array Configuration

An infinite close-packed hexagonal array is modeled for NCT conditions. No water is modeled inside of the package, although the water density is allowed to vary between packages. Based upon the analysis in Section 6.5, *Evaluation of Package Arrays Under Normal Conditions of Transport*, it is anticipated that the most reactive condition will be with no water between the packages.

Because the axial orientation of the Exxon and PNL rods will have an effect on the reactivity, cases are run in which the two rod types are both separate and combined. In both of these cases, void is modeled between packages. In Case H1, the rods are modeled in separate groups (like Case G1), while in Case H2, the rods are modeled in the same group (like Case G5). The results in Table C6.5-1 indicate that Case H2 is more reactive than Case H1.

Several additional cases are run with the internal configuration of Case H2 and variable water density between the packages. Only a limited number of cases are executed to confirm that reactivity is optimized with no water between the packages. As expected, the results in Table C6.5-1 confirm that adding water between the packages decreases reactivity.

In cases H1 through H5, the Exxon rods are modeled with 60 g Pu, and the PNL rods are modeled with 40 g Pu. To add conservatism, the most reactive case from above (Case H2) is rerun with 65 g Pu in the Exxon rods and 42 g Pu in the PNL rods (Case H6). Case H6 is the most reactive case, with $k_s = 0.49095$. This value is far below the USL of 0.9288.

C6.5.2 NCT Array Results

The results for the NCT array cases are provided in Table C6.5-1. The most reactive configuration is listed in boldface.

Table C6.5-1 – NCT Array Results

Case No.	Filename	Water Density Between Packages (g/cm ³)	k_{eff}	σ	k_s ($k_{eff}+2\sigma$)
H1	nac_o0_long	0	0.41430	0.00048	0.41526
H2	nac_o0	0	0.47132	0.00051	0.47234
H3	nac_o05	0.05	0.46488	0.00061	0.46610
H4	nac_o10	0.1	0.44628	0.00058	0.44744
H5	nac_o100	1.0	0.29218	0.00054	0.29326
Case H6 is Case H2 with increased Pu mass in the fuel rods					
H6	nac_o0h	0	0.48991	0.00052	0.49095

This page left intentionally blank.

C6.6 Package Arrays Under Hypothetical Accident Conditions

C6.6.1 HAC Array Configuration

The HAC array configuration is similar to the NCT array configuration. Reflective surfaces are placed around the package to simulate a close-packed hexagonal array, see Figure C6.6-1. The top and bottom package surfaces are also set as reflective boundaries.

Cases are run for various combinations of internal and external moderator density. Case J1 is simply the most reactive single package model (Case G1) with reflective boundary conditions. Because there could be axial interaction effects between the package arrays, in Case J2 the PNL rods are shifted all the way to the top of the package, while the Exxon rods remain at the bottom of the package. The reactivity is statistically equivalent to Case J1 and the internal configuration of Case J1 is used for the remainder of the cases.

It is apparent from the analysis in Section 6.6, *Package Arrays Under Hypothetical Accident Conditions*, that the reactivity is somewhat insensitive to the water density between the packages under HAC. Because the package is very large and the contents are poisoned on all sides, the packages are largely isolated from one another and the infinite array results are very close to the single package results. This observation is confirmed in Cases J3 through J6, in which the external moderator density is varied between 0.05 g/cm^3 and 1.0 g/cm^3 . The reactivity of these cases are statistically equivalent, although the maximum reactivity occurs for case J4.

In Cases J7 through J11, the internal moderator density is reduced while the external moderator is modeled as void. For simplicity, the homogenized steel/water mixture internal to the package is modeled as water for these cases. Comparison of Cases J1 and J7 indicates that removing the homogenized steel has a negligible effect on the reactivity. As expected, reactivity drops quickly as the internal moderation is reduced, indicating that full water moderation is the most reactive condition.

In cases J1 through J11, the Exxon rods are modeled with 60 g Pu, and the PNL rods are modeled with 40 g Pu. To add conservatism, the most reactive case from above (Case J4) is rerun with 65 g Pu in the Exxon rods and 42 g Pu in the PNL rods (Case J12). Case J12 is the most reactive case, with $k_s = 0.89913$. This value is below the USL of 0.9288.

In Cases J13 through J15, the effect on the reactivity of replacing an AFS-C with a dummy fuel assembly is investigated. A dummy fuel assembly is a hollow stainless steel box that mimics the weight of a standard fuel assembly. As a dummy fuel assembly filled with air could increase transmission between packages, cases are run in which an AFS-C is replaced by water (Case J13), void (Case J14), and steel (Case J15). Of course, replacing an AFS-C with a dummy fuel assembly will greatly reduce the fissile mass in a package, and the reactivity is expected to reduce. Case J4, with an external water density of 0.1 g/cm^3 , is used as the base model. As expected, the reactivity drops in all cases compared to the base model. Replacing two AFS-C containers with dummy assemblies would further reduce the reactivity.

C6.6.2 HAC Array Results

Results for the HAC single package are provided in Table C6.6-1. The most reactive case is listed in boldface.

Table C6.6-1 – Criticality Results for an Infinite Array of HAC Packages

Case No.	Filename	Water Density (g/cm ³)		k_{eff}	σ	k_s ($k_{eff}+2\sigma$)
		Internal	External			
J1	ha_i100_o0	1	0	0.88784	0.00098	0.88980
J2	ha_i100_o0c2	1	0	0.88767	0.00098	0.88963
J3	ha_i100_o05	1	0.05	0.88858	0.00102	0.89062
J4	ha_i100_o10	1	0.1	0.88883	0.00099	0.89081
J5	ha_i100_o50	1	0.5	0.88725	0.00099	0.88923
J6	ha_i100_o100	1	1	0.88639	0.00098	0.88835
J7	ha_i100b_o0	1	0	0.88636	0.00097	0.88830
J8	ha_i95_o0	0.95	0	0.86787	0.00093	0.86973
J9	ha_i90_o0	0.9	0	0.84513	0.00095	0.84703
J10	ha_i75_o0	0.75	0	0.77254	0.00097	0.77448
J11	ha_i50_o0	0.5	0	0.62899	0.00088	0.63075
Case J12 is Case J4 with increased Pu mass in the fuel rods						
J12	ha_i100_o10h	1	0.1	0.89717	0.00098	0.89913
Dummy Fuel Assembly Cases						
J13	ha_i100_o10_dw	1	0.1	0.86969	0.00097	0.87163
J14	ha_i100_o10_dv	1	0.1	0.87115	0.00098	0.87311
J15	ha_i100_o10_ds	1	0.1	0.87246	0.00097	0.87440

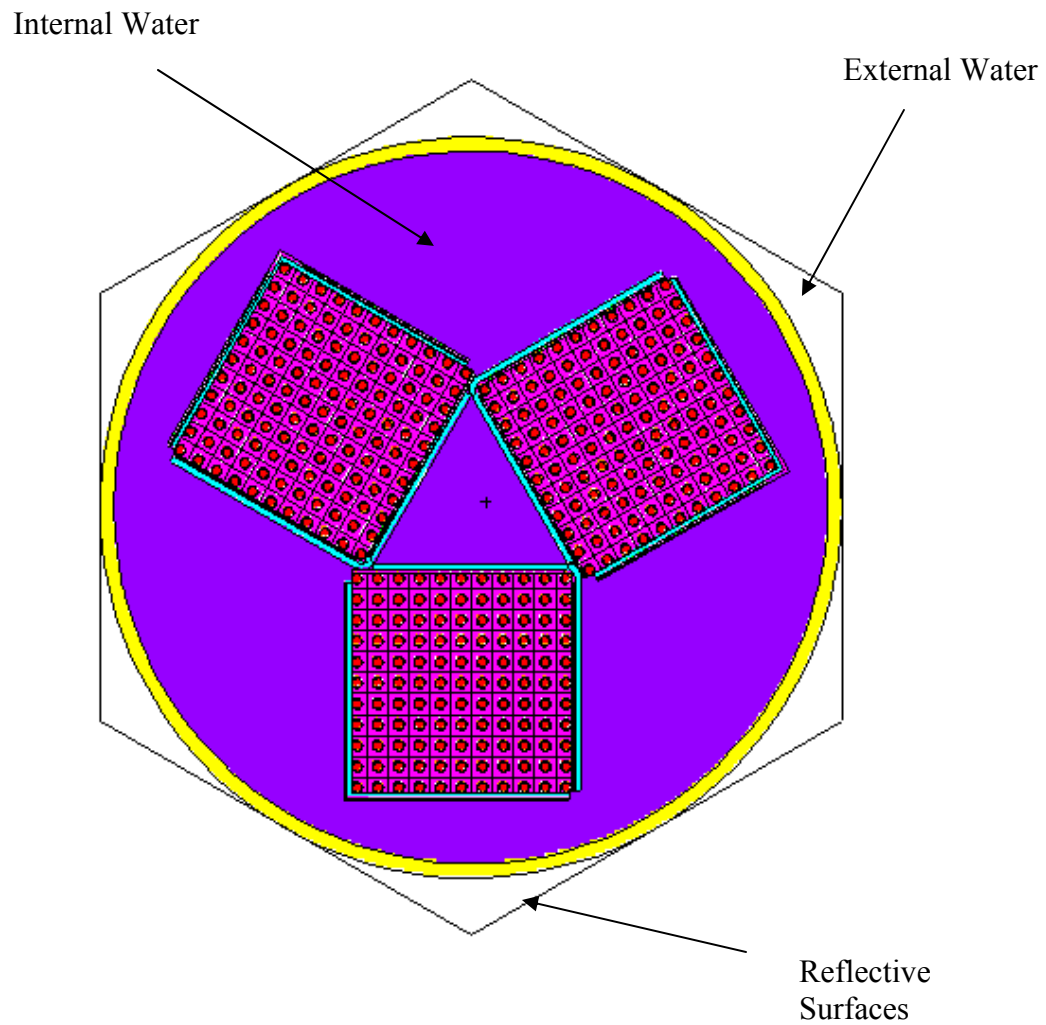


Figure C6.6-1 – HAC Array Geometry

This page left intentionally blank.

C6.7 Fissile Material Packages for Air Transport

This section does not apply for the MFFP, because air transport is not claimed.

This page left intentionally blank.

C6.8 Benchmark Evaluations

The benchmark evaluation is provided in Section 6.8, *Benchmark Evaluations*. A USL of 0.9288 is justified.

This page left intentionally blank.

C6.9 Appendices

Representative MCNP models are included in the following appendices:

C6.9.1 Single Package Model

C6.9.2 Infinite Array Model

This page left intentionally blank.

C6.9.1 Single Package Model

This file is for the worst-case HAC single package model (hsc_b11x11_t9x9h).

```

TA18
c
c *****Fuel Assembly*****
c cells 1 to 3 transform the 3 assemblies to their locations
c 1 4 -1.0 -21 22 -23 24 -25 6 imp:n=1 $ top nozzle, void
c 2 4 -1.0 -21 22 -23 24 -7 26 imp:n=1 $ bottom nozzle, void
c 7 0 -21 22 -23 24 126 -410 fill=20 imp:n=1 $ Exxon pins
c 8 0 -21 22 -23 24 410 -25 fill=21 imp:n=1 $ PNL pins
c
c 201 like 1 but trcl=53 $ assembly 2
c 202 like 2 but trcl=53
c 207 like 7 but trcl=53
c 208 like 8 but trcl=53
c 220 like 1 but trcl=54 $ assembly 3
c 221 like 2 but trcl=54
c 222 like 7 but trcl=54
c 223 like 8 but trcl=54
c
c -- "box" around fuel
c
c 301 0 (302 -303 300 -304 -906 26):
(303 -305 300 -301 -906 26) fill=30 imp:n=1 $ "box" cutout
c 302 like 301 but trcl=53
c 303 like 301 but trcl=54
c
c perimeter containing strongback #1 in -y
c 50 0 (26 -906 902 -909 904 -910):
(26 -906 909 -912 904 -901):
(26 -906 912 904 -908):
(26 -906 911 905 -904 -908):
(26 -906 905 -900 903 -911) fill=7 imp:n=1
c
c perimeter containing strongback #2
c 51 like 50 but trcl=53
c
c perimeter containing strongback #3
c 52 like 50 but trcl=54
c
c *****water beyond three units*****
c
c 131 9 -1.4 -61 -69 64 #7 #8 #50 #51 #52 #301 #302 #303
#207 #208 #222 #223 imp:n=1
c
c *****containment*****
c 141 5 -7.94 -62 -66 63 (61:65:-64) imp:n=1 $ outer steel
c 143 5 -7.94 -61 -70 69 imp:n=1 $ upper inner steel
c 145 4 -1.0 -61 -65 70 imp:n=1 $ upper void
c
c *****beyond containment*****
c 195 6 -7.94 -72 -76 73 (62:66:-63) imp:n=0.25 $ one foot refl
c 199 0 (72:76:-73) imp:n=0 $ outside world
c
c
c Universe 20: Exxon Fuel Lattice (lower)
c
c 200 4 -1.0 -12 11 -14 13 u=20 lat=1 trcl=30 fill=0:10 0:10 0:0
1 1 1 1 1 1 1 1 1 1 $ row 11
1 1 1 1 1 1 1 1 1 1 $ row 10
1 1 1 1 1 1 1 1 1 1 $ row 9
1 1 1 1 1 1 1 1 1 1 $ row 8
1 1 1 1 1 1 1 1 1 1 $ row 7
1 1 1 1 1 1 1 1 1 1 $ row 6
1 1 1 1 1 1 1 1 1 1 $ row 5
1 1 1 1 1 1 1 1 1 1 $ row 4
1 1 1 1 1 1 1 1 1 1 $ row 3
1 1 1 1 1 1 1 1 1 1 $ row 2
1 1 1 1 1 1 1 1 1 1 imp:n=1 $ row 1 (top)
c
c
c Universe 21: PNL Fuel Lattice (upper)
c
c 201 4 -1.0 -412 411 -414 413 u=21 lat=1 trcl=31 fill=0:8 0:8 0:0
2 2 2 2 2 2 2 2 $ row 9
2 2 2 2 2 2 2 2 $ row 8
2 2 2 2 2 2 2 2 $ row 7
2 2 2 2 2 2 2 2 $ row 6

```


C6.9.1-2

```

704      2    -2.713      720 -715 -716      u=7  imp:n=1  $ tan Al clad
706      2    -2.713      712 -722 -717      u=7  imp:n=1  $ rad Al clad
707     21  9.2244E-02    722 -723 -717
      770 771 772 773 774 775 776 777 778
      779 780 781 782 783 784 785 786 787
      790 791 792 793 794 795 796 797 798
      799 800 801 802 803 804 805 806 807 u=7  imp:n=1 $ radial boral
708      2    -2.713      723 -713 -717      u=7  imp:n=1 $ rad Al
710      4   -1.0      (710 711 -718):(716 -710 717 -715):
      (710 -713 717 -711)      u=7  imp:n=1
719      6   -7.94      ((-717 -712):(-716 -714 717))      -809 u=7  imp:n=1 $ poison holder
720      4   -1.0      ((-717 -712):(-716 -714 717))      809 -810 u=7  imp:n=1
721      6   -7.94      ((-717 -712):(-716 -714 717))      810 -811 u=7  imp:n=1
722      4   -1.0      ((-717 -712):(-716 -714 717))      811 -812 u=7  imp:n=1
723      6   -7.94      ((-717 -712):(-716 -714 717))      812 -813 u=7  imp:n=1
724      4   -1.0      ((-717 -712):(-716 -714 717))      813 -814 u=7  imp:n=1
725      6   -7.94      ((-717 -712):(-716 -714 717))      814 -815 u=7  imp:n=1
726      4   -1.0      ((-717 -712):(-716 -714 717))      815 -816 u=7  imp:n=1
727      6   -7.94      ((-717 -712):(-716 -714 717))      816 -817 u=7  imp:n=1
728      4   -1.0      ((-717 -712):(-716 -714 717))      817 -818 u=7  imp:n=1
729      6   -7.94      ((-717 -712):(-716 -714 717))      818 -819 u=7  imp:n=1
730      4   -1.0      ((-717 -712):(-716 -714 717))      819 -820 u=7  imp:n=1
731      6   -7.94      ((-717 -712):(-716 -714 717))      820 -821 u=7  imp:n=1
732      4   -1.0      ((-717 -712):(-716 -714 717))      821 -822 u=7  imp:n=1
733      6   -7.94      ((-717 -712):(-716 -714 717))      822 -823 u=7  imp:n=1
734      4   -1.0      ((-717 -712):(-716 -714 717))      823 -824 u=7  imp:n=1
735      6   -7.94      ((-717 -712):(-716 -714 717))      824 -825 u=7  imp:n=1
736      4   -1.0      ((-717 -712):(-716 -714 717))      825 -826 u=7  imp:n=1
737      6   -7.94      ((-717 -712):(-716 -714 717))      826 u=7  imp:n=1
c
750      6   -7.94      719 -720 -750      u=7  imp:n=1 $ screws in boral
751      6   -7.94      719 -720 -751      u=7  imp:n=1
752      6   -7.94      719 -720 -752      u=7  imp:n=1
753      6   -7.94      719 -720 -753      u=7  imp:n=1
754      6   -7.94      719 -720 -754      u=7  imp:n=1
755      6   -7.94      719 -720 -755      u=7  imp:n=1
756      6   -7.94      719 -720 -756      u=7  imp:n=1
757      6   -7.94      719 -720 -757      u=7  imp:n=1
758      6   -7.94      719 -720 -758      u=7  imp:n=1
759      6   -7.94      719 -720 -759      u=7  imp:n=1
760      6   -7.94      719 -720 -760      u=7  imp:n=1
761      6   -7.94      719 -720 -761      u=7  imp:n=1
762      6   -7.94      719 -720 -762      u=7  imp:n=1
763      6   -7.94      719 -720 -763      u=7  imp:n=1
764      6   -7.94      719 -720 -764      u=7  imp:n=1
765      6   -7.94      719 -720 -765      u=7  imp:n=1
766      6   -7.94      719 -720 -766      u=7  imp:n=1
767      6   -7.94      719 -720 -767      u=7  imp:n=1
c
770      6   -7.94      722 -723 -770      u=7  imp:n=1
771      6   -7.94      722 -723 -771      u=7  imp:n=1
772      6   -7.94      722 -723 -772      u=7  imp:n=1
773      6   -7.94      722 -723 -773      u=7  imp:n=1
774      6   -7.94      722 -723 -774      u=7  imp:n=1
775      6   -7.94      722 -723 -775      u=7  imp:n=1
776      6   -7.94      722 -723 -776      u=7  imp:n=1
777      6   -7.94      722 -723 -777      u=7  imp:n=1
778      6   -7.94      722 -723 -778      u=7  imp:n=1
779      6   -7.94      722 -723 -779      u=7  imp:n=1
780      6   -7.94      722 -723 -780      u=7  imp:n=1
781      6   -7.94      722 -723 -781      u=7  imp:n=1
782      6   -7.94      722 -723 -782      u=7  imp:n=1
783      6   -7.94      722 -723 -783      u=7  imp:n=1
784      6   -7.94      722 -723 -784      u=7  imp:n=1
785      6   -7.94      722 -723 -785      u=7  imp:n=1
786      6   -7.94      722 -723 -786      u=7  imp:n=1
787      6   -7.94      722 -723 -787      u=7  imp:n=1
c
790      6   -7.94      722 -723 -790      u=7  imp:n=1
791      6   -7.94      722 -723 -791      u=7  imp:n=1
792      6   -7.94      722 -723 -792      u=7  imp:n=1
793      6   -7.94      722 -723 -793      u=7  imp:n=1
794      6   -7.94      722 -723 -794      u=7  imp:n=1
795      6   -7.94      722 -723 -795      u=7  imp:n=1
796      6   -7.94      722 -723 -796      u=7  imp:n=1

```

```

797      6  -7.94      722 -723 -797      u=7  imp:n=1
798      6  -7.94      722 -723 -798      u=7  imp:n=1
799      6  -7.94      722 -723 -799      u=7  imp:n=1
800      6  -7.94      722 -723 -800      u=7  imp:n=1
801      6  -7.94      722 -723 -801      u=7  imp:n=1
802      6  -7.94      722 -723 -802      u=7  imp:n=1
803      6  -7.94      722 -723 -803      u=7  imp:n=1
804      6  -7.94      722 -723 -804      u=7  imp:n=1
805      6  -7.94      722 -723 -805      u=7  imp:n=1
806      6  -7.94      722 -723 -806      u=7  imp:n=1
807      6  -7.94      722 -723 -807      u=7  imp:n=1
c
810      6  -7.94      719 -720 -730      u=7  imp:n=1
811      6  -7.94      719 -720 -731      u=7  imp:n=1
812      6  -7.94      719 -720 -732      u=7  imp:n=1
813      6  -7.94      719 -720 -733      u=7  imp:n=1
814      6  -7.94      719 -720 -734      u=7  imp:n=1
815      6  -7.94      719 -720 -735      u=7  imp:n=1
816      6  -7.94      719 -720 -736      u=7  imp:n=1
817      6  -7.94      719 -720 -737      u=7  imp:n=1
818      6  -7.94      719 -720 -738      u=7  imp:n=1
819      6  -7.94      719 -720 -739      u=7  imp:n=1
820      6  -7.94      719 -720 -740      u=7  imp:n=1
821      6  -7.94      719 -720 -741      u=7  imp:n=1
822      6  -7.94      719 -720 -742      u=7  imp:n=1
823      6  -7.94      719 -720 -743      u=7  imp:n=1
824      6  -7.94      719 -720 -744      u=7  imp:n=1
825      6  -7.94      719 -720 -745      u=7  imp:n=1
826      6  -7.94      719 -720 -746      u=7  imp:n=1
827      6  -7.94      719 -720 -747      u=7  imp:n=1
c
c      Universe 30:  "box" around fuel
c
c 310      2  -2.713      -313 317      u=30 imp:n=1 $ radial left
c 311      2  -2.713      316 -310      u=30 imp:n=1 $ tangential bot
c 312      2  -2.713      314 -315 317 u=30 imp:n=1 $ radial right
c 315      2  -2.713      311 -312 316 u=30 imp:n=1 $ tangential top
316      6  -7.94      315 312      u=30 imp:n=1
317      4  -1.0      (312 -317 -315):(-316 -312) u=30 imp:n=1
c
320      4  -1.0      -315 317 -320      u=30 imp:n=1 $ radial water gap
321      21  9.2244E-02 313 -314 317 320 -321 u=30 imp:n=1 $ radial boral
322      4  -1.0      -315 317 321 -322 u=30 imp:n=1
323      21  9.2244E-02 313 -314 317 322 -323 u=30 imp:n=1
324      4  -1.0      -315 317 323 -324 u=30 imp:n=1
325      21  9.2244E-02 313 -314 317 324 -325 u=30 imp:n=1
326      4  -1.0      -315 317 325 -326 u=30 imp:n=1
327      21  9.2244E-02 313 -314 317 326 -327 u=30 imp:n=1
328      4  -1.0      -315 317 327 -328 u=30 imp:n=1
329      21  9.2244E-02 313 -314 317 328 -329 u=30 imp:n=1
330      4  -1.0      -315 317 329 -330 u=30 imp:n=1
331      21  9.2244E-02 313 -314 317 330 -331 u=30 imp:n=1
332      4  -1.0      -315 317 331 -332 u=30 imp:n=1
333      21  9.2244E-02 313 -314 317 332 -333 u=30 imp:n=1
334      4  -1.0      -315 317 333      u=30 imp:n=1
c
340      2  -2.713      -313 317 320 -321 u=30 imp:n=1 $ radial Al cladding
341      2  -2.713      -313 317 322 -323 u=30 imp:n=1
342      2  -2.713      -313 317 324 -325 u=30 imp:n=1
343      2  -2.713      -313 317 326 -327 u=30 imp:n=1
344      2  -2.713      -313 317 328 -329 u=30 imp:n=1
345      2  -2.713      -313 317 330 -331 u=30 imp:n=1
346      2  -2.713      -313 317 332 -333 u=30 imp:n=1
c
347      2  -2.713      314 -315 317 320 -321 u=30 imp:n=1 $ radial Al cladding
348      2  -2.713      314 -315 317 322 -323 u=30 imp:n=1
349      2  -2.713      314 -315 317 324 -325 u=30 imp:n=1
350      2  -2.713      314 -315 317 326 -327 u=30 imp:n=1
351      2  -2.713      314 -315 317 328 -329 u=30 imp:n=1
352      2  -2.713      314 -315 317 330 -331 u=30 imp:n=1
353      2  -2.713      314 -315 317 332 -333 u=30 imp:n=1
c
360      4  -1.0      -312 316 -320      u=30 imp:n=1 $ tangential water gap
361      21  9.2244E-02 310 -311 316 320 -321 u=30 imp:n=1 $ tangential boral
362      4  -1.0      -312 316 321 -322 u=30 imp:n=1

```

```

363 21 9.2244E-02 310 -311 316 322 -323 u=30 imp:n=1
364 4 -1.0 -312 316 323 -324 u=30 imp:n=1
365 21 9.2244E-02 310 -311 316 324 -325 u=30 imp:n=1
366 4 -1.0 -312 316 325 -326 u=30 imp:n=1
367 21 9.2244E-02 310 -311 316 326 -327 u=30 imp:n=1
368 4 -1.0 -312 316 327 -328 u=30 imp:n=1
369 21 9.2244E-02 310 -311 316 328 -329 u=30 imp:n=1
370 4 -1.0 -312 316 329 -330 u=30 imp:n=1
371 21 9.2244E-02 310 -311 316 330 -331 u=30 imp:n=1
372 4 -1.0 -312 316 331 -332 u=30 imp:n=1
373 21 9.2244E-02 310 -311 316 332 -333 u=30 imp:n=1
374 4 -1.0 -312 316 333 u=30 imp:n=1
c
380 2 -2.713 316 311 -312 320 -321 u=30 imp:n=1 $ horizontal Al cladding
381 2 -2.713 316 311 -312 322 -323 u=30 imp:n=1
382 2 -2.713 316 311 -312 324 -325 u=30 imp:n=1
383 2 -2.713 316 311 -312 326 -327 u=30 imp:n=1
384 2 -2.713 316 311 -312 328 -329 u=30 imp:n=1
385 2 -2.713 316 311 -312 330 -331 u=30 imp:n=1
386 2 -2.713 316 311 -312 332 -333 u=30 imp:n=1
c
387 2 -2.713 316 -310 320 -321 u=30 imp:n=1 $ horizontal Al cladding
388 2 -2.713 316 -310 322 -323 u=30 imp:n=1
389 2 -2.713 316 -310 324 -325 u=30 imp:n=1
390 2 -2.713 316 -310 326 -327 u=30 imp:n=1
391 2 -2.713 316 -310 328 -329 u=30 imp:n=1
392 2 -2.713 316 -310 330 -331 u=30 imp:n=1
393 2 -2.713 316 -310 332 -333 u=30 imp:n=1
c
c Universe 51: Dummy universe containing fuel
c
c 999 1 -10.31 -999 u=51 imp:n=1 $ for diagnostics only, not used
c 1000 1 -10.31 999 u=51 imp:n=1 $ for diagnostics only, not used
c
c *****Fuel Assembly*****
c Exxon fuel pin
401 cz 0.471932 $ fuel radius
402 cz 0.48387 $ radius inside clad
403 cz 0.57277 $ radius outside clad
404 pz 88.9 $ top of fuel
405 pz -88.9 $ bottom of fuel
406 pz 106.8404 $ top of fuel pin
407 pz -89.4 $ bottom of fuel pin
408 pz 106.3404 $ bottom of top cap
c
410 pz 2.46 $ divide between different pins
411 px -1.3074 $ PNL lattice definition (upper)
412 px 1.3074
413 py -1.3074
414 py 1.3074
c
421 cz 0.652145 $ fuel radius
422 cz 0.6604 $ radius inside clad
423 cz 0.71755 $ radius outside clad
424 pz 35.56 $ top of fuel
425 pz -35.56 $ bottom of fuel
c
11 px -1.0604 $ Exxon lattice definition (lower)
12 px 1.0604
13 py -1.0604
14 py 1.0604
c 200 pz -119.38
c guide tube
18 cz 0.57150
19 cz 0.61214
c perimeter of fuel assembly
21 px 10.2391 $ offset from surface 905
22 px -12.1116 $
23 py -6.6593 $ offset from surface 904
24 py -29.0113 $
25 pz 226.466
26 pz -190.95720
126 pz -193.776
c *****containment*****
61 cz 36.1950

```

```

62      cz      37.6174
63      pz      -197.5866  $ 1.5" thick
64      pz      -193.7766  $ 1.11" below bottom of fuel (strongback bottom not modeled)
65      pz      235.6866
66      pz      237.5916
c 67      pz      -203.0222
c 68      pz      -201.1172
69      pz      226.4664
70      pz      228.0666
c      *****outside of water refl****
72      cz      68.0974
73      pz      -228.0666  $ 1' water from 63
76      pz      268.0716  $ 1' water from 66
c
c -- "box"
c
300      py -29.7925  $ defining box in u=0
301      py -29.0114
302      px -12.8928
303      px -12.1117
304      py -7.5675
305      px 9.9672
c
310      25 py 0.04445
311      25 py 0.2604
312      25 py 0.3048
313      25 px 0.04445
314      25 px 0.2604
315      25 px 0.3048
316      25 px 2.54
317      25 py 2.54
c
320      pz -171.049
321      pz -119.532
322      pz -109.758
323      pz -67.412
324      pz -57.638
325      pz -15.316
326      pz -5.542
327      pz 36.855
328      pz 46.629
329      pz 89.002
330      pz 98.776
331      pz 141.097
332      pz 150.871
333      pz 193.548
c
c      strongback surfaces
c
710      22 px 0
711      22 py 0
712      22 px 0.476
713      22 px 0.7808
714      22 py 0.476
715      22 py 0.7808
716      22 px -0.3114  $ 0.43" less than surface 713
717      22 py -0.54
718      22 cz 0.7808
719      22 py 0.5205
720      22 py 0.7364
722      22 px 0.5205
723      22 px 0.7364
c
730      22 c/y -2.7752 -189.6872 0.47625
731      22 c/y -2.7752 -179.5526 0.47625
732      22 c/y -2.7752 -172.3187 0.47625
733      22 c/y -2.7752 -118.2624 0.47625
734      22 c/y -2.7752 -111.0285 0.47625
735      22 c/y -2.7752 -66.1416 0.47625
736      22 c/y -2.7752 -58.9077 0.47625
737      22 c/y -2.7752 -14.0462 0.47625
738      22 c/y -2.7752 -6.8123 0.47625
739      22 c/y -2.7752 38.1254 0.47625
740      22 c/y -2.7752 45.3593 0.47625
741      22 c/y -2.7752 90.2716 0.47625

```

742 22 c/y -2.7752 97.5055 0.47625
743 22 c/y -2.7752 142.3670 0.47625
744 22 c/y -2.7752 149.6009 0.47625
745 22 c/y -2.7752 194.8180 0.47625
746 22 c/y -2.7752 202.0519 0.47625
747 22 c/y -2.7752 213.8172 0.47625
c
750 22 c/y -16.7452 -189.6872 0.47625
751 22 c/y -16.7452 -179.5526 0.47625
752 22 c/y -16.7452 -172.3187 0.47625
753 22 c/y -16.7452 -118.2624 0.47625
754 22 c/y -16.7452 -111.0285 0.47625
755 22 c/y -16.7452 -66.1416 0.47625
756 22 c/y -16.7452 -58.9077 0.47625
757 22 c/y -16.7452 -14.0462 0.47625
758 22 c/y -16.7452 -6.8123 0.47625
759 22 c/y -16.7452 38.1254 0.47625
760 22 c/y -16.7452 45.3593 0.47625
761 22 c/y -16.7452 90.2716 0.47625
762 22 c/y -16.7452 97.5055 0.47625
763 22 c/y -16.7452 142.3670 0.47625
764 22 c/y -16.7452 149.6009 0.47625
765 22 c/y -16.7452 194.8180 0.47625
766 22 c/y -16.7452 202.0519 0.47625
767 22 c/y -16.7452 213.8172 0.47625
c
770 22 c/x -5.9248 -189.6872 0.47625
771 22 c/x -5.9248 -179.5526 0.47625
772 22 c/x -5.9248 -172.3187 0.47625
773 22 c/x -5.9248 -118.2624 0.47625
774 22 c/x -5.9248 -111.0285 0.47625
775 22 c/x -5.9248 -66.1416 0.47625
776 22 c/x -5.9248 -58.9077 0.47625
777 22 c/x -5.9248 -14.0462 0.47625
778 22 c/x -5.9248 -6.8123 0.47625
779 22 c/x -5.9248 38.1254 0.47625
780 22 c/x -5.9248 45.3593 0.47625
781 22 c/x -5.9248 90.2716 0.47625
782 22 c/x -5.9248 97.5055 0.47625
783 22 c/x -5.9248 142.3670 0.47625
784 22 c/x -5.9248 149.6009 0.47625
785 22 c/x -5.9248 194.8180 0.47625
786 22 c/x -5.9248 202.0519 0.47625
787 22 c/x -5.9248 213.8172 0.47625
c
790 22 c/x -16.9789 -189.6872 0.47625
791 22 c/x -16.9789 -179.5526 0.47625
792 22 c/x -16.9789 -172.3187 0.47625
793 22 c/x -16.9789 -118.2624 0.47625
794 22 c/x -16.9789 -111.0285 0.47625
795 22 c/x -16.9789 -66.1416 0.47625
796 22 c/x -16.9789 -58.9077 0.47625
797 22 c/x -16.9789 -14.0462 0.47625
798 22 c/x -16.9789 -6.8123 0.47625
799 22 c/x -16.9789 38.1254 0.47625
800 22 c/x -16.9789 45.3593 0.47625
801 22 c/x -16.9789 90.2716 0.47625
802 22 c/x -16.9789 97.5055 0.47625
803 22 c/x -16.9789 142.3670 0.47625
804 22 c/x -16.9789 149.6009 0.47625
805 22 c/x -16.9789 194.8180 0.47625
806 22 c/x -16.9789 202.0519 0.47625
807 22 c/x -16.9789 213.8172 0.47625
c
809 pz -188.417
810 pz -181.331 \$ PH 1 (bottom)
811 pz -170.541 \$ PH 1
812 pz -120.040 \$ PH 2
813 pz -109.250
814 pz -67.920 \$ PH 3
815 pz -57.130
816 pz -15.824 \$ PH 4
817 pz -5.034
818 pz 36.347 \$ PH 5
819 pz 47.137

```

820 pz 88.494 $ PH 6
821 pz 99.284
822 pz 140.589 $ PH 7
823 pz 151.379
824 pz 193.040 $ PH 8
825 pz 203.830 $ PH 8
826 pz 212.547
c
900 px 11.18006 $ FIXED for strongbacks touching
901 py -5.71956 $ FIXED for strongbacks touching
902 px -11.9593
903 py -28.7574 $ surface 901 minus 9.07"
c
c 904 is -7.1354 and 905 is 9.7633 for nominal case (with poison holders).
c they are shifted to cut off poison holders to allow for
c expansion for damaged cases.
c
c To completely "slice off" the poison holders, set
c 904 to -6.6593 and 905 to 10.2392.
c
904 py -6.6593 $ tangential strongback lower bound, surface 901 minus total thickness
905 px 10.2392 $ radial strongback left bound, surface 901 minus total thickness
906 pz 215.7222
908 c/z 9.87856 -7.02106 1.3015
909 px -9.9019
910 py -6.35448
911 py -7.1344 $ fixed
912 px 9.7653 $ fixed
c
998 so 10000
999 pz 345.5565

mode n
c print
kcode 2000 0.9 30 530
sdef cell=d1 pos=0 0 0 rad=d3 ext=d4 axs=0 0 1
si1 1 7:200:10 207:200:10 222:200:10 8:201:430 208:201:430 223:201:430
spl 121 121 121 81 81 81
si3 0.652145
si4 88.9
cut:n j j 0 0
c
c Materials
c
m1 92235 -0.592 $ Exxon fuel pellet
92238 -82.746
94239 -3.828
94240 -0.674
94241 -0.313
8016 -11.847
m2 13027 1.0 $ aluminum cladding for BORAL
m3 92235 -0.597 $ PNL fuel pellet
92238 -83.483
94239 -3.238
94240 -0.570
94241 -0.265
8016 -11.848
m4 1001 2 $ water
8016 1
mt4 lwtr.01t
m5 6000 -0.06 $ XM-19
7014 -0.4
14000 -0.75
15031 -0.04
16032 -0.03
23000 -0.3
24000 -23.5
25055 -6
28000 -13.5
41093 -0.3
42000 -3
26000 -52.12
m6 6000 -0.08 $ SS-304
14000 -1.0
15031 -0.045

```

```

24000      -19.0
25055      -2.0
26000     -68.375
28000      -9.5
m7  40000    -1.0  $ Cladding
c   41093    -0.030
m8  82000     1.0  $ lead
m9   6000    -25.1  $ water/steel mix, 5.8% steel by volume
      14000    -313.9
      15031    -14.1
      24000   -5964.9
      25055   -627.9
      26000  -21465.8
      28000  -2982.5
      1001   -7240.1
      8016   -57462.7
mt9  lwtr.01t
m21  5010    7.3123E-03 $ 35 mg/cm2 B-10, 75% credit
      5011    3.9244E-02
      6000    1.2248E-02
      13027    3.3439E-02
c     total 9.2244E-02
c
c     Translations
c
c     tr22 is the intersection of planes 904 and 905
c     when the poison holders are present (904 and 905 shift when it is
c     desired to "slice off" the poison holders).
c     Note that the origin of Universe 7 corresponds to the intersection
c     of these planes.
c
c     *tr22      9.7643 -7.1354 0.0
c
c     tr25 is the intersection of planes 300 and 302. The origin of Universe 30
c     corresponds to the intersection of these planes.
c
c     *tr25     -12.8928 -29.7925 0.0
c
c     tr30 is computed by taking the coordinates of the intersection of planes
c     22 and 24 and adding half the pitch (note: can't be exact or else planes will
c     overlap, causing program termination.)
c
c     *tr30     -11.5389 -28.4386 -104.38 $ lower fuel (Exxon lower)
c     *tr31     -11.3941 -28.2938 38.03  $ upper fuel (PNL upper)
c
c     tr53 and tr54 rotate the bottom assembly to create assemblies 2 and 3
c
c     *tr53      0 0 0           120 30 90   150 120 90   90 90 0  $ +x+y
c     *tr54      0 0 0           120 150 90   30 120 90   90 90 0  $ -x-y

```


This page left intentionally blank.

C6.9.2 Infinite Array Model

The infinite array models are geometrically the same as the single package models, although small changes have been made to the outer boundary to simulate the infinite array. Additional cells and surfaces are listed below.

```
195      0      -881 882 -886 885 -883 884 -66 63 62  imp:n=1 $ w between packages
199      0      (881:-882:886:-885:883:-884:66:-63)  imp:n=0 $ outside world
```

```
c      hexagonal boundary of one unit lattice cell, close packed
*881    px      37.6184
*882    px     -37.6184
*883    p     -0.5000000      0.866025404      0.0000000      37.6184
*884    p     -0.5000000      0.866025404      0.0000000     -37.6184
*885    p      0.5000000      0.866025404      0.0000000     -37.6184
*886    p      0.5000000      0.866025404      0.0000000      37.6184
```

This page left intentionally blank.

C7.0 PACKAGE OPERATIONS

C7.1 Package Loading

The AFS-C contents are loaded in the following manner:

1. Remove the 22 bolts that attach the lid of the AFS-C. Remove the AFS-C lid.
2. Load up to 116 Exxon rods and up to 69 PNL rods into the AFS-C. Place the Exxon rods into the Exxon cavity (long), and place the PNL rods into the PNL cavity (short). Within each cavity, add steel or aluminum dunnage rods until all space is filled. Alternately, the Exxon rods may be shipped with an empty PNL cavity, or the PNL rods may be shipped with an empty Exxon cavity. Ensure that the loaded AFS-C meets the applicable heat load limits.
3. Place the AFS-C lid on the body. Tighten the 22 bolts to the torque value specified on *Packaging General Arrangement Drawing 99008-61*. For each bolt, bend lock tab against bolt flat.

Once the AFS-C has been loaded, the package loading operations are essentially the same as the operations for fuel assembly loading described in Chapter 7.1, *Package Loading*. The AFS-C is handled in the same manner as a fuel assembly.

The only difference is the tightening of the swivel clamp pads. Because the AFS-C is constructed of aluminum, a thermal expansion gap is provided. Therefore, modify Step 18 of Section 7.1.2.1, *Loading of Fuel Assemblies into Strongback*, as follows:

- 7.1.2.1, Step 18: Tighten the four (4) 3/4-inch swivel clamp pads on the top plate until the screw pad contacts the AFS-C top. Then loosen each swivel clamp pad 1 – 1½ turns, and lock in place with a hex nut.

C7.2 Package Unloading

The package unloading operations are the same as the operations for fuel assembly unloading described in Chapter 7.2, *Package Unloading*. The AFS-C is handled in the same manner as a fuel assembly.

The AFS-C contents are unloaded in the following manner:

1. Remove the 22 bolts that attach the lid of the AFS-C. Remove the AFS-C lid.
2. Unload the fuel and dunnage rods present.
3. Place the AFS-C lid on the body. Tighten the 22 bolts to the torque value specified on *Packaging General Arrangement Drawing 99008-61*. For each bolt, bend lock tab against bolt flat.

C7.3 Preparation of an Empty Package for Transport

Previously used and empty MFFPs shall be prepared and transported per the requirements of 49 CFR §173.428¹.

C7.4 Preshipment Leakage Rate Test

The preshipment leakage rate test is the same as described in Section 7.4, *Preshipment Leakage Rate Test*.

¹ Title 49, Code of Federal Regulations, Part 173 (49 CFR 173), *Shippers—General Requirements for Shipments and Packagings*, 10-01-06 Edition.

C8.0 ACCEPTANCE TESTS AND MAINTENANCE PROGRAM

C8.1 Acceptance Tests

Per the requirements of 10 CFR §71.85¹, this section discusses the inspections and tests to be performed prior to first use of the AFS-C rod container.

C8.1.1 Visual Inspections and Measurements

Each AFS-C rod container shall be examined in accordance with the requirements delineated on the drawings in Appendix C1.4.2, *Packaging General Arrangement Drawings*, prior to use.

C8.1.2 Weld Inspections

All welds shall be inspected to the requirements delineated on the drawings in Appendix C1.4.2, *Packaging General Arrangement Drawings*.

C8.1.3 Structural and Pressure Tests

The AFS-C rod container does not require any lifting device load tests or pressure tests.

C8.1.4 Fabrication Leakage Rate Tests

The AFS-C rod container does not require any leakage rate tests.

C8.1.5 Component and Material Tests

The AFS-C rod container does not require any component or material tests.

C8.1.6 Shielding Tests

The AFS-C rod container does not require any shielding tests.

C8.1.7 Thermal Tests

The AFS-C rod container does not require any thermal tests.

¹ Title 10, Code of Federal Regulations, Part 71 (10 CFR 71), *Packaging and Transportation of Radioactive Material*, 01-01-06 Edition.

C8.2 Maintenance Program

The AFS-C rod container does not require a scheduled maintenance program. The parts which are routinely handled during use (the body, the lid, and the lid fasteners) are visually inspected prior to use. Damaged components shall be repaired or replaced prior to use.